1993

Fluid Dynamics Of High-temperature Bubble And Slurry Bubble Columns

Julie Chabot

FLUID DYNAMICS OF HIGH TEMPERATURE BUBBLE AND SLURRY BUBBLE COLUMNS

VOLUME 1

by

Julie Chabot

Department of Biochemical and Chemical Engineering

Submitted in partial fulfilment
of the requirements for the degree of
Doctor of Philosophy

Faculty of Graduate Studies
The University of Western Ontario
London, Ontario

February 1993

ISBN 0-315-81312-1

ABSTRACT

The present Ph.D. dissertation was focused on the study of the fluid dynamics of high temperature bubble and slurry bubble columns. The study was centred on a system of particular interest for the petrochemical industry, the liquid phase methanol synthesis process, for which very little information is currently available. Emphasis was placed on the study of important gas phase parameters, including the gas holdup, the bubble rise velocity, the bubble chord length and the bubble chord length distribution, which were measured using spherical bulb fibre optic sensors.

The experiments were conducted in a 0.2 m diameter and 2.4 m height carbon steel column operated in the batch mode with respect to the liquid or slurry suspension. The gas superficial velocity was varied between 2.2 and 14.7 cm/s, while the operating temperature ranged from 25 to 175°C. In order to reliably represent the system studied (methanol synthesis), the exact liquid (paraffinic oil) and solid (ZnO-CuO catalyst) phases encountered in this system were used. Nitrogen was used as the gas phase. The fibre optic sensors (two) were implemented using a newly designed insertion device that allowed flexible and precise radial and axial displacement of the sensors. This device provided the possibility to investigate the bubble characteristics at

several locations in the column, including the proximity to the gas distributor and the column wall.

Important information concerning the radial and axial profiles of crucial gas phase properties such as the gas holdup, the bubble velocity, the bubble frequency, the bubble axial chord length and the bubble axial chord length distribution was obtained under a significant range of operating conditions. The information and the mathematical modelling presented in this work unveil important fluid dynamics features of bubble and slurry bubble column reactors, such as the dual cell flow pattern and the bubble "coalescence-break-up" regime. This study contributes, in this sense, to a better understanding of the complex fluid dynamics and mixing patterns encountered in bubble and slurry bubble columns in general, while providing reliable data for a number of systems of prime interest for the petrochemical industry.

ACKNOWLEDGEMENTS

The author expresses her sincere gratitude to Prof. H.I. de Lasa for his excellent support and assistance in the supervision of this work.

Special thanks are due to Mr. Souheil Afara for his very valuable cooperation in various aspects of this study. Sincere appreciation is conveyed to Mr. Ahmet Pekediz for his precious support and technical advices. Thanks are also due to my fellow colleagues José Arandes, Alberto Blasetti, Mariano Del Pozo, Hany Farag, Aro Gervais, Paul Lee, Alberto Soria and many others for their support and friendship.

The Professors and the staff of the Department of Chemical and Biochemical Engineering, the staff of the University Machine Shop of the Faculty of Engineering Science and the staff of the Electronic Shop of the Faculty of Engineering Science deserve special thanks for their assistance.

The University of Western Ontario, the Government of Ontario, the Government of Quebec, and the National Sciences and Engineering Research Council of Canada are also recognized for their financial support.

Sincere acknowledgment is expressed to my family for their continual encouragement and solicitude.

Last, but not least, the author wishes to convey her gratitude to Dr. François Simard for his endless understanding and encouragement and his inestimable and caring advices.

TABLE OF CONTENTS

VOLUME 1

LIST OF TABLES

LIST OF FIGURES

VOLUME 2

APPENDICES

NOMENCLATURE

A	Cross-sectional area of fluidized bed
a	Gas-liquid interfacial area
Bo	Bond number
C_1	Parameter
$C(f)$	Normalized cumulative periodogram
C_{xy}	Normalized cross-correlation function
D_c	Column diameter
d_{avg}	Volume-based arithmetic average solid particle diameter
d_b	Bubble diameter
d_{bi}	Individual bubble diameter
d_{vs}	Sauter mean bubble diameter
f	Frequency
f_1	Parameter
Fr	Froude number
g	Gravitational acceleration
Ga	Galileo number
H	Height
H_b	Fluidized bed height
I	Luminous intensity
I_o	Luminous reference intensity
$I(\theta)$	Parameter
J_0	Parameter
J_1	Parameter
m	Parameter in Eq.(5.2)

M_s Total weight of solid particles

N_i Number of bubbles having diameter d_b

p(x) Probability distribution function

P Pressure

ΔP Pressure drop

r Radial position

R Column radius

s Thickness of the absorbing medium

t Time

Δt_i Fraction of the time during which the tip of the sensor is in contact with the gas phase

T Temperature

T_t Total data acquisition time

U_l Local liquid velocity

$U_{l,c}$ Local liquid velocity (center)

$U_{l,w}$ Local liquid velocity (wall)

u_x Mean value of time series x(t)

u_y Mean value of time series y(t)

V_g Superficial gas velocity

V_b Bubble rise velocity

V_l Superficial liquid velocity

$V_{l.b.}$ Large bubble rise velocity

$V_{s.b.}$ Small bubble rise velocity

V_{slip} Bubble slip velocity

V_{trans} Transition gas superficial velocity

v_l Volume of liquid drained from the column

x Random variable

$x(t)$ Time series of signals from the lower optical sensor

$y(t)$ Time series of signals from the upper optical sensor

z Axial position

Greek

α Population mean

δ Conductivity in the bed

δ_o Conductivity in the liquid alone

ϵ Holdup

$\epsilon_{g,avg}$ Average radial gas holdup

$\epsilon_{g,loc}$ Local gas holdup

ϵ_{repeat} Local gas holdup for every repeated runs

θ Dimensionless radial position (r/R)

λ Coefficient of mass absorption

μ Scale parameter

σ_g Gas viscosity

μ_l Liquid viscosity

ξ_{xy} Covariance function

ρ Density

σ Shape parameter

σ_l Liquid surface tension

σ_x Standard deviation of x series

σ_y Standard deviation of y series

τ Time lag

τ Parameter in Eq.(5.8)

τ_s Shear stress

ν_t Turbulent kinematic viscosity

Ω Drift flux velocity

Subscripts

g gas

l liquid

s solid

Superscript

n exponent

CHAPTER 1

GENERAL REVIEW

1.1 INTRODUCTION

The importance of multiphase contactors involving gas-liquid or gas-liquid-solid mixtures is well established in the chemical, petrochemical and biochemical engineering industries. Bubble column and slurry bubble column reactors, with concurrent upward flow of gas or gas and liquid (liquid being the continuous phase) have emerged in recent years as very promising devices for multiphase operation. Typical processes conducted in bubble and slurry bubble columns include hydrotreating and conversion of heavy petroleum residues, fermentation (production of ethanol and mammalian cells), biological waste water treatment, flue gas desulfurization, Fischer-Tropsch, methanol synthesis, dimethyl ether production, polymerization (production of polyolefins), oxidation (adiponitrile synthesis), hydrogenation (saturation of fatty acids) and chlorination (production of aliphatic and aromatic chlorinated compounds) (Fan, 1989; Dudukovic and Devanathan, 1992; Lewnard et al., 1990).

The interest for slurry bubble column reactor technology is particularly pronounced in the fuel processing industry for which a number of challenging slurry bubble column reactor technology applications have recently gained recognition.

This is indeed true of the Fischer-Tropsch and oxygenates synthesis processes. Actually, the slurry bubble column reactor technology application for these particular processes was recently reported (Zhou et al., 1992) to be a high priority research activity area for the indirect coal liquefaction program of the U.S. Department of Energy/Pittsburgh Energy Technology Center (DOE-PETC). The slurry phase Fischer-Tropsch synthesis is considered a potentially economical way of converting coal derived synthesis gas into liquid fuels due to its improved thermal efficiency and ability to process CO-rich synthesis gas. The slurry process presents substantial potential advantages over conventional vapour phase processes (fixed bed and entrained bed reactors) (Bukur and Daly, 1987; Bukur et al., 1987b).

The slurry bubble column reactor technology was also proposed as a promising alternative way to carry out the synthesis of methanol (Sherwin and Frank, 1976; Frank and Mednick, 1982; Brown, 1984; Roberts et al., 1985; Weimer et al., 1987; Frey et al., 1988; Roberts et al., 1990). This is particularly important knowing that methanol as an alternative fuel, fuel additive, fuel intermediate, and gas turbine fuel for power generation is becoming increasingly important. The Liquid-Phase Methanol Process (LPMEOH) constitutes a major departure from traditional process designs based on fixed-bed catalytic reactors. The heart of the LPMEOH Process is a slurry reactor containing an inert hydrocarbon liquid (paraffinic oil) in

which the methanol synthesis catalyst is suspended and through which the synthesis gas feed is sparged. The inert liquid hydrocarbon absorbs the heat of reaction very effectively from the relatively small (≈ 10 μm) catalyst particles, and the backmixing behaviour and the higher heat transfer rates per unit volume of the slurry reactor permits a very close approach to isothermal operation. The LPMEOH process was recently extended to the production of dimethyl ether (DME), an important intermediate in several alternative fuels processes, converting synthesis gas to liquid fuels. The new slurry based process (Lewnard et al, 1990; Gogate et al., 1992) yields DME and variable amounts of co-product methanol from synthesis gas in a single step. The water gas shift, methanol synthesis and methanol dehydration reactions proceed concurrently in the three phase reactor. The methanol synthesis catalyst ($ZnO-CuO-Al_2O_3$) and the methanol dehydration catalyst (gamma-alumina) are slurried in the inert liquid phase, while the synthesis gas and the products (methanol, water and dimethyl ether) constitute the vapour phase.

The above mentioned applications of the slurry bubble column technology undoubtedly offer great promises. The potential widespread application of bubble column systems in various areas of the chemical industry motivated substantial research activities. The abundant literature related to bubble and slurry bubble columns indeed confirms this fact. However, despite considerable research efforts, recent reviews of the

current literature (Shah et al., 1982; Deckwer and Schumpe, 1987; Yoshida, 1988; Fan, 1989; Dudukovic and Devanathan, 1992; Deckwer and Schumpe, 1992) revealed that the general understanding of bubble and slurry bubble column technology is far from complete. The design, scale-up and optimum operation of these technologies are still founded on empiricism and remain a major difficulty. Current bubble column and slurry bubble column reactor design and scale-up procedures involve time consuming and costly multistage and multi-scale pilot plant experimentation, thus limiting the economical competitiveness of these new technologies (Dudukovic and Devanathan, 1992).

The accurate design, scale-up and operation of bubble column reactors and slurry bubble column reactors is highly dependent upon the ability to understand and properly describe their respective hydrodynamics (Dudukovic and Devanathan, 1992). Actually, Tarmy and Coulaloglou (1992) recently stated that the most critical element in developing and scaling-up a gas/liquid/solid reactor is the thorough understanding of its hydrodynamics. The hydrodynamic characteristics of bubble and slurry bubble columns are intimately linked to the velocity, size, size distribution and spatial allocation of gas bubbles. Consequently, the clear understanding of these parameters (gas holdup, bubble size, bubble size distribution, bubble velocity and their respective spatial arrangement) is essential to the extensive knowledge and overall comprehension of bubble and

slurry bubble columns.

A number of research activities were devoted to the study of the gas phase hydrodynamic parameters in bubble and slurry bubble columns, as reviewed by Shah et al. (1982) and Fan (1989). However, these studies were mainly conducted in small scale laboratory units (D_c < 15 cm), in presence of aqueous liquids or polar liquids, under ambient temperature and atmospheric pressure conditions (Reilly et al., 1986). These conditions differ substantially from the ones to be encountered in systems of interest for the fuel industry (methanol synthesis, Fischer-Tropsch, hydrotreating ...). Actually, these systems operate under severe conditions (high temperature, high pressure), in presence of complex organic liquid mixtures. Because of the extreme and still poorly understood sensitivity of the gas phase hydrodynamic parameters (gas holdup, bubble size, bubble size distribution, bubble velocity, bubble spatial arrangement) on the "nature" and physical properties of the liquid media (Bukur and Daly, 1987), the measurements obtained in *ideal* systems (aqueous liquids, ambient temperature) can not be safely applied to *real* systems. Furthermore, given the importance of the operating conditions (temperature, pressure, gas superficial velocity ...) and the reactor design characteristics (gas distributor, column dimensions ...), experimental investigations in laboratory and pilot scale installations, for a given system, are essential (Deckwer and Schumpe, 1987).

This was actually emphasized by a number of authors, including Shah et al. (1982), and most recently by Zhou et al. (1992).

The precise measurement of local gas phase hydrodynamics parameters, under conditions of industrial interest, requires the availability of reliable measuring tools. The limited number of such dependable measuring techniques is highly responsible for the general lack of hydrodynamic knowledge in bubble and slurry bubble columns, especially under severe industrial like conditions. In this context, a spherical bulb optical fibre sensor was recently proposed and successfully tested under conditions of interest for the fuel industry (Chabot, 1989; Chabot et al., 1992). The principle of operation of this miniaturized sensor is based on the difference in refractive indices between the gas phase and the liquid phase, allowing the local observation of gas bubbles. Local gas phase hydrodynamic parameters such as gas holdup, bubble velocity, bubble axial chord length, bubble axial chord length distribution, and bubble frequency were successfully measured with such optical sensors.

In the present study, the spherical bulb dual fibre optic sensor was extensively used, in conjunction with a newly designed periscopic insertion system, to extensively investigate the local gas phase characteristics of the liquid phase methanol synthesis system. The objective of the present work was to measure important local gas phase parameters (gas

holdup, bubble velocity, bubble axial chord length, bubble axial chord length distribution and bubble frequency) under the *realistic* conditions inherent to a system of prime interest for the fuel industry: the liquid phase methanol synthesis process. The excellent performance and resistance of the fibre optic sensors were exploited in obtaining highly valuable local gas phase information in this system. The results obtained are not only of prime importance for the design and scale-up of the liquid phase methanol synthesis process but constitute a valuable source of information for systems of similar nature, including the Fischer-Tropsch system and the newly proposed methanol-dimethyl ether combined slurry process. Furthermore, the present study constitutes one of the few investigations of local gas phase hydrodynamic parameters in bubble and slurry bubble columns and certainly one of the first reported under *realistic* conditions. In this context, this study represents indeed a significant research contribution. Specific knowledge concerning a system of high industrial interest, and valuable understanding of the general fundamental fluid dynamic behaviour encountered in bubble and slurry bubble column reactors were obtained.

In the following pages (Sections 1.2 and 1.3), a review of the current literature concerning the hydrodynamics of bubble and slurry bubble column reactors, with stress assigned to the gas phase characteristics, is presented. This review emphasizes more extensively the motivation of the present work,

rationalises the experimental approach selected and summarizes previous findings of importance in the context of the present study. Chapters 2, 3 and 4 are devoted to the description of the experimental set-up and procedure, the presentation of the measuring techniques (including the fibre optic sensor) used, and the data analysis methodologies respectively. The experimental results and the discussion are elaborated in Chapter 5, while the conclusions and recommendations are presented in Chapter 6.

1.2 HYDRODYNAMICS OF BUBBLE AND SLURRY BUBBLE COLUMNS

Bubble column reactors are multiphase contacting devices in which a discontinuous gas phase moves in the form of discrete bubbles relative to a continuous liquid phase. In its most simple form, the bubble column is a vertical cylinder where the gas enters at the bottom through a gas distribution device. The column can be operated either in concurrent upflow, countercurrent or semi-batch (batch liquid phase) mode. When operated as a slurry bubble column or a three phase fluidized bed, catalyst particles are suspended in the liquid by the action of the rising gas bubbles. A three phase bubble column operating with small particles (terminal settling velocity of the particle in the liquid phase < 7 cm/s) is usually referred to as a slurry bubble column. A three phase bubble column operating with larger particles (terminal settling velocity of the particle in the liquid

phase < 50 cm/s) is normally termed a three phase fluidized bed. The flow of solids may be continuous or batch and the direction of flow, upward or downward (Fan, 1989; Dudukovic and Devanathan, 1992; Deckwer and Schumpe, 1992).

Normally, bubble columns operate with a reactor height to diameter ratio greater than five, and with gas superficial velocity of at least an order of magnitude greater than the superficial liquid velocity. Typical ranges of superficial velocities for bubble column operation are 1 to 30 cm/s for the gas phase and 0 to 2 cm/s for the liquid phase (Dudukovic and Devanathan, 1992). Coils or other internals may be inserted into the bubble column to promote heat transfer. In addition, the column may be sectionalized using baffle systems or perforated plates to inhibit liquid phase backmixing or bubble coalescence, two usually highly undesirable phenomena. Simplicity of operation, lack of moving parts (easy maintenance and sealing), excellent heat transfer (good temperature control), reasonable interphase mass transfer rates (at low energy input), easy solids handling, little floor space required, and low operating costs are among the major advantages of this technology (Deckwer and Schumpe, 1992).

1.2.1 Flow regimes

The existence of different gas phase flow regimes in bubble

columns is of great importance for the understanding and modelling of bubble column reactors. Actually, in bubble column reactors, the hydrodynamics, transport and mixing properties such as the pressure drop, the holdup of the various phases, the fluid-fluid interfacial areas, and the interphase mass and heat transfer coefficients depend strongly on the prevailing flow regime (Shah et al., 1982). The flow regimes are qualitatively classified as bubbling flow, churn turbulent flow, slug flow, and foaming flow. The bubbling flow regime is characterized by the presence of relatively uniformly sized bubbles, of slow and uniform rising velocities (18-30 cm/s), and equally distributed radially. This regime occurs at relatively low gas superficial velocities (< 5 cm/s) in presence of low viscosity media. The numbers just mentioned above should be regarded as a guideline, since they are particular to the air-water system.

At higher gas superficial velocities, coalescence of the bubbles occurs and a portion of the gas throughput, which increases with increasing the gas superficial velocity, is transported in the form of fast-rising large bubbles. Because of the appearance of clearly distinguishable classes of bubbles, this regime of flow is termed heterogeneous or, owing to the rotating turbulent motion of the large bubbles, churn turbulent. The large bubbles take the form of spherical caps with a very mobile and flexible interface. These large bubbles can grow up to a diameter of about 0.15 m (Shah et

al., 1982). In small diameter columns, at high gas flow rates, large bubbles are stabilized by the column wall, leading to the formation of bubble slugs. This regime is known as the slug flow regime. Bubble slugs can be observed in columns of diameters up to 0.15 m.

The occurrence of the various regimes depends on numerous factors, including: the velocity of the phases, their physical properties, the type of sparger used and the column dimensions (Shah et al., 1982). For example, Maruyama et al. (1981) observed that the transition gas superficial velocity between the bubbling and the churn turbulent regime, under uniformly sparged conditions, depended on the ungassed liquid height and was independent of the sparger geometry. The occurrence of the churn turbulent regime was however delayed under non-uniform gas distribution. In this context, the crucial knowledge of the transition from one regime to another becomes extremely complex. In this respect, the concept of drift flux, as discussed by Deckwer and Schumpe (1987), has been proven useful. The drift flux is defined as the volumetric flux of the gas phase relative to a surface moving with the average velocity of the dispersion:

$$\Omega = V_g(1-\epsilon_g) \pm V_l\,\epsilon_g \qquad (1.1)$$

Plotting Ω versus ϵ_g immediately reveals which regime of flow

is present or at which gas velocity the bubble flow switches over into the churn-turbulent region, since at that point the drift flux increases steeply. A typical illustration of the dependency of the flow regime on the gas superficial velocity and the column diameter for aqueous systems, is presented in Figure 1.1. This diagram should be used with caution, since the transition between flow regimes is dependent on the nature of the system. For example, Bukur and Daly (1987) observed the churn turbulent regime, for gas superficial velocities between 0.02 m/s and 0.15 m/s, under conditions simulating the slurry Fischer-Tropsch process. Other factors were also observed to have an influence on the transition between the bubbling to the churn turbulent flow regime. Actually, according to Krishna et al. (1991), the transition from the homogeneous bubble flow regime to the churn turbulent regime was accompanied by the formation of large fast-rising bubbles. As a consequence, all factors influencing the occurrence (coalescence versus break-up) and formation (gas sparger) of these large bubbles can, in principle, also influence the transition velocity between both flow regimes. For example, the formation of large bubbles can be delayed to higher gas superficial velocities when the coalescence rate is reduced by the addition of an electrolyte (Wilkinson et al., 1992). As reported by Wilkinson et al. (1992), higher liquid viscosity promotes coalescence of large bubbles, whereas bubble breakup rates decrease in the presence of a high liquid viscosity. Consequently, the appearance of larger bubbles is favoured in

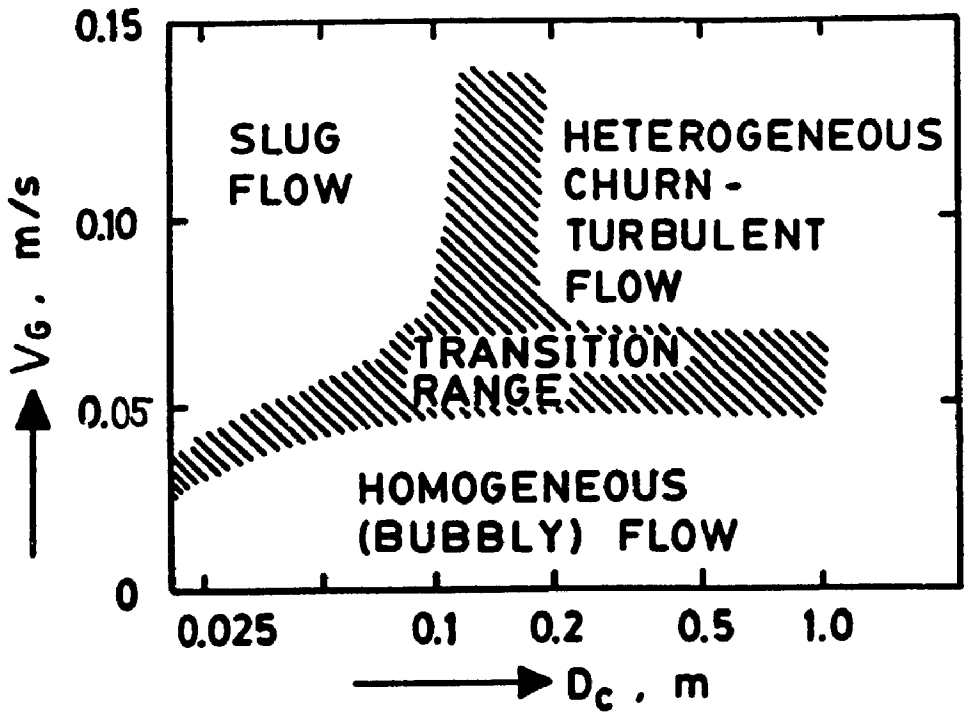

Figure 1.1: Approximate dependency of flow regime on gas velocity and column diameter (water and dilute aqueous solutions) (Shah et al., 1982)

the presence of high viscosity liquids and the transition to the churn turbulent regime thus promoted at lower gas superficial velocities. Furthermore, fewer large bubbles occur in the presence of lower surface tension liquids, since surface tension is known to oppose deformation and bubble break-up (Wilkinson et al., 1992). Consequently, the occurrence of large bubbles is minimal due to pronounced bubble breakup and poor coalescence activities, especially in the presence of liquids combining both, low surface tension and low viscosity. The transition to the churn turbulent regime in such systems would be delayed to higher gas superficial velocity. In addition, Krishna et al. (1991) and Wilkinson and van Dierendonck (1990) have demonstrated that a higher gas density increases the rate of bubble breakup, especially for large bubbles. The higher bubble break-up rate thus counteracts the formation of large bubbles due to coalescence. As a result, at high pressure, mainly small bubbles occur under homogeneous bubble flow, until very large gas holdups are observed and coalescence becomes important. This was also reported by Clark (1990), who observed a reduced tendency of the bubbles to coalesce under high pressure conditions. The reduced bubble coalescence resulted in an extended zone of homogeneous bubble flow occupying the bottom half of the column. The bubble column was seen to operate in a two regimes mode over a wide range of gas velocities: homogeneous bubble regime in the lower half and churn-turbulent regime in the top half. The addition of fine solids

to the liquid phase promoted rapid bubble coalescence resulting in the complete column operating in the churn-turbulent regime, over all the conditions studied. Kara et al. (1982) observed that an increase in the solid concentration, particle size and slurry velocity caused an earlier deviation from bubbly flow regime.

Foaming regime occurs in many systems of practical interest, including hydrocarbons based processes operated at high temperature and pressure, and fermentation processes. In general, foaming is not desirable as it increases the reactor space required, and thus the capital cost. Furthermore, foaming constitutes an undesirable operating regime for hydroprocessing reactors, where the high gas content of the foam considerably hinders the heat and mass transfer rates. In general, foams are constituted by thin liquid films joined at junctions. The stability of a foam is a consequence of the high resistance to elongation of the liquid films induced by the presence of tensoactive molecules adsorbed at the gas-liquid interface. The formation of foam depends on the chemical nature of the substance acting as tensoactive agent and its concentration. The operating conditions, sparger design and column diameter play an important role in the formation of foam in bubble columns. The presence of foam depends on the viscosity (temperature) of the liquid, gas sparger configuration, and on the flow patterns inside the column, which are strongly related to the velocities of the

phases. It is important to point out that, in some cases, foam only occupies a region at the upper part of the column, coexisting with another flow regime in the lower part of the column.

Bukur et al. (1987a, 1987b) and Bukur and Daly (1987) performed a series of gas holdup measurements in 0.051 m and 0.229 m diameter by 3.0 m long columns in presence of molten paraffin wax (FT-300) and Fischer-Tropsch reactor waxes. They reported that paraffinic waxes have a tendency to foam under some conditions. For the FT-300 wax, at temperatures between 230°C and 280°C, they observed a range of gas superficial velocities, where two different flow regimes were possible, the foamy and the turbulent bubbling flow regime. The start-up velocity determined which flow regime was to be present. For the increasing order of the gas superficial velocity, the foaming regime was present up to a superficial velocity of 3 cm/s. Foam break-up was observed as the gas superficial velocity was further increased (between 3 and 5 cm/s). When changes of the gas superficial velocity followed a decreasing order, from 15 cm/s to 3 cm/s, lower gas holdups were observed, mostly in the 3 cm/s to 5 cm/s range, for which no foam was observed. When the gas superficial velocity was further decreased from 3 cm/s to 2 cm/s, foaming reappeared. Transitions between these two flow regimes occurred and were influenced by the temperature and the gas distributor design. Lower temperatures and/or perforated plate distributors with

larger holes favoured the existence of the turbulent bubbling flow regime. Furthermore the use of high start-up velocity followed by a gradual decrease of the flowrate until the desired gas superficial velocity is reached, also reduced or prevented foaming by dispersing coalescence promoting impurities throughout the column. The addition of alcohol (1-octadecanol and octadecanoic acid, up to 10%$_{wt}$) to the FT-300 wax was not observed to have significant effect on the gas holdup and foaming behaviour, though an increase of the gas holdup was noticed for some cases. Foaming was however not observed in presence of reactor waxes, where an absence of fine bubbles (< 1 mm) was noticed.

1.2.2 Gas holdup

The gas hold-up is one of the most important parameters characterizing the hydrodynamics of bubble columns (Shah et al., 1982). It is defined as the percentage by volume of the gas in the two or three phase mixture in the column. Gas hold-up is a strong function of the gas superficial velocity, and is known to be very sensitive to the nature and physical properties of the liquid.

Bach and Pilhofer (1978) carried out experiments with different pure liquids in such a way that they could isolate the effect of the liquid viscosity from the rest of the physical properties. These authors argued that the viscosity

was the liquid physical property with the greatest influence on the gas holdup. They concluded that, for similar operating conditions, an increase in the viscosity of the liquid results in a decrease of the gas holdup. This trend has been consistently reported in subsequent works (Godbole et al., 1982; Kelkar et al., 1984; Zahradnik et al., 1987). The reduction of the gas hold-up with an increase in liquid viscosity is a consequence of two superimposed effects: an increase in bubble coalescence rate and the existence of larger stable bubbles. A larger value of the viscosity implies faster bubble coalescence rate, owing to the presence of larger drag forces (Zahradnik et al., 1982). Zahradnik et al. (1982) quantified the coalescence of the bubbles through the experimental measurement of the coalescence ratio, defined as the ratio between the number of bubble pairs that coalesce divided by the number of bubble pairs generated in a given period of time. They concluded that the coalescence ratio increases with liquid viscosity. Prince and Blanch (1990) observed that, in turbulent flow, higher liquid viscosities result in the formation of larger stable bubbles, since the resistance to elongation of a bubble is enhanced by an increase in liquid viscosity and bubble break-up occurs at a lower extent. It is interesting to note that, when the coalescence rate is high, the largest stable bubble size is reached in a region close to the gas distributor. In this case, the coalescence rate has no influence over the gas hold-up, and the capability of the system to form large stable

bubbles becomes the predominant factor. As the mean bubble size in the column is larger, the upward bubble velocity increases and this diminishes the mean residence time of the bubbles in the column, and consequently the gas holdup. On the contrary, Guy et al. (1986) reported only a slight influence of the liquid viscosity on the gas holdup. They however observed an increase of the gas holdup with an increase of the elastic properties of the liquid phase.

The effect of the liquid density on the gas hold-up in bubble columns has not been analyzed in detail in the literature. According to the experimental observations of Bach and Pilhofer (1978), an increase in the density of pure liquids results in an increase in the gas hold-up. This trend is consistent with the theory developed by Prince and Blanch (1990) for turbulent flow, which predicts that the maximum stable bubble size decreases as the density of the liquid increases.

The theory by Prince and Blanch (1990) also predicts that the surface tension of the liquid has a quantitative effect over the maximum stable bubble size, which is more pronounced than that of the viscosity and density. According to this theory, an increase in the surface tension results in an increase in the maximum stable bubble size which implies, in systems with high coalescence rates, a reduction in the gas hold-up. Similar conclusions were recently reported by Wilkinson et al.

20

(1992). In spite of this, Bach and Pilhofer (1978) (σ_l = 27.5 - 49.5 g/s^2) and Kelkar et al. (1983) (σ_l = 45 - 70 g/s^2) concluded that variations in the surface tension of the liquid have no appreciable effect over the gas hold-up.

Bach and Pilhofer (1978) argued that the effect of the liquid phase properties over the gas hold-up is different for pure liquids than for liquid mixtures. This indicates that the viscosity, density and surface tension of the liquid are not enough to quantify the effect of the nature of the liquid phase over the gas holdup. This fact has been acknowledged by more recent investigations (Zahradnik et al., 1987; Öztürk et al., 1987). Smith et al. (1984) and Kuo (1985) found that paraffin wax (FT-200) at 200°C gives higher hold-ups and smaller bubbles than hexadecane at room temperature even though their physical properties (viscosity and surface tension) were similar under these conditions. Quicker and Deckwer (1981a) determined the gas holdup for various types of spargers for hydrocarbon liquids. The authors demonstrated that the correlations from the literature failed to describe their data, though the physicochemical properties of the liquids were within the range recommended for the application of these correlations. These results confirmed that the liquid medium for hydrodynamic studies must be chosen very carefully in order to obtain valuable information for bubble column reactor design. Furthermore, the presence of surfactants decreases the upward bubble velocity and inhibits

the bubble coalescence, simultaneously decreasing the maximum stable bubble size. The net effect of the presence of surfactants is a reduction of the mean bubble size in the gas-liquid suspension. The reduction of the mean bubble size and the bubble velocity results in a high gas holdup in liquids that contain surfactants. Kelkar et al. (1984) also observed that the addition of a surfactant (Triton-114, 0-30 ppm) increased the gas hold-up. They claimed that the addition of the surfactant induced a non-coalescing tendency in the liquid media, while creating a surface tension gradient at the gas-liquid interface, thereby decreasing the bubble rise velocity. They also observed foaming of the liquid media at concentration of surfactant greater than 30 ppm. An increase of the gas holdup upon surfactant addition was recently reported by Bukur and Patel (1989) who observed that in foaming mixtures, the gas holdup increased with an increase in alcohol concentration (n-butanol, 0.5%$_{wt}$ and 1%$_{wt}$). The presence of alcohol in water acts as a surfactant which hinders the bubble coalescence by accumulating at the gas-liquid interface and orienting their hydrophilic group into the liquid film surrounding the gas bubble and thus creating repulsive electric forces when two bubbles come close to each other (Keitel and Onken, 1982). The concentration of the hydrophilic molecules at the surface increases with surfactant concentration up to a point and results in a lower surface tension. Actually it is expected that a specific surfactant composition exists at which the maximum gas holdup occurs.

Furthermore, it is believed that the surface active materials are swept to the rear of the rising bubble, creating a surfactant concentration gradient and consequently a surface tension gradient that favours an increase of the drag on the bubble and reduces its rising velocity. Consequently, the gas bubbles in the presence of surface active agents are small, rigid and have high residence time in the column. These small bubbles may accumulate at the top of the gas-liquid dispersion forming a stable cellular foam. This is in agreement with the recent findings of Pino et al. (1990) who observed that when kerosene is used as the liquid phase, already containing natural surfactants, the addition of additional surface active substances does not affect the gas holdup if foam is present. However, under conditions for which kerosene does not foam, the addition of a surfactant promotes foaming. Since the addition of surfactant does not change to a great extent the overall physical properties of the kerosene (density, viscosity, surface tension), this last fact indicates that the effect of the nature of the liquid phase on the fluid dynamics of foaming systems cannot be uniquely quantified in terms of the liquid physical properties. The previous discussion indicates that the empirical correlations for predicting gas holdup in bubble columns, which have been usually developed for pure liquids, are not adequate when used to represent liquid mixtures. And, the empirical correlations that have been developed to predict gas holdup in the presence of liquid mixtures are generally specific for the system considered.

23

A number of authors (Koide et al, 1979) have determined that gas holdup (under atmospheric conditions) is virtually independent of the column diameter provided its value is larger than 0.15 m, as reviewed by Shah et al. (1982). This was also recently confirmed for high pressure conditions (up to 2.0 MPa) by Wilkinson et al. (1992). These authors reported that even for liquids that are as viscous as mono-ethylene glycol (μ_l=0.021 Pa-s), a column diameter, which is larger than 0.15 m, has little or no effect on the gas holdup. However, for smaller column diameters, wall effects become important and are known to promote larger gas holdup values. For example, the experiments of Idogawa et al. (1987) in a 0.05 m diameter column in presence of water were between 30 and 50% higher than similar experimental data by Wilkinson and van Dierendonck (1990) in a 0.15 m diameter column for both low and high pressures. Deckwer et al. (1980) reported measurements of the gas hold-up in slurry bubble column reactors of 4.1 and 10 cm diameter. The column was operated batch wise with respect to the slurry with a suspension height varying between 60 and 100 cm. The gas (nitrogen) was sparged into both columns by metal sintered plates having a mean pore diameter of 75 μm. Molten paraffin was used as the liquid phase and powdered Al_2O_3 (diameter $\leq$ 5 μm) was suspended in the liquid at concentrations between 5.5 and 16%$_m$. The temperature was varied between 143 and 270°C, the pressure between 400 and 1100 kPa and the gas superficial velocity between 0.5 to 3.4 cm/s. The gas hold-up was measured by

means of constant temperature anemometry. They observed a substantial decrease of the gas hold-up as the temperature increased from 180 to 240°C in the 4.1 cm diameter column. Such a dependency of the gas hold-up on the temperature was not observed in the 10 cm column although the temperature range was even larger. This suggests, according to the authors, the existence of a "wall" effect in the small column. Furthermore, Pino et al. (1990) and Bukur and Patel (1989) (for gas superficial velocities between 0.01-0.12 m/s) observed that, for non-foaming systems, the gas holdup decreases as the column diameter increases. On the other hand, Pino et al. (1990) observed that the column diameter (0.10 m to 0.29 m) does not influence appreciably the gas holdup of foaming systems in semi-batch operation while Bukur and Patel (1989) reported an increase of the gas holdup with the column diameter (0.05 m to 0.23 m). Pino et al. (1990) found that in continuous operation, the tendency of a system to foam is diminished when the column diameter increases.

Gas holdup in a bubble column is usually not uniform. In general, three regions of different gas holdup are identified. At the top of the column, foam structure with relatively high gas holdup might be present, while the gas holdup near the distributor is sometimes found to be larger (porous sparger) or lower (single-nozzle sparger) than in the main central section of the column. The extent of the influence of the lower and upper regions on the overall average gas holdup

depends on the column height. Furthermore, the column height can also influence the value of the gas holdup due to the fact that liquid circulation patterns are not fully developed in short bubble columns ($H/D_c < 3$). However, most authors agree, as reported by Wilkinson et al. (1992), that the influence of the column height on the gas holdup is negligible for column heights greater than 1-3 m or height to diameter ratios above 5 ($H/D_c > 5$).

Furthermore, Bukur and Daly (1987) showed that the distributor type (19 x 1.85 mm perforated plate, 19 x 1 mm perforated plate, perforated pipe having a star shaped arrangement with 6 segments having 5 holes of 1.5 mm in diameter, each and 60° angle between segments) does not have significant effect on the gas hold-up values in the absence of foam. These results were recently complemented by the findings of Wilkinson et al. (1992). Actually, Wilkinson et al. (1992) observed that the influence of the gas sparger on the gas holdup was negligible (for various liquids under various pressures) provided the sparger hole diameters were larger than approximately 1-2 mm (and care is taken to prevent maldistribution of gas at the sparger). They reported that spargers with small hole diameters (< 1 mm), however, lead to the formation of smaller bubbles and thus to a higher gas holdup. However, in foaming system, the gas holdup was found to be a strong function of the gas distributor type. Incidentally, Bukur and Patel (1989) reported that in systems with foaming mixtures, the gas

holdup increases with a decrease in orifice size for the 0.05 m diameter column, whereas in experiments with pure liquids and/or with highly viscous aqueous solutions, the gas sparger design did not have significant effect on the gas holdup.

A number of authors, including Hills (1974), Ueyama et al. (1980) and Yao et al. (1991), have reported pronounced parabolic radial gas holdup profiles (central gathering distribution) in bubble columns under turbulent flow regime conditions. Several power law models have been used to describe locally varying gas voidage, but the most popular of these (Miyauchi and Shyu, 1970; Hills, 1974; Kato et al., 1975; Ueyama and Miyauchi, 1979; Walter and Blanch, 1983; Yang et al., 1986) takes the following form, in terms of the dimensionless radius θ (θ=r/R):

$$\epsilon_{g,loc}(\theta) = \epsilon_{g,avg} \frac{(m+2)}{m}(1-\theta^m) \qquad (1.2)$$

The values of m reported to date, in the recirculation flow regime, for the air/water system, indicate a value of m approximately equal to 2, in the average (since important discrepancies could be observed), as reviewed by Ueyama and Miyauchi (1979). However, no values of m were so far reported for different systems, operated under very different operating conditions (hydrocarbon systems, high temperature, high pressure). This is of most importance since the precise

knowledge or reliable prediction of gas holdup radial profiles is required in most liquid recirculation models, as recently emphasized by Rice and Geary (1990). Furthermore, axial variation in gas holdup can be observed at low gas velocities and at high conversions (Deckwer et al., 1978, 1980).

The dependence of the overall gas holdup on the gas velocity is generally represented by an equation of the form:

$$\epsilon_g \propto V_g^n \tag{1.3}$$

The value of n depends on the flow regime. For the bubbly flow regime, the value of n varies from 0.7 to 1.2 (Hammer and Rähse, 1973; Schügerl et al., 1977; Bach and Pilhofer, 1978; Deckwer et al., 1980), which indicates the relatively strong effect of V_g on ϵ_g. In the churn turbulent or the transition regime, the effect of V_g is less pronounced and the exponent n takes values from 0.4 to 0.7. This trend was also confirmed by Kara et al. (1982).

For the air-water system, the pressure dependency of the holdup was investigated by Kolbel et al. (1961) for the pressure range of 0.1 to 1.7 MPa. They found no effect of pressure. Similar results were also reported by Deckwer et al. (1980), who measured the gas holdup for the pressure range of 0.4 to 1.1 MPa in presence of molten paraffin in relatively small columns ($\leq$ 0.1 m) using a porous plate distributor.

28

However, Idogawa et al. (1987) observed an increase of the gas holdup with the pressure. This was also noted by Oyevaar et al. (1991), who observed an increase of the gas holdup with pressure (up to 8.0 MPa) in presence of water and DEA (diethanolamine) aqueous solutions. They observed differences in the magnitude of the gas holdup increase with the nature of the liquid and the gas sparger configuration. In presence of coal particles and kerosene, Chiba et al. (1989) noticed that the effect of pressure varied with the nature of tne gas. The gas holdup increased with pressure for hydrogen gas up to 1.0 MPa and stabilized for higher pressures (up to 12 MPa). On the other hand, the gas holdup in presence of nitrogen was found to be independent of pressure. However, Clark (1990) observed that published correlations for gas holdup in bubble columns were unable to predict the behaviour of bubble columns operating at high pressures and temperatures. The high gas holdup observed appeared to be the result of the reduced tendency of the bubbles to coalesce at higher pressures. The use of a sintered metal gas distributor produced small bubble sizes and could have masked any effect of the increased gas density occurring at high pressure.

In general, it appears that there is agreement in the sense that an increase of the temperature leads to an increase in the gas holdup (Renjun et al., 1988; Wilkinson et al., 1992). Both the liquid surface tension and viscosity decrease with an increase in the temperature, thus favouring smaller bubbles

29

and higher gas holdup values as previously mentioned. As reported by Renjun et al. (1988), the effect of the presence of an electrolyte substance (5% NaCl solution) on the gas holdup varies with the temperature. Furthermore, a higher temperature increases the liquid vapour pressure. Then, if the feed gas to the bubble column is not presaturated, the evaporation of the liquid phase can lead to a substantial increase in the gas volumetric flow rate, thus increasing the gas holdup. In addition, a higher liquid vapour pressure can influence the gas density, and consequently the gas holdup. The latter effect is particularly pronounced if the molecular weight of the liquid phase is different from the one of the gas.

Various studies on three phase slurry bubble columns have shown that the effect of solids on the gas holdup depends on a wide variety of factors, including: liquid properties, particle properties (density, size, concentration and wettability) (Bukur et al., 1990). Jeffrey and Acrivos (1976) found that for particles as small as a few (< 10 μm) microns, suspensions behave macroscopically as non-Newtonian fluids. Therefore, gas holdup values involving non-Newtonian liquids might be useful in analyzing the gas-slurry systems. However, some contradictory results were reported concerning the effect of the presence of solid particles on the gas holdup. Ostergaard and Michelsen (1968) observed that for particles less than 1 mm in size, the gas holdup was significantly

30

reduced by the presence of solid particles given the conditions for bubble coalescence. The effect of larger particles was found, however, to be less significant, since these particles tend to cause breakup of bubbles. However, Morooka et al. (1986) observed an increase in the gas holdup upon solids addition (44 and 113 μm) in presence of water (containing a surfactant). This was also recently observed by Khare and Joshi (1990), upon addition of fine particles (12 - 1300 μm). They observed that the extent of increase in the gas holdup depends on several parameters, a synergetic effect between these parameters being present. The extent of increase of the gas holdup (between two and three phase) becomes more significant with a decrease in the gas superficial velocity and the height to diameter ratio. It also increases with the non-coalescing behaviour of the liquid phase, as observed by Sada et al. (1986), who noted that the presence of suspended solid particles has a much smaller influence on gas holdup in electrolyte solutions (Na_2SO_4 0 - 1 mol/dm^3, NaCl 0 - 2.4 mol/dm^3, KCl 2.4 mol/dm^3) than in non-electrolyte solutions. Sauer and Hempel (1987), observed that the presence of small light particles (density < 1300 kg/m^3) at low gas superficial velocity (V_g < 0.04 m/s) resulted in optimum interaction between the particles and liquid turbulence, thus producing smaller bubbles and consequently higher gas holdup values. This was also noted by Wolff et al. (1990), who reported higher gas holdup (than the two phase system) at low gas flow rate and low solid concentration.

However, according to Sauer and Hempel (1987), high gas superficial velocities, solid concentrations and densities resulted in larger bubbles and consequently lower gas holdups, as also reported by Wolff et al. (1990). Kara et al. (1982) did not observe significant difference in gas holdup between gas-liquid and gas-liquid-solid systems when 10 μm size particles were used. They observed, however, that an increase in the solid particle size decreased the gas holdup, as also observed by Sada et al (1986) and Morooka et al. (1986). This effect was reduced for larger particle sizes and, as observed by Sada et al. (1986) for higher solid loading (up to 20%$_{wt}$). Kato et al. (1972), Deckwer et al. (1980), Kara et al. (1982), Capuder and Koloini, (1984), Sada et al. (1986), Yasunishi et al. (1986), Nigam and Schumpe (1987) and Ying et al. (1980) concluded that an increase in the solid concentration generally reduces the gas holdup. However, Kato et al. (1972) observed that this effect becomes insignificant at high gas velocities (> 0.1-0.2 m/s) and, at low gas velocities (< 3 cm/s), the existence of solids did not change the holdup according to Ying et al. (1980). Kojima et al. (1986) observed that an increase in solid holdup (solid concentration in feed 3.1-62 kg/m^3, glass beads with diameter: 0.105-0.125 mm) decreased the gas holdup when a porous plate (mean pore size = 185 μm) was used as gas distributor. They observed a trend of bubble coalescing behaviour in increasing the solid holdup when the porous plate distributor was used. When a perforated plate (31 x 1.05 mm; 7 x 1.05 mm) or a single

32

nozzle (3 mm i.d. x 10 mm o.d.) were employed as the gas distributors, an increase in solid concentration did not result in lower gas holdup. More recently, Saxena et al. (1990) reported a slight decrease of the gas holdup upon solid addition (magnetite powders with average diameter: 35.7, 49, 58, 69, 90.5, 115.5 and 137.5 μm, solid loading up to 30%$_{wt}$), while observing a weak dependence of the particle diameter and concentration. Clark (1990) observed that the addition of fine solids (glass beads, 43-65 μm, 10%$_{wt}$) to the liquid phase promoted rapid bubble coalescence. This resulted in a marked reduction of the overall gas holdup and an even gas distribution through the length of the column. However, Kelkar et al. (1984) observed that the phase holdups were not significantly affected by the particle size (40-250 μm) and the particle concentration (5-15%wt). However, they observed that solid wettability was a very important factor in enhancing the coalescence tendencies in the liquid phase and consequently reducing the gas holdup.

A number of authors, including Kojima and Asano (1981), Sauer and Hempel (1987) and Immich and Onken (1992) studied the influence of various parameters on the extent of complete and uniform solids fluidization. This is particularly important since a number of references stated the effect of the axial particle concentration gradient on the bubble size. For example, Wolff et al. (1990) observed that for dense particles and low gas superficial velocities, high solid concentrations

were present in the sparger vicinity, resulting in larger bubbles than the ones measured in the solid free system. Sauer and Hempel (1987) observed that the critical gas velocity for complete fluidization increases with increasing solids density, diameter and concentration.

More recently, Bukur et al. (1990) studied the effect of the operating regime on the gas holdup. They used two types of solids (iron oxide and silica) in two size ranges (0-5 and 20-44 μm), with solids concentrations of 10, 20 and 30%$_{wt}$. The experiments were conducted in a 0.05 m ID and 3 m high column equipped with a single-hole 2 mm orifice plate distributor. Both, batch and circulating modes were studied for the slurry. Nitrogen was used as the gas phase and the superficial gas velocity was varied between 0.02 and 0.12 m/s. FT-300 paraffin wax was employed as the liquid medium. They observed that even a small upward liquid flow (0.005 m/s) lowers the gas holdup markedly; however, a further increase in the liquid flow has only a marginal effect on the average gas holdup values. It appears that the significant differences in gas hold-ups between the batch and the continuous modes of operation are due to changes in the foaming characteristics of the medium. For the batch case, the foam accumulates at the top of the dispersion and increases the gas hold-up, whereas in the continuous mode of operation the foam is removed form the column by the circulating slurry. These results were recently confirmed by Pino et al. (1990) who found that the

operating mode strongly affects the gas holdup of foaming systems. In the semi-batch mode, the gas holdup is higher than in the continuous mode. They explain these observations by the effect of foam degradation owing to the drag forces at the column exit in the continuous mode, which are absent at the free surface in the semi-batch mode. This effect was so important that, in some cases, foaming occurs only in the semi-batch mode. They found that an increase in the liquid superficial velocity (0-3.21 cm/s) in foaming systems results, at first, in a decrease in gas holdup and, as the liquid velocity is further increased, the gas holdup goes through a minimum. They did not observe any influence of the liquid superficial velocity on the gas holdup for non-foaming system. Results obtained in the continuous mode of operation by other researchers indicate that liquid velocity either has no effect on the average gas hold-up (Shah et al. 1982; Kelkar et al., 1984; Ying et al., 1980) or decreases the gas hold-up slightly (Kara et al. 1982, Kelkar et al. 1984), as recently confirmed by Wilkinson et al. (1992). According to Kelkar et al. (1984), the effect of the slurry velocity on the gas holdup was more pronounced at lower gas velocities where the bubbly flow regime prevailed, being negligible in the case of a 10_{wt}% oil shale particle/water slurry for gas velocity greater than 6 cm/s. However, it should be noted that most previous studies were conducted with liquids that do not have the tendency to foam. In the case of foaming systems, the method used to measure the gas hold-up is very important. Local

measurements of the gas hold-up which have the ability to discriminate between foaming regime and other regimes should be preferred.

A large number of correlations for the prediction of gas hold-up in bubble and slurry bubble column have been proposed in the literature, as reviewed by Shah et al., (1982). These correlations contain variables such as liquid and gas density, liquid surface tension and liquid viscosity, implying that the proposed correlations are suitable for predicting most systems. However, a number of authors reported major discrepancies in using existing correlations to predict gas holdup. For example, Quicker and Deckwer (1981) noted that existing literature correlations did not describe their measurements on xylene, decaline, C_{10}-C_{14} paraffins or Vestowax. Even for the most studied system, air/water, fairly large differences in predicting gas holdups were encountered. The large scatter observed is partly due to the lack of knowledge about the nature of the flow patterns (Reilley et al., 1986; Tsuchiya and Nakanishi, 1992) and to the extreme sensitivity of the gas holdup on the system media, in particular the effect of trace impurities. Unfortunately, these effects are not well understood. Furthermore, and as stated above, the easily available liquid physical properties such as density, viscosity and surface tension are not necessarily sufficient to explain the observed scatter. Furthermore, most correlations developed in predicting the gas holdup show a

36

pronounced difference in the dependence of the gas holdup on the gas superficial velocity. It is well known that the gas holdup is proportional to the gas superficial velocity, the dependence varying with the flow regime. Consequently, a correlation developed with a fixed dependence of the gas holdup on the gas superficial velocity would be hardly applicable to different flow regimes. Moreover, the potential influence of the equipment design was usually ignored in most correlations. It appears, that in order to be able to moderate the influence of these factors, the bubble formed at the distributor should have a size close to the equilibrium bubble size or the medium must be coalescence promoting, and the bubble column must have a liquid height such that the stable bubble size is reached in a small fraction of the total liquid height.

Molerus and Kurtin (1985) proposed a relation between gas holdup, superficial velocities of the gas and the liquid and the mean bubble size. This relation predicts the maximum gas throughput in the uniform bubbling regime for a given bubble size. Such relation is however of limited applicability since most systems of industrial interest operate in the churn turbulent regime. The same authors (Molerus and Kurtin, 1986a, 1986b) proposed, based on the two bubble class model, a phenomenological model predicting some limited flow patterns characteristics in bubble columns from average gas holdup measurements. However, this model was based on the assumption

that large bubbles ascend uniquely in the core region. Such assumption can not be safely applied to the case of hydrocarbon type of systems, as discussed in the Chapter 5, for which large bubbles were observed to be present in the peripheral region of the column. Furthermore, based on recent experimental evidences (Dudukovic and Devanathan, 1992), the liquid velocity inversion point was found to be closer to 0.7 than 0.75, as suggested by Molerus and Kurtin (1986b). Finally, the model proposed by Molerus and Kurtin (1986b) was adjusted and validated from data obtained using the Dynamic Gas Disengagement (DGD) technique. They assumed that the initial drop in the suspension level was attributed to the disengagement of the large bubbles only. As previously discussed (Patel et al., 1990), the initial bed level decrease corresponds to the disengagement of all of the largest bubbles and a fraction of the small ones. Consequently, the small bubbles holdup obtained, following such analysis is, in some extent, underestimated. The model proposed was further validated from data exclusively obtained using the DGD technique.

Akita and Yoshida (1973) proposed the following dimensionless empirical equation for predicting the average gas holdup:

$$\frac{\epsilon}{(1-\epsilon)^4} = C_1 (Bo)^{\frac{1}{8}} (Ga)^{\frac{1}{12}} (Fr)^{1.0} \qquad (1.4)$$

38

where:

$$Bo = \frac{g D_c^2 \rho_l}{\sigma_l} \qquad (1.4.a)$$

$$Ga = \frac{g D_c^3}{\mu_l^2} \qquad (1.4.b)$$

$$Fr = \frac{V_s}{\sqrt{(g D_c)}} \qquad (1.4.c)$$

The value of C_1 is 0.2 for pure liquids and non-electrolyte solutions and 0.25 for electrolyte solutions. This correlation is known to provide for reliable and conservative estimates for low viscosity and coalescing liquids ($\mu_l \leq 0.02$ Pa s). It is however not recommended for hydrocarbon fluids, non-Newtonian fluids or noncoalescing liquids. Furthermore, for mixtures of liquids which have significant differences in one or more physical properties, it appears that only those holdup correlations derived by using direct measurements on the mixture should be used.

Hikita et al. (1980) reported on gas holdup measurements in a 10 cm diameter column using various gases and liquids. These authors proposed the following relation:

39

$$\epsilon_g = 0.672 f_1 \left(\frac{V_g \mu_l}{\sigma_l}\right)^{0.578} \left(\frac{\mu_l^4 g}{\rho_l \sigma_l^3}\right)^{-0.131} \left(\frac{\rho_g}{\rho_l}\right)^{0.062} \left(\frac{\mu_g}{\mu_l}\right)^{0.107} \qquad (1.5)$$

where f_1=1 for non-electrolyte and for salt solutions, f_1 is a function of the ionic strength. Hikita et al. (1980) were the first researchers to consider physical properties of the gas phase. As shown in Equation 1.5, the influence of the gas density is rather limited but, if omitted, the data fit may rise to 15% as opposed to 4.2%. This might be of particular importance for systems operating under high pressure conditions. Here again, caution is advised for complex mixture of fluids, non-Newtonian fluids, non-coalescing fluids and hydrocarbon liquids. Furthermore, the experiments conducted by Hikita et al. (1980) were performed in a small diameter column (D_c < 0.15 m), which could introduce further imprecisions, as previously discussed.

Bach and Pilhofer (1978) proposed the following equation to describe the holdup data for pure organic liquids. This equation does not apply to mixtures and electrolyte solutions:

$$\frac{\epsilon_g}{1-\epsilon_g} = 0.115 \left(\frac{V_g^3}{\mu_l g \frac{(\rho_l - \rho_g)}{\rho_l}}\right)^{0.23} \qquad (1.6)$$

However, since the data covered by this correlation were

40

obtained in a small diameter column (D_c < 0.15 m) equipped with small hole opening (≤ 1 mm) gas distributor, this correlation must be carefully used. This correlation was however proven satisfactory in representing gas holdup data obtained in presence of hydrocarbon waxes (Bukur et al., 1987b).

Krishna et al. (1991) proposed a gas holdup model based on the two-bubble class theory. For superficial gas velocities below the transition gas superficial velocity (V_{trans}), the gas holdup increases proportionally to the superficial gas velocity, whereas, for higher gas superficial velocities (churn turbulent regime) it was assumed that the gas velocity in excess of the transition velocity ($V_g - V_{trans}$) flows through the bubble column in the form of large bubbles. Recently, this theory was further developed by Wilkinson et al. (1992), and generalized to incorporate the effects of both the gas and liquid physical properties. For the transition and heterogeneous regimes, the gas holdup can be expressed as follows:

$$\epsilon_g = \frac{V_{trans}}{V_{s.b.}} + \frac{V_g - V_{trans}}{V_{l.b.}} \qquad (1.7)$$

where:

$V_{s.b.}$ is the rise velocity of the small bubbles and $V_{l.b.}$ is the rise velocity of the large bubbles. Furthermore, $V_{s.b.}$, $V_{l.b.}$ and V_{trans} could be obtained as follows:

$$\frac{V_{s.b.}\mu_l}{\sigma_l} = 2.25\left(\frac{\sigma^3\rho_l}{g\mu_l^4}\right)^{-0.273}\left(\frac{\rho_l}{\rho_g}\right)^{0.03} \qquad (1.7.a)$$

$$\frac{V_{l.b}\mu_l}{\sigma_l} = \frac{V_{s.b.}\mu_l}{\sigma_l} + 2.4\left(\frac{\mu_l(V_g - V_{trans})}{\sigma_l}\right)^{0.757}\left(\frac{\sigma^3\rho_l}{g\mu_l^4}\right)^{-0.077}\left(\frac{\rho_l}{\rho_g}\right)^{0.077} \qquad (1.7.b)$$

$$\frac{V_{trans}}{V_{s.b.}} = 0.5\ \exp^{-193\,\rho_l^{-0.61}\,\mu_l^{0.3}\,\sigma_l^{0.11}} \qquad (1.7.c)$$

These equations were found to give an excellent description of the experimental data for gas-liquid systems, the physical properties of which cover the subsequent ranges: σ_l: 0.02-0.073 N/m, μ_l: 0.0004-0.055 Pa s, ρ_l: 683-2960 Kg/m^3, and ρ_g: 0.09-38 Kg/m^3. The average error reported by the authors was only 10% and experimental gas holdup data up to 0.5 were successfully described by this new model. However, these equations, developed for pure liquids, would lead to a conservative estimate of the gas holdup, for both low and high pressure, in the presence of noncoalescing liquid mixtures and electrolyte solutions. Furthermore, the validity of this new gas holdup

42

model, rests on the validity of the two bubble class theory: 1) under the heterogeneous regime, the small bubble gas holdup is constant and corresponds with the end of the homogeneous flow regime, 2) increasing the gas velocity beyond the transition velocity (V_{trans}) from the homogeneous to the heterogeneous regime, increases only the large bubble holdup. This approach, though reasonable and promising in principle, can not be applicable to all cases, as recently discussed by Deckwer and Schumpe (1992). Therefore, the assumption of a constant small bubble holdup in the heterogeneous flow regime can not be generalized and caution is advised in applying this correlation.

1.2.3 Bubble characteristics

Bubble characteristics, such as bubble size, velocity, frequency, size distribution and spatial distribution constitute hydrodynamic parameters of prime importance in understanding and predicting the performance of bubble and slurry bubble columns.

Bubble size or formation dynamics are extremely complex and thus difficult to predict. Coalescence and break-up phenomena could be extremely important in determining the bubble size. Whether or not the size of a primary bubble will change depends on its size relative to the maximum equilibrium bubble size and whether the system is coalescing or non-coalescing

43

(Reilley et al., 1986).

In systems where coalescence rates are insignificant and the liquid motion is inadequate to break bubbles, the bubble formation process controls the bubble size and becomes critical. Terasaka and Tsuge (1991) and Tsuge et al. (1992) studied the bubble formation at a single orifice under various conditions. They observed that the bubble volume increased when decreasing the system pressure, increasing the orifice diameter and increasing the gas flowrate. Geary and Rice (1991) recently derived elementary force balances to predict bubble formation size.

Coalescence is affected by the presence of surfactants, contaminants, and the liquid properties, in fact by any substance altering the surface or interfacial properties of the gas bubble and the liquid. For example, high rates of bubble coalescence are common in highly viscous liquids while low viscosity liquid systems are observed to show significant bubble breakup. This was confirmed by Bukur and Patel (1989) who observed an increase of the bubble Sauter mean diameter with the viscosity of the liquid medium. Furthermore, mixtures were also found to show different coalescing behaviour than pure liquids. Bubble coalescence properties were also found to depend on the presence of added salts. If a bubble is generated, the concentrations of an electrolyte at the interface and in the bulk liquid are initially equal.

44

However, the ions have a tendency to move away from the interface. This results in an enrichment of the liquid phase, accompanied by an increase in the surface tension. Since the transport of ions in the bulk liquid requires some time, the coalescence hindering action is only pronounced at short residence times of the bubbles. Thus, if the bubble residence time is large, the influence of added electrolytes is much less pronounced (Shah, 1982). This could explain why Deckwer et al. (1978) did not find significant differences in bubble diameters for water and electrolytes in tall bubble columns. The addition of alcohols lowers the surface tension if these substances have enough time to accumulate at the surface. As they orient themselves with their hydrophobic group towards the gas phase, the generated dipole layer suppresses tha coalescence. The effect largely depends on the chain length of the alcohol. Prince and Blanch (1990) recently proposed a phenomenological model to predict the rates of bubble coalescence and bubble break-up in turbulent air-sparged bubble columns. They modeled bubble coalescence by considering bubble collisions due to turbulence, buoyancy, and laminar shear and by analyzing the bubble collision efficiency. Bubble break-up was analyzed in term of bubble interactions with turbulent eddies. The model allowed as well to predict equilibrium bubble size and bubble size distribution. However, this model, developed for water and salt solutions systems, was based on the assumption of isotropic turbulence, which was recently found to be

questionable (Dudukovic and Devanathan, 1992), particularly for smaller diameter columns. In addition, the bubble break-up coalescence phenomena were assumed homogeneously radially distributed, which, as discussed in Chapter 5, is not the case for the system presently studied.

Zaidi et al. (1979) and Deckwer et al. (1980) measured the hydrodynamic properties prevailing under the conditions of the Fischer-Tropsch process in the slurry phase (molten paraffin, 250-300°C, 900 KPa). The bubble size measurements were carried out in a bubble column of 5.0 cm diameter which was equipped with porous plate spargers (mean pore diameter: 60-90 μm). The Sauter bubble diameter in the molten paraffin wax was found to be about 0.7 mm and was not found to be significantly affected by the gas velocity (V_g). This is in agreement with numerous authors (Akita and Yoshida, 1974; Deckwer et al., 1978) who confirmed that when the gas is sparged by single orifices, perforated or sintered plates, the diameter of the generated bubbles are only slightly dependent on the gas velocity. Bukur and Patel (1989), however, found that the Sauter mean bubble diameter decreased monotonically with the superficial gas velocity and reached a constant value at higher gas velocities.

Substantial controversy arises on the effect of the gas distributor on the bubble size. Many researchers reported a dependency of the *initial* bubble sizes on the orifice diameter

46

(Akita and Yoshida, 1973; Bhavaraju et al., 1978; Tsuge et al., 1992), but the effect of the sparger is still not clarified for the Sauter bubble diameter of the fully established multi-phase flow. Actually, some researchers argued that the gas distributor has a significant effect on the bubble size (Satterfield and Huff, 1980; Bhavaraju et al., 1978; Kumar et al., 1976), while others denied this effect (Deckwer et al. 1978; Akita and Yoshida, 1974).

The bubble Sauter mean diameter correlation proposed by Akita and Yoshida (1974) indicated that the bubble sauter mean diameter was proportional to the column diameter. However, for columns of diameter larger than 0.3 m, the bubble diameter was found to be independent of the column diameter. Actually, in a general way, the effect of the column diameter on all the hydrodynamic parameters (except the dispersion coefficient) becomes insignificant for $D_c \geq 0.15$ m, for less viscous liquids. For highly viscous ($\mu_l > 0.02$ Pa·s) liquids, this effect should become insignificant for $D_c \geq 0.3$ m. These values of column diameter are independent of other liquid properties (Shah et al., 1982). The correlation proposed by Akita and Yoshida (1974) (Equation 1.8), can exclusively be recommended for systems equipped with single orifice spargers similar to the ones studied by these authors (1974). For instance, it is doubtful that bubble sizes in various hydrocarbon systems could satisfactorily be described by the correlation proposed by Akita and Yoshida (1974).

47

$$\frac{d_{vs}}{D_c} = 26\left(\frac{D_c^2 g \rho_l}{\sigma_l}\right)^{-0.5} \left(\frac{gD_c^3}{\mu_l^2}\right)^{-0.12} \left(\frac{V_g}{\sqrt{gD_c}}\right)^{-0.12} \qquad (1.8)$$

A significant number of researchers studied the bubble rise velocity in bubble columns, including Mendelson (1967), Berghmans (1973) and Abou-El-Hassan (1983). It was found that the bubble rise velocity was usually an increasing function of its size and correlations of the following form were proposed: $V_b \sim (d_b)^a$, as reviewed by Muroyama and Fan (1985). Recently, Bly and Worden (1992) studied the effect of the solids on the bubble rise velocity. The bubble rise velocity was found to decrease with increasing solids fraction and density and to increase with bubble size. A number of authors, including Hills and Darton (1976), studied the rise velocity of large bubbles in a bubble swarm. They concluded that in the presence of a swarm of smaller bubbles in a liquid, a cap bubble rises faster than it would do in isolation.

1.2.4 Gas-liquid interfacial area

The gas-liquid interfacial area is an important design variable which depends on the geometry of the apparatus, the operating conditions and the physical properties of the liquid media. The gas-liquid interfacial area can be determined at various locations in the multiphase reactor using the volume-to-surface mean bubble diameter and the gas hold-up in the

48

following way:

$$a = \frac{6\epsilon_g}{d_{vs}} \qquad (1.9)$$

with

$$d_{vs} = \frac{\Sigma\, N_i\, d_{bi}^3}{\Sigma\, N_i\, d_{bi}^2} \qquad (1.10)$$

As it can be appreciated, this technique, allowing the assessment of the mean gas-liquid interfacial area, a key parameter in multiphase reactors, requires a detailed knowledge of the bubble size distribution and thus, special techniques for the direct measurement of this distribution.

1.2.5 Liquid holdup

Kara et al. (1982) observed that the liquid holdup was influenced by both gas velocity and slurry velocity. For example, it was shown that liquid holdup decreased with an increase in the gas velocity and a decrease in slurry velocity. Furthermore, an effect of the particle size was noticed and this effect of the particle size on the liquid holdup was found to be more significant for the higher values of superficial gas velocities.

1.2.6 Mixing models

The problem of mixing in slurry reactors involve matters that pertain to the solid, liquid and gas phase. This review will consider them in this sequence.

1.2.6.1 Solid dispersion coefficient and solid concentration profile

Concerning the solid dispersion, Kojima et al. (1986) showed that the dispersion coefficient of the solid particles was not influenced by the distributor design. Kato et al. (1972) demonstrated that the axial solid dispersion coefficient was not a function of the liquid velocity and the average solid particle concentration. However, they have shown that the axial solid dispersion coefficient increases with an increase in V_g and is proportional to $D_c^{1-1.5}$. Kato et al., (1985) proposed a correlation for the longitudinal solid dispersion coefficient in slurry bubble columns. Kara et al. (1982) observed that the axial dispersion coefficient is dependent upon the gas and slurry velocities and the particle size but relatively independent of the solids concentration.

It appears that the liquid velocity is an important parameter in determining the homogeneity of the slurry phase. Kelkar et al. (1984) observed that as long as the liquid velocity is significantly higher than the settling velocity of the solid

50

particles, the slurry behaves as a pseudo-homogeneous liquid, irrespective of the gas velocity. The solids concentration profiles are usually represented by means of the sedimentation-dispersion model, which was developed by Cova (1966) and by Suganuma and Yamanishi (1966). This model is based on a macroscopic mass balance of solids that takes into account the mechanisms of solids sedimentation and solid dispersion due to the convective currents in the liquid phase.

Cova (1966) observed that higher gas and liquid velocities and high viscosities all tend to give more uniform solid distributions.

1.2.6.2 Liquid mixing

1.2.6.2.A Dispersion coefficient

Liquid phase mixing in bubble columns is due to the following combined effects: convective dispersion caused by nonuniform cross sectional liquid velocity profiles resulting from liquid recirculation, turbulent eddies, entrainment and shedding of the liquid in the wakes of bubbles and molecular diffusion. These mixing mechanisms are often lumped into a single parameter, the axial dispersion coefficient, which is usually evaluated from tracer experiments using electroconductivity and spectrophotometry techniques. The reported data on the liquid phase dispersion coefficient indicate that it depends

on the gas velocity and column diameter, as reviewed by Shah et al. (1982). The various correlations described in the literature show dependencies of the liquid dispersion coefficient on the column diameter which range from $D_c^{1.0}$ to $D_c^{1.5}$ and on the gas velocity which varies from $V_g^{0.3}$ to $V_g^{2.0}$. However, the influence of the liquid phase properties is not clearly understood. For Newtonian liquids, the effect is small and can usually be neglected. Concerning the effect of the liquid velocity, within the range of industrial interest (< 0.03 m/s), it appears to be insignificant, though at high liquid velocities, Kara et al. (1982) observed some effect of the liquid velocity.

Both Kara et al. (1982) and Kelkar et al. (1984) have shown that the effect of the gas distributor design on the liquid dispersion coefficient was pronounced at low gas velocity. This was more recently confirmed by Kojima et al. (1986). Another potential factor influencing the liquid dispersion coefficient is the effect of solid particles. Actually, the effect of the solid particles on the liquid dispersion coefficient is still not clearly understood. Kara et al. (1982) observed that the dispersion coefficient was dependent on the particle size while relatively independent of the solids concentration. Rice and Littlefield (1987) and Rice et al. (1990) reported order of magnitude lower axial dispersion coefficients than predicted by available correlations. They attributed this to their flexible spargers which maintained

bubble flow in perfect vertical alignment. These authors claimed that most of the liquid axial dispersion coefficient data in the literature reflect misalignment of columns. They reported that only 0.5 degree of misalignment from the vertical could lead to axial liquid dispersion coefficient differing in two orders of magnitude.

1.2.6.2.B Liquid recirculation

Phase recirculation or gulf streaming is commonly encountered in bubble column systems. The bubbles rising in a liquid entrain liquid upwards. Because of continuity, an equal amount of liquid must therefore flow downwards. This circulation is driven by the difference in density between the gas and liquid and it arises due to radially non-uniform gas holdup profiles. The scale of the macroscopic liquid circulation depends on the regime of bubble flow. For a heterogeneous distribution of bubbles (churn turbulent flow regime) in which the gas transport preferentially takes place in the form of fast-rising large bubbles, high rates of circulation occur in the liquid phase. The effect of column size (diameter and height), distributor and internals design, physical properties of the two-phase system and operating conditions (superficial gas velocity) on liquid recirculation is not still well understood. Since liquid recirculation affects mixing, interfacial transport and heat transfer, it needs to be properly quantified.

53

The prediction of liquid recirculation based on the early inviscid pressure balance model of Freedman and Davidson (1969) is limited to shallow tanks stirred with gas plumes, and low gas superficial velocities ($V_g \approx 1$ cm/s), and are thus not suitable for most bubble column systems. The laminar liquid circulation and "bubble street model" of Rietema and Ottengraph (1970) was developed, based on pressure balance, for high viscosity liquids. Predictions of this model were found to deviate as the liquid viscosity decreased, or as the liquid flow became turbulent. In commercial columns of practical interest, the liquid flow is turbulent in most cases and the theory of laminar circulation is limited to small diameter column and/or highly viscous liquids. Such limitations also applied to the laminar liquid circulation and bubble chain model of Crabtree and Bridgwater (1969). Bhavraju et al. (1978) analyzed the problem of laminar and turbulent liquid circulation and developed a liquid circulation model based on multiple liquid circulation cells in the transverse direction. However, since experimental measurements of the liquid velocity indicated the absence of multiple cells in the transverse direction, this model was unable to adequately predict the liquid velocity. Whalley and Davidson (1974) proposed an energy balance method to predict the liquid recirculation in shallow bubble columns ($H/D_c \approx 1$). This model was however proven unsuccessful in taller bubble column systems (Joshi and Sharma, 1979). Joshi and Sharma (1979), extending the so-called principle of

minimization of maximum vorticity to tall columns, modified the original energy balance model of Whalley and Davidson (1974). However, the application of the single phase vorticity transport equations to two phase flow, as suggested by both, Davidson and Whalley (1974) and Joshi and Sharma (1979) is highly questionable. Joshi and Sharma (1979), applying this theory, concluded, without experimental evidences, that multiple circulation cells of height equal to column diameter were present in bubble columns. However, since it is indeed physically impossible for streamlines of adjacent cells to oppose each other (Van den Akker and Rietema, 1982), this model was modified to allow for assisting streamlines which assures alternating sense of rotation in the cells along the column (Joshi and Sharma, 1982). This model, however, predicts that axial centerline velocity alternates in direction along the column which is contrary to experimental observations. Moreover, in such a flow pattern, inter-cell interaction is minimal and hence significant inter-cell concentration and temperature gradients can develop which has never been observed in bubble column systems. A number of experimental studies provided evidence of the existence of multiple recirculation cells (Chen, 1989). However, as suggested by Dudukovic and Devanathan (1992), no evidence that these cells are actually fixed in space were, so far, presented. It seems more likely, according to Dudukovic and Devanathan (1992), that these liquid circulation cells consist of travelling secondary vortices, superimposed over the

classical macroscopic liquid circulation pattern: liquid rising in the center and descending near the column wall. Experimental confirmation of such macroscopic liquid circulation pattern were indeed provided by a number of authors, including Hills (1974), Ueyama and Miyauchi (1979), Kojima et al. (1980), Franz et al. (1984), and more recently, Yao et al. (1991), and Dudukovic and Devanathan (1992). So, the multiple circulation cell model developed by Joshi and Sharma (1982) constitute a questionable representation of the liquid circulation in bubble columns. Furthermore, such approach could be misleading, since little interaction between adjacent cells is assumed. Thus, such liquid flow representation suggests that the tanks-in-series model is applicable for scale-up purposes, whereas a number of studies indeed suggest complete backmixing of the liquid phase (Dudukovic and Devanathan, 1992).

Miyauchi and co-workers (1970, 1979) developed a turbulent circulating flow model, based on pressure balance. The equation of motion for the liquid phase, assuming no end effects and constant radial pressure is as follows:

$$\frac{-1}{r}\frac{d}{dr}(r\tau_t) = \frac{dP}{dz} + (1-\epsilon_{g,loc})\rho_l g \qquad (1.11)$$

The shear stress τ_t is defined through the turbulent kinematic viscosity, while the molecular kinematic viscosity was assumed

to be negligible.

$$\tau_s = -\nu_t \rho_l \frac{dU_l}{dr} \qquad (1.11.a)$$

Furthermore, one boundary condition is obtained assuming axisymmetric liquid flow in the column:

$$\frac{dU_l}{dr} = 0 \quad at \quad r=0 \qquad (1.11.b)$$

Another boundary condition is obtained from the *Universal Velocity Distribution for Turbulent Flow*, assuming that the laminar sublayer can be neglected and the velocity at the wall is equal to $U_{l,w}$:

$$U_{l,w} = -11.63 \frac{\sqrt{|\tau_s|}}{\rho_l} \qquad (1.11.c)$$

Introducing an expression for the radial profile of the gas holdup (Equation 1.2), and assuming constant radial turbulent kinematic viscosity (Dudukovic and Devanathan, 1992), the following expressions for the liquid velocity are obtained, for batch system (no net liquid circulation):

57

$$|U_{l,w}| = (11.63)^2 \frac{\nu_l J_1}{R}\left(-1+\sqrt{1+\frac{(2J_0-(\frac{\epsilon_{g,avg}}{2}))}{(11.63)^2 J_1^2}\frac{R^3 g}{\nu_l^2}}\right) \quad (1.11.d)$$

$$U_l = (J_1(1-\theta^2)-1)|U_{l,w}| - \frac{R^2 g}{\nu_l}(J_0(1-\theta^2)-I(\theta)) \quad (1.11.e)$$

where:

$$J_0 = \frac{(m+6)\epsilon_{g,avg}}{4(m+4)} \frac{1-\frac{(m^2+10m+20)}{(m+2)(m+6)}\epsilon_{g,avg}}{1-\frac{(m+6)}{(m+4)}\epsilon_{g,avg}} \quad (1.11.f)$$

$$J_1 = \frac{2(1-\epsilon_{g,avg})}{1-\frac{(m+6)}{(m+4)}\epsilon_{g,avg}} \quad (1.11.g)$$

$$I(\theta) = (\frac{(m+2)}{m})(\frac{1-\theta^2}{4} - \frac{1-\theta^{m+2}}{(m+2)^2})\epsilon_{g,avg} \quad (1.11.h)$$

For uniformly distributed rising bubbles in a batch system (no net liquid circulation), the relationship between the mean gas holdup ($\epsilon_{g,avg}$) and the slip velocity of the bubbles relative to the liquid V_{slip} is given by:

$$\frac{V_g}{\epsilon_{g,avg}} = V_{slip} \qquad (1.11.i)$$

Moreover, Ueyama and Miyauchi (1979) proposed the following relationship to relate the slip velocity of the gas bubbles to the gas superficial velocity in the circulation flow regime (batch system):

$$V_{slip} = \frac{V_g}{\epsilon_{g,avg}} - \frac{1}{(1-\epsilon_{g,avg})}\left(\frac{U_{l,c}+U_{l,w}}{(m+4)}\right) \qquad (1.11.j)$$

Experimental values of the liquid radial profile are well accounted for by this model, as reviewed by Deckwer and Schumpe (1987) and more recently by Dudukovic and Devanathan (1992). This model requires, as shown in Equations 1.11, the gas holdup radial profile and eddy viscosity values as inputs. Different constitutive relations have been proposed for the eddy viscosity, ranging from purely empirical correlations, as reviewed by Deckwer and Schumpe (1987), to turbulence based models based on single phase mixing length (Clark et al., 1987) and von Karman's hypothesis (Anderson and Rice, 1989).

As recently discussed by Dudukovic and Devanathan (1992), the Ueyama and Miyauchi (1979) model provides a more satisfactory representation of the liquid radial velocity profile than the model proposed by Rice and Geary (1990).

Experimental measurements of liquid velocities in bubble columns are limited. A limited number of reliable techniques were proposed in the literature, including pitot tubes, Laser Doppler Velocimetry (limited to low gas holdup values), hot wire anemometer, ultrasonic Doppler technique (also limited to low gas holdup values), as reviewed by Dudukovic and Devanathan (1992). A new Computer Aided Radioactive Particle Tracking (CARPT) was recently adapted to bubble column systems by Dudukovic and Devanathan (1992). This technique allows one to track a single neutrally buoyant radioactive particle using an array of scintillation detectors. They observed that the primary flow pattern was constituted of a single recirculation cell, as illustrated in Figure 1.2(b). However, they observed the existence of a small secondary liquid cell close to the distributor at low gas superficial velocity (≈ 2.0 cm/s), as shown in Figure 1.2(a). Moreover, they concluded that simplified one dimensional liquid recirculation profile was applicable to most of the column investigated, though Drahos et al. (1992) recently claimed that none of the existing one-dimensional models were adequate in describing their observations. Their observations suggested the existence of spiral upward flow.

1.2.6.3 Gas mixing

Gas phase backmixing is one of the important hydrodynamic parameters to be considered in the scale-up of bubble columns.

60

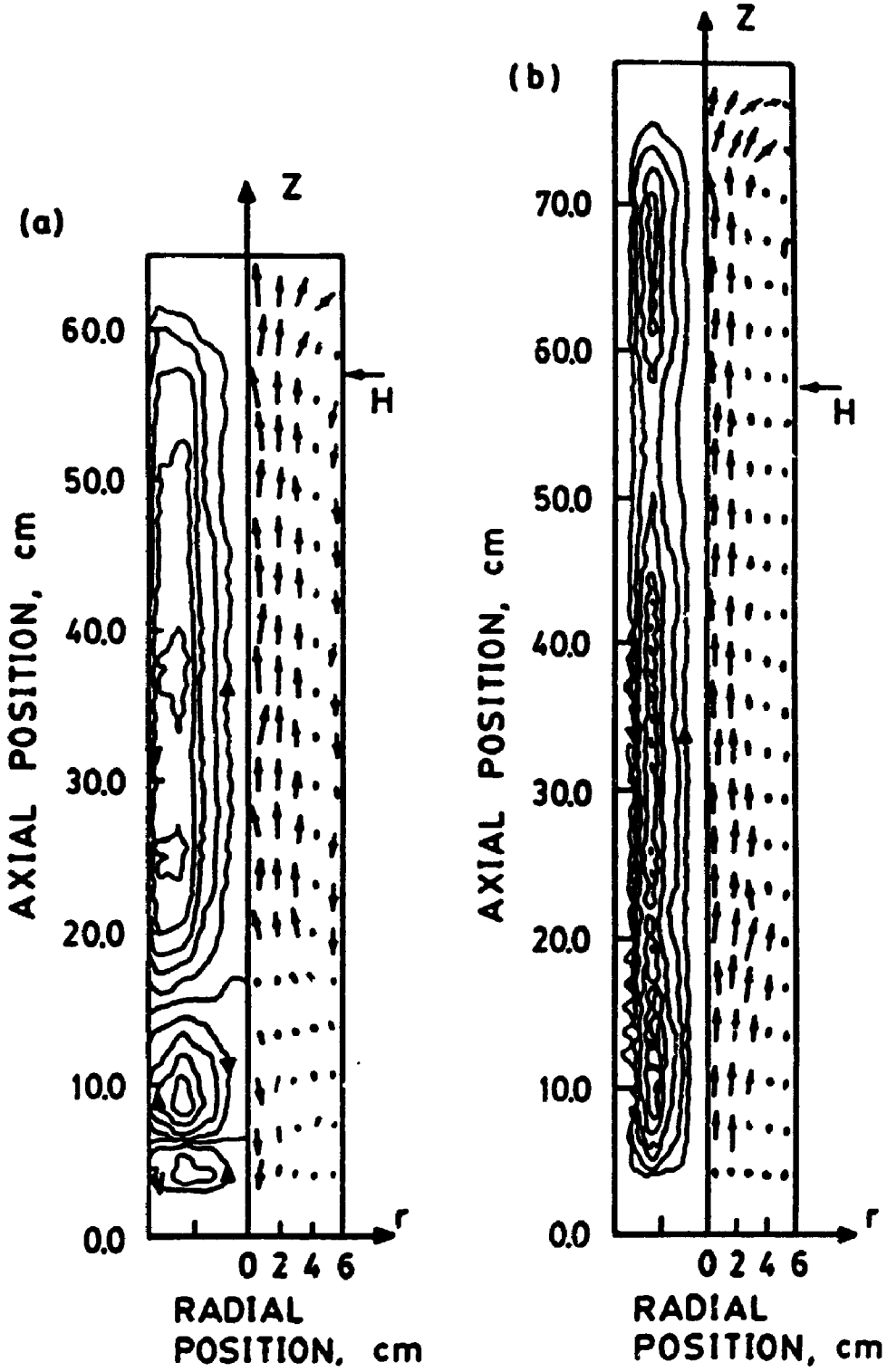

Figur 1.2: Liquid streamlines and velocity in a 0.114 m diameter column a) V_g=0.028 m/s; b) V_g=0.184 m/s (Dudukovic and Devanathan, 1992)

It can adversely affect the reaction rates and product selectivity. The mechanism of mixing of the gas phase in the homogeneous bubbling regime differs distinctly from the one existing in the heterogeneous mixing regime. In the homogeneous regime, uniform sized bubbles rise in the quiescent liquid without hindering each other, and with minimum backflow. At higher gas velocities, the flow becomes chaotic and is characterized by fast moving bubbles coexisting with smaller ones. The current and most widely used approach to characterize the gas phase mixing is to use the axial dispersion model, which allows for the effect of longitudinal mixing on the reactor performance. However, gas phase backmixing data presented in the literature, as reviewed by Shah et al. (1982), show considerable scatter, attributable to the measurement and analysis techniques. Furthermore, most data reported in the literature lie in the homogeneous regime, thus being of limited relevance for the industrially important churn-turbulent regime. Shah et al (1982) have recommended the correlations by Joshi (1982) and Mangartz and Pilhofer (1981) to predict gas phase backmixing. However, very little information is available in the literature regarding the effects of the physical and chemical properties of the gas and the liquid phases on the gas backmixing, as summarized by Shetty et al. (1992).

Shetty et al. (1992) recently proposed a two-bubble-class hydrodynamic model to predict gas-phase backmixing in bubble

62

column reactors. The model assumes a bimodal distribution of the gas phase with large bubbles flowing in a plug-flow manner and small bubbles being partially backmixed with a dispersion coefficient equal to the one of the liquid phase.

1.3 REVIEW OF EXPERIMENTAL MEASURING TECHNIQUES

The complete understanding of the hydrodynamic characteristics of bubble and slurry bubble columns, especially in systems of importance for the chemical industry (normally severe conditions; high temperature, high pressure ...) was and is still limited by the existence of reliable and precise observation techniques. In the following pages, a number of existing gas bubble measuring techniques will be reviewed, including the fibre optic sensors.

1.3.1 Two-dimensional bed

There have been several studies (Clift and Grace, 1972; Henriksen and Ostergaard, 1974; Kim et al., 1975; Saxena et al., 1984) of very wide, thin parallelepiped beds, which are usually referred to as two-dimensional beds. If the walls of the bed are transparent, the bubbles, wakes of the bubbles, and local hold-ups can be observed directly using photographic or cine camera techniques. These works in bi-dimensional beds have indeed provided a great insight into various aspects of fluidized bed behaviour, but their extension to quantify the

bubbling phenomenon and its associated details in a full three dimensional cylindrical three phase fluidized bed must be handled with some considerable caution. So, only at best qualitative observations and conclusions can be drawn from these studies.

Basically, there are two types of available measurement techniques in three-dimensional beds: non-invasive and invasive (with in-bed probes).

1.3.2 Non-invasive techniques

1.3.2.1 Pressure profile

1.3.2.1.A Bed Height

The height of the bed can be determined by direct observation. This method, only applicable to transparent plexiglass columns, is of rather poor precision. When high rates of gas flow are reached, the bed begins to pulsate and the surface of the bed (and consequently the total bed height) becomes undefined. Another method consists of measuring the pressure profile along the column: as the density of the solid is greater than that of the liquid, the pressure varies more rapidly in the dense phase section than in the freeboard region. The level where a change of slope of the pressure drop profile is observed provides a reference point to

determine the total height of the bed. This method also has some difficulties and inaccuracies for expanded beds with high gas holdups. The location of the reference point in these cases becomes quite uncertain.

1.3.2.1.B Determination of the phase holdups

A popular method for defining average phase hold-ups in the three phase (gas-liquid-solid) and two phase (gas-liquid) regions of the column can also be based on the pressure drop profile (Costa et al., 1986; Fan et al., 1987a; Kang and Kim, 1988; Patwari et al., 1986). The method uses the approximation that hold-ups of the gas, liquid and solid can be considered independent of the height in each one of these two regions of the column. Furthermore because the pressure varies quasi-linearly with the height of the bed: two straight lines may be defined, the intersection of which, as stated above, corresponds to the total bed height.

The mean hold-up of the solid ϵ_s is then obtained directly from the bed height and the mass of the dry particles as shown in the following equation:

$$\epsilon_s = \frac{M_s}{\rho_s A H_b} \qquad (1.12)$$

The two remaining unknowns (ϵ_l and ϵ_g) will then be found using Equation 1.13 (from the knowledge of the pressure profile) and Equation 1.14.

$$\frac{\Delta P}{H_b} = g(\rho_s \epsilon_s + \rho_g \epsilon_g + \rho_l \epsilon_l) \qquad (1.13)$$

$$\epsilon_g + \epsilon_l + \epsilon_s = 1 \qquad (1.14)$$

This method, which only yields the mean values over the entire bed, is precise as long as the flow rates of both gas and liquid remain small, small enough for the compositions of the two phases to be quite homogeneous. This method is then very sensitive to uncertainties in the determination of the pressure drop at the boundary between the two phase and three phase zones and in the assessment of the bed height. So, when pulsating conditions occur at the bed interface or when a ill defined transition between the three phase (gas-liquid-solid) and two phase system exists, this method is not suitable. In addition, this method requires that pressure has to be measured at several locations all along the wall of the column.

The implication of Equation 1.13 is that the pressure drops due to friction are negligible compared with the drop in static pressure. It has been shown by Kim et al. (1975) that

this is quite correct for almost all the flow rates encountered in three phase fluidization, even when the liquid viscosity reaches 80 cp.

1.3.2.2 Determination of the phase holdups by flow interruption

This method may be employed if the three phase fluidized bed occupies the entire test section. It involves simultaneously shutting off the liquid and gas flows to the column by means of fast-acting valves and subsequently draining the remaining liquid from the column. The volume of gas contained in the bed is equal to the reduction in the height of the liquid level after shutting off the flows multiplied by the column cross-sectional area A. The gas hold-up is therefore given by:

$$\epsilon_g = \frac{H}{H_b} \qquad (1.15)$$

Similarly, if v_l is the volume of liquid drained from the column:

$$\epsilon_l = \frac{V_l}{H_b A} \qquad (1.16)$$

Concerning the solid hold-up, it is determined from the knowledge of the mass of solids in the bed, as described in Equation 1.12.

This technique suffers from a number of disadvantages. First, it can only be employed when there is no solid-free zone above the three phase fluidized bed. Second, this technique requires close control on valve closing or errors will undoubtedly be introduced. This problem can become quite acute in beds of large diameter in which flowrates are relatively large. Furthermore, this technique could only be used in cold units and in set-ups where the flow disruption does not affect the reactor or process.

In a similar way, the Dynamic Gas Disengagement (DGD) technique was proposed (Patel et al., 1990) to study the bubble size distribution in bubble column. This technique is based on the measurement of the rate at which the level of the gas-liquid dispersion drops after the gas flow to the bubble column is shut off. Usually, the rate of the decrease of the bed level is determined from visual observation, which restrict its application to transparent column and medium. However, Daly et al. (1992) recently proposed the use of pressure transducer signals to measure the rate of liquid drop during the bubble disengagement process, which would extend the use of this technique to opaque systems. The bubble chord length distribution obtained, from DGD technique, is not

directly measured, but estimated from the bubble rise velocity distribution measured. Consequently, the precision of this technique is limited to the reliability of existing bubble rise velocity correlations, and to the validity of the main assumptions (no bubble-bubble interactions, constant rate disengagement process) involved in reconstructing the bubble rise velocity distribution.

1.3.2.3 Laser doppler anemometry

Laser-doppler velocimetry is based on the fact that in the intersection volume of two monochromatic laser beams, interference fringes are formed. A particle crossing these fringes scatters light, whose intensity varies with a high oscillation originated by passing light or dark areas. This oscillation can be detected by photodiodes or photomultipliers. The evaluation of the oscillation frequency of this so called doppler-signal and the fringe spacing known from the optical geometry gives the velocity information. The gas velocity can also be determined, assuming that very small particles follow the gas flow.

Laser doppler anemometry has been used by Levy and Lockwood, (1983) to perform the measurement of the gas and the elutriated particle velocities in the freeboard of a cold fluidized bed. Particle sizes have also been investigated based on the principle that there is a direct relation between

69

the particle size and the intensity of the scattered light (i.e. signal amplitude). Berkelmann and Renz, (1989) applied this technique to measure the particle velocity and size in the freeboard of a fluidized bed combustor.

Hamdullahpur and MacKay (1986) also used a laser doppler velocimeter to identify the flow behaviour of gas and particulates in the freeboard of a gas fluidized bed. They developed a technique based on fluorescence emission to discriminate between gas phase and particle phase velocity information. The principle of the technique is based on the discrimination between the scattered light from particles and the fluorescence emission from particles coated with a fluorescent dye. More recently, Hamdullahpur et al. (1987) applied this technique in a turbulent two phase flow (gas-solid) and succeeded in discriminating velocities from the two phases as well as from two different particle groups within the solid phase.

The measurement of bubbly flow using the laser-doppler anemometer is affected by the difference in the refractive indices of the gas and liquid phases. This difference in refractive index allows the measurement of the velocity and curvature of the bubble surface. Total reflection of light occurs if a light-beam intersects the bubble surface at an angle normal to the surface and larger than the critical angle. The light beam is only partially reflected and

partially refracted if the incident angle with the normal to the surface is smaller than the critical one. As a consequence of this fact, the two beams on an LDA system, incident on a bubble surface interfere beyond the bubble in space such that the doppler bursts recorded in the forward direction exhibit three peaks with sinusoidal oscillations in each part of the signal. The two side peaks are a result of the interference fringe pattern in space produced during the period of total reflection of the incident beam at the front and rear of the moving bubble. The central peak of the signal is a result of the interference of the partially refracted light beams that pass the bubble and interfere to produce the central peak of the signal burst. The bubble velocity is inferred from the doppler frequency of the burst signal. The bubble diameter or bubble axial cord is inferred from the time interval between the side peaks of the pedestal and the velocity. This method is known as the triple-peak technique of bubble sizing. Yu and Varty (1988) performed laser-doppler measurement to evaluate the velocity and diameter of bubbles using the triple-peak technique in a two-phase gas-liquid system.

It has to be pointed out that using additional streams of bubbles to generate an optical disturbance, similar to the one found in a bubbly bed, the probability of detecting a valid signal decreased linearly (with increasing bubble flowrate of the additional streams). Thus, this method (LDA) seems to

require a discrete phase which is generally of isolated nature rather than swarms of bubbles in close proximity with each other. Optical windows are also needed. All this highly limits its application in fluidized beds of different scale, including industrial scale units. In addition, this method has the obvious drawback that light transmission is required. Consequently, particle concentrations cannot exceed certain limits in order to prevent severe reduction of the light beam strength. Actually, no known applications of LDA in three phase fluidized beds have been reported in the literature.

1.3.2.4 Photographic techniques

Bruce and Revel-Chion (1974) used photography to investigate the porosity of a three-dimensional three phase fluidized bed. In order to minimize the distortion of the bubbles, they used a Perspex tank filled with water surrounding the circular bed of 46.3 mm i.d. and 1950 mm in height at the point were the pictures were taken. Some investigators (Page and Harrison, 1972; Sitthiphong et al., 1981) have used photographic studies to investigate the eruption bubble diameters in two and three phase fluidized beds. However, these measurements are only possible when the gas velocity is moderate.

More recently, Peterson et al. (1987) used off-axis holography to study the bubble behaviour in a three phase fluidized bed. The advantage, as compared to ordinary photography, of this

technique is that it allows measurement of the entire bubble size and location distribution within the bed at a single instant of time.

However this technique suffers from serious drawbacks. The solid phase used has to match the refractive index of the liquid phase or vice-versa. Also, this technique requires the presence of optical windows which can limit the use of this technique in laboratory units. In addition, this technique requires sophisticated and expensive instrumentation.

1.3.2.5 γ-rays

The attenuation of the γ-rays has been used by Lee et al. (1973) to measure the gas hold-up. The attenuation of the γ-rays obeys the Beer-Lambert law:

$$\ln\left(\frac{I}{I_o}\right) = \lambda \rho s \qquad (1.17)$$

Here, λ is the coefficient of mass absorption, whose value has been tabulated for most atoms, s is the thickness of the absorbing medium, and ρ is the density of the emulsion, from which it is simple to deduce the gas hold-up. However, this technique presents all the inconvenients of a radioactive technique, in terms of safety, and is thus restricted to laboratory studies. The technique also presents severe

problems in properly defining temporal properties such as bubble velocities, and bubble size in conjunction with local gas hold-ups.

1.3.2.6 X-rays

The X-rays technique has been widely used to view bubbles in fluidized bed system. Beds of any size or shape can be examined but it is more convenient to use beds of rectangular plan section with one face parallel to the beam axis so that the beam path length is equal over the whole field of view. However, since the picture is essentially a silhouette, interpretation at high bubble concentration may be difficult. The power of penetration of X-rays is a quite serious limitation. In practice the vessel walls must be made of materials such as aluminium and the powdered material forming the bed should contain small fractions or if possible no elements with atomic number greater than that of calcium. The thickness of the bed that can be penetrated depends entirely on the solids absorption properties and on the beam energy. For the majority of materials of practical interest the maximum penetration length is less than one meter.

Rowe and coworkers at University College in England pioneered the application of this technique. For example, Rowe and Everett, (1972) used this technique to investigate the interaction of bubbles with solid surfaces in a gas-solid

fluidized bed.

1.3.2.7 Neutron radiography

Neutron radiography has been recently used by Chiba et al. (1989) for visualization of the bed behaviour of a three phase fluidized bed at high pressure. The unit used for neutron generation is a cyclotron, which generates a 16 MeV proton beam. A beryllium target assembly is placed at the center of a moderator which converts initially produced fast neutrons to thermal neutrons. The thermal neutrons pass through the column wall and the fluidized bed, giving an image on a scintillation material screen. The image produced on the screen can be photographed by a highly sensitive camera and recorded on video film. This technique was also recently proposed (Chang and Harvel, 1992) to determine the gas-liquid bubble column instantaneous interfacial area and void fraction.

1.3.3 Invasive techniques

1.3.3.1 Electrical probes

The first requirement when using an electrical probe in multiphase flow is that the phases have significantly different electrical conductivities. Consequently, variations in conductance permit the measurement of the local void

fractions (local gas hold-ups) and the arrival frequency of the bubbles at a given point in a continuous, conducting fluid. Statistical information can be obtained to characterize the flow pattern. By using a double probe, a bubble velocity and bubble axial length can be measured.

1.3.3.1.A Electroresistivity / electroconductivity probes

These probes consist mainly of two electrodes. The relative position and shape of the electrodes differ according to different workers. For instance the tip of the probe may constitute the first electrode while the second electrode may be the metallic part protecting the sheath of the probe. The use of a second probe of the same type can allow rising bubble velocity measurements. Soria (1991), described a multi-electrode arrangement, including electrode guards to avoid detrimental distortion of the electrical field.

When the primary electrode is in contact with the conductive liquid, electrons flow freely to the secondary electrode; but, when the primary electrode is in contact with a gas bubble, the resistance to current flow is greatly increased and essentially no electrons can flow. So, the probe is able to distinguish the non-conductive bubble phase from the conductive dense phase working as an on-off switch.

Electroconductivity as well as electroresistivity probes have

been extensively used to obtain the local gas porosity, the bubble frequency, the distribution of bubble size and rising bubble velocity as well as the average bubble size and average rising bubble velocity. It can also be used very effectively for the determination of volume averaged hydrodynamic parameters, as recently proposed by Soria (1991). This device has been mainly employed in two-phase systems (gas-liquid) (Soria, 1991; Soria and de Lasa, 1992), in three phase fluidized beds (Fan et al., 1987a; Kim and Kim, 1987; Sun and Furusaki S., 1988; Zrymiak and Hill, 1986; Soria, 1991; Soria and de Lasa, 1992) and in slurry bubble columns (Yasunishi et al., 1986) using the electroconductivity properties of the liquid. Furthermore, this type of probe has been adopted in two-phase system studies (gas-solid) (Park et al., 1969) where electrically conductive solid particles are used. The main disadvantage of this technique is that the continuous phase has to be an electrical conductor, which highly restricts the application of this sensor to real systems and industrial scale reactors frequently dealing with non-conductive liquids or\and solids.

Conductivity probes have been also used to directly measure the liquid hold-up. The conductivity of a liquid system with a fixed concentration of ions at a fixed temperature is proportional to the cross-sectional area of conducting material and inversely proportional to the length of the path between two electrodes. The fraction of the cross-sectional

area occupied by the liquid in a multi-phase system is equal to the volumetric fraction of the liquid. The length of the path in a multiphase system is obtained by multiplying the distance between the electrodes by a tortuosity factor. It has to be pointed out that this tortuosity factor is not substantially affected by the amount of gas in a ternary system gas-liquid-solid. Then, the conductivity should vary in proportion to the liquid hold-up in the bed only.

$$\epsilon_l = \frac{\delta}{\delta_o} \qquad (1.18)$$

where δ represents the conductivity in the bed and δ_o represents the conductivity in the liquid alone. Soria (1991) reported various precisions concerning the previous equation and calibration methodology.

Achwal and Stepanek (1975) used this technique to determine the gas hold-up in a gas-liquid system ($\epsilon_g + \epsilon_l = 1$). Begovich and Watson (1978) applied this method in three phase fluidized beds to determine the axial profile of the gas hold-up. Thus, measurement of the conductivity and pressure at various heights in the bed and application of Equations 1.12, 1.13 and 1.14 or 1.13, 1.14 and 1.18 to incremental sections of the bed allows each of the three phase hold-ups to be calculated as functions of height in the bed.

More recently, Tang and Fan (1989) studied the hydrodynamics of a three-phase fluidized bed containing low-density particles. They used a conductivity probe to study the axial holdup of gas and liquid phases and the bubble distribution. They tested the applicability of several literature equations.

This method, with valuable capabilities for defining volume averaged properties, has to be used with caution. It can be used only for electroconductive liquids. Also a maldistribution of the liquid can lead to erroneous results, e.g. in situations where a significant fraction of liquid bypass the electrode leaving most of the electrode out of action. This effect will probably not be serious in relatively long beds.

Conductivity probes were also used in combination with tracers (potassium chloride solution 1.0 N) to determine the axial and radial dispersion characteristics of the liquid phase in three phase fluidized beds (Kang and Kim, 1986; Kojima et al., 1986). The definition of these parameters are of crucial importance for reactor modelling. Unfortunately, the extrapolation of these results to fluidized beds with different properties (viscosity, surface tension, rheological properties) is uncertain. Other direct methods would be advisable for these cases.

1.3.3.1.B Capacitance probes

Capacitance probes have been extensively adopted (Abed, 1985; Gunn and Al-Doori, 1985; Hilligardt and Werther, 1986; Zhang et al., 1987) to characterize the hydrodynamics in laboratory gas-solid fluidized beds. However, capacitance probes suffer from three major shortcomings :

1 - Signal to noise ratio becomes unacceptably low when probes and associated cables are long,

2 - Probe calibration strongly depends on bed material as well as reactor temperature and pressure,

3 - Expensive equipment is needed to carry out sophisticated signal analysis.

More recently, Weluda et al., (1987) developed a cooled capacitance bubble probe to investigate the bubble phase behaviour in a high temperature (850°C) fluidized reactor with coal combustion. An important advantage of the cooled sensor is that the capacity changes due to temperature are compensated. They observed that characteristic bubble parameters, such as frequency and rising bubble velocity were temperature dependent. Also Schweinzer and Molerus (1987) investigated the bubble behaviour in a pressurized gas-solid fluidized bed using miniaturized capacitance probes. They

concluded that there is a strong indication of a complex variation of bubble properties with pressure. These conclusions confirm the need of hydrodynamic studies in more realistic systems (high pressure, high temperature) to improve the design, modelling and operation of industrial fluidized bed reactors. These conclusions also confirm the need of effective tools for hydrodynamic observations under severe conditions.

1.3.3.1.C Inductance probes

Cranfield (1972) used an inductance probe to perform bubble measurement in large gas-solid fluidized beds. The inductance probe comprised of a single needle-like rod of approximately the same diameter as the bed particles (2 mm). This technique, which requires no calibration, is based on the principle that the particles of the bed act as an "armature" to close a miniature inductance coil placed in the bed. The sequence of particle transition, i.e. during the passage of a bubble, is detected as a change in inductance. However, this technique requires the bed material to be susceptible to a magnetic field, which severely restricts its application to industrial units, and also requires extensive instrumentation.

1.3.3.1.D Electrical discharge

Yoshida et al. (1982) developed an electrical discharge probe

to investigate bubble behaviour in gas-solid fluidized beds. The detecting device is based on the principle that the voltage of dielectric breakdown of dielectric particles is higher in the emulsion phase than in the bubble phase. The probe can be applied at temperatures as high as 1000°C without restriction of particle properties. However, the electrode materials should be oxidation resistant at high temperature, which may limit the probe application in FCC regenerators. If oxidation is allowed, an oxide film is formed, which interrupts the electrical discharge and disturbs the sensor operation.

1.3.3.2 Static pressure

Pressure fluctuations are known to occur in fluidized beds and are known to be associated with the presence of bubbles, or other local bed non-homogeneities, as well as with the circulation of solids. Several authors (Abed, 1985; Atkinson and Clark, 1988) measured, using pressure probes, the fluctuating static pressure in fluidized beds. One of the main advantages of this technique is that it requires simple instrumentation commonly found or easily installed in most fluidized beds. However, proper connections between the tip of the tube and the pressure transducer are crucial to avoid signal deterioration. Also special care must be taken to avoid the backflow of the particles into the tube which can influence the pressure signal spectrum. This technique also

requires very fast response time and the use of a proper deconvolution analysis for data interpretation. In fact, the pressure signal at a given bed level is a complex integration of various bubbles evolving in the vicinity of the measuring port.

1.3.3.3 Thermal methods

1.3.3.3.A Thermal response probes

Several authors, including Morooka et al.(1980) and Wittmann et al. (1981), used thermal response probes to measure the local particle velocities in fluidized beds. The method applies a temperature pulse of very short duration to a group of particles and follows the movement of the latter with the aid of a rapid-response thermocouple. Interpretation of thermocouple data involves important difficulties due to the complex fluid dynamic and heat transfer phenomena involved. In this respect, Thimmapuram et al. (1992) recently proposed the statistical analysis of temperature-history records of a heat transfer surface immersed in a bubble column, as a mean to characterize the hydrodynamic regimes.

1.3.3.3.B Hot wire anemometer

Hot wire anemometers have an advantage over electrical and optical probes in that they can measure mean and fluctuating

characteristics of the superficial fluid velocity as well as temperature and void fractions. Hot wire anemometry was used for gas velocity measurements by several authors, including Oki et al. (1977) and Briens et al. (1978). Furthermore, the value of this technique for assessing gas recirculation in a novel Riser Simulator was recently demonstrated by Pekediz et al. (1992). However, problems were reported with the impingement of solids on the wire as well as with high temperature operation. In addition, the extreme fragility of the sensors, the complex data analysis resulting from the fact that temperature oscillations are a complex combination of thermal and fluid dynamic phenomena acting simultaneously in the bed, and the need for calibration must also be carefully considered when selecting this technique.

1.3.3.4 Light probes

1.3.3.4.A Light probes

Light probes have the advantages of being extremely simple in construction, installation and versatile in application. For example, the light probe constructed by Dutta and Wen (1979) can be described as follows: a tiny light emitting diode (LED) acts as the light source with a sensing element (photo-cell) of about 1 mm in diameter and 8 mm in length. The LED and the photo-cell are separated from each other by a distance of about 3 mm and encased in a stainless pressure tubing having

an inside diameter of 2.4 mm. Slots of 3.5 mm length are cut through near the end of the stainless steel tube for face-to-face positioning of the LED and the photo-cell. The design of the probe allows, in theory, undisturbed movement of solid-fluid mixture through the LED-photo-cell assembly when the probe is positioned horizontally in the bed. The left-hand end of the stainless tube which holds the LED is thus connected to the remaining portion of the tube by two very thin uncut strips of the tube about 1 mm wide.

Light probes have been used to investigate the jet behaviour in gas fluidized beds, bubble behaviour in gas fluidized beds and particle volume-fractions. However, determination of particle hold-ups requires a complex probe calibration. Also, in order to accurately track the temporal variations in particle volume fraction, the recording system requires a very fast sampling rate (600 Hz).

1.3.3.4.B Optical fibre probes

An optical probe is based on the change of the refractive index of the probe surrounding medium. These probes consist of a fibre light-guide which conveys light to a specially-shaped terminal. If the probe is immersed in the gas phase of low refractive index, a significant fraction of the light beam is internally reflected and returned through the guide to a photodetector. If, however, the fibre optic sensor is

immersed in a liquid (emulsion) of high refractive index, the light is mostly transmitted through the medium and dissipated. The transition from one mode to the other mode of operation (state of fibre optic interface) produces a step-change in reflected light intensity which is used to detect the passage of a bubble boundary. The optical probe is thus affected by variations of probe-medium interfacial conditions enabling measurement of local void fraction or interface passage frequencies. This probe system theoretically gives an on-off signal corresponding to the phase change with sensor time-on-stream. Thus the only requirement is a sufficient difference between the indices of refraction of the emulsion and gaseous phases. By using more than one sensor, properly located, information may be extracted from the time-on-stream records on bubble velocity, bubble chord length, bubble chord length distribution and bubble velocity distribution. These measurements can be conducted even in non-electrically conducting fluids which give special possibilities of applications to these sensors.

These probes are also effective in gas-solid fluidized beds, although here the polarity of the signal is reversed. Light is reflected back up to the guide when its end is immersed in reflective particles but is dissipated when the terminal is in a particle-free volume fraction, as demonstrated by Huskey (1990).

A number of applications of the fibre optic sensor technique for the gas fluid dynamic study of bubble column systems were reported. However, the totality of these applications, with the exception of Chabot (1989) and Chabot et al. (1992), were referring to fluid dynamic studies performed in "cold-flow" ideal systems (mostly aqueous systems). Furthermore, despite the fact that a rather limited number of studies were devoted to the development and use of fibre optic sensors in bubble column systems, important divergences were reported in the characteristics and overall general performance of these sensors. For example, differences were reported concerning the type of light guides, detecting tips design, spacing and size, light sources characteristics, photodetector characteristics, probes implementation methodology, data acquisition procedure and signal analysis methodology. As a consequence, important divergences were reported concerning the general bubble detection performance of the fibre optic sensors proposed. For example, Wachi et al. (1987) reported average discrepancies of 30% between fibre optic sensors gas holdup measurements and manometrically measured gas holdups. Bruck (1984) reported very significant discrepancies (more than 50%) between gas holdup, bubble velocity and bubble size measured photographically, from electrical sensors, and from two different fibre optic sensors. These examples clearly illustrates the fact that extreme care must be taken in developing, designing, implementing and using the fibre optic sensor measuring technique, even in relatively simple "cold-

flow" aqueous systems.

As previously mentioned, Wachi et al. (1987) studied the effect of the liquid flow on the gas holdup of an air/water system using a fibre optic sensor. They measured the local gas holdup and compared the integrated average gas holdup values with manometrically measured average gas holdup values. They reported that the numerical integration of the local gas holdup measured with the fibre optic sensor gave, on average, 70% of the value observed manometrically. The authors claimed that the reason for the discrepancy was the existence of small bubbles which were not detected by the optical sensor. However, such discrepancy could be more realistically assigned to the fact that the fibre optic sensor used by Wachi et al. (1987) was inserted in such a way that the detecting tip of the sensor was parallel to the axis of the column, pointing downward. Then, the fibre optic sensor used by Wachi et al. (1987) was blind to descending gas bubbles, most likely to be encountered at higher gas superficial velocities (liquid circulation regime) in the peripheral region of the column. Since Wachi et al. (1987) actually worked under very high gas superficial velocities (0.21-0.87 m/s), the gas holdup radial profiles reported by Wachi et al. (1987) should be considered with extreme caution. This indeed suggests that probes insertion angles are most critical, especially in the liquid circulation regime.

Kago et al. (1989) used a similar fibre optic sensors' implementation technique than the one suggested by Wachi et al. (1987). However, the authors did not present an independent validation of the fibre optic sensors gas holdup measurements. Consequently, the local gas holdup measurements reported by Kago et al. (1989) should be considered with extreme caution. Kago et al. (1989) measured the chord length and velocity of individual bubbles. However, since no precise and valid assessment was provided concerning the exact proportion of the total bubble population actually seen by the sensors (most of the descending bubbles were presumably not detected by the optical sensors), it is not possible to determine if the measurements provided are representative of the bubble population.

Bruck (1984) studied the effect of the physical properties of suspended particles on the fluid dynamic of aqueous systems, using two different optical sensors, the AID sensor (developed by the Firme Assistance Industrielle Dauphinoise) and the FRA sensor (developed by the Fraunhofer Institute in Freiburg). They have reported significant deviations (up to 50%) between the gas holdup, bubble velocity and bubble size measured by two different optical sensors (FRA, AID) and photography or electric sensors. The AID sensor, in particular, comprising two detecting tips converging towards the measurement space from opposite locations, systematically underestimated gas holdup, bubble size and bubble velocity. This indeed suggests

important hindrance of the gas bubble flow, which reiterates the extreme importance of careful design and proper implementation methodology of the fibre optic sensors. Consequently, the results reported by Bruck (1984), particularly the ones obtained with the AID sensor, should be considered with extreme caution.

Lee (1986) and Lee and de Lasa (1987) developed a U-shaped fibre optic probe to perform hydrodynamic studies in a cylindrical three phase fluidized bed. A single core silica optical fibre of 400 μm diameter was bent in a U-shape. The radius selected for each U was approximately 0.5 mm at the tip of the probe. The fibre was placed in a stainless steel tube so that only the tip of the U was exposed to the fluidized bed. A helium-neon laser was used as the light source (wavelength of 632.8 nm). Lee and de Lasa also used an array of 5 optical fibres to investigate the shape of the gas bubbles. They also measured the radial and axial distribution of gas hold-up and bubble properties.

More recently, Yu and Kim (1988) studied the radial distribution of bubble characteristics in a three phase fluidized bed using a plastic U-shaped optical fibre of 250 μm diameter. Mann and Hackett (1985), developed a miniature, U-shaped fibre optic probe to gather gas hold-up, bubble intercept chord, frequency distributions and bubble separation frequency distributions in a two-phase gas-liquid system. The

fibre had a diameter of 40 μm and provided a sensing tip of about 100 μm diameter. The fibre was mounted in a 3mm diameter stainless steel tube. Ishida and Tanaka (1982) developed an optical probe to detect both bubbles and suspended particles in a three phase fluidized bed. The probe was made of a single quartz optical fibre (350 μm diameter) with two others connected. The single fibre has the dual functions of projecting light and receiving its reflection. The end of the fibre was cut to create a uniform plane. Tuominen (1987) developed a 100 μm optical fibre to study three-phase fluidized bed columns with various organic liquid mixtures. Several authors, including Glicksman et al. (1987), applied optical fibre sensors to study the hydrodynamics of two-phase gas-solid fluidized beds. The sensors were designed using the principles described above.

Optical fibres offer the prospect of application to non-aqueous systems which are extremely important to the chemical industry, based largely on hydrocarbons. Also, special silica optical fibres are well suited for high temperature operation (500-600°C). Glass fibres would not be however applicable to corrosive environments such as high pressure steam-water flows which readily dissolve the glass or in very high temperature systems (>700°C). In these cases, other fibre optic materials should be used (quartz for high temperature operation, plastic for corrosive environment), as reported by Chabot et al. (1992) and Chabot (1989).

Mudde et al. (1992) recently compared successfully the results obtained from optic sensors and a non-intrusive light transmission technique, thus reinforcing the validity of the optical sensors, when properly designed and implemented, as a reliable mean of measuring gas bubbles.

1.3.3.4.C Image-carrying fibre optic probes

The image-carrying fibre optic probes are different from conventional fibre optic probes in that the optical signal is not converted to an electrical signal for detection, but instead, the optical image is directly recorded on photographic film. Peters et al. (1983) have used an image-carrying probe to study the particle ejection velocity at the top surface of a gas-fluidized bed. The bed surface was illuminated by external lights and the input end of the probe was positioned at the center, just above the bed surface, where bubbles were ejected. The image of the erupting bubbles was transported to the output end of the probe and was recorded by a high-speed camera. However, such a probe cannot be employed to investigate the interior of a bed due to the necessity of external lighting. Saxena et al. (1987) used an image-carrying fibre optic probe to investigate solids distribution around an immersed surface in a gas-fluidized bed. They developed a mobile light source that is connected to the optical system by a flexible light guide. The light from the light source illuminates the surface to be

investigated after being reflected from a mirror. The images of the illuminated particles are focused by objective lenses and transmitted for viewing on a TV monitor. Chen and Fan (1992) recently proposed a particle image velocimetry technique to characterize the flow structure in gas-liquid-solid fluidized beds.

1.3.3.5 Tracer (detection probes)

The real velocity of the gas, liquid or solid phases can be determined from the mean time passage of a tracer between two points. The ratio of the superficial velocity to the real velocity of this phase is equal to its hold-up.

These tracer techniques make possible, in principle, the determination of local values of the hold-ups by moving the two measurement points closer together. However, various problems arise:

1 - The tracers must be easily detectable and must not change either the properties of the phase whose hold-up is to be measured or the interfacial properties. Usually saline tracers are used in the aqueous phase with measurements of the electrical conductivity (see electrical probes), or radioactive tracers;

2 - Devices which measure the concentration with a very short

response time are necessary.

Apart from the hold-ups, axial dispersion coefficient can be determined in this way, with adequate treatment of the signals.

Yang et al. (1986) studied the solids circulation pattern and the particle mixing in a large jetting fluidized bed. They used a pulse injection of tracer particles with characteristics similar to those inside the bed but with sizes larger than those in the bed. By taking solids samples continuously at different locations and analyzing by sieving the concentration of the tracer particles in the samples, the rate of particle mixing and circulation can be calculated. Also radioactive tracers provide a direct measurement of particle velocity, but require a nuclear radiation source, which limits the technique to research applications. Radioactive tracers have been used to monitor the particle flow in fluidized beds.

Dry et al. (1984) studied the bubble velocities in fluidized beds of fine, dense powder. They injected a small amount of methane into the bed immediately above the distributor, and a continuous analysis was performed higher up in the bed. The sampling probe was connected to a flame ionization detector (FID) via a short sample line. The bubble velocity was obtained from the time elapsed between the tracer injection

and its detection at the other probe, since gas usually flows faster with the bubbles than through the emulsion. However, this method does not distinguish between single bubbles and groups of bubbles undergoing coalescence and/or splitting. Also, the experiment should be repeated several times to ensure that in at least one case, the tracer is injected just as a bubble passes by.

More recently, Guo (1987) used hydrogen as a tracer to determine the residence time distribution and values of dispersion efficiency of gas in a fine-powder fluidized bed.

Lubbert et al. (1987) developed a new tracer method to measure the local velocities of the continuous liquid phase in gas-liquid multiphase reactors. They introduced heat pulses, instead of material tracer. The input of heat pulses and measurement of temperature at an adjacent point is performed by small probes. As an intermediate result, the flow time distribution of the heat-labelled fluid elements is calculated on-line as a cross-correlation function between the pseudo-random input and the measured output signals. This method has the advantage of low costs, while allowing measurements at high gas flows. However, this method has some important restrictions because the measured output signals (temperatures) are the result of a number of heat and hydrodynamic phenomena of no simple interpretation.

1.3.3.6 Interaction probe-bubble

Invasive techniques deal with in-bed probes. These techniques present the advantage of allowing local measurements of the bed properties. However, probes can interfere with bubbles so that the quantities measured might be different from those that would exist in a probe-free bed. Even if several invasive techniques have been successfully implemented in fluidized beds, only a few researchers studied the interaction between probes and bubbles and/or developed special efforts regarding probe miniaturization. The design of the probes (size and shape) as well as the orientation of the probes in the fluidized beds are important parameters to optimize in order to minimize the perturbation of the bubble flow and to increase the quality of the probes detection. However, guidelines are still missing, and only a few studies discuss these important topics.

Rowe and Masson (1981) analyzed the interaction of bubbles with several probes in a gas fluidized bed using X-ray cine photography. They concluded that probes, and particularly their supporting stems, are liable to alter the position, shape and velocity of a detected bubble. They advised that the stem should be as slender as is compatible with rigidity. They also mentioned that with the knowledge of the disturbance caused by a probe it may be possible to partially correct the interpretation of the signal generated. Chabot et al. (1992)

96

investigated the interaction between gas bubbles and fibre optic sensors in a bubble column. They concluded that the sensors performed extremely well in presence of bubbles having a diameter larger than 5 mm. The detection was observed to be satisfactory in presence of smaller bubbles, 0.5 to 2 mm in oil and 3 to 4 mm in water.

1.4 CONCLUSION

In the present chapter, significant challenges and difficulties related to the design and scale-up of bubble and slurry bubble column reactors were highlighted. Most particularly, relevant matters concerning the importance of a better understanding of the fluid dynamics of these reactors were stressed. However, as reviewed in Section 1.3, the availability of proper measuring techniques still represents a major drawback in fully understanding the complex fluid dynamics of bubble and slurry bubble columns, notably under the severe operating conditions encountered frequently in the chemical and petrochemical industries.

The objective of the Ph.D. dissertation was to further advance the understanding of the fluid dynamics of bubble and slurry bubble columns, particularly under conditions of interest for the liquid phase methanol synthesis or other systems involving hydrocarbon media. In order to allow precise and reliable measurements of the gas phase characteristics, fibre optic

sensors were developed, tested and extensively used. In the following Chapters, details of the experimental procedure, the sensors description and significant results concerning the fluid dynamics of bubble and slurry bubble columns are reported.

CHAPTER 2

EXPERIMENTAL SYSTEM AND PROCEDURE

As thoroughly reviewed in Chapter 1, the clear understanding of the fluid dynamic behaviour of bubble and slurry bubble column reactors still suffers from a lack of reliable and precise hydrodynamic observations. This is particularly true for systems of industrial interest for which only scarce and incomplete information is currently available. In this context, the objectives of the present study were to obtain, as already mentioned in detail in Section 1.1, reliable and precise gas phase hydrodynamics information related to the three-phase methanol synthesis system. Consequently, the experimental procedure and equipment were designed and constructed in such a way to ensure precision and generalization of the data collected, based on criteria (column dimension, gas distributor, fluids selection ...) reported and discussed in Section 1.2.

The experiments reported were carried out in a 0.2 m diameter and 2.4 m height carbon steel column. The column was operated in the batch mode with respect to the liquid or the slurry suspension. In order to mimic the hydrodynamic conditions encountered in the three-phase slurry methanol synthesis reactor, the fluids used (gas, liquid and solid) were chosen carefully. First of all, in the three-phase methanol synthesis process, an inert liquid phase is added to the

synthesis gas/catalyst mixture to provide better temperature control and thus higher conversion per pass while permitting recovery of the heat of reaction (Sherwin and Frank, 1976). In the present study, the liquid phase chosen was not a simulated liquid phase with similar matching physical properties but the exact liquid paraffinic oil (LP-100, manufactured by Witco Co.) used in the actual methanol synthesis process (Frey et al, 1988; Fox, 1990). This approach is particularly critical since Bukur et al. (1987) have shown that, despite similar physical properties, different hydrocarbon fluids have dissimilar hydrodynamic behaviour. The complete characteristics and physical properties of the paraffinic oil LP-100 are presented in Appendix 1. The influence of the temperature on the density, viscosity and surface tension, presented respectively in Figures A1.1, A1.2 and A1.3, was provided by the manufacturer (Witco Corporation). The extrapolation of the influence of the temperature on density, viscosity and surface tension to higher temperatures (100-175°C) was performed using measurements performed by Air Products and Chemicals Inc., as shown in Table A1.1a.

For the slurry experiments, a non-activated zinc-copper oxide catalyst (volume-based arithmetic average particle diameter: d_{avg}=13.85 μm) (Air Products and Chemicals) Inc. was suspended in the paraffinic oil at a concentration of 10%$_{wt}$. The particle size distribution as well as density and pore volume

values are reported in Appendix 1.

Nitrogen was selected, as the gas phase, for safety reasons. Liquid nitrogen cylinders (Canox) were used as the nitrogen source. The gaseous nitrogen was produced by evaporation of the liquid nitrogen. Thus, particularly at high gas flowrate, relatively cold gaseous nitrogen emanated from the liquid nitrogen cylinder, due to the important heat of evaporation and the very limited heat transfer between the room and the cylinder. Thus, a relatively long tubing length (≈ 6 m) was installed between the nitrogen cylinder and the gas flowmeter to allow the gas temperature to approach ambient temperature condition prior to the gas flowrate measurement. A thermocouple was inserted prior to the gas flowmeter to allow for any temperature correction, if necessary. The nitrogen flowrate was measured using a Brooks flowmeter, model 1307DO8F1A1A equipped with two needle valves (Whitey 1RM4). A second similar flowmeter was also available at the exit of the bubble column. This second flowmeter was used periodically to validate the first flowmeter measurements and to ensure that the complete system was free of leaks. Both flowmeters were calibrated using a wet test meter (GCA Precision Scientific), as reported in Appendix 2. The gas was preheated to the temperature of the bed (± 5°C) using five flexible electric heating tapes (Sybron Thermolyne BWH051-020, 156 Watts) surrounding the copper gas line. The heating tapes were controlled using a variable autotransformer (Staco Energy

Products Co., 3PN1010). The gas was then introduced into the column, and most of the experiments were performed using a steel perforated plate gas distributor consisting of 40 holes, 1.59 mm in diameter, arranged in a triangular pitch of 2.8 cm. For the slurry experiments, a substantial gas flowrate was continuously maintained after the introduction of the solid particles to prevent plugging of the gas distributor holes by the settling of the small solid particles. A few experiments (as discussed in Section 5.1.1) were conducted (bubble column condition) using a steel porous plate (20 μm) in order to assess the influence of the gas distributor. At the exit of the reactor, the gas was cooled down using a packed bed water (steel beads, 1/4") condenser. Then, the gas was sent to the fume hood to prevent escape of the non-condensable oil vapour into the laboratory environment.

Four band heaters (Molders Supply, 500 Watts/heater, width: 6", i.d.: 8.625") were positioned around the external diameter of the column and carefully distributed along the length of the column. The heaters were regulated using a temperature controller (Omega CN5001K2) connected to a thermocouple (Omega TJ36 CASS 166G-8) located in the center (axial position) of the bed at approximately 2.5 cm from the wall of the column (radial position). Several thermocouples were also implemented to monitor the temperature at various strategic points in the column, including the gas entry and exit lines. All the thermocouples were tested and calibrated prior to

being implemented in the system, using both an ice/water mixture (0°C) and boiling water (100°C). Ceramic fibre (Fiberfrax Durablanket S) was used to insulate the column and the adjacent high temperature gas lines. A detailed schematic of the column and the overall set-up characteristics are presented in Figures 2.1 and 2.2 respectively.

The column was operated under atmospheric pressure, in the batch mode with respect to the liquid phase or the slurry suspension (no liquid or slurry circulation). The static liquid height or the static slurry suspension height was kept constant throughout the experiments at 96 cm (H/D ≈ 5) above the gas distributor. Three operating temperatures were investigated: 25°C, 100°C and 175°C. For a given series of experiments, the band heaters were turned on and the column was allowed to reach the proper operating temperature. During the heating process (≈ 3 hours), a gas flowrate was continuously maintained to ensure proper heat transfer from the wall of the column to the center of the bed and minimize overheating of the hydrocarbon liquid along the wall. The gas flowrate selected for this purpose was identical to the one to be investigated during this particular phase of experiments, so that the heating period also served as a hydrodynamic stabilization period (minimum of ≈ 3 hours). During this period, the heating tapes were also activated so that the gas entered the column at approximately the same temperature as the bed (± 5°C), thus minimizing heat transfer effects and

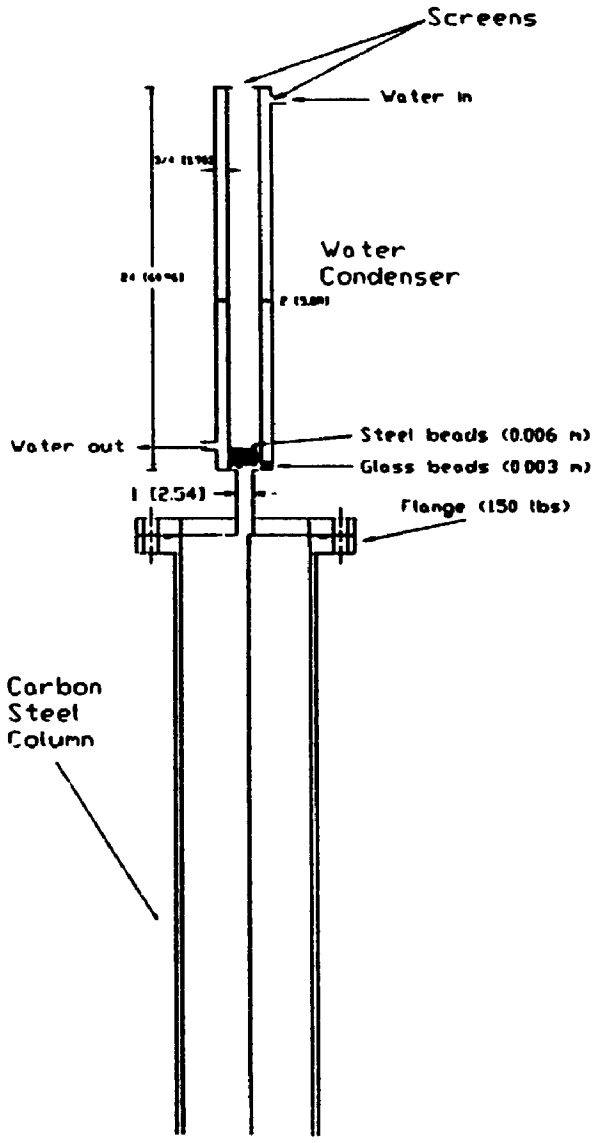
Screens
Water in
Water
Condenser
Water out
Steel beads (0.006 m)
Glass beads (0.003 m)
1 (2.54)
Flange (150 lbs)
Carbon
Steel
Column

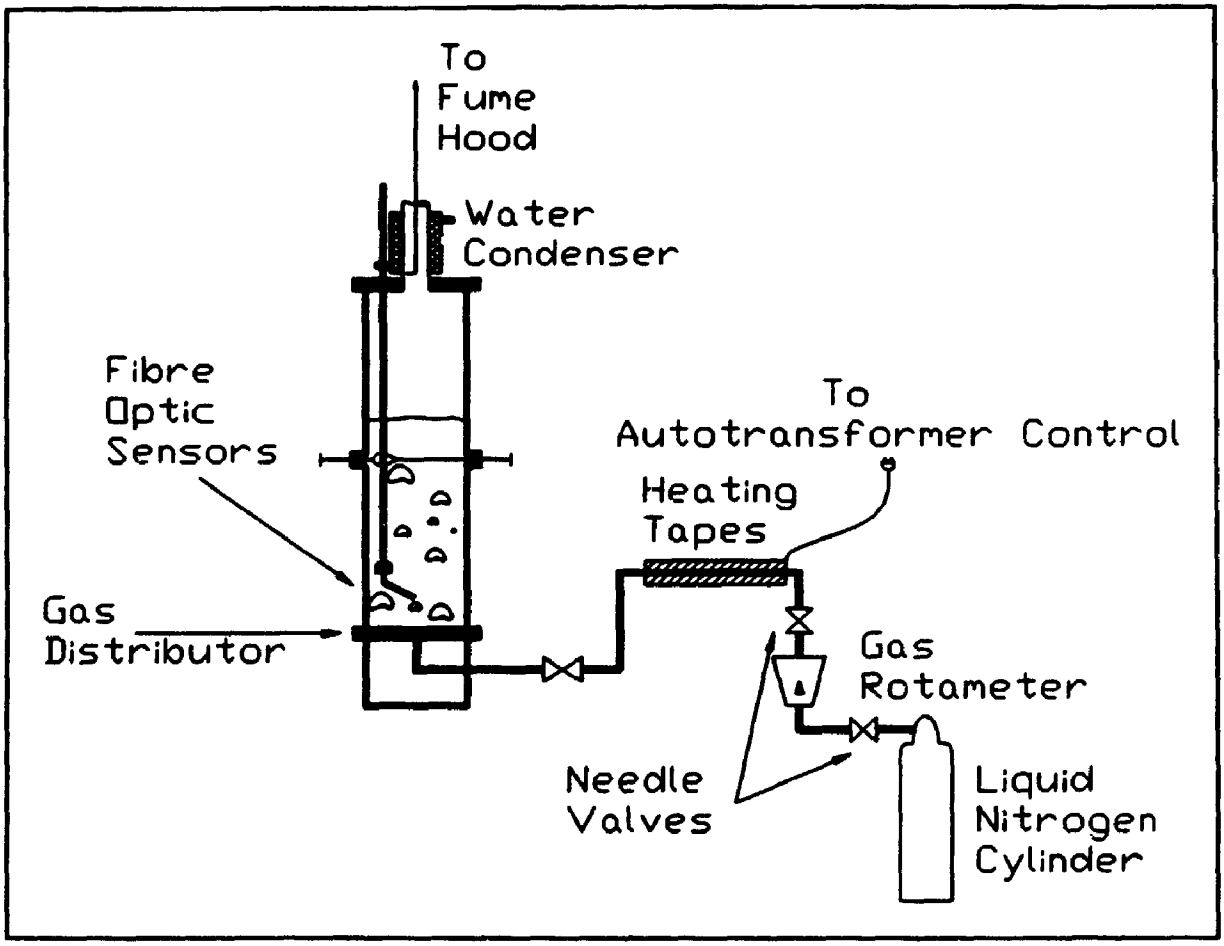

Figure 2.2: Process Flowsheet

possible variations in the gas volumetric flowrate. Four different gas superficial velocities were investigated: 2.2, 4.1, 9.0 and 14.7 cm/s. Special care was taken to adjust the gas flowrate for any oil vapour pressure effects. As shown in Appendix 1, the liquid phase vapour pressure was negligible below 100°C. However, for the experiments conducted at 175°C, adjustment of the gas flowrate was required. For this particular condition, it was assumed that the gas had reached saturation prior to being injected into the column, the column windbox (downstream of the gas distributor) acting as a saturation chamber. During the heating process and the actual operation period, the water packed bed condenser was put into operation to avoid any excessive paraffinic oil loss and minimize the hydrocarbon emission to the fume hood. During the actual operation period of the column, the gas flowrate and the temperature of the system were closely monitored to ensure maximum precision of the data collected. After completion of a series of experiments, the heaters (band heaters and heating tapes) were turned off. However, the gas flowrate and the cooling water flowrate (condenser) were maintained until ambient temperature was reached to ensure fast and safe cooling of the system.

Thus, as discussed in this section, a set-up and a fluid system, closely matching the characteristics of the liquid phase methanol synthesis process, were adopted for the experiments. Moreover, appropriate selected techniques were

106

used for various calibrations of auxiliary equipment to secure reliable results.

CHAPTER 3

INSTRUMENTAL MEASURING TECHNIQUES

3.1 FIBRE OPTIC SENSORS

3.1.1 Introduction

As thoroughly discussed in Section 1.1, the objectives of the present study were to obtain detailed local gas hydrodynamic information pertinent to the liquid methanol synthesis process. In order to fulfil this task, a reliable gas bubble measuring technique was needed. Based on the promising results obtained in a previous study (Chabot, 1989), the fibre optic sensor technique was selected. This technique was proven (Chabot, 1989; Chabot et al., 1992) to be fully compatible with the liquid phase methanol synthesis environment (high temperature, hydrocarbon liquid, presence of catalyst particles) while providing reliable local gas phase observations (gas holdup, bubble velocity, bubble chord length, bubble chord length distribution, bubble velocity distribution), when properly designed and implemented, as discussed in Chapter 1. In the following sections, a complete description of the sensors, including principle of operation, manufacturing process, implementation, testing and operation will be provided.

108

3.1.2 Description and principle of operation

The design of the fibre optic sensor was based on the difference in refractive indices between the gas phase and the liquid phase. According to Snell's law, the angle of total reflection is larger in the liquid than in the gas phase. If this principle is applied to a fibre optic having a U-shape, the fibre has to be bent as follows: the radius of curvature of the U has to be large enough so that the angle of incidence of the light at the turning point is greater than the angle of total reflection when the same fibre is exposed to a gas phase. If this condition is met, the source light is conserved in the fibre at the turning point and light can be detected at the extremity of the detecting fibre. However, the radius of curvature of the U-shape fibre has to be, at the same time, curved in such a way that the radius is small enough to secure an angle of incidence at the turning point smaller than the angle of total reflection for the same fibre exposed to the liquid phase. Therefore, a significant fraction of the source light is lost at the turning point and only small light intensity is perceivable at the extremity of the detecting fibre. Then, substantial differences in the intensity of the light detected at the extremity of the detecting fibre can be perceived depending on the phase present (gas or liquid) at the turning point of the fibre (detecting tip). Consequently, if such fibre is properly inserted at a given position in a bubble column or a slurry

bubble column, local real-time discrimination between the gas phase (gas bubbles) and the liquid phase is possible. Thus, individual gas bubbles, as they contact the detecting tip of the fibre optic sensor can be detected and analyzed. Furthermore, considering the speed of light (3.0×10^8 m/s) and the moderate length of the detecting fibre (in the present case approximately 20 m), the presence of a gas bubble at the detecting tip of the fibre optic sensor is thus perceived instantaneously, without significant delay, at the extremity of the detecting fibre optic. Furthermore, since direct contact between the gas bubbles and the small detecting tip (< 1 mm) of the sensor is required for bubble detection, the measurements are essentially considered local measurements in comparison to measurements effected in a given control volume (e.g. reflection optical sensors). Thus, no imprecision is incorporated due to an erroneous evaluation of the control or measurement volume.

As shown in Figure 3.1, the main components of the photometric measuring system included a single light source, two photodetectors, two fibre optic sensors (to be described in detail in the following section) and the related data acquisition system. A Spectra Physics helium-neon laser (35 mW), model no. 124B-255, provided a very stable source of visible red light (wavelength = 632.8 nm). Two EG&G photodetectors, model no: 460-1A, were used to measure the intensity of light returned by the detecting fibre optic.

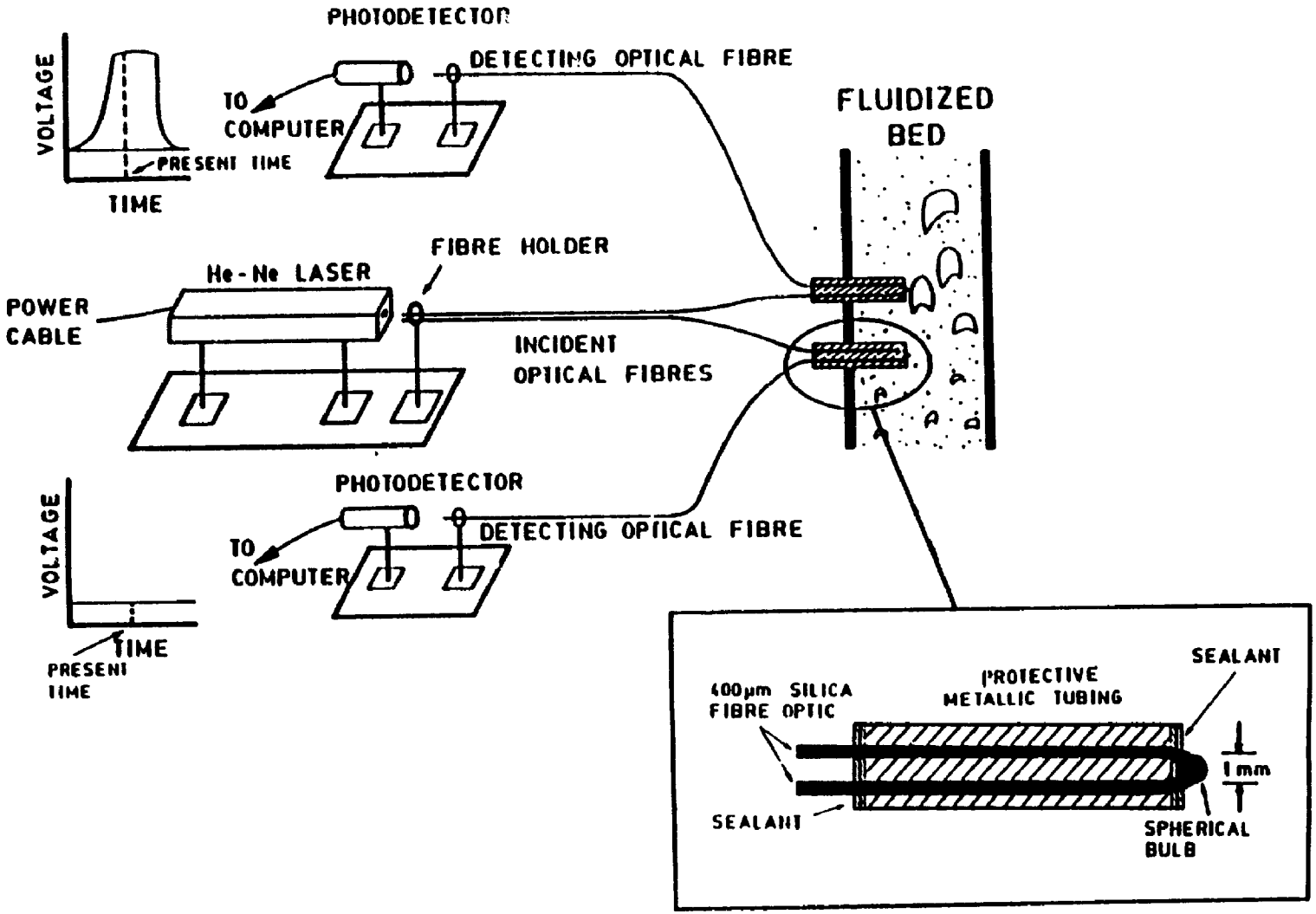

Figure 3.1: Fibre optic sensor: principle of operation

These photodetectors provided a selective and highly sensitive light detection performance at precisely 632.8 nm, so that any parasite light (mostly visible) present in the optical chamber would be poorly perceived by the photodetectors. Furthermore, the photodetectors were characterized by an extremely fast response time, in the order of a few picoseconds, thus taking full advantage of the inherent rapid response time of the fibre optic sensors.

In order to provide optimum alignment between the laser source light and the incident fibre optics, and the photodetectors and the detecting fibre optics, all the photometric components were installed on an optical bench. This optical bench was then covered by a wood box to protect the optical components against parasite light, dust and potential spills from the adjacent column. The laser tube was mounted on two alignment supports which were attached to the optical bench. The incident fibre optics (two) were precisely held by a single specially designed mechanical holder. This holder provided three dimensional adjustment so that the laser beam could be properly focused on the extremity of the incident fibres, to forward maximum light intensity to the detecting tips. This adjustment was critical so that optimum source light intensity could be directed toward the fibre optic sensors' detecting tips, for optimum gas bubble detection sensitivity. The light directed into the incident fibres was guided up to the fibre optic sensors detection tips and the conserved light was

returned to the extremity of the detecting fibres (two) which were held by two individual mechanical holders. Each detecting fibre was carefully aligned to its respective photodetector, which translated the light intensity received to an analog signal. No calibration of the photodetectors was required since only light intensity differences were analyzed. The analog signals were then processed via the data acquisition system, which will be described in detail in Section 3.1.6.

3.1.3 Miniaturized fibre optic sensor design and manufacturing process

As discussed in the previous Section, the fibre optic sensors consisted of an incident fibre optic connected to a detecting fibre optic via a sharp U-shape turning point. One way to manufacture such sensor is to use a single strand of fibre optic which is then slowly bent under a high temperature torch to a perfect U-shape. This process is not only extremely delicate but generates, for a given fibre optic diameter, a relatively large U-shape detection tip, which is highly undesirable to detect smaller bubbles. In the present study, a different manufacturing process was suggested for sensor miniaturization, based on previous results (Chabot, 1989; Chabot et al., 1992). The two miniaturized fibre optic sensors used in the present study were manufactured using two fibre optic strands that were joined at one extremity by

fusion, as shown in Figure 3.2. A 400 μm silica core fibre optic (manufactured by Tasso inc.), surrounded by a silica cladding and an ETFE (copolymers of ethylene and tetrafluoroethylene) protective coating was selected for the present study. This fibre optic, essentially made of silica (core and cladding) provided excellent temperature resistance and chemical resistance to the methanol synthesis environment. Furthermore, it was found (Chabot, 1989) that a 400 μm core diameter fibre optic provided an optimum compromise between minimum flow disturbance (miniaturization of the detection tip) and optimum transmission of light to the detecting tip. Actually, it was observed (Chabot, 1989) that a smaller fibre optic core diameter limited the quantity of light transmitted to the detecting tip and presented substantially detrimental effects on the bubble detection sensitivity. Typically, ETFE polymers soften between 200°C and 300°C. Samples of the fibre optics were exposed to a high temperature oven and the coating was found to withstand excellent dimensional stability below 200°C. However, the coating was observed to soften and shrink at approximately 200°C, while complete melting of the coating was observed at 256°C. Consequently, such fibre would not be recommended above 200°C, since modification of the coating structure would induce detrimental stresses to the fragile glass core, while reducing the protective capability of the coating. However, for applications of the fibre optic sensor under such conditions (> 200°C), silica fibre optics equipped with high temperature coating (polyimide, aluminum, gold) are

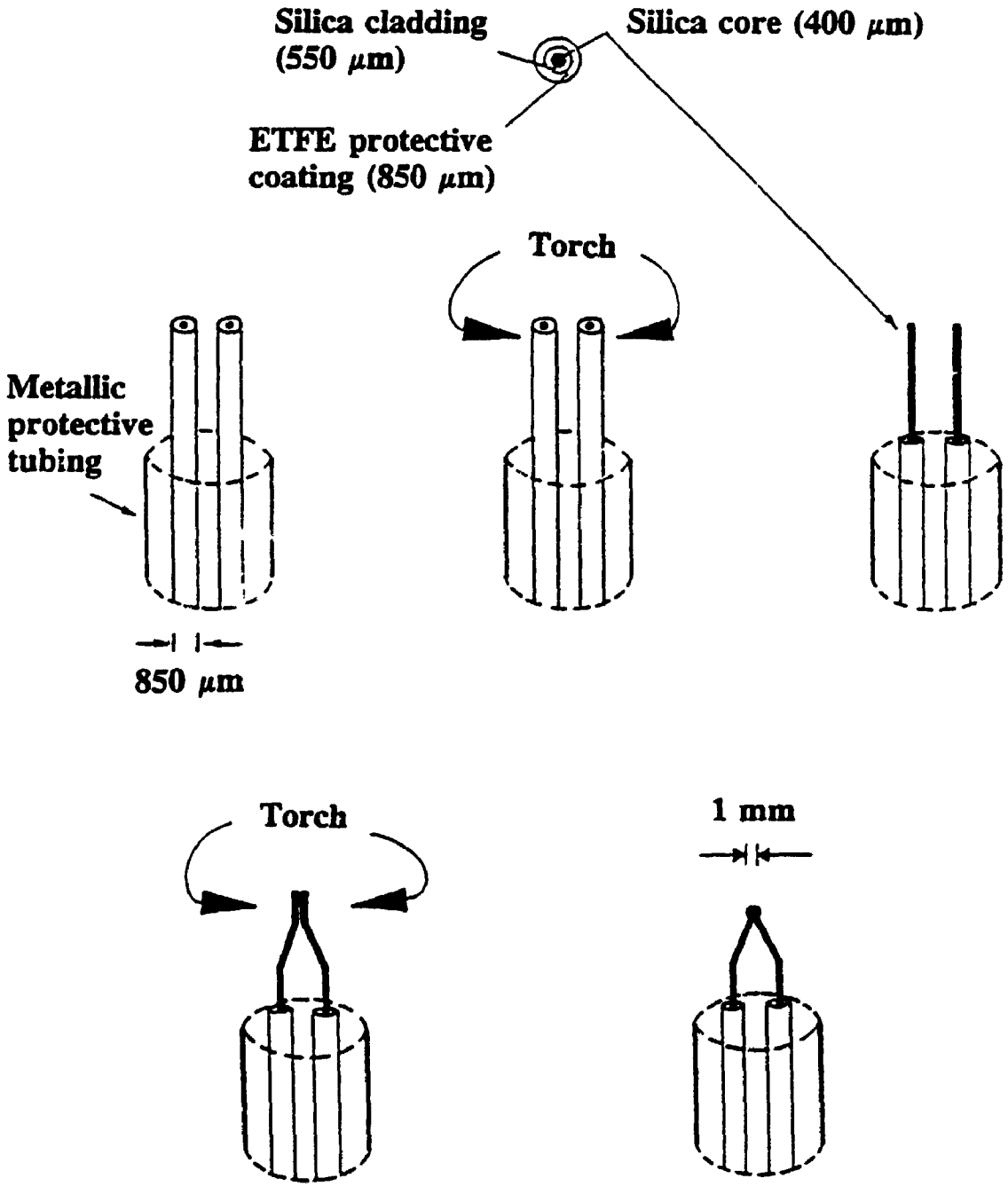

Figure 3.2: Fibre optic sensor: manufacturing process

currently available (Fibre Guide Industries, Stirling, NJ).

To manufacture the miniaturized fibre optic sensors, as shown in Figure 3.2, the protective polymer coating was first removed at one extremity of each fibre strand using a high temperature acetylene/oxygen torch. The two fibres' extremities, now free of coating, were held together in a parallel position. The same torch was slowly brought near the point of contact between the two fibres for a few seconds. Extreme care was taken at this stage to avoid damage or distortion of the small glass rods. A small spherical bulb (≈ 1 mm in diameter) was then created, joining the two fibres together. This spherical tip, called the detecting tip of the optical sensor, was relatively optically equivalent to the U-shape curvature issued from the single strand fibre manufacture, but substantially smaller and thus less perturbing to the bubble flow. Careful visual inspection of the detection tips was performed under microscope (Wild type 355110, 40x) to detect any failure or imperfections in the glass tip. Following a successful inspection, the fibre optic sensors were then inserted into individual stainless steel tubing (HTX-13). Only the spherical detection tip of the probe was left out of the tube, as shown in Figure 3.1, to ensure sufficient mechanical protection of the sensors. In order to adequately protect the tip of the sensor and properly seal the tubing, a high temperature cement (Omega, CC high temperature) rated for temperatures up to 1000°C, was used.

The sealant was placed in a conical way in proximity of the detecting tip of the sensor to minimize the size of the detecting tip. The optical sensor was left immobile for a minimum of 24 hours to allow the sealant to dry. Prior to being used, the two optical sensors were tested at ambient temperature in presence of the LP-100 oil to ensure proper and reliable response of the sensor. The time series processing software (described in Chapter 4) was fine tuned at this stage to incorporate any particularity of the two manufactured sensors.

3.1.4 Implementation of the sensors

In order to optimize the use of the two optical sensors manufactured, a proper implementation method was needed. As discussed in Chapter 1, the insertion angle of the optical sensors' detecting tips can have tremendous importance on the general performance of the sensors. Since the present study was conducted in the liquid circulation regime, as discussed in Chapter 5, the sensors were inserted at a 45° pointing downward to ensure optimum and equal visibility of both, ascending and descending bubbles. This angle was preferred over the vertical downward insertion angle, which does not provide proper detection of descending bubbles. This can severely impair the detection performance of the sensor, since under the liquid circulation regime, an important fraction of the gas bubbles are indeed recirculated downward with the

liquid in the peripheral area of the column, as discussed in Chapter 1. Furthermore, as the gas superficial velocity is increased, turbulent eddies are induced, which, as well, promote gas bubble movements in multiple directions. Furthermore, the 45° downward angle provided minimum flow disturbance, as compared to horizontal insertion. Furthermore, the two fibre optic sensors' tips were located along each other to minimize bubble flow disturbance. Bruck (1984) reported very severe hindrance of the bubble flow in implementing the two fibre optic sensors' tips in a converging manner from opposite locations.

Because of the significant and particular difficulties inherent to the system investigated (high temperature, hydrocarbon medium, presence of very small solid particles), the sensors had to be implemented using a minimum of windows for safety reasons. This consideration actually is valid for most systems of industrial interest for which the viability of a measuring technique, even remarkably reliable, is limited by its safe and convenient implementation in actual conditions. The implementation method should as well provide, using a minimum of sensors and windows, a maximum of flexibility in terms of radial and axial displacements of the sensors. The following implementation method was designed. The two optical sensors, mounted on individual HTX-13 tubing, were attached to a single 1/4" tubing, which was soldered to a solid metallic bloc, as shown in Figure 3.3. The two optical sensors were

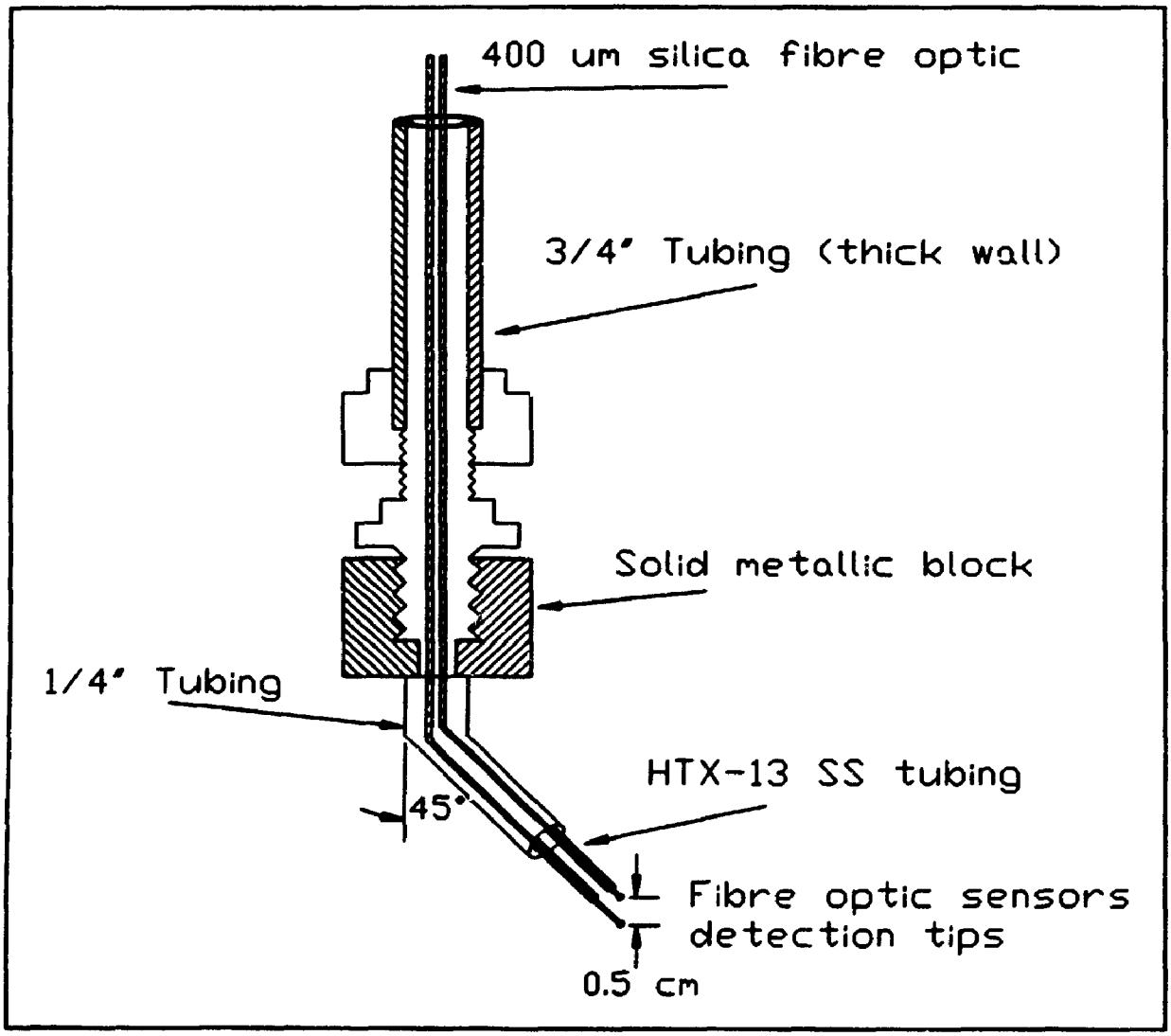

Figure 3.3: Fibre optic sensors implementation system

mounted to the 1/4" tubing in such a way that their respective detecting tips were separated by a vertical distance of 0.5 cm (discussed in more detail in Chapter 4), and were pointing downward with a 45° angle with respect to the vertical position. As previously discussed, the 45° angle was previously found (Chabot, 1989) to provide maximum gas bubble detection sensitivity in comparison to fully horizontal or vertical insertion. The solid metallic block could then be attached to a specially designed insertion system. This system consisted of a 2.75 m long, 0.0191 m diameter stainless steel tube. This tube was inserted into the column through the top flange of the column, in a median point between the center of the column and the wall of the column (please refer to Figure 2.2). The system was designed in such a way that when performing a 180° rotation of the long vertical tube, the detecting tips of the two sensors were displaced from the vicinity of the center to the vicinity of the column wall, as shown in Figure 3.4. The detecting tips of the sensors could also be displaced axially by moving the insertion tube up or down. The long vertical tube then served the purpose of both controlling the axial and radial positions of the detecting tips of the sensors, while serving as a protection chamber for the incident and detecting fibres. Consequently, the four fibre optics (two incident fibres, two detecting fibres) were perfectly isolated from the column environment and were fully protected during displacement of the insertion system. Because of limited clearance between the top of the column and

120

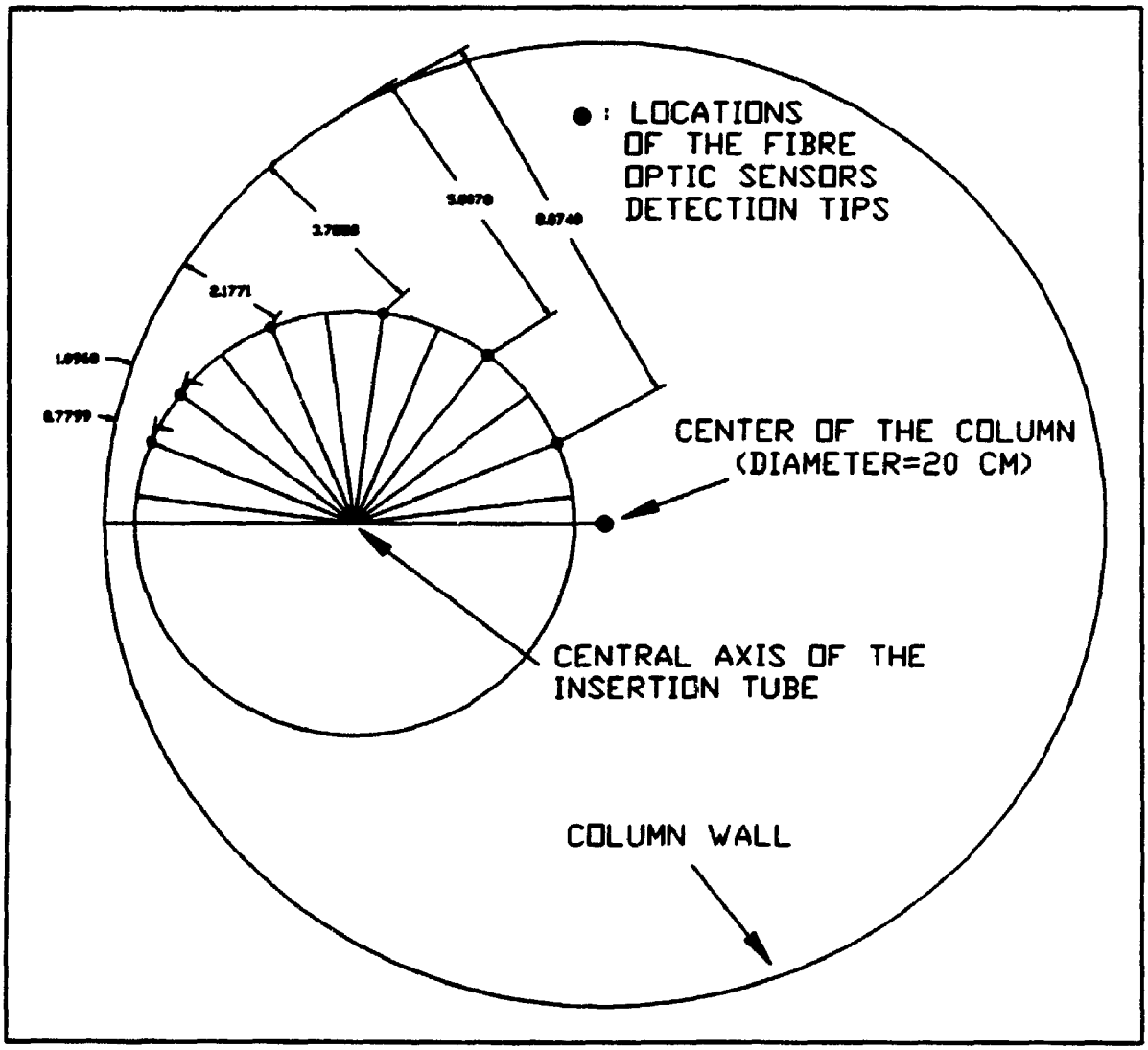

Figure 3.4: Fibre optic sensors radial positions

the laboratory ceiling, the long insertion tube was split in 4 sections of approximately 0.7 m. Each section could be solidly screwed to each other using fine and very tight threads. This was particularly important to avoid percolation of oil or fine particles inside the insertion tube, interfering with the operation of the device. When the tips of the optical sensors were positioned in the bottom of the column (gas distribution zone), the four tube sections were inserted into the column. As the tips of the sensors were moved upward, the top section of the insertion tube was gradually pulled outside the column and detached as the top of the second section was pulled outside. The top section was then unscrewed from the insertion tube and hold in a horizontal position using a specially designed support device located just below the laboratory ceiling. As needed, other sections of the long insertion tube were detached to investigate higher axial positions. The special support device allowed the unused tube sections to be held in a safe and stable manner so that the fibre optics could remain inside the unused sections without any risk of being damaged. This special procedure allowed investigation of the full axial span of the bed without any need to disconnect the fibre optics (incident and detecting) from the photometric system, thus avoiding dangerous fibre optics manipulation and time consuming optical adjustments. In order to secure the radial and axial positioning of the fibre optic sensors, special support systems were implemented. First of all, at the top of

the column, a two level attachment system was implemented to ensure perfect vertical alignment of the insertion tube and to secure appendage of the optical sensors. This was particularly important given the substantial weight of the optical sensors insertion device and the serious problems to be faced in case of accidental detachment of the insertion tube. Then, the insertion tube was first anchored to the column using a standard 3/4" Swagelok fitting screwed directly (pipe thread) into the top flange of the column. This fitting, equipped with teflon ferrules, allowed precise radial and axial positioning of the tubes while tightened, and easy rotation and axial displacement of the tube while untightened. A second anchorage station was located 16 cm above the top flange. This device consisted of a solid metallic block screwed solidly into the top flange. The block was provided with a circular opening of a diameter identical to the exterior diameter of the insertion tube. Then, the insertion tube was enclosed into the circular opening of the block prior to being inserted into the column via the top flange of the column (Swagelok fitting). The block was then carefully positioned to ensure perfect vertical alignment of the insertion tube. This device was as well equipped with a lock system to hold the insertion tube in position (second level safety lock) and of a precise graduated compass used to adjust the radial position of the optical sensors' tips. The axial position of the optical sensors detecting tips was adjusted using marks drawn directly on the insertion tube during a

calibration experiment. Furthermore, because of the substantial length of the insertion tube, a stabilizer was implemented, 1.2 m below the insertion point of the support tube to prevent any excessive vibrations of the detecting tips of the two sensors (please refer to Figure 2.2), and provide maximum radial position precision. The stabilizer consisted of two V-shape rods introduced from opposite sides of the middle flange. One of the rods was locked in position at exactly the median point of the column. The other rod could then be horizontally displaced to squeeze the insertion tube solidly during experiments or be taken away to allow free displacement of the insertion tube between experiments. Furthermore, a special guard was implemented to protect the tips of the optical sensors while positioned in proximity of the wall. This guard, slightly longer than the fibre optic sensors prevented the tips of the sensors from being knocked to the wall in case of excessive vibrations of the insertion device. As shown in Figure 3.4, several radial positions were investigated (6), and the precision of the radial and axial detecting tips locations was experimentally determined to be approximately ± 1 mm.

3.1.5 Data acquisition system

The data acquisition system was used to digitize the optical sensors' analog signals generated by the photodetectors. The core of this system consisted of a Hewlett Packard (HP-1000

124

model A600+) computer equipped with a ram memory of three mega bytes and a fifteen mega bytes fixed disk. The computer was equipped with a high speed (55 Khz) analog to digital converter. The digitized data were first collected and stored on a 3M data cartridge (65 mega bytes) to be later retrieved for further analysis. Prior to being sent to the computer, the analog signals generated by each photodetector were preconditioned (amplified and pulsed at the desired frequency) to avoid impedance matching problems. The frequency generator and amplifier was designed and built in the University of Western Ontario Electronic Shop.

For every series of experiments, the laser tube was first warmed up for at least one hour to ensure stable light emission. The incident and detecting tips of the optical sensors were carefully aligned with the laser beam and the photodetectors respectively. External resistors for the photodetectors were selected to provide maximum sensitivity of the optic sensors. The tips of the optical sensors were then located at the desired axial and radial positions and the operating conditions of the column properly adjusted (Chapter 2). The data acquisition system was then activated. In order to take full advantage of the optical sensors' capabilities, the data acquisition criteria (data acquisition frequency and total time of data acquisition) were carefully selected. The frequency of data acquisition was carefully adjusted to the frequency of the phenomenon studied, given this frequency is

within the frequency of the apparatus involved. From preliminary experimental testing and previous experience (Chabot, 1989) it was found that the shortest bubble-probe contact time was approximately 2 ms. Consequently, a data acquisition frequency of 1000 data points per second (1 khz) allows one to follow the shortest phenomena encountered. Furthermore, in order to secure the hydrodynamic parameters extracted from the optical sensors' time series, the total time period of data acquisition was based on stationary criteria. Qualitatively, a stationary time series is one that has reached some form of statistical equilibrium (Bendat and Piersol, 1986). Under such condition, the statistical properties of the time series are independent of absolute time, and the results derived from such series of data are highly reproducible. In the present case, a data acquisition period of 50 seconds was found to provide satisfactorily qualifications for stationarity. This was actually confirmed by analyzing the reproducibility of the hydrodynamic parameters derived from the fibre optic sensors time series, as discussed in Chapter 5. It has to be mentioned that the benefits provided by using a longer data acquisition time period are seriously counterbalanced by the substantial size of the data files collected under such conditions and the related problems in terms of data storage and processing. Consequently, for every experiment (data files) collected, 100,000 data points (2 sensors x 1000 data/s x 50 s) were registered. A copy of the computer software used in

collecting the fibre optic sensors measurements (getad, ad2) are presented in Appendix 3.

3.2 STATIC PRESSURE PROFILE

3.2.1 Introduction

In order to validate the fibre optic sensors' gas holdup measurements, static pressure profiles were measured along the column. Theoretical considerations regarding the implementation of this technique and the derivation of the gas holdup values from pressure measurements are discussed in Chapter 5. Due to the risk that small catalyst particles contaminate the pressure lines and damage the fragile switching wafer or pressure transducer diaphragm, the pressure profiles were only collected under bubble column conditions (two phases; gas-liquid).

3.2.2 Description of the experimental system

Seven pressure taps, located along the rear side of the column were used to measure the static pressure profile. The pressure taps' location was precisely indicated in Figure 2.1. An eighth pressure tap was implemented along the gas entry line to measure the pressure drop across the gas distributor. Details of the grid pressure drop measurements are discussed in Appendix 5. The pressure measuring system consisted of

127

four main components, one pressure transducer, a switch wafer valve with power supply and controller, seven pressure lines and the data acquisition system. A pressure transducer (Data Instrument Inc., model AB) was used to measure the absolute pressure at different levels in the column. However, given the cost of pressure transducers, and the substantial number of pressure measurements required, it was proven more economical to use a switching device so that every pressure tap could be connected in sequence with the unique pressure transducer. This arrangement has the disadvantage that the individual pressure measurements were not simultaneous. However, under steady-state operation, given that the total data acquisition time was sufficient to satisfy stationarity qualification, this disadvantage was unimportant. However, the use of a single pressure transducer provided extra precision in the pressure measurements since a single calibration curve was used in determining the pressure for several locations. The calibration curve of the pressure transducer used in the present study is presented in Appendix 2. Due to the limited sensitivity of the pressure transducer used in the present study, pressure measurements were limited to cases where the gas holdup was inferior to 20%. Above this limiting value, the pressure drop between adjacent pressure taps was found to be at the limit of the sensitivity level of the instrument. The switching device used in the present study consisted of a mechanical switch wafer manufactured by Scanivalve Corporation. The switch wafer was equipped with a

128

twelve channels disk connected in sequence to a single output, related to the pressure transducer. Consequently, the seven pressure taps were connected to the pressure transducer sequentially. The wafer was turned by a solenoid drive, periodically activated by a time controller. The power supply and the controller for the solenoid were designed and built in the University of Western Ontario Electronic Shop. The period of excitation of the solenoid drive could be adjusted from a fraction of a second to thirty seconds in order to leave enough time for pressure equilibration after switching channels.

3.2.3 Experimental procedure

In order to register an accurate value of the static pressure, extreme care was taken to purge the pressure lines, as well as the switching wafer lines from any gas pockets. This procedure was repeated prior to any measurements and periodically during every series of experiments to ensure gas free lines. In order to verify the purging process, the gas flowrate was stopped in the column and a static pressure profile was taken. Under such condition, if the gas lines were properly purged, a zero gas holdup value was observed. Any discrepancy from this expected value indicated an improper purge of the lines. The analog signal generated form the pressure transducer was connected to the same data acquisition system used in the case of the fibre optic sensors (Section

129

3.1.4). The data acquisition system was carefully synchronized to the switching wafer frequency. The switching wafer was allowed to reach the pressure tap no. 1. Five seconds were allowed for stabilization of the prassure. Then, the data acquisition system was activated and data were registered for a total period of 5 seconds at a rate of 100 data per second. The data acquisition system was then stopped to allow the switching wafer to connect the pressure tap no. 2 to the pressure transducer and the pressure to stabilize. Then, the data acquisition system was once again activated to collect the data for the pressure tap no. 2. This process was continued until pressure measurements of the seven taps were completed. Consequently, the pressure measured at a given axial position, represents the arithmetical average of 500 data points collected over a time period of 5 seconds. The software used in collecting the data from the pressure measuring system (ppf) and the software used in processing the collected data to evaluate the gas holdup for every series of measurements (ppc) are presented in Appendix 3.

In summary, the experimental equipment used in this research included miniaturized fibre optic sensors for minimum intrusion effects, auxiliary equipment (insertion tube) for fibre optic sensors' implementation, optical equipment, data acquisition and storage devices, and pressure transducer. Altogether, the advanced experimental techniques provided the needed tools for assessing fluid dynamic parameters in slurry

reactors and bubble columns at high temperature.

CHAPTER 4

FIBRE OPTIC SENSORS - DATA ANALYSIS

4.1 INTRODUCTION

In order to derive valuable gas fluid dynamic parameters (gas holdup, bubble velocity, bubble chord length...) from the fibre optic sensors' raw signals, a series of data analysis methodologies were developed. As explained in Chapter 3, special care was taken to ensure that the raw signals collected from the optical sensors were as significant and precise as possible. However, such efforts in collecting the raw signals would be simply useless if reliable signal analysis algorithms were not available. In the present Chapter, the methodology used in deriving important gas phase fluid dynamic parameters will be described.

As explained in Chapter 3, the fibre optic sensors' measurements were first collected and stored on magnetic tapes for further analysis. This procedure was selected so that maximum time and attention could be devoted to the proper operation of the column and the photometric system, and thus ensure high quality raw data. After the completion of a number of experiments, the raw data files, each containing 100,000 data points, were retrieved individually for complete analysis. Typical raw time series obtained, under bubble column condition, for both, the lower and upper optical

sensors, are presented in Figure 4.1. As shown on this Figure (abscissa: time; ordinate: signal intensity (volt)), excellent correspondence (emergence of bubble detection peaks was similar) between both sensors' observations was obtained, or, in other words, both sensors viewed very similar bubble flow patterns. This was expected since the vertical spacing between the two sensors (lower and upper) was carefully chosen to provide optimum signal statistical resolution, while allowing good correspondence between both time series (Chapter 3). Based on previous results (Chabot, 1989), and according to the guidelines reported by Mudde et al. (1992) regarding the digitalization parameter, a vertical spacing of 0.5 cm was found to be optimum. Due to the qualitative nature of the raw time series obtained from the fibre optic sensors and the important number of experiments performed, it was decided not to present all the time series obtained in the Appendices. However, the important fluid dynamic parameters derived from these raw time series are extensively reported in the Appendix section as mentioned in Chapter 5.

4.2 LOCAL GAS HOLDUP

The gas holdup constitutes one of the most important fluid dynamic parameters to be measured in a bubble or slurry bubble column. The gas holdup at a particular position in the column can be derived from the fibre optic measurements by evaluating the fraction of the total data acquisition time during which

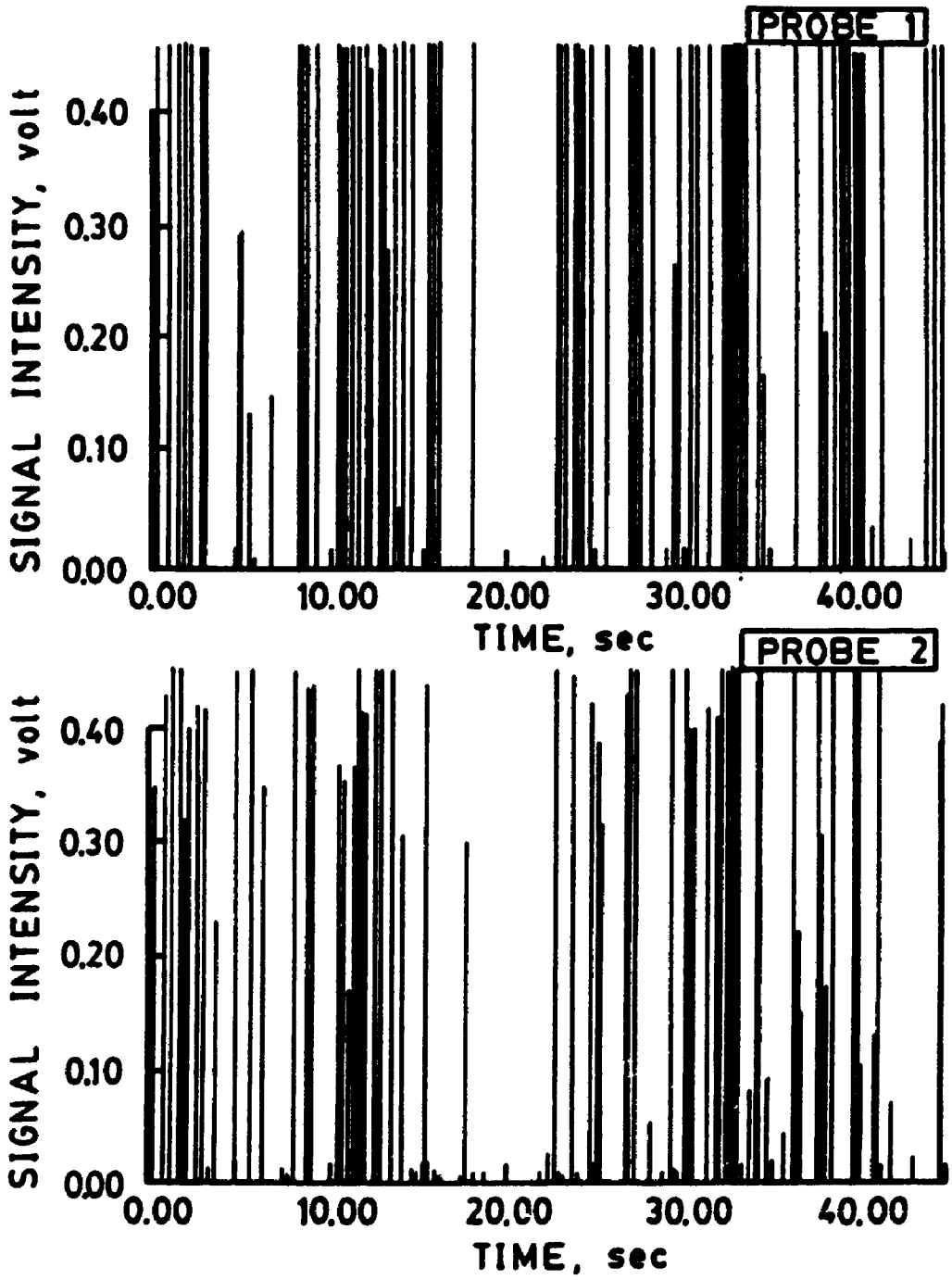

Figure 4.1: Typical fibre optic sensors output signals (time series) (T=100°C, V_g=4.1 cm/s, z=15 cm, θ=0.92)

the tip of the sensor was in contact with the gas phase, as represented by the following equation:

$$\epsilon_{g,loc} = \sum_{i=1}^{n} \frac{\Delta t_i}{T_i} \qquad (4.1)$$

The software developed to evaluate the gas holdup value for a given fibre optic sensors' time series (C2HR) is presented in Appendix 3. The value thus obtained represents a time averaged (averaged over the total data acquisition time: 50 s) local gas holdup value. The determination of the fraction of the time during which the tip of the sensor is in contact with the gas phase is done through the summation of the duration of individual bubble contacts. Individual bubbles are identified using a multi-criteria analysis of the change of the slope of the raw time series baseline: 1) when the slope of the signal increases (positive slope) above a preset value (criterion #1) the bubble detection algorithm is activated, 2) if the slope of the signal (positive slope) is maintained for one more time interval above a preset value (criterion #2), a bubble is identified, 3) the ascending portion of the bubble detection peak is monitored until a change of slope is encountered (negative slope), 4) the descending section of the detection peak is monitored until a change in the sign of the slope is encountered (end of the detection peak), 5) two additional criteria (criteria # 3 and #4) are incorporated to account for oscillations in the bubble detection peaks (multiple change of

slopes) and ensure that the bubble detection time termination is properly assessed. The criteria were selected based on the individual response of the sensor (established during the pre-testing phase) and the noise present in the system. Blank runs (experiments performed without any gas flows), allowed quantitative assessment of the level of the parasite noises present in the overall system (analog cable, photometric system, amplifier, data acquisition card). These parasite noises were typically always kept below 0.625 mV. More details concerning the bubble identification procedure are presented in Appendix 3 (software: C2HR).

4.3 BUBBLE VELOCITY AND BUBBLE CHORD LENGTH

The average bubble velocity for a given data file was obtained by applying the cross correlation analysis to the two time series obtained (lower optical sensor and upper optical sensor). Thus, the average time delay needed for the gas bubbles to move from the lower sensor tip to the upper one can be determined. The normalized cross correlation function is defined as follows:

$$C_{xy} = \frac{\xi_{xy}(\tau)}{\sigma_x \sigma_y} \qquad (4.2)$$

where x(t) and y(t) are the signals from the lower and the

136

$$\xi_{xy}(\tau) = \frac{1}{T_t}\int_0^{T_t}(x(t)-u_x)\,(y(t+\tau)-u_y)\,dt \qquad (4.3)$$

upper optical sensor respectively, and u_x and u_y are the mean values of the lower and upper optical sensors' time series respectively. A cross correlogram was constructed by plotting the normalized cross correlation function against the time lag. The average time required for the gas bubbles to pass through the two probes was obtained from the maximum time delay which was established by noting the time lag at the peak of the cross correlogram. Since the distance between the two probes was known, the average bubble velocity was obtained by dividing the distance by the most probable time delay.

The average bubble axial chord length was obtained by multiplying the average bubble velocity by the average bubble-sensor contact time duration. As previously reported (Chabot, 1989; Chabot et al., 1992), satisfactory bubble detection was reported for bubbles as small as 0.5-2 mm in diameter in oil at room temperature. Improved detection efficiency was however observed for bubbles of similar size under lower viscosity conditions (higher temperature), where better bubble-sensor contacts are possible. However, the fibre optic sensors used in the present study do not have any limitations concerning possible maximum bubble size or maximum gas holdup to be detected. The optical sensors were also found to

efficiently performed under high solid loading conditions (up to 35%$_{wt}$), as previously reported (Chabot, 1989).

4.4 BUBBLE AXIAL CHORD LENGTH DISTRIBUTION

The previous measurements were obtained through a global statistical approach and thus represent an overall description of the bubble population present at a given position and operating condition. However, much interest lies in obtaining a more thorough description of the total bubble population. In this context, an analysis methodology was developed to obtain the bubble axial chord length distribution. This analysis was based on the analysis of individual bubbles. Actually, the bubble chord length distribution was obtained by carefully screening the two time series obtained from the lower and the upper optical sensors respectively. Bubble detection peaks were first identified (using the identical approach used in the gas holdup evaluation) for the lower optical sensor. The upper optical sensor time series was then screened to identify similar peaks, corresponding to the detection of the same bubble. Similarity was based on several severe criteria including the duration of the peak, the normalized voltage intensity and the normalized average signal intensity. Thus, special care was taken to insure that the bubble detection peaks successfully retained (typically between 20-80% of the total peaks detected on the lower sensor) were most likely generated by the same bubble. The

138

software written to perform the bubble axial chord length distribution analysis (bsize) is presented in Appendix 3.

All the bubble chord length distributions reported above were obtained from fibre optic sensor measurements. Generally, if a sensor is used in investigating the bubble population, the sensor intersects the bubble with a chord length other than the diameter of the largest vertical chord length of the bubble (the true bubble diameter). Consequently, a bubble chord length smaller than the largest vertical bubble dimension is typically measured, resulting in a skewed bubble chord length distribution shifted toward smaller bubble sizes (Clark and Turton, 1988). So, if the general conclusions presented above concerning the dependence of the bubble chord length distribution on the operating parameters would indeed be valid for bubble diameter distribution (since no major probe disturbance effects were noticed for all operating conditions), the bubble diameter distribution would be expected to be somewhat shifted to the right (larger bubbles), while being less skewed. The reconstruction of the bubble diameter distribution from the bubble chord length distribution does require an assumed bubble shape. Since, in the present case, a very wide bubble chord length distribution was observed (long tail), the assumption of a unique bubble shape might represent a risky assumption.

Thus, the present research included significant effort to

determine key fluid dynamic parameters such as gas phase holdup, bubble velocity, bubble chord length, and bubble axial chord length distribution from the time series obtained from the fibre optic sensors. These methodologies were applied consistently throughout the experimental program.

CHAPTER 5

RESULTS AND DISCUSSION

5.1 BUBBLE COLUMN

5.1.1 Gas holdup radial profiles

The local gas holdup was measured, using the fibre optic technology previously described, at six different radial positions (θ=0.19, 0.42, 0.62, 0.78, 0.89, 0.92) and at several axial positions (z=10, 15, 30, 46, 61, 76 cm). The local gas holdup values presented in this study were derived from the measurements obtained with the optical sensor no.1, located upstream (considering the gas dominant vertical upward flow direction) with respect to the optical sensor no.2. The measurements obtained with the fibre optic sensor no.1 are subjected to a minimum of hydrodynamic perturbations in comparison to the ones derived from the upper fibre optic sensor (sensor no.2), potentially more susceptible to minor gas flow upsets introduced by the presence of the lower optic sensor. The extent of these possible gas flow hydrodynamic perturbations was studied by comparing the gas holdup values derived from both fibre optic sensors (fibre optic sensor no.1 and no.2). The comparison between the two fibre optic sensors' performance is presented, for all the experiments performed, in Figure 5.1 for T=100°C and in Figure 5.2 for T=175°C. As illustrated on these Figures, the presence of the

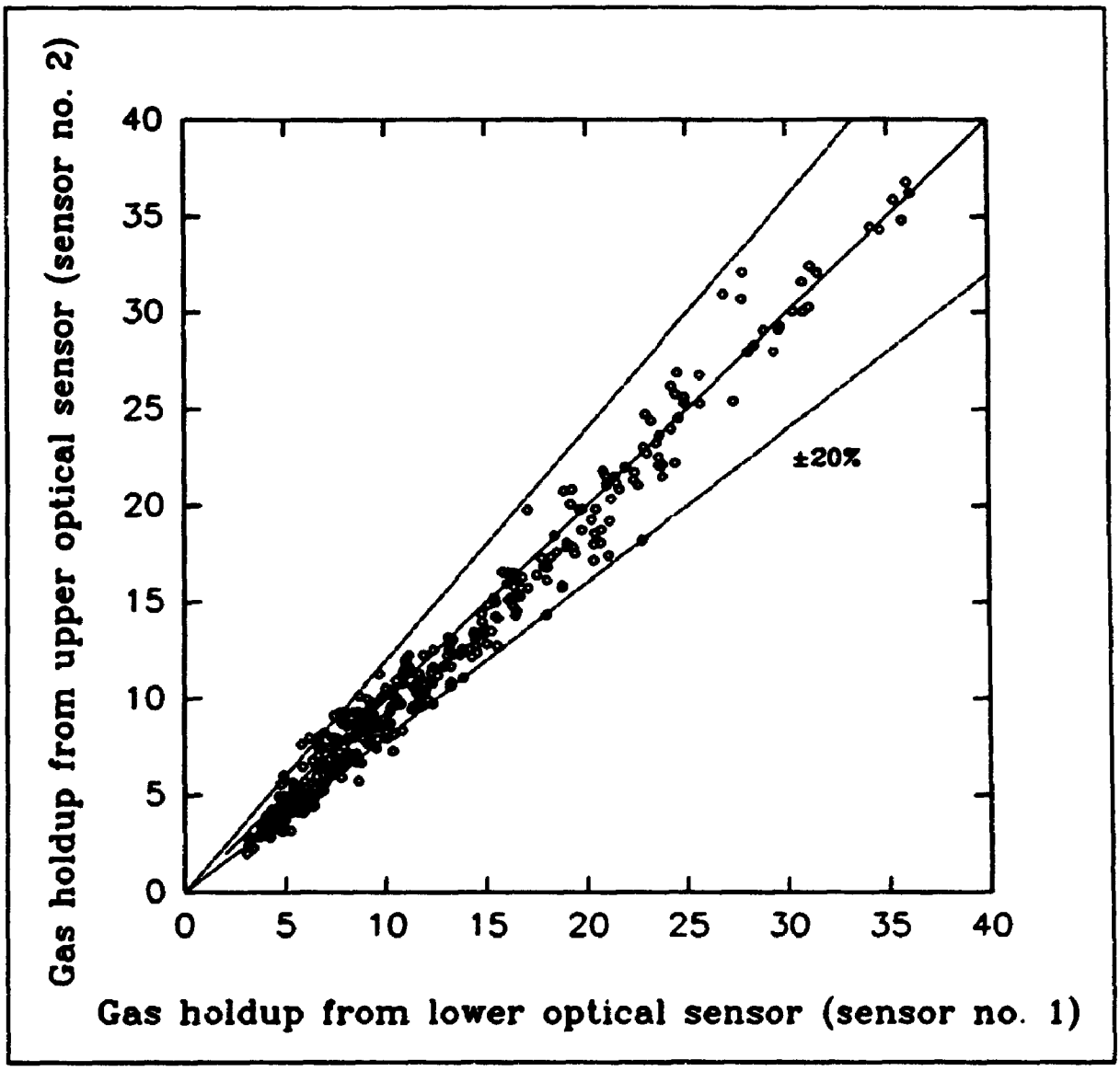

Figure 5.1: Gas holdups from fibre optic sensor no.2 (upper) vs gas holdups from fibre optic sensor no.1 (lower) (T=100°C)

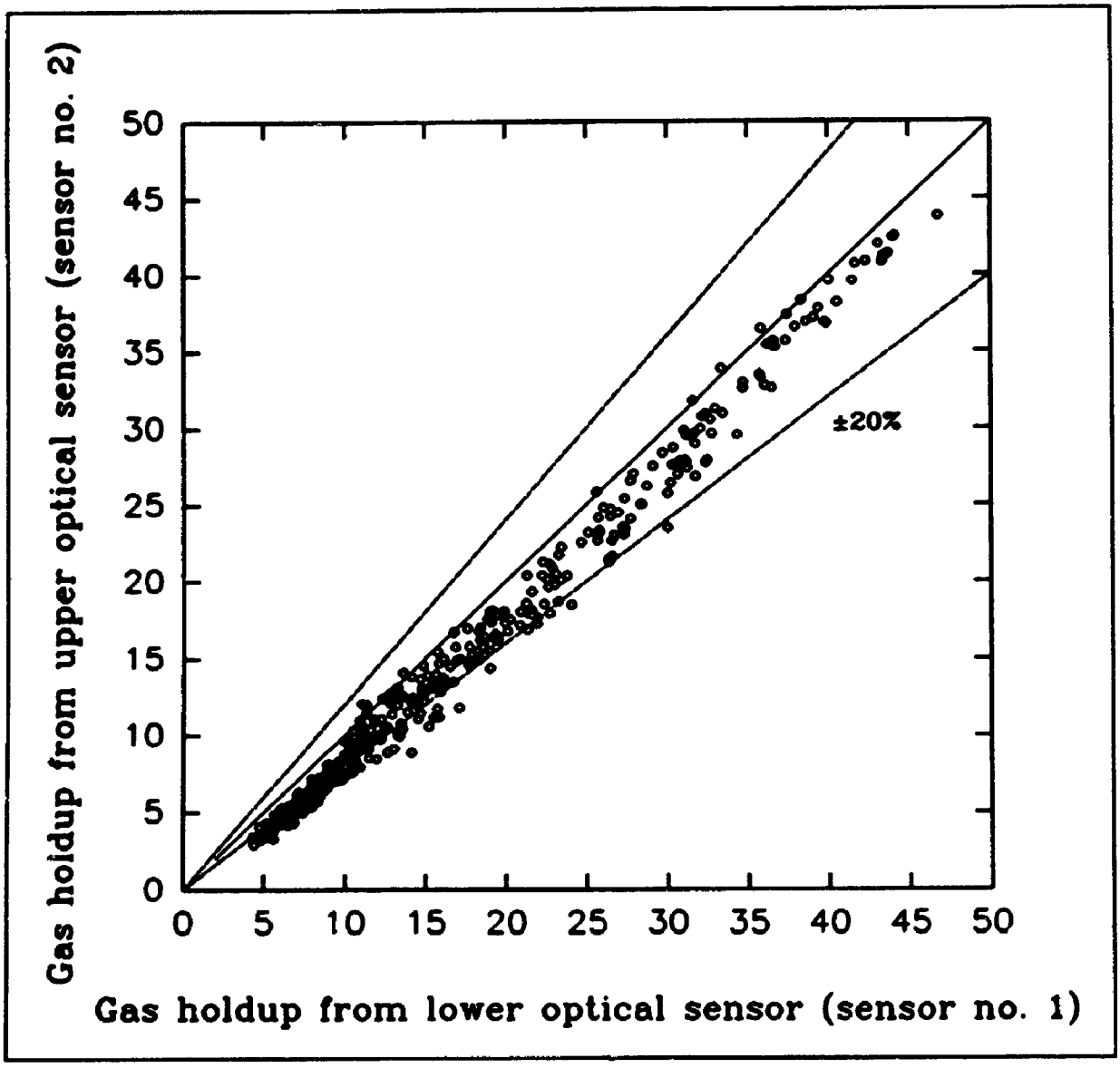

Figure 5.2: Gas holdups from fibre optic sensor no.2 (upper) vs gas holdups from fibre optic sensor no.1 (lower) (T=175°C)

lower fibre optic sensor generally contributed to the detection of slightly lower gas holdups by the fibre optic sensor no.2 (upper). This difference was however found to be very small, the majority of the readings from both sensors being safely within 10% of each other, and most of them being within 20% of each other. In summary, the negligible disturbance caused by the presence of the lower probe on the upper sensor measurements was confirmed for the different experiments and conditions studied during this research.

The gas holdup radial profiles obtained at various axial positions (A.P.) are presented, for V_g=2.2, 4.1, 9.0 and 14.7 cm/s, in Figures 5.3 to 5.6 for T=100°C and in Figures 5.7 to 5.10 for T=175°C. Each local gas holdup value ($\epsilon_{g,loc}$) reported in these Figures represents the average of a minimum of 3 experimental gas holdup repeats ($\epsilon_{g,repeat}$) obtained after steady state hydrodynamic conditions were reached (as verified following the procedure described in section 2.3.3). A summary of all the results obtained is presented in Appendix 4. In order to assess the consistency of the fibre optic measurements, the relative percentage errors (equation 1) between the local gas holdup ($\epsilon_{g,loc}$) and the gas holdup experimental repeats ($\epsilon_{g,repeat}$) were evaluated.

$$err = \left| \frac{\epsilon_{g,loc} - \epsilon_{g,repeat}}{\epsilon_{g,loc}} \right| \qquad (5.1)$$

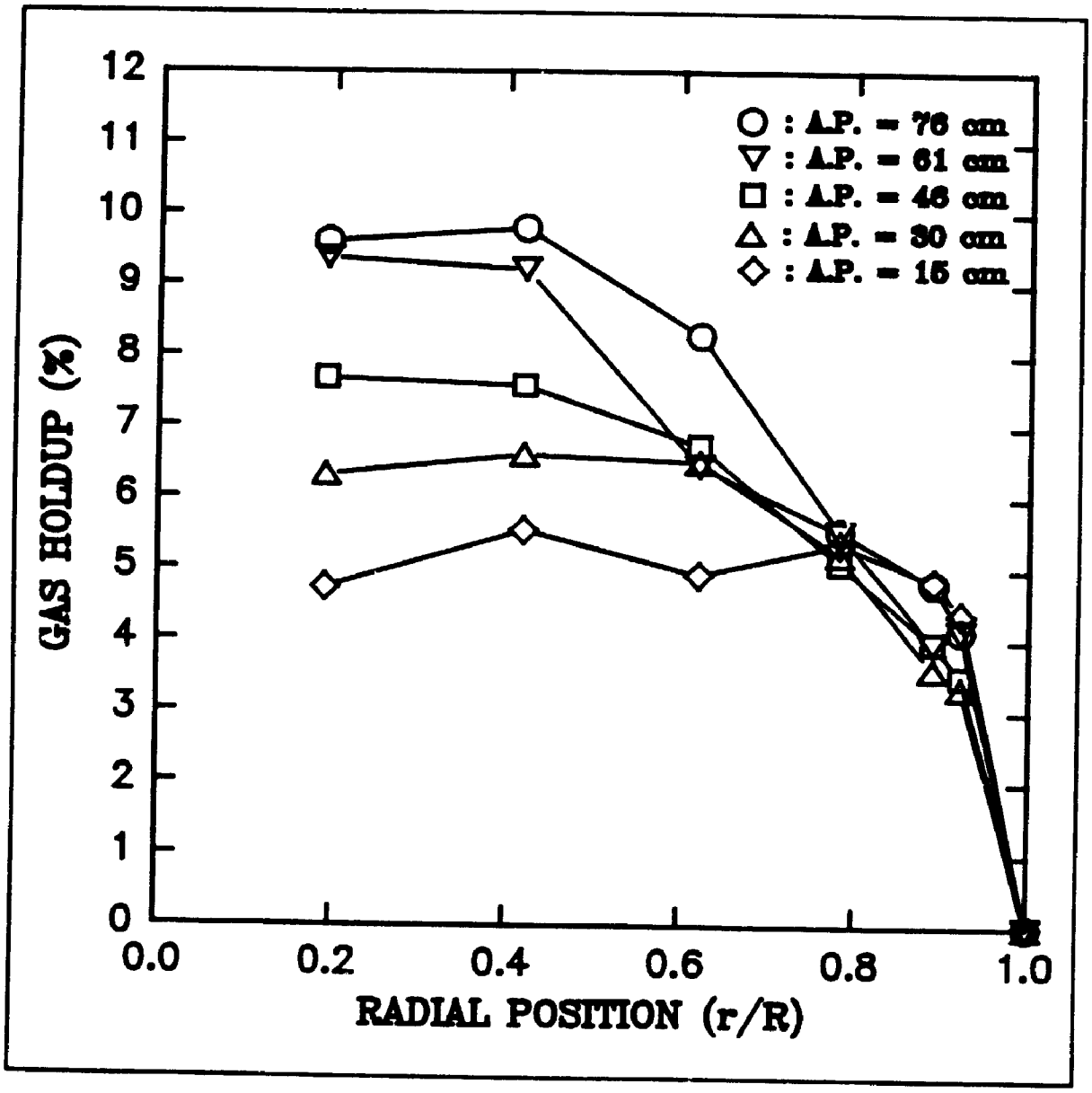

Figure 5.3: Gas holdup radial profile (T=100°C, V_g=2.2 cm/s)

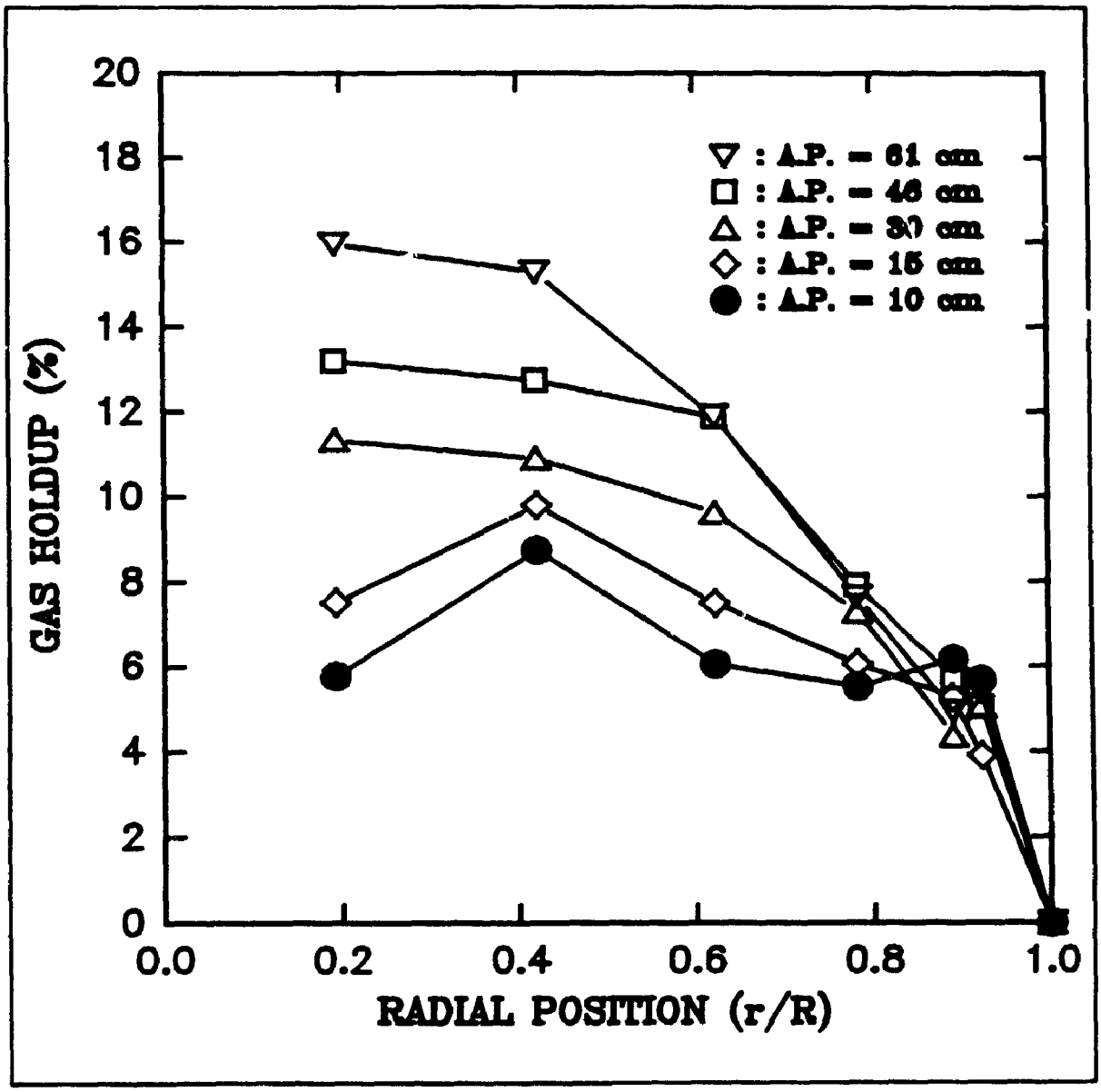

Figure 5.4: Gas holdup radial profile (T=100°C, V_g=4.1 cm/s)

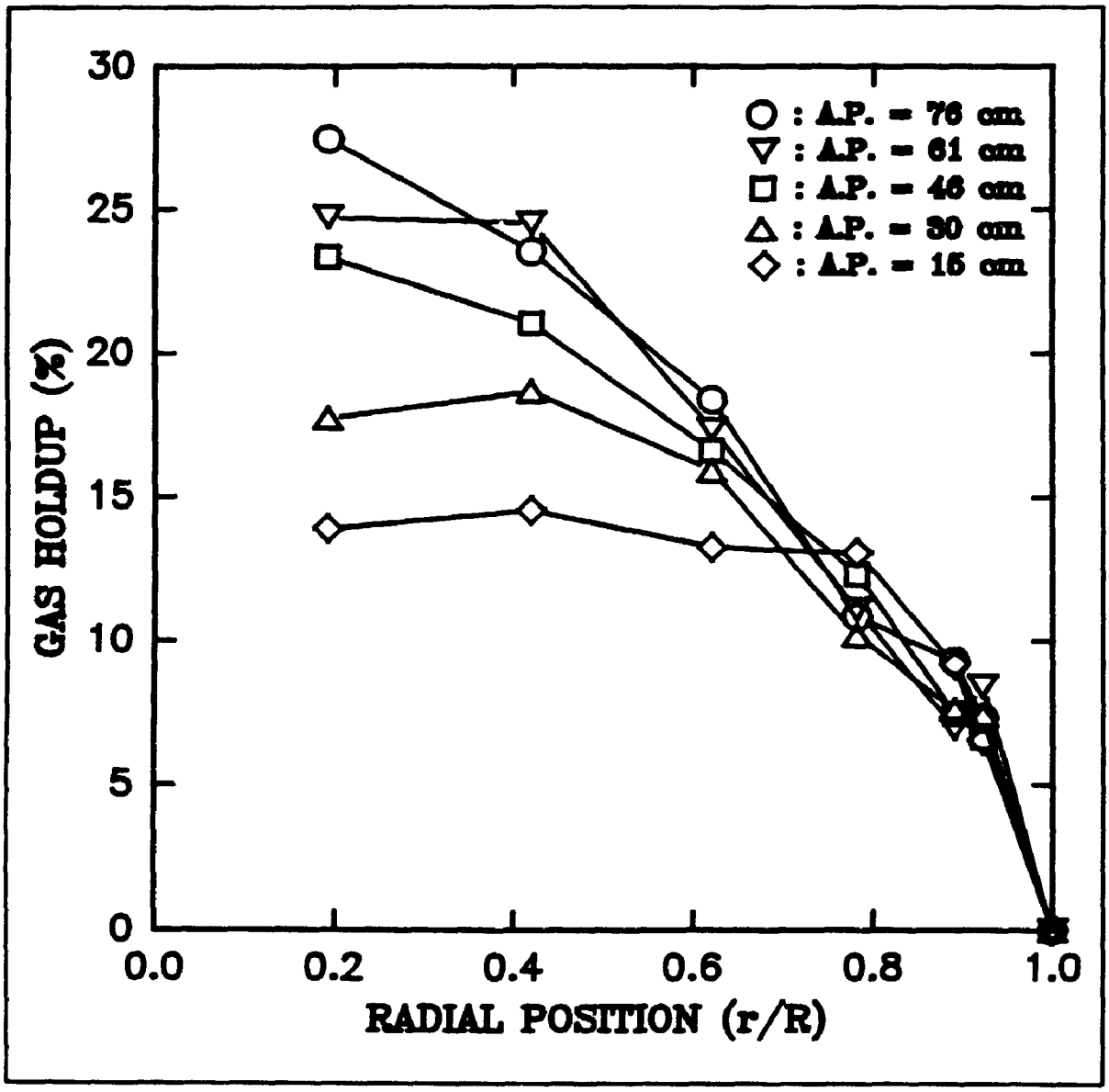

Figure 5.5: Gas holdup radial profile (T=100°C, V_g=9.0 cm/s)

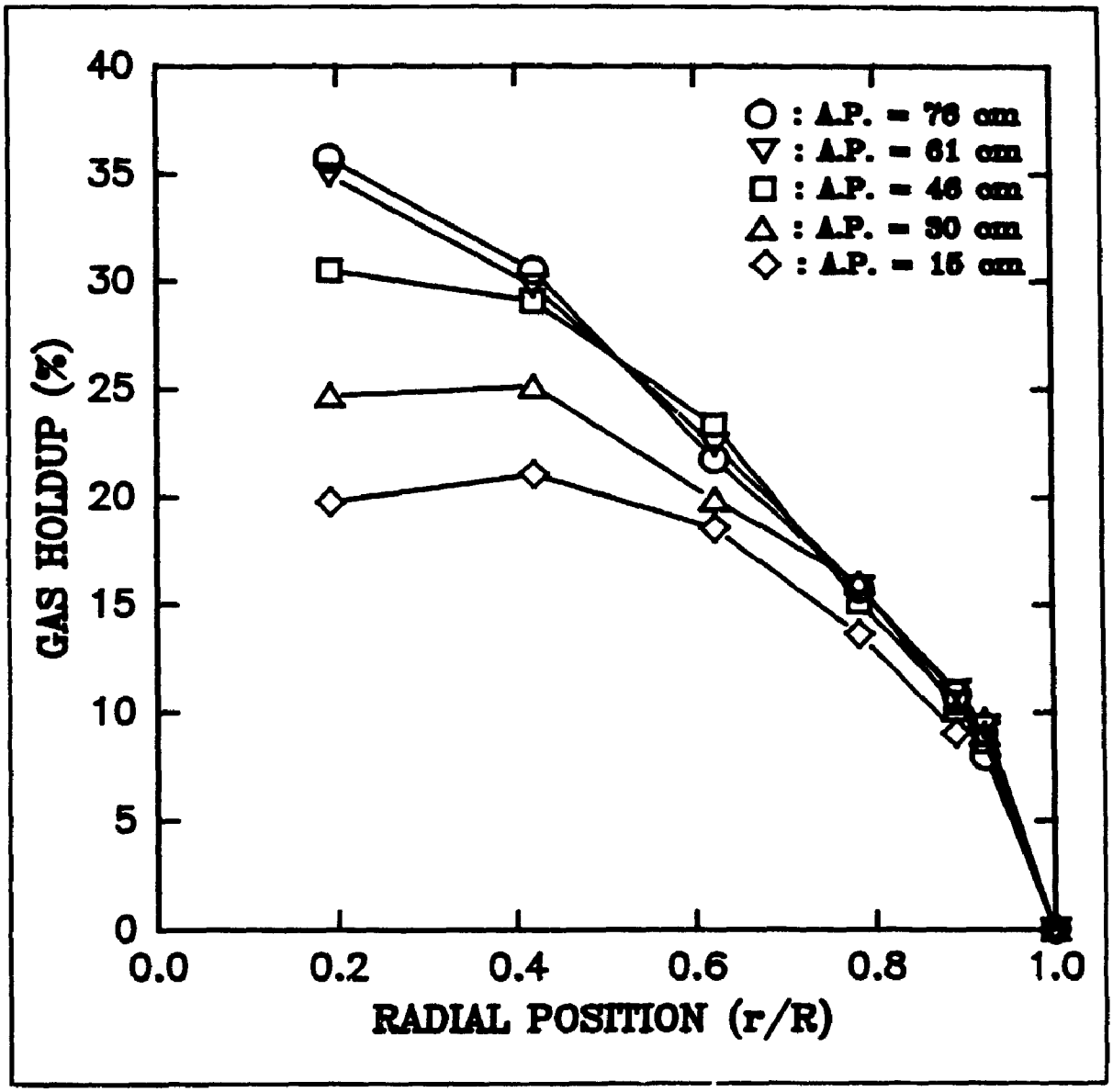

Figure 5.6: Gas holdup radial profile (T=100°C, V_g=14.7 cm/s)

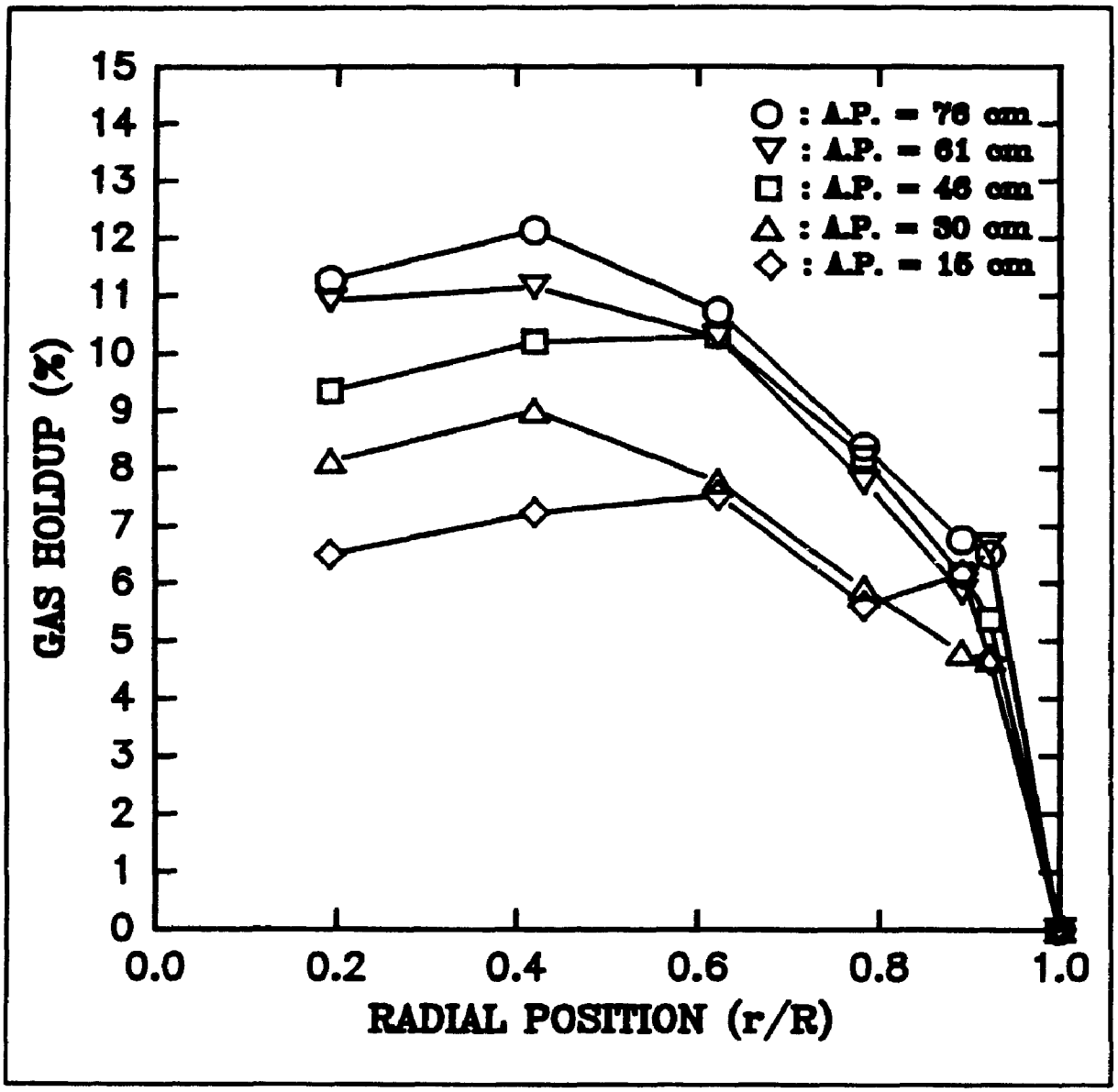

Figure 5.7: Gas holdup radial profile (T=175°C, V_g=2.2 cm/s)

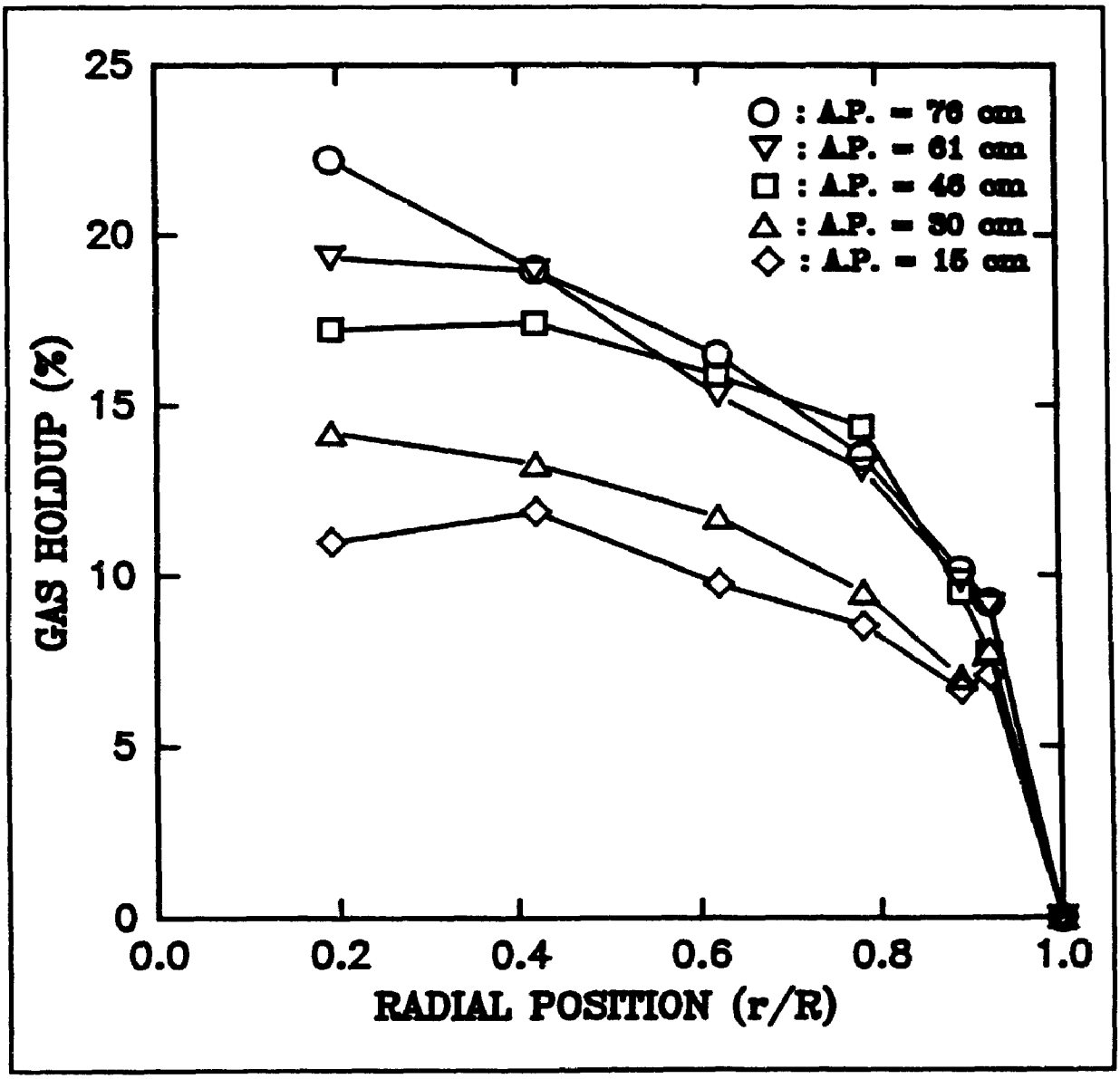

Figure 5.8: Gas holdup radial profile (T=175°C, V_g=4.1 cm/s)

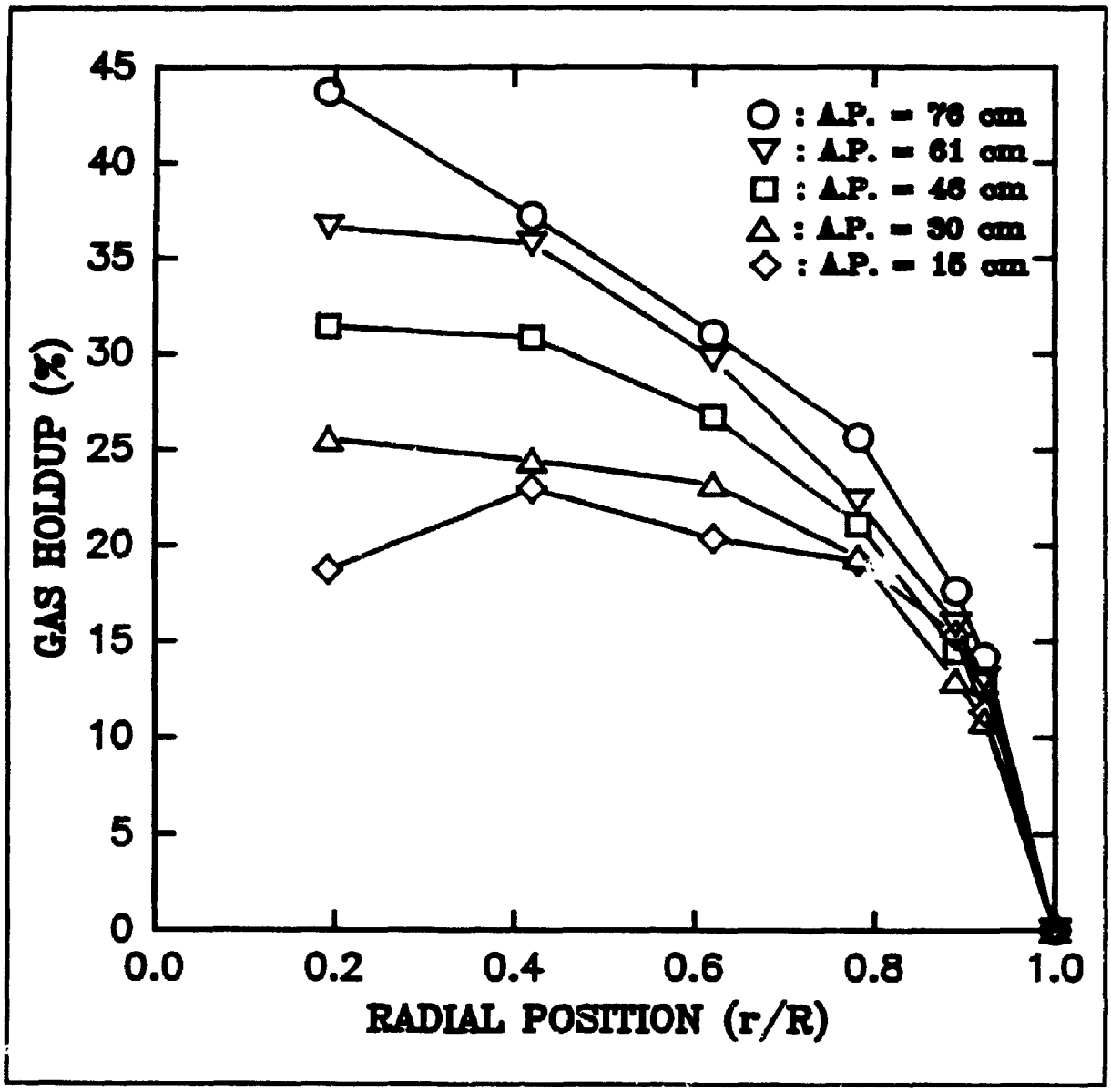

Figure 5.9: Gas holdup radial profile (T=175°C, V_g=9.0 cm/s)

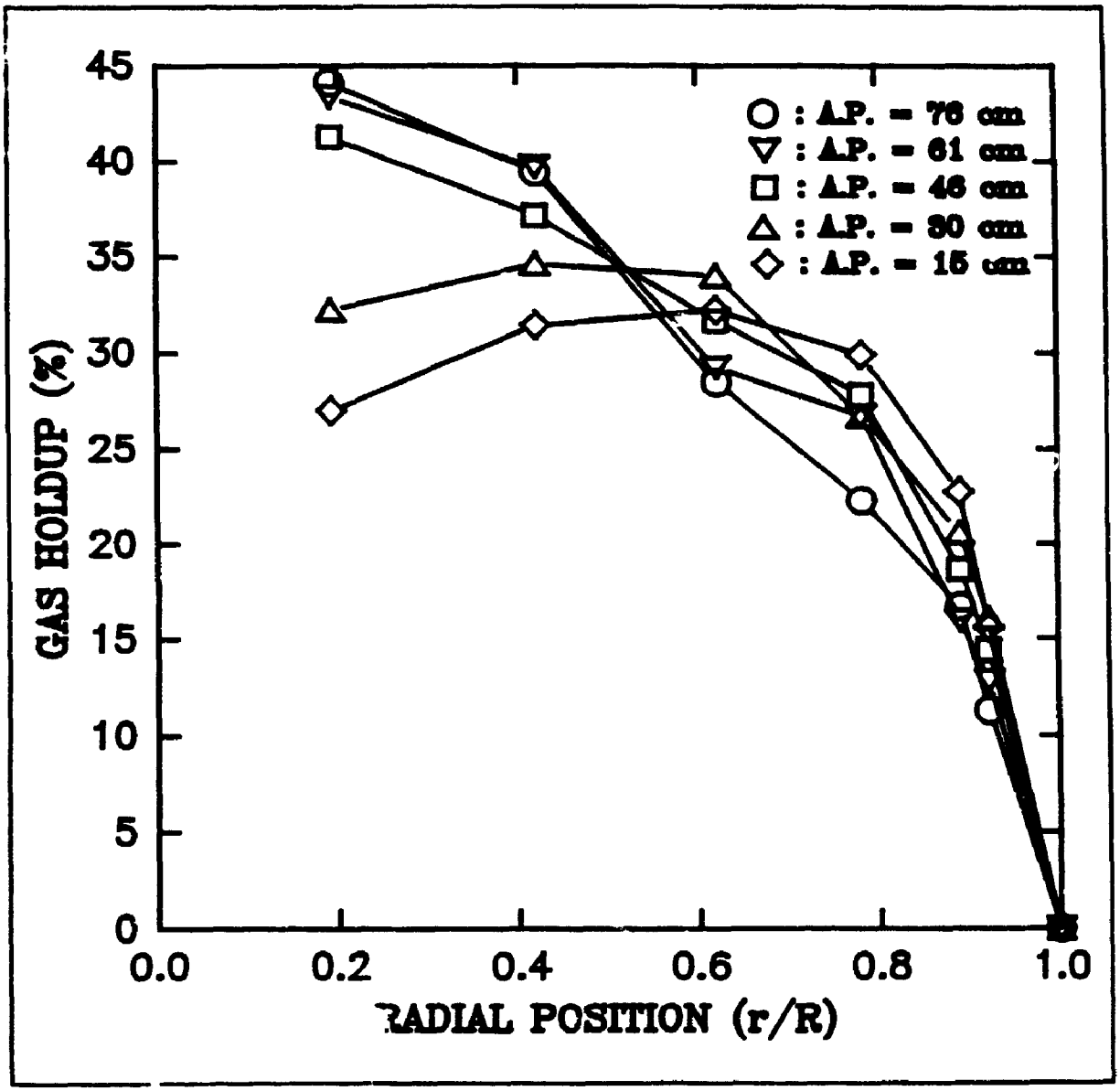

Figure ..10: Gas holdup radial profile (T=175°C, V_g=14.7 cm/s)

The relative percentage errors are reported in Tables 5.1 and 5.2 for the experiments conducted at T=100°C and in Tables 5.3 and 5.4 for the ones performed at T=175°C. The results presented in the top row correspond to the average relative percentage error for all the experimental repeats performed at a given operating condition, while the results presented in the bottom row correspond to the maximum percentage error observed for this particular set of repeats. As shown in Tables 5.1 to 5.4, the average relative percentage errors were in general very satisfactory, being equal on average to 6.42%, 5.81%, 5.14% and 3.84% at T=100°C and 4.27%, 3.38%, 3.29% and 3.27% at T=175°C for V_g=2.2, 4.1, 9.0 and 14.7 cm/s respectively. Furthermore, the average maximum relative percentage errors were safely within 10%, being equal to 9.59%, 8.79%, 7.81%, 5.78% at T=100°C and 6.28%, 6.59%, 5.09% and 4.94% at T=175°C for V_g=2.2, 4.1, 9.0 and 14.7 cm/s respectively. These results demonstrate the excellent consistency of the fibre optic sensor experimental gas holdup measurements under all the operating conditions investigated. In fact, the low discrepancies observed between experimental measurements support the adequacy of the fibre optic sensor data acquisition procedure implemented. Actually, repeatability of the measurements require a sufficient data acquisition time to ensure a representative visualization of the phenomenon studied. An insufficient data acquisition time would favour statistically unstable time series and consequently important inconsistencies between experimental

153

Table 5.1

Average (top row) and maximum (bottom row) relative percentage errors between calculated average gas holdups ($\epsilon_{g,lm}$) and gas holdups (repeats) (T=100°C)

V_s cm/s	z cm	θ=0.19 %	θ=0.42 %	θ=0.62 %	θ=0.78 %	θ=0.89 %	θ=0.92 %
2.2	15	2.82 4.23	7.02 10.61	6.63 9.84	13.19 19.78	8.88 13.22	5.57 8.45
2.2	30	4.81 7.29	8.93 13.3	4.87 7.23	6.53 9.79	16.96 25.64	7.11 10.48
2.2	46	3.17 4.69	2.05 2.11	8.77 13.08	1.83 2.75	15.33 22.86	6.95 10.29
2.2	61	7.65 11.53	2.82 4.23	5.32 8.06	3.19 4.88	6.30 9.57	2.82 4.35
2.2	76	1.04 1.56	5.64 8.48	3.50 5.19	4.27 6.50	6.17 9.36	12.32 18.36
4.1	10	10.11 15.08	2.94 4.35	10.46 15.69	6.72 10.08	4.79 7.18	9.97 14.96
4.1	15	4.72 7.07	5.33 8.00	5.28 7.92	4.07 6.10	7.90 11.84	5.21 7.83
4.1	30	5.05 10.15	2.60 3.94	2.77 4.16	10.61 15.91	5.06 7.59	6.27 9.50
4.1	46	0.60 0.90	2.12 3.14	2.33 3.54	7.25 10.87	1.69 2.63	8.55 12.72
4.1	61	0.66 1.00	4.10 6.15	5.69 8.49	19.37 29.06	6.02 8.92	6.02 8.94

154

Table 5.2

Average (top row) and maximum (bottom row) relative percentage errors between calculated average gas holdups ($\epsilon_{g,av}$) and gas holdups (repeats) (T=100°C)

V_s cm/s	z cm	θ=0.19 %	θ=0.42 %	θ=0.62 %	θ=0.78 %	θ=0.89 %	θ=0.92 %
9.0	15	4.01 5.98	1.42 2.13	5.01 7.55	5.03 7.50	8.82 13.18	1.99 7.50
9.0	30	3.50 5.25	2.23 3.37	5.47 8.18	9.21 13.86	6.97 10.39	4.42 6.62
9.0	46	1.02 1.56	4.49 6.74	1.75 2.65	4.79 7.23	6.15 7.48	8.41 12.69
9.0	61	2.34 3.52	0.93 1.38	4.86 7.32	7.72 11.63	7.90 11.78	11.60 17.46
9.0	76	1.52 2.26	2.79 4.16	4.85 7.24	7.05 10.62	12.09 18.19	5.85 8.77
14.7	15	2.21 3.29	1.11 1.66	4.29 6.42	9.69 14.54	4.02 6.09	4.94 7.46
14.7	30	3.00 4.49	5.85 8.76	8.87 13.33	8.23 12.38	1.12 1.68	2.33 3.44
14.7	46	3.64 5.48	4.01 6.02	2.67 4.03	5.49 8.27	4.07 6.14	1.12 1.73
14.7	61	2.01 2.99	1.22 1.85	3.88 6.02	2.58 3.87	4.71 7.02	12.67 19.06
14.7	76	0.77 1.15	1.89 2.85	3.26 4.92	2.64 4.00	0.28 0.28	2.72 4.09

Table 5.3

Average (top row) and maximum (bottom row) relative percentage errors between calculated average gas holdups ($\epsilon_{g,ave}$) and gas holdups (repeats) (T=175°C)

V_s cm/s	z cm	θ=0.19 %	θ=0.42 %	θ=0.62 %	θ=0.78 %	θ=0.89 %	θ=0.92 %
2.2	15	1.90 2.92	2.58 3.87	4.95 7.43	10.15 15.33	4.00 6.01	1.22 1.93
2.2	30	2.63 3.94	0.63 0.89	0.82 1.29	2.54 3.89	7.29 11.04	4.20 6.20
2.2	46	4.88 7.27	1.31 1.98	1.26 1.84	1.59 2.44	3.85 5.69	3.79 5.78
2.2	61	2.17 3.21	3.50 5.20	3.60 5.35	9.40 14.16	7.40 11.08	1.55 2.40
2.2	76	3.52 5.24	8.81 13.18	6.83 10.25	9.47 10.25	7.55 11.27	4.62 6.92
4.1	15	1.67 2.55	4.12 6.22	3.35 5.03	4.73 7.17	10.61 15.84	6.57 9.79
4.1	30	3.36 5.00	3.99 6.02	3.38 5.03	3.30 4.95	1.86 2.86	4.08 6.19
4.1	46	1.997 3.02	6.21 9.29	3.55 5.35	7.03 10.58	3.33 5.05	8.67 13.0
4.1	61	2.02 3.05	2.38 3.54	3.16 4.71	2.31 3.50	2.34 3.56	9.66 14.49
4.1	76	1.85 2.75	1.99 2.95	4.93 7.398	5.99 9.02	7.36 11.05	5.70 8.60

Table 5.4

Average (top row) and maximum (bottom row) relative percentage errors between calculated average gas holdups ($\epsilon_{g,av}$) and gas holdups (repeats) (T=175°C)

V_s cm/s	z cm	θ=0.19 %	θ=0.42 %	θ=0.62 %	θ=0.78 %	θ=0.89 %	θ=0.92 %
9.0	15	2.90 4.38	3.99 5.96	1.83 2.75	5.96 8.92	7.81 11.75	4.98 7.42
9.0	30	1.16 1.72	5.73 8.60	1.77 2.67	2.49 3.71	5.41 8.11	5.18 7.73
9.0	46	2.20 7.73	2.39 3.57	2.46 3.71	3.61 5.44	3.75 5.66	7.31 11.00
9.0	61	2.34 3.52	1.93 2.91	3.07 4.61	3.33 4.97	2.85 4.28	1.61 2.45
9.0	76	0.57 0.85	2.04 3.06	2.25 3.38	2.51 3.74	2.80 4.20	2.56 3.81
14.7	15	2.92 4.38	6.20 9.32	0.94 1.43	3.32 4.98	1.03 1.54	2.65 3.98
14.7	30	2.45 3.66	2.42 3.64	3.52 5.29	1.67 2.51	7.05 10.55	4.83 7.28
14.7	46	1.99 2.98	0.96 1.45	1.16 1.74	5.41 8.09	2.67 3.97	8.36 12.57
14.7	61	0.48 0.71	0.48 0.71	3.55 5.34	1.42 2.14	4.12 6.21	2.06 2.90
14.7	76	3.99 5.98	1.89 2.84	7.75 11.61	2.86 4.27	9.75 14.63	0.11 1.60

measurements. Consequently, the total data acquisition time selected (50 seconds), according to the procedure described in Section 3.1.6, appeared to be adequate under all the operating conditions investigated, even for the cases where the total number of bubbles detected is minimum (lower temperature and lower gas superficial velocities).

The gas holdup radial profiles obtained at V_g=2.2 cm/s and T=100°C are presented in Figure 5.3. As shown on this Figure, the gas holdup radial profile was relatively uniform throughout the cross section area of the column, in the proximity of the gas distributor (z=15 cm). It has to be stressed that uniform gas holdup throughout the cross section of the column, in the vicinity of the gas distributor, indicates an effective uniform gas distribution throughout the cross section of the perforated plate. Moreover, the uniform distribution of the gas through the perforated plate was corroborated by the measurements of the pressure drop across the gas distributor, as explicitly described in Appendix 5, and summarized in Table 5.5. Kunii and Levenspiel (1984) suggested the following criterion for minimum pressure drop across distributor:

$\Delta P_{(grid,\ minimum)}$ ≥ of the largest of these three conditions:

$0.1\ \Delta P_{bed}$

35 cm H2O

158

100 $\Delta P_{\text{expansion into vessel}}$

The pressure drop across the column (bed), neglecting the dynamic component of the measured pressure and the frictional losses, as supported by the work of Kim et al. (1975), was evaluated to be equal, under the conditions prevailing during the perforated plate pressure drop measurements, to 8200 Pa ($\Delta P = \rho\ g\ h = 870\ kg/m^3 \times 9.81\ m/s^2 \times 0.96\ m = 8200\ Pa$). The vessel pressure drop due to expansion was evaluated (refer to Appendix 5: friction losses for a sudden enlargement) to be equal to 9.9 Pa, for V_g=2.2 cm/s. Then, the maximum of the three criteria previously mentioned, for V_g=2.2 cm/s, would be:

$$\Delta P_{\text{grid, minimum}} = \text{MAX}(820\ Pa,\ 3432\ Pa,\ 994\ Pa) = 3432\ Pa$$

As shown in Table 5.5, for V_g=2.2 cm/s, the measured pressure drop across the perforated plate was found to be equal to 3980 Pa, which is 13.8% larger than the recommended minimum pressure drop, thus insuring efficient distribution of the gas. For the two other gas superficial velocities studied, respectively 4.1 and 9.0 cm/s, the measured pressure drops across the perforated plate were found to be 82.2% and 95.6% larger than the recommended minimum grid pressure drop. The grid pressure drop measurements could not be performed at V_g=14.7 cm/s, since the pressure, before the grid, exceeded the recommended pressure range for the mechanical switch wafe:

Table 5.5

Pressure drop through perforated plate distributor
T=25°C

V_g cm/s	ΔP KPa
2.2	3.98
4.1	19.27
9.0	77.55

160

device operation.

As the axial position (distance from the gas distributor) was increased, the relatively uniform radial distribution of the gas holdup present at V_g=2.2 cm/s and z=15 cm was replaced by the typical parabolic gas holdup radial profile, characterized by maximum gas holdup values in the central region of the bed and minimum gas holdup values in the proximity of the column wall. This typical parabolic gas holdup radial profile was also present under the other operating conditions studied (Figures 5.4 to 5.10). However, for all the operating conditions investigated, a clear evolution of the gas holdup parabolic radial profile was observed as the axial position was increased. Actually, the gas holdup radial profile evolved gradually from a more uniform radial profile in the vicinity of the gas distributor to a more pronounced parabolic gas holdup radial profile at a higher axial position. The axial evolution of the gas holdup radial profile appeared however to have approached or completely reached stabilization at the axial position equal to 76 cm.

These experimental observations suggested, for the gas holdups, an evolving parabolic radial profile changing with the axial position. Thus, the gas holdup radial profiles observed for all the operating conditions studied were proposed to be represented by the following mathematical expression:

$$\epsilon_{g,loc}(\theta) = \epsilon_{g,avg} \left(\frac{m+2}{m}\right)(1-\theta^m) \qquad (5.2)$$

where the measured local gas holdup ($\epsilon_{g,loc}$) was expressed in terms of the dimensionless radial distance (θ=r/R), and the average gas holdup ($\epsilon_{g,avg}$), which was calculated using the following expression:

$$\epsilon_{g,avg} = \frac{2}{R^2}\int_0^R \epsilon_{g,loc}\, r dr \qquad (5.3)$$

In fact, all the radial gas holdup profiles obtained were successfully depicted by the equation 5.2, with correlation coefficients (Kleinbaum and Kupper, 1978) in excess of 0.964 and average correlation coefficient equal to 0.987. A Marquart-Levenberg algorithm (non-linear least squares fitting) was used in obtaining the parameter m in equation 5.2. This method introduces a smooth variation between the extremes given by the inverse-Hessian method and the steepest descent method. The latter method is used far from the minimum, switching continuously to the former as the minimum is approached (Press et al., 1989). The values of the parameter m found, and the corresponding standard deviation of this parameter are presented in Tables 5.6 and 5.7 for the experiments performed at T=100°C and at T=175°C respectively. In general, the standard deviation of the

Table 5.6

Variation of the parameter m (Equation 5.2) with the axial position and gas superficial velocity (T=100°C)

Temperature (°C)	V_g (cm/s)	A.P. (cm)	m	Std. Dev.
100	2.2	15	23.87	4.801
100	2.2	30	7.52	0.582
100	2.2	46	5.92	0.726
100	2.2	61	4.32	0.916
100	2.2	76	4.86	0.772
100	4.1	15	7.08	1.533
100	4.1	30	4.83	0.618
100	4.1	46	4.60	0.433
100	4.1	61	3.04	0.351
100	9.0	15	8.60	0.673
100	9.0	30	4.34	0.594
100	9.0	46	3.12	0.248
100	9.0	61	2.72	0.395
100	9.0	76	2.52	0.330
100	14.7	15	5.43	0.674
100	14.7	30	4.34	0.399
100	14.7	46	3.13	0.232
100	14.7	61	2.59	0.293
100	14.7	76	2.34	0.235

Table 5.7

Variation of the parameter m (Equation 5.2) with the axial position and gas superficial velocity (T=175°C)

Temperature (°C)	V_g (cm/s)	A.P. (cm)	m	Std. Dev.
175	2.2	15	15.05	3.360
175	2.2	30	7.32	1.260
175	2.2	46	8.59	0.819
175	2.2	61	7.62	1.436
175	2.2	76	7.79	1.211
175	4.1	15	9.21	1.857
175	4.1	30	6.93	1.356
175	4.1	46	7.05	0.331
175	4.1	61	6.13	0.995
175	4.1	76	5.28	0.945
175	9.0	15	10.52	1.463
175	9.0	30	6.37	0.318
175	9.0	46	5.22	0.462
175	9.0	61	4.36	0.392
175	9.0	76	4.07	0.577
175	14.7	15	10.58	1.716
175	14.7	30	7.66	0.600
175	14.7	46	5.06	0.585
175	14.7	61	3.64	0.489
175	14.7	76	2.95	0.391

estimated parameter m was found to be satisfactory, being equal on average to 12.6% and 13.8% of the m values, for T=100°C and T=175°C respectively.

The distinct axial evolution of the gas holdup radial profile was also corroborated by the values of the parameters m found, as observed in Tables 5.6 and 5.7. Actually, for all the operating conditions explored, as shown in Figure 5.11, a pronounced decrease of the parameter m with the axial position was observed, particularly for the lower axial positions ($z < 61$ cm) studied. This distinct decrease of the parameter m corresponds to the emergence and/or development of the parabolic gas holdup radial profile. For the higher axial positions ($z \geq 61$ cm), the gas holdup radial profile was found to have reached or have approached stabilization. In fact, for these particular values of z, the parameter m appeared to be a weak function of the axial position, showing a relatively constant value or slightly decreasing with a further increase in the axial position. Consequently, it appeared that the established or final form of the gas holdup radial profile was in general achieved at the axial position $z = 76$ cm, corresponding to a H/D ratio equal to 3.8. Then, assessment of hydrodynamic parameters below this level, or in shallow columns that do not allow the complete development of gas holdup radial profiles (and consequently do not allow the complete development of liquid circulation patterns), could lead to erroneous estimations of the parameter m and

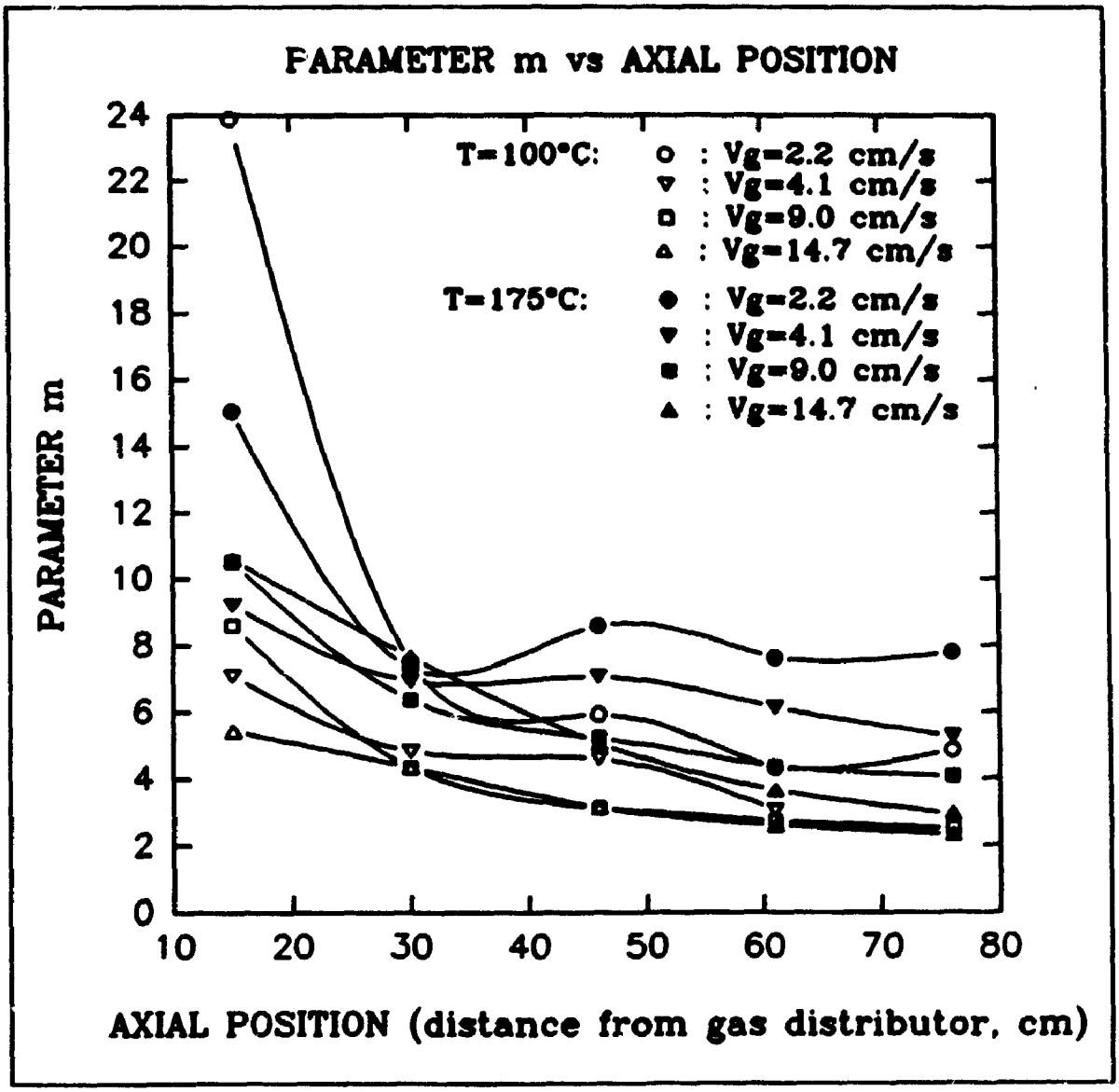

Figure 5.11: Parameter m versus axial position.

166

inadequate representation of the established gas holdup radial profile. These findings are actually in agreement with the findings of Wilkinson et al. (1992), who suggested a minimum H/D ratio equal to 3.0.

Furthermore, in a general way for all the axial positions investigated, the parameter m was found to diminish with an increase in the gas superficial velocity. This is more clearly illustrated, for z = 46, 61 and 76 cm, in Figure 5.12. Actually, the influence of the gas superficial velocity on the parameter m was found to be more pronounced for the lower gas superficial velocities studied (< 9.0 cm/s), while a weaker dependence was observed for the higher gas superficial velocities investigated (≥ 9.0 cm/s). So, as the gas superficial velocity was increased, the gas holdup radial profile became progressively steeper. However, the influence of the gas superficial velocity on the characteristics of the gas holdup radial profile was more apparent for the lower gas superficial velocities studied (< 9.0 cm/s) as compared to the higher ones (≥ 9.0 cm/s). These results are in close agreement with the recent findings of Dudukovic and Devanathan (1992). Dudukovic and Devanathan (1992) studied, using CARPT (Computer Automated Radio-Active Particle Tracking) measurements, the liquid circulation patterns in a 0.19 m diameter bubble column (air-water system). They observed a strong influence of the gas superficial velocity on the axial liquid velocity radial profile at low gas superficial gas

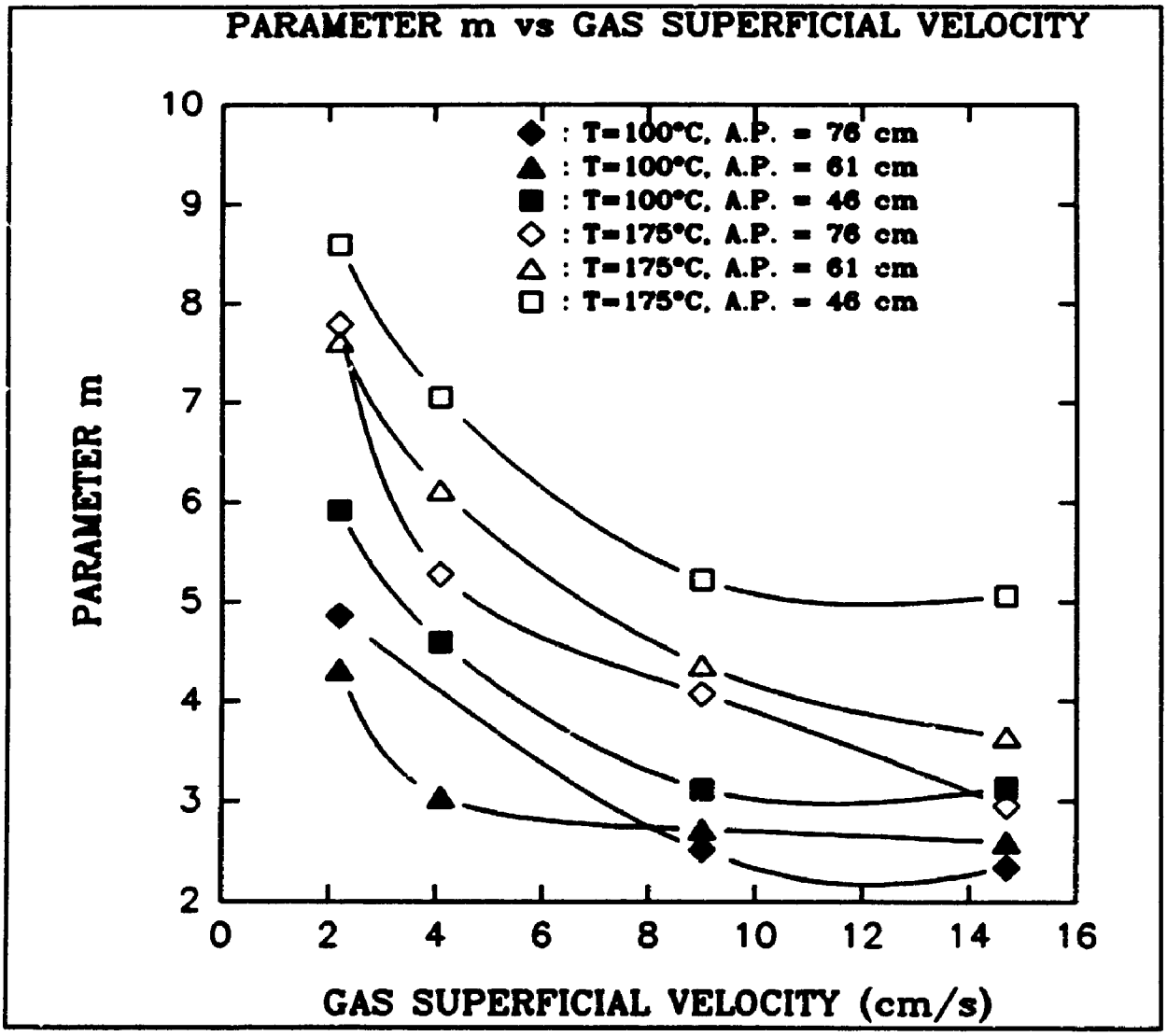

Figure 5.12: Parameter m versus gas superficial velocity.

velocities (< 10 cm/s), while they reported a weaker dependence of the liquid circulation flow rates on the gas superficial velocity for higher gas superficial velocities (> 10 cm/s).

The operating temperature was also found to have a strong influence on the shape of the gas holdup radial profile. Actually, as shown in Tables 5.6 and 5.7, for identical gas superficial velocity and axial position, the parameters m were found to be substantially lower at T=100°C compared to T=175°C. In fact, on average, the parameters m were found to be 35.1% larger at T=175°C than at T=100°C. Hence, less uniform gas holdup radial profiles were observed at the lower temperature investigated, for which condition higher liquid viscosity and consequently larger bubbles, as discussed in a further section, were present.

Ueyama and Miyauchi (1979) suggested a value of m equal to 2 for the air-water system in small diameter columns (≤ 0.15 m) with perforated plate distributors or in larger columns with a single nozzle gas distributor. Since, in the present study, a larger diameter column (0.20 m) and smaller gas bubbles were observed (Section 5.4) as compared to the typical air-water system (presence of a bubble disintegrating regime as compared to the air-water bubble coalescing regime), the gas holdup radial profiles were consequently more uniform, and the values of m consequently larger. Hence, the final values of m,

corresponding to the fully developed gas holdup radial profiles (z = 76 cm) were found to be higher than 2, varying from 4.86 to 2.34 at T=100°C and from 7.79 to 2.95 at T=175°C for gas superficial velocities ranging from 2.2 to 14.7 cm/s.

The influence of the gas superficial velocity on the local values of the gas holdup is illustrated, for z=15 cm and z=46 cm, in Figures 5.13 and 5.14 for T=100°C and in Figures 5.15 and 5.16 for T=175°C. As clearly depicted in these Figures, an increase of the gas superficial velocity favoured an increase of the local gas holdup. However, the influence of the gas superficial velocity on the local gas holdup was found to be a strong function of the radial position. A more pronounced increase of the gas holdup with an increase in the gas superficial velocity was indeed observed in the central section of the column as compared to the area located in proximity to the column wall, as clearly illustrated in Figures 5.17 and 5.18, for T=100°C and T=175°C and z=76 cm and z=30 cm respectively. As shown in these Figures, a gradual decrease of the gas superficial velocity influence on the local values of the gas holdup was observed as the radial position $\theta=r/R$ augmented. For example, for T=100°C and z=46 cm (Figure 5.14), the local gas holdup increased by 297.7% from V_g=2.2 to 14.7 cm/s in the center of the column (θ=0.19), while increasing by 148.0% in the vicinity of the column wall (θ=0.92). This phenomenon was present at all the axial positions studied, including z=76 cm, for which fully

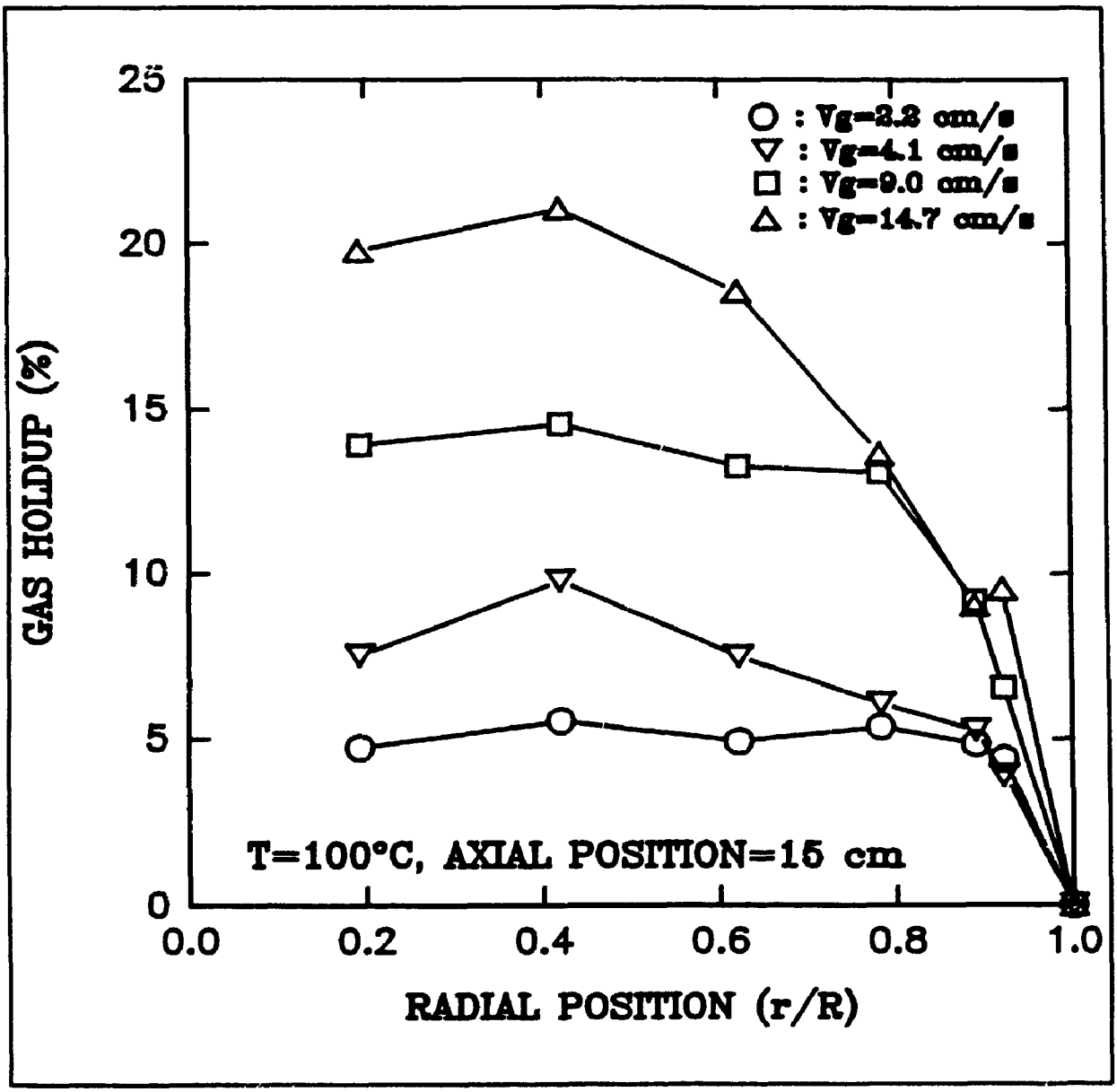

Figure 5.13: Gas holdup vs radial position (T=100°C, z=15 cm)

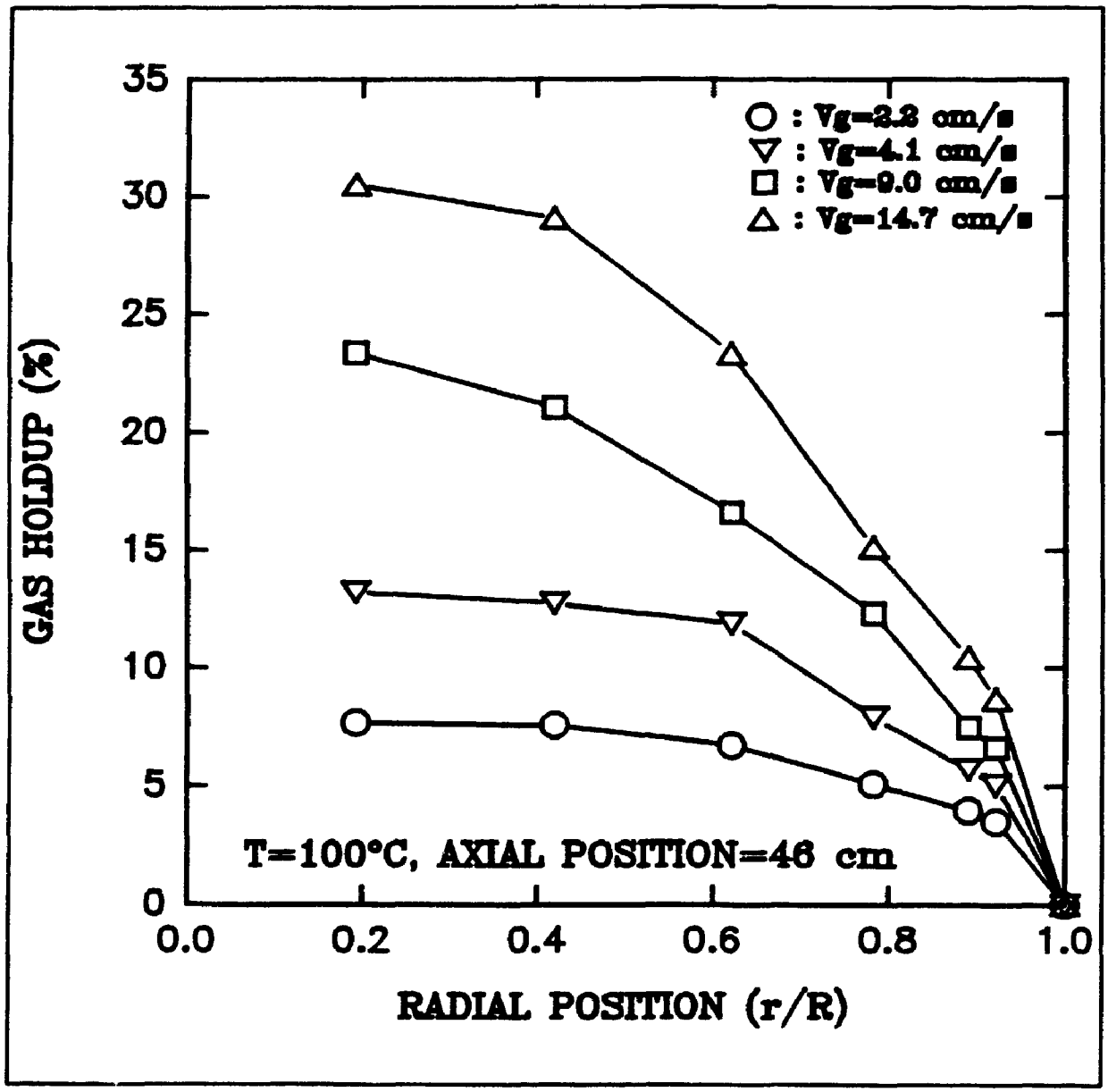

Figure 5.14: Gas holdup vs radial position (T=100°C, z=46 cm)

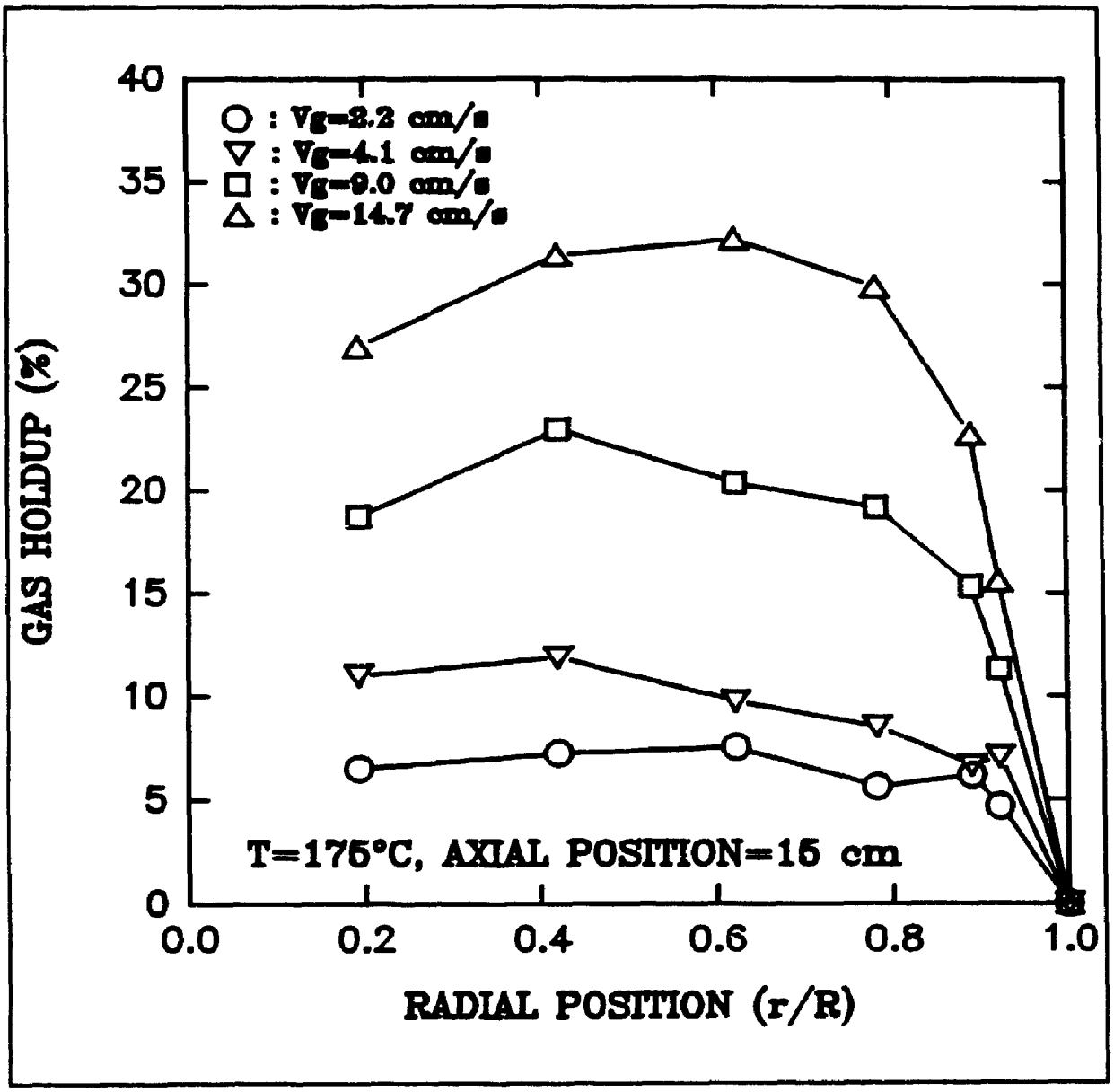

Figure 5.15: Gas holdup vs radial position (T=175°C, z=15 cm)

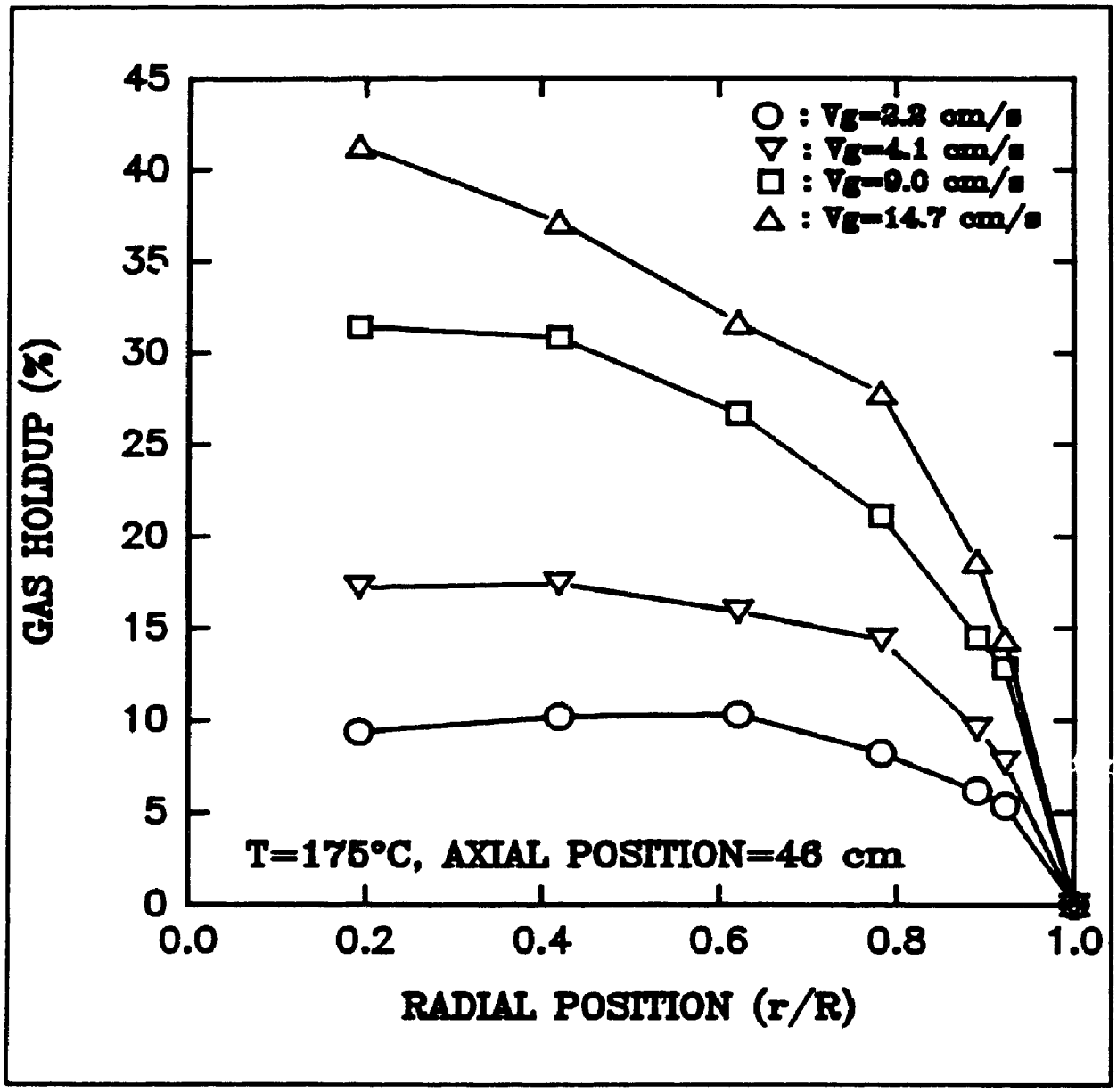

Figure 5.16: Gas holdup vs radial position (T=175°C, z=46 cm)

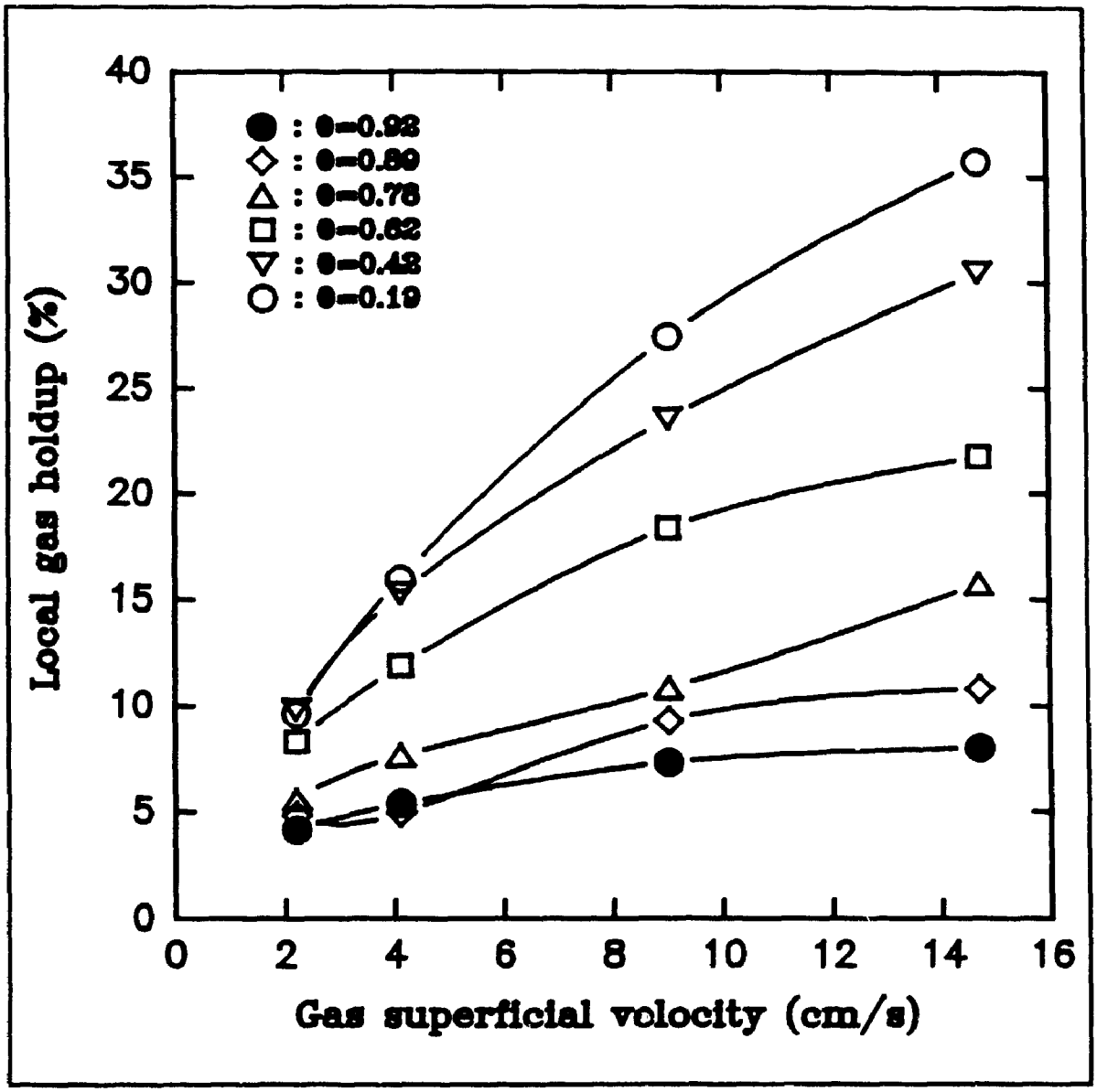

Figure 5.17: Local gas holdup vs gas superficial velocity (T=100°C, z=76 cm)

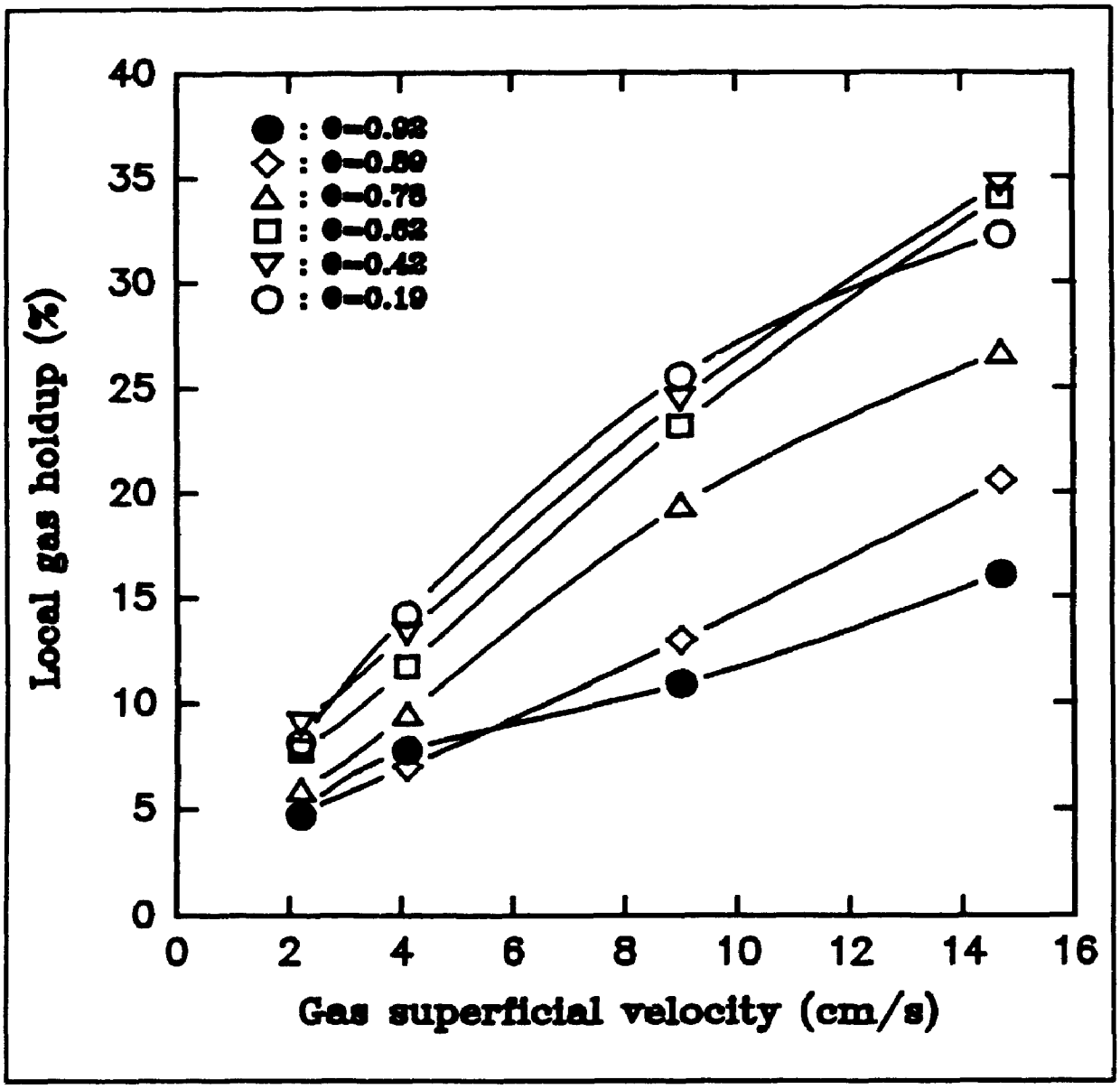

Figure 5.18: Local gas holdup vs gas superficial velocity (T=175°C, z=30 cm)

established gas holdup radial profiles were observed. Consequently, an increase of the gas superficial velocity would influence the radial distribution of the gas holdup in addition to the average gas holdup, as discussed in Section 5.1.2. The influence of the temperature on the local gas holdup was found to be significant for all the operating conditions studied. Actually, as shown in Figure 5.19, the local gas holdup increased as the operating temperature was raised from 100°C to 175°C. In fact, on average, the local gas holdup was found to be 46.9% higher at T=175°C as compared to T=100°C. Furthermore, since, as previously discussed, the gas holdup radial profiles were found to be less uniform at T=100°C than at T=175°C and that the local gas holdup was found to increase with the operating temperature, it was expected that a more pronounced influence of the operating temperature would be perceived in the vicinity of the column wall in comparison to the central region of the column. Such phenomenon was indeed noticed, with an increase of gas holdup of 29.4%, on average, in the central region of the column (θ=0.19) and 55.9% in proximity of the column wall (θ=0.92).

In summary, the consistency of the gas holdup measurements obtained from both sensors (lower and upper) was found to be highly satisfactory, thus confirming minimum disturbance of the flow pattern by the sensors. The gas holdup radial profiles were found to evolve from a relatively uniform profile in the proximity of the gas distributor to a more

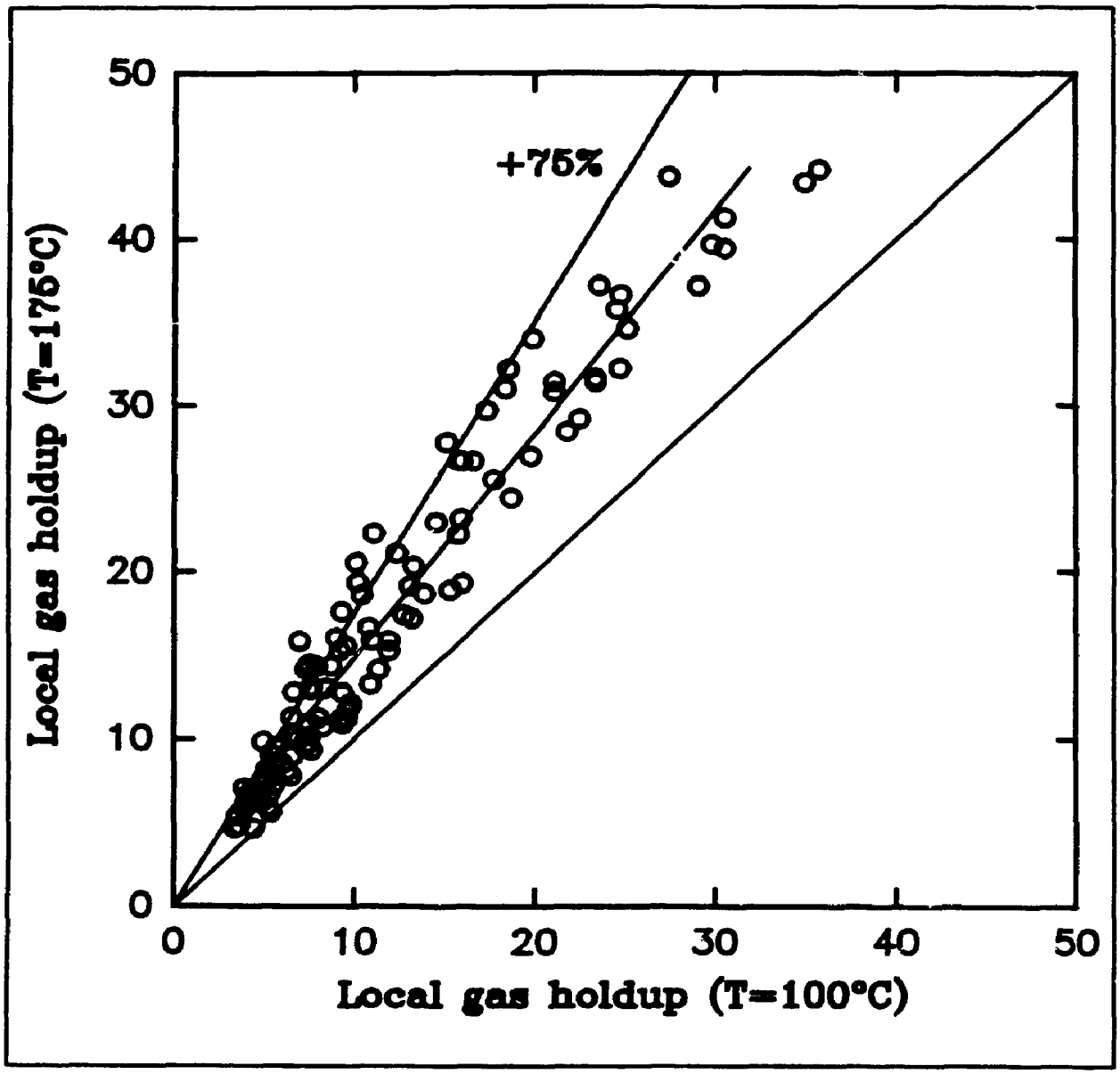

Figure 5.19: Local gas holdup (T=175°C) vs local gas holdup (T=100°C)

pronounced parabolic profile at higher axial positions. However, all profiles were successfully represented by the parabolic equation. The stabilized gas holdup radial profiles observed, for all the operating conditions, were found to be sharper close to the column wall and flatter in the central area than the ones observed in aqueous systems. These original findings (no information concerning gas holdup radial profile was known to have been previously reported for systems of relevance to methanol synthesis reactors and other reactors dealing with hydrocarbon media) are particularly important given the significance of assessments of gas holdup radial profiles in deriving the liquid mixing flow patterns in bubble columns. The stabilization of the gas holdup radial profiles was observed at a height of approximately z=76 cm. This confirms the importance of a minimum liquid height in properly assessing bubble column hydrodynamic characteristics. The gas holdup radial profiles were found to become less uniform as the temperature was decreased and the gas superficial velocity increased, while the local gas holdup values were noted to increase with both, an increase of the gas superficial velocity and the temperature.

5.1.2 Average gas holdup

The average gas holdup, for a given axial position, was calculated using Equation 5.3. For all the operating conditions studied, the average gas holdup was found to slightly increase with the axial position, as illustrated in Figure 5.20.

The average gas holdup derived from the fibre optic local gas holdup measurements were validated by performing static pressure profile measurements along the column. As described in Section 3.2, seven pressure taps, located at 2.5, 15.2, 25.4, 40.6, 55.9, 71.1 and 91.4 cm above the gas distributor were connected to a pressure transducer via a mechanical switch wafer. Details concerning the static pressure measuring system as well as calibration and testing methodologies were given in Section 3.2.

All the static pressure profiles recorded were successfully fitted to a straight line with linear regression coefficients in excess of 0.991 and an average linear regression coefficient equal to 0.998. The constant pressure drop observed along the column height was indeed consistent with the fibre optic measurements, for which only a slight increase of the radial average gas holdup with the axial position was observed. A summary of the results obtained for all the pressure profiles recorded are presented in Appendix 6. The

180

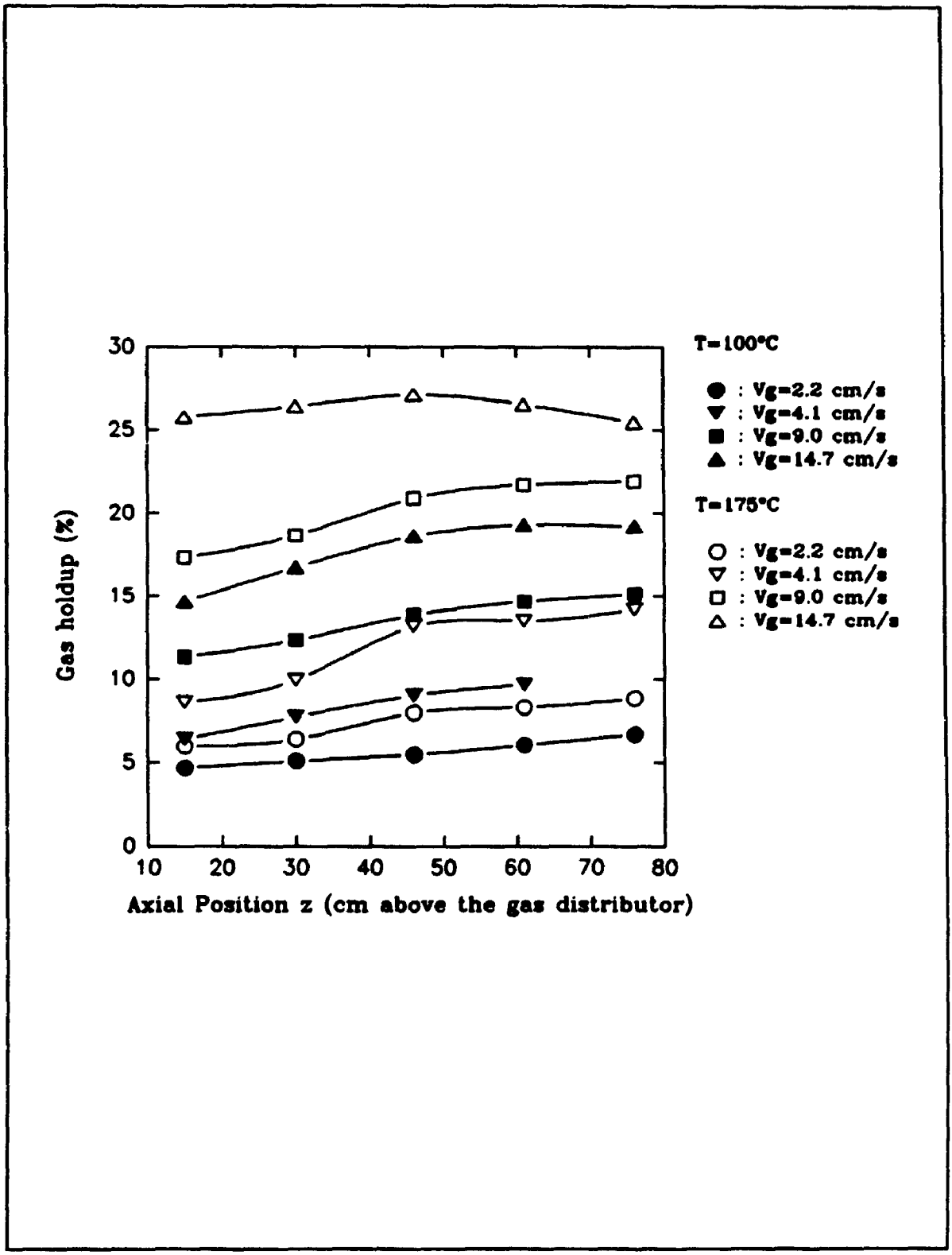

Figure 5.20: Average gas holdup vs axial position.

average gas holdup can be derived from the static pressure profile using the two following equations:

$$\epsilon_g + \epsilon_l = 1 \qquad (5.4)$$

$$\frac{\Delta P}{H_b} = g(\epsilon_g \rho_g + \epsilon_l \rho_l) \qquad (5.5)$$

The average gas holdup values derived from the static pressure profile measurements are presented in Table 5.8.

For all the experiments performed at T=100°C and T=175°C, good agreement was obtained between the gas holdup derived from pressure profile measurements and fibre optic sensor measurements. Actually, as illustrated in Figure 5.21, the fibre optic sensor radial average gas holdup values obtained at z=46 cm (□) (corresponding to the axial position located approximately in the middle of the window investigated by static pressure measurements: ≈ 46 cm) as well as the axial average of the fibre optic sensor radial average gas holdup values obtained for all the axial positions studied were found to be approximately within 10% of the gas holdup values derived from pressure profile measurements. These results demonstrated the validity of the fibre optic sensors' gas holdup measurements performed at T=100°C and T=175°C. For the measurements conducted at ambient temperature (T=25°C), more significant discrepancies were observed between the gas holdup

182

Table 5.8

Gas holdup derived from pressure profile measurements

Temperature (°C)	V_g (cm/s)	Gas holdup (%)
25	2.2	3.8
25	4.1	5.3
25	9.0	11.0
25	14.7	12.7
100	2.2	6.2
100	4.1	9.1
100	9.0	14.7
100	14.7	17.9
175	2.2	7.2
175	4.1	14.8

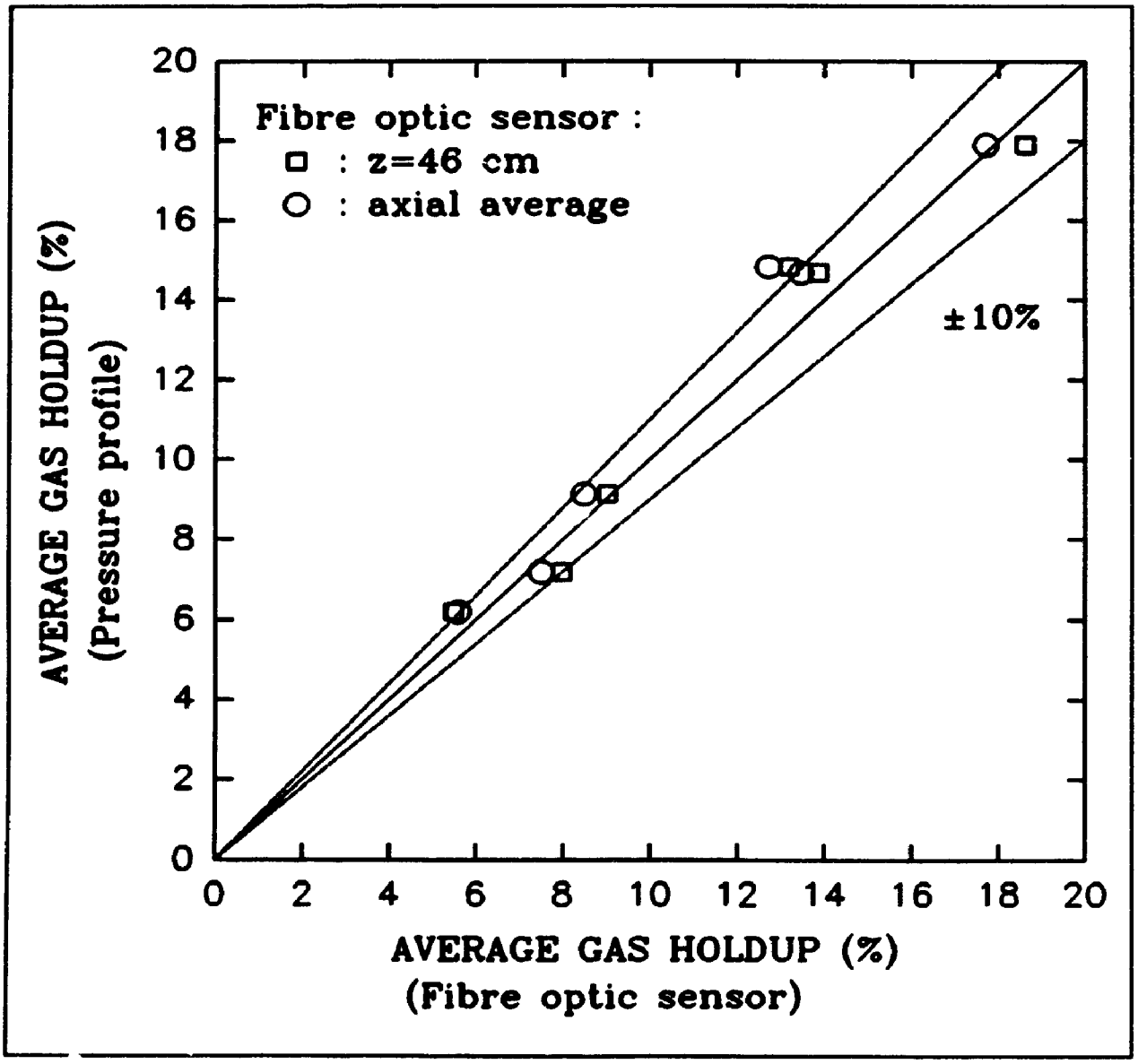

Figure 5.21: Average gas holdup derived from pressure profile measurements vs average gas holdup derived from fibre optic sensor measurements (results obtained at T=100°C and T=175°C)

values generated from pressure profiles and fibre optic sensors' measurements. In fact, the gas holdup values derived from fibre optic sensors' measurements were found to be, on average, 48.8% lower than the ones obtained from pressure profile experiments. In order to assess the cause of this inconsistency, a series of experiments were conducted in a 16 cm by 21 cm rectangular plexiglas column, having an approximately similar cross section (336 cm^2) as the main column (314 cm^2). The plexiglas column, 82 cm in height, was equipped with a gas pipe sparger with hole diameters (1.59 mm) equal to the ones of the perforated plate present in the main column. The column was filled with the paraffinic oil LP-100 up to a height of 50 cm above the gas sparger. The nitrogen flow rate was adjusted to match the gas superficial velocities previously studied in the main column (2.2 - 14.7 cm/s).

Visual observation of the column allowed one to immediately notice that under all the gas superficial velocities studied, a significant fraction of the gas was present in the form of very small gas bubbles, estimated to be between 0.3-0.5 mm in diameter, as well as fine bubbles (0.5-2 mm in diameter). In order to approximately evaluate the contribution to the total gas holdup of these particular fractions of the gas bubble population, the dynamic gas disengagement (DGD) technique was applied. The liquid level, free of gas, was visually determined. Then, the gas supply was turned on and the column was operated under this particular condition for a sufficient

period of time for steady state condition to be reached (constant bed level). The bed level was then visually evaluated after which the gas supply was quickly interrupted by simply disconnecting the entry gas line. The decrease in the bed level was monitored until the initial liquid level (free of gas) was reached. For all the gas superficial velocities studied (2.2, 4.1, 9.0 and 14.7 cm/s), the gas disengagement process followed a similar pattern. The bed level rapidly decreased to reach approximately 30% to 40% of the total bed expansion. This initial contraction of the bed was then followed by a calm and slow bed level decrease until the initial liquid level was reached. The initial contraction phase corresponded to the disengagement of the larger and then faster gas bubbles accompanied by an entrained fraction of the very small and fine gas bubbles. The second bed contraction phase corresponded to the disengagement of the very small and fine gas bubbles, or in other words, the slower gas bubbles. Consequently, it could be safely stated that the very small bubbles and the fine bubbles contributed to a minimum of 30 to 40% of the total gas holdup and possibly more since an unknown portion of these small bubbles were more rapidly entrained during the initial disengagement phase. As discussed in previous publications (Chabot, 1989; Chabot et al., 1992), the limiting smaller bubble size to be detected by the actual fibre optic sensors, in cold oil (μ_l=0.0155 Kg/m-s), is approximately 0.5-2 mm. Furthermore, since the very small gas bubbles present in the plexiglas column were visually

186

estimated to be below this range (0.3-0.5 mm), while the fine bubbles were within this range (0.5-2 mm), these fractions of the total gas bubble population were difficultly seen by the fibre optic sensors. Since these difficultly detected fractions of the total bubble population, at room temperature, were found to represent at least 30% to 40% of the gas volumetric fraction, it would be logical to expect that the gas holdup derived from fibre optic sensors be at least 30 to 40% lower than the one obtained from pressure profile measurements. Actually, as previously mentioned, an average negative deviation of 48.8% was observed between the fibre optic sensor and pressure profile derived gas holdup values. Consequently, considering the fact that the fibre optic sensors' measurements are representative of only approximately 40-50% of the total gas volumetric fraction, and are clearly discriminatory toward a particular gas bubble population (very small bubbles), the fibre optic sensors' measurements performed at ambient temperature were not considered further and only qualitative reference to these results will be made in the present study. Such small bubbles (0.3-2 mm) were indeed present at T=100°C and T=175°C. However, the lower viscosity of the oil (μ_l=0.00086 Kg/m-s at T=175°C, μ_l=0.003 Kg/m-s at T=100°C) under these conditions, allowed a better contact between these small bubbles and the fibre optic sensors' detecting tips. Thus, bubbles as small as 0.2 mm were satisfactorily viewed by the optical sensors at higher temperatures.

The influence of the operating temperature on the average gas holdup is illustrated in Figure 5.22. Both, gas holdup values derived from pressure profile measurements (including 95% confidence interval) and gas holdup values derived from fibre optic sensor (z=46 cm) were represented. First, significant agreement between measurements coming from pressure profiles and fibre optic sensors were observed. These results confirmed the validity of the fibre optic sensor technology in assessing gas phase parameters, as recently corroborated by Mudde et al. (1992). Secondly, and as shown in this Figure, the average gas holdup was found to increase with an increase of the operating temperature. It is well documented in the literature (Prince and Blanch, 1990) that higher liquid viscosity promotes coalescence of bubbles, whereas bubble breakup rates decrease for high liquid viscosity. Consequently, on the basis of both these trends, it can be argued that higher liquid viscosity promotes the existence of larger bubbles and then faster bubbles, thus favouring lower gas holdup. Hence, knowing that the liquid viscosity is an inverse function of the temperature (Figure A1.2), an increase of the temperature promoted lower liquid viscosity and consequently higher gas holdup values. Furthermore, the liquid surface tension was also found to have a pronounced effect on bubble breakup and thus on gas holdup (Wilkinson et al., 1992). At lower surface tension, fewer large bubbles occur and consequently higher gas holdup is observed, due to the fact that surface tension forces oppose deformation and

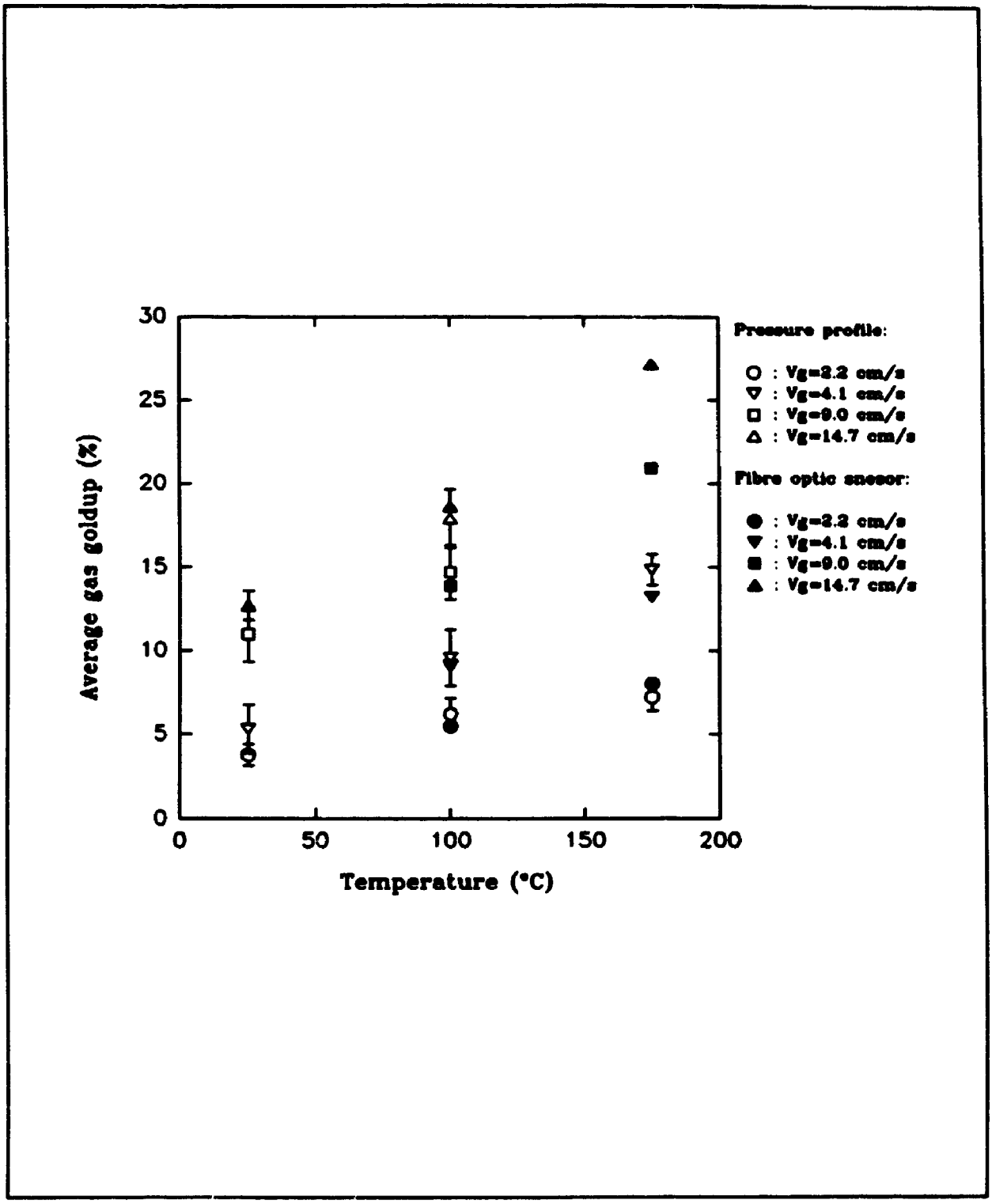

Figure 5.22: Average gas holdup vs temperature

189

bubble breakup (Prince and Blanch, 1990). Since, as shown in Figure A1.3, the surface tension of the liquid is an inverse function of the temperature, higher temperature favoured lower surface tension and thus higher gas holdup. Consequently, the increase of the gas holdup with the operating temperature observed in the present study was consistent with the additive influence of both the liquid viscosity and the liquid surface tension.

The influence of the gas superficial velocity on the average gas holdup is presented in Figures 5.23, 5.24 and 5.25 for T=25°C, T=100°C and T=175°C respectively. As shown in these Figures, the average gas holdup increased with an increase of the gas superficial velocity. The increase of the average gas holdup with the gas superficial velocity was found to be proportional to $V_g^{0.64}$, $V_g^{0.61}$ and $V_g^{0.60}$ for T=25°C, T=100°C and T=175°C respectively. This consistent dependency of the gas holdup on V_g is typical of the presence of the churn turbulent regime, where $\epsilon_g \approx V_g^{0.4-0.6}$. This indeed suggests that all the experiments performed were done under the churn turbulent regime. In the homogeneous bubbling regime, a linear increase of the gas holdup with the gas superficial velocity would be expected. The suspected presence of the churn turbulent regime under all the operating conditions investigated ($V_g \geq$ 2.2 cm/s) was also consistent with the correlation by Wilkinson et al. (1992), which predicted a gas superficial transition velocity between the homogeneous bubbling regime

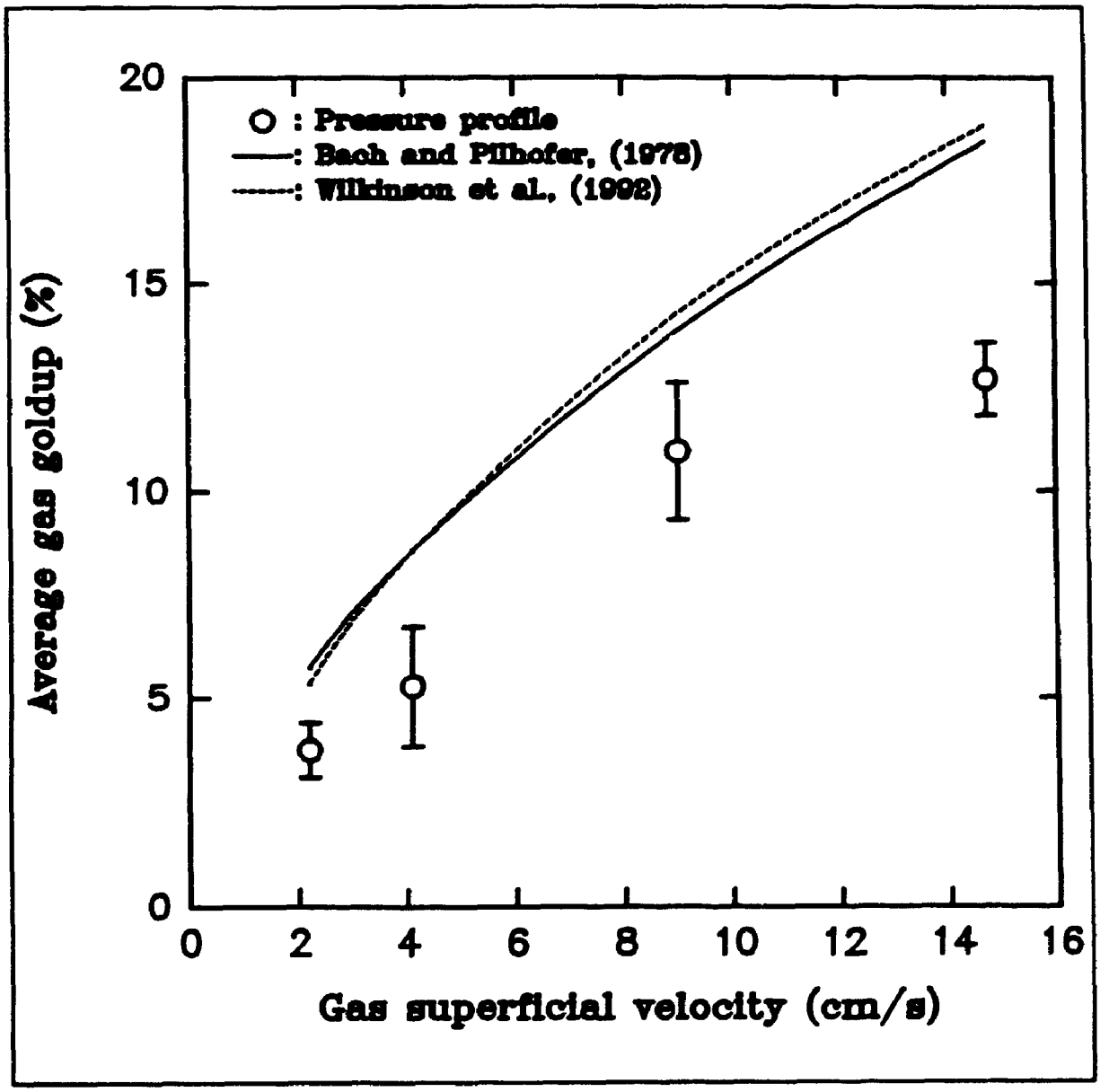

Figure 5.23: Average gas holdup vs gas superficial velocity (T=25°C)

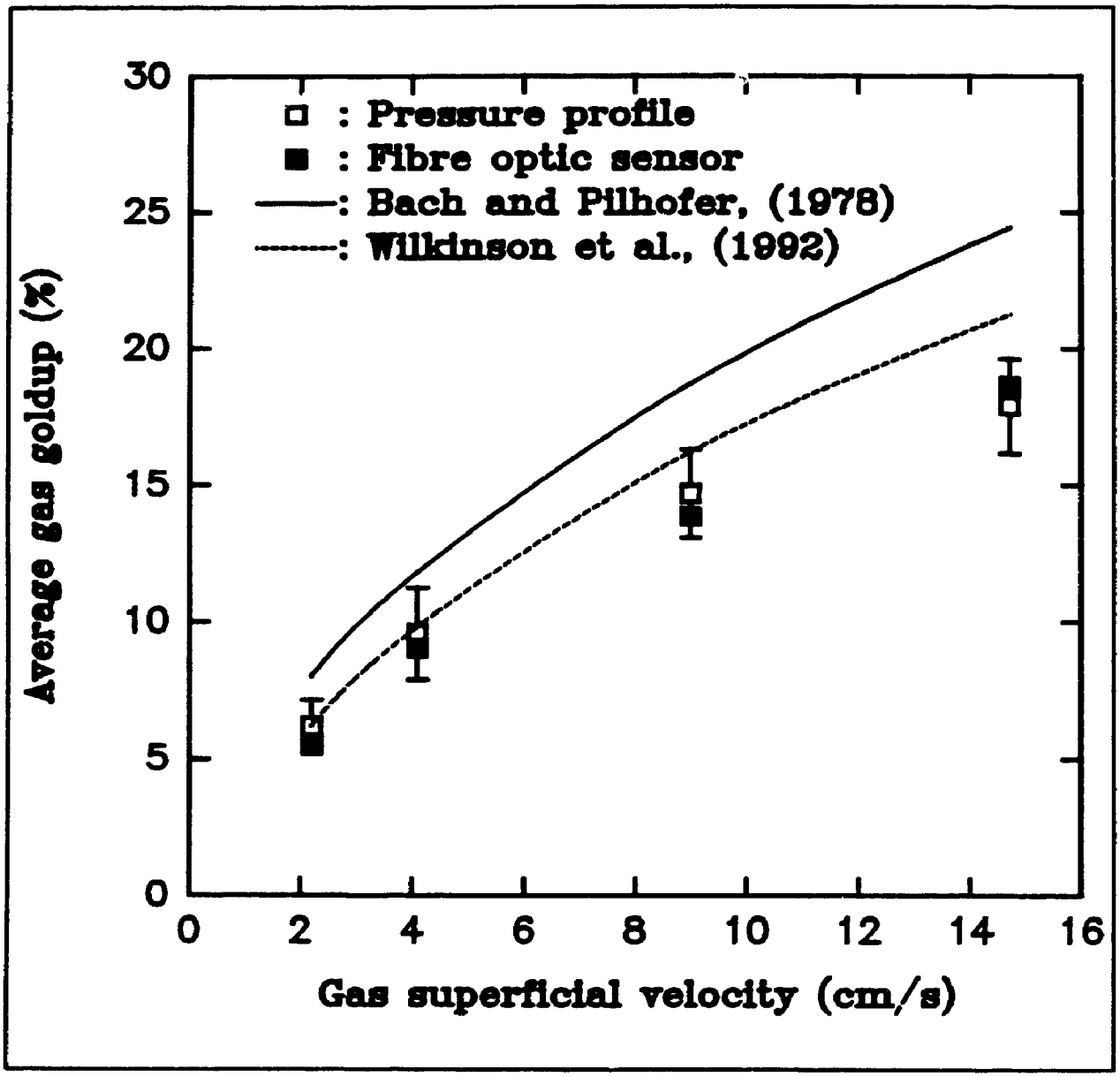

Figure 5.24: Average gas holdup vs gas superficial velocity (T=100°C)

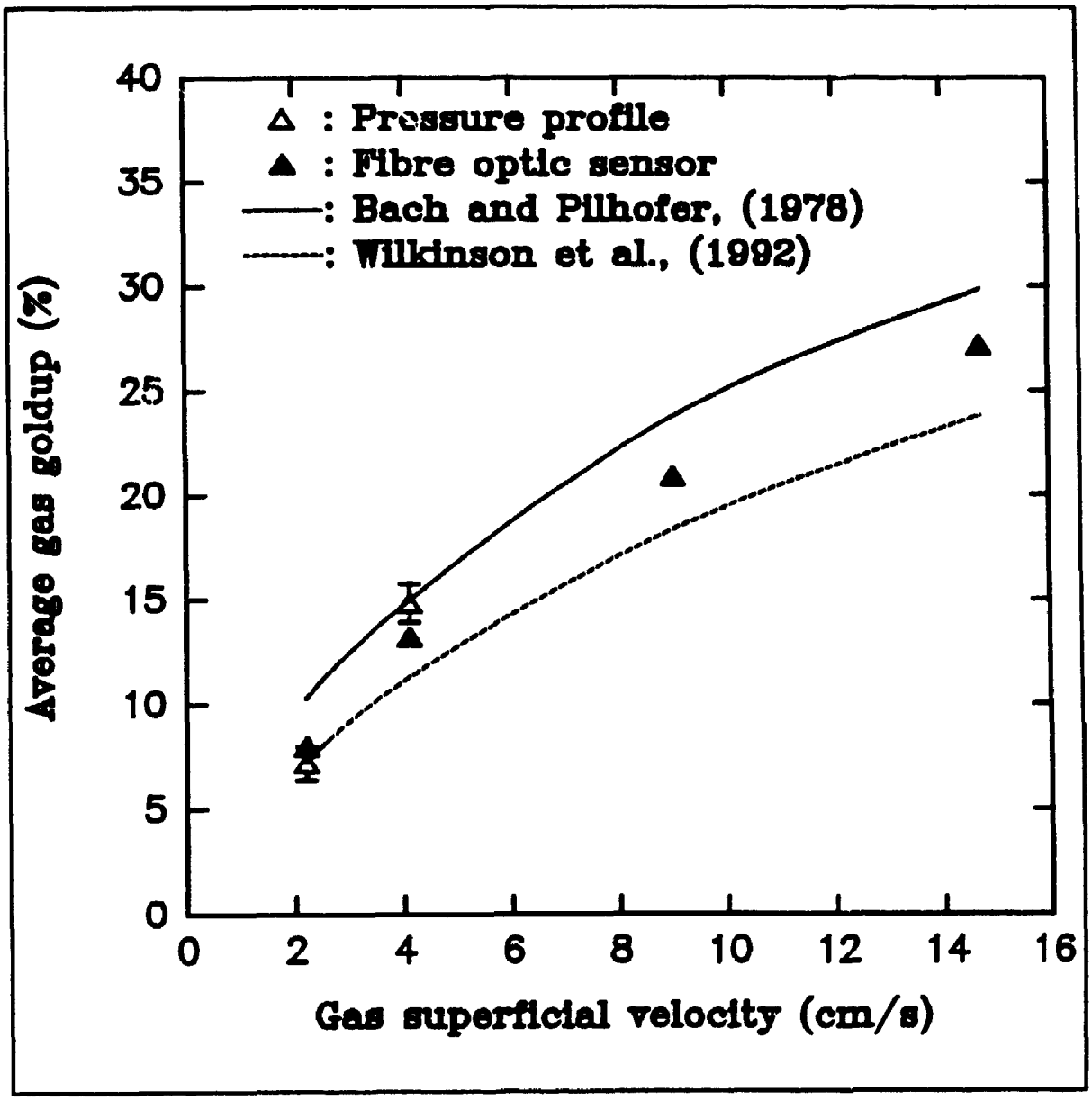

Figure 5.25: Average gas holdup vs gas superficial velocity (T=175°C)

and the churn turbulent regime equal to: $V_{g,trans}$=4.89 x 10^{-4} cm/s, 0.00699 cm/s and 0.137 cm/s for T=25°C, T=100°C and T=175°C respectively. The presence of the churn turbulent regime was also reported in a similar system (Fischer-Tropsch) for the same range of gas superficial velocity (Bukur and Daly, 1987).

The experimental average gas holdup values obtained at T=100°C and T=175°C were satisfactorily depicted by the correlation recently proposed by Wilkinson et al. (1992). This correlation, incorporating the effects of liquid density, viscosity and surface tension as well as gas density, represented the measured gas holdups with an average deviation equal to 13.3% and 12.0% at T=100°C and T=175°C respectively. However, poor representation of the experimental gas holdup measurements was observed at ambient temperature, with average deviations in excess of 45%, despite the fact that the liquid physical properties (density, viscosity, surface tension) were well within the recommended range for this correlation. Similar partial agreements between predictions from available gas holdup correlations and experimental data in presence of hydrocarbons were previously reported (Quicker and Deckwer, 1981a), suggesting that the readily measurable physico-chemical properties of the liquid phase (density, viscosity, surface tension) are insufficient to describe the fluid dynamic characteristics of a gas/liquid system. This was also verified in the case of the correlation by Bach and Pilhofer (1978), which overestimated the experimental gas holdup values

with average deviations equal to 46.6%, 35.9% and 16.0% at T=25°, T=100°C and T=175°C respectively. This systematic positive deviation could be due, in the present case, to the relatively small column diameter, below the recommended 15 cm, and the small perforated plate gas distributor hole sizes (0.5 mm) used in the study by Bach and Pilhofer (1978). The use of small sparger openings (below the recommended 1-2 mm minimum range) is known to contribute to the formation of smaller gas bubbles, thus favouring higher gas holdup values (Wilkinson et al., 1992). Furthermore, the wall effects in a small diameter column (below the recommended 15 cm diameter) was recently reported to promote larger gas holdup values (Wilkinson et al., 1992). Both correlations were found to represent somewhat differently the experimental gas holdup values for the two temperatures investigated. Both correlations were developed for pure liquids, while, in the present study, a complex liquid hydrocarbon mixture was used. Bach and Pilhofer (1978) indeed demonstrated that liquid mixtures behave differently from pure liquids, which could explain the overall changes in the quality of fitting as the temperature varied. The correlation proposed by Hikita et al. (1980) systematically overestimated the measured gas holdup values. Positive deviations in excess of 30% were observed. This correlation, as discussed in Chapter 1, was developed from data obtained in a small diameter column (D_c < 0.15 m), for which higher gas holdup values are expected. The correlation proposed by Akita and Yoshida (1973) was found to provide a

conservative representation of the experimental gas holdups, with negative deviations in excess of 20%. These two correlations (Hikita et al., 1980; Akita and Yoshida, 1973) were not advised, as discussed in Chapter 1, for complex hydrocarbon mixtures.

A definite influence of the gas distributor, for gas distributors providing with pore size openings smaller than 1 mm, was suggested (Quicker and Deckwer, 1981a; Wilkinson et al., 1992). Consequently, when performing experiments using, as gas distributor, a metallic porous distributor with average pore opening equal to 20 μm, a substantial change in the hydrodynamic characteristics of the system should be observed. Effectively, at z=76 cm, T=100°C, Θ=0.19, and V_g=2.2 cm/s, a gas holdup value equal to 21.0% was observed with the porous distributor, as compared to a value of 9.6% in presence of the perforated plate distributor (hole diameter = 1.59 mm) under the same conditions. As, expected, the average bubble chord length was found to be substantially smaller in presence of the porous distributor (0.6 mm) as compared to the one observed in presence of the perforated plate distributor (3.2 mm). These results were confirmed using pressure profile measurements. Actually, the average gas holdup observed at T=100°C and V_g=2.2 cm/s, using this technique, was equal to 18.8% as compared to 6.2% for tne perforated plate experiments under identical conditions. The distinct influence of the gas distributor configurations on the fluid dynamic

196

characteristics of the system, even at a significant distance from the gas distributor (z=76 cm), certainly suggests the presence of a non-coalescing or slowly coalescing system, typical of foaming systems. Bukur et al. (1987) indeed mentioned that in systems which have foaming capacity, the gas holdup is strongly affected by the distributor type. Sintered metal plates and orifice plate distributors with small holes give high holdups, whereas orifice plates with large openings give lower gas holdups. Similar conclusions were obtained by Quicker and Deckwer (1981a) in presence of hydrocarbons. Having literature warnings concerning the extreme influence of the porous plate gas distributor on the fluid dynamic characteristics of the present system, and the risky generalization of any results obtained under such conditions, all the experimental measurements performed in this study were done under the more reliable influence of the perforated plate gas distributor with hole diameter larger than the recommended minimum value (1 mm).

Excellent correspondence (within 10%) was observed between pressure profiles and fibre optic sensors' gas holdup measurements at T=100°C and T=175°C, thus validating the optical sensor technology measurements. In general, poor agreement was observed between the existing correlations (Akita and Yoshida, 1973; Hikita et al., 1980; Bach and Pilhofer, 1978) and the experimentally measured gas holdup values, with the exception of the Wilkinson et al. (1992)

model. This model provided satisfactory representation of the data, with average deviations equal to 13.3% and 12.0% at T=100°C and T=175°C respectively. These previous results reiterate the importance of direct experimental measurements in obtaining good assessment of the gas holdup and other gas phase parameters, especially in presence of complex liquid mixtures.

5.1.3 Bubble velocity

As discussed in Section 4.1.3, the bubble rise velocity was obtained by dividing the vertical spacing between the two optical sensors (5 mm) by the time delay observed at the peak of the normalized cross correlation function (Chabot et al., 1992). This bubble velocity represents a time averaged (over the total data acquisition time: 50 seconds) average absolute (with respect with the column wall) local bubble velocity in the upward axial position. The validity of the cross correlation technique in giving a true representation of the bubble rise velocity was verified by a number of authors. For example, Lubbesmeyer (1984) has shown that in the case of bubbly flow, the velocity that can be constructed from the time delay obtained through cross correlation analysis and the known distance between the two sensors is very close to the true bubble velocity. Several other authors have reported experimental evidences supporting this fact, including, among others, Van der Hagen (1989) for an air/water loop, Miyzaki et al. (1973) for N_2/water, and Matsumoto et al. (1986) for solid particles suspensions. Nevertheless, in order to confirm the validity of the cross correlation technique in giving a true representation of the bubble velocity under the actual operating conditions investigated in the present study, verifications were performed. For every radial and axial position, temperature and gas superficial velocity studied, the individual bubble velocity distributions (based on number

of bubbles) were constructed. The individual bubble velocity distributions were extracted from the bubble axial chord length distribution analysis, as discussed in Sections 4.4 and 5.1.5. As shown in a typical example, Figure 5.26, the individual bubble rise velocity distributions were, as it was also the case for the bubble axial chord length distributions (Section 5.1.4), skewly distributed (narrow peak, followed by a long slowly declining tail). These individual bubble rise velocity distributions were used to validate the average bubble rise velocity derived from the cross correlation analysis. The first moment (arithmetic average) of every individual bubble rise velocity distribution was calculated and compared to the average bubble rise velocity obtained from the cross correlation analysis. On average, for all the conditions studied, both, the average bubble rise velocities derived from the cross correlation analysis and the ones obtained from the individual bubble rise velocity distributions were safely within 10%, thus validating the ability of the cross correlation analysis in providing a true representation of the bubble rise velocity.

The ability of the fibre optic sensor to measure local bubble rise velocity provides the possibility to perform a gas mass balance. Actually, for a given axial position, a cross-sectional average gas superficial velocity can be evaluated using the following expression:

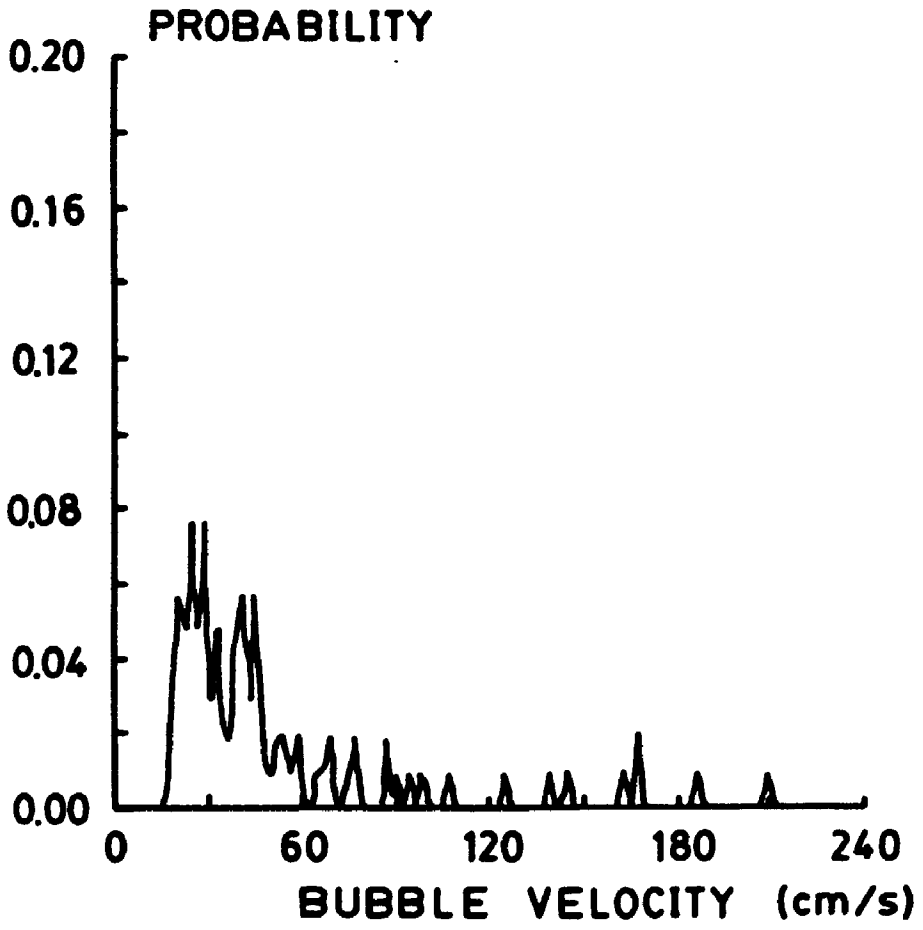

Figure 5.26: Typical bubble velocity distribution
(T=100°C, V_g=2.2 cm/s, z=30 cm, θ=0.92)

$$V_g = \frac{1}{\pi R^2} \int_0^R V_{b,loc}\ \epsilon_{g,loc}\ 2\pi r dr \qquad (5.6)$$

where V_g is the cross-sectional average gas superficial velocity, $V_{b,loc}$ is the local average bubble rise velocity measured by the optical sensors, and $\epsilon_{g,loc}$ is the local gas holdup value also obtained from the fibre optic measurements. This analysis implies, of course, that all the gas present at a given location ($\epsilon_{g,loc}$) rises with an average velocity $V_{b,loc}$. Since, as previously discussed, the individual bubble rise velocity distributions observed were, in general, relatively wide, the gas present at a given location was actually rising with a wide distribution of velocity. In order to verify that such phenomenon was not introducing undue imprecisions in the gas mass balance analysis, the following verification was performed. The gas holdup based individual bubble rise velocity distribution was constructed and used to perform the gas mass balance. This analysis allowed to confirm that the fact of using average quantities ($\epsilon_{g,loc}$, $V_{b,loc}$) in Equation 5.6 did not, in the present case, introduce error in excess of 5%.

Equation 5.6 is based on the assumption of symmetrical or very close to symmetrical gas flow in the radial direction. This assumption thus requires an effective gas distribution system providing both the appropriate pressure drop and a symmetrical distribution of openings throughout the cross section of the

column. As discussed in Section 5.1.1, both these conditions were met under all the operating conditions investigated and thus symmetrical gas flow at the distributor level was safely assumed. In addition, the vertical alignment of the column was carefully verified using precise level measurements, thus insuring symmetrical circulation flow patterns in the system.

The superficial gas velocity obtained from Equation 5.6 was compared to the actual gas superficial velocity, taking special care to correct the former one for any pressure and/or vapour pressure effects. As recently reported by Dudukovic and Devanathan (1992), typical liquid circulation patterns, normally characterized by upward liquid circulation in the center of the column and downward liquid circulation in the vicinity of the column wall were observed in the bulk of the column, most particularly for the cases where important radial non-uniformities of the gas holdup profiles exist (higher axial positions, higher gas superficial velocities). Under such conditions, a fraction of the gas bubbles is entrained downward with the liquid current, as reported by Dudukovic and Devanathan (1992). Since only the average upward dominant gas bubble velocity vector (forward cross correlation) is considered in the mass balance, any gas bubbles travelling downward with the liquid (particularly in the vicinity of the column wall) are considered to be travelling with the average upward velocity vector evaluated from the forward cross correlation analysis. This procedure leads to an

overestimation of the gas flow rate in cases where gas bubble recirculation is important since both, bubbles travelling upward and downward are seen by the optical sensors ($\epsilon_{g,loc}$, Equation 5.6), but are all assumed to travel upward with the average upward velocity vector derived from the forward cross correlation analysis ($V_{g,loc}$, Equation 5.6). Then, the results of the gas balance analysis have to be considered carefully. In this respect, the gas balance analysis was limited to cases where liquid recirculation flow patterns, though present, were minimum, and consequently the contribution of downward gas recirculation was minimum: the lower axial position (z=15 cm). The presence of any downward liquid circulation current, inducing gas recirculation, would favour overestimation of the calculated (Equation 5.6) gas superficial velocity.

The deviation between the calculated and the actual gas superficial velocity, obtained at z=15 cm under various operating conditions, is presented in Table 5.9. In general, reasonable agreement was observed between the calculated and the actual gas superficial velocity, with average deviations between both values equal to 10.9% and 18.3% for T=100°C and T=175°C respectively. For most cases, as expected in presence of liquid circulation induced gas bubbles downward recirculation, the calculated gas superficial velocity was systematically higher than the actual gas superficial velocity. The highest deviations were obtained at the lowest gas superficial velocity (V_g=2.2 cm/s), for which, as

204

Table 5.9

Mass Balance of gas phase (z=15 cm)
(% error of calculated vs actual gas superficial velocity)

Superficial Gas Velocity (cm/s)	T=100°C	T=175°C
2.2	+ 27.9%	+ 32.7%
4.1	- 4.9%	+ 3.8%
9.0	+ 9.8%	+ 14.9%
14.7	+ 1.1%	+ 21.9%

discussed in a further section, a distinct liquid recirculation cell was observed, thus promoting gas recirculation and consequently overestimation of the gas superficial velocity (Equation 5.6). The deviations between the calculated and the actual gas superficial velocities were slightly higher at T=175°C as compared to T=100°C. This can be explained by the presence of smaller gas bubbles (Section 5.1.4), which are more easily being entrained with the descending liquid circulation patterns, already present in the bottom of the column under these conditions, as discussed later in this Chapter. The gas holdup values implemented in Equation 5.6, measured with the fibre optic sensors, were already independently successfully validated using pressure profile measurements, as discussed in Section 5.1.2. Thus, the satisfactory agreement between actual and calculated (Equation 5.6) gas superficial velocities provided a verification of the ability of the fibre optic sensor to perform local bubble velocity measurements. As expected, as the axial position increased, a more pronounced positive deviation was observed between the calculated (Equation 5.6) and the actual gas superficial velocity. In some cases (highest axial position and gas superficial velocity: z=76 cm, V_g=14.7 cm/s), due to the presence of more vigorous liquid circulation induced gas recirculation, positive deviations of up to 60% was observed. These results clearly emphasized the extreme importance of using and interpreting gas mass balance analysis testing with extreme caution. In the present study,

however, the proper implementation of the gas mass balance analysis (z=15 cm), allowed verification of the excellent ability of the optical sensor technology to measure gas bubble characteristics in bubble column systems.

Typical radial profiles of the bubble rise velocities are presented in Figures 5.27a to 5.27d for T=100°C and in Figures 5.27e to 5.27h for T=175°C. Each local bubble rise velocity presented in these Figures represents, in general, the average of at least three experiments. A summary of the cross correlation analysis results used in deriving the bubble rise velocities for all the experiments presented in Figures 5.27a to 5.27h are summarized in Appendix 7, while two examples of typical cross correlograms obtained at T=100°C and T=175°C are presented in Figures 5.28a and 5.28b respectively. As illustrated in these Figures, and presented in detail in Appendix 7, the amplitude of the cross correlation peak varied with the radial and axial positions as well as the gas superficial velocity. This is consistent with the fact that the cross correlation peak amplitude is a function of the statistical correspondence between the two time series evaluated (obtained from the lower and upper sensors respectively). This statistical correspondence is a function of the probability that a particular bubble or group of bubbles will successfully be detected by the two sensors. This probability is in turn a function of the total bubble population considered and of the main bubble velocity vector

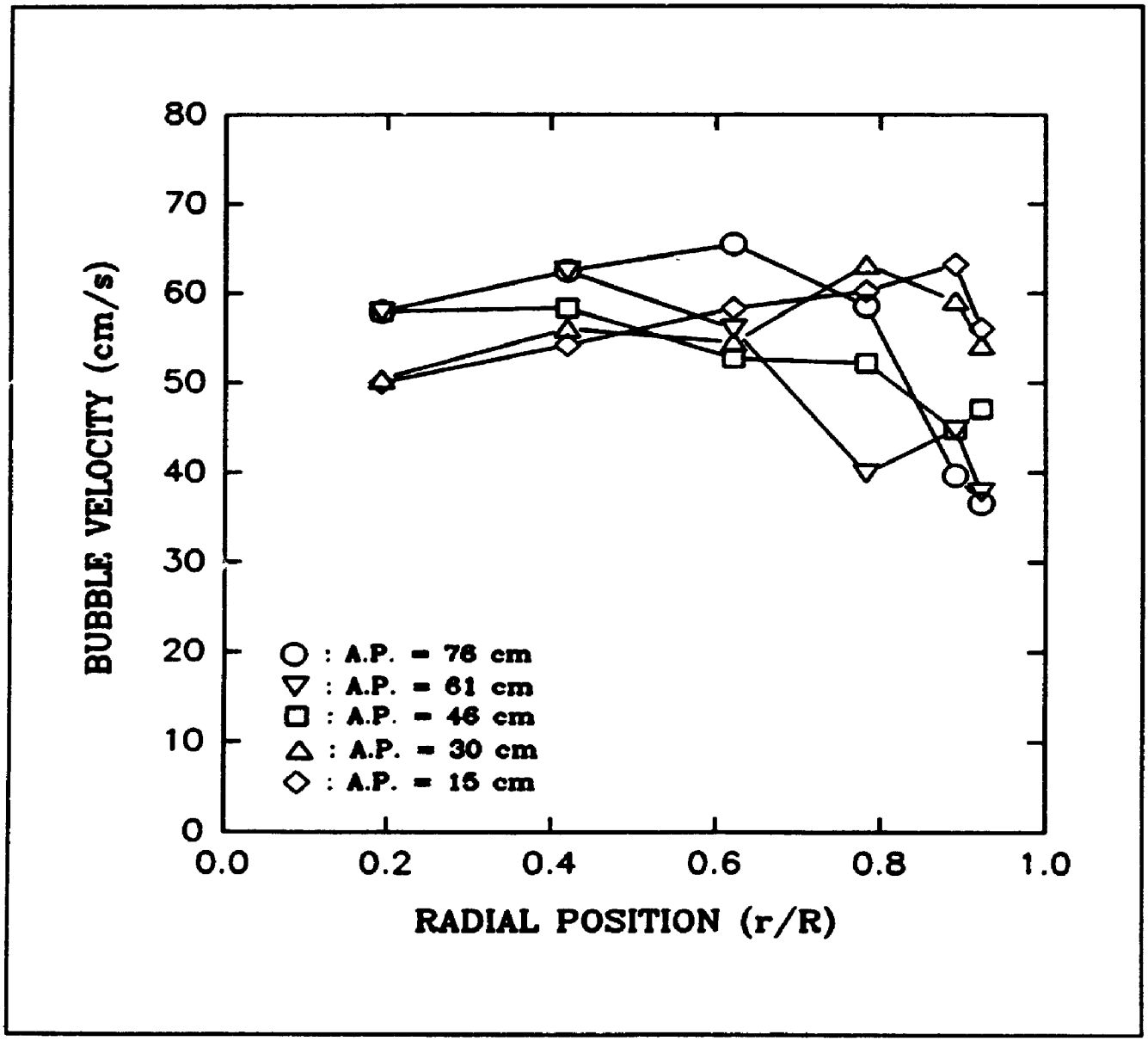

Figure 5.27a: Bubble rise velocity vs radial position
(T=100°C, V_g=2.2 cm/s)

208

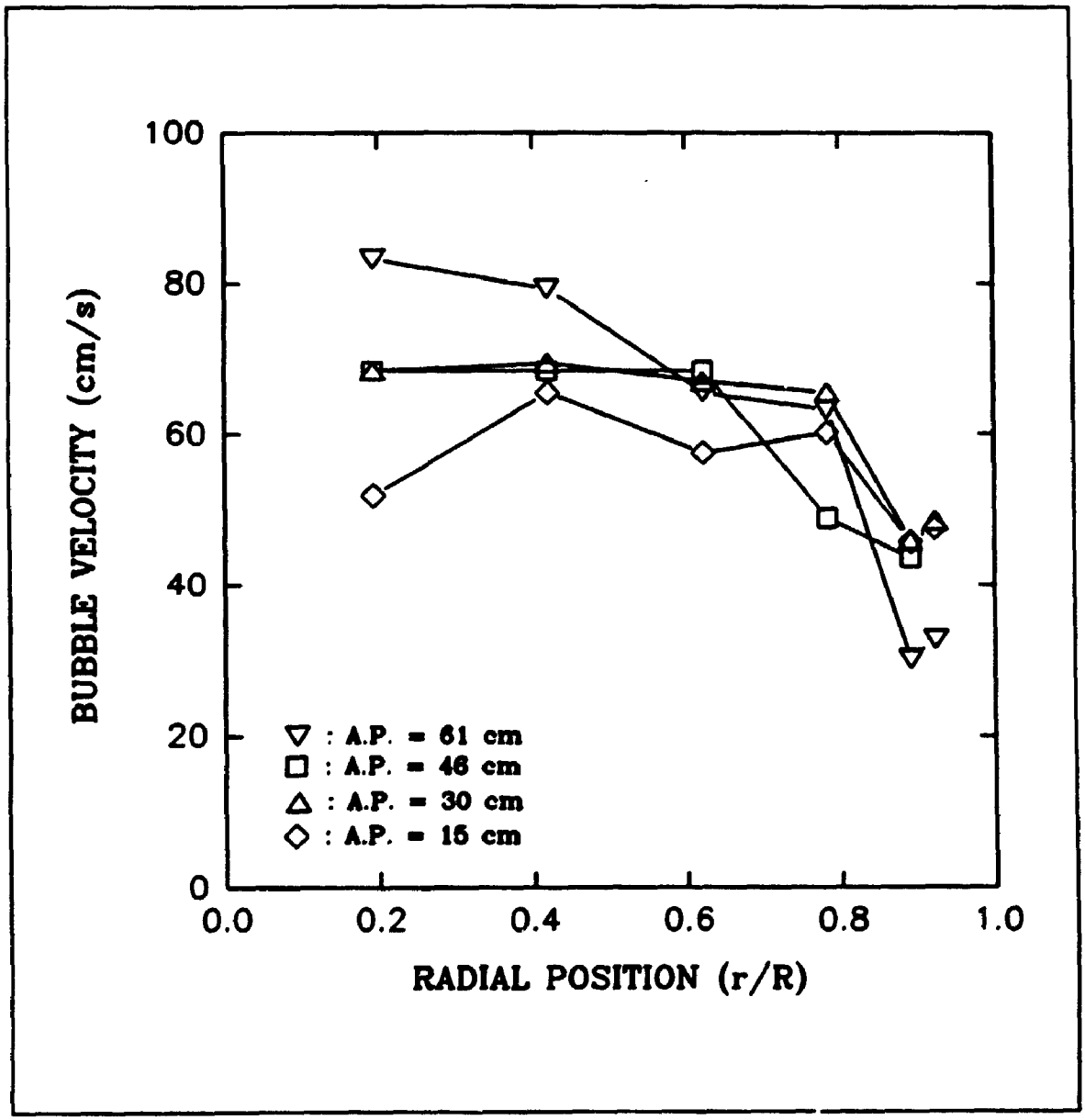

Figure 5.27b: Bubble rise velocity vs radial position
(T=100°C, V_g=4.1 cm/s)

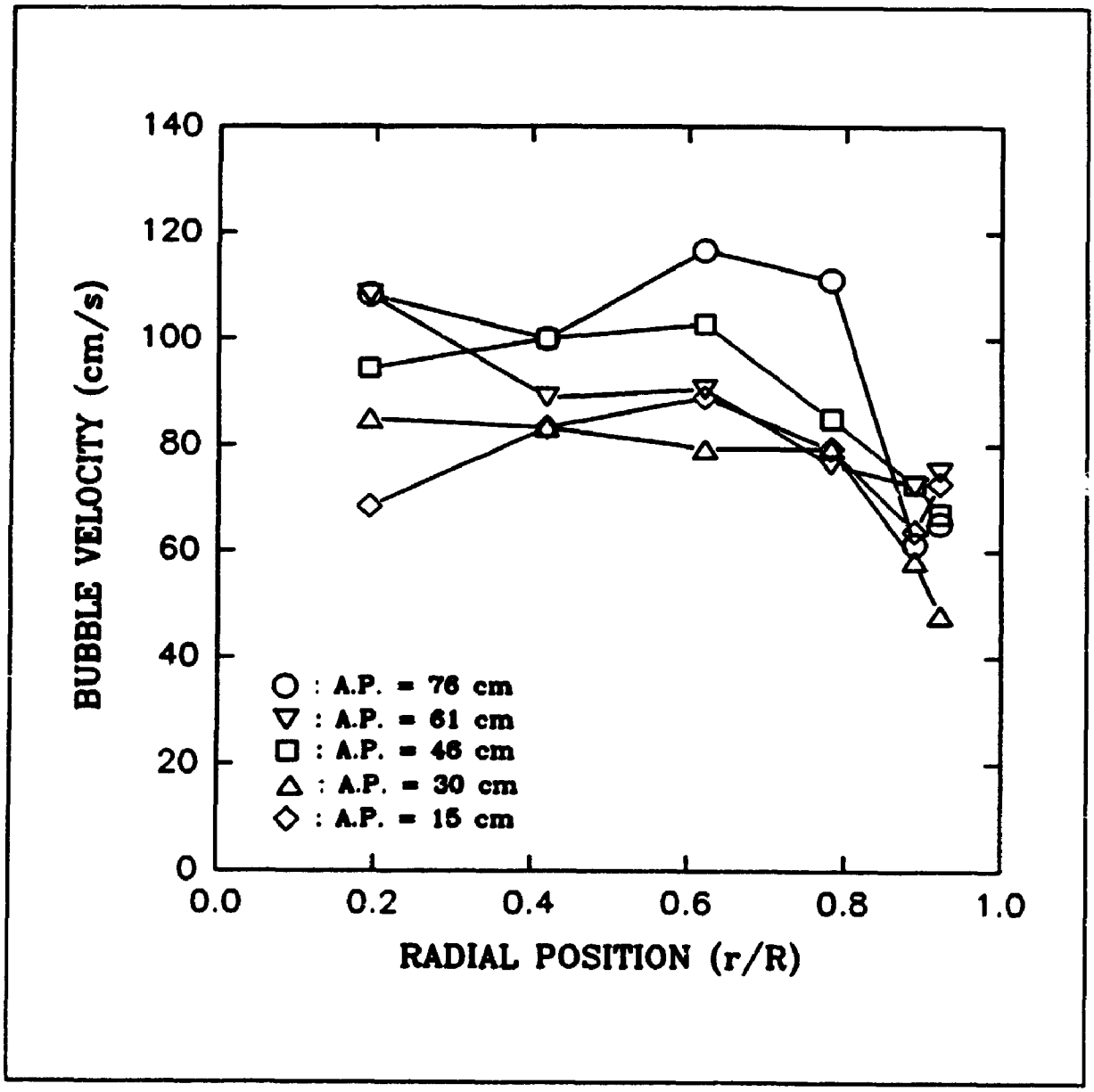

Figure 5.27c: Bubble rise velocity vs radial position (T=100°C, V_g=9.0 cm/s)

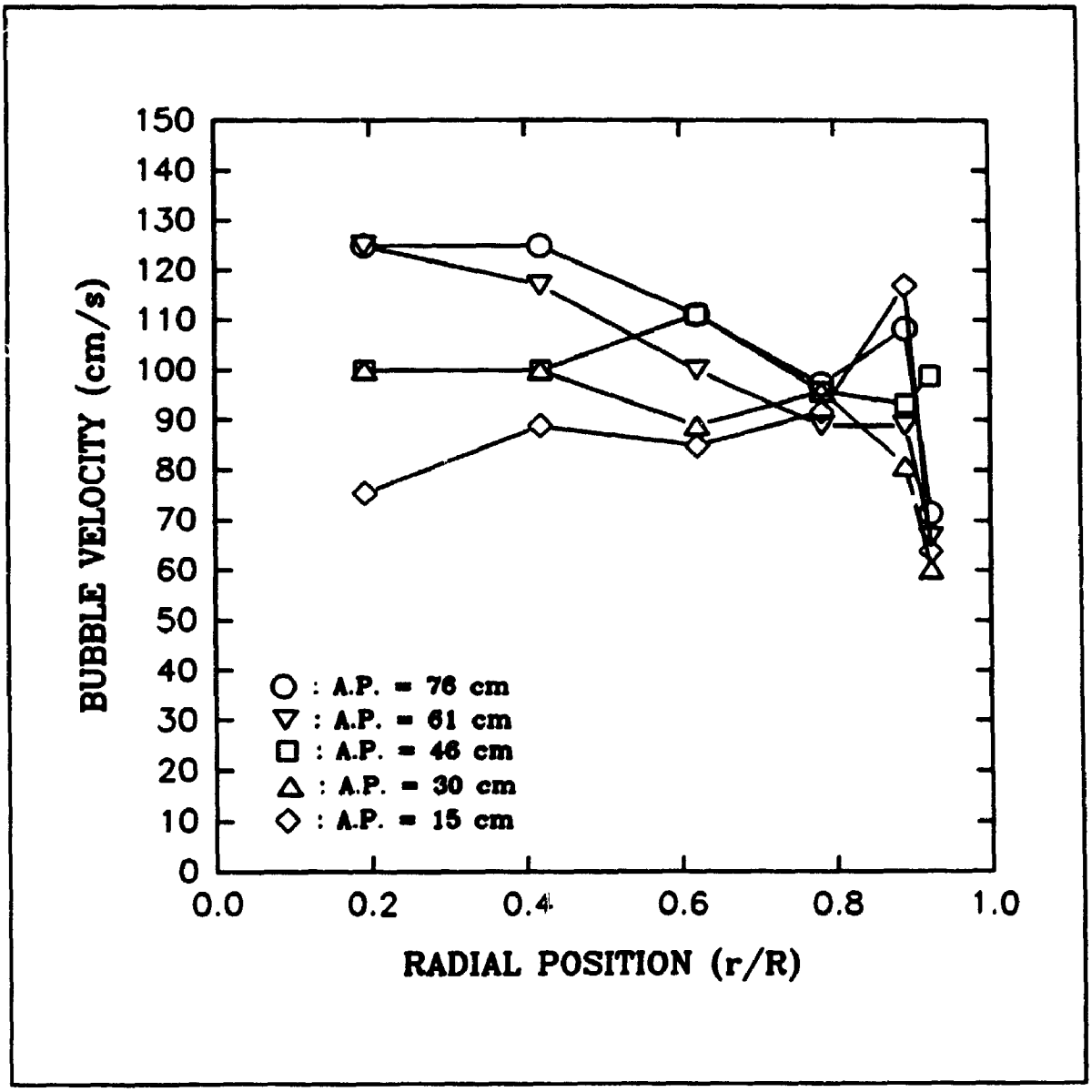

Figure 5.27d: Bubble rise velocity vs radial position (T=100°C, V_g=14.7 cm/s)

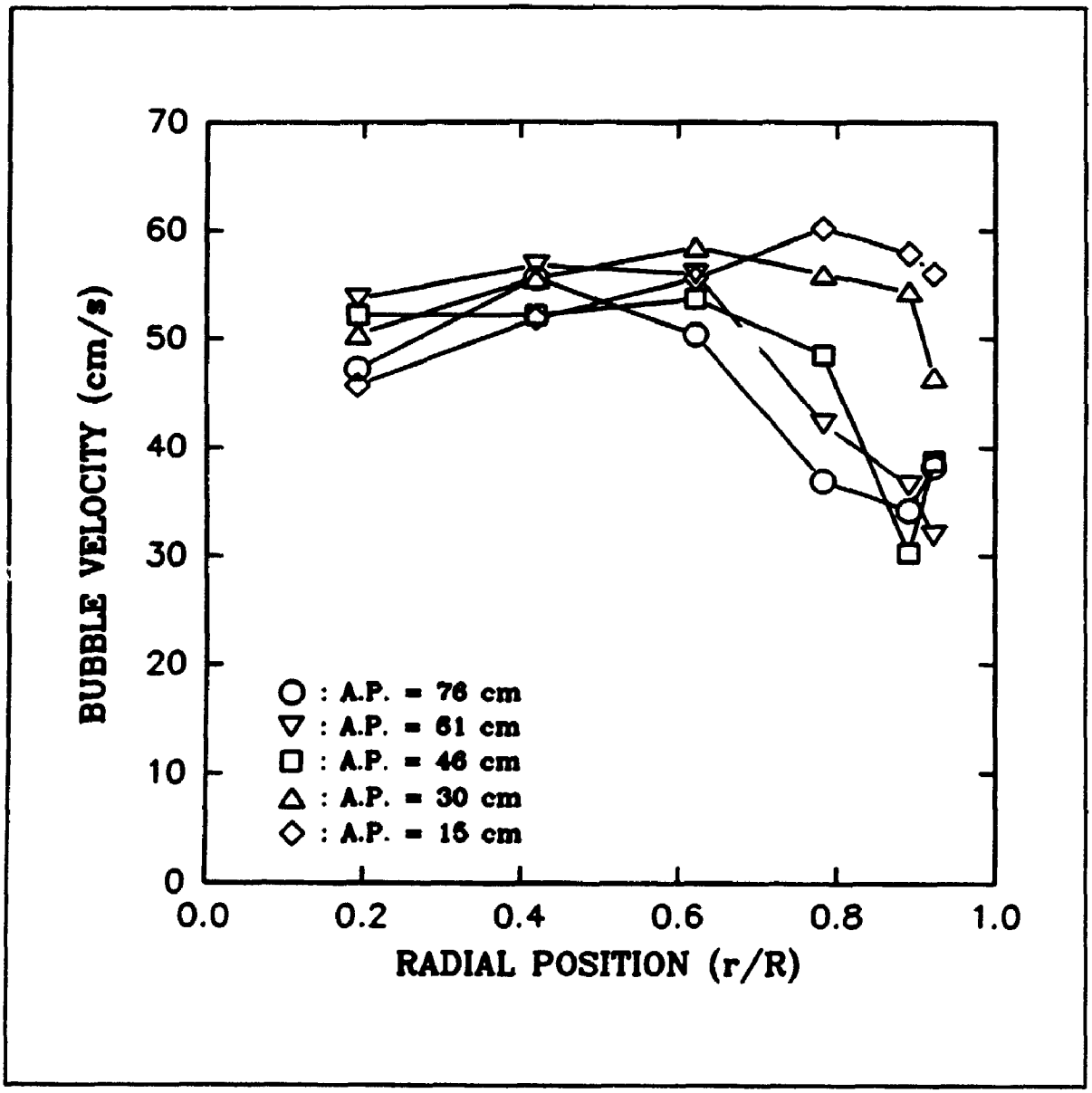

Figure 5.27e: Bubble rise velocity vs radial position
(T=175°C, V_g=2.2 cm/s)

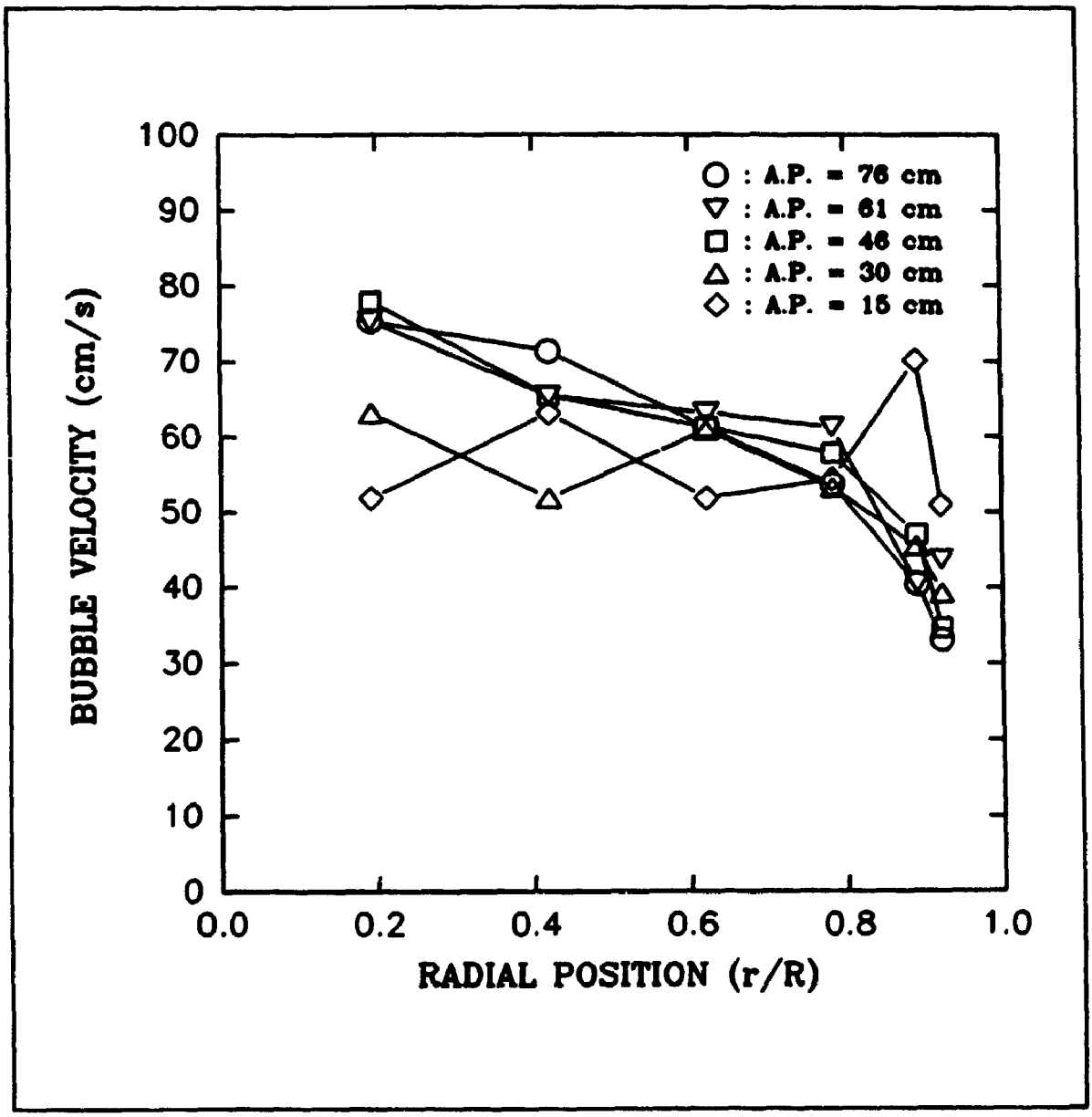

Figure 5.27f: Bubble rise velocity vs radial position
(T=175°C, V_t=4.1 cm/s)

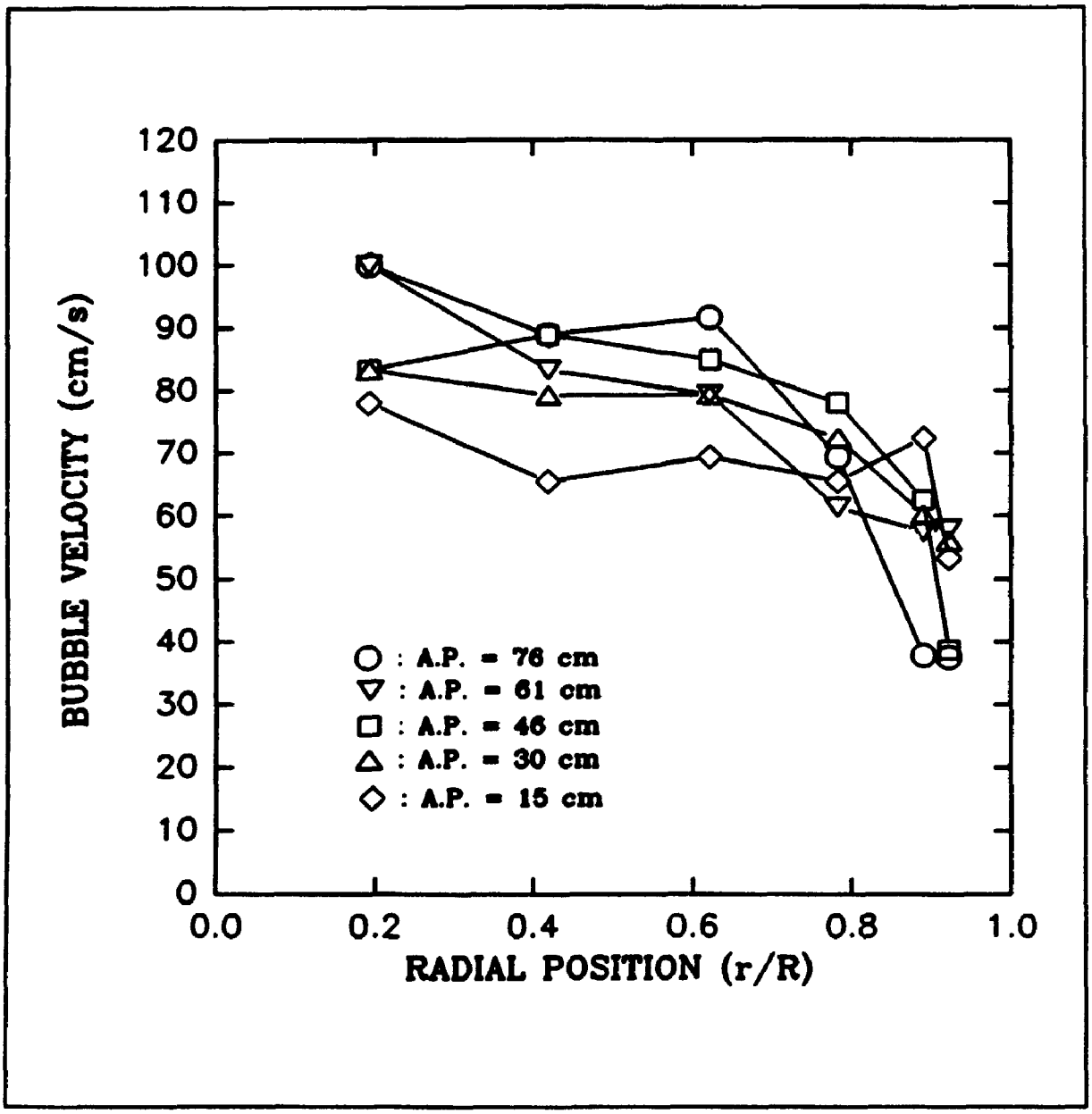

Figure 5.27g: Bubble rise velocity vs radial position
(T=175°C, V_s=9.0 cm/s)

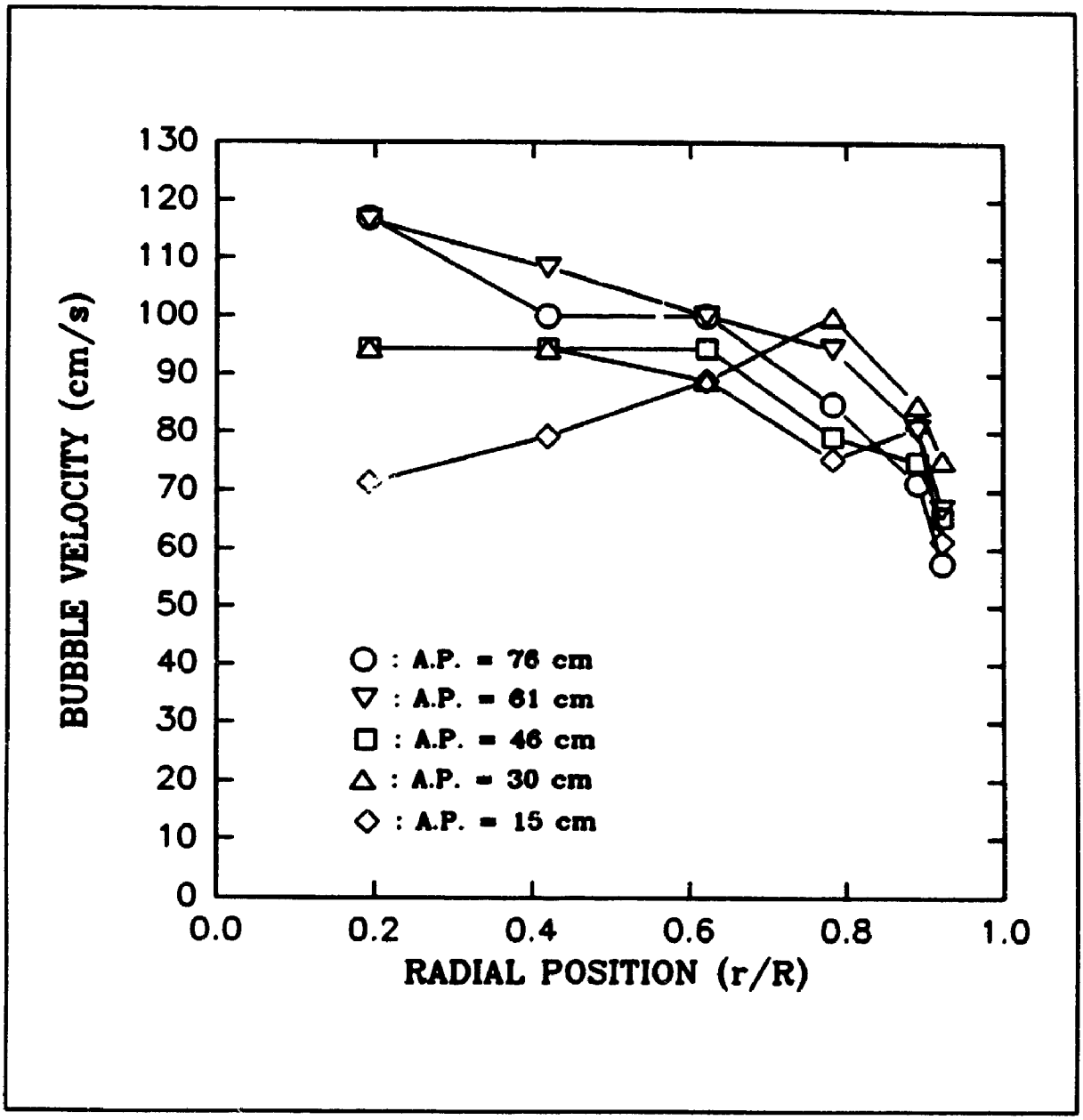

Figure 5.27h: Bubble rise velocity vs radial position
(T=175°C, V_g=14.7 cm/s)

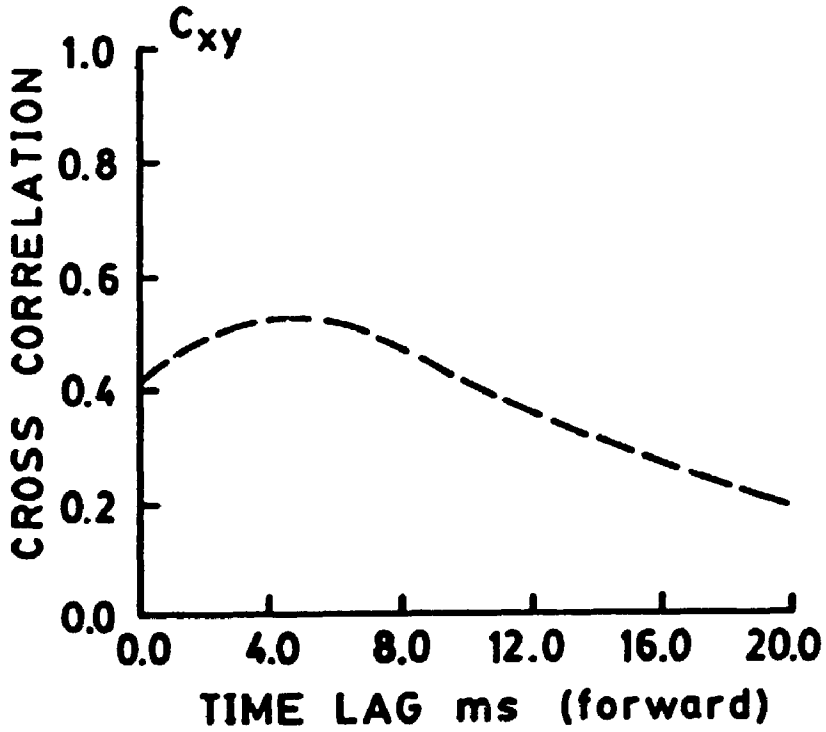

Figure 5.28a: Cross correlogram, forward analysis (T=100°C, V_s=14.7 cm/s, z=61 cm, θ=0.19)

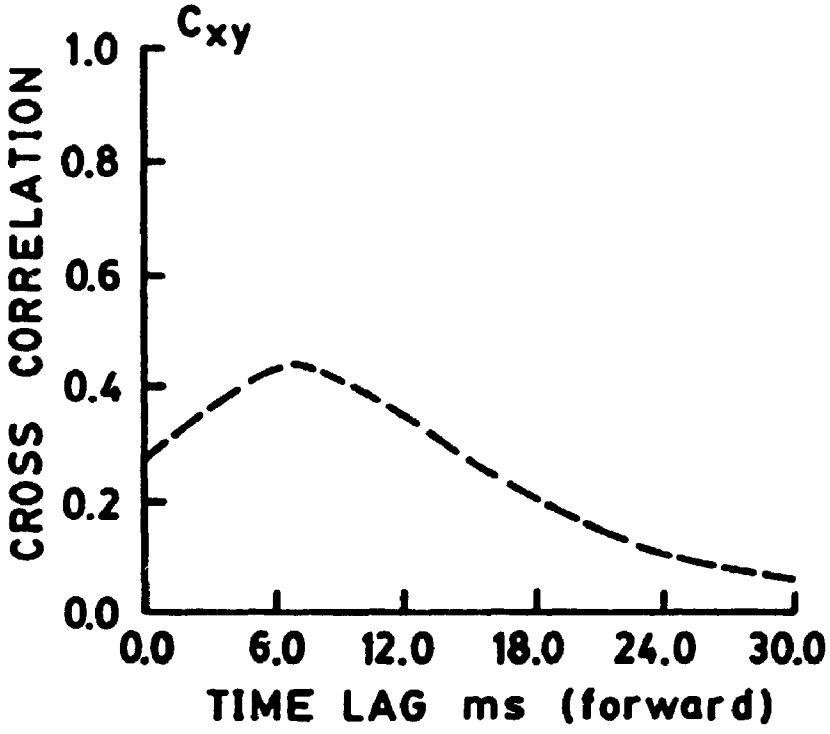

Figure 5.28b: Cross correlogram, forward analysis (T=100°C, V_g=4.1 cm/s, z=76 cm, θ=0.19)

217

present at the point of detection. Actually, as the number of bubbles considered increases, the number of successful detection processes (same bubble detected by both sensors) increases, and so is the information included in the cross correlation analysis. Furthermore, as the dominant bubble velocity vector resembles a perfectly upward vertical velocity vector, the probability that the same bubble be detected, with the proper sequence, by the two optical sensors increases (see optical sensors configuration, Section 3.1.4) and consequently, for a given bubble population, the cross correlation peak amplitude increases. The cross correlation peak amplitude was actually plotted, for all the gas superficial velocities studied at T=100°, against the bubble frequency for the particular column regions where dominant vertical upward gas flow was expected (○) (z=46 cm, θ=0.19; z=61 cm, θ=0.19; z=76 cm, θ=0.19) and where downward gas flow was suspected (▲) (z=76 cm, θ=0.92; z=61 cm, θ=0.92; z=46 cm, θ=0.92). As shown in Figure 5.29, the cross correlation peak amplitude was found to increase with the bubble frequency in both cases (upward gas flow vector and downward flow vector). However, substantially lower amplitude in the cross correlation peak was observed, for equivalent bubble frequency, for the cases recorded in the proximity of the column wall, suggesting the presence of less pronounced gas upflow circulation at this particular location. Similar results were obtained for the experiments conducted at T=175°C. A backward cross correlation analysis was also

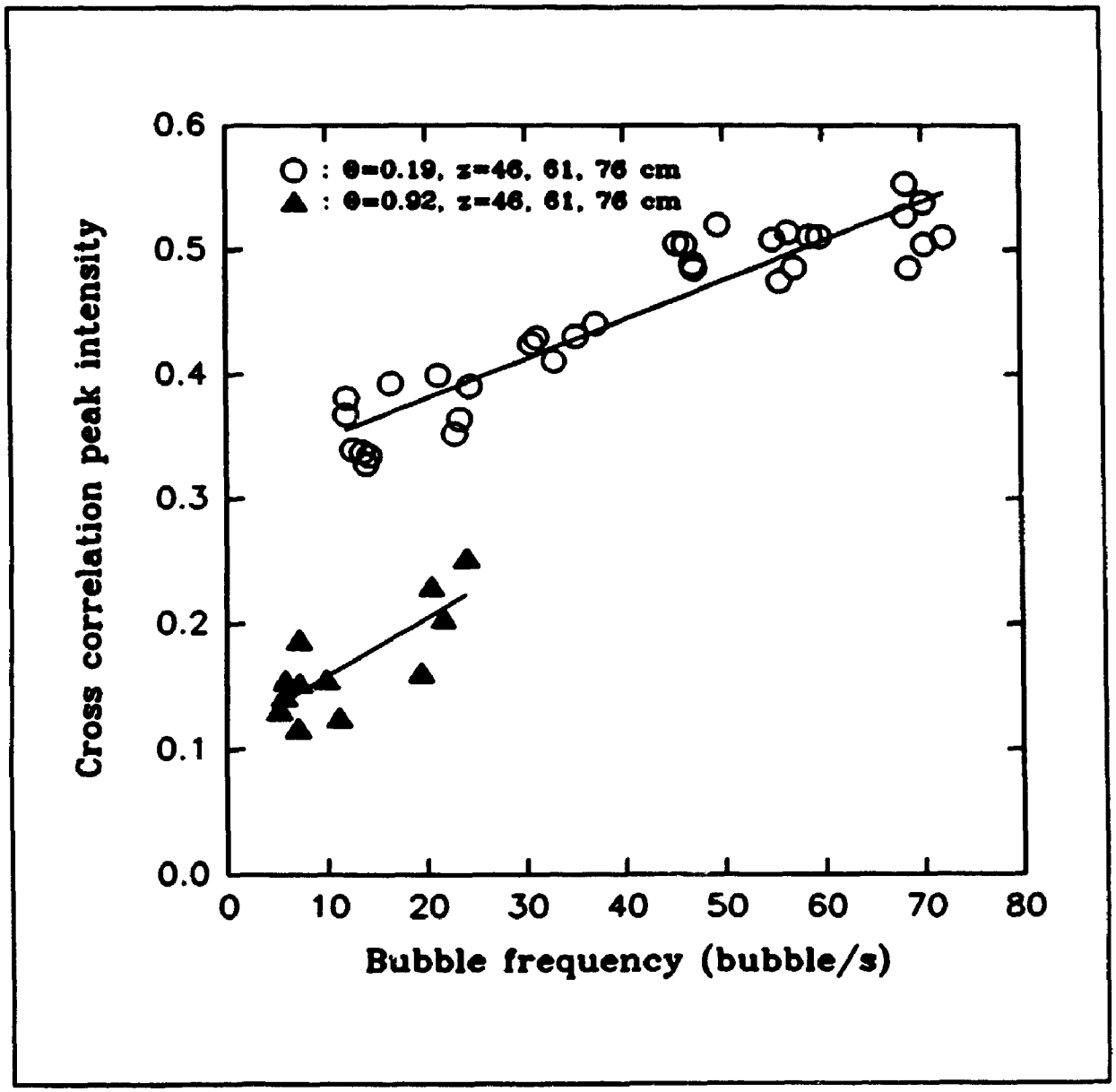

Figure 5.29: Cross correlation peak intensity vs bubble frequency (T=100°C)

applied for these particular locations to confirm the presence of downward bubble flow. However, due to the nature of the bubble flow in these locations (erratic bubble movements and low bubble frequency), a very distinct backward cross correlation peak could not be observed. However, several low intensity cross correlation peaks, as shown in Figure 5.30a, were present, suggesting the presence of disorganized gas bubble downward displacements. Thus, close to the wall, downflow bubble circulation took place together with upflow gas displacement. These secondary peaks could not be observed under the same operating conditions in the center of the column, where dominant upward gas flow is expected, as shown in Figure 5.30b.

Furthermore, the consistency of the fibre optic sensors' bubble rise velocity measurements was studied by evaluating, for a given operating condition, the relative percentage error between the average time lags (values used in the calculation of the bubble rise velocities reported in Figures 5.27a to 5.27h) and the experimental time lags (repeats). The relative percentage errors are reported in Tables 5.10 and 5.11 for the experiments conducted at T=100°C and in Tables 5.12 and 5.13 for the ones performed at T=175°C. The results presented in the top row correspond to the average relative percentage error for all the experimental repeats performed at this particular condition, while the results presented in the

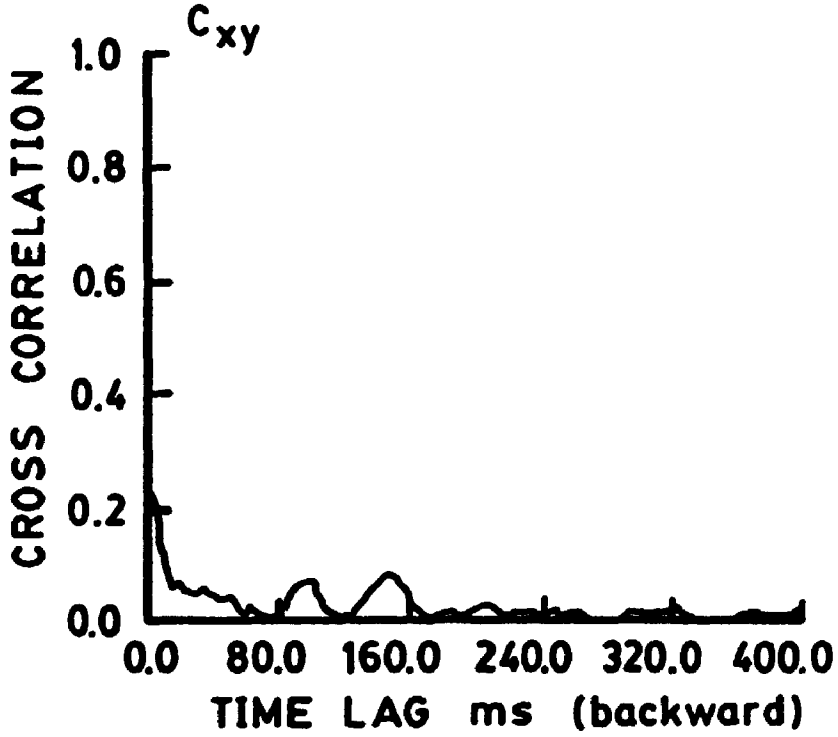

Figure 5.30a: Cross correlogram, backward analysis (T=175°C, V_t=14.7 cm/s, z=76 cm, θ=0.92)

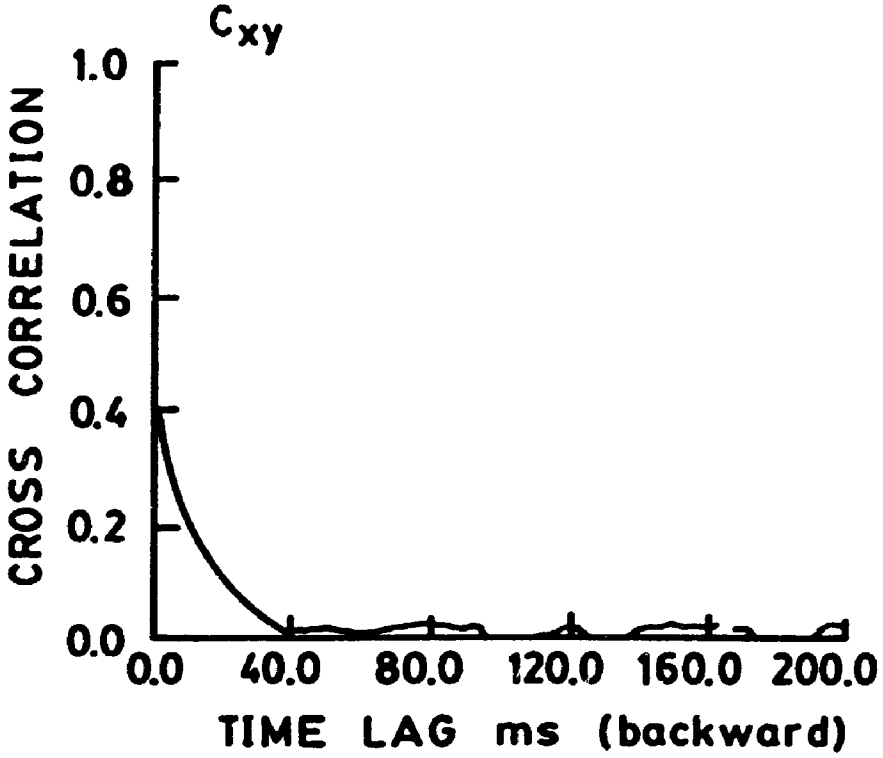

Figure 5.30b: Cross correlogram, backward analysis (T=175°C, V_g=14.7 cm/s, z=76 cm, θ=0.19)

Table 5.10

Average (top row) and maximum (bottom row) relative percentage errors between average time lag and time lags (repeats)
T=100°C

V_s cm/s	z cm	θ=0.19 %	θ=0.42 %	θ=0.62 %	θ=0.78 %	θ=0.89 %	θ=0.92 %
2.2	15	0 0	9.5 14.3	10.3 15.4	5.3 8.0	8.3 12.5	7.4 11.1
2.2	30	6.7 10.0	7.4 11.1	11.9 17.9	8.3 12.5	28.6 42.9	9.5 14.3
2.2	46	5.1 7.7	10.3 15.4	11.5 17.2	9.2 13.8	19.1 28.6	18.2 27.3
2.2	61	5.3 8.0	0 0	7.4 11.1	15.4 23.1	22.2 33.3	8.3 12.5
2.2	76	5.3 8.0	0 0	5.8 8.7	22.2 33.3	15.4 23.1	3.3 4.9
4.1	10	6.7 10.0	4.8 7.1	0 0	8.3 12.5	14.6 21.9	9.5 14.3
4.1	15	4.6 6.9	5.8 8.7	14.8 22.2	5.3 8.0	6.1 9.1	10.4 15.6
4.1	30	6.1 9.1	12.1 18.2	5.8 8.7	6.7 6.7	9.1 9.1	24.3 36.4
4.1	46	6.1 9.1	6.1 9.1	6.1 9.1	8.6 12.9	4.3 4.3	- -
4.1	61	0 0	7.0 10.5	5.8 8.7	8.3 12.5	7.1 7.1	27.3 27.3

Table 5.11

Average (top row) and maximum (bottom row) relative percentage errors between average time lag and time lags (repeats)
T=100°C

V_s cm/s	z cm	θ=0.19 %	θ=0.42 %	θ=0.62 %	θ=0.78 %	θ=0.89 %	θ=0.92 %
9.0	15	6.1 9.1	0 0	7.8 11.8	7.0 10.5	21.3 32.0	21.2 31.8
9.0	30	11.1 16.7	0 0	7.0 10.5	7.0 10.5	23.8 35.7	14.6 21.9
9.0	46	8.3 12.5	0 0	13.3 20.0	11.1 16.7	21.2 31.8	14.5 21.7
9.0	61	9.5 14.3	7.8 11.8	15.7 23.5	13.3 20.0	9.5 14.3	19.1 28.6
9.0	76	9.5 14.3	0 0	10.3 15.4	19.1 28.6	13.3 20.0	4.8 4.8
14.7	15	6.7 10.0	7.8 11.8	11.1 16.7	9.1 9.1	10.3 15.4	21.3 32.0
14.7	30	0 0	0 0	7.8 11.8	27.5 41.2	14.0 21.1	5.3 8.0
14.7	46	0 0	0 0	19.1 28.6	27.5 41.2	19.6 29.4	20.8 31.3
14.7	61	0 0	10.3 15.4	0 0	7.8 11.8	7.8 11.8	25.0 25.0
14.7	76	0 0	0 0	19.1 28.6	16.7 25.0	9.5 14.3	0 0

Table 5.12

Average (top row) and maximum (bottom row) relative percentage errors between average time lag and time lags (repeats)
T=175°C

V_s cm/s	z cm	θ=0.19 %	θ=0.42 %	θ=0.62 %	θ=0.78 %	θ=0.89 %	θ=0.92 %
2.2	15	6.1 9.1	4.6 6.9	0 0	5.3 8.0	5.1 7.7	7.4 11.1
2.2	30	6.7 10.0	0 0	22.2 33.3	7.4 11.1	18.4 27.6	12.1 18.2
2.2	46	9.2 13.8	9.2 13.8	4.7 7.1	4.3 6.5	9.3 14.0	28.6 42.9
2.2	61	4.8 7.1	14.8 22.2	7.4 11.1	11.1 16.7	14.3 21.4	21.3 32.0
2.2	76	8.3 12.5	0 0	6.7 10.0	8.1 12.2	18.9 28.3	13.3 20.0
4.1	15	4.6 6.9	8.3 12.5	4.6 6.9	18.4 27.6	15.1 22.7	13.3 20.0
4.1	30	8.3 12.5	4.6 6.9	10.7 16.0	16.1 24.1	0 0	31.0 46.5
4.1	46	16.7 25.0	5.8 8.7	13.3 20.0	5.1 7.7	18.2 27.3	20.0 20.0
4.1	61	6.7 10.0	5.8 8.7	8.3 12.5	13.3 20.0	3.6 5.4	13.3 20.0
4.1	76	6.7 10.0	0 0	12.8 19.2	4.7 7.1	28.6 42.9	35.3 52.9

Table 5.13

Average (top row) and maximum (bottom row) relative percentage errors between average time lag and time lags (repeats)
T=175°C

V_s cm/s	z cm	θ=0.19 %	θ=0.42 %	θ=0.62 %	θ=0.78 %	θ=0.89 %	θ=0.92 %
9.0	15	16.7 25.0	5.8 8.7	12.1 18.2	5.8 8.7	9.5 14.3	16.1 24.1
9.0	30	0 0	7.0 10.5	7.0 10.5	9.5 14.3	5.3 8.0	7.4 11.1
9.0	46	0 0	7.8 11.8	11.1 16.7	16.7 25.0	25.7 38.5	7.7 7.7
9.0	61	0 0	0 0	7.0 10.5	13.3 20.0	26.2 39.3	5.1 7.7
9.0	76	0 0	7.8 11.8	13.3 20.0	12.1 18.2	8.3 12.5	11.1 11.1
14.7	15	0 0	7.0 10.5	7.8 11.8	6.7 10.0	14.1 21.1	13.3 20.0
14.7	30	8.3 12.5	8.3 12.5	7.8 11.8	0 0	11.1 16.7	6.7 10.0
14.7	46	8.3 12.5	8.3 12.5	8.3 12.5	7.0 10.5	19.1 28.6	5.8 8.7
14.7	61	10.3 15.4	9.5 14.3	0 0	8.3 12.5	- -	6.7 6.7
14.7	76	10.3 15.4	0 0	0 0	11.1 16.7	0 0	14.8 22.2

bottom row correspond to the maximum percentage error observed for this particular set of repeats. As shown in Tables 5.10 to 5.13, the average relative percentage errors were in general satisfactory, being equal on average to 9.8% at T=100°C and 9.5% at T=175°C, thus confirming the validity of the fibre optic sensors' bubble rise velocity measurements.

In general, the bubble rise velocity decreased with an increase of the radial position, with the exception, for both temperatures investigated, of the two lower axial positions (z=15 cm and z=30 cm) at V_g=2.2 cm/s, for which the bubble rise velocity was higher in the vicinity of the column wall as compared to the central region of the column. This phenomenon seemed to be in agreement with the recent observations of Dudukovic and Devanathan (1992) and Devanathan et al. (1990). Actually, for a bubble column of similar diameter (19 cm) than the one used in the present study (20 cm), they observed, for the air-water system at low gas superficial velocity (≈ 2 cm/s), the presence, in the proximity of the gas distributor, of a small liquid circulation cell for which liquid flows towards the distributor in the center of the column and upward in the vicinity of the column wall. The presence of such cell in the region of the gas distributor at V_g=2.2 cm/s, would favour faster bubble rise velocities in the proximity of the column wall as compared to the central area of the column, as effectively observed in the present work. Dudukovic and Devanathan (1992) observed that the small circulation cell in

the gas distributor region was followed, at higher axial position, by a single larger circulation cell in which the classical and expected liquid circulation patterns (upward in the center and downward at the wall) were observed (Figure 5.31a). This was consistent with the bubble rise velocity profiles observed at higher axial positions for V_g=2.2 cm/s for which the bubble rise velocity was smaller in the vicinity of the wall as compared to the central area of the column. At higher gas superficial velocity, Dudukovic and Devanathan (1992) did not observe the presence of a small secondary liquid circulation cell in the gas distributor region, but the presence of a single large circulation cell characterized by the classical upward liquid velocity in the center of the column and downward liquid velocity in the periphery of the column wall (Figure 5.31b). These observations are in agreement with the bubble rise velocity radial profiles observed at higher gas superficial velocity (4.1 to 14.7 cm/s), for which the bubble rise velocity was found to decrease with an increase in the radial position, even at the gas distributor level (z=15 cm).

It can be speculated that the presence of a downward liquid circulation flow in the central region of the column would induce gas recirculation in this particular area, thus reducing, in the central section of the column, the cross correlation peak intensity. Furthermore, it can be argued that in the vicinity of the wall region, where upward liquid

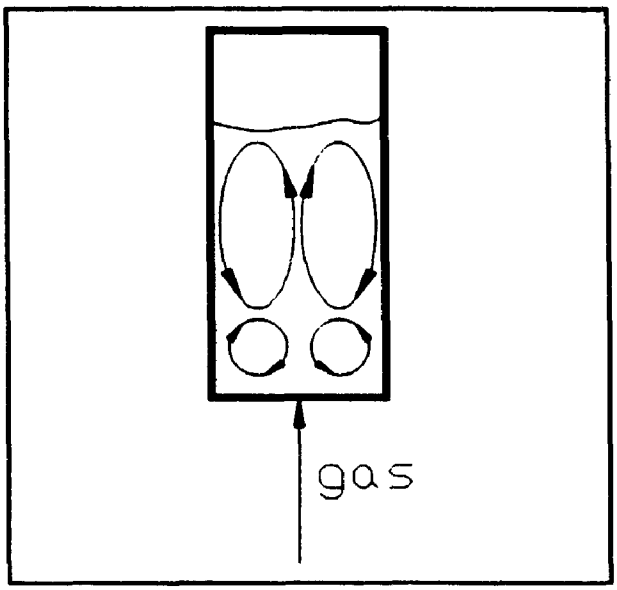

Figure 5.31a: Dual liquid circulation cells

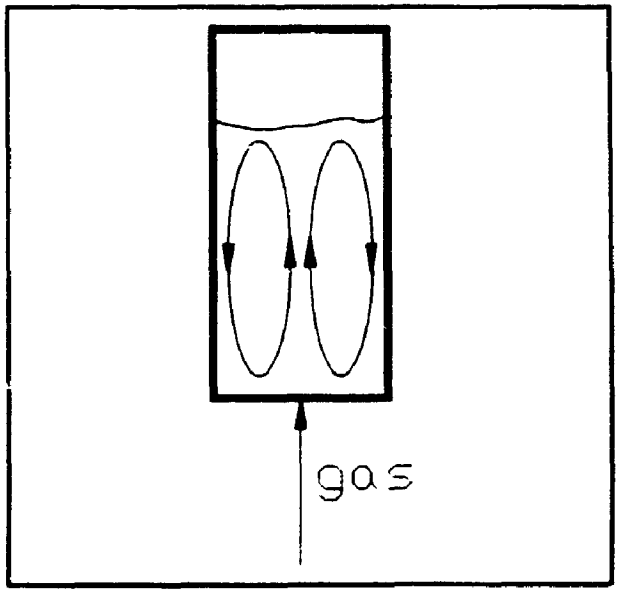

Figure 5.31b: Single liquid circulation cell

flow and then minimum gas recirculation is present, higher cross correlation peak amplitude would be observed. These facts, as shown in Table 5.14, for V_g=2.2 cm/s, were confirmed with a cross correlation peak intensity indeed smaller in the center of the column (θ=0.19) at z=15 cm as compared to the wall periphery (θ=0.92). However, for all the other superficial gas velocities investigated (V_g=4.1, 9.0, 14.7 cm/s), for which the small circulation cell was not observed, the cross correlation peak intensity was smaller in the periphery of the column wall, as compared to the center of the column, suggesting the emergence of the classical liquid circulation cell (upward liquid flow in the center and downward liquid flow at the wall). As shown in Table 5.14, for θ=0.19, the cross correlation peak amplitude gradually increased as the gas superficial velocity augmented due to an increase of the bubble frequency with the gas superficial velocity. However, at θ=0.92, the increase in the bubble frequency induced by an increase of the gas superficial velocity was counterbalanced by an increase in the magnitude of the downward liquid circulation current. So, the cross correlation peak intensity remained approximately constant for this particular position as the gas superficial velocity increased.

As shown in Figures 5.27a to 5.27h, the bubble rise velocity radial profiles became steeper as the axial position increased, or as the gas holdup radial parabolic profile

Table 5.14

Cross correlation peak intensity vs radial position
z=15 cm

Temperature (°C)	V_g (cm/s)	θ=0.19	θ=0.92
100	2.2	0.2977	0.4013
100	4.1	0.3438	0.3222
100	9.0	0.3803	0.3548
100	14.7	0.4277	0.3128
175	2.2	0.3084	0.4082
175	4.1	0.3533	0.2889
175	9.0	0.3679	0.3442
175	14.7	0.3904	0.2938

became more pronounced (Section 5.1.1), thus promoting stronger liquid circulation. These results are in agreement with the observations reported by Dudukovic and Devanathan (1992), who measured the liquid velocity profiles. They indeed noticed the emergence of steeper radial liquid velocity profiles (prior to stabilization) as the axial position increased.

The local bubble rise velocity was found to increase with an increase of the gas superficial velocity, this increase being more pronounced in the central section of the column as compared to the proximity of the column wall. Actually, as shown in Figure 5.32, for V_g=2.2 cm/s to 14.7 cm/s, the bubble rise velocity increased from 57.9 cm/s to 125.0 cm/s and from 47.2 cm/s to 117.0 cm/s for T=100°C and T=175°C respectively in the central region of the column (θ=0.19). In the vicinity of the column wall, for V_g=2.2 cm/s to 14.7 cm/s, the bubble rise velocity increased in a more moderate way, from 36.6 cm/s to 71.4 cm/s and from 38.2 cm/s to 57.5 cm/s for T=100°C and T=175°C respectively. The average radial bubble rise velocity (calculated assuming radial symmetry) was found to increase with the gas superficial velocity, as shown in Figure 5.32 (dash lines). The increase of the bubble rise velocity with the gas superficial velocity is the result of both, the presence of less uniform gas holdup profiles and consequently more vigorous liquid circulation and the presence of larger gas bubbles as discussed in Section 5.1.4.

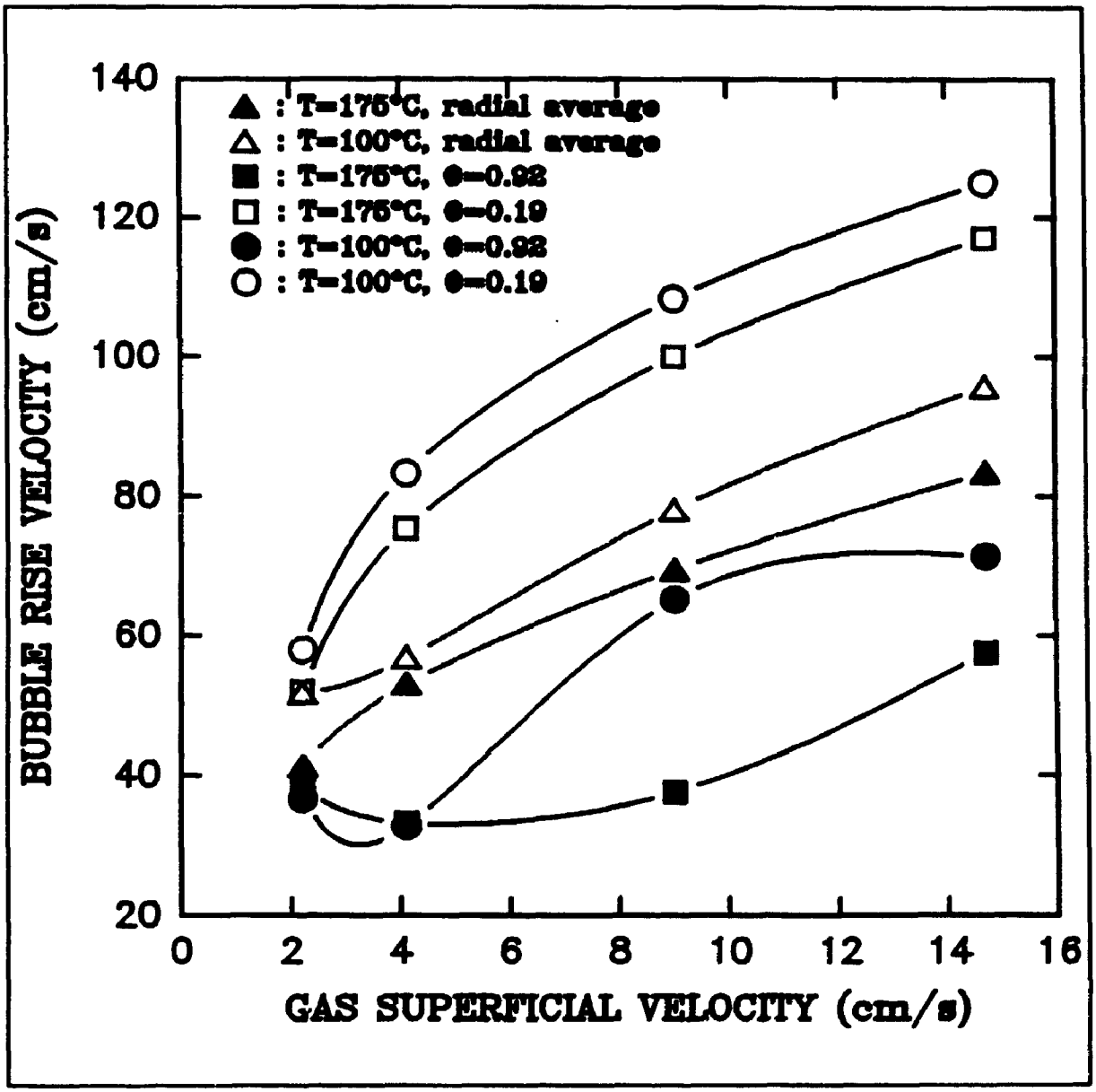

Figure 5.32: Bubble rise velocity vs gas superficial velocity (z=76 cm).

233

Furthermore, the bubble rise velocity radial profiles became steeper as the gas superficial velocity increased, as shown in Figure 5.33. These results, in spite of significant differences in the gas-liquid medium used in the two studies, were found to be, in general, consistent with the findings of Dudukovic and Devanathan (1992). These authors observed that as the gas superficial velocity augmented, stronger liquid velocity currents emerged. This liquid circulation pattern suggests that faster bubble rise velocity in the column central region and slower ascension of the gas bubbles at the wall should be promoted. This bubble phase behaviour was indeed precisely obtained in the present study. These findings are, in this respect, particularly important since they constitute valuable bubble phase information in general, but also unique observations of a system of extreme importance for the fuel industry, for which very scarce bubble phase knowledge is available.

Since sharper gas holdup profiles (and consequently more intense liquid circulation patterns) were observed at T=100°C, as compared to T=175°C (Section 5.1.1), and since larger gas bubbles were present at T=100°C as compared to T=175°C (Section 5.1.4), higher bubble rise velocities should be expected at T=100°C than at T=175°C. In fact, bubble rise velocities were found to be on average 4.8% and 15% higher at T=100°C as compared to T=175°C for θ=0.19 and θ=0.92 respectively.

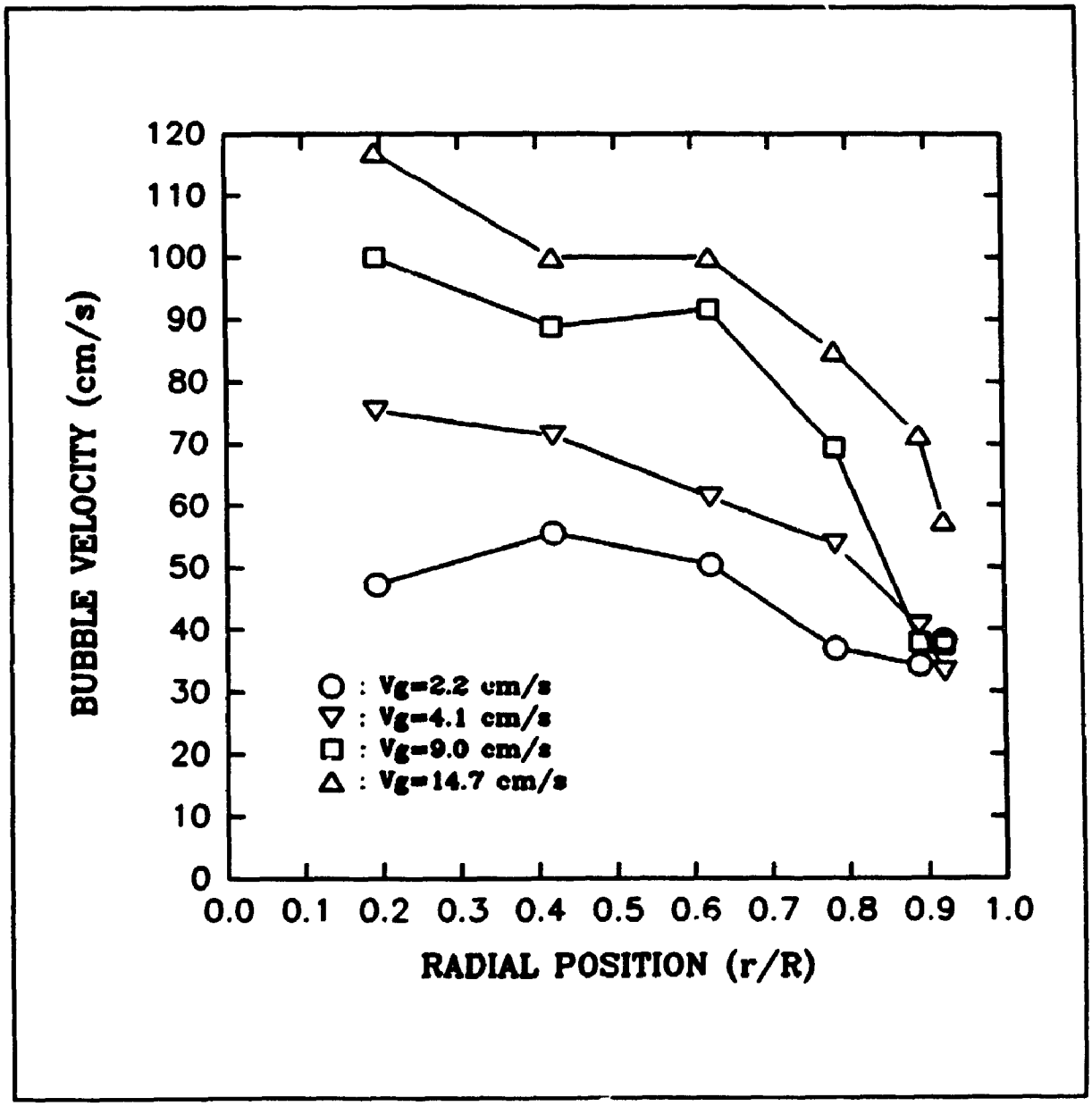

Figure 5.33: Bubble rise velocity vs radial position (z=76 cm, T=175°C).

In order to further validate the bubble rise velocity experimentally measured and studied more thoroughly the flow regime observed, the turbulent liquid circulating flow model proposed by Ueyama and Miyauchi (1979) was tested. As discussed in Chapter 1, this model, based on pressure balance, was found to provide excellent representation of the flow pattern in air/water systems. Dudukovic and Devanathan (1992) recently confirmed the validity of the Ueyama and Miyauchi (1979) model in satisfactorily representing liquid velocity measurements in an air/water system. However, no applications of the Ueyama and Miyauchi (1979) model were so far reported for hydrocarbon high temperature type systems.

As thoroughly discussed in Chapter 1, the application of the Ueyama and Miyauchi (1979) model requires the knowledge of two parameters, namely the gas holdup radial profile and the turbulent kinematic viscosity. In the present case, since precise and validated measurements of the gas holdup radial profiles were available, the experimentally derived values of the parameter m (gas holdup radial profile power law representation, Equation 5.2) were used. Only limited information is available concerning the turbulent kinematic viscosity in two-phase bubble column system. A few empirical correlations, as reviewed by Deckwer and Schumpe (1987), were proposed for estimating the turbulent kinematic viscosity in bubble column conditions (two-phase system). For example, Ueyama and Miyauchi (1979) presented the following empirical

equation:

$$\nu_t = 0.0322 D_c^{1.7} \qquad (5.6.a)$$

Miyauchi et al. (1981) considered the dependence of the turbulent viscosity on column diameter and superficial gas velocity, and presented the following empirical equation:

$$\nu_t = 0.0345 V_g^{\frac{1}{3}} D_c^{\frac{3}{2}} \qquad (5.6.b)$$

However, such correlations, developed exclusively for air/water systems, and based on very limited experimental data, could not provide a precise and reliable evaluation of the turbulent kinematic viscosity under the present operating conditions. So, the following procedure was adopted. The bubble velocity could be related to the liquid velocity in the following way:

$$U_l = V_b - V_{slip} \qquad (5.6.c)$$

The bubble slip velocity V_{slip} was assumed to be radially constant. Such assumption was experimentally validated by a number of authors, including Koide et al. (1979) and Ueyama and Miyauchi (1979). The bubble slip velocity (V_{slip}) and the

237

liquid velocity (U_l) were calculated, using respectively Equations 1.11.j and 1.11.e. The bubble velocity was obtained from Equation 5.6.c. The only unknown, the turbulent kinematic viscosity, was optimized, using a Marquart-Levenberg algorithm, to provide the best possible closure of the gas mass balance, as depicted by Equation 5.6. For all the cases studied, the gas mass balances were closed within ± 2%.

The calculated liquid velocity and bubble velocity radial profiles obtained for all the gas superficial velocities studied, using the above described procedure, are presented in Figures 5.34a to 5.34d for T=100°C. As shown in Figures 5.34b to 5.34d, the correspondence between calculated gas velocity and measured bubble rise velocity was very good, being within 10%, for V_g=4.1 to 14.7 cm/s, and z=30 cm. These results indeed confirmed the validity of the experimentally measured bubble rise velocities. However, since a secondary liquid circulation cell (upward liquid flow along the wall of the column, downward liquid flow in the central region of the column) was present in the bottom of the column (z=30 cm) at V_g=2.2 cm/s, poorer correspondence between the predicted and measured gas velocities was expected. Since the liquid velocity profile predicted by the Ueyama and Miyauchi (1979) model could not predict this particular flow phenomenon, the measured bubble rise velocities were larger than the predicted ones in the peripheral area. Furthermore, as the distance from the gas distributor (z) increased, the liquid circulation

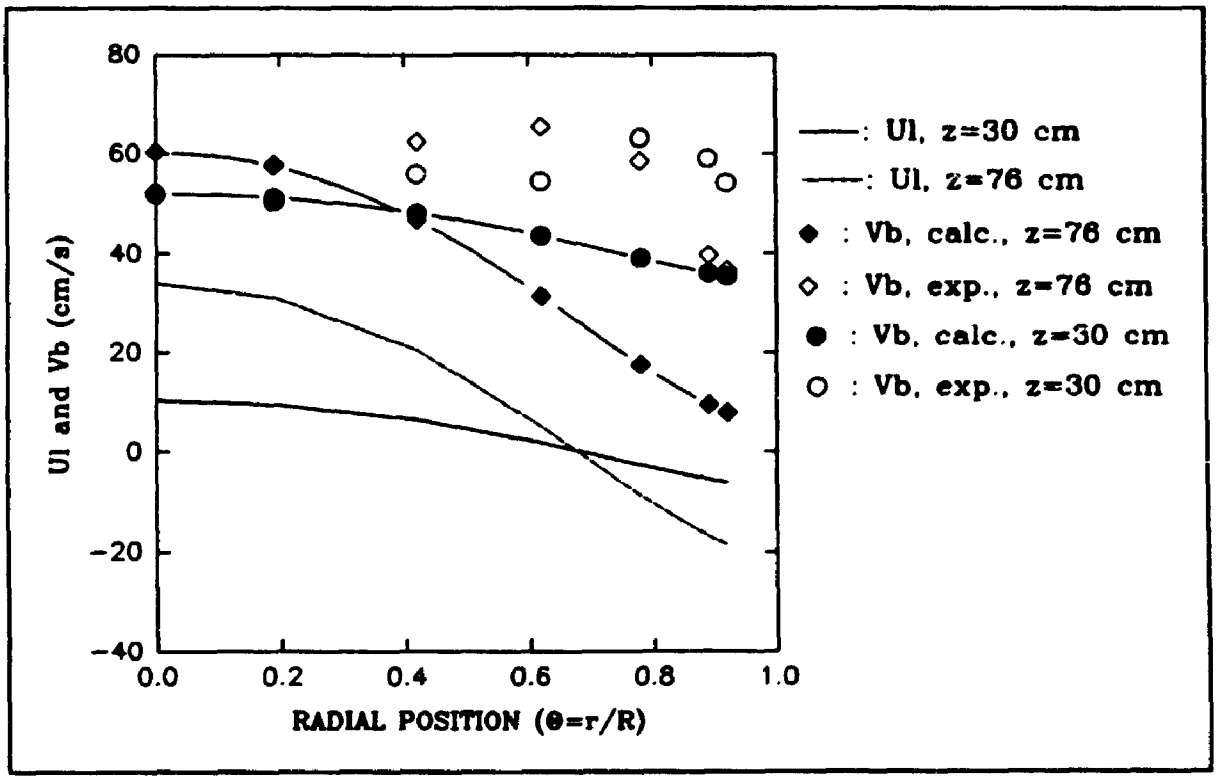

Figure 5.34a: Calculated U_l, V_b and experimental V_b, T=100°C, V_g=2.2 cm/s

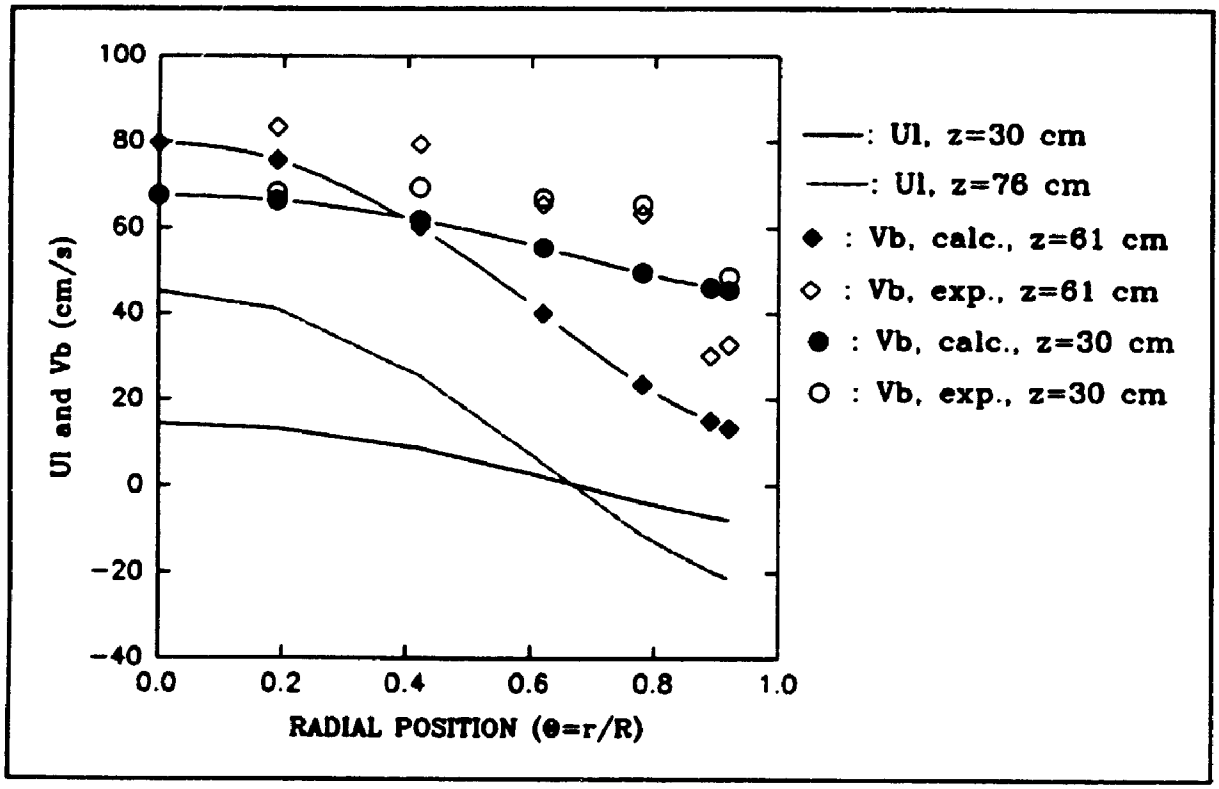

Figure 5.34b: Calculated U_l, V_b and experimental V_b, T=100°C, V_s=4.1 cm/s

240

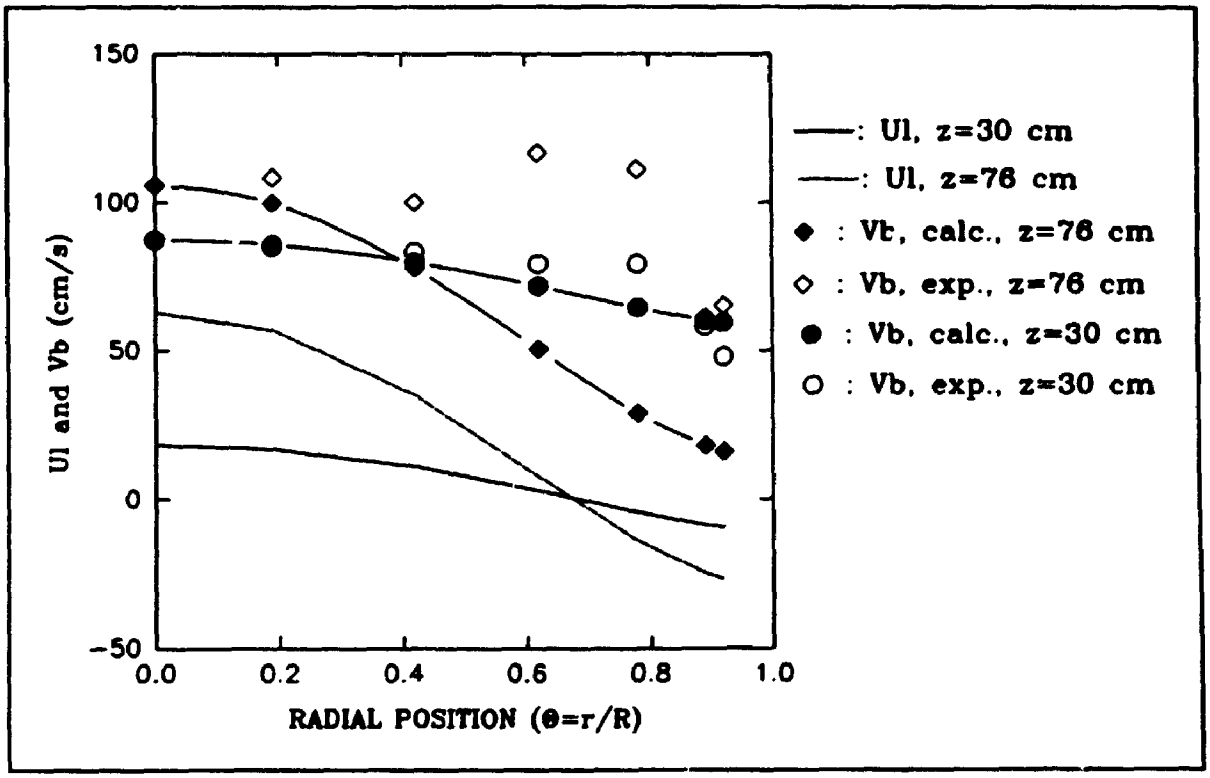

Figure 5.34c: Calculated U_l, V_b and experimental V_b, T=100°C, V_g=9.0 cm/s

241

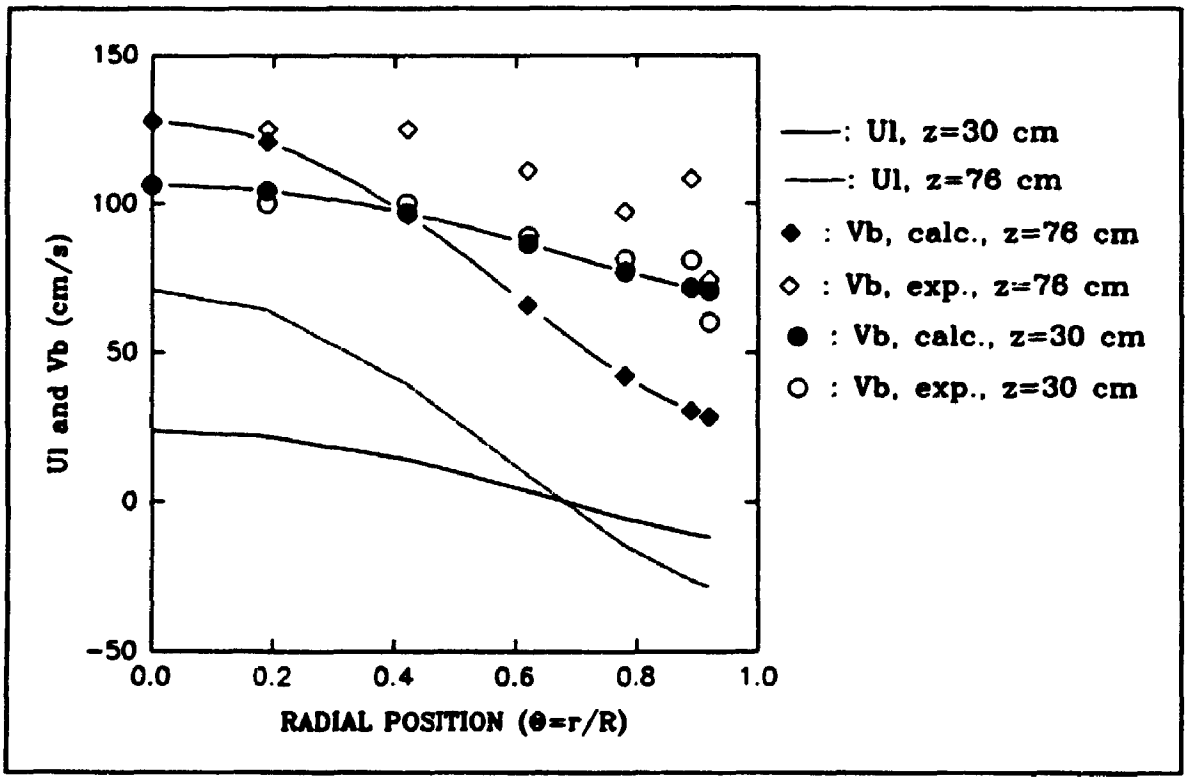

Figure 5.34d: Calculated U_l, V_b and experimental V_b, T=100°C, V_g=14.7 cm/s

242

flow predicted by the Ueyama and Miyauchi (1979) model increased, to reach stability at a distance of approximately 61 cm above the gas distributor. This distance corresponded to the establishment of the gas holdup radial profiles, as discussed in Section 5.1.1. Under the influence of the fully established liquid circulation regime, as previously discussed, important gas recirculation was expected. Under such conditions, the bubble rise velocities measured were expected to be actually higher than the net gas velocity (including both, upward and downward bubble velocity). As shown in Figures 5.34a to 5.34b, for z=76 cm, the measured bubble rise velocities were indeed higher than the calculated net gas velocities, especially in the peripheral region of the column. This indeed confirmed the presence of strong gas bubble backmixing under established liquid circulation regime. However, and for all the conditions studied, excellent correspondence was observed between the measured bubble rise velocities and the calculated ones in the central section of the column (θ=0.19), where bubble recirculation is minimum, as confirmed by Yao et al. (1991). On average, for all the gas superficial velocities studied, the discrepancy between calculated and measured bubble velocities was equal to 5.7% for θ=0.19, z=76 cm and T=100°C. This further confirmed the validity of the measured bubble rise velocities. The occurrence of gas backmixing was found to gradually increase from the bottom of the column to the top of the column as the liquid circulation flow reached the fully established regime,

243

as shown in Figure 5.36. Differences between measured bubble rise velocity and net gas velocity in the peripheral region of the column were also reported by Kago et al. (1989). However, these authors failed to recognize the possible presence of gas recirculation and rather suggested that the discrepancy could be due to entry effects. The measurements were however performed at a distance of 194 cm above the gas distributor (H/D_c=10.2), where entry effects should be minimum, as recently emphasized by Dudukovic and Devanathan (1992).

Similar trends as the ones observed at T=100°C were observed at T=175°C, as shown in Figures 5.35a and 5.35b. However, for this particular condition, gas backmixing was observed at the lower axial positions, as a result of both, stronger liquid circulation pattern at the bottom of the column and the presence of smaller bubbles, more susceptible to downward entrainment. Actually, the liquid circulation flow was observed to develop more quickly at T=175°C, as compared to T=100°C, thus suggesting more complete backmixing of the liquid flow at T=175°C, as shown in Figure 5.37. However, only slightly stronger established liquid circulation flow rate was observed at T=100°C, as compared to T=175°C, as shown in Figure 5.37. This is indeed consistent with the results of Ueyama and Miyauchi (1977) who did not observe a strong effect of the liquid viscosity under low liquid viscosity conditions (< 2 stokes). Under such condition, they claimed that the internal flow of liquid was a fully developed turbulent flow.

244

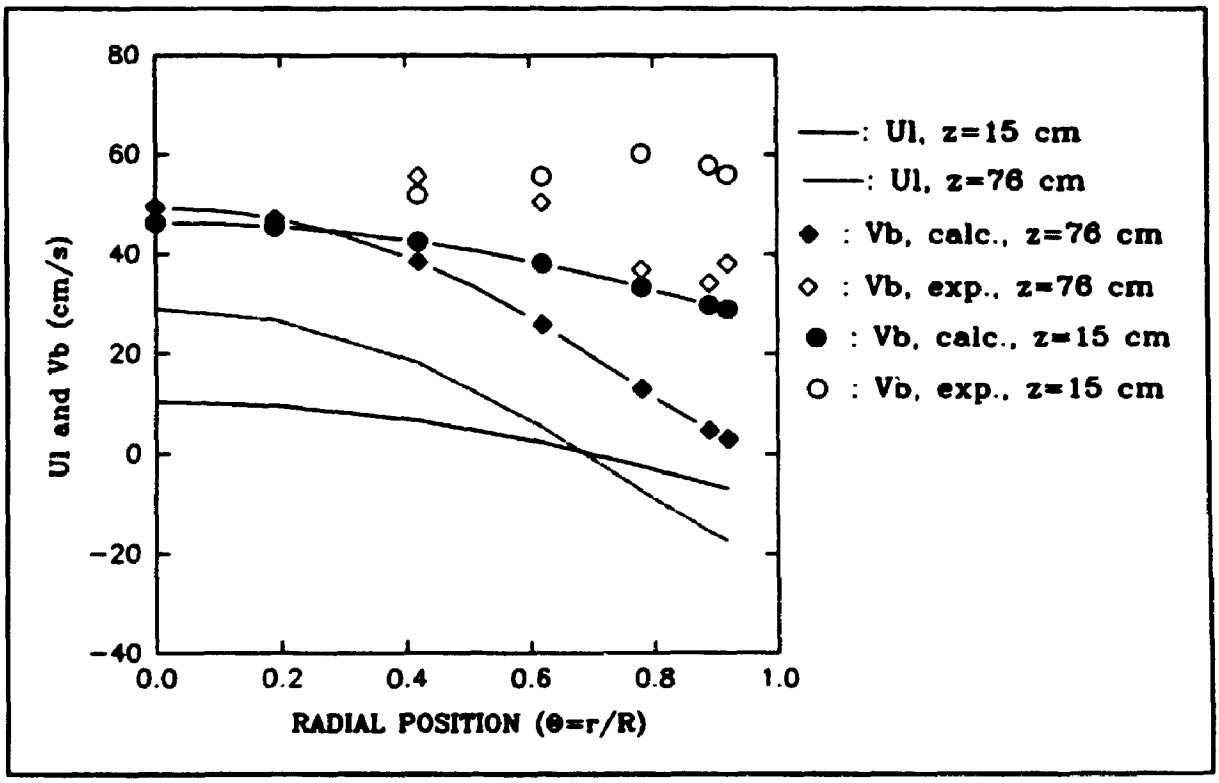

Figure 5.35a: Calculated U_l, V_b and experimental V_b, T=175°C, V_s=2.2 cm/s

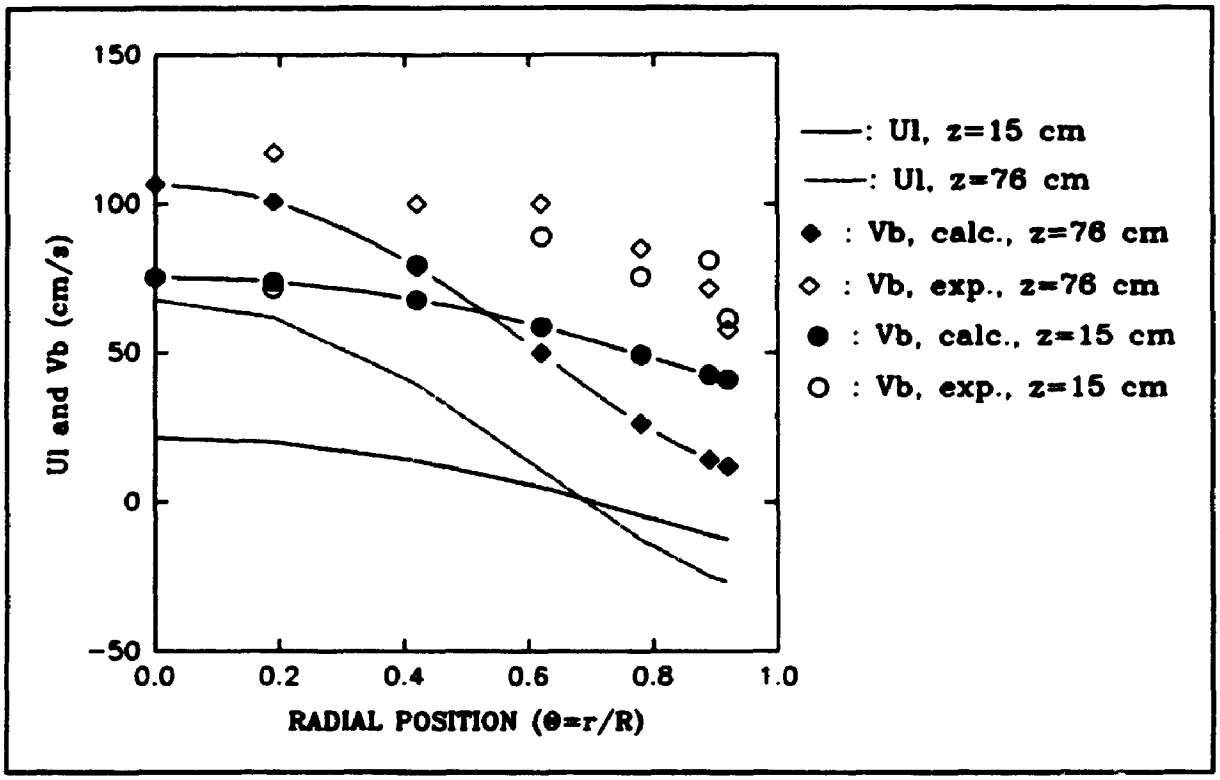

Figure 5.35b: Calculated U_l, V_b and experimental V_b, T=175°C, V_g=14.7 cm/s

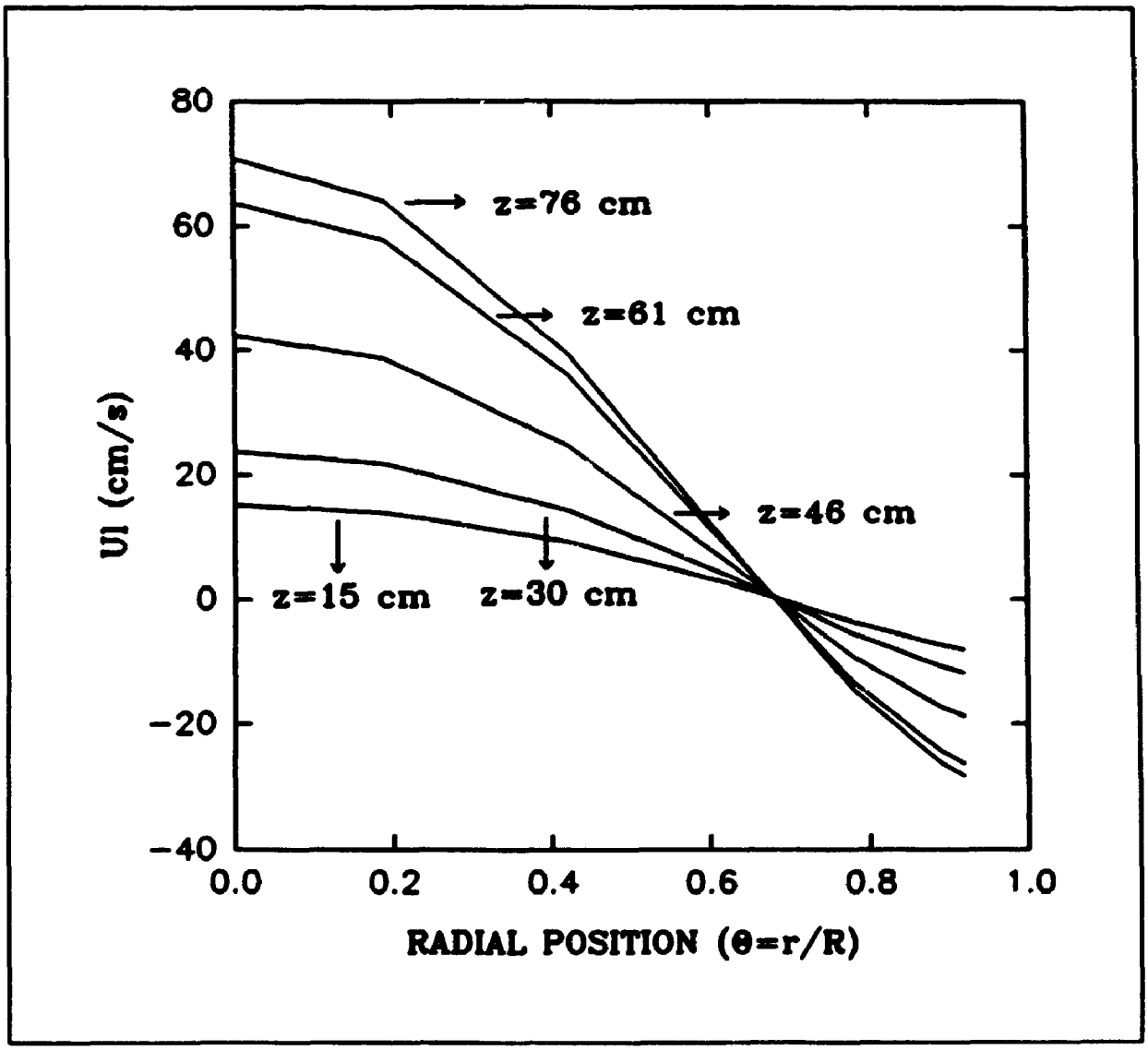

Figure 5.36: Liquid velocity vs radial position (V_g=14.7 cm/s, T=100°C)

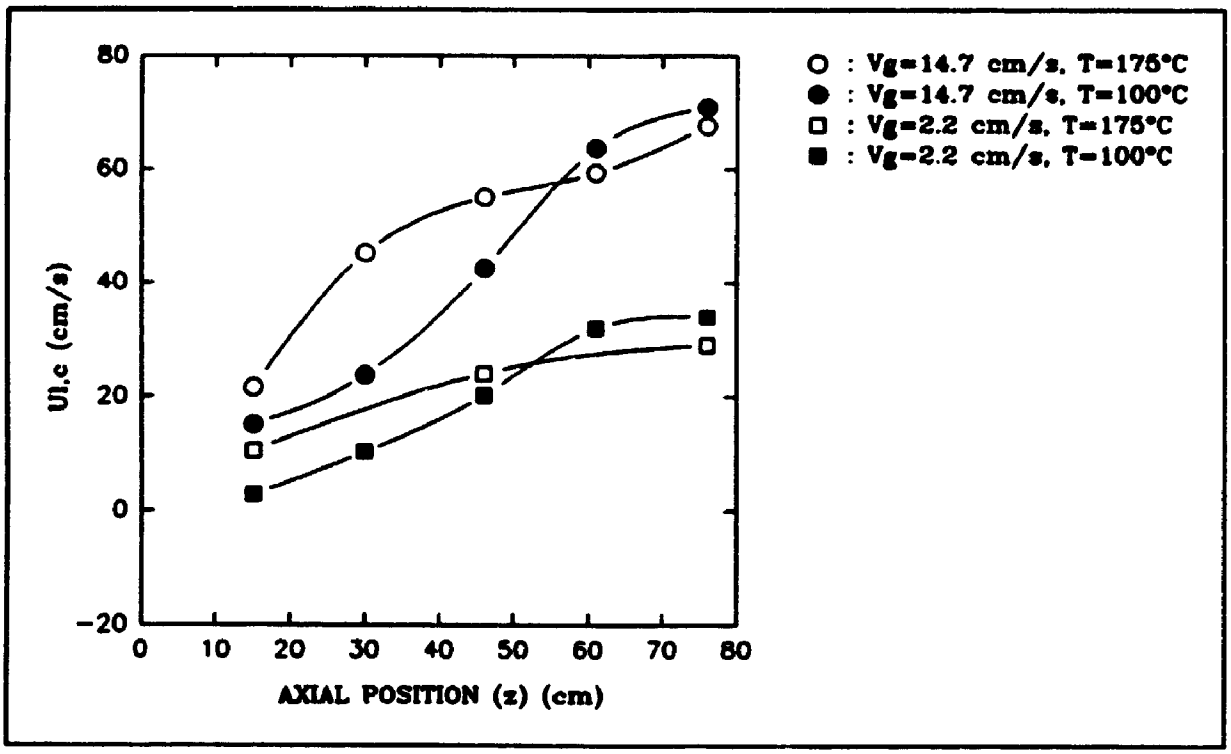

Figure 5.37: Axial evolution of the central liquid velocity

248

This is also in agreement with the fact that the turbulent liquid circulation model of Ueyama and Miyauchi (1979) predicted very well the experimental measurements.

The radial average slip velocities obtained, under fully established conditions (z=76 cm), from the Ueyama and Miyauchi (1979) model application are presented in Figure 5.38. As expected in the liquid circulation regime, the slip velocity increased with an increase of the gas superficial velocity. Furthermore, the slip velocity observed at T=175°C were smaller than the ones observed at T=100°C, since smaller gas bubbles were observed at T=175°C.

As previously explained, the turbulent kinematic viscosity was optimized to ensure the best possible closure of the gas mass balance. The values of the turbulent kinematic viscosity obtained for the fully established liquid circulation regime (z=76 cm) are presented in Figure 5.39a. As shown on this Figure, the turbulent kinematic viscosity was found to increase with the gas superficial velocity. The dependence of the turbulent kinematic viscosity on the gas superficial velocity was found to be well represented by a power law relationship, as shown in Figure 5.39a. The turbulent kinematic viscosity as well as the dependence of the turbulent kinematic viscosity on the gas superficial velocity were found to be slightly more pronounced at T=175°C, as compared to T=100°C. The turbulent kinematic viscosity is known to be a

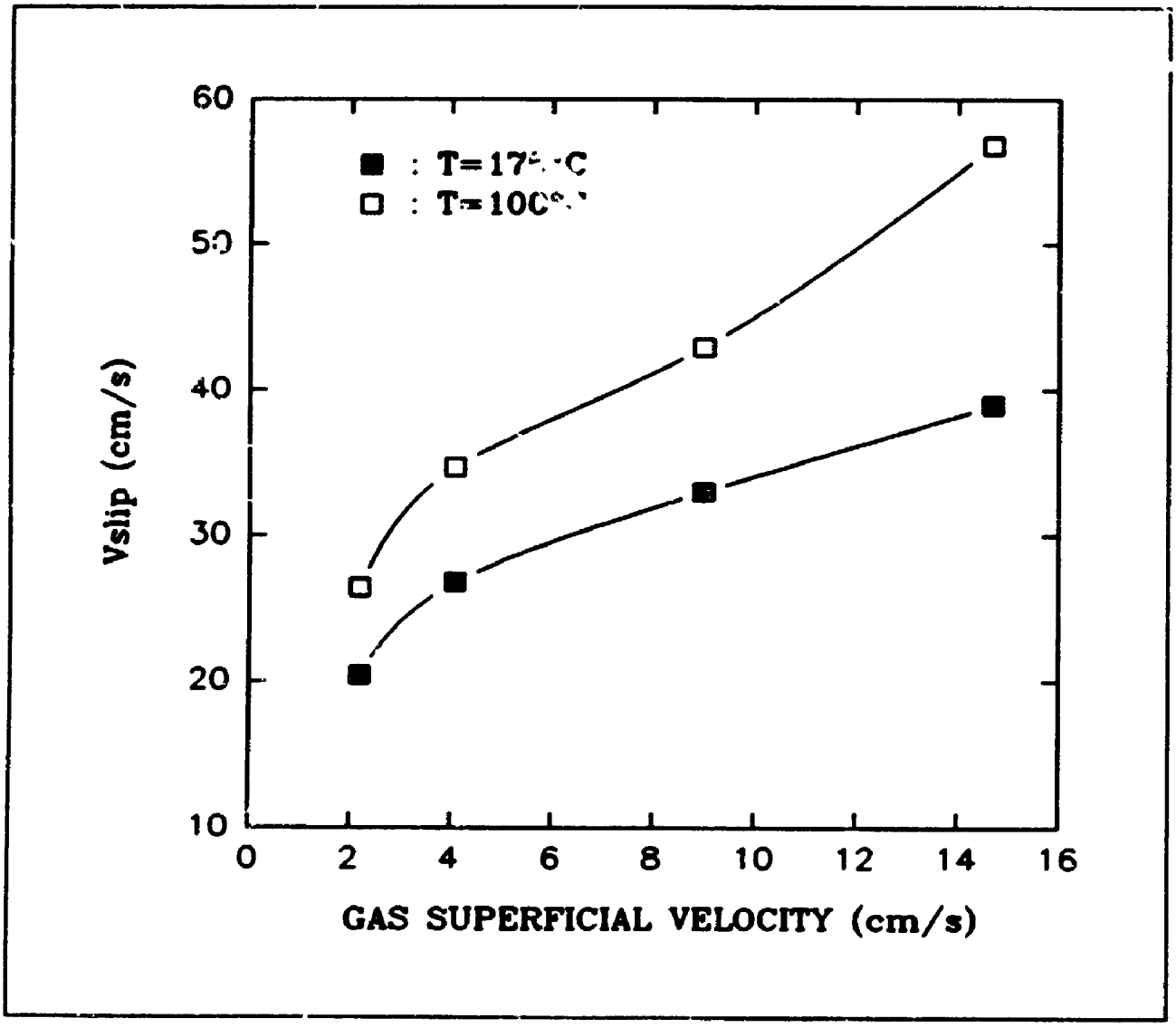

Figure 5.38: Gas slip velocity vs gas superficial velocity

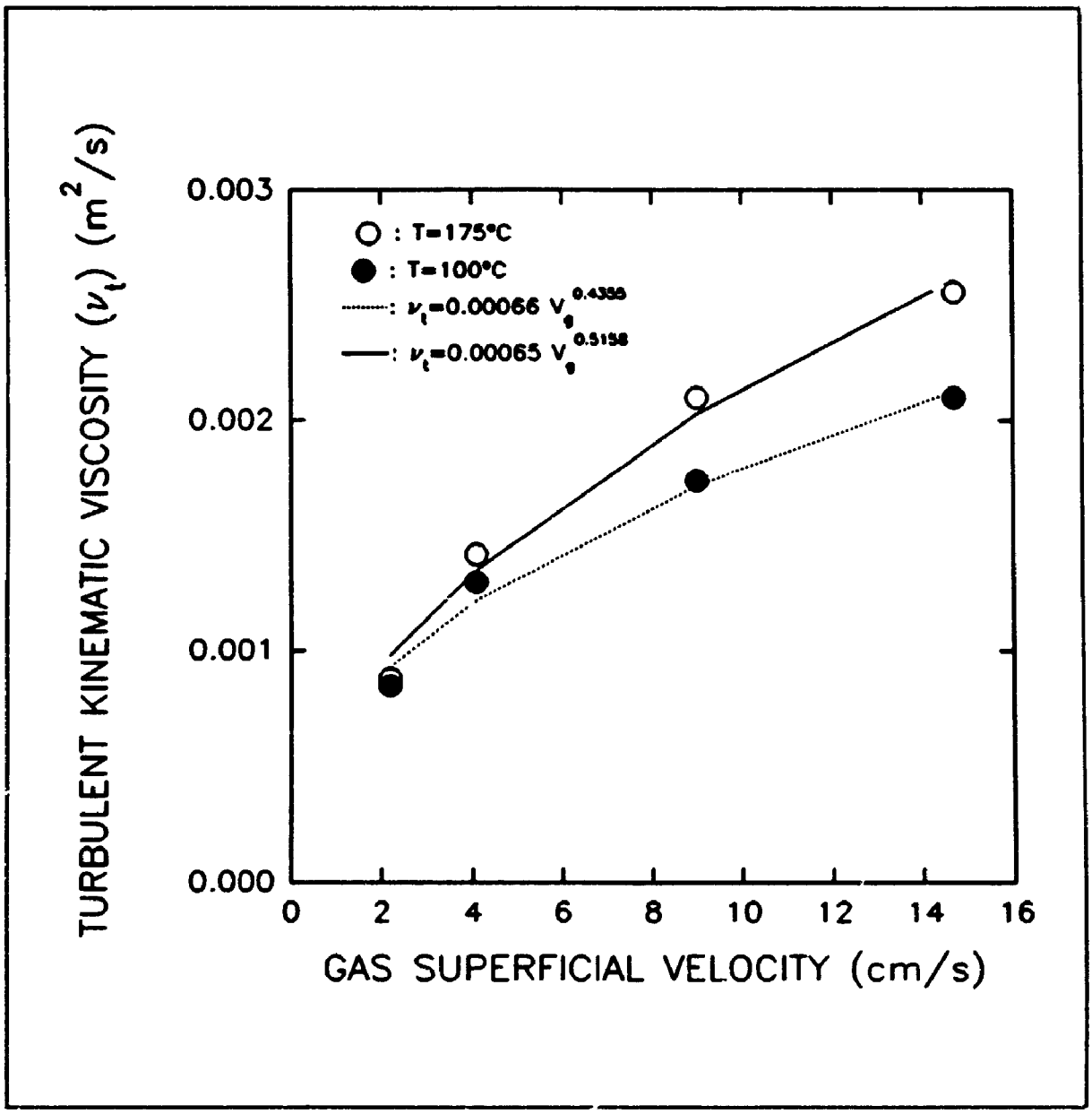

Figure 5.39a: Turbulent kinematic viscosity vs gas superficial velocity (z=76 cm)

251

function of the eddy scale. As discussed by Rice and Geary (1990), the scale of turbulent eddies in two-phase turbulent flow is expected to lie between the bubble average size and the diameter of the column. Furthermore, the number population density of bubbles is expected to enhance eddy scaling, becoming larger as bubble concentration (hence number of interactions) increases (Rice and Geary, 1990). So, as the temperature increases, the bubble size slightly decreases, while the number population density of bubbles increases considerably. As a consequence, the turbulent kinematic viscosity was found to increase with the temperature. In the same way, the bubble size and the bubble density were both found to increase with the gas superficial velocity, and, as a consequence, an increase of the turbulent kinematic viscosity was observed. It is interesting to note that, under the conditions investigated in the present study, the dependence of the turbulent kinematic viscosity on the gas superficial velocity was found to be higher than the one suggested by Miyauchi et al. (1981). However, the values of the turbulent kinematic viscosities observed in the present study were found to be, in general, smaller than the values observed in air/water systems (Ueyama and Miyauchi, 1979) and, on average, smaller than the values predicted by both empirical equations previously mentioned (Equations 5.6.b and 5.6.c). This could be due to the fact that in the present system, smaller bubbles than the ones typically observed in air/water systems were present. Furthermore, as shown in

Figures 5.39b and 5.39c, the turbulent kinematic viscosity was found to be a function of the axial position. As shown in Figures 5.39b and 5.39c, the eddy kinematic viscosity was found to be larger in the bottom of the column than at higher axial positions. The larger turbulent kinematic viscosity observed in the bottom of the column was due to entry effects. These entry effects were found to be more pronounced at T=100°C than at T=175°C, which is consistent with the fact that liquid circulation patterns are evolving more rapidly at the higher temperature.

In summary, cautious gas mass balance and mathematical analysis were implemented and led to the confirmation of the fibre optic sensors' ability to perform bubble phase measurements, even under severe conditions. Important insights concerning the general utilization of gas mass balance analysis in validating experimental gas phase measurements in bubble column systems were also obtained. Local bubble rise velocities were found, in general, to decrease with the radial position, suggesting upward liquid circulation patterns in the center and downward liquid circulation at the wall. In fact, strong evidence of downward bubble displacement along the wall of the column was provided. Furthermore, for some particular conditions, (low gas superficial velocity: V_g=2.2 cm/s; lower axial positions: z=15 cm, z=30 cm), a larger bubble rise velocity was observed in the vicinity of the wall than in the central section of the

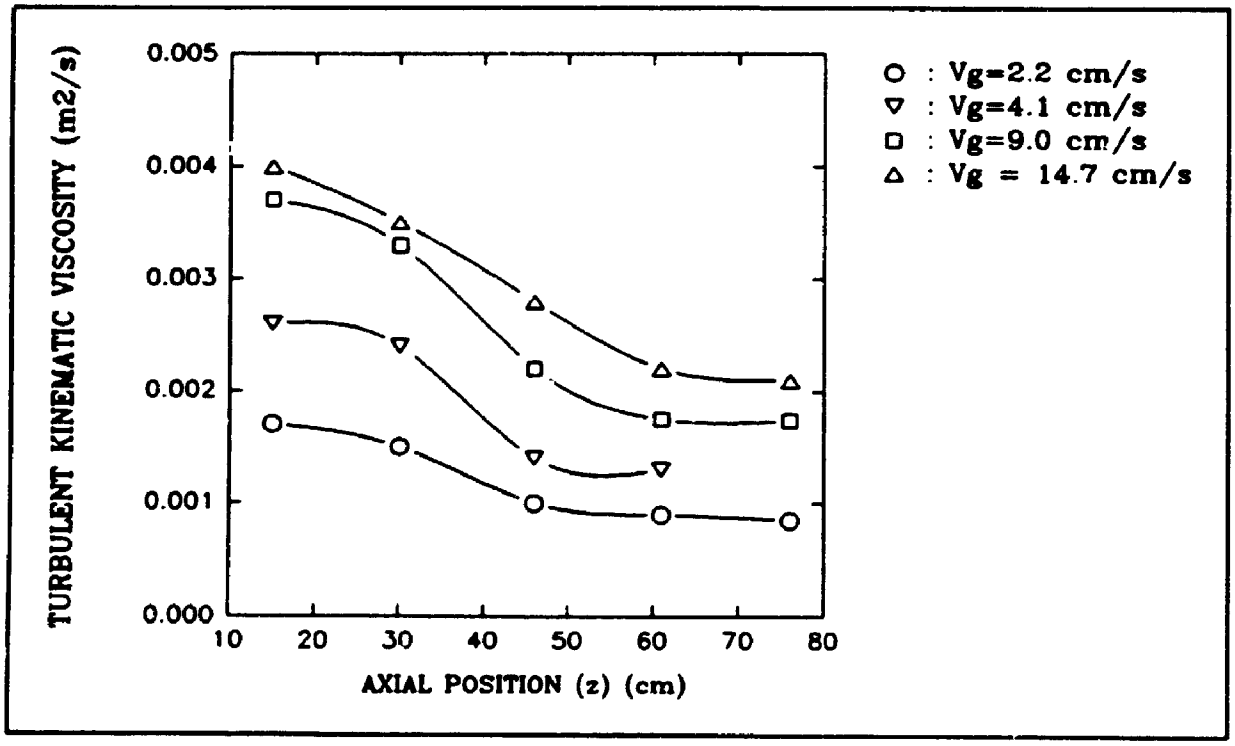

Figure 5.39b: Turbulent kinematic viscosity vs axial position (T=100°C)

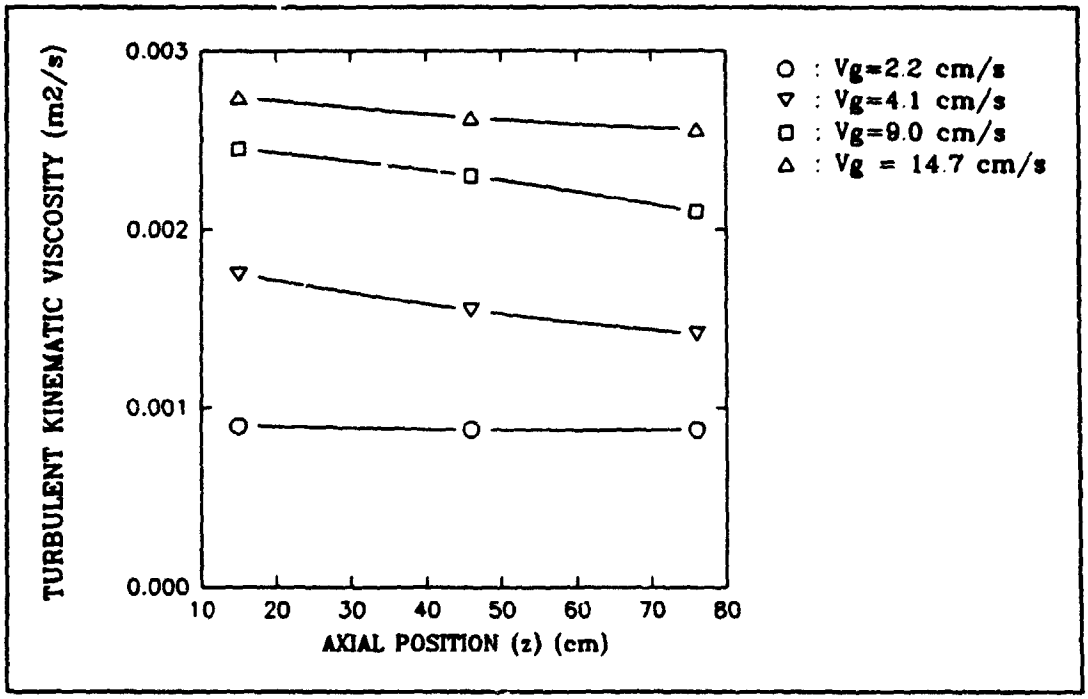

Figure 5.39c: Turbulent kinematic viscosity vs axial position (T=175°C)

column. This important observation supported the conclusion that a secondary countercurrent liquid circulation cell indeed was present. Evidence of this phenomenon through bubble detection was never reported before for bubble column system of significant importance for the methanol synthesis process. Furthermore, the identification of the secondary liquid circulation cell under severe operating conditions (T=100-200°C) confirmed the sensitivity and precision of the optical sensors in tracking bubble behaviour. In addition, the bubble rise velocity profiles were found to become steeper as both, the gas superficial velocity and the axial position increased. Faster bubble rise velocities were also noted as the superficial velocity augmented and the operating temperature decreased. Furthermore, the ability of the Ueyama and Miyauchi (1979) model in representing properly the trend of the experimentally measured bubble rise velocities was satisfactorily verified. The implementation of this model allowed, for the first time, to obtain important insight concerning the influence of the axial position, gas superficial velocity and temperature on the turbulent kinematic viscosity of hydrocarbon systems.

5.1.4 Bubble chord length and "coalescence-break-up" bubble flow regime

The average bubble chord length, for a given operating condition and position, was obtained by multiplying the average bubble rise velocity by the average bubble detection peaks duration measured at this same condition and position. The bubble chord length radial profiles obtained for the various gas superficial velocities studied (V_g=2.2, 4.1, 9.0 and 14.7 cm/s) are presented in Figures 5.40 to 5.43 for the experiments conducted at T=100°C and in Figures 5.44 to 5.47 for the ones performed at T=175°C. As expected, the bubble chord length decreased as the radial position increased, with the exception, for both temperatures investigated (T=100°C and T=175°C), the two lower axial position (z=15 cm) and V_g=2.2 cm/s. Actually, for this particular condition, the bubble chord length was found to be 22.7% and 22.4% larger, for T=100°C and T=175°C respectively, in the periphery of the column wall as compared to the central region of the column. These results are indeed consistent with the particular secondary liquid circulation cell proven (section 5.1.3) to be present in the bottom section of the column under these same conditions. The upward liquid velocity vector present in the vicinity of the column wall induced a preferential current, with lower slip velocities than would normally be expected at this particular location, and thus unfavourable conditions for bubble break-up phenomena. On the contrary, in the central

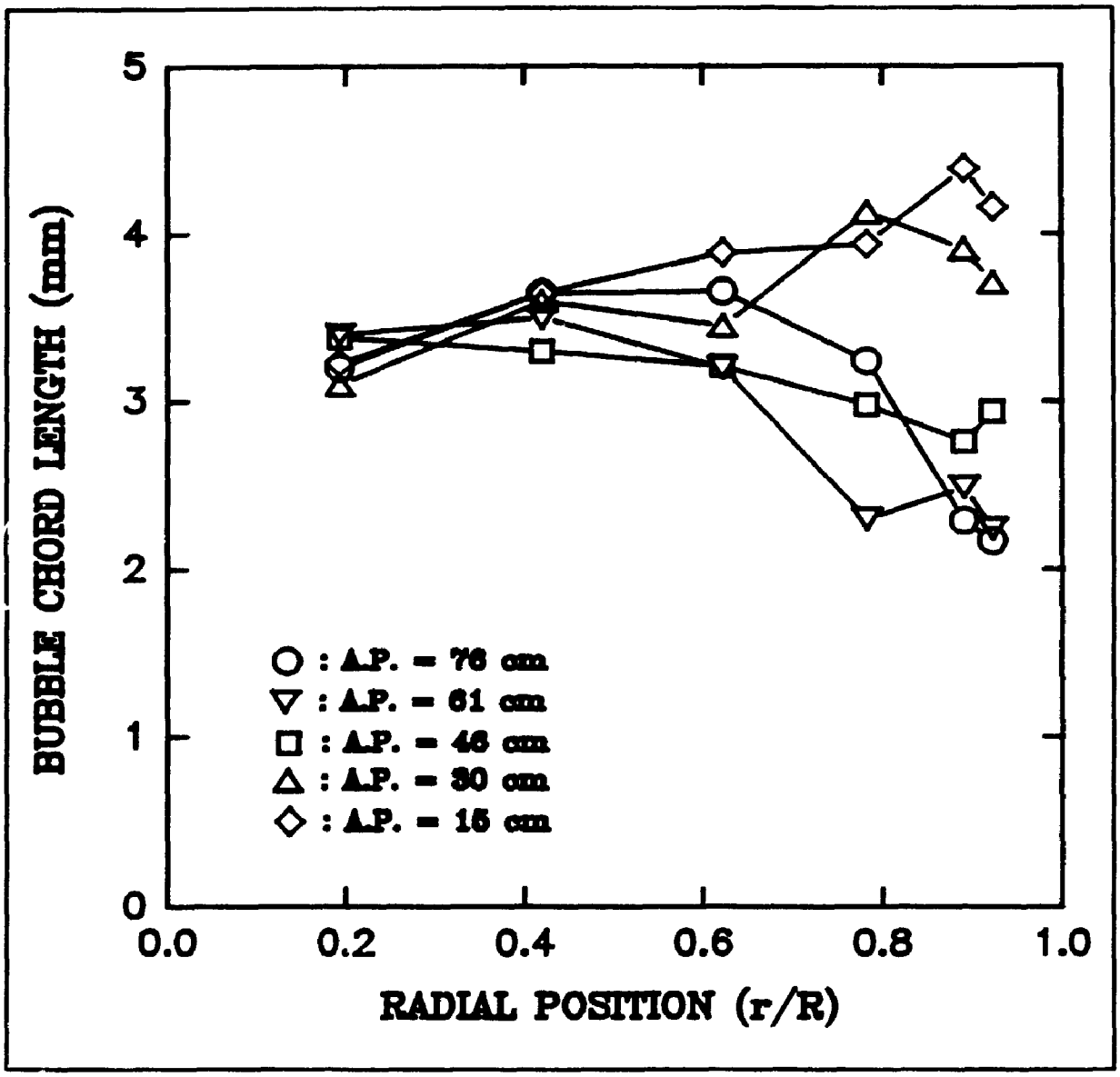

Figure 5.40: Bubble chord length vs radial position
(T=100°C, V_g=2.2 cm/s)

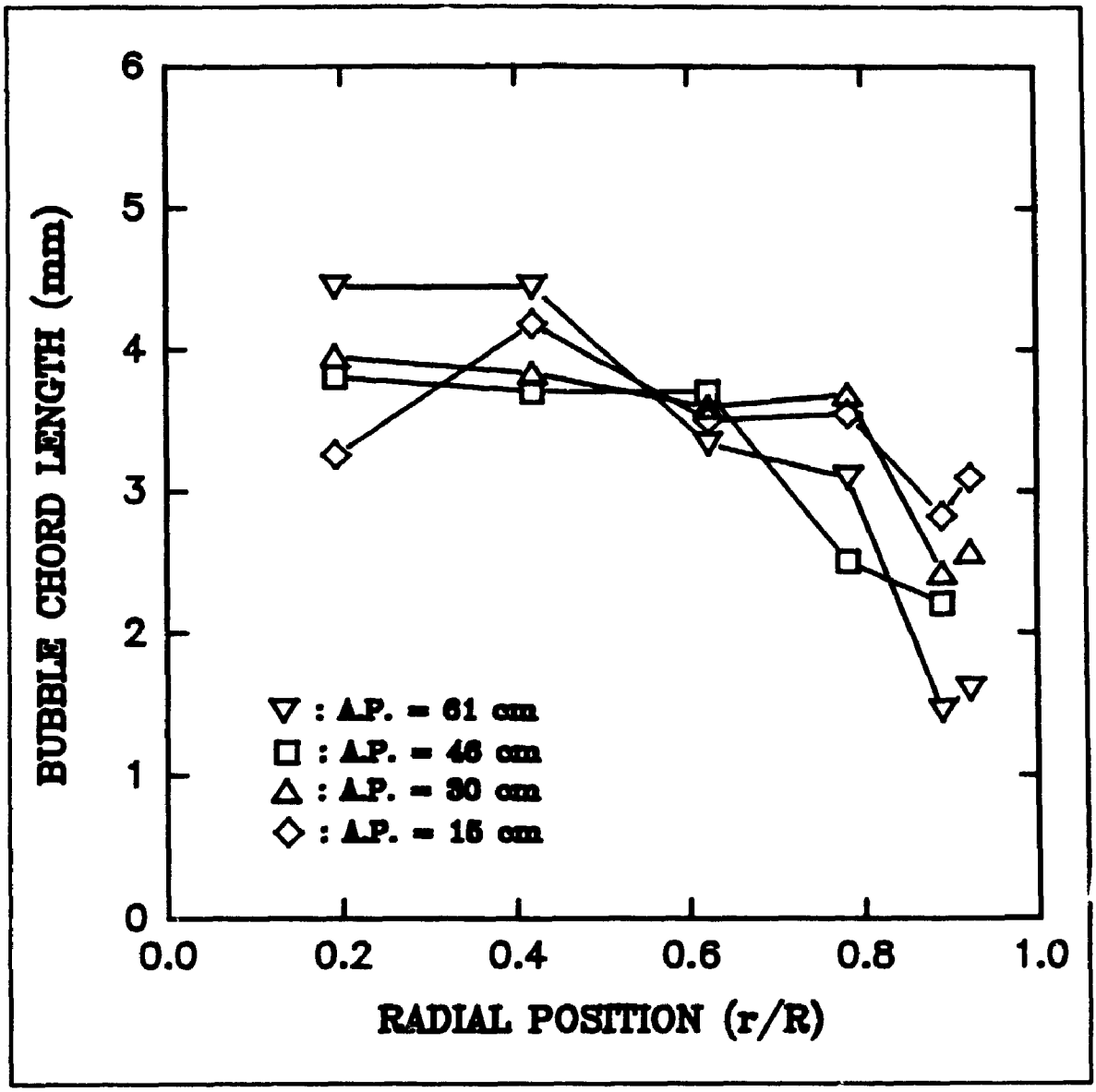

Figure 5.41: Bubble chord length vs radial position
(T=100°C, V_g=4.1 cm/s)

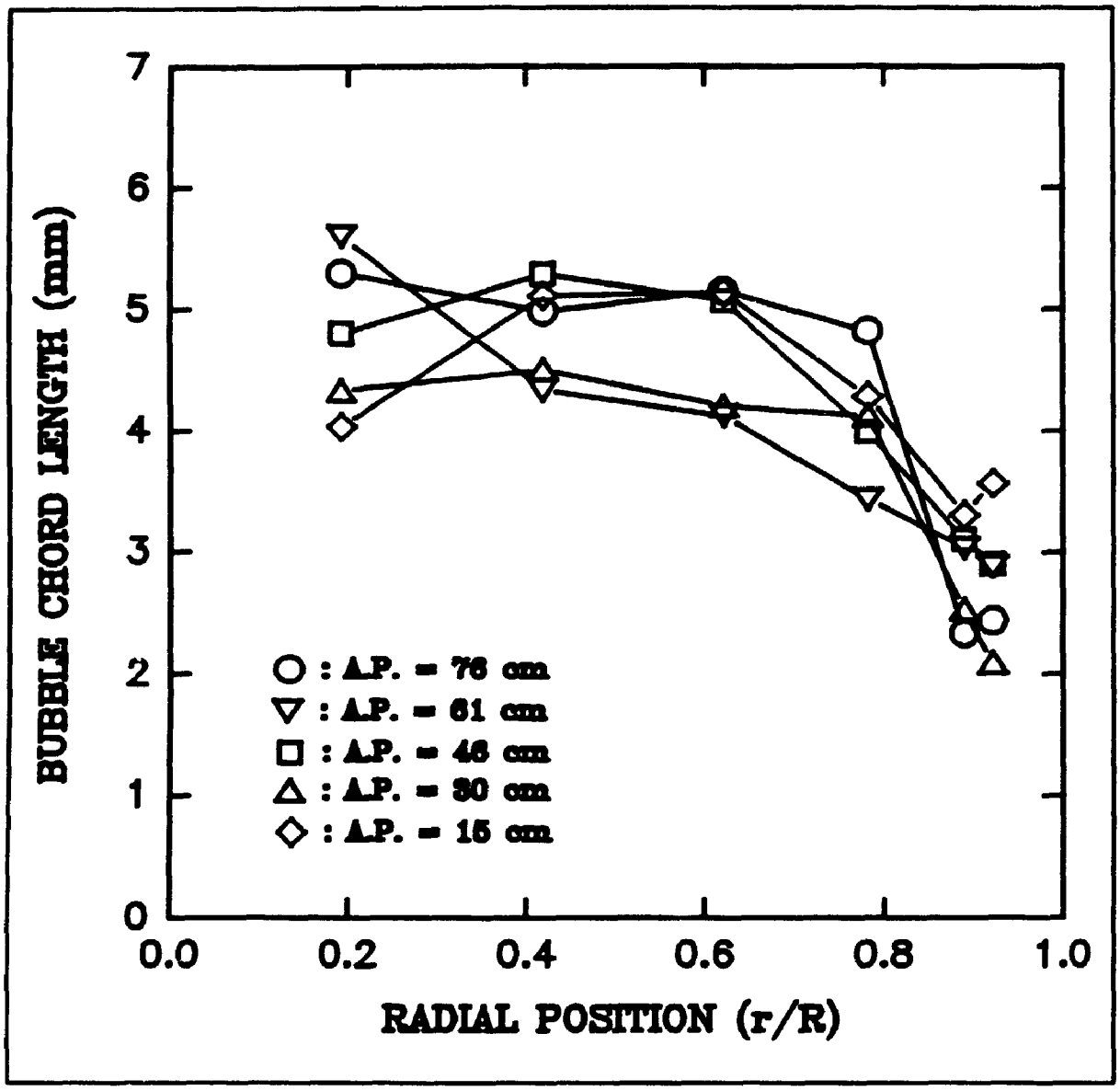

Figure 5.42: Bubble chord length vs radial position
(T=100°C, V_g=9.0 cm/s)

260

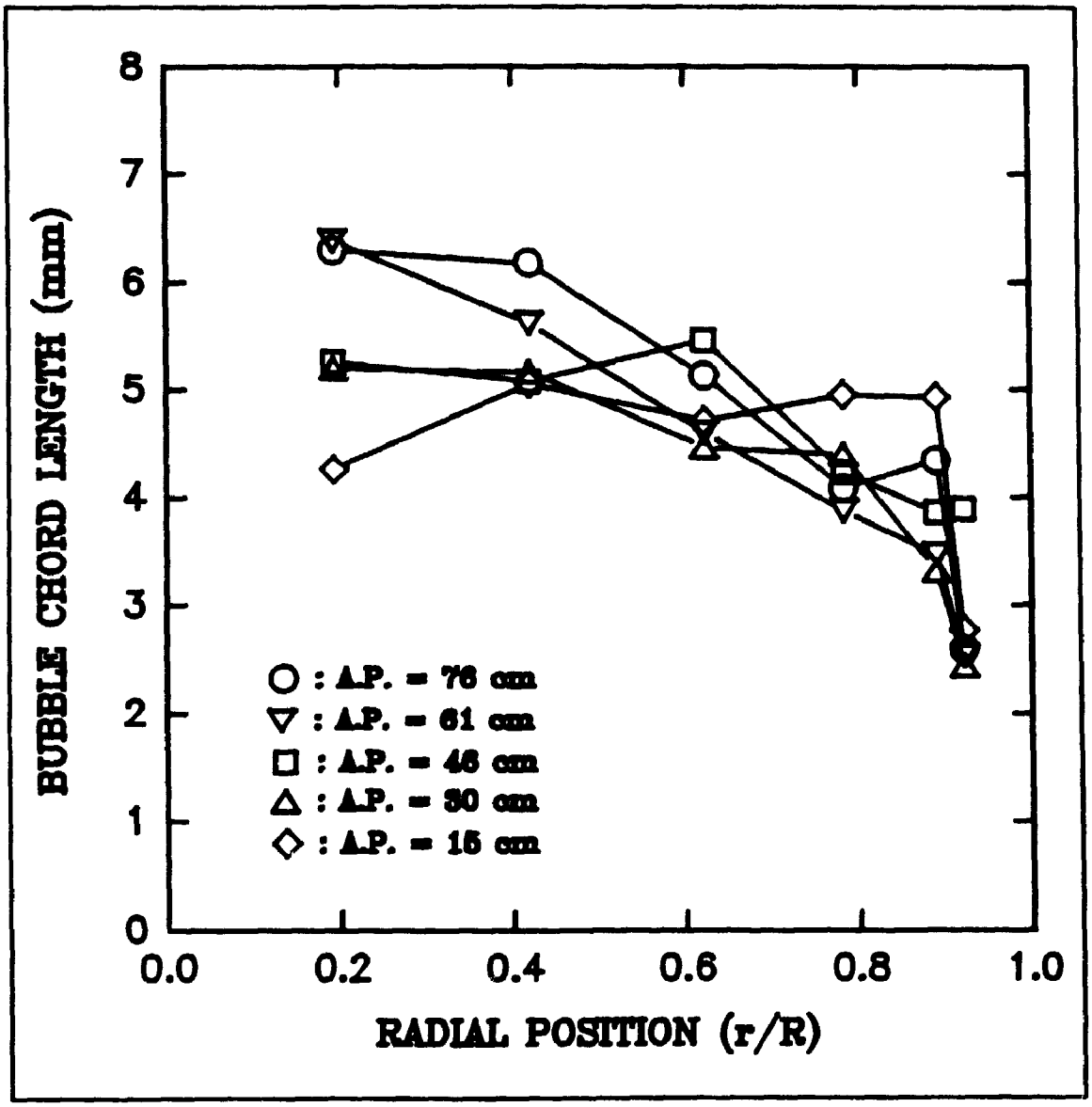

Figure 5.43: Bubble chord length vs radial position
(T=100°C, V_t=14.7 cm/s)

261

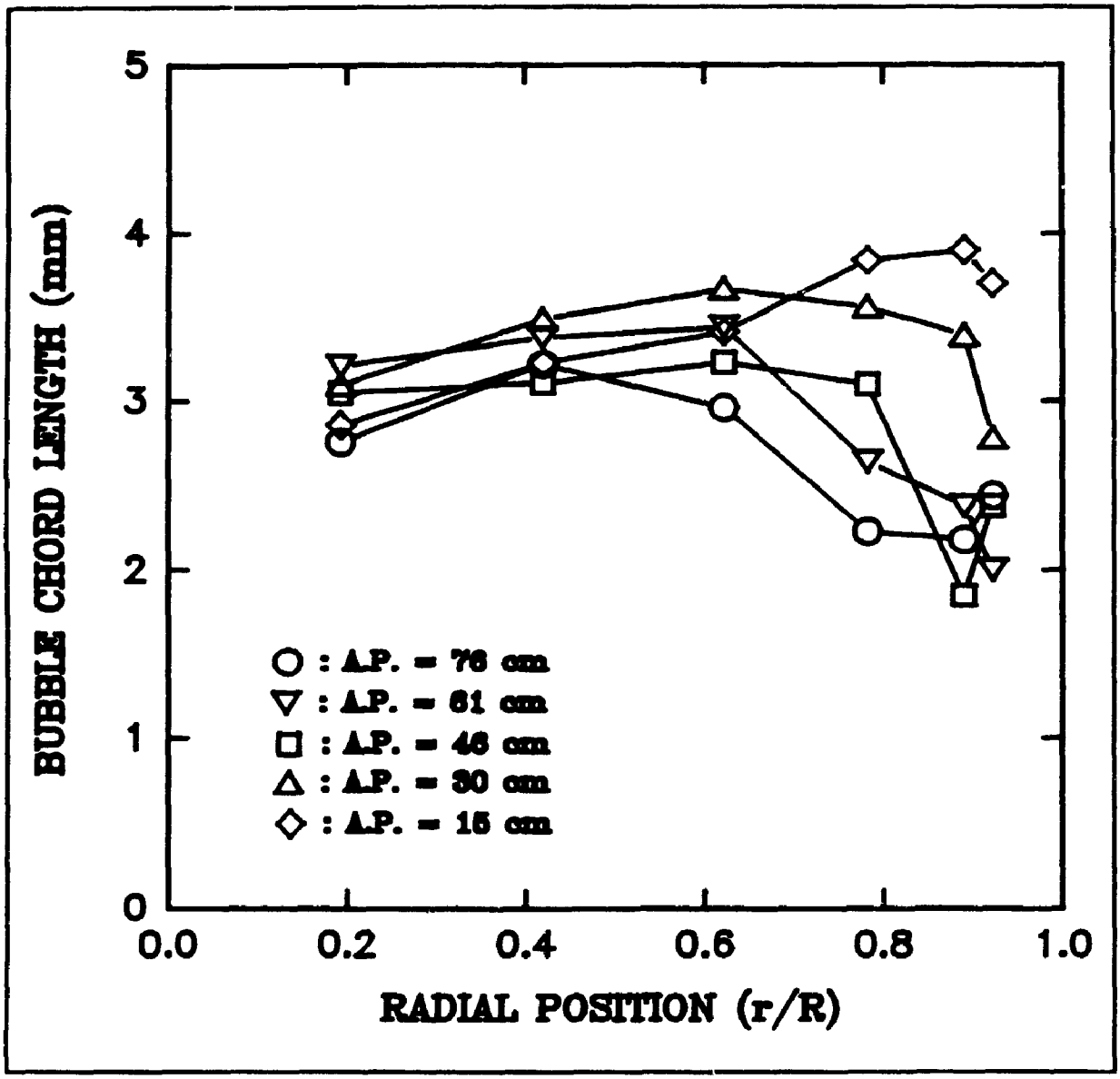

Figure 5.44: Bubble chord length vs radial position
(T=175°C, V_g=2.2 cm/s)

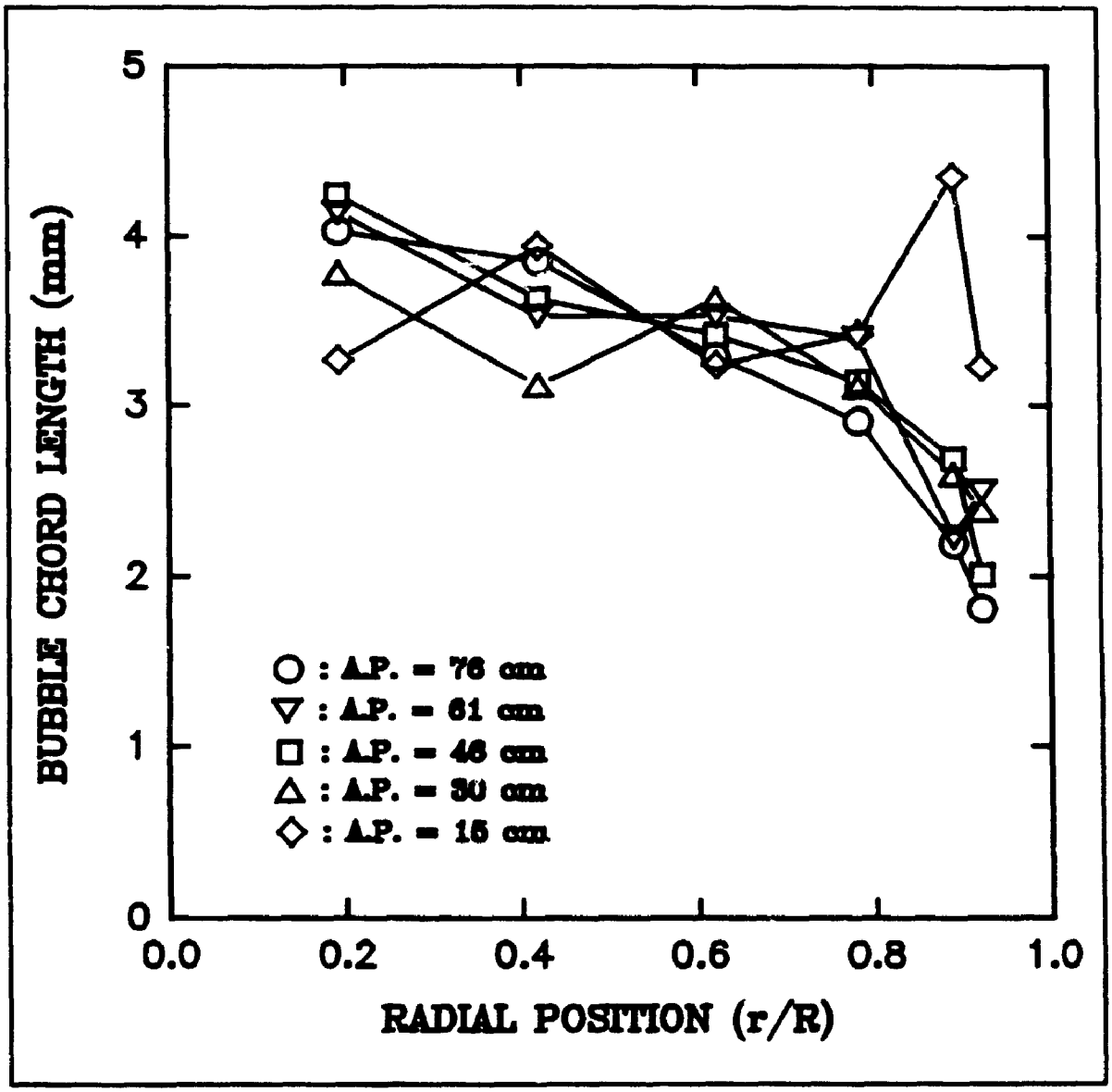

Figure 5.45: Bubble chord length vs radial position
(T=175°C, V_g=4.1 cm/s)

263

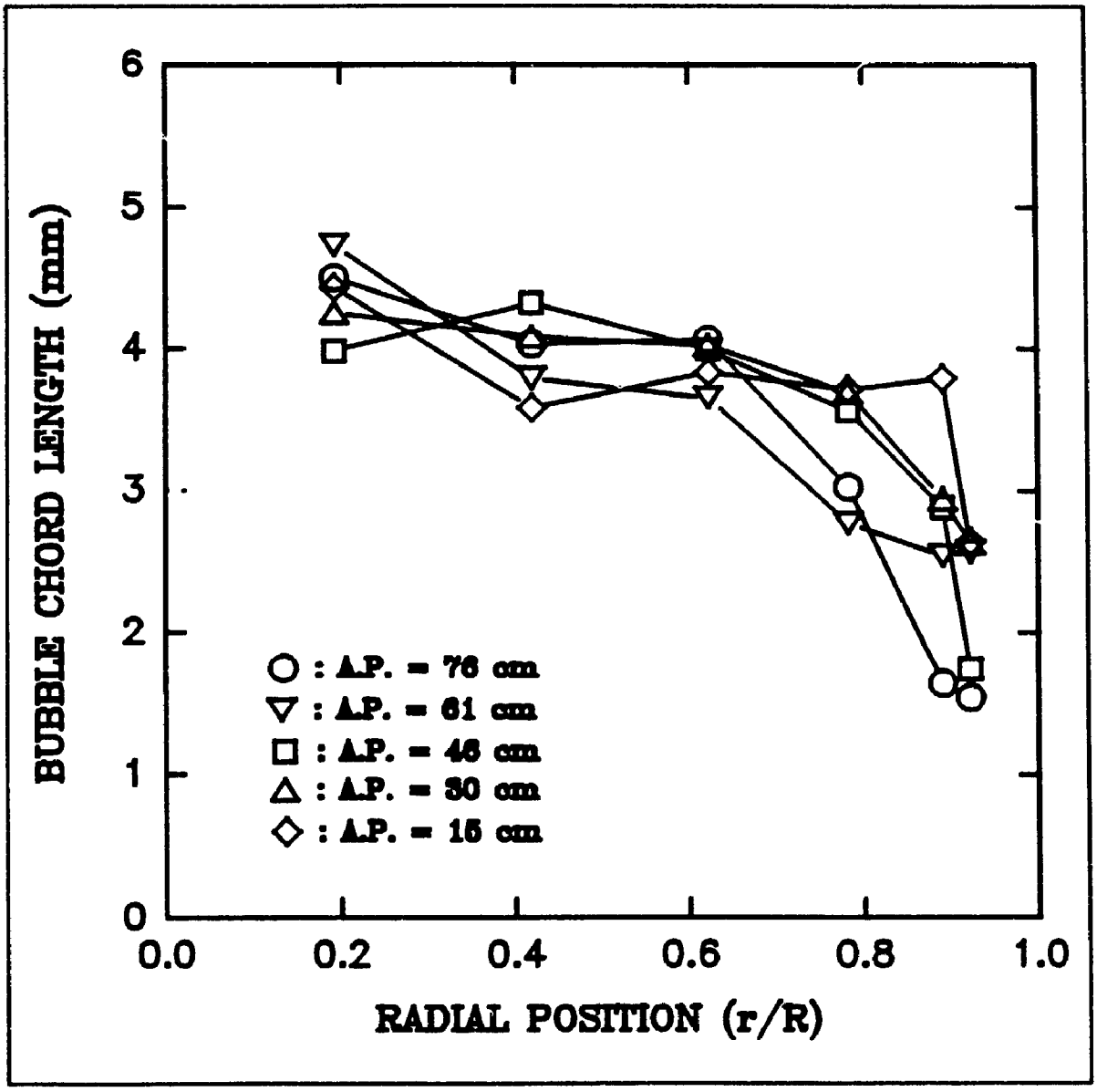

Figure 5.46: Bubble chord length vs radial position
(T=175°C, V_g=9.0 cm/s)

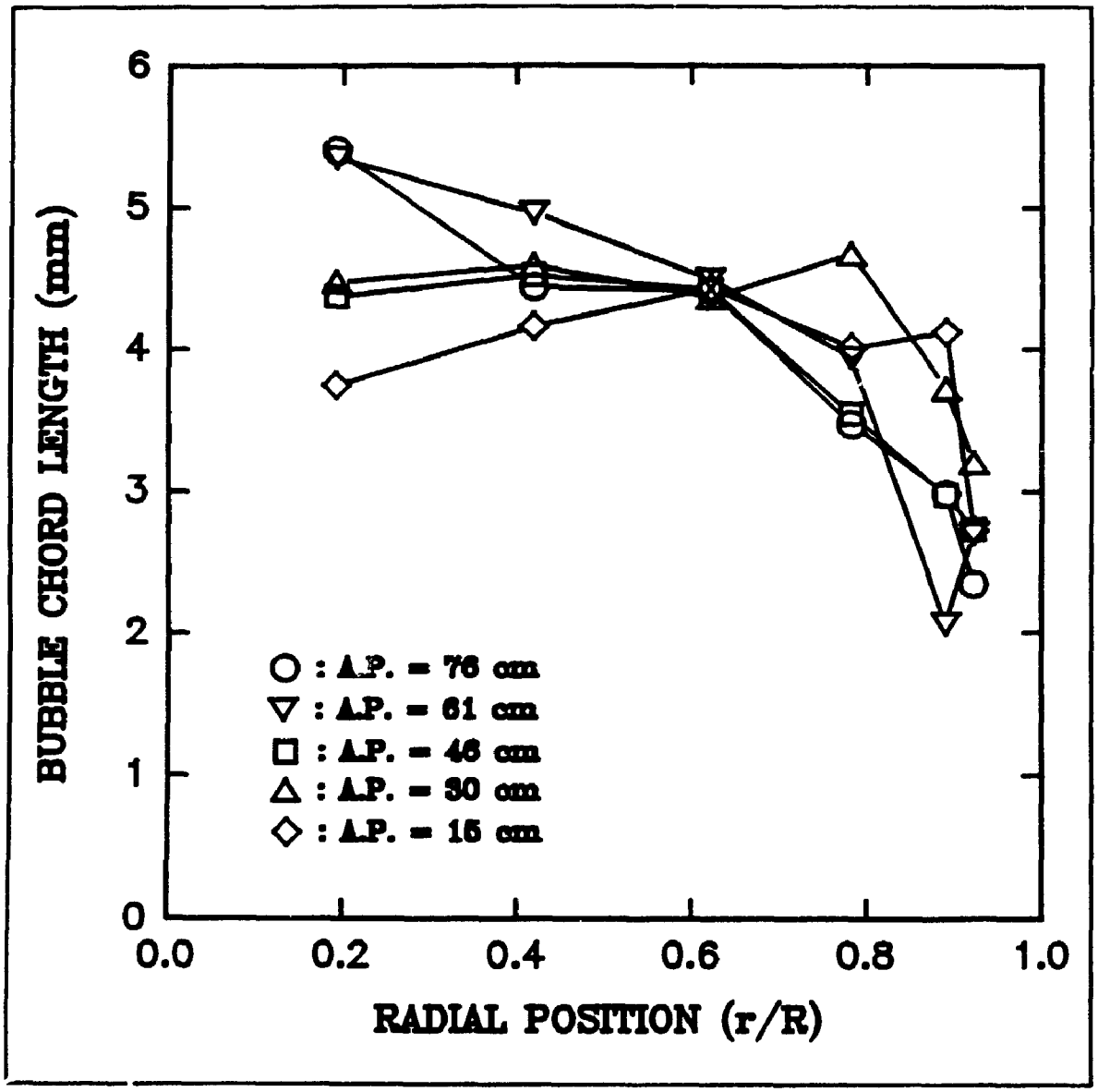

Figure 5.47: Bubble chord length vs radial position
(T=175°C, V_g=14.7 cm/s)

region of the column, a downward liquid velocity vector, and consequently higher slip velocities than normally encountered at this location was present, thus inducing extra turbulence and consequently contributing to bubble break-up phenomena and small bubbles recirculation. For all the other operating conditions, the bubble chord length was found to decrease with an increase in the radial position, as expected when upward liquid circulation is present in the central portion of the column and downward liquid velocity vector is present in the proximity of the wall. Actually, under such conditions, larger bubbles tend to rise in the center while smaller bubbles remain in the vicinity of the column wall.

The average radial bubble chord length was found to decrease with the axial position, for the lower gas superficial velocities (V_g=2.2, 4.1 and 9.0 cm/s), or remain relatively constant for the highest gas superficial velocity studied (V_g=14.7 cm/s). These observations indicated the dominance of bubble break-up phenomena over bubble coalescence phenomena for the lower gas superficial velocities, and a relative equilibrium between both phenomena at the higher gas superficial velocity. Thus, for the lower gas superficial velocities, the presence of an overall bubble disintegrating regime was observed. The average radial bubble axial chord length is represented as a function of the axial position in Figure 5.48 for the experiments conducted at T=100°C and in Figure 5.49 for the experiments performed at T=175°C. It is

interesting to note, on these Figures, the presence of larger bubbles at V_g=2.2 cm/s as compared to V_g=4.1 cm/s for the two lower axial positions investigated (z=15 cm, z=30 cm). Such observation could be justified considering the effect of tne secondary liquid circulation cell present under these particular conditions (V_g=2.2 cm/s; z=15 cm, z=30 cm). Actually, the presence of the secondary liquid circulation cell (characterized by upward liquid velocity vector at the wall and downward liquid velocity current in the central region of the column) in the bottom of the column and the existence of the main *classical* liquid circulation cell in the upper section of the column, created two distinct and relatively isolated regions. These two separated cells favoured segregation between the bubble population present in the bottom region of the column (secondary liquid cell region) and the one present in the upper region of the column (classical liquid circulation cell). Consequently, the overall smaller bubble population present in the upper section of the column (generated along the length of the column from break-up events, as discussed in detail in the following pages) was segregated from the larger bubble population (still relatively unaffected by bubble break-up events occurring at relatively small rates under low gas superficial velocity) present in the bottom of the column. Then, the smaller bubbles present in the upper section and recirculated downward along the wall of the column under the influence of the main classical liquid circulation cell (downward liquid velocity

vector along the wall of the column) could not be mixed with the ones present within the secondary liquid circulation cell. In consequence, the bubble population observed within the secondary liquid circulation cell region, was relatively unaffected by the smaller bubbles normally recirculated downward by the downward liquid circulation pattern present along the wall of the column. Then, larger bubbles were observed at this particular location, as opposed to the case (V_g=4.1 cm/s) where the single liquid circulation cell allowed more complete (toward lower axial position) backmixing of the small bubbles at the lower axial positions. However, as the gas superficial velocity was further increased, larger bubbles were generated at the gas distributor, as shown in Figures 5.48 and 5.49.

As illustrated in Figures 5.48 and 5.49, the decrease in the bubble axial chord length with the axial position appeared to be more pronounced at the lower gas superficial velocities studied. Actually, such observation was found to be in agreement with the axial variation of the bubble frequency. In fact, as typically shown in Figures 5.50 and 5.51, the bubble frequency was found to increase with the axial position, for all the conditions investigated. This indicated the presence of overall dominant break-up phenomena over coalescence phenomena. However, the increase of the bubble frequency with the axial position was found to become less pronounced as the gas superficial velocity augmented, as shown in Figures 5.50

268

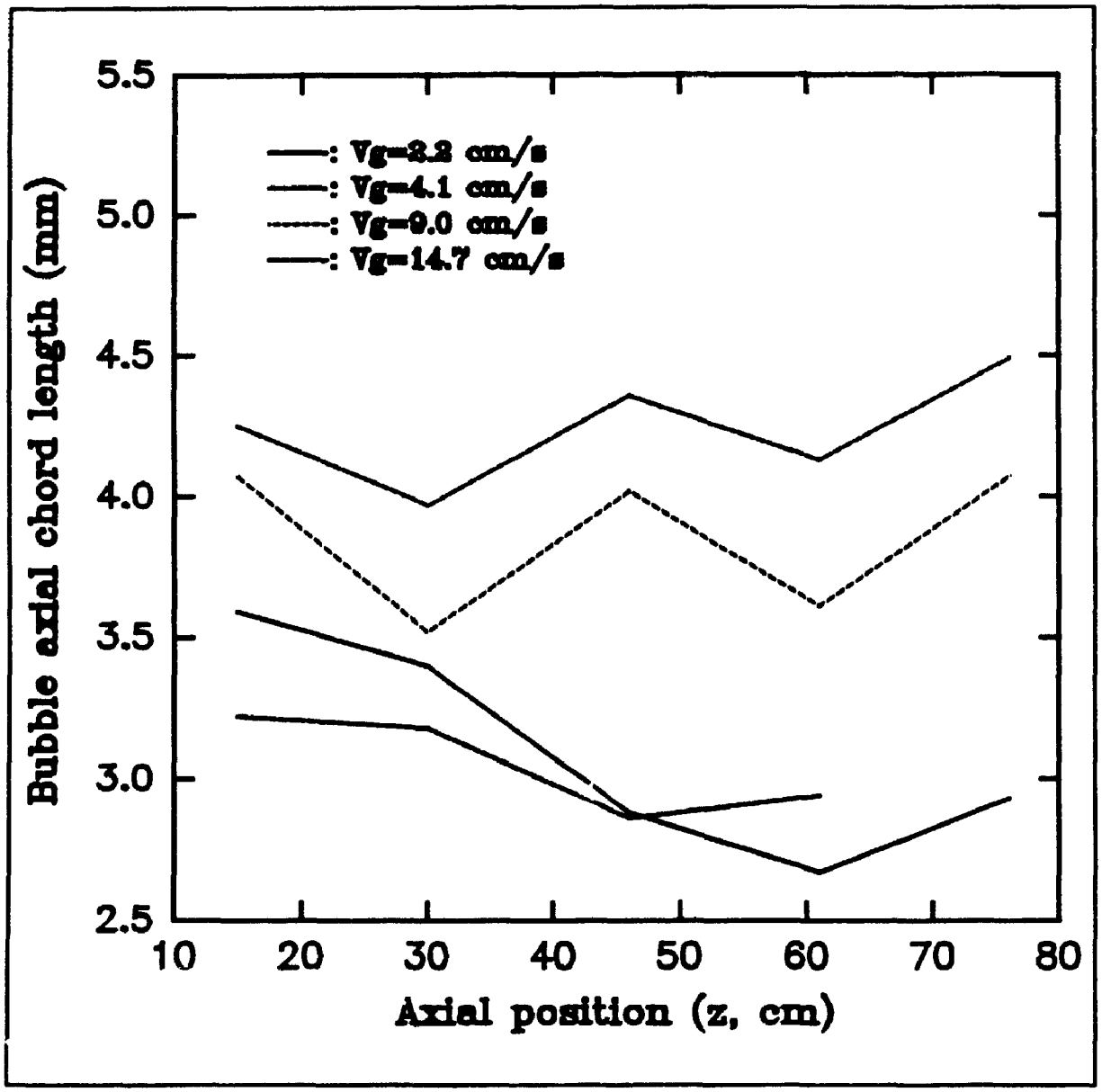

Figure 5.48: Average radial bubble axial chord length vs axial position (T=100°C)

269

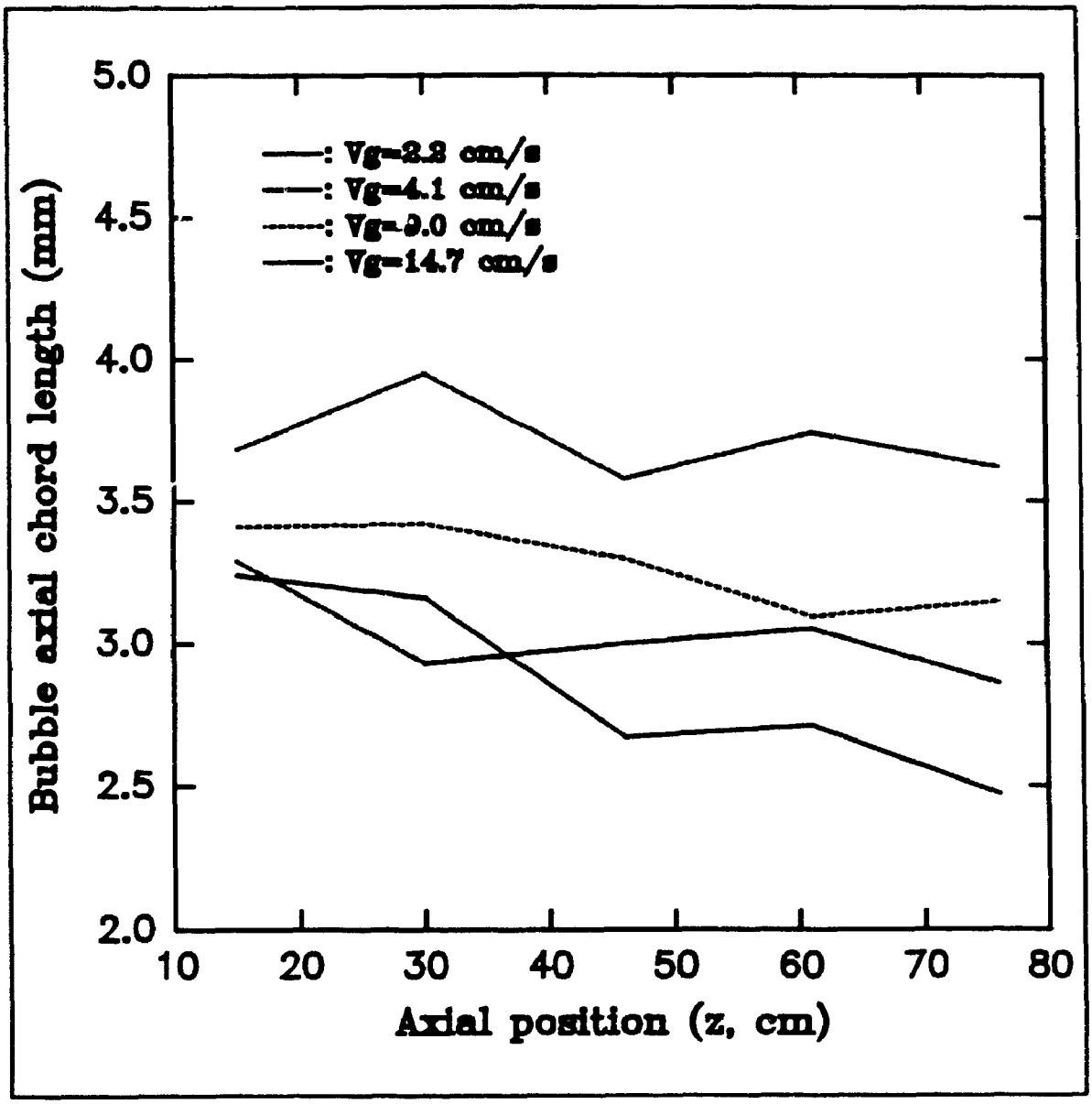

Figure 5.49: Average radial bubble axial chord length vs axial position (T=175°C)

270

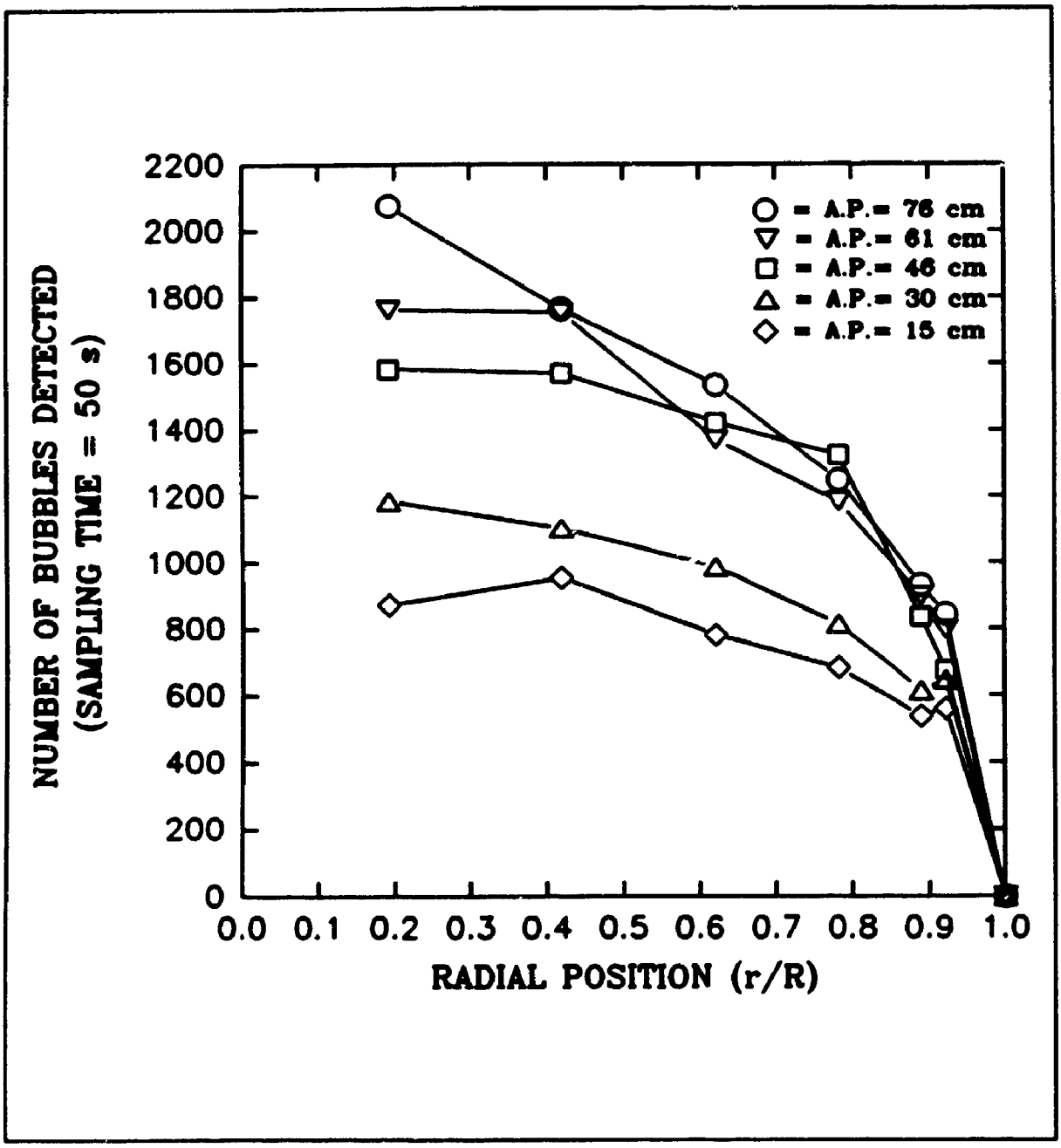

Figure 5.50: Bubble frequency vs radial position (T=175°C, V_g=4.1 cm/s)

271

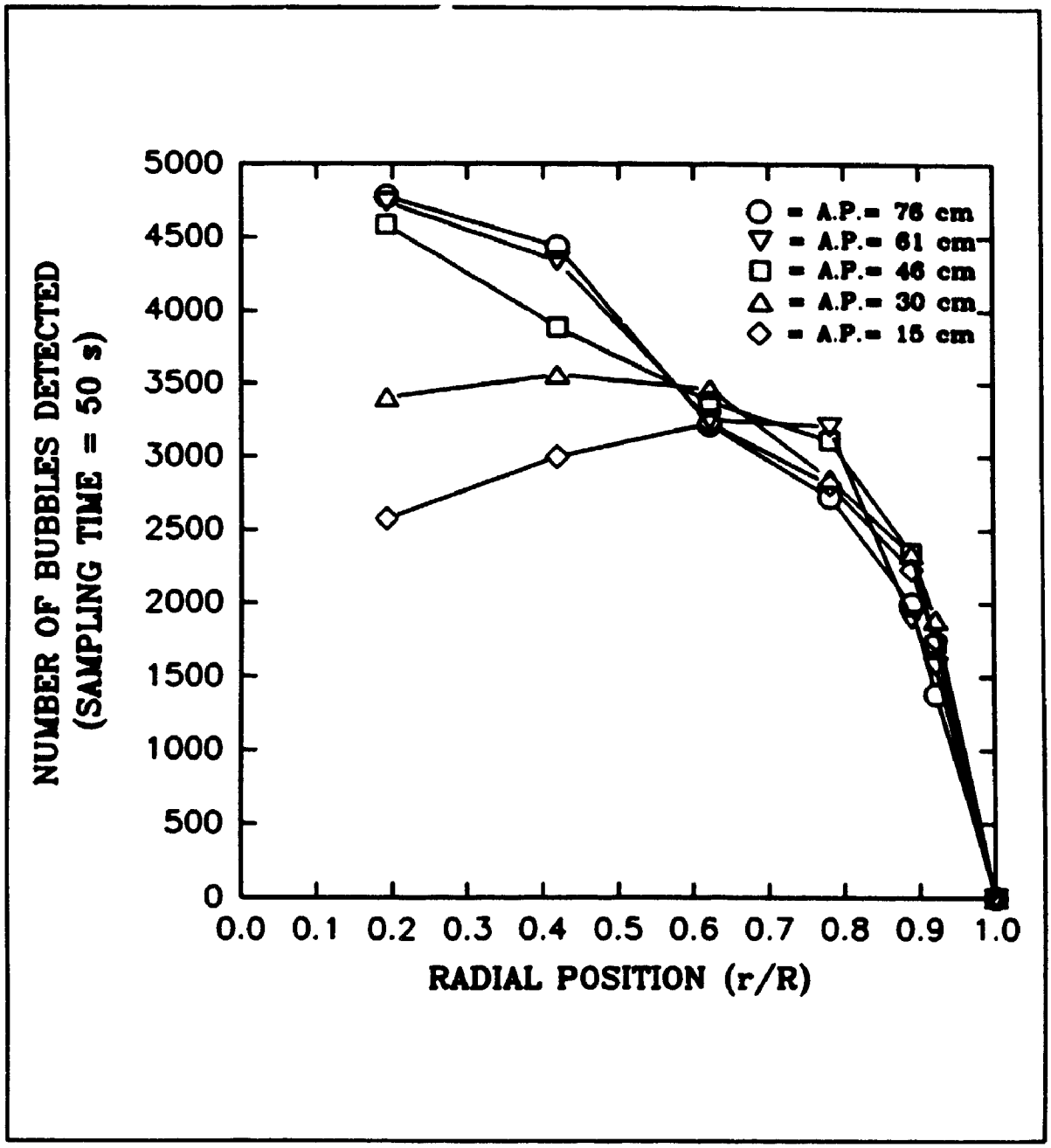

Figure 5.51: Bubble frequency vs radial position (T=175°C, V_g=14.7 cm/s)

and 5.51. The pronounced dominance of break-up events at low gas superficial velocities resulted in a decrease of the average radial bubble axial chord length with the axial position, which in turn favoured an increase of the average radial gas holdup with the axial position, as discussed in section 5.1.2. In other words, the presence of more smaller gas bubbles as the axial position increased indicated the presence of the bubble disintegrating regime and provided a forceful justification for the increase of the gas holdup with the axial position reported in section 5.1.2. At the highest gas superficial velocities, the increase of the bubble frequency with the axial position was more moderate. This could be explained by the fact that under this condition, very high bubble break-up rate and more substantial coalescence rate are present, as suggested by Prince and Blanch (1990). As the gas superficial velocity increases, bubbles are subjected to a higher bubble density environment. Such situation favours the probability of contact between bubbles and consequently increases the probability of coalescence, as compared to lower gas superficial velocity conditions. However, as the gas superficial velocity increases, the turbulence intensity increases and so does the probability of break-up events. Consequently, in a system where break-up events are naturally highly favoured (as shown by the high incidence of break-up events even at low gas superficial velocity), an increase of the turbulence intensity induced by an increase of the gas superficial velocity would be

translated in high bubble break-up rates. Under such high bubble break-up rate, it is possible that a number of bubble break-up events had already been taking place below the first measurement window investigated (z=15 cm) (this hypothesis will actually be verified in the next pages). These phenomena would then explain the lower increase of the bubble frequency and the more uniform average bubble chord length size with the axial position observed. These, in turn, contributed to a more uniform average gas holdup along the length of the column, as discussed in Section 5.1.2.

The overall decrease of the average radial bubble axial chord length with the axial position was however found to be non-uniform throughout the cross section of the column, and was noted to change with the operating conditions. As previously mentioned, an increase of the local bubble axial chord length with the axial position was consistently observed in the central region of the column, while a decrease of the local bubble axial chord length with the axial position was noticed in the vicinity of the column wall, as illustrated in Figure 5.52a and 5.52b. As shown in Figures 5.40 to 5.47, the radial profiles of the bubble chord length were found to become steeper (less uniform) as the axial position was increased. This is indeed in agreement with the increase of the bubble chord length with the axial position in the central section of the column, and the decrease of the bubble chord length with the axial position in the periphery of the column wall. This

274

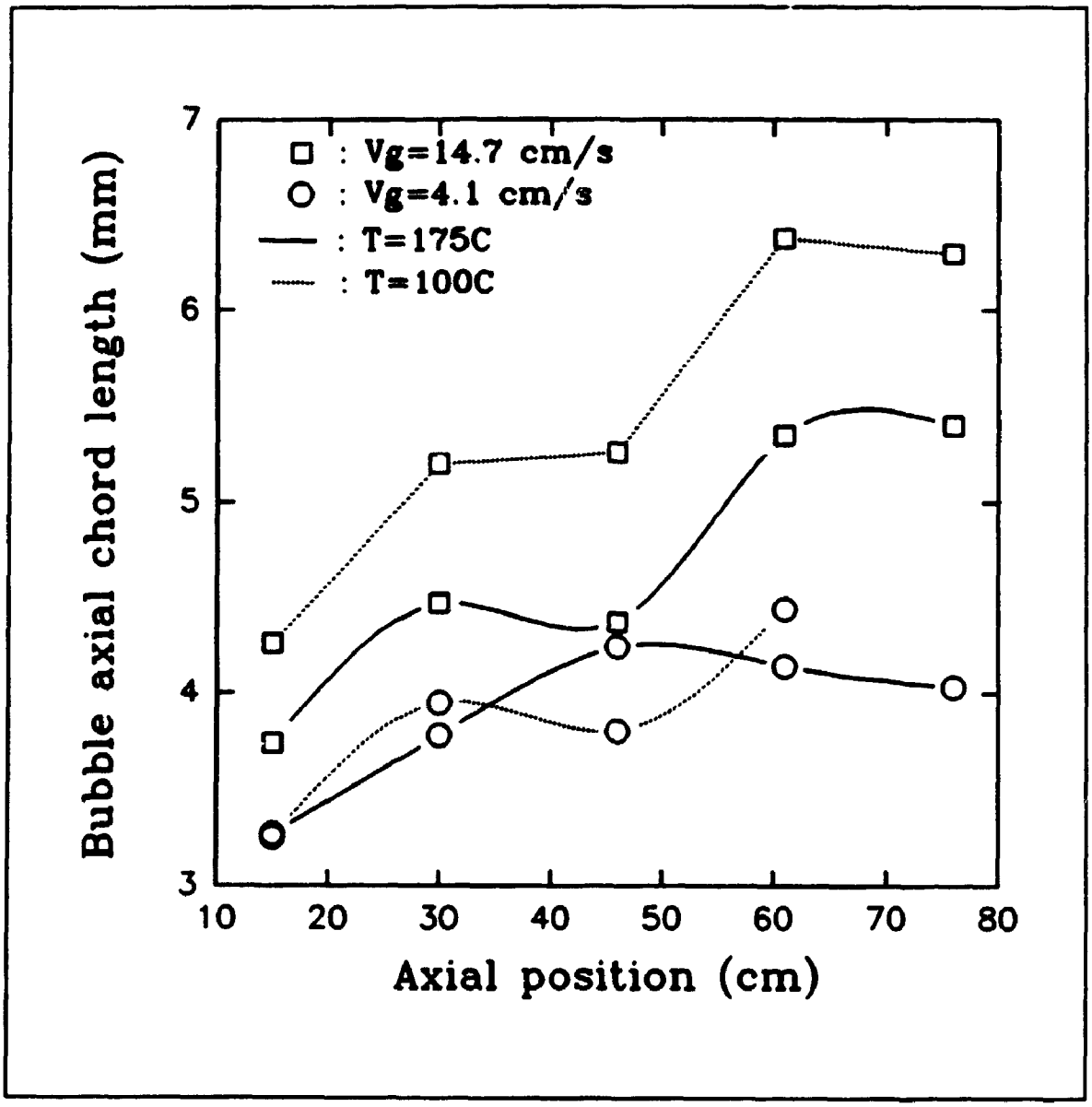

Figure 5.52a: Local bubble axial chord length vs axial position (θ=0.19)

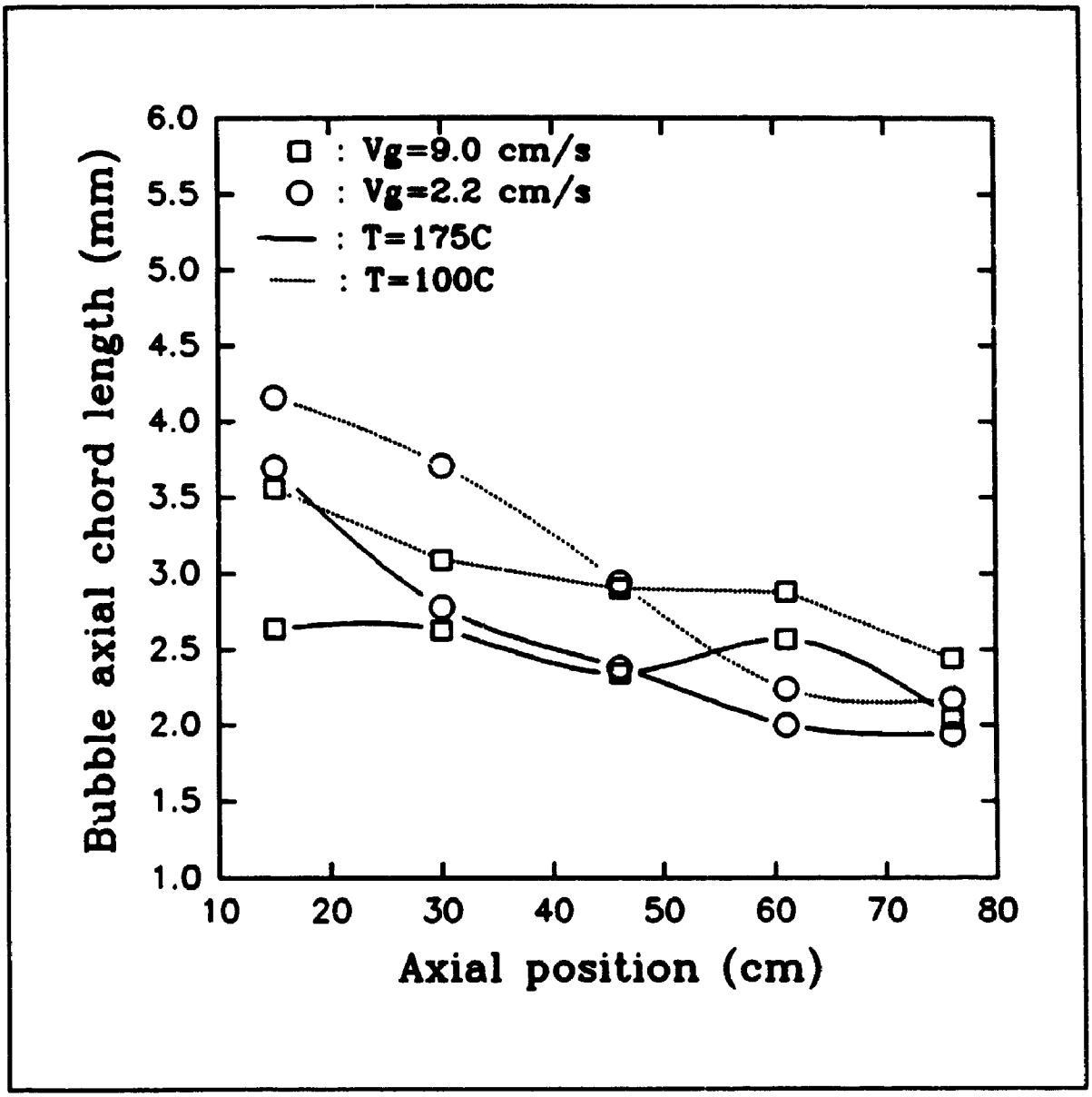

Figure 5.52b: Local axial bubble chord length vs axial position (θ=0.92)

regime with dominant bubble coalescence in the center and bubble break-up in the walls was named "coalescence bubble break-up" regime. It is important to stress that these two regimes coexist in well identified regions of the column under a significant range of conditions studied.

Furthermore, the magnitude of the central increase and the peripheral decrease of the bubble chord length with the axial position were found to be both highly dependent on the gas superficial velocity. Actually, the central increase of the local bubble axial chord length with the axial position was found to be more dominant as the gas superficial velocity augmented. This appeared to be in agreement with the fact that as the gas superficial velocity augmented, the frequency of the gas bubbles increased in the center of the column, as shown in Figures 5.53a and 5.53b for T=100°C and T=175°C respectively. Thus, as the bubble frequency augmented in the central portion of the column, or in other words as the bubble density increased, the probability of contact or collision events between bubbles augmented. In addition, an increase of the gas throughput promoted higher relative bubble velocities and thus higher probability of collision events between bubbles. So, as the gas superficial velocity increased, despite a reduced bubble contact time associated with higher turbulent intensities in the liquid phase, the rate of coalescence was found to gain importance, as previously suggested by Prince and Blanch (1990). So, as the gas

277

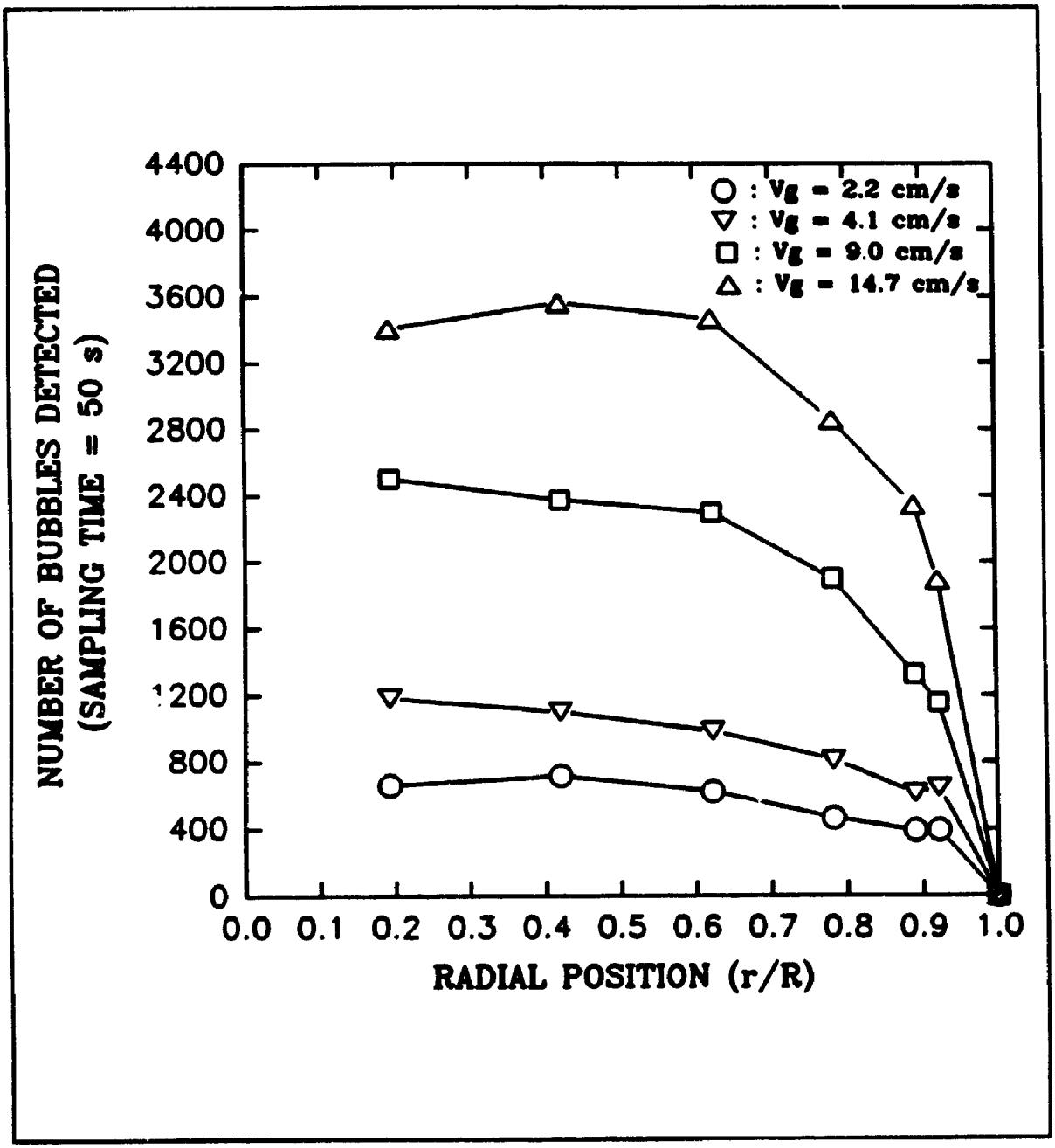

Figure 5.53a: Bubble frequency vs radial position (T=175°C, z=30 cm)

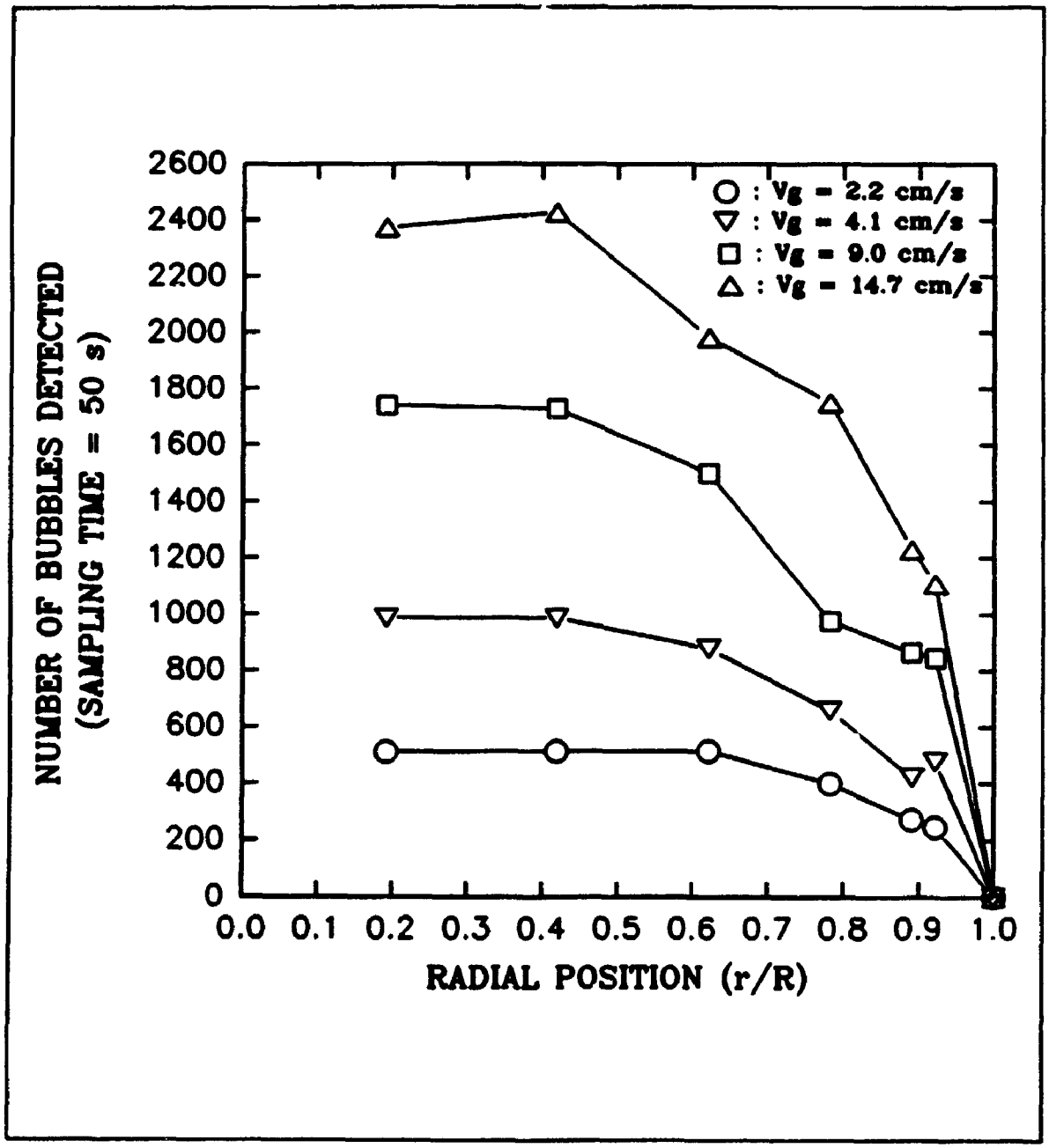

Figure 5.53b: Bubble frequency vs radial position (T=100°C, z=30 cm)

superficial velocity increased, more intense coalescing phenomena were encountered in the central portion of the column, thus favouring a more pronounced increase of the bubble axial chord length with the axial position, as shown in Table 5.15. Since, as shown above, an increase of the local bubble axial chord length was observed in the central portion of the column, a decrease of the local bubble axial chord length with the axial position was needed in the column peripheral zone, to give an overall decrease or stagnation of the average bubble chord length consistent with the ones reported in Figures 5.48 and 5.49. Actually, a pronounced decrease of the bubble axial chord length with the axial position was recorded at the lower gas superficial velocity, while a weaker decrease was observed at higher gas superficial velocities, as shown in Table 5.16. This could be explained by the following facts. In the vicinity of the column wall, minimum bubble frequency was encountered (except in the cases where the secondary liquid circulation cell was observed). This effect contributed to an overall unfavourable environment for bubble coalescing phenomena. Furthermore, as the gas superficial velocity increased, liquid circulation currents became more vigorous even at low axial positions, as confirmed by the presence of already pronounced radial gas holdup parabolic profiles (section 5.1.1), and by the observations of a number of researchers including Hills (1974) and Dudukovic and Devanathan (1992). Under such conditions, as confirmed by Prince and Blanch (1990), high break-up rates should be

280

Table 5.15

% increase of the local bubble axial chord length between z=15 cm and z=61 cm at θ=0.19

V_g (cm/s)	% increase z=15-61 cm T=100°C	% increase z=15-61 cm T=175°C
2.2	5.3	12.2
4.1	36.6	26.6
9.0	39.0	23.7
14.7	49.8	43.0

281

Table 5.16

% decrease of the local bubble axial chord length between z=15 cm and z=61 cm at θ=0.92

V_g (cm/s)	% decrease z=15-61 cm T=100°C	% decrease z=15-61 cm T=175°C
2.2	46.2	45.9
4.1	48.2	22.6
9.0	19.1	2.7
14.7	8.7	0.7

present due to high probability of contact between bubbles and powerful turbulent liquid eddies. Therefore, a significant number of bubble break-up phenomena might have already occurred below the first measurement window (z=15 cm), thus contributing to the observation of lower percentage bubble chord length decrease than normally present under this particular condition. Actually, the local bubble axial chord length was measured via fibre optic sensors at θ=0.92, z=10 cm, T=100°C and V_g=14.7 cm/s to test the validity of this hypothesis. As expected, the percentage of decrease of the bubble axial chord length with the axial position at θ=0.92 was substantially larger between z=10 cm and z=61 cm (29.7%) as compared to the one observed for the same conditions between z=15 cm and z=61 cm (8.7%). Therefore, the lower percentage of decrease observed at higher gas throughput at θ=0.92, could be partially attributed to a higher bubble break-up rate inducing a substantial fraction of the bubble break-up phenomena below the first measurement window. At lower gas throughput, lower bubble break-up rates were present, thus distributing the bubble break-up phenomena over a more extended column height. Actually, this is confirmed by looking at the rate of increase of the bubble frequency over the column height. While the rate of increase of the bubble frequency is well distributed along the column height (between z=15 cm and z=76 cm) at low gas superficial velocity, the rate of increase of the bubble frequency is substantially more pronounced in the lower portion of the column at higher gas

superficial velocities. Furthermore, the small decrease in the bubble axial chord length with the axial position observed at θ=0.92 under high gas superficial velocity could also be partially the result of the strong liquid circulation current present under large gas throughput. Actually, very efficient recirculation of the small bubbles generated though breakup phenomena was accomplished at higher gas superficial velocity. Then, a more homogeneous axial mixing or dispersion of these small bubbles was possible at higher gas superficial velocity, resulting in the presence of a more uniform local bubble axial chord length population throughout the axial section investigated in proximity of the column wall. As a result of both high coalescence rate (larger bubbles promoting high bubble rise velocity), excellent recirculation of small bubbles, and early break-up phenomena (prior to the first measurement window) the axial increase of the overall bubble frequency was found to be smaller at higher gas superficial velocity as compared to lower gas superficial velocity. Moreover, only a slight decrease of the average radial bubble chord length was observed under this condition, as shown in Figure 5.48 and 5.49. And, as a result, very moderate increase in the average radial gas holdup was observed with the axial position at higher gas superficial velocity. However, at lower gas superficial velocity, liquid circulation currents were not sufficient to recirculate efficiently the small bubbles produced from break-up phenomena along the column. In addition, lower bubble break-up rate, due to low

284

energy liquid turbulent eddy, was present under low gas superficial velocity. Therefore, bubble break-up phenomena were occurring over the complete column axial section investigated. As a consequence, as the axial position increased, the presence of smaller bubbles was observed along the column wall. Then, a substantial decrease in the local bubble axial chord length was observed at θ=0.92 as the axial position increased, as shown in Table 5.16. Then, due to low coalescence rate (low bubble frequency), poor recirculation of smaller bubbles generated from bubble break-up event) and continuous bubble break-up events along the column height, the bubble frequency was found to increase substantially with the axial position at lower gas superficial velocity. Then, a more pronounced decrease in the average radial bubble axial chord length was observed along the column, as shown in Figures 5.48 and 5.49. The presence of more smaller bubbles as the axial position increased, favoured a more pronounced increase in the average radial gas holdup with the axial position, as reported in section 5.1.2..

Despite the fact that a clear dominance of the bubble break-up phenomena was observed in the present system, the column could be divided in two distinct zones. A first one, located in the central region of the column (core region), in which the manifestation of bubble coalescence phenomena dominated, especially at higher gas superficial velocity. The second zone (peripheral zone), located in the periphery of the

column, where evidence of bubble break-up phenomena was major, especially at lower gas superficial velocity due to poor recirculation of small bubbles and continuous bubble break-up events along the column height. The existence of a peripheral zone where manifestation of break-up events dominates, does not imply that break-up phenomena is limited to the peripheral zone, though, as reported by Franz et al. (1984), a slight increase of the axial turbulent intensity was observed in proximity of the column wall (close to the liquid velocity inversion point), as opposed to other radial locations, thus favouring extra bubble break-up in proximity to the column wall. An illustration of the local bubble axial chord length dynamic mapping, under both low and high gas superficial velocities, is presented in Figures 5.54 and 5.55 respectively.

It is highly interesting to note the effect of the rates of bubble coalescence and bubble break-up on the shape of the gas bubble axial chord length radial profile. At low gas throughput, the gas holdup radial profile was found to be quite uniform at z=15 cm, the bubble characteristics being dominantly governed by the distributor design (with the exception of the conditions for which the secondary liquid circulation cell was present) due to slow bubble coalescence and bubble breakup rates. At higher gas superficial velocities, the higher rates of bubble coalescence and bubble break-up influenced the bubble characteristics at a very early

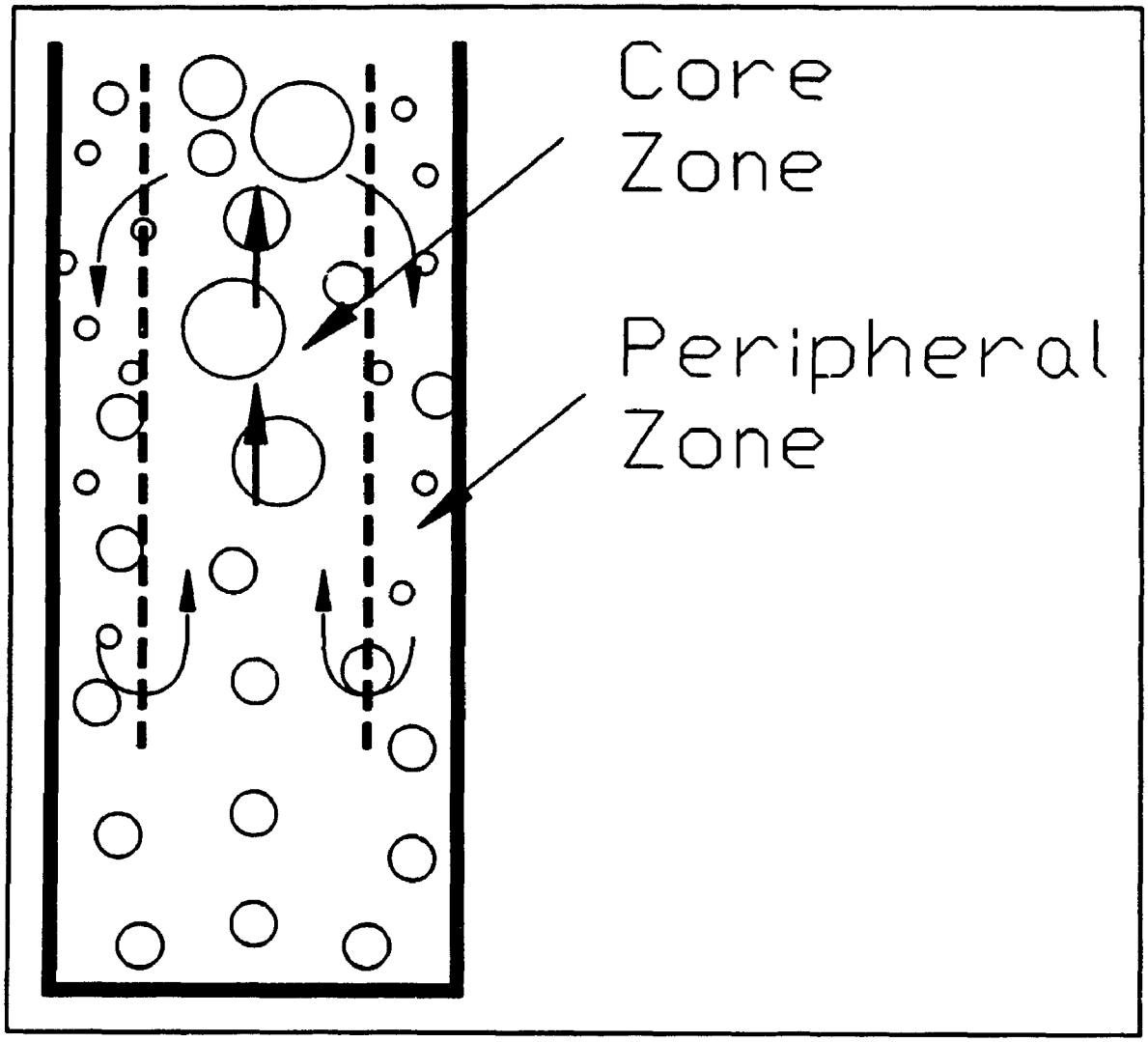

Figure 5.54: Schematic representation of the bubble chord length mapping (low gas superficial velocity)

287

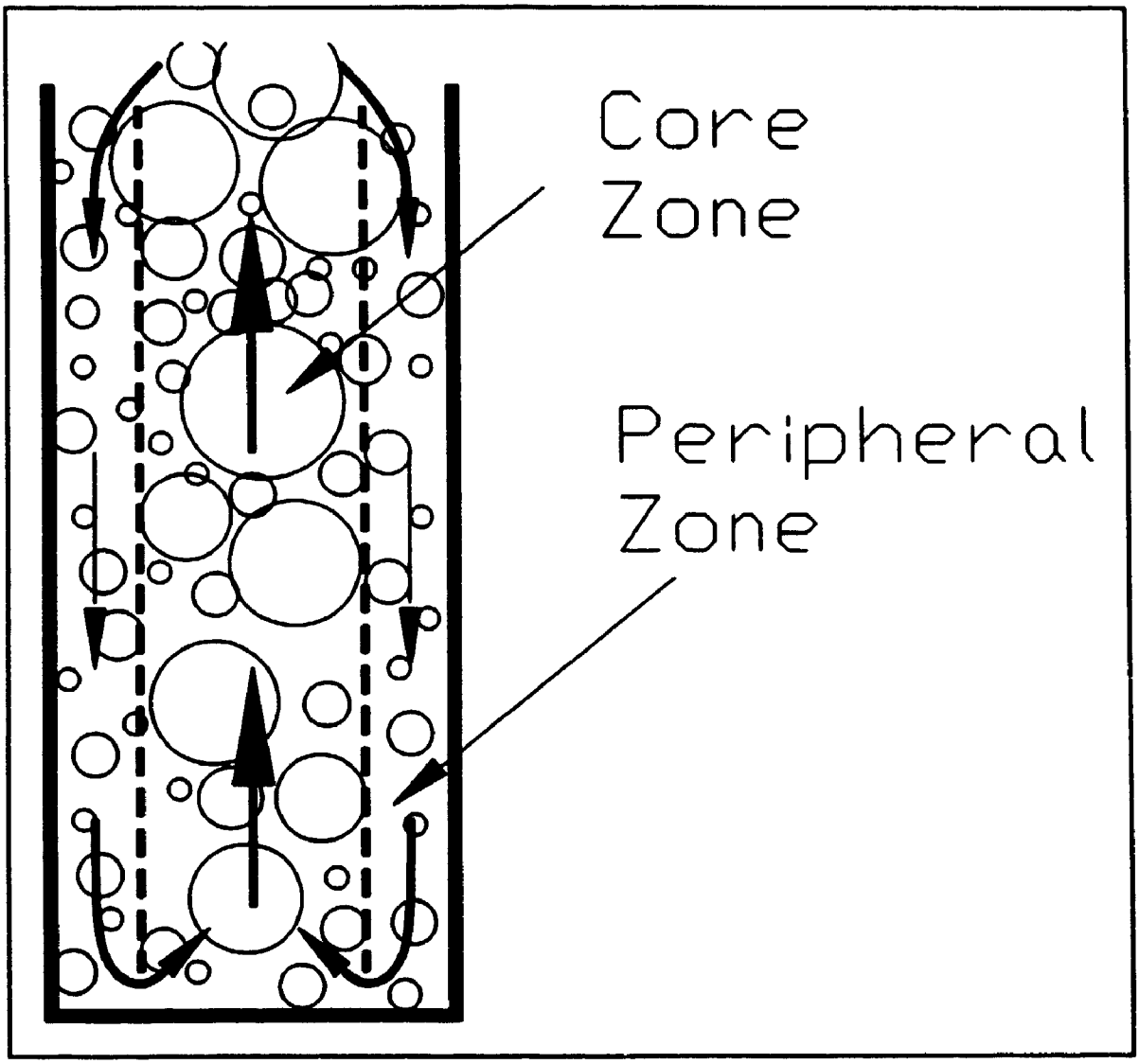

Figure 5.55: Schematic representation of the bubble chord length mapping (high gas superficial velocity)

axial position, thus inducing early pronounced bubble axial chord length radial profiles.

The radial average bubble axial chord length was found to augment with an increase in the gas superficial velocity, as shown in Figure 5.56 (dash lines). It is interesting to note the repercussions of the presence of the secondary liquid circulation cell at V_g=2.2 cm/s (θ=0.92), even at z=76 cm. Actually, as shown in Figure 5.56 for θ=0.92, larger local bubble axial chord length was observed at V_g=2.2 cm/s as compared to V_g=4.1 cm/s. This is due to the fact that unusually large gas bubbles were present in the vicinity of the column wall at z=15 cm and z=30 cm, due to the presence of the secondary liquid circulation cell. These atypical larger bubbles persisted along the length of the column, despite pronounced decrease of the bubble axial chord length with the axial position in the periphery of the column at V_g=2.2 cm/s (as discussed above).

The influence of the gas superficial velocity was found to be maximum in the central part of the column (Figure 5.56, θ=0.19) while being less pronounced in the vicinity of the column wall (Figure 5.56, θ=0.92). This is indeed consistent with the previously discussed fact that the bubble coalescence phenomena in the center of the column became more intense as the gas superficial velocity increased, thus amplifying the effect of the gas superficial velocity on the bubble axial

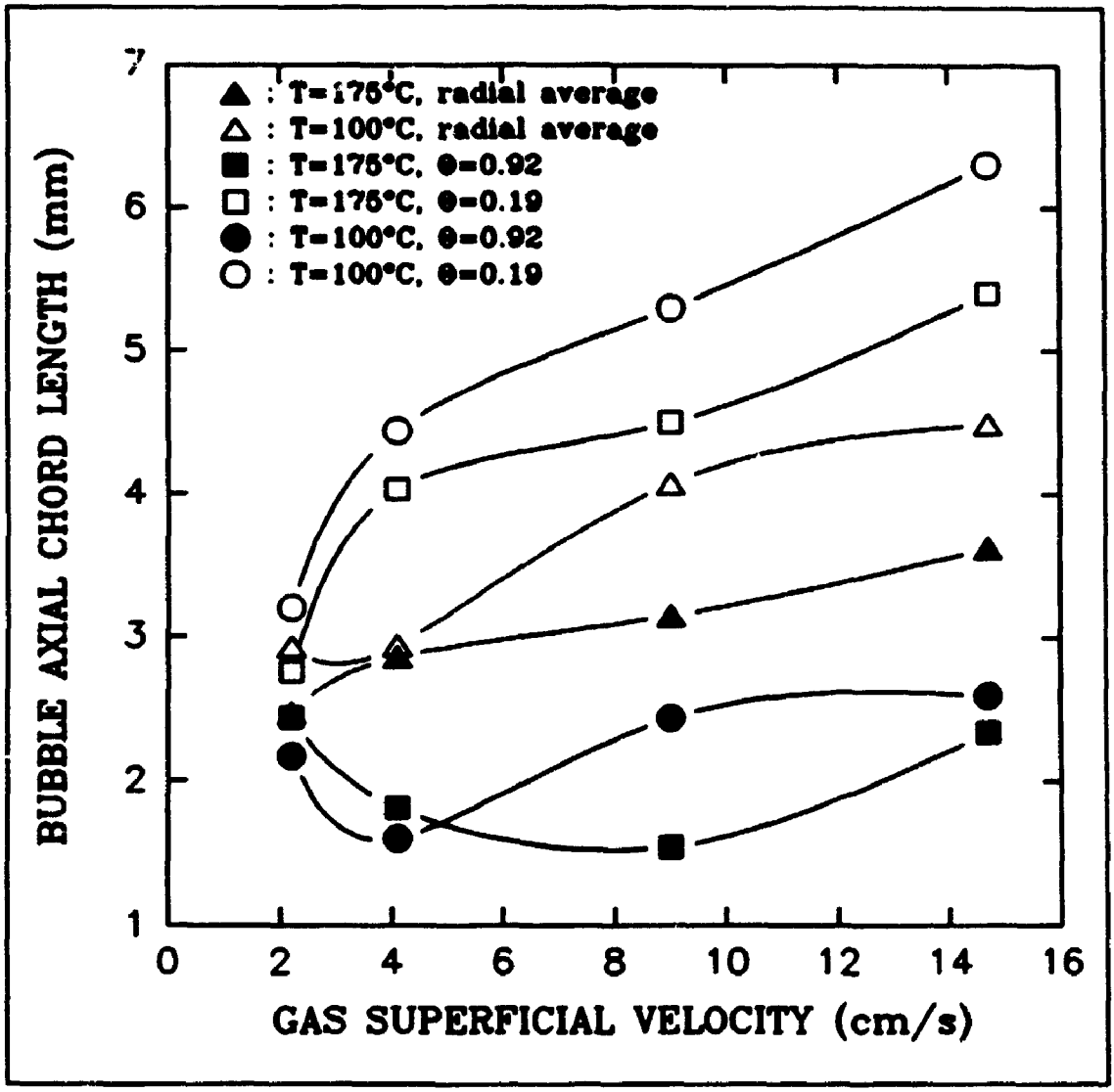

Figure 5.56: Axial bubble chord length vs gas superficial velocity (z=76 cm).

290

chord length in the center of the column. On the contrary, in proximity of the column wall (θ=0.92), more moderate effects of the gas superficial velocity were observed due to the dominance of the manifestation of the bubble break-up phenomena at this particular location.

The bubble chord length was found in general to decrease with an increase in the operating temperature, as shown in Figure 5.56. This is due to the fact that a substantial decrease in the liquid viscosity and surface tension was observed as the temperature increased (Appendix 1). An increase of the liquid viscosity and the surface tension are known to respectively decrease bubble breakup rates and promote coalescence of large bubbles and promote the existence of larger stable bubble size (Wilkinson et al., 1992), thus to encourage overall larger bubble sizes. Actually, as shown in Table 5.15, lower percentage increase in the bubble axial chord length with the axial position was observed for most superficial gas velocities in the bubble coalescing dominant zone (center of the column) at T=175°C as compared T=100°C, despite a substantially higher bubble frequency and a resulting higher probability of contact. Furthermore, as shown in Table 5.16, the percentage of decrease of the bubble axial chord length with the axial position was found to be less pronounced at T=175°C as compared to T=100°C, indicating a more uniform mixing of the bubble population at T=175°C as compared to T=100°C and an earlier presence of bubble break-up events, due

291

to higher bubble break-up rates.

In general, the bubble chord length was found to decrease with the axial position, except for the cases where the secondary liquid circulation cell was present. Overall, the average axial bubble chord length was observed to decrease (lower gas superficial velocities) or remain approximately constant (higher gas superficial velocities) with the axial position, thus suggesting the dominance of bubble break-up events over coalescence phenomena in this particular system. However and as it was the case at lower temperature, two distinct zones were observed: a first one (core zone) located in the central region of the column where bubble coalescence dominated and a second one (peripheral zone) located along the wall of the column where manifestation of break-up events dominated.

In summary, a so-called "coalescence-break-up" bubble regime, where conditions favoured coalescence in the center of the column and bubble break-up in the vicinity of the wall was found for most conditions investigated. These findings are extremely important for a better understanding of the fluid dynamic behaviour of bubble columns and for controlling the bubble coalescence and gas recirculation effects.

292

5.1.5 Bubble chord length distribution

The bubble chord length distribution analysis was applied for the various operating conditions (T, V_g) as well as axial and radial positions investigated. The bubble chord length distribution was obtained for every particular data file, following the procedure outlined in section 4.1.5. A copy of the software used in generating the bubble chord length distribution is presented in Appendix 3.

Two typical bubble chord length distributions obtained respectively at T=100°C and T=175°C are presented in Figures 5.57 and 5.58. As shown in these Figures, the bubble chord length distribution appeared to be non-gaussian. Actually, the typical bubble chord length distribution obtained, characterized by a relatively sharp and narrow peak, followed by a long and slowly decaying tail, was typical of a skewed probability distribution function. This type of bubble chord length distribution suggested the presence of numerous small bubbles (0.3 - 3 mm) accompanied by a wide chord length distribution of fewer large bubbles (3 mm - 5 cm). The observation of such bubble chord length distribution was found to be highly consistent with the findings reported in the previous section (section 5.1.4). Actually, as mentioned in the previous section, the present system was characterized by a distinct dominance of bubble break-up phenomena over coalescence phenomena, resulting in the presence of an overall

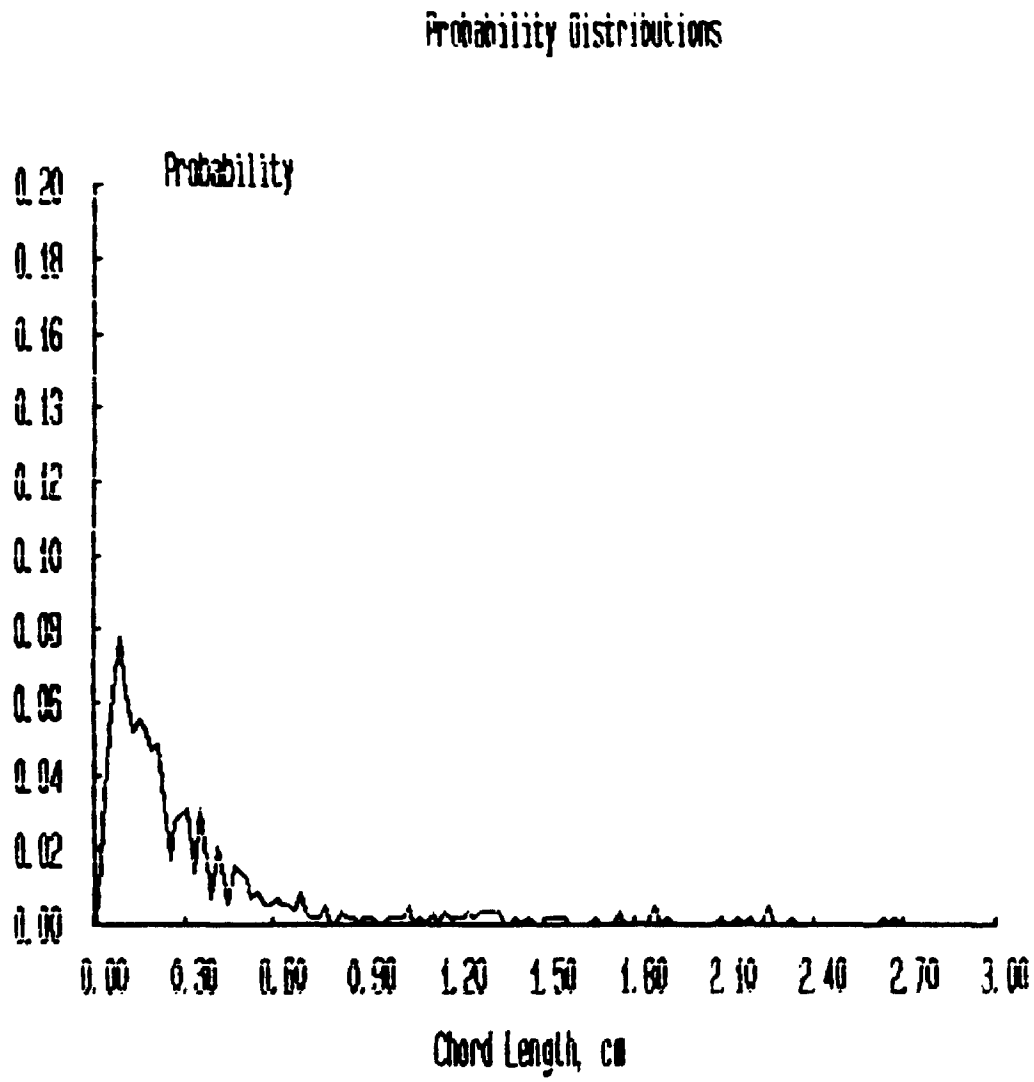

Figure 5.57: Bubble axial chord length distribution (T=175°C, V_g=4.1 cm/s, z=30 cm, θ=0.42)

294

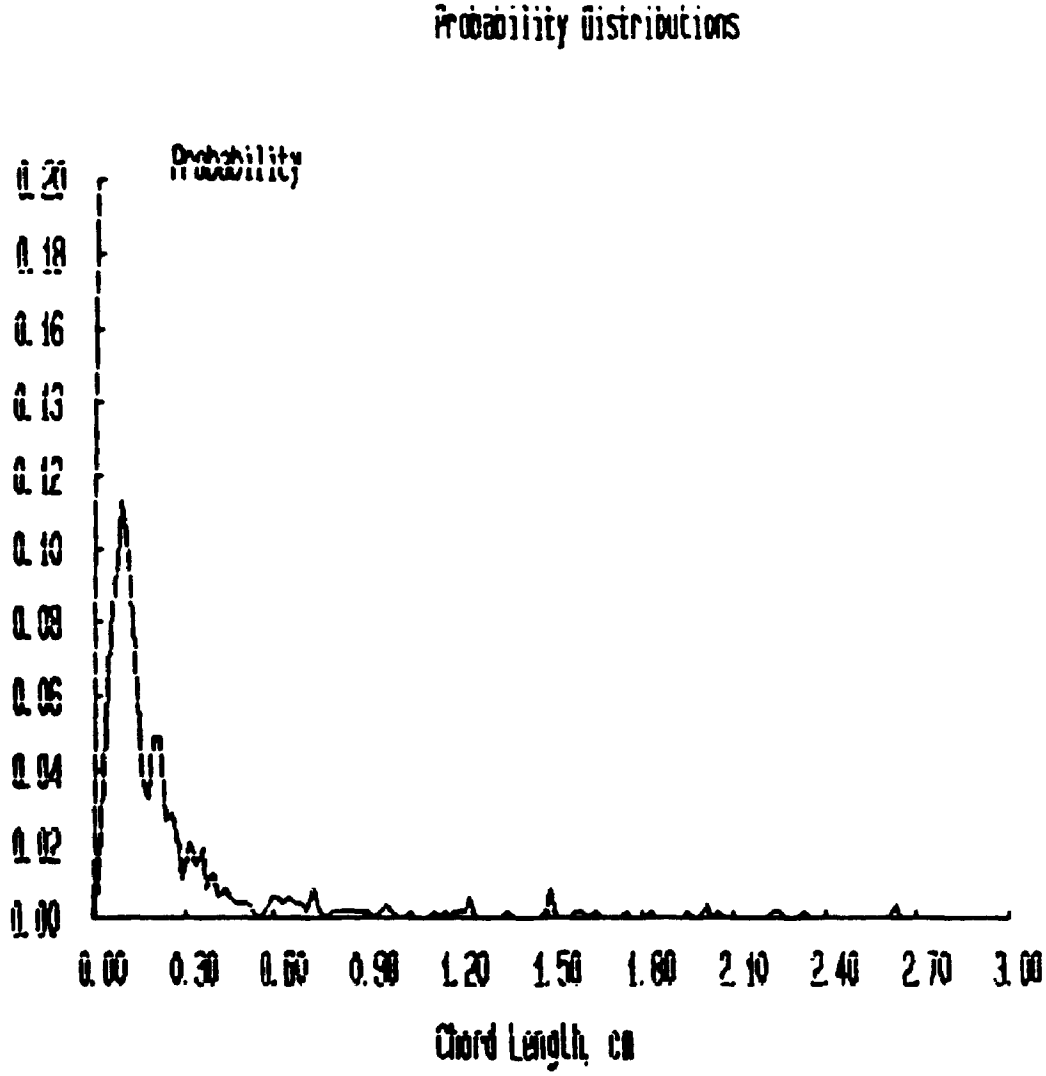

Figure 5.58: Bubble axial chord length distribution (T=175°C, V_g=4.1 cm/s, z=76 cm, θ=0.89)

bubble disintegrating regime. Consequently, such regime highly favoured the massive presence of small bubbles. On the other hand, the less likely occurrence of successful coalescence events, arising at a relatively slow rate, favoured a wide distribution of sparse larger bubbles. Thus, the preferential existence of small bubbles as opposed to larger bubbles resulted in an asymmetrical bubble chord length distribution, clearly favouring smaller bubbles. Actually, a number of authors also observed the presence of skewed bubble size distribution. For example, Patel et al., (1990) reported a log-normal bubble size distribution in a Fischer-Tropsch derived waxes system, a system having quite similar liquid phase properties to the one used in the present study. Furthermore, Prince and Blanch (1990) predicted, using their phenomenological bubble coalescence-break-up model, a skewed bubble volume distribution in a turbulent gas-liquid dispersion. They satisfactorily validated the model using experimental measurements.

Due to thesis length limitation, only one bubble chord length distribution per condition was presented in Appendix 8, despite the fact that a minimum of three experimental repeats were performed for every condition investigated. However, in order to verify the reproducibility of the bubble chord length distribution analysis, a minimum of two bubble chord length distributions were generated for every operating condition. In general, excellent correspondence was obtained between

these two bubble chord length distributions, as exemplified by comparing respectively Figure 5.59 with Figure 5.60 and Figure 5.61 with Figure 5.62.

As thoroughly discussed in section 4.1.5, the bubble chord length distribution analysis involved a careful analysis of the bubbles detected by both, the lower optical sensor and the upper one. Following this analysis, only a fraction (typically between 20 and 80%) of the total bubbles detected by the bottom sensor successfully qualified as being detected by both optical sensors with the proper sequence. This conservative approach guaranteed a safe coupling of the bubble detection peaks, thus insuring that no make-up match was erroneously incorporated to the bubble chord length distribution. However, special care must be taken to insure that the selective bubble population retained and included in the bubble chord length distribution is well representative of the whole bubble population present at the point of measurement. This verification is crucial to confirm that the severe bubble matching process was not discriminatory toward a specific class of bubbles, most likely the smaller bubbles that are less susceptible to be detected by both optical sensors. So, for the lower sensor, the average bubble-sensor contact time duration of the bubble population retained for the bubble chord length distribution was compared with the average bubble-sensor contact time duration obtained for the totality of the bubbles viewed by the lower sensor. On

297

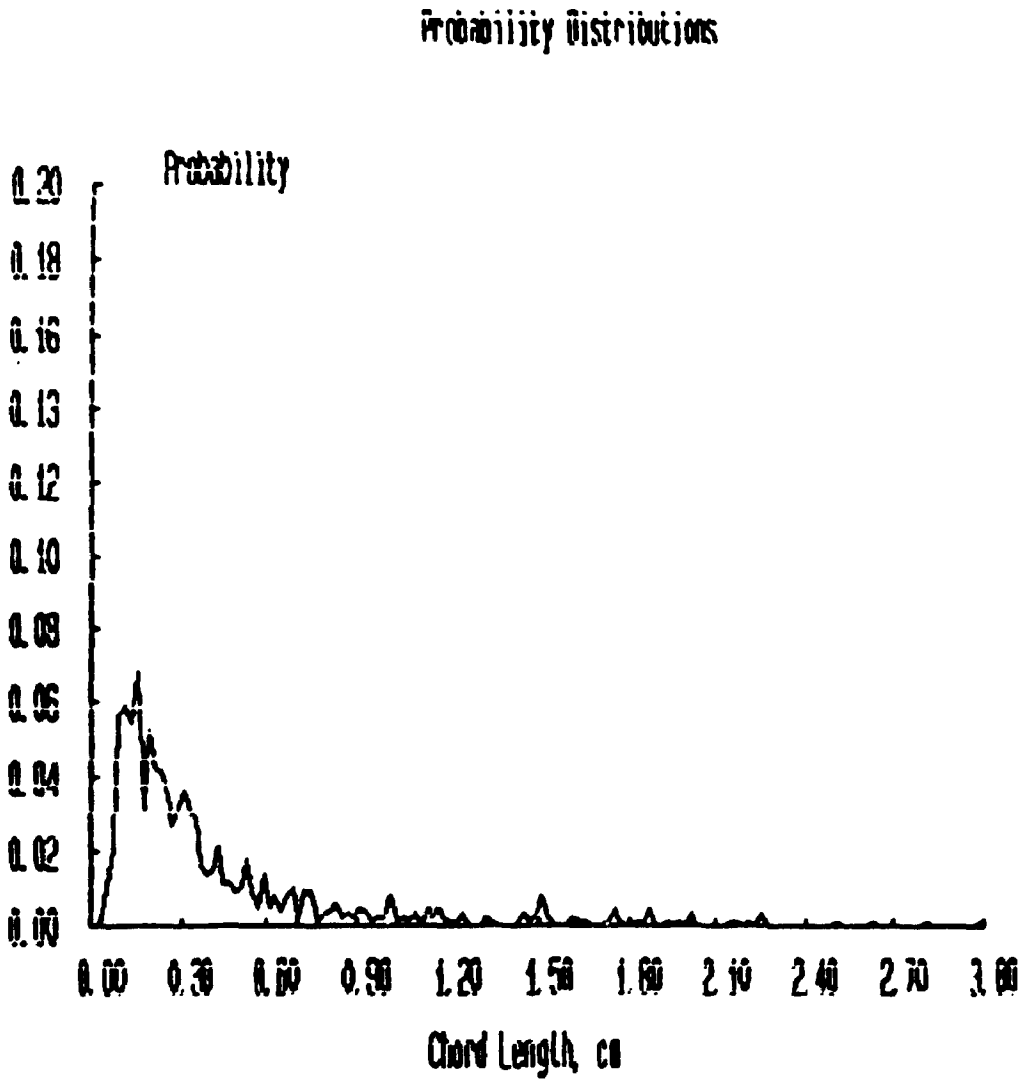

Figure 5.59: Bubble axial chord length distribution (T=175°C, V_g=4.1 cm/s, z=46 cm, θ=0.19)

298

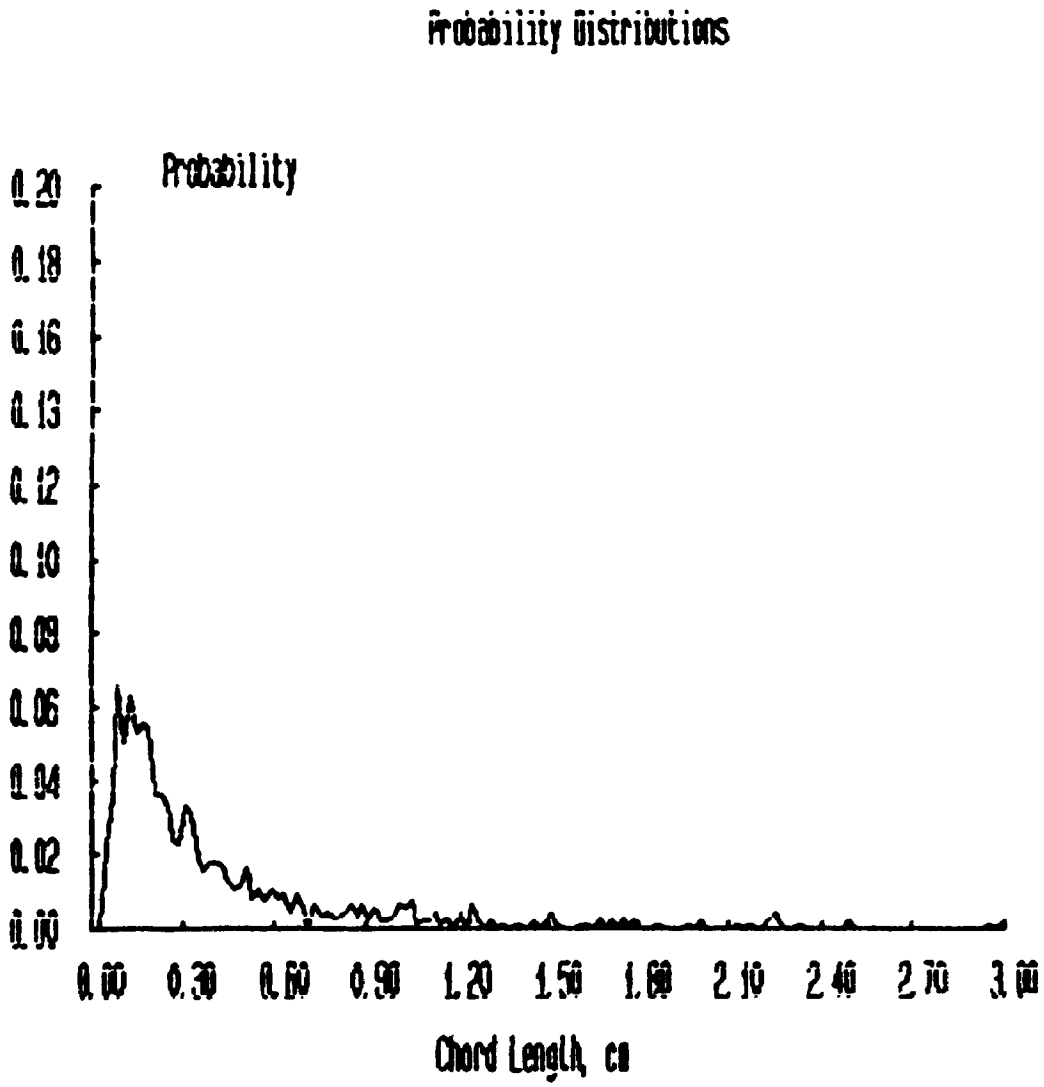

Figure 5.60: Bubble axial chord length distribution (T=175°C, V_g=4.1 cm/s, z=46 cm, θ=0.19)

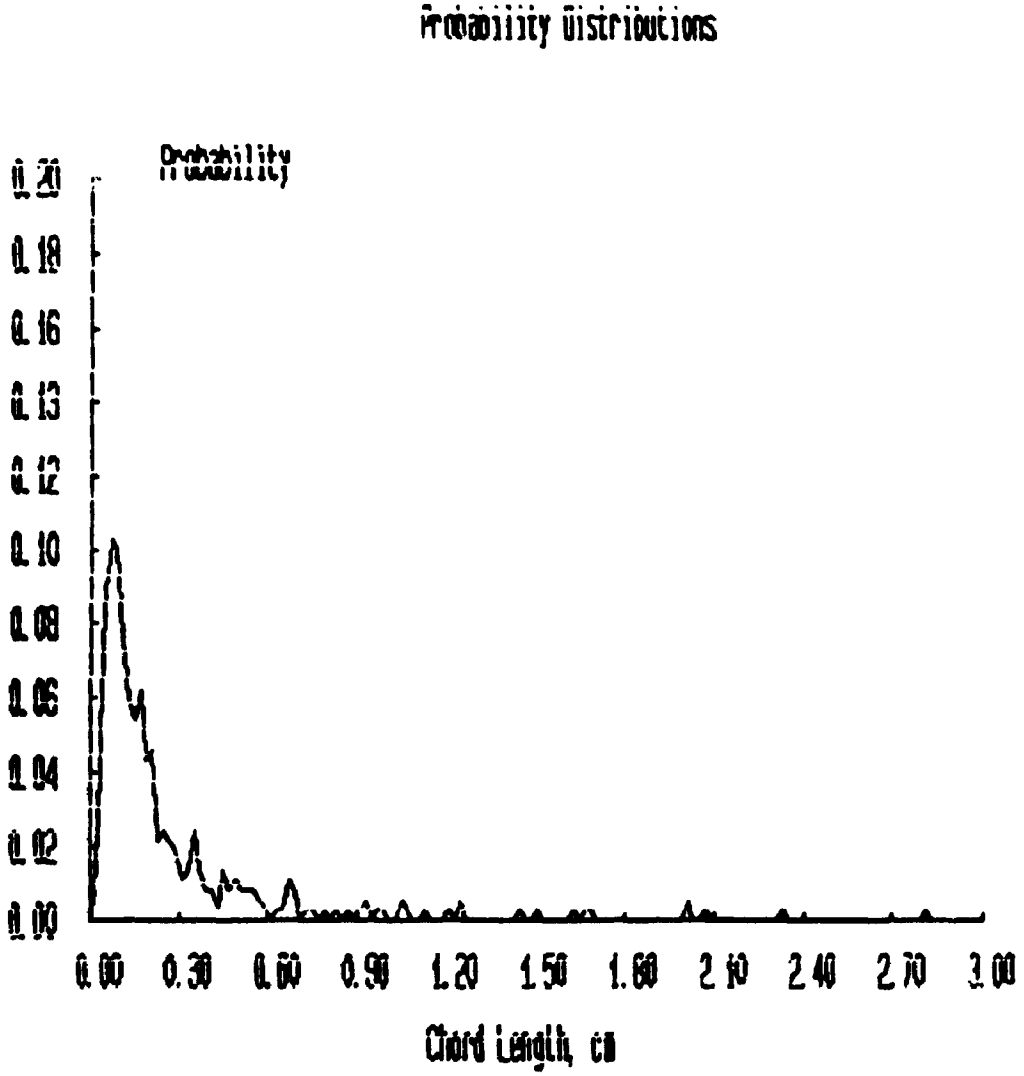

Figure 5.61: Bubble axial chord length distribution (T=175°C, V_g=4.1 cm/s, z=61 cm, θ=0.89)

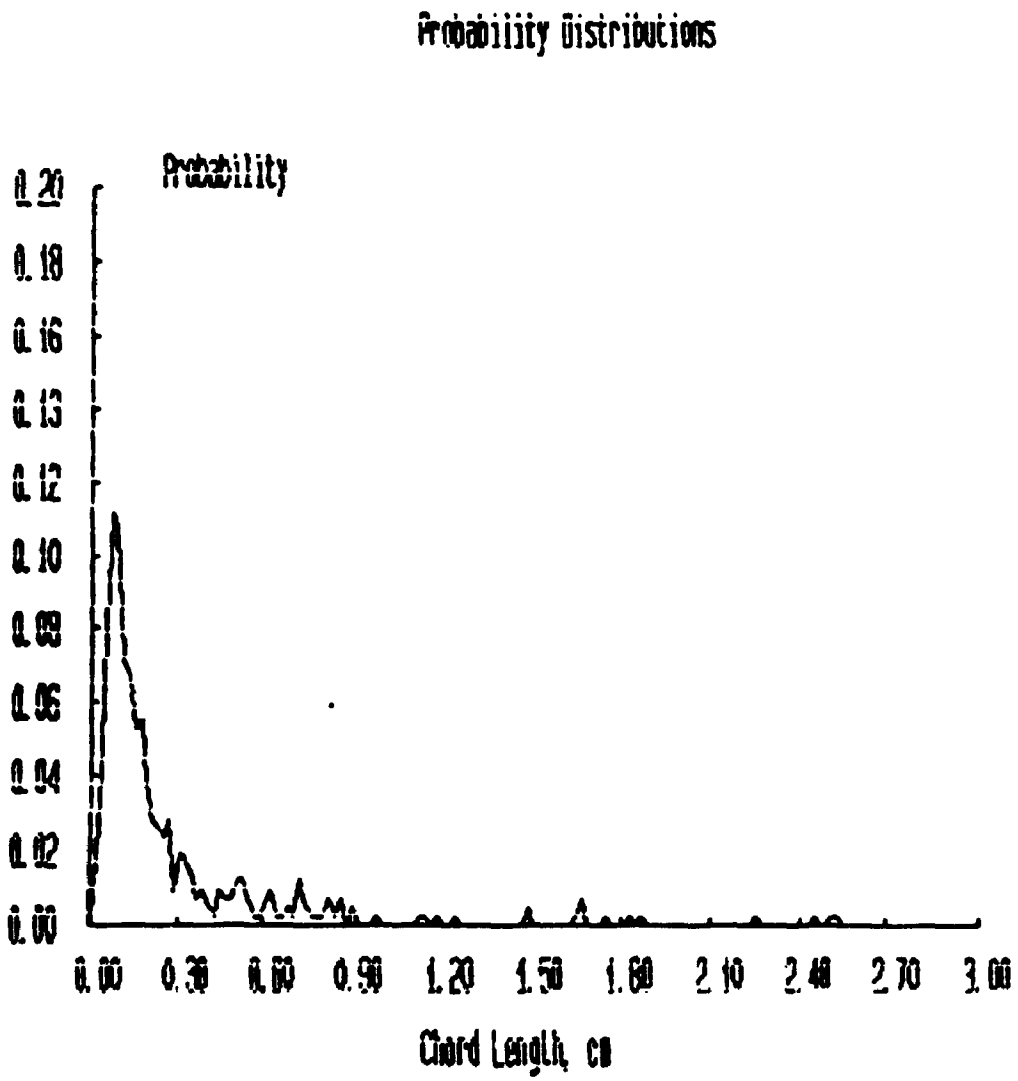

Figure 5.62: Bubble axial chord length distribution (T=175°C, V_g=4.1 cm/s, z=61 cm, θ=0.89)

average, the average bubble-sensor contact time duration of the bubble population retained for the bubble chord length distribution was within 12% (3.3% and 11.2% average deviation for T=175°C and T=100°C respectively) of the one obtained considering the entire bubble population. Thus, the bubble chord length distribution analysis could be safely assumed to have been constructed from a bubble population well representative of the complete bubble population viewed by the lower optical sensor. It is highly interesting to note however that the percentage of bubbles retained for the bubble chord length distribution varied with the axial and radial position, as well as the gas superficial velocity. Actually, as typically shown in Figure 5.63 and 5.64, the percentage of bubbles retained for the bubble chord length distribution decreased with the radial position, except for the condition where the secondary liquid circulation cell was present. This is consistent with the fact that where downward liquid circulation currents were present, a number of bubbles were entrained downward with the liquid, thus being automatically disqualified from the selection process. Furthermore, as the axial position increased (for the central section of the column only) and as the gas superficial velocity increased, as illustrated in Figures 5.63 and 5.64, the percentage of bubbles retained rose. This is consistent with the fact that under both these effects, the bubble chord length increased, thus making adequate bubble detection by both sensors easier.

302

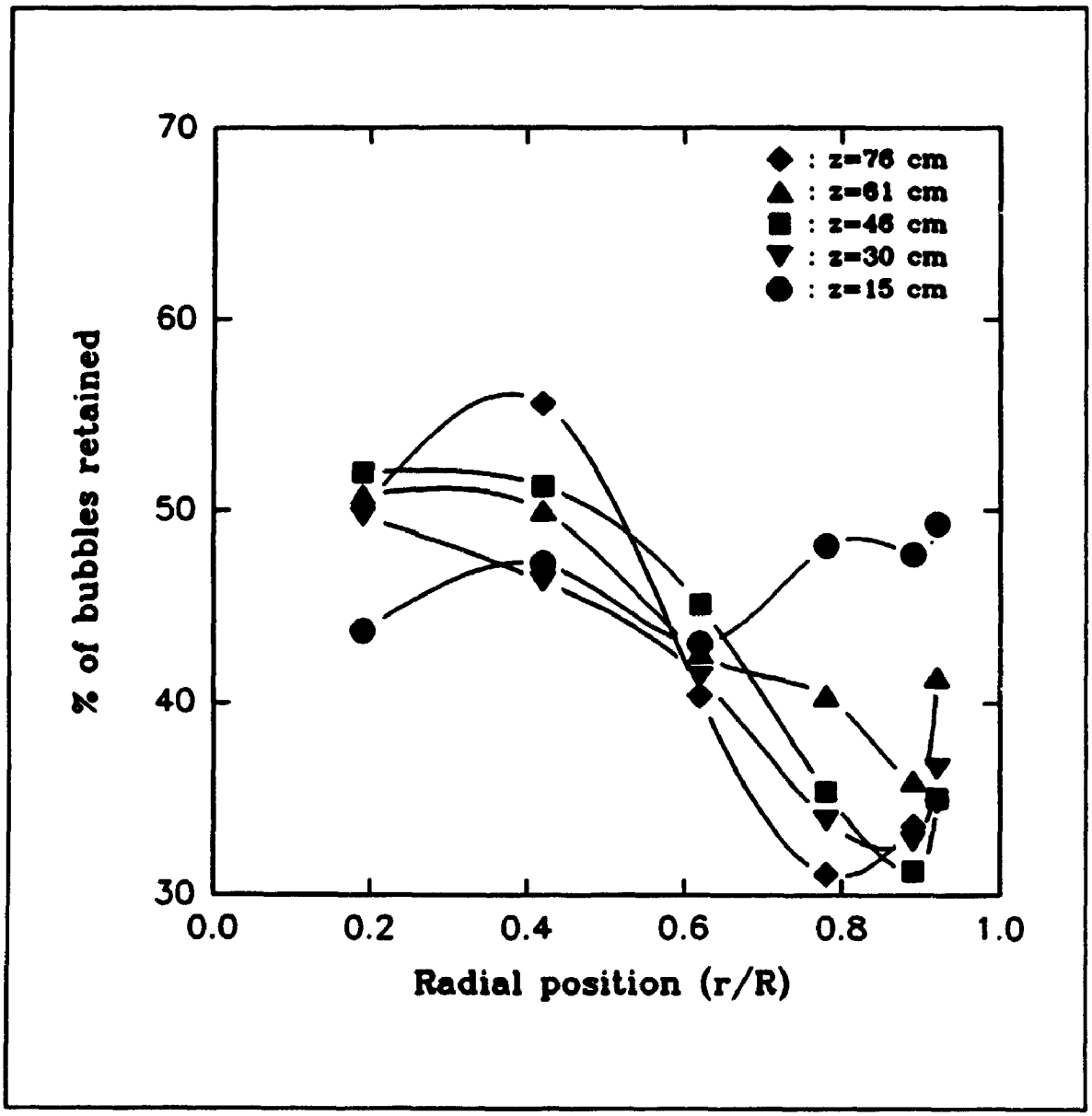

Figure 5.63: Percentage of bubbles retained (bubble chord length distribution analysis versus radial position (T=100°C, V_g=2.2 cm/s)

303

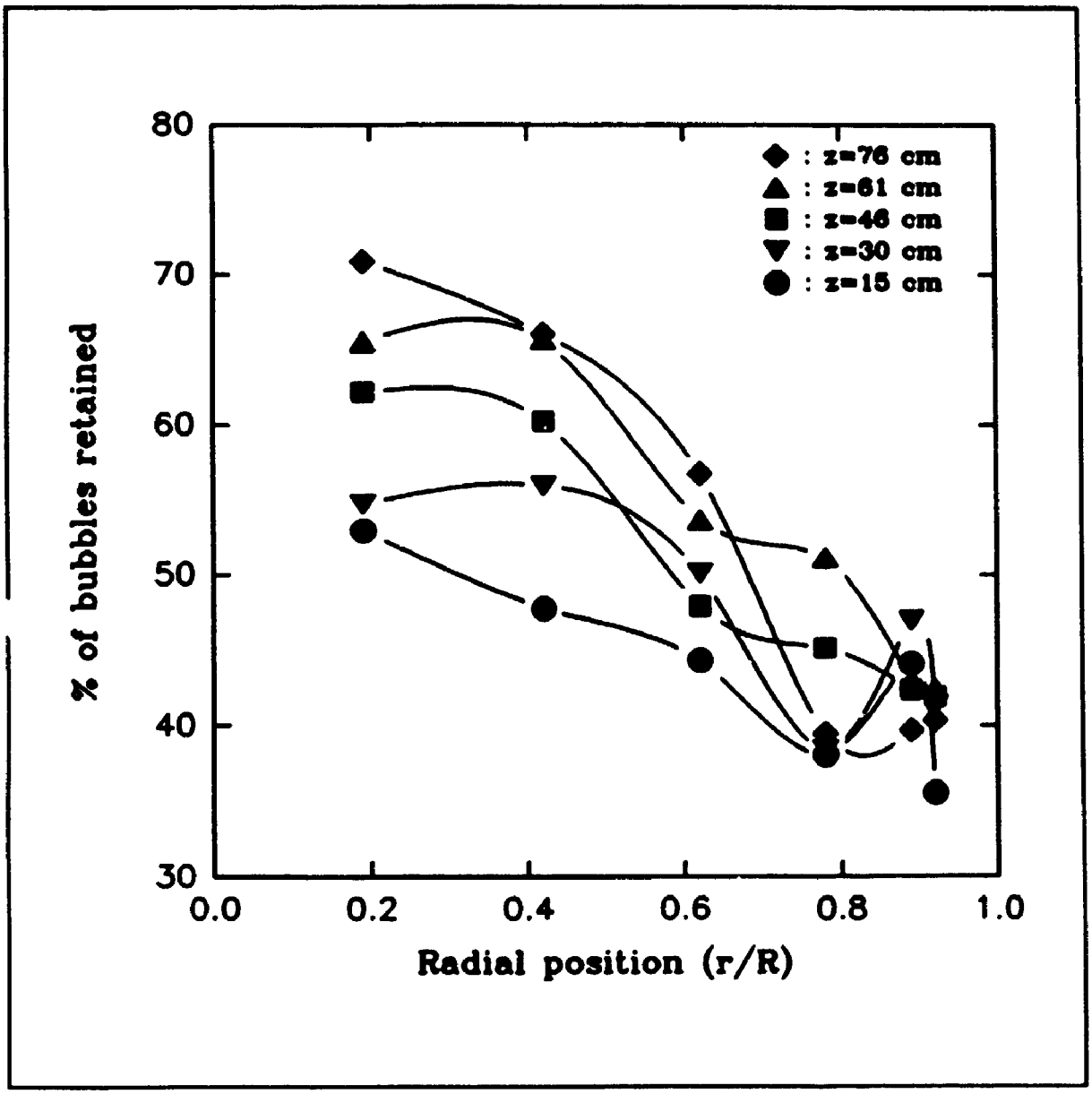

Figure 5.64: Percentage of bubbles retained (bubble chord length distribution analysis) versus radial position (T=100°C, V_g=9.0 cm/s)

In order to adequately represent the experimental bubble chord length distributions obtained, two classical skewed probability distribution functions were investigated, the log normal distribution and the inverse gaussian distribution. The log normal distribution and the inverse gaussian distribution are presented in equations 5.7 and 5.8 respectively.

$$p(x) = \frac{1}{\sigma x \sqrt{2\pi}} \exp\left(-\frac{1}{2\sigma^2} (\ln(x)-\mu)^2\right) \qquad (5.7)$$

where μ and σ are the scale and shape parameters respectively, and:

$$\begin{array}{c} x > 0 \\ -\infty < \mu > \infty \\ \sigma > 0 \end{array}$$

$$p(x) = \sqrt{\frac{\tau}{2\pi x^3}} \exp\left(\frac{-\tau (x-\alpha)^2}{2\alpha^2 x}\right) \qquad (5.8)$$

where α = population mean, α^3/τ = variance, and:

$$\begin{array}{c} x > 0 \\ \alpha > 0 \\ \tau > 0 \end{array}$$

Due to the similarities in the characteristics of these two equations, including both two parameters and an exponential term, the general shape of these two functions was expected to be analogous. Both expressions were fitted to the experimental data using a Marquart-Levenberg optimization algorithm (non-linear least squares fitting). As illustrated for two typical cases in Figures 5.65 and 5.66, both

305

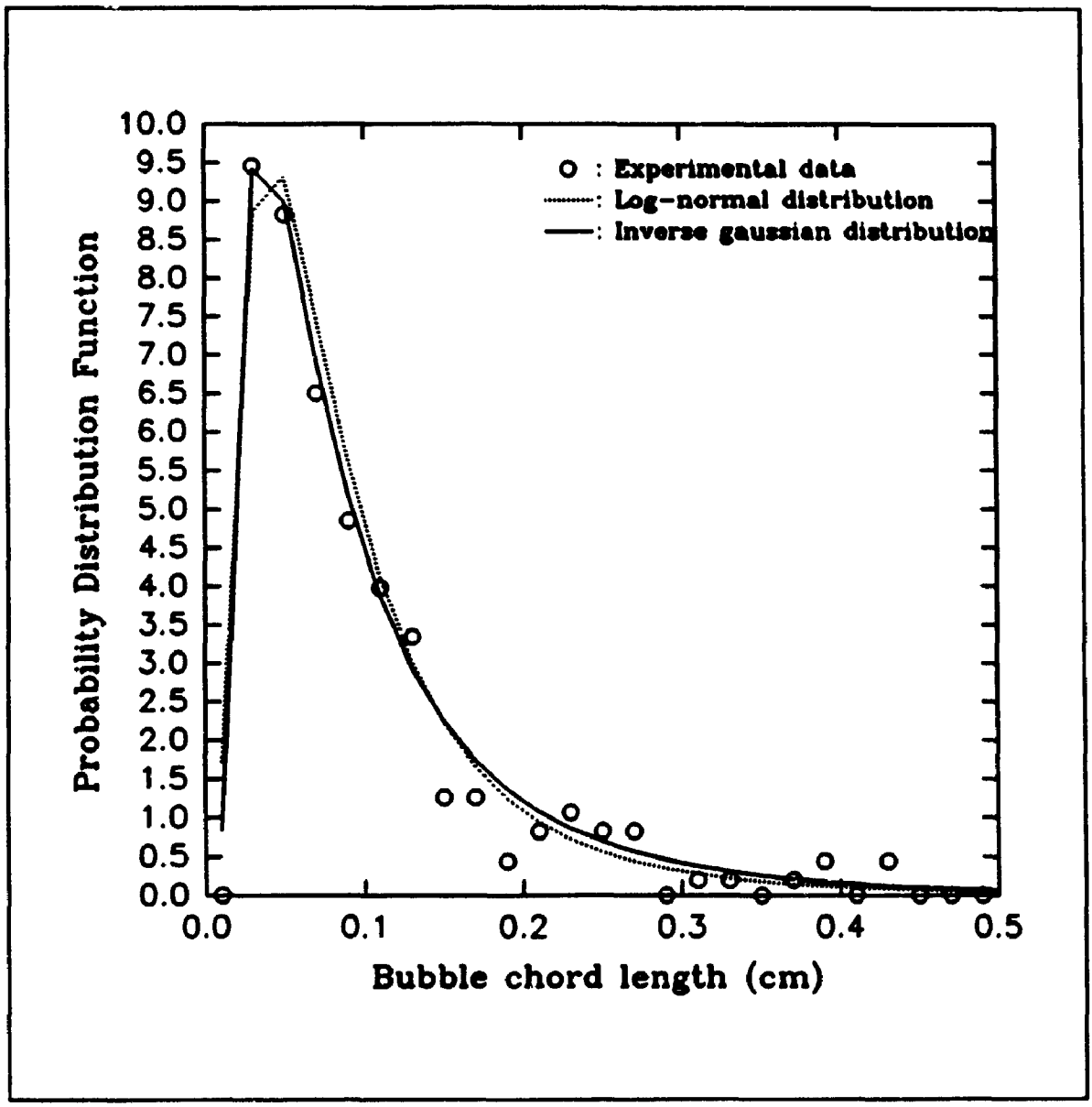

Figure 5.65: Bubble chord length distribution (T=100°C, V_g=4.1 cm/s, z=61 cm, θ=0.89)

306

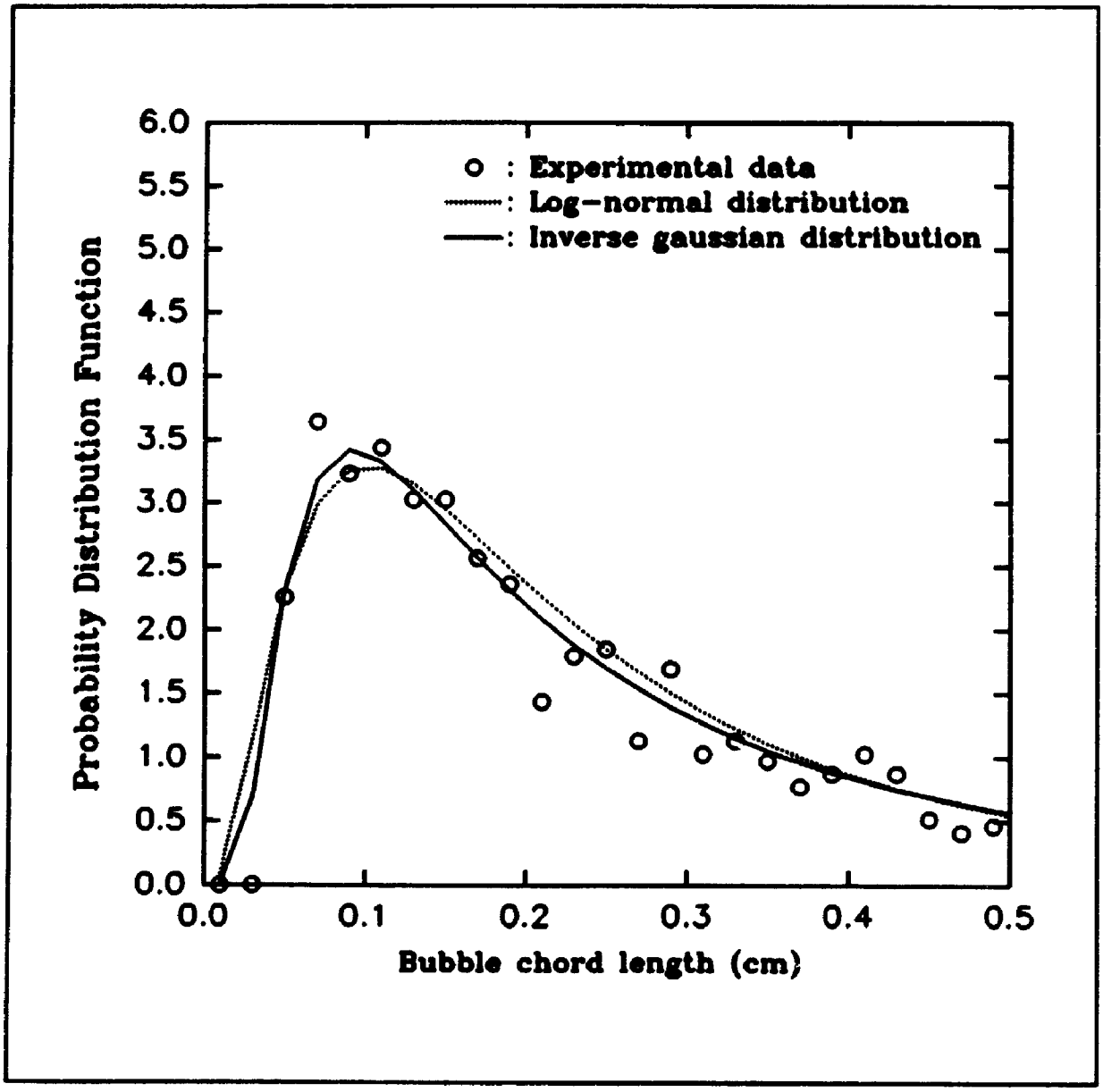

Figure 5.66: Bubble chord length distribution (T=100°C, V_g=9.0 cm/s, z=15 cm, θ=0.78)

probability distribution functions captured the general trends of the experimental data, giving globally very comparable curves. However, and as shown in Figures 5.65 and 5.66, the inverse gaussian distribution function appeared superior in representing the very sharp and narrow initial peak, while following very closely the long and slowly decaying tail. For all the experimental bubble chord length distributions obtained, the log-normal distribution seemed to lack flexibility in incorporating the data points located along the initial rather sharp peak, while systematically underestimating the long tail of the experimental bubble chord length distribution. So, because of a general superior capability in closely representing the data, the inverse gaussian distribution was retained over the log-normal distribution for further examinations and a complete assessment of the statistical goodness of fit. First of all, the residuals (inverse gaussian fitted function - experimental points) were examined. As shown in a typical example presented in Figure 5.67, the residuals were small and well distributed around zero. An autocorrelation analysis was applied to the residuals to ensure that no fundamental information was left behind or overlooked by the inverse gaussian model. In other words, if the inverse gaussian model provides a satisfactory representation of the experimental data, it should incorporate all the essential information contained within these data. Consequently, any discrepancies remaining after optimum fitting process between the model and

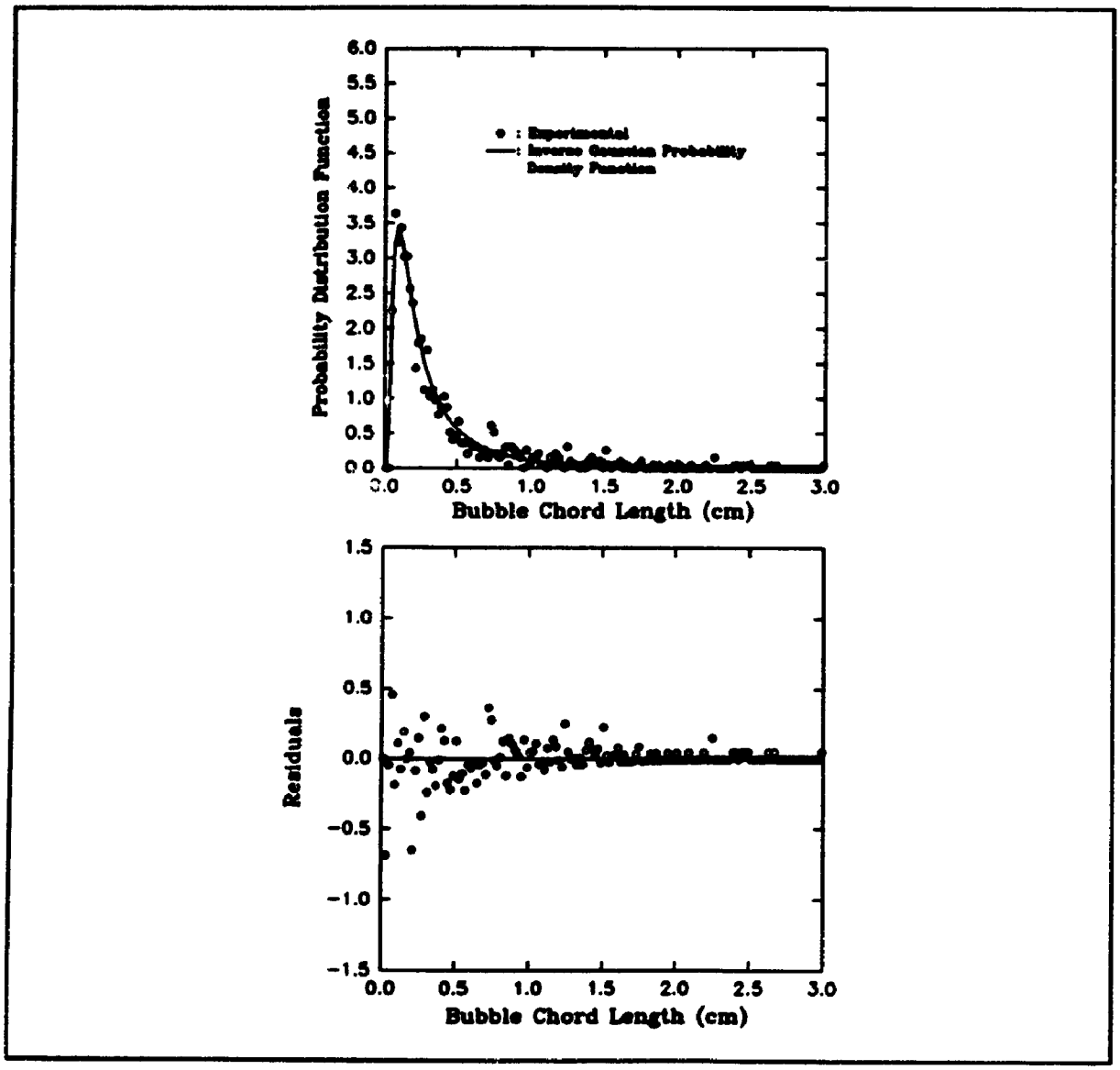

Figure 5.67. Bubble chord length probability distribution function and residuals (T=175°C, V_g=8.7 cm/s, A.P.=15 cm, r/R=0.78)

309

the experimental points (residuals) should be of a random nature. Then the residuals should be, using a well established statistical terminology: pure white noise. By definition, white noise constitutes a purely random series of numbers, then a non-autocorrelated series of numbers. An autocorrelation (20 lags) analysis was applied to the residuals. As typically shown in Figure 5.68, the residuals were found to be essentially non-autocorrelated.

To investigate the presence of any periodicity effects in the residuals, a cumulative periodogram check was performed. The autocorrelation function is not a sensitive indicator of such departure from randomness, because periodic effects are typically diluted among several autocorrelations. The periodogram, on the other hand, is specifically designed for the detection of periodic patterns in a background of white noise. If the residuals are white noise, the plot of the cumulative periodogram against the period should be scattered about a straight line joining the points (0,0) and (f_{max},1) (Box and Jenkins, 1976). As shown in Figure 5.69, such behaviour was indeed observed, thus confirming the randomness of the residuals.

Furthermore, the standard deviation of each one of the two optimum parameters derived from the inverse gaussian model fitting exercise was found to be highly satisfactorily. Actually, standard deviations safely within 10% of the

310

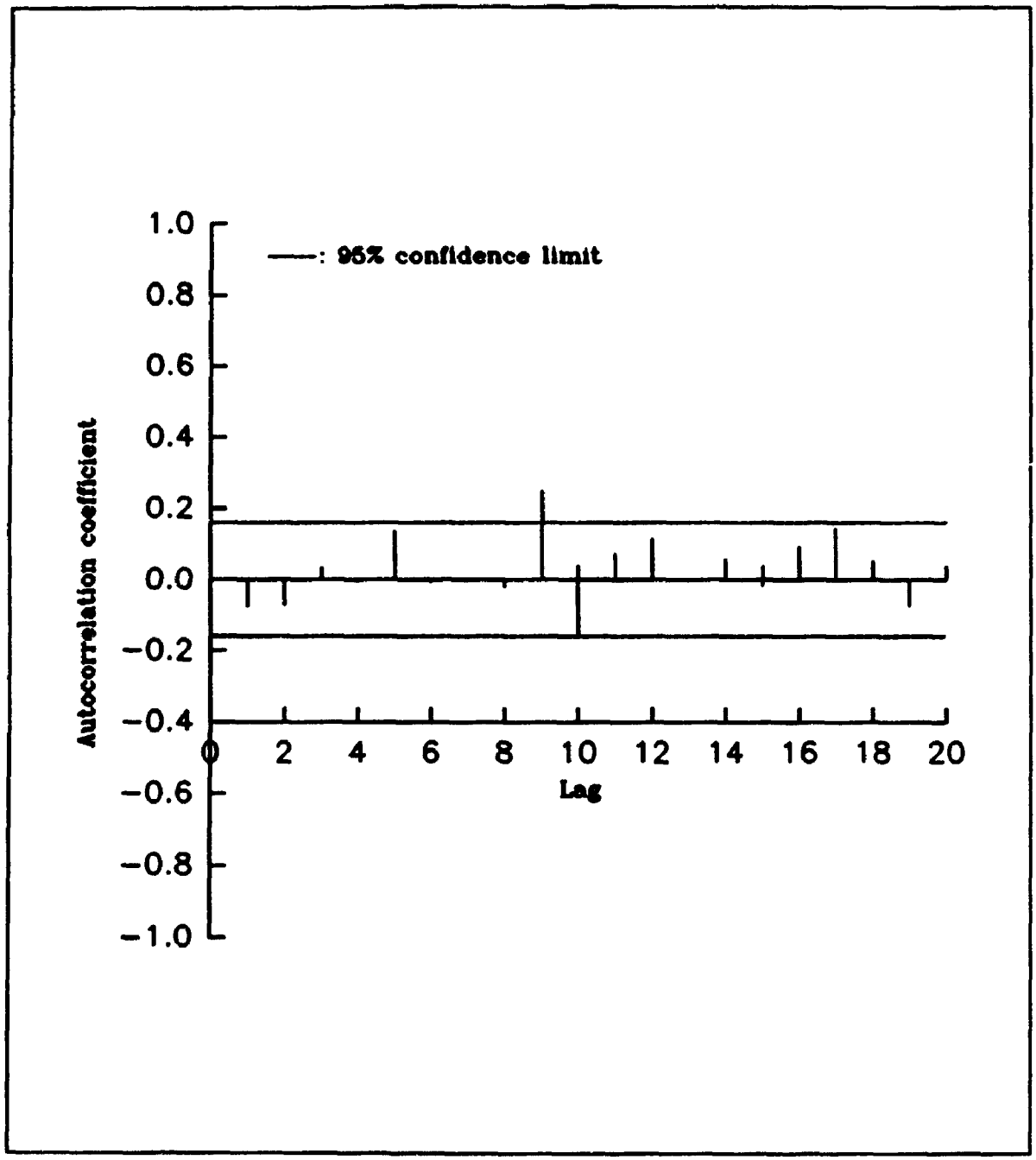

Figure 5.68: Autocorrelation of the residuals (inverse gaussian function)

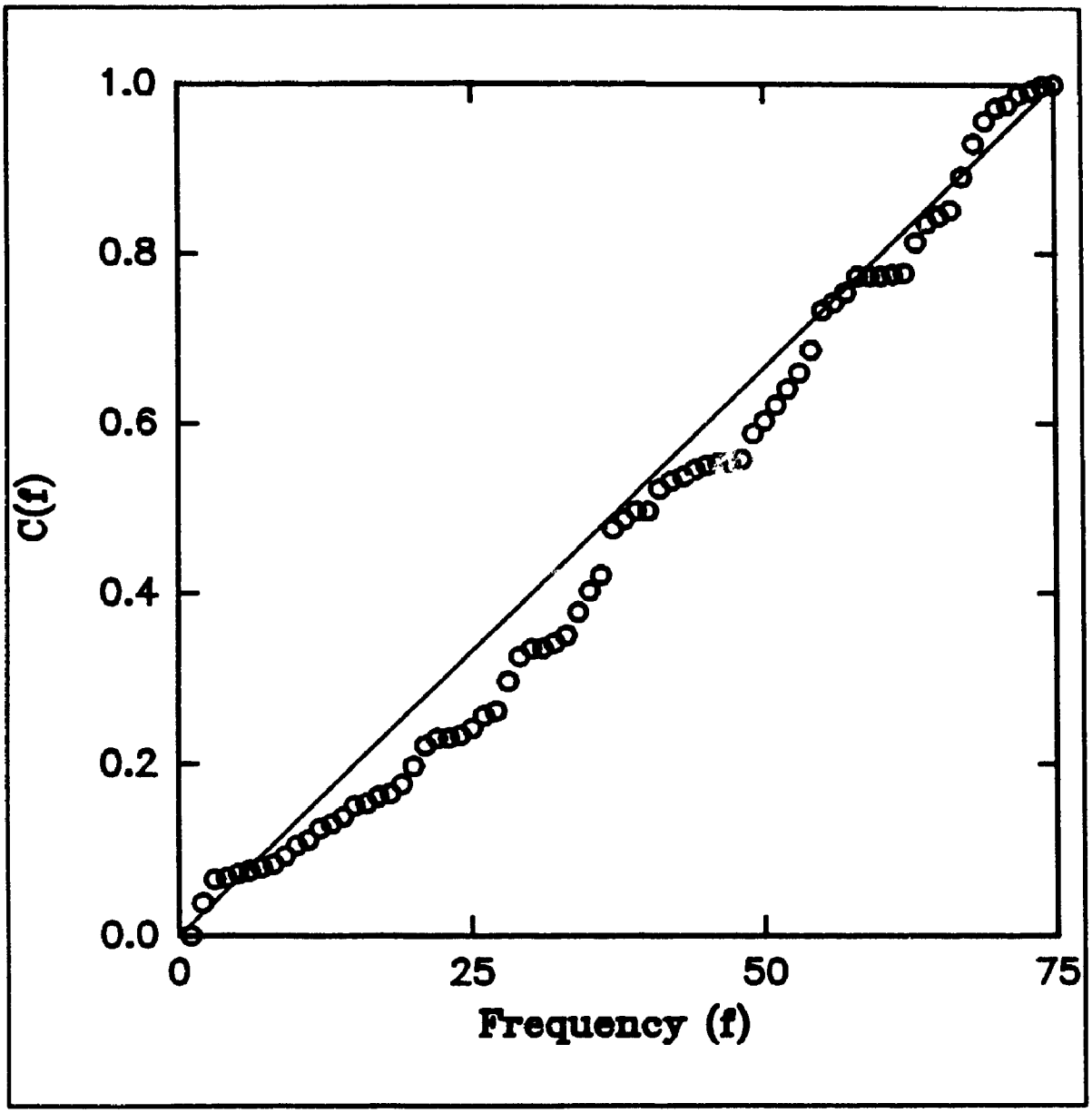

Figure 5.69: Cumulative periodogram of the residuals (inverse gaussian distribution function)

parameter value were obtained for the totality of the experiments. A complete listing of the parameters obtained and their respective standard deviation is presented in Appendix 9 (please refer to Appendix 4 for more details concerning the operating conditions corresponding to each data file).

Consequently, considering the successful model behaviour, the adequate standard deviation of the optimum parameters obtained, and the successful residuals checks (autocorrelation and cumulative periodogram), the inverse gaussian distribution function was considered to represent the experimental bubble chord length distributions. It is however important to stress that the inverse gaussian function was selected over the well established log-normal distribution for its slight superiority in representing the experimental data, though both models appeared to capture the general shape of the bubble chord length distribution.

The characteristics of the bubble chord length distributions were found to be a pronounced function of the radial position. Actually, both, the standard deviation and the average of the bubble chord length distribution decreased as the radial position increased, as shown in detail in Appendix 9. Consequently, the bubble chord length distributions were found to gradually broaden when moving from the vicinity of the column wall to the center of the column, while simultaneously

being shifted toward larger average bubble chord length. Two illustrations of this phenomenon are presented in Figures 5.70 and 5.71. This particular behaviour of the bubble chord length distribution was observed for all the operating conditions and locations, with the exception of the lower axial positions (z=15 cm, z=30 cm) at V_g=2.2 cm/s, for which the bubble chord length distribution was found to be wider, while having a larger average value, in the vicinity of the column wall than in the central section of the column, as shown in Figure 5.72. This phenomenon indeed confirmed the presence of a secondary liquid circulation cell under these particular conditions. Actually, the presence of two distinct liquid circulation cells, the secondary liquid circulation cell in the bottom of the column followed, at higher axial positions, by the main (classical) liquid circulation cell, favoured segregation of the bubble population between the bottom and the top section of the bed. Such segregated flow patterns prevented complete backmixing of the small bubbles (generated from break-up events along the column length) along the wall of the column and favoured the presence of larger bubbles in the bottom of the column, close to the wall. The small bubbles recirculated downward along the length of the column by the main liquid circulation cell were pushed toward the column center at the transition point between the two cells. Furthermore, the presence of the downward liquid circulation vector in the center of the column due to the presence of the secondary liquid circulation cell, retarded

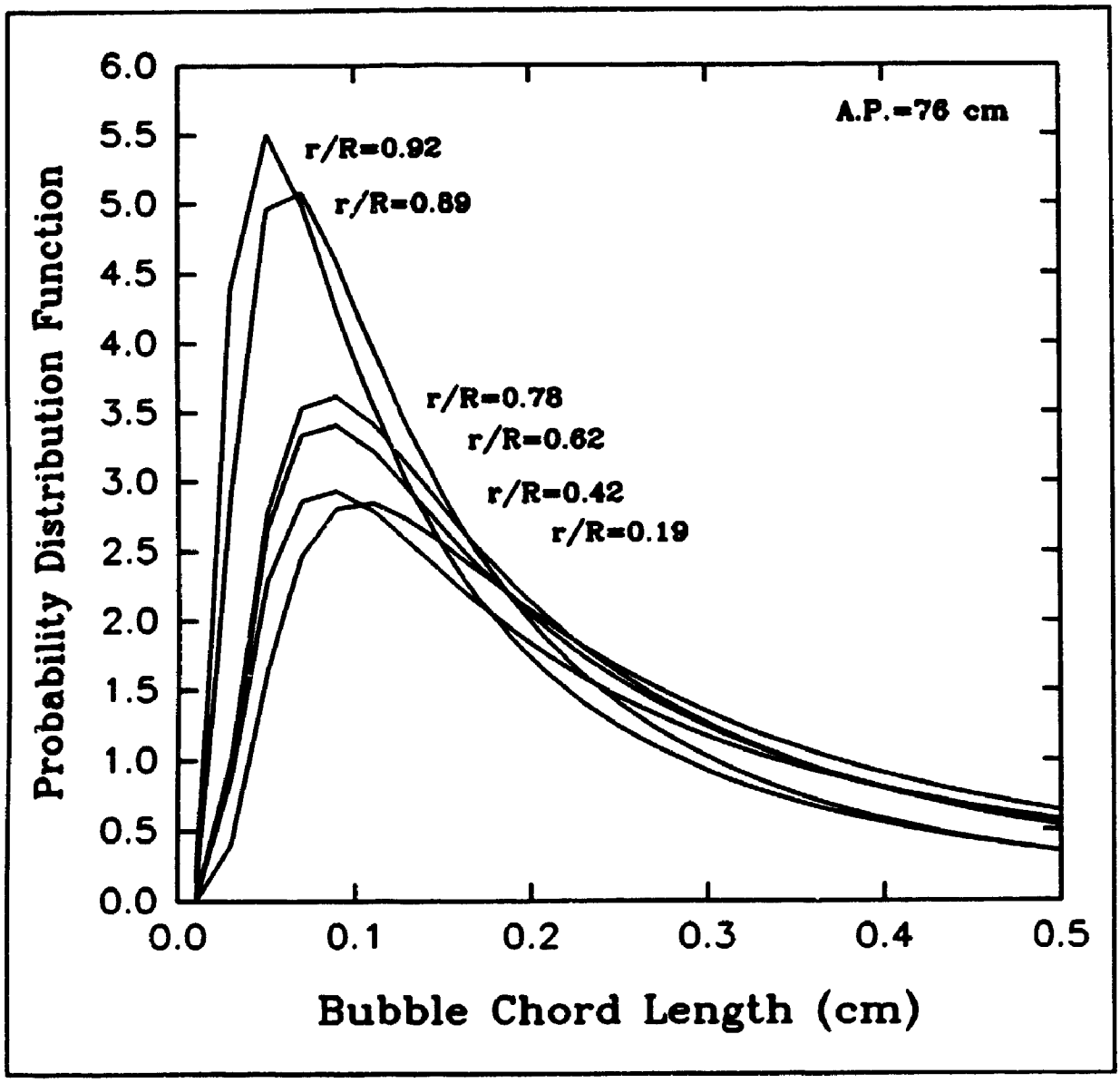

Figure 5.70: Bubble chord length distribution function (T=100°C, V_g=2.2 cm/s, z=76 cm)

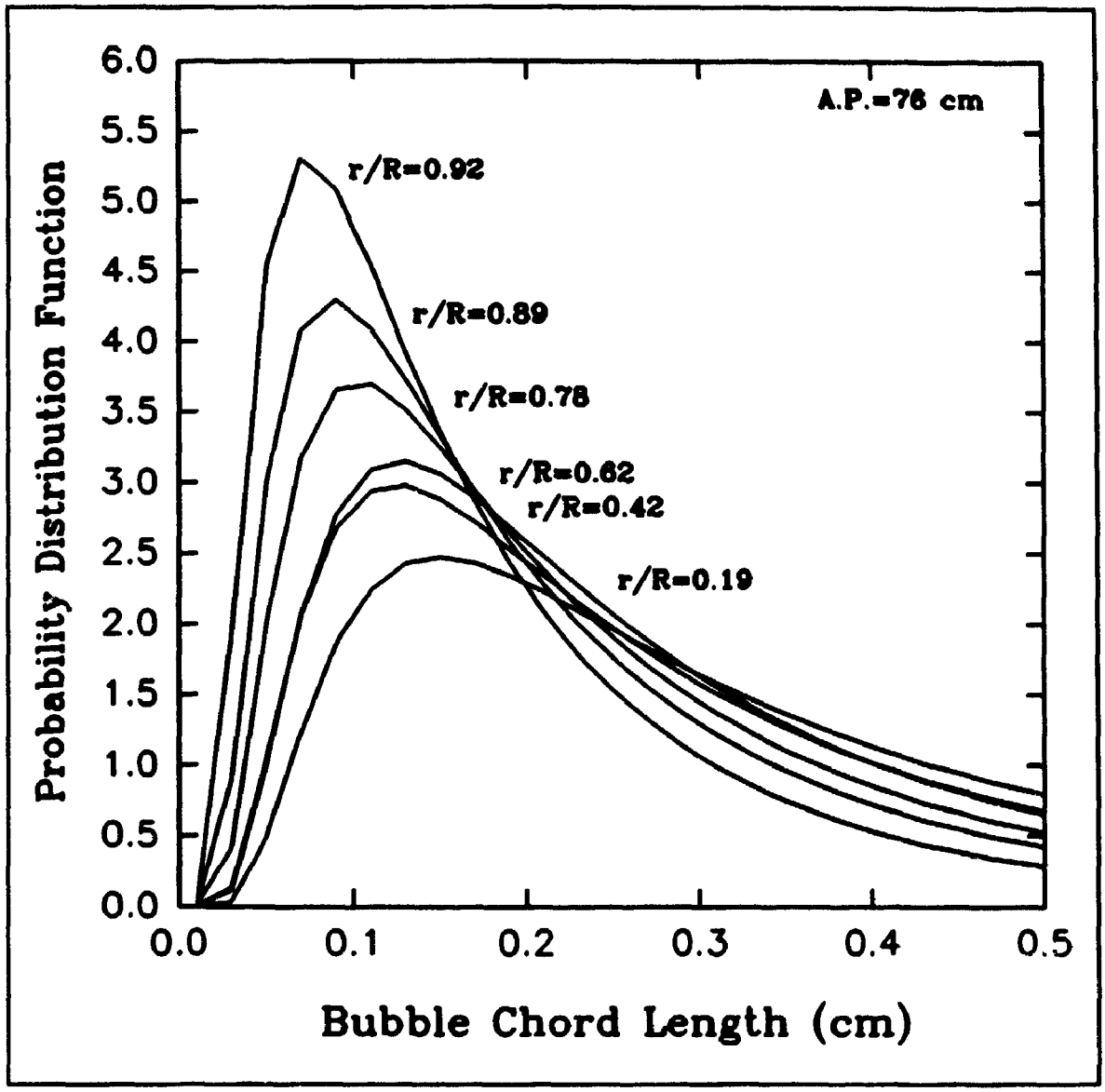

Figure 5.71: Bubble chord length distribution (T=175°C, V_g=14.7 cm/s, z=76 cm)

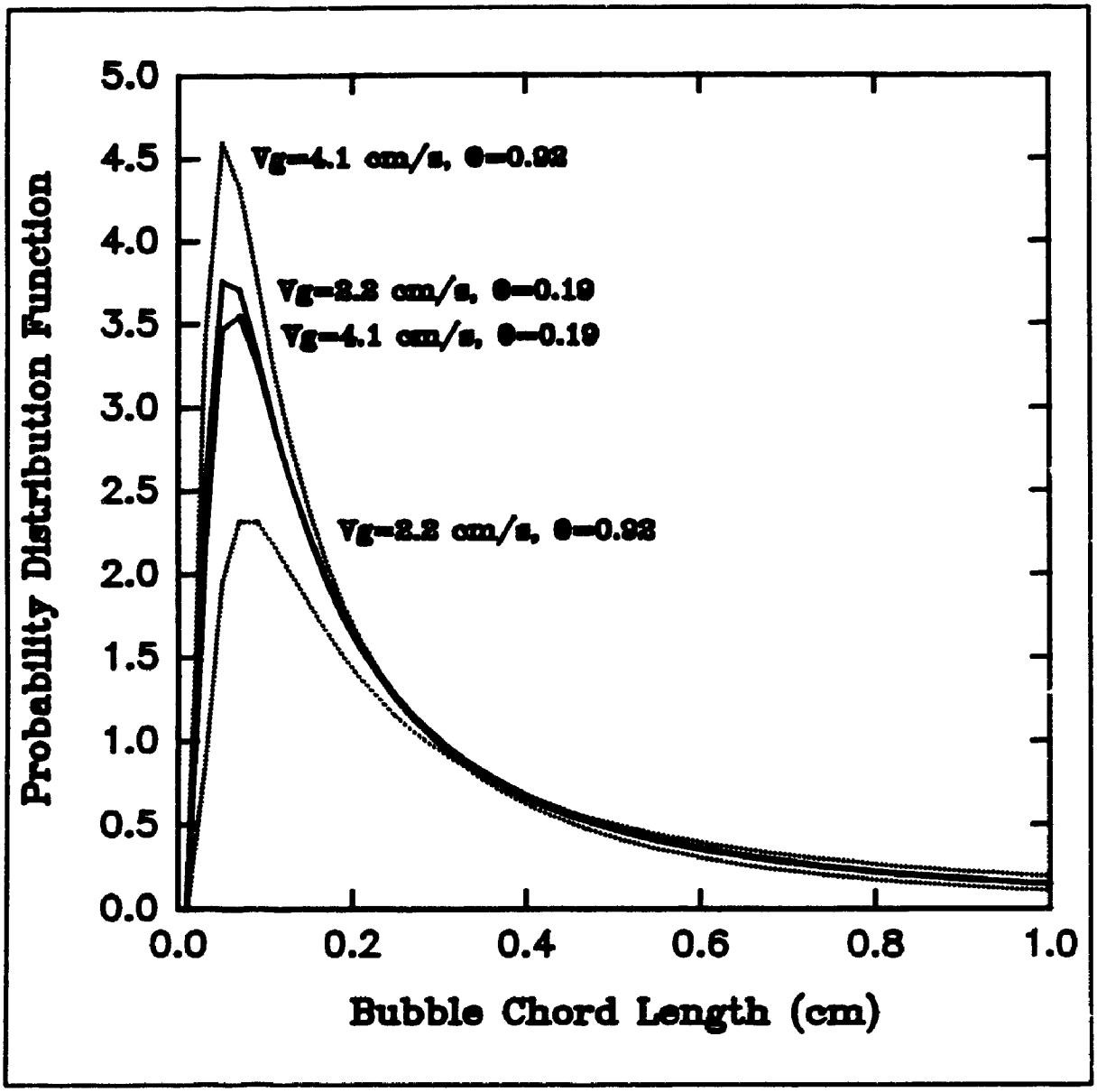

Figure 5.72: Bubble chord length distribution (T=100°C, z=15 cm)

the migration of the bubbles toward the center, as confirmed by extremely uniform gas holdup radial profile at this location. This, in turn, favoured a more diluted gas flow (lower bubble frequency), lower probability of contact between bubbles and thus a lower incidence of bubble coalescence events. This particular phenomenon however disappeared with an increase in the axial position, or as the primary liquid circulation cell (upward liquid velocity in the center and downward liquid velocity at the column wall) emerged, as confirmed in Figure 5.70.

The axial evolution of the bubble chord length probability distribution function was also found to be dependent on the radial position. Actually, since the average bubble chord length was found to increase with the axial position in the central section of the column (core zone) due to a dominant manifestation of bubble coalescence events in this region, it was expected that a wider bubble chord length distribution with a higher proportion of larger bubbles be observed as the axial position increased. This was actually observed for all the operating conditions, and one example, in terms of the cumulative probability distribution function is presented in Figure 5.73. So, in the center of the column (core zone), the bubble chord length distribution function was found to widen with the axial position, as larger bubbles appeared as a result of coalescence events. On the other hand, since the bubble chord length was found to decrease with the axial

318

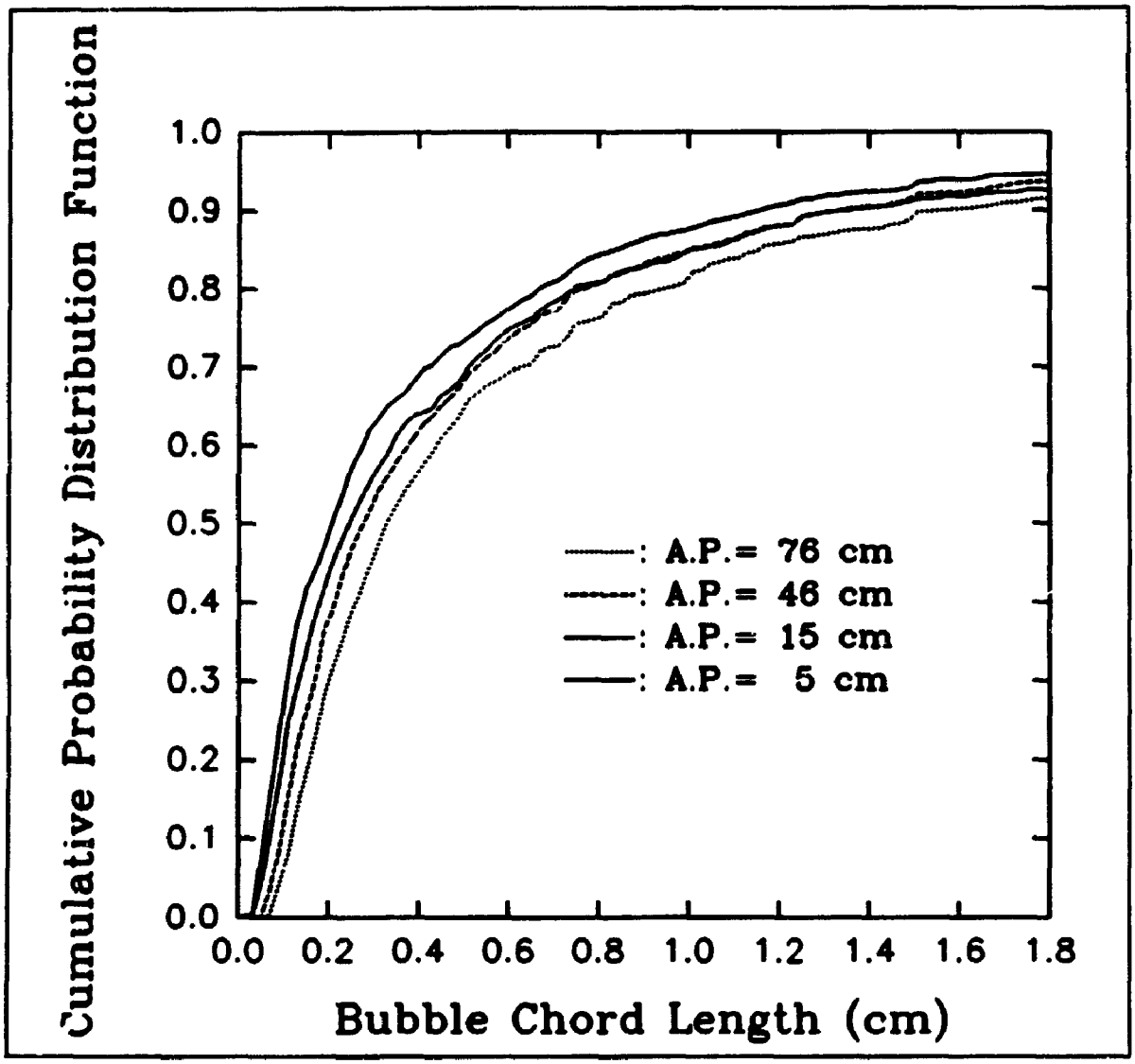

Figure 5.73: Cumulative bubble chord length distribution (T=100°C, V_g=14.7 cm/s, θ=0.19)

position in the vicinity of the column wall (peripheral zone), narrower bubble chord length distributions with smaller average bubble chord length were observed at the wall as the axial position increased, as shown in Figure 5.74.

The influence of the gas superficial velocity on the bubble chord length distribution in the central region of the column (core zone) is illustrated in Figure 5.75. As shown in this Figure, the standard deviation of the bubble chord length distribution was found to gradually diminish as the gas superficial velocity decreased, while the location of the distribution was shifted to smaller bubbles. Then, for the same radial and axial position, wider bubble chord length distributions were observed as the gas superficial velocity augmented. This phenomenon was generally present for all radial and axial positions, though the influence of the gas superficial velocity on the bubble chord length distribution was less pronounced in the proximity of the column wall, as shown in Figure 5.76.

The temperature of operation was also found to have an influence on the bubble chord length distribution. Actually, for the same radial and axial position, the bubble chord length distribution was found to be wider as the temperature decreased, as shown in Figure 5.77.

As mentioned previously, the presence of large bubbles was

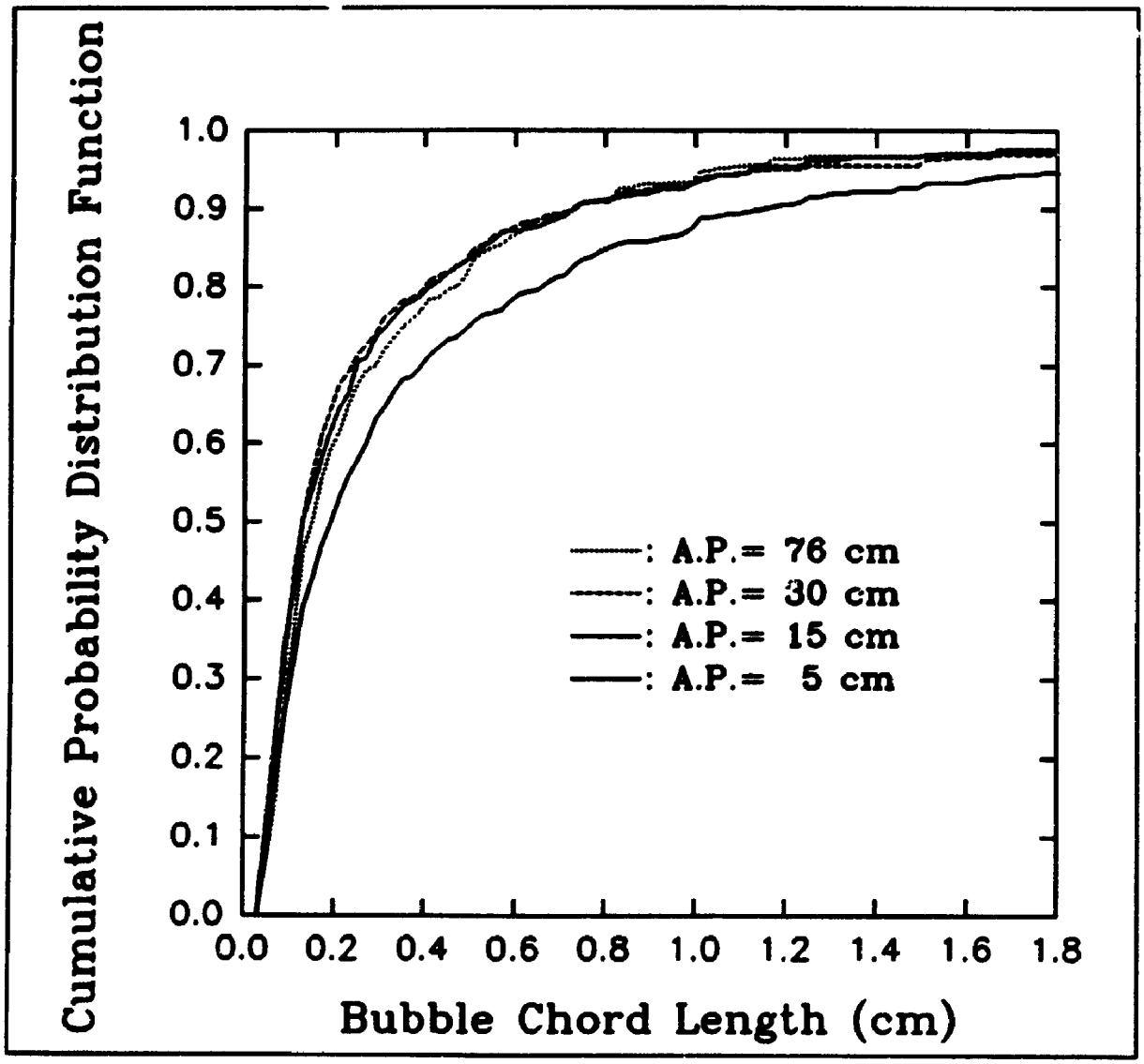

Figure 5.74: Cumulative bubble chord length distribution (T=100°C, V_g=14.7 cm/s, θ=0.92)

321

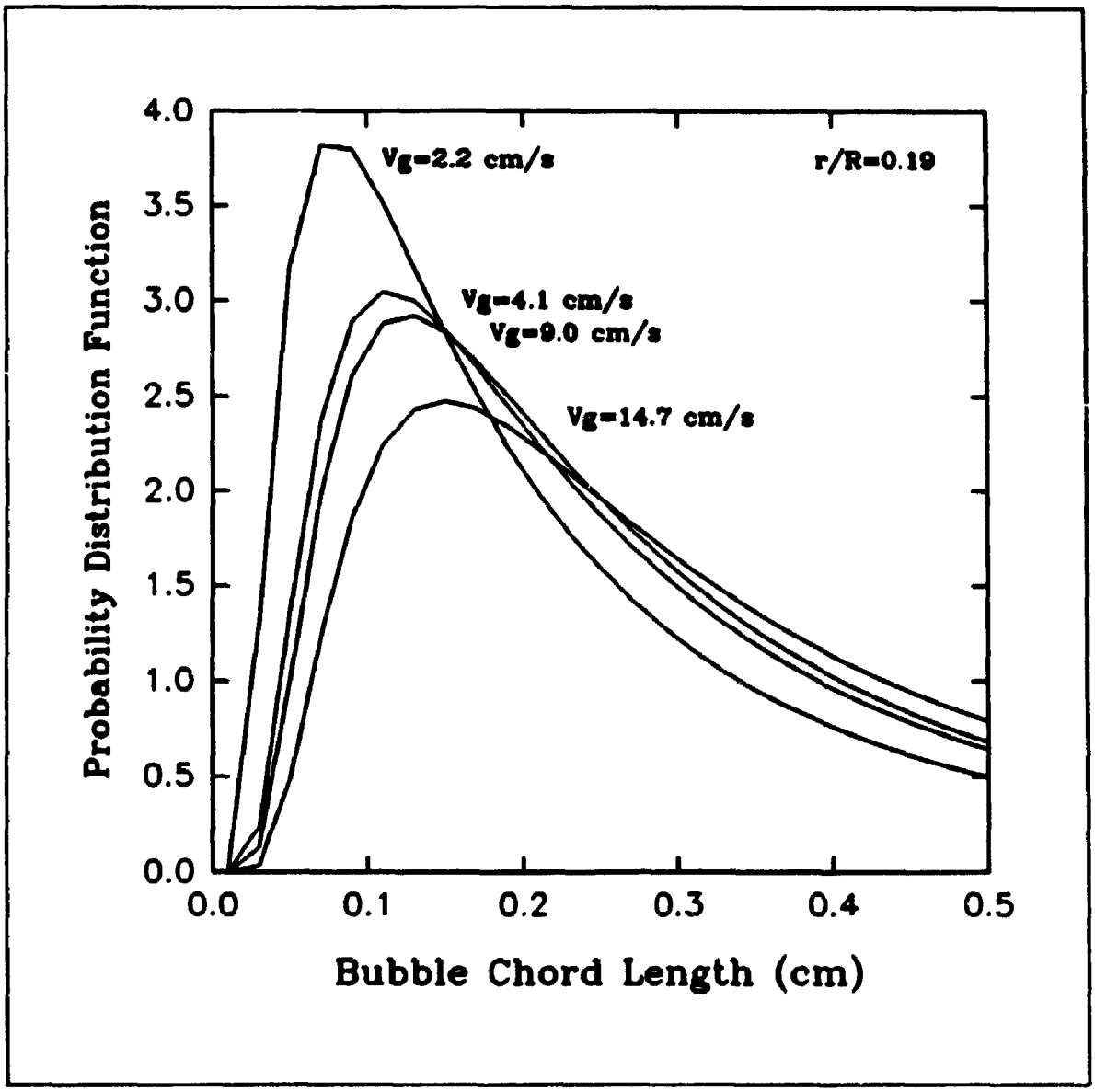

Figure 5.75: Bubble chord length distribution (T=175°C, z=76 cm, θ=0.19)

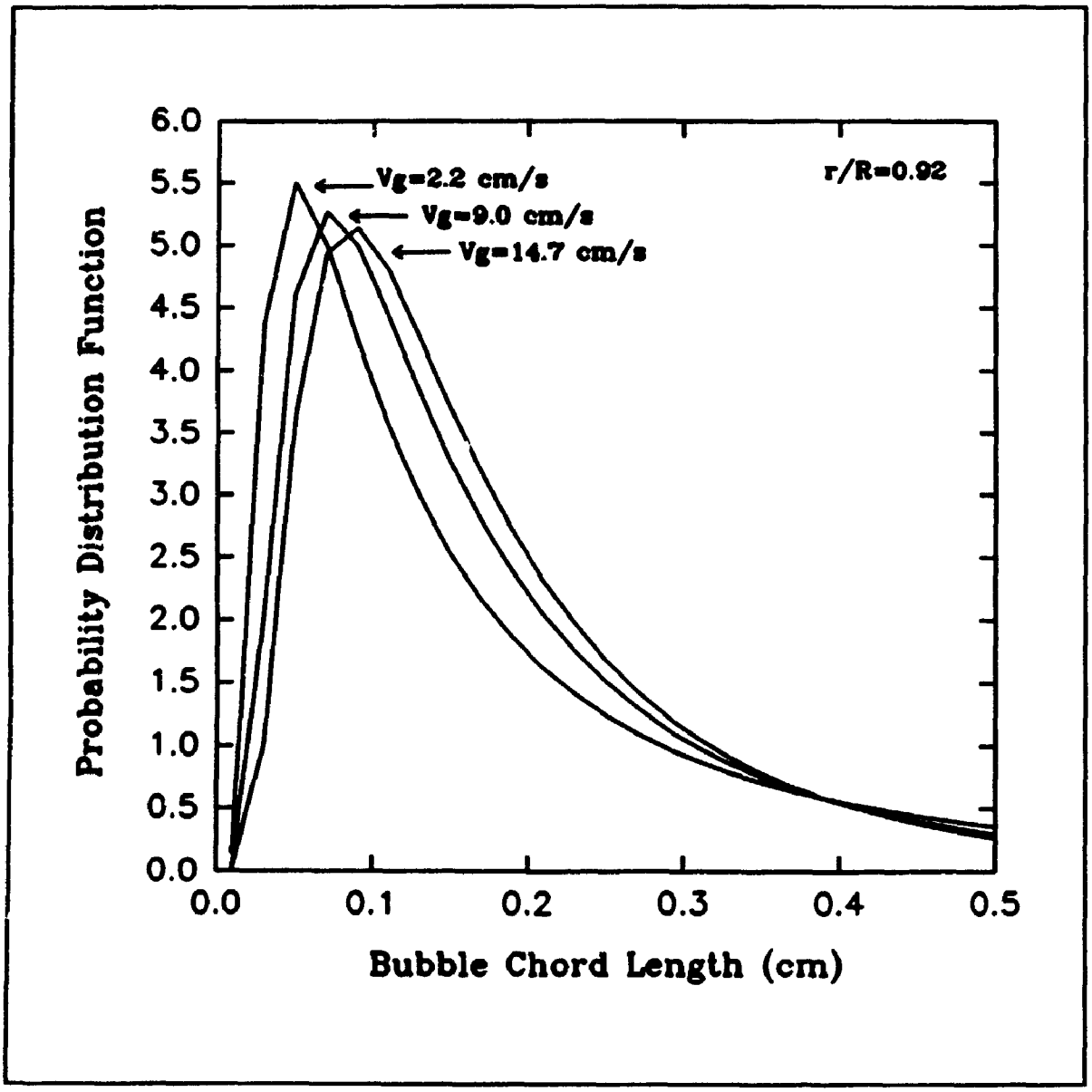

Figure 5.76: Bubble chord length distribution (T=100°C, z=76 cm, θ=0.92)

323

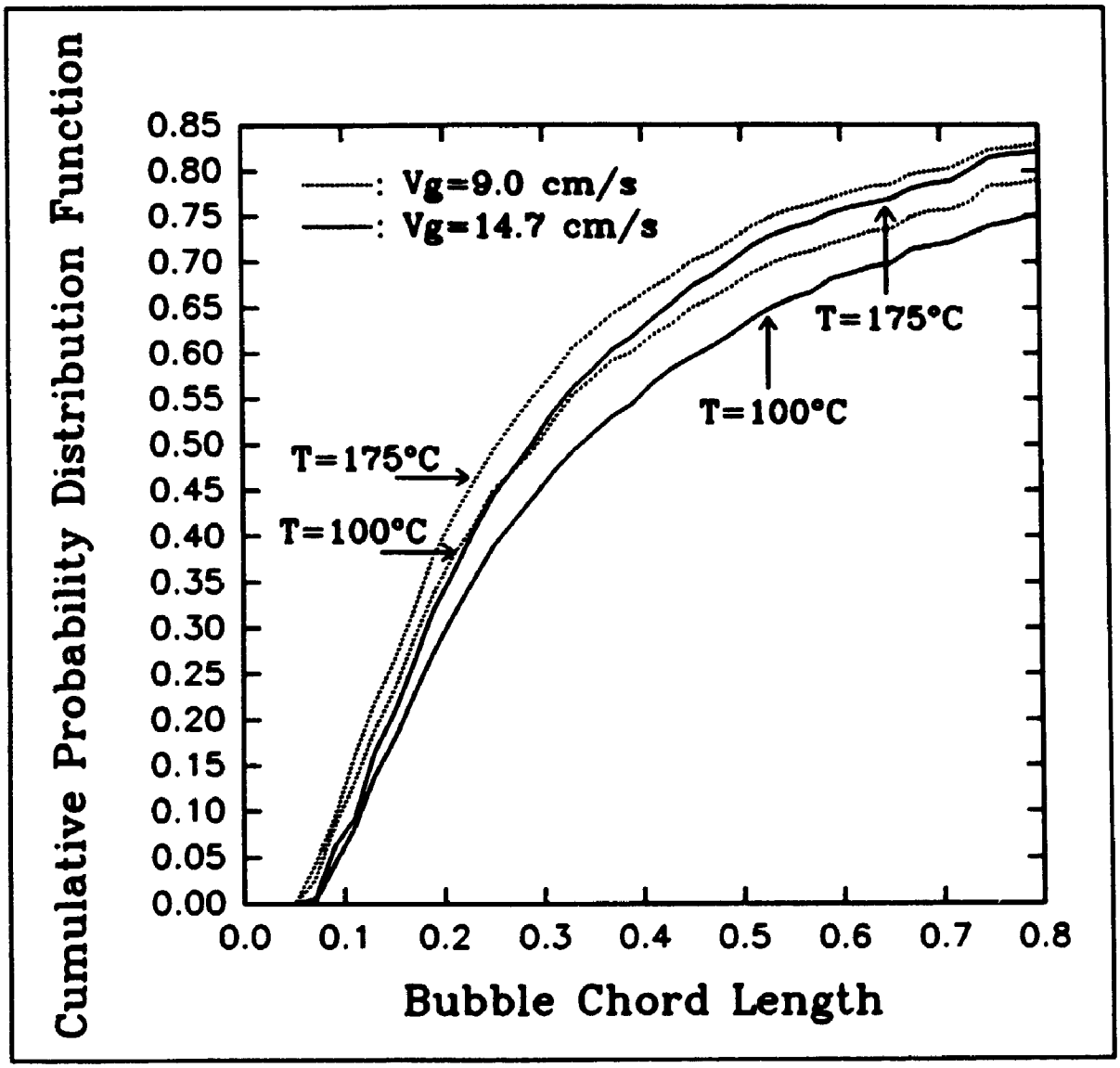

Figure 5.77: Cumulative bubble chord length probability distribution (θ=0.19, z=76 cm)

relatively small as compared to the one of smaller bubbles (highly skewed bubble axial chord length distribution). However, even in small proportion, very large bubbles (bubble having chord length > 3 cm) were indeed present in the system. These very large bubbles, as shown in Figure 5.78, represented, in general, less than 4% of the total bubble population. Furthermore, and as shown in Figure 5.78, the proportion of these very large bubbles decreased with a decrease of the gas superficial velocity. In addition, the proportion of these very large bubbles augmented with the axial position in the center of the column, while slightly decreasing at the column wall. The proportion of very large bubbles (axial bubble chord length > 3 cm) was also found to be systematically higher in the center of the column than in the vicinity of the column wall. However, even in smaller proportion, these very large bubbles were seen in the periphery of the column wall for the higher gas superficial velocities. At very low gas superficial velocity (V_g=2.2 cm/s), an extremely small occurrence of large bubbles was observed at the column wall, as illustrated in Figure 5.78. In addition, it is interesting to note (Figure 5.78) that as the axial position increased, a larger difference between the proportion of very large bubbles observed was noted between the wall and the central region of the column. Actually, in the bottom of the column, a relatively similar occurrence of very large bubbles was observed throughout the cross section of the column.

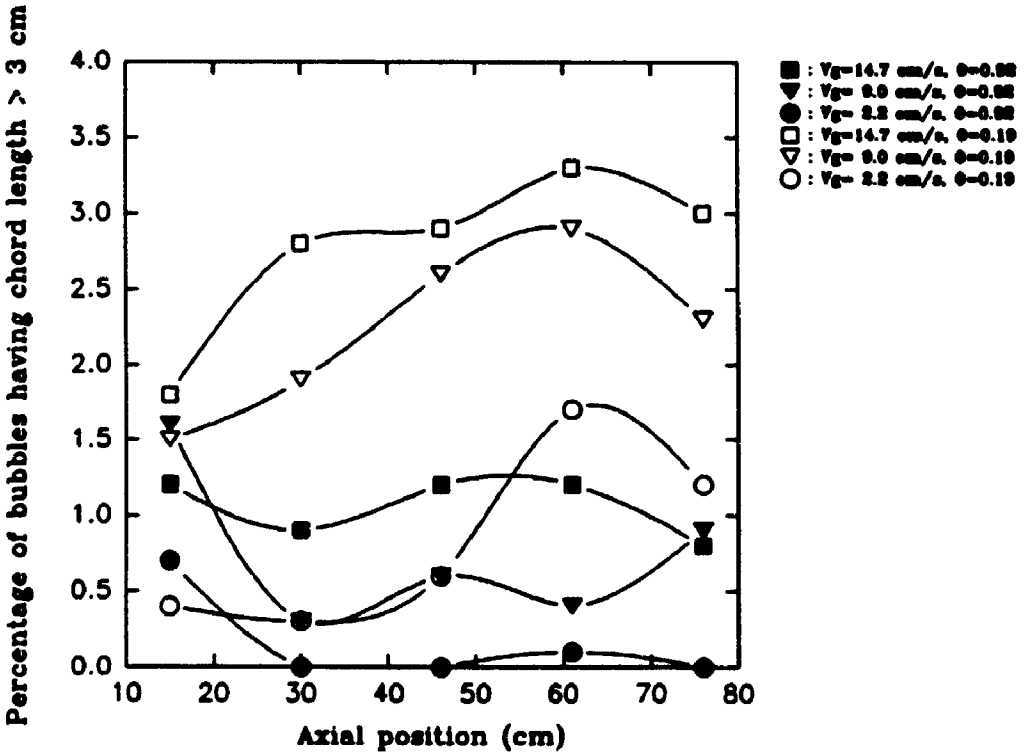

Figure 5.78: Percentage of bubbles having axial chord length larger than 3 cm vs axial position (T=100°C)

These findings indeed confirm the dominance of coalescing events in the center of the column (central zone), and the poor incidence of coalescing events in the peripheral region of the column (peripheral zone), the so-called "coalescence-break-up" bubble regime as discussed in the previous section.

In order to study the respective contribution of small and large bubbles to the gas holdup, the following analysis was undertaken. The total range of bubble chord lengths observed was divided in two categories, namely small and large bubbles. The large bubbles were defined as the ones having an axial chord length bigger than 0.3 cm, while the small bubbles were classified as having a chord length smaller or equal to 0.3 cm. Then, the contribution to the gas holdup of each one of these two bubbles classes was analyzed for various conditions.

As shown in Figure 5.79, the contribution to the gas holdup of large bubbles was higher in the center of the bed (θ=0.19) than at the column wall (θ=0.92), and systematically increased with the gas superficial velocity. At the column wall, the large bubbles contributed for less than 50% of the gas holdup, and this contribution decreased with an increase of the gas superficial velocity between 2.2 and 9.0 cm/s, and slightly increased with a further increase of the gas superficial velocity (V_g=14.7 cm/s). These findings are consistent with the dominance of coalescing events in the center of the column (core zone) and bubble break-up manifestations dominance in

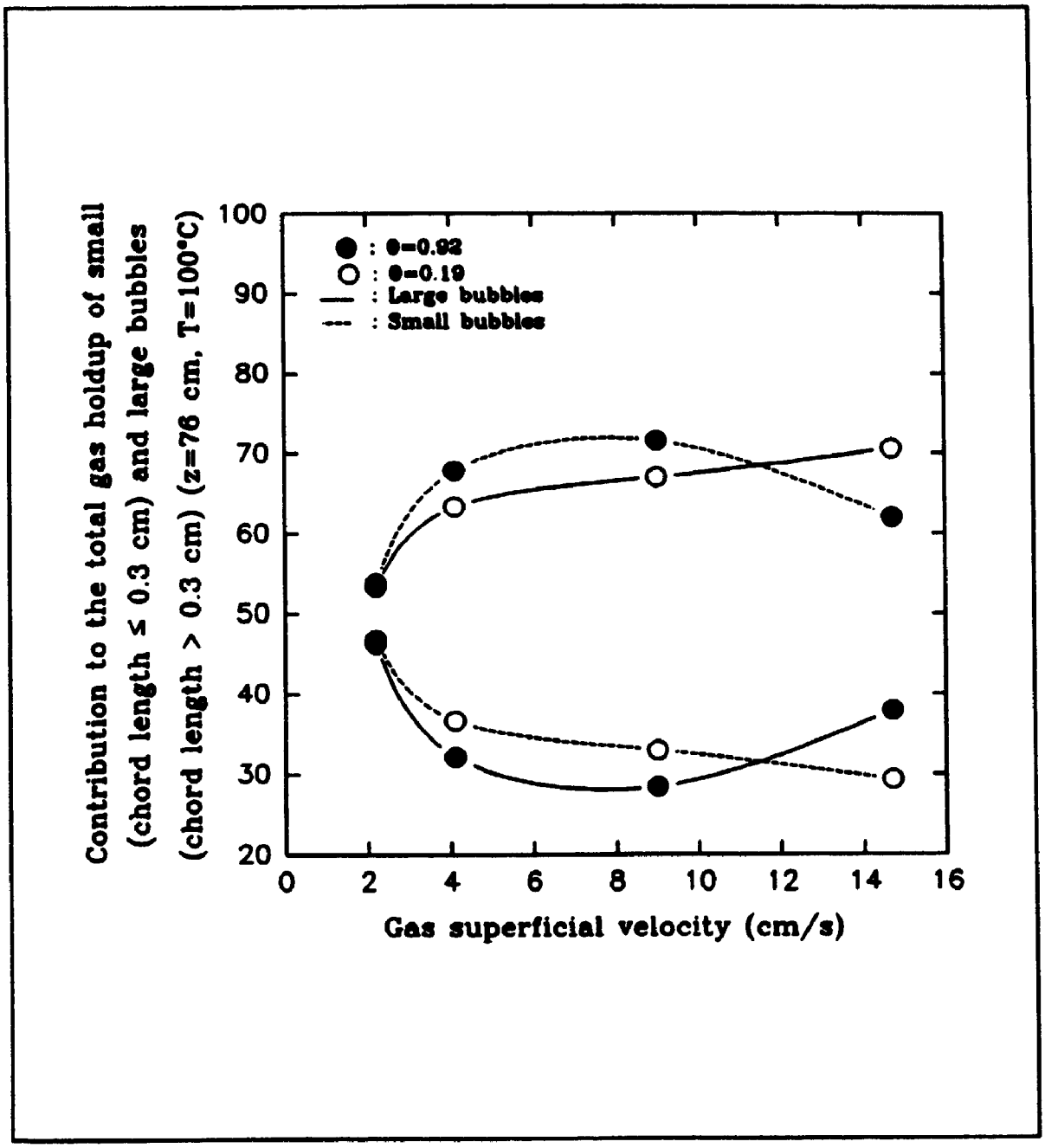

Figure 5.79: Contribution (%) to the gas holdup of small bubbles (axial chord length ≤ 0.3 cm) and large bubbles (axial chord length > 0.3 cm) vs gas superficial velocity (T=100°C, z=76 cm)

the peripheral zone of the column. Then, as the gas superficial velocity increased, the contribution to the gas holdup was dominated in the center of the column by large bubbles, and by small ones at the column wall. For example, at V_g=14.7 cm/s (T=100°C, z=76 cm), the large bubbles contributed to 70.6% of the gas holdup in the center and only to 37.9% of the gas holdup at the column wall. At lower gas superficial velocity, small and large bubbles contributed more equally to the gas holdup throughout the cross section of the column. The more balanced contribution to the gas holdup of small and large bubbles observed at V_g=14.7, as compared to V_g=9.0 cm/s, might be due to an overall increase of the mixing intensity which contributed to a more homogeneous repartition of the bubbles.

The same overall behaviour was observed at T=175°C, though a systematic increase of the contribution of small bubbles was observed for all the conditions, particularly in the center of the column.

It is important to note that, in general, the contribution of a particular class of bubbles (small or large) to the gas holdup was not equal to its contribution to the total number of bubbles. In other words, if a class of bubbles represents 10% of the bubble population, these particular bubbles will not contribute to 10% of the gas holdup. In order to study more thoroughly this question, the ACGH (Ability to Contribute

to the Gas Holdup) factor was introduced. The ACGH factor is defined as the ratio of the contribution of a particular class of bubbles (small or large) to the gas holdup over the contribution of this same class of bubbles to the bubble population (in numbers). This factor is then a measure of the relative contributiona by a particular class of bubbles to the gas holdup. A ACGH factor of 1.0 would mean an equal contribution to the gas holdup and to the bubble population of a particular group of bubbles. As shown in Figure 5.80, the small bubbles were found to have systematically a poor ability to contribute to the gas holdup (ACGH < 1.0). They then participated to the gas holdup with a smaller proportion than they contributed to the overall bubble population, and this phenomenon was found to be maximum in the center of the column. Actually, at this particular radial location, the small bubbles are entrained with the large fast rising bubbles slugs and liquid upward currents, and are then carried up the column with a large rise velocity. Consequently, their contribution to the gas holdup becomes less important. On the contrary, at the column wall, descending liquid currents favoured a longer retention of the small bubbles, thus allowing them to contribute more generously to the gas holdup. In consequence, higher ACGH factors were observed in the vicinity of the column wall than in the center of the column. Despite a larger participation of the small bubbles class to the gas holdup at the higher temperature (T=175°C), the ACGH factors were found to be of similar magnitude than the ones

330

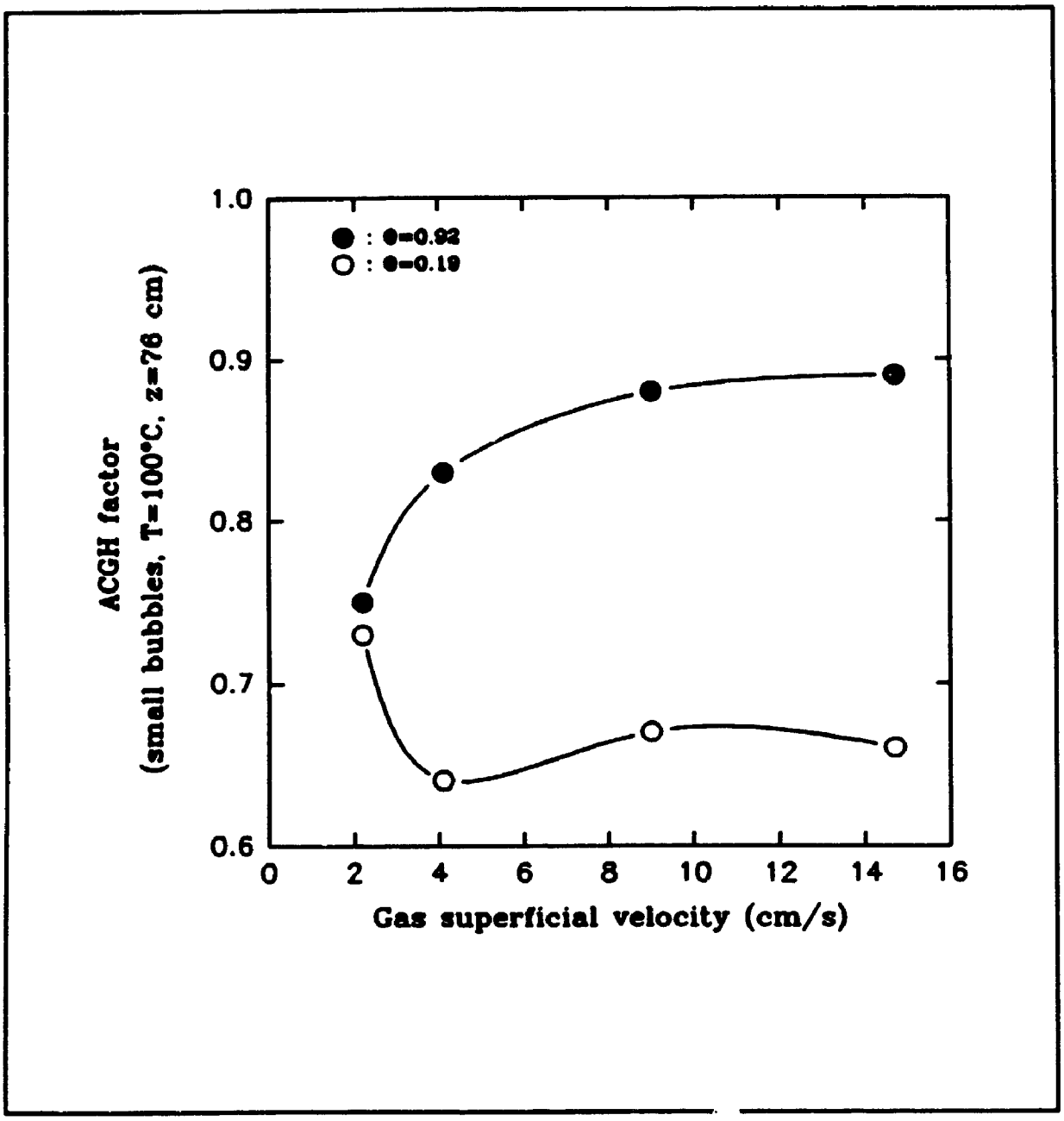

Figure 5.80: ACGH factor vs gas superficial velocity (T=100°C, z=76 cm)

observed at T=100°C for identical locations in the column. This is consistent with the observation of similar overall flow patterns at these two temperatures.

In conclusion, the information obtained from the bubble chord length distribution analysis provided extremely interesting insights about the nature of the bubble population in a system of high interest for the fuel industry. First of all, all the bubble chord length distributions observed in the present study were characterized by the dominant presence of small bubbles and the scarce presence of larger ones. These skewed distributions were adequately represented by the inverse gaussian probability distribution function. In general, the average and standard deviations of the bubble chord length distributions were found to decrease with the radial position, except for the cases where the secondary liquid circulation cell was present. The axial evolution of the bubble chord length distribution was consistent with the existence of a central coalescence dominated zone (core zone) and a bubble break-up dominated zone (peripheral zone) in the vicinity of the column wall, as explained in the previous section. These results confirmed the important axial and radial variations of the bubble population and point toward the need to implement such local variations in the theoretical representation of the gas phase behaviour in bubble column systems. Furthermore, the average and standard deviations of the bubble axial chord length distribution were observed, in general, to increase

with an increase of the gas superficial velocity and a decrease of the operating temperature.

333

5.2 SLURRY BUBBLE COLUMN

As extensively discussed in Chapter 1, the effect of solids on the gas phase hydrodynamics of bubble columns still represents a particularly critical issue. Various studies were conducted on the effect of the solids characteristics (size, density, wettability, sphericity), and loading on the gas holdup, bubble size and general flow patterns. However, contradictory conclusions were frequently reported and only scarce data are currently available for systems of similar nature to the liquid phase methanol system or other systems involving hydrocarbon liquids.

In the present study, the influence of solid particles on the general gas phase characteristics of the system was investigated. A typical slurry methanol synthesis catalyst (zinc-copper oxide catalyst, d_{avg}=13.85 μm) was suspended in the paraffinic oil at a concentration of 10%$_{wt}$. A complete description of the solid particles used in this study is presented in Appendix 1, while details concerning the operation of the system in presence of solids are discussed in Chapter 2. The operating parameters (gas superficial velocity, temperature, radial and axial positions) selected for the slurry experiments were identical to the ones studied during the bubble column experimental phase. The study was however focused on assessing the overall effects of solid particles addition, while confirming the presence of important

334

flu'd dynamics observations found under bubble column conditions. The fibre optic sensors were also used, in the present section, to investigate the bubble phase characteristics. Despite the presence of a dark and opaque medium, resulting in stronger light absorption and thus lower returning light intensities, the optical sensors performed satisfactorily, as shown in typical fibre optic sensors' output signals presented in Figure 5.81.

In general, it was found that the addition ($10\%_{wt}$) of the solid particles favoured a slight decrease of the average radial gas holdup. Actually, the presence of the solid particles contributed to an increase of the apparent viscosity of the system. This, in turn, favoured bubble coalescence and resulted in smaller gas holdups. A typical comparison between the average radial gas holdup measured in the two-phase and the three-phase systems is presented in Figure 5.82, for z=76 cm. As shown on this Figure, the influence of the solid particles, though very clear and consistent, was found to be relatively small. Actually, the maximum decrease of the gas holdup observed upon solid addition was not in excess of 3%. ($\Delta\epsilon_g < 0.03$). However, the influence of the solid was found to be higher for the lower gas superficial velocities studied (2.2 cm/s), while gradually decreasing with an increase of the gas superficial velocity. The difference became imperceptible at the highest gas superficial velocity (14.7 cm/s), as shown in Figure 5.82. The same trend, diminution of the effect of

335

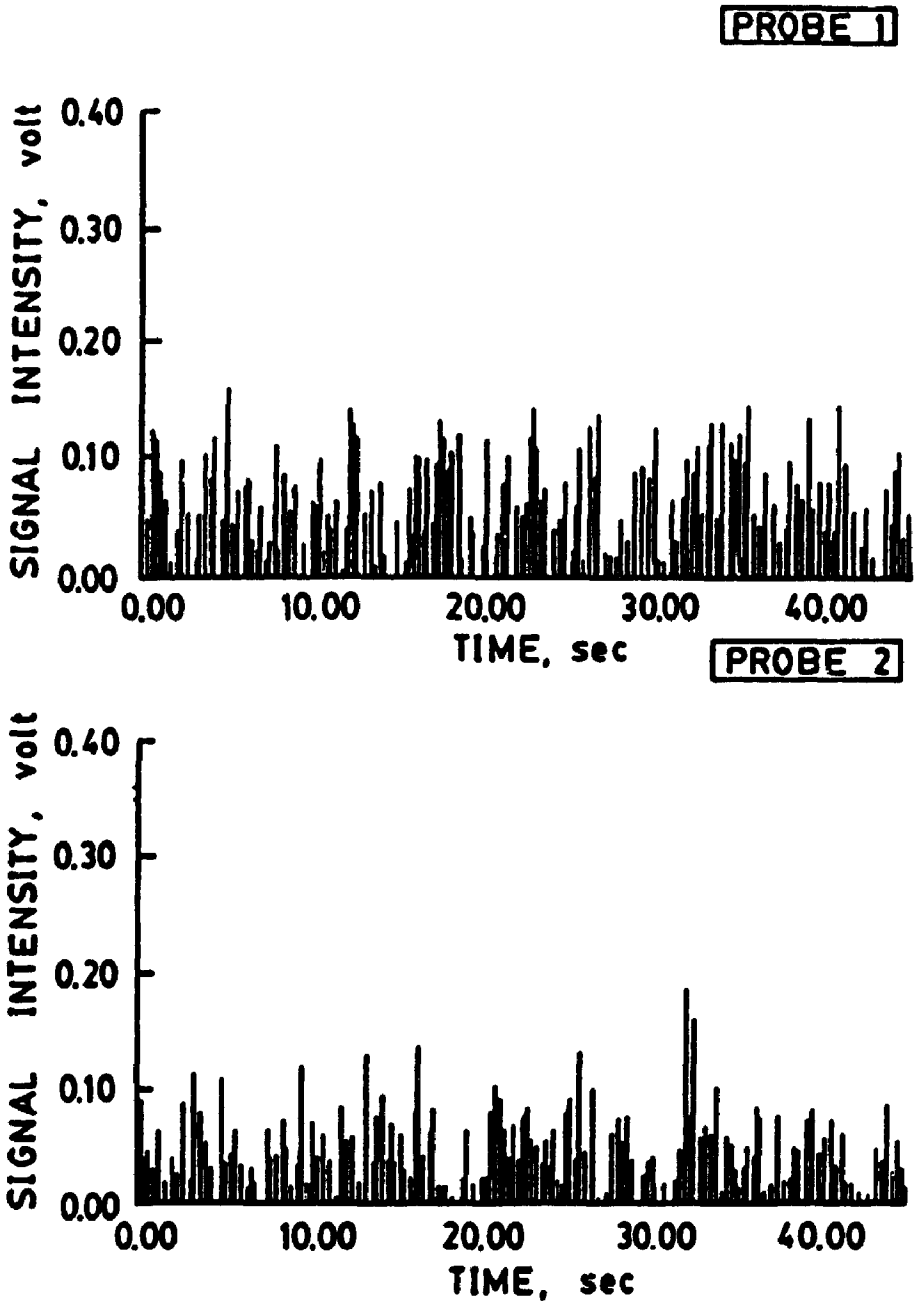

Figure 5.81: Typical fibre optic sensors output signals (time series) in slurry bubble column conditions (T=100°C, V_g=14.7 cm/s, z=15 cm, θ=0.19)

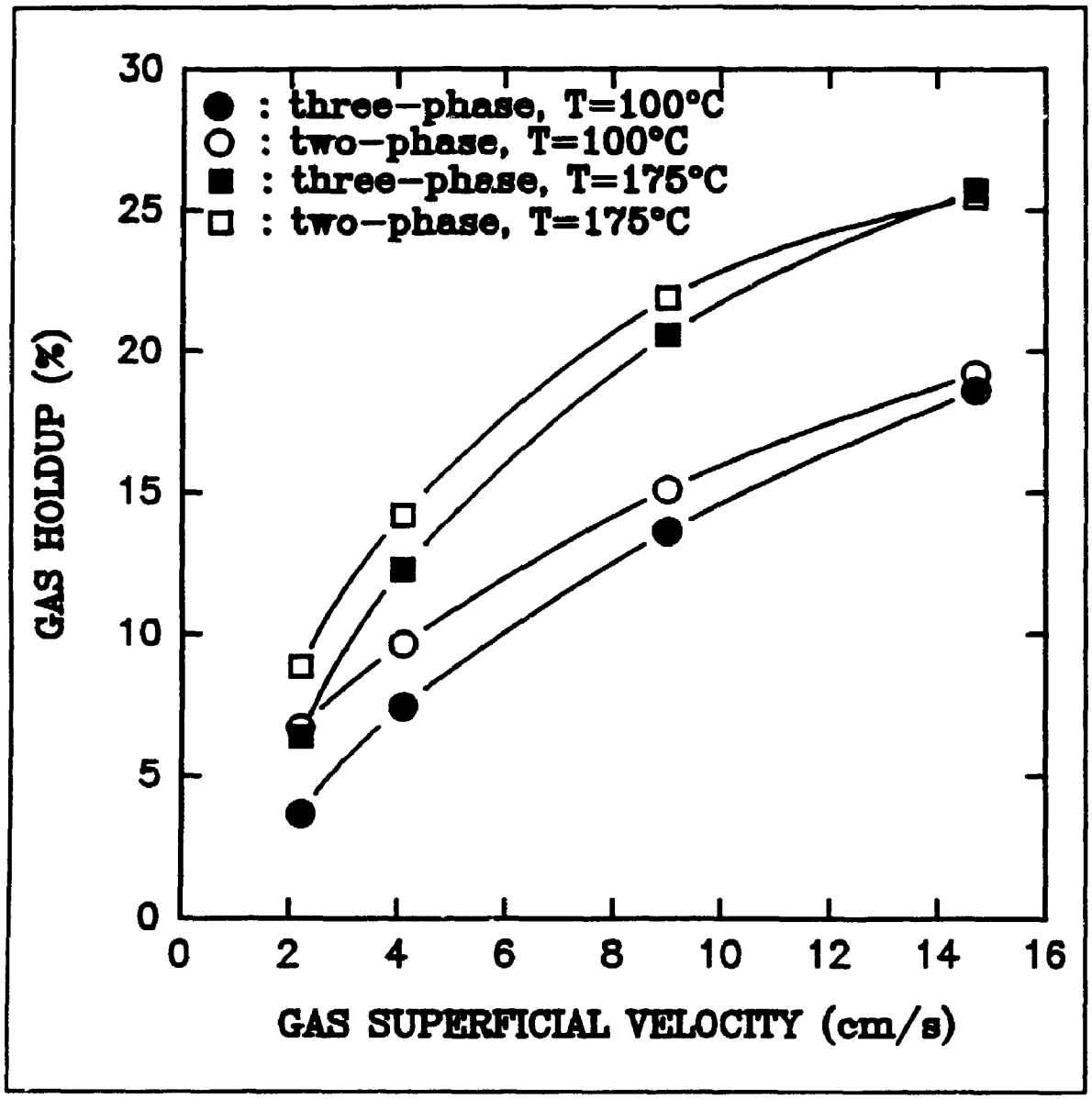

Figure 5.82: Effect of the presence of solid particles ($10\%_{wt}$) on the average gas holdup (z = 76 cm)

solids with the increase of the gas superficial velocity, was observed for both temperatures studied. However, no clear influence of the temperature on the effect of solids addition was detected.

The observation of a systematic decrease of the gas holdup upon solids addition was found to be consistent with the general increase of the bubble chord length, noted for the operating conditions and locations studied. For example, the average bubble chord length measured in bubble column conditions (T=100°C, V_g=14.7 cm/s, z=15 cm, θ=0.19) was equal to 4.3 mm, as compared to 5.4 mm in slurry bubble column conditions. At T=100°C, V_g=9.0 cm/s, z=76 cm and θ=0.19, the average bubble axial chord length measured in bubble and slurry bubble conditions respectively, were equal to 5.3 mm and 6.1 mm. Increase of the bubble axial chord length upon solids addition was also observed along the wall of the column. For example, the average bubble axial chord length increased from 2.8 mm to 3.9 mm (T=100°C, V_g=14.7 cm/s, z=15 cm) and from 2.4 mm to 3.8 mm (T=100°C, V_g=9.0 cm/s, z=76 cm) between 0%$_{wt}$ and 10%$_{wt}$ solids loadings at θ=0.92. Then, the addition of solids particles contributed to an overall increase of the system apparent viscosity, which, in turn, favoured more rapid and efficient bubble coalescence events.

A clear influence of the solids on the bubble axial chord length distribution was also observed. In general, for the

338

conditions and locations studied, the axial bubble chord length distributions were found to be satisfactorily represented by the inverse-gaussian distribution function. Then, the addition of solid particles did not affect the actual configuration of the bubble axial chord length distribution. However, a distinct increase of the bubble axial chord length parameters (average and standard deviation) was observed for all the cases studied, as shown in Figures 5.83 and 5.84. Actually, a fraction of the small bubbles, though still present, were shifted toward larger bubble sizes, under the effect of more efficient bubble coalescence phenomena. Furthermore, the higher apparent viscosity of the system induced upon solids addition allowed the presence of a higher fraction of very large bubbles (bubble axial chord length > 3 cm), which represented, in some cases, up to 6% of the bubble population.

The presence of the secondary liquid circulation cell was also observed at low gas superficial velocity in the proximity of the gas distributor, as reported for the bubble column system (Section 5.1.3). Actually, for this particular condition, bubble rise velocities were found to be larger at the wall than in the center of the column, as shown in Table 5.17. The presence of the secondary liquid circulation cell was replaced, at higher axial position by the classical liquid circulation cell characterized by upward liquid velocity in the column central region and downward liquid circulation

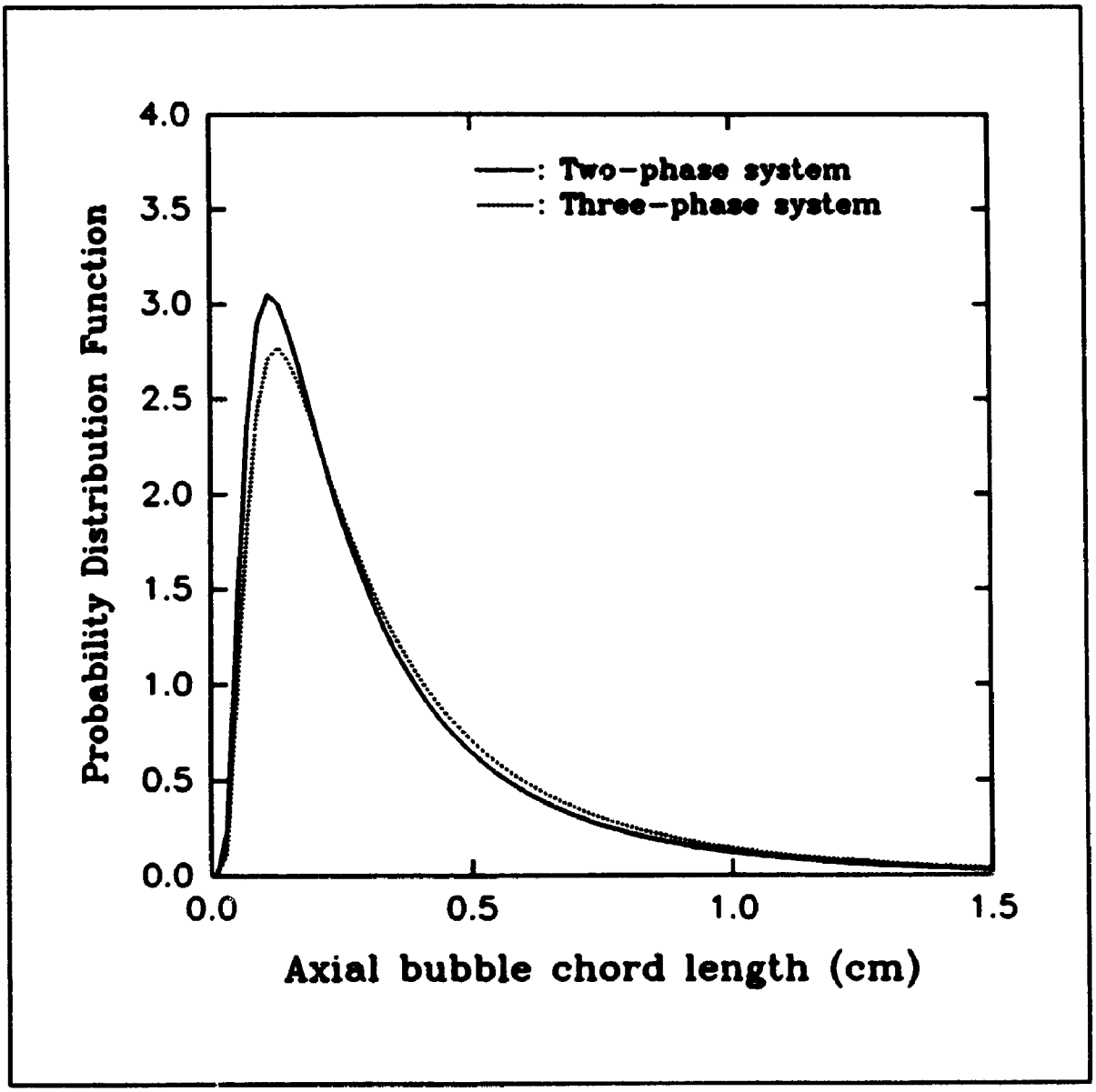

Figure 5.83: Bubble axial chord length distribution function (T=175°C, V_g=4.1 cm/s, z=76 cm, θ=0.19)

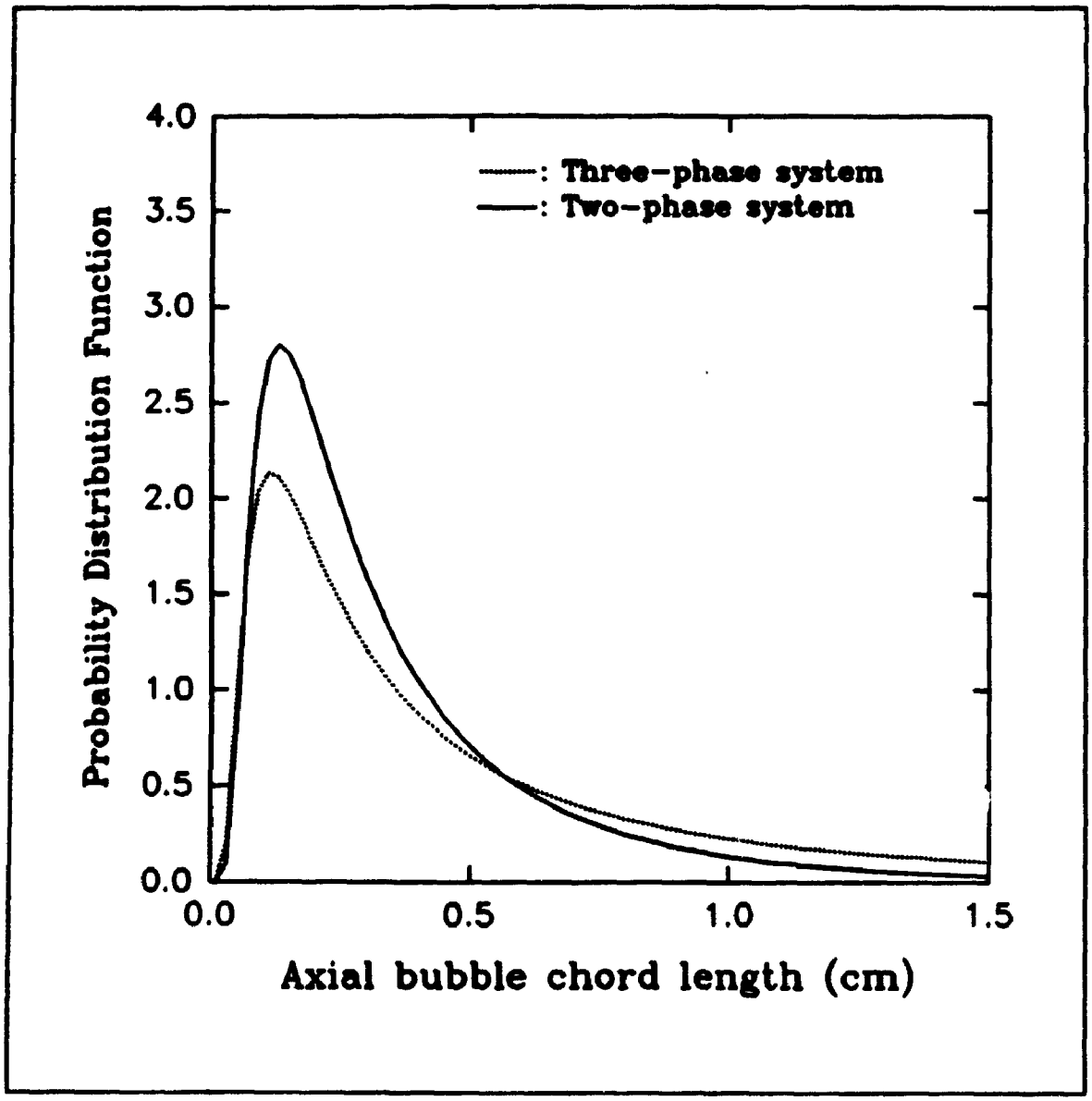

Figure 5.84: Bubble axial chord length distribution function (T=100°C, V_g=9.0 cm/s, z=76 cm, θ=0.19)

current in the vicinity of the column wall. Under such condition, as shown in Table 5.17, higher bubble rise velocities were observed in the center of the column as compared to the column periphery. Such behaviour was also seen in bubble column conditions. It is interesting to note, however, that the bubble rise velocity, for corresponding conditions, was higher under bubble conditions in proximity of the gas distributor. Actually, bubble rise velocity was reported to decrease in presence of solid particles (Bly and Worden, 1992). However, as the axial position increased, promoted coalescence due to the presence of the solid particles favoured the existence of larger and faster bubbles in the slurry system, particularly in the center of the column. As a consequence, the detrimental effect of the presence of solids on the bubble rise velocity was compensated by an increase in the bubble size. In consequence, as the axial position increased, smaller differences between the bubble rise velocity in bubble and slurry bubble column were observed, in the center of the column, as shown in Table 5.17.

The existence of a central zone where coalescence phenomena dominates over bubble break-up events was also observed in the slurry system. Actually, as it was observed in the two phase system, and as shown in Table 5.18, the bubble chord length was found to increase with the axial position in the center of the column, while decreasing along the wall periphery.

Table 5.17

Bubble rise velocity (cm/s)
(T=100°C, V_g=2.2 cm/s)

Axial position (cm)	System studied	θ=0.19	θ=0.92
15	Two-phase	50.0	56.0
15	Three-phase	33.3	45.5
76	Two-phase	57.9	36.6
76	Three-phase	58.1	29.5

343

Table 5.18

Bubble chord length (mm)
(T=175°C, V_g=14.7 cm/s)

Axial position (cm)	System studied	θ=0.19	θ=0.92
15	Two-phase	3.74	2.72
15	Three-phase	3.98	2.88
76	Two-phase	5.40	2.34
76	Three-phase	6.60	2.42

344

The gas holdup radial profiles were found, in general, to be flatter in the slurry bubble column than in the bubble column system for a similar axial position. Typical examples of this fact are illustrated in Figure 5.85. This visual observation was confirmed by analyzing the values of the parameter m (Equation 5.2), as shown in Table 5.19. Actually, the parameters m were higher for the slurry system than for the bubble column system, which may point out a still non-stabilized gas holdup profile. These results were reported for the axial position z=76 cm, for which the gas holdup profiles were found to be already stabilized in the bubble column system. It is interesting to note that, as it was the case in the two phase system, the values of the parameter m decreased with an increase of the gas superficial velocity.

In summary, the slurry column (hydrocarbon medium containing 10%$_{wt}$ solids) behaved in a similar way than the bubble column, showing the main features of secondary liquid circulation cell at low gas superficial velocity in the bottom of the column and the "coalescence-break-up" bubble regime.

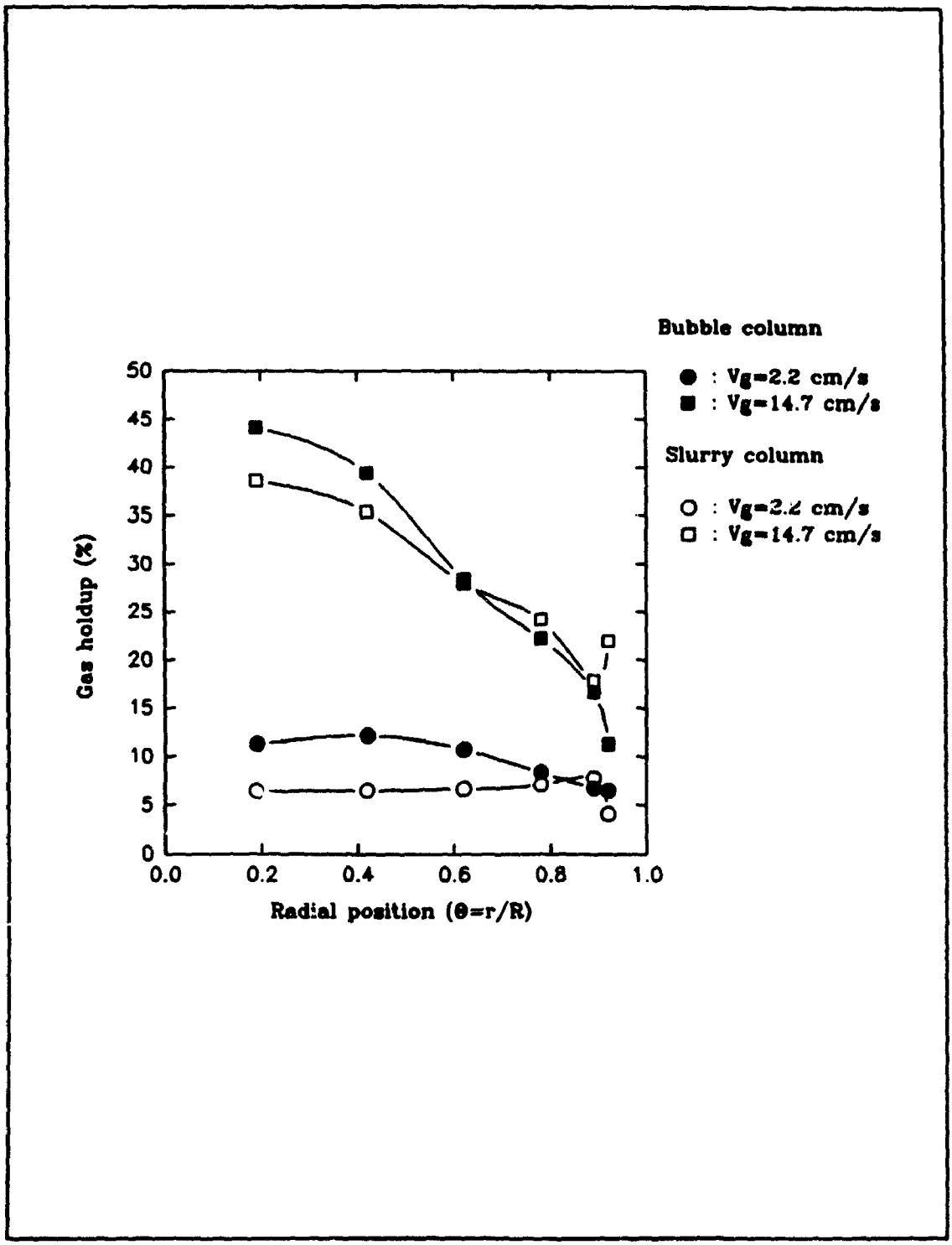

Figure 5.85: Gas holdup radial profiles (T=175°C, z=76 cm)

Table 5.19

Values of the parameter m (Equation 5.2)
(T=175°C, z=76 cm)

Gas superficial velocity (cm/s)	m values two-phase	m values three-phase
2.2	7.79	9.25
9.0	4.07	8.91
14.7	2.95	6.68

CHAPTER 6

CONCLUSIONS AND RECOMMENDATIONS

6.1 CONCLUSIONS

1. New miniaturized fibre optic sensors were successfully developed and extensively used in this research project. It was demonstrated that the consistency of the gas holdup measurements obtained from both sensors (lower and upper) was highly satisfactory, thus confirming minimum disturbance of the flow pattern by the sensors. Furthermore, excellent correspondence was observed between pressure profiles and fibre optic sensors derived gas holdup measurements at T=100°C and T=175°C, thus validating the optical sensors measurements.

2. Using the advanced miniaturized fibre optic sensors, the gas holdup radial profiles were found to evolve from a relatively uniform profile in the proximity of the gas distributor to a more pronounced parabolic profile at higher axial positions. However, all profiles were successfully represented by a power law equation. The stabilized gas holdup radial profiles observed, for all the operating conditions, were found to be sharper close to the column wall and flatter in the central area than the ones observed in aqueous systems. The stabilization of the gas holdup radial profiles was observed in the bubble column at a height of approximately z=76 cm for all the operating conditions

studied, thus confirming the importance of a minimum liquid height in properly assessing bubble column hydrodynamic characteristics. The gas holdup radial profiles were found to become less uniform as the temperature was decreased and the gas superficial velocity increased, while the local gas holdup values were noted to increase with both, an increase of the gas superficial velocity and the temperature.

3. Concerning the available models proposed to predict gas holdups, questionable agreement was observed between these existing correlations and the experimentally measured gas holdup values, with the exception of the Wilkinson et al. (1992) model, which offered more reliable predictions of the measured gas holdup. This certainly reiterates the importance of direct experimental measurements in obtaining adequate assessment of the gas holdup and other gas phase parameters, particularly in presence of complex liquid mixtures.

4. Cautious gas mass balance analysis was implemented in this study and led to the additional confirmation of the fibre optic sensors' ability to perform bubble phase measurements, even under severe conditions. Important insights concerning the proper utilization of gas mass balance analysis in validating experimental gas phase measurements in bubble column systems were also obtained.

5. Local bubble rise velocities were found, in general, to

decrease with the radial position, suggesting upward liquid circulation patterns in the center and downward liquid circulation at the wall. In fact, strong evidence of downward bubble displacement along the wall of the column were provided. Furthermore, for some particular conditions, (low gas superficial velocity: V_g=2.2 cm/s; lower axial positions: z=15 cm, z=30 cm), it was observed a larger bubble rise velocity in the vicinity of the wall than in the central section of the column. This observation, consistent for both, bubble column and slurry bubble column, allowed to conclude about the existence of a secondary countercurrent liquid circulation cell. Evidence of this phenomenon through bubble detection was not known to have been reported previously for bubble and slurry bubble column systems of significant importance for the methanol synthesis process. Furthermore, the identification of the secondary liquid circulation cell under severe operating conditions (T=100-200°C) confirmed the value of the optical sensors in tracking bubble behaviour.

6. In addition, the bubble rise velocity profiles were found to become steeper as both, the gas superficial velocity and the axial position increased. Faster bubble rise velocities were also noted as the superficial velocity augmented and the operating temperature decreased.

7. The overall performance of the fibre optic sensors in measuring the bubble rise velocity was further validated by

using the turbulent liquid circulation model proposed by Ueyama and Miyauchi (1979). This model, based on pressure balance, was found satisfactory in representing the measured bubble rise velocity for the cases where minimum gas recirculation was present and for the cases where the classical liquid recirculation pattern was present. This constitutes the first analysis of the turbulent circulation model theory in a system other than the air/water system. The implementation of the turbulent liquid circulation model allowed to obtain important information concerning the dependence of the turbulent kinematic viscosity on the gas superficial velocity, the temperature and the axial position in hydrocarbon systems. The turbulent kinematic viscosity was found to be, in general, smaller than in the typical air/water system.

8. In general, the bubble chord length was found to decrease with the axial position, except for the cases where the secondary liquid circulation cell was present. Overall, the average axial bubble chord length was observed to decrease (lower gas superficial velocities) or remain approximately constant (higher gas superficial velocities) with the axial position, thus suggesting the dominance of bubble break-up events over coalescence phenomena in this particular system. However, two distinct zones were observed: a first one (core zone) located in the central region of the column where bubble coalescence dominated and a second one (peripheral zone)

located along the wall of the column where manifestation of break-up events dominated. These findings, concerning the existence of a "coalescence-break-up" bubble regime, are extremely important in better understanding the fluid dynamic behaviour of bubble column and controlling bubble coalescence and gas recirculation effects. Effective model of the fluid dynamic of bubble and slurry bubble columns should incorporate the flow pattern identified in the course of this research.

9. The information obtained from the bubble chord length distribution analysis provided extremely interesting insights about the nature of the typical bubble population present in the system studied. First of all, all the bubble chord length distributions observed in the present study were characterized by the dominant presence of small bubbles (< 0.3 cm) and the scarce presence of larger ones. These skewed distributions were adequately represented by the inverse gaussian probability distribution function. In general, the average and standard deviations of the bubble chord length distributions were found to decrease with the radial position, except for the cases where the secondary liquid circulation cell was present. The axial evolution of the bubble chord length distribution was consistent with the existence of a central coalescence dominated zone (core zone) and a bubble break-up dominated zone (peripheral zone) in the vicinity of the column wall, as explained in the previous section. These results confirmed the important axial and radial variations of

the bubble population and point toward the need to implement such local variations in the theoretical representation of the gas phase behaviour in bubble column systems. Furthermore, the average and standard deviations of the bubble axial chord length distribution were observed, in general, to increase with an increase of the gas superficial velocity and a decrease of the operating temperature. The contribution to the total gas holdup of small (bubble axial chord length $\leq$ 0.3 cm) and large (bubble axial chord length > 0.3 cm) bubbles was studied. It was found that small bubbles contributed more strongly in the bubble column to the gas holdup in the vicinity of the column as compared to the central section of the column. However, small bubbles were found to have a lower ability to contribute to the total gas holdup in the center of the column as opposed to the periphery of the column.

10. The effect of solid particles was studied by suspending a typical methanol synthesis catalyst in the paraffinic oil ($10\%_{wt}$). Case studies were selected to compare trends between the bubble and the slurry column. The presence of the solid particles favoured a slight decrease of the gas holdup, this effect becoming almost imperceptible as the gas superficial velocity increased to V_g=14.7 cm/s. The decrease of the gas holdup resulted from an increase of the gas bubble size caused by an overall augmentation of the system apparent viscosity. Measurements of the average bubble axial chord length confirmed this hypothesis. Furthermore, the bubble axial

chord length distributions obtained in presence of the solid particles were also found to be well represented by the inverse-gaussian distribution function. However, both, the average and the standard deviation of the bubble axial chord length distributions were found to be larger in the three phase system than the bubble column (two phase). In addition, a larger proportion of very large bubbles (axial chord length > 3 cm) was observed in presence of the solid particles, confirming the stronger coalescing properties of the three phase system as compared to the two phase bubble column. In addition, the radial gas holdup profiles were found, for identical axial position (below a maximum axial position = 76 cm), to be flatter in the slurry bubble column than in the bubble column system.

11. Finally, the slurry bubble column was found to retain the main characteristics of the flow behaviour observed in the bubble column: secondary liquid circulation cell at low gas superficial velocity in proximity of the gas distributor and the presence of a "coalescence-break-up" flow pattern.

6.2 RECOMMENDATIONS

The convincing performance of the fibre optic sensors developed in the present study offers promising grounds for further study. On the basis of the results obtained in the present study, the literature currently available (as reviewed

in Chapter 1) and the actual and expected needs of the industry regarding bubble and slurry bubble column systems, as recently discussed by a number of authors (Zhu et al., 1992; Dudukovic and Devanathan, 1992 ...), the following recommendations are made:

1. The data acquisition procedure (frequency of data acquisition, total time of data acquisition) used in the present study was found to be highly satisfactory (as demonstrated by the reproducibility of the measurements: gas holdup, bubble rise velocity) and well adapted to the system studied. However, given a more powerful computer system is available, further expansion could be made in this area. For example, the total time of data acquisition could be increased for further approach to statistical stationarity.

2. As clearly discussed in the Chapter 1, the proper design, scale-up and operation of bubble and slurry bubble column systems require the comprehensive knowledge of the hydrodynamic characteristics encountered under actual operating conditions. In this respect, special care, as emphasized in the thesis, was taken to properly design the set-up unit (diameter, gas distributor ...) and simulate as closely as possible the conditions encountered in the liquid phase methanol synthesis system (exact liquid and solid phases encountered in the liquid phase methanol synthesis system were used, high temperature). However, high pressure or exact

reactive conditions could not be simulated, in the present study, due to the important cost involved with the construction and operation of such systems. Further efforts in this direction, though extremely expensive, would certainly be highly valuable in gaining a more thorough and precise understanding of the hydrodynamic characteristics of the liquid phase methanol synthesis system or other systems of similar nature.

REFERENCES

Abed R., "Characterization of Hydrodynamic Nonuniformity in Large Fluidized Beds", Ind. Eng. Chem. Fundam. 24, 78-82, (1985).

Abou-El-Hassan M.E., "A Generalized Bubble Rise Velocity Correlation", Chem. Eng. Commun. 22, 243-250, (1983).

Achwal S.K., Stepanek J.B., "An Alternative Method of Determining Hold-Up in Gas-Liquid Systems", Chem. Eng. Sci 30, 1443-1444, (1975).

Akita K., Yoshida F., "Gas Holdup and Volumetric Mass Transfer Coefficient in Bubble Columns", Ind. Eng. Chem. Process Des. Develop. 12(1), 76-80, (1973).

Akita K., Yoshida F., "Bubble Size, Interfacial Area, and Liquid-Phase Mass Transfer Coefficient in Bubble Columns", Ind. Eng. Chem. Process Des. Develop. 13(1), 84-91, (1974).

Anderson K.G., Rice R.G., "Local Turbulence Model for Predicting Circulation Rates in Bubble Columns", AIChE J. 35, 514-518, (1989).

Atkinson C.M., Clark N.N., "Gas Sampling from Fluidized Beds: A Novel Probe System", Powder Technology 54, 59-70, (1988).

Bach H.F., Pilhofer T., "Variation of Gas Hold-Up in Bubble Columns with Physical Properties of Liquids and Operating Parameters of Columns", Ger. Chem. Eng. 1, 270-275, (1978).

Begovich J.M., Watson J.S., "An Electroconductivity Technique for the Measurement of Axial Variation of Holdups in Three-Phase Fluidized Beds", AIChE J. 24(2), 351-354, (1978).

Bendat J.S., Piersol A.G., Random Data. Analysis and Measurement Procedures", John Wiley & Sons, New-York, (1986).

Berghmans J., "Stability of Gas Bubbles Rising in Inviscid Fluids", Chem Eng. Sci. 28, 2005-2011, (1973).

Berkelmann K.G., Renz U., The Fluid Dynamics in the Freeboard of an FBC; The Use of LDV to Determine Particle Velocity and Size", Proceedings 6th International Conference on Fluidization, Banff, Canada, 105-112, (1989).

Bhavaraju S.M., Russel T.W.F., Blanch H.W., "The Design of Gas Sparged Devices for Viscous Liquid Systems", AIChE J. 24(3), 454-466, (1978).

Bly M.J., Worden R.M., "The Effects of Solids Density and Void Fraction on the Bubble Rise Velocity in a Liquid-Solid

Fluidized Bed", Chem. Eng. Sci. 47(13-14), 3281-3288, (1992).

Box G.E.P., Jenkins G.M., "Time Series Analysis. Forecasting and Control", Holden-Day Inc. Publishing, Oakland, CA, (1976).

Briens C.L., Bergougnou M.A., Baker C.G.J., "Leakage of Solids (Weeping, Dumping) at the Grid of a 0.6 m Diameter Gas Fluidized Bed", Fluidization, Cambridge University Press, (1978).

Brown D.M., "Modelling of Methanol Synthesis in the Liquid Phase", I. Chem. E. Symposium Series No. 87, 699-708, (1984).

Bruce P.N., Revel-Chion L., "Bed Porosity in Three-Phase Fluidization", Powder Technology 10, 243-249, (1974).

Bruck F.J., "Investigation with Microprobes of the Effect of the Physical Properties of Suspended Particles on the Hydrodynamic Characteristics of Bubble Columns", Ph.D. Thesis, Aachen, Germany, (1984).

Bukur D.B., Petrovic D., Daly J.G., "Flow Regime Transitions in a Bubble Column with a Paraffin Wax as the Liquid Medium", Ind. Eng. Chem. Res. 26, 1087-1092, (1987a)

Bukur D.B., Daly J.G., "Gas Hold-Up in Bubble Columns for Fischer-Tropsch Synthesis", Chem. Eng. Sci. 42(12), 2967-2969, (1987).

Bukur D.B., Patel S.A., Matheo R., "Hydrodynamics Studies in Fischer-Tropsch Derived Waxes in a Bubble Column", Chem. Eng. Comm. 60, 63-78, (1987b).

Bukur D.B., Patel S.A., "Hydrodynamic Studies with Foaming and Non-Newtonian Solutions in Bubble Columns", Can. J. Chem. Eng. 67, 741-751, (1989).

Bukur D.B., Patel S.A., Daly J.G., "Gas Holdup and Solids Dispersion in a Three-Phase Slurry Bubble Column", AIChE J. 36(11), 1731-1735, (1990).

Capuder E., Koloini T., "Gas Hold-Up and Interfacial Area in Aerated Suspensions of Small Particles", Chem. Eng. Res. Des. 62, 255-260, (1984).

Chabot J., "Fibre Optic Sensors for Fluid Dynamic Studies in Multiphase Reactors", M.E.Sc., The University of Western Ontario, 438, (1989).

Chabot J., Lee S.L.P., Soria A., de Lasa H.I., "Interaction between Bubbles and Fibre Optic Probes in a Bubble Column", Can. J. Chem. Eng. 70, 61-68, (1992).

Chang J.-S., Harvel G.D., "Determination of Gas-Liquid Bubble

Column Instantaneous Interfacial Area and Void Fraction by a real-Time Neutron radiography Method", Chem. Eng. Sci. 47(13-14), 3639-3646, (1992).

Chen J.J.J., Jamialahmadi M., Li S.M., "Effect of Liquid Depth on Circulation in Bubble Columns: A Visual Study", Chem. Eng. Res. Des. 67, 203-207, (1989).

Chen R.C., Fan L.-S., "Particle Image Velocimetry for Characterizing the Flow Structure in Three-Dimensional Gas-Liquid-Solid Fluidized Beds", Chem. Eng. Sci. 47(13-14), 3615-3622, (1992).

Chiba S., Idogawa K., Maekawa Y., Moritomi H., Kato N., Chiba T., "Neutron Radiographic Observation of High Pressure Three-Phase Fluidization", Proceedings 6th International Conference on Fluidization, Banff, Canada, 523-530, (1989).

Clark K.N., "The Effect of High Pressure and Temperature on Phase Distributions in a Bubble Column", Chem. Eng. Sci. 45(8), 2301-2307, (1990).

Clark N.N., Atkinson C.M., Flemmer R.L.C., "Turbulent Circulation in Bubble Columns", AIChE J. 33, 575-578, (1987).

Clark N.N., Turton R., "Chord Length Distributions Related to Bubble Size Distributions in Multiphase Flows", Int. J. Multiphase Flow 14(4), 413-424, (1988).

Clift R., Grace J.R., "The Mechanism of bubble break-up in Fluidized Beds", Chem. Eng. Sci. 27, 2309-2310, (1972).

Costa E., de Lucas A., Garcia P., "Fluid Dynamics of Gas-Liquid-Solid FLuidized Beds", Ind. Eng. Process Des. Dev. 25, 849-854, (1986).

Cova D.R., "Catalyst Suspension in Gas-Agitated Tubular Reactors", I&EC Process. Des. Dev., 5, 1, 20-25, (1966).

Crabtree J.R., Bridgwater J., J. Chem. Eng. Sci. 24, 1755, (1969).

Cranfield R.R., "A Probe for Bubble Detection and Measurement in Large Particle Fluidized Beds", Chem. Eng. Sci. 27, 239-245, (1972).

Daly J.G., Patel S.A., Bukur D.B., "Measurement of Gas Holdups and Sauter Mean Bubble Diameters in Bubble Column Reactors by Dynamic Gas Disengagement Method", Chem. Eng. Sci. 47(13-14), 3647-3654, (1992).

Deckwer W.-D., Adler I., Zaidi A., "A Comprehensive Study on CO_2-Interphase Mass Transfer in Vertical Cocurrent and

Countercurrent gas Flow," Can. J. Chem. Eng., 56, 43 (1978).

Deckwer W.-D., Louisi Y., Zaidi A., Ralek M., "Hydrodynamic Properties of the Fischer-Tropsch Slurry Process", Ind. Eng. Chem. Process Des. Dev. 19, 699-708, (1980).

Deckwer W.-D., Schumpe A., "Bubble Columns - The State of the Art and Current Trends", Int. Chem. Eng. 27(3), 405-422, (1987).

Deckwer W.-D., Schumpe A., "Improved Tools for Bubble Column Reactor Design and Scale-Up", First International Conference on Gas-Liquid and Gas-Liquid-Solid Reactor Engineering, Columbus, OH, Keynote Paper K5, September 13-16, (1992).

Devanathan N., Moslemian D., Dudukovic M.P., "Flow Mapping in Bubble Columns Using Carpt", Chem. Eng. Sci 45(8), 2285-2291, (1990).

Drahos J., Zahradnik J., Fialova M., Bradka F., "Identification and Modelling of Liquid Flow Structures in Bubble Column Reactors", Chem. Eng. Sci. 47(13-14), 3313-3320, (1992).

Dry R.J., Judd M.R., "Fluidized Beds of Fine, Dense Powders: Scale-Up and Reactor Modelling", Powder Technology 39, 69-75, (1984).

Dudukovic M.P., Devanathan N., "Bubble Column Reactors: Some Recent Developments", Nato-ASI Symposium Series, Kluwer Publishing, (1992).

Dutta S., Wen C.Y., "A Simple Probe for Fluidized Bed Measurements", Can. J. Chem. Eng. 57, 115-119, (1979).

Fan L.-S., "Gas-Liquid-Solid Fluidization Engineering", Butterworth, Boston, (1989).

Fan L.-S., Jean R.-H., Kitano K., "On the Operating Regimes of Cocurrent upward Gas-Liquid-Solid Systems with Liquid as the Continuous Phase", Chem. Eng. Sci. 42(7), 1853-1855, (1987a).

Fan L.-S., Kitano K., Kreischer B.E., "Hydrodynamics of Gas-Liquid-Solid Annular Fluidization", AIChE J. 33(2), 225-231, (1987b).

Fox J.M., "A Comparison of Slurry versus Fixed-Bed Reactor Design Principles for Methanol and Fischer-Tropsch Distillate Production", AIChE Spring National Meeting, Fischer-Tropsch Symposium, Paper No. 91c, March 21, (1990).

Frank M.E., Mednick R.L., "Liquid-Phase Methanol Project Status and Laboratory Results", 7th Annual EPRI Contractor's Conf. on Coal Liquefaction, Palo Alto, (1982).

Franz K., Borner T., Kantorek H.J., Buchholz R., "Flow Structures in Bubble Columns", Ger. Chem. Eng. 7, 365-374, (1984).

Freedman W., Davidson J.F., "Holdup and Liquid Circulation in Bubble Columns", Trans. Instn. Chem. Engrs. 47, T251-T262, (1969).

Frey J.H., Studer D.W., Henderson J.L., Weimer R.F., Further Process Improvements at the Laporte Liquid Phase Methanol Facility", DOE Indirect Liquefaction Contractors Review Meeting, Pittsburgh, November 15-17, (1988).

Gasche H.-E., Edinger Ch., Kompel H., Hofmann H., "Hydrodynamics in Bubble Columns", Chem. Eng. Process 26, 101-109, (1989).

Geary N.W., Rice R.G., "Bubble Size Prediction for Rigid and Flexible Spargers", AIChE J. 37(2), 161-168, (1991).

Gibra I.N., "Probability and Statistical Inference for Scientists and Engineers", Prentice-Hall Inc., Englewood Cliffs, New-Jersey, (1973).

Glicksman L.R., Lord W.K., Sakagami M., "Bubble Properties in Large-Particle Fluidized Beds", Chem. Eng. Sci. 42(3), 479-491, (1987).

Godbole S.P., Honath M.F., Shah Y.T., "Holdup Structure in Highly Viscous Newtonian and Non-Newtonian Liquids in Bubble Columns", Chem. Eng. Commun. 16, 119, (1982).

Gogate M.R., Vijayaraghavan P., Lee S., Kulik C.J., "A Single-Stage, Liquid-Phase Dimethyl Ether Synthesis Process from Syngas", Fuel Science and Technology Int'l 10(3), 281-311, (1992).

Gunn D.J., Al-Doori H.H., "The Measurement of Bubble Flows in Fluidized Beds by Electrical Probe", Int. J. Multiphase Flow 11(4), 535-551, (1985).

Guo F., "Gas Flow and Mixing Behavior in Fine-Powder Fluidized Bed", AIChE J. 33(11), 1895-1898, (1987).

Guy C., Carreau P.J., Paris J., "Mixing Characteristics and Gas Hold-Up of a Bubble Column", Can. J. Chem. Eng. 64, 23-35, (1986).

Hamdullahpur F., Mackay G.D.M., "Two-Phase Flow Behavior in the Freeboard of a Gas-Fluidized Bed", AIChE J. 32(12) 2047-2055, (1986).

Hamdullahpur K.C., Pegg M.J., Mackay G.D.M., "A Laser-Fluorescence Technique for Turbulent Two-Phase Flow

Measurements", Int. J. Multiphase Flow 13(3), 379-385, (1987).

Hahn G.J., Shapiro S.S., "Statistical Models in Engineering", John Wiley & Sons, New-York, (1967).

Hammer H., Rähse W., "Blasengrößen-Häufigkeits-Verteilungen und Phasengrenzflächen in Blasensäulen", Chem.-Ing.-Tech., 50, 623 (1973).

Henriksen H.K., Ostergaard K., "Characteristics of Large Two-Dimensional Air Bubbles in Liquids and in Three-Phase Fluidized Beds", Chem. Eng. J. 7, 141-146, (1974).

Hikita H., Asai S., Tanigawa K., Segawa K., Kitao M., "Gas Hold-Ups in Bubble Columns", Chem. Eng. J. 20, 59-67, (1980).

Hilligardt K., Werther J., "Local Bubble Gas Hold-Up and Expansion of Gas/Solid Fluidized Beds", Ger. Chem. Eng. 9, 215-221, (1986).

Hills J.H., "Radial Non-Uniformity of Velocity and Voidage in a Bubble Column", Trans. Instn. Chem. Engrs. 52, 1-9, (1974).

Hills J.H., Darton R.C., "The Rising Velocity of a Large Bubble in a Bubble Swarm", Trans. Instn. Chem. Engrs 54, 258-264, (1976).

Huskey D., "Evaluation of a Multitubular-Cracker-Exchanger FCC Unit", M.E.Sc. Thesis, The University of Western Ontario, (1990).

Idogawa K., Ikeda K., Fukuda F., Morooka S., "Effect of Gas and Liquid Properties on the Behavior of Bubbles in a Bubble Column under High Pressure", Int. Chem. Eng. 27, 93, (1987).

Immich M., Onken U., "Prediction of Minimum Gas Velocity in Suspended Bubble Columns and Airlift Reactors", Chem Eng. Sci. 47(13-14), 3379-3386, (1992).

Ishida M., Tanaka H., "An Optical Probe to Detect both Bubbles and Suspended Particles in a Three-Phase Fluidized Bed", J. Chem. Eng. Japan 15(5), 389-391, (1982).

Jeffrey D.J., Acrivos A., "The rheological Properties of Suspensions of Rigid Particles", AIChE J., 222(3), 417 (1976).

Joshi J.B., "Gas Phase Dispersion in Bubble Columns", Chem. Eng. J. 24, 213, (1982).

Joshi J.B., Shah Y.T., "Hydrodynamic and Mixing Models for Bubble Column Reactors", Chem. Eng. Commun. 11, 165-199, (1981).

Joshi J.B., Sharma M.M., "A Circulation Cell Model for Bubble

Columns", Trans. Inst. Chem. Engrs. 57, 244-251, (1979).

Joshi J.B., Sharma M.M., "Liquid Phase Flow Pattern in Bubble Columns", Trans. Inst. Chem. Engrs. 60, 255-256, (1982).

Kang Y., Kim S.D., "Radial Dispersion Characteristics of Two- and Three-Phase Fluidized Beds", Ind. Eng. Chem. Process Des. Dev. 25, 717-722, (1986).

Kang Y., Kim S.D., "Solid Flow Transition in Liquid and Three-Phase Fluidized Beds", Part. Sci. Technol. 6, 133-144, (1988).

Kara S., Kelkar B.G., Shah Y.T., Carr N.L., "Hydrodynamics and Axial Mixing in a Three-Phase Bubble Column", Ind. Eng. Chem. Process Des. Dev. 21, 584-594, (1982).

Kago T., Sasaki Y., Kondo T., Morooka S., Kato Y., "Gas Holdup and Axial Dispersion of Gas and Liquid in Bubble Columns of Homogeneous Bubble Flow Regime", Chem. Eng. Comm. 75, 23-38, (1989).

Kato Y., Morooka S., Kago T., Saruwatari T., Yang S.-Z., "Axial Holdup Distributions of Gas and Solid Particles in Three-Phase Fluidized Bed for Gas-Liquid (Slurry)-Solid Systems", J Chem. Eng. Japan, 18(4), 308-313, (1985).

Kato Y., Nishinaka M., Morooka S., "Distribution of Gas Holdup in a Bubble Column", Kagaku Kogaku Ronbunshu 1, 530, (1975).

Kato Y., Nishiwaki A., Takashi F., Tanaka S., "The Behavior of Suspended Particles and Liquid in Bubble Columns", J. Chem. Eng. Japan., 5, 112 (1972).

Kelkar B.G., Godbole S.P., Honath M.F., Shah Y.T., Carr N.L., Deckwer W.-D., "Effect of Addition of Alcohols on Gas Holdup and Backmixing in Bubble Columns", AIChE J. 29(3), 361-369, (1983).

Kelkar B.G., Shah Y.T., Carr N.L., "Hydrodynamics and Axial Mixing in a Three-Phase Bubble Column. Effect of Slurry Properties", Ind. Eng. Chem. Process Des. Dev. 23(2), 308-313, (1984).

Khare A.S., Joshi J.B., "Effect of Fine Particles on Gas Hold-up in Three-Phase Sparged Reactors", Chem. Eng. J. 44, 11-25, (1990).

Kim S.D., Baker C.G.J., Bergougnou M.A., "Phase Holdup Characteristics of Three Phase Fluidized Beds", Can. J. Chem. Eng. 53, 134-139, (1975).

Kim J.O., Kim S.D., "Bubble Characteristics in Three Phase Fluidized Beds of Floating Bubble Breaker", Particulate Sci. Technol. 5, 309-321, (1987).

Kleinbaum D.G., Kupper L.L., "Applied Regression Analysis and other Multivariable Methods", Duxbury Press, North Scituate, Massachusetts, 556 p, (1978).

Koide K., Morooka S., Ueyama K., Matsuura A., Yamashita F., Iwamoto S., Kato Y., Inoue H., Shigeta M., Suzuki S., Akehata T., "Behavior of Bubbles in Large Scale Bubble Column", J. Chem. Eng. Japan 12(2), 98-104, (1979).

Kojima E., Unno H., Sato Y., Chida T., Imai H., Endo K., Inoue I., Kobayashi J., Kaji H., Nakanishi H., Yamamoto K., "Liquid Phase Velocity in a 5.5 m Diamater Bubble Column", J. Chem. Eng. Japan 13(1), 16-21, (1980).

Kojima H., Anjyo H., Mochizuki Y., "Axial Mixing in Bubble Column with Suspended Solid Particles", J. Chem. Eng. Japan 19(3), 232-234, (1986).

Kojima H., Asano K., "Hydrodynamic Characteristics of a Suspension-Bubble Column", Int. Chem. Eng. 21(3), 473-481, (1981).

Kölbel H., Borchers E., Langemann H., "Größenverteilung der Gasblasen in Blasensäulen", Chem.-Ing.-Tech., 33, 668 (1961).

Krishna R., Wilkinson P.M., van Dierendonck L.L., "A Model for Gas Holdup in Bubble Columns Incorporating the Influence of Gas Density on Flow Regime Transitions", Chem. Eng. Sci 16(10), 2491-2496, (1991).

Kumar A., Dagalessan T.T., Laddha G.S., Hoelsher H.E., "Bubble Swarm Characteristics in Bubble Columns", Can. J. Chem. Eng., 54, 503 (1976).

Kunii D., Levenspiel O., "Fluidization Engineering", Robert E. Krieger Publising Co. Inc., Florida, (1984).

Kuo J.C.W., "Two-Stage Process for Conversion of Synthesis Gas to High Quality Transportation Fuels", Mobil Research and Development's Final Report to the Dep. of Energy Contract DE-AC22-83PC60019 (1985)

Lee S.L.P., "Bubble Dynamics in Three Phase Fluidized Beds", Ph.D. Thesis, The University of Western Ontario, London, Ontario, (1986).

Lee S.L.P., de Lasa H.I., "Phase Holdups in Three-Phase Fluidized Beds", AIChE J. 33(8), 1359-1370, (1987).

Lee J.C., Sherrard A.J., Buckley P.S., "Optimum Particle Size in Three Phase Fluidized Bed Reactors", Proceeding International Symposium on Fluidization and its Application, Cepades-Editions, Toulouse, 407-416, (1973).

Levy Y., Lockwood F.C., "Laser Doppler Measurements of Flow in the Freeboard of a Gas Fluidized Bed", AIChE J. 29(6), 889-895, (1983).

Lewnard J.J., Hsiung T.H., White J.F., Brown D.M., Single-Step Synthesis of Dimethyl Ether in a Slurry Reactor", Chem. Eng. Sci. 45(8), 2735-2741, (1990).

Lubbert A., Larson B., "A New Method for Measuring Local Velocities of the Continuous Liquid Phase in Strongly Aerated Gas-Liquid Multiphase Reactors", Chem. Eng. Technol. 10, 27-32, (1987).

Lubbesmeyer D., "Experimental Reactor noise - A Review on Noise-Analytic Measurements of Thermore-Hydraulic Parameters in Operating BWRs and their Interpretation", Prog. Nucl. Energy 14, 41-93, (1984).

Mangartz K.H., Pilhofer T., "Interpretation of Mass-Transfer Measurements in Bubble Columns Considering Dispersion of both Phases", Chem. Eng. Sci. 36, 1969, (1981).

Mann R., Hackett L.A., "Interpretation of Bubble Cloud Statistics Gathered by Fibre Optic Phase Detection", 2nd International Conference on Multi-Phase Flow, London, England, 19-21 June, 345-360, (1985).

Maruyama T., Yoshida S., Mizushina T., "The Flow Transition in a Bubble Column", J. Chem. Eng. Japan, 14(5), 352-357, (1981).

Matsumoto S., Harakawa H., Susuki H., Ohtani S., "Solid Particle Velocity in Vertical Gaseous Suspension Flows", Int. J. Multiphase Flow 12, 445-458, (1986).

Mendelson H.D., "The Prediction of Bubble Terminal Velocities from Wave Theory", AIChE J. 13(2), 250-252, (1967).

Miyauchi T., Furusaki S., Morooka S., Ikeda Y., "Advances in Chemical Engineering", 11, 275-448, Academic Press, New-York, (1981).

Miyauchi T., Shyu C.N., "Flow of Fluid in Gas Bubble Columns", Kagaku Kogaku 34, 958, (1970).

Molerus O., Kurtin M., "Hydrodynamics of Bubble Columns in the Uniform Bubbling Regime", Chemical Engineering Science 40(4), 647-652, (1985).

Molerus O., Kurtin M., "Hydrodynamics of Bubble Columns in the Liquid Circulation Regime", Chem. Eng. Sci. 41(10), 2685-2692, (1986a).

Molerus O., Kurtin M., "Modelling of Residence Time Distributions of the Gas Phase in Bubble Columns in the Liquid

Circulation Regime", Chem. Eng. Sci. 41(10), 2693-2698, (1986b).

Morooka S., Kawazuishi K., Kato Y., "Holdup and Flow Pattern of Solid Particles in Freeboard of Gas-Solid Fluidized Bed with Fine Particles", Powder Technology 26, 75-82, (1980).

Morooka S., Mizoguchi T., Kago T., Kato Y., Hidaka N., "Effect of Fine Bubbles on Flow Properties in Bubble Column with Suspended Solid Particles", J. Chem. Eng. Japan 19(6), 507-512, (1986).

Mudde R.F., Bakker R.A., van den Akker H.E.A., "Noise Analysis of Transmitted Light Beams fro Determining Bubble Velocity and Gas Holdup Profiles in a Bubble Column", Chem. Eng. Sci. 47(13-14), 3631-3638, (1992).

Muroyama K., Fan L.-S., "Fundamentals of Gas-Liquid-Solid Fluidization", AIChE J. 31(1), 1-34, (1985).

Miyzaki K., Isogai K., Fuziine K., Suita T., "Measurements of Propagation Velocities of Pressure and Voidfractions in Nitrogen-Water Flow", J. Nucl. Sci. Techn. 10, 323, (1973).

Nigam K.D.P., Schumpe A., "Gas-Liquid Mass Transfer in a Bubble Column with Suspended Solids", AIChE J. 33(2), 328-330, (1987).

Oki K., Walawender W.P., Fan L.T., "The Measurement of Local Velocity of Solid Particles", Powder Technology 18, 171-178, (1977).

Ostergaard K., Michelsen M.L., "Holdup and Axial Dispersion in Gas-Liquid Fluidized Bed: The Effect of Fluid Velocities and Particle Size", Joint AIChE-I.I.Q.P.R. Mtg., Tampa, FL (1968).

Oyevaar M.H., Bos R., Westerterp K.R., "Interfacial Areas and Gas Hold-Ups in Gas-Liquid Contactors at Elevated Pressures from 0.1 to 8.0 MPa", Chem. Eng. Sci. 46(5-6), 1217-1231, (1991).

Öztürk S.S., Schumpe A., Deckwer W.-D., "Organic Liquids in a Bubble Column: Hold-ups and Mass Transfer Coefficients", AIChE J., 33, 1473-1480, (1987).

Page R.E., Harrison D., "The Size Distribution of Gas Bubbles Leaving a Three-Phase Fluidized Bed", Powder Technology 6, 245-249, (1972).

Park W.H., Kang W.K., Capes C.E., Osberg G.L., The Properties of Bubbles in Fluidized Beds of Conducting Particles as Measured by an Electroresistivity Probe", Chem. Eng. Sci. 24, 851-865, (1969).

Pass G., Holzhauser C., Akgerman A., Anthony R.G., "Methanol Synthesis in a0Trick|e-Bed Reactor", AIChE J. 36(7), 1054-1060, (1990).

Patel S.A., Daly J.G., Bukur D.B., Bubble-Size Distribution in Fischer-Tropsch Derived Waxes in a Bubble Column", AIChE J. 36(1), 93-105, (1990).

Patwari A.N., Nguyen-Tien K., Schumpe A., Deckwer W.-D., "Three-Phase Fluidized Beds with Viscous Liquid: Hydrodynamics and Mass Transfer", Chem. Eng. Commun. 40, 49-65, (1986).

Pekediz A., Kraemer D., Chabot J., de Lasa H.I., "Mixing Effects in Nove` Riser Simulator", NATO-ASI Proceedings, Kluwer Publishing Co., In Press, (1992).

Peters M.H., Fan L.-S., Sweeney T.L., "Study of Particle Ejections in the Freeboard region of a Fluidized Bed with an Image-Carrying probe", Chem. Eng. Sci. 38(3), 481-485, (1983).

Peterson D.A., Tankin R.S., Bankoff S.G., "Bubble Behavior in a Three-Phase Fluidized Bed", Int. J. Multiphase Flow 13(4), 477-491, (1987).

Pino L.Z., Yepez M.M., Saez A.E., de Drago G., "An Experimental Study of Gas Holdup in Two-Phase Bubble Columns with Foaming Liquids", Chem. Eng. Comm. 89, 155-175, (1990).

Press W.H., Flannery B.P., Teukolsky S.A., Vetterling W.T., "Numerical Recipes", Cambridge University Press, 702 p, (1989).

Prince M.J., Blanch H.W., "Bubble Coalescence and Break-Up in Air-Sparged Bubble Columns", AIChE J. 36(10), 1485-1499, (1990).

Quicker G., Deckwer W.-D., "Gas Holdup and Interfacial Area in Aerated Hydrocarbons", Ger. Chem. Eng. 4, 363-370, (1981a).

Quicker G., Deckwer W.-D., "A Further Note on Mass Transfer Limitations in the Fischer-Tropsch Slurry Process", Chem. Eng. Sci 36(9), 1579-1582, (1981b).

Reilly I.G., Scott D.S., DE Bruijn T., Jain A., Piskorz J., "A Correlation fro Gas Holdup in Turbulent Coalescing Bubble Columns", Can. J. Chem. Eng. 64, 705-717, (1986).

Renjun Z., Xinzhen J., Baozhang L., Yong Z., Laiqi Z., "Studies on Gas Holdup in a Bubble Column Operated at Elevated Temperatures", Ind. Eng. Chem. Res. 27, 1910-1916, (1988).

Rice R.G., Barbe D.T., Geary N.W., "Correlation of Nonverticality and Entrance Effects in Bubble Columns", AIChE J. 36(9), 1421-1424, (1990).

Rice R.G., Geary N.W., "Prediction of Liquid Circulation in Viscous Bubble Columns", AIChE J. 36(9), 1339-1348, (1990).

Rice R.G. and Littlefield M.A., "Dispersion Coefficients for Ideal Bubbly Flow in Truly Vertical Bubble Columns", Chem. Eng. Sci. 42, 2045-2053, (1987).

Rietema K., Ottengraph S.P.P., Trans. Instn. Chem. Engrs. 48, T54, (1970).

Roberts G.W., Brown D.M., Hsiung T.H., Lewnard J.J., "Catalyst Poisoning during the Synthesis of Methanol in a Slurry Reactor", Chem. Eng. Sci. 45(8), 2713-2720, (1990).

Roberts G.W., Dicciani N.K., Klosek J., "The LPMEOH Process - an Efficient Route to Methanol from Coal", Conference on Coal Gasification and Synthetic Fuels for Power Generation, San Francisco, CA, April 14-18, (1985).

Rowe P.N., Everett D.J., "Fluidized Bed Bubbles Viewed by X-Rays", Trans. Instn. Chem. Eng. 50, 42-48, (1972).

Rowe P.N., Masson H., "Fluidized Bed Bubbles Observed Simultaneously by Probe and by X-Rays", Chem. Eng. Sci. 35, 177-185, (1980).

Sada E., Kumazawa H., Lee C., Iguchi T., "Gas Holdup and Mass-Transfer Characteristics in a Three-Phase Bubble Column", Ind. Eng. Chem. Process Des. Dev. 25, 472-476, (1986).

Satterfield C.N., huff G.A., "Effects of Mass Transfer on Fischer-Tropsch Synthesis in Slurry Reactors", chem. Eng. Sci 35, 195-202, (1980).

Sauer T., Hempel D.-C., "Fluid Dynamics and Mass Transfer in a Bubble Column with Suspended Particles", Chem. Eng. Technol. 10, 180-189, (1987).

Saxena S.C., Mathur A., Sharma G.K., "Bubble Dynamics and Elutriation Studies in Gas-Fluidized Beds", Chem. Eng. Commun. 29, 35-61, (1984).

Saxena S.C., Patel D.C., Kathuria D., "An Image-Carrying Fiber Optic Probe to Investigate Solids Distribution around an Immersed Surface in a Gas-Fluidized Bed", AIChE J. 33(4), 672-676, (1987).

Saxena S.C., Rao N.S., Saxena A.C., Heat Transfer from a Cylindrical Probe Immersed in a Three-Phase Slurry Bubble Column", Chem. Eng. J. 44, 141-156, (1990).

Schumpe A., Saxena A.K., Fang L.K., Gas-Liquid Mass Transfer in a Slurry Bubble Column", Chem. Eng. Sci. 42(7), 1787-1796, (1987).

Schügerl K., Lücke J., Oels U., "Bubble Column Bioreactors", Adv. Biochem. Eng., ed., T.K. Ghose, A. Fiechter, N. Blakeborogh, 7, 1 (1977).

Schweinzer J., Molerus O., "Bubble Flow y~ Pressurized Gas/Solid Fluidized Beds", Chem. Eng. Technol. 10, 368-375, (1987).

Shah Y.T., Kelkar B.G., Godbole S.P., Deckwer W.-D., "Design Parameters Estimations for Bubble Column Reactors", AIChE J. 28(3) 353-379, (1982).

Sherwin M.B., Frank M.E., "Make Methanol by Three Phase Reaction", Hydrocarbon Processing, November, 122-124, (1976).

Shetty S.A., Kantak M.V., Kelkar B.G., "Gas-Phase Backmixing in Bubble-Column Reactors", AIChE J. 38(7), 1013-1026, (1992).

Sitthiphong N., George A.H., Bushnell D., "Bubble eruption Diameter in a Fluidized Bed of Large Particles at Elevated Temperatures", Chem. Eng. Sci. 36, 1259-1260, (1981).

Smith D.N., Fuchs W., Lynn R.J., Smith D.H., Hess M., "Bubble Behavior in a Slurry Bubble Column Reactor Model", Chemical and Catalytic Reactor Modelling, ACS Symp. Ser., M.P. Dudukovic and P.L. Mills, eds., 237, 125 (1984).

Soria A., "Kinematic Waves and Governing Equations in Bubble Columns and Three-Phase Fluidized Beds", Ph.D. Thesis, The University of Western Ontario, (1991).

Soria A., de Lasa H.I., "Kinematic Waves and Flow Patterns in Bubble Columns and Three-Phase Fluidized Beds", Chem. Eng. Sci. 47(13-14), 3403-3410, (1992).

Stangle G.C., Mahalingam R., "Mass Transfer with Chemical Reaction in a three-Phase Foam-Slurry reactor", AIChE J. 36(1), 117-125, (1990).

Suganuma T., Yamanishi T., Kogaku Kōgaku, 30, 1136 (1966).

Sun Y., Furusaki S., "Mean Bubble Diameter and Oxygen Transfer Coefficient in a Three-Phase Fluidized Bed Bioreactor", J. Chem. Eng. Japan 21(1), 20-24, (1988).

Tang W.-T., Fan L.-S., "Hydrodynamics of a Three-Phase Fluidized Bed Containing Low-Density Particles", AIChE J. 35(3), 355-364, (1989).

Tarmy B.L., Coulaloglou C.A., "Alpha-Omega and Beyond - Industrial View of Gas/Liquid/Solid Reactor Development", Chem. Eng. Sci. 47(13-14), 3231--3246, (1992).

Terasaka K., Tsuge H., "Bubble Formation at a Single Orifice

in Non-Newtonian Liquids", Chem. Eng. Sci 46(1), 85-93, (1991).

Thimmapuram P.R., Rao N.S., Saxena S.C., "Characterization of Hydrodynamic Regimes in a Bubble Column", Chem. Eng. Sci. 47(13-14), 3355-3362, (1992).

Tsuchiya K, Nakanishi O., "Gas Holdup Behavior in a Tall Bubble Column with Perforated Plate Distributors", Chem. Eng. Sci. 47(13-14), 3347-3354, (1992).

Tsuge H., Nakajima Y., Terasaka K., "Behavior of Bubbles Formed from a Submerged Orifice under High System Pressure", Chem. Eng. Sci. 47(13-14), 3273-3280, (1992).

Tuominen O.-P., "Zur Hydrodynamik von Blasensaulen: Messungen mit Optischen Zweipunkt-Mikrosonden in Binaren und Ternaren Gemischen Organisch-Chemischer Flussigkeiten und in Suspensionen", Doktor-Ingenieurs Thesis, Helsinki, Finland, 160 Pages, (1987).

Ueyama K., Miyauchi T., "Properties of Recirculating Turbulent Two Phase Flow in Gas Bubble Columns", AIChE J. 25(2), 258-266, (1979).

Van Den Akker and Rietema K., "Comments on Paper by Joshi and Sharma", Trans. Inst. Chem. Engrs. 60, 255-256, (1982).

Van der Hagen T.H.J.J., "Stability Monitoring of a Natural-Circulation-Cooled Boiling Water Reactor", Thesis TU Delft, The Netherlands, (1989).

Wachi S., Morikawa H., Ueyama K., "Gas Holdup and Axial Dispersion in Gas-Liquid Concurrent Bubble Column", J. Chem. Eng. Japan 20(3), 309-316, (1987).

Weimer R.F., Terry D.M., Stepanoff P., "Laboratory Kinetics and Mass Transfer in the Liquid-Phase Methanol Process", Paper 25d, AIChE Annual Meeting, New-York, (1987).

Weluda K.D., Schutte K., Wittler W., Wingelsdorf R., Schugerl K., "Investigations of the Bubble Phase Behavior in a High Temperature Fluidized Bed Reactor with Coal Combustion", Chem. Eng. Commun. 62, 161-185, (1987).

Whalley P.B., Davidson J.F., "Liquid Circulation in Bubble Columns", Proc. Symp. Two Phase Flow Systems, Inst. Chem. Engrs. Symp. Ser. 38, Paper J5, 1-29, (1974).

Wild G., Saberian M., Schwartz J.-L., Charpentier J.-C., "Gas-Liquid-Solid Fluidized Bed Reactors. State of the Art and Industrial Possibilities", Int. Chem. Eng. 24(4), 639-678, (1984).

Wilkinson P.M., van Dierendonck L.L., "Pressure and Gas Density Effects on Bubble Breakup and Gas Holdup in Bubble Columns", Chem. Eng. Sci. 45, 2309, (1990).

Wilkinson P.M., Spek A.P. van Dierendonck L.L., "Design Parameters Estimation for Scale-Up of High Pressure Bubble Columns", AIChE J. 38(4), 544-554, (1992).

Wittmann K., Helmrich H., Schugerl K., "Measurements of Bubble Properties in Continuously Operated Fluidized Bed Reactor at Elevated Temperatures", Chem. Eng. Sci. 36(10), 1673-1677, (1981).

Wolff C., Briegleb F.U., Bader J., Hektor K., Hammer H., "Measurements with Multi-Point Microprobes", Chem. Eng. Technol., 13, 172-184, (1990).

Yang W.-C., Ettehadieh B., Haldipur G.B., "Solids Circulation Pattern and Particles Mixing in a Large Jetting Fluidized Bed", AIChE J. 32(12), 1994-2001, (1986).

Yang Y.B., Devanathan N., Dudukovic M.P., "Liquid Backmixing in Bubble Columns", Chem. Eng, Sci. 47(9-11), 2859-2864, (1992).

Yao B.P., Zheng C., Gasche H.E., Hofmann H., Bubble Behaviour and Flow Structure of Bubble Columns", Chem. Eng. Process 29, 65-75, (1991).

Yasunishi A., Fukuma M., Muroyama K., "Measurement of Behavior of Gas Bubbles and Gas Holdup in a Slurry Bubble Column by a Dual Electroresistivity Probe Method", J. Chem. Eng. Japan 19(5), 444-449, (1986).

Ying D.H., Givens E.N., Weimer R.F., "Gas Holdup in Gas-Liquid and Gas-Liquid-Solid Flow Reactors", Ind. Eng. Chem. Process Des. Dev. 19, 635-638, (1980).

Yoshida K., Sakane J.-I., Shimizu F., "A New Probe for Measuring Fluidized Bed Characteristics at High Temperatures", Ind. Eng. Chem. Fundam. 21, 83-85, (1982).

Yoshida F., "Bubble Column Research in Japan", Chem. Eng. Technol. 11, 205-212, (1988).

Yu Y.H., Kim S.D., "Bubble Characteristics in the Radial Direction of Three-Phase Fluidized Beds", AIChE J. 34(12) 2069-2072, (1988).

Yu P.Y.W., Varty R.L., "Laser-Doppler Measurement of the Velocity and Diameter of Bubbles using Triple-Peak Technique", Int. J. Multiphase Flow 14(6), 765-776, (1988).

Zaidi A., Louisi Y., Ralek M., Deckwer W.-D., "Mass Transfer

in the Liquid Phase Fischer-Tropsch Synthesis", Ger. Chem. Eng. 2, 94-102, (1979).

Zahradnik J., Kastanek F., Kratochvil J., "Hydrodynamics and Mass Transfer in Uniformly Aerated Bubble Column Reactors", Collection Czechoslovak Chem. Commun. 47, 262, (1982).

Zahradnik J., Peter R., Kastánek F., "The Effect of Liquid Phase Properties on Gas Holdup in Bubble Column Reactors", Collection of Czechoslovak Chemical Communications, 52, 335 (1987)

Zhang X.-R., Homsy G.M., Ropchan W.T., "Bubble Formation in a Single-Jet Gas-Solid Fluidized Bed", Int. J. Multiphase Flow 13(5), 649-660, (1987).

Zhou P., Srivastava R.D., Bose A.C., Stiegel G.J., "Applied Hydrodynamics in Three-Phase Bubble-Column Reactors for Indirect Coal Liquefaction Processes", AIChE Annual Meeting, Miami Beach, Florida, November 2-6, Paper 55h, (1992).

Zrymiak T.L., Hill G.A., "Probe for Measuring Local Holdups in Saline Potash Pulps", Can. J. Chem. Eng. 64, 341-345, (1986).

FLUID DYNAMICS OF HIGH TEMPERATURE BUBBLE AND SLURRY BUBBLE COLUMNS

VOLUME 2

by

Julie Chabot

Department of Biochemical and Chemical Engineering

Submitted in partial fulfilment
of the requirements for the degree of
Doctor of Philosophy

Faculty of Graduate Studies
The University of Western Ontario
London, Ontario

February 1993

TABLE OF CONTENTS

VOLUME 2

APPENDICES

APPENDIX 1

LIQUID AND SOLID PHYSICAL PROPERTIES

LP-100 OIL

PHYSICAL PROPERTIES

Table A1.1
LP-100 Properties

	LP-100 (Witco Corporation)
Average molecular weight	340
Distillation (ASTM D1160) °C 18P 10% 50% 90% EP	 263 317 369 428 473
Hydrocarbon Type (PONA) % Paraffinic/Naphthenic	100
Pour point (°C)	-37
Flash point (°C)	>110
Heat capacity (cal/g-°C)	0.78

Table A1.1a

Properties of the Paraffinic Oil (LP-100) (from: Air Product and Chemicals Inc.)

Temperature (°C)	Density (Kg/m^3)	Viscosity (Kg/m-s)	Surface Tension (Kg/s^2)
100	827	0.003	0.0265
175	783	0.00086	0.0213

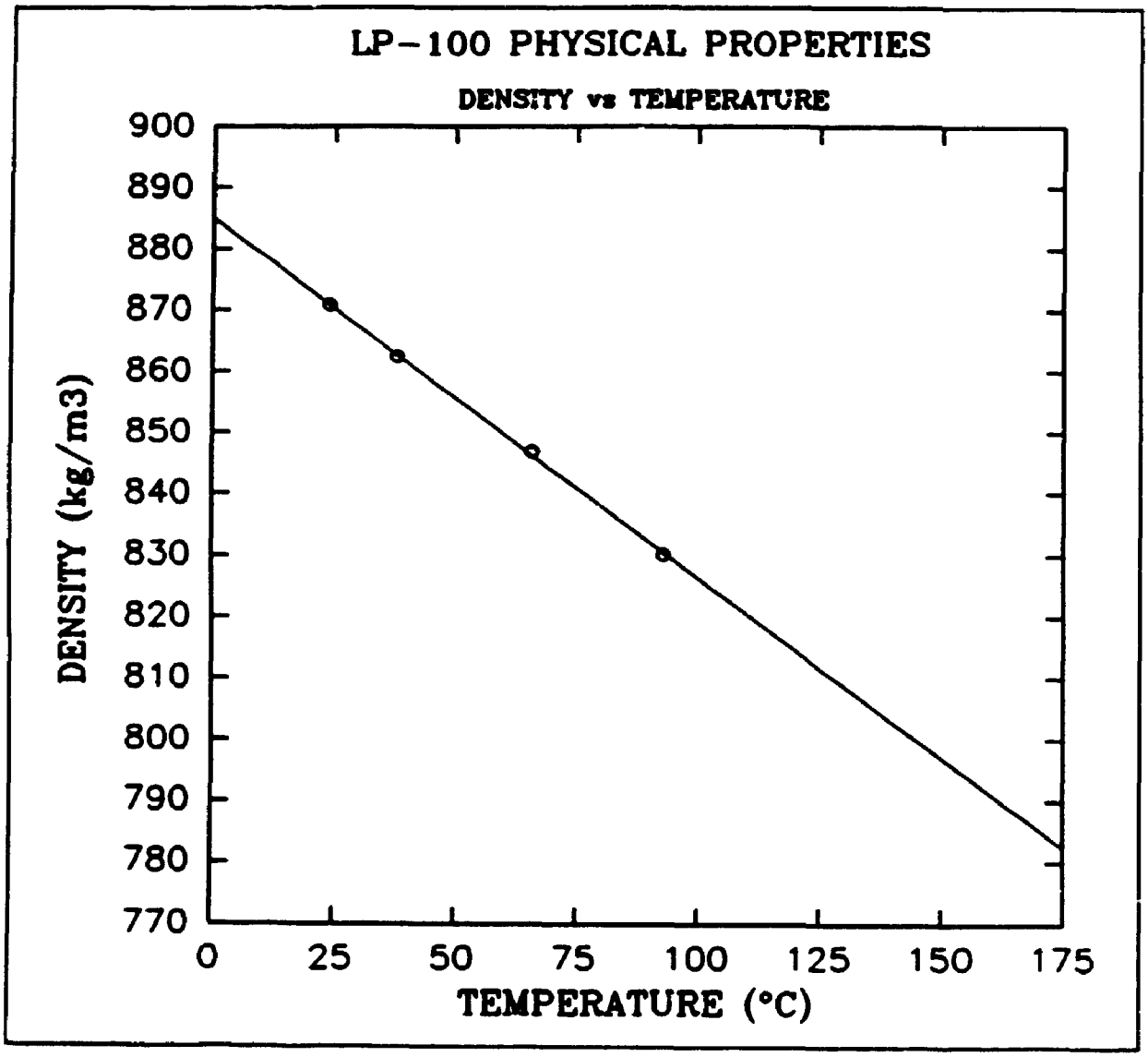

Figure A1.1: LP-100 density vs temperature

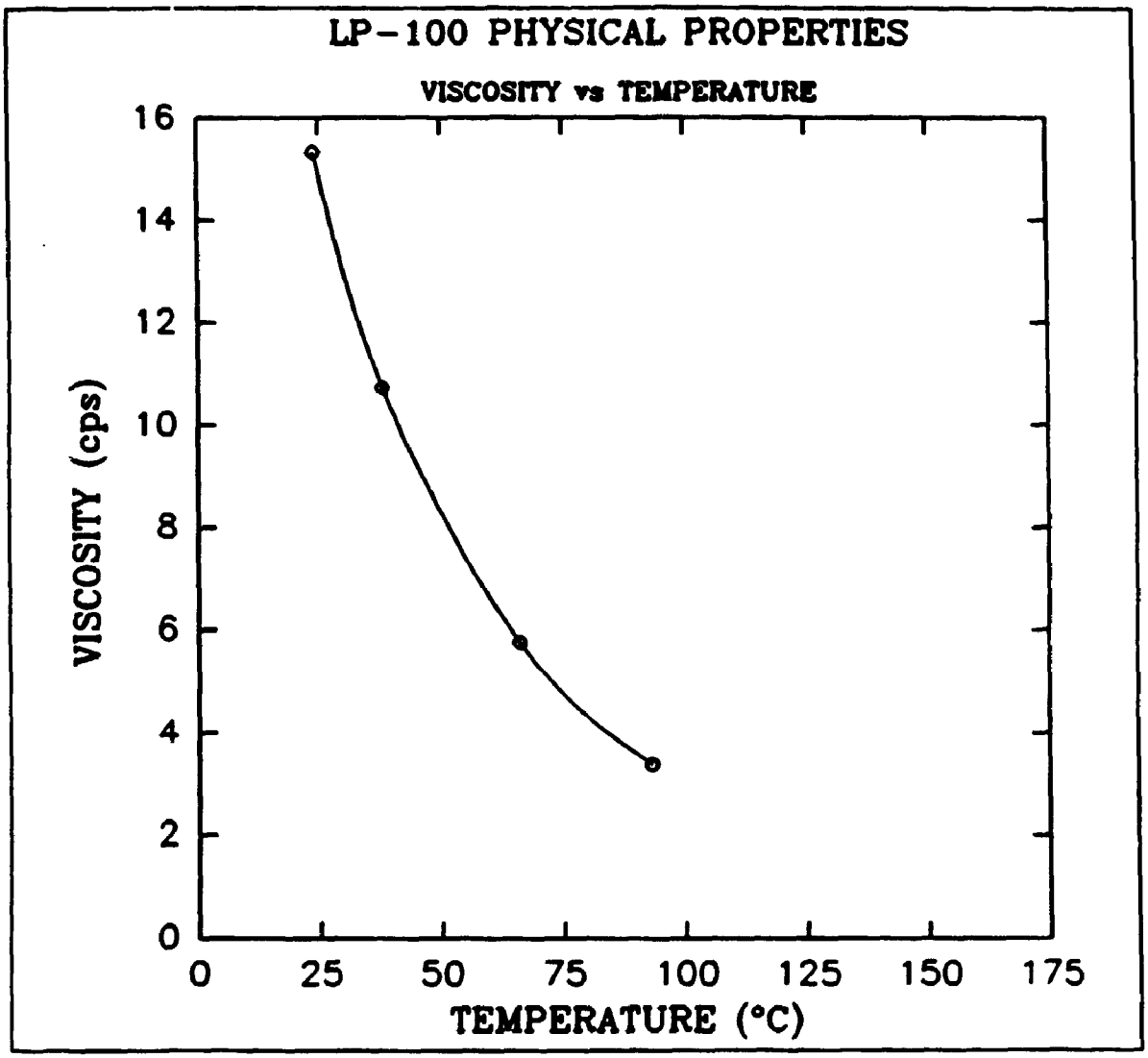

Figure A1.2: LP-100 viscosity vs temperature

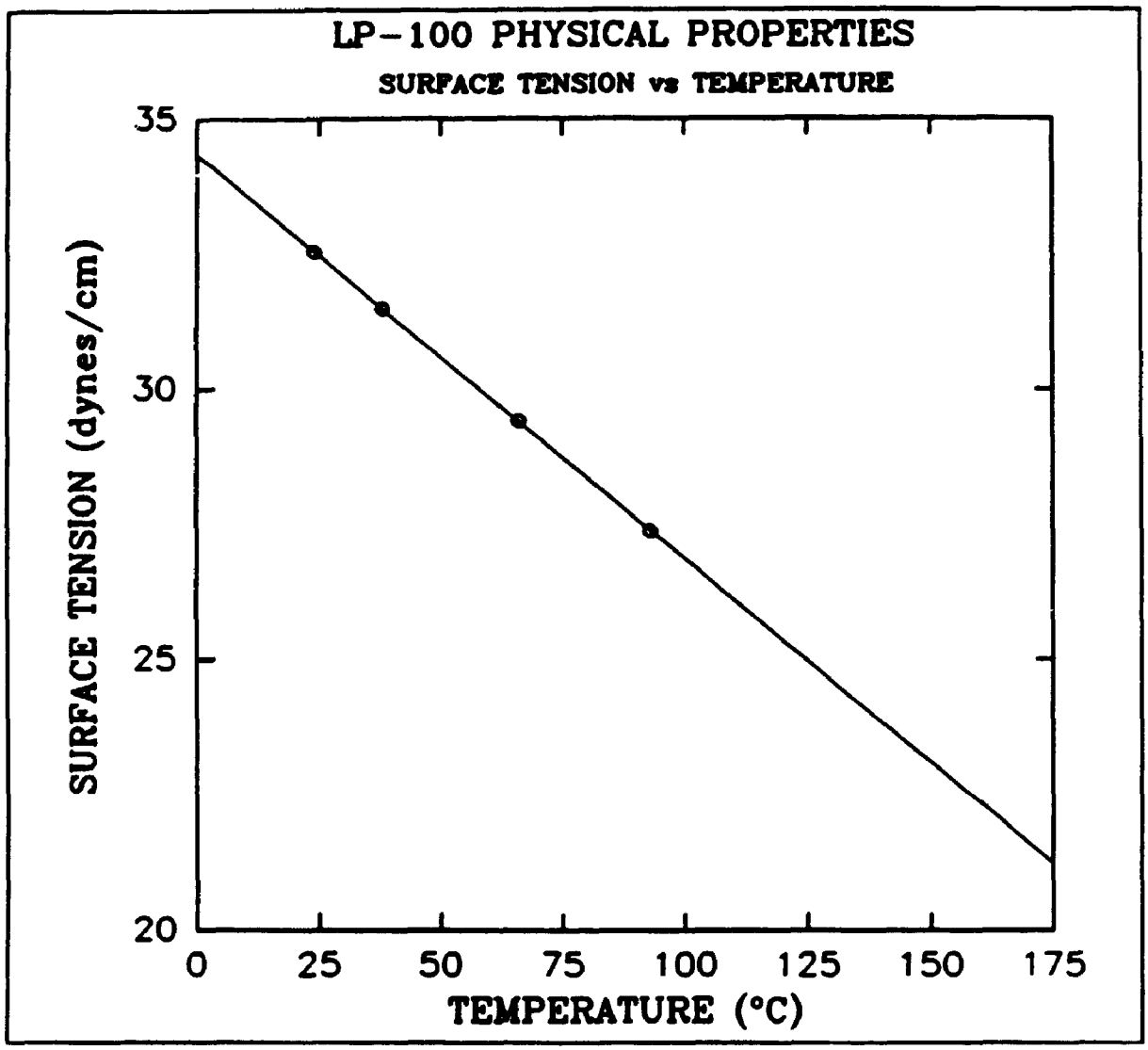

Figure A1.3: LP-100 surface tension vs temperature

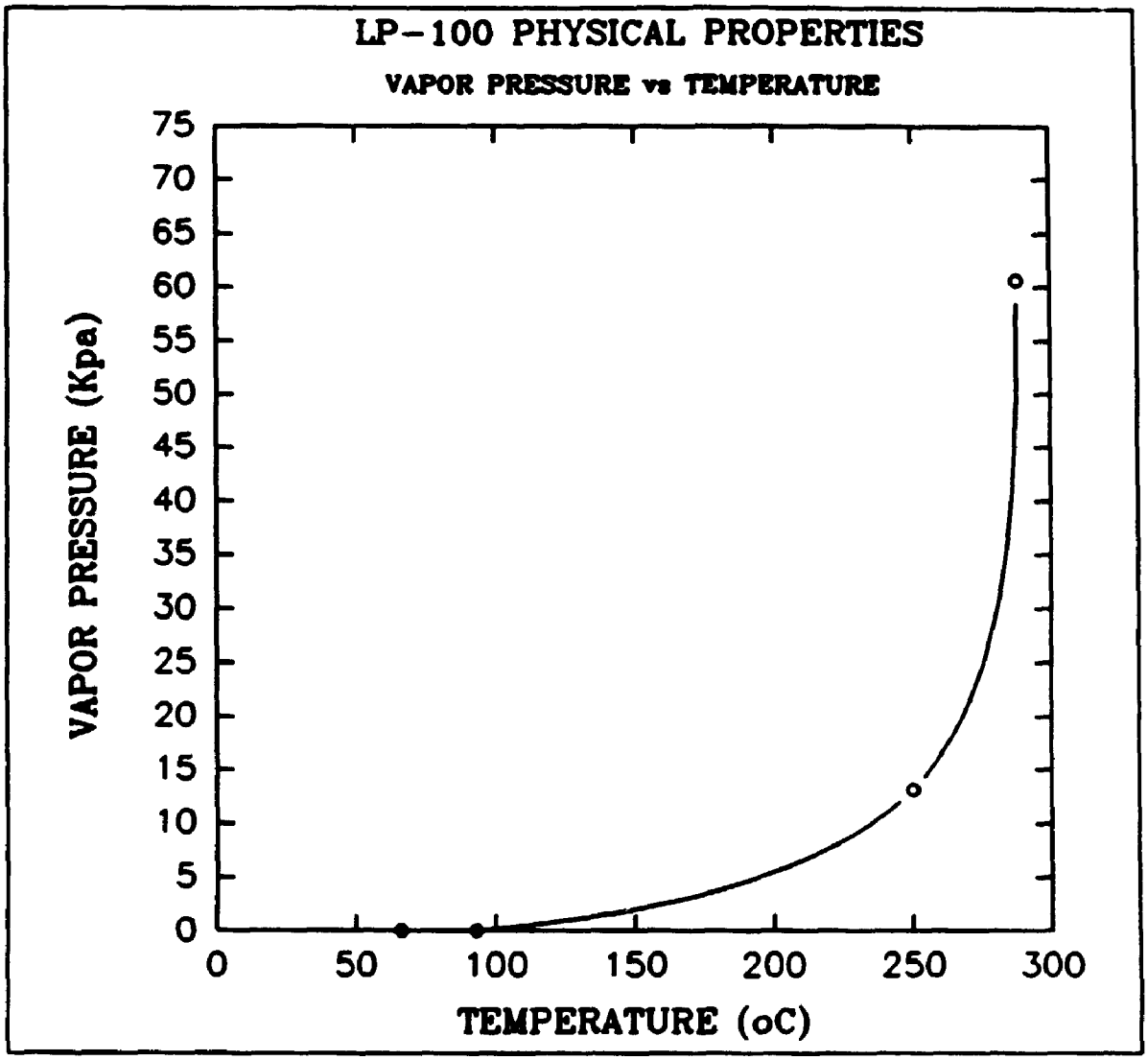

Figure A1.4: LP-100 vapor pressure vs temperature

SOLID PHYSICAL PROPERTIES

Table A1.2
Catalyst properties

Bulk density (kg/m^3)	1300
Pore volume (cm^3/g)	0.38
Average particle diameter (μm)	13.85

CATALYST PARTICLE SIZE DISTRIBUTION
(Obtained from: Malvern Instrument, Master Sizer MS-20)

MALVERN Instruments S8.09 Sat 19 Sep 1992 Time 1:46 pm

Slurry sample #2

Dispersant	: Naptha
Additives	: None
Ultrasound	: None
Pump speed	:
Stir speed	:3/4
Notes	:

High Size	Under %	High Size	Under %	High Size	Under %	High Size	Under %	High Size	Under %	High Size	Under %	Span 1.00
600	100	283	100	68.5	99.7	23.1	87.5	7.82	26.9	2.64	1.6	D[4,3] 13.85µm
544	100	184	100	62.1	99.5	21.0	84.3	7.08	21.6	2.39	1.3	
493	100	166	100	56.2	99.2	19.0	80.5	6.42	16.9	2.17	1.0	
446	100	151	100	50.9	98.9	17.2	76.1	5.82	13.1	1.97	0.8	D[3,2] 9.83µm
404	100	137	100	46.2	98.4	15.6	71.0	5.27	10.1	1.78	0.7	
366	100	124	100	41.8	97.7	14.1	65.4	4.77	7.7	1.61	0.6	
332	100	112	100	37.9	96.8	12.8	59.2	4.33	5.9	1.46	0.4	D[v,0.9] 25.37µm
301	100	102	100	34.3	95.6	11.6	52.7	3.93	4.5	1.32	0.3	
273	100	92.1	99.9	31.1	94.2	10.5	46.0	3.56	3.4	1.20	0.2	
247	100	83.4	99.9	28.2	92.4	9.52	39.3	3.22	2.6			D[v,0.1] 5.26µm
224	100	75.6	99.8	25.5	90.2	8.63	32.9	2.92	2.1			

Source =	:Sample	Mean length = 2.2 mm	Model indp
		Residual = 1.0%	
Focal length = 300 mm		Obscuration = 0.210%	Volume Conc. = 0.838%
Presentation = stnd		Volume distribution	Sp. S.A 0.6647 m²/cc.

D[v,0.5] 11.15µm

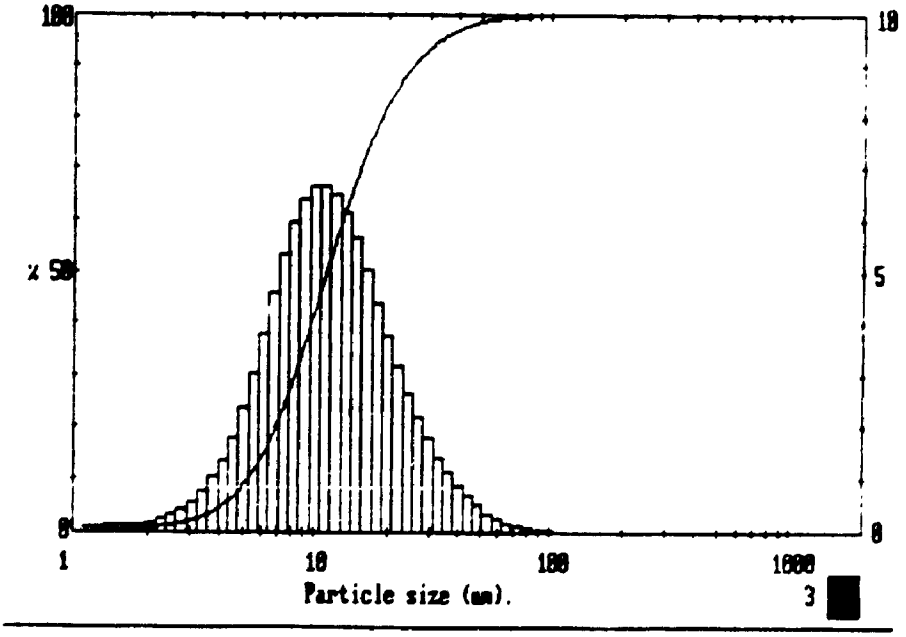

Malvern Instruments

APPENDIX 2

EQUIPMENT CALIBRATION

GAS FLOW METER CALIBRATION

Table A2.1
Gas flow meter calibration

Flow meter reading SCFM	Pressure Psig	Flow rate Wet flow meter (cm^3/s)
0.1	1.5	279.6
0.1	2.0	299.4
0.1	2.5	305.3
0.1	3.0	310.4
0.1	3.5	313.8
0.1	4.0	316.1
0.1	4.5	322.9
0.1	5.0	327.9
0.1	6.5	331.5
0.1	8.5	348.8
0.1	13.0	377.4
0.1	15.0	398.7
0.3	2.0	413.8
0.3	4.0	431.7
0.3	5.0	438.0
0.3	6.0	445.1
0.3	8.5	457.7
0.3	11.5	469.9
0.3	16.5	478.1
0.5	2.0	460.1
0.5	5.0	470.6
0.5	11.5	481.2
0.75	2.5	491.8
0.75	4.5	493.8
0.75	9.0	504.2
1.0	4.0	1029.7
1.0	12.5	1056.6
1.4	15.0	1418.5

PRESSURE TRANSDUCER CALIBRATION

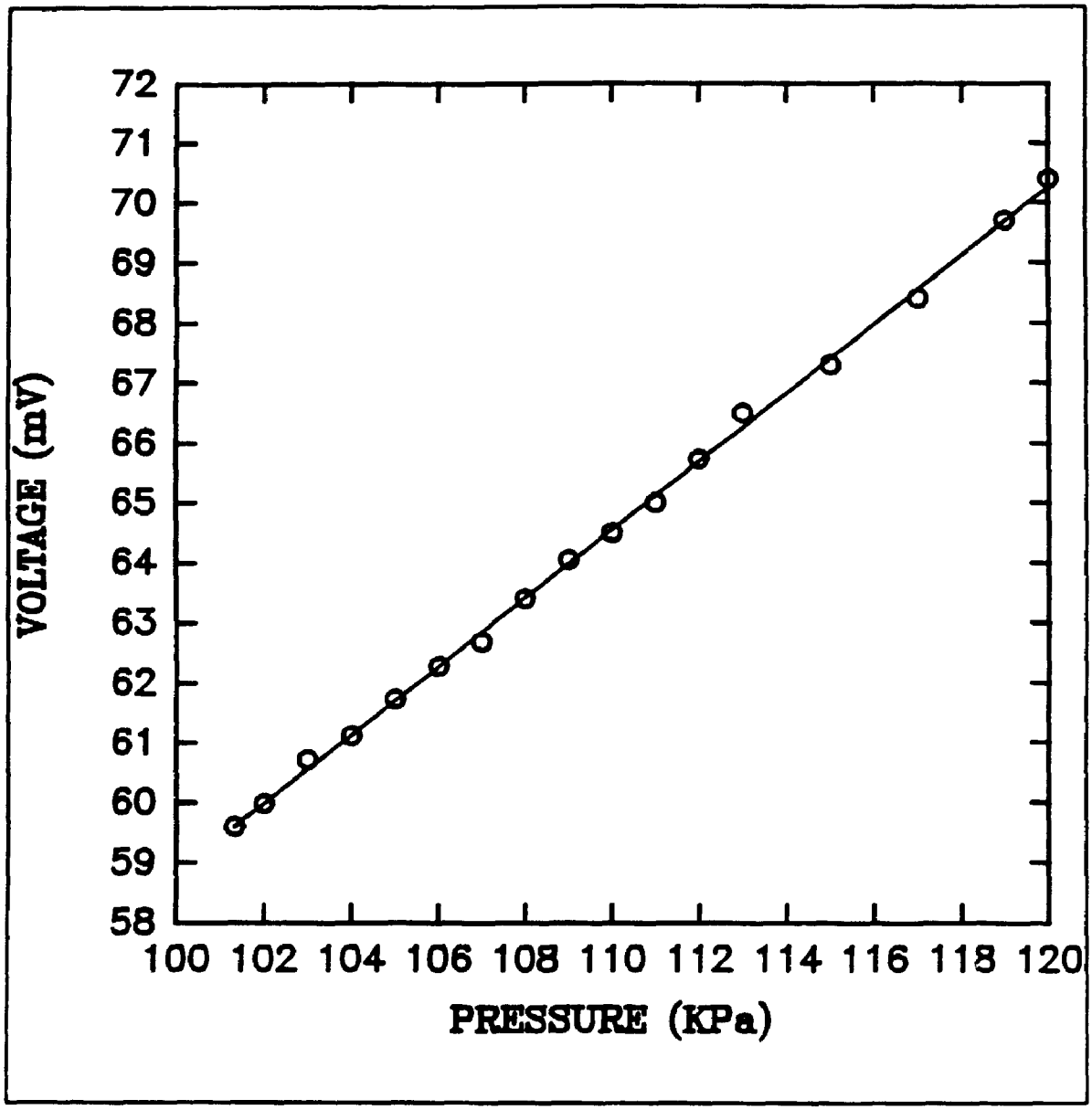

Figure A2.1: Pressure transducer calibration

APPENDIX 3

COMPUTER SOFTWARES

GETAD/AD2

FIBRE OPTIC SENSORS DATA ACQUISITION

```
ftn7x,l,s
$ema /shared_area/
$mseg 17
      program getad
c
c ***************************************************************************
c This program works in combination with ad2 program to perform the
c data acquisition task for the optical probes.
c ***************************************************************************
c
      integer*2 idcb(144), iparm(5), iad_lu, ilen, VmaRead
      integer FmpOpen, FmpReportError, VmaWrite, FmpClose
      character*8 open_opt, parm1, parm2
      character*64 filedesc
      common /shared_area/ ibuffa(16384), ibuffb(16384)
      data ibuff_length /100000b/           ! buffer length in bytes
c
   10 call rmpar (iparm)
c
      if (iparm(1) .eq. 1) then
          call fparm (parm1, parm2, filedesc)
          open_opt = 'orwf'
          itype = FmpOpen (idcb, ierror, filedesc, open_opt, 1)
          if (ierror .lt. 0) then
              write (1,'(//" GETAD cannot open data file")')
              call FmpReportError (ierror, filedesc)
              stop
          endif
c         ilen = VmaRead (idcb, ierror, ibuffa, 2048)
          call VmaRead (idcb, ierror, ibubba, 2048)
          if (ierror .lt. 0) then
              write (1,'(//" GETAD readover of header block failed",
     $            i5)') ierror
              call FmpReportError (ierror, filedesc)
              stop
          endif
          iold_seq = 0
          read (parm2,'(i5)') iad_lu
      elseif (iparm(1) .eq. iad_lu) then

c         write (1,'(5i7)') iparm
          iseq = iparm(2)
c
          if (iseq .ne. iold_seq+1) then
              write (1,'(//" GETAD has missed a schedule from driver")')
              ierror = FmpClose (idcb, ierror)
              stop
          endif
c
          if (iseq-2*(iseq/2) .ne. 0) then
              call VmaWrite (idcb, ierror, ibuffa, ibuff_length)
          else
              call VmaWrite (idcb, ierror, ibuffb, ibuff_length)
          endif
c
          if (ierror .lt. 0) then
              call FmpReportError (ierror, filedesc)
              stop
          endif
c
          iold_seq = iseq
c         write (1,'(" seq = ",i3)') iseq
c
c
```

```
c
      elseif (iparm(1) .eq. 999) then
c
c
          ierror = FmpClose (idcb)
          stop
c
c
      else
c
c
          write (1,'(" GETAD had a bad schedule")')
          ierror = FmpClose (idcb, ierror)
          stop
      endif
      call exec (6, 0, 1, 0, 0, 0, 0, 0)
      goto 10
      end
```

```
ftn7x,1,s
$ema /shared_area/
      program ad2
c
c ***************************************************************************
c This program collects data and creates a file to hold the data
c posting in the first 1024 words of the experiment.  The program
c GETAD pick up data as they become available from id.51, the
c continous ADC driver.
c This program and GETAD must be loaded using the same shared
c EMA area or it will not succeed.
c
c Sampling speed of 1000/s-channel for two channels.  Total sampling
c time is equal to 57s.
c ***************************************************************************
c
      integer*2 idcb(144), icnwd(2), iparm(5), ibuff(1024), iname(3)
      integer*2 ip(5), length, FmpWrite
      integer FmpworkingDir, FmpBuildPath, FmpOpen, FmpReportError
      integer FmpClose, FmpPurge, FmpRunProgram
      character*64 dir, dirpath, filedesc
      character*100 runstrng
      character*80 cbuff
      character*20 open_opt
      character*16 file_name, file
      character*15 run
      character*6 cname
      character*4 cad_lu
      character*1 cans
      logical existed
      common /shared_area/ ibuffa(32768)
      equivalence (icnwd(1),iadlu), (icnwd(2),ioption)
      equivalence (rbuffr,ibuff(108))
      equivalence (iname(1), cname)
      equivalence (cbuff, ibuff(1))
      data ibuff_length /16384/
      data ilen /100000b/
      data run /'XQ,GETAD.RUN,1,'/
      data iadlu /20/, nchan /2/, igain /8/, datarate /2000/, imode /1/
      data iseconds /57/, triggerate /1000/, ihiaddr /7/
      data Bini /17.5/, Weight /20000/, Spacing /0.375/
c
c ***************************************************************************
c ADC lu supplied is an ADC so try locking the lu for exclusive use.
c ***************************************************************************
c
      call lurq (100001b,iadlu,1)
      call abreg (ia, ib)
      if (ia .eq. 1) then
          write (1,'(//" Unable to lock lu ",i5," someone else is ",
     $        "using the ADC use program WH to see who")') iadlu
          stop
      endif
c
      total_samples = iseconds*datarate
      itotal_buffers = total_samples/ibuff_length+1
c
c ***************************************************************************
c Write out summary of experiment information.
c ***************************************************************************
c
      call write_summary (iadlu, imode, nchan, igain, istart,
     $    triggerate, datarate, iseconds, total_samples)
      ibuffer_time = ibuff_length*('00./datarate)  !buffer time in 10's
```

```
msec
      if (iseconds .eq. 0) then
          iblocks = 32767
      else
          iblocks = itotal_buffers*(ibuff_length/128)+8
      endif
c
c *****************************************************************
c Ask for file name info and if exists ask if okay to overlay.
c *****************************************************************
c
   60 write (1,'(//" Enter file name for storing data _")')
      read (1,'(a16)') file_name
      ierror = FmpworkingDir (dir)
      iend_dir = index(dir,' ')
      dirpath = dir(1:iend_dir-1) // '/'
      call FmpBuildPath (filedesc, dirpath, file_name, 'dat', ' ',
     $    0, 2, iblocks, 1024, ' ')
      open_opt = 'orw'
      existed = .true.
   70 itype = FmpOpen (idcb, ierror, filedesc, open_opt, 1)
      if (ierror .lt. 0) then
          if (ierror .eq. -6) then
              open_opt = 'crw'
              existed = .false.
              goto 70
          else
              call FmpReportError (ierror, filedesc)
              goto 60
          endif
      endif
      if (existed) then
          write (1,'(//" File exists do you want to overlay ? _")')
          read (1,'(a1)') cans
          if (cans .eq.'y' .or. cans .eq. 'Y') then
              ierror = FmpClose (idcb, ierror)
              ierror = FmpPurge (filedesc)
              if (ierror .ne. 0) then
                  write (1,'(//" Cannot overlay file")')
                  goto 60
              endif
              existed = .false.
              open_opt = 'crw'
              goto 70
          endif
      goto 60
      endif
c
c *****************************************************************
c Post header record into the file.  Rbuffr is equivalenced to
c ibuff(108) in order to get a real quantity into header.
c Any program that uses the data file as a VMA backing store file
c should have a common block of form:
c common /vma_area/ iheader(1024), idata (32000000)
c *****************************************************************
c
      write (1,'(//" Enter a description for the data file"//"? _")')
      read (1,'(a80)') cbuff
      call ftime (ibuff(81))
      ibuff(101) = iadlu
      ibuff(102) = imode
      ibuff(103) = ihiaddr+1
      ibuff(104) = nchan
      ibuff(105) = istart
```

```
      ibuff(106) = igain
      rbuffr = triggerate
c
      write (1,'(/"  ** >> Liquid Velocity ? ( GPM )")')
      Vliq = readans (1)
c     Convert liquid velocity to unit of cm/sec with Scale factor 10000
      Vliq = int (1945*Vliq)
      write (1,'(/"  ** >> Gas Velocity ? ( Flow meter Reading )")')
      Vgread = readans (1)
      write (1,'(/"  ** >> Pressure of Gas ? ( Psi )")')
      Press = readans (1)
c     Convert gas velocity to unit of cm/sec with scale factor of
c     10000 based on 740 mm Hg
      Vgas = 35.915 * ( 14.31 + Press ) * Grate ( Vgread )
c     Convert pressure to SI unit of Pa, N/(m*m)
      Press = INT ( 689.12 * ( 14.31 + Press ))
c     Convert initial bed height to SI unit of meter with scale factor
c     of 10000
      Bini = INT ( 254 * Bini )
      ibuff (110) = Vliq
      ibuff (111) = Vgas
      ibuff (112) = Vgread
      ibuff (113) = Press
      ibuff (114) = Bint
c
      length = FmpWrite (idcb, ierror, ibuff, 2048)
      ierror = FmpClose (idcb,ierror)
c
c ***************************************************************************
c Get program GETAD ready to receive data.
c ***************************************************************************
c
      write (cad_lu,'(i3,",")') iadlu
      runstrng = run//cad_lu//filedesc
      ierror = FmpRunProgram (runstrng, ips, cname)
      if (ierror .ne. 0 .and. ierror .ne. 32767) then
          write (1,'(//" Could not schedule GETAD program")')
          stop
      endif
c
c ***************************************************************************
c Program ADC timeout values.
c ***************************************************************************
c
      ito = ibuffer_time/5
      ito_count = 0
      ioption = 2200b
      call xluex (3, icnwd, ito, ito_count)
      ioption = 2500b
      call xluex (3, icnwd, itotal_buffers)
c
c ***************************************************************************
c Program ADC card control word.
c ***************************************************************************
c
      iextrig = 20000b
      iauto = 40000b
      if (igain .eq. 1) then
          jgain = 0
      elseif (igain .eq. 2) then
          jgain = 1
      elseif (igain .eq. 4) then
          jgain = 2
      elseif (igain .eq. 8) then
```

```
            jgain = 3
        endif
        if (nchan .eq. 1) then
            icard = (512*jgain)+istart
        else
            icard = iauto+(512*jgain)+(ihiaddr-nchan+1)
        endif
        if (imode .eq. 1) then
            icard = icard+iextrig
        endif
c
c ***************************************************************************
c Set up driver with name of program to schedule.
c ***************************************************************************
c
        ioption = 2000b
        call xluex (3, icnwd, iname(1), iname(2), iname(3), 1)
c
c ***************************************************************************
c Get on with taking the readings.
c ***************************************************************************
c
    80 write (1,'(//" Are you ready to start experiment _")')
        read (1,'(a1)') cans
            if (cans .eq.'y' .or. cans .eq. 'Y') then
                ioption = 200b
                call vmaio (1, icnwd, ibuffa, ilen, icard)
            elseif (cans .eq.'a' .or. cans .eq. 'A') then
                stop
            else
                goto 80
            endif
        call abreg (ia,ib)
        write (1,'(/" Collected",i6," buffers")') ib
        write (1,*) CHAR(7)
        call exec (100000b+23, 6hGETAD , 999, *100)
        stop
100     write (1,'(//" Could not terminate GETAD program")')
c
        stop
        end
c
c ***************************************************************************
c Routine to read an integer answer or terminate on a or A.
c ***************************************************************************
c
        function ireadans (lu)
        integer*2 ireadans
        character*8 cvalue
        read (lu,'(a8)') cvalue
        if (cvalue(1:1) .eq. 'a' .or. cvalue(1:1) .eq. 'A') then
            write (1,'(//" ADC program aborting")')
            stop
        endif
        read (cvalue,'(i8)') ireadans
        return
        end
c
        function readans (lu)
        read (lu,*) readans
        return
        end
c
        function grate (vg)
```

```
      grate = - 0.0546 + 0.2029 * vg + 0.001 * vg ** 2
     *- 2.7304E-6 * vg ** 3 + 6.0177E-9 * vg ** 4
      return
      end
c
      subroutine write_summary (iadlu, imode, nchan, igain, istart,
     $    triggerate, datarate, iseconds, total_samples)
      character*1 cans
      write (1,'(//" ADC sampling will occur on lu",i4," using",i4,
     $    " channels")') iadlu, nchan
      if (imode .eq. 0) then
          write (1,'(" The ADC will be free-run at 55 kHz")')
      else
          write (1,'(" The ADC will be externally triggered ",
     $        "at",f10.3," Hz ")') triggerate
      endif
      write (1,'(" The gain is set for",i3," on",i3," channels")')
     $    igain, nchan
          if (nchan .eq. 1) then
              write (1,'(" Single channel sampling is on channel ",i3)')
     $            istart
          endif
      write (1,'(" The experiment will produce",f20.3" samples",
     $    /," in",i8," seconds for a data rate of",f10.3," samples/sec"
     $    )') total_samples, iseconds, datarate
      return
      end
```

PPF

PRESSURE TRANSDUCER DATA ACQUISITION

```
FTN7X,L,S
$FILES 2,2
c
c @Copyright Julie Chabot July 28, 1992
c ***************************************************************
c This program is written for pressure profile mesurement.
c The sampling time is five seconds.
c Five seconds are reserved for switching channels.  In order to have
c trouble free operation, the following procedure is recommended:
c
c     1. check the LU for A/D card
c        eg. CI> IO 20
c        make sure it is "UP".
c
c     2. set the frequency generator at 280/s.
c
c     3. adjust the timer for scanning valve so that it is synchronized
c        with the frequency generator.
c
c     4. use channel 3
c
c ***************************************************************
c
      Program ppf
      Integer*2 iv(500,8), isp(500)
      Integer*2 icntwd, ivl, icrdcw, ispl, idcm, iend
      Character*16 file, file_name, null
c
      data null /'                '/
c
      call fparm ( file )
c
      ENCODE ( 16, 5, name ) file
    5 format ( a16 )
c
      if ( file .lt. null ) then
          write (1,'(//" Enter name of the data file !")')
          read (1,'(a16)') file
      end if
c
      idcm = index ( file, '.')
      if (idcm .eq. 0) then
          iend = index ( file, ' ')
          file_name = file(1:iend-1) // '.DAT'
      else
          file_name = file
      end if
c
      ICNTWD = 20       ! LU NUMBER
      IVL = 500      ! ONE CHANNEL, FIVE SECONDS AT 100/S
      ISPL = 500
      ICRDCW = 23002B     ! SINGLE CHANNEL, EXTER TRIG, CHANNEL 1
c
c
      DO J = 1, 7
          WRITE (1,*) '** >> SCANNER #', J, ' << **  ACTIVATED **'
          CALL EXEC (1,ICNTWD,IV(1,J),IVL,ICRDCW)
          WRITE (1,*) 'SWITCHING CHANNEL'
          CALL EXEC (1,ICNTWD,ISP,ISPL,ICRDCW) ! SKIP (ISPL/100) SECONDS
      END DO
c
      WRITE (1,*) '--- >> STORING DATA << ---'
      OPEN (100,FILE=file_name)
      WRITE (100,*) IV
```

```
CLOSE (100)
STOP
END
```

PPC

PRESSURE PROFILE

AVERAGE GAS HOLDUP MEASUREMENT

```
FTN7X,L,S
$FILES 2,2
c
c
c @Copyright Julie Chabot, April 15,1992
c
c*************************************************************************
c This program is written for the pressure profile calculation using the
c data collected by ppf.
c*************************************************************************
c
      PROGRAM ppc
      INTEGER*2 iv(500,8), i, y, a, h
      INTEGER*2 idcm, iend, col, bloc, nature
      REAL pres(10), lden, gden, pcor(10), x(10)
      REAL rtempc, mole, psum, avg(10), value(10)
      REAL eg, el
      REAL slope, sxy, sx, sxs, sy, sys, asyy, asxx, asxy, r
      CHARACTER*16 file, filename, null
c
c*************************************************************************
c Data File Characteristics
c*************************************************************************
c
      write (1,'("Enter Temperature of Operation oC ?")')
      read(1,*) rtempc
c
      write (1,'("Nature of gas ? air (1), nitrogen (2)")')
      read(1,*) nature
c
      if (rtempc .eq. 25) then
      lden=870
      else if (rtempc .eq. 100) then
      lden=827
      else if (rtempc .eq. 175) then
      lden=783
      end if
c
      if (nature .eq. 1) then
      mole = 28.9
      else
      mole = 28
      end if
c
      gden= 1000 * mole / (82.05 * (rtempc + 273.15))
c
      pcor(1)=6.5641
      pcor(2)=4.8274
      pcor(3)=3.5248
      pcor(4)=2.2222
      pcor(5)=0.9197
      pcor(6)=0.05129
      pcor(7)=-1.03425
c
c*************************************************************************
c Data file retrieving
c*************************************************************************
c
      write (1,'("Enter name of the data file ?")')
      read (1,'(a16)') filename
c
      open (100, file=filename)
      read (100,*)((iv(col,bloc), col=1,500), bloc=1,7)
      y=1
```

```
c
      do bloc=1,7,1
            psum=0
            do col=1,500,1
            psum=psum + abs(iv(col,bloc))
            end do
          avg(y)=psum/500
          value(y)=avg(y) * 0.0390625
          pres(y) = (1.7295 * value(y)) - 1.6868
          pres(y) = pres(y) - pcor(y)
          y=y+1
       end do
       close (100)
c
c*************************************************************************
c Holdup calculation
c*************************************************************************
c
      X(1)=91.4
      X(2)=71.1
       X(3)=55.9
       X(4)=40.6
       X(5)=25.4
       X(6)=15.2
       X(7)=2.5
c
       SX=0
       SXS=0
       SY=0
       SYS=0
       SXY=0
c
       DO Y=1,7,1
       SXS=SXS+(X(Y)**2)
       SX=SX+X(Y)
       SYS=SYS+(PRES(Y)**2)
       SY=SY+PRES(Y)
       SXY=SXY+(X(Y)*PRES(Y))
       END DO
c
       ASXX=SXS-((SX**2)/7)
       ASYY=SYS-((SY**2)/7)
       ASXY=SXY-((SX*SY)/7)
       SLOPE=abs((ASXY/ASXX)*100)
       R=ASXY/((ASXX*ASYY)**0.5)
c
       el=((slope * 1000 /(9.81))-gden)/(lden-gden)
       eg=1-el
       if (eg .lt. 0.0) then
       eg = 0
       else
       eg = eg
       end if
c
       write (6,*)
       write (6,*) '************************************************'
       write (6,*) ' '
       write (6,*) 'Filename = ', filename
       write (6,*) ' '
       do h=1,7
       write(6,11)h,x(h),Pres(h)
11     format(/,2x,' Tap = ',i2,4x,' Location = ',f4.1,' cm',4x,
     $  ' Pressure = ',f7.2,' Kpa')
       end do
       write (6,*) ' '
       write (6,*) '************************************************'
```

```
      write (6,*) ' '
      write (6,*) 'Liquid Porosity = ', el
      write (6,*) 'Gas Porosity    = ', eg
      write (6,*) 'Linear Regression Correlation Coefficient = ',r
      write (6,*) ' '
      write (6,*) '************************************************'
c
      stop
      end
```

C2HR

FIBRE OPTIC SENSORS

BUBBLES IDENTIFICATION (FREQUENCY / DURATION) / GAS HOLDUP

```
ftn7x,l,s
$ema /big/
$cds on
$files 0,2
c
c @Copyright Julie Chabot fall 1991
c
c ***************************************************************************
c This program was developed to draw the signal spectrum with a wide
c flexibility of resolution and to perform gas holdup analysis
c for a frequency of data acquisition of 1000 points/second-channel.
c ***************************************************************************
c
c ***************************************************************************
c Variables identification.
c ***************************************************************************
c
      program C2HR
      integer VmaRead, iend
      integer FmpOpen, FmpClose, idcb (144), OPTION, LUARY(2), NUMLUS
      integer FmpworkingDir, FmpBuildPath, Vmaopen
      integer IASC(5), ii, bouja, boujb, boujc
      integer lu, contrl, name(8), unit
      integer head(1024), skipdata(1024), iblocks
      integer pox(2,20), iv(2,55000)
      integer*4 i, ia, Nsta, Nsto, l(2), end(2,50), top
      integer*4 ilen, Nb(2), j, ic(2), fst(2,50), k
      integer  Nxtic, Nix, Ndx, Nytic, Niy, Ndy
      real bot1, bot2, start1, start2, stop1, stop2
      real slope1, slope2, slope3, slope4, bob(2)
      real noise(2), square(2), avg(2)
      real sq(2), Ndu(2), poro(2), moy(2)
      real v(2,50000), factor
      real Nk, freq(2), avgdur(2)
      real botc1, botc2, ban2, cr(2)
      real dum, hope, bodya(2), bodyb(2)
      real maxint(2), y(2), vf(2,20)
      real int(2,5000), cont(2,5000), contr(2,20)
      real var(2), bs(2)
      real Xpos, Ypos, width, height, size, base
      real Xmin, Xsta, Xend, Xmax, ban1
      real Ymin, Ysta, Yend, Ymax
      character*1 apos, ans, answ, rep1, rep2, answ1, answ2
      character*1 answ3
      character*8 open_opt
      character*16 file, file_out, null, file_or
      character*64 dir, filedesc, dirpath
      common/big/head,iv,v,int,cont,vf,contr,pox,fst,end,Nb,Ndu,poro
     $var, bs, cr, bob, bodya, bodyb, Nsto, Nsta, slope1, slope2
     $slope3, slope4, top, freq, avgdur, factor, dum
      common /Xaxis/ Xmin, Xsta, Xend, Xmax, Nxtic, Nix, Ndx, Xsp
      common /Yaxis/ Ymin, Ysta, Yend, Ymax, Nytic, Niy, Ndy, Ysp
      common /Fback/ width, height
      data iblocks /904/, lu /6/, contrl /400b/, hope /0/
      data null /'                '/
c
c ***************************************************************************
c Data file retrieving.
c ***************************************************************************
c
      call fparm ( file )
c
      ENCODE ( 16, 5, name ) file
5     format ( a16 )
```

```
c
      if ( file .lt. null ) then
          write (1,'(//" Enter name of the data file !")')
          read (1,'(a16)') file
      end if
c
      iend = index ( file, ' ')
c
c ***************************************************************************
c Data verification.
c ***************************************************************************
c
      ierror = FmpworkingDir (dir)
      iend_dir = index (dir,' ')
      dirpath = dir (1:iend_dir-1) // '/'
      call FmpBuildPath (filedesc, dirpath, file, 'DAT', ' ',
     *0, 2, iblocks, 1024, ' ')
c
      open_opt = 'orwf'
      call FmpOpen (idcb, ierror, filedesc, open_opt, 1)
      write (1,*) '*** FmpOpen ierror = ', ierror
c
      ilen = VmaRead (idcb, ierror, head, 2048)
      write (1,*) '***** ierror = ',ierror
      write (1,*) '*** Total number of bytes read = ',ilen
c
      ilen = VmaRead (idcb, ierror, skipdata, 2048)
      write (1,*) '***** ierror = ',ierror
      write (1,*) '*** Total number of bytes read = ',ilen
c
      do j = 1, 10
      ia = (j-1) * 5120. + 1
      ilen = VmaRead (idcb, ierror, iv(1,ia), 20480)
      write (1,*) '******** ierror = ',ierror
      write (1,*) '***** Total number of bytes read = ',ilen
      end do
c
      ia = 10. * 5120. + 1
      ilen = Vmaread (idcb, ierror, iv(1,ia), 15200)
      write (1,*) '********** ierror = ', ierror
      write (1,*) '***** Total number of bytes read = ', ilen
c
      ierror = FmpClose (idcb, ierror)
c
c ***************************************************************************
c Data reading and conversion.
c ***************************************************************************
c
c
c     factor for converting raw data into volt.
c
      factor = 5./(16.*8.*1000.)
c
c
      write (1, '(/"  *****  Converting Data  *****")')
c
      do i = 1, 50000
          do j= 1, 2
              dum = iv (j,i) * factor
              v(j,i) = ABS (dum)
          end do
      end do
c
c ***************************************************************************
```

```
c Baseline identification
c ************************************************************************
c
      do j = 1, 2
          bs(j) = 0.
          do i = 1, 50000
              bs(j) = bs(j) + v(j,i)
          end do
          bs(j) = bs(j) / 50000
      end do
c
      do j = 1, 2
          var(j) = 0.
          do i = 1, 50000
              var(j) = var(j) + ((v(j,i) - bs(j)) ** 2)
          end do
          var(j) = var(j) / 50000.
      end do
c
c
12    format('1')
40    format(//,20x,'******** Filename : ',a16, ' ********')
c
c
c
      boujb=0
      write(1,'(/"Do you want hardcopies of the spectrums ?")')
      read (1, '(a1)') answ2
      if (answ2 .eq. 'N' .or. answ2 .eq. 'n') then
      boujb=1
      end if
c
      boujc=0
      write (1,'(/"Do you want holdup/data distribution analysis ?")')
      read (1, '(a1)') answ3
      if (answ3 .eq. 'N' .or. answ3 .eq. 'n') then
      boujc=1
      end if
c
      bouja=0
      write (1,'(/"Do you want to perform criteria check ?")')
      read (1, '(a1)') answ
      if (answ .eq. 'N' .or.  answ .eq. 'n' ) then
      bouja=1
      end if
c
c
c ************************************************************************
c Locking printer
c ************************************************************************
c
      OPTION = 040001B
      LUARY(1) = 6
      NUMLUS = 1
c
      CALL LURQ (OPTION, LUARY, NUMLUS)
c
c
c
c ************************************************************************
c Check
c ************************************************************************
c
c
```

```
      write(1,'(/" ***** Printer locked *****")')
c
      if (boujb .eq. 1 .and. bouja .eq. 1) then
      goto 6500
      end if
c
      if (boujb .eq. 0 .and. bouja .eq. 0) then
      hope=1
      end if
c
c*************************************************************************
c Spectrums drawing
c*************************************************************************
c
      CALL ZBEGN
      CALL ZDINT (LU, CONTRL, IERR )
      CALL ZASPK ( 0.6, 1.0 )
      CALL ZDLIM ( 30.0, 180.0, 30.0, 265.0 )
c
c
c*************************************************************************
c Output Results
c*************************************************************************
c
      write(6,12)
      write(6,40) file
c
c ********************
c Channel #1
c ********************
c
      j = 1
c
c
2001  continue
c
c
      if (hope .eq. 1) then
      write (1, '(/"Please enter the time interval to consider ?")')
      write (1, '(/"minimum time (s)")')
      read(1,'(f4.2)') bot1
      write (1, '(/"maximum time (s)")')
      read(1,'(f4.2)') bot2
      end if
c
c
      if (hope .eq. 1) then
c
      ban1 = bot2 - bot1
      Xmin = bot1 - (4 * ban1 / 45.0)
      Xsta = bot1
      Xend = bot2
      Xmax = bot2 + (5 * ban1 / 45.0)
      Nxtic = 10
      Nix = 2
      Ndx = 3
c
      else
c
      bot1 = 0.001
      bot2 = 45.0
      Xmin = -4.0
      Xsta = 0.0
      Xend = 45.0
```

```
      Xmax = 50.0
      Nxtic = 9
      Nix = 2
      Ndx = 2
c
      end if
c
      Ymin = -0.072
      Ysta = 0.0
      Yend = 0.4
      Ymax = 0.44
      Nytic = 4
      Niy = 1
      Ndy = 2
c
      CALL ZVIEW ( 0.0, 0.6, 0.52, 0.90 )
      CALL ZWIND (Xmin, Xmax, Ymin, Ymax)
c
      Size = 0.5
      Base = 1.0
c
      call zaxes ( Size, Base )
      width = 1000. * width
      CALL ZCSIZ ( width, height )
c
      start1 = bot1 * 1000
      stop1 = bot2 * 1000
c
      if (hope .eq. 1) then
c
      Xmin = start1 - (1000.0 * 4 * ban1 / 45.0)
      Xsta = start1
      Xend = stop1
      Xmax = stop1 + (1000.0  * 5 * ban1 / 45.0)
c
      else
c
      Xmin = - 4000.0
      Xsta = 0.0
      Xend = 45000.0
      Xmax = 50000.0
c
      end if
c
      CALL ZWIND ( Xmin, Xmax, Ymin, Ymax )
c
      Xpos = start1
      Ypos = v(1,start1)
      CALL ZMOVE ( Xpos, Ypos )
c
      if (hope .eq. 1) then
c
      do i = start1, stop1, 1
         Xpos = i
         Ypos = v(1,i)
         CALL ZDRAW (Xpos, Ypos)
      end do
c
      else
c
      do i = 1, 45000, 1
         Xpos = i
         Ypos = v(1,i)
         CALL ZDRAW ( Xpos, Ypos )
```

```
      end do
c
      end if
c
      call ZMOVE ( Xsta + 31.0 * width, Ymin )
      call ZTEXT ( 12, 12HTime, second)
      call ZMOVE ( Xsta + 3.0 * width, Yend )
      call ZTEXT ( 6, 6HSignal)
      call ZMOVE ( Xsta + 3.0 * width, Yend - height )
      call ZTEXT ( 16, 16HIntensity, Volt.)
      call ZMOVE ( Xend - 15. * width, Yend )
      call ZTEXT ( 8, 8HProbe #1)
c
c **********************
c Channel #2
c **********************
c
      j = 2
c
c
      if (hope .eq. 1) then
c
      ban2=bot2-bot1
      Xmin = bot1 - (4 * ban2 / 45.0)
      Xsta = bot1
      Xend = bot2
      Xmax = bot2 + (5 * ban2 / 45.0)
      Nxtic = 10
      Nix = 2
      Ndx = 3
c
      else
c
      bot1 = 0.001
      bot2 = 45.0
      Xmin = -4.0
      Xmax = 50.0
      Xsta = 0.0
      Xend = 45.0
      Nxtic = 9
      Nix = 2
      Ndx = 2
c
      end if
c
      CALL ZVIEW ( 0.0, 0.6, .12, 0.50 )
      CALL ZWIND (Xmin, Xmax, Ymin, Ymax)
c
      call zaxes ( Size, Base )
      width = 1000. * width
      CALL ZCSIZ ( width, height )
c
      start2 = bot1 * 1000
      stop2 = bot2 * 1000
c
c
      if (hope .eq. 1) then
c
      Xmin = start2 - (1000.0 * 4 * ban2 / 45.0)
      Xsta = start2
      Xend = stop2
      Xmax = stop2 + (1000.0 * 5 * ban2 / 45.0)
c
      else
```

```
c
      Xmin = - 4000.0
      Xend = 45000.0
      Xsta = 0
      Xmax = 50000.0
c
      end if
c
      CALL ZWIND ( Xmin, Xmax, Ymin, Ymax )
c
      Xpos = start2
      Ypos = v(2,start2)
c
      CALL ZMOVE ( Xpos, Ypos )
c
      if (hope .eq. 1) then
c     if (rep2 .eq. 'Y' .or. rep2 .eq. 'y') then
c
      do i = start2, stop2, 1
         Xpos = i
         Ypos = v(2,i)
         CALL ZDRAW (Xpos, Ypos)
      end do
c
      else
c
      do i = 1, 45000, 1
         Xpos = i
         Ypos = v(2,i)
         CALL ZDRAW ( Xpos, Ypos )
      end do
c
      end if
c
      call ZMOVE ( Xsta + 31 * width, Ymin )
      call ZTEXT ( 12, 12HTime, second)
      call ZMOVE ( Xsta + 3.0 * width, Yend )
      call ZTEXT ( 6, 6HSignal)
      call ZMOVE ( Xsta + 3.0 * width, Yend - height )
      call ZTEXT ( 16, 16HIntensity, Volt.)
      call ZMOVE ( Xend - 15.0 * width, Yend )
      call ZTEXT ( 8, 8HProbe #2)
c
      call ZDEND
      call ZEND
c
c
6500  continue
c
       if (boujc .eq. 1 .and. bouja .eq. 1) then
       go to 7000
       end if
c
c
c
c*************************************************************************
c Identification of the gas bubbles
c*************************************************************************
c
c*************************************************************************
c Criteria identification
c*************************************************************************
c
c *****************
```

```
c Interactive
c ******************
c
c     write(1,'(/" Enter Criteria 4 for channel 1 ?")')
c     read(1,'(f7.3)') cr(1), bob(1), bodya(1), bodyb(1)
c     write(1,'(/" Enter Criteria 1 to 4 for channel 2 ?")')
c     read(1,'(f7.3)') cr(2), bob(2), bodya(2), bodyb(2)
c
c ************************
c Non-interactive
c ************************
c
      cr(1) = 2.50
      cr(2) = 2.50
      bob(1) = 5.0
      bob(2) = 5.0
      bodya(1) = 0.75
      bodya(2) = 0.75
      bodyb(1) = 2.5/1000.
      bodyb(2) = 2.5/1000.
c
c
c  ***************************************************************************
c Counting gas bubbles
c  ***************************************************************************
c
       write(1,'(/" ***** Counting gas bubbles *****")')
c
       do j=1,2
       l(j) = 0
       maxint(j)=0
       Ndu(j)=0
       Nb(j)=0
       i = 1
c
c
1010   continue
c
c
       i = i + 1
       if (i .gt. 50000) go to 1030
       slope1 = ((v(j,i)-v(j,i-1))/0.001)
       if (slope1 .le. cr(j)) go to 1010
c
       if (slope1 .gt. bob(j)) then
       Nsta = i-1
       go to 1020
       end if
c
       i = i + 1
       if (i .gt. 50000) go to 1030
       if (v(j,i) .le. v(j,i-1)) go to 1010
       slope2 = (v(j,i) - v(j,i-2)) / 0.002
       if (slope2 .le. (bob(j)/2)) go to 1010
       Nsta = i-2
       i = i - 1
c
c
1020   continue
c
c
       i = i + 1
       if (i .gt. 50000) go to 1040
       slope3 = (v(j,i) - v(j,i-1)) / 0.001
```

```
      if (slope3 .gt. 0) go to 1020
      top = i - 1
c
c
1024  continue
c
c
      i = i + 1
      if (i .gt. 50000) go to 1040
      slope4 = (v(j,i) - v(j,i-1)) / 0.001
      if (slope4 .lt. 0) go to 1024
      if ((v(j,top) - v(j,Nsta)) .gt.  0.1) then
        if (v(j,i-1).gt.(v(j,top)-(bodya(j)*v(j,top))))go to 1024
      else
        if (v(j,i-1) .gt. (v(j,Nsta) + bodyb(j))) go to 1024
      end if
c
c
1040  continue
c
c
      Nsto = i - 1
      Nb(j) = Nb(j) + 1
      Ndu(j) = Ndu(j) + (Nsto-Nsta)
c
      if (bouja .eq. 0) then
c
      if (j .eq. 1) then
c
       if (Nsta .ge. (bot1 * 1000) .and. Nsta .le. (bot2 * 1000)) then
       l(j) = l(j) + 1
       fst(j,l(j)) = Nsta
       end(j,l(j)) = Nsto
       end if
c
      else
c
       if (Nsta .ge. (bot1*1000) .and. Nsta .le. (bot2*1000)) then
       l(j) = l(j) + 1
       fst(j,l(j)) = Nsta
       end(j,l(j)) = Nsto
       end if
c
      end if
      end if
c
      int(j,Nb(j))=0
c
      do k = Nsta, Nsto
c
      if (v(j,k) .gt. int(j,Nb(j))) then
      int(j,Nb(j)) = v(j,k)
      else
      int(j,Nb(j))=int(j,Nb(j))
      end if
c
      end do
c
      cont(j,Nb(j))=(Nsto-Nsta)
c
      if (int(j,Nb(j)) .gt. maxint(j)) then
      maxint(j) = int(j,Nb(j))
      else
      maxint(j) = maxint(j)
```

```
      end if
c
      i = i - 1
      go to 1010
c
c
c
1030  continue
c
c
c
      end do
c
c
c**********************************************************************
c Check
c**********************************************************************
c
      if (boujc .eq. 1) then
      goto 5000
      end if
c
c  ********************************************************************
c Calculating porosity
c  ********************************************************************
c
      write(1,'(/" ***** Calculating porosity *****")')
      do j=1,2
      poro(j) = Ndu(j) / 50000
      freq(j) = Nb(j) /50.
      avgdur(j) = Ndu(j)/(Nb(j)*1000)
      end do
c
c  ********************************************************************
c Signal intensity distribution analysis
c  ********************************************************************
c
c     write(1,'(/" ** Performing Signal distribution analysis **")')
c
c     do j = 1,2
c     y(j) = maxint(j) / 20
c
c     do k=1,20
c     contr(j,k) = 0
c     pox(j,k) = 0
c     end do
c
c    do k = 1, Nb(j)
c
c     if (int(j,k) .ge. 0 .and. int(j,k) .lt. y(j)) then
c     contr(j,1) = contr(j,1) + cont(j,k)
c     pox(j,1) = pox(j,1) + 1
c     else
c
c     if (int(j,k).ge.y(j).and.int(j,k).lt.(2*y(j)))then
c     contr(j,2) = contr(j,2) + cont(j,k)
c     pox(j,2) = pox(j,2) + 1
c     else
c
c     if(int(j,k).ge.(2*y(j)).and.int(j,k).lt.(3*y(j)))then
c     contr(j,3) = contr(j,3) + cont(j,k)
c     pox(j,3) = pox(j,3) + 1
c     else
c
```

```
c     if(int(j,k).ge.(3*y(j)).and.int(j,k).lt.(4*y(j)))then
c     contr(j,4) = contr(j,4) + cont(j,k)
c     pox(j,4) = pox(j,4) + 1
c     else
c
c     if(int(j,k).ge.(4*y(j)).and.int(j,k).lt.(5*y(j)))then
c     contr(j,5) = contr(j,5) + cont(j,k)
c     pox(j,5) = pox(j,5) + 1
c     else
c
c     if(int(j,k).ge.(5*y(j)).and.int(j,k).lt.(6*y(j)))then
c     contr(j,6) = contr(j,6) + cont(j,k)
c     pox(j,6) = pox(j,6) + 1
c     else
c
c     if (int(j,k).ge.(6*y(j)).and.int(j,k).lt.(7*y(j)))then
c     contr(j,7) = contr(j,7) + cont(j,k)
c     pox(j,7) = pox(j,7) + 1
c     else
c
c     if (int(j,k).ge.(7*y(j)).and.int(j,k).lt.(8*y(j)))then
c     contr(j,8) = contr(j,8) + cont(j,k)
c     pox(j,8) = pox(j,8) + 1
c     else
c
c     if (int(j,k).ge.(8*y(j)).and.int(j,k).lt.(9*y(j)))then
c     contr(j,9) = contr(j,9) + cont(j,k)
c     pox(j,9) = pox(j,9) + 1
c     else
c
c     if (int(j,k).ge.(9*y(j)).and.int(j,k).lt.(10*y(j)))then
c     contr(j,10) = contr(j,10) + cont(j,k)
c     pox(j,10) = pox(j,9) + 1
c     else
c
c     if(int(j,k).ge.(10*y(j)).and.int(j,k).lt.(11*y(j)))then
c     contr(j,11) = contr(j,11) + cont(j,k)
c     pox(j,11) = pox(j,11) + 1
c     else
c
c     if(int(j,k).ge.(11*y(j)).and.int(j,k).lt.(12*y(j)))then
c     contr(j,12) = contr(j,12) + cont(j,k)
c     pox(j,12) = pox(j,12) + 1
c     else
c
c     if(int(j,k).ge.(12*y(j)).and.int(j,k).lt.(13*y(j)))then
c     contr(j,13) = contr(j,13) + cont(j,k)
c     pox(j,13) = pox(j,13) + 1
c     else
c
c     if(int(j,k).ge.(13*y(j)).and.int(j,k).lt.(14*y(j)))then
c     contr(j,14) = contr(j,14) + cont(j,k)
c     pox(j,14) = pox(j,14) + 1
c     else
c
c     if(int(j,k).ge.(14*y(j)).and.int(j,k).lt.(15*y(j)))then
c     contr(j,15) = contr(j,15) + cont(j,k)
c     pox(j,15) = pox(j,15) + 1
c     else
c
c     if(int(j,k).ge.(15*y(j)).and.int(j,k).lt.(16*y(j)))then
c     contr(j,16) = contr(j,16) + cont(j,k)
c     pox(j,16) = pox(j,16) + 1
c     else
```

```
c
c     if(int(j,k).ge.(16*y(j)).and.int(j,k).lt.(17*y(j)))then
c     contr(j,17) = contr(j,17) + cont(j,k)
c     pox(j,17) = pox(j,17) + 1
c     else
c
c     if(int(j,k).ge.(17*y(j)).and.int(j,k).lt.(18*y(j)))then
c     contr(j,18) = contr(j,18) + cont(j,k)
c     pox(j,18) = pox(j,18) + 1
c     else
c
c     if(int(j,k).ge.(18*y(j)).and.int(j,k).lt.(19*y(j)))then
c     contr(j,19) = contr(j,19) + cont(j,k)
c     pox(j,19) = pox(j,19) + 1
c     else
c
c     if(int(j,k).ge.(19*y(j)).and.int(j,k).le.(20*y(j)))then
c     contr(j,20) = contr(j,20) + cont(j,k)
c     pox(j,20) = pox(j,20) + 1
c
c     end if
c     end if
c     end if
c     end if
c     end if
c     end if
c     end if
c     end if
c     end if
c     end if
c     end if
c     end if
c     end if
c     end if
c     end if
c     end if
c     end if
c     end if
c     end if
c     end if
c     end if
c     end do
c     end do
c
c
c ***************************************************************************
c Output results
c ***************************************************************************
c
      write(6,40) file
      do j=1,2
      write(6,50) j
50    format(///,25x, '******** Probe No :', i2, ' ********',/)
      write(6,52) bs(j)
52    format(//,15x, '***** Average intensity:',f9.6, ' volts *****')
      write(6,53) cr(j)
      write(6,54) bob(j)
      write(6,55) bodya(j)
      write(6,51) bodyb(j)
53    format(/,15x,'******** Criteria 1 : ',f7.4, ' ********')
54    format(/,15x,'******** Criteria 2 : ',f7.4, ' ********')
55    format(/,15x,'******** Criteria 3 : ',f7.5, ' ********')
51    format(/,15x,'******** Criteria 4 : ',f7.5, ' ********')
      write(6,56) Nb(j)
56    format(/,15x,'** Total number of bubbles detected :',i6 ' **')
```

```
      write(6,57) avgdur(j)
57    format(/,15x,'**** Average bubble duration :',f9.6, ' s ****')
      write(6,58) poro(j)
58    format(/,15x,'******** Gas porosity :', f9.6, ' ********')
      write(6,60) freq(j)
60    format(/,15x,'******* Bubble frequency : ',f9.6,' 1/s *******')
      end do
c
c
c     write(6,12)
c     write(6,40) file
c     do j=1,2
c     write (6,50) j
c     vf(j,0)=0
c     do k=1,20
c     vf(j,k) = (y(j) / 2) + vf(j,k-1)
c     contr(j,k)=contr(j,k)/50000
c     contr(j,k) = (contr(j,k)/poro(j)) * 100
c     write(6,70) vf(j,k), contr(j,k), pox(j,k)
c70   format( 4x,  ' * Intensity: ',  f6.3, 2x, '  * Holdup: ', f6.3,
c    $'   * Nb. of bubbles: ',i5)
c     end do
c     end do
c
c ***************************************************************************
c Criteria Check Display
c ***************************************************************************
c
5000   continue
c
c
c ***************************************************************************
c Check
c ***************************************************************************
c
       if (bouja .eq. 1) then
       goto 7000
       end if
c
c**************************************************************************
c
      write(6,40) file
c
      do j=1,2
      write(6,50) j
c
      do i=1,l(j)
      write(6,92) i, fst(j,i), end(j,i)
92    format(15x,' ** Bubble # ',i2,2x,'  ** Start: ',i5,2x,
     $'  ** End: ',i5)
      end do
      end do
c
7000  OPTION = 140000B
      CALL LURQ (OPTION, LUARY, NUMLUS)
c
      stop
      end
```

CROSS

FIBRE OPTIC SENSORS

CROSS CORRELATION ANALYSIS

```
ftn7x,l,s
$sma /big/
$cds on
$files 0,2
c
c @Copyright Julie Chabot fall 1991
c
c ***************************************************************************
c This program was developed to perform cross correlation calculation
c forward and backward with a wide flexibility of time lag selection
c and to perform the auto-correlation analysis for each spectrum
c for a frequency of data acquisition of 1000 points/second-channel.
c ***************************************************************************
c
c ***************************************************************************
c Variables identification.
c ***************************************************************************
c
      program Cross
      integer VmaRead, iend, acqui
      integer FmpOpen, FmpClose, idcb (144), OPTION, LUARY(2), NUMLUS
      integer FmpworkingDir, FmpBuildPath, Vmaopen
      integer IASC(5), ii, bouja, boujb, boujc, boujd
      integer Ns, lu, contrl, name(8)
      integer head(1024), skipdata(1024), iv(2,46080), iblocks, Ninj
      integer*4 Np, Ne, Na, i, ia, lag1, lag2, lag3, k
      integer*4 ilen, i1, i2, j, space1, space2, space3
      integer  Nxtic, Nix, Ndx, Nytic, Niy, Ndy
      real Rxymax, Ryxmax, Rxxmax
      real gmax, kmax
      real v(2,45100), Rxy(45000), Ryx(45000), Cxy(0:50), Qxy(0:50)
      real Rxx(2,5000)
      real par, dum, dumx, dumy, b(1024), Ga(50), tau(50)
      real Grate, deno
      real f(2,55), pb(2,0:36), var(2), bs(2)
      real Xpos, Ypos, width, height, size, base, pos
      real Xmin, Xsta, Xend, Xmax, Xsp, ban1, gur1
      real Ymin, Ysta, Yend, Ymax, Ysp
      complex*8 Gxy(0:511)
      character*1 apos, ans, answ, rep1, rep2, answ1, answ2
      character*1 answ3, answ4
      character*8 open_opt
      character*16 file, file_out, null, file_or
      character*64 dir, filedesc, dirpath
      common/big/ head, iv, v, Rxy, Ryx, Rxx, deno, var
      common /Xaxis/ Xmin, Xsta, Xend, Xmax, Nxtic, Nix, Ndx, Xsp
      common /Yaxis/ Ymin, Ysta, Yend, Ymax, Nytic, Niy, Ndy, Ysp
      common /Fback/ width, height
      data iblocks /904/, lu /6/, contrl /400b/, Np /45000/
      data null /'                '/
c
c ***************************************************************************
c Data file retrieving.
c ***************************************************************************
c
      call fparm ( file )
c
      ENCODE ( 16, 5, name ) file
5     format ( a16 )
c
      if ( file .lt. null ) then
          write (1,'(//" Enter name of the data file !")')
          read (1,'(a16)') file
      end if
```

```
c
      iend = index ( file, ' ')
c
c ***************************************************************************
c Data verification.
c ***************************************************************************
c
      ierror = FmpworkingDir (dir)
      iend_dir = index (dir,' ')
      dirpath = dir (1:iend_dir-1) // '/'
      call FmpBuildPath (filedesc, dirpath, file, 'DAT', ' ',
     *0, 2, iblocks, 1024, ' ')
c
c     open_opt = 'rwxou'
c     call Vmaopen ( ierror, filedesc, open_opt )
c     write (1,*) '*** VmaOpen ierror = ', ierror
c
      open_opt = 'orwf'
      call FmpOpen (idcb, ierror, filedesc, open_opt, 1)
      write (1,*) '*** FmpOpen ierror = ', ierror
c
      ilen = VmaRead (idcb, ierror, head, 2048)
      write (1,*) '***** ierror = ',ierror
      write (1,*) '*** Total number of bytes read = ',ilen
c
      ilen = VmaRead (idcb, ierror, skipdata, 2048)
      write (1,*) '***** ierror = ',ierror
      write (1,*) '*** Total number of bytes read = ',ilen
c
      do j = 1, 9
      ia = (j-1) * 5120. + 1
      ilen = VmaRead (idcb, ierror, iv(1,ia), 20480)
      write (1,*) '******** ierror = ',ierror
      write (1,*) '***** Total number of bytes read = ',ilen
      end do
c
      ierror = FmpClose (idcb, ierror)
c
c ***************************************************************************
c Data reading and conversion.
c ***************************************************************************
c
c
c     factor for converting raw data into volt.
c
      factor = 5./(16.*8.*1000.)
c
c
      write (1, '(/"  *****  Converting Data  *****")')
      do i = 1, 50000
          do j= 1, 2
              dum = iv (j,i) * factor
              v(j,i) = ABS (dum)
          end do
      end do
c
c ***************************************************************************
c Baseline selection.
c ***************************************************************************
c
      do j = 1, 2
          bs(j) = 0.
          do i = 1, 50000
              bs(j) = bs(j) + v(j,i)
```

```
            end do
            bs(j) = bs(j) / 50000
        end do
c
        do j = 1, 2
            var(j) = 0.
            do i = 1, 50000
                var(j) = var(j) + ((v(j,i) - bs(j)) ** 2)
            end do
            var(j) = var(j) / 50000.
        end do
c
        deno = SQRT ( var(1) * var(2) )
        write(1,*) deno
c
12      format('1')
40      format(//,17x,'******** Filename : ',a16, ' ********')
c
c  ***************************************************************************
c Information
c  ***************************************************************************
c
        write (1,'(/"What was the data acquisition frequency ?")')
        read (1,'(i5)') acqui
c
        bouja = 0
        write (1,'(/"Do you want cross correlation FORWARD ?")')
        read (1, '(a1)') answ1
        if (answ1 .eq. 'N' .or.  answ1 .eq. 'n' ) then
        bouja = 1
        end if
c
        if (bouja .eq. 0) then
        write (1,'(/"Enter the total time lag to be used ?")')
        read (1, '(i5)') lag1
        write (1,'(/"Enter the resolution ?")')
        read (1, '(i5)') space1
        end if
c
        boujb = 0
        write (1,'(/"Do you want cross correlation BACKWARD ?")')
        read (1, '(a1)') answ2
        if (answ2 .eq. 'N' .or. answ2 .eq. 'n') then
        boujb = 1
        end if
c
        if (boujb .eq. 0) then
        write (1,'(/"Enter the total time lag to be used ?")')
        read (1, '(i5)') lag2
        write (1,'(/"Enter the resolution ?")')
        read (1, '(i5)') space2
        end if
c
        boujc = 0
        write (1,'(/"Do you want cross spectral analysis ?")')
        read (1, '(a1)') answ3
        if (answ3 .eq. 'N' .or. answ3 .eq. 'n') then
        boujc = 1
        end if
c
        boujd=0
        write (1,'(/"Do you want auto-correlation analysis?")')
        read (1, '(a1)') answ4
        if (answ4 .eq. 'N' .or. answ4 .eq. 'n') then
```

```
      boujd = 1
      end if
c
      if (boujd .eq. 0) then
      write (1,'(/"Enter the total time lag to be used ?")')
      read (1, '(i5)') lag3
      write (1,'(/"Enter the resolution ?")')
      read (1, '(i5)') space3
      end if
c
      if (bouja .eq. 1) then
      go to 2000
      end if
c
c
c ***************************************************************************
c Cross correlation calculation.
c ***************************************************************************
c
      write (1,'(/" *** Calculating Cross Correlation Function ***")')
c
c ***************************************************************************
c Calculating the cross correlation function (forward)
c ***************************************************************************
c
      write (1, '(/" *** Forward ***")')
c
c
      k = 0
      Rxy(k) = 0.
      do i = 1, (50000)
          Rxy(k) = Rxy(k) + ((v(1,i)-bs(1)) * (v(2,i+k)-bs(2)))
      end do
      Rxy(k) = abs(Rxy(k) / ((50000) * deno))
      write(1,*) Rxy(k)
1000  continue
      k = k + space1
      Rxy(k) = 0.
      do i = 1, (50000 - k)
          Rxy(k) = Rxy(k) + ((v(1,i)-bs(1)) * (v(2,i+k)-bs(2)))
      end do
      Rxy(k) = abs(Rxy(k) / ((50000 - k) * deno))
      write(1,*) Rxy(k)
c
c***************************************************************************
c Check
c***************************************************************************
c
      if ( k .lt. lag1) then
      go to 1000
      end if
c
      Rxymax = Rxy(0)
      kmax = 0
      do k = 0, lag1, space1
      if (Rxymax .lt. Rxy(k)) then
      Rxymax = Rxy(k)
      kmax = k
      else
      kmax = kmax
      Rxymax = Rxymax
      end if
      end do
c
```

```
c
2000  continue
c
c
c
      if (boujb .eq. 1) then
      go to 3000
      end if
c
c
c ***************************************************************************
c Calculating cross correlation function (Backward)
c ***************************************************************************
c
      write(1,'(/" *** Backward ***")')
c
      g = 0
      Ryx(g) = 0
      do i = 1, (50000)
         Ryx(g) = Ryx(g) + ((v(1,i+g)-bs(1)) * (v(2,i)-bs(2)))
      end do
      Ryx(g) = abs(Ryx(g) / ((50000) * deno))
      write(1,*) Ryx(g)
1001  continue
      g = g + space2
      Ryx(g) = 0
      do i=1, (50000 - g)
      Ryx(g) = Ryx(g) + ((v(1,i+g)-bs(1)) * (v(2,i)-bs(2)))
      end do
      Ryx(g) = abs(Ryx(g) /((50000 - g) * deno))
      write(1,*) Ryx(g)
c
c***************************************************************************
c Check
c***************************************************************************
c
c
      if (g .lt. lag2) then
      go to 1001
      end if
c
      Ryxmax = Ryx(0)
      gmax = 0
      do g = 0, lag2, space2
      if(Ryxmax .lt. Ryx(g)) then
      Ryxmax = Ryx(g)
      gmax = g
      else
      Ryxmax = Ryxmax
      gmax = gmax
      end if
      end do
c
3000  continue
c
c
c
      if (boujc .eq. 1) then
      go to 4000
      end if
c
c
c  ***************************************************************************
c Calculating the cross spectral density function
```

```
c  ********************  ************************************************
c
      write (1,'(/"Calculating Cross Spectral density function")')
c
      par = 2 * 3.14159
c
      do k = 0, 50
          Cxy(k) = 0.
          do i = 0, lag1, space1
              Cxy(k) = Cxy(k) + Rxy(i) * COS (par*k*i*0.5*space1)
          end do
          Cxy(k) = Cxy(k) * ( 2 * space1)
c
          Qxy(k) = 0.
          do i = 0, lag1, space1
              Qxy(k) = Qxy(k) + Rxy(i) * SIN (par*k*i*0.5*space1)
          end do
          Qxy(k) = Qxy(k) * ( 2 * space1 )
      end do
c
      do i = 1, 50
          Ga(i) = SQRT ( (Cxy(i)**2) + (Qxy(i)**2) )
          rad = ATAN ( Qxy(i)/Cxy(i) )
          if ( rad .le. 0 ) rad = rad + 3.14159
          tau(i) = rad / ( 2 * 3.14159 * 0.5)
      end do
c
c
4000  continue
c
c
c
c ***************************************************************************
c Locking printer
c ***************************************************************************
c
      OPTION = 040001B
      LUARY(1) = 6
      NUMLUS = 1
c
      CALL LURQ (OPTION, LUARY, NUMLUS)
c
c
c
c
c
      write (1,'(/"Printer is locked")')
c
c ***************************************************************************
c
      if (boujd .eq. 1) then
      go  o 5000
      en . if
c
c***************************************************************************
c Autocorrelation analysis
c***************************************************************************
c
c
      write (1,'(/"Autocorrelation analysis")')
      do j=1,2
c
      do k = 0, lag3, space3
      Rxx(j,k) = 0
```

```
      do i = 1, (50000-k)
      Rxx(j,k) = Rxx(j,k) + ((v(j,i)-bs(j)) * (v(j,i+k)-bs(j)))
      end do
      Rxx(j,k) = abs(Rxx(j,k) / (50000-k))
      Rxx(j,k) = Rxx(j,k) / Rxx(j,0)
      write(1,*) j, k, Rxx(j,k)
      end do
      end do
c
c
c
5000  continue
c
c
c
      if (boujb .eq. 1 .and. bouja .eq. 1) then
      go to 6250
      end if
      if (boujb .eq. 1 .and. bouja .eq. 0) then
      write(1,'(/"Cross correlation function drawing (Forward)")')
      end if
      if (boujb .eq. 0 .and. bouja .eq. 0) then
      write (1,'(/"Cross correlation drawing (Both)")')
      end if
      if (bouja .eq. 1 .and. boujb .eq. 0) then
      write(1,'(/"Cross correlation function drawing (Backward)")')
      end if
c
c ***************************************************************************
c Cross correlation function drawing (Backward)
c ***************************************************************************
c
      call ZBEGN
      call ZDINT (LU, CONTkL, IERR)
      call ZASPK (0.6, 1.0)
      call ZDLIM (10.0, 180.0, 30.0, 265.0)
c
      if (boujb .eq. 1) then
      go to 6100
      end if
c
      Xmin = 0.0 - (0.1 * lag2)
      Xsta = 0.0
      Xend = lag2
      Xmax = lag2 + (0.1 * lag2)
      Nxtic = 5
      Nix = 5
      Ndx = 1
c
      Ymin = -0.25
      Ysta = 0.0
      Yend = 1.0
      Ymax = 1.1
      Nytic = 5
      Niy = 1
      Ndy = 1
c
      Size=0.5
      Base=1.0
c
      width = 1000 * width
      call ZCSIZ (width, height)
c
      call ZVIEW (0.0, 0.3, 0.55, 0.85)
```

```
      call ZWIND (Xmin, Xmax, Ymin, Ymax)
      call ZAXES (Size, Base)
      call ZWIND (Xmin, Xmax, Ymin, Ymax)
c
      Xpos = 0
      Ypos = Ryx(0)
      Call ZMOVE (Xpos, Ypos)
      do k = 0, lag2, space2
           Xpos=k
           Ypos=Ryx(k)
      Call ZDRAW (Xpos, Ypos)
      end do
c
      Call ZMOVE (Xsta + 25 * width, Ymin)
      Call ZTEXT (25, 25HTime Lag, ms ( Backward ))
      Call ZMOVE (Xsta + 8 * width, Yend - height)
      Call ZTEXT (3,3HRyx)
c
      if (bouja .eq. 1) then
      Call ZMOVE (Xsta + 15 * width, Ymax + height)
      Call ZTEXT (17, 17HCross Correlation)
      end if
c
c
6100  continue
c
c
c
      if (bouja .eq. 1) then
      go to 6200
      end if
c
c
      Xmin = 0.0 - (0.1 * lag1)
      Xsta = 0.0
      Xend = lag1
      Xmax = lag1 + (0.1 * lag1)
      Nxtic = 5
      Nix = 5
      Ndx = 1
c
      Ymin = -0.25
      Ysta = 0.0
      Yend = 1.0
      Ymax = 1.1
      Nytic = 5
      Niy = 1
      Ndy = 1
c
      Size = 0.5
      Base = 1.0
c
c
      width = 1000 * width
      call ZCSIZ (width, height)
c
      Call ZVIEW (0.30, 0.60, 0.55, 0.85)
      Call ZWIND (Xmin, Xmax, Ymin, Ymax)
      Call ZAXES (size, Base)
      Call ZWIND (Xmin, Xmax, Ymin, Ymax)
c
      Xpos = 0
      Ypos = Rxy(0)
      Call ZMOVE (Xpos, Ypos)
```

```
c
      do k = 0, lag1, space1
           Xpos = k
           Ypos = Rxy(k)
      Call ZDRAW (Xpos, Ypos)
      end do
c
      Call ZMOVE ( Xsta + 25 * width, Ymin )
      Call ZTEXT ( 24, 24HTime Lag, ms ( Forward ))
      Call ZMOVE ( Xsta + 8.0 * width, Yend - height )
      Call ZTEXT ( 3, 3HRxy)
c
      Call ZMOVE ( Xmin - 15 * width, Ymax + height )
      Call ZTEXT ( 17, 17HCross Correlation )

6200  continue
c
c
c
c ***************************************************************************
c Output file
c ***************************************************************************
c
       write(6,40) file
c
       if (bouja .eq. 0) then
       write(6,10) kmax, Rxymax
       end if
c
       if (boujb .eq. 0) then
       write(6,11) gmax, Ryxmax
       end if
c
10     format(//,' * Time lag (forward) : ',f9.5,' ms  *  C.C. :',f9.5)
11     format(//,' * Time lag (backward): ',f9.5,' ms  *  C.C. :',f9.5)
c
c
c
6250   continue
c
c
c
       if (boujc .eq. 1) then
       go to 6300
       end if
c
       write(1,'(/"Power spectra drawing")')
c
c ***************************************************************************
c Power spectra
c ***************************************************************************
c
c
      Xmin = -6.0
      Xsta = 0.0
      Xend = 50.0
      Xmax = 56.0
      Nxtic = 10
      Nix = 2
      Ndx = 0
c
      Ymin = -0.25
      Ysta = 0.0
      Yend = 1.0
```

```
      Ymax = 1.1
      Nytic = 5
      Niy = 1
      Ndy = 1
c
      CALL ZVIEW (0.0, 0.3, 0.20, 0.50)
      CALL ZWIND (Xmin, Xmax, Ymin, Ymax)
      CALL ZAXES (Size, Base)
c
      Xpos = 0
      Ypos = Ga(o)
      CALL ZMOVE (Xpos, Ypos)
      do k = 1,50
      Xpos = k
      Ypos = Ga(k)
      CALL ZDRAW (Xpos, Ypos)
      end do
c
      Call ZMOVE (Xsta + 25.0 * width, Ymin )
      Call ZTEXT (13, 13HFrequency, ms)
      Call ZMOVE (Xsta + 8.0 * width, Yend - height)
      Call ZTEXT (5,5HGx(f))
c
      Ymin = -0.0125
      Ysta = 0.0
      Yend = 0.05
      Ymax = 0.055
      Nytic = 5
      Niy = 1
      Ndy = 3
c
      call ZVIEW (0.3, 0.6, 0.20, 0.50)
      call ZWIND (Xmin, Xmax, Ymin, Ymax)
      call Zaxes (size, Base)
c
      Xpos = 0
      Ypos = Tau(0)
      Call ZMOVE (Xpos, Ypos)
      do k = 1,50
      Xpos = k
      Ypos = Tau(k)
      Call ZDRAW (Xpos, Ypos)
      end do
c
      Call ZMOVE (Xsta + 25.0 * width, Ymin )
      Call ZTEXT (13, 13HFrequency, ms)
      Call ZMOVE (Xsta + 8.0 * width, Yend - height)
      Call ZTEXT (16, 16HTime Lag, second)
      Call ZMOVE (Xmin - 15 * width, Ymax + height)
      Call ZTEXT (13,13HPower Spectra)
c
c
6300  continue
c
c
c
      call ZDEND
      call ZEND

c
c
      if (boujd .eq. 1) then
      go to 7000
      end if
```

```
c
c*************************************************************************
c Auto-correlation drawing
c*************************************************************************
c
c
      write(1,'(/"Auto-correlation drawing")')
c
      call ZBEGN
      call ZDINT (LU, CONTRL, IERR)
      call ZASPK (0.6, 1.0)
      call ZDLIM (10.0, 180.0, 30.0, 265.0)
c
      do j=1,2
c
      Xmin = 0.0 - (0.1 * lag3)
      Xsta = 0.0
      Xend = lag3
      Xmax = lag3 + (0.1 * lag3)
      Nxtic = 5
      Nix = 5
      Ndx = 1
c
      Ymin = -0.25
      Ysta = 0.0
      Yend = 1.0
      Ymax = 1.1
      Nytic = 5
      Niy = 1
      Ndy = 1
c
      Size = 0.5
      Base = 1.0
c
      width = 1000 * width
      call ZCSIZ (width, height)
c
      if (j .eq. 1) then
      call ZVIEW (0.0, 0.6, 0.10, 0.45)
      else
      call ZVIEW (0.0, 0.6, 0.50, 0.85)
      end if
c
      call ZWIND (Xmin, Xmax, Ymin, Ymax)
      call ZAXES (Size, Base)
      call ZWIND (Xmin, Xmax, Ymin, Ymax)
c
      Xpos = 0.0
      Ypos = Rxx(j,0)
      call ZMOVE (Xpos, Ypos)
c
      do k = 0, lag3, space3
      Xpos=k
      Ypos=Rxx(j,k)
      call ZDRAW (Xpos, Ypos)
      end do
c
c
      call ZMOVE (Xsta + 32.0 * width, Ymin)
      call ZTEXT (12, 12HTime Lag, ms)
      call ZMOVE (Xsta + 6 * width, Yend)
      call ZTEXT (3,3HRxx)
c
      end do
```

```
c
      call ZMOVE (Xmin + 60 * width, Yend - height)
      call ZTEXT (9, 9HChannel 1)
      call ZMOVE (Xmin + 60 * width, Yend - 17 * height)
      call ZTEXT (9, 9HChannel 2)
      call ZMOVE (Xmin + 40 * width, Ymax + height)
      call ZTEXT (16, 16HAuto-Correlation)

c
      write(6,40) file

c
      call ZDEND
      call ZEND
c
7000  OPTION = 140000B
      CALL LURQ (OPTION, LUARY, NUMLUS)
c
      stop
      end
```

BSIZE

FIBRE OPTIC SENSORS

BUBBLE CHORD LENGTH DISTRIBUTION ANALYSIS

```
ftn7x,l,s
$ema /big/
$cds on
$files 0,2
c
c Copyright Julie Chabot, May 1992
c  ***************************************************************************
c This program was created to perform bubble to bubble analysis
c and generate the bubble chord length distribution.
c  ***************************************************************************
c
c  ***************************************************************************
c Variables identification
c  ***************************************************************************
c
c
      program bsize
      integer VmaRead, iend, OPTION, LUARY(2), NUMLUS, skipdata(1024)
      integer FmpOpen, FmpClose, idcb (144)
      integer FmpworkingDir, FmpBuildPath, Vmaopen
      integer Nxtic, Nix, Ndx, Nytic, Niy, Ndy, IASC(5), ii
      integer lu, contrl, name(8), unit, lomin, lo(6000)
      integer head(1024), iv(2,55000), iblocks, dodo
      integer*4 i, ia, i1, i2, Ntot, b(2,5000,2)
      integer*4 ilen, bb(2,6000,50,2), icount(2),ic(2),x1,x2
      integer*4 Nsta, Nsto, m, j, k, ib, top, Nb(2)
      real v(2,50000), mx(2), area(2), ma, mb
      real dum, var(2), vari(2), sdv(2), tm(2), dmean
      real Vind(2), tdu(2), chord(6000), Ndut(2)
      real bs(2), cr(2), dm(2), supvel, window
      real bou, du(2), tsta(2), tend(2), a(155), fra
      real mtdu(2,50), mtsta(2,50), mtend(2,50), mbou(50)
      real mdu(2,50), gromin, gro(50), ver(6000), mdev1(50), mdev2(50)
      real mdev3(50), dev1, dev2, dev3, poro(2), slope4
      real dada, dar, w, bodya(2), bodyb(2), totaldur, avgdur
      real Xpos, Ypos, width, height, size, base, siz, avgcd, totalcd
      real Xmin, Xsta, Xend, Xmax, Ymin, Ysta, Yend, Ymax
      real bob(2), slope1, slope2, slope3, h, factor
      character*1 apos, ans, pp
      character*8 open_opt
      character*16 file, file_out, null, file_or
      character*64 dir, filedesc, dirpath
      common/big/head,iv,v,bb,b,Ndut,z,Rxy,chord,a,Nb,lo,ver
     $w,dar,dada,siz, cr, bob, bodya, bodyb, slope4, slope3, slope2
     $slope1, fra, avgdur, totaldur, avgcd, totalcd
      common /Xaxis/ Xmin, Xsta, Xend, Xmax, Nxtic, Nix, Ndx
      common /Yaxis/ Ymin, Ysta, Yend, Ymax, Nytic, Ndy, Niy
      common /Fback/ width, height
      data iblocks /904/, lu /6/, contrl /400b/
      data null /'                '/
c
c
*******************************************************************************
c Data file information
c
*******************************************************************************
c
      call fparm ( file )
c
      ENCODE ( 16, 5, name ) file
5     format ( a16 )
c
      iend = index ( file, ' ')
c
```

```
c  ***************************************************************** *********
c Data retrieving
c  ***************************************************************************
c
      ierror = FmpworkingDir (dir)
      iend_dir = index (dir,' ')
      dirpath = dir (1:iend_dir-1) // '/'
      call FmpBuildPath (filedesc, dirpath, file, 'DAT', ' ',
     *0, 2, iblocks, 1024, ' ')
c
      open_opt = 'orwf'
      call FmpOpen (idcb, ierror, filedesc, open_opt, 1)
      write (1,*) '**  FmpOpen ierror = ', ierror
c
      ilen = VmaRead (idcb, ierror, head, 2048)
      write (1,*) '***** ierror = ',ierror
      write (1,*) '*** Total number of bytes read = ',ilen
c
      ilen = VmaRead (idcb, ierror, skipdata, 2048)
      write (1,*) '***** ierror = ',ierror
      write (1,*) '*** Total number of bytes read = ',ilen
c
      do j = 1, 10
      ia = (j-1) * 5120. + 1
      ilen = VmaRead (idcb, ierror, iv(1,ia), 20480)
      write (1,*) '******** ierror = ',ierror
      write (1,*) '***** Total number of bytes read = ',ilen
      end do
c
      ia = 10. * 5120. + 1
      ilen = VmaRead (idcb, ierror, iv(1,ia), 15200)
      write (1,*) '******** ierror = ',ierror
      write (1,*) '***** Total number of bytes read = ', ilen
c
      ierror = FmpClose (idcb, ierror)
c
c  ***************************************************************************
c Data reading and conversion
c  ***************************************************************************
c
c     factor for converting raw data into mV
c
      factor = 5./(16.*8.*1000)
      totaldur = 0.0
      totalcd = 0.0
c
      write (1, '(/" ***** Enter average bubble velocity ? *****")')
      read(1,'(f8.2)') supvel
c
      write (1, '(/" *****  Spectrum analysis  *****")')
c
      do i=1,50000
       do j=1,2
        dum=iv(j,i) * factor
        v(j,i)=ABS(dum)
       end do
      end do
c
      do j=1,2
       bs(j)=0
       do i=1,50000
       bs(j) = bs(j) + v(j,i)
       end do
      bs(j) = bs(j) / 50000
```

```
      end do
c
      do j=1,2
       var(j)=0
       do i=1,50000
       var(j) = var(j) + ((v(j,i) - ba(j)) ** 2)
       end do
      var(j) = var(j) /50000
      end do
c
c  ***************************************************************************
c Criteria identification
c  ***************************************************************************
c
      cr(1) = 2.50
      cr(2) = 2.50
c
      bob(1) = 5.0
      bob(2) = 5.0
c
      bodya(1) = 0.75
      bodya(2) = 0.75
c
      bodyb(1) = 2.5/1000.
      bodyb(2) = 2.5/1000.

c
c  ***************************************************************************
c Counting gas bubbles
c  ***************************************************************************
c
c
      write (1, '(/" *****  Counting Bubbles  *****")')
c
      do j = 1, 2
      Ndut(j)=0
      Nb(j) = 0
      i = 1
c
c
1010  continue
c
c
      i = i + 1
      if (i .gt. 50000) go to 1030
      slope1 = ((v(j,i)-v(j,i-1))/0.001)
      if (slope1 .le. cr(j)) go to 1010
c
      if (slope1 .gt. bob(j)) then
      Nsta = i-1
      go to 1020
      end if
c
      i = i + 1
      if (i .gt. 50000) go to 1030
      if (v(j,i) .le. v(j,i-1)) go to 1010
      slope2 = (v(j,i) - v(j,i-2)) / 0.002
      if (slope2 .le. (bob(j)/2)) go to 1010
      Nsta = i-2
      i = i - 1
c
c
1020  continue
c
```

```
c
      i = i + 1
      if (i .gt. 50000) go to 1040
      slope3 = (v(j,i) - v(j,i-1)) / 0.001
      if (slope3 .gt. 0) go to 1020
      top = i - 1
c
c
1024  continue
c
c
      i = i + 1
      if (i .gt. 50000) go to 1040
      slope4 = (v(j,i) - v(j,i-1)) / 0.001
      if (slope4 .lt. 0) go to 1024
      if ((v(j,top) - v(j,Nsta)) .gt. 0.1) then
         if (v(j,i-1) .gt. (v(j,top)-(bodya(j)*v(j,top)))) go to 1024
      else
         if (v(j,i-1) .gt. (v(j,Nsta) + bodyb(j))) go to 1024
      end if
c
c
1040  continue
c
c
      Nsto = i - 1
      Nb(j) = Nb(j) + 1
      Ndut(j) = Ndut(j) + (Nsto - Nsta)
      b(j,Nb(j),1) = Nsta
      b(j,Nb(j),2) = Nsto
c
c
      i = i - 1
      go to 1010
c
c
1030  continue
c
c
      end do
c
      do j=1,2
      poro(j) = Ndut(j) /50000
      end do
c
      write(1, '(/" ***** Bubbles Screening *****")')
c
      write(1,*) Nb(1), poro(1)
      write(1,*) Nb(2), poro(2)
c
      window = (500/(supvel/3.0))
      dodo = nint(window)
      m = 1
      do x1= 1, Nb(1)
          ver(m) = 0
          do x2 = 1, Nb(2)
              if ( b(2,x2,1) .GT. b(1,x1,1) ) then
                  if ( (b(2,x2,1)-dodo) .LT. b(1,x1,1) ) then
                      ver(m) = ver(m) + 1
                      bb(1,m,ver(m),1) = b(1,x1,1)
                      bb(1,m,ver(m),2) = b(1,x1,2)
                      bb(2,m,ver(m),1) = b(2,x2,1)
                      bb(2,m,ver(m),2) = b(2,x2,2)
                  end if
```

```
                end if
            end do
        m = m + 1
        end do
c
c  ***************************************************************************
c Locking printer
c  ***************************************************************************
c
        OPTION = 040001B
        LUARY(1) = 6
        NUMLUS = 1
c
        CALL LURQ (OPTION, LUARY, NUMLUS)
c
c  ***************************************************************************
c
c***************************************************************************
c Comparing bubbles
c***************************************************************************
c
        write (1, '(/" ***** Comparing bubbles *****")')
c
        w=0
c       write(1,'(/" ***** Do you want detail output ? *****")')
c       read (1,'(a1)') pp
c
        do i = 1, m
        lo(i) = 0
c
        if (ver(i) .eq. 0) then
        go to 6000
        end if
c
        do k = 1, ver(i)
c
            do j = 1, 2
                du(j) = bb(j,i,k,2) - bb(j,i,k,1)
                tsta(j)=bb(j,i,k,1)/1000.
                tend(j)=bb(j,i,k,2)/1000.
                tdu(j)=du(j)/1000.
                tm(j)=(bb(j,i,k,2) + bb(j,i,k,1)) /(2.*1000.)
            end do
c
            bou=tm(2)-tm(1)
            if (bou .eq. 0) then
            go to 2111
            end if
            if ((tsta(2)-tsta(1)) .eq. 0) then
            go to 2111
            end if
c
            if ( du(1) .GT. du(2) ) then
                dev1 = 1.0 - du(2)/du(1)
            else
                dev1 = 1.0 - du(1)/du(2)
            end if
c
            if ( dev1 .LT. 0.1 ) then
c
                do j = 1, 2
                    mx(j) = 0.0
                    vari(j)=0
                    do i1 = bb(j,i,k,1), bb(j,i,k,2)
```

```
                        if (v(j,il) .gt. mx(j)) then
                        mx(j) = v(j,il)
                        end if
                        vari(j) = vari(j) + v(j,il)
                    end do
                    vari(j) = vari(j)/du(j)
c
                    sdv (j) = vari(j)/bs(j)
                end do
c
                if ( sdv(1) .GT. sdv(2) ) then
                    dev2 = 1.0 - sdv(2)/sdv(1)
                else
                    dev2 = 1.0 - sdv(1)/sdv(2)
                end if
c
                if ( dev2 .LT. 0.1 ) then
c
                    ma = mx(1) / bs(1)
                    mb = mx(2) / bs(2)
                    if ( ma .GT. mb ) then
                        dev3 = 1.0 - mb/ma
                    else
                        dev3 = 1.0 - ma/mb
                    end if
                    if ( dev3 .LT. 0.1 ) then
c
                            lo(i) = lo(i) + 1
                            mdu(1,lo(i)) = du(1)
                            mdu(2,lo(i)) = du(2)
                            mtdu(1,lo(i)) = tdu(1)
                            mtdu(2,lo(i)) = tdu(2)
                            mtsta(1,lo(i)) = tsta(1)
                            mtsta(2,lo(i)) = tsta(2)
                            mtend(1,lo(i)) = tend(1)
                            mtend(2,lo(i)) = tend(2)
                            mdev1(lo(i)) = dev1
                            mdev2(lo(i)) = dev2
                            mdev3(lo(i)) = dev3
                            mbou(lo(i)) = bou
                            bb(1,i,lo(i),1) = bb(1,i,k,1)
                            bb(2,i,lo(i),1) = bb(2,i,k,1)
                            bb(1,i,lo(i),2) = bb(1,i,k,2)
                            bb(2,i,lo(i),2) = bb(2,i,k,2)
c
c
                        end if
                    end if
                end if
c
 111  continue
      end do
c
                            if (lo(i) .lt. 1) then
                            go to 6000
                            end if
c
                            do j = 1, lo(i)
                            gro(j) = mdev1(j)+mdev2(j)+mdev3(j)
                            gro(j) = gro(j) / 3
                            end do
c
                            gromin = gro(1)
                            lomin = 1
```

```
c
                              do j = 1, lo(i)
                              if (gro(j) .lt. gromin) then
                              gromin = gro(j)
                              lomin = j
                              else
                              gromin = gromin
                              lomin = lomin
                              end if
                              end do
c
c
                              do j = 1,2
                              du(j) = mdu(j, lomin)
                              tdu (j) = mtdu(j,lomin)
                              tsta(j) = mtsta(j,lomin)
                              tend(j) = mtend(j,lomin)
                              bb(j,i,k,1) = bb(j,i,lomin,1)
                              bb(j,i,k,2) = bb(j,i,lomin,2)
                              end do
                              bou = mbou(lomin)
c
c
                              w = w + 1
c
                              Vind(1)=0.5*1000/(bb(2,i,k,1)-bb(1,i,k,1))
                              Vind(2) = 0.5 / bou
                              dmean =  du(1)
                              totaldur=totaldur+dmean
                              chord(w) = 0
                              do j = 1, 2
                                  dm(j) = dmean * Vind(j) / 1000.0
                                  chord(w) = chord(w) + dm(j)
                              end do
                              chord(w) = chord(w)/2
                              totalcd = totalcd + chord(w)
c
c                         if (pp .eq. 'N' .or. pp .eq. 'n') then
c                         go to 6000
c                         end if
c
c                         call output(file,w,Vind,dm,tsta,tend,tdu)
c
c
6000                      continue
c
c
c
      end do
c
c
c
      dar = w / Nb(1)
      dada = dar * 100.0
      avgdur=totaldur/(w*1000)
      avgcd=totalcd/w
c
c
      do j = 1, 153
      a(j) = 0.0
      end do
c
      do j = 1, w
c
```

```
if (chord(j) .ge. 0 .and. chord(j) .lt. 0.02) then
a(1) = a(1) + 1
else
if (chord(j) .ge. 0.02 .and. chord(j) .lt.  0.04) then
a(2) = a(2) + 1
else
if (chord(j) .ge. 0.04 .and. chord(j) .lt. 0.06) then
a(3) = a(3) + 1
else
if (chord(j) .ge. 0.06 .and. chord(j) .lt. 0.08) then
a(4) = a(4) + 1
else
if (chord(j) .ge. 0.08 .and. chord(j) .lt. 0.1) then
a(5) = a(5) + 1
else
if (chord(j) .ge. 0.1 .and. chord(j) .lt. 0.12) then
a(6) = a(6) + 1
else
if (chord(j) .ge. 0.12 .and. chord(j) .lt. 0.14) then
a(7) = a(7) + 1
else
if (chord(j) .ge. 0.14 .and. chord(j) .lt. 0.16) then
a(8) = a(8) + 1
else
if (chord(j) .ge. 0.16 .and. chord(j) .lt. 0.18) then
a(9) = a(9) + 1
else
if (chord(j) .ge. 0.18 .and. chord(j) .lt. 0.2) then
a(10) = a(10) + 1
else
if (chord(j) .ge. 0.2 .and. chord(j) .lt. 0.22) then
a(11) = a(11) + 1
else
if (chord(j) .ge. 0.22 .and. chord(j) .lt. 0.24) then
a(12) = a(12) + 1
else
if (chord(j) .ge. 0.24 .and. chord(j) .lt. 0.26) then
a(13) = a(13) + 1
else
if (chord(j) .ge. 0.26 .and. chord(j) .lt. 0.28) then
a(14) = a(14) + 1
else
if (chord(j) .ge. 0.28 .and. chord(j) .lt. 0.3) then
a(15) = a(15) + 1
else
if (chord(j) .ge. 0.3 .and. chord(j) .lt. 0.32) then
a(16) = a(16) + 1
else
if (chord(j) .ge. 0.32 .and. chord(j) .lt. 0.34) then
a(17) = a(17) + 1
else
if (chord(j) .ge. 0.34 .and. chord(j) .lt. 0.36) then
a(18) = a(18) + 1
else
if (chord(j) .ge. 0.36 .and. chord(j) .lt. 0.38) then
a(19) = a(19) + 1
else
if (chord(j) .ge. 0.38 .and. chord(j) .lt. 0.4) then
a(20) = a(20) + 1
else
if (chord(j) .ge. 0.4 .and. chord(j) .lt. 0.42) then
a(21) = a(21) + 1
else
if (chord(j) .ge. 0.42 .and. chord(j) .lt. 0.44) then
```

```
a(22) = a(22) + 1
else
if (chord(j) .ge. 0.44 .and. chord(j) .lt. 0.46) then
a(23) = a(23) + 1
else
if (chord(j) .ge. 0.46 .and. chord(j) .lt. 0.48) then
a(24) = a(24) + 1
else
if (chord(j) .ge. 0.48 .and. chord(j) .lt. 0.5) then
a(25) = a(25) + 1
else
if (chord(j) .ge. 0.5 .and. chord(j) .lt. 0.52) then
a(26) = a(26) + 1
else
if (chord(j) .ge. 0.52 .and. chord(j) .lt. 0.54) then
a(27) = a(27) + 1
else
if (chord(j) .ge. 0.54 .and. chord(j) .lt. 0.56) then
a(28) = a(28) + 1
else
if (chord(j) .ge. 0.56 .and. chord(j) .lt. 0.58) then
a(29) = a(29) + 1
else
if (chord(j) .ge. 0.58 .and. chord(j) .lt. 0.6) then
a(30) = a(30) + 1
else
if (chord(j) .ge. 0.6 .and. chord(j) .lt. 0.62) then
a(31) = a(31) + 1
else
if (chord(j) .ge. 0.62 .and. chord(j) .lt. 0.64) then
a(32) = a(32) + 1
else
if (chord(j) .ge. 0.64 .and. chord(j) .lt. 0.66) then
a(33) = a(33) + 1
else
if (chord(j) .ge. 0.66 .and. chord(j) .lt. 0.68) then
a(34) = a(34) + 1
else
if (chord(j) .ge. 0.68 .and. chord(j) .lt. 0.7) then
a(35) = a(35) + 1
else
if (chord(j) .ge. 0.7 .and. chord(j) .lt. 0.72) then
a(36) = a(36) + 1
else
if (chord(j) .ge. 0.72 .and. chord(j) .lt. 0.74) then
a(37) = a(37) + 1
else
if (chord(j) .ge. 0.74 .and. chord(j) .lt. 0.76) then
a(38) = a(38) + 1
else
if (chord(j) .ge. 0.76 .and. chord(j) .lt. 0.78) then
a(39) = a(39) + 1
else
if (chord(j) .ge. 0.78 .and. chord(j) .lt. 0.8) then
a(40) = a(40) + 1
else
if (chord(j) .ge. 0.8 .and. chord(j) .lt. 0.82) then
a(41) = a(41) + 1
else
if (chord(j) .ge. 0.82 .and. chord(j) .lt. 0.84) then
a(42) = a(42) + 1
else
if (chord(j) .ge. 0.84 .and. chord(j) .lt. 0.86) then
a(43) = a(43) + 1
```

```
else
if (chord(j) .ge. 0.86 .and. chord(j) .lt. 0.88) then
a(44) = a(44) + 1
else
if (chord(j) .ge. 0.88 .and. chord(j) .lt. 0.9) then
a(45) = a(45) + 1
else
if (chord(j) .ge. 0.9 .and. chord(j) .lt. 0.92) then
a(46) = a(46) + 1
else
if (chord(j) .ge. 0.92 .and. chord(j) .lt. 0.94) then
a(47) = a(47) + 1
else
if (chord(j) .ge. 0.94 .and. chord(j) .lt. 0.96) then
a(48) = a(48) + 1
else
if (chord(j) .ge. 0.96 .and. chord(j) .lt. 0.98) then
a(49) = a(49) + 1
else
if (chord(j) .ge. 0.98 .and. chord(j) .lt. 1.0) then
a(50) = a(50) + 1
else
if (chord(j) .ge. 1.0 .and. chord(j) .lt. 1.02) then
a(51) = a(51) + 1
else
if (chord(j) .ge. 1.02 .and. chord(j) .lt. 1.04) then
a(52) = a(52) + 1
else
if (chord(j) .ge. 1.04 .and. chord(j) .lt. 1.06) then
a(53) = a(53) + 1
else
if (chord(j) .ge. 1.06 .and. chord(j) .lt. 1.08) then
a(54) = a(54) + 1
else
if (chord(j) .ge. 1.08 .and. chord(j) .lt. 1.1) then
a(55) = a(55) + 1
else
if (chord(j) .ge. 1.1 .and. chord(j) .lt. 1.12) then
a(56) = a(56) + 1
else
if (chord(j) .ge. 1.12 .and. chord(j) .lt. 1.14) then
a(57) = a(57) + 1
else
if (chord(j) .ge. 1.14 .and. chord(j) .lt. 1.16) then
a(58) = a(58) + 1
else
if (chord(j) .ge. 1.16 .and. chord(j) .lt. 1.18) then
a(59) = a(59) + 1
else
if (chord(j) .ge. 1.18 .and. chord(j) .lt. 1.2) then
a(60) = a(60) + 1
else
if (chord(j) .ge. 1.2 .and. chord(j) .lt. 1.22) then
a(61) = a(61) + 1
else
if (chord(j) .ge. 1.22 .and. chord(j) .lt. 1.24) then
a(62) = a(62) + 1
else
if (chord(j) .ge. 1.24 .and. chord(j) .lt. 1.26) then
a(63) = a(63) + 1
else
if (chord(j) .ge. 1.26 .and. chord(j) .lt. 1.28) then
a(64) = a(64) + 1
else
```

```
if (chord(j) .ge. 1.28 .and. chord(j) .lt. 1.3) then
a(65) = a(65) + 1
else
if (chord(j) .ge. 1.3 .and. chord(j) .lt. 1.32) then
a(66) = a(66) + 1
else
if (chord(j) .ge. 1.32 .and. chord(j) .lt. 1.34) then
a(67) = a(67) + 1
else
if (chord(j) .ge. 1.34 .and. chord(j) .lt. 1.36) then
a(68) = a(68) + 1
else
if (chord(j) .ge. 1.36 .and. chord(j) .lt. 1.38) then
a(69) = a(69) + 1
else
if (chord(j) .ge. 1.38 .and. chord(j) .lt. 1.4) then
a(70) = a(70) + 1
else
if (chord(j) .ge. 1.4 .and. chord(j) .lt. 1.42) then
a(71) = a(71) + 1
else
if (chord(j) .ge. 1.42 .and. chord(j) .lt. 1.44) then
a(72) = a(72) + 1
else
if (chord(j) .ge. 1.44 .and. chord(j) .lt. 1.46) then
a(73) = a(73) + 1
else
if (chord(j) .ge. 1.46 .and. chord(j) .lt. 1.48) then
a(74) = a(74) + 1
else
if (chord(j) .ge. 1.48 .and. chord(j) .lt. 1.5) then
a(75) = a(75) + 1
else
if (chord(j) .ge. 1.5 .and. chord(j) .lt. 1.52) then
a(76) = a(76) + 1
else
if (chord(j) .ge. 1.52 .and. chord(j) .lt. 1.54) then
a(77) = a(77) + 1
else
if (chord(j) .ge. 1.54 .and. chord(j) .lt. 1.56) then
a(78) = a(78) + 1
else
if (chord(j) .ge. 1.56 .and. chord(j) .lt. 1.58) then
a(79) = a(79) + 1
else
if (chord(j) .ge. 1.58 .and. chord(j) .lt. 1.6) then
a(80) = a(80) + 1
else
if (chord(j) .ge. 1.6 .and. chord(j) .lt. 1.62) then
a(81) = a(81) + 1
else
if (chord(j) .ge. 1.62 .and. chord(j) .lt. 1.64) then
a(82) = a(82) + 1
else
if (chord(j) .ge. 1.64 .and. chord(j) .lt. 1.66) then
a(83) = a(83) + 1
else
if (chord(j) .ge. 1.66 .and. chord(j) .lt. 1.68) then
a(84) = a(84) + 1
else
if (chord(j) .ge  1.68 .and. chord(j) .lt. 1.70) then
a(85) = a(85) +
else
if (chord(j) .ge. 1.70 .and. chord(j) .lt. 1.72) then
```

```
a(86) = a(86) + 1
else
if (chord(j) .ge. 1.72 .and. chord(j) .lt. 1.74) then
a(87) = a(87) + 1
else
if (chord(j) .ge. 1.74 .and. chord(j) .lt. 1.76) then
a(88) = a(88) + 1
else
if (chord(j) .ge. 1.76 .and. chord(j) .lt. 1.78) then
a(89) = a(89) + 1
else
if (chord(j) .ge. 1.78 .and. chord(j) .lt. 1.80) then
a(90) = a(90) + 1
else
if (chord(j) .ge. 1.80 .and. chord(j) .lt. 1.82) then
a(91) = a(91) + 1
else
if (chord(j) .ge. 1.82 .and. chord(j) .lt. 1.84) then
a(92) = a(92) + 1
else
if (chord(j) .ge. 1.84 .and. chord(j) .lt. 1.86) then
a(93) = a(93) + 1
else
if (chord(j) .ge. 1.86 .and. chord(j) .lt. 1.88) then
a(94) = a(94) + 1
else
if (chord(j) .ge. 1.88 .and. chord(j) .lt. 1.90) then
a(95) = a(95) + 1
else
if (chord(j) .ge. 1.90 .and. chord(j) .lt. 1.92) then
a(96) = a(96) + 1
else
if (chord(j) .ge. 1.92 .and. chord(j) .lt. 1.94) then
a(97) = a(97) + 1
else
if (chord(j) .ge. 1.94 .and. chord(j) .lt. 1.96) then
a(98) = a(98) + 1
else
if (chord(j) .ge. 1.96 .and. chord(j) .lt. 1.98) then
a(99) = a(99) + 1
else
if (chord(j) .ge. 1.98 .and. chord(j) .lt. 2.0) then
a(100) = a(100) + 1
else
if (chord(j) .ge. 2.0 .and. chord(j) .lt. 2.02) then
a(101) = a(101) + 1
else
if (chord(j) .ge. 2.02 .and. chord(j) .lt. 2.04) then
a(102) = a(102) + 1
else
if (chord(j) .ge. 2.04 .and. chord(j) .lt. 2.06) then
a(103) = a(103) + 1
else
if (chord(j) .ge. 2.06 .and. chord(j) .lt. 2.08) then
a(104) = a(104) + 1
else
if (chord(j) .ge. 2.08 .and. chord(j) .lt. 2.1) then
a(105) = a(105) + 1
else
if (chord(j) .ge. 2.1 .and. chord(j) .lt. 2.12) then
a(106) = a(106) + 1
else
if (chord(j) .ge. 2.12 .and. chord(j) .lt. 2.14) then
a(107) = a(107) + 1
```

```
else
if (chord(j) .ge. 2.14 .and. chord(j) .lt. 2.16) then
a(108) = a(108) + 1
else
if (chord(j) .ge. 2.16 .and. chord(j) .lt. 2.18) then
a(109) = a(109) + 1
else
if (chord(j) .ge. 2.18 .and. chord(j) .lt. 2.2) then
a(110) = a(110) + 1
else
if (chord(j) .ge. 2.2 .and. chord(j) .lt. 2.22) then
a(111) = a(111) + 1
else
if (chord(j) .ge. 2.22 .and. chord(j) .lt. 2.24) then
a(112) = a(112) + 1
else
if (chord(j) .ge. 2.24 .and. chord(j) .lt. 2.26) then
a(113) = a(113) + 1
else
if (chord(j) .ge. 2.26 .and. chord(j) .lt. 2.28) then
a(114) = a(114) + 1
else
if (chord(j) .ge. 2.28 .and. chord(j) .lt. 2.3) then
a(115) = a(115) + 1
else
if (chord(j) .ge. 2.3 .and. chord(j) .lt. 2.32) then
a(116) = a(116) + 1
else
if (chord(j) .ge. 2.32 .and. chord(j) .lt. 2.34) then
a(117) = a(117) + 1
else
if (chord(j) .ge. 2.34 .and. chord(j) .lt. 2.36) then
a(118) = a(118) + 1
else
if (chord(j) .ge. 2.36 .and. chord(j) .lt. 2.38) then
a(119) = a(119) + 1
else
if (chord(j) .ge. 2.38 .and. chord(j) .lt. 2.4) then
a(120) = a(120) + 1
else
if (chord(j) .ge. 2.4 .and. chord(j) .lt. 2.42) then
a(121) = a(121) + 1
else
if (chord(j) .ge. 2.42 .and. chord(j) .lt. 2.44) then
a(122) = a(122) + 1
else
if (chord(j) .ge. 2.44 .and. chord(j) .lt. 2.46) then
a(123) = a(123) + 1
else
if (chord(j) .ge. 2.46 .and. chord(j) .lt. 2.48) then
a(124) = a(124) + 1
else
if (chord(j) .ge. 2.48 .and. chord(j) .lt. 2.50) then
a(125) = a(125) + 1
else
if (chord(j) .ge. 2.50 .and. chord(j) .lt. 2.52) then
a(126) = a(126) + 1
else
if (chord(j) .ge. 2.52 .and. chord(j) .lt. 2.54) then
a(127) = a(127) + 1
else
if (chord(j) .ge. 2.54 .and. chord(j) .lt. 2.56) then
a(128) = a(128) + 1
else
```

```
if (chord(j) .ge. 2.56 .and. chord(j) .lt. 2.58) then
a(129) = a(129) + 1
else
if (chord(j) .ge. 2.58 .and. chord(j) .lt. 2.6) then
a(130) = a(130) + 1
else
if (chord(j) .ge. 2.6 .and. chord(j) .lt. 2.62) then
a(131) = a(131) + 1
else
if (chord(j) .ge. 2.62 .and. chord(j) .lt. 2.64) then
a(132) = a(132) + 1
else
if (chord(j) .ge. 2.64 .and. chord(j) .lt. 2.66) then
a(133) = a(133) + 1
else
if (chord(j) .ge. 2.66 .and. chord(j) .lt. 2.68) then
a(134) = a(134) + 1
else
if (chord(j) .ge. 2.68 .and. chord(j) .lt. 2.7) then
a(135) = a(135) + 1
else
if (chord(j) .ge. 2.7 .and. chord(j) .lt. 2.72) then
a(136) = a(136) + 1
else
if (chord(j) .ge. 2.72 .and. chord(j) .lt. 2.74) then
a(137) = a(137) + 1
else
if (chord(j) .ge. 2.74 .and. chord(j) .lt. 2.76) then
a(138) = a(138) + 1
else
if (chord(j) .ge. 2.76 .and. chord(j) .lt. 2.78) then
a(139) = a(139) + 1
else
if (chord(j) .ge. 2.78 .and. chord(j) .lt. 2.8) then
a(140) = a(140) + 1
else
if (chord(j) .ge. 2.8 .and. chord(j) .lt. 2.82) then
a(141) = a(141) + 1
else
if (chord(j) .ge. 2.82 .and. chord(j) .lt. 2.84) then
a(142) = a(142) + 1
else
if (chord(j) .ge. 2.84 .and. chord(j) .lt. 2.86) then
a(143) = a(143) + 1
else
if (chord(j) .ge. 2.86 .and. chord(j) .lt. 2.88) then
a(144) = a(144) + 1
else
if (chord(j) .ge. 2.88 .and. chord(j) .lt. 2.9) then
a(145) = a(145) + 1
else
if (chord(j) .ge. 2.9 .and. chord(j) .lt. 2.92) then
a(146) = a(146) + 1
else
if (chord(j) .ge. 2.92 .and. chord(j) .lt. 2.94) then
a(147) = a(147) + 1
else
if (chord(j) .ge. 2.94 .and. chord(j) .lt. 2.96) then
a(148) = a(148) + 1
else
if (chord(j) .ge. 2.96 .and. chord(j) .lt. 2.98) then
a(149) = a(149) + 1
else
if (chord(j) .ge. 2.98 .and. chord(j) .lt  3.0) then
```

```
a(150) = a(150) + 1
else
if (chord(j) .ge. 3.0 .and. chord(j) .lt. 4.0) then
a(151) = a(151) + 1
else
if (chord(j) .ge. 4.0 .and. chord(j) .lt. 5.0) then
a(152) = a(152) + 1
else
if (chord(j) .ge. 5.0) then
a(153) = a(153) + 1
end if
end if
end if
```

```
end if
end if
end if
```

```
      end if
      end if
      end if
```

```
c
      Size = 0.5
      Base = 1.0
c
      width = 1000 * width
      call ZCSIZ (width, height)
c
      call ZVIEW (0.0, 0.6, 0.4, 0.9)
      call ZWIND (Xmin, Xmax, Ymin, Ymax)
      call ZAXES (Size, Base)
      call ZWIND (Xmin, Xmax, Ymin, Ymax)
c
      a(0) = 0
      Xpos = 0
      Ypos = a(0)
      call ZMOVE (Xpos, Ypos)
c
      do j = 1, 150
       fra = j
       fra = ((fra / 100)*2) - 0.01
       if (j .eq. 150) then
       fra = 3.0
       end if
       Xpos = fra
       Ypos = a(j)
       call ZDRAW (Xpos, Ypos)
      end do
c
      call ZMOVE (Xsta + 29 * width, Ymin - 1 * height)
      call ZTEXT (16,16HChord Length, cm)
      call ZMOVE (Xsta + 6 * width, Yend )
      call ZTEXT (11, 11HProbability)
      call ZMOVE (Xsta + 28 * width, Ymax + height)
      call ZTEXT (25, 25HProbability Distributions)
c
c     Xmin = -21.0
c     Xsta = 0.0
c     Xend = 210.0
c     Xmax = 231.0
c     Nxtic = 7
c     Nix = 3
c     Ndx = 0
c
c     Ymin = -0.05
c     Ysta = 0.0
c     Yend = 0.5
c     Ymax = 0.55
c     Nytic = 5
c     Niy = 2
c     Nix = 2
c
c     Size = 0.5
c     Base = 1.0
c
c     width = 1000 * width
c     call ZCSIZ (width, height)
c
c     call ZVIEW (0.0, 0.6, 0.05, 0.45)
c     call ZWIND (Xmin, Xmax, Ymin, Ymax)
c     call ZAXES (Size, Base)
c     call ZWIND (Xmin, Xmax, Ymin, Ymax)
c
c     z(0) = 0.0
c     xpos = 0
```

```
c      Ypos = z(0)
c      call ZMOVE (Xpos, Ypos)
c
c      do j=5,205,10
c      Xpos = j
c      Ypos = z(j)
c      call ZDRAW (Xpos, Ypos)
c      end do
c
c      call ZMOVE (Xsta + 27 * width, Ymin - 1 * height)
c      call ZTEXT (21, 21HBubble Velocity, cm/s)
c      call ZMOVE (Xsta + 6 * width, Yend)
c      call ZTEXT (11, 11HProbability)
c
c
       write(6,40) file
40     format(20x, ' ****** FILENAME ****** : ', a16)
       write(6,42) Nb(1)
42     format(/,15x, ' **** Bubbles detected by probe 1 : ',i5)
       write(6,41) dada
41     format(15x, ' **** Percentage of bubbles retained : ',f7.2)
       write(6,39) avgdur
39     format(15x, ' **** Average bubble duration : ',f9.6,' s')
       write(6,38) avgcd
38     format(15x, ' **** Average bubble chord length : ',f9.6,' cm',/)
c
c
       call ZDEND
       call ZEND
c
       write(6,40) file
       do j = 1,150
       siz=j
       siz = ((siz/100)*2)-0.01
       write(6,43) siz, a(j)
43     format(15x,' * bubble size (cm):',f7.3,'   * probability:',f7.3)
       end do
       write(6,44) a(151)
       write(6,45) a(152)
       write(6,46) a(153)
44     format(/,15x,' * bubbles between 3 to 4 cm:',f7.3)
45     format(15x,' * bubbles between 4 to 5 cm:',f7.3)
46     format(15x,' * bubbles larger than 5 cm :',f7.3)
c
c
       OPTION = 140000B
c
       CALL LURQ (OPTION, LUARY, NUMLUS)
c
c
c
       stop
       end
c ***************************************************************************
       subroutine output (file, w, Vind, dm, tsta, tend, tdu)
       integer i
       real Vind(3), dm(3), tsta(2), tend(2), tdu(2), w
       character*16 file
c
       write (6,10) file
       write (6,55) w
       do i = 1, 2
           write (6,60) i
           write (6,70) tsta(i)
```

```
            write (6,80) tend(i)
            write (6,75) tdu(i)
          end do
          write (6,81)
          write (6,91) Vind(1), dm(1)
          write (6,82)
          write (6,92) Vind(2), dm(2)
          write (6,83)
          write (6,93) Vind(3), dm(3)
          write (6,99)
c
10        format ( 9x, '*****  Data File : ', a16 )
55        format ( //, 9x, '*  Bubble No. ', i3)
60        format ( //, 9x, '*** Probe No.', i2)
70        format ( /, 9x, '* Starting Point : ', f7.3, '  second')
75        format ( /, 9x, '* Duration : ', f5.3, '  second')
80        format ( /, 9x, '* Ending Point : ', f7.3, '  second')
81        format ( ///, 9x, '* Method 1 : Starting Point Shift')
82        format ( ///, 9x, '* Method 2 : Mean Time Shift')
83        format ( ///, 9x, '* Method 3 : Cross Correlation')
91        format ( /, 9x, '** Bubble Velocity = ', f5.1, ' cm/s ',
     *  '    Bubble Size = ', f4.2, ' cm')
92        format ( /, 9x, '** Bubble Velocity = ', f5.1, ' cm/s ',
     *  '    Bubble Size = ', f4.2, ' cm')
93        format ( /, 9x, '** Bubble Velocity = ', f5.1, ' cm/s ',
     *  '    Bubble Size = ', f4.2, ' cm')
99        format ('1')
c
          return
          end
```

APPENDIX 4

BUBBLE DURATION, GAS HOLDUP, BUBBLE FREQUENCY

SUMMARY OF EXPERIMENTS

Table A4.1
T=100°C, V_g=2.2 cm/s, z=15 cm

Filename	Θ=r/R	Average Signal Intensity volt	Total Number of Bubbles	Average Bubble Duration s	Gas Holdup	Bubble Freq. 1/s
jan13d1a	0.19	0.01399 0.00475	366 285	0.006730 0.005723	0.04926 0.03262	7.32 5.70
jan13d1b	0.19	0.01360 0.00488	383 288	0.006078 0.005774	0.04656 0.03326	7.66 5.76
jan13d1c	0.19	0.01539 0.00610	351 350	0.006553 0.005889	0.04600 0.04122	7.02 7.00
jan13d2a	0.42	0.01919 0.00775	377 353	0.006968 0.006439	0.05254 0.04546	7.54 7.06
jan13d2b	0.42	0.01935 0.00695	407 364	0.006447 0.005874	0.05248 0.04276	8.14 7.28
jan13d2c	0.42	0.02171 0.00710	452 352	0.006779 0.006241	0.06128 0.04394	9.04 7.04
jan13d3a	0.62	0.01738 0.00751	339 314	0.006543 0.006752	0.04436 0.04240	6.78 6.28
jan13d3b	0.62	0.02033 0.00757	380 349	0.006787 0.006258	0.05158 0.04368	7.60 6.98
jan13d3c	0.62	0.01820 0.00784	389 381	0.006653 0.006312	0.05176 0.04810	7.78 7.62
jan13d4a	0.78	0.02169 0.00728	409 353	0.006548 0.006249	0.05356 0.04412	8.18 7.06
jan13d4b	0.78	0.02812 0.00978	465 434	0.006903 0.006187	0.06420 0.05370	9.30 8.68
jan13d4c	0.78	0.01646 0.00750	350 327	0.006149 0.006514	0.04304 0.04260	7.00 6.54
jan13d5a	0.89	0.02019 0.00704	325 274	0.007323 0.007047	0.04760 0.03862	6.50 5.48
jan13d5b	0.89	0.01557 0.00776	321 280	0.006645 0.006911	0.04266 0.03870	6.42 5.60
jan13d5c	0.89	0.02299 0.00719	394 327	0.006952 0.006428	0.05478 0.04204	7.88 6.54
jan13d6a	0.92	0.01693 0.00551	288 223	0.007639 0.007408	0.04400 0.03304	5.76 4.46
jan13d6b	0.92	0.01784 0.00568	328 226	0.007192 0.007071	0.04718 0.03196	6.56 4.52
jan13d6c	0.92	0.01598 0.00467	270 223	0.007419 0.006731	0.04006 0.03002	5.40 4.46

Table A4.2
T=100°C, V_g=2.2 cm/s, z=30 cm

Filename	Θ=r/R	Average Signal Intensity volt	Total Number of Bubbles	Average Bubble Duration s	Gas Holdup	Bubble Freq. 1/s
jan13c1a	0.19	0.01964 0.00732	491 441	0.006242 0.005741	0.06130 0.05064	9.82 8.82
jan13c1b	0.19	0.02059 0.00810	538 477	0.006290 0.005669	0.06768 0.05408	10.76 9.54
jan13c1c	0.19	0.01809 0.00815	504 445	0.005990 0.005699	0.06038 0.05072	10.08 8.90
jan13c2a	0.42	0.02009 0.00825	460 418	0.006583 0.006079	0.06056 0.05082	9.20 8.36
jan13c2b	0.42	0.02151 0.00865	495 496	0.006317 0.005669	0.06254 0.05624	9.90 9.92
jan13c2c	0.42	0.02674 0.01087	584 581	0.006402 0.005861	0.07478 0.06810	11.68 11.62
jan13c3a	0.62	0.01822 0.00758	469 396	0.006429 0.006104	0.06030 0.04834	9.38 7.92
jan13c3b	0.62	0.02019 0.00880	561 463	0.006061 0.005911	0.06800 0.05474	11.22 9.26
jan13c3c	0.62	0.02068 0.00590	516 453	0.006473 0.006172	0.06680 0.05992	10.32 9.06
jan13c4a	0.78	0.01358 0.00518	372 330	0.006495 0.005858	0.04832 0.03866	7.44 6.60
jan13c4b	0.78	0.01825 0.00688	459 351	0.006227 0.006293	0.05716 0.04418	9.18 7.02
jan13c4c	0.78	0.01554 0.00692	370 341	0.006859 0.006311	0.05076 0.04304	7.40 6.82
jan13c5a	0.89	0.00969 0.00372	247 235	0.006381 0.006153	0.03152 0.02892	4.94 4.70
jan13c5b	0.89	0.00817 0.00363	237 223	0.006620 0.006112	0.03138 0.02726	4.74 4.46
jan13c5c	0.89	0.01370 0.00471	331 269	0.006828 0.006138	0.04520 0.03302	6.62 5.38
jan13c6a	0.92	0.00978 0.00400	287 236	0.006436 0.006119	0.03694 0.02888	5.74 4.72
jan13c6b	0.92	0.00827 0.00371	247 217	0.006474 0.006203	0.03198 0.02692	4.94 4.34
jan13c6c	0.92	0.00997 0.00292	202 198	0.007713 0.006030	0.03116 0.02388	4.04 3.96

Table A4.3
T=100°C, V_g=2.2 cm/s, z=46 cm

Filename	θ=r/R	Average Signal Intensity volt	Total Number of Bubbles	Average Bubble Duration s	Gas Holdup	Bubble Freq. 1/s
jan13b1a	0.19	0.02317 0.00916	679 621	0.005719 0.009161	0.07766 0.06656	13.58 12.42
jan13b1b	0.19	0.02304 0.00821	597 618	0.006121 0.005155	0.07308 0.06372	11.94 12.36
jan13b1c	0.19	0.02098 0.00957	707 640	0.005615 0.005417	0.07940 0.06934	14.14 12.80
jan13b2a	0.42	0.02362 0.00994	657 657	0.005874 0.005262	0.07718 0.06914	13.14 13.14
jan13b2c	0.42	0.02368 0.01072	635 624	0.005831 0.005617	0.07406 0.07010	12.70 12.48
jan13b3a	0.62	0.01579 0.00737	490 461	0.005967 0.005510	0.05848 0.05080	9.80 9.22
jan13b3b	0.62	0.01958 0.00929	557 556	0.006169 0.005831	0.06872 0.06484	11.14 11.12
jan13b3c	0.62	0.02225 0.01043	611 589	0.006124 0.005744	0.07484 0.06766	12.22 11.78
jan13b4a	0.78	0.01167 0.00638	441 400	0.005868 0.006015	0.05176 0.04812	8.82 8.00
jan13b4b	0.78	0.01273 0.00613	451 409	0.005703 0.005594	0.05144 0.04576	9.02 8.18
jan13b4c	0.78	0.01071 0.00466	445 335	0.005562 0.005484	0.04950 0.03674	8.90 6.70
jan13b5a	0.89	0.01032 0.00388	349 288	0.006249 0.005917	0.04362 0.03408	6.98 5.76
jan13b5b	0.89	0.00975 0.00480	366 363	0.006180 0.005504	0.04524 0.03996	7.32 7.26
jan13b5c	0.89	0.00559 0.00180	255 183	0.006027 0.005481	0.03074 0.02006	5.10 3.66
jan13b6a	0.92	0.00859 0.00311	297 246	0.006074 0.005764	0.03608 0.02836	5.94 4.92
jan13b6b	0.92	0.00844 0.00329	289 236	0.006505 0.006047	0.03760 0.02854	5.78 4.72
jan13b6c	0.92	0.00573 0.00231	258 213	0.006085 0.005653	0.03140 0.02408	5.16 4.26

Table A4.4
T=100°C, V_g=2.2 cm/s, z=61 cm

Filename	θ=r/R	Average Signal Intensity volt	Total Number of Bubbles	Average Bubble Duration s	Gas Holdup	Bubble Freq. 1/s
jan13a1a	0.19	0.02260 0.01129	698 672	0.005749 0.005473	0.08026 0.07356	13.96 13.44
jan13a1b	0.19	0.02393 0.01165	713 735	0.005801 0.005390	0.08272 0.07924	14.26 14.70
jan13a1c	0.19	0.02138 0.00953	648 715	0.005801 0.005176	0.07518 0.07402	12.96 14.30
jan13a2a	0.42	0.02734 0.01293	840 817	0.005617 0.005196	0.09436 0.08490	16.80 16.34
jan13a2b	0.42	0.02564 0.01104	804 790	0.005483 0.005011	0.08816 0.07918	16.08 15.80
jan13a2c	0.42	0.02819 0.01278	844 876	0.005552 0.005162	0.09372 0.09044	16.88 17.52
jan13a3a	0.62	0.01207 0.00710	526 540	0.005639 0.005307	0.05932 0.05732	10.52 10.80
jan13a3b	0.62	0.01518 0.00709	581 574	0.005627 0.005202	0.06538 0.05972	11.62 11.48
jan13a3c	0.62	0.01700 0.00908	597 593	0.005755 0.005417	0.06872 0.06424	11.94 11.86
jan13a4a	0.78	0.00901 0.00439	458 390	0.005742 0.005277	0.05260 0.04116	9.16 7.80
jan13a4b	0.78	0.01107 0.00571	494 479	0.005773 0.005710	0.05704 0.04974	9.88 9.58
jan13a4c	0.78	0.01156 0.00435	484 392	0.005808 0.005311	0.05622 0.04164	9.68 7.84
jan13a5a	0.89	0.00756 0.00362	395 343	0.005506 0.005271	0.04350 0.03616	7.90 6.86
jan13a5b	0.89	0.00559 0.00309	339 318	0.005593 0.005535	0.03792 0.03520	6.78 6.36
jan13a5c	0.89	0.00510 0.00321	337 318	0.005608 0.005374	0.03780 0.03418	6.74 6.36
jan13a6a	0.92	0.00869 0.00466	358 323	0.006028 0.006313	0.04316 0.04078	7.16 6.46
jan13a6b	0.92	0.00750 0.00415	334 337	0.006033 0.005801	0.04030 0.03910	6.68 6.74
jan13a6c	0.92	0.00713 0.00389	359 350	0.005685 0.005469	0.04082 0.03828	7.18 7.00

Table A4.5
T=100°C, V_g=2.2 cm/s, z=76 cm

Filename	θ=r/R	Average Signal Intensity volt	Total Number of Bubbles	Average Bubble Duration s	Gas Holdup	Bubble Freq. 1/s
jan13e1a	0.19	0.02412 0.01034	871 788	0.005502 0.005011	0.09584 0.07898	17.42 15.76
jan13e1b	0.19	0.02657 0.01197	910 814	0.005359 0.005316	0.09754 0.08654	18.20 16.28
jan13e1c	0.19	0.02908 0.01263	823 835	0.005751 0.005315	0.09466 0.08876	16.46 16.70
jan13e2a	0.42	0.03427 0.01391	865 900	0.006016 0.005364	0.10408 0.09656	17.30 18.00
jan13e2b	0.42	0.02506 0.01156	795 764	0.005635 0.005414	0.08960 0.08272	15.90 15.28
jan13e2c	0.42	0.02897 0.01218	852 826	0.005866 0.005262	0.09996 0.08692	17.04 16.52
jan13e3a	0.62	0.02096 0.00895	686 637	0.005720 0.005422	0.07848 0.06908	13.72 12.74
jan13e3b	0.62	0.02220 0.00834	761 660	0.005636 0.005189	0.08578 0.06850	15.22 13.20
jan13e3c	0.62	0.02151 0.00857	780 696	0.005399 0.004986	0.08422 0.06940	15.60 13.92
jan13e4a	0.78	0.01105 0.00407	502 417	0.005667 0.005137	0.05690 0.04284	10.04 8.34
jan13e4b	0.78	0.01076 0.00486	461 401	0.005616 0.005536	0.05178 0.04440	9.22 8.02
jan13e4c	0.78	0.01031 0.00562	534 432	0.005376 0.005451	0.05742 0.04710	10.68 8.64
jan13e5a	0.89	0.00943 0.00287	435 297	0.005998 0.005340	0.05218 0.03172	8.70 5.94
jan13e5b	0.89	0.00882 0.00334	421 300	0.005751 0.005560	0.04842 0.03336	8.42 6.00
jan13e5c	0.89	0.00826 0.00310	402 347	0.005425 0.005150	0.04362 0.03574	8.04 6.94
jan13e6a	0.92	0.00889 0.00305	418 265	0.005766 0.005928	0.04820 0.03142	8.36 5.30
jan13e6b	0.92	0.00676 0.00235	352 235	0.006014 0.006009	0.04234 0.02824	7.04 4.70
jan13e6c	0.92	0.00510 0.00168	281 214	0.006014 0.005327	0.03380 0.02280	5.62 4.28

Table A4.6
T=100°C, V_g=4.1 cm/s, z=10 cm

Filename	θ=r/R	Average Signal Intensity volt	Total Number of Bubbles	Average Bubble Duration s	Gas Holdup	Bubble Freq. 1/s
jan11a1a	0.19	0.01611 0.00622	412 353	0.006631 0.005943	0.05464 0.00594	8.24 7.06
jan11a1b	0.19	0.02191 0.00890	477 398	0.006960 0.006405	0.06640 0.05098	9.54 7.96
jan11a1c	0.19	0.01567 0.00607	400 363	0.006495 0.005906	0.05196 0.04288	8.00 7.26
jan11a2a	0.42	0.03192 0.01362	699 603	0.006524 0.006310	0.09120 0.07610	13.98 12.06
jan11a2b	0.42	0.03041 0.00903	585 482	0.007369 0.005948	0.08622 0.05734	11.70 9.64
jan11a2c	0.42	0.02665 0.01207	638 578	0.006638 0.006197	0.08470 0.07164	12.76 11.56
jan11a3a	0.62	0.01489 0.00681	479 402	0.005904 0.005920	0.05656 0.04760	9.58 8.04
jan11a3b	0.62	0.01973 0.00923	552 479	0.006339 0.006002	0.06998 0.06002	11.04 9.58
jan11a3c	0.62	0.01619 0.00852	439 450	0.006257 0.006069	0.05494 0.05462	8.78 9.00
jan11a4a	0.78	0.01809 0.00712	462 420	0.006574 0.006098	0.06074 0.05122	9.24 8.40
jan11a4b	0.78	0.01333 0.00645	390 394	0.006633 0.005751	0.05174 0.04532	7.80 7.88
jan11a4c	0.78	0.01517 0.00568	420 390	0.006317 0.005510	0.05306 0.04298	8.40 7.80
jan11a5a	0.89	0.02085 0.00759	464 434	0.007110 0.005903	0.06598 0.05124	9.28 8.68
jan11a5b	0.89	0.01886 0.00675	433 375	0.006829 0.006219	0.05914 0.04664	8.66 7.50
jan11a5c	0.89	0.01973 0.00710	436 358	0.006830 0.006489	0.05956 0.04646	8.72 7.16
jan11a6a	0.89	0.02129 0.00746	383 387	0.007598 0.006271	0.05820 0.04854	7.66 7.74
jan11a6b	0.92	0.02209 0.00767	402 364	0.007915 0.006459	0.06364 0.05102	8.04 7.28
jan11a6c	0.92	0.01580 0.00687	361 364	0.006676 0.006277	0.04820 0.04570	7.22 7.28

Table A4.7
T=100°C, V_g=4.1 cm/s, z=15 cm

Filename	Θ=r/R	Average Signal Intensity volt	Total Number of Bubbles	Average Bubble Duration s	Gas Holdup	Bubble Freq. 1/s
jan11b1a	0.19	0.02257 0.00978	602 486	0.006058 0.006379	0.07294 0.06200	12.04 9.72
jan11b1b	0.19	0.02732 0.01049	631 540	0.006369 0.006156	0.08038 0.06648	12.62 10.80
jan11b1c	0.19	0.02208 0.01041	559 481	0.006429 0.006509	0.07188 0.06262	11.18 9.62
jan11b2a	0.42	0.02893 0.01216	737 677	0.006110 0.005693	0.09006 0.07708	14.74 13.54
jan11b2b	0.42	0.03582 0.01224	772 612	0.006690 0.005948	0.10330 0.07280	15.44 12.24
jan11b2c	0.42	0.03249 0.01205	797 705	0.006301 0.005637	0.10044 0.07948	15.94 14.10
jan11b3a	0.62	0.02249 0.00953	637 483	0.006085 0.006157	0.07752 0.05948	12.74 9.66
jan11b3b	0.62	0.01929 0.00834	577 490	0.005976 0.005710	0.06896 0.05596	11.54 9.80
jan11b3c	0.62	0.02653 0.01018	623 525	0.006276 0.006114	0.07820 0.06420	12.46 10.50
jan11b4a	0.78	0.01459 0.00477	524 399	0.005611 0.005426	0.05880 0.05426	10.48 7.98
jan11b4b	0.78	0.01465 0.00645	495 412	0.005915 0.005959	0.05856 0.04910	9.90 8.24
jan11b4c	0.78	0.01709 0.00643	526 374	0.006105 0.005941	0.06422 0.04444	10.52 7.48
jan11b5a	0.89	0.01838 0.00460	451 371	0.006506 0.005504	0.05868 0.04084	9.02 7.42
jan11b5b	0.89	0.01495 0.00630	419 440	0.005850 0.005636	0.04902 0.04960	8.38 8.80
jan11b5c	0.89	0.01214 0.00446	407 331	0.006106 0.005900	0.04970 0.03906	8.14 6.62
jan11b6a	0.92	0.01252 0.00269	313 258	0.006709 0.005566	0.04200 0.02872	6.26 5.16
jan11b6b	0.92	0.01015 0.00328	323 268	0.005817 0.005634	0.03758 0.03020	6.46 5.36
jan11b6c	0.92	0.00682 0.00321	326 266	0.005718 0.005669	0.03728 0.03016	6.52 5.32

Table A4.8
T=100°C, V_g=4.1 cm/s, z=30 cm

Filename	θ=r/R	Average Signal Intensity volt	Total Number of Bubbles	Average Bubble Duration s	Gas Holdup	Bubble Freq. 1/s
jan11c1a	0.19	0.02927 0.01237	866 869	0.005878 0.005354	0.10180 0.09306	17.32 17.38
jan11c1b	0.19	0.03233 0.01583	1039 933	0.005605 0.005494	0.11648 0.10252	20.78 18.66
jan11c1c	0.19	0.03753 0.01495	1017 987	0.005860 0.005303	0.11920 0.10468	20.34 19.74
jan11c2a	0.42	0.02929 0.01059	966 781	0.005591 0.005348	0.10802 0.08354	19.32 15.62
jan11c2b	0.42	0.03432 0.01337	1019 923	0.005557 0.005207	0.11326 0.09612	20.38 18.46
jan11c2c	0.42	0.03221 0.01461	976 893	0.005422 0.005536	0.10584 0.09888	19.52 17.86
jan11c3a	0.62	0.01655 0.00442	592 508	0.005539 0.005012	0.06558 0.05092	11.84 10.16
jan11c3b	0.62	0.01246 0.00424	664 525	0.005167 0.005000	0.06862 0.05250	13.28 10.50
jan11c3c	0.62	0.02244 0.00871	721 620	0.005859 0.005421	0.08448 0.06722	14.42 12.40
jan11c4a	0.78	0.02456 0.008712	867 714	0.005487 0.005199	0.09514 0.07424	17.34 14.28
jan11c4b	0.78	0.02377 0.00846	844 727	0.005525 0.005219	0.09326 0.07588	16.88 14.54
jan11c4c	0.78	0.02821 0.01094	922 764	0.005432 0.005402	0.10016 0.08254	18.44 15.28
jan11c5a	0.89	0.00554 0.00272	418 334	0.004892 0.005168	0.04090 0.03452	8.36 6.68
jan11c5b	0.89	0.00809 0.00346	408 394	0.005250 0.005292	0.04284 0.04170	8.16 7.88
jan11c5c	0.89	0.00766 0.00269	441 364	0.005306 0.004940	0.04680 0.03596	8.82 7.28
jan11c6a	0.92	0.01016 0.00411	464 406	0.005291 0.005384	0.04910 0.04372	9.28 8.12
jan11c6b	0.92	0.00777 0.00251	438 388	0.005384 0.005142	0.04716 0.03990	8.76 7.76
jan11c6c	0.92	0.01176 0.00462	533 450	0.005191 0.005322	0.05534 0.04790	10.66 9.00

Table A4.9
T=100°C, V_g=4.1 cm/s, z=46 cm

Filename	e=r/R	Average Signal Intensity volt	Total Number of Bubbles	Average Bubble Duration s	Gas Holdup	Bubble Freq. 1/s
jan11d1a	0.19	0.04427 0.01795	1221 1259	0.005456 0.005172	0.13324 0.13022	24.42 25.18
jan11d1b	0.19	0.04378 0.01917	1158 1210	0.005683 0.005300	0.13162 0.12826	23.16 24.20
jan11d1c	0.19	0.04083 0.01693	1211 1217	0.005416 0.005156	0.13118 0.12550	21.22 24.34
jan11c2a	0.42	0.03751 0.01597	1214 1191	0.005360 0.005135	0.13014 0.12232	24.28 23.82
jan11d2b	0.42	0.03639 0.01528	1207 1121	0.005337 0.005214	0.12884 0.11690	24.14 22.42
jan11d2c	0.42	0.03880 0.01716	1122 1176	0.005501 0.005323	0.12344 0.12520	22.44 23.52
jan11d3a	0.62	0.03166 0.01350	1119 910	0.005497 0.005352	0.12302 0.09740	22.38 18.20
jan11d3b	0.62	0.02755 0.01289	1091 930	0.005369 0.005194	0.11716 0.09660	21.82 18.60
jan11d3c	0.62	0.02688 0.01237	1059 950	0.005491 0.005278	0.11630 0.10028	21.18 19.00
jan11d4a	0.78	0.01384 0.00582	847 682	0.005161 0.004881	0.08742 0.06658	16.94 13.64
jan11d4b	0.78	0.01223 0.00556	685 622	0.005145 0.005061	0.07048 0.06296	13.70 12.44
jan11d4c	0.78	0.01321 0.00734	803 670	0.004941 0.005282	0.01936 0.07078	16.06 13.40
jan11d5a	0.89	0.00869 0.00417	538 478	0.005264 0.005207	0.05664 0.04978	10.76 9.56
jan11d5b	0.89	0.00946 0.00359	556 497	0.005263 0.004966	0.05852 0.04936	11.12 9.94
jan11d5c	0.89	0.00826 0.00411	556 489	0.005036 0.005135	0.05600 0.05022	11.12 9.78
jan11d6a	0.92	0.00744 0.00374	601 558	0.004719 0.004871	0.05672 0.05436	12.02 11.16
jan11d6b	0.92	0.00744 0.00374	601 558	0.004719 0.004871	0.05672 0.05436	12.02 11.16
jan11d6c	0.92	0.00762 0.00287	409 412	0.005543 0.005051	0.04534 0.04162	8.18 8.24

Table A4.10
T=100°C, V_g=4.1 cm/s, z=61 cm

Filename	e=r/R	Average Signal Intensity volt	Total Number of Bubbles	Average Bubble Duration s	Gas Holdup	Bubble Freq. 1/s
jan11e1a	0.19	0.04966 0.02189	1561 1573	0.005125 0.005076	0.16000 0.15968	31.22 31.46
jan11e1b	0.19	0.04913 0.02206	1534 1737	0.005149 0.004769	0.15796 0.16566	30.68 34.74
jan11e1c	0.19	0.05693 0.02316	1483 1611	0.005422 0.005122	0.16082 0.16504	29.66 32.22
jan11e2a	0.42	0.04546 0.02123	1513 1524	0.005363 0.004994	0.16228 0.15222	30.26 30.48
jan11e2b	0.42	0.04129 0.01937	1323 1422	0.005578 0.005061	0.14760 0.14394	26.46 28.44
jan11e2c	0.42	0.04278 0.01694	1271 1384	0.005854 0.004923	0.14882 0.13626	25.42 27.68
jan11e3a	0.62	0.02622 0.01310	1112 1139	0.005070 0.004982	0.11276 0.11348	22.24 22.78
jan11e3b	0.62	0.02579 0.01299	1163 1078	0.004936 0.004942	0.11480 0.10654	23.26 21.56
jan11e3c	0.62	0.03131 0.01459	1237 1180	0.005214 0.004976	0.12900 0.11744	24.74 23.60
jan11e4a	0.78	0.01359 0.00647	814 804	0.004993 0.004922	0.08128 0.07914	16.28 16.08
jan11e4b	0.78	0.00721 0.00261	539 570	0.005026 0.004677	0.05418 0.05332	10.78 11.40
jan11e4c	0.78	0.01668 0.00864	1002 927	0.004674 0.004970	0.09366 0.09214	20.04 18.54
jan11e5a	0.89	0.00651 0.00307	487 588	0.004875 0.004726	0.04748 0.05558	9.74 11.76
jan11e5b	0.89	0.00684 0.00296	541 578	0.004961 0.004680	0.05368 0.05410	10.82 11.56
jan11e5c	0.89	0.00488 0.00314	496 521	0.004702 0.004735	0.04664 0.04934	9.92 10.42
jan11e6a	0.92	0.00697 0.00339	495 607	0.004954 0.004932	0.04904 0.05988	9.90 12.14
jan11e6b	0.92	0.00698 0.00460	614 641	0.004765 0.005030	0.05852 0.06448	12.28 12.82
jan11e6c	0.92	0.00583 0.00347	559 590	0.004789 0.004807	0.05354 0.05672	11.18 11.80

Table A4.11
T=100°C, V_g=9.0 cm/s, z=15 cm

Filename	e=r/R	Average Signal Intensity volt	Total Number of Bubbles	Average Bubble Duration s	Gas Holdup	Bubble Freq. 1/s
jan16e1a	0.19	0.04047 0.02098	1144 1169	0.005708 0.005639	0.13060 0.13184	22.88 23.38
jan16e1b	0.19	0.04896 0.01873	1169 1091	0.006100 0.005576	0.14262 0.12166	23.38 21.82
jan16e1c	0.19	0.04774 0.02134	1232 1213	0.005830 0.005500	0.14364 0.13344	24.64 24.26
jan16e2a	0.42	0.04550 0.01910	1208 1183	0.005972 0.005533	0.14428 0.13090	24.16 23.66
jan16e2b	0.42	0.05206 0.02110	1190 1203	0.006240 0.005554	0.14852 0.13362	23.80 24.06
jan16e2c	0.42	0.05134 0.02132	1160 1172	0.006182 0.005732	0.14342 0.13436	23.20 23.44
jan16e3a	0.62	0.03925 0.01805	1213 1181	0.005654 0.005214	0.13716 0.12316	24.26 23.62
jan16e3b	0.62	0.05190 0.01996	1083 1122	0.006359 0.005586	0.13774 0.12536	21.66 22.44
jan16e3c	0.62	0.03436 0.01779	1132 1045	0.005411 0.005435	0.12250 0.11360	22.64 20.90
jan16e4a	0.78	0.03216 0.01334	1155 976	0.005228 0.005076	0.12076 0.09908	23.10 19.52
jan16e4b	0.78	0.03756 0.01556	1256 1085	0.005508 0.005112	0.13836 0.11092	25.12 21.70
jan16e4c	0.78	0.04124 0.01871	1220 1100	0.005440 0.005590	0.13274 0.12298	24.40 22.00
jan16e5a	0.89	0.01952 0.00956	886 812	0.005126 0.004999	0.09084 0.08118	17.72 16.24
jan16e5b	0.89	0.02710 0.01004	960 822	0.005409 0.004964	0.10386 0.08160	19.20 16.44
jan16e5c	0.89	0.01847 0.00894	791 720	0.005097 0.005004	0.08064 0.07206	15.82 14.40
jan16e6a	0.92	0.01375 0.00744	683 777	0.004855 0.004821	0.06632 0.07492	13.66 15.54
jan16e6b	0.92	0.01257 0.00708	645 713	0.004909 0.004752	0.06332 0.06776	12.90 14.26
jan16e6c	0.92	0.01612 0.00775	670 712	0.004940 0.004949	0.06620 0.07048	13.40 14.24

Table A4.12
T=100°C, V_g=9.0 cm/s, z=30 cm

Filename	θ=r/R	Average Signal Intensity volt	Total Number of Bubbles	Average Bubble Duration s	Gas Holdup	Bubble Freq. 1/s
jan16d1a	0.19	0.05296 0.02399	1750 1660	0.005137 0.005114	0.17978 0.16978	35.00 33.20
jan16d1b	0.19	0.05222 0.02305	1624 1583	0.005167 0.005142	0.16782 0.16278	32.48 31.66
jan16d1c	0.19	0.05448 0.02588	1849 1820	0.004967 0.005063	0.18368 0.18428	36.98 36.40
jan16d2a	0.42	0.05791 0.02494	1696 1646	0.005317 0.005099	0.18036 0.16786	33.92 32.92
jan16d2b	0.42	0.06138 0.02628	1789 1676	0.005305 0.005317	0.18980 0.17822	35.78 33.52
jan16d2c	0.42	0.06876 0.02619	1703 1739	0.005574 0.005185	0.18984 0.18034	34.06 34.78
jan16d3a	0.62	0.05494 0.02262	1509 1423	0.005516 0.005365	0.16648 0.15270	30.18 28.46
jan16d3b	0.62	0.04271 0.01827	1419 1321	0.005145 0.005048	0.14602 0.13338	28.38 26.42
jan16d3c	0.62	0.04938 0.01940	1573 1471	0.005231 0.004903	0.16458 0.14426	31.46 29.42
jan16d4a	0.78	0.02886 0.01068	1059 967	0.005312 0.004880	0.11250 0.09438	21.18 19.34
jan16d4b	0.78	0.02515 0.01078	1000 1083	0.005244 0.004637	0.10488 0.10044	20.00 21.66
jan16d4c	0.78	0.01939 0.01036	869 880	0.005040 0.004841	0.08760 0.08520	17.38 17.60
jan16d5a	0.89	0.01078 0.00724	928 861	0.004085 0.004598	0.07582 0.07918	18.56 17.22
jan16d5b	0.89	0.01013 0.00583	787 850	0.004332 0.004372	0.06818 0.07432	15.74 17.00
jan16d5c	0.89	0.01429 0.00707	879 897	0.004774 0.004466	0.08392 0.08012	17.58 17.94
jan16d6a	0.92	0.00917 0.00592	810 838	0.004586 0.004494	0.07430 0.07532	16.20 16.76
jan16d6b	0.92	0.01114 0.00600	863 884	0.004556 0.004261	0.07864 0.07534	17.26 17.68
jan16d6c	0.92	0.00716 0.00425	866 806	0.002988 0.004140	0.06908 0.06674	17.32 16.12

Table A4.13
T=100°C, V_g=9.0 cm/s, z=46 cm

Filename	θ=r/R	Average Signal Intensity volt	Total Number of Bubbles	Average Bubble Duration s	Gas Holdup	Bubble Freq. 1/s
jan16c1a	0.19	0.07914 0.03550	2307 2324	0.005082 0.005000	0.23448 0.23238	46.14 46.48
jan16c1b	0.19	0.07922 0.03273	2317 2436	0.005098 0.004854	0.23622 0.23650	46.34 48.72
jan16c1c	0.19	0.07890 0.03303	2266 2351	0.005074 0.004833	0.22996 0.22724	45.32 47.02
jan16c2a	0.42	0.07417 0.03279	2135 2160	0.005135 0.005095	0.21928 0.22010	42.70 43.20
jan16c2b	0.42	0.07691 0.03022	1962 2071	0.005507 0.005028	0.21608 0.20828	39.24 41.42
jan16c2c	0.42	0.06281 0.02608	1874 2039	0.005241 0.004845	0.19644 0.19756	37.48 40.78
jan16c3a	0.62	0.04841 0.01983	1709 1619	0.004984 0.004852	0.17036 0.15712	34.18 32.38
jan16c3b	0.62	0.04291 0.01887	1675 1533	0.004868 0.004822	0.16308 0.14784	33.50 30.66
jan16c3c	0.62	0.04398 0.02110	1677 1676	0.004908 0.004843	0.16460 0.16234	33.54 33.52
jan16c4a	0.78	0.02424 0.01102	1324 1201	0.004639 0.004524	0.12284 0.10866	26.48 24.02
jan16c4b	0.78	0.02292 0.01109	1244 1126	0.004606 0.004576	0.11460 0.10306	24.88 22.52
jan16c4c	0.78	0.03186 0.01305	1345 1264	0.004908 0.004621	0.13202 0.11682	26.90 25.28
jan16c5a	0.89	0.01205 0.00625	920 936	0.004387 0.004259	0.08072 0.07972	18.40 18.72
jan16c5b	0.89	0.00976 0.00668	855 914	0.004432 0.004216	0.07578 0.07706	17.10 18.28
jan16c5c	0.89	0.00819 0.00579	828 892	0.004103 0.004239	0.06794 0.07562	16.56 17.84
jan16c6a	0.92	0.00887 0.00580	696 905	0.004154 0.004221	0.05782 0.07640	13.92 18.10
jan16c6b	0.92	0.01236 0.00297	830 955	0.004488 0.004162	0.07450 0.07950	16.60 19.10
jan16c6c	0.92	0.00765 0.00558	753 874	0.004396 0.004368	0.06620 0.07636	15.06 17.48

Table A4.14
T=100°C, V_g=9.0 cm/s, z=61 cm

Filename	e=r/R	Average Signal Intensity volt	Total Number of Bubbles	Average Bubble Duration s	Gas Holdup	Bubble Freq. 1/s
jan16b1a	0.19	0.08229 0.03631	2354 2664	0.005141 0.004919	0.24206 0.26208	47.08 53.28
jan16b1b	0.19	0.08326 0.03472	2348 2750	0.005199 0.004689	0.24416 0.25788	46.96 55.00
jan16b1c	0.19	0.09027 0.03796	2472 2721	0.005183 0.004923	0.25624 0.26790	49.44 54.42
jan16b2a	0.42	0.07380 0.03380	2451 2446	0.004939 0.004900	0.24210 0.23972	49.02 48.92
jan16b2b	0.42	0.07791 0.03587	2548 2673	0.004877 0.004793	0.24852 0.25622	50.96 53.46
jan16b2c	0.42	0.07641 0.03542	2566 2533	0.004793 0.004845	0.24596 0.24546	51.32 50.66
jan16b3a	0.62	0.04645 0.02158	1973 1861	0.004679 0.004721	0.18464 0.17572	39.46 37.22
jan16b3b	0.62	0.03970 0.01827	1949 1796	0.004484 0.004562	0.17478 0.16386	38.98 35.92
jan16b3c	0.62	0.03593 0.01767	1793 1676	0.004481 0.004517	0.16070 0.15140	35.86 33.52
jan16b4a	0.78	0.02010 0.01012	1280 1348	0.004351 0.004316	0.11138 0.11636	25.60 26.96
jan16b4b	0.78	0.02799 0.01320	1334 1273	0.004618 0.004571	0.12320 0.11638	26.68 25.46
jan16b4c	0.78	0.01928 0.00938	1094 1183	0.004479 0.004278	0.09800 0.10122	21.88 23.66
jan16b5a	0.89	0.00696 0.00568	772 971	0.003990 0.004097	0.06160 0.07956	15.44 19.42
jan16b5b	0.89	0.01170 0.00829	900 964	0.004323 0.004529	0.07782 0.08732	18.00 19.28
jan16b5c	0.89	0.00940 0.00696	809 963	0.004284 0.004271	0.06932 0.08226	16.18 19.26
jan16b6a	0.92	0.00753 0.00569	970 1129	0.003816 0.004043	0.07404 0.09130	19.40 22.58
jan16b6b	0.92	0.01398 0.00633	1199 1102	0.004124 0.004056	0.09890 0.08940	23.98 22.04
jan16b6c	0.92	0.00588 0.00499	1090 1115	0.003661 0.003882	0.07982 0.08656	21.80 22.30

Table A4.15
T=100°C, V_g=9.0 cm/s, z=76 cm

Filename	θ=r/R	Average Signal Intensity volt	Total Number of Bubbles	Average Bubble Duration s	Gas Holdup	Bubble Freq. 1/s
jan16a1a	0.19	0.08740 0.04718	2823 3426	0.004925 0.004687	0.27804 0.32112	56.46 68.52
jan16a1b	0.19	0.08395 0.04131	2856 3334	0.004855 0.004603	0.27734 0.30690	57.12 66.68
jan16a1c	0.19	0.08200 0.04078	2746 3355	0.004886 0.004609	0.26834 0.30928	54.92 67.10
jan16a2a	0.42	0.06086 0.03028	2395 2723	0.004845 0.004483	0.23206 0.24414	47.90 54.46
jan16a2b	0.42	0.06462 0.03048	2319 2749	0.004942 0.004501	0.22920 0.24746	46.38 54.98
jan16a2c	0.42	0.07771 0.03702	2381 2904	0.005154 0.004633	0.24544 0.26910	47.62 58.08
jan16a3a	0.62	0.03462 0.02082	1998 2295	0.004265 0.004304	0.17042 0.19756	39.96 45.90
jan16a3b	0.62	0.04143 0.02222	2098 2389	0.004489 0.004342	0.18836 0.20744	41.96 47.78
jan16a3c	0.62	0.04570 0.02463	2141 2318	0.004493 0.004494	0.19238 0.20834	42.82 46.36
jan16a4a	0.78	0.01277 0.01004	1206 1339	0.004014 0.004217	0.09682 0.11292	24.12 26.78
jan16a4b	0.78	0.02024 0.01139	1212 1411	0.004524 0.004278	0.10966 0.12072	24.24 28.22
jan16a4c	0.78	0.02204 0.01235	1307 1429	0.004524 0.004293	0.11826 0.12268	26.14 28.58
jan16a5a	0.89	0.01473 0.00914	1360 1439	0.004038 0.004125	0.10984 0.11872	27.20 28.78
jan16a5b	0.89	0.00808 0.00578	1107 1179	0.003732 0.003821	0.08262 0.09010	22.14 23.58
jan16a5c	0.89	0.00988 0.00688	1181 1289	0.003657 0.003928	0.08638 0.10126	23.62 25.78
jan16a6a	0.92	0.00552 0.00468	1023 1004	0.003584 0.003969	0.07332 0.07970	20.46 20.08
jan16a6b	0.92	0.00483 0.00408	942 1056	0.003537 0.003799	0.06664 0.08024	18.84 21.12
jan16a6c	0.92	0.00857 0.00643	1006 1133	0.003932 0.004117	0.07912 0.09330	20.12 22.66

Table A4.16
T=100°C, V_g=14.7 cm/s, z=15 cm

Filename	θ=r/R	Average Signal Intensity volt	Total Number of Bubbles	Average Bubble Duration s	Gas Holdup	Bubble Freq. 1/s
jan17a1a	0.19	0.05485 0.03027	1647 1971	0.005818 0.005094	0.19166 0.20080	32.94 39.42
jan17a1b	0.19	0.05949 0.03072	1758 1927	0.005613 0.005138	0.19734 0.19800	35.16 38.54
jan17a1c	0.19	0.05788 0.03158	1856 1895	0.005503 0.005228	0.20426 0.19814	37.12 37.90
jan17a2a	0.42	0.06670 0.03366	1786 1985	0.005869 0.005310	0.20964 0.21082	35.72 39.70
jan17a2b	0.42	0.06462 0.03267	1911 2118	0.005601 0.005079	0.21406 0.21514	38.22 42.36
jan17a2c	0.42	0.06361 0.03436	1843 2099	0.005647 0.005200	0.20814 0.21828	36.86 41.98
jan17a3a	0.62	0.04793 0.02421	1659 1745	0.005479 0.004963	0.18180 0.17322	33.18 34.90
jan17a3b	0.62	0.05007 0.02574	1587 1682	0.005582 0.005133	0.17718 0.17268	31.74 33.64
jan17a3c	0.62	0.05878 0.02979	1760 1792	0.005607 0.005223	0.19736 0.18718	35.20 35.84
jan17a4a	0.78	0.02523 0.01250	1186 1257	0.004906 0.004492	0.11636 0.11294	23.72 25.14
jan17a4b	0.78	0.04466 0.02020	1368 1499	0.005505 0.004950	0.15062 0.14840	27.36 29.98
jan17a4c	0.78	0.03740 0.01593	1334 1307	0.005307 0.004818	0.14160 0.12594	26.68 26.14
jan17a5a	0.89	0.01455 0.00891	1059 1027	0.004428 0.004380	0.09378 0.08996	21.18 20.54
jan17a5b	0.89	0.01082 0.00745	1014 1064	0.004180 0.004013	0.08478 0.08540	20.28 21.28
jan17a5c	0.89	0.01365 0.00877	1122 1115	0.004108 0.004283	0.09218 0.09550	22.44 22.30
jan17a6a	0.92	0.01215 0.00554	1086 1083	0.004165 0.004012	0.09046 0.08690	21.72 21.66
jan17a6b	0.92	0.01836 0.00867	1153 1059	0.004436 0.004529	0.10230 0.09592	23.06 21.18
jan17a6c	0.92	0.01485 0.00853	1066 1043	0.004357 0.004533	0.09290 0.09456	21.32 20.86

Table A4.17
T=100°C, V_g=14.7 cm/s, z=30 cm

Filename	θ=r/R	Average Signal Intensity volt	Total Number of Bubbles	Average Bubble Duration s	Gas Holdup	Bubble Freq. 1/s
jan17b1a	0.19	0.08821 0.03580	2425 2533	0.005130 0.004997	0.24880 0.25316	48.50 50.66
jan17b1b	0.19	0.07699 0.03090	2336 2311	0.005050 0.004877	0.23592 0.22542	46.72 46.22
jan17b1c	0.19	0.09310 0.03957	2359 2449	0.005432 0.005169	0.25630 0.25320	47.18 48.98
jan17b2a	0.42	0.07541 0.03069	2345 2273	0.005029 0.004805	0.23588 0.22130	46.90 45.46
jan17b2b	0.42	0.08300 0.03227	2377 2241	0.005137 0.004958	0.24420 0.22222	47.54 44.82
jan17b2c	0.42	0.09852 0.03909	2560 2445	0.005334 0.005199	0.27310 0.25422	51.20 48.90
jan17b3a	0.62	0.04901 0.02224	1845 1763	0.004833 0.004774	0.17832 0.16834	36.90 35.26
jan17b3b	0.62	0.05168 0.02425	1974 1845	0.004886 0.004828	0.19290 0.17816	39.48 36.90
jan17b3c	0.62	0.07419 0.03003	2128 2123	0.005293 0.004967	0.22528 0.21090	42.56 42.46
jan17b4a	0.78	0.03103 0.01666	1657 1534	0.004463 0.004557	0.14790 0.13982	33.14 30.68
jan17b4b	0.78	0.04387 0.01978	1903 1762	0.004722 0.004574	0.17972 0.16120	38.06 35.24
jan17b4c	0.78	0.03371 0.01587	1689 1486	0.004506 0.004542	0.15222 0.13500	33.78 29.72
jan17b5a	0.89	0.01670 0.01099	1244 1224	0.004126 0.004258	0.10266 0.01099	24.88 24.48
jan17b5b	0.89	0.01547 0.00902	1214 1292	0.004105 0.004077	0.09966 0.10536	24.28 25.84
jan17b5c	0.89	0.01625 0.00956	1232 1204	0.004083 0.004237	0.10060 0.10202	24.64 24.08
jan17b6a	0.92	0.00761 0.00638	1131 1089	0.003902 0.004082	0.08826 0.08890	22.62 21.78
jan17b6b	0.92	0.01372 0.00689	1095 1128	0.004039 0.004095	0.08846 0.09238	21.90 22.56
jan17b6c	0.92	0.01574 0.00866	1099 1144	0.004236 0.004267	0.09310 0.09764	21.98 22.88

Table A4.18
T=100°C, V_g=14.7 cm/s, z=46 cm

Filename	e=r/R	Average Signal Intensity volt	Total Number of Bubbles	Average Bubble Duration s	Gas Holdup	Bubble Freq. 1/s
jan17c1a	0.19	0.09786 0.04119	2779 3007	0.005187 0.004841	0.28828 0.29114	55.58 60.14
jan17c1b	0.19	0.11389 0.04507	2936 3296	0.005305 0.004918	0.31152 0.32418	58.72 65.92
jan17c1c	0.19	0.11415 0.04633	2984 3312	0.005280 0.004844	0.31510 0.32084	59.68 66.24
jan17c2a	0.42	0.09600 0.03952	2739 2981	0.005174 0.004750	0.28344 0.28318	54.78 59.62
jan17c2b	0.42	0.09761 0.03994	2749 2925	0.005103 0.004783	0.28054 0.27978	54.98 58.50
jan17c2c	0.42	0.10352 0.04375	3092 3074	0.004984 0.004886	0.30822 0.30040	61.84 61.48
jan17c3a	0.62	0.06093 0.02794	2325 2269	0.004815 0.004790	0.22390 0.21736	46.50 45.38
jan17c3b	0.62	0.07493 0.03155	2383 2255	0.004994 0.004903	0.23800 0.22114	47.66 45.10
jan17c3c	0.62	0.07087 0.02887	2394 2244	0.004968 0.004794	0.23788 0.21516	47.88 44.88
jan17c4a	0.78	0.03080 0.01570	1639 1354	0.004434 0.004574	0.14536 0.12386	32.78 27.08
jan17c4b	0.78	0.02738 0.01363	1681 1467	0.004296 0.004342	0.14444 0.12740	33.62 29.34
jan17c4c	0.78	0.03832 0.02014	1830 1691	0.004470 0.004665	0.16362 0.15776	36.60 33.82
jan17c5a	0.89	0.01838 0.01087	1348 1361	0.004079 0.004205	0.10998 0.1144+	26.96 27.22
jan17c5b	0.89	0.01949 0.01015	1260 1272	0.004165 0.004303	0.10496 0.10948	25.20 25.44
jan17c5c	0.89	0.01766 0.00893	1180 1226	0.004150 0.004095	0.09794 0.10042	23.60 24.52
jan17c6a	0.92	0.00996 0.00696	1126 1170	0.003839 0.003940	0.08646 0.09220	22.52 23.40
jan17c6b	0.92	0.01072 0.00774	1069 1121	0.004009 0.004158	0.08572 0.09322	21.38 22.42
jan17c6c	0.92	0.01025 0.00688	1129 1077	0.003910 0.004072	0.08828 0.08772	22.58 21.54

Table A4.19
T=100°C, V_g=14.7 cm/s, z=61 cm

Filename	e=r/R	Average Signal Intensity volt	Total Number of Bubbles	Average Bubble Duration s	Gas Holdup	Bubble Freq. 1/s
jan17d1a	0.19	0.11825 0.04909	3437 3647	0.005044 0.004701	0.34670 0.34288	68.74 72.94
jan17d1b	0.19	0.13833 0.05818	3420 3687	0.005263 0.004986	0.35996 0.36770	68.40 73.74
jan17d1c	0.19	0.11957 0.04900	3417 3545	0.004999 0.004859	0.34166 0.34448	68.34 70.90
jan17d2a	0.42	0.09654 0.03841	3037 3011	0.004829 0.004649	0.29334 0.27994	60.74 60.22
jan17d2b	0.42	0.10117 0.04206	3127 3127	0.004851 0.004807	0.30336 0.30066	62.54 62.54
jan17d2c	0.42	0.09397 0.04024	3114 3097	0.004770 0.004727	0.29710 0.29276	62.28 61.94
jan17d3a	0.62	0.06397 0.02743	2579 2408	0.004608 0.004600	0.23770 0.22154	51.58 48.16
jan17d3b	0.62	0.06015 0.02640	2433 2300	0.004592 0.004637	0.22344 0.21330	48.66 46.00
jan17d3c	0.62	0.05795 0.02279	2302 2202	0.004591 0.004359	0.21136 0.19196	46.04 44.04
jan17d4a	0.78	0.03177 0.01522	1784 1628	0.004363 0.004348	0.15566 0.14156	35.68 32.56
jan17d4b	0.78	0.03664 0.01623	1871 1754	0.004381 0.004360	0.16392 0.15294	37.42 35.08
jan17d4c	0.78	0.03070 0.01612	1776 1775	0.004331 0.004285	0.15384 0.15212	35.52 35.50
jan17d5a	0.89	0.01698 0.00969	1364 1334	0.003973 0.004050	0.10838 0.10806	27.28 26.68
jan17d5b	0.89	0.01335 0.00697	1339 1299	0.003855 0.003931	0.10324 0.10212	26.78 25.98
jan17d5c	0.89	0.01585 0.00932	1517 1361	0.003869 0.004044	0.11740 0.11008	30.34 27.22
jan17d6a	0.92	0.01585 0.00961	1436 1570	0.003872 0.003902	0.11120 0.12252	28.72 31.40
jan17d6b	0.92	0.00874 0.00599	1206 1318	0.003750 0.003788	0.09046 0.09984	24.12 26.36
jan17d6c	0.92	0.00623 0.00441	1083 1246	0.003630 0.003624	0.07862 0.09030	21.66 24.92

Table A4.20
T=100°C, V_g=14.7 cm/s, z=76 cm

Filename	e=r/R	Average Signal Intensity volt	Total Number of Bubbles	Average Bubble Duration s	Gas Holdup	Bubble Freq. 1/s
jan17e1a	0.19	0.12983 0.04896	3612 3817	0.005004 0.004742	0.36150 0.36204	72.24 76.34
jan17e1b	0.19	0.12547 0.04766	3515 3826	0.005025 0.004686	0.35328 0.35856	70.30 76.52
jan17e1c	0.19	0.13429 0.04914	3510 3597	0.005091 0.004838	0.35742 0.34802	70.20 71.94
jan17e2a	0.42	0.10295 0.03939	3091 3331	0.005020 0.004545	0.31084 0.30280	61.82 66.62
jan17e2b	0.42	0.09957 0.04249	3132 3409	0.004914 0.004633	0.30780 0.31586	62.64 68.18
jan17e2c	0.42	0.09314 0.03765	3029 3185	0.004890 0.004570	0.29626 0.29114	60.58 63.70
jan17e3a	0.62	0.04706 0.02333	2317 2471	0.004520 0.004365	0.20944 0.21570	46.34 49.42
jan17e3b	0.62	0.05557 0.02448	2326 2394	0.004623 0.004420	0.21504 0.21162	46.5 47.9
jan17e3c	0.62	0.05925 0.02734	2427 2653	0.004701 0.004342	0.22820 0.23038	48.54 53.06
jan17e4a	0.78	0.03039 0.01571	1975 1997	0.004147 0.004121	0.16382 0.16458	39.50 39.94
jan17e4b	0.78	0.02667 0.01500	1842 1670	0.004195 0.004268	0.15454 0.14254	36.84 33.40
jan17e4c	0.78	0.02982 0.01554	1796 1789	0.004297 0.004186	0.15434 0.14978	35.92 35.78
jan17e5a	0.89	0.01494 0.00958	1422 1423	0.003792 0.003935	0.10784 0.11200	28.44 28.46
jan17e5b	0.89	0.01482 0.00810	1387 1497	0.003906 0.003824	0.10836 0.11450	27.74 29.94
jan17e6a	0.92	0.00824 0.00656	1065 1216	0.003599 0.003818	0.07666 0.09286	21.30 24.32
jan17e6b	0.92	0.00923 0.00596	1071 1109	0.003735 0.003862	0.08000 0.08566	21.42 22.18
jan17e6c	0.92	0.00877 0.00657	1135 1208	0.003664 0.003851	0.08318 0.09304	22.70 24.16

Table A4.21
T=175°C, V_g=2.2 cm/s, z=15 cm

Filename	θ=r/R	Average Signal Intensity volt	Total Number of Bubbles	Average Bubble Duration s	Gas Holdup	Bubble Freq. 1/s
jan18e1a	0.19	0.11944 0.01175	522 437	0.006358 0.005554	0.06638 0.04854	10.44 8.74
jan18e1b	0.19	0.11362 0.01169	523 437	0.006031 0.005588	0.06308 0.04884	10.46 8.74
jan18e1c	0.19	0.11655 0.01206	515 423	0.006350 0.005813	0.06540 0.04918	10.30 8.46
jan18e2a	0.42	0.11725 0.01554	538 452	0.006467 0.006334	0.06958 0.05726	10.76 9.04
jan18e2b	0.42	0.11696 0.01662	587 516	0.006167 0.006037	0.07240 0.06230	11.74 10.32
jan18e2c	0.42	0.11686 0.01317	621 503	0.006052 0.005511	0.07516 0.05544	12.42 10.06
jan18e3a	0.62	0.11520 0.01493	643 501	0.006103 0.005609	0.07848 0.05620	12.86 10.02
jan18e3b	0.62	0.11158 0.01371	555 410	0.006292 0.005229	0.06984 0.04862	11.10 8.20
jan18e3c	0.62	0.11571 0.01981	648 534	0.006014 0.006086	0.07794 0.06500	12.96 10.68
jan18e4a	0.78	0.10647 0.01303	504 367	0.006367 0.005970	0.06418 0.04382	10.08 7.34
jan18e4b	0.78	0.09998 0.00960	370 369	0.006422 0.005463	0.04752 0.04032	7.40 7.38
jan18e4c	0.78	0.10270 0.01340	444 394	0.006367 0.006155	0.05654 0.04850	8.88 7.88
jan18e5a	0.89	0.10875 0.01297	432 350	0.006771 0.006091	0.05850 0.04264	8.64 7.00
jan18e5b	0.89	0.10912 0.01705	526 441	0.006205 0.006181	0.06528 0.05452	10.52 8.82
jan18e5c	0.89	0.11209 0.01718	425 408	0.007179 0.006461	0.06102 0.05272	8.50 8.16
jan18e6a	0.92	0.10034 0.00948	363 275	0.006375 0.005909	0.04628 0.03250	7.26 5.50
jan18e6b	0.92	0.10675 0.01085	362 275	0.006569 0.006342	0.04756 0.03488	7.24 5.50
jan18e6c	0.92	0.11126 0.01238	335 256	0.006910 0.006734	0.04630 0.03448	6.70 5.12

Table A4.22
T=175°C, V_g=2.2 cm/s, z=30 cm

Filename	Θ=r/R	Average Signal Intensity volt	Total Number of Bubbles	Average Bubble Duration s	Gas Holdup	Bubble Freq. 1/s
jan18d1a	0.19	0.11269 0.01814	664 648	0.006002 0.005557	0.07970 0.07202	13.28 12.96
jan18d1b	0.19	0.11464 0.01564	629 606	0.006335 0.005630	0.07970 0.06824	12.58 12.12
jan18d1c	0.19	0.11761 0.01703	687 656	0.006147 0.005549	0.08446 0.07280	13.74 13.12
jan18d2a	0.42	0.12856 0.02160	694 727	0.006537 0.005608	0.09074 0.08154	13.88 14.54
jan18d2b	0.42	0.12449 0.01990	723 633	0.006174 0.005983	0.08928 0.07574	14.46 12.66
jan18d2c	0.42	0.12316 0.02020	737 692	0.006134 0.005720	0.09042 0.07916	14.74 13.84
jan18d3a	0.62	0.11137 0.01399	623 557	0.006270 0.005671	0.07812 0.06318	12.46 11.14
jan18d3b	0.62	0.10924 0.01579	645 585	0.006078 0.005622	0.07840 0.06578	12.90 11.70
jan18d3c	0.62	0.10694 0.01323	600 502	0.006398 0.005661	0.07678 0.05684	12.00 10.04
jan18d4a	0.78	0.10320 0.01287	474 384	0.006209 0.006539	0.05886 0.05022	9.48 7.68
jan18d4b	0.78	0.10703 0.01085	469 418	0.006550 0.005952	0.06144 0.04976	9.38 8.36
jan18d4c	0.78	0.10564 0.01004	453 422	0.006305 0.005758	0.05712 0.04860	9.06 8.44
jan18d5a	0.89	0.10462 0.00700	374 308	0.006503 0.005666	0.04864 0.03490	7.48 6.16
jan18d5b	0.89	0.10123 0.00530	437 349	0.006021 0.004897	0.05262 0.03418	8.74 6.98
jan18d5c	0.89	0.09757 0.00556	353 291	0.006051 0.005842	0.04272 0.03400	7.06 5.82
jan18d6a	0.92	0.09543 0.00533	383 268	0.005726 0.005422	0.04386 0.02906	7.66 5.36
jan18d6b	0.92	0.09419 0.00719	395 305	0.006089 0.005407	0.04810 0.03298	7.90 6.10
jan18d6c	0.92	0.09433 0.00706	393 285	0.006168 0.005670	0.04848 0.03232	7.86 5.70

Table A4.23
T=175°C, V_g=2.2 cm/s, z=46 cm

Filename	θ=r/R	Average Signal Intensity volt	Total Number of Bubbles	Average Bubble Duration s	Gas Holdup	Bubble Freq. 1/s
jan18c1a	0.19	0.10679 0.01451	769 652	0.005889 0.005452	0.09058 0.07110	15.38 13.04
jan18c1b	0.19	0.10590 0.01666	778 774	0.005751 0.005220	0.08948 0.08080	15.56 15.48
jan18c1c	0.19	0.11038 0.01960	853 831	0.005880 0.005279	0.10032 0.08774	17.06 16.62
jan18c2a	0.42	0.12470 0.02230	859 893	0.005984 0.005413	0.10280 0.09668	17.18 17.86
jan18c2b	0.42	0.12413 0.02144	889 867	0.005807 0.005358	0.10324 0.09290	17.78 17.34
jan18c2c	0.42	0.12452 0.01995	830 818	0.006023 0.005345	0.09998 0.08744	16.60 16.36
jan18c3a	0.62	0.12682 0.01628	869 706	0.005970 0.005482	0.10376 0.07740	17.38 14.12
jan18c3b	0.62	0.12543 0.01552	815 687	0.006202 0.005435	0.10110 0.07468	16.30 13.74
jan18c3c	0.62	0.12237 0.02056	892 793	0.005842 0.005474	0.10422 0.08682	17.84 15.86
jan18c4a	0.78	0.10894 0.01297	666 490	0.006291 0.005798	0.08380 0.05682	13.32 9.80
jan18c4b	0.78	0.11164 0.00990	595 494	0.006718 0.005409	0.07994 0.05344	11.90 9.88
jan18c4c	0.78	0.11618 0.01215	662 524	0.006184 0.005414	0.08188 0.05674	13.24 10.48
jan18c5a	0.89	0.10984 0.00759	524 372	0.006202 0.005610	0.06500 0.04174	10.48 7.44
jan18c5b	0.89	0.10771 0.00702	505 386	0.006032 0.005479	0.06092 0.04230	10.10 7.72
jan18c5c	0.89	0.10847 0.00764	483 356	0.006058 0.005966	0.05852 0.04248	9.66 7.12
jan18c6a	0.92	0.10114 0.00687	438 360	0.005995 0.005553	0.05252 0.03998	8.76 7.20
jan18c6b	0.92	0.10447 0.00632	441 361	0.006424 0.005374	0.05666 0.03880	8.82 7.22
jan18c6c	0.92	0.10457 0.00852	430 378	0.006012 0.005720	0.05170 0.04324	8.60 7.56

Table A4.24
T=175°C, V_g=2.2 cm/s, z=61 cm

Filename	θ=r/R	Average Signal Intensity volt	Total Number of Bubbles	Average Bubble Duration s	Gas Holdup	Bubble Freq. 1/s
jan18b1a	0.19	0.11107 0.01938	891 889	0.005932 0.005190	0.10570 0.09228	17.82 17.78
jan18b1b	0.19	0.11049 0.01947	947 862	0.005919 0.005419	0.11210 0.09342	18.94 17.24
jan18b1c	0.19	0.11308 0.02201	908 906	0.006054 0.005465	0.10994 0.09902	18.16 18.12
jan18b2a	0.42	0.11618 0.02259	956 1003	0.005860 0.005239	0.11204 0.10510	19.12 20.06
jan18b2b	0.42	0.11526 0.01992	983 902	0.005947 0.005315	0.11692 0.09588	19.66 18.04
jan18b2c	0.42	0.11581 0.02213	880 856	0.006008 0.005514	0.10574 0.09440	17.60 17.12
jan18b3a	0.62	0.11055 0.01457	796 701	0.006114 0.005411	0.09734 0.07586	15.92 14.02
jan18b3b	0.62	0.11559 0.01525	868 749	0.006118 0.005300	0.10620 0.07940	17.36 14.98
jan18b3c	0.62	0.11825 0.01798	849 778	0.006185 0.005513	0.10502 0.08578	16.98 15.56
jan18b4a	0.78	0.10275 0.00900	680 566	0.006240 0.005314	0.08486 0.06016	13.60 11.32
jan18b4b	0.78	0.10154 0.01106	659 600	0.006179 0.005362	0.08144 0.06434	13.18 12.00
jan18b4c	0.78	0.09622 0.00729	523 468	0.006380 0.005519	0.06674 0.05166	10.46 9.36
jan18b5a	0.89	0.09728 0.00413	425 308	0.006600 0.005351	0.05610 0.03296	8.50 6.16
jan18b5b	0.89	0.10448 0.00688	499 450	0.006511 0.005364	0.06498 0.04828	9.98 9.00
jan18b5c	0.89	0.10358 0.00355	426 337	0.006380 0.005356	0.05436 0.03610	8.52 6.74
jan18b6a	0.92	0.10867 0.00732	509 438	0.006397 0.005345	0.06512 0.04682	10.18 8.76
jan18b6b	0.92	0.10777 0.00555	549 419	0.006215 0.005215	0.06824 0.04370	10.98 8.38
jan18b6c	0.92	0.10636 0.00770	541 458	0.006157 0.005539	0.06662 0.05074	10.82 9.16

Table A4.25
T=175°C, V_g=2.2 cm/s, z=76 cm

Filename	θ=r/R	Average Signal Intensity volt	Total Number of Bubbles	Average Bubble Duration s	Gas Holdup	Bubble Freq. 1/s
jan18a1a	0.19	0.11053 0.01855	903 899	0.006034 0.005253	0.10898 0.09444	18.06 17.98
jan18a1b	0.19	0.10992 0.02034	986 999	0.005597 0.005115	0.11038 0.10220	19.72 19.98
jan18a1c	0.19	0.11623 0.02320	1001 1039	0.005924 0.005307	0.11860 0.11028	20.02 20.78
jan18a2a	0.42	0.12111 0.02063	919 989	0.005736 0.005208	0.10542 0.10302	18.38 19.78
jan18a2b	0.42	0.13141 0.02530	1125 1079	0.005758 0.005278	0.12956 0.11390	22.50 21.58
jan18a2c	0.42	0.13211 0.02688	1103 1151	0.005859 0.005304	0.12926 0.12210	22.06 23.02
jan18a3a	0.62	0.10560 0.01637	801 770	0.006010 0.005383	0.09628 0.08290	16.02 15.40
jan18a3b	0.62	0.11102 0.01984	1002 912	0.005733 0.005303	0.11488 0.09672	20.04 18.24
jan18a3c	0.62	0.11191 0.02144	937 919	0.005905 0.005533	0.11066 0.10170	18.74 18.38
jan18a4a	0.78	0.09582 0.00725	617 470	0.006125 0.005640	0.07558 0.05302	12.34 9.40
jan18a4b	0.78	0.10187 0.01381	793 712	0.006033 0.005506	0.09568 0.07840	15.86 14.24
jan18a4c	0.78	0.09864 0.01023	667 650	0.006001 0.005358	0.08006 0.06966	13.34 13.00
jan18a5a	0.89	0.10076 0.00600	513 385	0.006673 0.005565	0.06846 0.04296	10.26 7.72
jan18a5b	0.89	0.10136 0.00866	592 442	0.006285 0.005627	0.07442 0.04974	11.84 8.84
jan18a5c	0.89	0.09779 0.00697	481 441	0.006235 0.005660	0.05998 0.04992	9.62 8.82
jan18a6a	0.92	0.10002 0.00524	469 370	0.006580 0.005714	0.06172 0.04228	9.38 7.40
jan18a6b	0.92	0.10595 0.00697	500 427	0.006382 0.005506	0.06382 0.04702	10.00 8.54
jan18a6c	0.92	0.11041 0.00863	559 434	0.006213 0.005795	0.06946 0.05030	11.18 8.68

Table A4.26
T=175°C, V_g=4.1 cm/s, z=15 cm

Filename	θ=r/R	Average Signal Intensity volt	Total Number of Bubbles	Average Bubble Duration s	Gas Holdup	Bubble Freq. 1/s
jan20a1a	0.19	0.12819 0.02266	913 806	0.006170 0.005710	0.11266 0.09204	18.26 16.12
jan20a1b	0.19	0.12030 0.01990	862 672	0.006224 0.005884	0.10730 0.07908	17.24 13.44
jan20a1c	0.19	0.12195 0.01957	842 699	0.006518 0.005674	0.10976 0.07932	16.84 13.98
jan20a2a	0.42	0.13608 0.02437	979 871	0.006267 0.005591	0.12270 0.09740	19.58 17.42
jan20a2b	0.42	0.13176 0.02708	892 907	0.006250 0.005612	0.11150 0.10180	17.84 18.14
jan20a2c	0.42	0.13583 0.02547	991 898	0.006175 0.005601	0.12238 0.10060	19.82 17.96
jan20a3a	0.62	0.12880 0.02030	812 718	0.006303 0.005877	0.10236 0.08440	16.24 14.36
jan20a3b	0.62	0.11898 0.01779	784 772	0.006209 0.005400	0.09736 0.08338	15.68 15.44
jan20a3c	0.62	0.11672 0.01431	743 646	0.006237 0.005526	0.09268 0.07140	14.86 12.92
jan20a4a	0.78	0.12127 0.01490	697 629	0.006527 0.005412	0.09098 0.06808	13.94 12.58
jan20a4b	0.78	0.11653 0.01288	701 561	0.006078 0.005590	0.08522 0.06272	14.02 11.22
jan20a4c	0.78	0.11568 0.01116	642 584	0.006154 0.005442	0.07902 0.06356	12.84 11.68
jan20a5a	0.89	0.10424 0.00606	442 425	0.006312 0.005113	0.05580 0.04346	8.84 8.50
jan20a5b	0.89	0.10653 0.01028	552 475	0.006214 0.005625	0.06860 0.05344	11.04 9.50
jan20a5c	0.89	0.11059 0.00895	612 478	0.006096 0.005437	0.07462 0.05198	12.24 9.56
jan20a6a	0.92	0.11220 0.01163	584 445	0.006358 0.005730	0.07426 0.05100	11.68 8.90
jan20a6b	0.92	0.10579 0.00811	500 409	0.006362 0.005506	0.06362 0.04504	10.00 8.18
jan20a6c	0.92	0.11560 0.01132	587 444	0.006278 0.005725	0.07370 0.05084	11.74 8.88

Table A4.27
T=175°C, V_g=4.1 cm/s, z=30 cm

Filename	Θ=r/R	Average Signal Intensity volt	Total Number of Bubbles	Average Bubble Duration s	Gas Holdup	Bubble Freq. 1/s
jan20b1a	0.19	0.13842 0.02755	1135 1199	0.005939 0.005257	0.13482 0.12606	22.70 23.98
jan20b1b	0.19	0.14122 0.02761	1235 1158	0.005898 0.005304	0.14568 0.12284	24.70 23.16
jan20b1c	0.19	0.13882 0.02637	1184 1115	0.006136 0.005364	0.14530 0.11962	23.68 22.30
jan20b2a	0.42	0.12570 0.02359	1122 1089	0.006194 0.005286	0.13900 0.11512	22.44 21.78
jan20b2b	0.42	0.12077 0.02262	1053 977	0.005930 0.005390	0.12488 0.10532	21.06 19.54
jan20b2c	0.42	0.12466 0.02300	1135 1011	0.005933 0.005331	0.13468 0.10780	22.70 20.22
jan20b3a	0.62	0.12511 0.02266	1058 1008	0.005819 0.005493	0.12314 0.11074	21.16 20.16
jan20b3b	0.62	0.12448 0.01735	939 876	0.006050 0.005301	0.11362 0.09288	18.78 17.52
jan20b3c	0.62	0.13022 0.01586	962 884	0.005966 0.005155	0.11478 0.09114	19.24 17.68
jan20b4a	0.78	0.10300 0.01117	790 718	0.005928 0.005175	0.09366 0.07432	15.80 14.36
jan20b4b	0.78	0.11156 0.01127	851 731	0.005854 0.005066	0.09964 0.07406	17.02 14.62
jan20b4c	0.78	0.11204 0.01022	796 763	0.005740 0.005983	0.09138 0.07604	15.92 15.26
jan20b5a	0.89	0.11194 0.00645	569 553	0.005963 0.005002	0.06786 0.05532	11.38 11.06
jan20b5b	0.89	0.10689 0.00863	634 615	0.005634 0.005135	0.07144 0.06316	12.68 12.30
jan20b5c	0.89	0.10562 0.00718	630 619	0.005579 0.007179	0.07030 0.00614	12.60 12.40
jan20b6a	0.92	0.10187 0.00749	653 578	0.005807 0.005050	0.07584 0.05838	13.06 11.56
jan20b6b	0.92	0.09842 0.00827	620 549	0.006027 0.005222	0.07474 0.05734	12.40 10.98
jan20b6c	0.92	0.10595 0.00882	660 602	0.006242 0.005264	0.08240 0.06338	13.20 12.04

Table A4.28
T=175°C, V_g=4.1 cm/s, z=46 cm

Filename	Θ=r/R	Average Signal Intensity volt	Total Number of Bubbles	Average Bubble Duration s	Gas Holdup	Bubble Freq. 1/s
jan20c1a	0.19	0.13294 0.03082	1578 1500	0.005433 0.004995	0.17146 0.14984	31.56 30.00
jan20c1b	0.19	0.13925 0.03504	1646 1541	0.005389 0.005125	0.17742 0.15794	32.92 30.82
jan20c1c	0.19	0.14099 0.03780	1524 1623	0.005518 0.005148	0.16784 0.16710	30.48 32.46
jan20c2a	0.42	0.13627 0.02623	1427 1389	0.005540 0.004829	0.15812 0.13416	28.54 27.78
jan20c2b	0.42	0.14340 0.02854	1585 1482	0.005606 0.005011	0.17772 0.14854	31.70 29.64
jan20c2c	0.42	0.14697 0.03056	1702 1526	0.005498 0.004999	0.18716 0.15256	34.04 30.52
jan20c3a	0.62	0.13005 0.01670	1403 1120	0.005546 0.004991	0.15562 0.11180	28.06 22.40
jan20c3b	0.62	0.13419 0.02288	1353 1281	0.005684 0.005102	0.15382 0.13072	27.06 25.62
jan20c3c	0.62	0.13902 0.02742	1506 1315	0.005558 0.005129	0.16742 0.13488	30.12 26.30
jan20c4a	0.78	0.12567 0.01318	1297 883	0.005455 0.005033	0.14150 0.08888	25.94 17.66
jan20c4b	0.78	0.12898 0.01896	1469 1113	0.005404 0.005026	0.15876 0.11188	29.38 22.26
jan20c4c	0.78	0.11824 0.01272	1203 926	0.005426 0.004931	0.13056 0.09132	24.06 18.52
jan20c5a	0.89	0.10970 0.00928	852 734	0.005829 0.004955	0.09932 0.07274	17.04 14.68
jan20c5b	0.89	0.10617 0.00845	795 672	0.005675 0.005113	0.09024 0.06872	15.90 13.44
jan20c5c	0.89	0.10821 0.00957	854 789	0.005588 0.004981	0.09544 0.07860	17.08 15.78
jan20c6a	0.92	0.10514 0.00709	660 563	0.005932 0.005032	0.07830 0.05666	13.20 11.26
jan20c6b	0.92	0.09942 0.00506	599 555	0.005586 0.004831	0.06692 0.05362	11.98 11.10
jan20c6c	0.92	0.10138 0.00774	758 620	0.005641 0.005058	0.08552 0.06272	15.16 12.40

485

Table A4.29
T=175°C, V_g=4.1 cm/s, z=61 cm

Filename	Θ=r/R	Average Signal Intensity volt	Total Number of Bubbles	Average Bubble Duration s	Gas Holdup	Bubble Freq. 1/s
jan20d1a	0.19	0.14365 0.03591	1810 1827	0.005503 0.004946	0.19920 0.18074	36.20 36.54
jan20d1b	0.19	0.14406 0.03644	1756 1822	0.005470 0.004969	0.19212 0.18106	35.12 36.44
jan20d1c	0.19	0.14467 0.03606	1721 1734	0.005481 0.005067	0.18866 0.17572	34.42 34.68
jan20d2a	0.42	0.15120 0.03327	1786 1638	0.005468 0.005015	0.19530 0.16428	35.72 32.76
jan20d2b	0.42	0.14188 0.02855	1734 1528	0.005272 0.004933	0.18282 0.15074	34.68 30.56
jan20d2c	0.42	0.15003 0.03189	1743 1616	0.005464 0.004944	0.19046 0.15978	34.86 32.32
jan20d3a	0.62	0.12974 0.02327	1402 1298	0.005556 0.005131	0.15580 0.13320	28.04 25.96
jan20d3b	0.62	0.11769 0.01558	1295 1125	0.005628 0.004912	0.14576 0.11052	25.90 22.50
jan20d3c	0.62	0.12223 0.01877	1411 1201	0.005582 0.004888	0.15752 0.11740	28.22 24.02
jan20d4a	0.78	0.11731 0.01453	1214 993	0.005527 0.005003	0.13420 0.09936	24.28 19.86
jan20d4b	0.78	0.12056 0.01381	1207 1049	0.005507 0.004794	0.13294 0.10058	24.14 20.98
jan20d4c	0.78	0.11735 0.01147	1125 902	0.005632 0.004937	0.12672 0.08906	22.50 18.04
jan20d5a	0.89	0.10751 0.00714	867 708	0.005475 0.004956	0.09494 0.07018	17.34 14.16
jan20d5b	0.89	0.10867 0.00762	912 767	0.005568 0.004875	0.10156 0.07478	18.24 15.34
jan20d5c	0.89	0.10489 0.00761	910 739	0.005418 0.004811	0.09860 0.07110	18.20 14.78
jan20d6a	0.92	0.10817 0.01016	911 865	0.005724 0.004884	0.10430 0.08450	18.22 17.30
jan20d6b	0.92	0.10091 0.00576	706 641	0.005673 0.004788	0.08010 0.06138	14.12 12.82
jan20d6c	0.92	0.10778 0.00832	770 709	0.005770 0.004865	0.08886 0.06898	15.40 14.18

Table A4.30
T=175°C, V_g=4.1 cm/s, z=76 cm

Filename	θ=r/R	Average Signal Intensity volt	Total Number of Bubbles	Average Bubble Duration s	Gas Holdup	Bubble Freq. 1/s
jan20e1a	0.19	0.14724 0.03869	2011 1990	0.005372 0.004857	0.21606 0.19332	40.22 39.80
jan20e1b	0.19	0.15594 0.04324	2111 2233	0.005283 0.004765	0.22304 0.21282	42.22 44.66
jan20e1c	0.19	0.15625 0.04362	2104 2199	0.005408 0.004802	0.22758 0.21118	42.08 43.98
jan20e2a	0.42	0.14363 0.03352	1735 1846	0.005490 0.004898	0.19050 0.18082	34.70 36.92
jan20e2b	0.42	0.13908 0.03184	1707 1751	0.005398 0.004855	0.18430 0.17002	34.14 35.02
jan20e2c	0.42	0.14267 0.03130	1849 1876	0.005274 0.004752	0.19504 0.17828	36.98 37.52
jan20e3a	0.62	0.13279 0.02366	1664 1537	0.005320 0.004744	0.17706 0.14584	33.28 30.74
jan20e3b	0.62	0.12812 0.01746	1453 1351	0.005470 0.004779	0.15896 0.12912	29.06 27.02
jan20e3c	0.62	0.12955 0.02327	1486 1550	0.005336 0.004735	0.15858 0.14680	29.72 31.00
jan20e4a	0.78	0.11326 0.01557	1361 1192	0.005410 0.004799	0.14726 0.11442	27.22 23.84
jan20e4b	0.78	0.11009 0.01487	1243 1094	0.005437 0.004916	0.13516 0.10756	24.86 21.88
jan20e4c	0.78	0.11092 0.01115	1141 1039	0.005390 0.004714	0.12300 0.09796	22.82 20.78
jan20e5a	0.89	0.10726 0.00923	1027 919	0.005213 0.004890	0.10708 0.08988	20.54 18.38
jan20e5b	0.89	0.10591 0.00832	959 896	0.005576 0.004669	0.10694 0.08366	19.18 17.92
jan20e5c	0.89	0.10095 0.00627	803 782	0.005619 0.004813	0.09024 0.07528	16.06 15.64
jan20e6a	0.92	0.10633 0.00762	921 789	0.005418 0.004693	0.09980 0.07406	18.42 15.78
jan20e6b	0.92	0.10372 0.00668	823 729	0.005281 0.004840	0.08692 0.07056	16.46 14.58
jan20e6c	0.92	0.10482 0.00626	783 658	0.005687 0.004926	0.08906 0.06482	15.66 13.16

Table A4.31
T=175°C, V_g=9.0 cm/s, z=15 cm

Filename	θ=r/R	Average Signal Intensity volt	Total Number of Bubbles	Average Bubble Duration s	Gas Holdup	Bubble Freq. 1/s
jan21e1a	0.19	0.14345 0.03657	1616 1470	0.005642 0.005269	0.18236 0.15490	32.32 29.40
jan21e1b	0.19	0.14355 0.03807	1593 1400	0.005766 0.005333	0.18370 0.14932	31.86 28.00
jan21e1c	0.19	0.14838 0.04070	1735 1517	0.005627 0.005340	0.19526 0.16202	34.70 30.34
jan21e2a	0.42	0.17147 0.04591	2264 1772	0.005315 0.005212	0.24066 0.18472	45.28 35.44
jan21e2b	0.42	0.17008 0.04935	2109 1736	0.005516 0.005385	0.23266 0.18696	42.18 34.72
jan21e2c	0.42	0.16529 0.04504	1931 1723	0.005595 0.005265	0.21608 0.18144	38.62 34.46
jan21e3a	0.62	0.15644 0.04167	1904 1763	0.005494 0.005120	0.20920 0.18052	38.08 35.26
jan21e3b	0.62	0.15331 0.04550	1795 1717	0.005538 0.005220	0.19882 0.17924	35.90 34.34
jan21e3c	0.62	0.15336 0.04219	1833 1711	0.005531 0.005126	0.20278 0.17542	36.66 34.22
jan21e4a	0.78	0.15264 0.03905	1841 1674	0.005673 0.005130	0.20888 0.17174	36.82 33.48
jan21e4b	0.78	0.14632 0.03431	1570 1416	0.005744 0.005201	0.18036 0.14728	31.40 28.32
jan21e4c	0.78	0.14247 0.03557	1663 1568	0.005591 0.005022	0.18596 0.15748	33.26 31.36
jan21e5a	0.89	0.12219 0.01998	1266 1079	0.005372 0.004829	0.13602 0.10422	25.32 21.58
jan21e5b	0.89	0.13367 0.02095	1625 1262	0.005268 0.004676	0.17122 0.11802	32.50 25.24
jan21e5c	0.89	0.13025 0.01871	1493 1126	0.005109 0.004702	0.15254 0.10588	29.86 22.52
jan21e6a	0.92	0.11161 0.01035	1109 838	0.004723 0.004506	0.10476 0.07552	22.18 16.76
jan21e6b	0.92	0.11829 0.01271	1171 909	0.005120 0.004652	0.11992 0.08458	23.42 18.18
jan21e6c	0.92	0.11674 0.01476	1128 898	0.005097 0.004756	0.11498 0.08542	22.56 17.96

Table A4.32
T=175°C, V_g=9.0 cm/s, z=30 cm

Filename	e=r/R	Average Signal Intensity volt	Total Number of Bubbles	Average Bubble Duration s	Gas Holdup	Bubble Freq. 1/s
jan21d1a	0.19	0.17419 0.04679	2536 2505	0.005096 0.004637	0.25846 0.23230	50.72 50.10
jan21d1b	0.19	0.17078 0.04692	2492 2378	0.005157 0.004762	0.25700 0.22650	49.84 47.56
jan21d1c	0.19	0.16649 0.04942	2479 2411	0.005065 0.004807	0.25112 0.23178	49.58 48.22
jan21d2a	0.42	0.17534 0.05672	2622 2531	0.005059 0.004874	0.26530 0.24672	52.44 50.62
jan21d2b	0.42	0.16255 0.04767	2280 2329	0.005145 0.004774	0.23462 0.22236	45.60 46.58
jan21d2c	0.42	0.15967 0.04402	2224 2272	0.005239 0.004778	0.23302 0.21712	44.48 45.44
jan21d3a	0.62	0.15353 0.04163	2330 2163	0.005112 0.004708	0.23820 0.20366	46.60 43.26
jan21d3b	0.62	0.14631 0.03484	2203 2121	0.005143 0.004627	0.22660 0.19628	44.06 42.42
jan21d3c	0.62	0.13840 0.03914	2356 2245	0.004909 0.004563	0.23130 0.20490	47.12 44.90
jan21d4a	0.78	0.13817 0.03109	1900 1799	0.005097 0.004614	0.19368 0.16600	38.00 35.98
jan21d4b	0.78	0.13733 0.03118	1943 1805	0.005176 0.004655	0.20114 0.16804	38.86 36.10
jan21d4c	0.78	0.12896 0.02656	1864 1825	0.005010 0.004496	0.18678 0.16412	37.28 36.50
jan21d5a	0.89	0.11787 0.01969	1392 1377	0.004895 0.004564	0.13628 0.12568	27.84 27.54
jan21d5b	0.89	0.11081 0.01433	1231 1245	0.004830 0.004373	0.11892 0.10890	24.62 24.90
jan21d5c	0.89	0.11246 0.01517	1351 1416	0.004922 0.004222	0.13300 0.11958	27.02 28.32
jan21d6a	0.92	0.10121 0.01217	1096 1114	0.004575 0.004322	0.10028 0.09638	21.92 22.28
jan21d6b	0.92	0.11037 0.01187	1198 1222	0.004860 0.004241	0.11644 0.10364	23.96 24.44
jan21d6c	0.92	0.10713 0.01414	1173 1272	0.004667 0.004312	0.10948 0.10970	23.46 25.44

Table A4.33
T=175°C, V_g=9.0 cm/s, z=46 cm

Filename	θ=r/R	Average Signal Intensity volt	Total Number of Bubbles	Average Bubble Duration s	Gas Holdup	Bubble Freq. 1/s
jan21c1a	0.19	0.18462 0.05613	3273 3246	0.004812 0.004538	0.31502 0.29462	65.46 64.92
jan21c1b	0.19	0.19303 0.06692	3408 3282	0.004751 0.004707	0.32380 0.30894	68.16 65.64
jan21c1c	0.19	0.17740 0.05559	3191 3126	0.004762 0.004594	0.30394 0.28720	63.82 62.52
jan21c2a	0.42	0.19199 0.06161	3227 3494	0.004893 0.004542	0.31580 0.31738	64.54 69.88
jan21c2b	0.42	0.17968 0.05321	3077 3114	0.004830 0.004555	0.29726 0.28366	61.54 62.28
jan21c2c	0.42	0.18138 0.05642	3201 3265	0.004872 0.004523	0.31190 0.29536	64.02 65.30
jan21c3a	0.62	0.15776 0.04310	2881 2736	0.004682 0.004470	0.26978 0.24458	57.62 54.72
jan21c3b	0.62	0.15041 0.03685	2822 2678	0.004553 0.004297	0.25696 0.23016	56.44 53.56
jan21c3c	0.62	0.15493 0.04609	2831 2790	0.004833 0.004550	0.27362 0.25390	56.62 55.80
jan21c4a	0.78	0.13060 0.02510	2355 2079	0.004552 0.004302	0.21438 0.17888	47.10 41.58
jan21c4b	0.78	0.13680 0.02478	2361 2026	0.004650 0.004357	0.21958 0.17654	47.22 40.52
jan21c4c	0.78	0.12598 0.02085	2211 2076	0.004519 0.004170	0.19984 0.17314	44.22 41.52
jan21c5a	0.89	0.11163 0.01489	1509 1515	0.004527 0.004138	0.13662 0.12538	30.18 30.30
jan21c5b	0.89	0.11374 0.01374	1568 1538	0.004773 0.004147	0.14968 0.12756	31.36 30.76
jan21c5c	0.89	0.11495 0.01523	1609 1579	0.004599 0.004142	0.14798 0.13080	32.18 31.58
jan21c6a	0.92	0.09902 0.00885	1231 1222	0.004705 0.004029	0.11584 0.09848	24.62 24.44
jan21c6b	0.92	0.10141 0.01407	1591 1460	0.004473 0.004262	0.14234 0.12446	31.82 29.20
jan21c6c	0.92	0.09700 0.01056	1403 1289	0.004510 0.004088	0.12656 0.10540	28.06 25.78

Table A4.34
T=175°C, V_g=9.0 cm/s, z=61 cm

Filename	e=r/R	Average Signal Intensity volt	Total Number of Bubbles	Average Bubble Duration s	Gas Holdup	Bubble Freq. 1/s
jan21b1a	0.19	0.21400 0.07230	4031 4094	0.004704 0.004468	0.37926 0.36588	80.62 81.88
jan21b1b	0.19	0.20294 0.07007	3774 4096	0.004745 0.004454	0.35816 0.36486	75.48 81.92
jan21b1c	0.19	0.20398 0.07079	3826 3923	0.004728 0.004516	0.36180 0.35434	76.52 78.46
jan21b2a	0.42	0.18284 0.05703	3796 3724	0.004573 0.004371	0.34722 0.32552	75.92 74.48
jan21b2b	0.42	0.18719 0.05641	4016 3768	0.004543 0.004323	0.36190 0.32576	80.32 75.36
jan21b2c	0.42	0.18926 0.05551	3987 3774	0.004522 0.004337	0.36062 0.32736	79.74 75.48
jan21b3a	0.62	0.15060 0.03743	3153 2930	0.004496 0.004264	0.28350 0.24988	63.06 58.60
jan21b3b	0.62	0.15786 0.04143	3292 3056	0.004592 0.004321	0.30236 0.26412	65.84 61.12
jan21b3c	0.62	0.16794 0.04427	3247 3178	0.004707 0.004341	0.30570 0.27592	64.94 63.56
jan21b4a	0.78	0.12960 0.02461	2659 2481	0.004408 0.004048	0.23440 0.20088	53.18 49.62
jan21b4b	0.78	0.12787 0.02646	2462 2467	0.004521 0.004133	0.22260 0.20390	49.24 49.34
jan21b4c	0.78	0.12017 0.01981	2316 2291	0.004594 0.004055	0.21280 0.18582	46.32 45.82
jan21b5a	0.89	0.10725 0.01330	1758 1787	0.004460 0.003909	0.15680 0.13972	35.16 35.74
jan21b5b	0.89	0.10624 0.01255	1893 1876	0.004373 0.003861	0.16556 0.14486	37.86 37.52
jan21b5c	0.89	0.10448 0.01310	1732 1661	0.004446 0.003993	0.15400 0.13264	34.64 33.22
jan21b6a	0.92	0.10678 0.01300	1476 1615	0.004509 0.004058	0.13312 0.13106	29.52 32.30
jan21b6b	0.92	0.10163 0.01182	1475 1547	0.004442 0.004045	0.13104 0.12514	29.50 30.94
jan21b6c	0.92	0.10100 0.01126	1464 1591	0.004347 0.003884	0.12728 0.12358	29.28 31.82

Table A4.35
T=175°C, V_g=9.0 cm/s, z=76 cm

Filename	θ=r/R	Average Signal Intensity volt	Total Number of Bubbles	Average Bubble Duration s	Gas Holdup	Bubble Freq. 1/s
jan21a1a	0.19	0.23290 0.07897	4849 4865	0.004548 0.004367	0.44110 0.42492	96.98 97.30
jan21a1b	0.19	0.22385 0.07366	4836 4723	0.004517 0.004374	0.43684 0.41314	96.72 94.46
jan21a1c	0.19	0.21914 0.07354	4909 4760	0.004422 0.004326	0.43418 0.41188	98.18 95.20
jan21a2a	0.42	0.18432 0.06200	4020 4042	0.004546 0.004371	0.36550 0.35338	80.40 80.84
jan21a2b	0.42	0.19324 0.06738	4221 4359	0.004542 0.004395	0.38340 0.38316	84.42 84.18
jan21a2c	0.42	0.17531 0.05686	4076 4157	0.004504 0.004243	0.36714 0.35274	81.52 83.14
jan21a3a	0.62	0.15223 0.04398	3560 3567	0.004505 0.004198	0.32074 0.29946	71.20 71.34
jan21a3b	0.62	0.14274 0.04061	3506 3266	0.004325 0.004224	0.30326 0.27588	70.12 65.32
jan21a3c	0.62	0.14505 0.03655	3417 3255	0.004487 0.004144	0.30662 0.26976	68.34 65.10
jan21a4a	0.78	0.12812 0.02618	2795 2772	0.004414 0.004065	0.24676 0.22536	55.90 55.44
jan21a4b	0.78	0.13768 0.03192	3046 2912	0.004352 0.004163	0.26510 0.24244	60.92 58.24
jan21a4c	0.78	0.13108 0.02754	3002 2946	0.004286 0.004096	0.25736 0.24136	60.04 58.92
jan21a5a	0.89	0.11345 0.01566	2169 2123	0.004234 0.003941	0.18368 0.16732	43.38 42.46
jan21a5b	0.89	0.10936 0.01380	1958 2057	0.004312 0.003832	0.16886 0.15766	39.16 41.14
jan21a5c	0.89	0.11394 0.01646	1980 2166	0.004453 0.003916	0.17634 0.16966	39.60 43.32
jan21a6a	0.92	0.10470 0.01155	1695 1812	0.004181 0.003816	0.14174 0.13828	33.90 36.24
jan21a6b	0.92	0.10287 0.01050	1710 1910	0.003989 0.003680	0.13642 0.14058	34.20 38.20
jan21a6c	0.92	0.10577 0.01077	1781 1778	0.004131 0.003840	0.14716 0.13656	35.62 35.56

Table A4.36
T=175°C, V_g=14.7 cm/s, z=15 cm

Filename	e=r/R	Average Signal Intensity volt	Total Number of Bubbles	Average Bubble Duration s	Gas Holdup	Bubble Freq. 1/s
jan22a1a	0.19	0.16104 0.05143	2474 2376	0.005211 0.004914	0.25786 0.23350	49.48 47.52
jan22a1b	0.19	0.16638 0.05079	2647 2389	0.005176 0.004897	0.27404 0.23396	52.94 47.78
jan22a1c	0.19	0.18018 0.05442	2607 2412	0.005316 0.004987	0.27718 0.24056	52.14 48.24
jan22a2a	0.42	0.18979 0.06317	2626 2572	0.005473 0.005095	0.28746 0.26210	52.52 51.44
jan22a2b	0.42	0.19280 0.06820	3021 2708	0.005162 0.005129	0.31188 0.27780	60.42 54.16
jan22a2c	0.42	0.20444 0.07363	3353 2871	0.005124 0.005140	0.34362 0.29516	67.06 57.42
jan22a3a	0.62	0.19138 0.06122	3236 2803	0.005019 0.004978	0.32484 0.27904	64.72 56.06
jan22a3b	0.62	0.18164 0.06495	3239 2658	0.004901 0.005050	0.31746 0.26848	64.78 53.16
jan22a3c	0.62	0.19093 0.06259	3212 2792	0.005042 0.004971	0.32388 0.27760	64.24 55.84
jan22a4a	0.78	0.17514 0.05328	2729 2567	0.005205 0.004875	0.28410 0.25028	54.58 51.34
jan22a4b	0.78	0.19502 0.06011	2809 2593	0.005350 0.004961	0.30054 0.25730	56.18 51.86
jan22a4c	0.78	0.20101 0.06543	2900 2656	0.005387 0.005156	0.31242 0.27388	58.00 53.12
jan22a5a	0.89	0.14952 0.03204	2239 1961	0.005081 0.004574	0.22752 0.17940	44.78 39.22
jan22a5b	0.89	0.14850 0.03686	2163 1928	0.005173 0.004805	0.22380 0.18530	43.26 38.56
jan22a5c	0.89	0.15138 0.04360	2294 2039	0.005026 0.004850	0.23058 0.19778	45.88 40.78
jan22a6a	0.92	0.11925 0.01891	1764 1585	0.004471 0.004205	0.15772 0.13330	35.28 31.70
jan22a6b	0.92	0.11648 0.01600	1675 1423	0.004466 0.004299	0.14962 0.12234	33.50 28.46
jan22a6c	0.92	0.11839 0.01657	1833 1514	0.004368 0.004248	0.16012 0.12862	36.66 30.28

Table A4.37
T=175°C, V_g=14.7 cm/s, z=30 cm

Filename	θ=r/R	Average Signal Intensity volt	Total Number of Bubbles	Average Bubble Duration s	Gas Holdup	Bubble Freq. 1/s
jan22b1a	0.19	0.18442 0.05809	3445 3331	0.004743 0.004583	0.32678 0.30532	68.90 66.62
jan22b1b	0.19	0.18200 0.06172	3279 3132	0.004734 0.004761	0.31048 0.29826	65.58 62.64
jan22b1c	0.19	0.19332 0.06337	3490 3318	0.004723 0.004709	0.32966 0.31246	69.80 66.36
jan22b2a	0.42	0.19996 0.07233	3449 3649	0.004835 0.004638	0.33354 0.33850	68.98 72.98
jan22b2b	0.42	0.20556 0.06996	3520 3454	0.004933 0.004765	0.34728 0.32918	70.40 69.08
jan22b2c	0.42	0.21124 0.06871	3719 3603	0.004805 0.004645	0.35742 0.33470	74.38 72.06
jan22b3a	0.62	0.20908 0.06969	3630 3478	0.004933 0.004748	0.35812 0.33282	72.60 69.56
jan22b3b	0.62	0.19307 0.05908	3333 3159	0.004915 0.004690	0.32766 0.19630	66.66 63.18
jan22b3c	0.62	0.19541 0.06235	3433 3300	0.004873 0.004684	0.33456 0.30912	68.66 66.00
jan22b4a	0.78	0.14851 0.03787	2849 2564	0.004669 0.004416	0.26604 0.22644	56.98 51.28
jan22b4b	0.78	0.15433 0.03959	2864 2645	0.004773 0.004358	0.27338 0.23052	57.28 52.90
jan22b4c	0.78	0.15901 0.04119	2852 2812	0.004570 0.004408	0.26070 0.24790	57.04 56.24
jan22b5a	0.89	0.13061 0.02269	2548 2026	0.004190 0.004167	0.21350 0.16886	50.96 40.52
jan22b5b	0.89	0.12903 0.02487	2064 1878	0.004456 0.004316	0.18396 0.16212	41.28 37.56
jan22b5c	0.89	0.14089 0.02621	2407 2025	0.004563 0.004261	0.21968 0.17256	48.14 40.50
jan22b6a	0.92	0.10749 0.01568	1908 1725	0.004227 0.003995	0.16132 0.13784	38.16 34.50
jan22b6b	0.92	0.10726 0.01563	1773 1806	0.004202 0.004029	0.14900 0.14554	35.46 36.12
jan22b6c	0.92	0.10881 0.01668	1994 1839	0.004306 0.004073	0.17172 0.14982	39.88 36.78

Table A4.38
T=175°C, V_g=14.7 cm/s, z=46 cm

Filename	θ=r/R	Average Signal Intensity volt	Total Number of Bubbles	Average Bubble Duration s	Gas Holdup	Bubble Freq. 1/s
jan22c1a	0.19	0.22847 0.07910	4617 4525	0.004583 0.004514	0.42324 0.10848	92.34 90.50
jan22c1b	0.19	0.22577 0.07968	4466 4376	0.004644 0.004522	0.41484 0.39576	89.32 87.52
jan22c1c	0.19	0.21590 0.07758	4286 4428	0.004672 0.004475	0.40050 0.39630	85.72 88.56
jan22c2a	0.42	0.20695 0.07054	3923 3958	0.004665 0.004508	0.36598 0.35686	78.46 79.16
jan22c2b	0.42	0.21973 0.07472	3827 3831	0.004881 0.004659	0.37362 0.35694	76.54 76.62
jan22c2c	0.42	0.21351 0.07590	3916 4030	0.004781 0.004636	0.37446 0.37366	78.32 80.60
jan22c3a	0.62	0.18183 0.06201	3388 3381	0.004744 0.004546	0.32148 0.30742	67.76 67.62
jan22c3b	0.62	0.17698 0.05371	3327 3277	0.004764 0.004525	0.31700 0.29660	66.54 65.54
jan22c3c	0.62	0.16600 0.04860	3421 3110	0.004545 0.004488	0.31098 0.27914	68.42 62.20
jan22c4a	0.78	0.15514 0.03520	2980 2689	0.004486 0.004272	0.26734 0.22976	59.60 53.78
jan22c4b	0.78	0.16763 0.03974	3273 2621	0.004591 0.004479	0.30054 0.23480	65.46 52.42
jan22c4c	0.78	0.15211 0.03616	3085 2505	0.004313 0.004317	0.26612 0.21626	61.70 50.10
jan22c5a	0.89	0.11882 0.01700	2447 1830	0.003890 0.003933	0.19038 0.14396	48.94 36.60
jan22c5b	0.89	0.11852 0.01795	2382 1925	0.003985 0.004022	0.18986 0.15486	47.64 38.50
jan22c5c	0.89	0.11864 0.02126	2218 1906	0.004035 0.004004	0.17898 0.15264	44.36 38.12
jan22c6a	0.92	0.09948 0.01308	1537 1565	0.004183 0.003862	0.12858 0.12088	30.74 31.30
jan22c6b	0.92	0.10584 0.01495	1909 1694	0.004247 0.004001	0.16214 0.13556	38.18 33.88
jan22c6c	0.92	0.10010 0.01361	1735 1558	0.004076 0.003906	0.14142 0.12172	34.70 31.16

Table A4.39
T=175°C, V_g=14.7 cm/s, z=61 cm

Filename	e=r/R	Average Signal Intensity volt	Total Number of Bubbles	Average Bubble Duration s	Gas Holdup	Bubble Freq. 1/s
jan22d1a	0.19	0.24098 0.07956	4754 4456	0.004565 0.004580	0.43400 0.40820	95.08 89.12
jan22d1b	0.19	0.24588 0.07890	4795 4498	0.004556 0.004599	0.43696 0.41372	95.90 89.96
jan22d1c	0.19	0.24397 0.07944	4672 4577	0.004615 0.004586	0.43124 0.41982	93.44 91.54
jan22d2a	0.42	0.21041 0.06623	4377 4320	0.004501 0.004374	0.39402 0.37790	87.54 86.40
jan22d2b	0.42	0.22075 0.06959	4286 4025	0.004640 0.004585	0.39772 0.36912	85.72 80.50
jan22d2c	0.42	0.21318 0.07121	4352 4038	0.004581 0.004560	0.39876 0.36826	87.04 80.76
jan22d3a	0.62	0.15948 0.04322	3284 3206	0.004436 0.004290	0.29134 0.27508	65.68 64.12
jan22d3b	0.62	0.16115 0.04545	3079 3013	0.004501 0.004406	0.27720 0.26550	61.58 60.26
jan22d3c	0.62	0.16777 0.04555	3389 3200	0.004539 0.004348	0.30762 0.27830	67.78 64.00
jan22d4a	0.78	0.15427 0.03628	3261 2807	0.004180 0.004189	0.27264 0.23516	65.22 56.14
jan22d4b	0.78	0.15009 0.03045	3101 2592	0.004255 0.004134	0.26390 0.21432	62.02 51.84
jan22d4c	0.78	0.14379 0.02897	3253 2616	0.004060 0.004065	0.26416 0.21268	65.06 52.32
jan22d5a	0.89	0.11674 0.01717	1992 1915	0.004249 0.003873	0.11674 0.14832	39.84 38.30
jan22d5b	0.89	0.11893 0.01913	1848 1946	0.004260 0.003969	0.15746 0.15446	36.96 38.92
jan22d5c	0.89	0.11102 0.01471	1841 1804	0.004116 0.003856	0.15154 0.13912	36.82 36.08
jan22d6a	0.92	0.10498 0.01135	1618 1753	0.004063 0.003715	0.13148 0.13026	32.36 35.06
jan22d6b	0.92	0.10450 0.01202	1510 1588	0.004104 0.003756	0.12394 0.11920	30.20 31.76
jan22d6c	0.92	0.10589 0.01239	1600 1698	0.004004 0.003741	0.12814 0.12704	32.00 33.96

Table A4.40
T=175°C, V_g=14.7 cm/s, z=76 cm

Filename	θ=r/R	Average Signal Intensity volt	Total Number of Bubbles	Average Bubble Duration s	Gas Holdup	Bubble Freq. 1/s
jan22e1a	0.19	0.23971 0.07682	4423 4453	0.004709 0.004568	0.41660 0.40686	88.46 89.06
jan22e1b	0.19	0.24992 0.08272	4796 4531	0.004588 0.004680	0.44012 0.42410	95.92 90.62
jan22e1c	0.19	0.25983 0.08277	5109 4749	0.004581 0.004613	0.46804 0.43812	102.18 94.98
jan22e2a	0.42	0.20964 0.06604	4385 4205	0.004459 0.004425	0.39104 0.37212	87.70 84.10
jan22e2b	0.42	0.21881 0.06701	4510 4347	0.004494 0.004392	0.40536 0.38188	90.20 86.94
jan22e2c	0.42	0.20500 0.06157	4417 4243	0.004271 0.004351	0.38616 0.36922	88.34 84.86
jan22e3a	0.62	0.15536 0.04337	3236 3205	0.004314 0.004215	0.27918 0.27016	64.72 64.10
jan22e3b	0.62	0.14640 0.03740	2948 3134	0.004346 0.004121	0.25626 0.25832	58.96 62.68
jan22e3c	0.62	0.17411 0.04858	3466 3309	0.004578 0.004380	0.31732 0.28984	69.32 66.18
jan22e4a	0.78	0.13228 0.02693	2831 2554	0.004047 0.004088	0.22912 0.20880	56.62 51.08
jan22e4b	0.78	0.13489 0.02478	2794 2529	0.004042 0.003982	0.22586 0.20140	55.88 50.58
jan22e4c	0.78	0.13124 0.02761	2560 2473	0.004164 0.004122	0.21318 0.20388	51.20 49.46
jan22e5a	0.89	0.10685 0.01589	1966 1975	0.004099 0.003792	0.16116 0.14980	39.32 39.50
jan22e5b	0.89	0.11454 0.02024	2273 2199	0.004207 0.003944	0.19124 0.17344	45.46 43.98
jan22e5c	0.89	0.10427 0.01555	1751 1668	0.004226 0.003859	0.14798 0.12872	35.02 33.36
jan22e6a	0.92	0.10363 0.01101	1355 1615	0.004191 0.003716	0.11358 0.12004	27.10 32.30
jan22e6b	0.92	0.09790 0.01181	1370 1610	0.004048 0.003743	0.11092 0.12052	27.40 32.20
jan22e6c	0.92	0.10117 0.01265	1422 1515	0.003994 0.003772	0.11360 0.11428	28.44 30.30

APPENDIX 5

GRID PRESSURE DROP

PERFORATED PLATE GAS DISTRIBUTOR
PRESSURE DROP MEASUREMENTS

The pressure drop across the perforated plate gas distributor was measured using a pressure transducer (Data Instrument, Model AB, absolute pressure) coupled to a mechanical switch wafer (Scanivalve Corporation). The two pressure taps, downstream and upstream of the perforated plate, were located as indicated on Figure A5.1.

In order to obtain the net pressure drop across the perforated plate, a number of contributions to the pressure drop measured at the existing taps locations had to be subtracted. These contributions include the friction losses in the gas inlet pipe (26.99 cm of pipe length, 1 elbow, 1 sudden enlargement) (the friction losses in the main column were assumed negligible), the difference in static pressure between the pressure tap no. 2 and the pressure tap no. 1, and the change in kinetic energy between positions 2 and 1:

$$\Delta P_{grid} = \Delta P_{measured} - (\Delta P_{friction} + \Delta P_{potential\ energy} + \Delta P_{kinetic\ energy}) \qquad (A5.1)$$

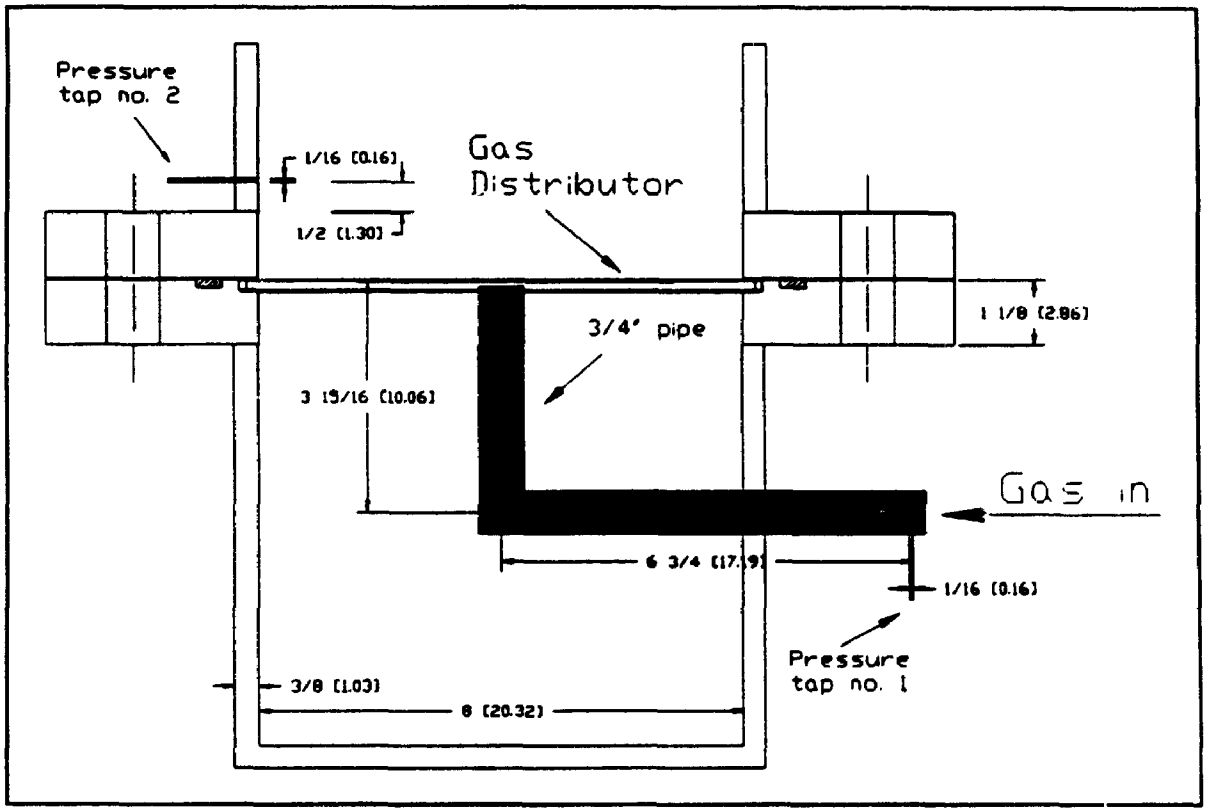

Figure A5.1: Pressure taps locations for the pressure drop measurement across the perforated plate distributor (dimensions: inch [cm])

1. Friction losses

(V_g=2.2 cm/s; q=691.2 cm^3/s):

ρ_g=1.243 kg/m^3 (P_{avg}=110.03 Kpa; average pressure between tap no.1 and tap no. 2)

μ=0.0000178 kg/m-s

d=0.0209 m (3/4" pipe, sch. 40 : i.d. = 0.824" = 2.09 cm)

v=2.01 m/s

Re=2933 (d v ρ_g / μ)

f_f=0.011 (with relative roughness = 454)

L_{eq}=(pipe length + elbow + sudden enlargement)

L_{eq}=(0.27 + 0.86 + 0.94)=2.34

$\Delta P_{friction}$ = 2 f_f (L_{eq} / D) v^2 ρ_g = 12.4 Pa

(V_g=4.0 cm/s; q=1288.1 cm^3/s):

ρ_g=1.355 kg/m^3 (P_{avg}=119.95 Kpa)

v=3.75 m/s

Re=5966

f_f=0.0092

$\Delta P_{friction}$ = 53.2 Pa

(V_g=9.0 cm/s; q=2827.4 cm^3/s):

ρ_g=1.763 kg/m^3 (P_{avg}=156.1 Kpa)

v=8.24 m/s

Re=17057

f_f=0.0078

$\Delta P_{friction}$ = 209.1 Pa

2. Potential energy pressure drop

$\underline{V_g=2.2\ cm/s:}$

$\Delta P_{potential\ energy}$ = (gas pipe level variation) + (liquid height between end of gas pipe and pressure tap no. 2)

$\Delta P_{potential\ energy} = (\rho_g\ g\ h_g) + (\rho_l\ g\ h_l)$

$\Delta P_{potential\ energy} = (1.243*9.81*0.0984) + (870*9.81*0.0437)$

$\Delta P_{potential\ energy} = 374.2$ Pa

$\underline{V_g=4.0\ cm/s:}$

$\Delta P_{potential\ energy} = 374.3$ Pa

$\underline{V_g=9.0\ cm/s:}$

$\Delta P_{potential\ energy} = 374.7$ Pa

3. Kinetic energy pressure drop

$\Delta P_{kinetic\ energy} = \rho_g\ (v_2^2 - v_1^2)\ /\ 2$

$\underline{V_g=2.2\ cm/s:}$ $\Delta P_{kinetic\ energy} = -2.3$ Pa

$\underline{V_g=4.1\ cm/s:}$ $\Delta P_{kinetic\ energy} = -9.2$ Pa

$\underline{V_g=9.0\ cm/s:}$ $\Delta P_{kinetic\ energy} = -59.4$ Pa

So, the total pressure drop contributions to be subtracted from the overall pressure drop measured between the pressure tap no. 1 and the pressure tap no.2 are the addition of the friction losses, the static pressure drop and the loss in

kinetic energy:

V_g=2.2 cm/s : 384.3 Pa

V_g=4.1 cm/s : 418.3 Pa

V_g=9.0 cm/s : 524.4 Pa

Then, the net pressure drop across the perforated plate distributor is:

V_g=2.2 cm/s: ΔP_{grid} = 4359.8 - 384.3 = 3975.5 Pa

V_g=4.1 cm/s: ΔP_{grid} = 19687.2 - 418.3 = 19268.8 Pa

V_g=9.0 cm/s: ΔP_{grid} = 78070.8 - 524.4 = 77546.4 Pa

APPENDIX 6

PRESSURE PROFILES

Table A6.1
Summary of pressure profile measurements
T=25°C

Filename	Temperature °C	V_g cm/s	Regression Coefficient	Slope
Ap161	25	2.2	0.9993	-0.0821
Ap162	25	2.2	0.9995	-0.0825
Ap163	25	2.2	0.9998	-0.0826
Ap164	25	2.2	0.9993	-0.0818
Ap165	25	4.1	0.9991	-0.0821
Ap166	25	4.1	0.9999	-0.0825
Ap167	25	4.1	0.9999	-0.0812
Ap168	25	4.1	0.9999	-0.0797
Ap169	25	4.1	0.9996	-0.0797
Ap1610	25	4.1	0.9995	-0.0807
Ap1611	25	9.0	0.9999	-0.0750
Ap1612	25	9.0	0.9998	-0.0750
Ap1613	25	9.0	0.9996	-0.0776
Ap1614	25	9.0	0.9992	-0.0763
Ap1615	25	9.0	0.9989	-0.0766
Ap194	25	14.7	0.9976	-0.0747
Ap195	25	14.7	0.9959	-0.0749
Ap197	25	14.7	0.9971	-0.0743

Table A6.2
Summary of pressure profile measurements
T=100°C

Filename	Temperature °C	V_s cm/s	Regression Coefficient	Slope
Ma0101	100	2.2	0.9995	-0.0747
Ma0102	100	2.2	0.9986	-0.0771
Ma0103	100	2.2	0.9987	-0.0751
Ma0104	100	2.2	0.9992	-0.0744
Ma0105	100	2.2	0.9993	-0.0794
Ma0106	100	2.2	0.9994	-0.0762
Ma0107	100	2.2	0.9975	-0.0763
Ma0160	100	2.2	0.9997	-0.0766
Ma0161	100	2.2	0.9990	-0.0759
Ma0162	100	2.2	0.9982	-0.0745
Ma0163	100	2.2	0.9985	-0.0763
Ma0164	100	2.2	0.9993	-0.0747
Ma0165	100	2.2	0.9996	-0.0748
Ma0166	100	2.2	0.9988	-0.0775
Ma0167	100	2.2	0.9990	-0.0770
Ma0110	100	4.1	0.9982	-0.0711
Ma0111	100	4.1	0.9967	-0.0681
Ma0112	100	4.1	0.9996	-0.0741
Ma0113	100	4.1	0.9987	-0.0741
Ma0114	100	4.1	0.9992	-0.0743
Ma0115	100	4.1	0.9987	-0.0737
Ma0116	100	4.1	0.9969	-0.0760
Ma0150	100	4.1	0.9934	-0.0771
Ma0151	100	4.1	0.9986	-0.0727
Ma0152	100	4.1	0.9950	-0.0713
Ma0153	100	4.1	0.9990	-0.0732
Ma0154	100	4.1	0.9980	-0.0739
Ma0155	100	4.1	0.9991	-0.0738

Table A6.3
Summary of pressure profile measurements
T=100°C

Filename	Temperature °C	V_g cm/s	Regression Coefficient	Slope
Ma0120	100	9.0	0.9973	-0.0684
Ma0121	100	9.0	0.9977	-0.0726
Ma0122	100	9.0	0.9971	-0.0668
Ma0123	100	9.0	0.9987	-0.0684
Ma0124	100	9.0	0.9942	-0.0687
Ma0141	100	9.0	0.9978	-0.0678
Ma0142	100	9.0	0.9963	-0.0675
Ma0143	100	9.0	0.9976	-0.0679
Ma0144	100	9.0	0.9979	-0.0705
Ma0145	100	9.0	0.9990	-0.0698
Ma0130	100	14.7	0.9993	-0.0668
Ma0131	100	14.7	0.9985	-0.0659
Ma0132	100	14.7	0.9991	-0.0679
Ma0133	100	14.7	0.9940	-0.0641
Ma0134	100	14.7	0.9974	-0.0684
Ma0135	100	14.7	0.9996	-0.0678
Ma0136	100	14.7	0.9983	-0.0642
Ma0137	100	14.7	0.9929	-0.0673

Table A6.4
Summary of pressure profile measurements
T=175°C

Filename	Temperature °C	V_s cm/s	Regression Coefficient	Slope
Ma0601	175	2.2	0.9999	-0.0719
Ma0602	175	2.2	0.9994	-0.0706
Ma0603	175	2.2	0.9999	-0.0716
Ma0604	175	2.2	0.9994	-0.0706
Ma0605	175	2.2	0.9998	-0.0727
Ma0606	175	2.2	0.9998	-0.0722
Ma0660	175	2.2	0.9998	-0.0711
Ma0661	175	2.2	0.9999	-0.0711
Ma0662	175	2.2	0.9995	-0.0718
Ma0663	175	2.2	0.9983	-0.0694
Ma0664	175	2.2	0.9999	-0.0708
Ma0611	175	4.1	0.9991	-0.0666
Ma0613	175	4.1	0.9997	-0.0654
Ma0614	175	4.1	0.9996	-0.0642
Ma0615	175	4.1	0.9994	-0.0665
Ma0616	175	4.1	0.9998	-0.0663
Ma0650	175	4.1	0.9987	-0.0647
Ma0651	175	4.1	0.9995	-0.0657
Ma0652	175	4.1	0.9993	-0.0647
Ma0654	175	4.1	0.9996	-0.0645

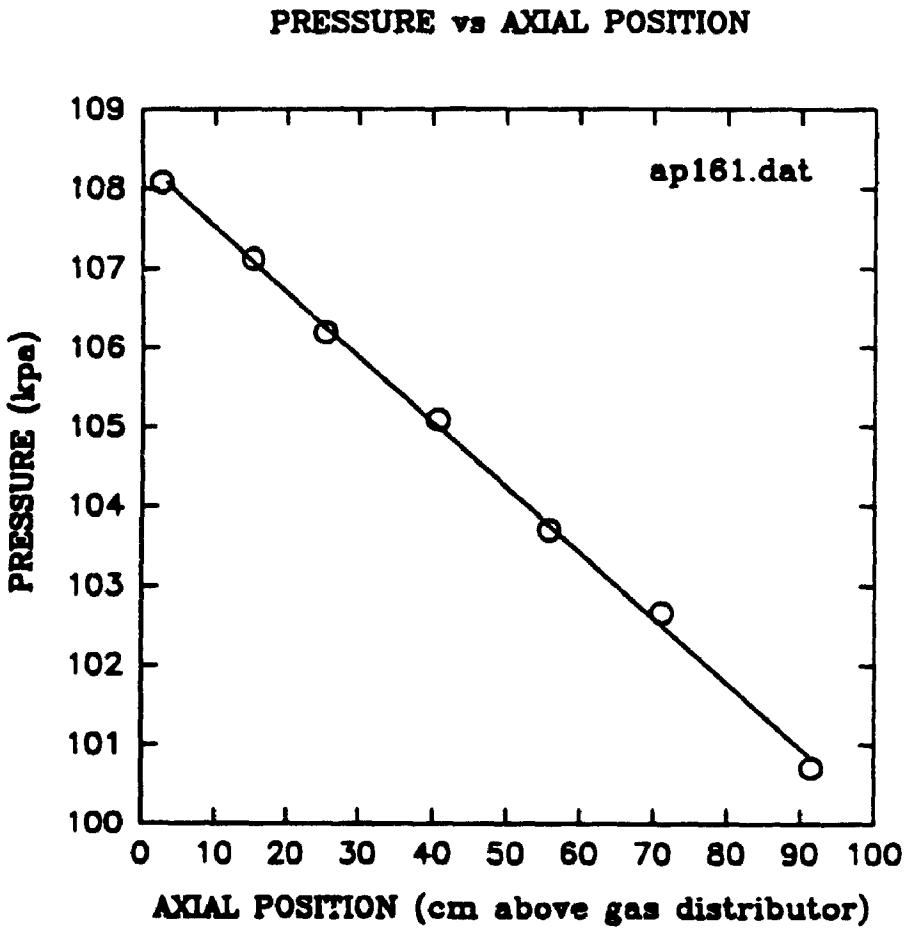
PRESSURE vs AXIAL POSITION
ap161.dat
PRESSURE (kpa)
109
108
107
106
105
104
103
102
101
100
0
10
20
30
40
50
60
70
80
90
100
AXIAL POSITION (cm above gas distributor)

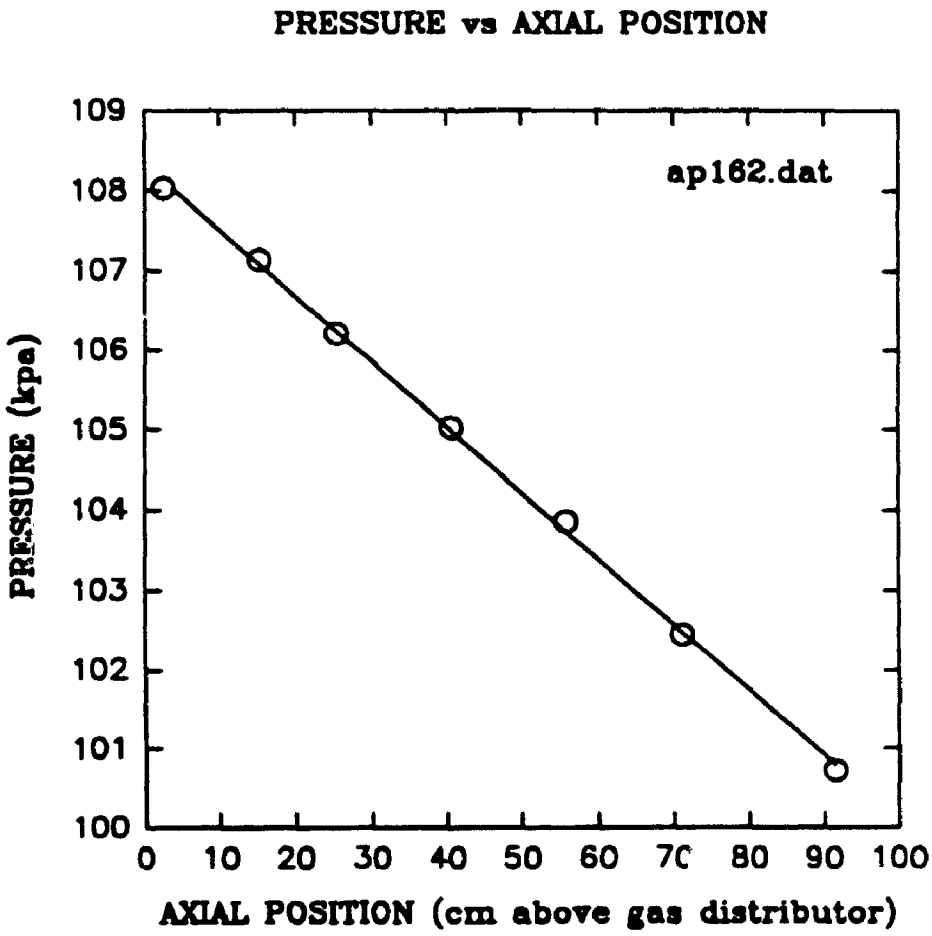
PRESSURE vs AXIAL POSITION
ap162.dat
PRESSURE (kpa)
109
108
107
106
105
104
103
102
101
100
0
10
20
30
40
50
60
70
80
90
100
AXIAL POSITION (cm above gas distributor)

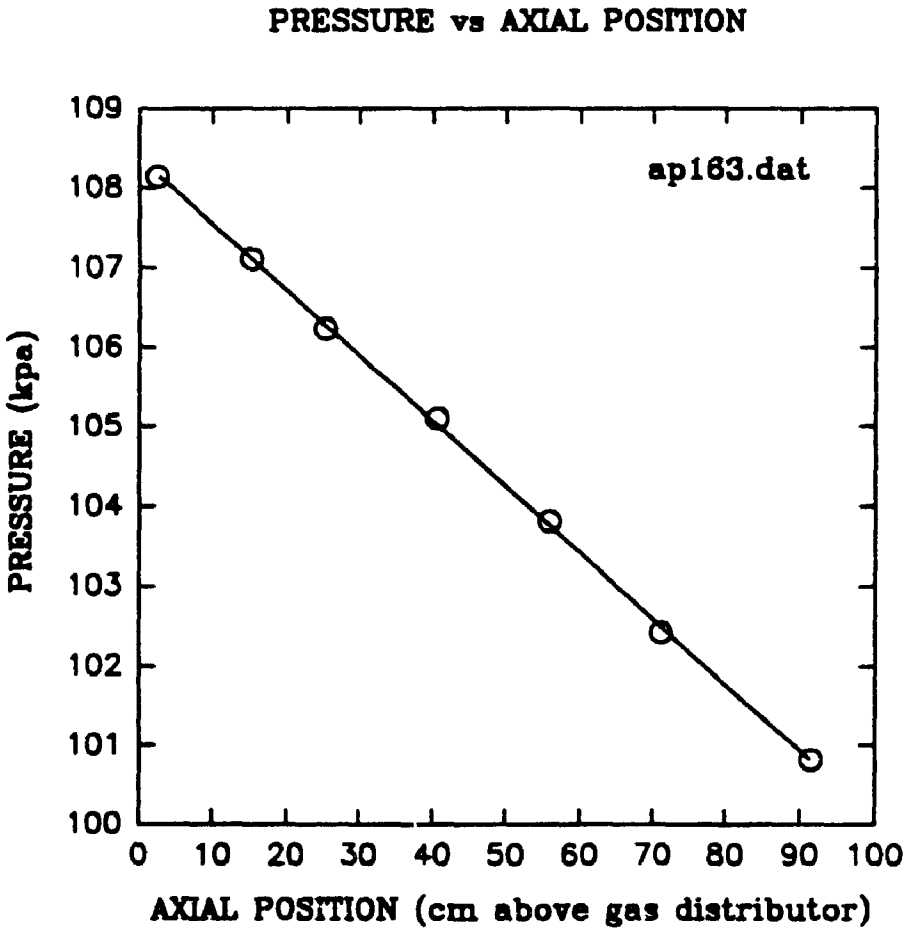
PRESSURE vs AXIAL POSITION
ap163.dat
PRESSURE (kpa)
109
108
107
106
105
104
103
102
101
100
0
10
20
30
40
50
60
70
80
90
100
AXIAL POSITION (cm above gas distributor)

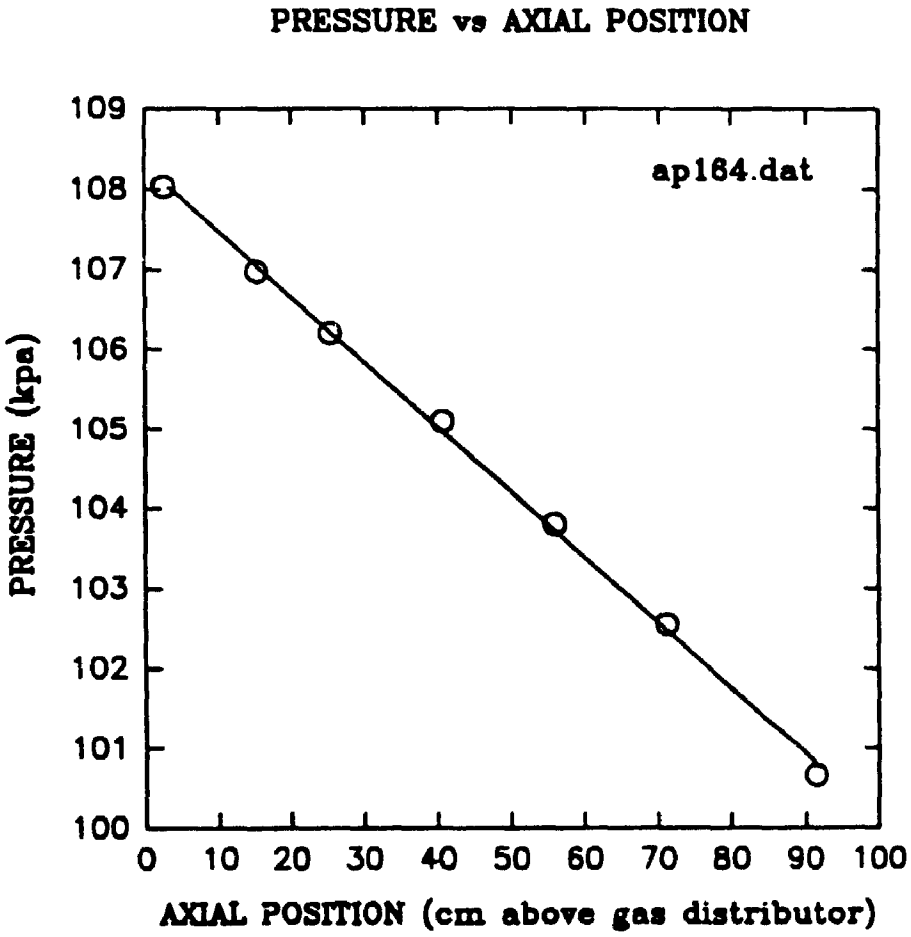
PRESSURE vs AXIAL POSITION
ap164.dat
PRESSURE (kpa)
109
108
107
106
105
104
103
102
101
100
0
10
20
30
40
50
60
70
80
90
100
AXIAL POSITION (cm above gas distributor)

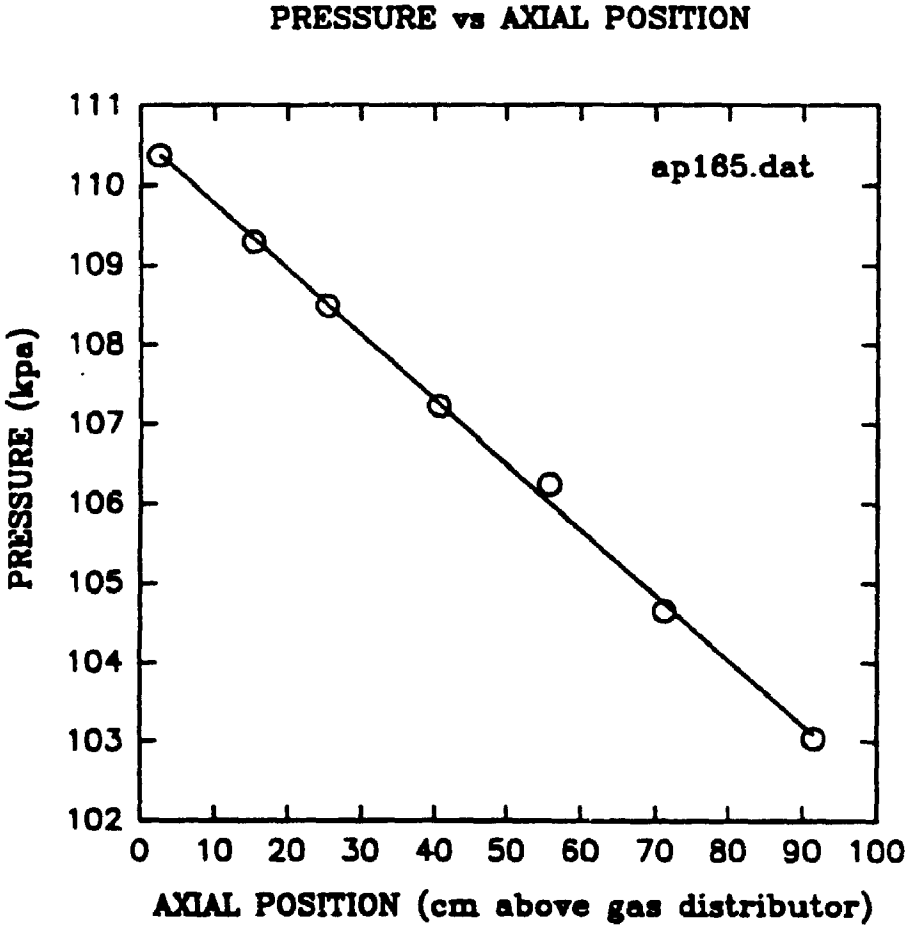
PRESSURE vs AXIAL POSITION
ap165.dat
PRESSURE (kpa)
111
110
109
108
107
106
105
104
103
102
0
10
20
30
40
50
60
70
80
90
100
AXIAL POSITION (cm above gas distributor)

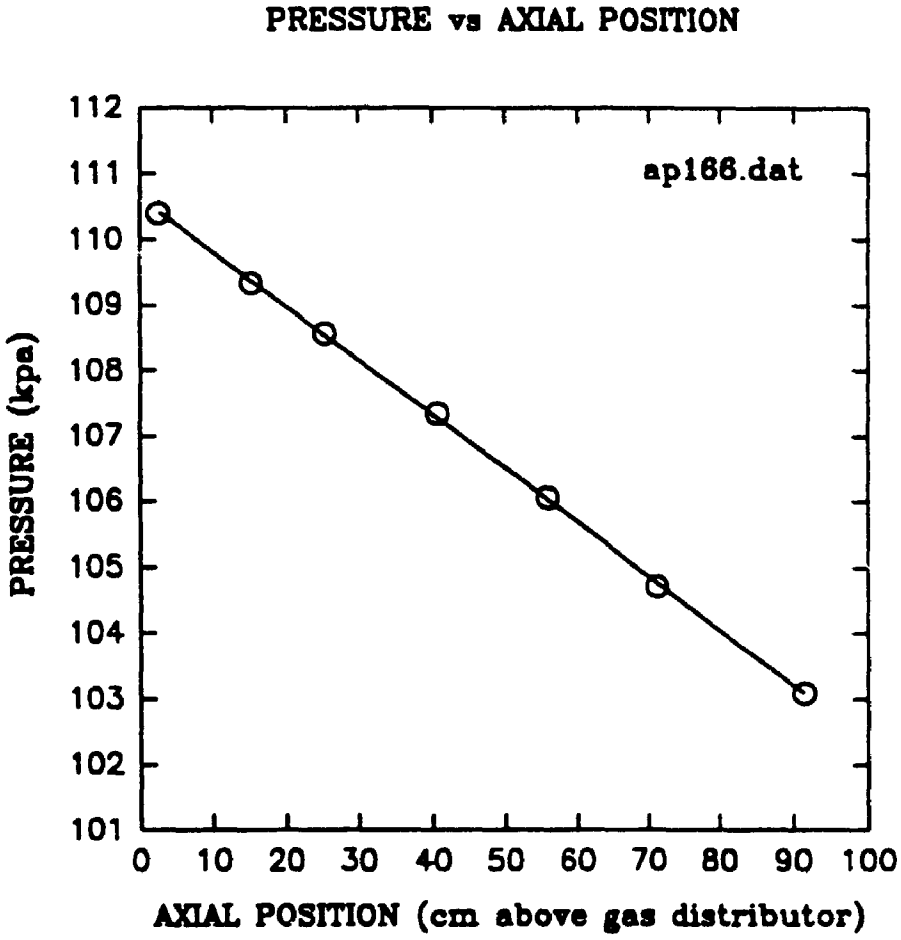
PRESSURE vs AXIAL POSITION
ap166.dat
PRESSURE (kpa)
112
111
110
109
108
107
106
105
104
103
102
101
0
10
20
30
40
50
60
70
80
90
100
AXIAL POSITION (cm above gas distributor)

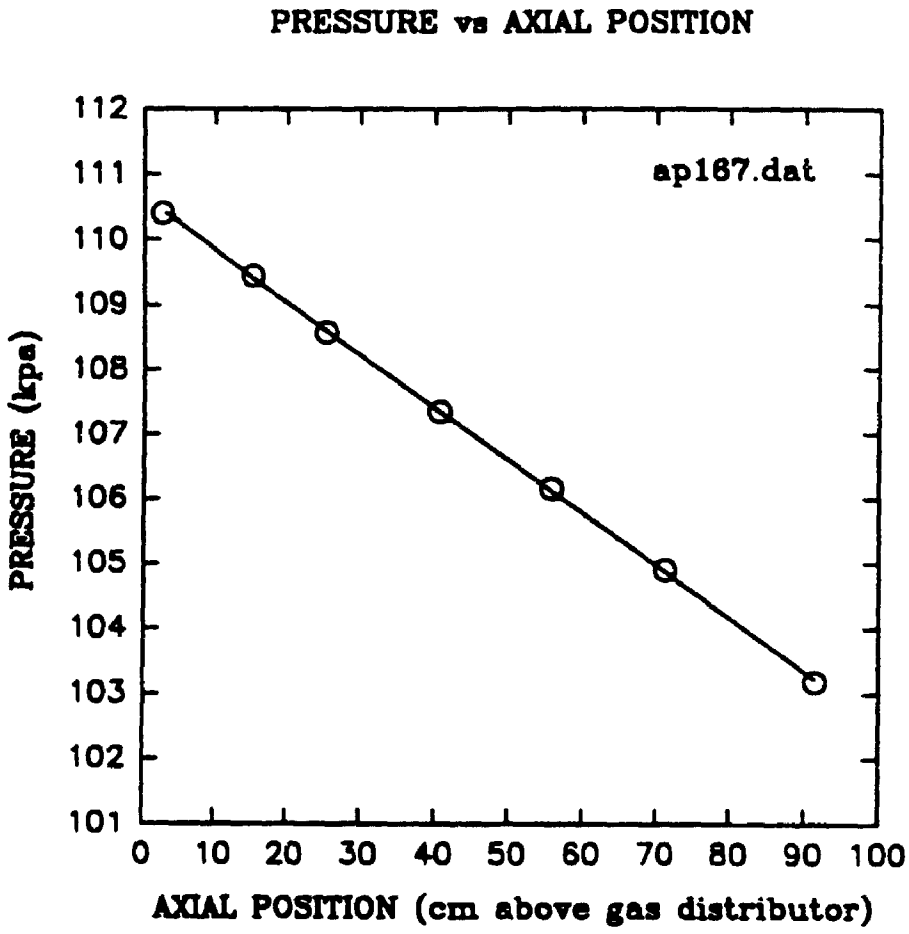
PRESSURE vs AXIAL POSITION
ap167.dat
PRESSURE (kpa)
112
111
110
109
108
107
106
105
104
103
102
101
0
10
20
30
40
50
60
70
80
90
100
AXIAL POSITION (cm above gas distributor)

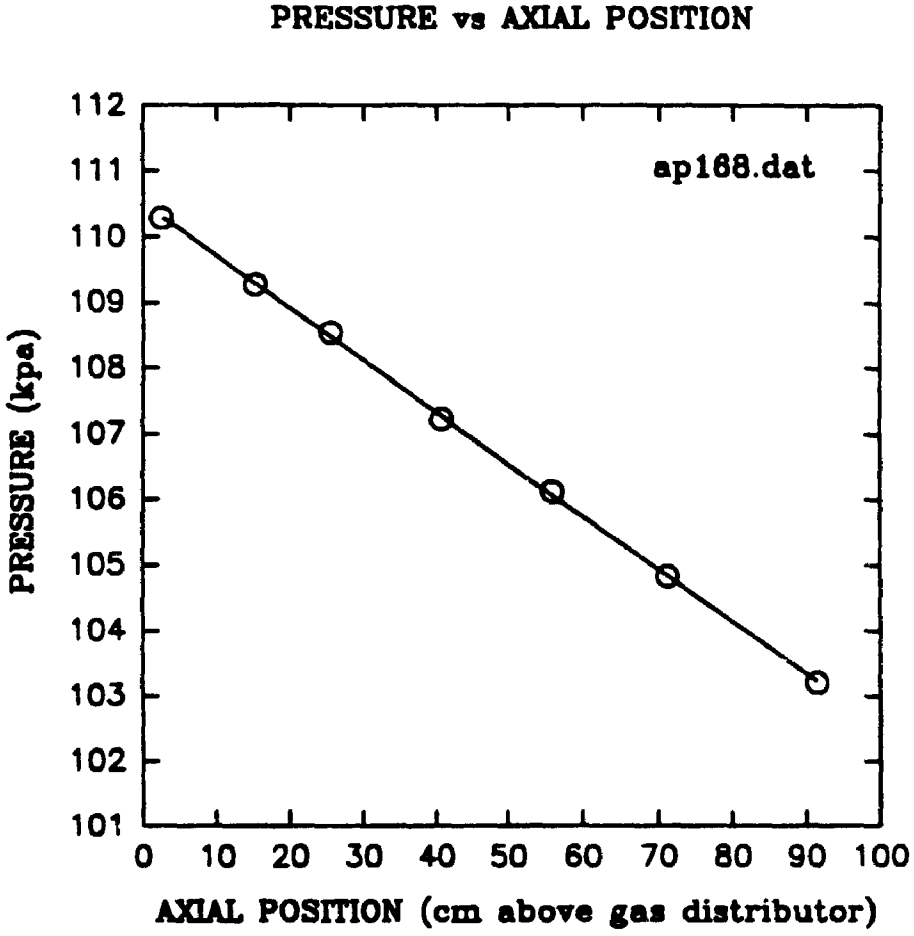
PRESSURE vs AXIAL POSITION
ap168.dat
PRESSURE (kpa)
112
111
110
109
108
107
106
105
104
103
102
101
0
10
20
30
40
50
60
70
80
90
100
AXIAL POSITION (cm above gas distributor)

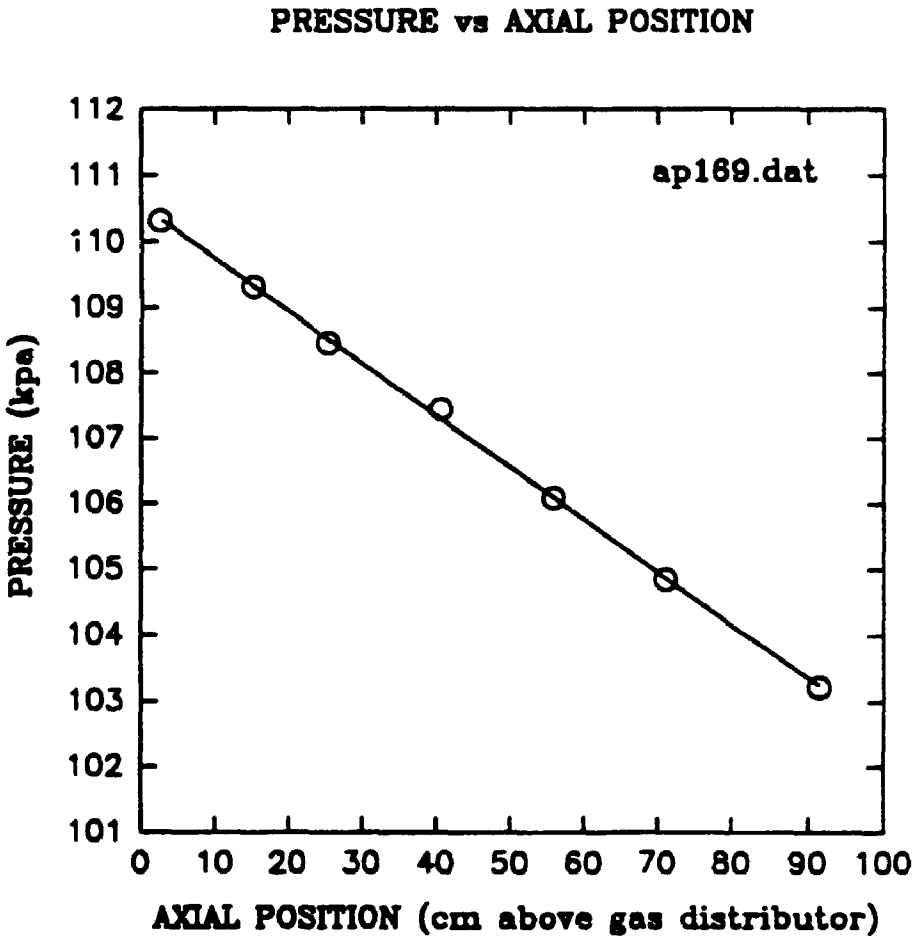
PRESSURE vs AXIAL POSITION
ap169.dat
PRESSURE (kpa)
112
111
110
109
108
107
106
105
104
103
102
101
0
10
20
30
40
50
60
70
80
90
100
AXIAL POSITION (cm above gas distributor)

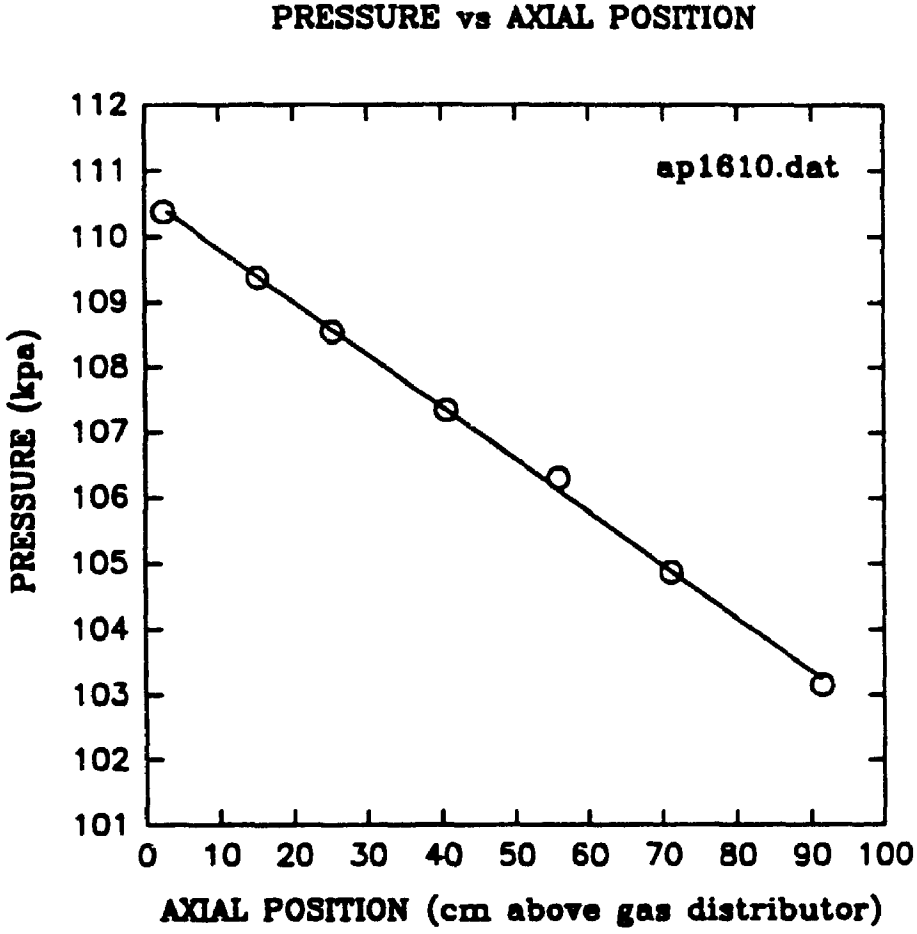
PRESSURE vs AXIAL POSITION
ap1610.dat
PRESSURE (kpa)
112
111
110
109
108
107
106
105
104
103
102
101
0
10
20
30
40
50
60
70
80
90
100
AXIAL POSITION (cm above gas distributor)

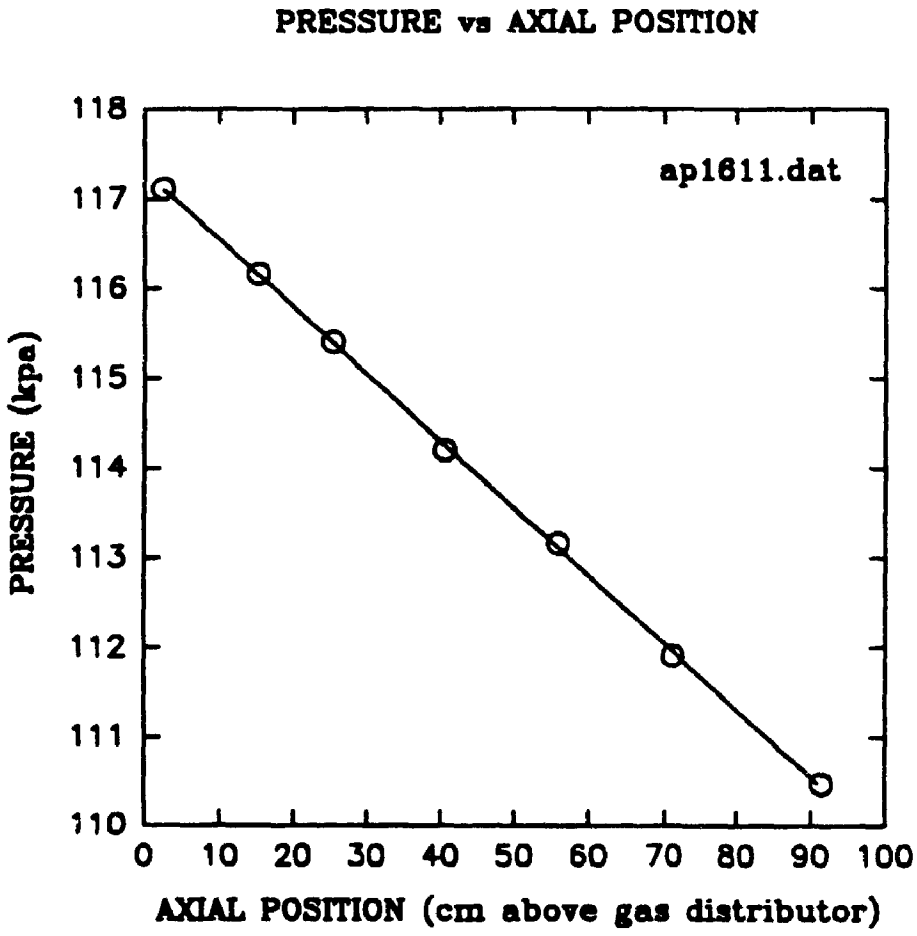
PRESSURE vs AXIAL POSITION
ap1611.dat
PRESSURE (kpa)
118
117
116
115
114
113
112
111
110
0
10
20
30
40
50
60
70
80
90
100
AXIAL POSITION (cm above gas distributor)

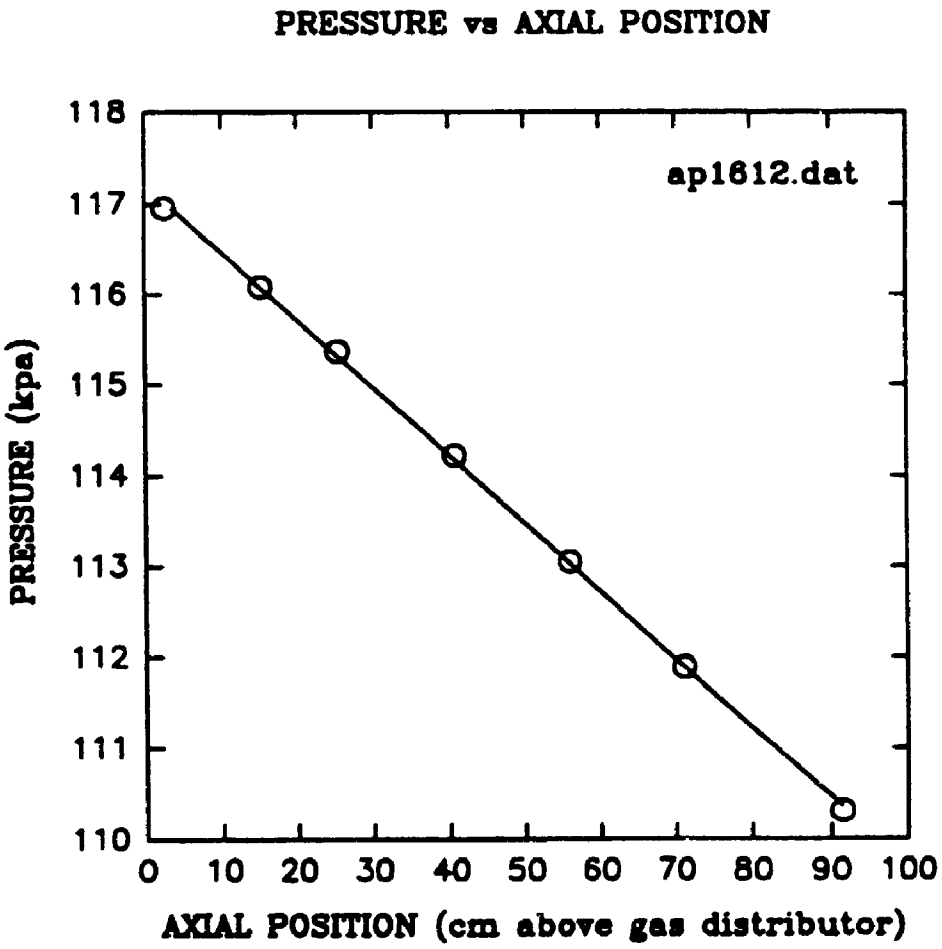
PRESSURE vs AXIAL POSITION
ap1612.dat
PRESSURE (kpa)
118
117
116
115
114
113
112
111
110
0
10
20
30
40
50
60
70
80
90
100
AXIAL POSITION (cm above gas distributor)

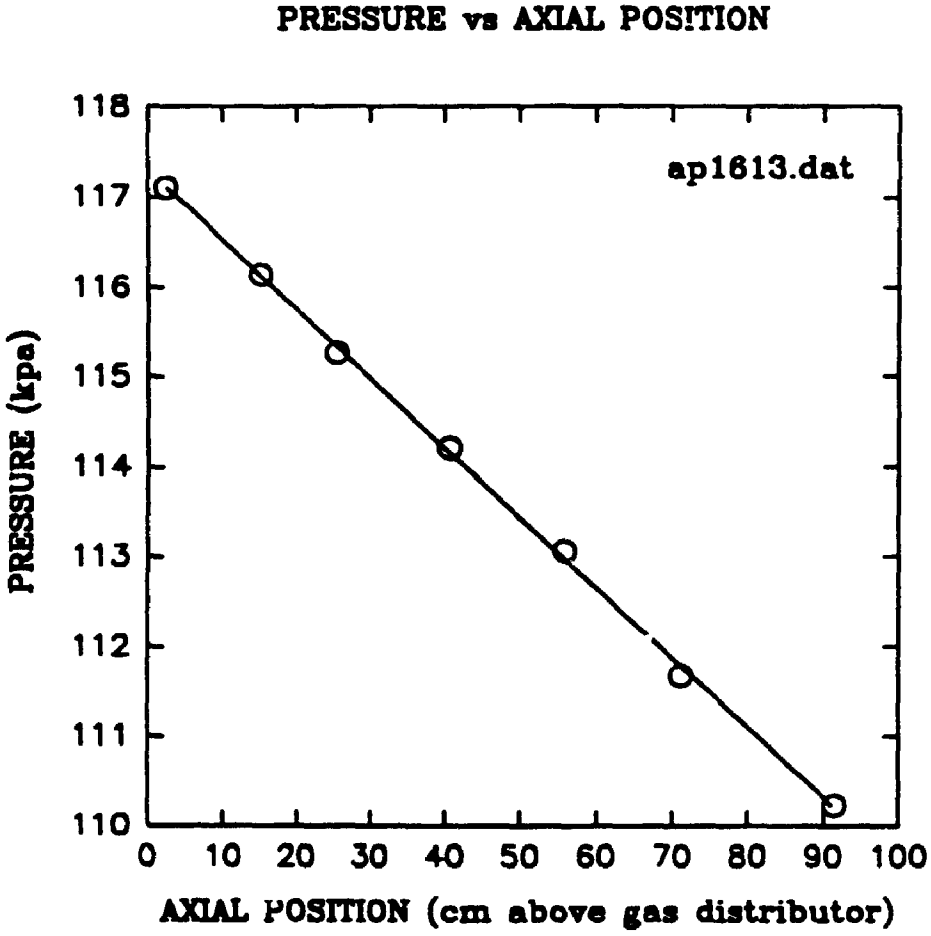
PRESSURE vs AXIAL POSITION
ap1613.dat
PRESSURE (kpa)
118
117
116
115
114
113
112
111
110
0
10
20
30
40
50
60
70
80
90
100
AXIAL POSITION (cm above gas distributor)

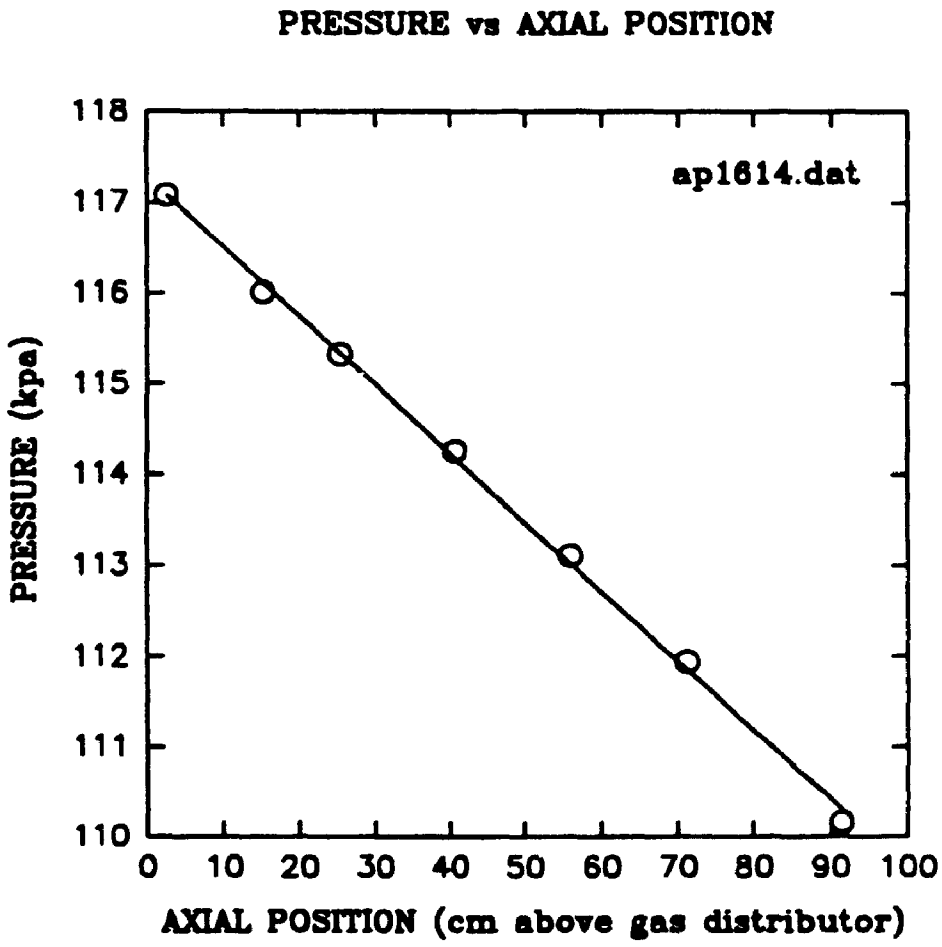
PRESSURE vs AXIAL POSITION
ap1614.dat
PRESSURE (kpa)
118
117
116
115
114
113
112
111
110
0
10
20
30
40
50
60
70
80
90
100
AXIAL POSITION (cm above gas distributor)

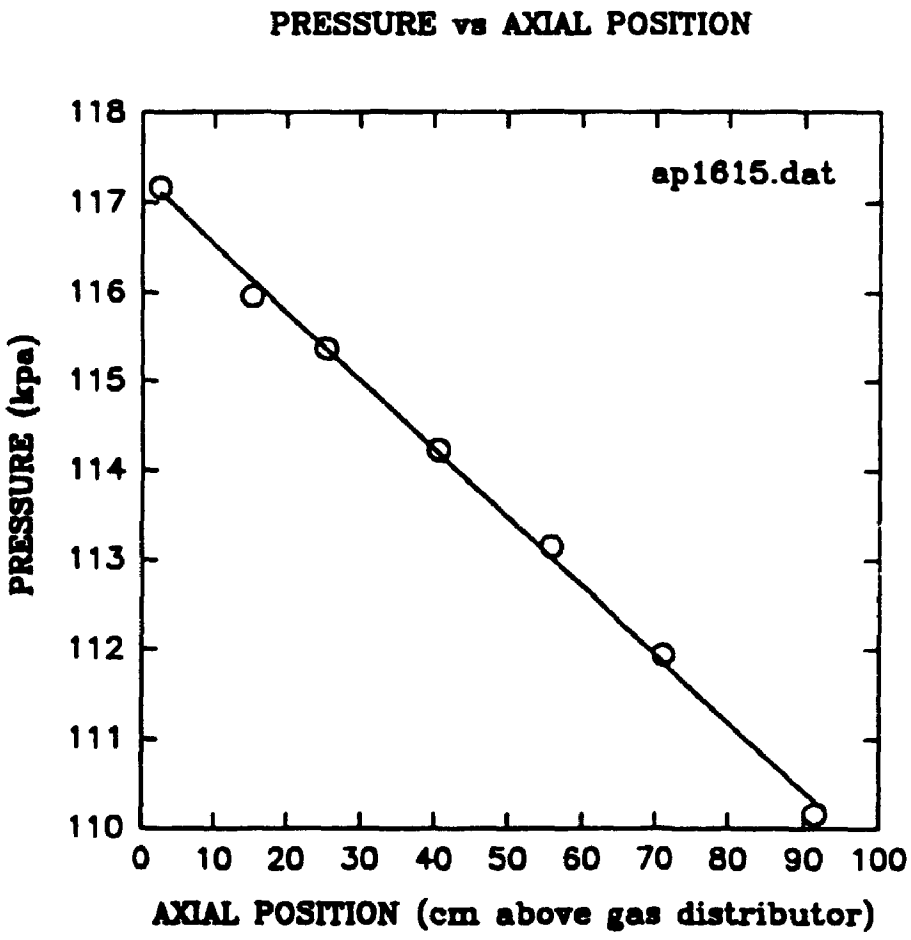
PRESSURE vs AXIAL POSITION
ap1615.dat
PRESSURE (kpa)
118
117
116
115
114
113
112
111
110
0
10
20
30
40
50
60
70
80
90
100
AXIAL POSITION (cm above gas distributor)

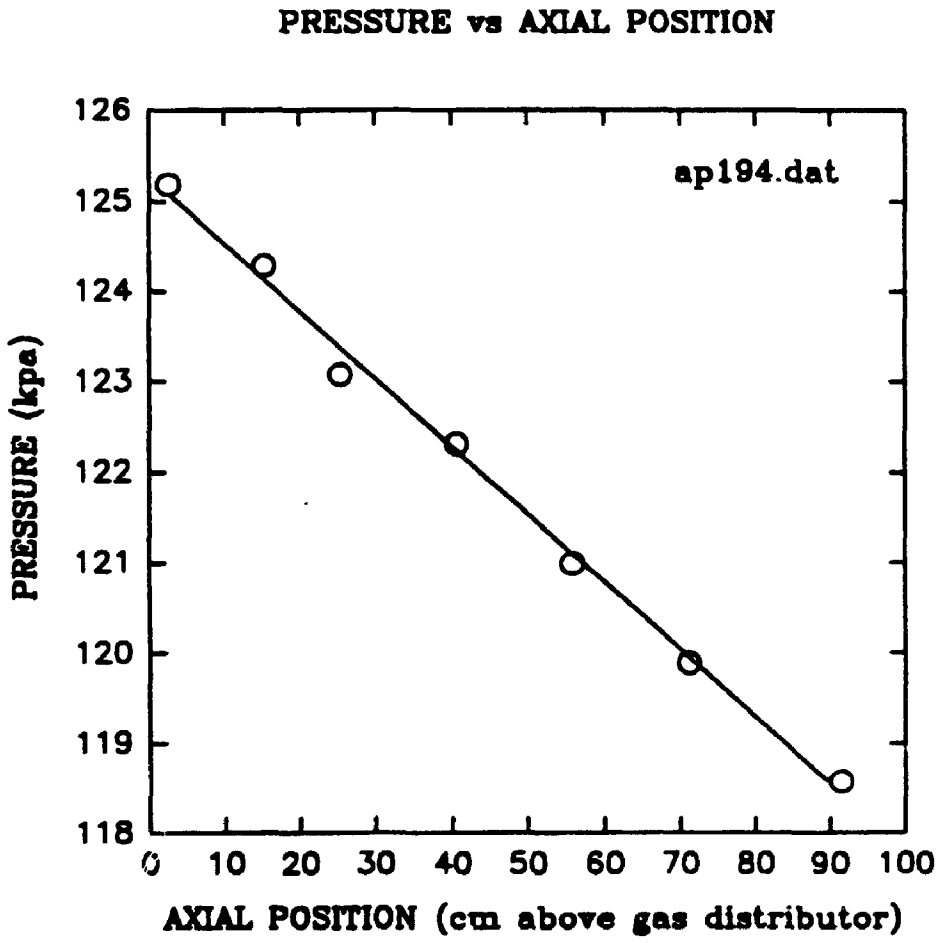
PRESSURE vs AXIAL POSITION
ap194.dat
PRESSURE (kpa)
126
125
124
123
122
121
120
119
118
0
10
20
30
40
50
60
70
80
90
100
AXIAL POSITION (cm above gas distributor)

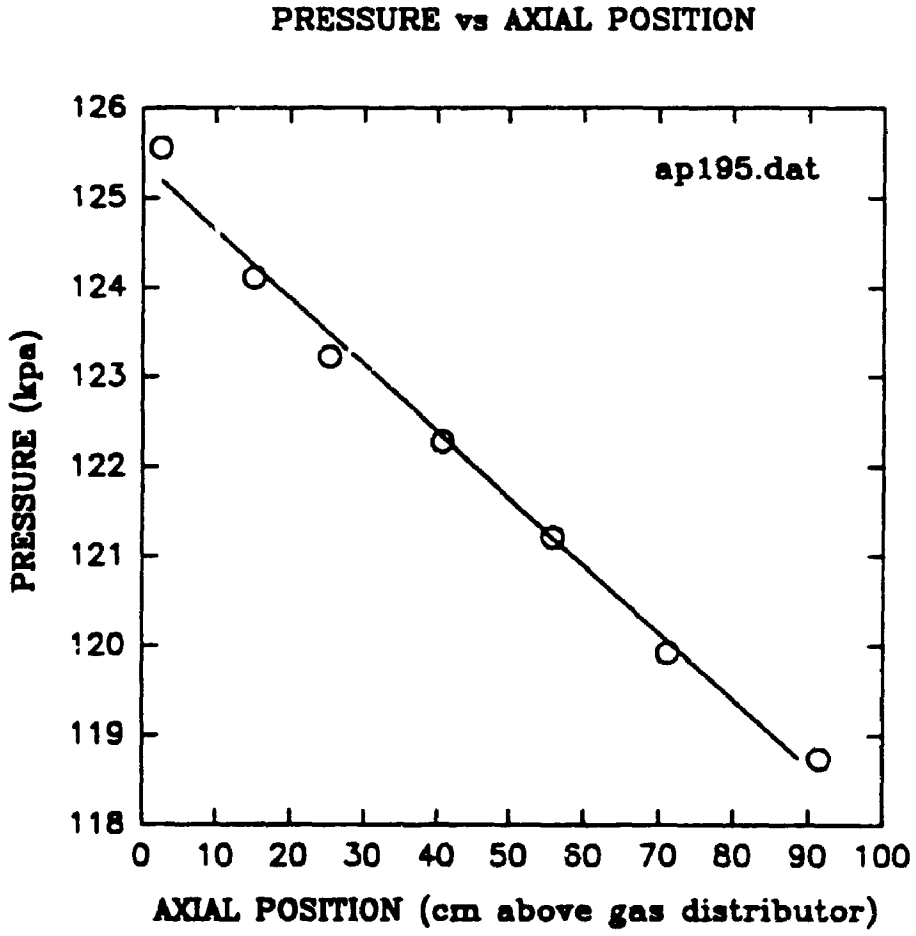
PRESSURE vs AXIAL POSITION
ap195.dat
PRESSURE (kpa)
126
125
124
123
122
121
120
119
118
0
10
20
30
40
50
60
70
80
90
100
AXIAL POSITION (cm above gas distributor)

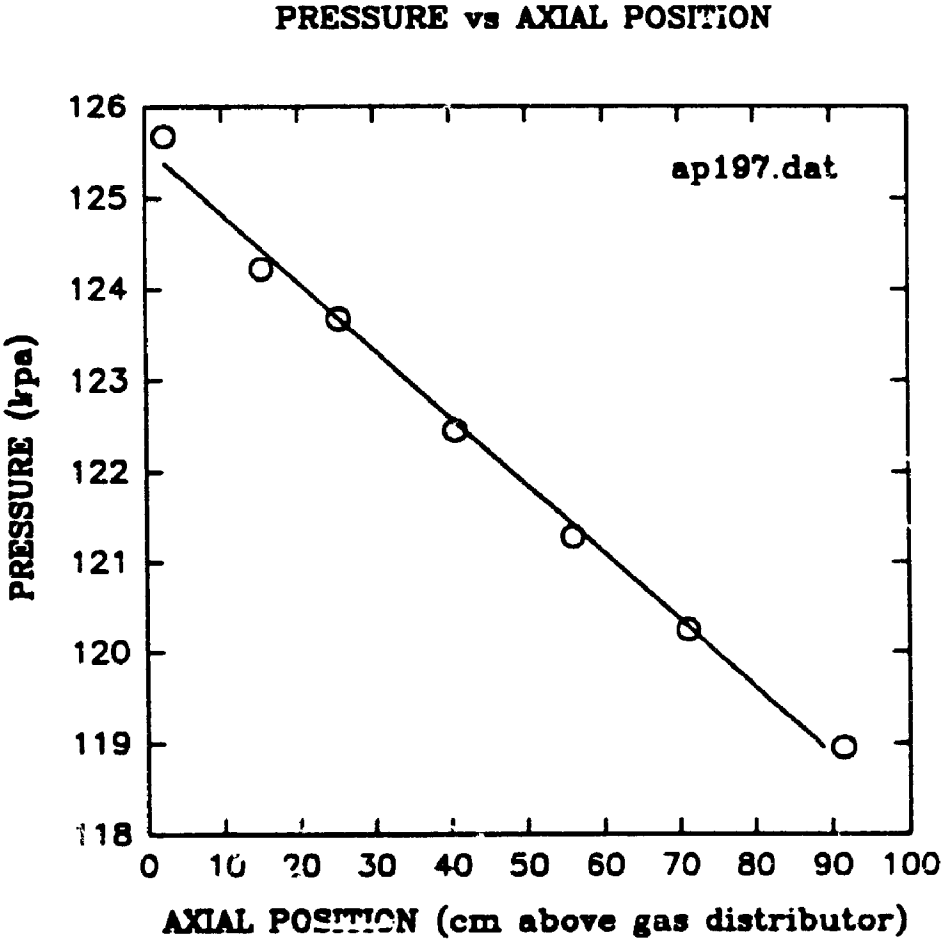
PRESSURE vs AXIAL POSITION
ap197.dat
PRESSURE (kpa)
126
125
124
123
122
121
120
119
118
0
10
20
30
40
50
60
70
80
90
100
AXIAL POSITION (cm above gas distributor)

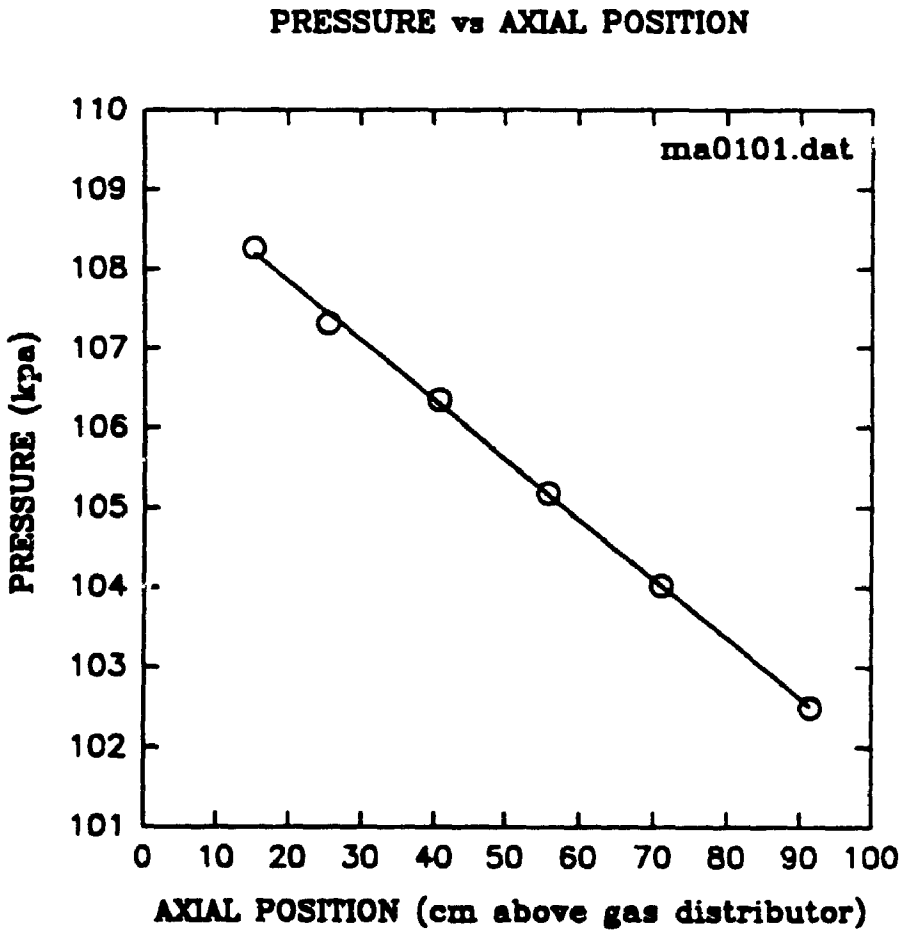
PRESSURE vs AXIAL POSITION
ma0101.dat
PRESSURE (kpa)
110
109
108
107
106
105
104
103
102
101
0
10
20
30
40
50
60
70
80
90
100
AXIAL POSITION (cm above gas distributor)

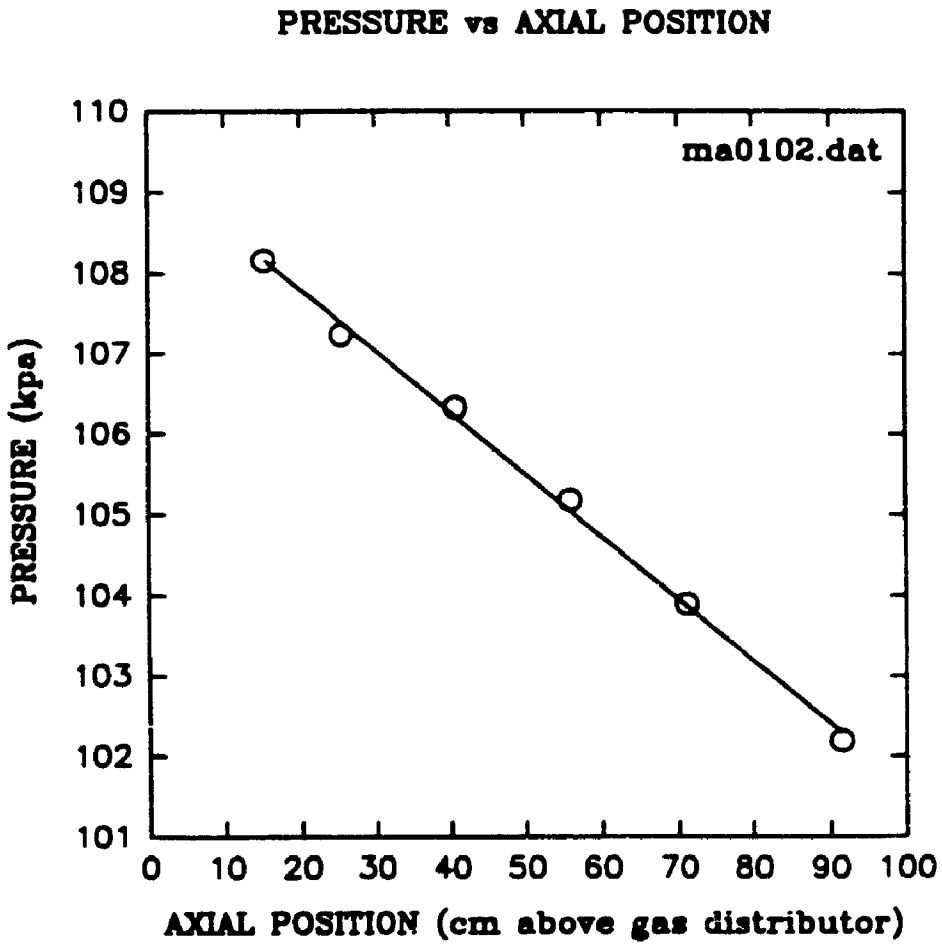
PRESSURE vs AXIAL POSITION
ma0102.dat
PRESSURE (kpa)
110
109
108
107
106
105
104
103
102
101
0
10
20
30
40
50
60
70
80
90
100
AXIAL POSITION (cm above gas distributor)

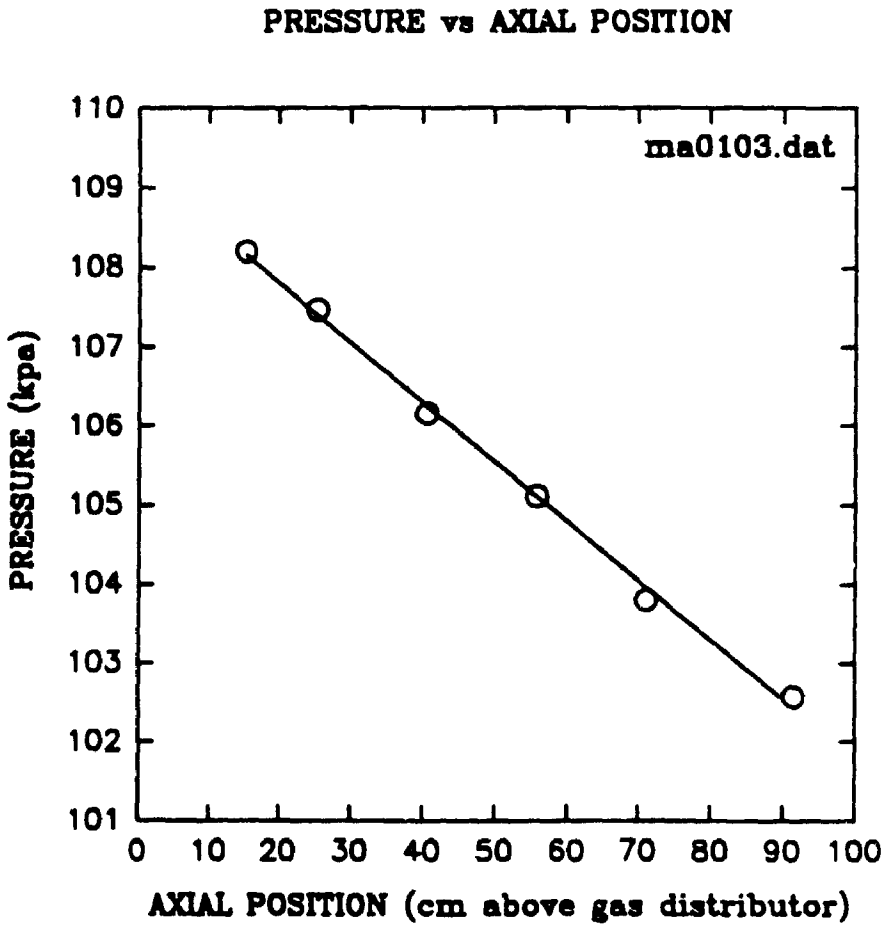
PRESSURE vs AXIAL POSITION
ma0103.dat
PRESSURE (kpa)
110
109
108
107
106
105
104
103
102
101
0
10
20
30
40
50
60
70
80
90
100
AXIAL POSITION (cm above gas distributor)

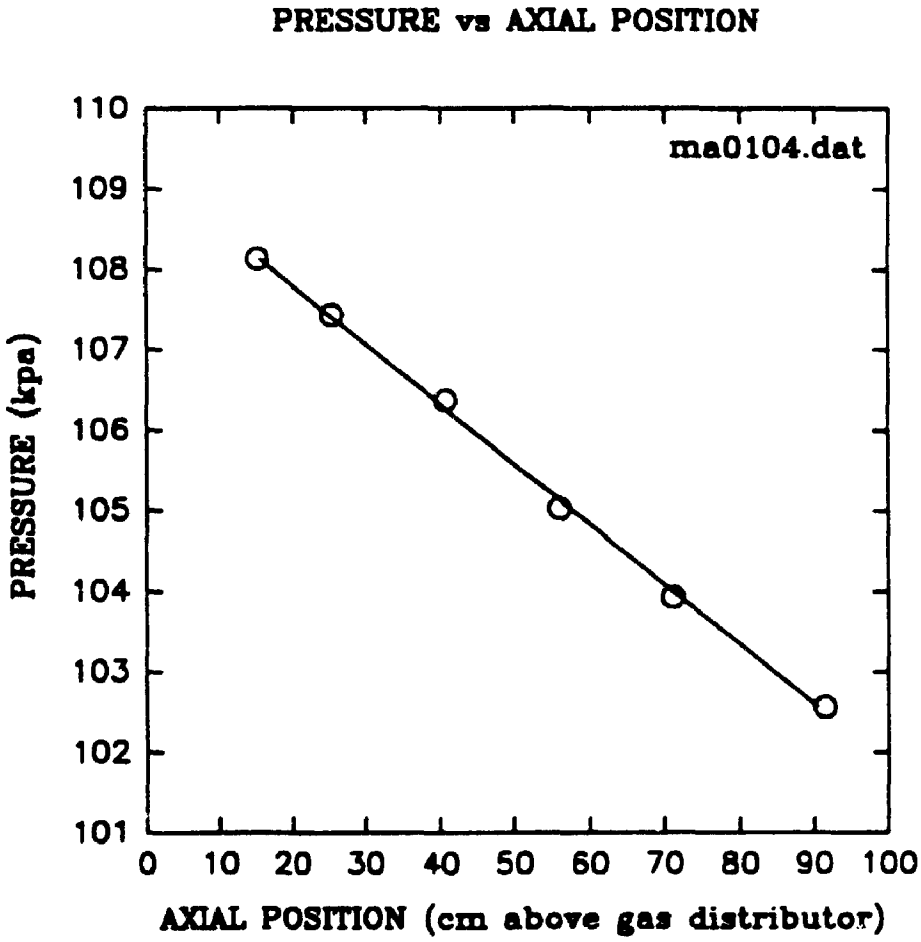
PRESSURE vs AXIAL POSITION
ma0104.dat
PRESSURE (kpa)
110
109
108
107
106
105
104
103
102
101
0
10
20
30
40
50
60
70
80
90
100
AXIAL POSITION (cm above gas distributor)

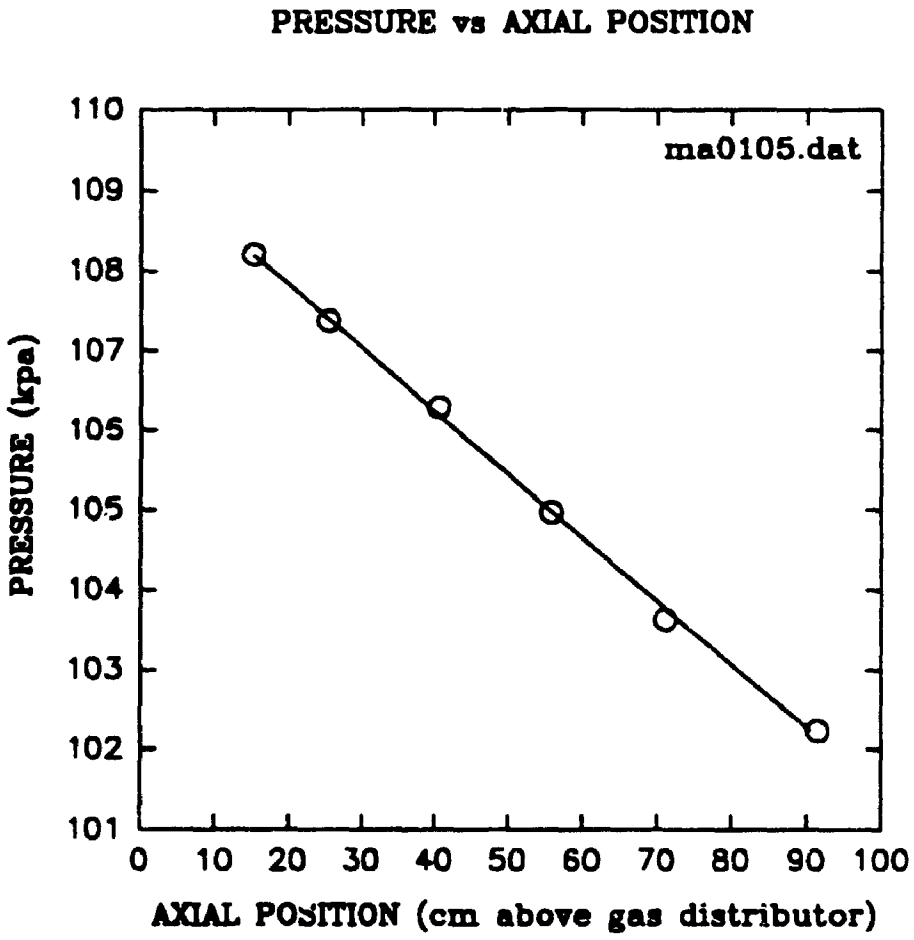
PRESSURE vs AXIAL POSITION
ma0105.dat
PRESSURE (kpa)
110
109
108
107
106
105
104
103
102
101
0
10
20
30
40
50
60
70
80
90
100
AXIAL POSITION (cm above gas distributor)

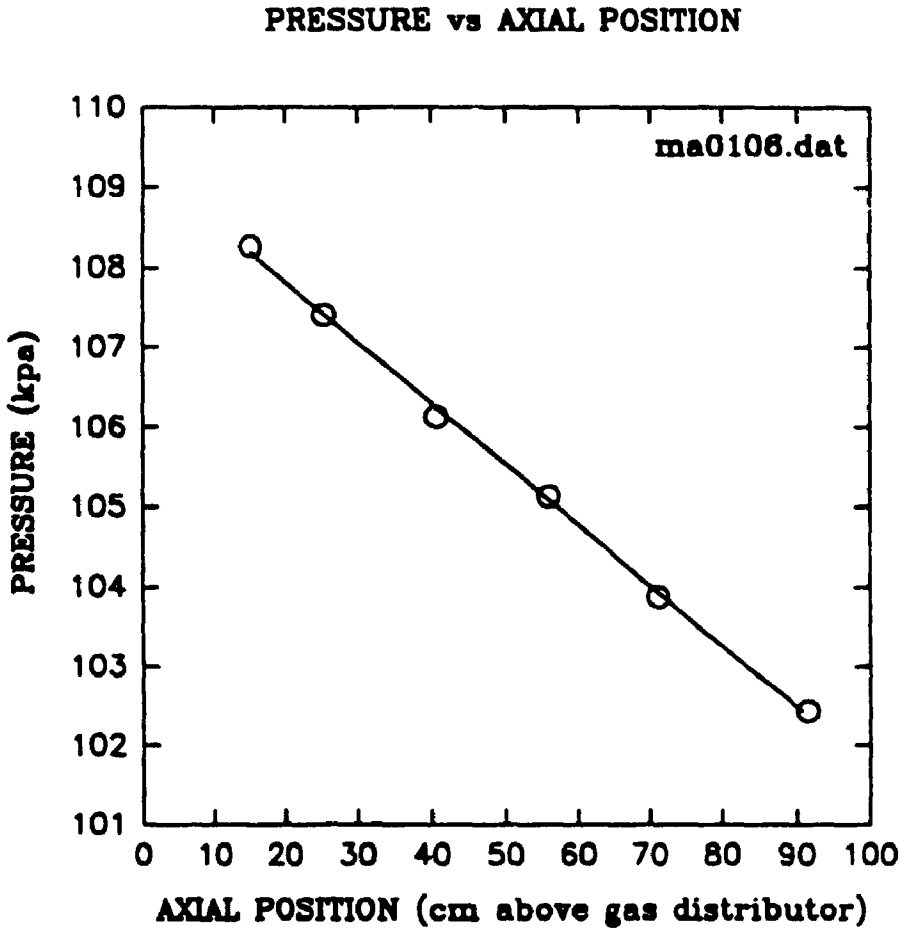
PRESSURE vs AXIAL POSITION
ma0106.dat
PRESSURE (kpa)
110
109
108
107
106
105
104
103
102
101
0
10
20
30
40
50
60
70
80
90
100
AXIAL POSITION (cm above gas distributor)

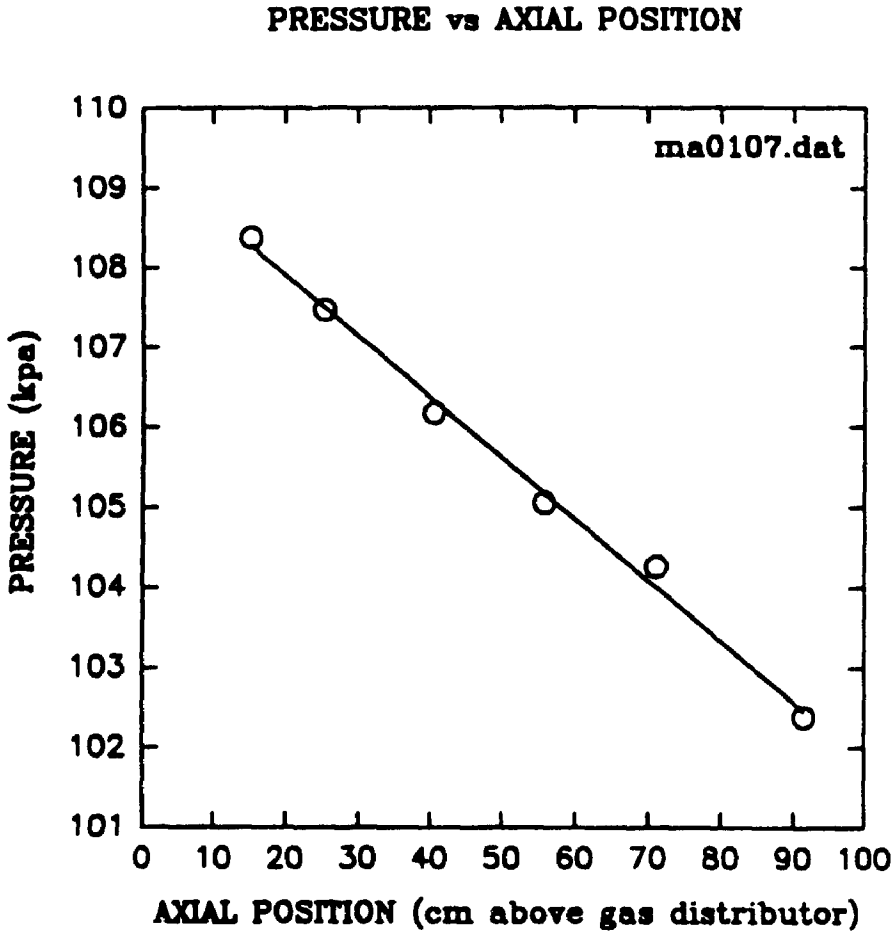
PRESSURE vs AXIAL POSITION
ma0107.dat
PRESSURE (kpa)
110
109
108
107
106
105
104
103
102
101
0
10
20
30
40
50
60
70
80
90
100
AXIAL POSITION (cm above gas distributor)

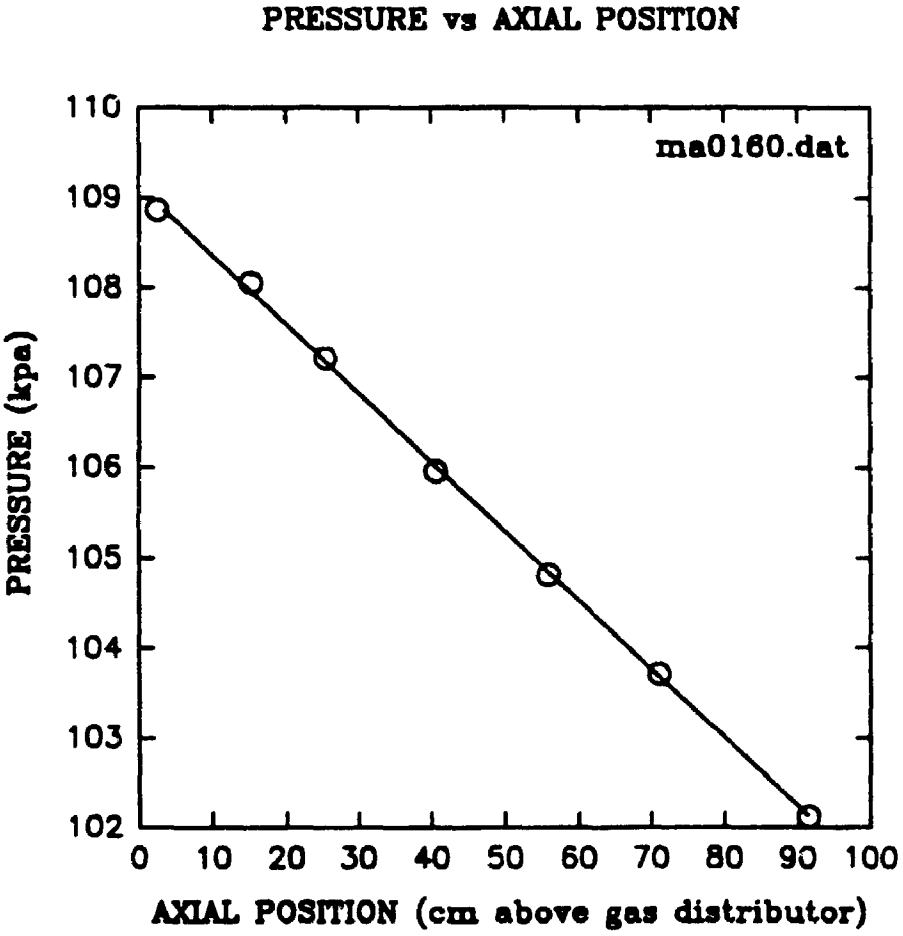
PRESSURE vs AXIAL POSITION
ma0160.dat
PRESSURE (kpa)
110
109
108
107
106
105
104
103
102
0
10
20
30
40
50
60
70
80
90
100
AXIAL POSITION (cm above gas distributor)

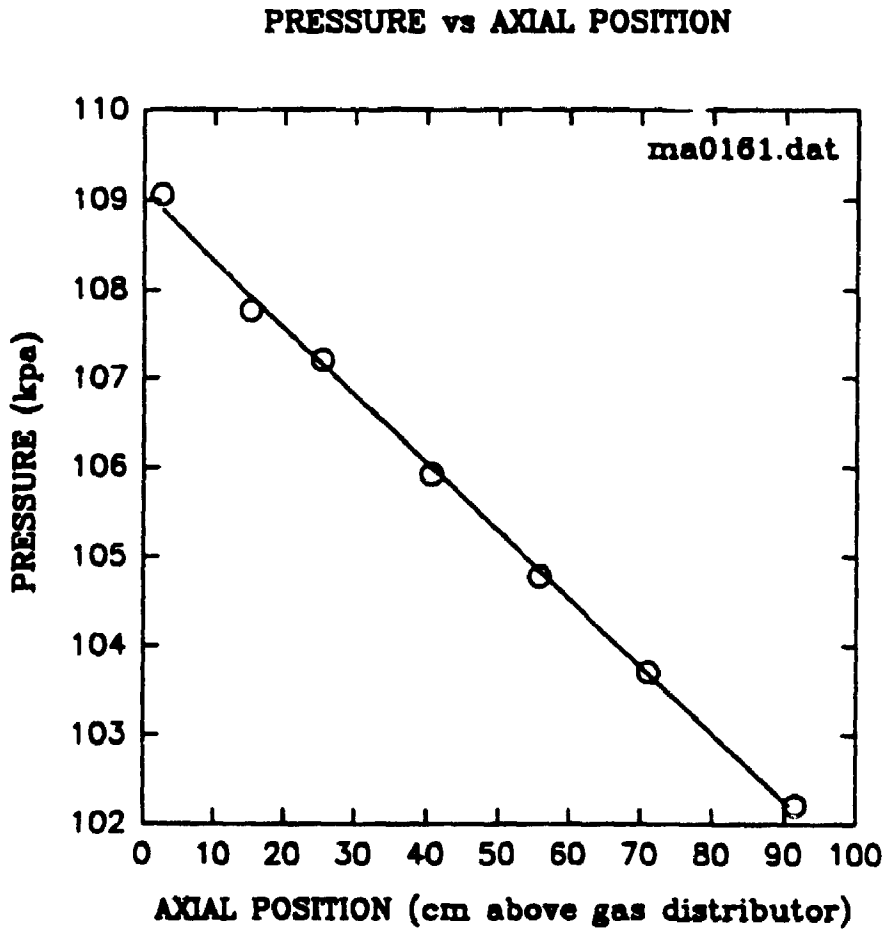
PRESSURE vs AXIAL POSITION
ma0161.dat
PRESSURE (kpa)
110
109
108
107
106
105
104
103
102
0
10
20
30
40
50
60
70
80
90
100
AXIAL POSITION (cm above gas distributor)

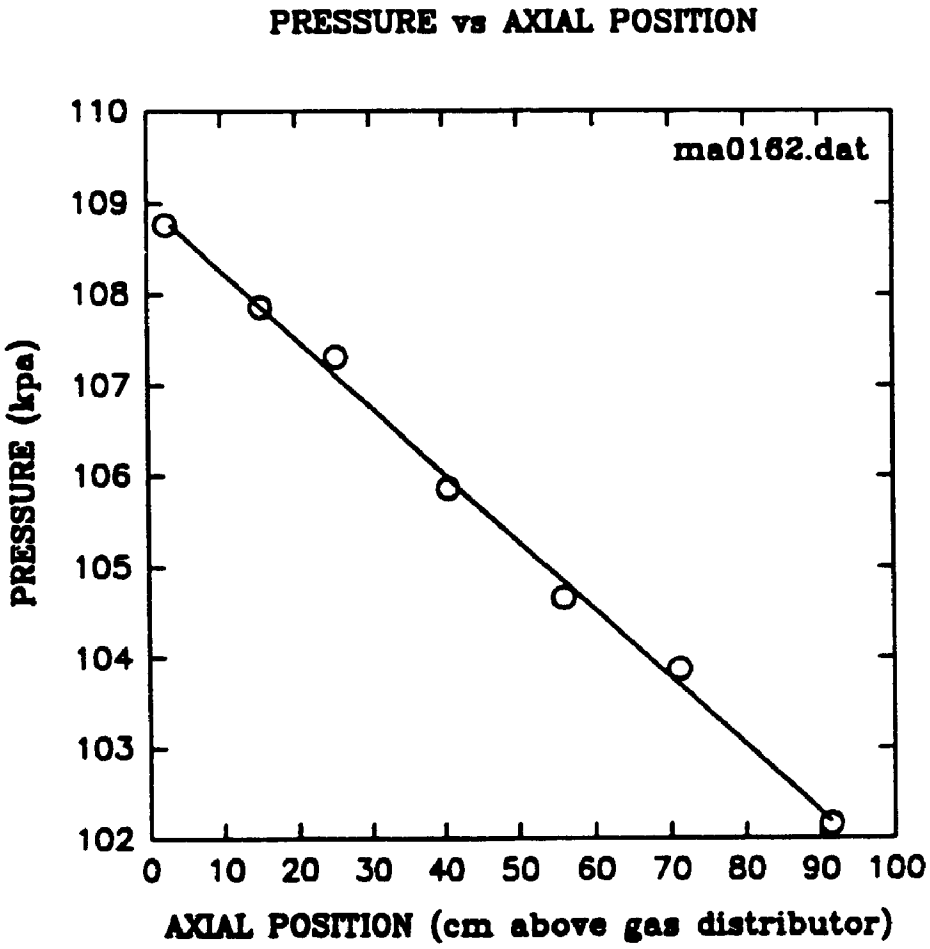
PRESSURE vs AXIAL POSITION
ma0162.dat
PRESSURE (kpa)
110
109
108
107
106
105
104
103
102
0
10
20
30
40
50
60
70
80
90
100
AXIAL POSITION (cm above gas distributor)

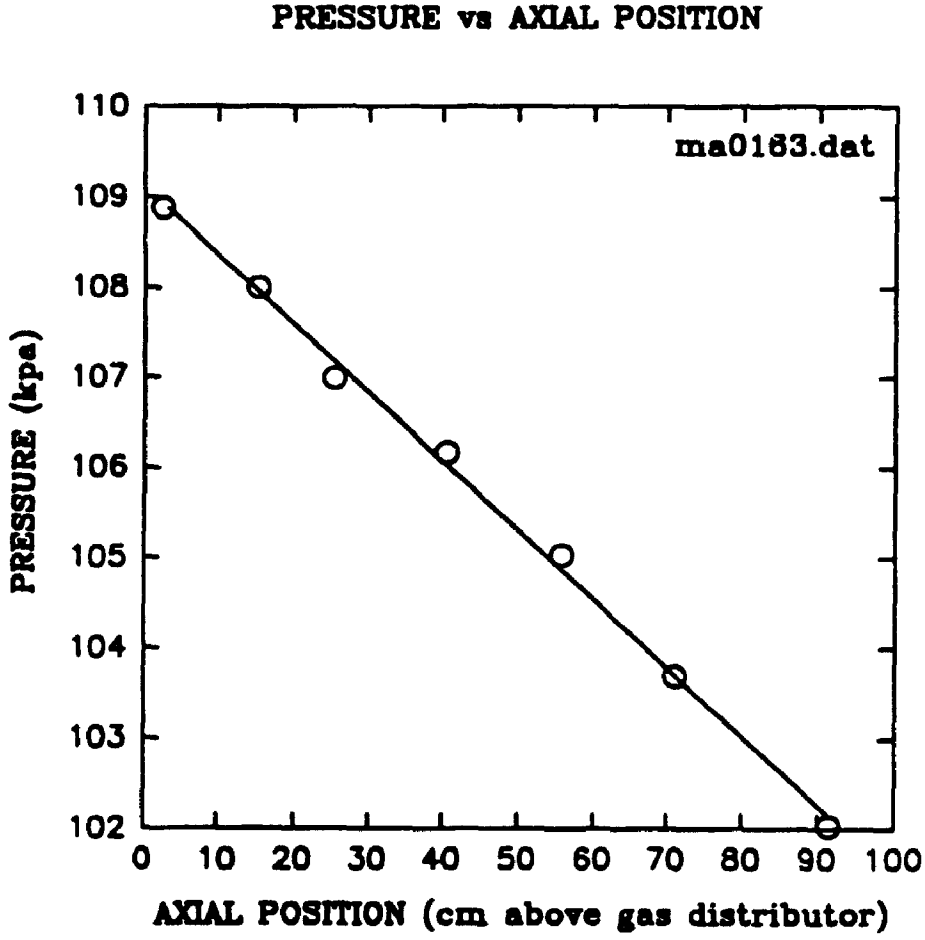
PRESSURE vs AXIAL POSITION
ma0163.dat
PRESSURE (kpa)
110
109
108
107
106
105
104
103
102
0
10
20
30
40
50
60
70
80
90
100
AXIAL POSITION (cm above gas distributor)

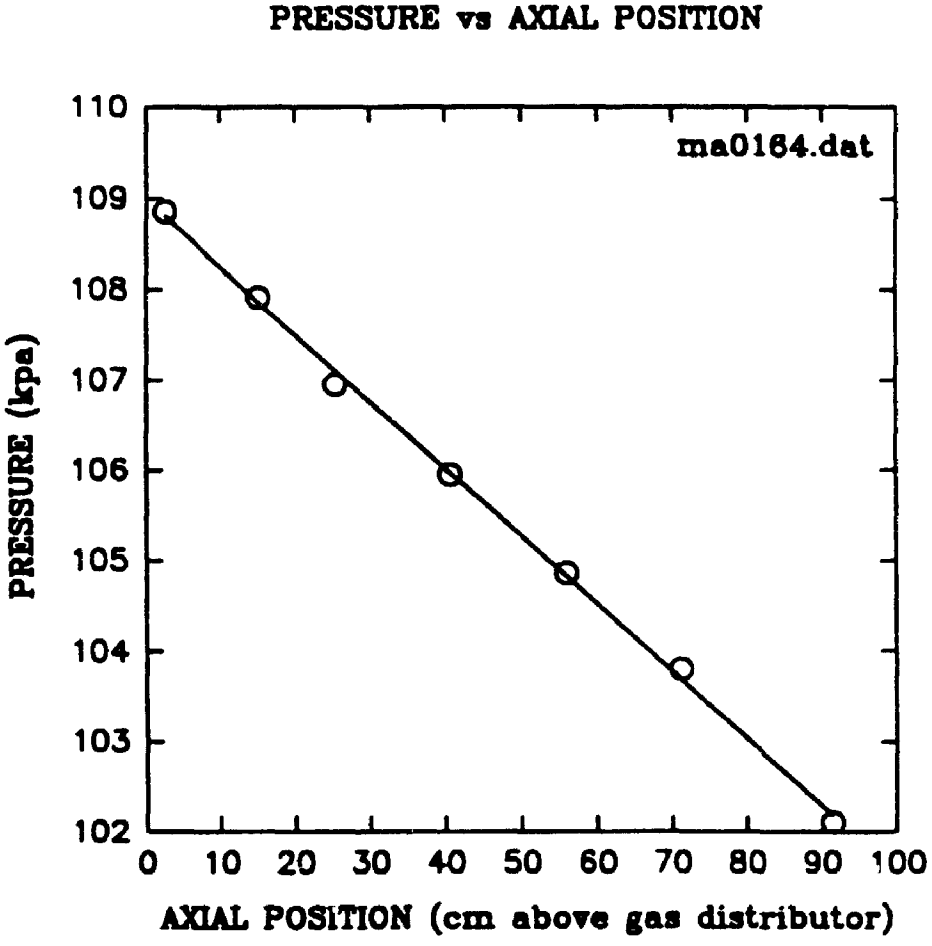
PRESSURE vs AXIAL POSITION
ma0164.dat
PRESSURE (kpa)
110
109
108
107
106
105
104
103
102
0
10
20
30
40
50
60
70
80
90
100
AXIAL POSITION (cm above gas distributor)

PRESSURE vs AXIAL POSITION

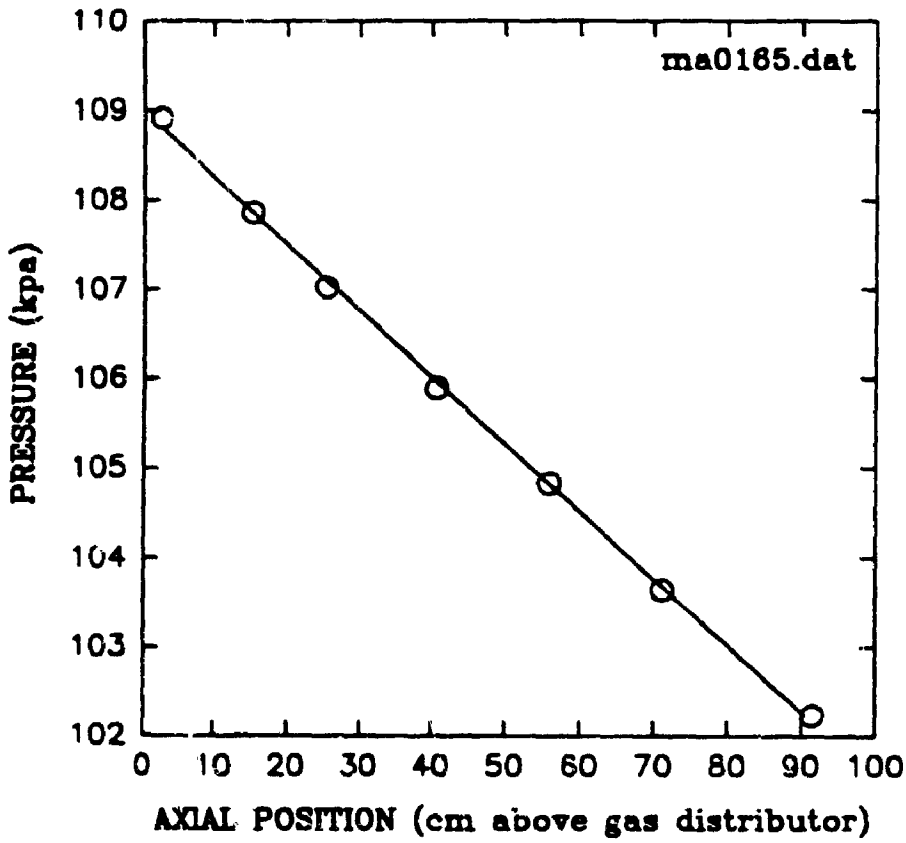

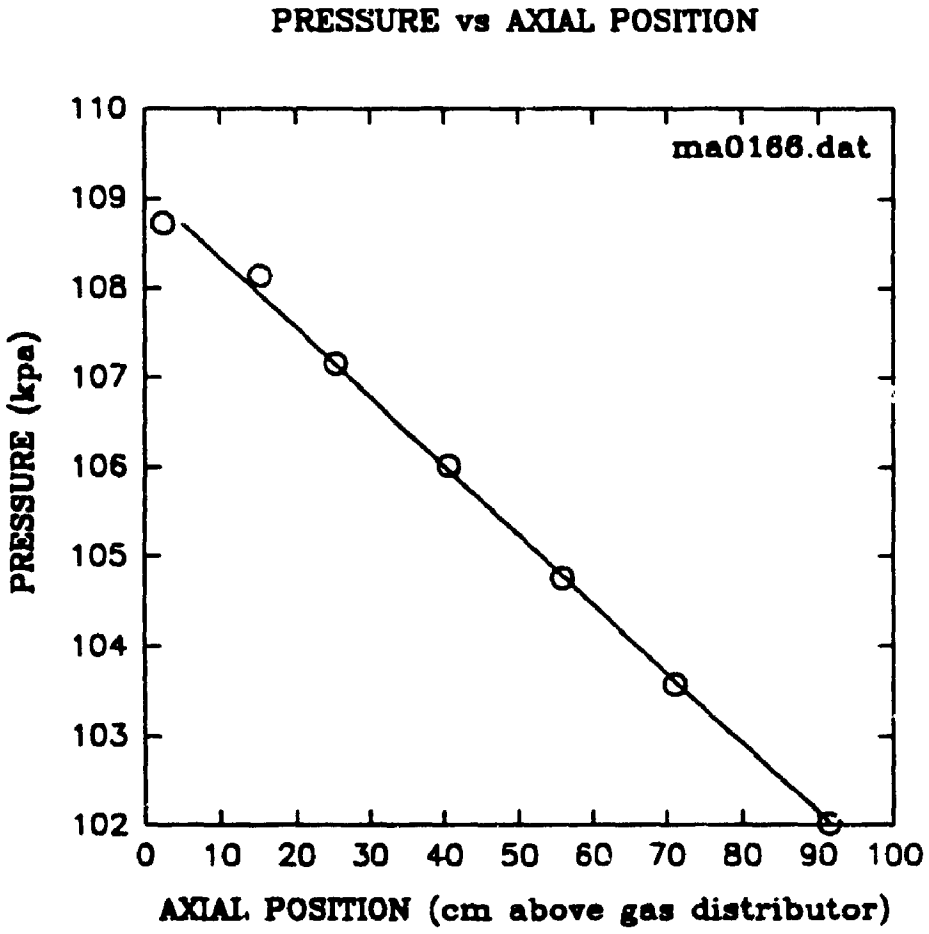
PRESSURE vs AXIAL POSITION
ma0166.dat
PRESSURE (kpa)
110
109
108
107
106
105
104
103
102
0
10
20
30
40
50
60
70
80
90
100
AXIAL POSITION (cm above gas distributor)

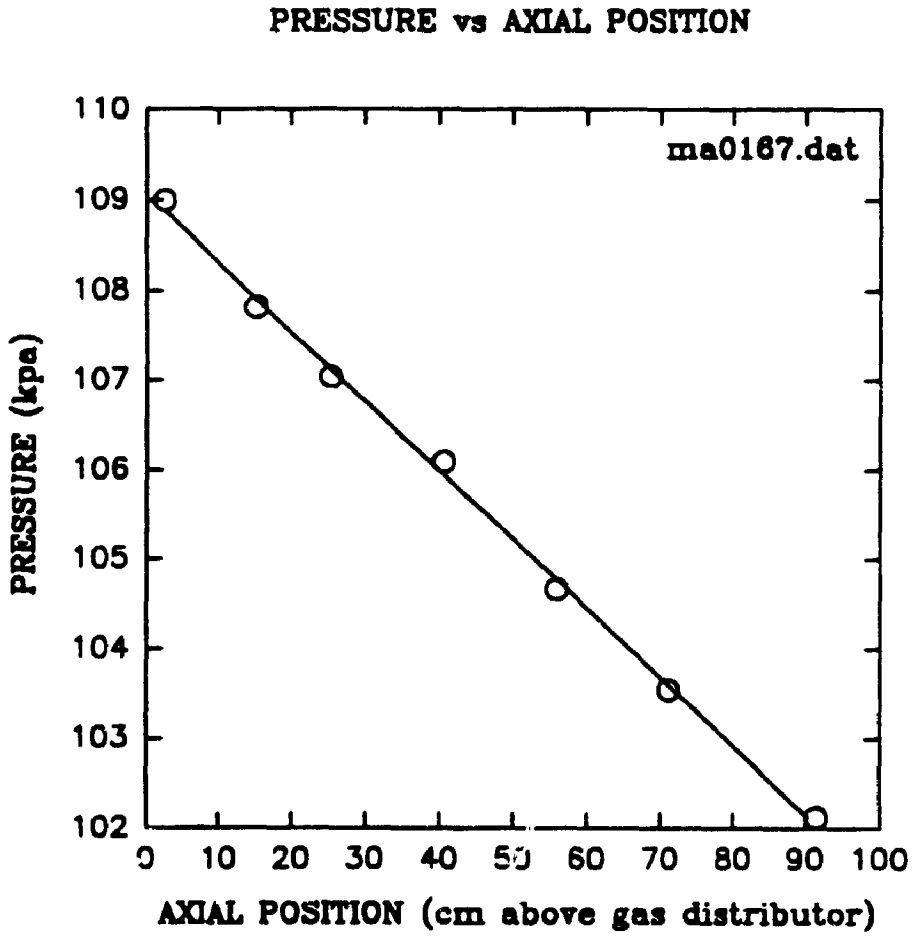
PRESSURE vs AXIAL POSITION
ma0167.dat
PRESSURE (kpa)
110
109
108
107
106
105
104
103
102
0
10
20
30
40
50
60
70
80
90
100
AXIAL POSITION (cm above gas distributor)

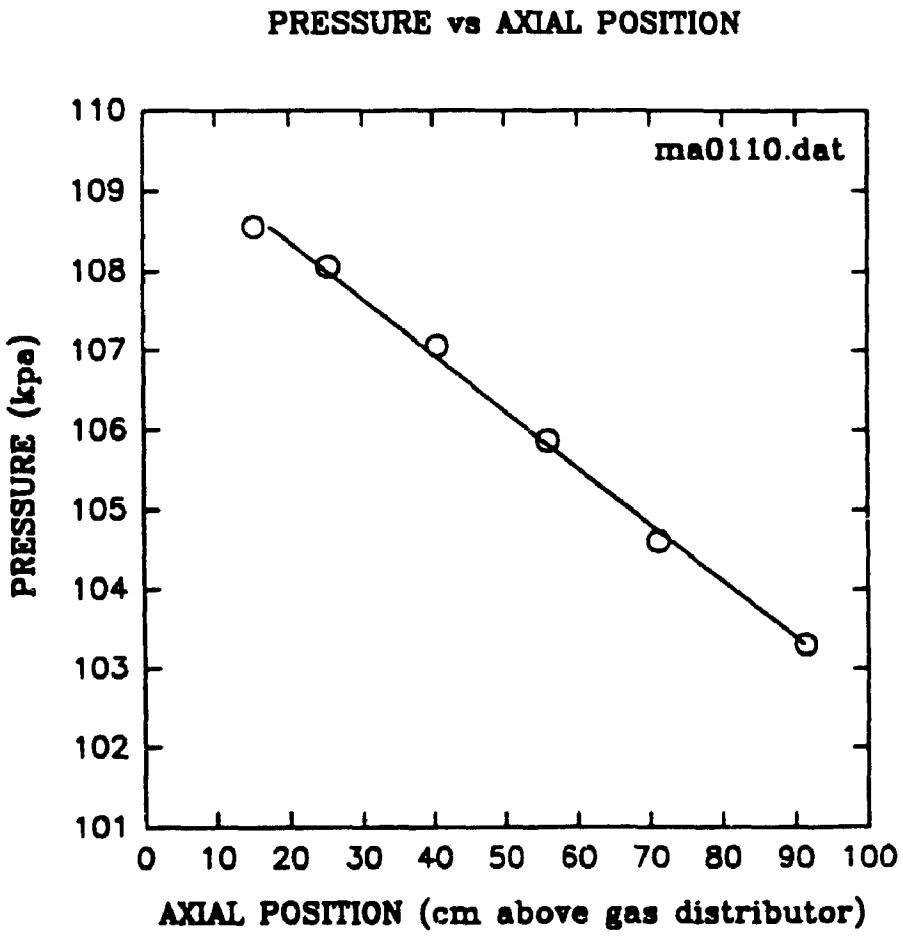
PRESSURE vs AXIAL POSITION
ma0110.dat
PRESSURE (kpa)
110
109
108
107
106
105
104
103
102
101
0
10
20
30
40
50
60
70
80
90
100
AXIAL POSITION (cm above gas distributor)

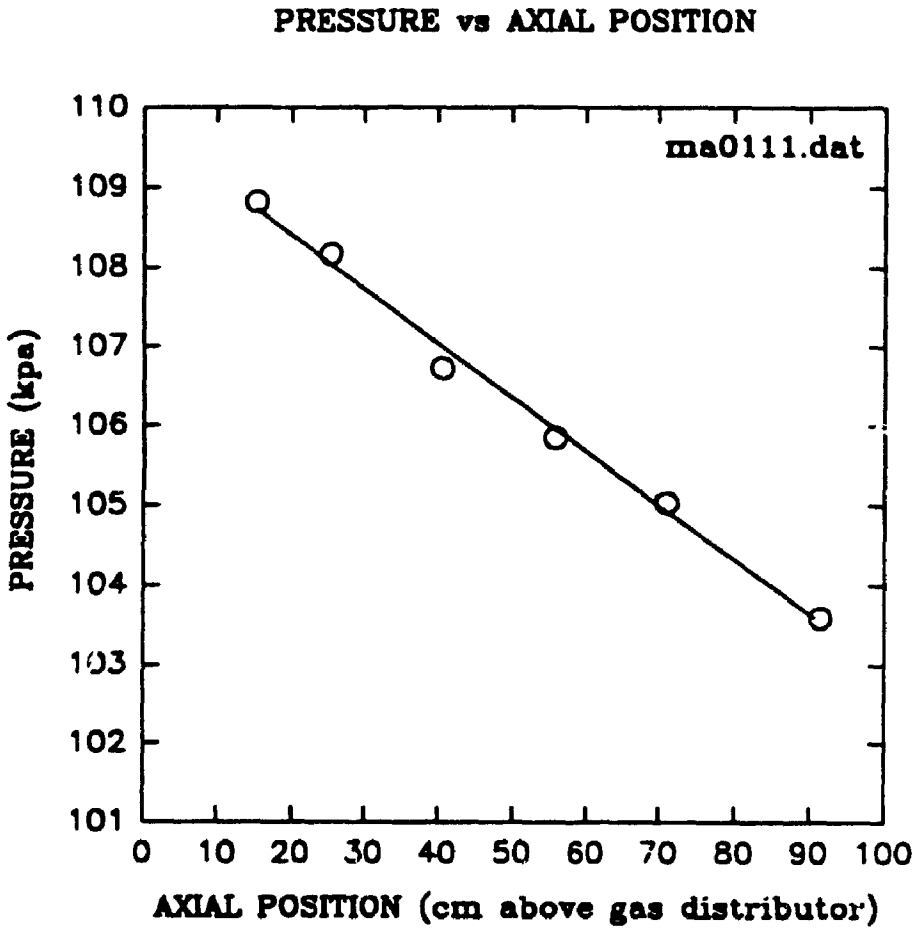
PRESSURE vs AXIAL POSITION
ma0111.dat
PRESSURE (kpa)
110
109
108
107
106
105
104
103
102
101
0
10
20
30
40
50
60
70
80
90
100
AXIAL POSITION (cm above gas distributor)

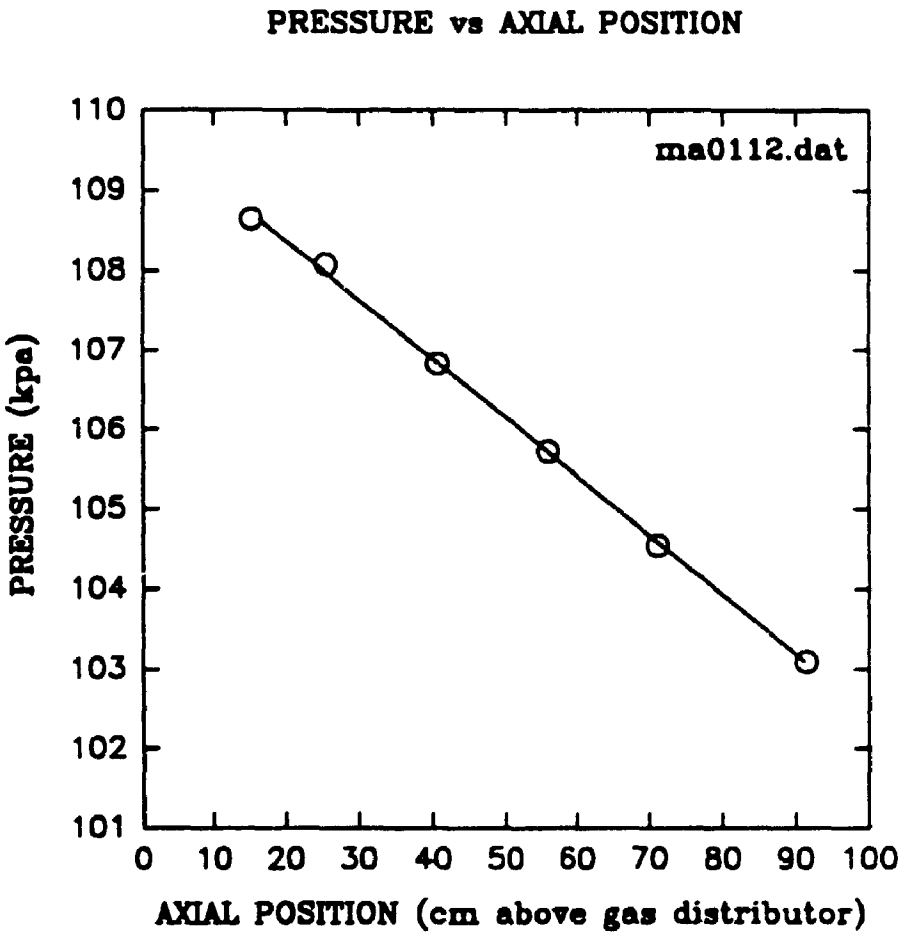
PRESSURE vs AXIAL POSITION
ma0112.dat
PRESSURE (kpa)
110
109
108
107
106
105
104
103
102
101
0
10
20
30
40
50
60
70
80
90
100
AXIAL POSITION (cm above gas distributor)

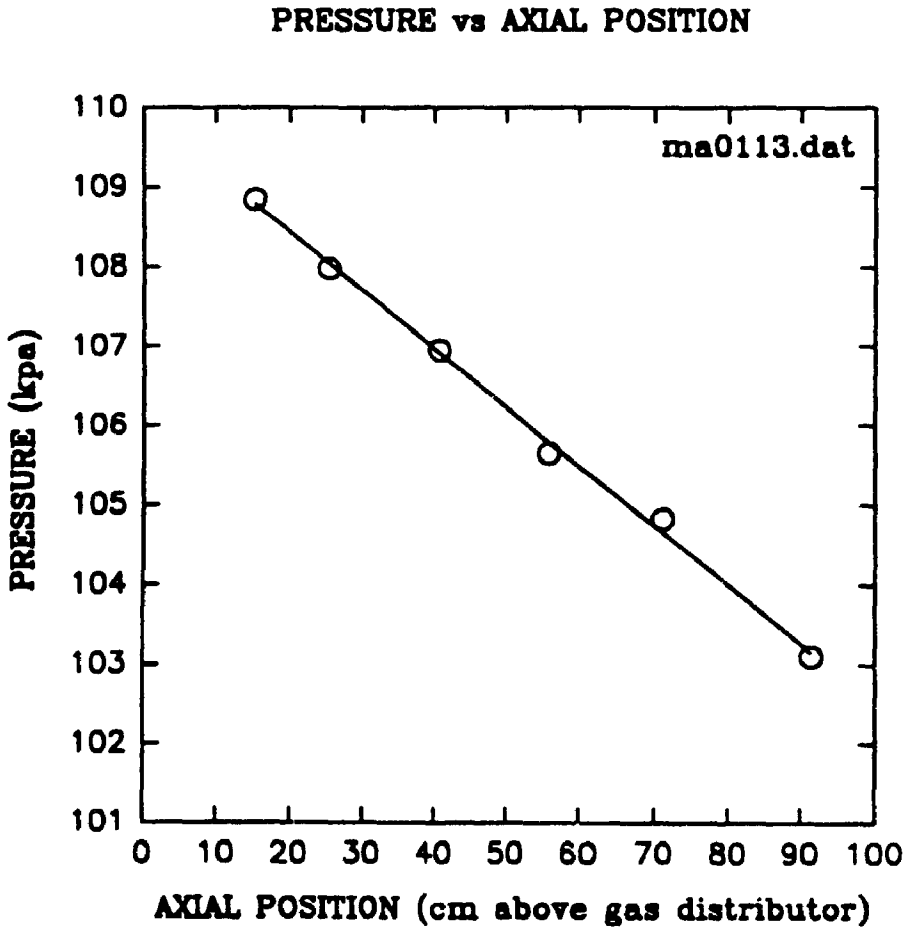
PRESSURE vs AXIAL POSITION
ma0113.dat
PRESSURE (kpa)
110
109
108
107
106
105
104
103
102
101
0
10
20
30
40
50
60
70
80
90
100
AXIAL POSITION (cm above gas distributor)

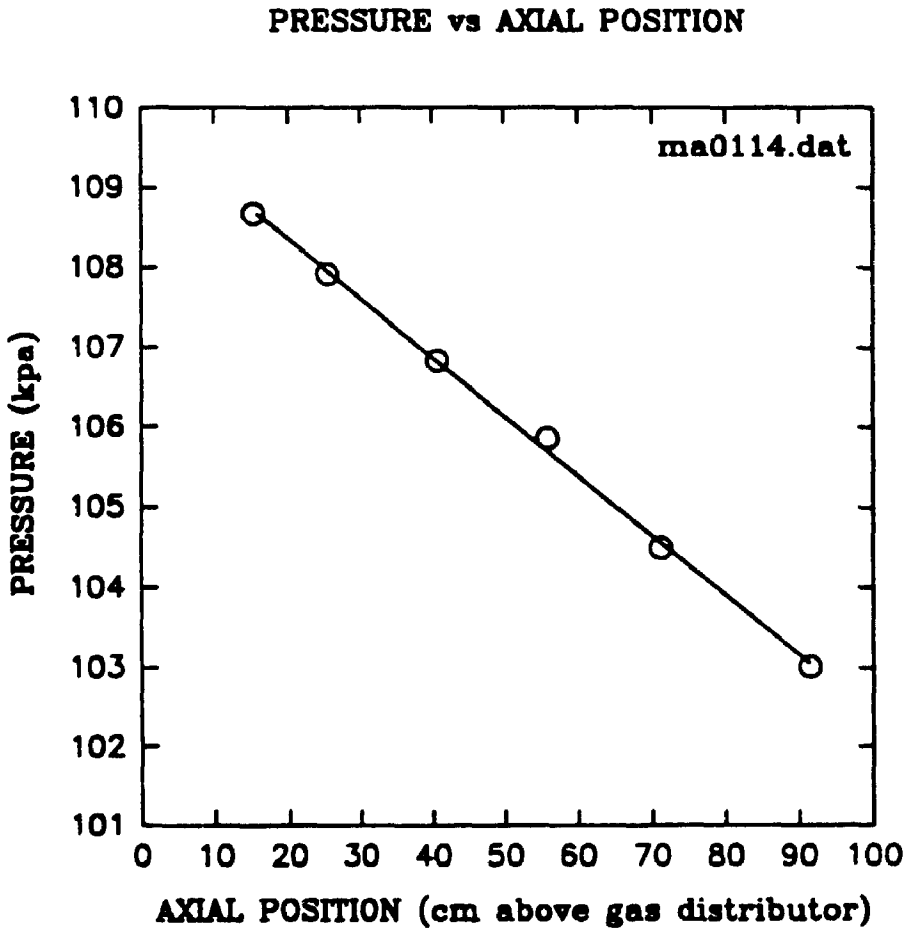
PRESSURE vs AXIAL POSITION
ma0114.dat
PRESSURE (kpa)
110
109
108
107
106
105
104
103
102
101
0
10
20
30
40
50
60
70
80
90
100
AXIAL POSITION (cm above gas distributor)

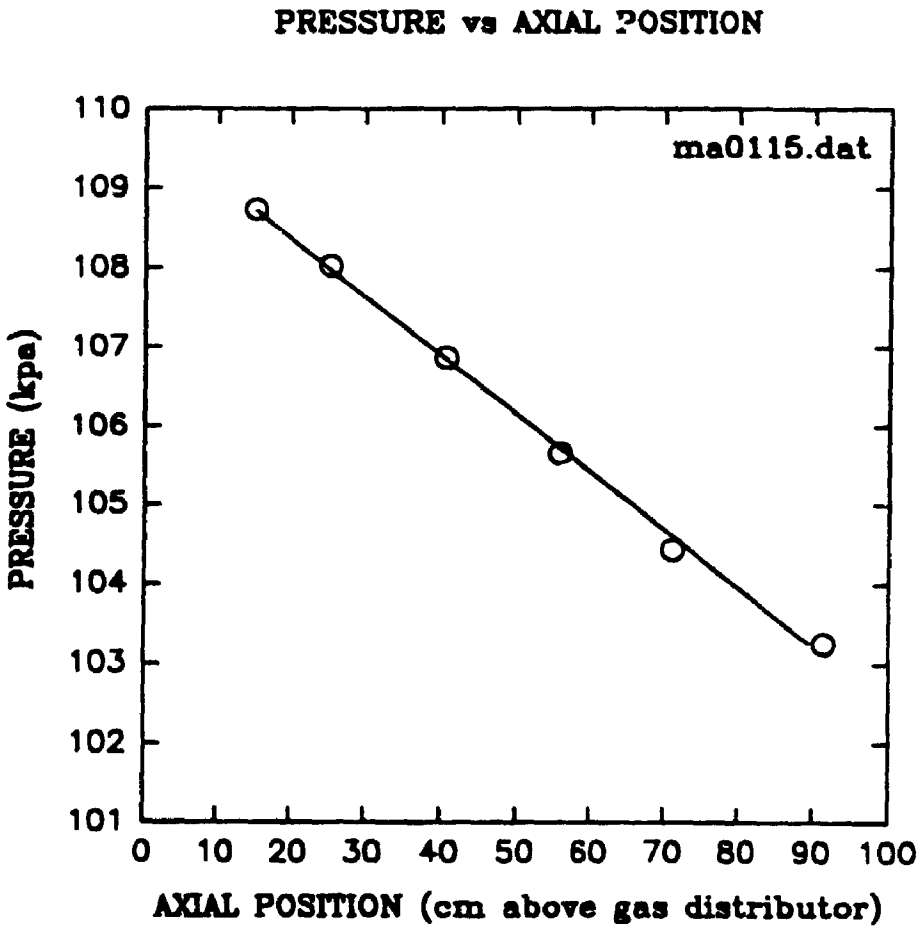
PRESSURE vs AXIAL POSITION
ma0115.dat
PRESSURE (kpa)
110
109
108
107
106
105
104
103
102
101
0
10
20
30
40
50
60
70
80
90
100
AXIAL POSITION (cm above gas distributor)

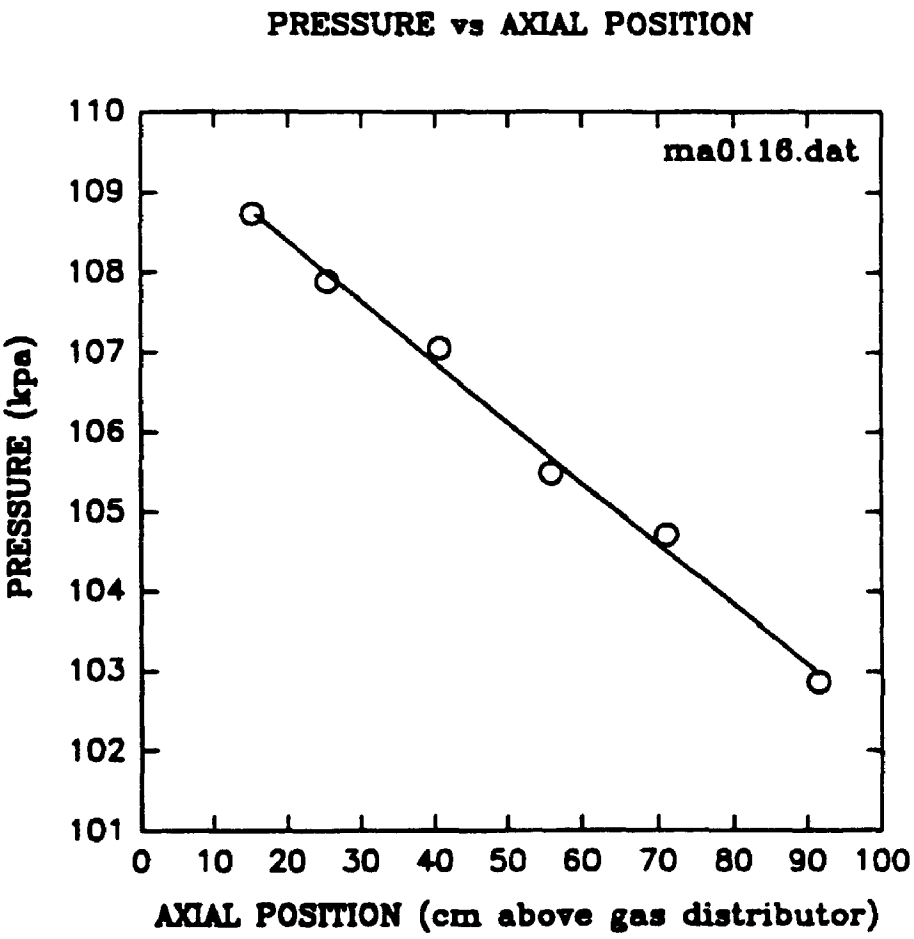
PRESSURE vs AXIAL POSITION
ma0116.dat
PRESSURE (kpa)
110
109
108
107
106
105
104
103
102
101
0
10
20
30
40
50
60
70
80
90
100
AXIAL POSITION (cm above gas distributor)

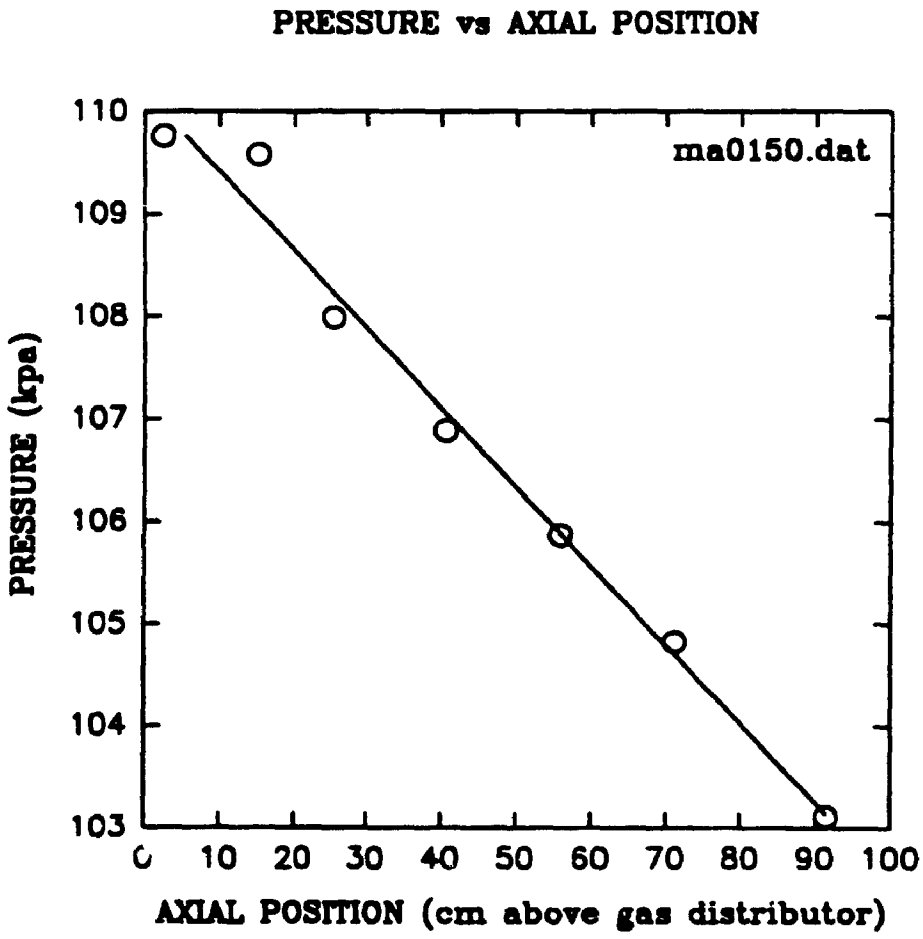
PRESSURE vs AXIAL POSITION
ma0150.dat
PRESSURE (kpa)
110
109
108
107
106
105
104
103
0
10
20
30
40
50
60
70
80
90
100
AXIAL POSITION (cm above gas distributor)

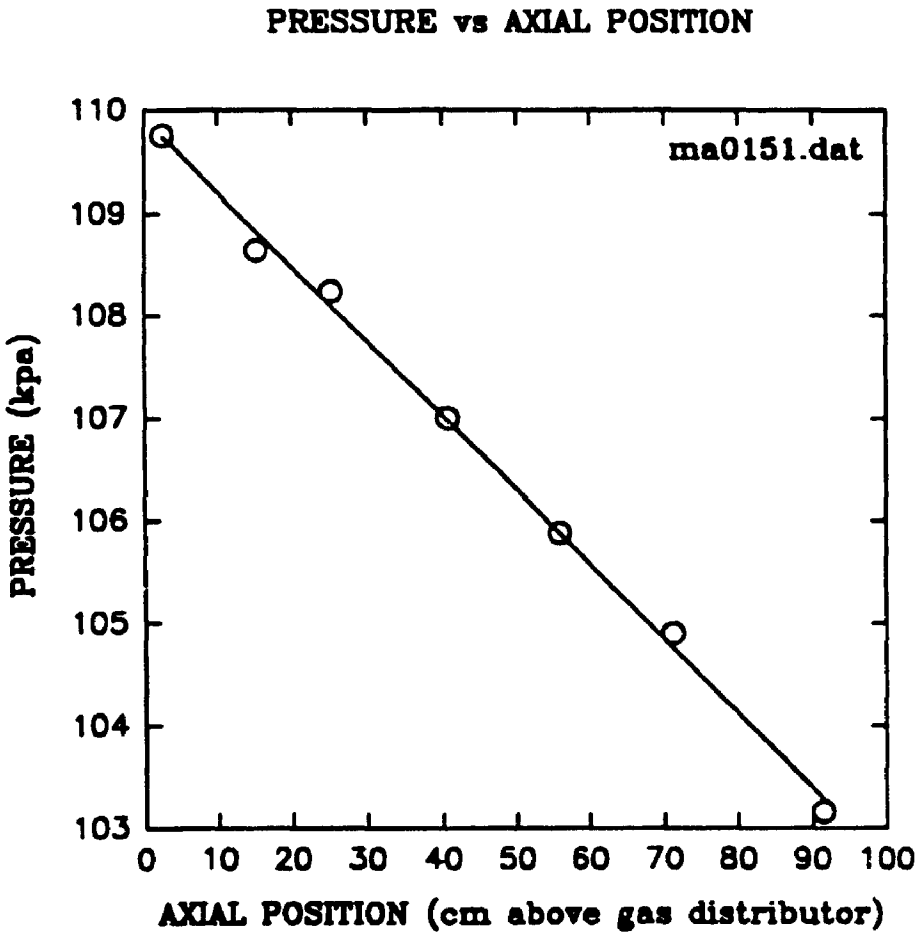
PRESSURE vs AXIAL POSITION
ma0151.dat
PRESSURE (kpa)
110
109
108
107
106
105
104
103
0
10
20
30
40
50
60
70
80
90
100
AXIAL POSITION (cm above gas distributor)

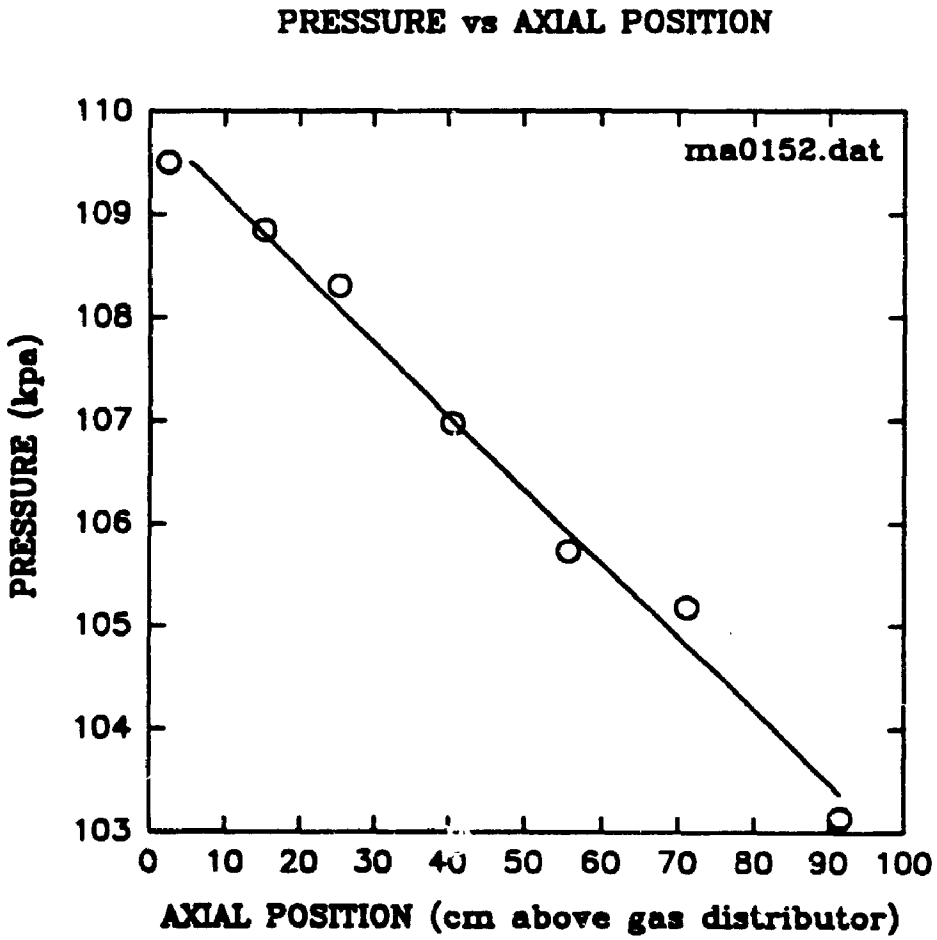
PRESSURE vs AXIAL POSITION
ma0152.dat
PRESSURE (kpa)
110
109
108
107
106
105
104
103
0
10
20
30
40
50
60
70
80
90
100
AXIAL POSITION (cm above gas distributor)

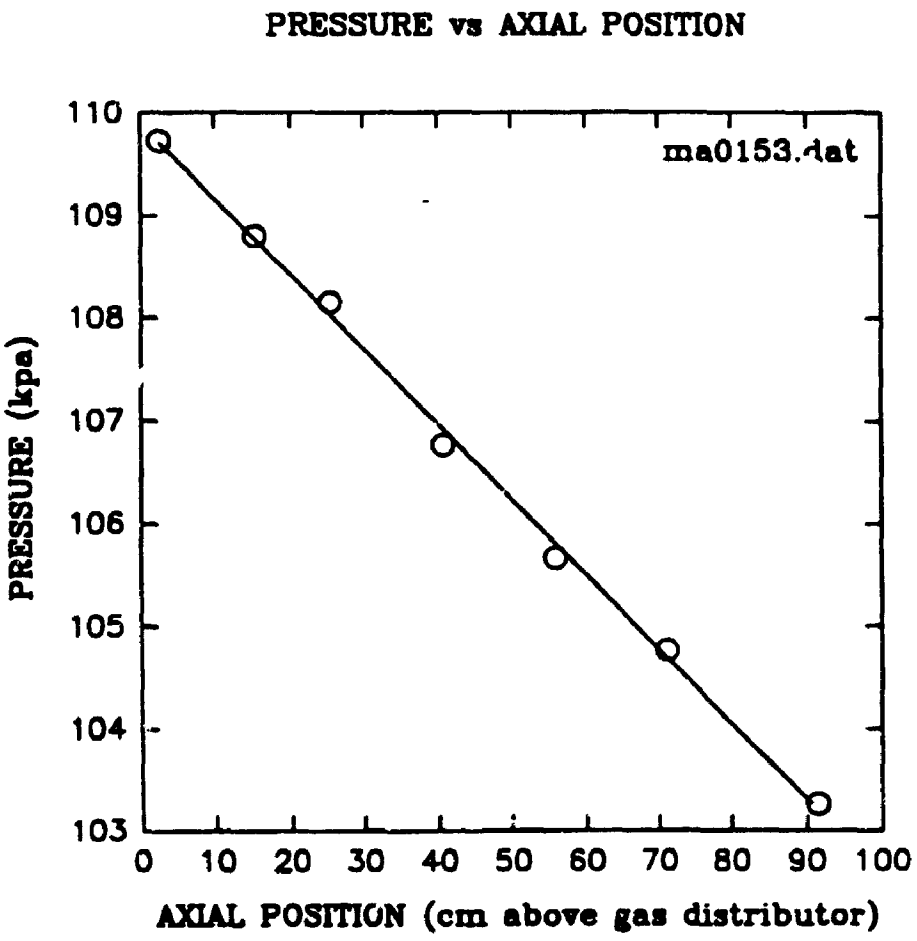
PRESSURE vs AXIAL POSITION
ma0153.dat
PRESSURE (kpa)
110
109
108
107
106
105
104
103
0
10
20
30
40
50
60
70
80
90
100
AXIAL POSITION (cm above gas distributor)

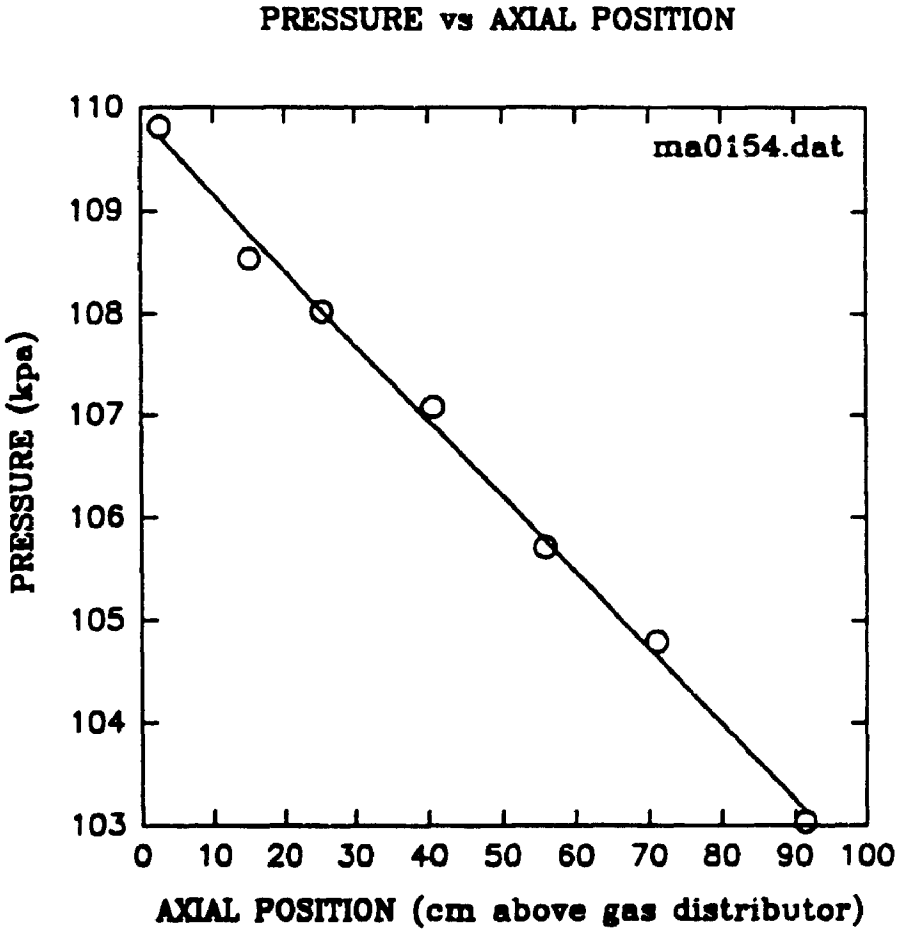
PRESSURE vs AXIAL POSITION
ma0154.dat
PRESSURE (kpa)
110
109
108
107
106
105
104
103
0
10
20
30
40
50
60
70
80
90
100
AXIAL POSITION (cm above gas distributor)

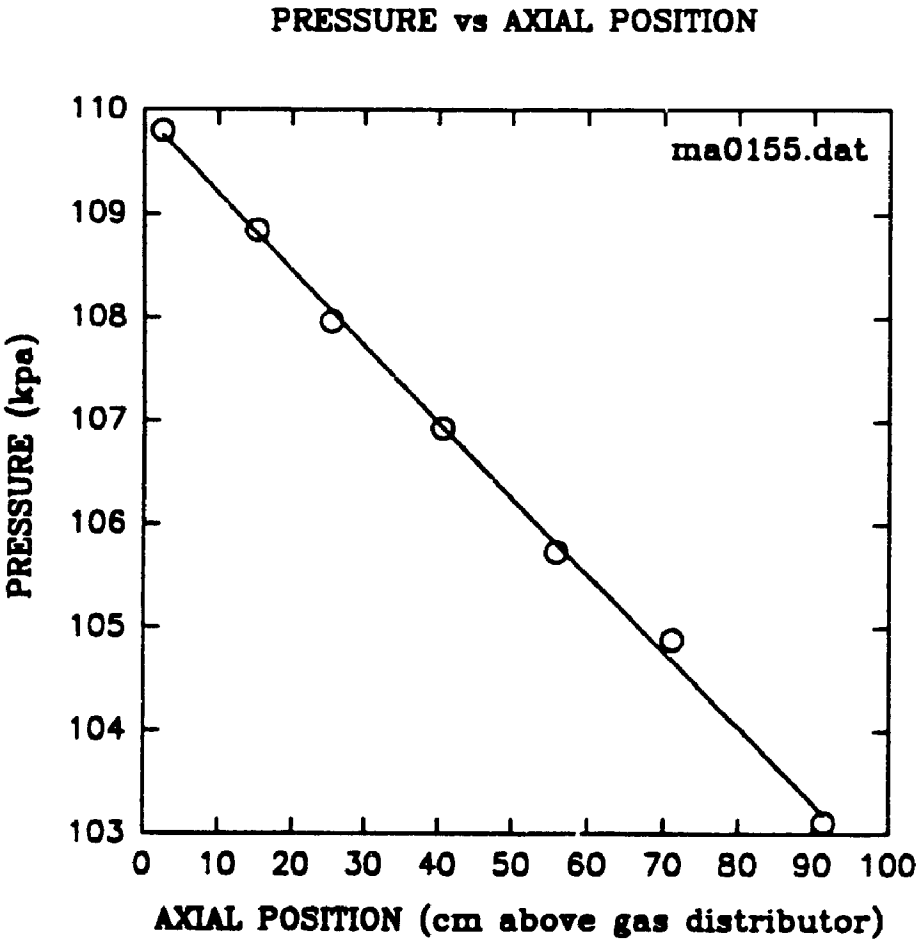
PRESSURE vs AXIAL POSITION
ma0155.dat
PRESSURE (kpa)
110
109
108
107
106
105
104
103
0
10
20
30
40
50
60
70
80
90
100
AXIAL POSITION (cm above gas distributor)

PRESSURE vs AXIAL POSITION

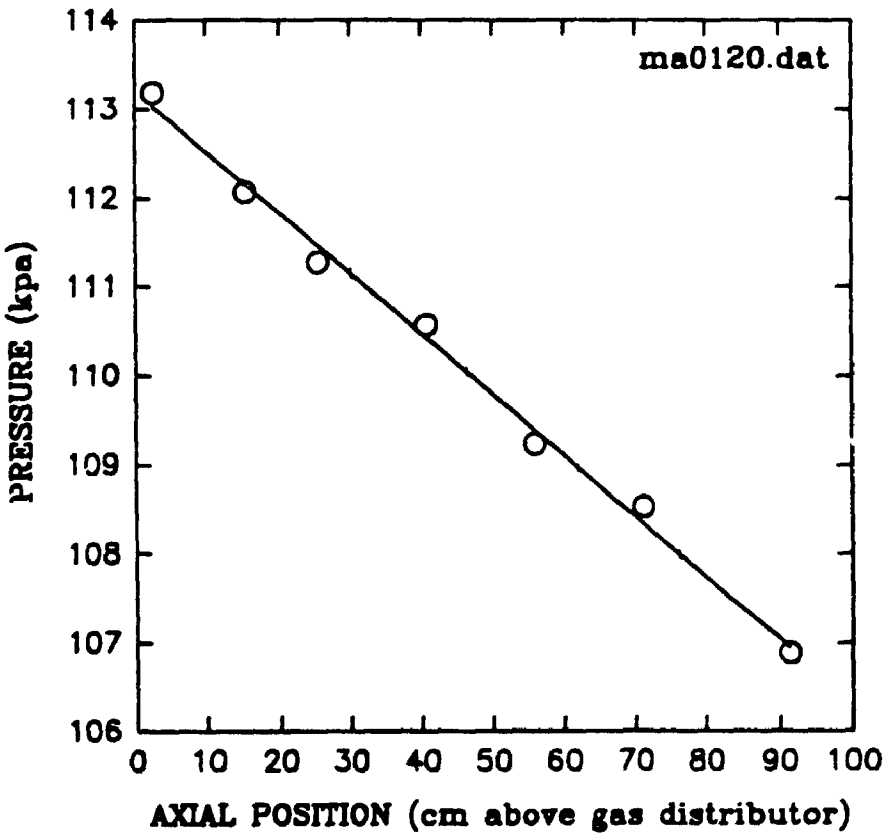

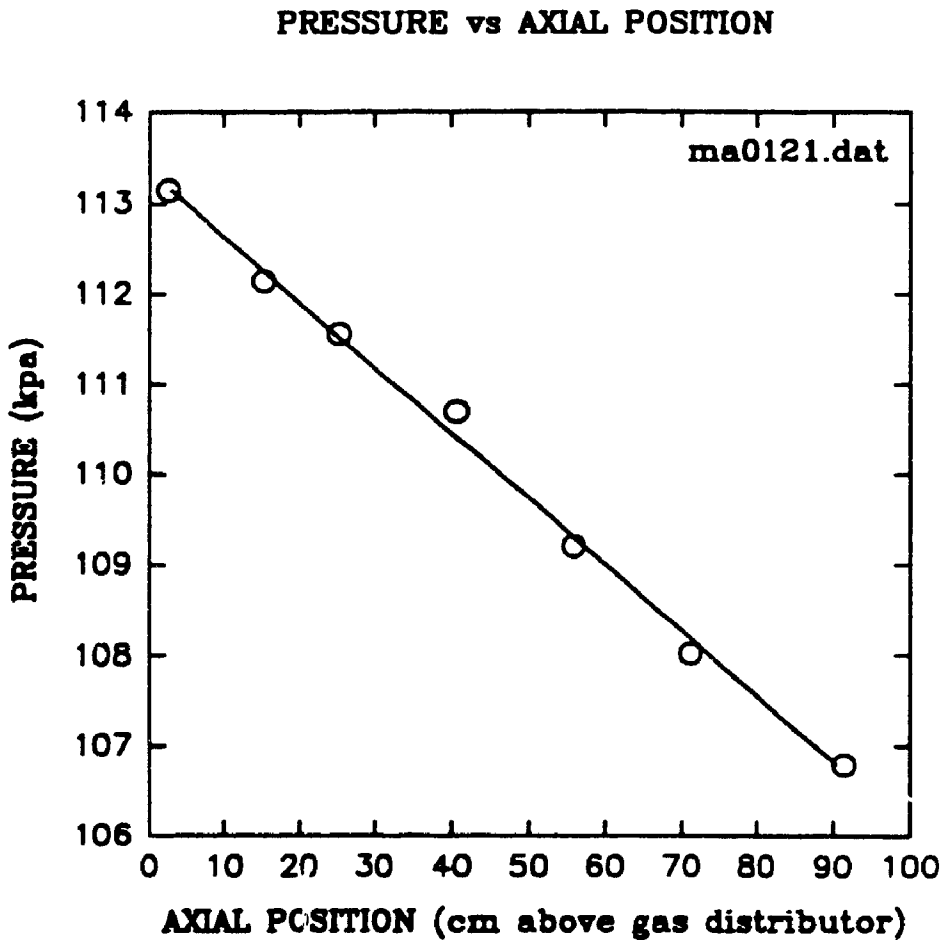
PRESSURE vs AXIAL POSITION
ma0121.dat
PRESSURE (kpa)
114
113
112
111
110
109
108
107
106
0
10
20
30
40
50
60
70
80
90
100
AXIAL POSITION (cm above gas distributor)

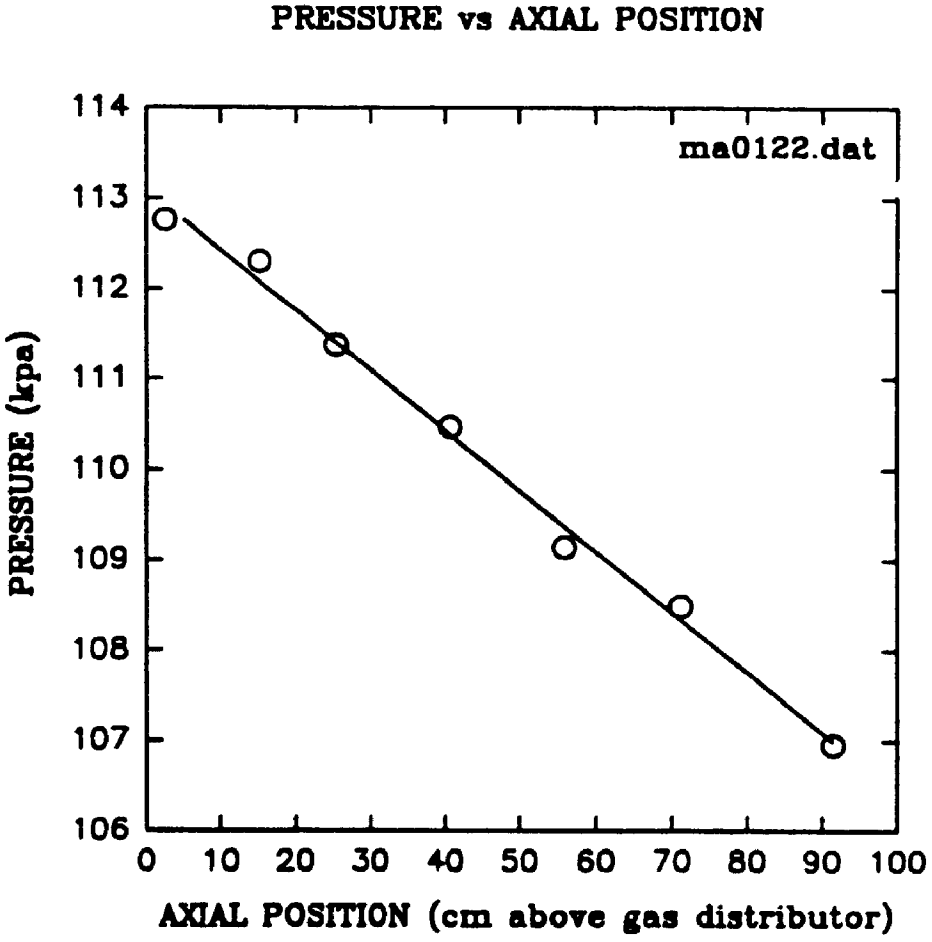
PRESSURE vs AXIAL POSITION
ma0122.dat
PRESSURE (kpa)
114
113
112
111
110
109
108
107
106
0
10
20
30
40
50
60
70
80
90
100
AXIAL POSITION (cm above gas distributor)

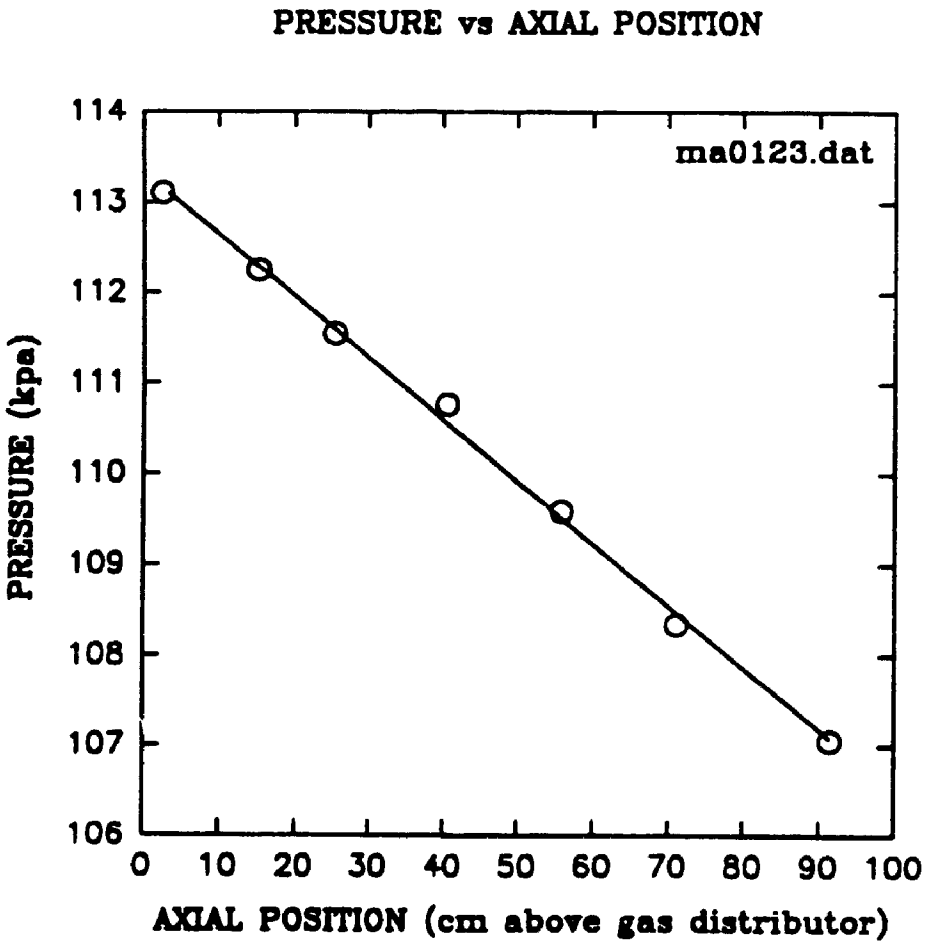
PRESSURE vs AXIAL POSITION
ma0123.dat
PRESSURE (kpa)
114
113
112
111
110
109
108
107
106
0
10
20
30
40
50
60
70
80
90
100
AXIAL POSITION (cm above gas distributor)

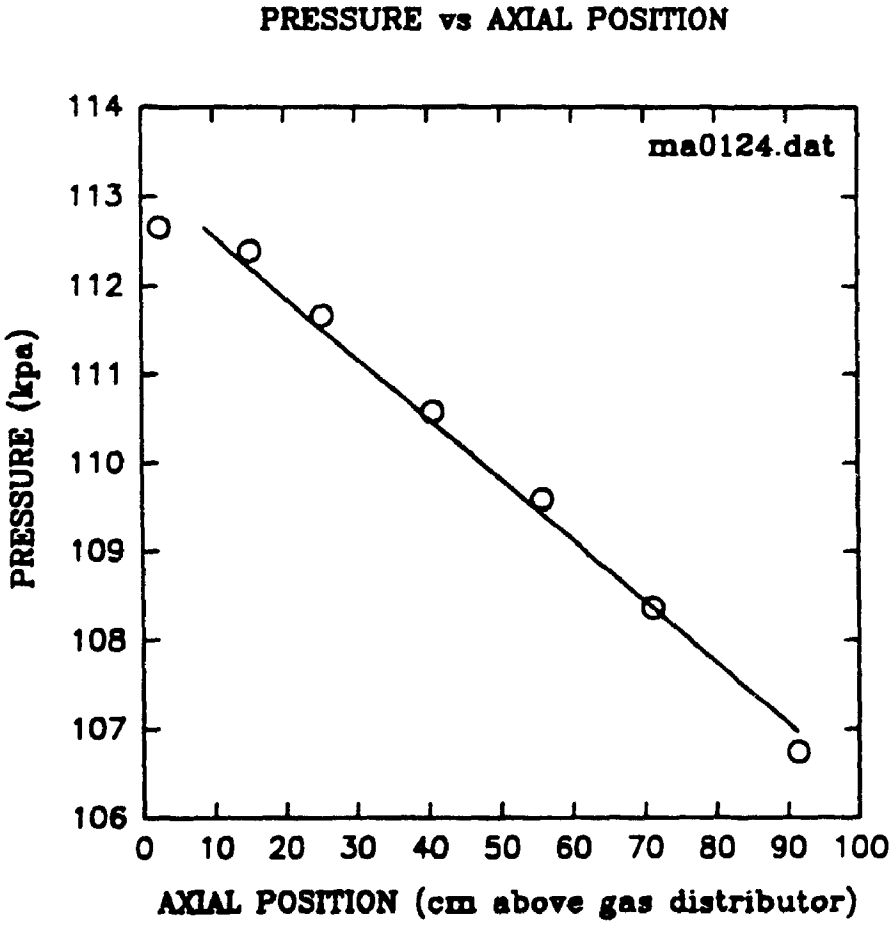
PRESSURE vs AXIAL POSITION
ma0124.dat
PRESSURE (kpa)
114
113
112
111
110
109
108
107
106
0
10
20
30
40
50
60
70
80
90
100
AXIAL POSITION (cm above gas distributor)

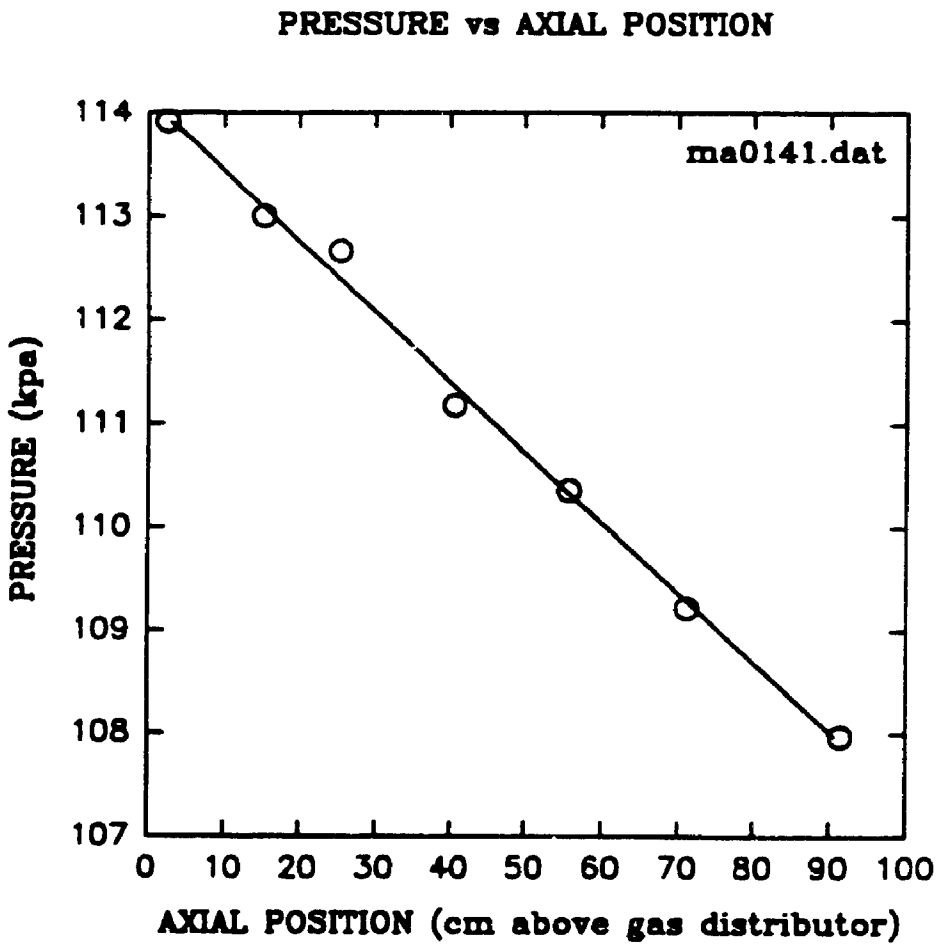
PRESSURE vs AXIAL POSITION
ma0141.dat
PRESSURE (kpa)
114
113
112
111
110
109
108
107
0
10
20
30
40
50
60
70
80
90
100
AXIAL POSITION (cm above gas distributor)

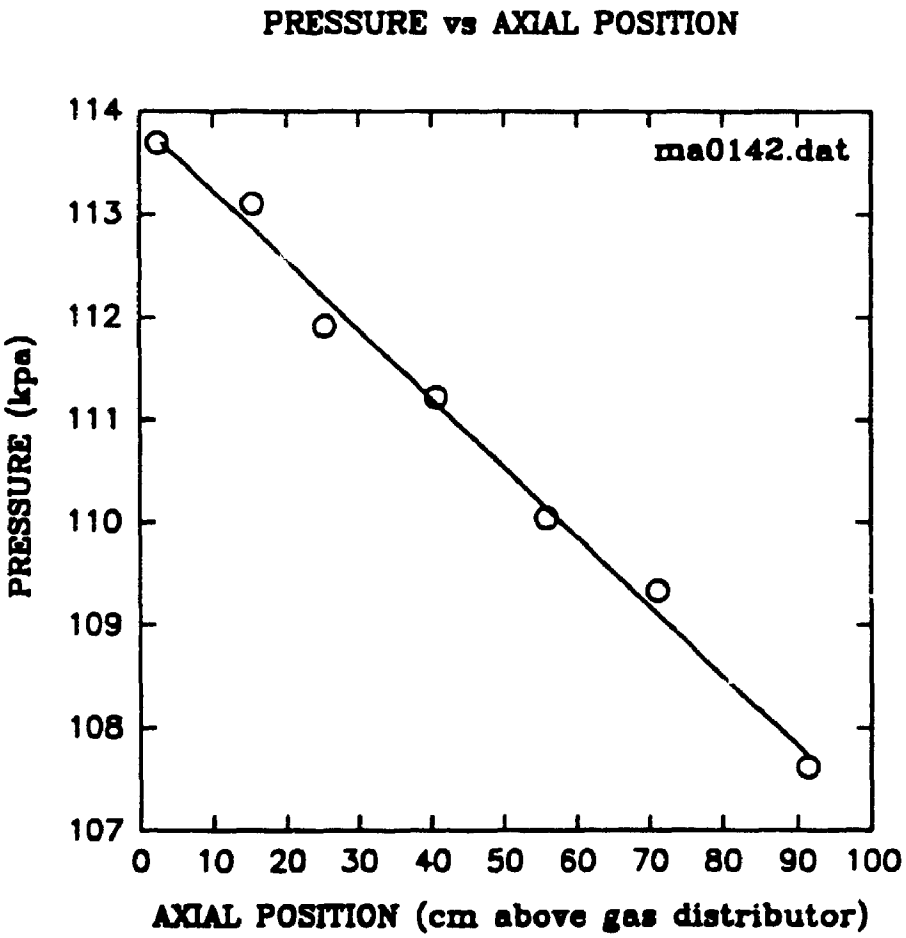
PRESSURE vs AXIAL POSITION
ma0142.dat
PRESSURE (kpa)
114
113
112
111
110
109
108
107
0
10
20
30
40
50
60
70
80
90
100
AXIAL POSITION (cm above gas distributor)

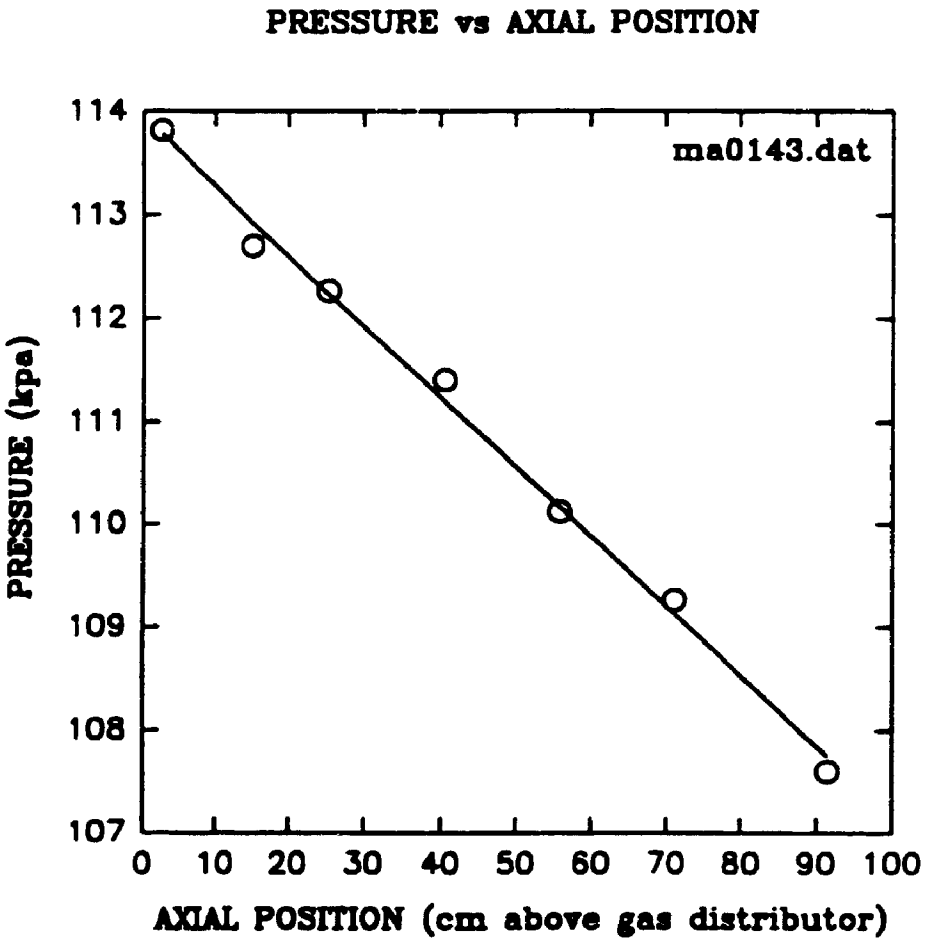
PRESSURE vs AXIAL POSITION
ma0143.dat
PRESSURE (kpa)
114
113
112
111
110
109
108
107
0
10
20
30
40
50
60
70
80
90
100
AXIAL POSITION (cm above gas distributor)

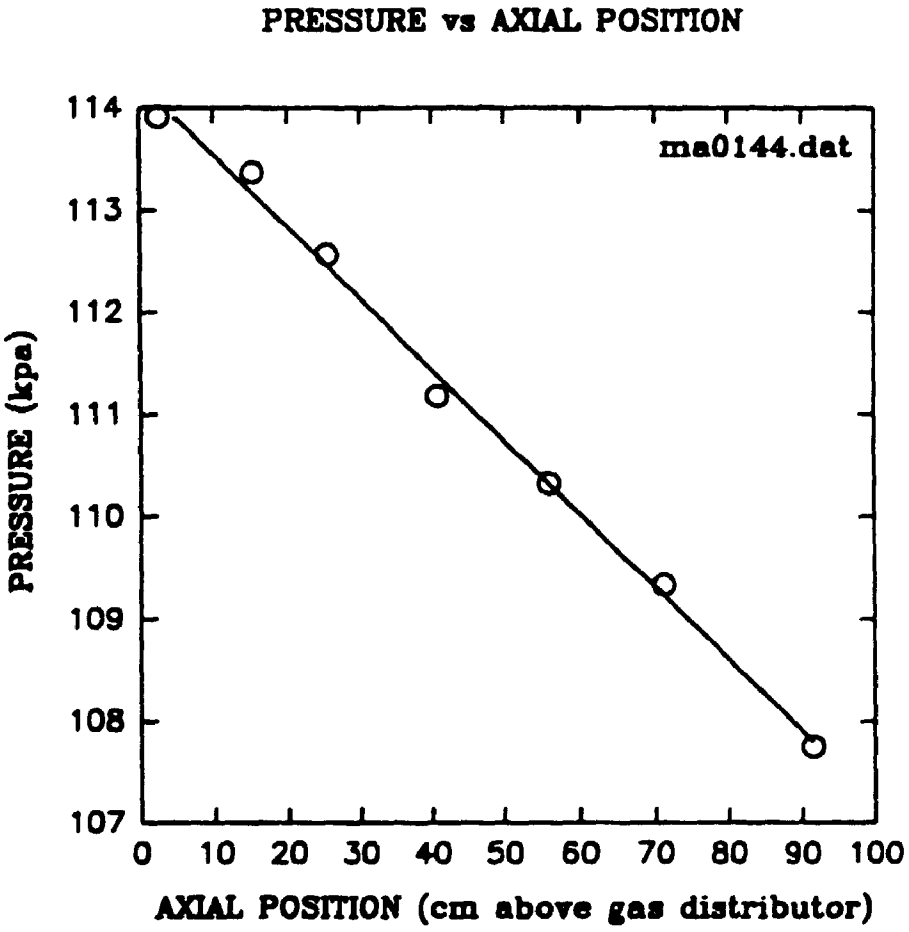
PRESSURE vs AXIAL POSITION
ma0144.dat
PRESSURE (kpa)
114
113
112
111
110
109
108
107
0
10
20
30
40
50
60
70
80
90
100
AXIAL POSITION (cm above gas distributor)

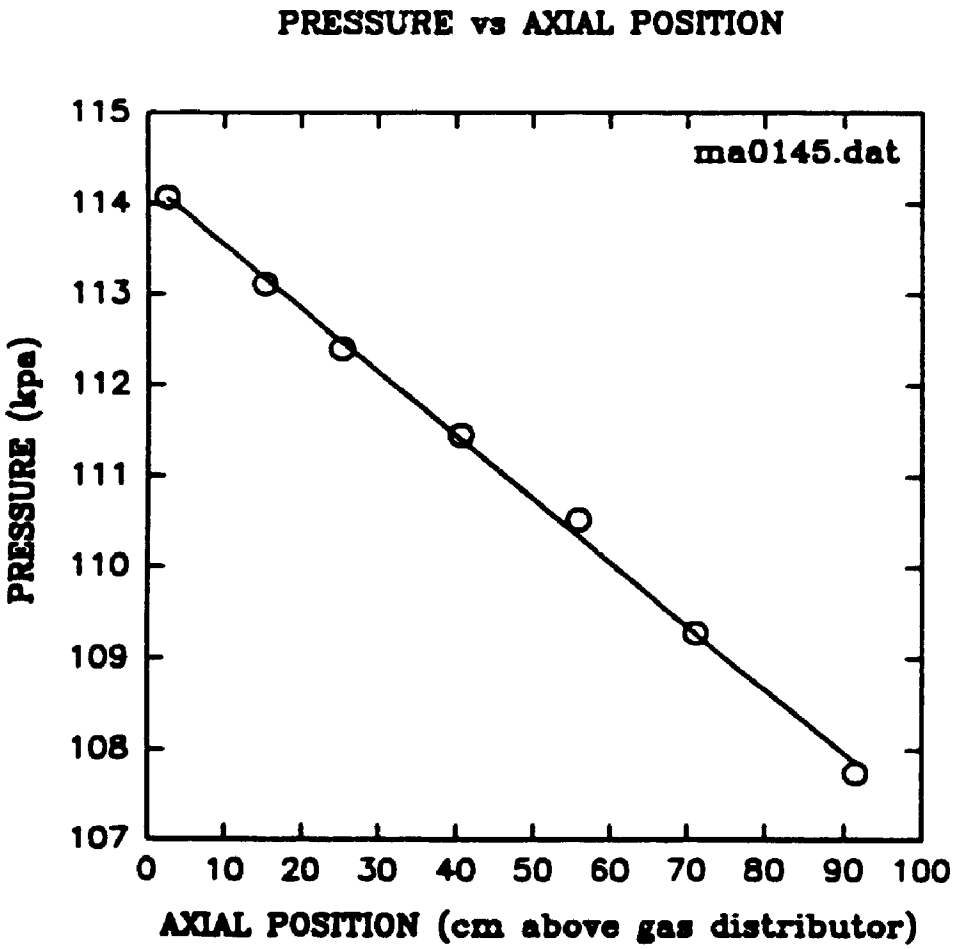
PRESSURE vs AXIAL POSITION
ma0145.dat
PRESSURE (kpa)
115
114
113
112
111
110
109
108
107
0
10
20
30
40
50
60
70
80
90
100
AXIAL POSITION (cm above gas distributor)

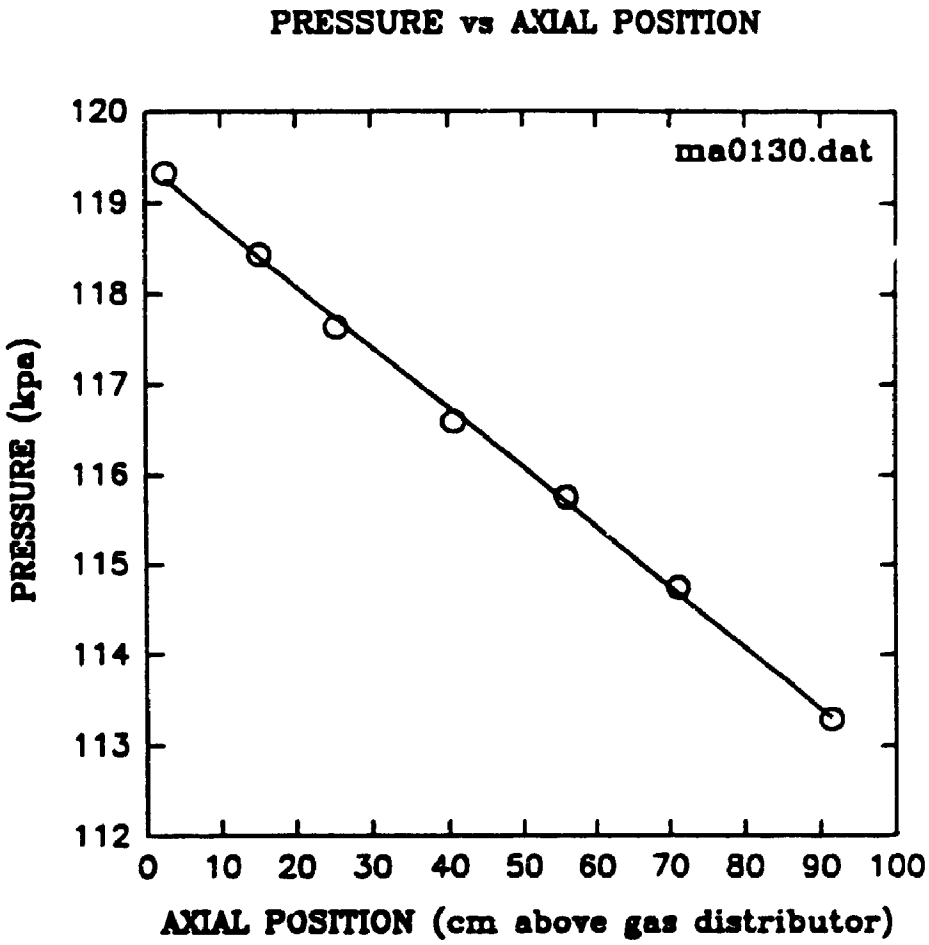
PRESSURE vs AXIAL POSITION
ma0130.dat
PRESSURE (kpa)
120
119
118
117
116
115
114
113
112
0
10
20
30
40
50
60
70
80
90
100
AXIAL POSITION (cm above gas distributor)

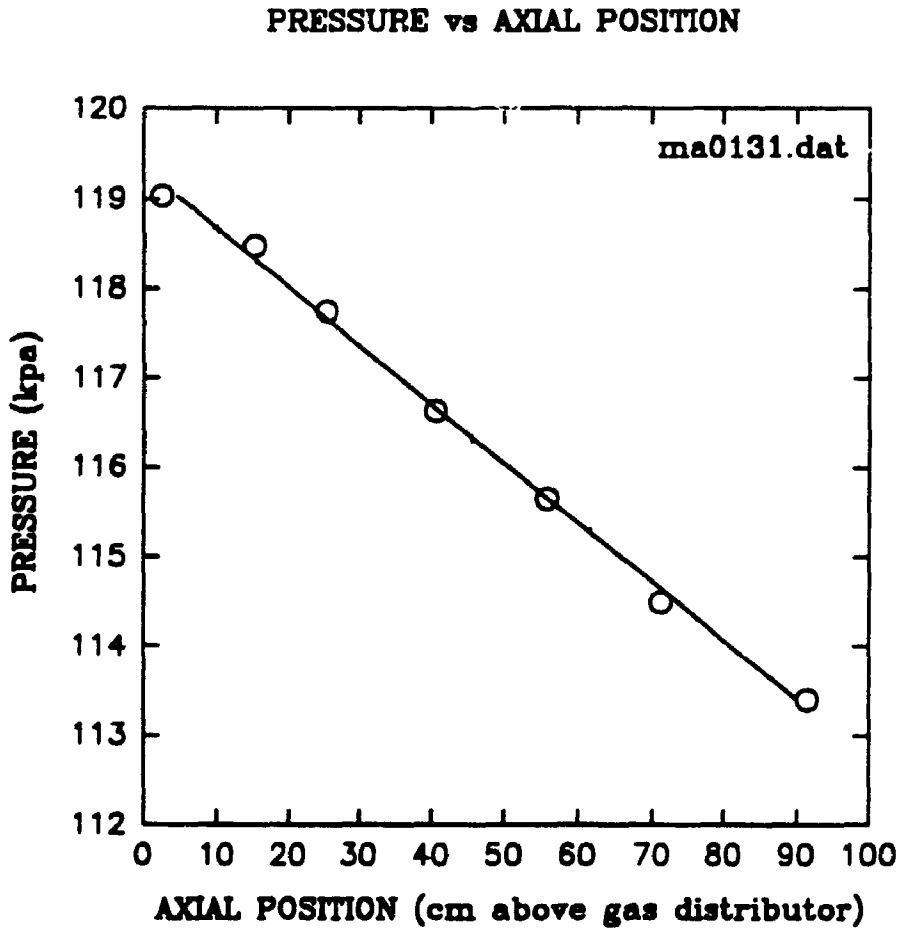
PRESSURE vs AXIAL POSITION
ma0131.dat
PRESSURE (kpa)
120
119
118
117
116
115
114
113
112
0
10
20
30
40
50
60
70
80
90
100
AXIAL POSITION (cm above gas distributor)

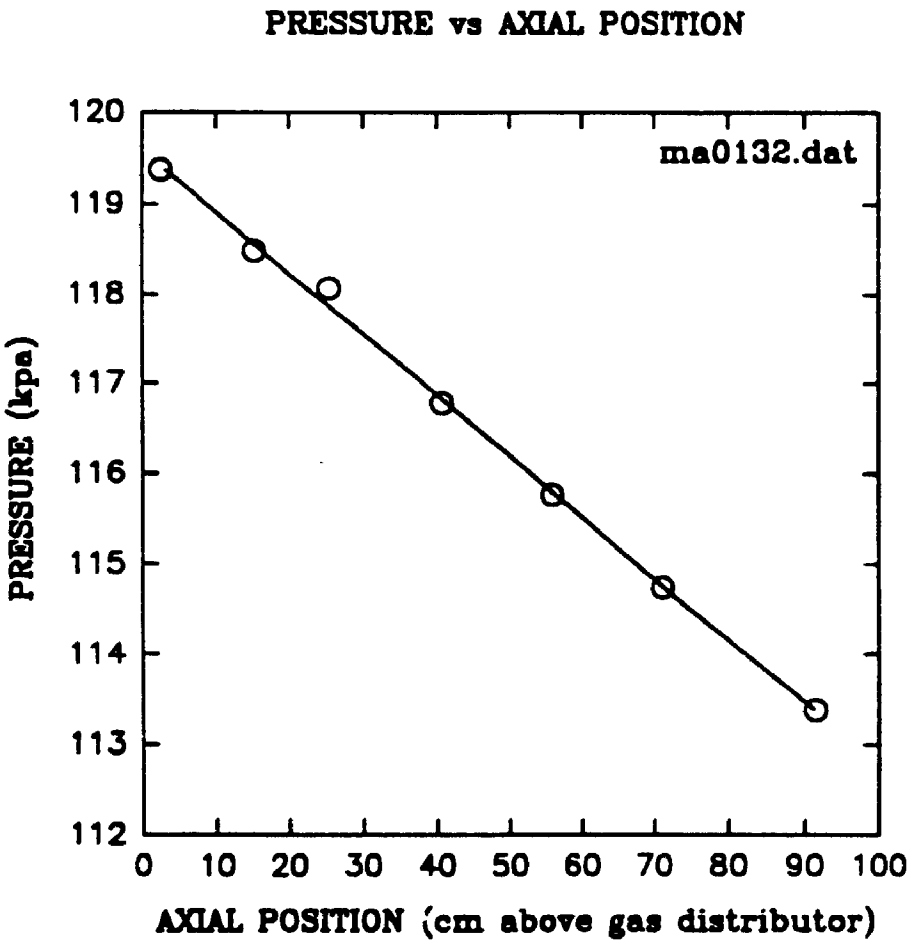
PRESSURE vs AXIAL POSITION
ma0132.dat
PRESSURE (kpa)
120
119
118
117
116
115
114
113
112
0
10
20
30
40
50
60
70
80
90
100
AXIAL POSITION (cm above gas distributor)

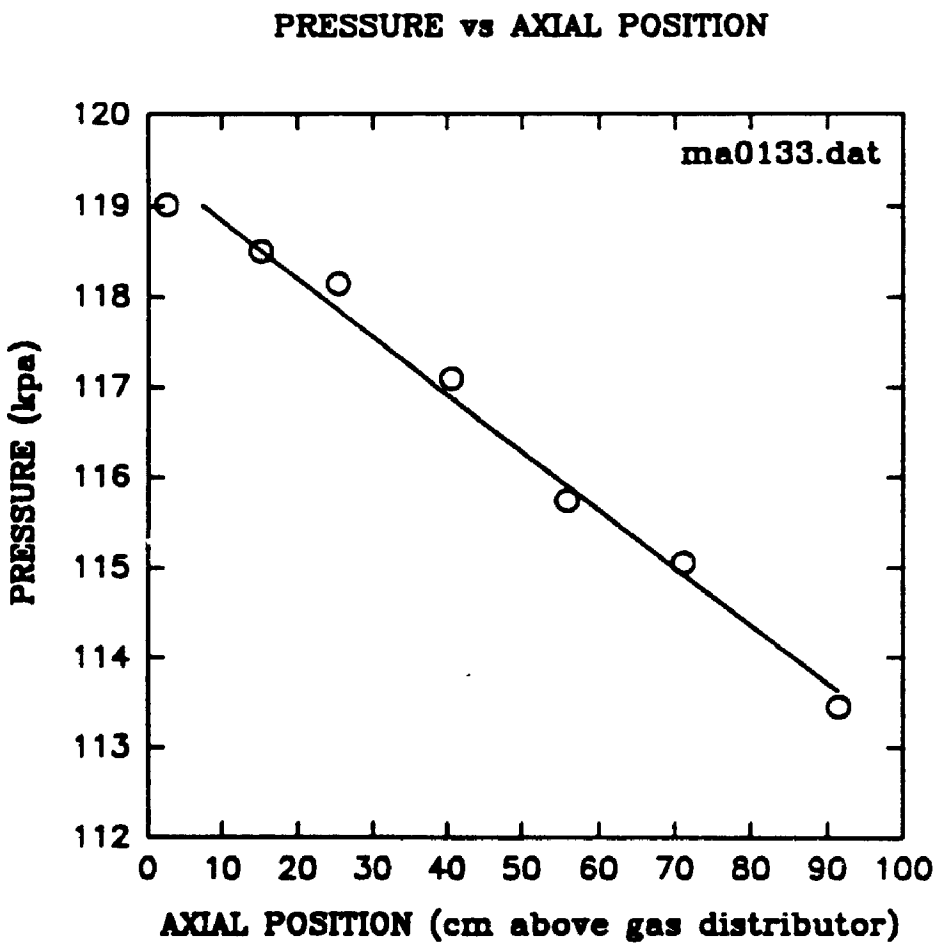
PRESSURE vs AXIAL POSITION
ma0133.dat
PRESSURE (kpa)
120
119
118
117
116
115
114
113
112
0
10
20
30
40
50
60
70
80
90
100
AXIAL POSITION (cm above gas distributor)

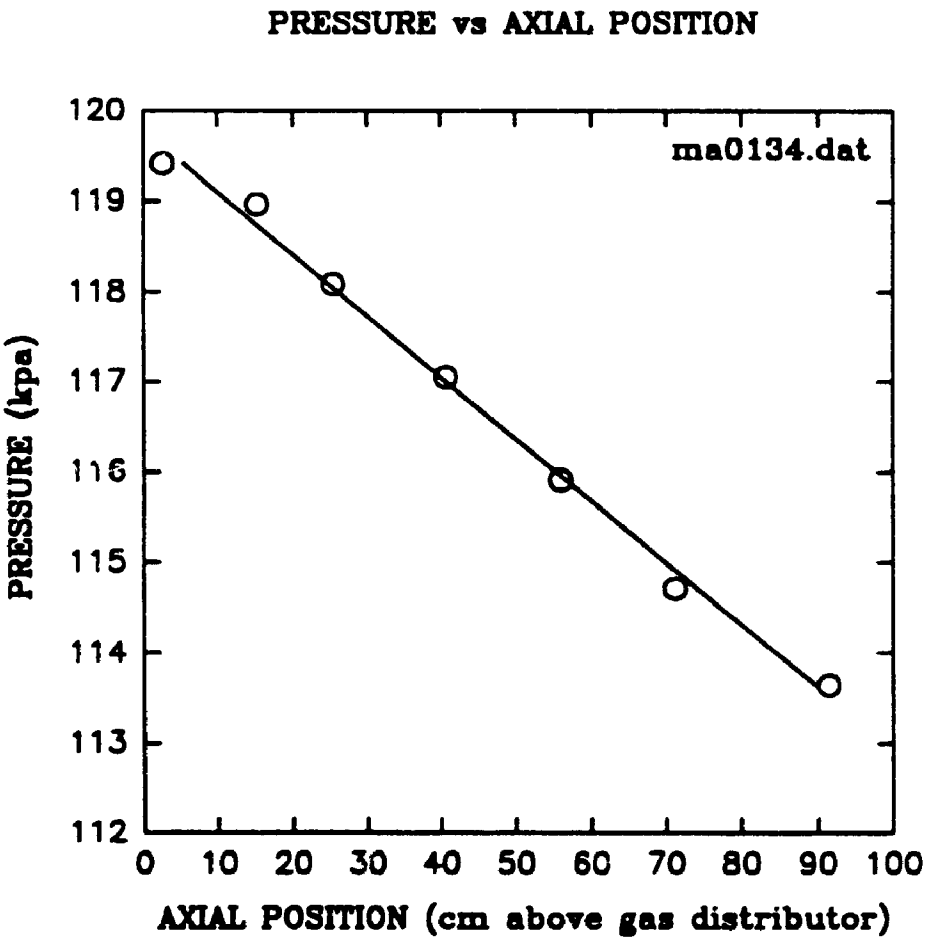
PRESSURE vs AXIAL POSITION
ma0134.dat
PRESSURE (kpa)
120
119
118
117
116
115
114
113
112
0
10
20
30
40
50
60
70
80
90
100
AXIAL POSITION (cm above gas distributor)

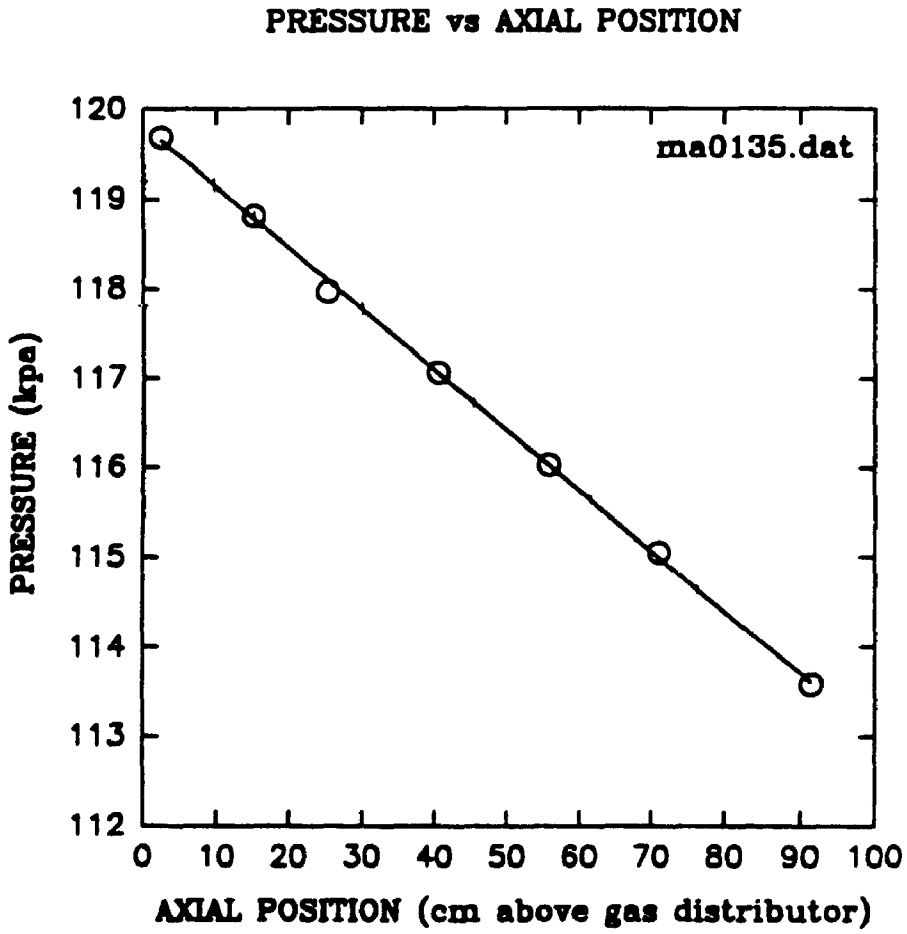
PRESSURE vs AXIAL POSITION
ma0135.dat
PRESSURE (kpa)
120
119
118
117
116
115
114
113
112
0
10
20
30
40
50
60
70
80
90
100
AXIAL POSITION (cm above gas distributor)

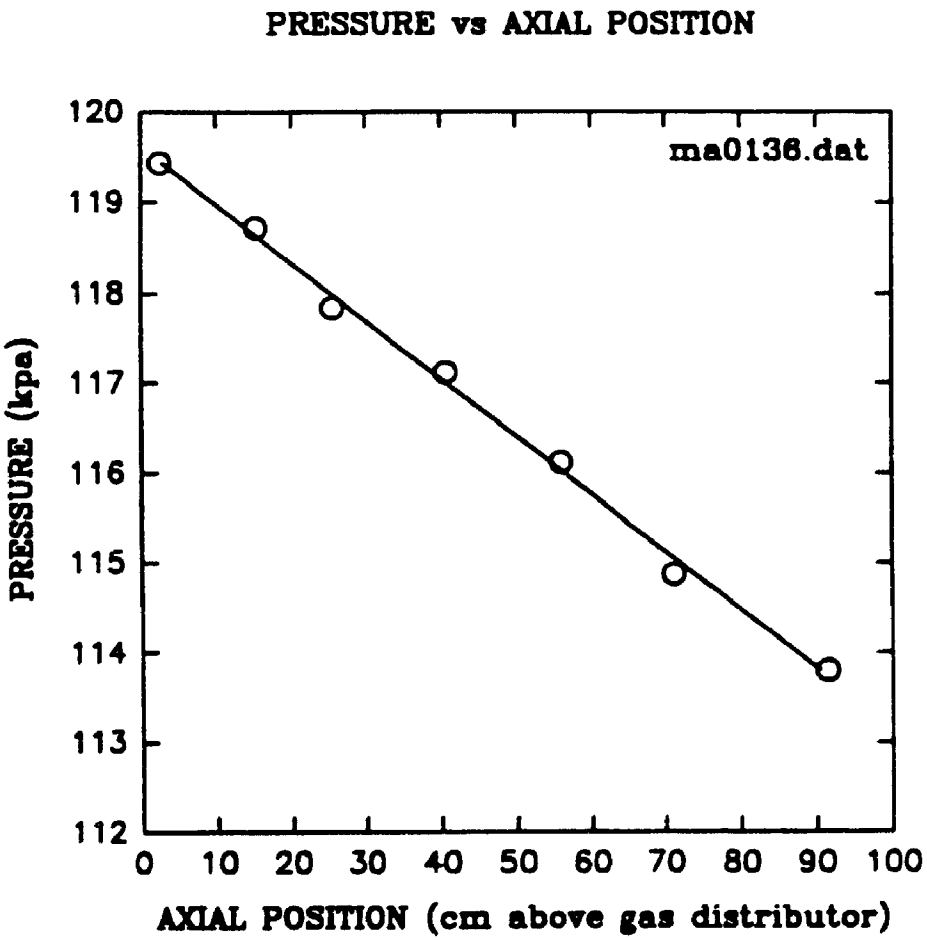
PRESSURE vs AXIAL POSITION
ma0136.dat
PRESSURE (kpa)
120
119
118
117
116
115
114
113
112
0
10
20
30
40
50
60
70
80
90
100
AXIAL POSITION (cm above gas distributor)

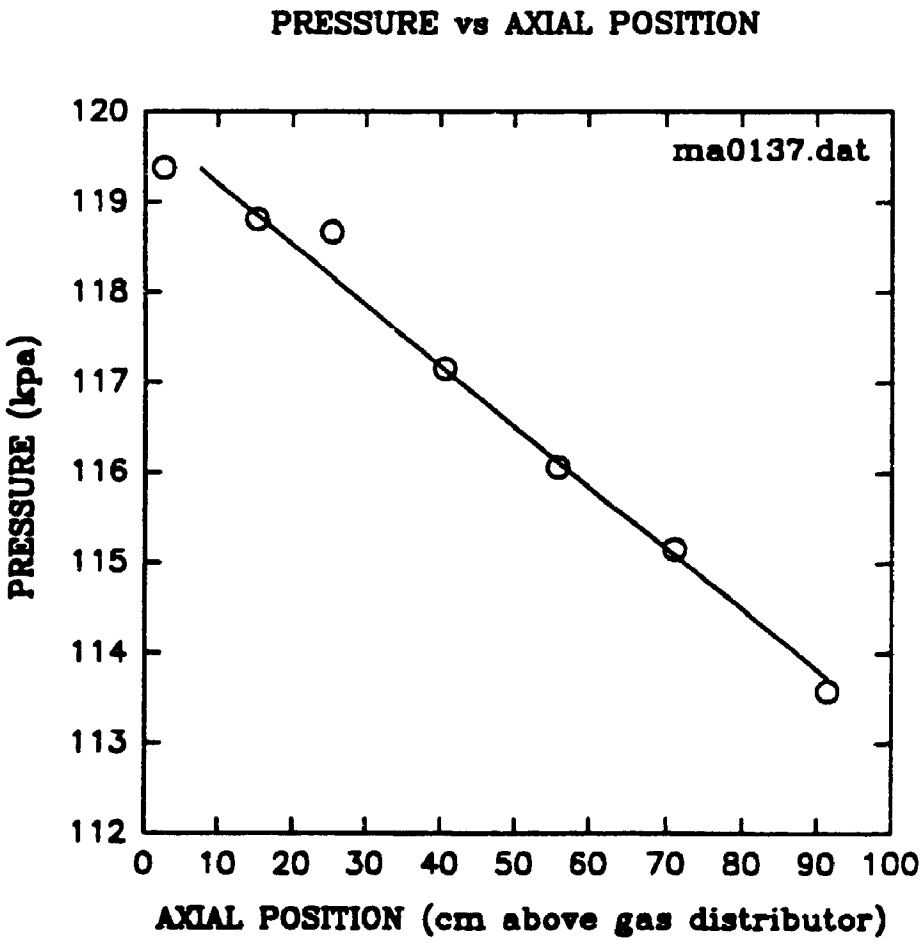
PRESSURE vs AXIAL POSITION
ma0137.dat
PRESSURE (kpa)
120
119
118
117
116
115
114
113
112
0
10
20
30
40
50
60
70
80
90
100
AXIAL POSITION (cm above gas distributor)

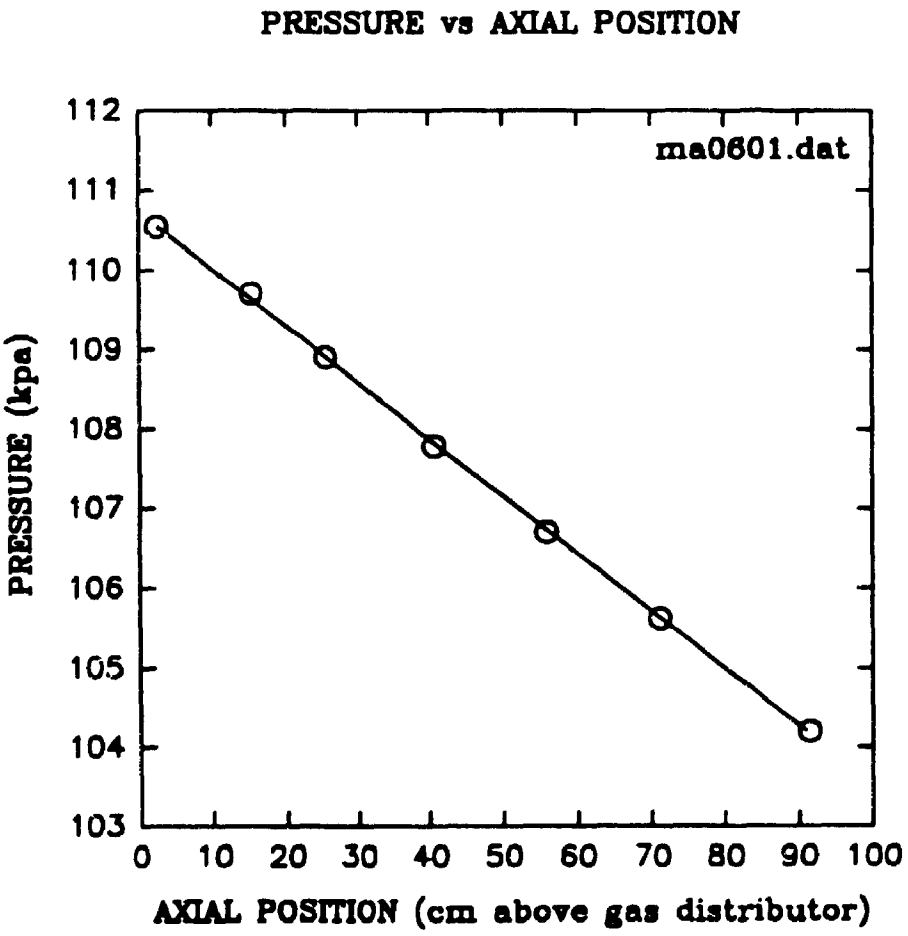
PRESSURE vs AXIAL POSITION
ma0601.dat
PRESSURE (kpa)
112
111
110
109
108
107
106
105
104
103
0
10
20
30
40
50
60
70
80
90
100
AXIAL POSITION (cm above gas distributor)

PRESSURE vs AXIAL POSITION

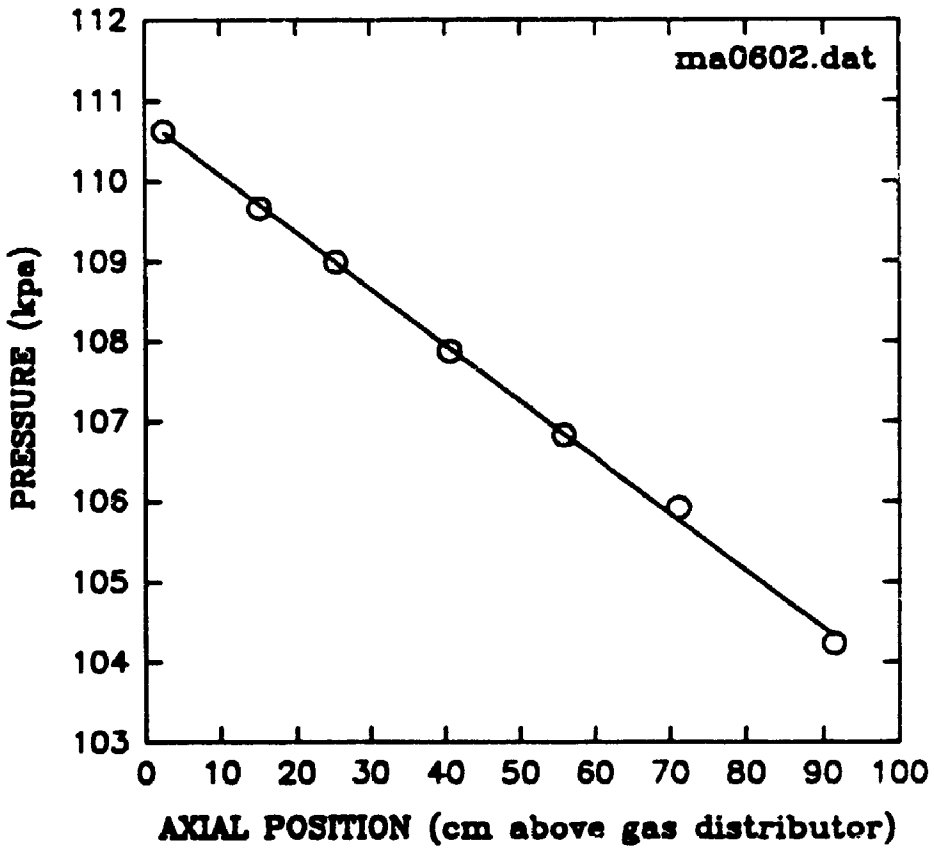

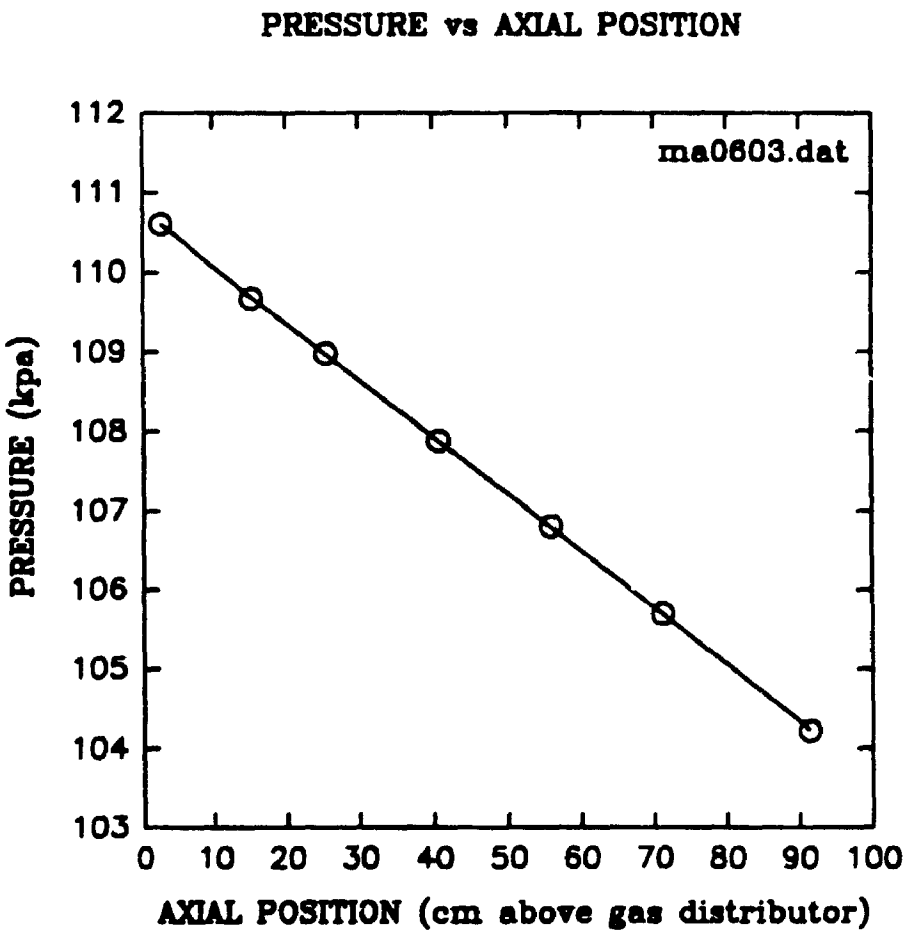
PRESSURE vs AXIAL POSITION
ma0603.dat
PRESSURE (kpa)
112
111
110
109
108
107
106
105
104
103
0
10
20
30
40
50
60
70
80
90
100
AXIAL POSITION (cm above gas distributor)

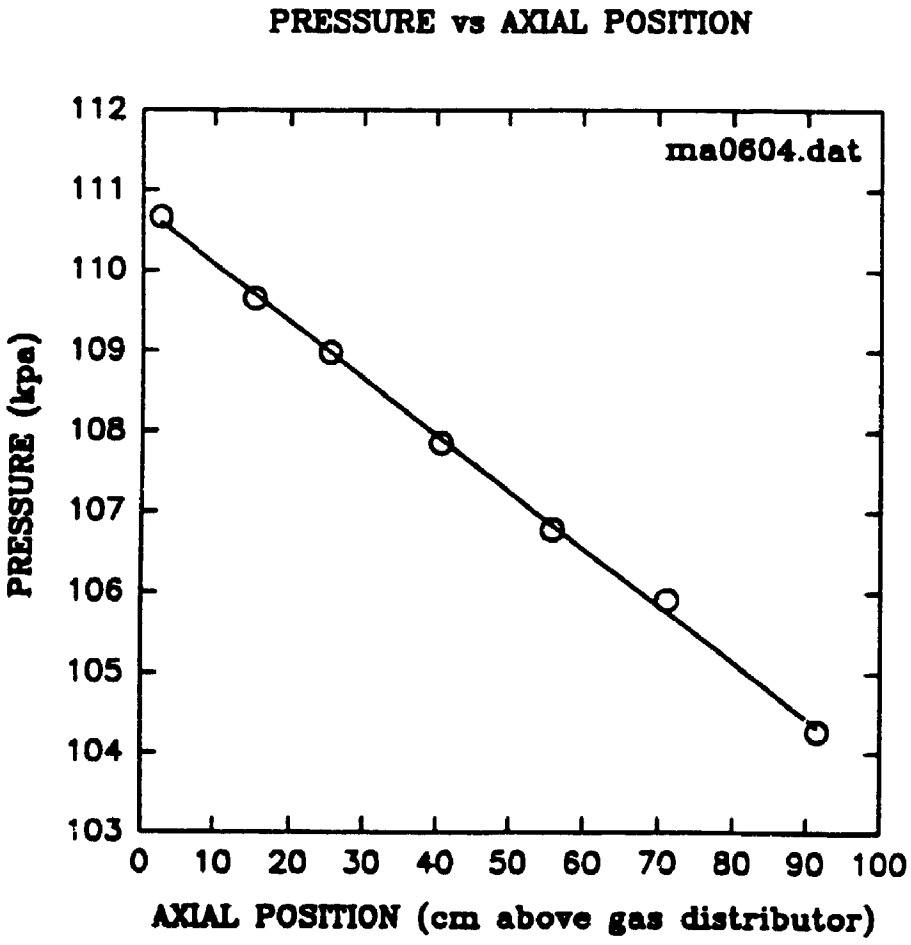
PRESSURE vs AXIAL POSITION
ma0604.dat
PRESSURE (kpa)
112
111
110
109
108
107
106
105
104
103
0
10
20
30
40
50
60
70
80
90
100
AXIAL POSITION (cm above gas distributor)

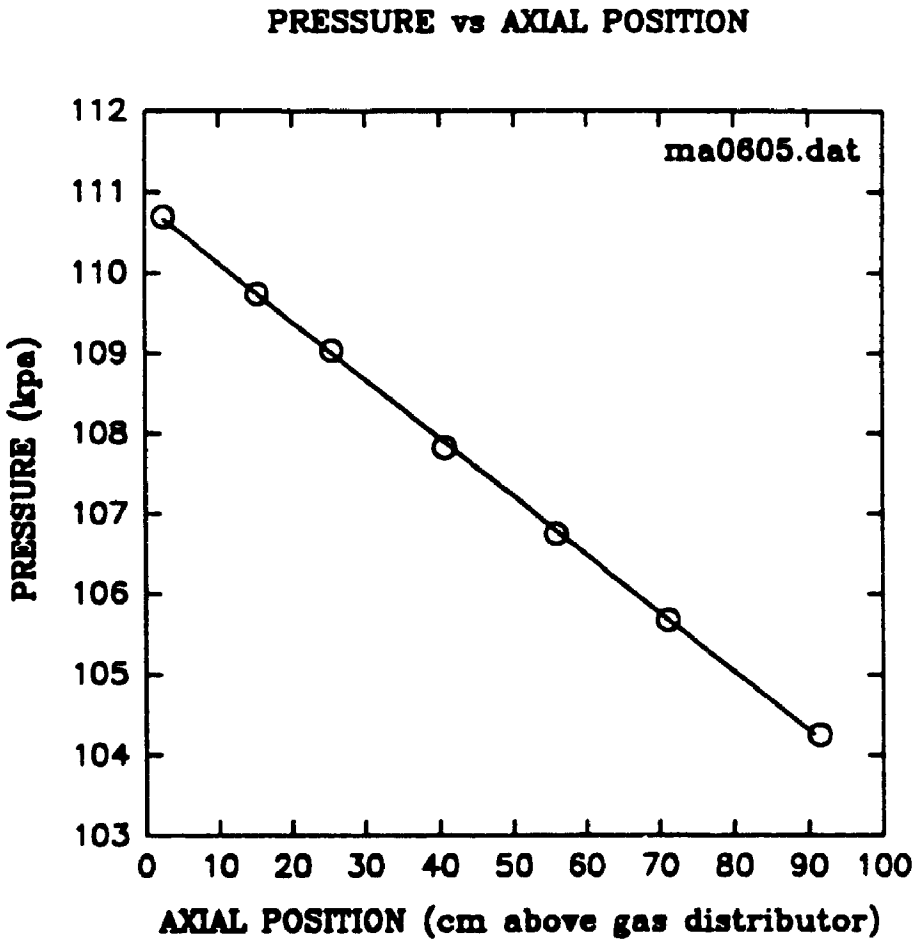
PRESSURE vs AXIAL POSITION
ma0605.dat
PRESSURE (kpa)
112
111
110
109
108
107
106
105
104
103
0
10
20
30
40
50
60
70
80
90
100
AXIAL POSITION (cm above gas distributor)

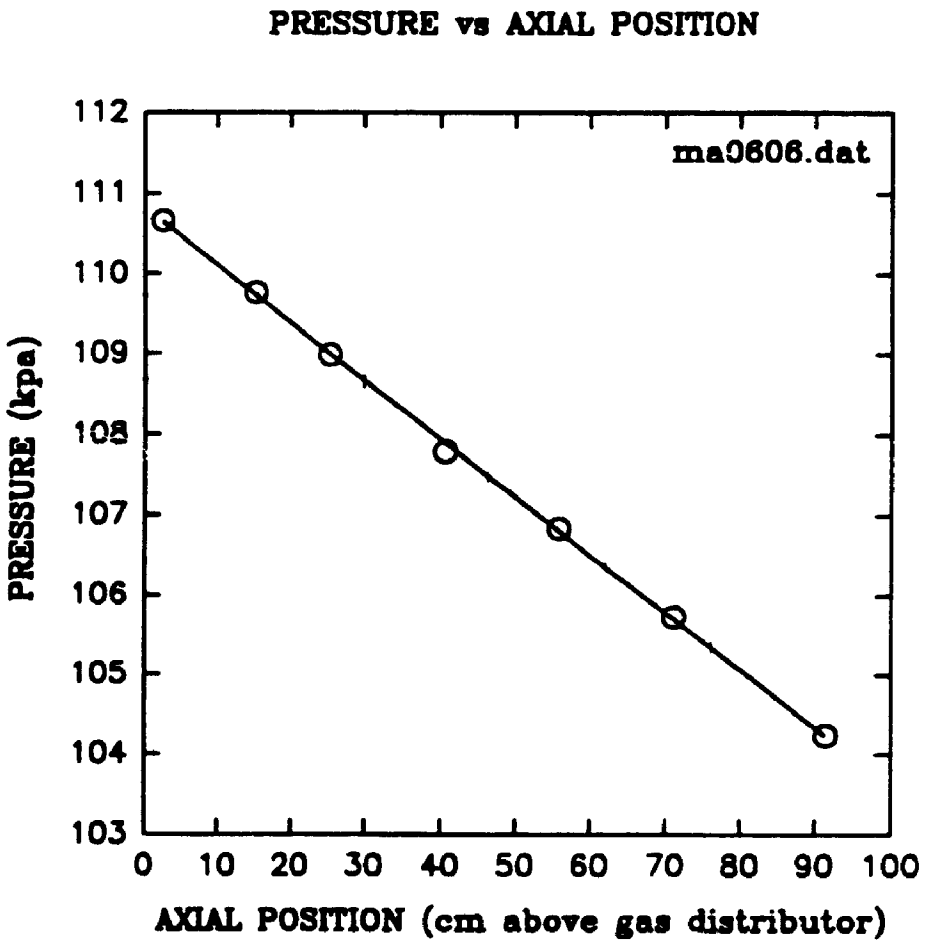
PRESSURE vs AXIAL POSITION
ma0606.dat
PRESSURE (kpa)
112
111
110
109
108
107
106
105
104
103
0
10
20
30
40
50
60
70
80
90
100
AXIAL POSITION (cm above gas distributor)

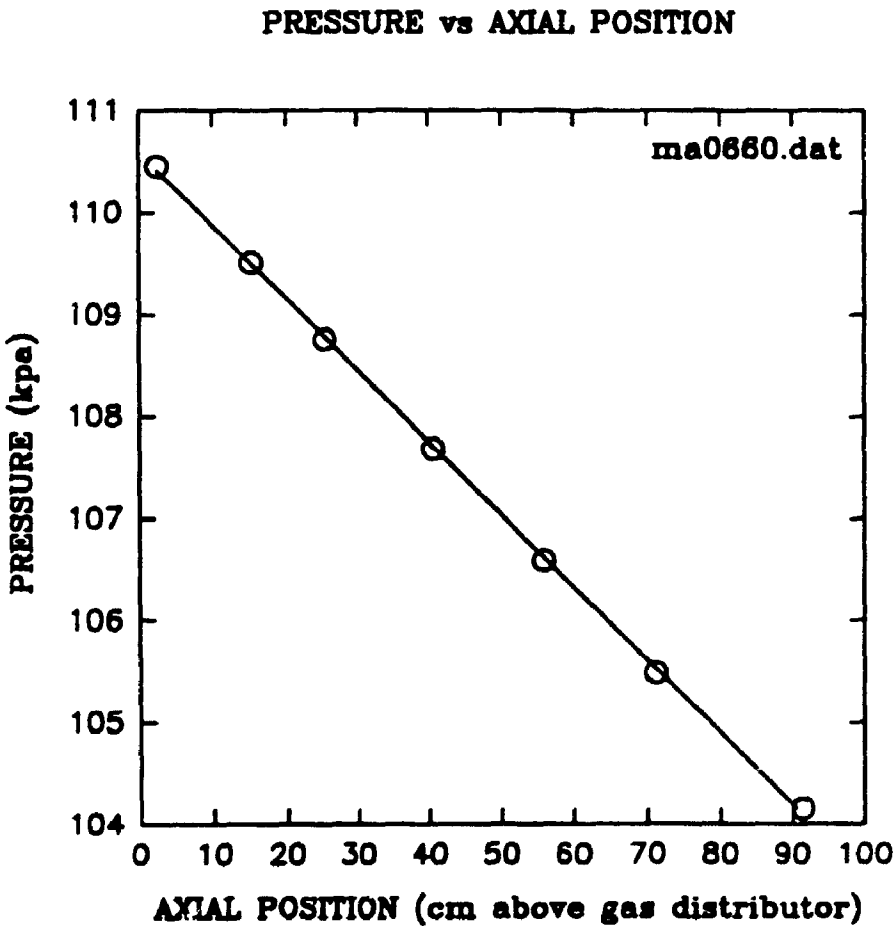
PRESSURE vs AXIAL POSITION
ma0660.dat
PRESSURE (kpa)
111
110
109
108
107
106
105
104
0
10
20
30
40
50
60
70
80
90
100
AXIAL POSITION (cm above gas distributor)

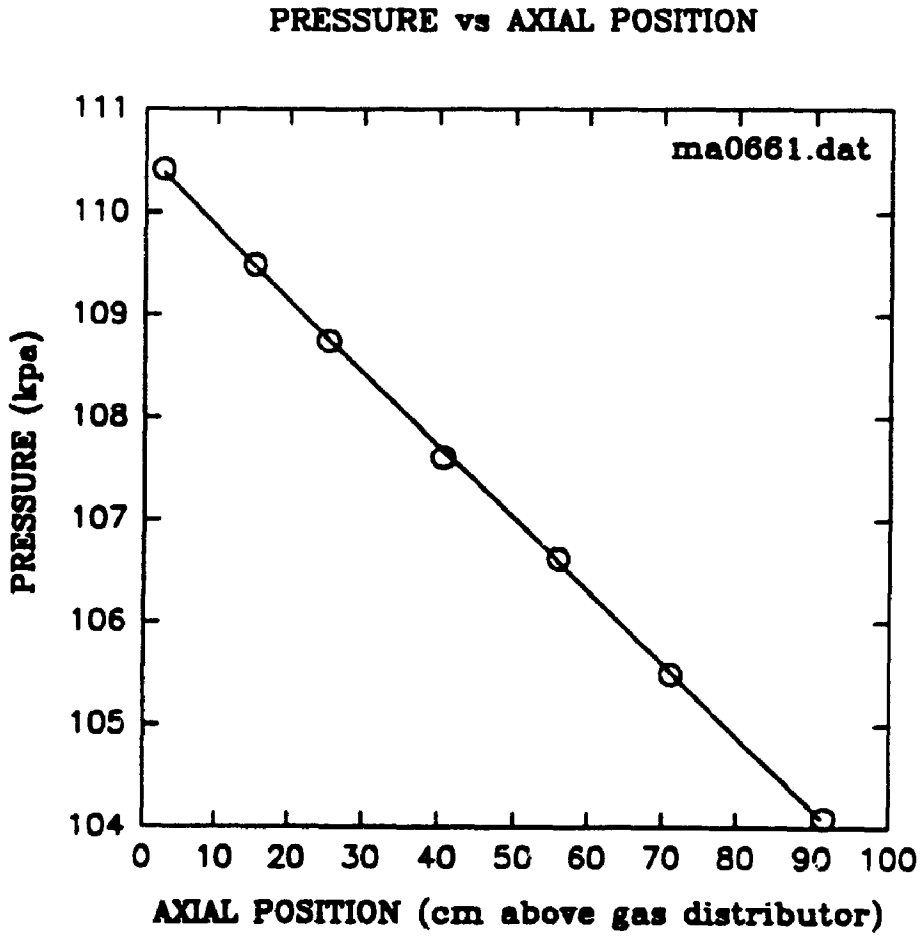
PRESSURE vs AXIAL POSITION
ma0661.dat
PRESSURE (kpa)
111
110
109
108
107
106
105
104
0
10
20
30
40
50
60
70
80
90
100
AXIAL POSITION (cm above gas distributor)

PRESSURE vs AXIAL POSITION

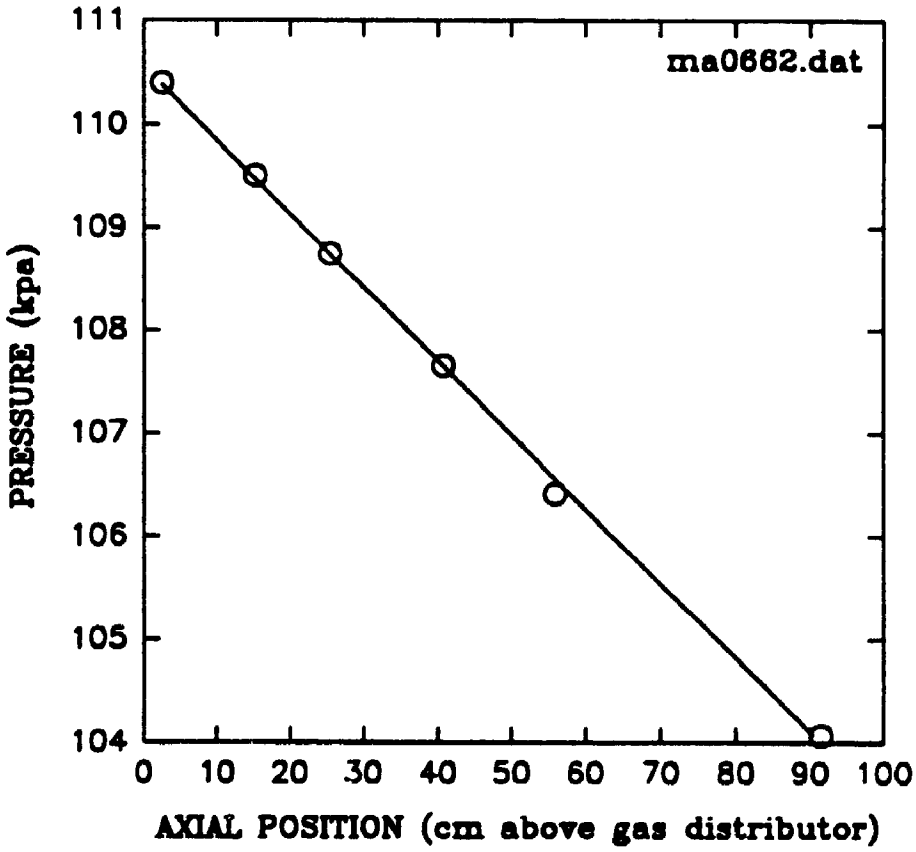

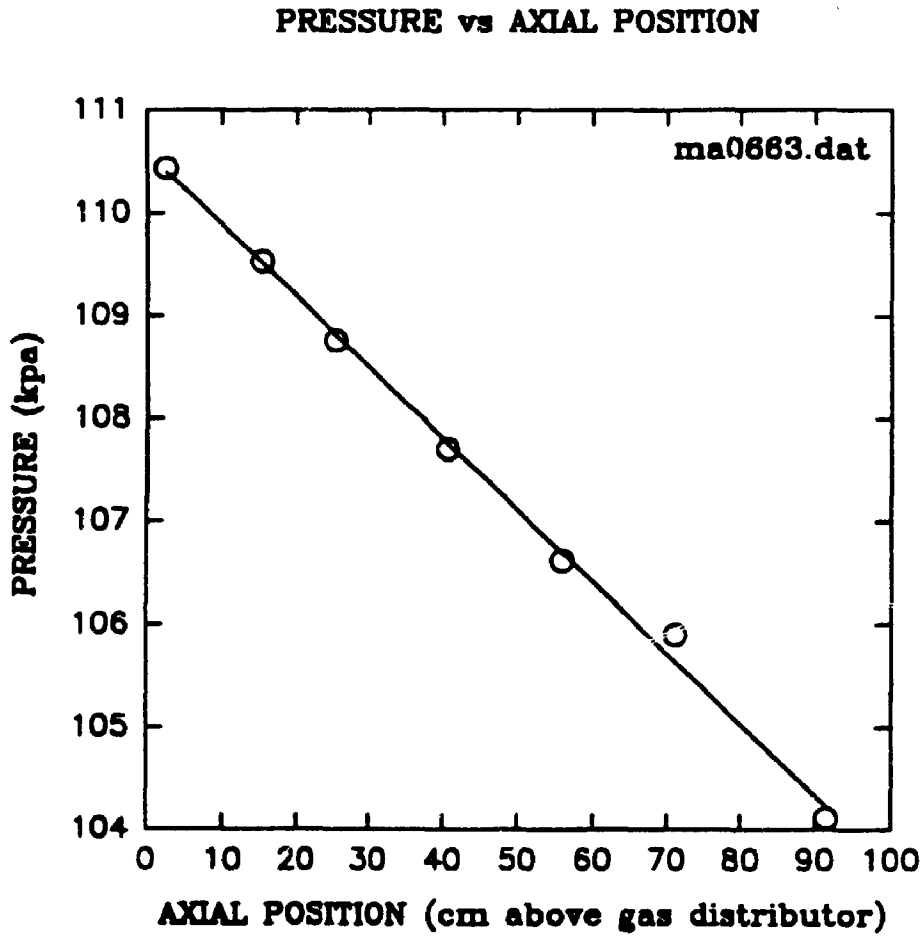
PRESSURE vs AXIAL POSITION
ma0663.dat
PRESSURE (kpa)
111
110
109
108
107
106
105
104
0
10
20
30
40
50
60
70
80
90
100
AXIAL POSITION (cm above gas distributor)

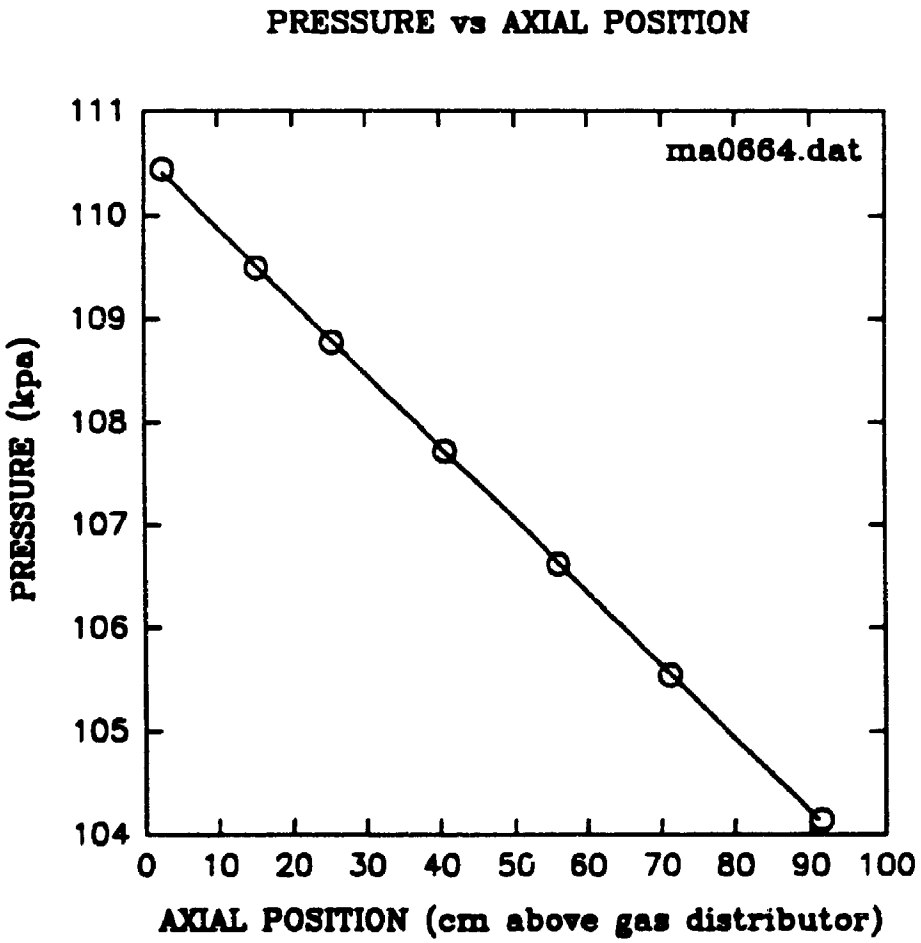
PRESSURE vs AXIAL POSITION
ma0664.dat
PRESSURE (kpa)
111
110
109
108
107
106
105
104
0
10
20
30
40
50
60
70
80
90
100
AXIAL POSITION (cm above gas distributor)

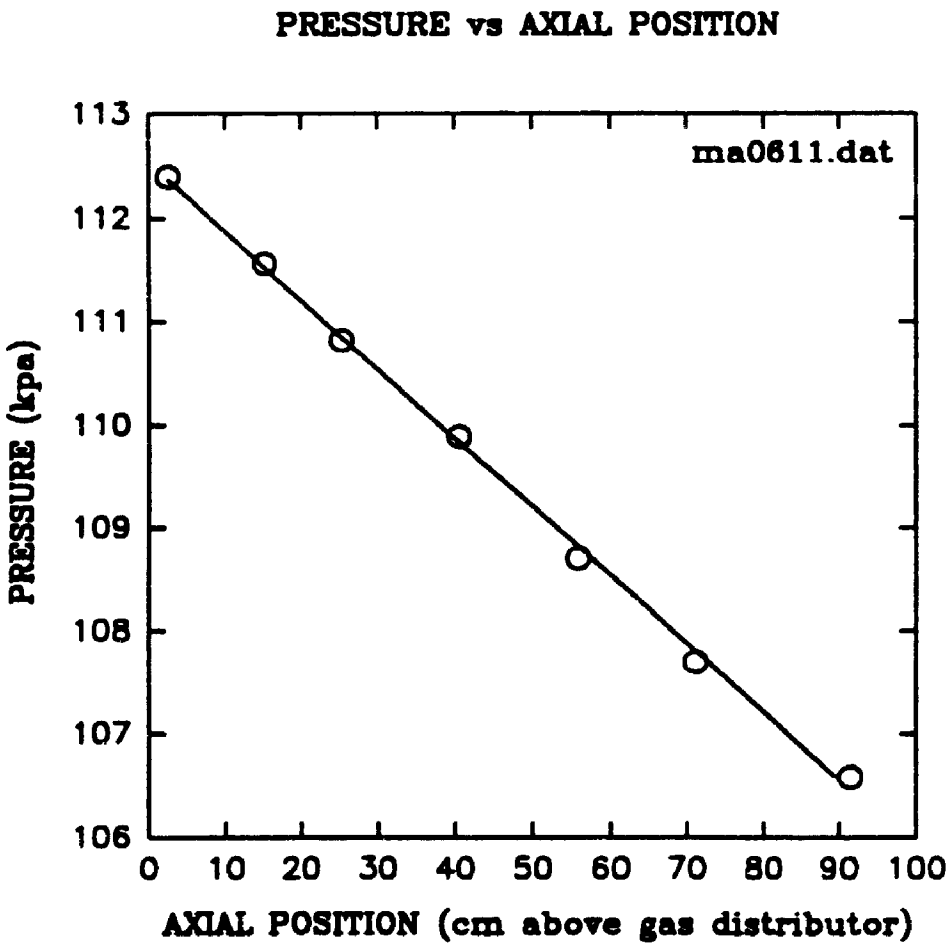
PRESSURE vs AXIAL POSITION
ma0611.dat
PRESSURE (kpa)
113
112
111
110
109
108
107
106
0
10
20
30
40
50
60
70
80
90
100
AXIAL POSITION (cm above gas distributor)

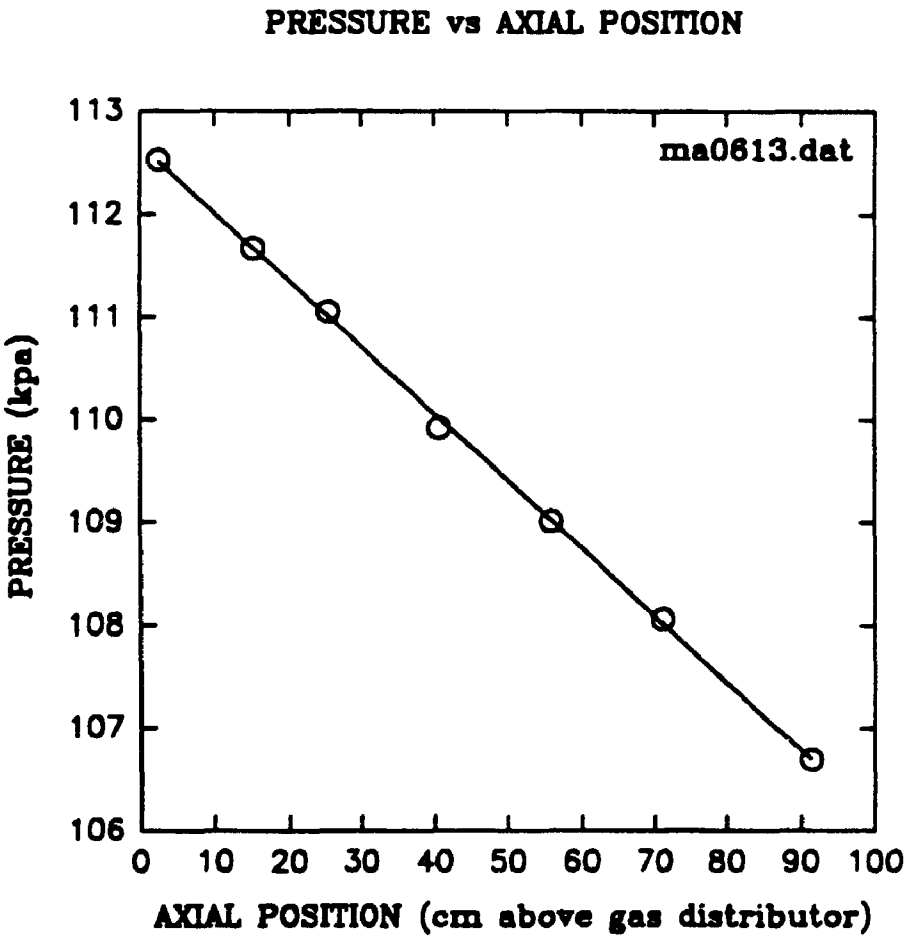
PRESSURE vs AXIAL POSITION
ma0613.dat
PRESSURE (kpa)
113
112
111
110
109
108
107
106
0
10
20
30
40
50
60
70
80
90
100
AXIAL POSITION (cm above gas distributor)

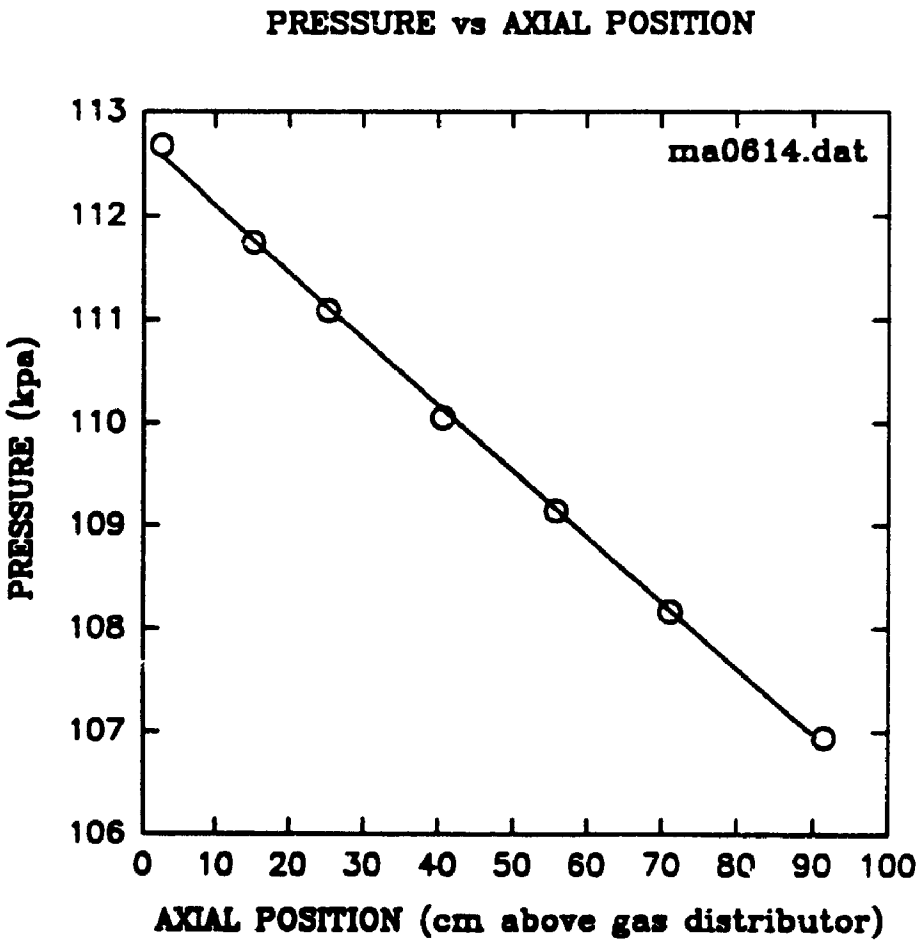
PRESSURE vs AXIAL POSITION
ma0614.dat
PRESSURE (kpa)
113
112
111
110
109
108
107
106
0
10
20
30
40
50
60
70
80
90
100
AXIAL POSITION (cm above gas distributor)

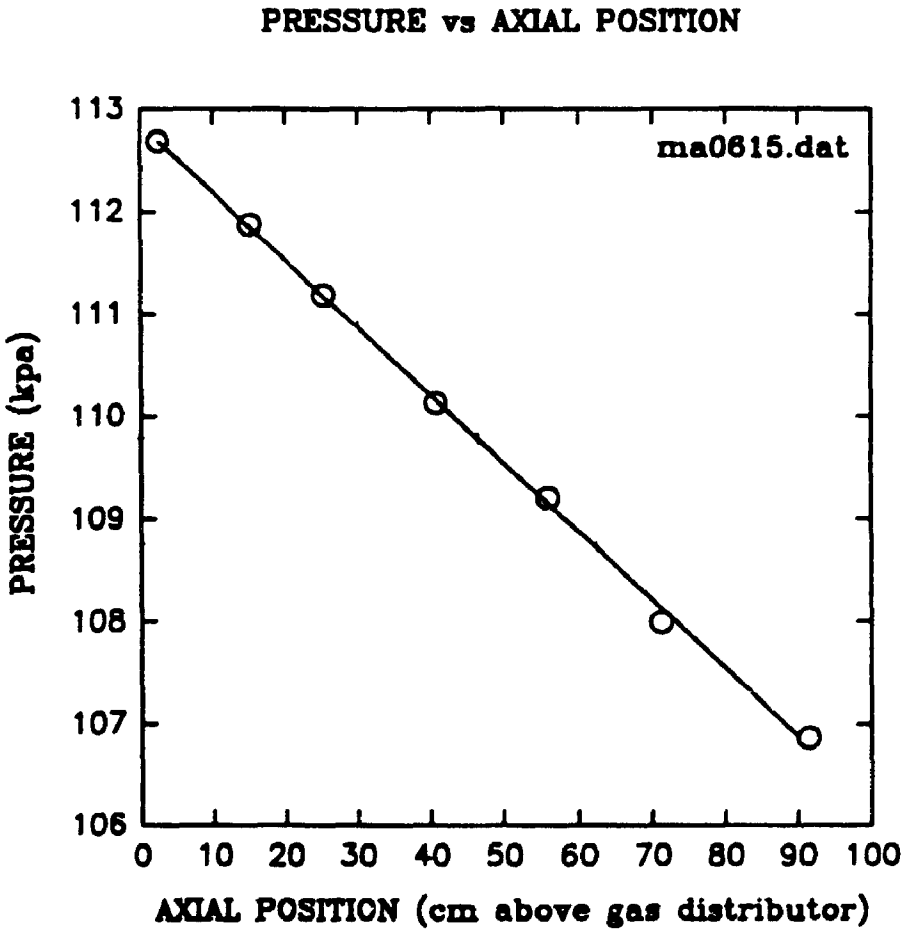
PRESSURE vs AXIAL POSITION
ma0615.dat
PRESSURE (kpa)
113
112
111
110
109
108
107
106
0
10
20
30
40
50
60
70
80
90
100
AXIAL POSITION (cm above gas distributor)

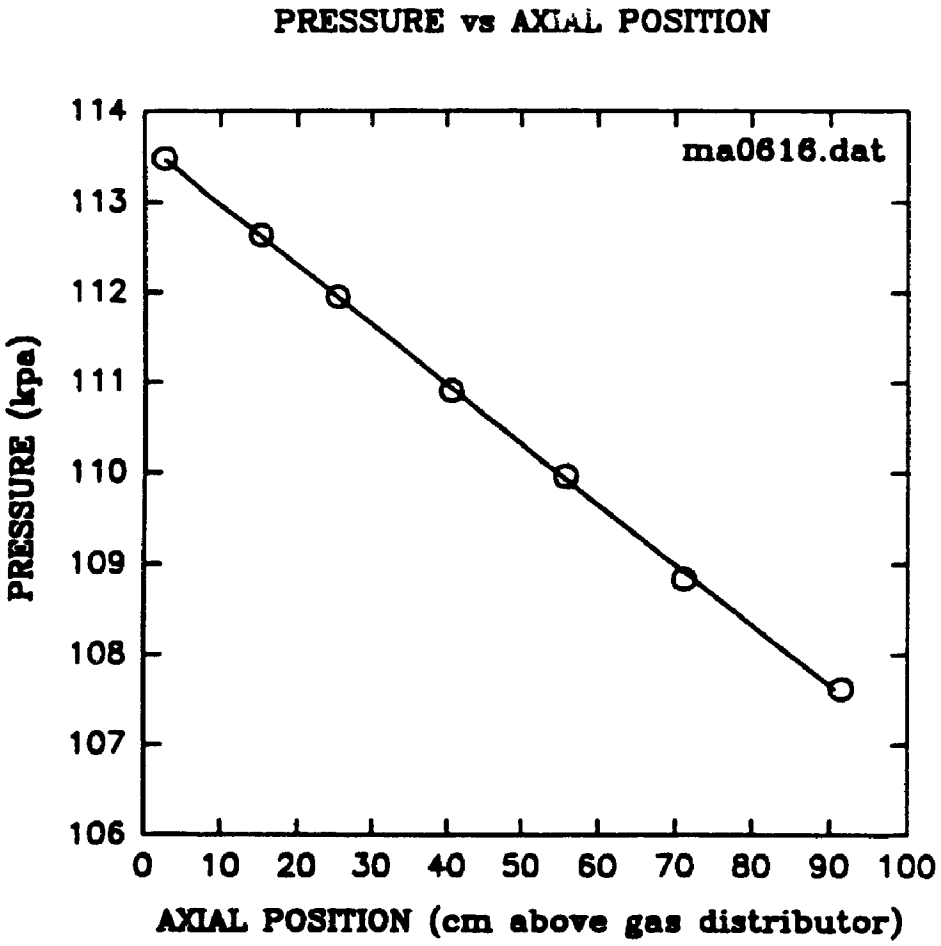
PRESSURE vs AXIAL POSITION
ma0616.dat
PRESSURE (kpa)
114
113
112
111
110
109
108
107
106
0
10
20
30
40
50
60
70
80
90
100
AXIAL POSITION (cm above gas distributor)

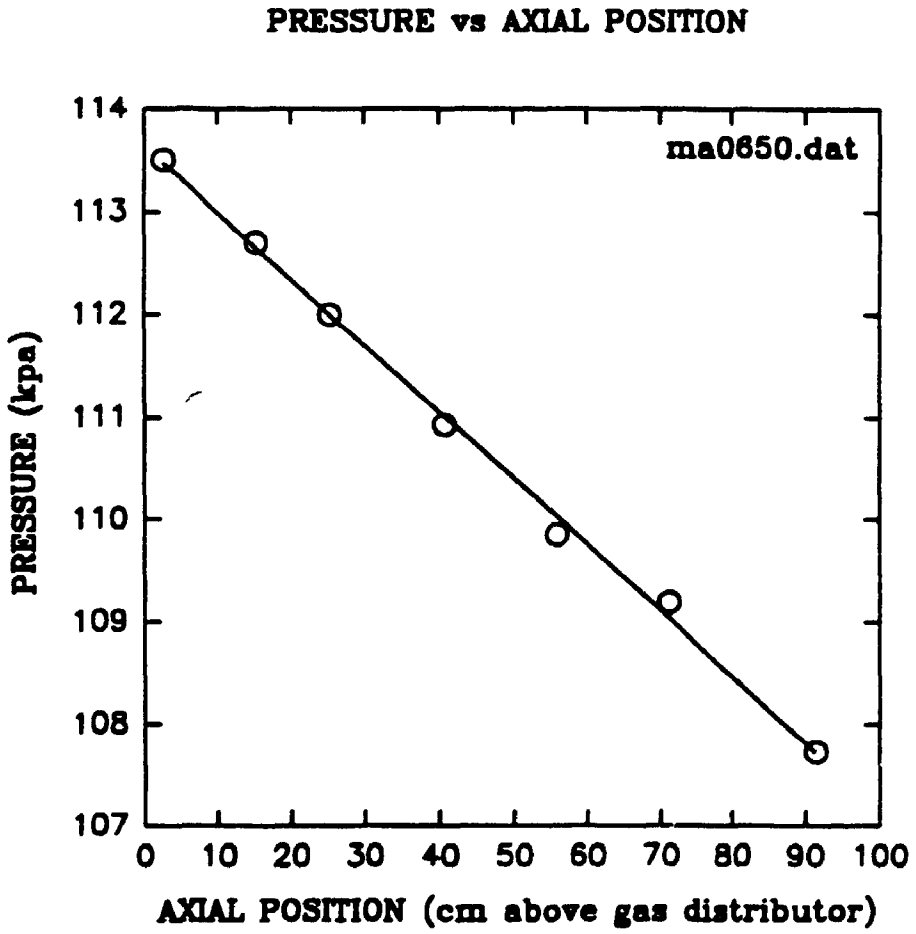
PRESSURE vs AXIAL POSITION
ma0650.dat
PRESSURE (kpa)
114
113
112
111
110
109
108
107
0
10
20
30
40
50
60
70
80
90
100
AXIAL POSITION (cm above gas distributor)

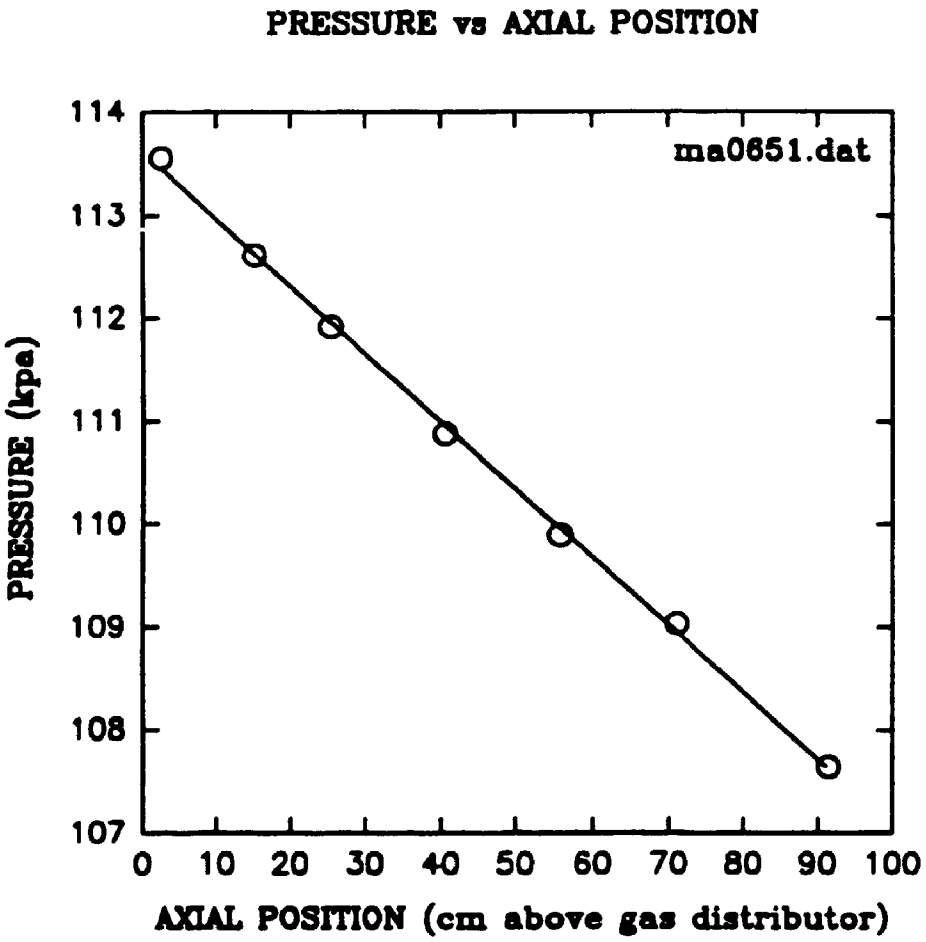
PRESSURE vs AXIAL POSITION
ma0651.dat
PRESSURE (kpa)
114
113
112
111
110
109
108
107
0
10
20
30
40
50
60
70
80
90
100
AXIAL POSITION (cm above gas distributor)

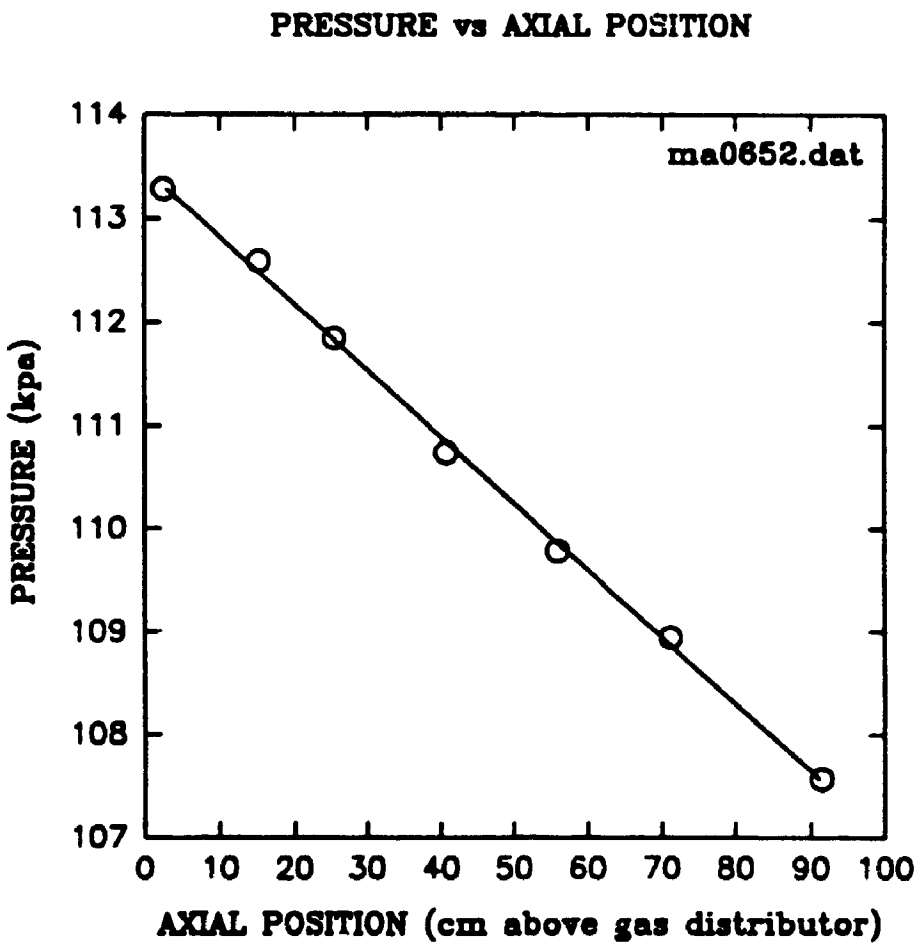
PRESSURE vs AXIAL POSITION
ma0652.dat
PRESSURE (kpa)
114
113
112
111
110
109
108
107
0
10
20
30
40
50
60
70
80
90
100
AXIAL POSITION (cm above gas distributor)

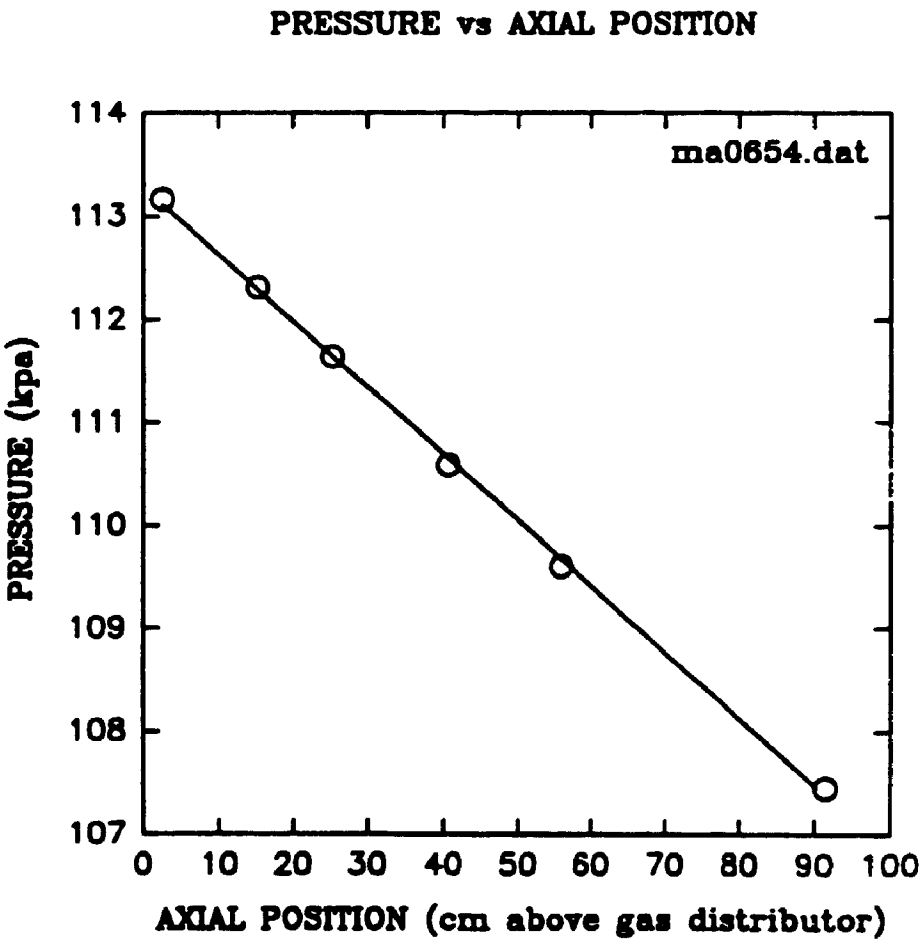
PRESSURE vs AXIAL POSITION
ma0654.dat
PRESSURE (kpa)
114
113
112
111
110
109
108
107
0
10
20
30
40
50
60
70
80
90
100
AXIAL POSITION (cm above gas distributor)

APPENDIX 7

CROSS CORRELATION ANALYSIS

Table A7.1
T=100°C, V_g=2.2 cm/s, z=15 cm

Filename	e=r/R	Cross correlation peak	Time lag (ms)	Bubble rise velocity (cm/s)
jan13d1a	0.19	0.25198	10	50.0
jan13d1b	0.19	0.30796	10	50.0
jan13d1c	0.19	0.33320	10	50.0
jan13d2a	0.42	0.29438	10	50.0
jan13d2b	0.42	0.38066	10	50.0
jan13d2c	0.42	0.36068	8	62.5
jan13d3a	0.62	0.31951	8	62.5
jan13d3b	0.62	0.34649	8	62.5
jan13d3c	0.62	0.30732	10	50.0
jan13d4a	0.78	0.36652	8	62.5
jan13d4b	0.78	0.38995	8	62.5
jan13d4c	0.78	0.30955	9	55.6
jan13d5a	0.89	0.42304	9	55.6
jan13d5b	0.89	0.38457	7	71.4
jan13d5c	0.89	0.42860	8	62.5
jan13d6a	0.92	0.33928	8	62.5
jan13d6b	0.92	0.39941	9	55.6
jan13d6c	0.92	0.46524	10	50.0

Table A7.2
T=100°C, V_g=2.2 cm/s, z=30 cm

Filename	θ=r/R	Cross correlation peak	Time lag (ms)	Bubble rise velocity (cm/s)
jan13c1a	0.19	0.31700	10	50.0
jan13c1b	0.19	0.32675	11	45.5
jan13c1c	0.19	0.31758	9	55.6
jan13c2a	0.42	0.26562	9	55.6
jan13c2b	0.42	0.32666	10	50.0
jan13c2c	0.42	0.31810	8	62.5
jan13c3a	0.62	0.29156	8	62.5
jan13c3b	0.62	0.32866	9	55.6
jan13c3c	0.62	0.29492	11	45.5
jan13c4a	0.78	0.25684	9	55.6
jan13c4b	0.78	0.34657	8	62.5
jan13c4c	0.78	0.31768	7	71.4
jan13c5a	0.89	0.36014	9	55.6
jan13c5b	0.89	0.24987	4	125.0
jan13c5c	0.89	0.40451	8	62.5
jan13c6a	0.92	0.35855	10	50.0
jan13c6b	0.92	0.16403	8	62.5
jan13c6c	0.92	0.18742	10	50.0

Table A7.3
T=100°C, V_g=2.2 cm/s, z=46 cm

Filename	θ=r/R	Cross correlation peak	Time lag (ms)	Bubble rise velocity (cm/s)
jan13b1a	0.19	0.33759	9	55.6
jan13b1b	0.19	0.36754	8	62.5
jan13b1c	0.19	0.29953	9	55.6
jan13b2a	0.42	0.37133	8	62.5
jan13b2b	0.42	0.36412	8	62.5
jan13b2c	0.42	0.36554	10	50.0
jan13b3a	0.62	0.26115	10	50.0
jan13b3b	0.62	0.30855	11	45.5
jan13b3c	0.62	0.31003	8	62.5
jan13b4a	0.78	0.19139	11	45.5
jan13b4b	0.78	0.29397	9	55.6
jan13b4c	0.78	0.27076	9	55.6
jan13b5a	0.89	0.32122	9	55.6
jan13b5b	0.89	0.28023	11	45.5
jan13b5c	0.89	0.15608	15	33.3
jan13b6a	0.92	0.29984	10	50.0
jan13b6b	0.92	0.15466	9	55.6
jan13b6c	0.92	0.13137	14	35.7

Table A7.4
T=100°C, V_g=2.2 cm/s, z=61 cm

Filename	θ=r/R	Cross correlation peak	Time lag (ms)	Bubble rise velocity (cm/s)
jan13a1d	0.19	0.32797	9	55.6
jan13a1e	0.19	0.33459	8	62.5
jan13a1e	0.19	0.22511	8	62.5
jan13a2a	0.42	0.38000	8	62.5
jan13a2b	0.42	0.36087	8	62.5
jan13a2c	0.42	0.37866	8	62.5
jan13a3a	0.62	0.22584	9	55.6
jan13a3b	0.62	0.25697	10	50.0
jan13a3c	0.62	0.33449	8	62.5
jan13a4a	0.78	0.15244	13	38.5
jan13a4b	0.78	0.18132	16	31.3
jan13a4c	0.78	0.24993	10	50.0
jan13a5a	0.89	0.19677	8	62.5
jan13a5b	0.89	0.12350	13	38.5
jan13a5c	0.89	0.17704	15	33.3
jan13a6a	0.92	0.18738	12	41.7
jan13a6b	0.92	0.09322	13	38.5
jan13a6c	0.92	0.15242	15	33.3

Table A7.5
T=100°C, V_g=2.2 cm/s, z=76 cm

Filename	θ=r/R	Cross correlation peak	Time lag (ms)	Bubble rise velocity (cm/s)
jan13e1a	0.19	0.26336	9	55.6
jan13e1b	0.19	0.31629	8	62.5
jan13e1c	0.19	0.39292	8	62.5
jan13e2a	0.42	0.39212	8	62.5
jan13e2b	0.42	0.32165	8	62.5
jan13e2c	0.42	0.30090	8	62.5
jan13e3a	0.62	0.28724	8	62.5
jan13e3b	0.62	0.27888	7	71.4
jan13e3c	0.62	0.27262	8	62.5
jan13e4a	0.78	0.17406	12	41.7
jan13e4b	0.78	0.23140	7	71.4
jan13e4c	0.78	0.20045	8	62.5
jan13e5a	0.89	0.14482	10	50.0
jan13e5b	0.89	0.15985	15	33.3
jan13e5c	0.89	0.21545	14	35.7
jan13e6a	0.92	0.20935	13	38.5
jan13e6b	0.92	0.11705	14	35.7
jan13e6c	0.92	0.14210	14	35.7

Table A7.6
T=100°C, V_g=4.1 cm/s, z=10 cm

Filename	θ=r/R	Cross correlation peak	Time lag (ms)	Bubble rise velocity (cm/s)
jan11a1a	0.19	0.23982	11	45.5
jan11a1b	0.19	0.29185	9	55.6
jan11a1c	0.19	0.28801	10	50.0
jan11a2a	0.42	0.34204	9	55.6
jan11a2b	0.42	0.30861	9	55.6
jan11a2c	0.42	0.36195	10	50.0
jan11a3a	0.62	0.28445	8	62.5
jan11a3b	0.62	0.30862	8	62.5
jan11a3c	0.62	0.27000	8	62.5
jan11a4a	0.78	0.33494	9	55.6
jan11a4b	0.78	0.23965	7	71.4
jan11a4c	0.78	0.25618	8	62.5
jan11a5a	0.89	0.38143	9	55.6
jan11a5b	0.89	0.35383	13	38.5
jan11a5c	0.89	0.34301	10	50.0
jan11a6a	0.92	0.40548	10	50.0
jan11a6b	0.92	0.43107	10	50.0
jan11a6c	0.92	0.38084	8	62.5

Table A7.7
T=100°C, V_g=4.1 cm/s, z=15 cm

Filename	θ=r/R	Cross correlation peak	Time lag (ms)	Bubble rise velocity (cm/s)
jan11b1a	0.19	0.38108	9	55.6
jan11b1b	0.19	0.33955	10	50.0
jan11b1c	0.19	0.31078	10	50.0
jan11b2a	0.42	0.36903	8	62.5
jan11b2b	0.42	0.30167	7	71.4
jan11b2c	0.42	0.35277	8	62.5
jan11b3a	0.62	0.40404	9	55.6
jan11b3b	0.62	0.32537	7	71.4
jan11b3c	0.62	0.32024	11	45.5
jan11b4a	0.78	0.33068	8	62.5
jan11b4b	0.78	0.29507	9	55.6
jan11b4c	0.78	0.33836	8	62.5
jan11b5a	0.89	0.26565	10	50.0
jan11b5b	0.89	0.33422	11	45.5
jan11b5c	0.89	0.21074	12	41.7
jan11b6a	0.92	0.39738	11	45.5
jan11b6b	0.92	0.28896	9	55.6
jan11b6c	0.92	0.28022	12	41.7

Table A7.8
T=100°C, V_g=4.1 cm/s, z=30 cm

Filename	θ=r/R	Cross correlation peak	Time lag (ms)	Bubble rise velocity (cm/s)
jan11c1a	0.19	0.30367	8	62.5
jan11c1b	0.19	0.34823	7	71.4
jan11c1c	0.19	0.35204	7	71.4
jan11c2a	0.42	0.32963	8	62.5
jan11c2b	0.42	0.36974	8	62.5
jan11c2c	0.42	0.38514	6	83.3
jan11c3a	0.62	0.30088	7	71.4
jan11c3b	0.62	0.28324	8	62.5
jan11c3c	0.62	0.36245	8	62.5
jan11c4b	0.78	0.23714	7	71.4
jan11c4c	0.78	0.43503	8	62.5
jan11c5b	0.89	0.43438	10	50.0
jan11c5c	0.89	0.24237	12	41.7
jan11c6a	0.92	0.15418	8	62.5
jan11c6b	0.92	0.18651	15	33.3
jan11c6c	0.92	0.29243	10	50.0

Table A7.9
T=100°C, V_g=4.1 cm/s, z=46 cm

Filename	θ=r/R	Cross correlation peak	Time lag (ms)	Bubble rise velocity (cm/s)
jan11d1a	0.19	0.39047	7	71.4
jan11d1b	0.19	0.42274	7	71.4
jan11d1c	0.19	0.39972	8	62.5
jan11d2a	0.42	0.37856	7	71.4
jan11d2b	0.42	0.35738	8	62.5
jan11d2c	0.42	0.42111	7	71.4
jan11d3a	0.62	0.47482	8	62.5
jan11d3b	0.62	0.31238	7	71.4
jan11d3c	0.62	0.37190	7	71.4
jan11d4a	0.78	0.21486	11	45.5
jan11d4b	0.78	0.31451	11	45.5
jan11d4c	0.78	0.29581	9	55.6
jan11d5b	0.89	0.27579	12	41.7
jan11d5c	0.89	0.29483	11	45.5

Table A7.10
T=100°C, V_g=4.1 cm/s, z=61 cm

Filename	Θ=r/R	Cross correlation peak	Time lag (ms)	Bubble rise velocity (cm/s)
jan11e1a	0.19	0.42964	6	83.3
jan11e1b	0.19	0.42479	6	83.3
jan11e1c	0.19	0.46950	6	83.3
jan11e2a	0.42	0.41049	6	83.3
jan11e2b	0.42	0.41533	7	71.4
jan11e2c	0.42	0.40609	6	83.3
jan11e3a	0.62	0.36254	8	62.5
jan11e3b	0.62	0.38102	8	62.5
jan11e3c	0.62	0.39502	7	71.4
jan11e4a	0.78	0.33375	9	55.6
jan11e4b	0.78	0.23503	8	62.5
jan11e4c	0.78	0.31146	7	71.4
jan11e5b	0.89	0.08958	15	33.3
jan11e5c	0.89	0.15574	13	38.5
jan11e6a	0.92	0.19639	12	41.7
jan11e6b	0.92	0.12529	21	23.8

Table A7.11
T=100°C, V_g=9.0 cm/s, z=15 cm

Filename	e=r/R	Cross correlation peak	Time lag (ms)	Bubble rise velocity (cm/s)
jan16e1a	0.19	0.35236	8	62.5
jan16e1b	0.19	0.36398	7	71.4
jan16e1c	0.19	0.42452	7	71.4
jan16e2a	0.42	0.37120	6	83.3
jan16e2b	0.42	0.39828	6	83.3
jan16e2c	0.42	0.40314	6	83.3
jan16e3a	0.62	0.34358	6	83.3
jan16e3b	0.62	0.40265	6	83.3
jan16e3c	0.62	0.36526	5	100.0
jan16e4a	0.78	0.42407	7	71.4
jan16e4b	0.78	0.38739	6	83.3
jan16e4c	0.78	0.48062	6	83.3
jan16e5a	0.89	0.36604	8	62.5
jan16e5b	0.89	0.48197	11	45.5
jan16e5c	0.89	0.43809	6	83.3
jan16e6a	0.92	0.34065	5	100.0
jan16e6b	0.92	0.34976	9	55.6
jan16e6c	0.92	0.37389	8	62.5

Table A7.12
T=100°C, V_g=9.0 cm/s, z=30 cm

Filename	θ=r/R	Cross correlation peak	Time lag (ms)	Bubble rise velocity (cm/s)
jan16d1a	0.19	0.39307	5	100.0
jan16d1b	0.19	0.41061	6	83.3
jan16d1c	0.19	0.42976	7	71.4
jan16d2a	0.42	0.46469	6	83.3
jan16d2b	0.42	0.47699	6	83.3
jan16d2c	0.42	0.45279	6	83.3
jan16d3a	0.62	0.47321	6	83.3
jan16d3b	0.62	0.45086	6	83.3
jan16d3c	0.62	0.39256	7	71.4
jan16d4a	0.78	0.47125	7	71.4
jan16d4b	0.78	0.30087	6	83.3
jan16d4c	0.78	0.33461	6	83.3
jan16d5a	0.89	0.30310	12	41.7
jan16d5b	0.89	0.29006	6	83.3
jan16d5c	0.89	0.28245	10	50.0
jan16d6a	0.92	0.13226	10	50.0
jan16d6b	0.92	0.27058	13	38.5
jan16d6c	0.92	0.16330	9	55.6

Table A7.13
T=100°C, V_g=9.0 cm/s, z=46 cm

Filename	θ=r/R	Cross correlation peak	Time lag (ms)	Bubble rise velocity (cm/s)
jan16c1a	0.19	0.50427	5	100.0
jan16c1b	0.19	0.45590	5	100.0
jan16c1c	0.19	0.50484	6	83.3
jan16c2a	0.42	0.46479	5	100.0
jan16c2b	0.42	0.50242	5	100.0
jan16c2c	0.42	0.44565	5	100.0
jan16c3a	0.62	0.43723	4	125.0
jan16c3b	0.62	0.49085	6	83.3
jan16c3c	0.62	0.48160	5	100.0
jan16c4a	0.78	0.35989	5	100.0
jan16c4b	0.78	0.19322	6	83.3
jan16c4c	0.78	0.37765	7	71.4
jan16c5a	0.89	0.19254	9	55.6
jan16c5b	0.89	0.33642	8	62.5
jan16c5c	0.89	0.28228	5	100.0
jan16c6a	0.92	0.30937	6	83.3
jan16c6b	0.92	0.31663	9	55.6
jan16c6c	0.92	0.10318	8	62.5

Table A7.14
T=100°C, V_g=9.0 cm/s, z=61 cm

Filename	θ=r/R	Cross correlation peak	Time lag (ms)	Bubble rise velocity (cm/s)
jan16b1a	0.19	0.48454	4	125.0
jan16b1b	0.19	0.48854	5	100.0
jan16b1c	0.19	0.51968	5	100.0
jan16b2a	0.42	0.49425	6	83.3
jan16b2b	0.42	0.52736	5	100.0
jan16b2c	0.42	0.52100	6	83.3
jan16b3a	0.62	0.48031	5	100.0
jan16b3b	0.62	0.43052	7	71.4
jan16b3c	0.62	0.45201	5	100.0
jan16b4a	0.78	0.27892	8	62.5
jan16b4b	0.78	0.45840	6	83.3
jan16b4c	0.78	0.30982	6	83.3
jan16b5a	0.89	0.24080	6	83.3
jan16b5b	0.89	0.33439	8	62.5
jan16b5c	0.89	0.16642	7	71.4
jan16b6a	0.92	0.16091	8	62.5
jan16b6b	0.92	0.25239	8	62.5
jan16b6c	0.92	0.26767	5	100.0

Table A7.15
T=100°C, V_g=9.0 cm/s, z=76 cm

Filename	θ=r/R	Cross correlation peak	Time lag (ms)	Bubble rise velocity (cm/s)
jan16a1a	0.19	0.51362	5	100.0
jan16a1b	0.19	0.48550	4	125.0
jan16a1c	0.19	0.50792	5	100.0
jan16a2a	0.42	0.46348	5	100.0
jan16a2b	0.42	0.48774	5	100.0
jan16a2c	0.42	0.51284	5	100.0
jan16a3a	0.62	0.42000	4	125.0
jan16a3b	0.62	0.47318	5	100.0
jan16a3c	0.62	0.43310	4	125.0
jan16a4a	0.78	0.35143	4	125.0
jan16a4b	0.78	0.37179	4	125.0
jan16a4c	0.78	0.37866	6	83.3
jan16a5a	0.89	0.29826	8	62.5
jan16a5b	0.89	0.27972	10	50.0
jan16a5c	0.89	0.34566	7	71.4
jan16a6a	0.92	0.23001	11	45.5
jan16a6b	0.92	0.32867	10	50.0

Table A7.16
T=100°C, V_g=14.7 cm/s, z=15 cm

Filename	θ=r/R	Cross correlation peak	Time lag (ms)	Bubble rise velocity (cm/s)
jan17a1a	0.19	0.41110	6	83.3
jan17a1b	0.19	0.43103	7	71.4
jan17a1c	0.19	0.44090	7	71.4
jan17a2a	0.42	0.38140	6	83.3
jan17a2b	0.42	0.42452	5	100.0
jan17a2c	0.42	0.44922	6	83.3
jan17a3a	0.62	0.39456	5	100.0
jan17a3b	0.62	0.41051	7	71.4
jan17a3c	0.62	0.41024	6	83.3
jan17a4b	0.78	0.38537	6	83.3
jan17a4c	0.78	0.41342	5	100.0
jan17a5a	0.89	0.39185	5	100.0
jan17a5b	0.89	0.23073	4	125.0
jan17a5c	0.89	0.28609	4	125.0
jan17a6a	0.92	0.28430	11	45.5
jan17a6b	0.92	0.32095	8	62.5
jan17a6c	0.92	0.33316	6	83.3

Table A7.17
T=100°C, V_g=14.7 cm/s, z=30 cm

Filename	θ=r/R	Cross correlation peak	Time lag (ms)	Bubble rise velocity (cm/s)
jan17b1a	0.19	0.44586	5	100.0
jan17b1b	0.19	0.46610	5	100.0
jan17b1c	0.19	0.53821	5	100.0
jan17b2a	0.42	0.46624	5	100.0
jan17b2b	0.42	0.44411	5	100.0
jan17b2c	0.42	0.50303	5	100.0
jan17b3a	0.62	0.41181	6	83.3
jan17b3b	0.62	0.41018	6	83.3
jan17b3c	0.62	0.47499	5	100.0
jan17b4a	0.78	0.42583	5	100.0
jan17b4b	0.78	0.45628	4	125.0
jan17b4c	0.78	0.33601	8	62.5
jan17b5a	0.89	0.21755	7	71.4
jan17b5b	0.89	0.25583	7	71.4
jan17b5c	0.89	0.27877	5	100.0
jan17b6a	0.92	0.09657	8	62.5
jan17b6b	0.92	0.27474	8	62.5
jan17b6c	0.92	0.29725	9	55.6

Table A7.18
T=100°C, V_g=14.7 cm/s, z=46 cm

Filename	θ=r/R	Cross correlation peak	Time lag (ms)	Bubble rise velocity (cm/s)
jan17c1a	0.19	0.47471	5	100.0
jan17c1b	0.19	0.51048	5	100.0
jan17c1c	0.19	0.50995	5	100.0
jan17c2a	0.42	0.49358	5	100.0
jan17c2b	0.42	0.46935	5	100.0
jan17c2c	0.42	0.50320	5	100.0
jan17c3a	0.62	0.44138	4	125.0
jan17c3b	0.62	0.50335	6	83.3
jan17c3c	0.62	0.42409	4	125.0
jan17c4a	0.78	0.43484	4	125.0
jan17c4b	0.78	0.31500	8	62.5
jan17c4c	0.78	0.47319	5	100.0
jan17c5a	0.89	0.40490	7	71.4
jan17c5b	0.89	0.36385	4	125.0
jan17c5c	0.89	0.34530	6	83.3
jan17c6a	0.92	0.18802	7	71.4
jan17c6b	0.92	0.28803	4	125.0
jan17c6c	0.92	0.26488	5	100.0

Table A7.19
T=100°C, V_g=14.7 cm/s, z=61 cm

Filename	θ=r/R	Cross correlation peak	Time lag (ms)	Bubble rise velocity (cm/s)
jan17d1a	0.19	0.48520	4	125.0
jan17d1b	0.19	0.55287	4	125.0
jan17d1c	0.19	0.52693	4	125.0
jan17d2a	0.42	0.49531	4	125.0
jan17d2b	0.42	0.52071	4	125.0
jan17d2c	0.42	0.47399	5	100.0
jan17d3a	0.62	0.43992	5	100.0
jan17d3b	0.62	0.50426	5	100.0
jan17d3c	0.62	0.39708	5	100.0
jan17d4a	0.78	0.38399	6	83.3
jan17d4b	0.78	0.38348	5	100.0
jan17d4c	0.78	0.38592	6	83.3
jan17d5a	0.89	0.37294	5	100.0
jan17d5b	0.89	0.23790	6	83.3
jan17d5c	0.89	0.26257	6	83.3
jan17d6a	0.92	0.29547	6	83.3
jan17d6c	0.92	0.20444	10	50.0

Table A7.20
T=100°C, V_g=14.7 cm/s, z=76 cm

Filename	θ=r/R	Cross correlation peak	Time lag (ms)	Bubble rise velocity (cm/s)
jan17e1a	0.19	0.50972	4	125.0
jan17e1b	0.19	0.50436	4	125.0
jan17e1c	0.19	0.53781	4	125.0
jan17e2a	0.42	0.47823	4	125.0
jan17e2b	0.42	0.47716	4	125.0
jan17e2c	0.42	0.48284	4	125.0
jan17e3a	0.62	0.42636	4	125.0
jan17e3b	0.62	0.41397	4	125.0
jan17e3c	0.62	0.46694	6	83.3
jan17e4a	0.78	0.38847	4	125.0
jan17e4b	0.78	0.39748	6	83.3
jan17e4c	0.78	0.43664	6	83.3
jan17e5a	0.89	0.50078	5	100.0
jan17e5b	0.89	0.34686	4	125.0
jan17e5c	0.89	0.37977	5	100.0
jan17e6a	0.92	0.35976	7	71.4
jan17e6c	0.92	0.28281	7	71.4

Table A7.21
T=175°C, V_g=2.2 cm/s, z=15 cm

Filename	θ=r/R	Cross correlation peak	Time lag (ms)	Bubble rise velocity (cm/s)
jan18e1a	0.19	0.34936	11	45.5
jan18e1b	0.19	0.25793	12	41.7
jan18e1c	0.19	0.31798	10	50.0
jan18e2a	0.42	0.30641	10	50.0
jan18e2b	0.42	0.33258	9	55.6
jan18e2c	0.42	0.21015	10	50.0
jan18e3a	0.62	0.34921	9	55.6
jan18e3b	0.62	0.29836	9	55.6
jan18e3c	0.62	0.38533	9	55.6
jan18e4a	0.78	0.31794	8	62.5
jan18e4b	0.78	0.31650	9	55.6
jan18e4c	0.78	0.31423	8	62.5
jan18e5a	0.89	0.38803	9	55.6
jan18e5b	0.89	0.33361	9	55.6
jan18e5c	0.89	0.31557	8	62.5
jan18e6a	0.92	0.38860	8	62.5
jan18e6b	0.92	0.45951	10	50.0
jan18e6c	0.92	0.37657	9	55.6

Table A7.22
T=175°C, V_g=2.2 cm/s, z=30 cm

Filename	θ=r/R	Cross correlation peak	Time lag (ms)	Bubble rise velocity (cm/s)
jan18d1a	0.19	0.23030	10	50.0
jan18d1b	0.19	0.28052	11	45.5
jan18d1c	0.19	0.32141	9	55.6
jan18d2a	0.42	0.34578	9	55.6
jan18d2b	0.42	0.32707	9	55.6
jan18d2c	0.42	0.28755	9	55.6
jan18d3a	0.62	0.22399	8	62.5
jan18d3b	0.62	0.29542	12	41.7
jan18d3c	0.62	0.29264	7	71.4
jan18d4a	0.78	0.27666	10	50.0
jan18d4b	0.78	0.25665	9	55.6
jan18d4c	0.78	0.20635	8	62.5
jan18d5a	0.89	0.30262	7	71.4
jan18d5b	0.89	0.24258	10	50.0
jan18d5c	0.89	0.06753	12	41.7
jan18d6a	0.92	0.15121	9	55.6
jan18d6b	0.92	0.18869	13	38.5
jan18d6c	0.92	0.23226	11	45.5

Table A7.23
T=175°C, V_g=2.2 cm/s, z=46 cm

Filename	θ=r/R	Cross correlation peak	Time lag (ms)	Bubble rise velocity (cm/s)
jan18c1a	0.19	0.24350	11	45.5
jan18c1b	0.19	0.25419	9	55.6
jan18c1c	0.19	0.27879	9	55.6
jan18c2a	0.42	0.26932	9	55.6
jan18c2b	0.42	0.29760	11	45.5
jan18c2c	0.42	0.33989	9	55.6
jan18c3a	0.62	0.29165	9	55.6
jan18c3b	0.62	0.30111	9	55.6
jan18c3c	0.62	0.29561	10	50.0
jan18c4a	0.78	0.31070	10	50.0
jan18c4b	0.78	0.21090	11	45.5
jan18c4c	0.78	0.26050	10	50.0
jan18c5a	0.89	0.14298	15	33.3
jan18c5b	0.89	0.16521	19	26.3
jan18c5c	0.89	0.22193	16	31.3
jan18c6a	0.92	0.13113	20	25.0
jan18c6b	0.92	0.12764	11	45.5
jan18c6c	0.92	0.12520	11	45.5

Table A7.24
T=175°C, V_g=2.2 cm/s, z=61 cm

Filename	Θ=r/R	Cross correlation peak	Time lag (ms)	Bubble rise velocity (cm/s)
jan18b1a	0.19	0.28398	9	55.6
jan18b1b	0.19	0.18966	10	50.0
jan18b1c	0.19	0.30959	9	55.6
jan18b2a	0.42	0.33010	8	62.5
jan18b2b	0.42	0.27613	11	45.5
jan18b2c	0.42	0.26463	8	62.5
jan18b3a	0.62	0.24511	9	55.6
jan18b3b	0.62	0.31627	10	50.0
jan18b3c	0.62	0.27017	8	62.5
jan18b4a	0.78	0.16035	11	45.5
jan18b4b	0.78	0.18072	11	45.5
jan18b4c	0.78	0.10904	14	35.7
jan18b5a	0.89	0.16460	13	38.5
jan18b5b	0.89	0.20003	12	41.7
jan18b5c	0.89	0.03966	17	29.4
jan18b6a	0.92	0.17112	12	41.7
jan18b6b	0.92	0.07566	22	22.7
jan18b6c	0.92	0.08618	16	31.3

Table A7.25
T=175°C, V_g=2.2 cm/s, z=76 cm

Filename	θ=r/R	Cross correlation peak	Time lag (ms)	Bubble rise velocity (cm/s)
jan18a1a	0.19	0.18521	10	50.0
jan18a1b	0.19	0.20493	10	50.0
jan18a1c	0.19	0.20925	12	41.7
jan18a2a	0.42	0.30411	9	55.6
jan18a2b	0.42	0.31820	9	55.6
jan18a2c	0.42	0.34479	9	55.6
jan18a3a	0.62	0.22344	11	45.5
jan18a3b	0.62	0.22165	9	55.6
jan18a3c	0.62	0.29562	10	50.0
jan18a4a	0.78	0.12743	12	41.7
jan18a4b	0.78	0.16818	15	33.3
jan18a4c	0.78	0.17706	14	35.7
jan18a5a	0.89	0.07435	17	29.4
jan18a5b	0.89	0.27891	11	45.5
jan18a5c	0.89	0.23915	18	27.8
jan18a6a	0.92	0.14068	12	41.7
jan18a6b	0.92	0.05342	16	31.3
jan18a6c	0.92	0.14317	12	41.7

Table A7.26
T=175°C, V_g=4.1 cm/s, z=15 cm

Filename	θ=r/R	Cross correlation peak	Time lag (ms)	Bubble rise velocity (cm/s)
jan20a1a	0.19	0.33030	9	55.6
jan20a1b	0.19	0.35691	10	50.0
jan20a1c	0.19	0.37279	10	50.0
jan20a2a	0.42	0.37890	8	62.5
jan20a2b	0.42	0.36628	7	71.4
jan20a2c	0.42	0.33684	9	55.6
jan20a3a	0.62	0.36989	9	55.6
jan20a3b	0.62	0.34573	10	50.0
jan20a3c	0.62	0.33147	10	50.0
jan20a4a	0.78	0.34319	7	71.4
jan20a4b	0.78	0.30110	10	50.0
jan20a4c	0.78	0.28417	12	41.7
jan20a5a	0.89	0.28408	7	71.4
jan20a5b	0.89	0.32956	9	55.6
jan20a5c	0.89	0.28650	6	83.3
jan20a6a	0.92	0.35120	9	55.6
jan20a6b	0.92	0.21066	9	55.6
jan20a6c	0.92	0.30475	12	41.7

Table A7.27
T=175°C, V_g=4.1 cm/s, z=30 cm

Filename	θ=r/R	Cross correlation peak	Time lag (ms)	Bubble rise velocity (cm/s)
jan20b1a	0.19	0.32981	9	55.6
jan20b1b	0.19	0.33107	7	71.4
jan20b1c	0.19	0.39937	8	62.5
jan20b2a	0.42	0.26705	10	50.0
jan20b2b	0.42	0.32333	9	55.6
jan20b2c	0.42	0.35786	10	50.0
jan20b3a	0.62	0.38094	9	55.6
jan20b3b	0.62	0.30856	7	71.4
jan20b3c	0.62	0.32222	9	55.6
jan20b4a	0.78	0.25822	9	55.6
jan20b4b	0.78	0.16780	12	41.7
jan20b4c	0.78	0.22888	8	62.5
jan20b5a	0.89	0.37140	11	45.5
jan20b5b	0.89	0.20318	11	45.5
jan20b5c	0.89	0.17824	11	45.5
jan20b6a	0.92	0.13037	21	23.8
jan20b6b	0.92	0.22819	13	38.5
jan20b6c	0.92	0.38389	9	55.6

Table A7.28
T=175°C, V_g=4.1 cm/s, z=46 cm

Filename	θ=r/R	Cross correlation peak	Time lag (ms)	Bubble rise velocity (cm/s)
jan20c1a	0.19	0.35494	5	100.0
jan20c1b	0.19	0.35833	8	62.5
jan20c1c	0.19	0.40071	7	71.4
jan20c2a	0.42	0.38208	7	71.4
jan20c2b	0.42	0.37685	8	62.5
jan20c2c	0.42	0.41709	8	62.5
jan20c3a	0.62	0.29557	7	71.4
jan20c3b	0.62	0.32298	10	50.0
jan20c3c	0.62	0.32737	8	62.5
jan20c4a	0.78	0.35541	8	62.5
jan20c4b	0.78	0.24842	9	55.6
jan20c4c	0.78	0.30456	9	55.6
jan20c5a	0.89	0.26596	9	55.6
jan20c5b	0.89	0.15654	14	35.7
jan20c5c	0.89	0.37892	10	50.0
jan20c6a	0.92	0.21351	12	41.7
jan20c6b	0.92	0.11937	18	27.8

Table A7.29
T=175°C, V_g=4.1 cm/s, z=61 cm

Filename	θ=r/R	Cross correlation peak	Time lag (ms)	Bubble rise velocity (cm/s)
jan20d1a	0.19	0.40612	7	71.4
jan20d1b	0.19	0.37520	7	71.4
jan20d1c	0.19	0.39024	6	83.3
jan20d2a	0.42	0.41307	8	62.5
jan20d2b	0.42	0.33223	7	71.4
jan20d2c	0.42	0.40748	8	62.5
jan20d3a	0.62	0.35971	8	62.5
jan20d3b	0.62	0.26644	9	55.6
jan20d3c	0.62	0.33639	7	71.4
jan20d4a	0.78	0.23984	8	62.5
jan20d4b	0.78	0.26879	7	71.4
jan20d4c	0.78	0.27792	10	50.0
jan20d5a	0.89	0.09377	12	41.7
jan20d5b	0.89	0.19972	12	41.7
jan20d5c	0.89	0.09791	13	38.5
jan20d6a	0.92	0.22926	11	45.5
jan20d6b	0.92	0.13304	10	50.0
jan20d6c	0.92	0.20322	14	35.7

Table A7.30
T=175°C, V_g=4.1 cm/s, z=76 cm

Filename	θ=r/R	Cross correlation peak	Time lag (ms)	Bubble rise velocity (cm/s)
jan20e1a	0.19	0.39903	7	71.4
jan20e1b	0.19	0.41873	6	83.3
jan20e1c	0.19	0.43408	7	71.4
jan20e2a	0.42	0.35937	7	71.4
jan20e2b	0.42	0.38898	7	71.4
jan20e2c	0.42	0.31857	7	71.4
jan20e3a	0.62	0.32695	7	71.4
jan20e3b	0.62	0.26311	10	50.0
jan20e3c	0.62	0.33485	9	55.6
jan20e4a	0.78	0.31493	9	55.6
jan20e4b	0.78	0.41252	9	55.6
jan20e4c	0.78	0.19076	10	50.0
jan20e5a	0.89	0.13543	8	62.5
jan20e5b	0.89	0.10659	16	31.3
jan20e5c	0.89	0.06670	18	27.8
jan20e6a	0.92	0.08203	26	19.2
jan20e6b	0.92	0.10713	13	38.5
jan20e6c	0.92	0.10779	12	41.7

Table A7.31
T=175°C, V_g=9.0 cm/s, z=15 cm

Filename	θ=r/R	Cross correlation peak	Time lag (ms)	Bubble rise velocity (cm/s)
jan21e1a	0.19	0.36192	8	62.5
jan21e1b	0.19	0.40214	7	71.4
jan21e1c	0.19	0.33972	5	100.0
jan21e2a	0.42	0.41375	7	71.4
jan21e2b	0.42	0.39199	8	62.5
jan21e2c	0.42	0.38220	8	62.5
jan21e3a	0.62	0.39597	6	83.3
jan21e3b	0.62	0.41138	8	62.5
jan21e3c	0.62	0.41506	8	62.5
jan21e4a	0.78	0.38671	8	62.5
jan21e4b	0.78	0.51232	8	62.5
jan21e4c	0.78	0.42164	7	71.4
jan21e5a	0.89	0.35894	8	62.5
jan21e5b	0.89	0.36773	7	71.4
jan21e5c	0.89	0.36102	6	83.3
jan21e6a	0.92	0.34756	8	62.5
jan21e6b	0.92	0.29976	12	41.7
jan21e6c	0.92	0.38538	9	55.6

Table A7.32
T=175°C, V_g=9.0 cm/s, z=30 cm

Filename	θ=r/R	Cross correlation peak	Time lag (ms)	Bubble rise velocity (cm/s)
jan21d1a	0.19	0.40320	6	83.3
jan21d1b	0.19	0.41845	6	83.3
jan21d1c	0.19	0.37474	6	83.3
jan21d2a	0.42	0.46829	6	83.3
jan21d2b	0.42	0.45210	6	83.3
jan21d2c	0.42	0.43243	7	71.4
jan21d3a	0.62	0.37278	6	83.3
jan21d3b	0.62	0.43839	6	83.3
jan21d3c	0.62	0.41096	7	71.4
jan21d4a	0.78	0.45487	6	83.3
jan21d4b	0.78	0.45236	8	62.5
jan21d4c	0.78	0.37899	7	71.4
jan21d5a	0.89	0.41675	8	62.5
jan21d5b	0.89	0.21506	8	62.5
jan21d5c	0.89	0.27366	9	55.6
jan21d6a	0.92	0.33826	8	62.5
jan21d6b	0.92	0.30849	10	50.0
jan21d6c	0.92	0.34320	9	55.6

Table A7.33
T=175°C, V_g=9.0 cm/s, z=46 cm

Filename	θ=r/R	Cross correlation peak	Time lag (ms)	Bubble rise velocity (cm/s)
jan21c1a	0.19	0.44779	6	83.3
jan21c1b	0.19	0.51002	6	83.3
jan21c1c	0.19	0.44475	6	83.3
jan21c2a	0.42	0.48952	6	83.3
jan21c2b	0.42	0.46660	5	100.0
jan21c2c	0.42	0.45257	6	83.3
jan21c3a	0.62	0.45313	6	83.3
jan21c3b	0.62	0.42852	7	71.4
jan21c3c	0.62	0.37279	5	100.0
jan21c4a	0.78	0.36978	8	62.5
jan21c4b	0.78	0.45422	7	71.4
jan21c4c	0.78	0.33069	5	100.0
jan21c5a	0.89	0.52962	6	83.3
jan21c5b	0.89	0.26939	12	41.7
jan21c5c	0.89	0.19220	8	62.5
jan21c6b	0.92	0.19501	14	35.7
jan21c6c	0.92	0.28091	12	41.7

Table A7.34
T=175°C, V_g=9.0 cm/s, z=61 cm

Filename	θ=r/R	Cross correlation peak	Time lag (ms)	Bubble rise velocity (cm/s)
jan21b1a	0.19	0.53024	5	100.0
jan21b1b	0.19	0.53126	5	100.0
jan21b1c	0.19	0.54198	5	100.0
jan21b2a	0.42	0.46696	6	83.3
jan21b2b	0.42	0.47501	6	83.3
jan21b2c	0.42	0.46502	6	83.3
jan21b3a	0.62	0.40988	6	83.3
jan21b3b	0.62	0.40188	7	71.4
jan21b3c	0.62	0.47895	6	83.3
jan21b4a	0.78	0.32428	8	62.5
jan21b4b	0.78	0.35356	10	50.0
jan21b4c	0.78	0.30359	7	71.4
jan21b5a	0.89	0.24694	7	71.4
jan21b5b	0.89	0.11411	8	62.5
jan21b5c	0.89	0.23891	13	38.5
jan21b6a	0.92	0.33855	8	62.5
jan21b6b	0.92	0.13387	9	55.6
jan21b6c	0.92	0.09675	9	55.6

Table A7.35
T=175°C, V_g=9.0 cm/s, z=76 cm

Filename	θ=r/R	Cross correlation peak	Time lag (ms)	Bubble rise velocity (cm/s)
jan21a1a	0.19	0.52433	5	100.0
jan21a1b	0.19	0.48220	5	100.0
jan21a1c	0.19	0.50008	5	100.0
jan21a2a	0.42	0.50970	5	100.0
jan21a2b	0.42	0.48970	6	83.3
jan21a2c	0.42	0.42973	6	83.3
jan21a3a	0.62	0.44593	5	100.0
jan21a3b	0.62	0.45903	6	83.3
jan21a3c	0.62	0.42584	4	125.0
jan21a4a	0.78	0.34332	8	62.5
jan21a4b	0.78	0.46978	6	83.3
jan21a4c	0.78	0.38096	8	62.5
jan21a5a	0.89	0.38130	12	41.7
jan21a5b	0.89	0.18176	13	38.5
jan21a5c	0.89	0.11968	15	33.3
jan21a6a	0.92	0.21620	12	41.7
jan21a6b	0.92	0.14508	15	33.3

Table A7.36
T=175°C, V_g=14.7 cm/s, z=15 cm

Filename	θ=r/R	Cross correlation peak	Time lag (ms)	Bubble rise velocity (cm/s)
jan22a1a	0.19	0.39787	7	71.4
jan22a1b	0.19	0.38048	7	71.4
jan22a1c	0.19	0.39279	7	71.4
jan22a2a	0.42	0.41420	7	71.4
jan22a2b	0.42	0.48046	6	83.3
jan22a2c	0.42	0.47425	6	83.3
jan22a3a	0.62	0.44248	5	100.0
jan22a3b	0.62	0.45007	6	83.3
jan22a3c	0.62	0.42226	6	83.3
jan22a4a	0.78	0.37669	7	71.4
jan22a4b	0.78	0.42103	6	83.3
jan22a4c	0.78	0.47654	7	71.4
jan22a5a	0.89	0.36388	5	100.0
jan22a5b	0.89	0.45863	7	71.4
jan22a5c	0.89	0.49083	7	71.4
jan22a6a	0.92	0.31862	7	71.4
jan22a6b	0.92	0.31017	10	50.0
jan22a6c	0.92	0.25267	8	62.5

Table A7.37
T=175°C, V_g=14.7 cm/s, z=30 cm

Filename	θ=r/R	Cross correlation peak	Time lag (ms)	Bubble rise velocity (cm/s)
jan22b1a	0.19	0.38550	5	100.0
jan22b1b	0.19	0.44167	5	100.0
jan22b1c	0.19	0.45933	6	83.3
jan22b2a	0.42	0.48455	5	100.0
jan22b2b	0.42	0.47734	6	83.3
jan22b2c	0.42	0.48993	5	100.0
jan22b3a	0.62	0.47817	5	100.0
jan22b3b	0.62	0.50223	6	83.3
jan22b3c	0.62	0.47323	6	83.3
jan22b4a	0.78	0.44924	5	100.0
jan22b4b	0.78	0.46407	5	100.0
jan22b4c	0.78	0.37785	5	100.0
jan22b5a	0.89	0.38517	5	100.0
jan22b5b	0.89	0.44104	7	71.4
jan22b5c	0.89	0.41816	6	83.3
jan22b6a	0.92	0.33585	7	71.4
jan22b6b	0.92	0.47858	7	71.4
jan22b6c	0.92	0.34539	6	83.3

Table A7.38
T=175°C, V_g=14.7 cm/s, z=46 cm

Filename	θ=r/R	Cross correlation peak	Time lag (ms)	Bubble rise velocity (cm/s)
jan22c1a	0.19	0.51368	5	100.0
jan22c1b	0.19	0.50296	5	100.0
jan22c1c	0.19	0.47938	6	83.3
jan22c2a	0.42	0.49991	6	83.3
jan22c2b	0.42	0.52194	5	100.0
jan22c2c	0.42	0.50869	5	100.0
jan22c3a	0.62	0.47707	6	83.3
jan22c3b	0.62	0.49213	5	100.0
jan22c3c	0.62	0.48681	5	100.0
jan22c4a	0.78	0.40042	6	83.3
jan22c4b	0.78	0.45177	7	71.4
jan22c4c	0.78	0.52520	6	83.3
jan22c5a	0.89	0.27700	5	100.0
jan22c5b	0.89	0.25789	8	62.5
jan22c5c	0.89	0.46544	8	62.5
jan22c6a	0.92	0.18542	7	71.4
jan22c6b	0.92	0.29977	8	62.5
jan22c6c	0.92	0.23455	8	62.5

Table A7.39
T=175°C, V_g=14.7 cm/s, z=61 cm

Filename	θ=r/R	Cross correlation peak	Time lag (ms)	Bubble rise velocity (cm/s)
jan22d1a	0.19	0.52465	5	100.0
jan22d1b	0.19	0.52753	4	125.0
jan22d1c	0.19	0.52891	4	125.0
jan22d2a	0.42	0.47770	5	100.0
jan22d2b	0.42	0.52069	4	125.0
jan22d2c	0.42	0.51985	5	100.0
jan22d3a	0.62	0.46347	5	100.0
jan22d3b	0.62	0.49472	5	100.0
jan22d3c	0.62	0.43802	5	100.0
jan22d4a	0.78	0.46031	5	100.0
jan22d4b	0.78	0.40545	5	100.0
jan22d4c	0.78	0.35728	6	83.3
jan22d5c	0.89	0.24116	10	50.0
jan22d6a	0.92	0.19668	7	71.4
jan22d6c	0.92	0.26858	8	62.5

Table A7.40
T=175°C, V_g=14.7 cm/s, z=76 cm

Filename	θ=r/R	Cross correlation peak	Time lag (ms)	Bubble rise velocity (cm/s)
jan22e1a	0.19	0.50467	4	125.0
jan22e1b	0.19	0.54508	4	125.0
jan22e1c	0.19	0.51639	5	100.0
jan22e2a	0.42	0.53397	5	100.0
jan22e2b	0.42	0.48240	5	100.0
jan22e2c	0.42	0.47235	5	100.0
jan22e3a	0.62	0.43469	5	100.0
jan22e3b	0.62	0.45173	5	100.0
jan22e3c	0.62	0.48816	5	100.0
jan22e4a	0.78	0.41682	7	71.4
jan22e4b	0.78	0.39123	6	83.3
jan22e4c	0.78	0.38231	5	100.0
jan22e5a	0.89	0.21856	7	71.4
jan22e5b	0.89	0.39762	7	71.4
jan22e5c	0.89	0.17288	7	71.4
jan22e6a	0.92	0.21703	9	55.6
jan22e6b	0.92	0.17219	11	45.5
jan22e6c	0.92	0.30849	7	71.4

APPENDIX 8

BUBBLE CHORD LENGTH DISTRIBUTION

Table A8.1
Summary of operating conditions
(T=100°C)

Filename	Temperature (°C)	V_s (cm/s)	z (cm)
jan11a...	100	4.1	10
jan11b...	100	4.1	15
jan11c...	100	4.1	30
jan11d...	100	4.1	46
jan11e...	100	4.1	61
jan13a...	100	2.2	61
jan13b...	100	2.2	46
jan13c...	100	2.2	30
jan13d...	100	2.2	15
jan13e...	100	2.2	76
jan16a...	100	9.0	76
jan16b...	100	9.0	61
jan16c...	100	9.0	46
jan16d...	100	9.0	30
jan16e...	100	9.0	15
jan17a...	100	14.7	15
jan17b...	100	14.7	30
jan17c...	100	14.7	46
jan17d...	100	14.7	61
jan17e...	100	14.7	76

jan11a... # *

↓ ↓

radial position: repeats:

1: θ=0.19
2: θ=0.42
3: θ=0.62
4: θ=0.78
5: θ=0.89
6: θ=0.92

a: repeat no. 1
b: repeat no. 2
c: repeat no. 3

Table A8.2
Summary of operating conditions
(T=175°C)

Filename	Temperature (°C)	V_g (cm/s)	z (cm)
jan18a...	175	2.2	76
jan18b...	175	2.2	61
jan18c...	175	2.2	46
jan18d...	175	2.2	30
jan18e...	175	2.2	15
jan20a...	175	4.1	15
jan20b...	175	4.1	30
jan20c...	175	4.1	46
jan20d...	175	4.1	61
jan20e...	175	4.1	76
jan21a...	175	9.0	76
jan21b...	175	9.0	61
jan21c...	175	9.0	46
jan21d...	175	9.0	30
jan21e...	175	9.0	15
jan22a...	175	14.7	15
jan22b...	175	14.7	30
jan22c...	175	14.7	46
jan22d...	175	14.7	61
jan22e...	175	14.7	76

jan18a... # *

↓ ↓

radial position: repeats:

1: θ=0.19
2: θ=0.42
3: θ=0.62
4: θ=0.78
5: θ=0.89
6: θ=0.92

a: repeat no. 1
b: repeat no. 2
c: repeat no. 3

****** FILENAME ****** : JAN11A1A

**** Bubbles detected by probe 1 : 412
**** Percentage of bubbles retained : 41.26
**** Average bubble duration : .007376 s

Probability Distributions

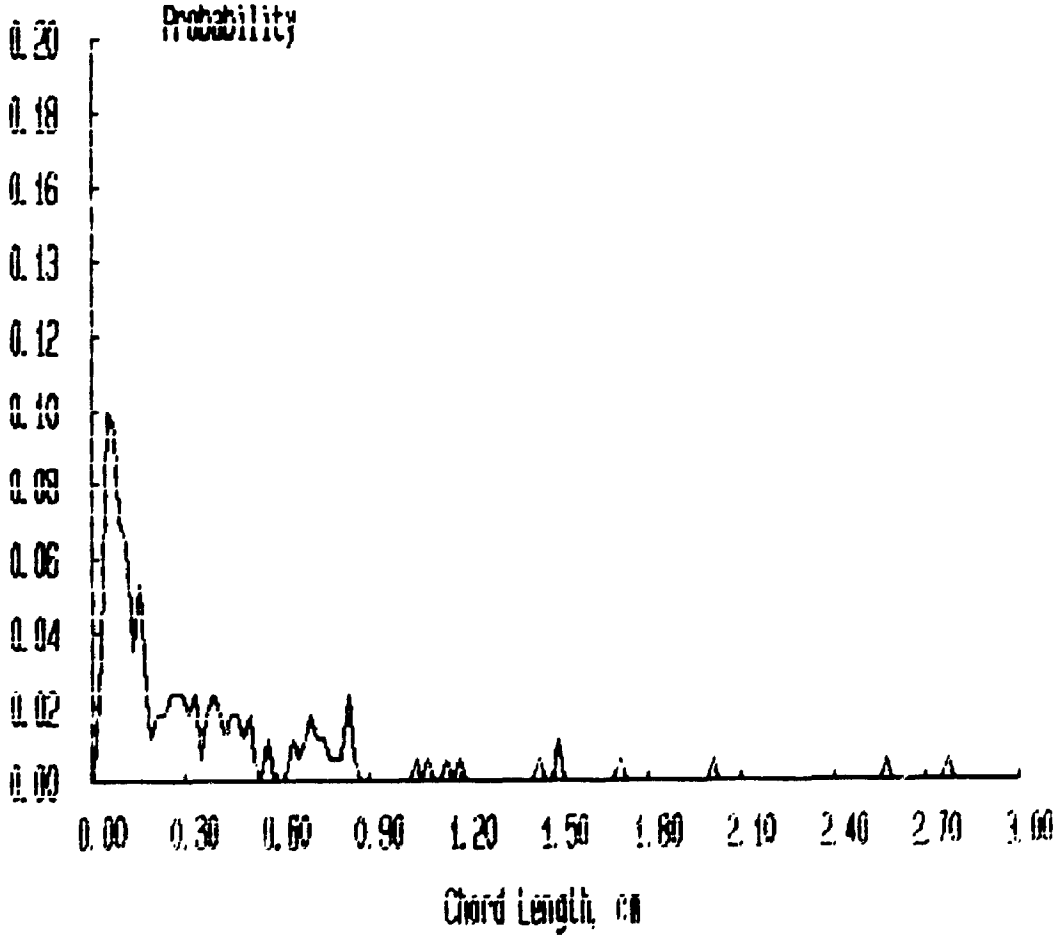

****** FILENAME ****** : JAN11A2A

**** Bubbles detected by probe 1 : 699
**** Percentage of bubbles retained : 47.93
**** Average bubble duration : .007466 s

Probability Distributions

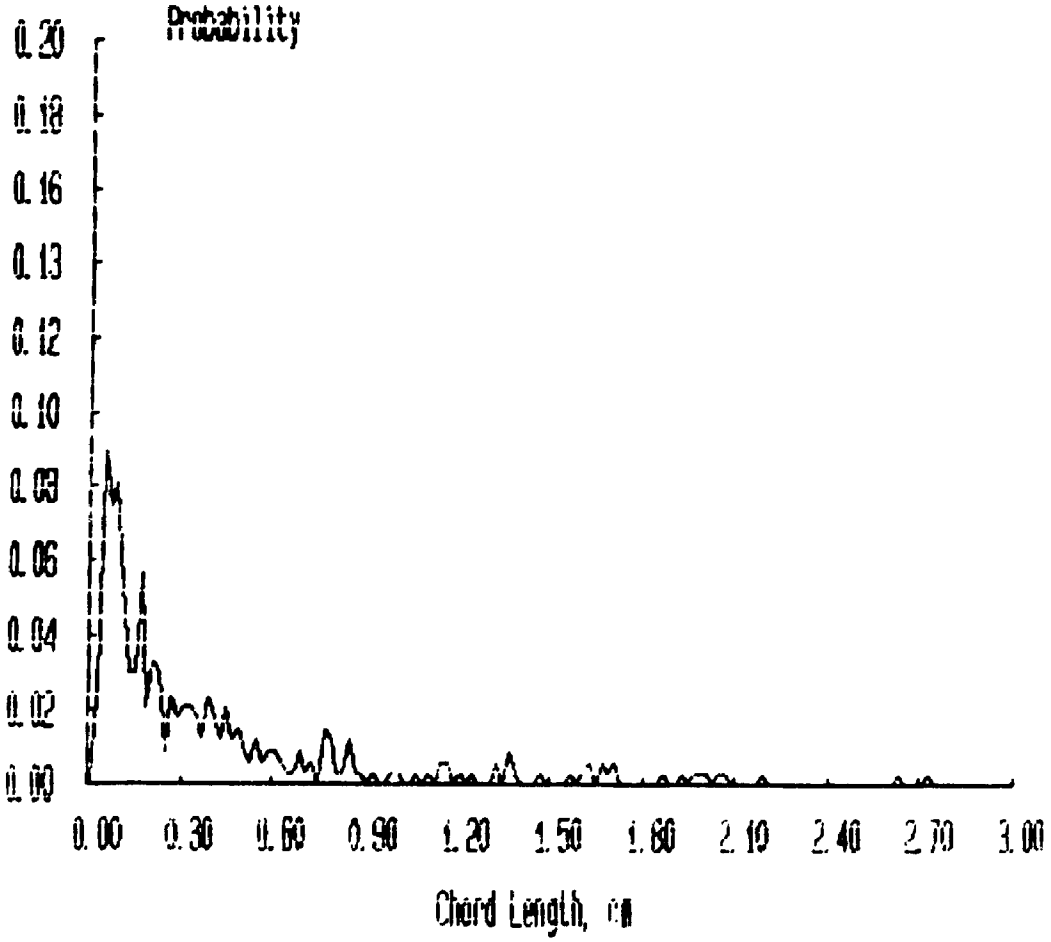

****** FILENAME ****** : JAN11A3A

**** Bubbles detected by probe 1 : 479
**** Percentage of bubbles retained : 33.40
**** Average bubble duration : .006494 s

Probability Distributions

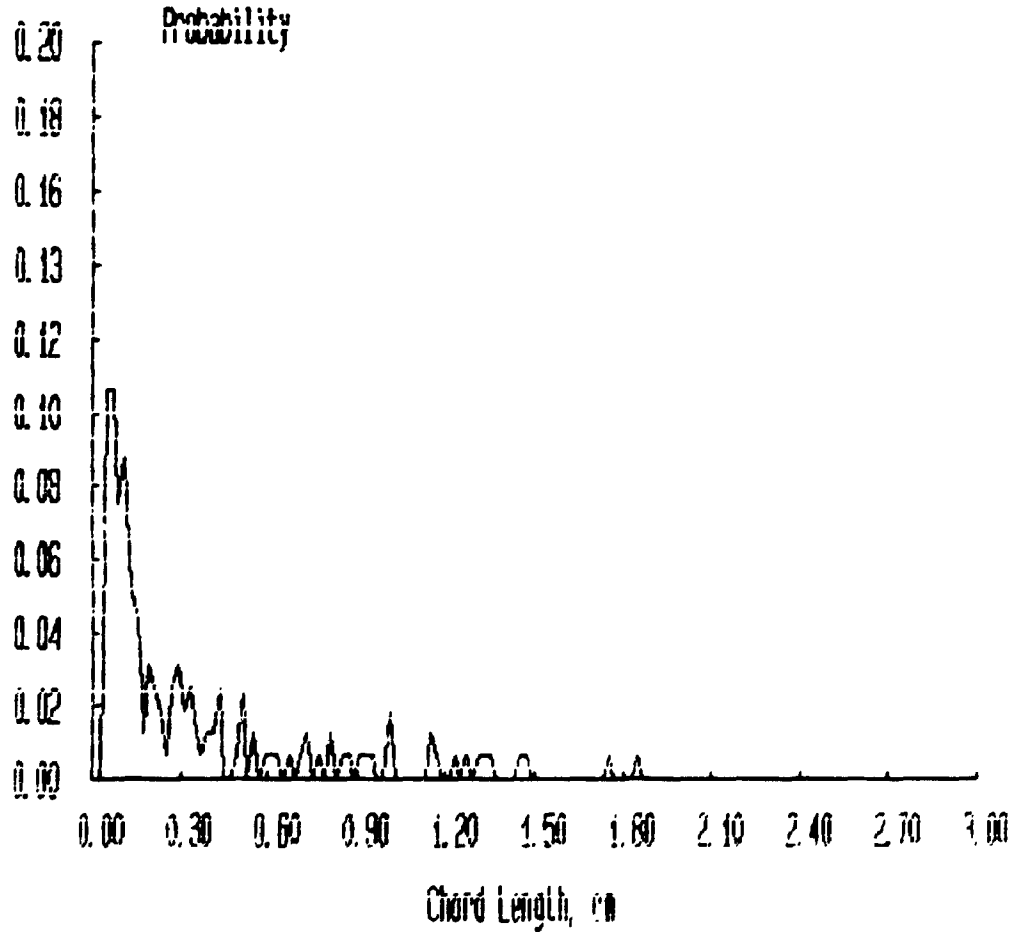

****** FILENAME ****** : JAN11A4A

**** Bubbles detected by probe 1 : 462
**** Percentage of bubbles retained : 34.63
**** Average bubble duration : .007944 s

Probability Distributions

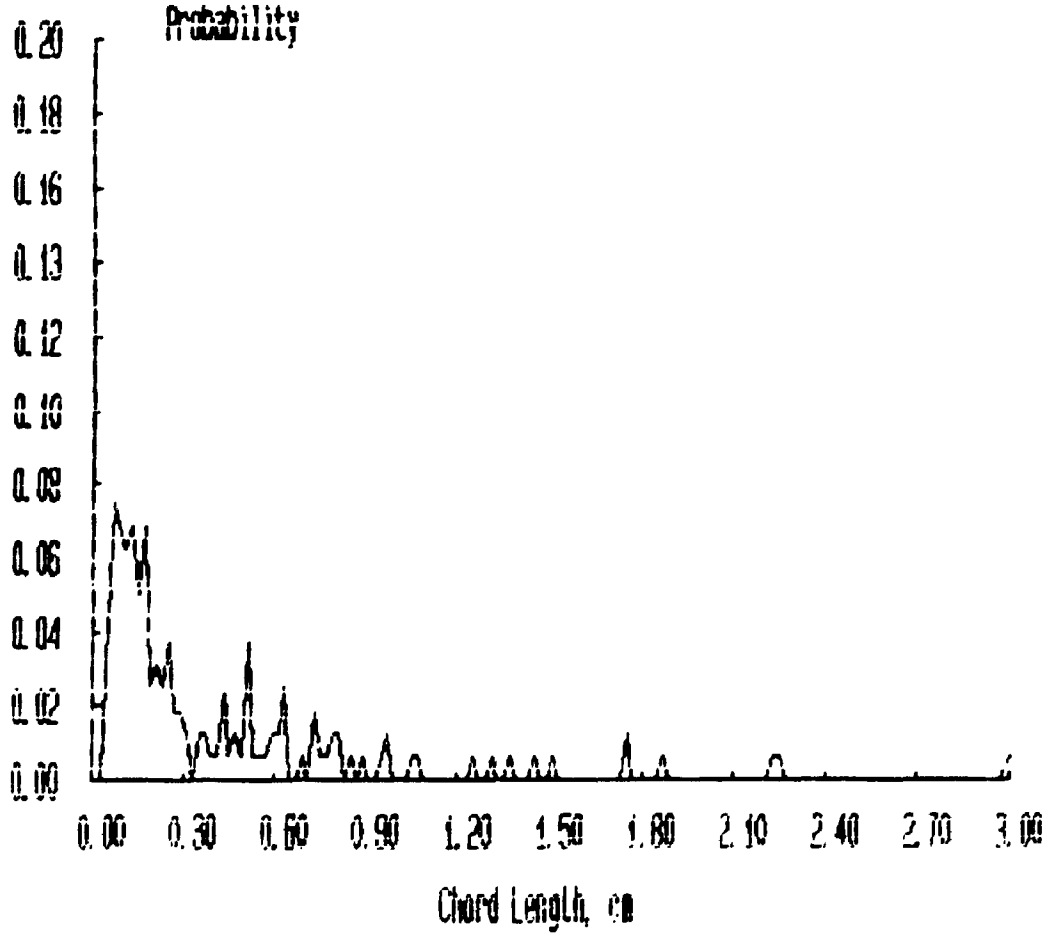

****** FILENAME ****** : JAN11A5A

**** Bubbles detected by probe 1 : 464
**** Percentage of bubbles retained : 38.58
**** Average bubble duration : .008827 s

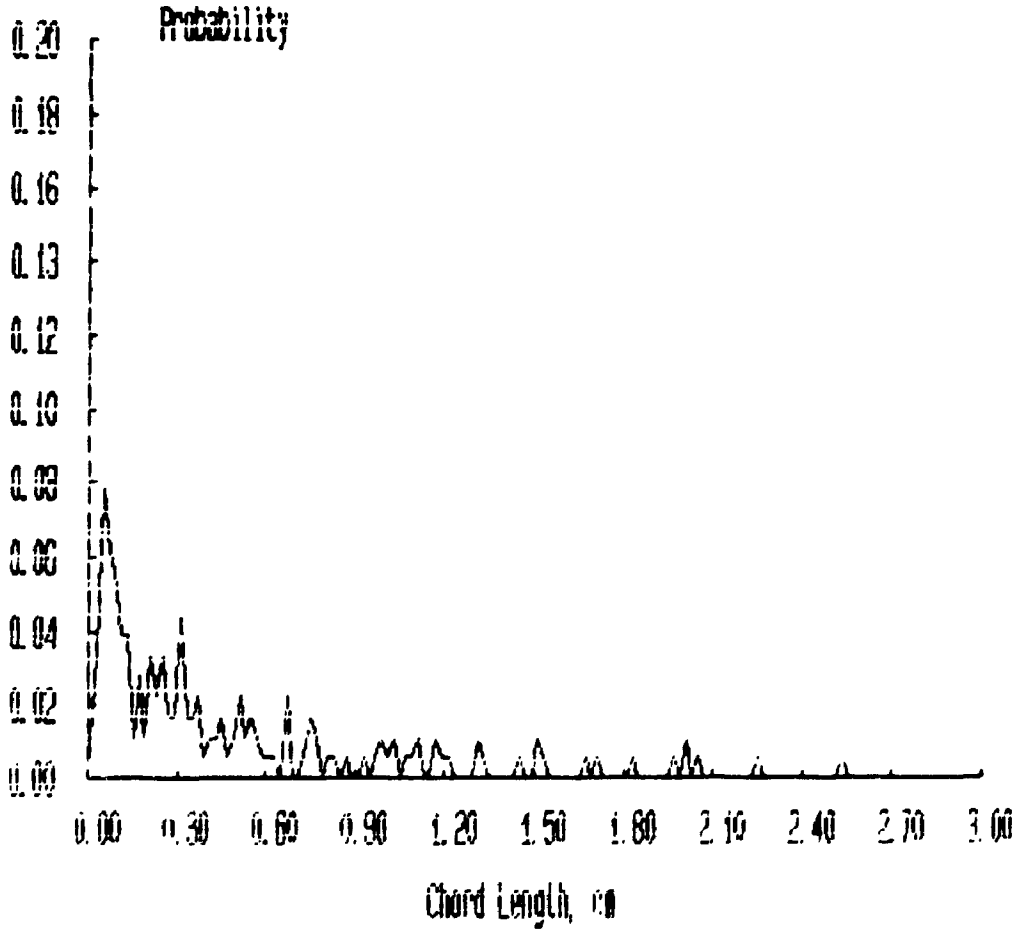

****** FILENAME ****** : JAN11A6A

**** Bubbles detected by probe 1 : 383
**** Percentage of bubbles retained : 38.90
**** Average bubble duration : .008953 s

Probability Distributions

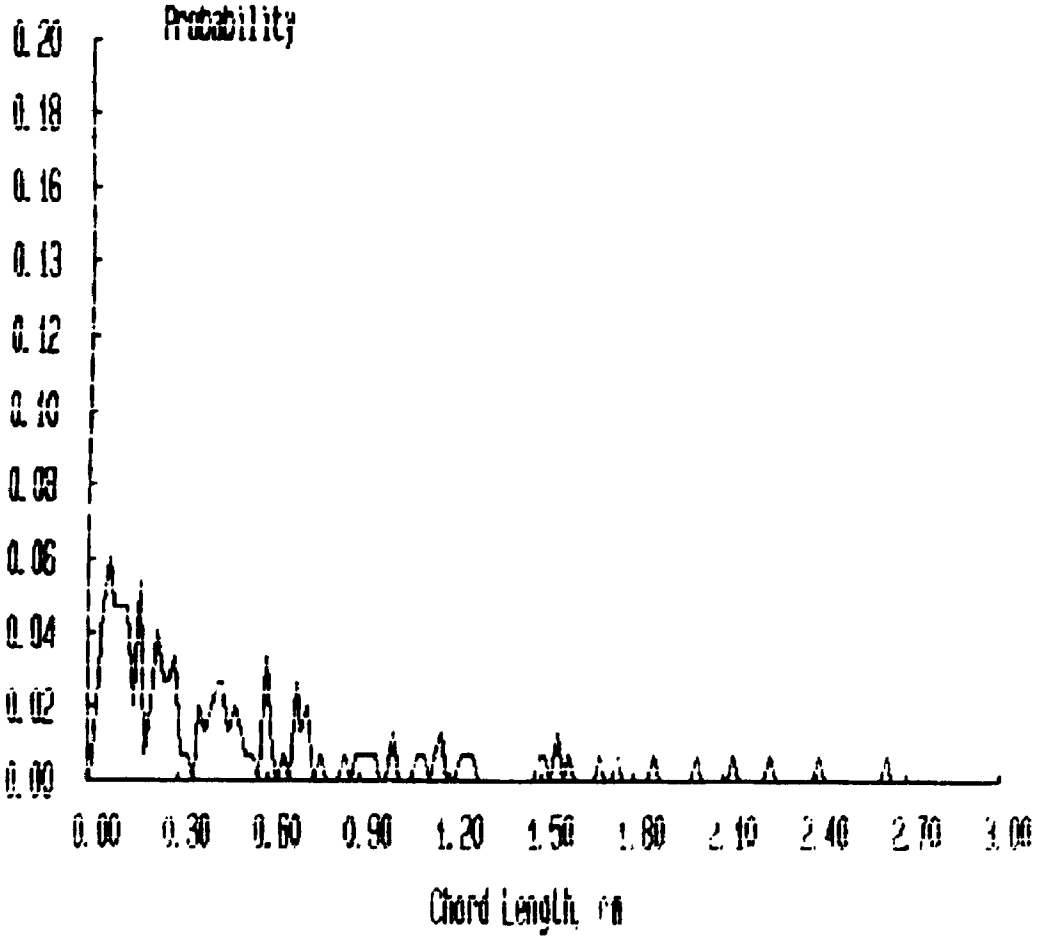

****** FILENAME ****** : JAN11B1A

**** Bubbles detected by probe 1 : 602
**** Percentage of bubbles retained : 41.86
**** Average bubble duration : .007690 s

Probability Distributions

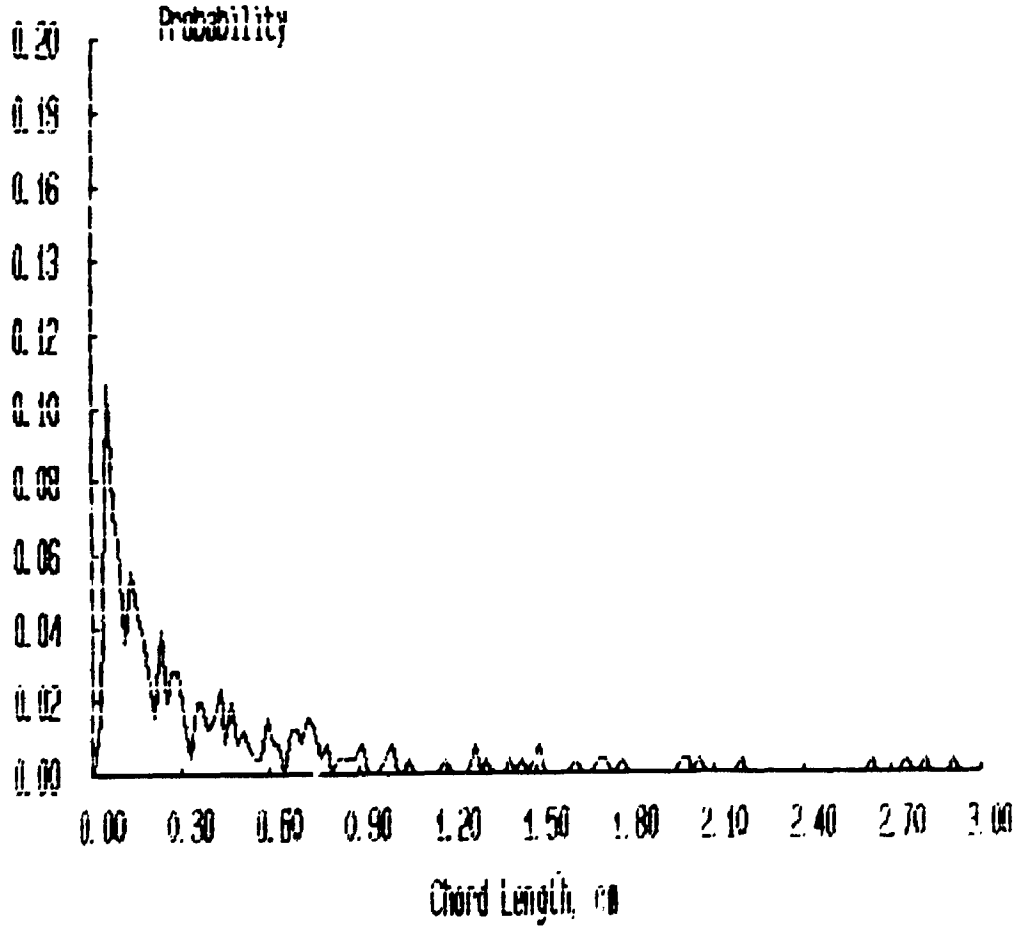

****** FILENAME ****** : JAN1182A

**** Bubbles detected by probe 1 : 737
**** Percentage of bubbles retained : 42.47
**** Average bubble duration : .007339 s

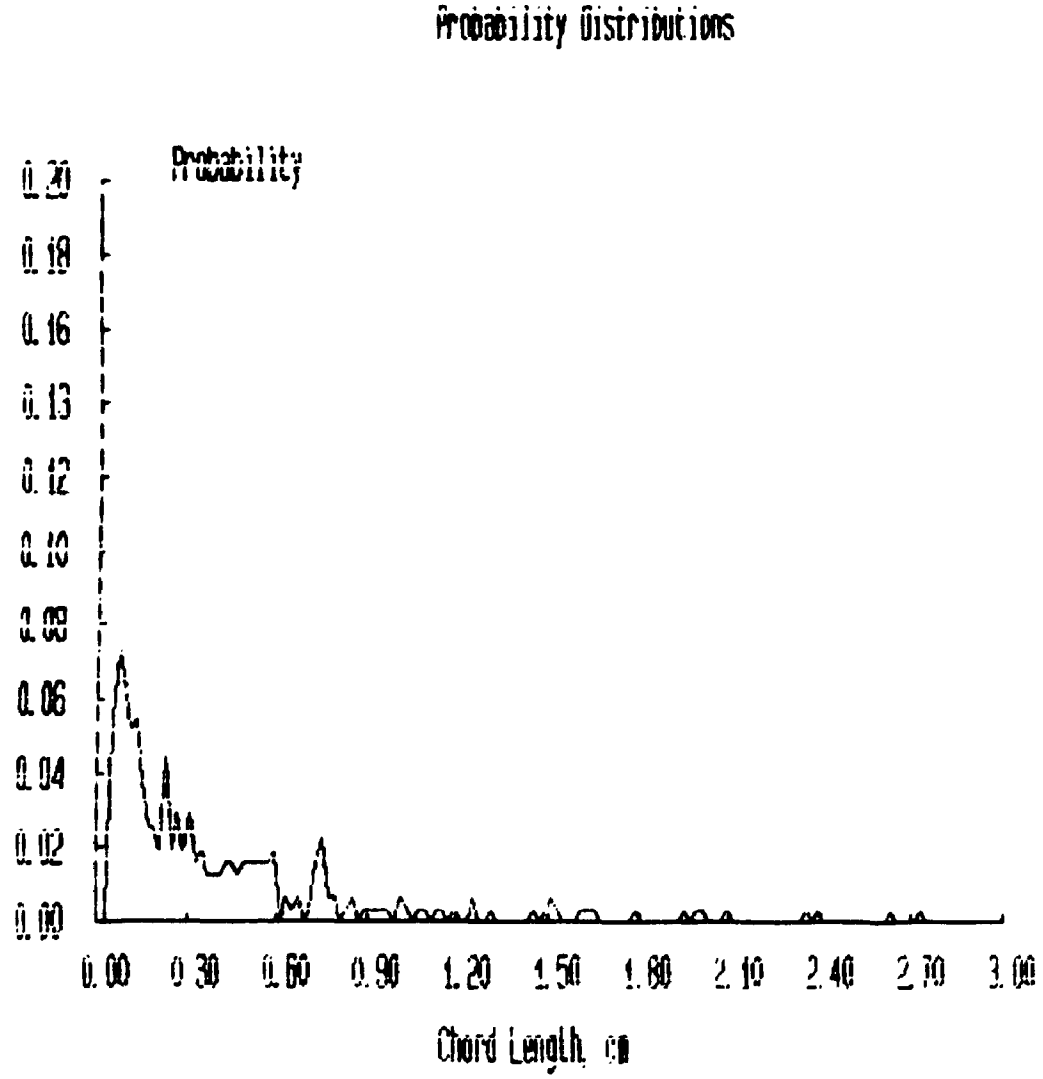

****** FILENAME ****** : JAN11B3A

**** Bubbles detected by probe 1 : 657
**** Percentage of bubbles retained : 35.16
**** Average bubble duration : .007621 s

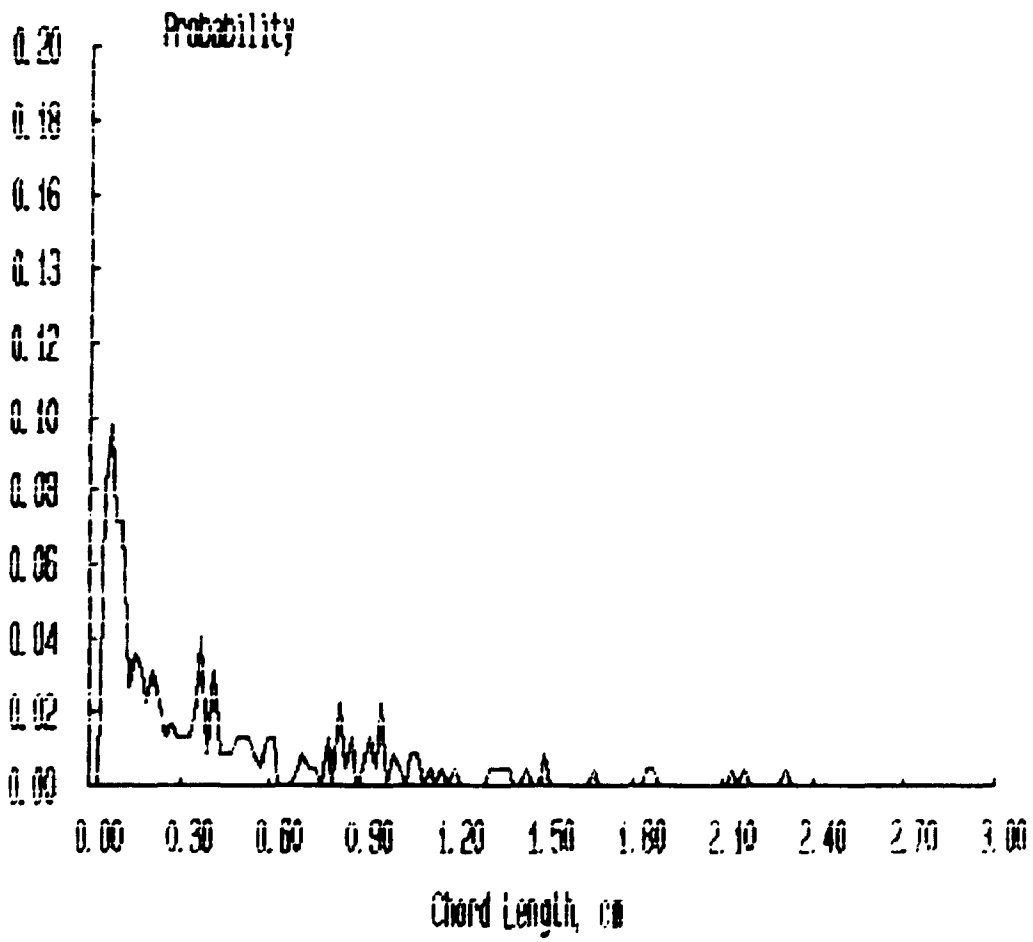

****** FILENAME ****** : JAN1184A

**** Bubbles detected by probe 1 : 524
**** Percentage of bubbles retained : 29.58
**** Average bubble duration : .006865 s

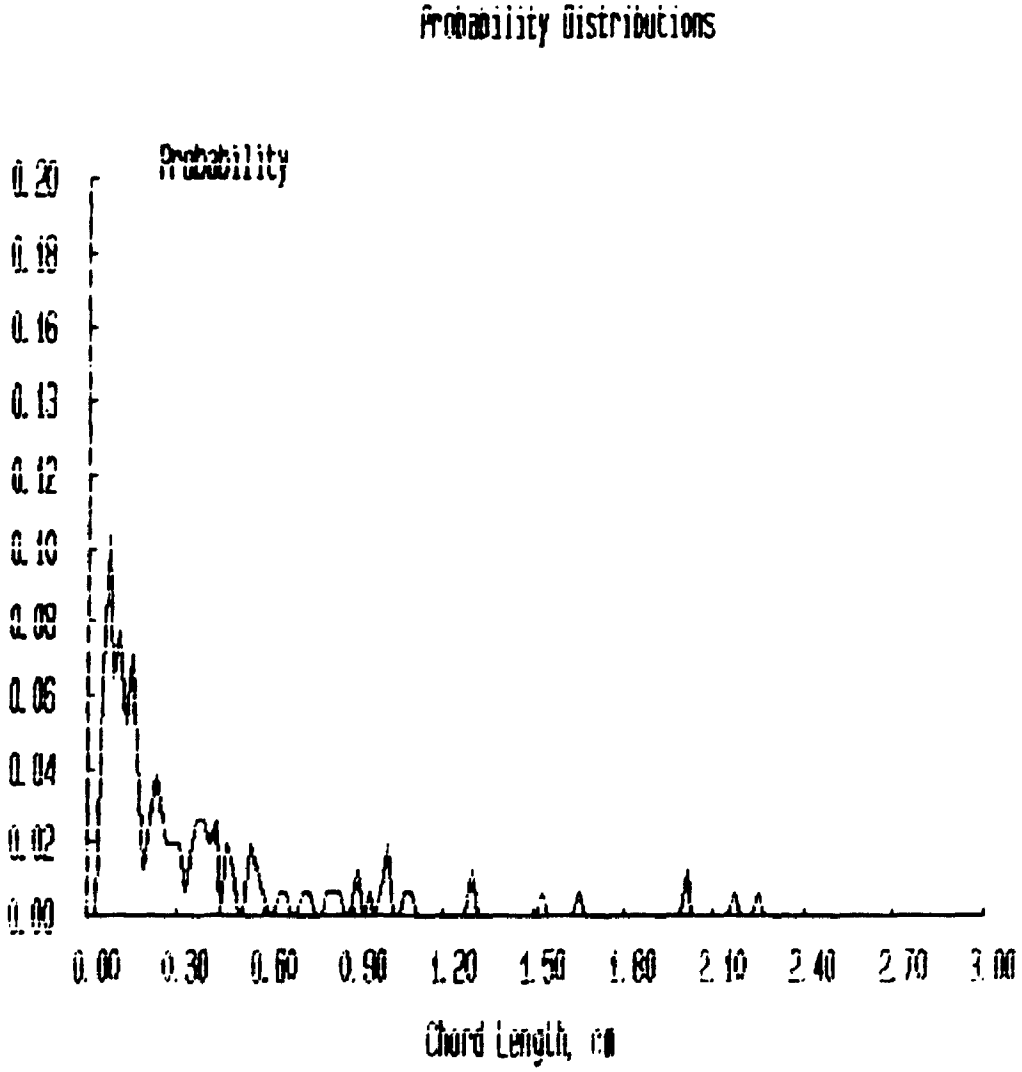

****** FILENAME ****** : JAN11B5A

**** Bubbles detected by probe 1 : 451
**** Percentage of bubbles retained : 36.36
**** Average bubble duration : .007616 s

Probability Distributions

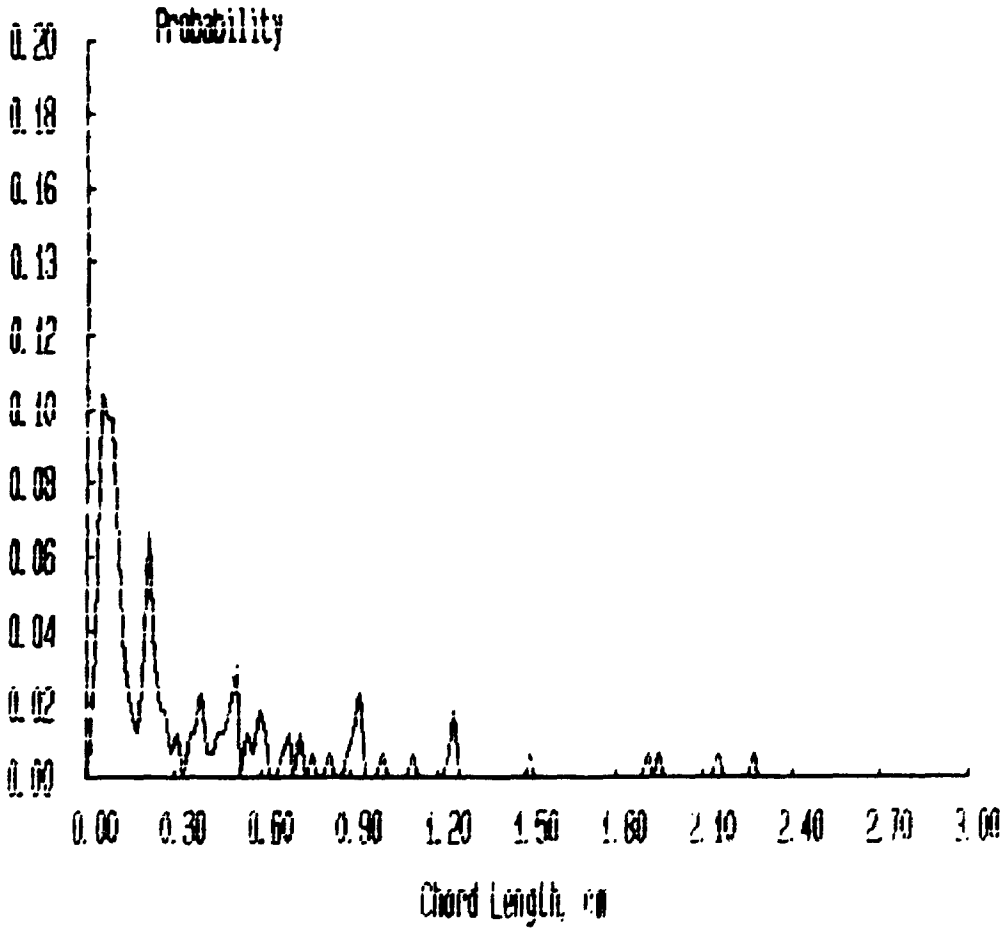

****** FILENAME ****** : JAN1186A

**** Bubbles detected by probe 1 : 313
**** Percentage of bubbles retained : 31.95
**** Average bubble duration : .008410 s

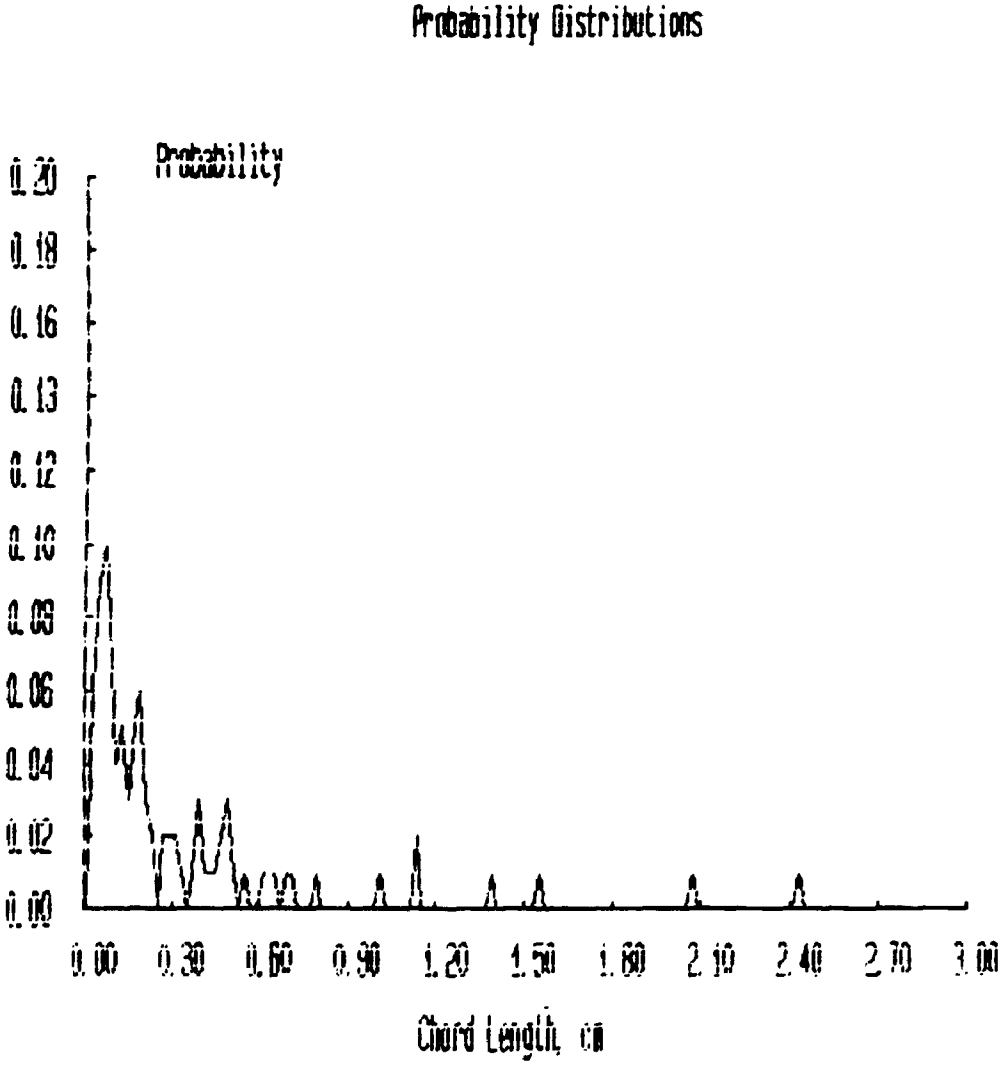

****** FILENAME ****** : JAN11C1A

**** Bubbles detected by probe 1 : 866
**** Percentage of bubbles retained : 47.46
**** Average bubble duration : .006594 s

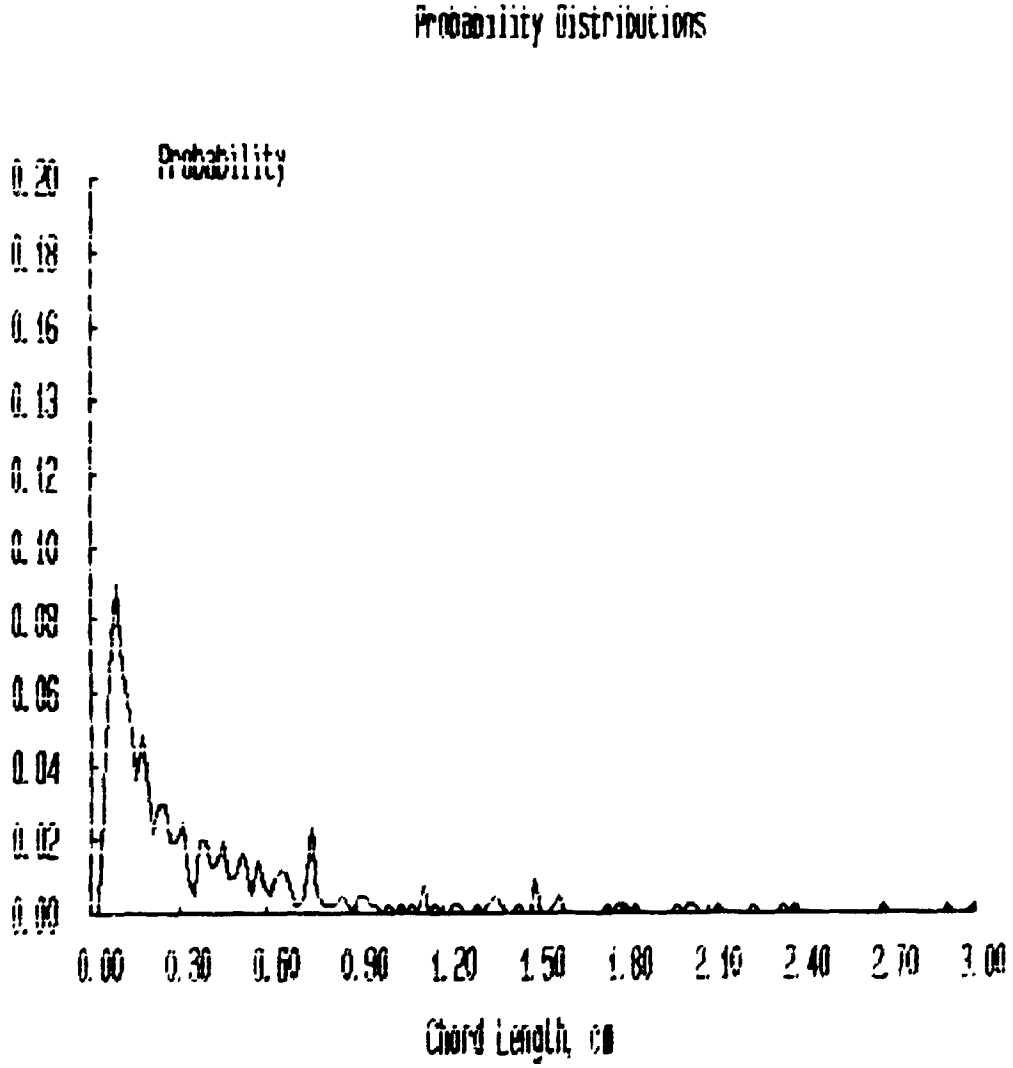

****** FILENAME ****** : JAN11C2A

**** Bubbles detected by probe 1 : 966
**** Percentage of bubbles retained : 42.55
**** Average bubble duration : .006406 s

Probability Distributions

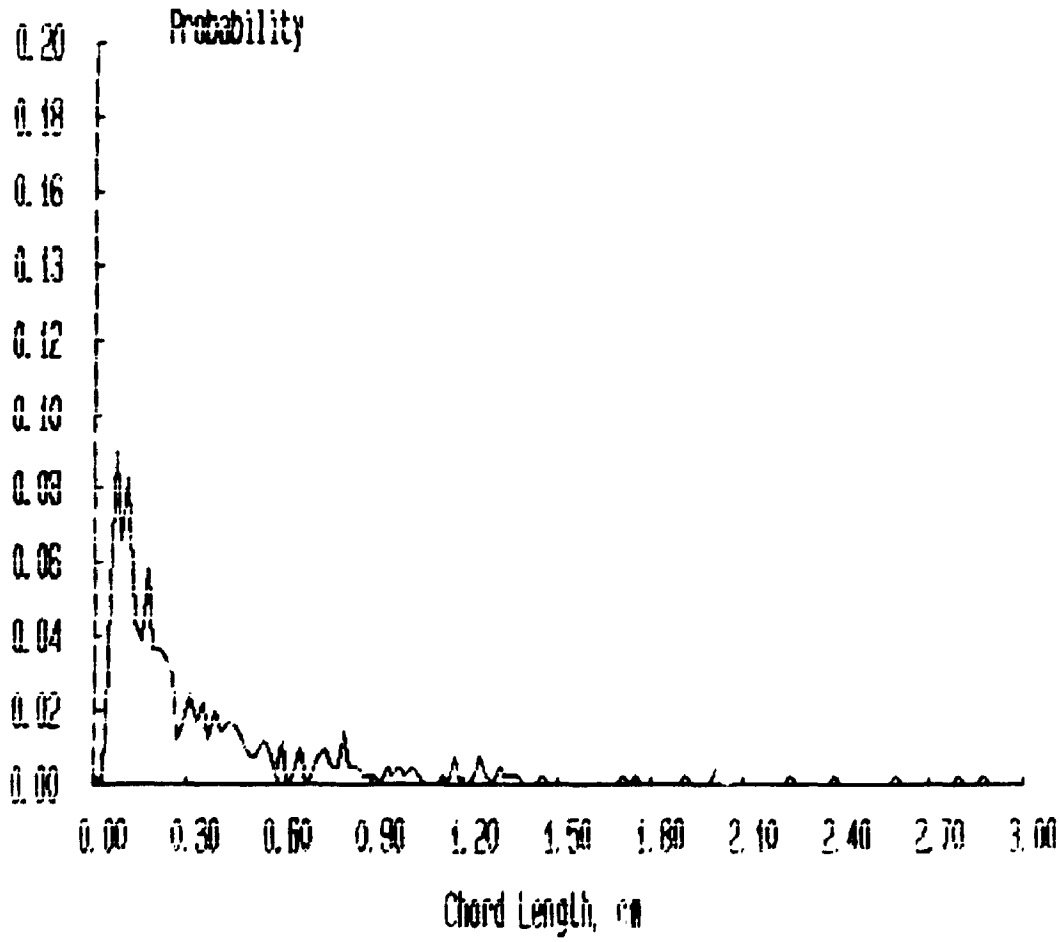

****** FILENAME ****** : JAN11C3A

**** Bubbles detected by probe 1 : 592
**** Percentage of bubbles retained : 28.89
**** Average bubble duration : .006006 s

Probability Distributions

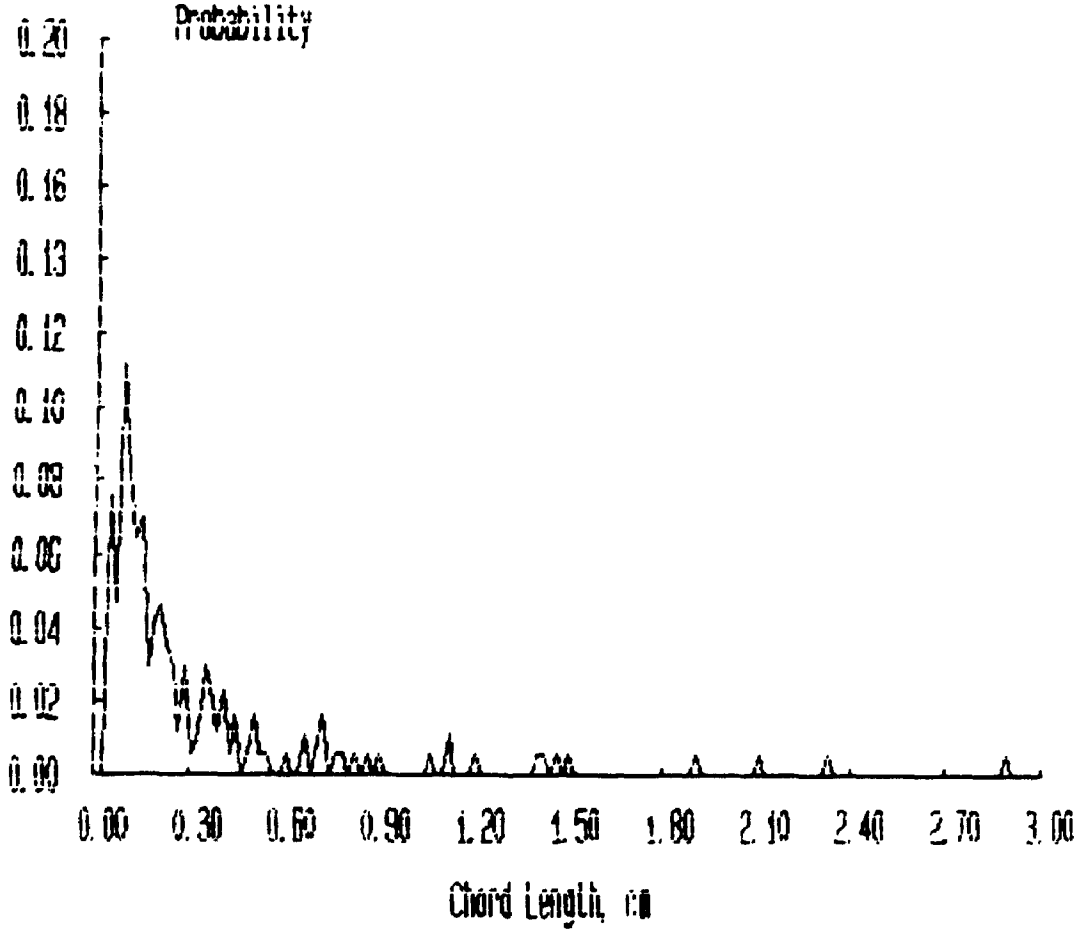

****** FILENAME ****** : JAN11C4A

**** Bubbles detected by probe 1 : 867
**** Percentage of bubbles retained : 36.33
**** Average bubble duration : .005816 s

Probability Distributions

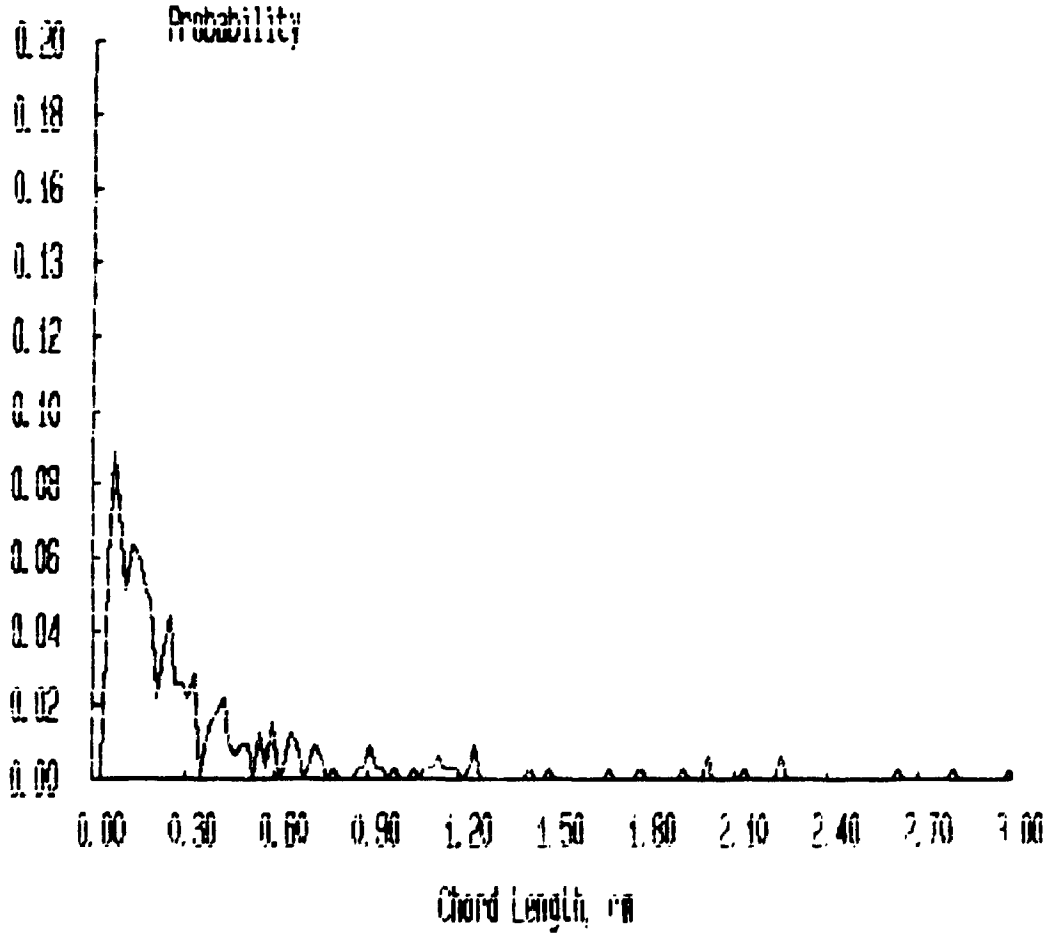

****** FILENAME ****** : JAN11C5B

**** Bubbles detected by probe 1 : 408
**** Percentage of bubbles retained : 35.54
**** Average bubble duration : .006338 s

Probability Distributions

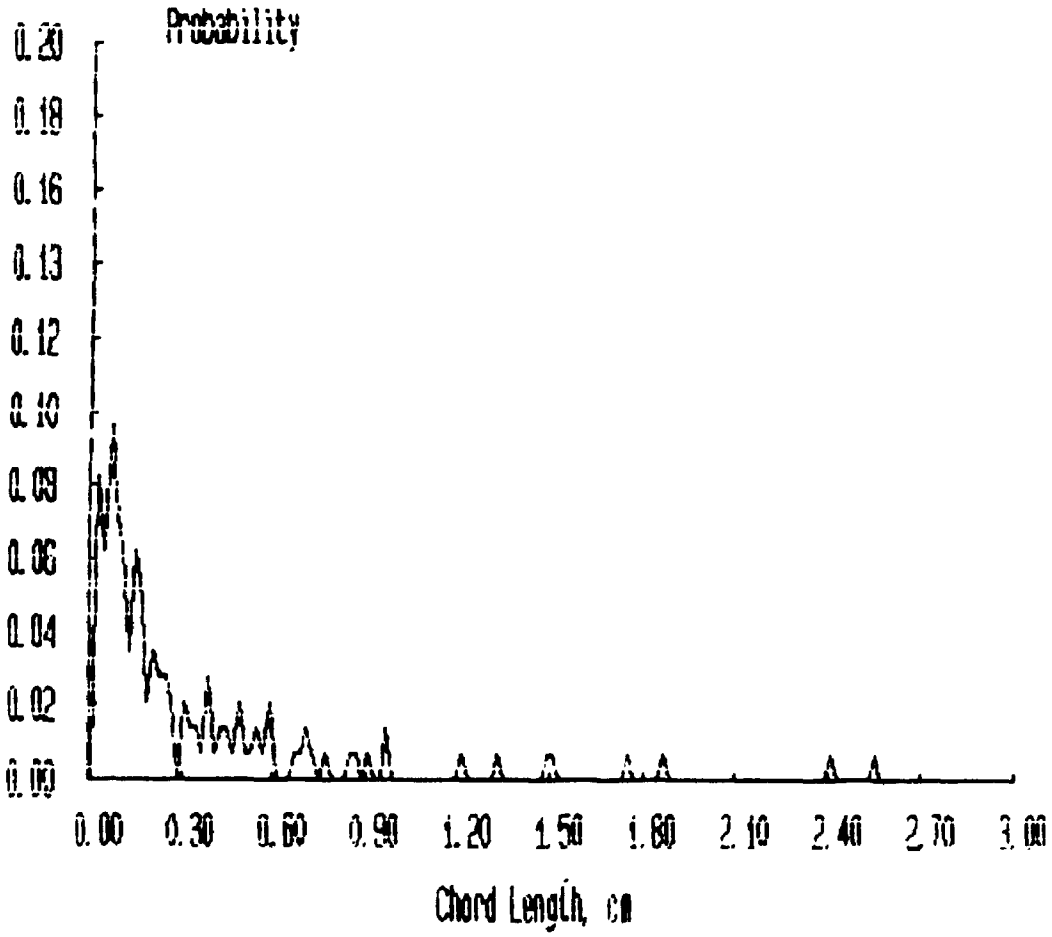

****** FILENAME ****** : JAN11C6A

**** Bubbles detected by probe 1 : 464
**** Percentage of bubbles retained : 31.68
**** Average bubble duration : .006184 s

Probability Distributions

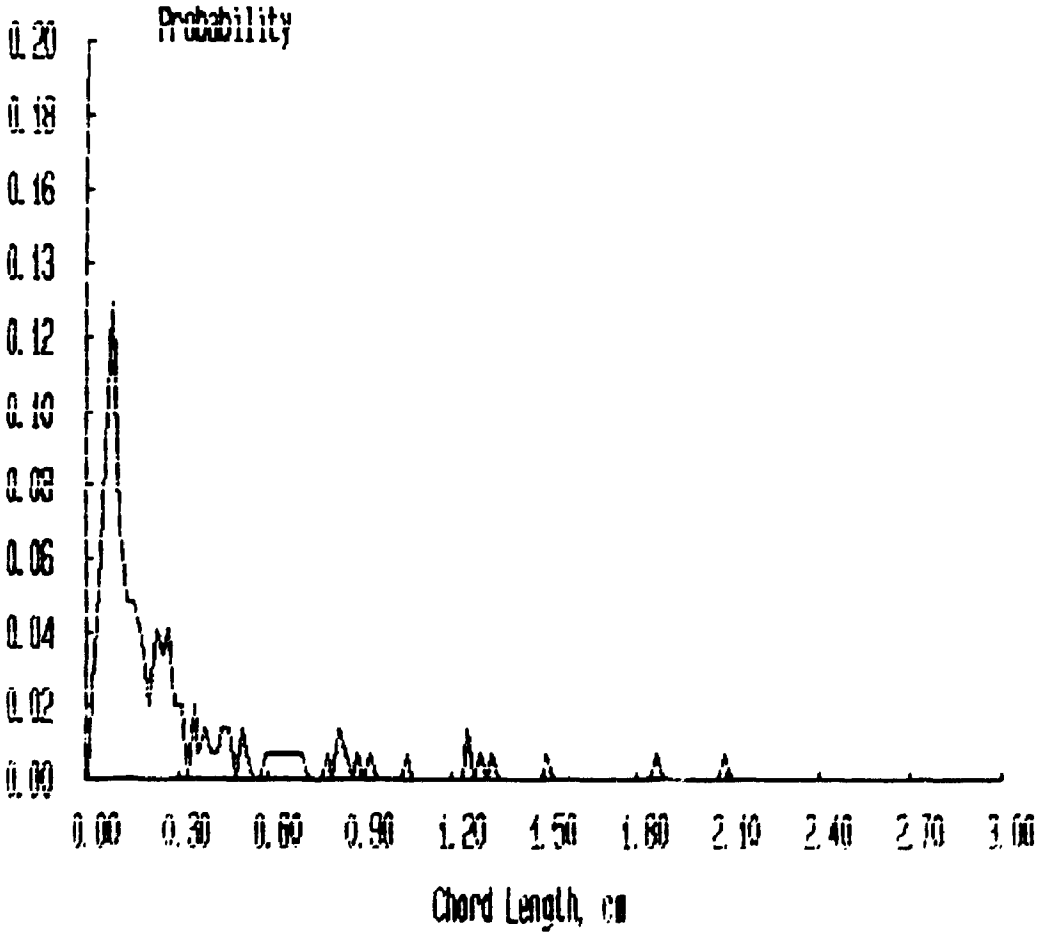

****** FILENAME ****** : JAN11D1A

**** Bubbles detected by probe 1 : 1221
**** Percentage of bubbles retained : 55.94
**** Average bubble duration : .005899 s

Probability Distributions

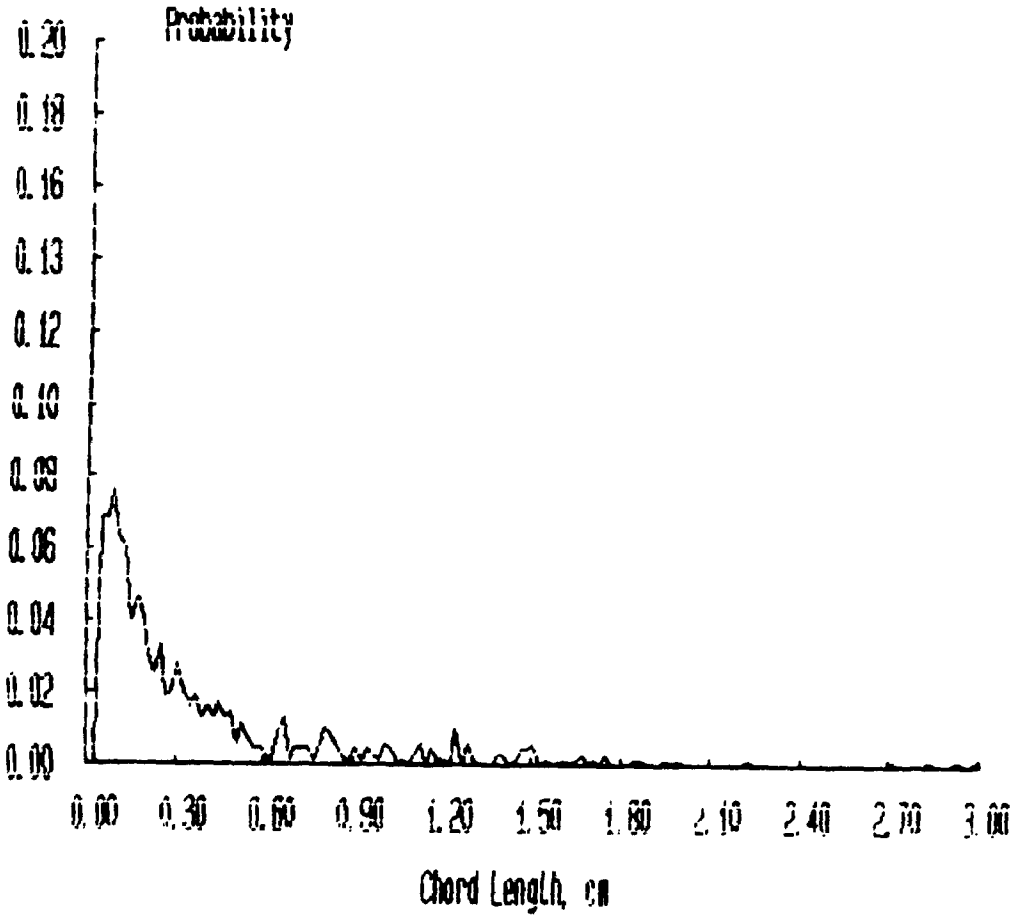

****** FILENAME ****** : JAN11D2A

**** Bubbles detected by probe 1 : 1214
**** Percentage of bubbles retained : 50.25
**** Average bubble duration : .005995 s

Probability Distributions

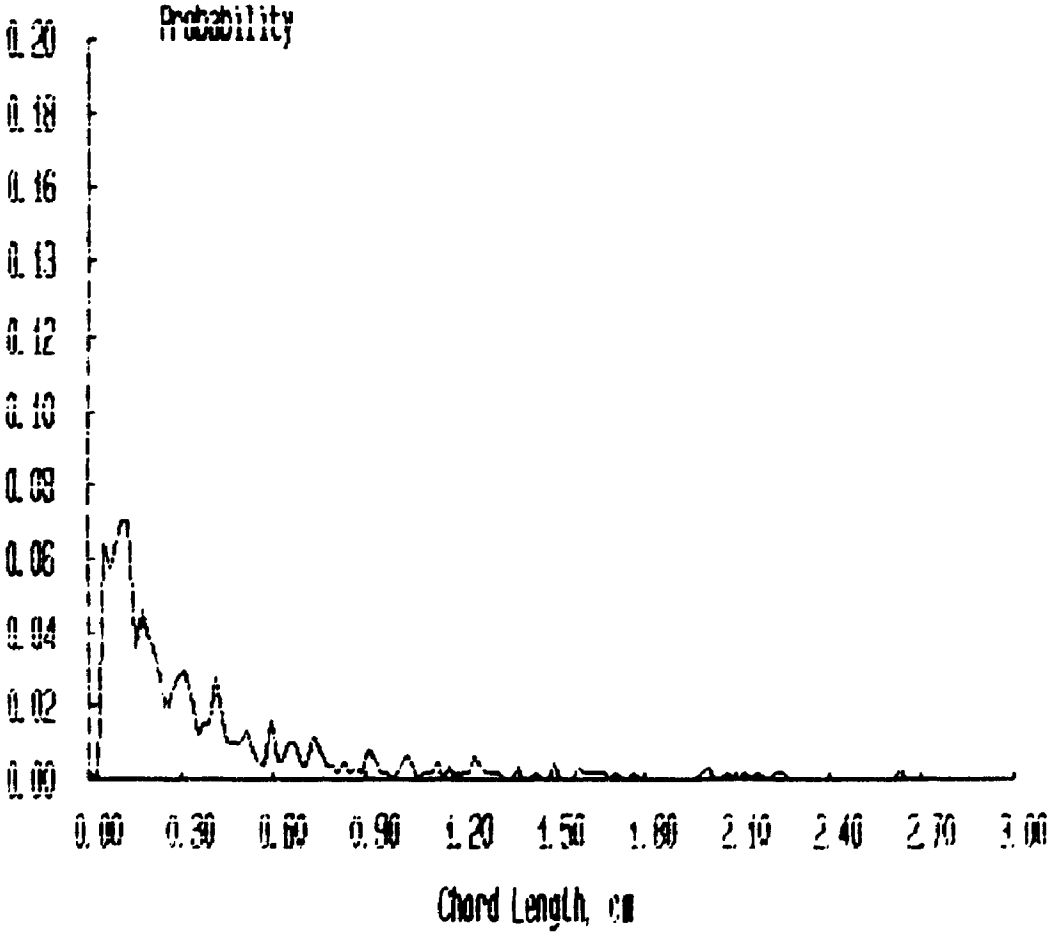

****** FILENAME ****** : JAN11D3A

**** Bubbles detected by probe 1 : 1119
**** Percentage of bubbles retained : 44.24
**** Average bubble duration : .006228 s

Probability Distributions

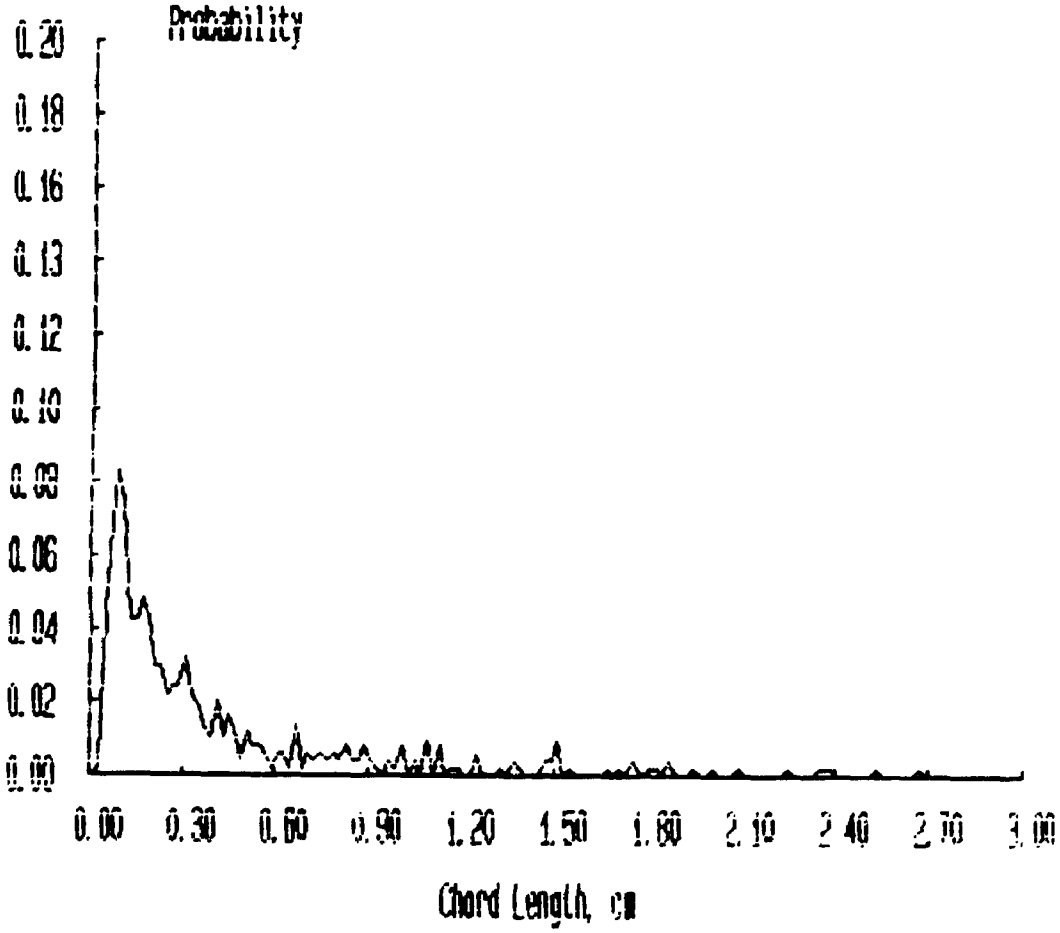

****** FILENAME ****** : JAN11D4A

**** Bubbles detected by probe 1 : 847
**** Percentage of bubbles retained : 411.97
**** Average bubble duration : .005562 s

Probability Distributions

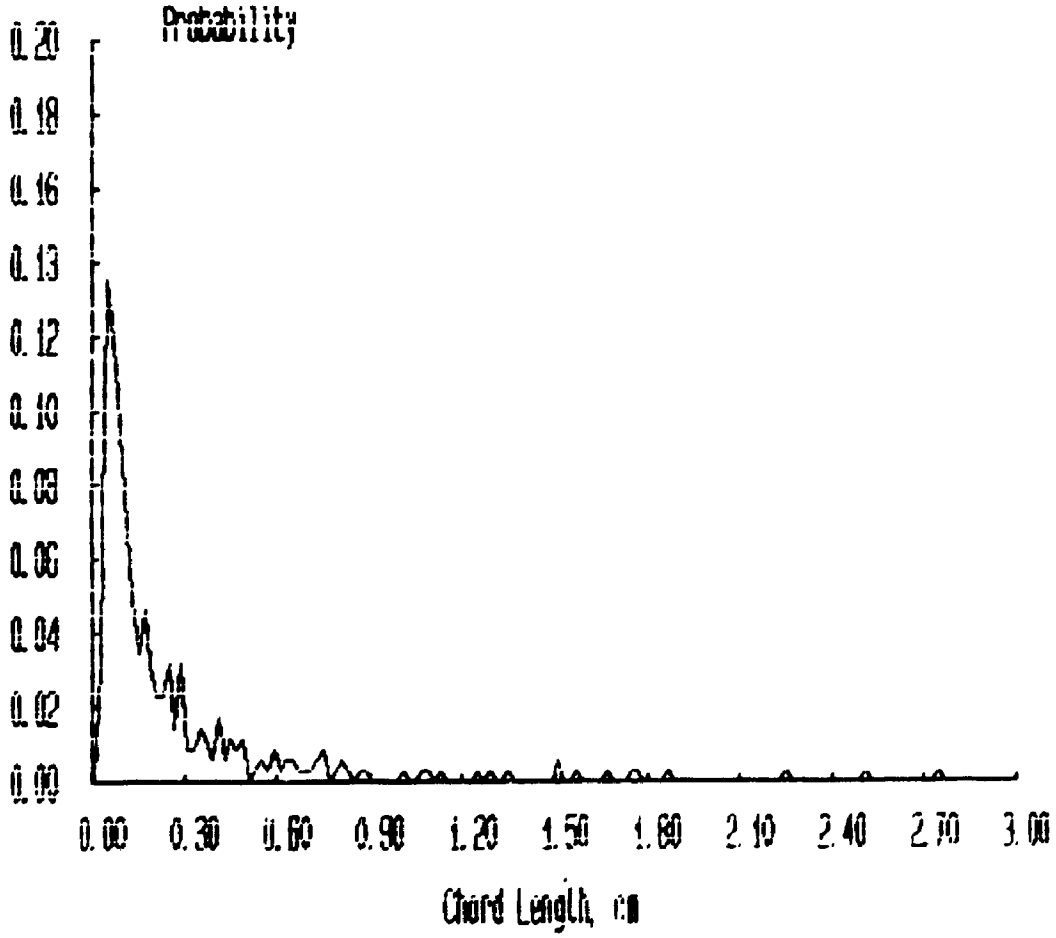

****** FILENAME ****** : JAN11D5A

**** Bubbles detected by probe 1 : 538
**** Percentage of bubbles retained : 37.36
**** Average bubble duration : .005259 s

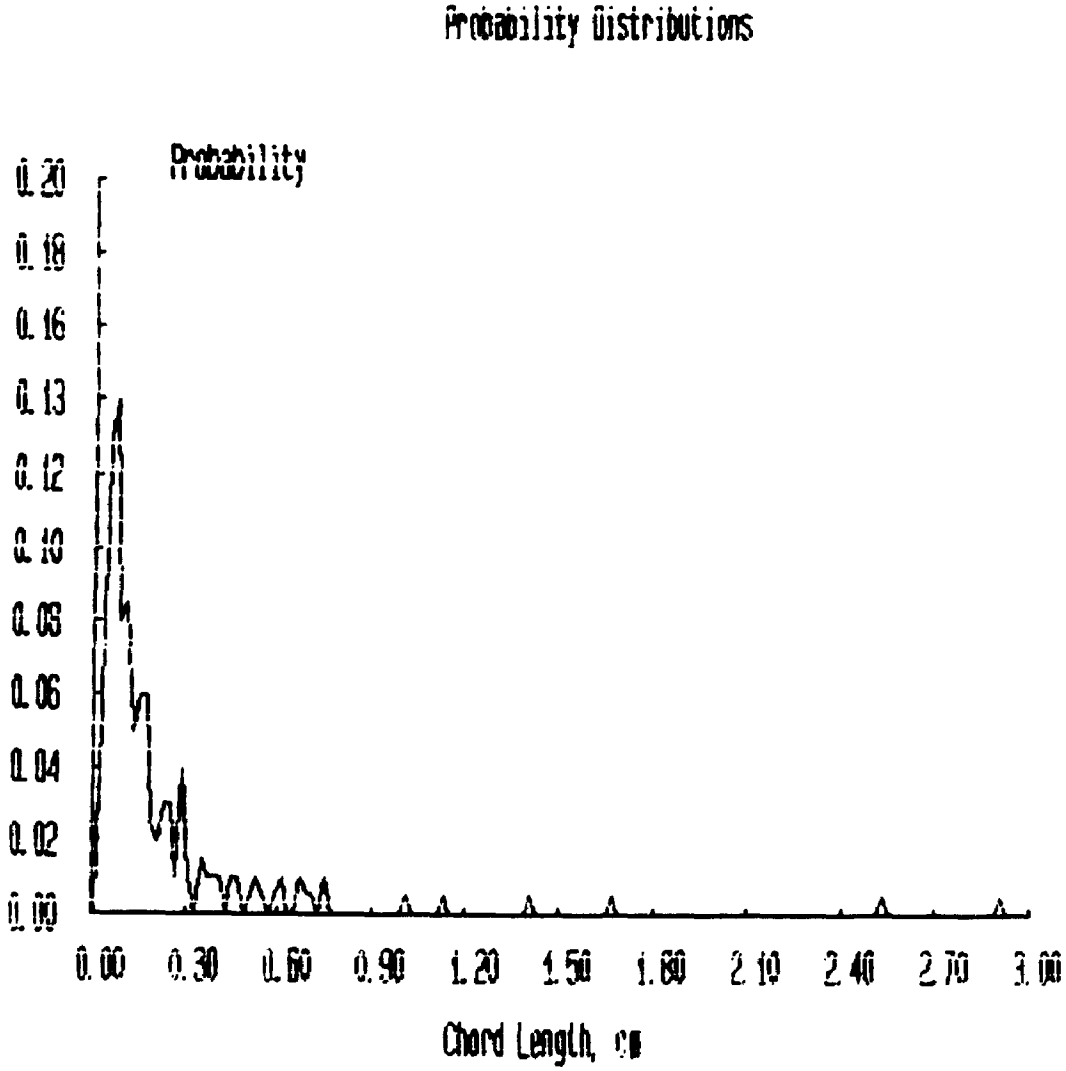

****** FILENAME ****** : JAN11D6A

**** Bubbles detected by probe 1 : 601
**** Percentage of bubbles retained : 41.10
**** Average bubble duration : .004640 s

Probability Distributions

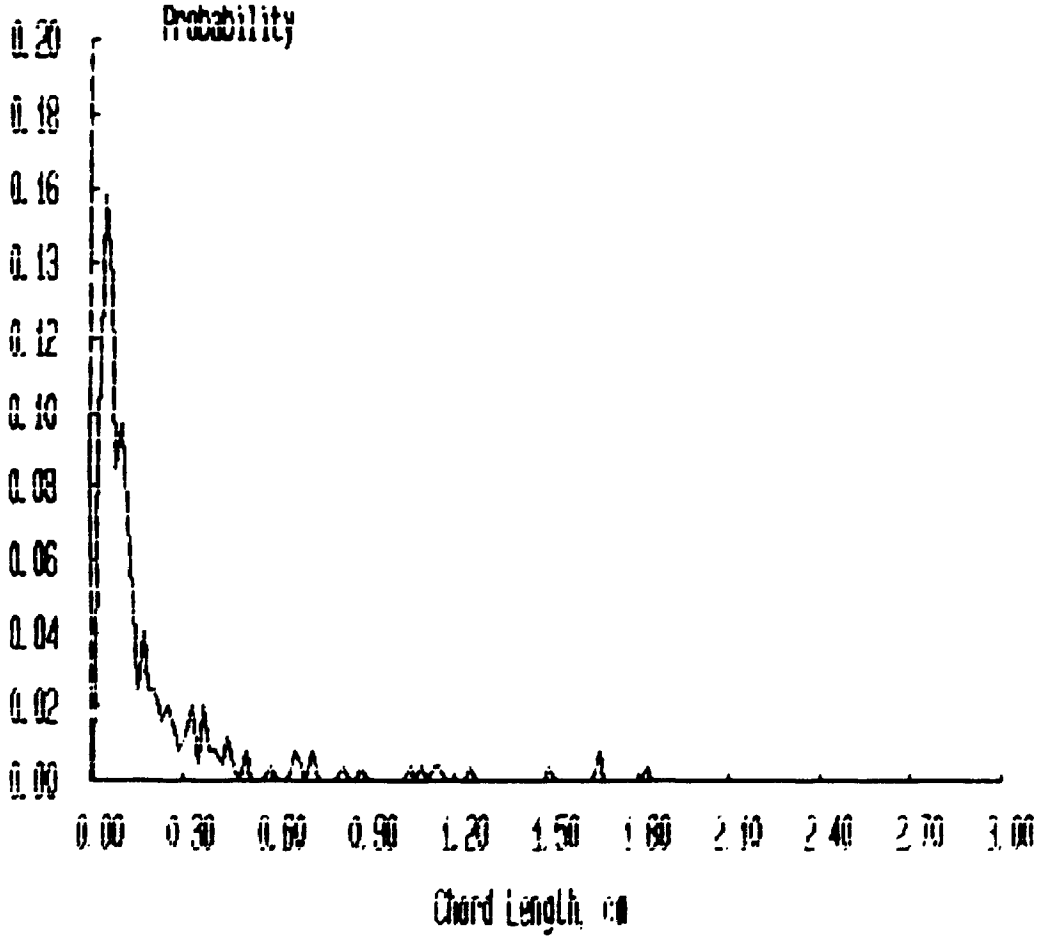

****** FILENAME ****** : JAN11E1A

**** Bubbles detected by probe 1 : 1561
**** Percentage of bubbles retained : 57.08
**** Average bubble duration : .005617 s

Probability Distributions

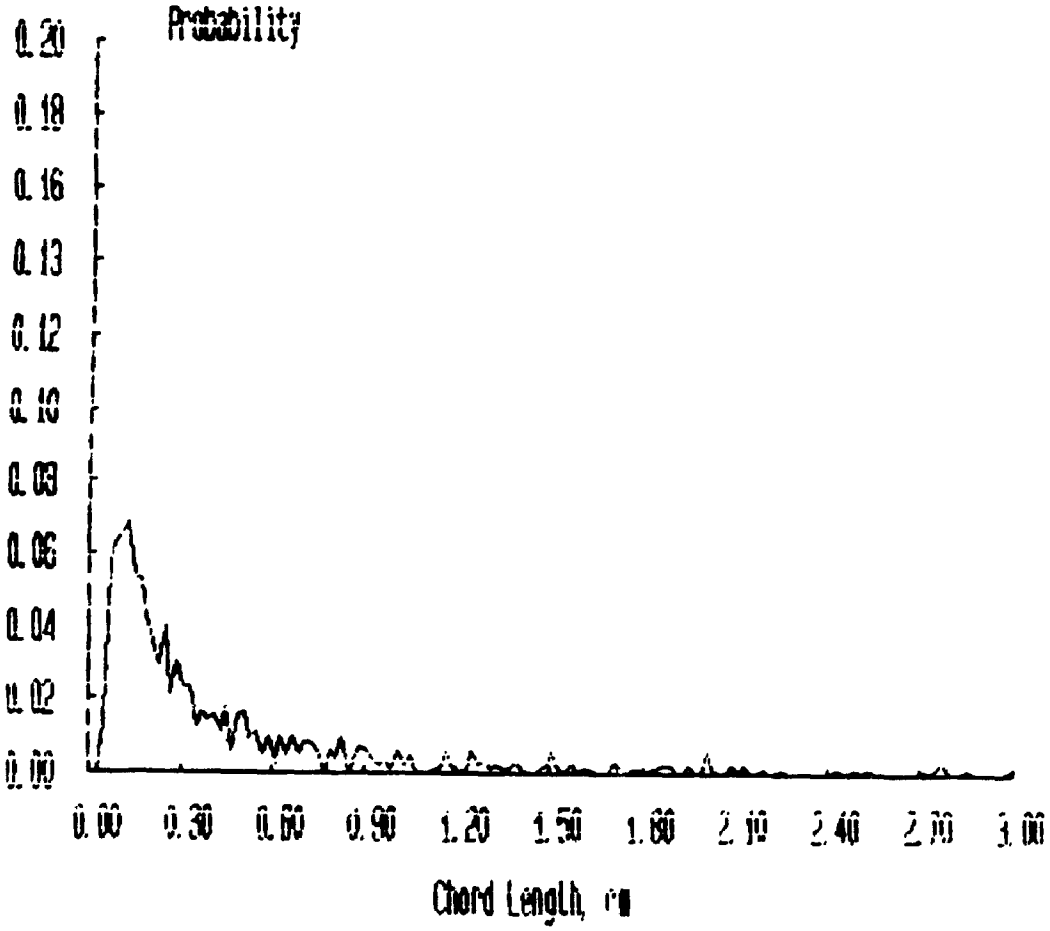

****** FILENAME ****** : JAN11E2A

**** Bubbles detected by probe 1 : 1513
**** Percentage of bubbles retained : 53.34
**** Average bubble duration : .005865 s

Probability Distributions

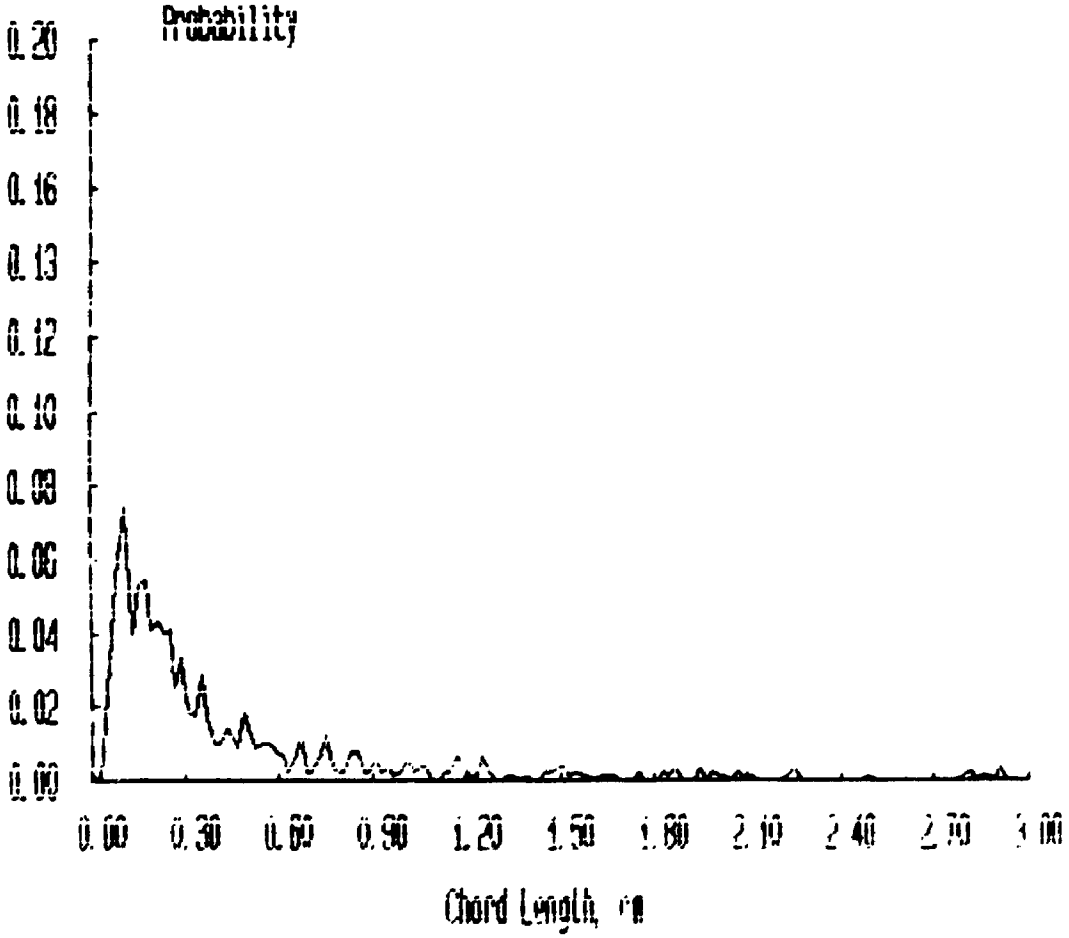

****** FILENAME ****** : JAN1163A

**** Bubbles detected by probe 1 : 1112
**** Percentage of bubbles retained : 51.53
**** Average bubble duration : .005274 s

Probability Distributions

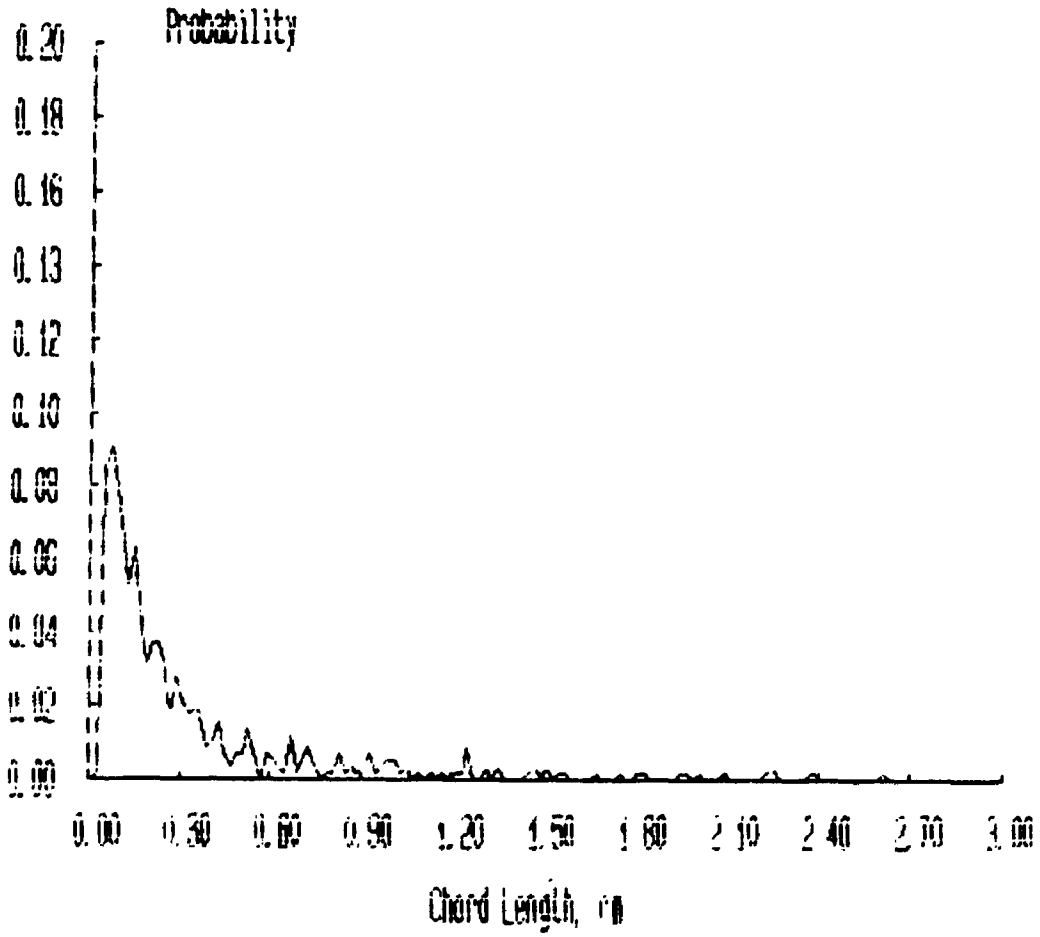

****** FILENAME ****** : JAN11E4A

**** Bubbles detected by probe 1 : 814
**** Percentage of bubbles retained : 40.66
**** Average bubble duration : .005767 s

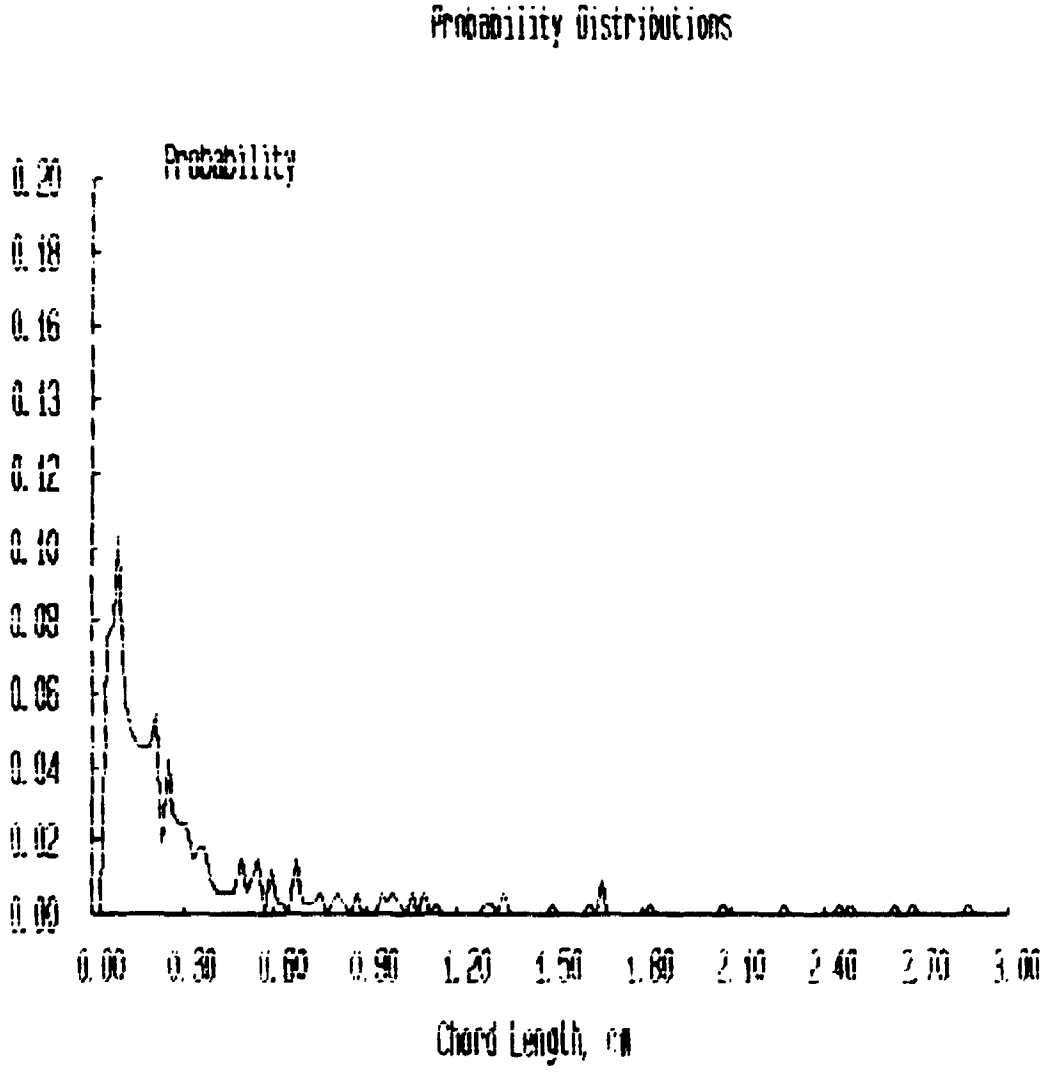

****** FILENAME ****** : JAN11E5A

**** Bubbles detected by probe 1 : 487
**** Percentage of bubbles retained : 47.43
**** Average bubble duration : .004831 s

Probability Distributions

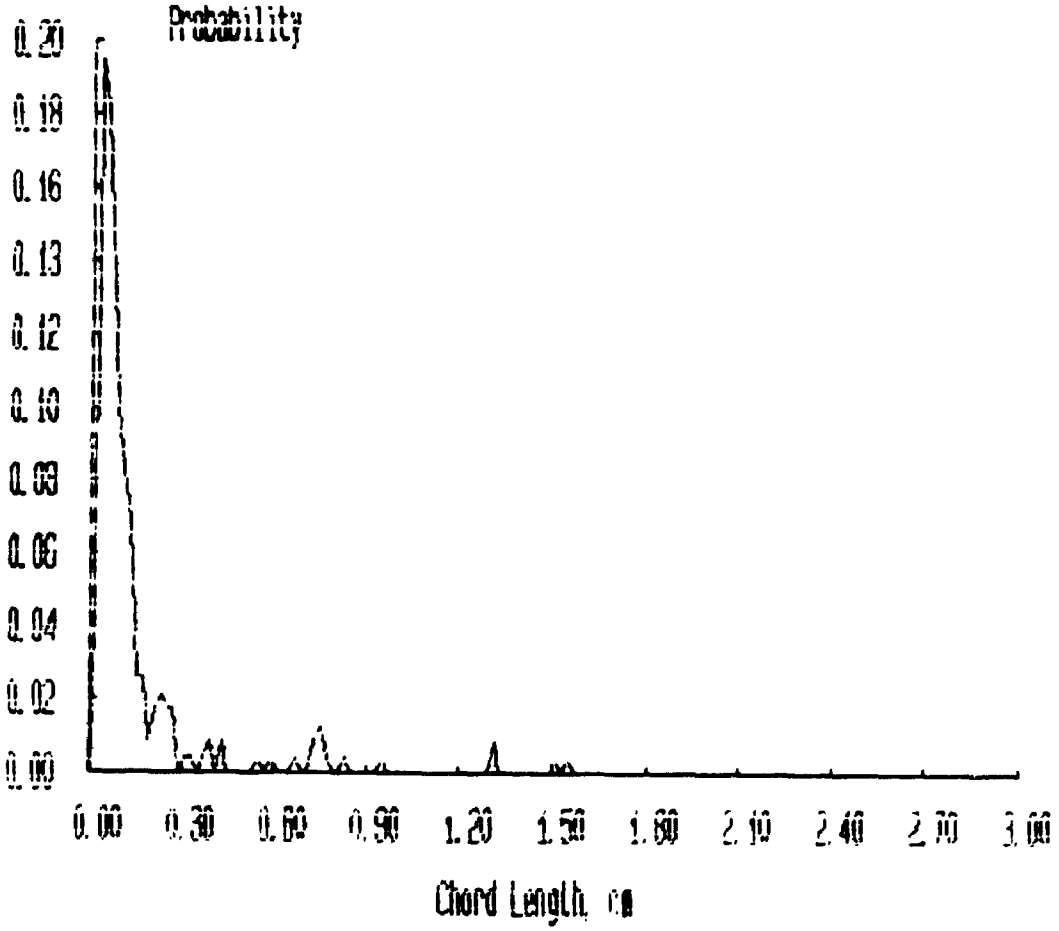

****** FILENAME ****** : JAN11E6A

**** Bubbles detected by probe 1 : 495
**** Percentage of bubbles retained : 41.82
**** Average bubble duration : .005290 s

Probability Distributions

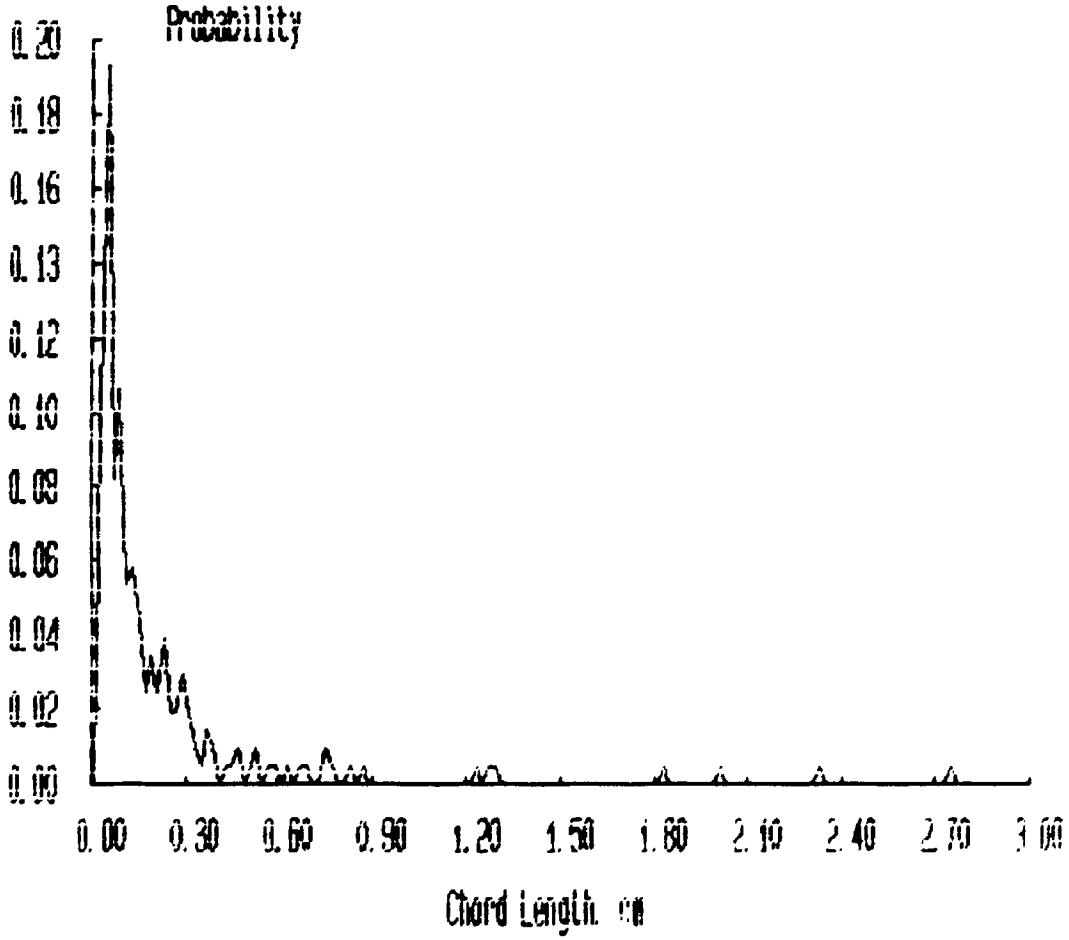

****** FILENAME ****** : JAN13A1U

**** Bubbles detected by probe 1 : 858
**** Percentage of bubbles retained : 50.82
**** Average bubble duration : .006640 s

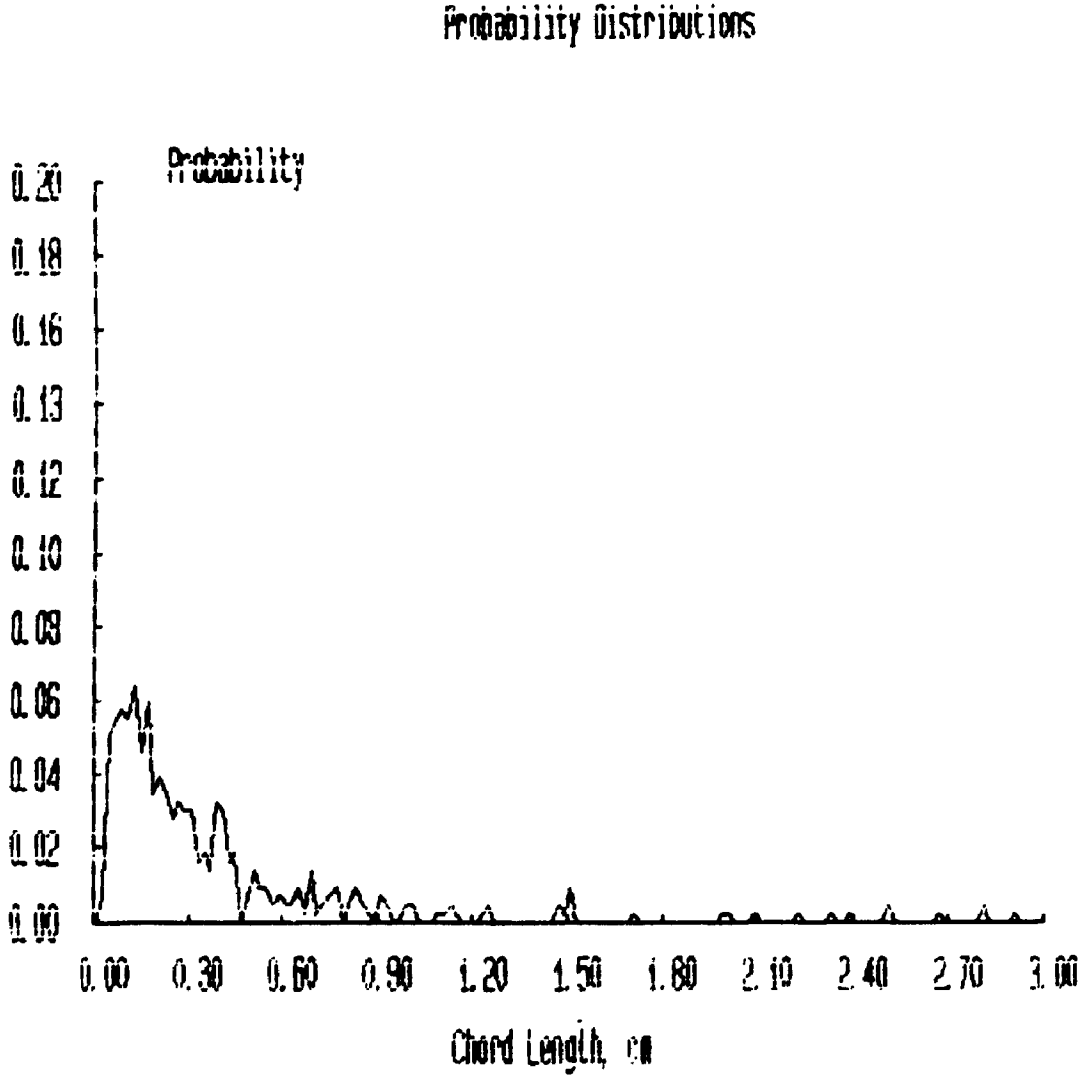

****** FILENAME ****** : JAN13A2A

**** Bubbles detected by probe 1 : 840
**** Percentage of bubbles retained : 50.00
**** Average bubble duration : .006529 s

Probability Distributions

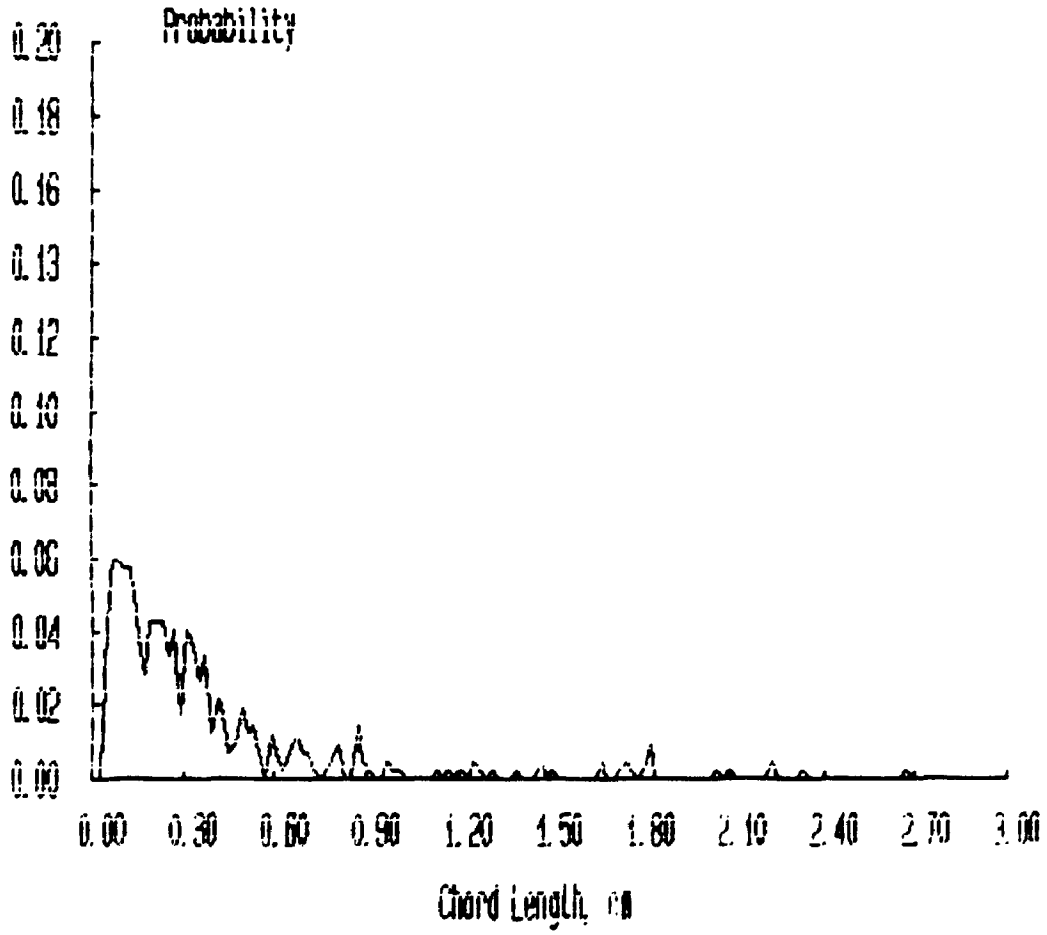

666

****** FILENAME ****** : JAN13A3A

**** Bubbles detected by probe 1 : 526
**** Percentage of bubbles retained : 42.59
**** Average bubble duration : .006058 s

Probability Distributions

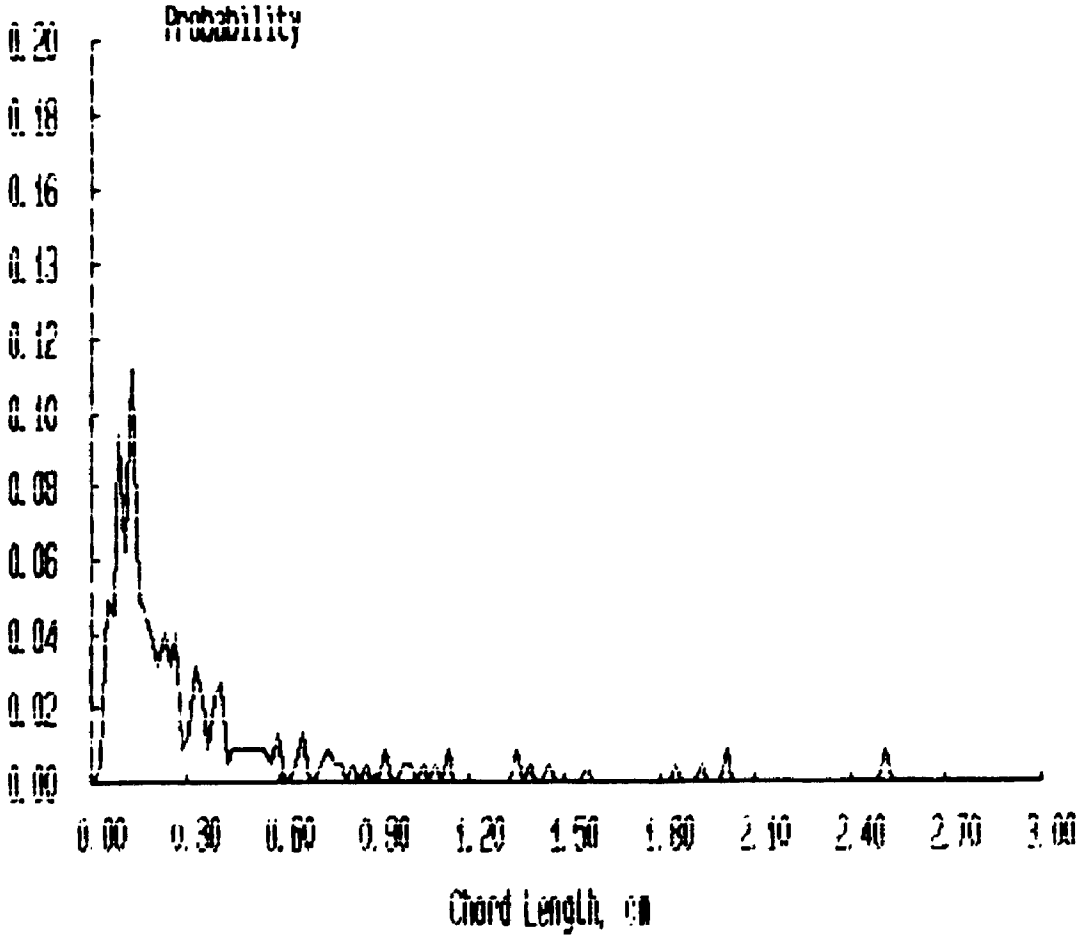

****** FILENAME ****** : JAN13A4A

**** Bubbles detected by probe 1 : 458
**** Percentage of bubbles retained : 40.39
**** Average bubble duration : .005649 s

Probability Distributions

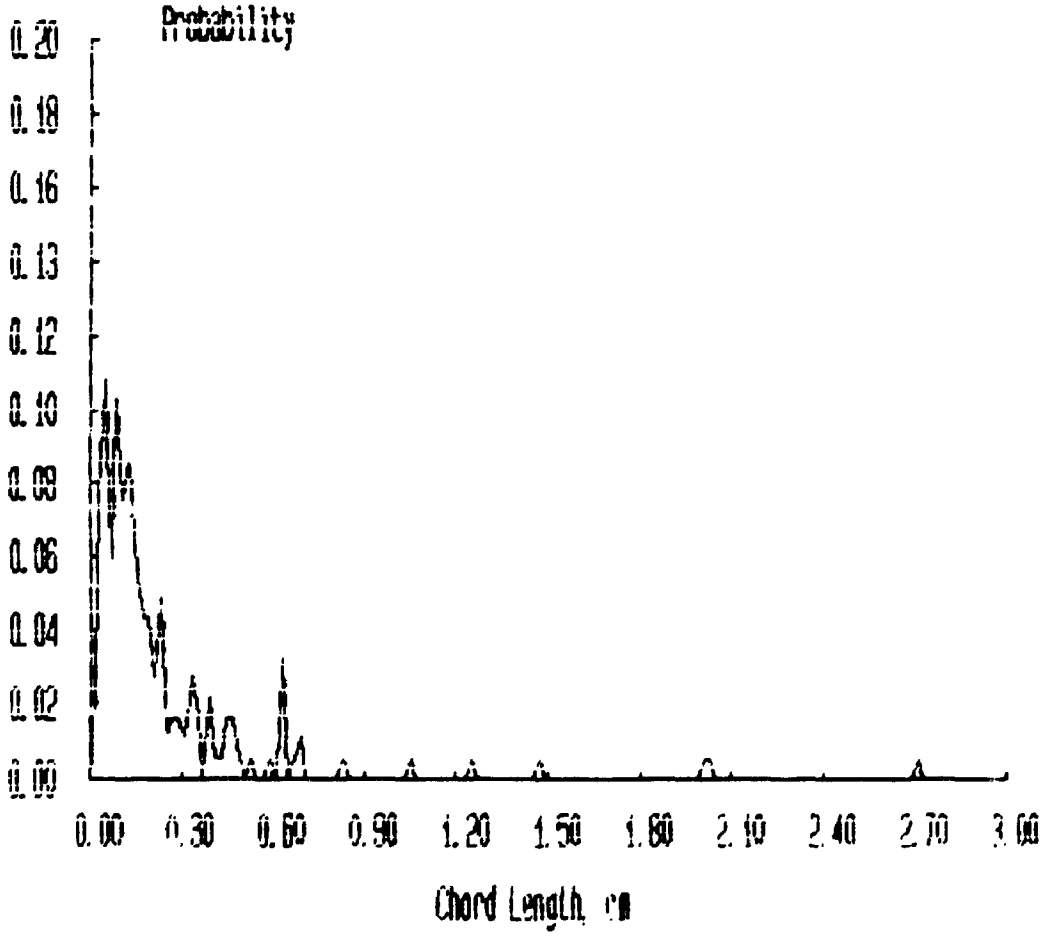

****** FILENAME ****** : JAN13A5A

**** Bubbles detected by probe 1 : 595
**** Percentage of bubbles retained : 35.95
**** Average bubble duration : .005831 s

Probability Distributions

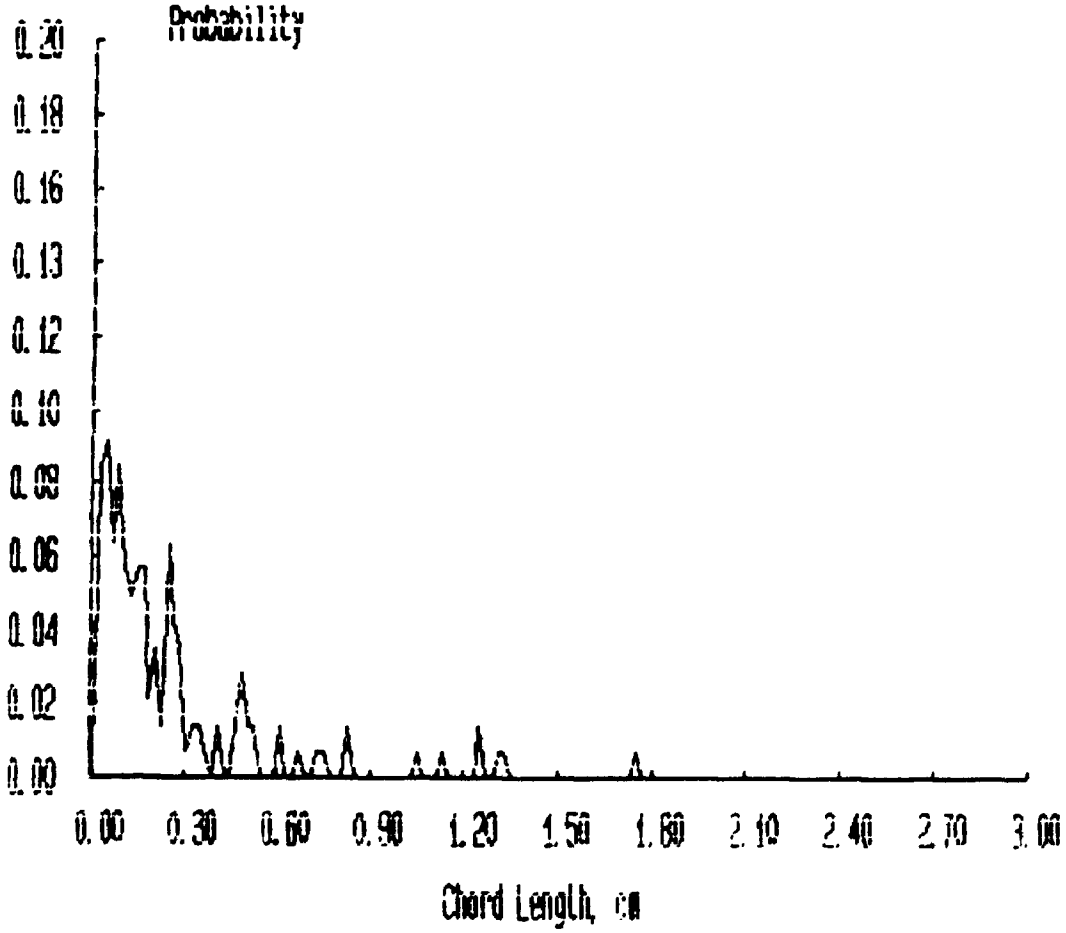

****** FILENAME ****** : JAN13A6A

**** Bubbles detected by probe 1 : 598
**** Percentage of bubbles retained : 41.34
**** Average bubble duration : .006797 s

Probability Distributions

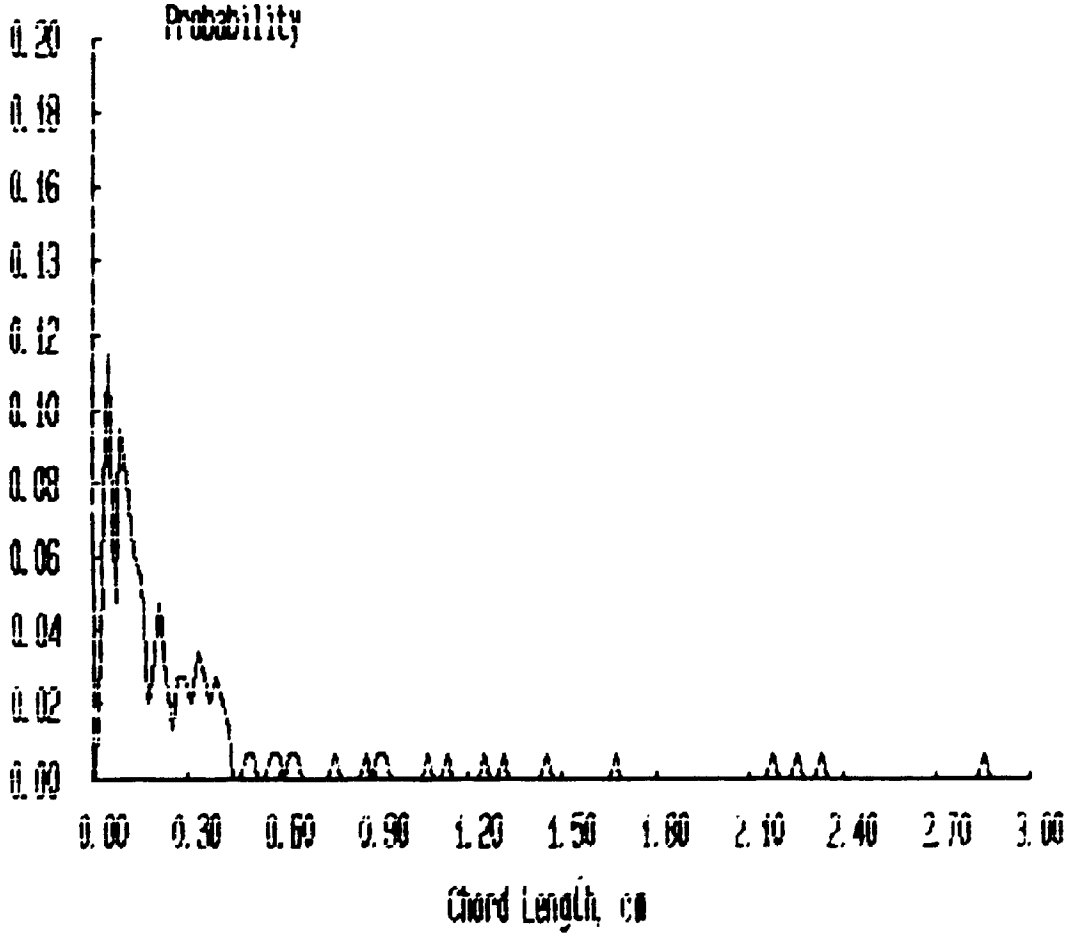

620

****** FILENAME ****** : JAN13B1A

**** Bubbles detected by probe 1 : 629
**** Percentage of bubbles retained : 51.99
**** Average bubble duration : .006433 s

Probability Distributions

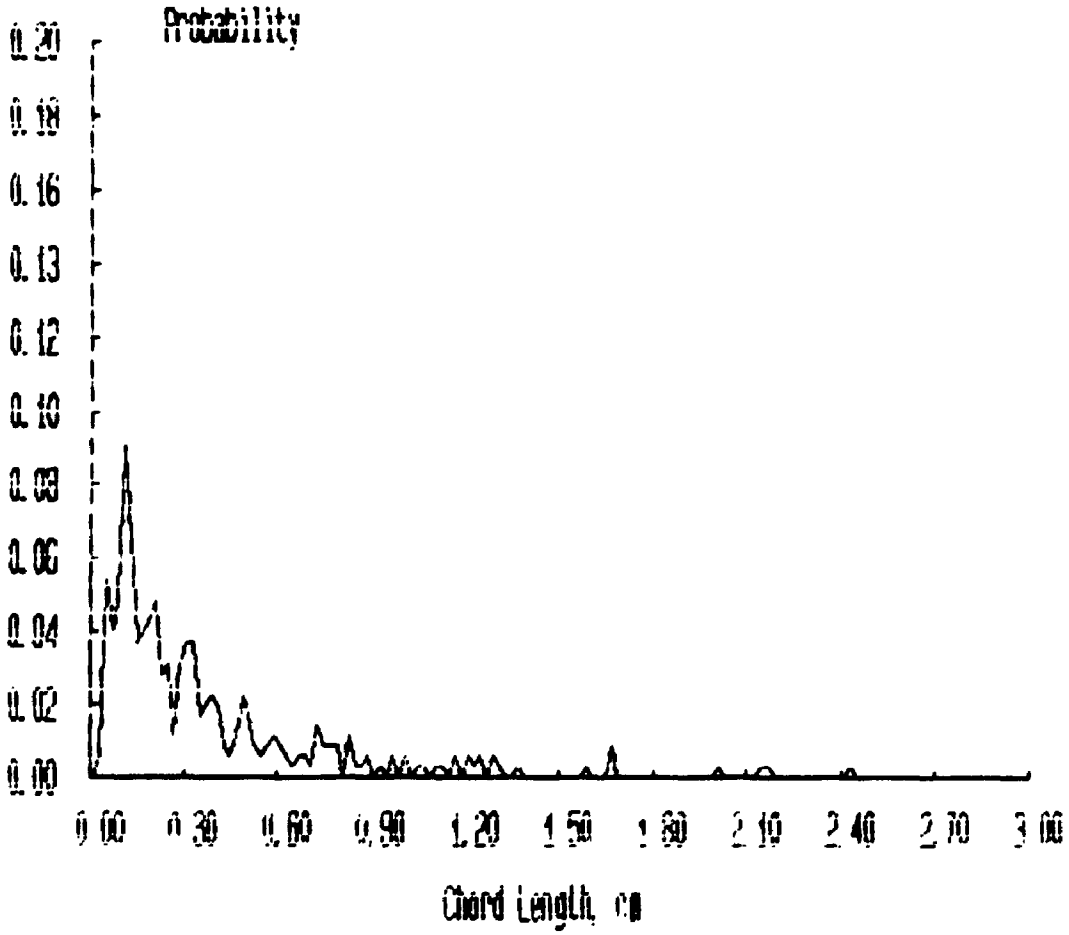

****** FILENAME ****** : JAN13B2A

**** Bubbles detected by probe 1 : 657
**** Percentage of bubbles retained : 41.29
**** Average bubble duration : .006605 s

Probability Distributions

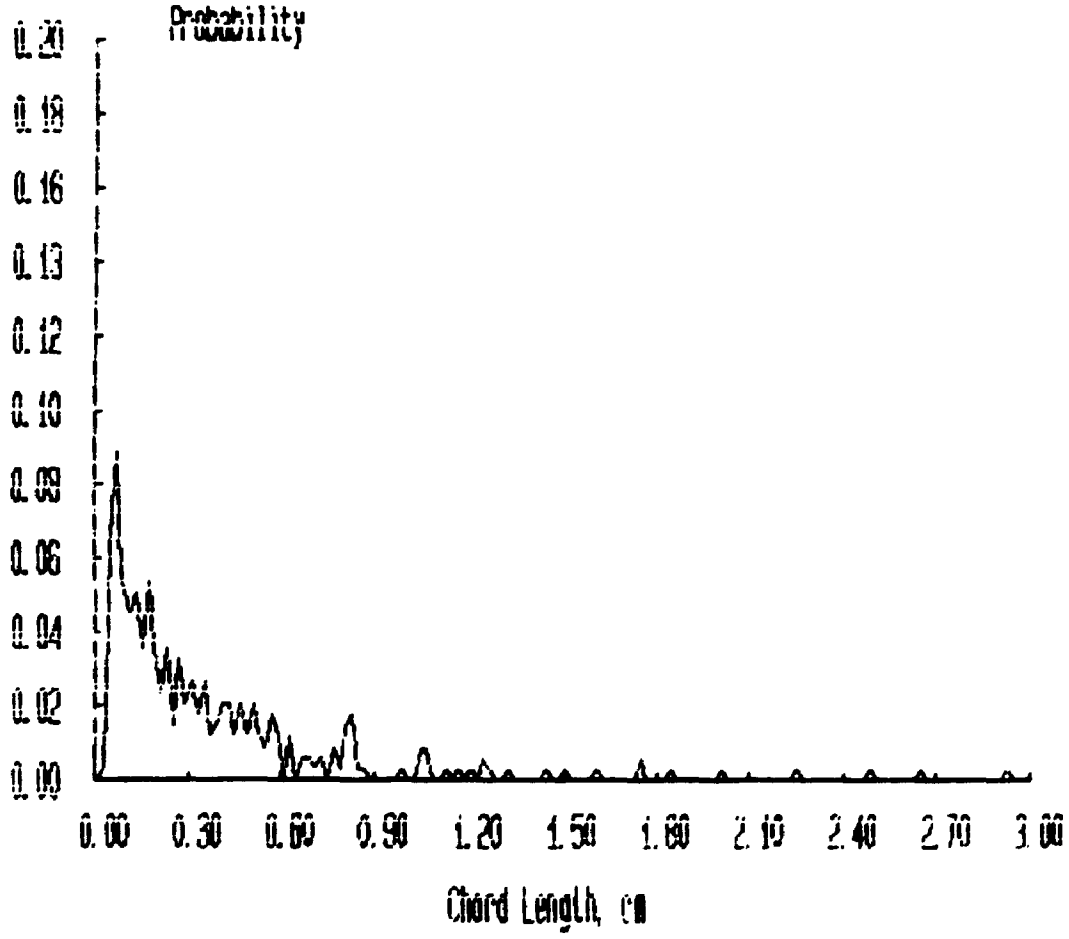

****** FILENAME ****** : JAN1383A

**** Bubbles detected by probe 1 : 490
**** Percentage of bubbles retained : 45.10
**** Average bubble duration : .006538 s

Probability Distributions

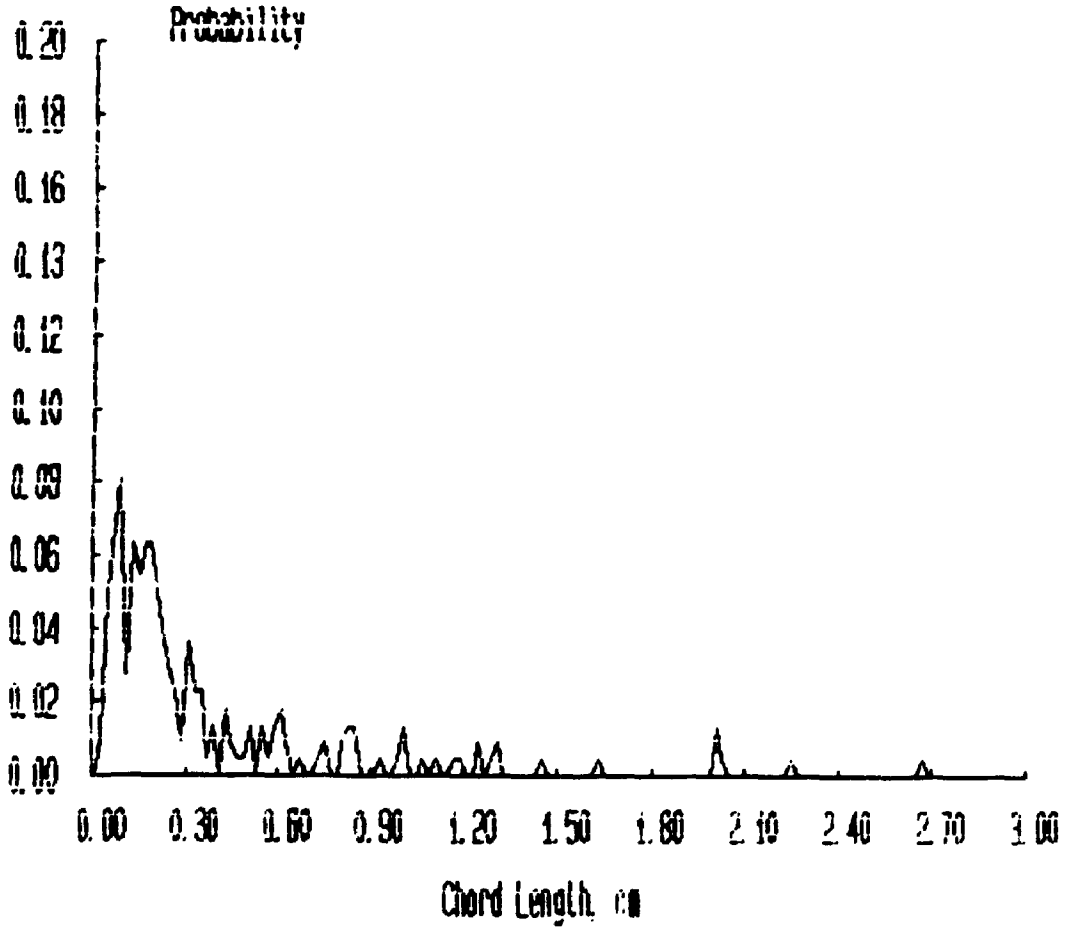

623

****** FILENAME ****** : JAN13B4A

**** Bubbles detected by probe 1 : 441
**** Percentage of bubbles retained : 35.37
**** Average bubble duration : .006865 s

Probability Distributions

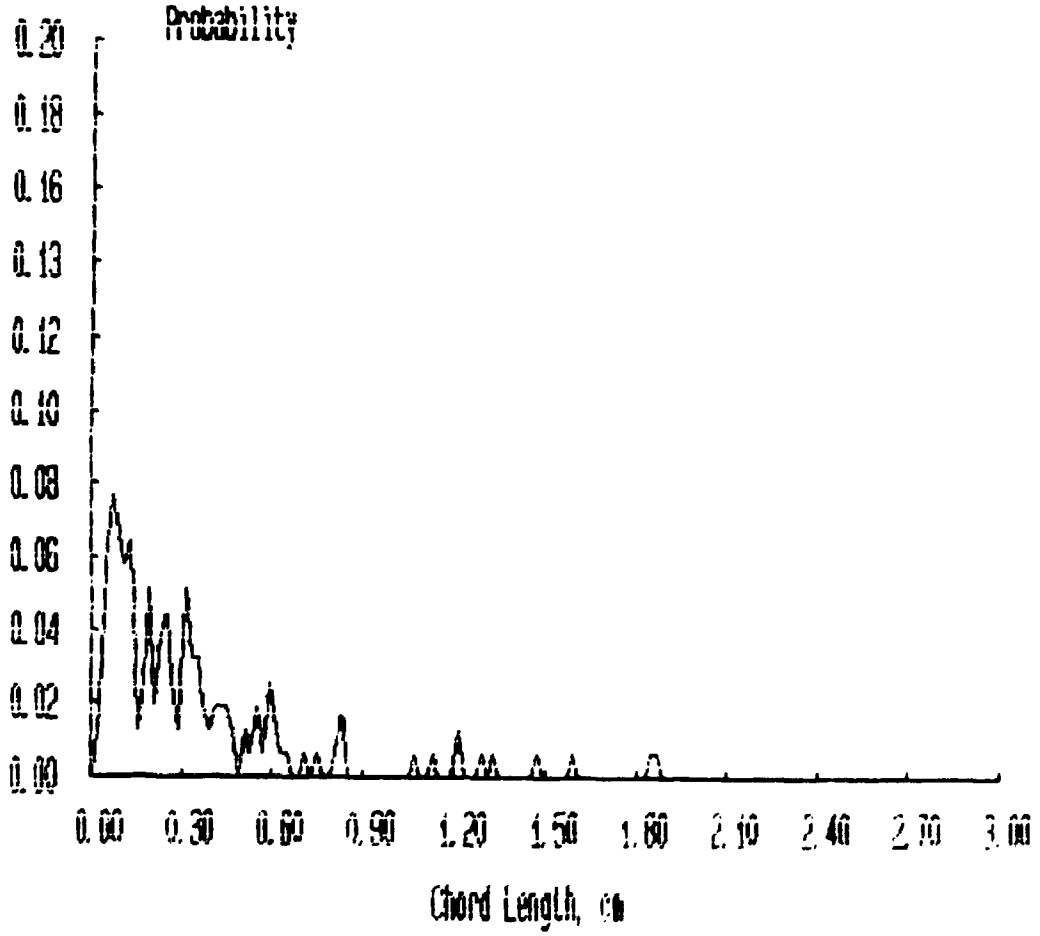

****** FILENAME ****** : JAN13B5A

**** Bubbles detected by probe 1 : 349
**** Percentage of bubbles retained : 31.23
**** Average bubble duration : .007569 s

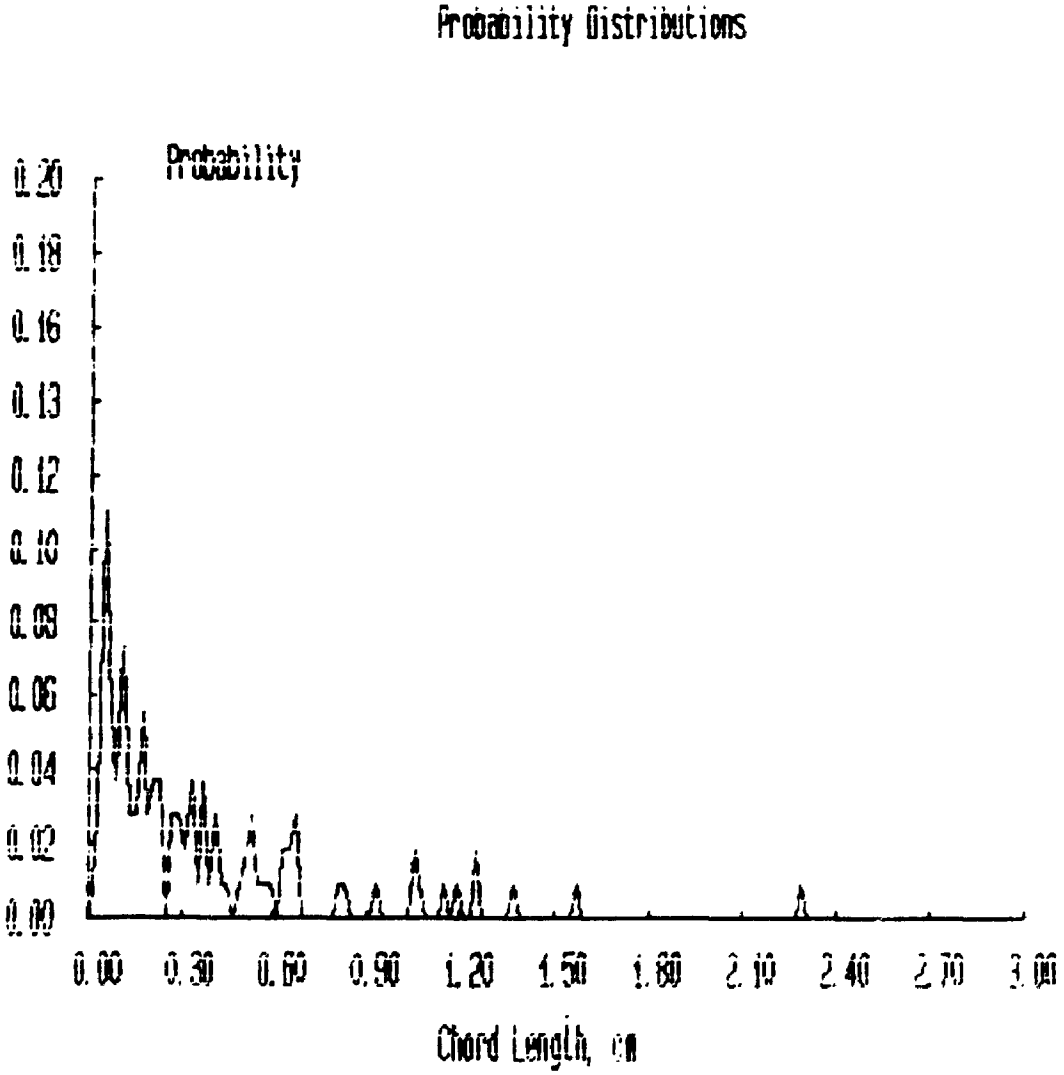

****** FILENAME ****** : JAN13B6A

**** Bubbles detected by probe 1 : 297
**** Percentage of bubbles retained : 35.02
**** Average bubble duration : .006462 s

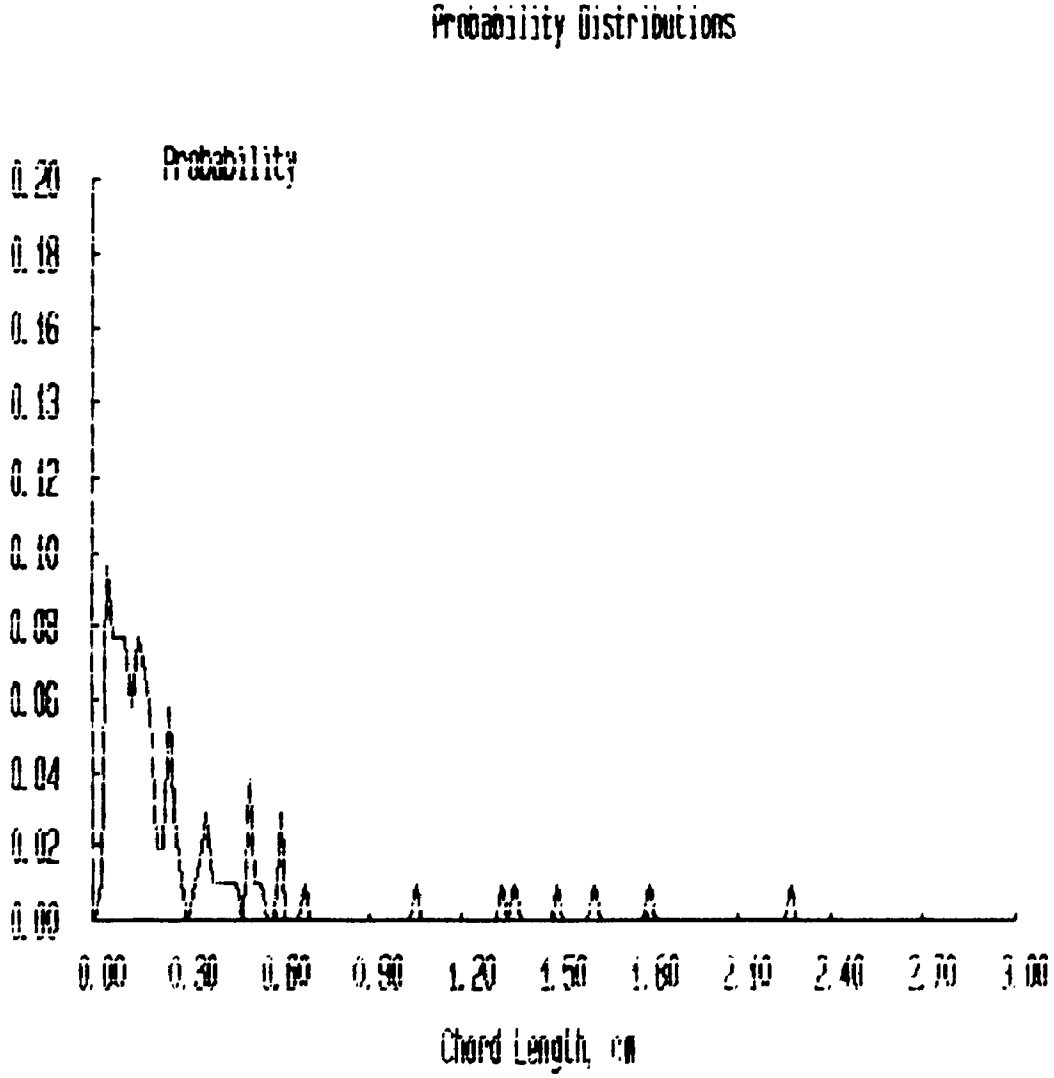

****** FILENAME ****** : JAN13C1A

**** Bubbles detected by probe 1 : 491
**** Percentage of bubbles retained : 49.69
**** Average bubble duration : .007029 s

Probability Distributions

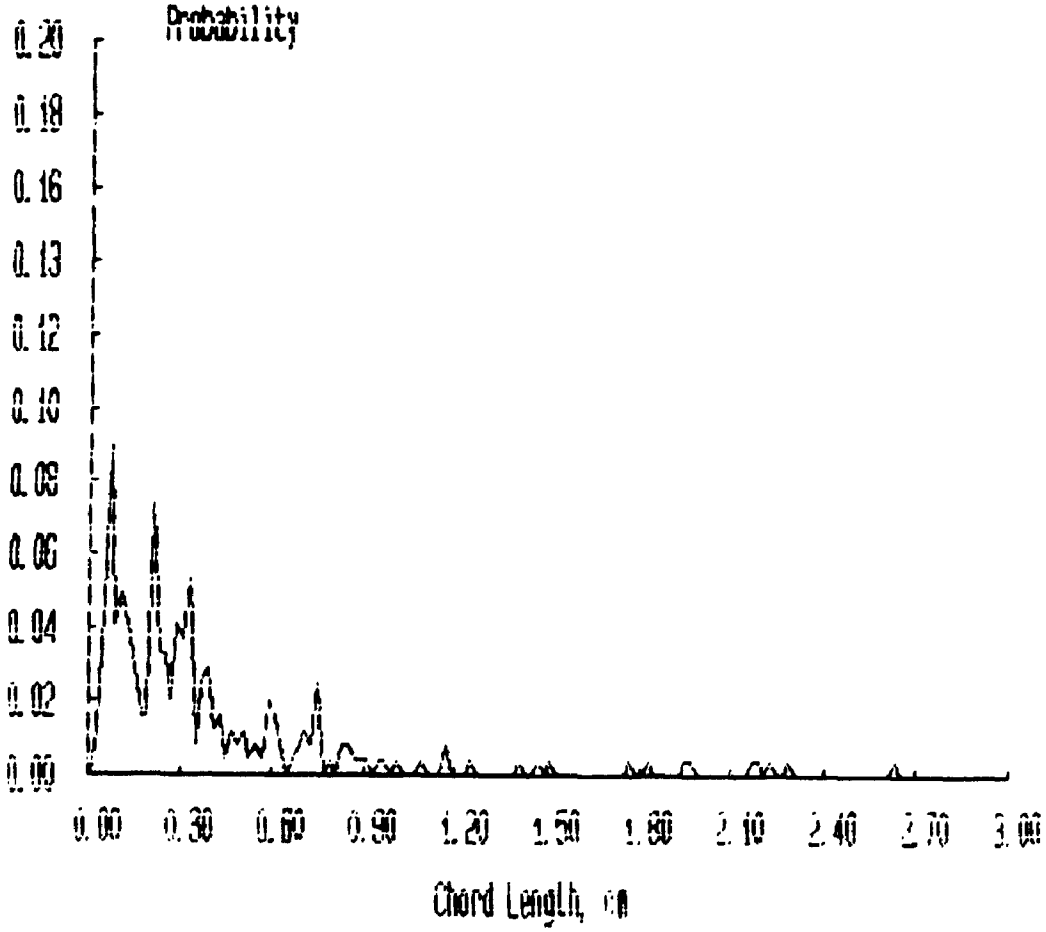

****** FILENAME ****** : JAN13C2A

**** Bubbles detected by probe 1 : 460
**** Percentage of bubbles retained : 46.30
**** Average bubble duration : .007592 s

Probability Distributions

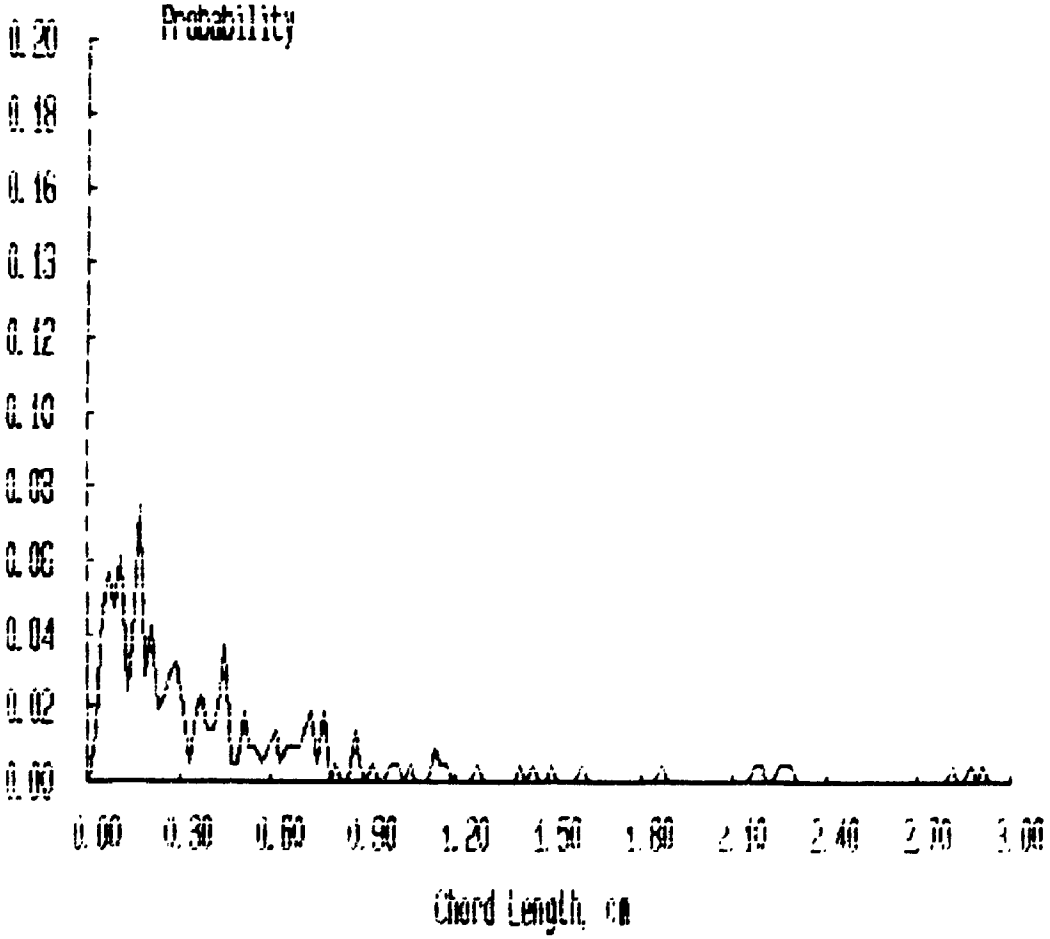

****** FILENAME ****** : JAN13C3A

**** Bubbles detected by probe 1 : 469
**** Percentage of bubbles retained : 41.36
**** Average bubble duration : .007320 s

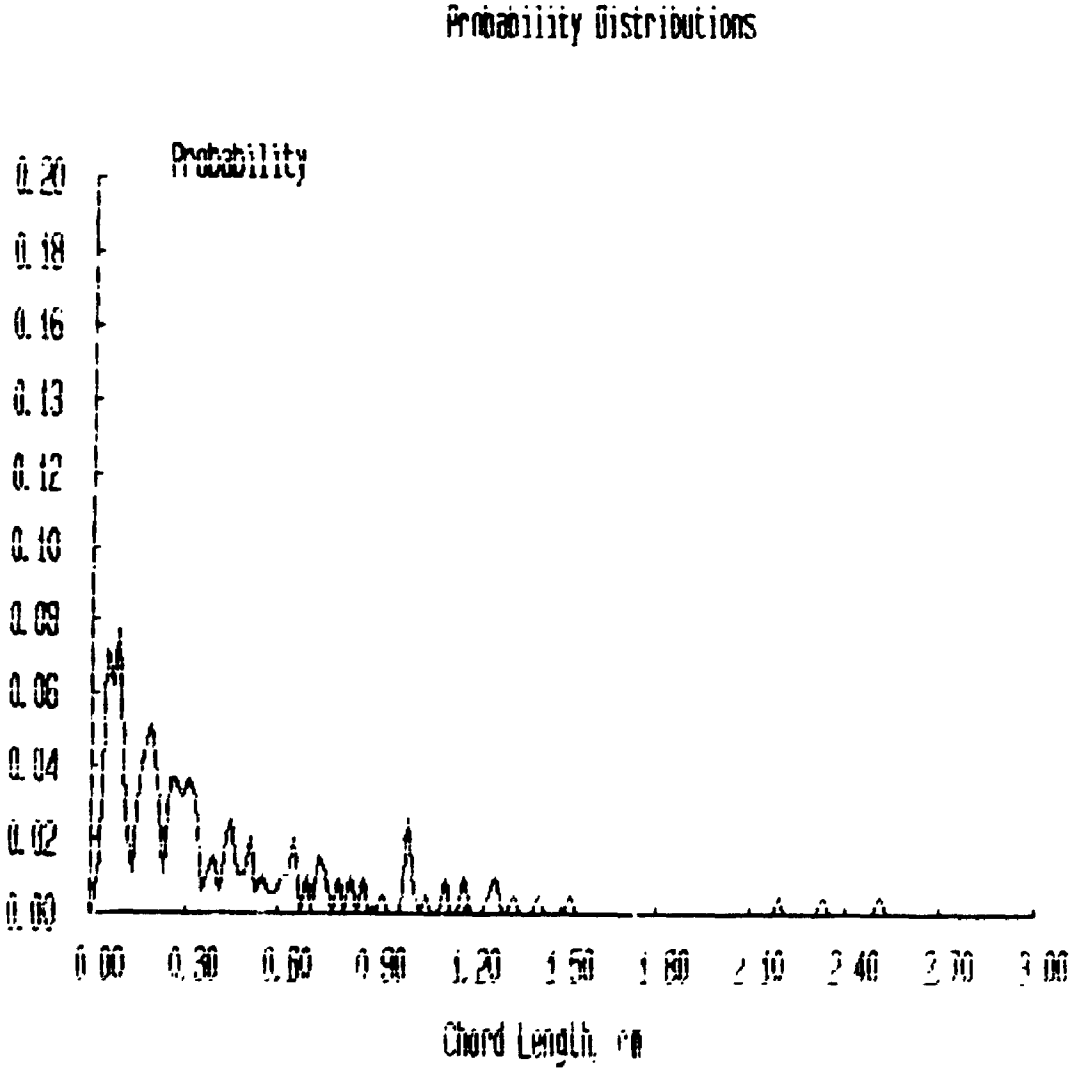

****** FILENAME ****** : JAN13C4A

**** Bubbles detected by probe 1 : 372
**** Percentage of bubbles retained : 33.87
**** Average bubble duration : .007690 s

Probability Distributions

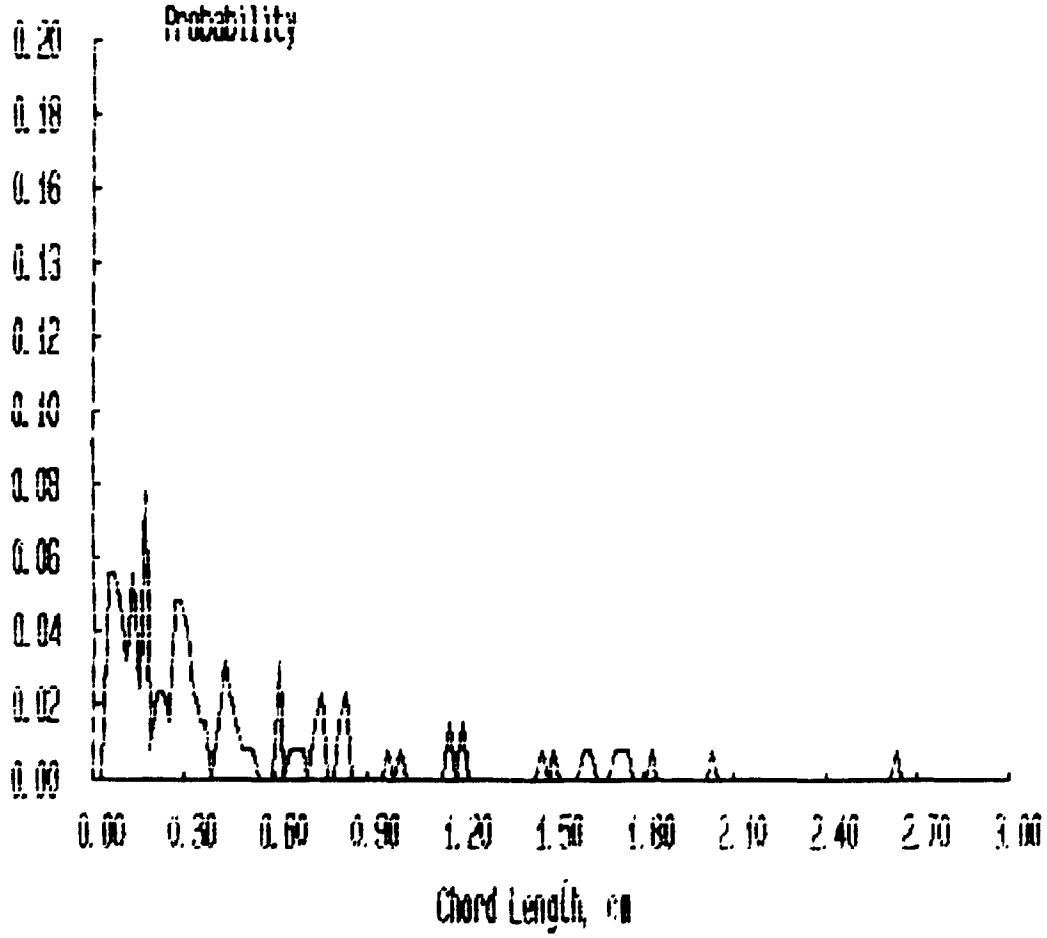

****** FILENAME ****** : JAN13C5A

**** Bubbles detected by probe 1 : 247
**** Percentage of bubbles retained : 32.79
**** Average bubble duration : .008136 s

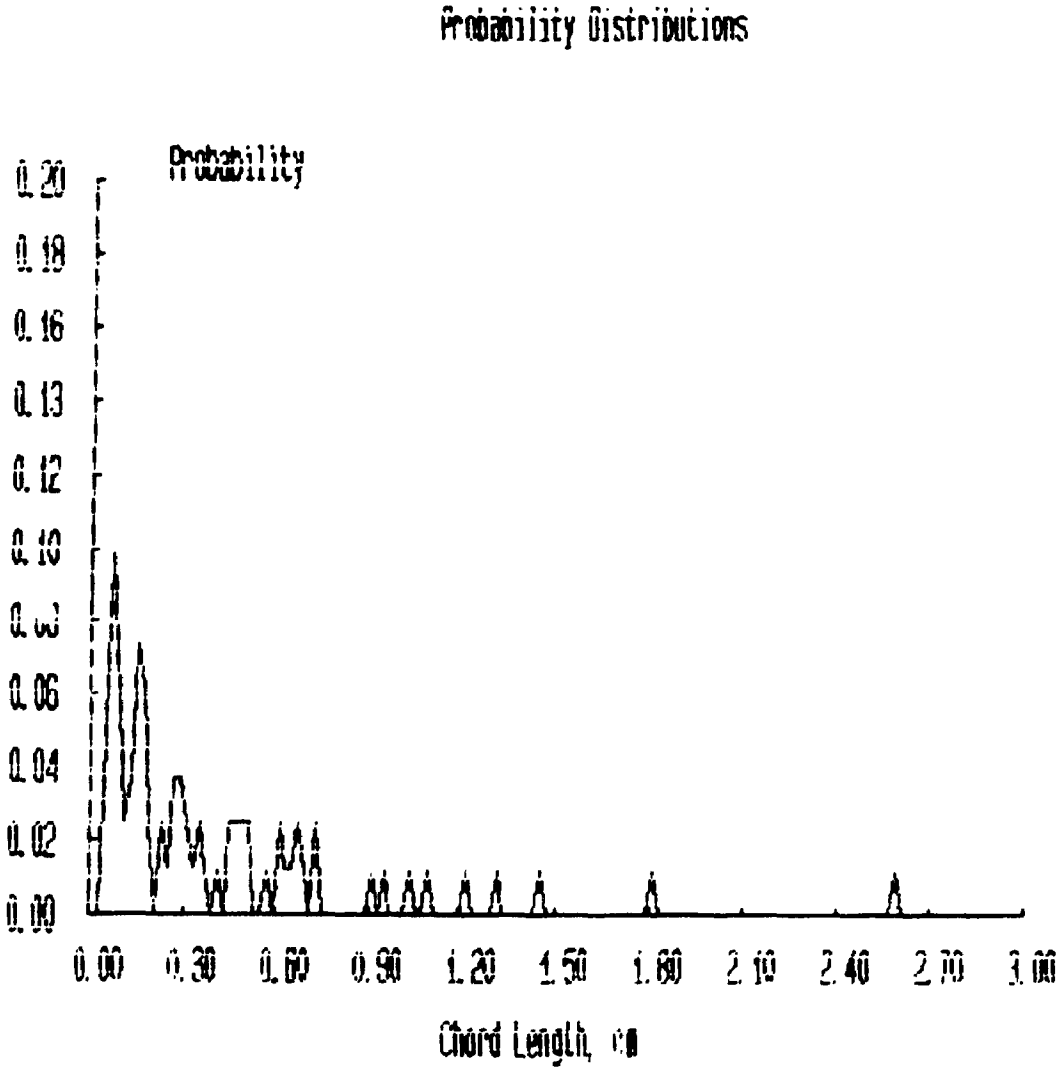

****** FILENAME ****** : JAN13C6A

**** Bubbles detected by probe 1 : 287
**** Percentage of bubbles retained : 36.59
**** Average bubble duration : .002810 s

Probability Distributions

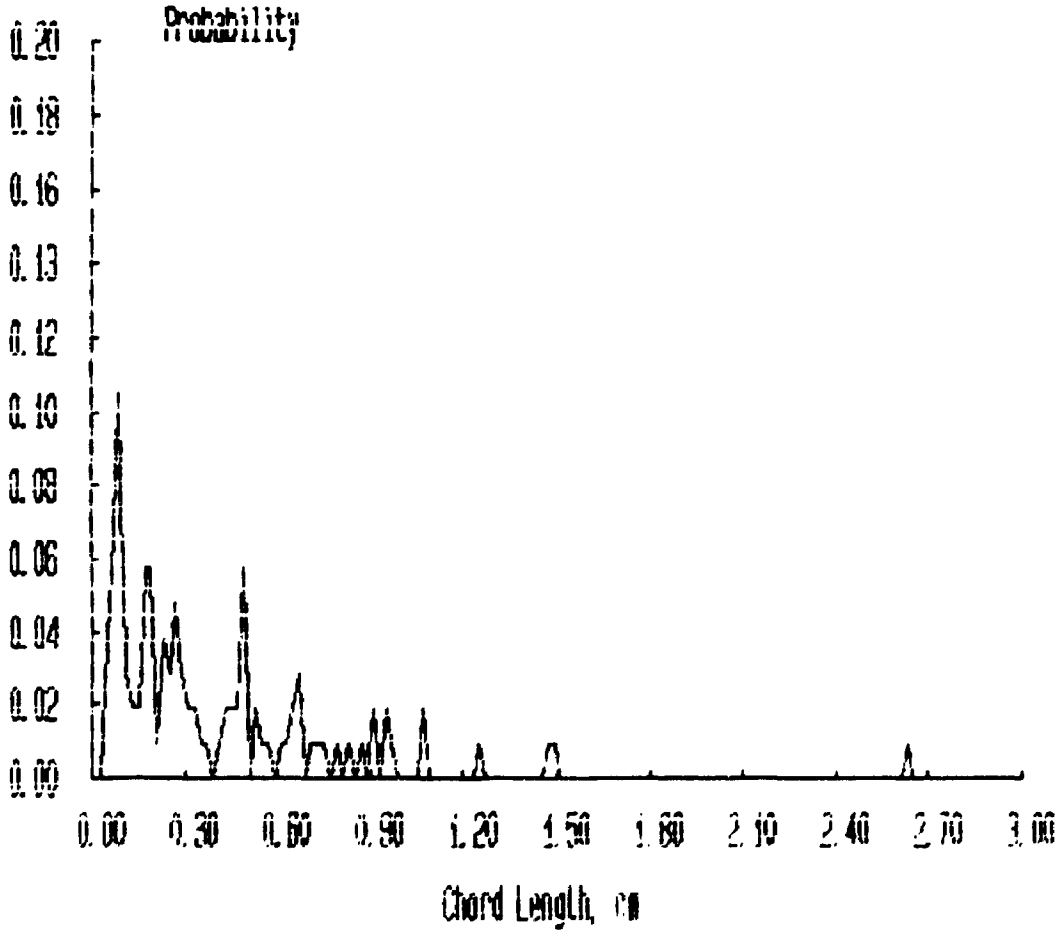

****** FILENAME ****** : JAN13D1A

**** Bubbles detected by probe 1 : 366
**** Percentage of bubbles retained : 43.72
**** Average bubble duration : .007306 s

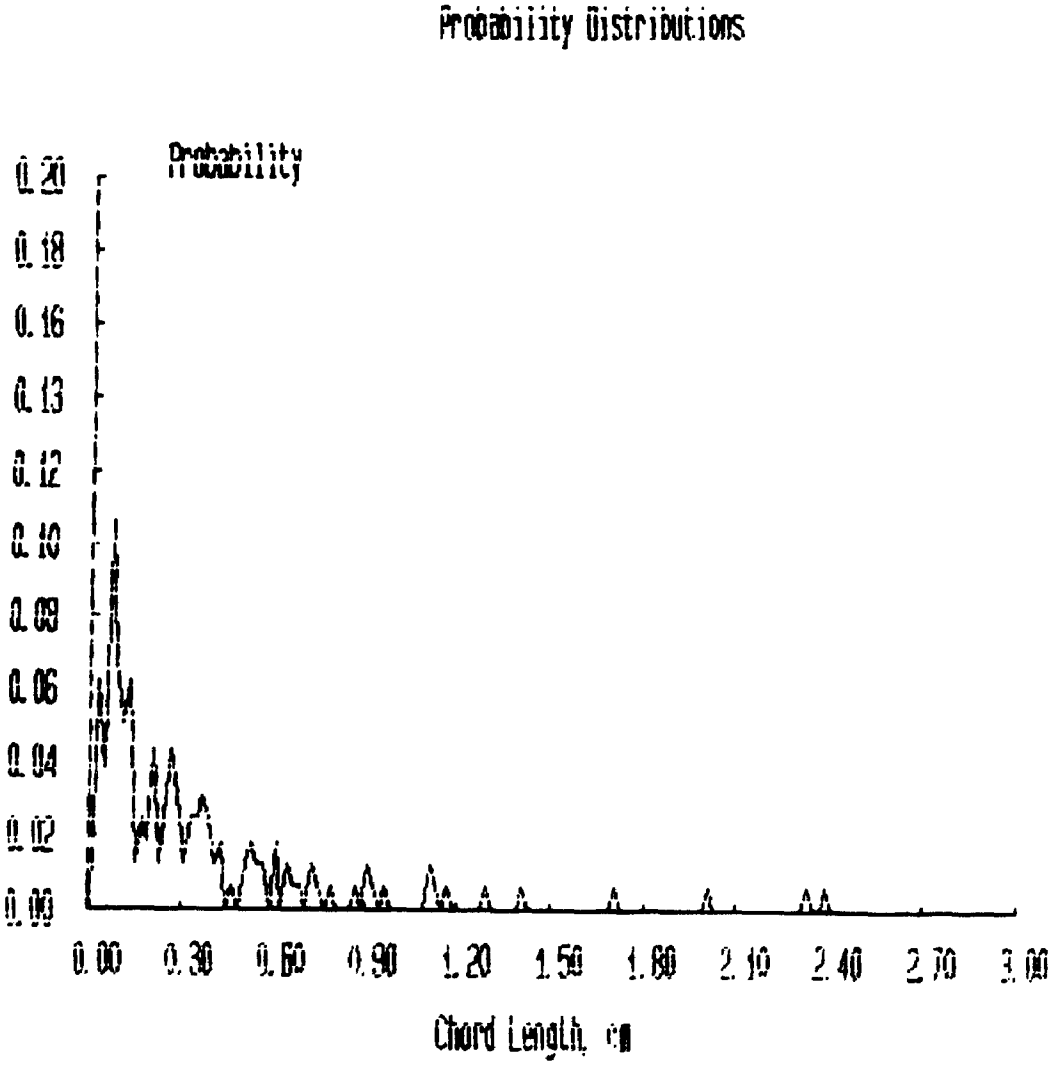

****** FILENAME ****** : JAN13D2A

**** Bubbles detected by probe 1 : 377
**** Percentage of bubbles retained : 47.21
**** Average bubble duration : .008640 s

Probability Distributions

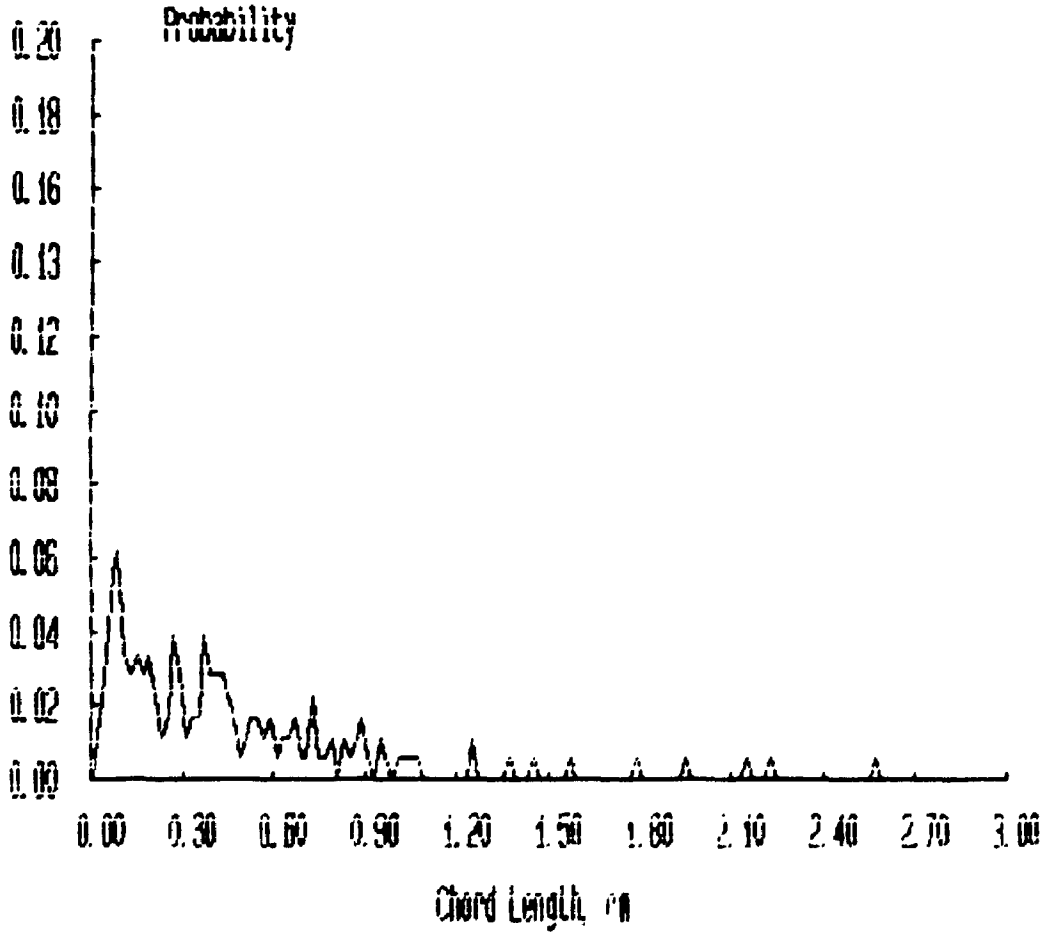

****** FILENAME ****** : JAN13D3A

**** Bubbles detected by probe 1 : 339
**** Percentage of bubbles retained : 43.07
**** Average bubble duration : .007774 s

Probability Distributions

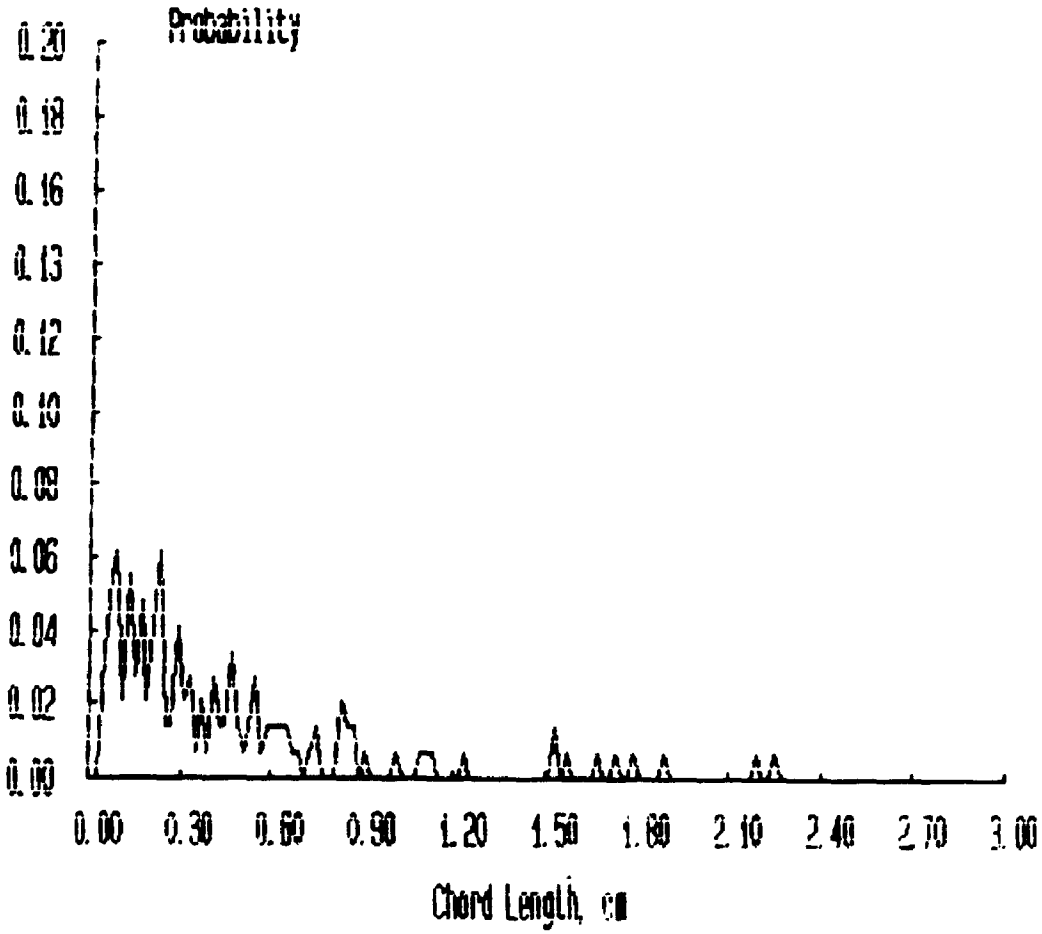

****** FILENAME ****** : JAN13D4A

**** Bubbles detected by probe 1 : 409
**** Percentage of bubbles retained : 48.17
**** Average bubble duration : .007772 s

Probability Distributions

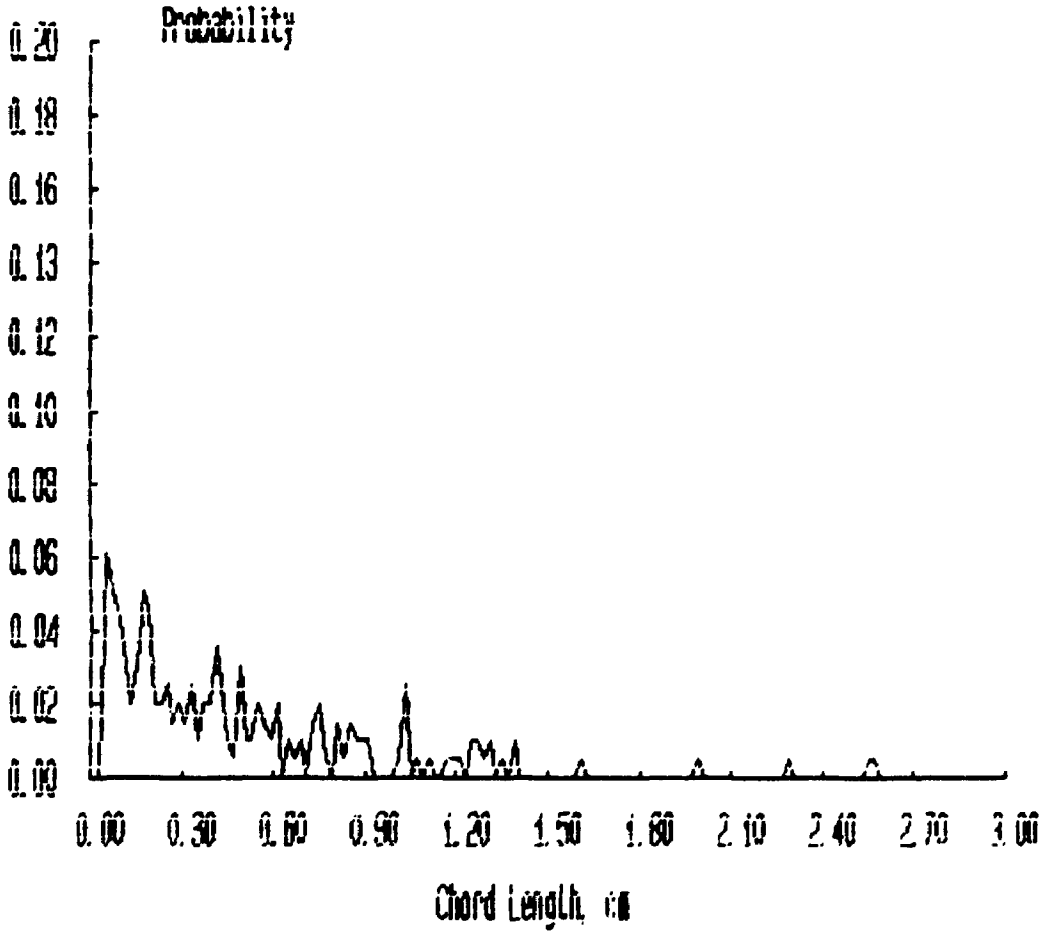

****** FILENAME ****** : JAN13D5A

**** Bubbles detected by probe 1 : 325
**** Percentage of bubbles retained : 47.69
**** Average bubble duration : .008361 s

Probability Distributions

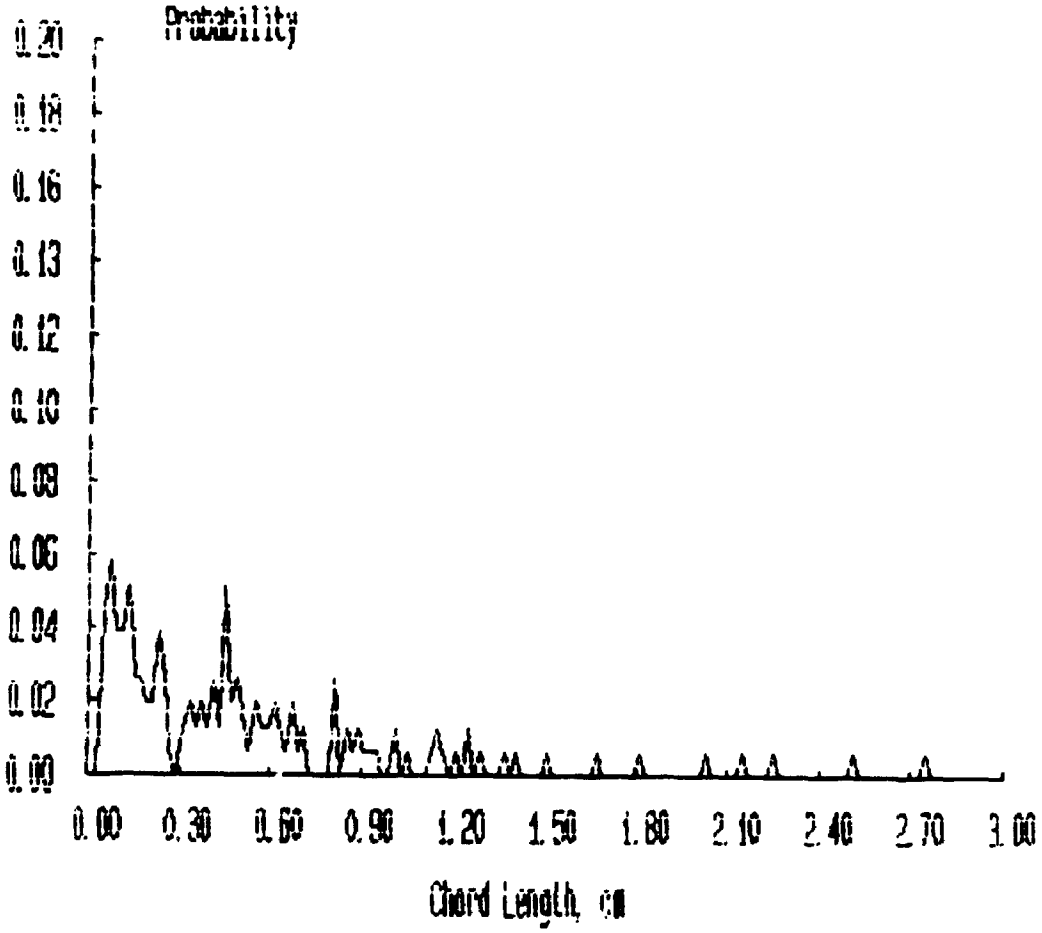

****** FILENAME ****** : JAN13D6A

**** Bubbles detected by probe 1 : 288
**** Percentage of bubbles retained : 49.31
**** Average bubble duration : .009422 s

Probability Distributions

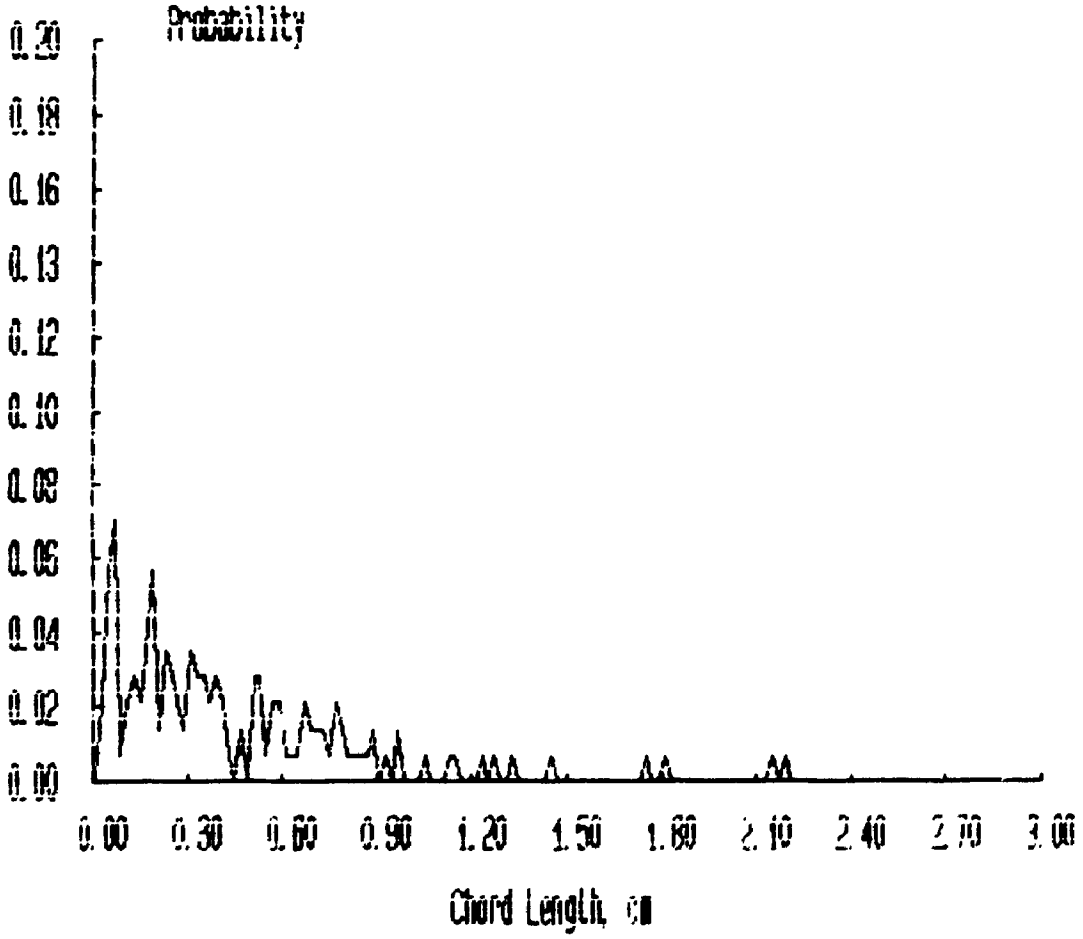

****** FILENAME ****** : JAN13E1A

**** Bubbles detected by probe 1 : 871
**** Percentage of bubbles retained : 50.06
**** Average bubble duration : .005856 s

Probability Distributions

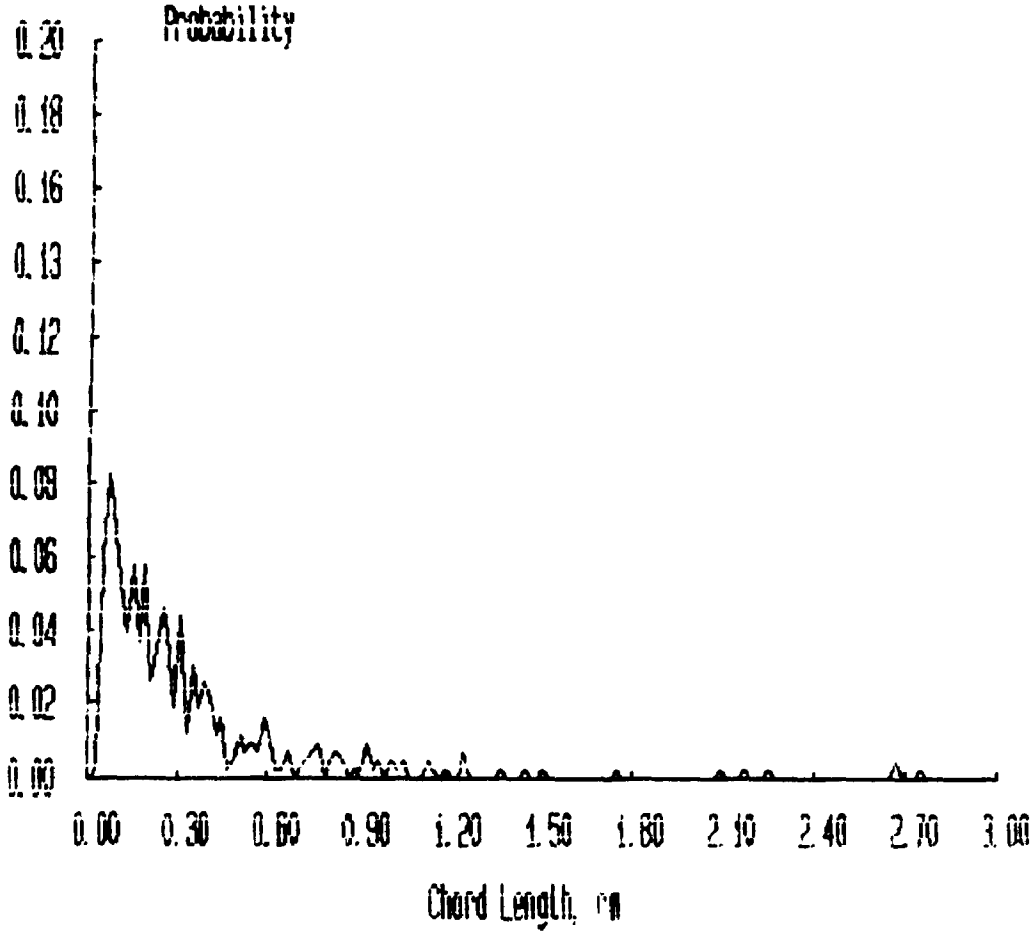

****** FILENAME ****** : JAN13E2A

**** Bubbles detected by probe 1 : 865
**** Percentage of bubbles retained : 55.61
**** Average bubble duration : .006778 s

Probability Distributions

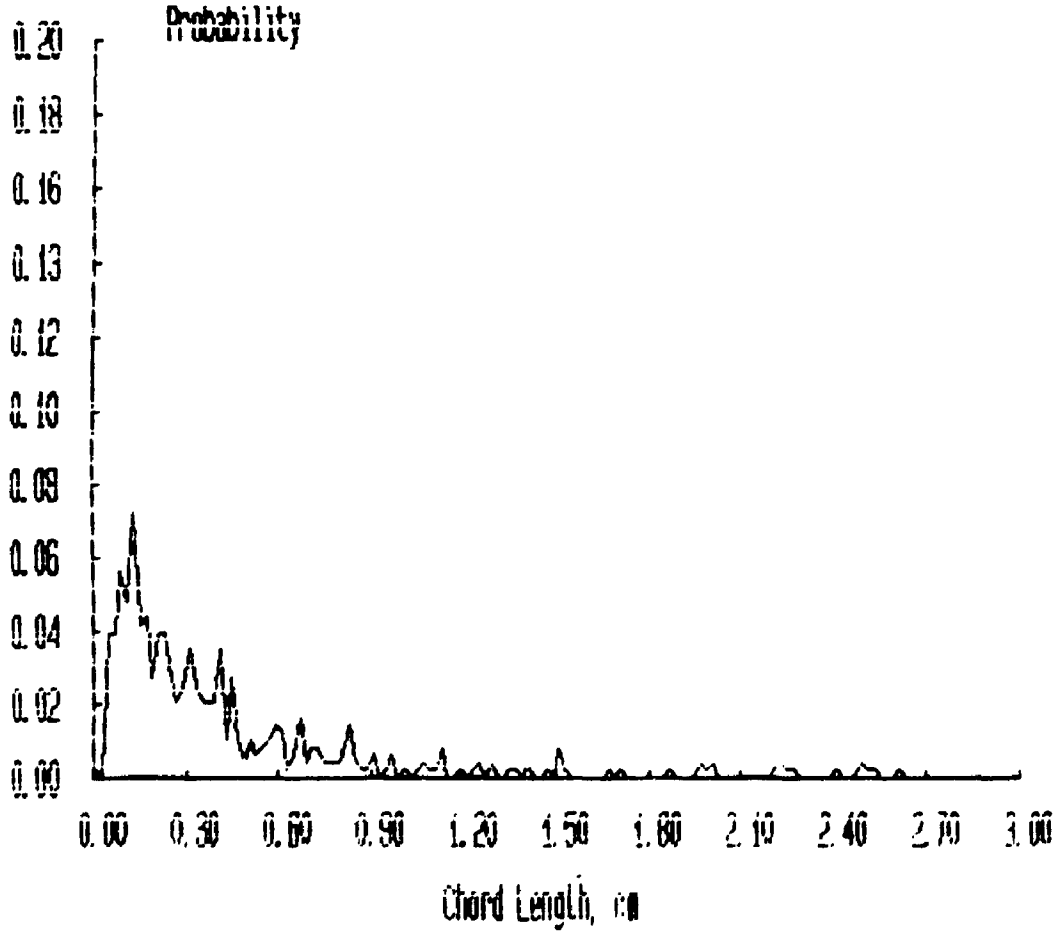

****** FILENAME ****** : JAN13E3A

**** Bubbles detected by probe 1 : 686
**** Percentage of bubbles retained : 40.38
**** Average bubble duration : .006542 s

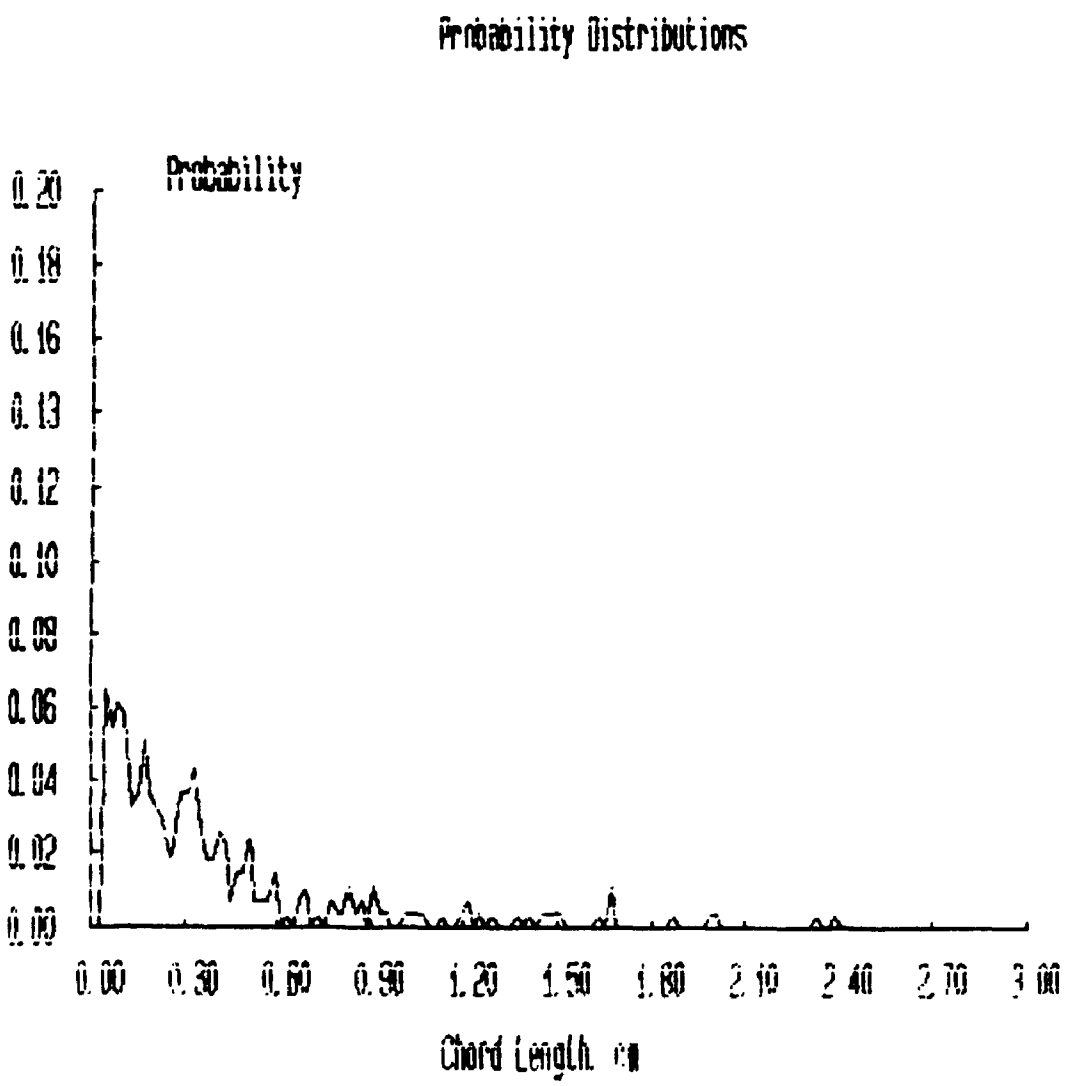

****** FILENAME ****** : JAN13E4A

**** Bubbles detected by probe 1 : 502
**** Percentage of bubbles retained : 31.08
**** Average bubble duration : .005981 s

Probability Distributions

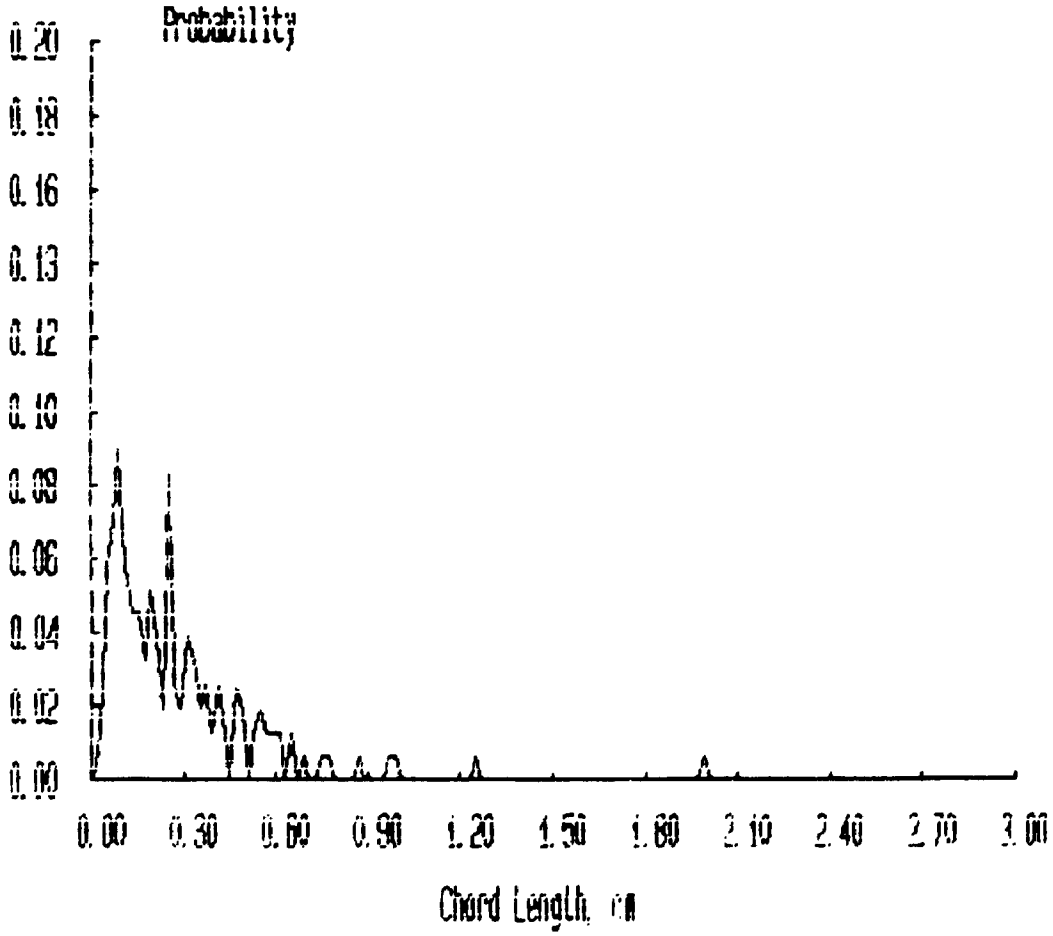

****** FILENAME ****** : JAN13E5A

**** Bubbles detected by probe 1 : 435
**** Percentage of bubbles retained : 55.56
**** Average bubble duration : .006082 s

Probability Distributions

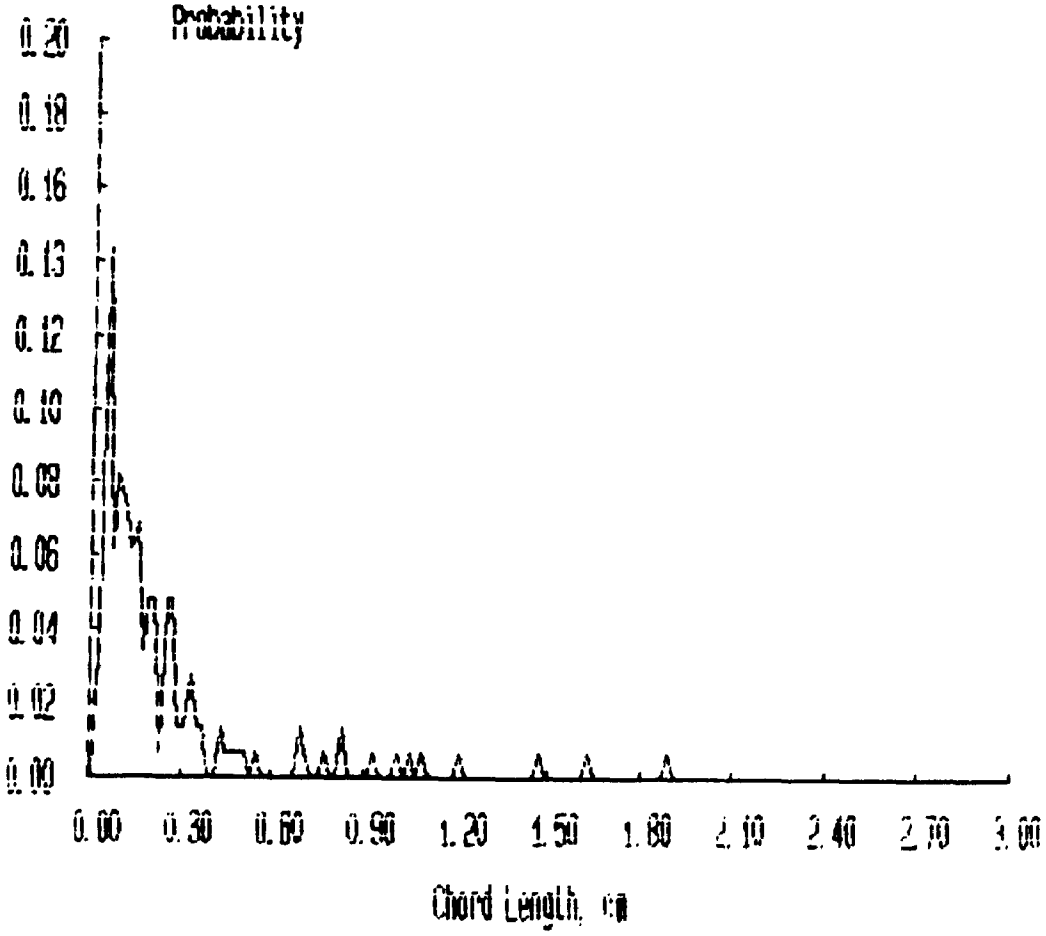

****** FILENAME ****** : JAN13E6A

**** Bubbles detected by probe 1 : 418
**** Percentage of bubbles retained : 34.93
**** Average bubble duration : .006630 s

Probability Distributions

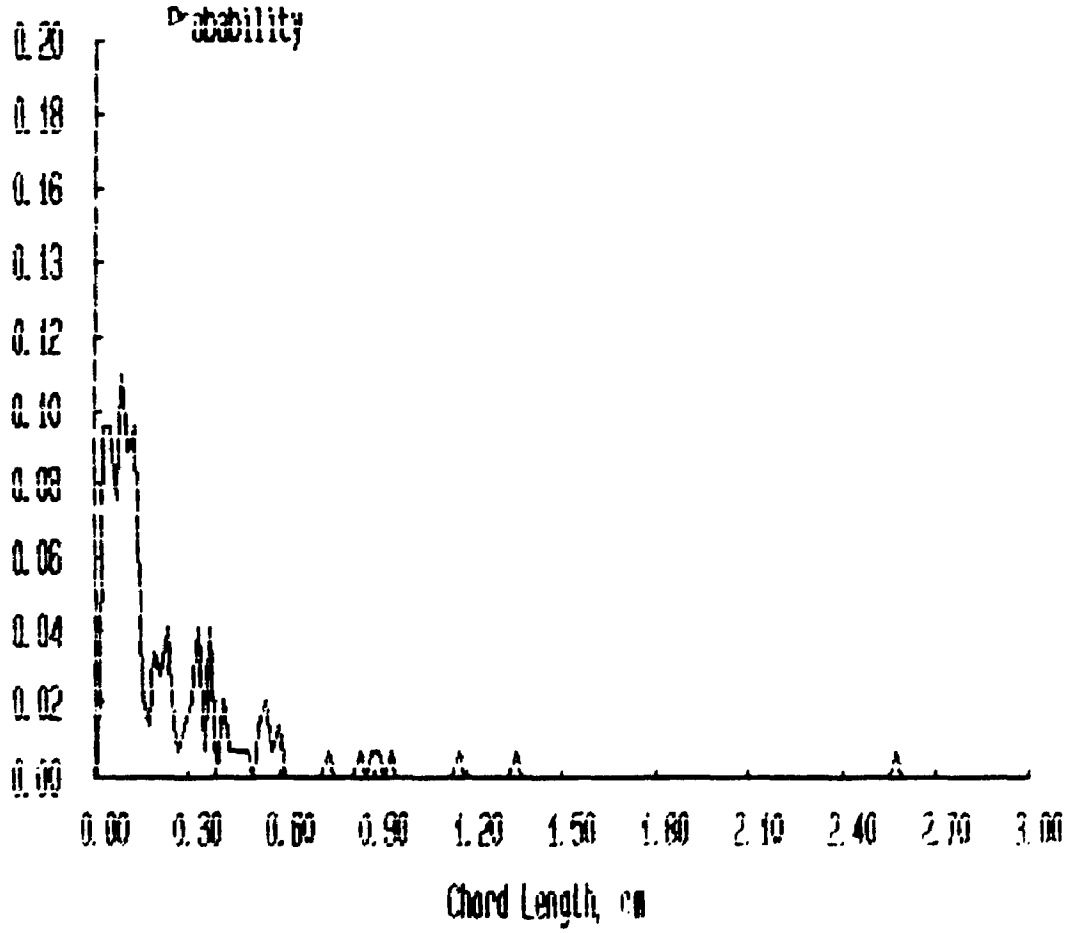

****** FILENAME ****** : JAN16A1A

**** Bubbles detected by probe 1 : 2823
**** Percentage of bubbles retained : 70.88
**** Average bubble duration : .005106 s

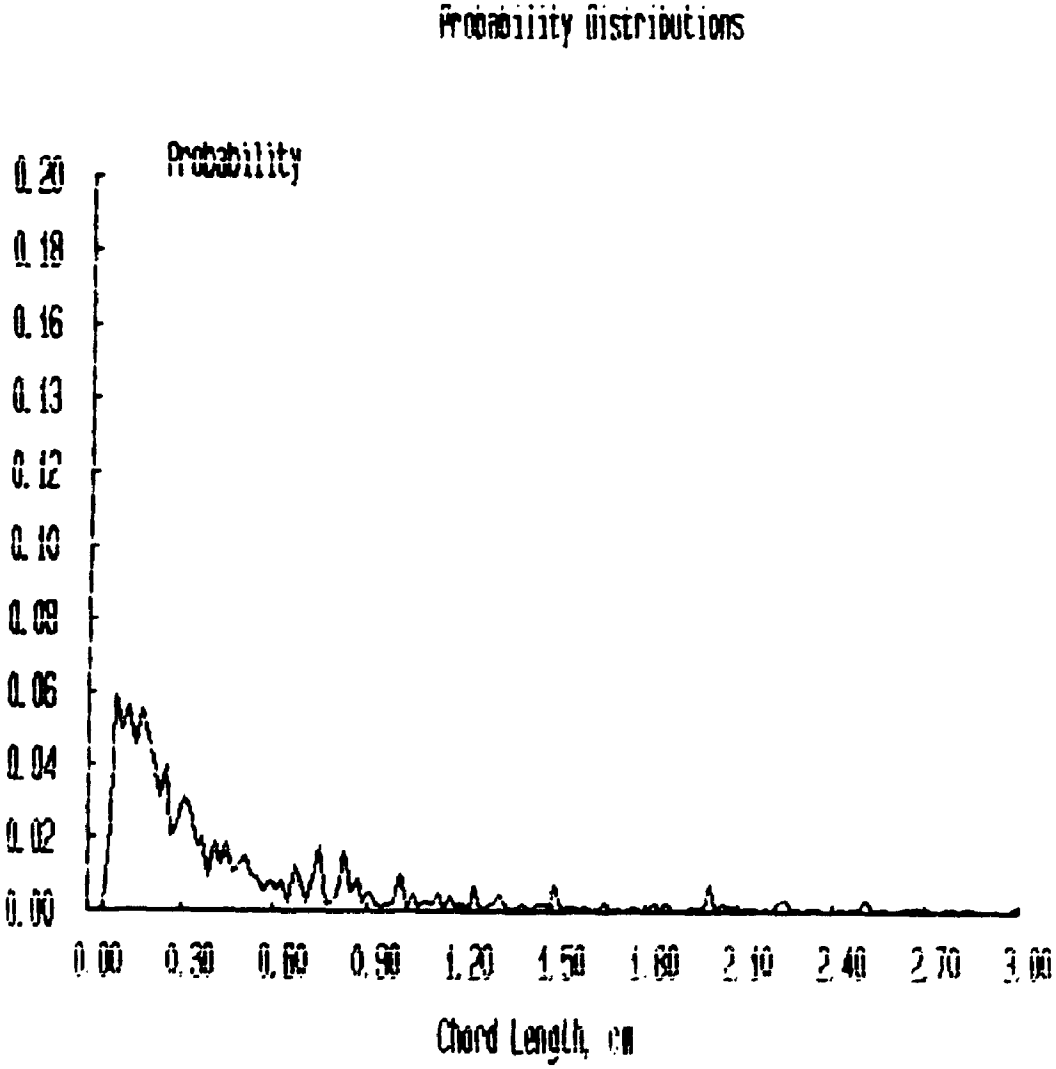

****** FILENAME ****** : JAN16A2A

**** Bubbles detected by probe 1 : 2395
**** Percentage of bubbles retained : 66.05
**** Average bubble duration : .005028 s

Probability Distributions

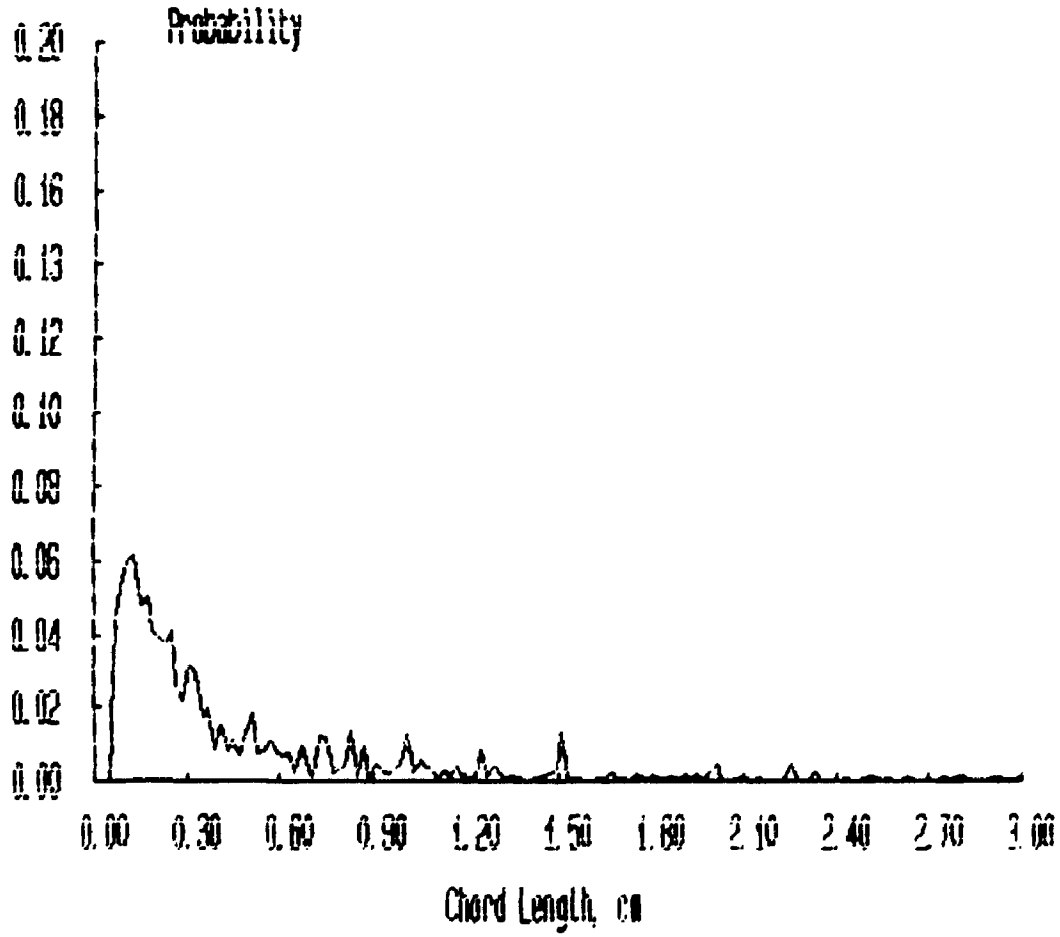

****** FILENAME ****** : JAN16A3A

**** Bubbles detected by probe 1 : 1998
**** Percentage of bubbles retained : 56.76
**** Average bubble duration : .004582 s

Probability Distributions

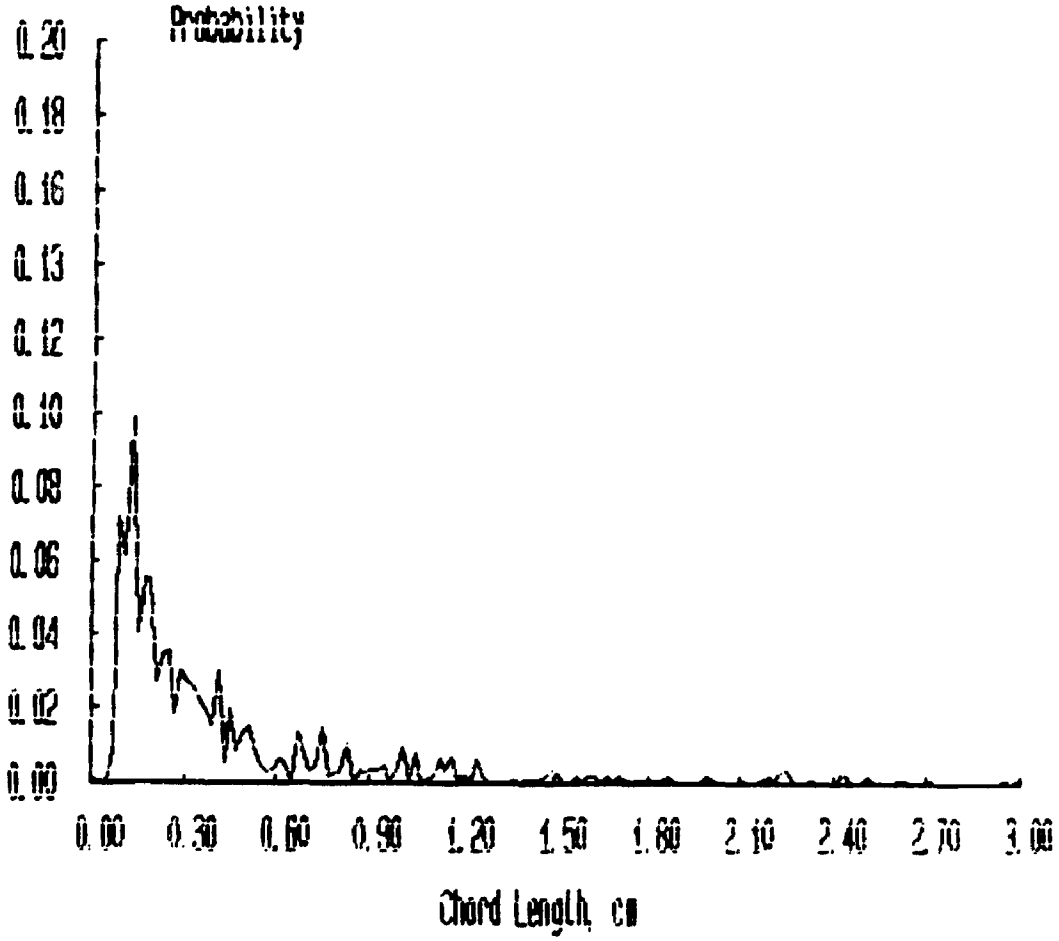

****** FILENAME ****** : JAN16A4A

**** Bubbles detected by probe 1 : 1206
**** Percentage of bubbles retained : 39.47
**** Average bubble duration : .004454 s

Probability Distributions

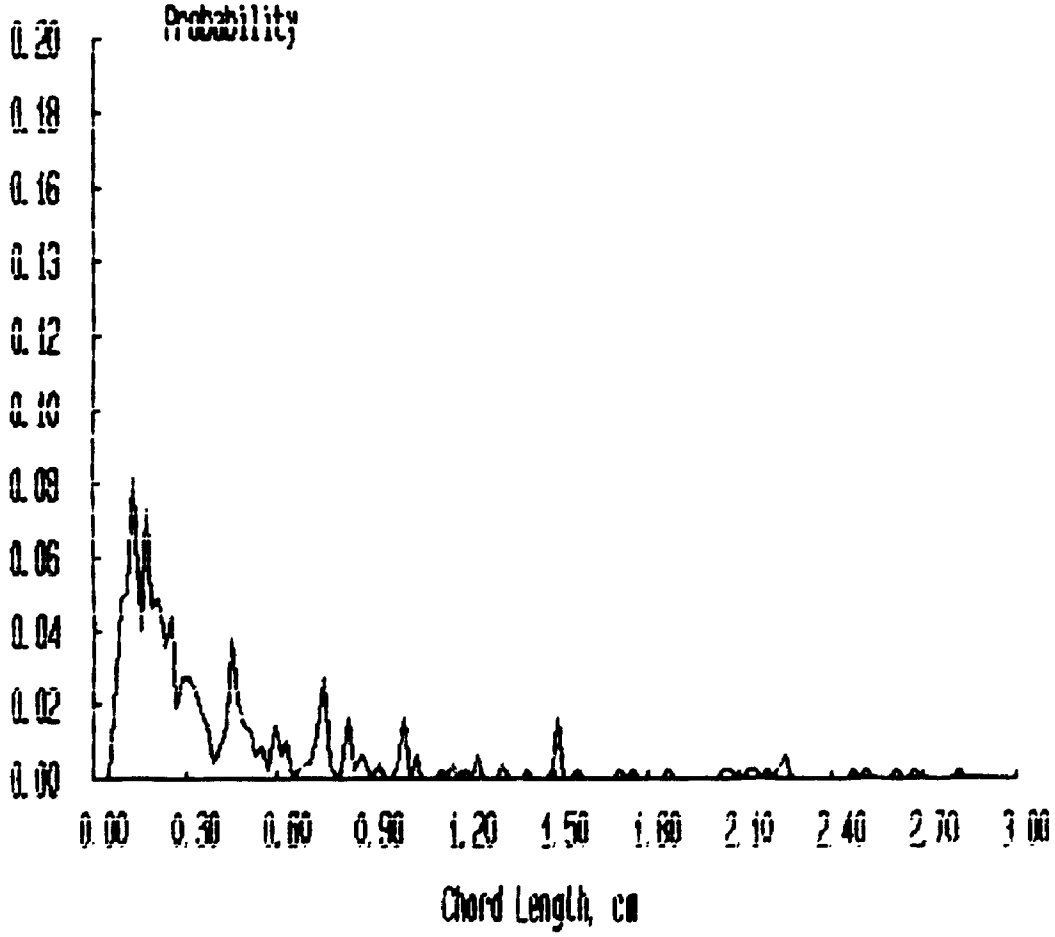

****** FILENAME ****** : JAN16A5A

**** Bubbles detected by probe 1 : 1360
**** Percentage of bubbles retained : 56.18
**** Average bubble duration : .004251 s

Probability Distributions

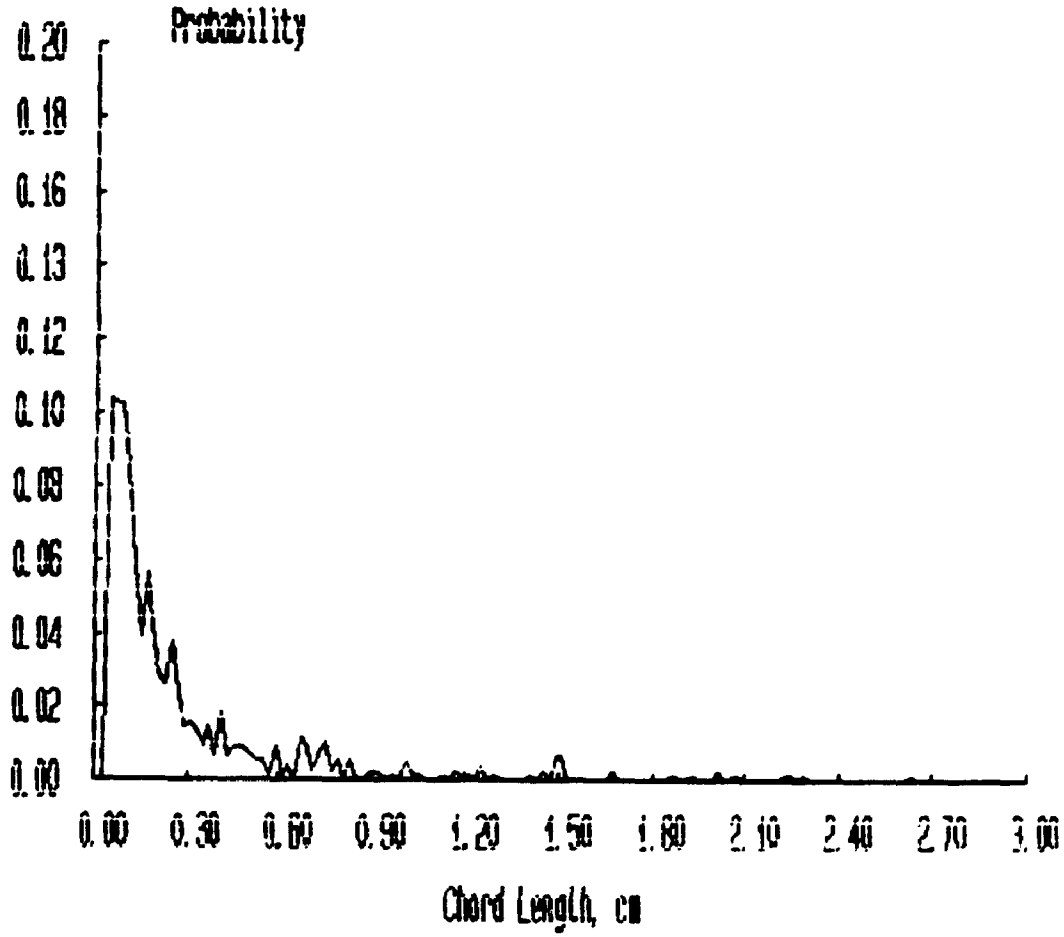

****** FILENAME ****** : JAN16A6A

**** Bubbles detected by probe 1 : 1023
**** Percentage of bubbles retained : 40.37
**** Average bubble duration : .003867 s

Probability Distributions

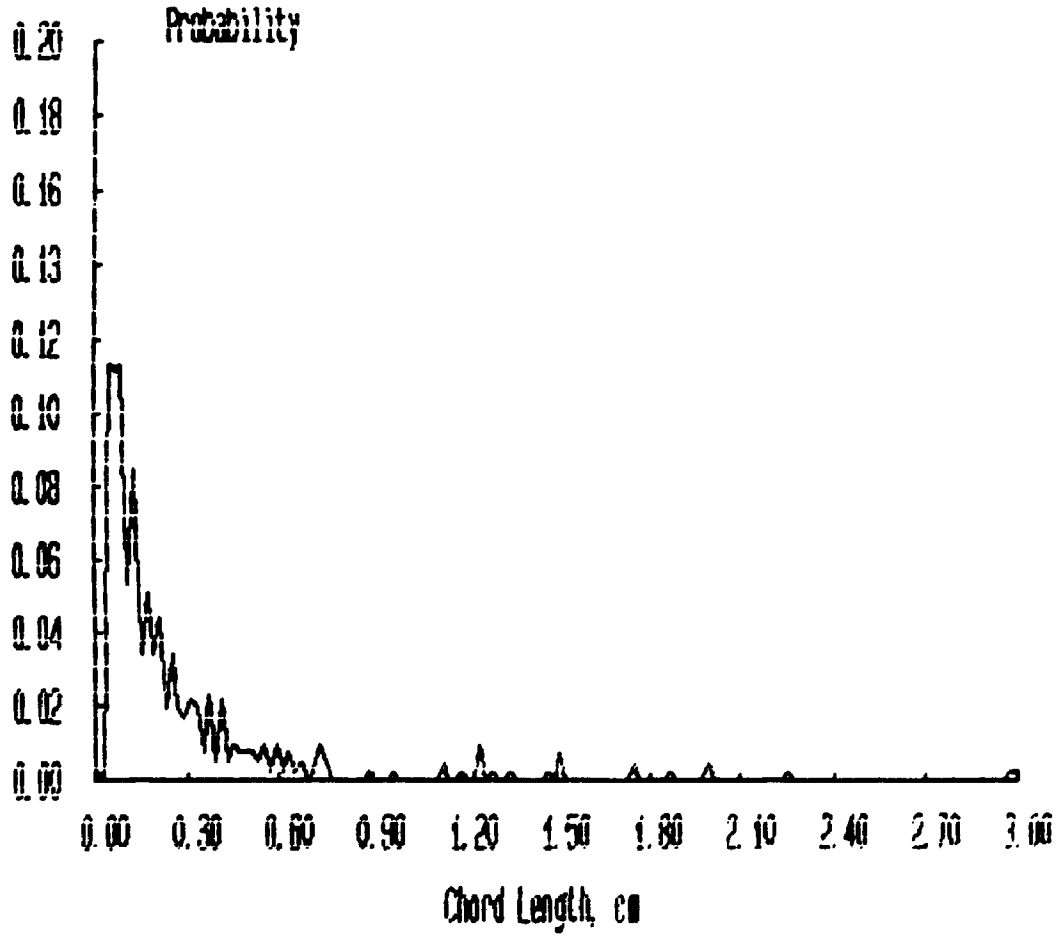

****** FILENAME ****** : JAN16B1A

**** Bubbles detected by probe 1 : 2354
**** Percentage of bubbles retained : 65.55
**** Average bubble duration : .005498 s

Probability Distributions

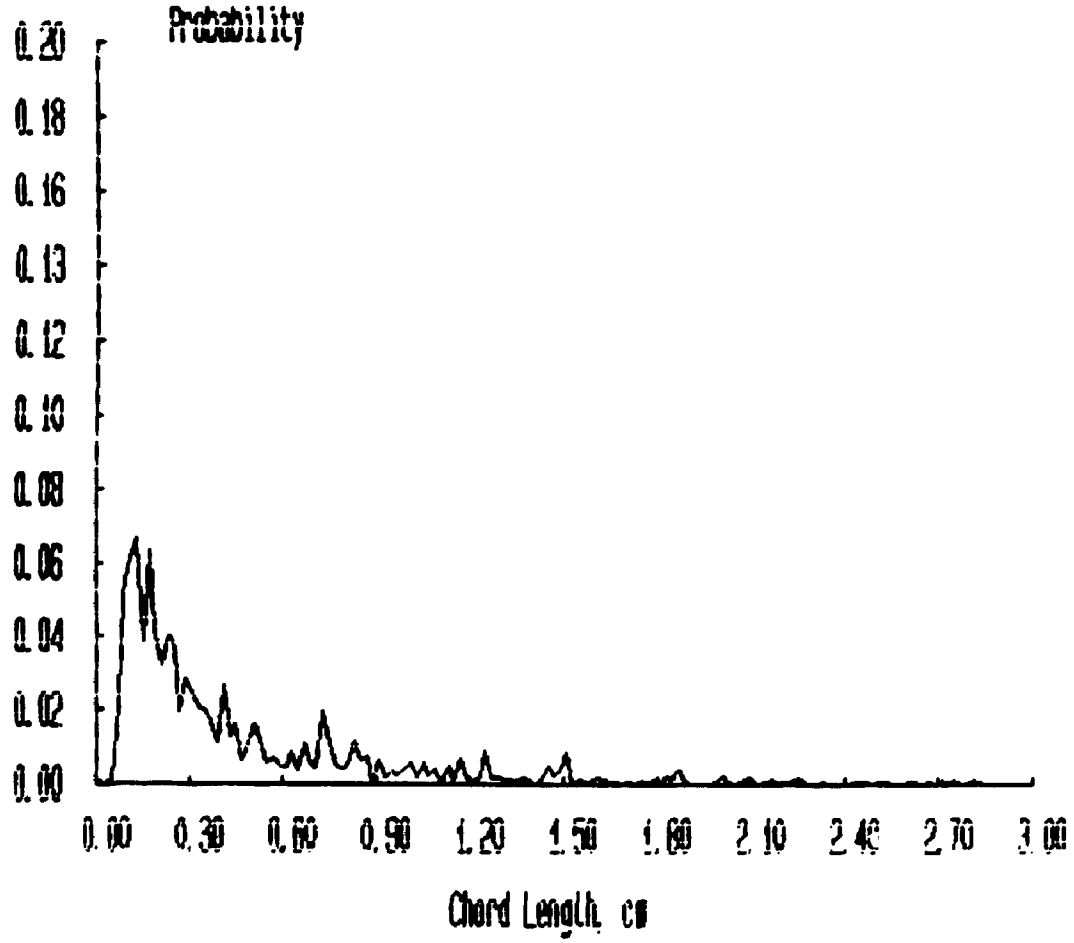

****** FILENAME ****** : JAN16B2A

**** Bubbles detected by probe 1 : 2451
**** Percentage of bubbles retained : 65.69
**** Average bubble duration : .005400 s

Probability Distributions

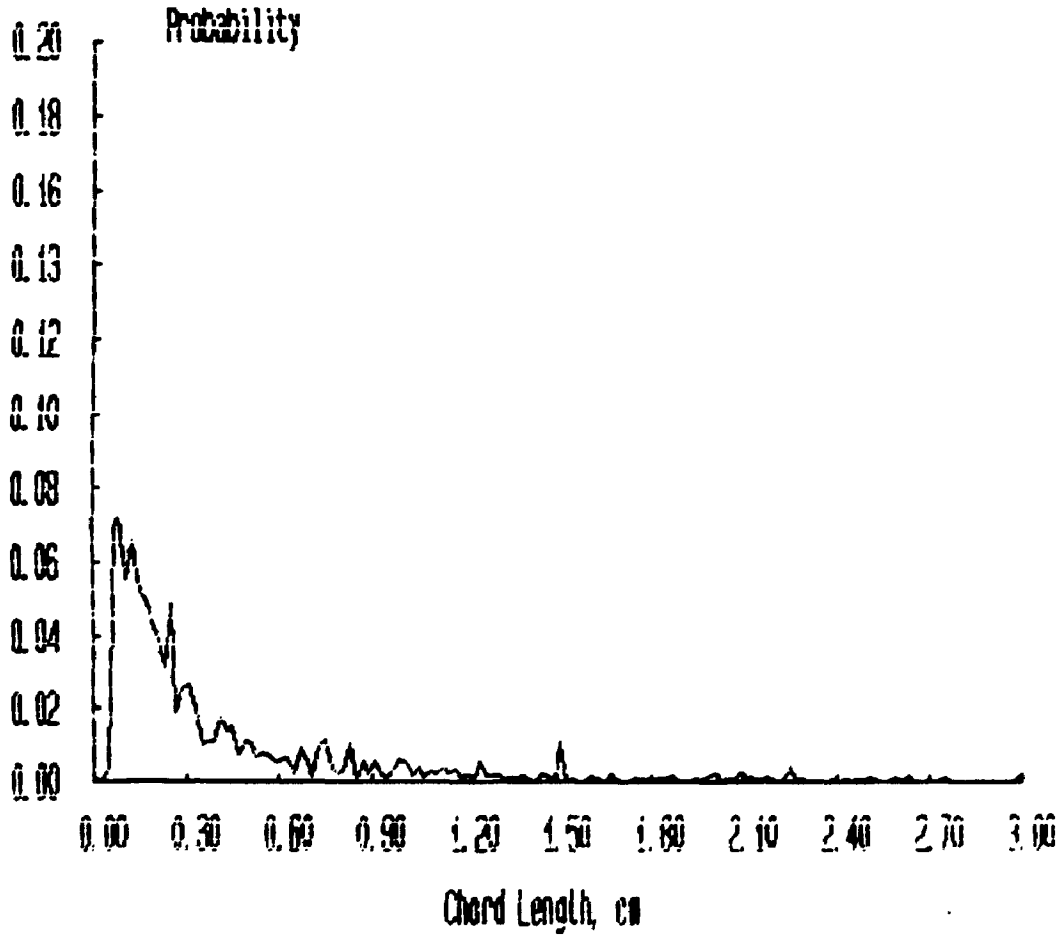

****** FILENAME ****** : JAN16B3A

**** Bubbles detected by probe 1 : 1973
**** Percentage of bubbles retained : 53.67
**** Average bubble duration : .005142 s

Probability Distributions

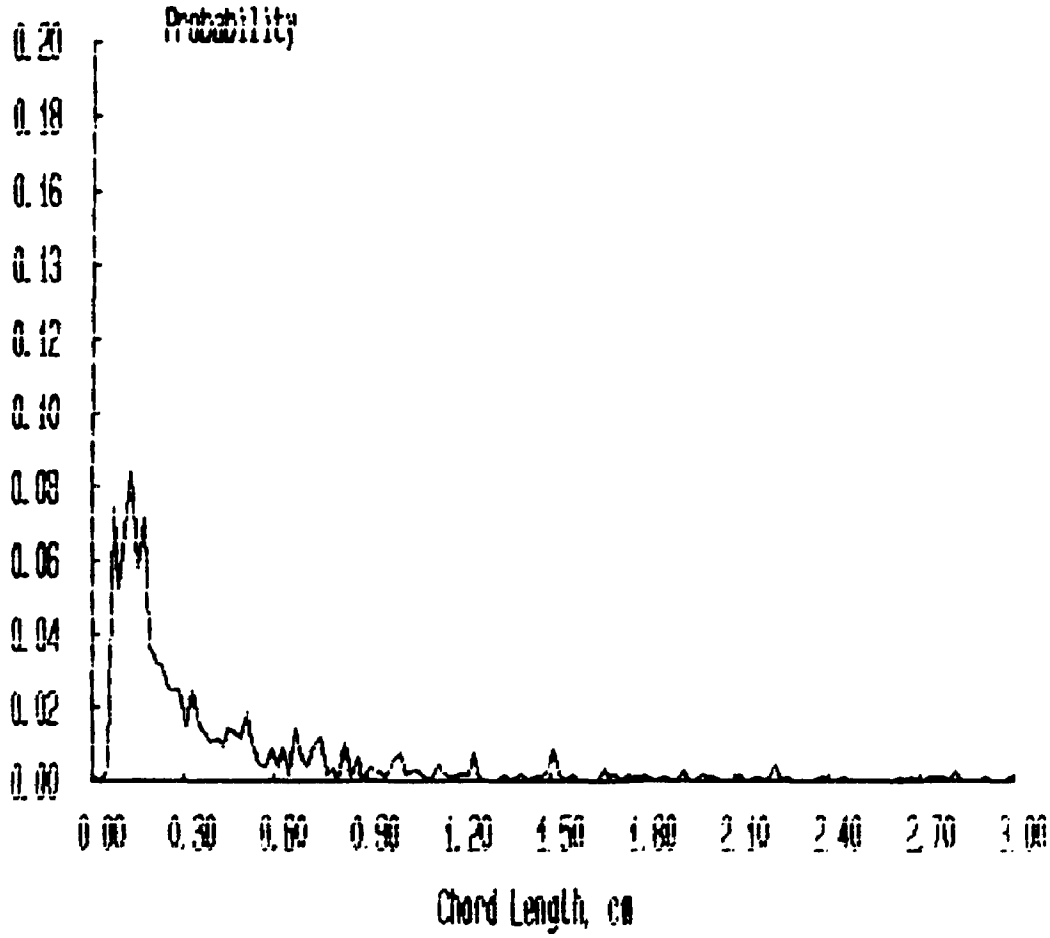

****** FILENAME ****** : JAN16B4A

**** Bubbles detected by probe 1 : 1280
**** Percentage of bubbles retained : 51.17
**** Average bubble duration : .004579 s

Probability Distributions

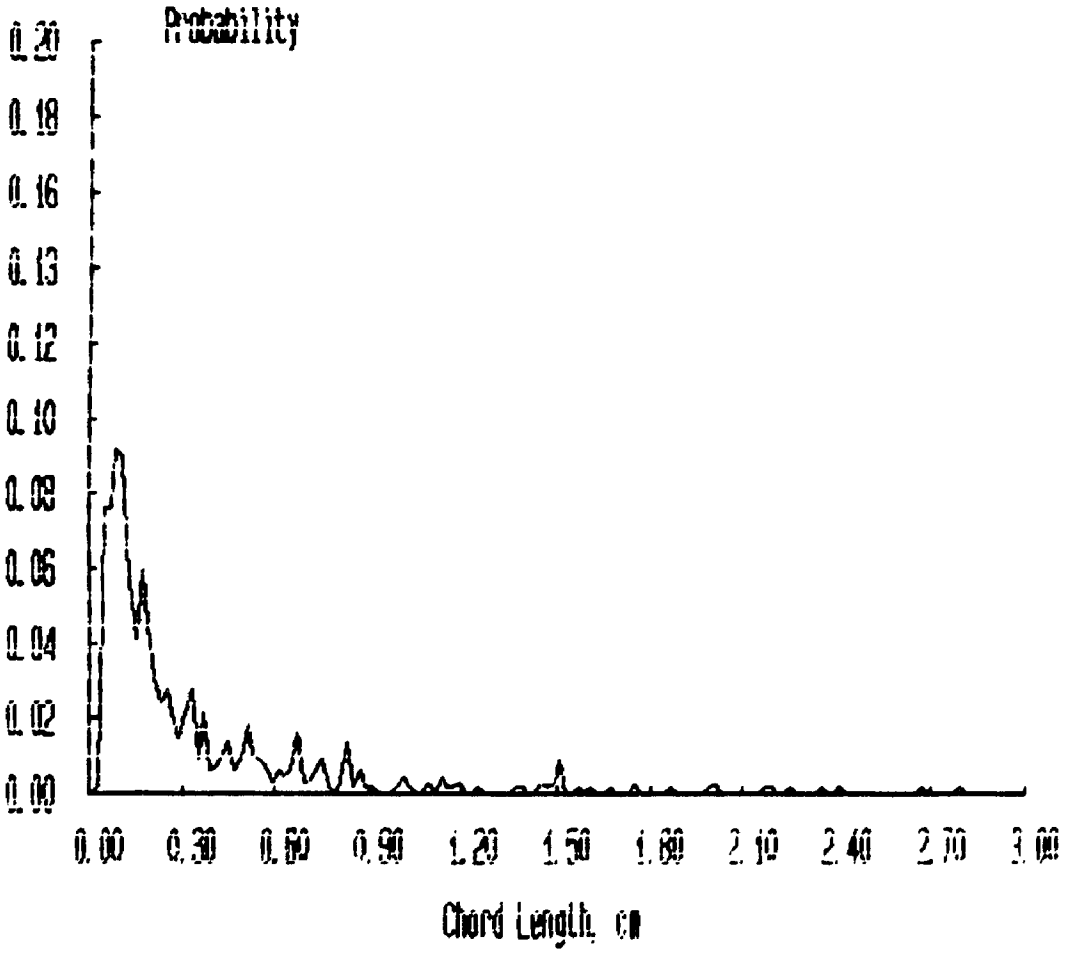

****** FILENAME ****** : JAN16B5A

**** Bubbles detected by probe 1 : 272
**** Percentage of bubbles retained : 45.01
**** Average bubble duration : .004105 s

Probability Distributions

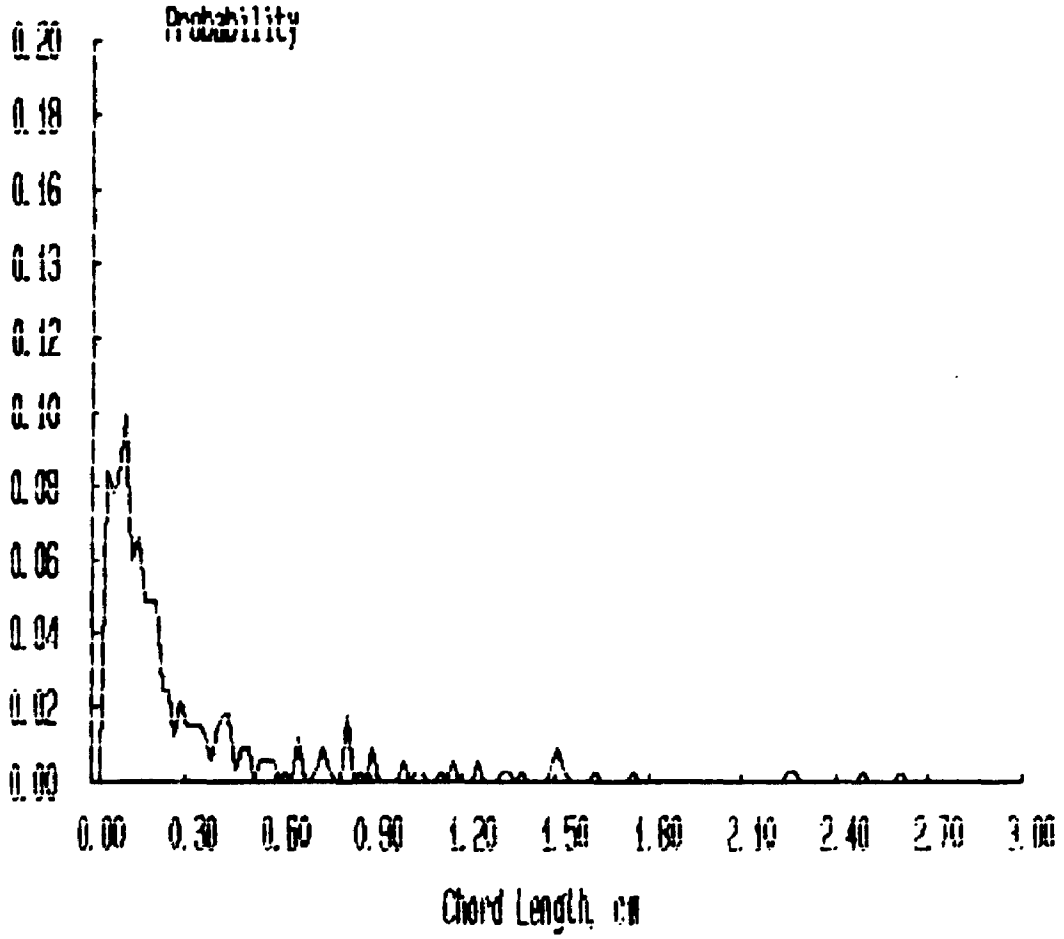

****** FILENAME ****** : JAN16B6A

**** Bubbles detected by probe 1 : 970
**** Percentage of bubbles retained : 42.47
**** Average bubble duration : .003864 s

Probability Distributions

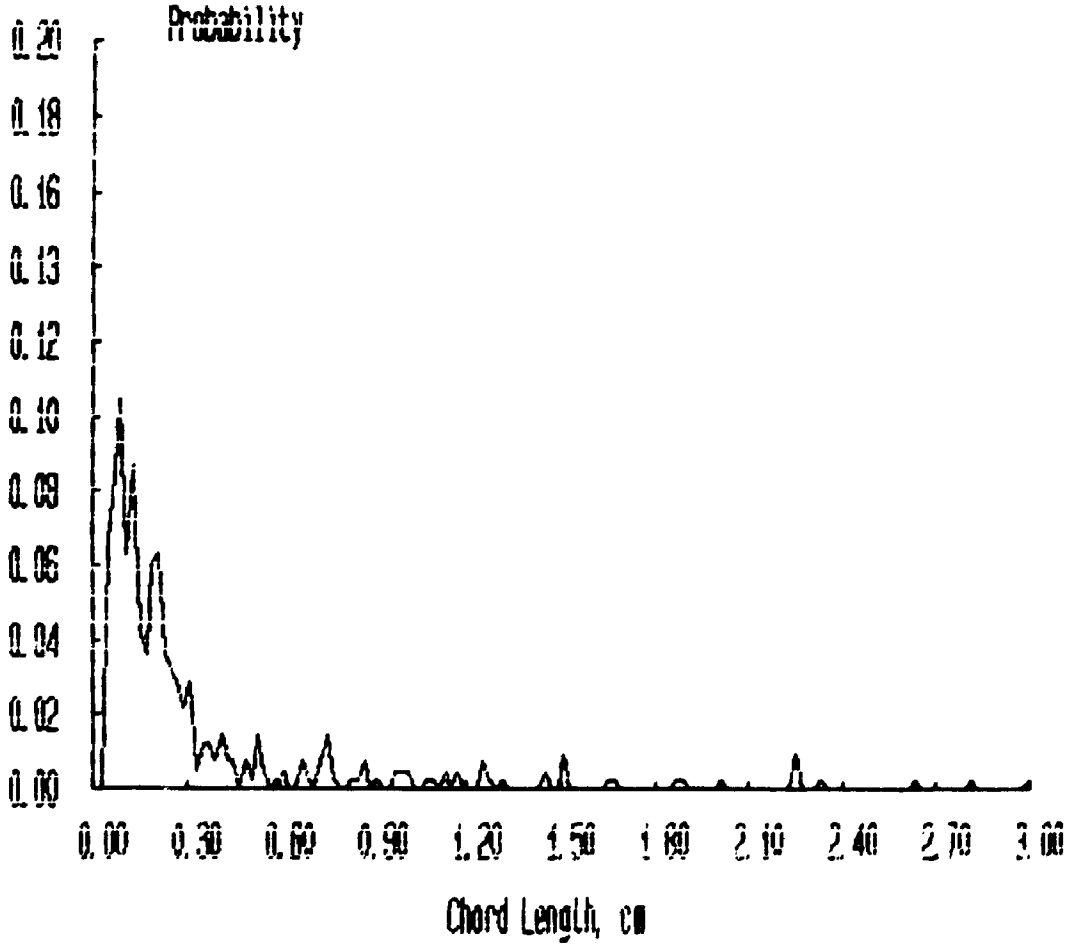

****** FILENAME ****** : JAN16C1A

**** Bubbles detected by probe 1 : 2307
**** Percentage of bubbles retained : 62.20
**** Average bubble duration : .005583 s

Probability Distributions

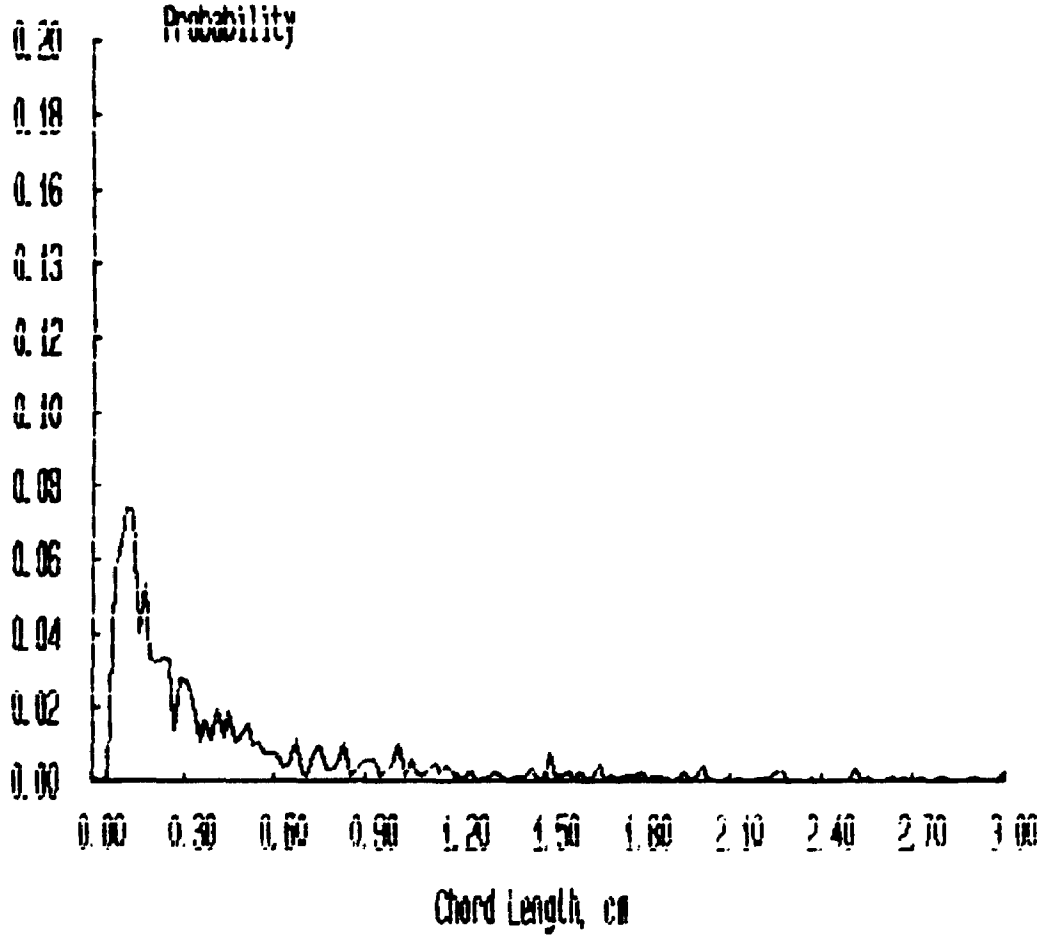

****** FILENAME ****** : JAN16C2A

**** Bubbles detected by probe 1 : 2135
**** Percentage of bubbles retained : 60.28
**** Average bubble duration : .005477 s

Probability Distributions

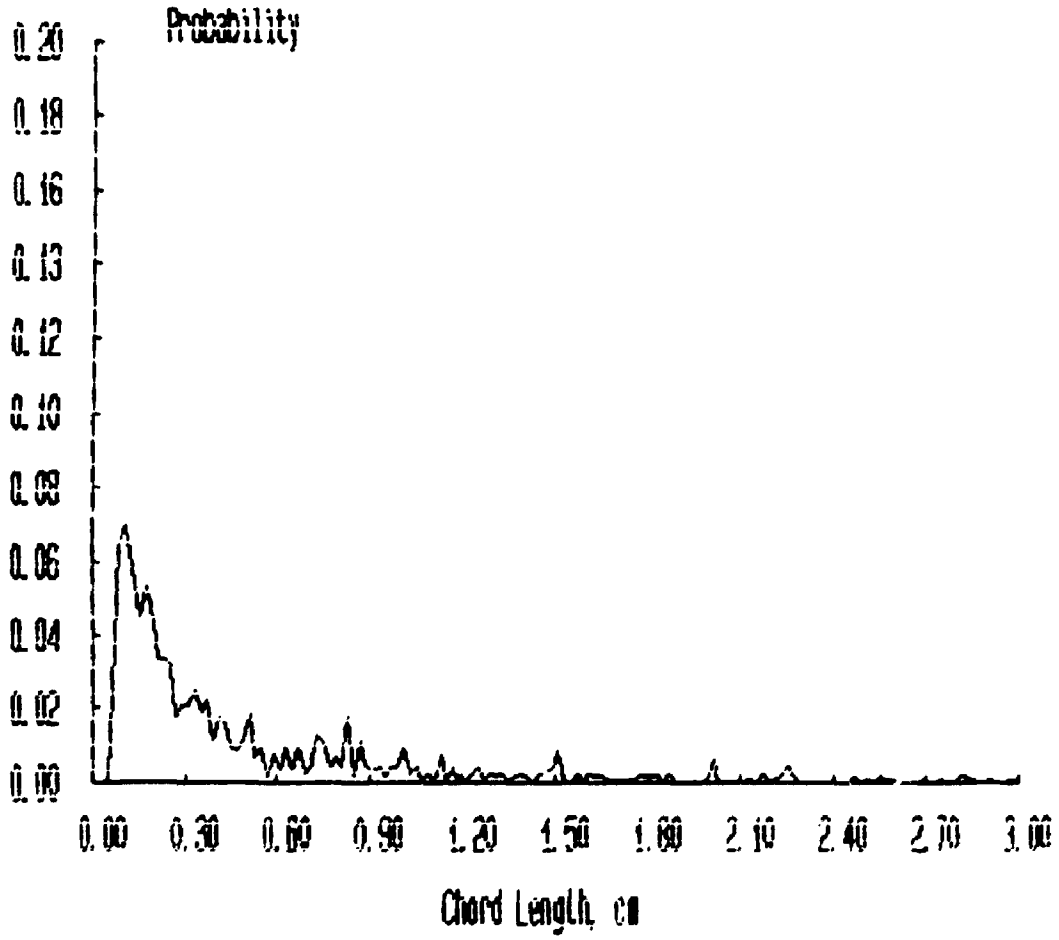

****** FILENAME ****** : JAN16C3A

**** Bubbles detected by probe 1 : 1709
**** Percentage of bubbles retained : 47.92
**** Average bubble duration : .005663 s

Probability Distributions

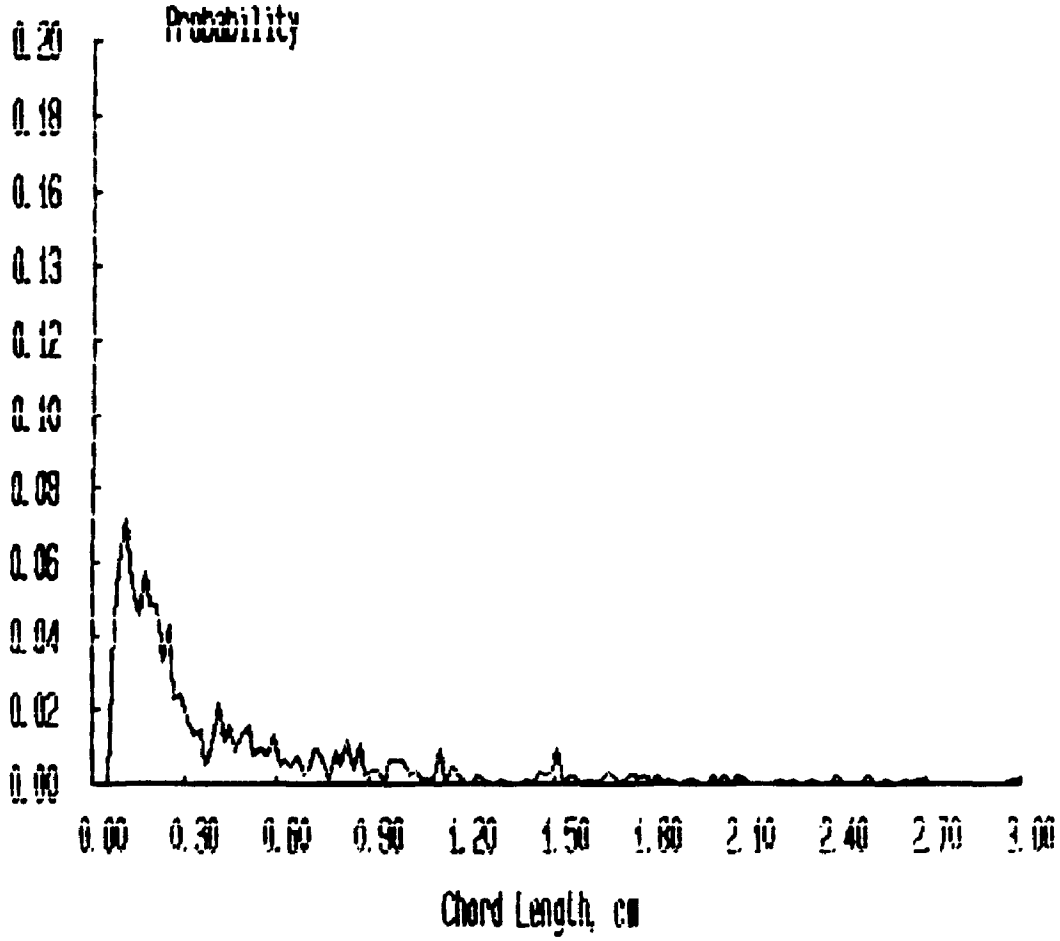

****** FILENAME ****** : JAN16C4A

**** Bubbles detected by probe 1 : 1924
**** Percentage of bubbles retained : 45.17
**** Average bubble duration : .005201 s

Probability Distributions

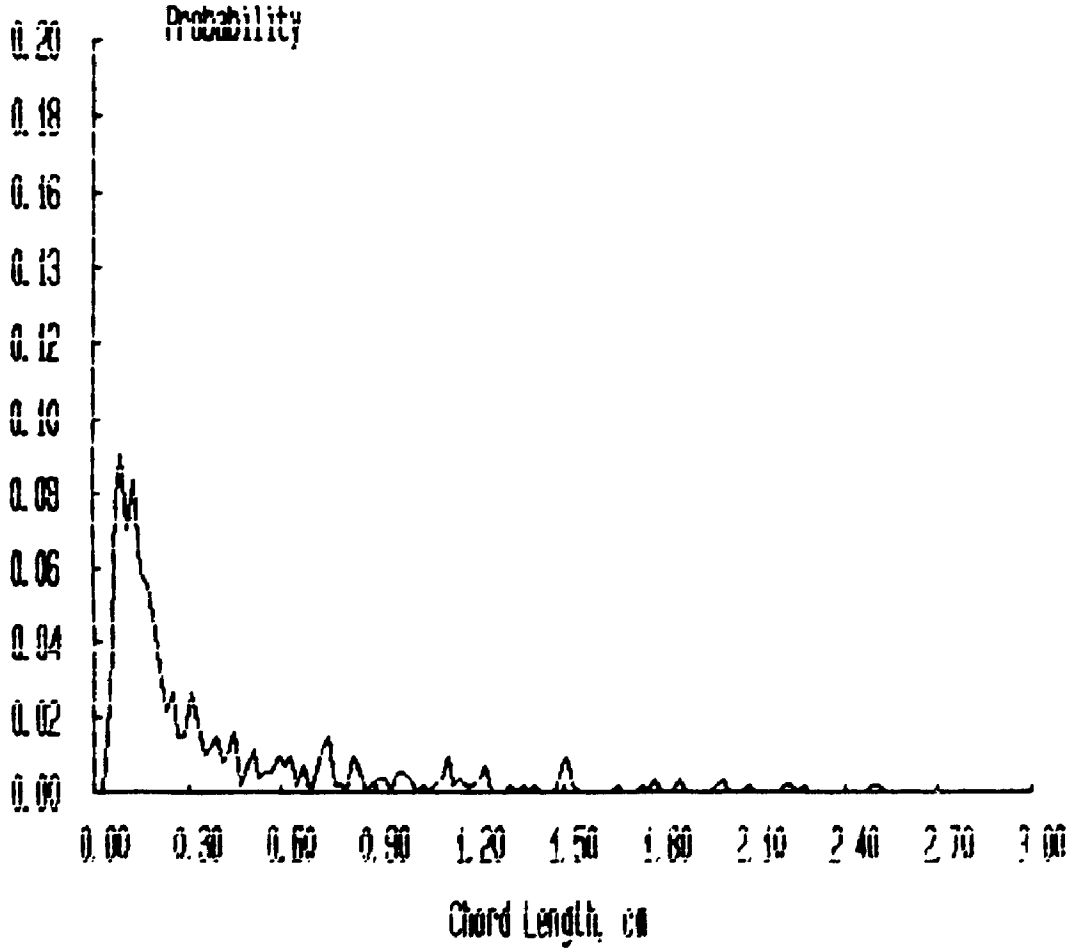

****** FILENAME ****** : JAN16C5A

**** Bubbles detected by probe 1 : 920
**** Percentage of bubbles retained : 42.39
**** Average bubble duration : .004797 s

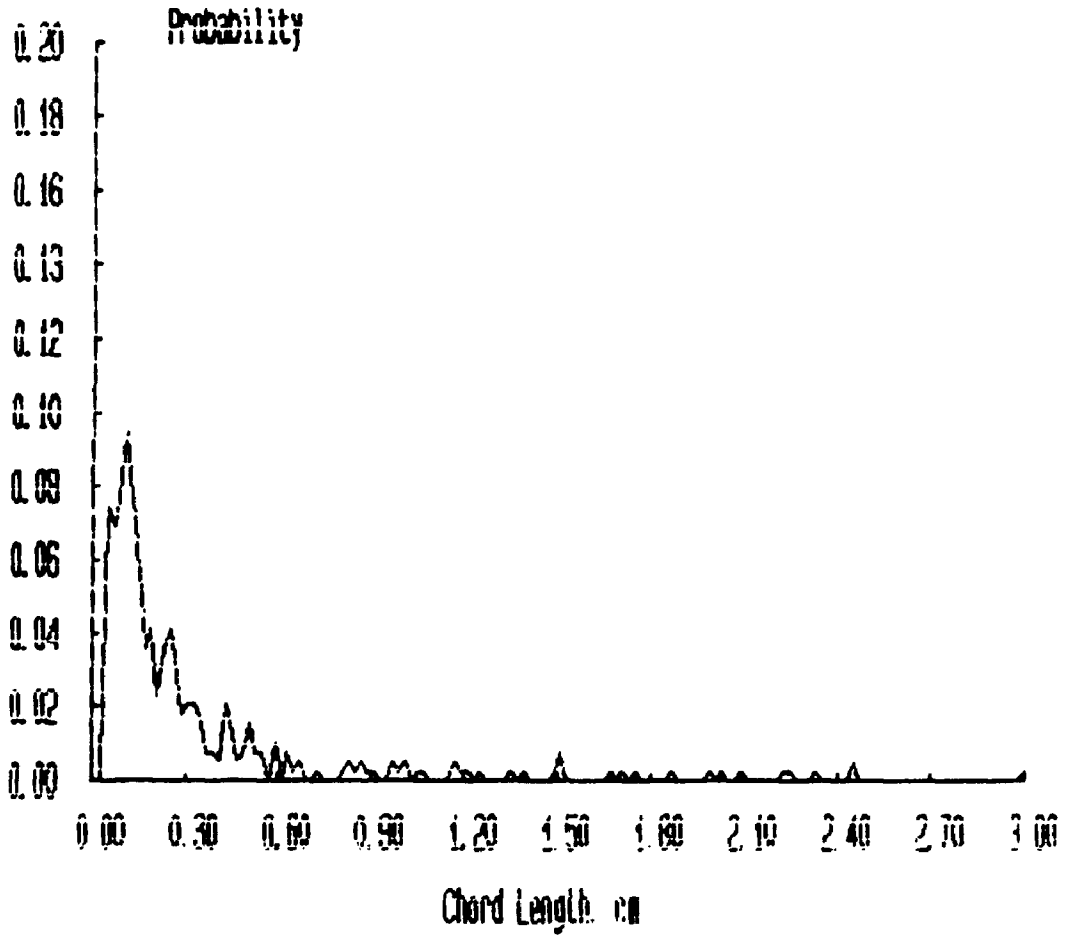

211

****** FILENAME ****** : JAN16C6A

**** Bubbles detected by probe 1 : 696
**** Percentage of bubbles retained : 41.95
**** Average bubble duration : .004342 s

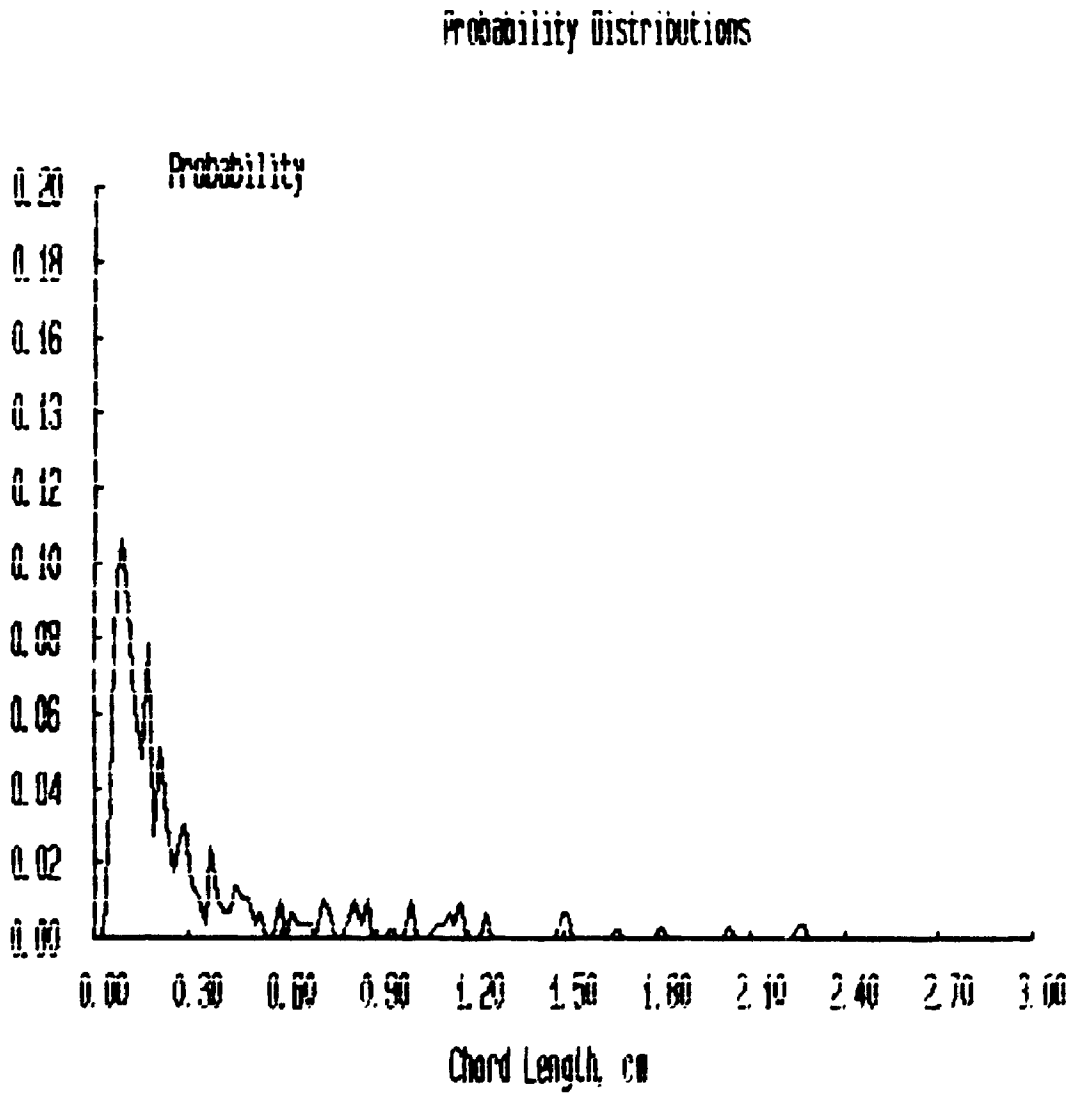

****** FILENAME ****** : JAN16D1A

**** Bubbles detected by probe 1 : 1750
**** Percentage of bubbles retained : 54.74
**** Average bubble duration : .005530 s

Probability Distributions

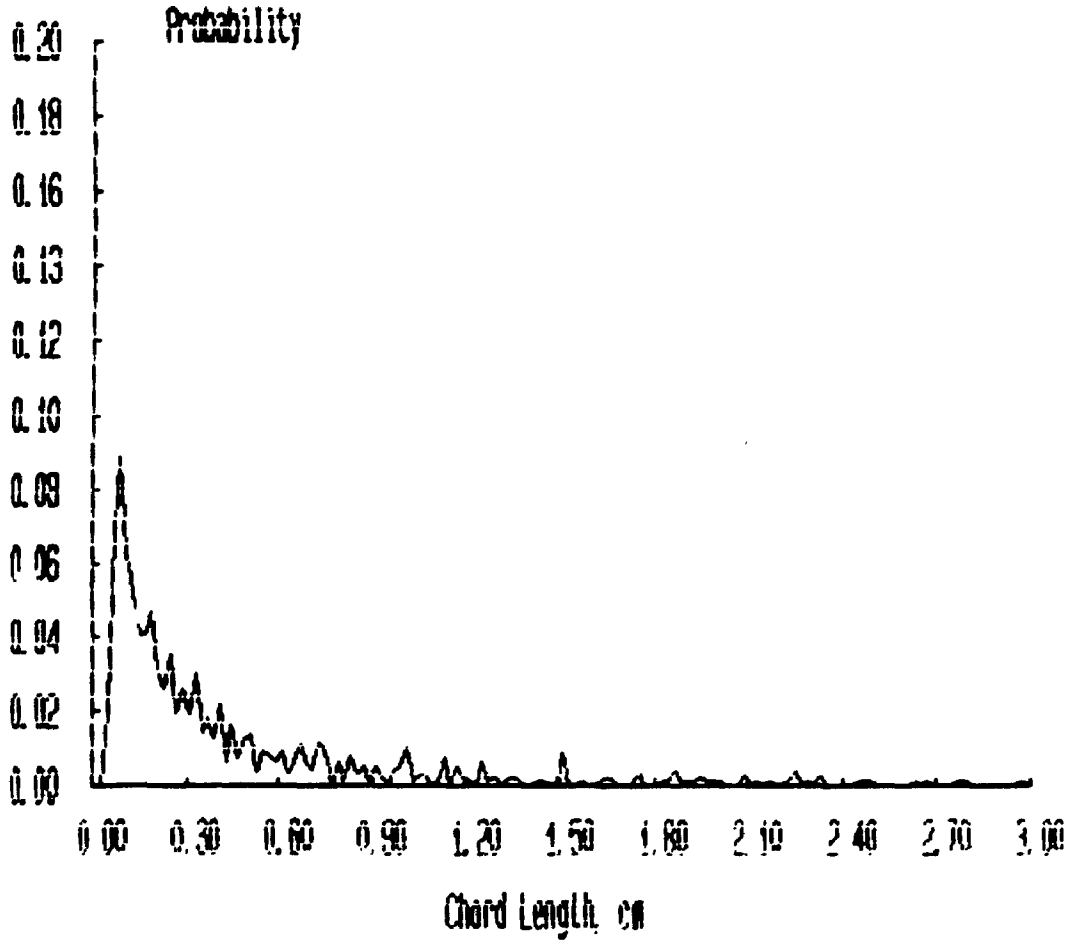

****** FILENAME ****** : JAN16D2A

**** Bubbles detected by probe 1 : 1696
**** Percentage of bubbles retained : 55.96
**** Average bubble duration : .005787 s

Probability Distributions

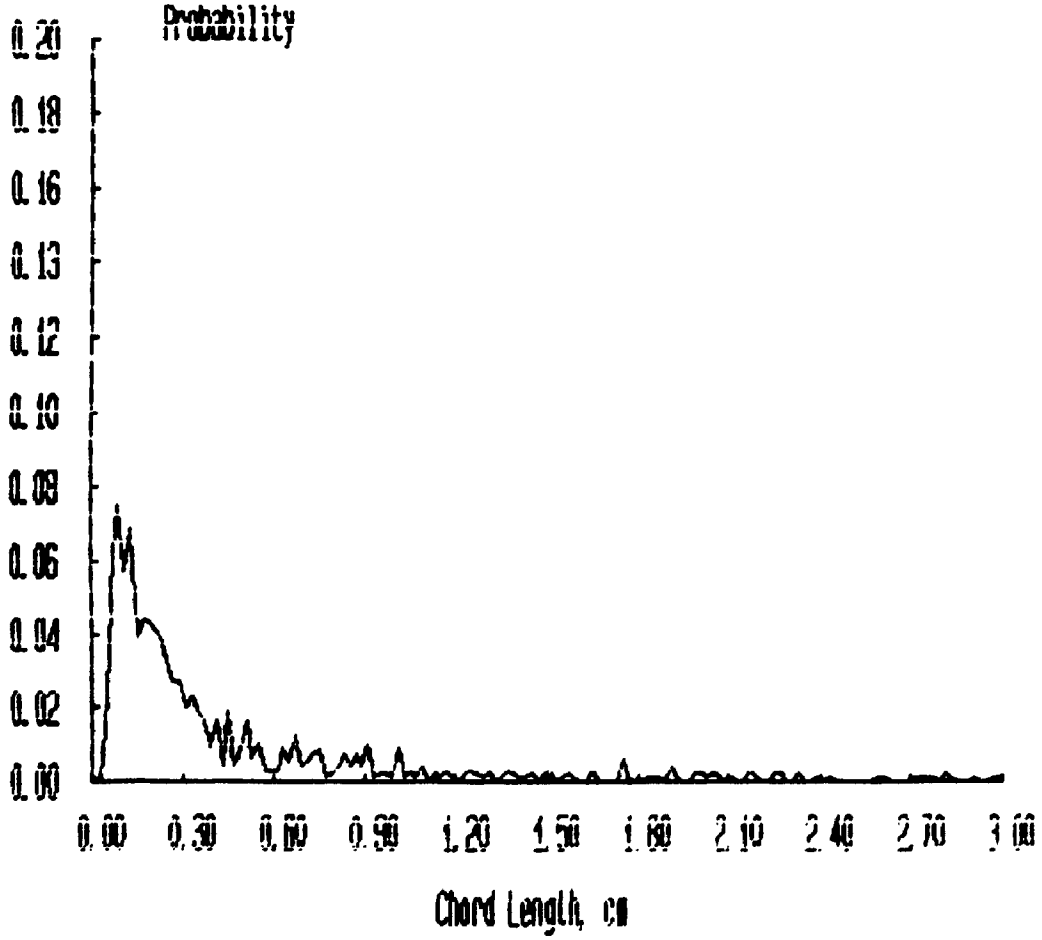

****** FILENAME ****** : JAN16D3A

**** Bubbles detected by probe 1 : 1509
**** Percentage of bubbles retained : 50.11
**** Average bubble duration : .006396 s

Probability Distributions

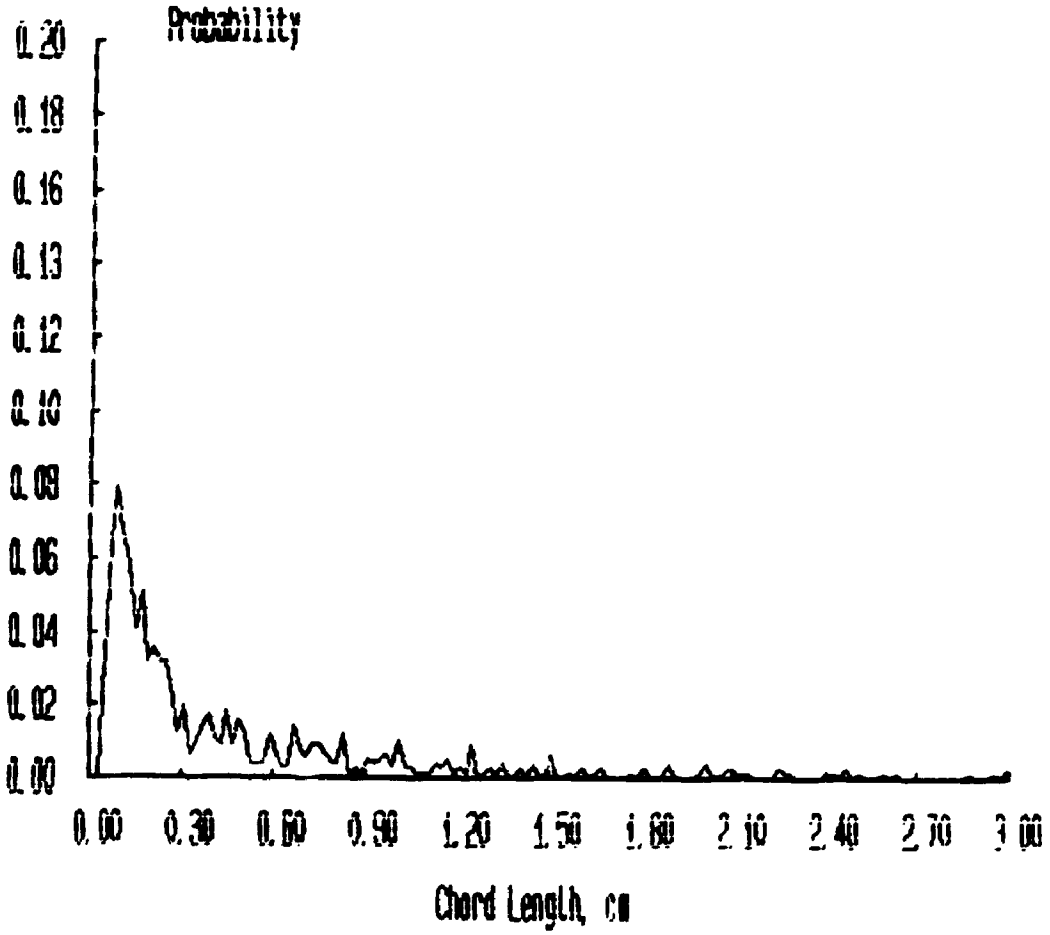

****** FILENAME ****** : JAN16D4A

**** Bubbles detected by probe 1 : 1059
**** Percentage of bubbles retained : 38.43
**** Average bubble duration : .006224 s

Probability Distributions

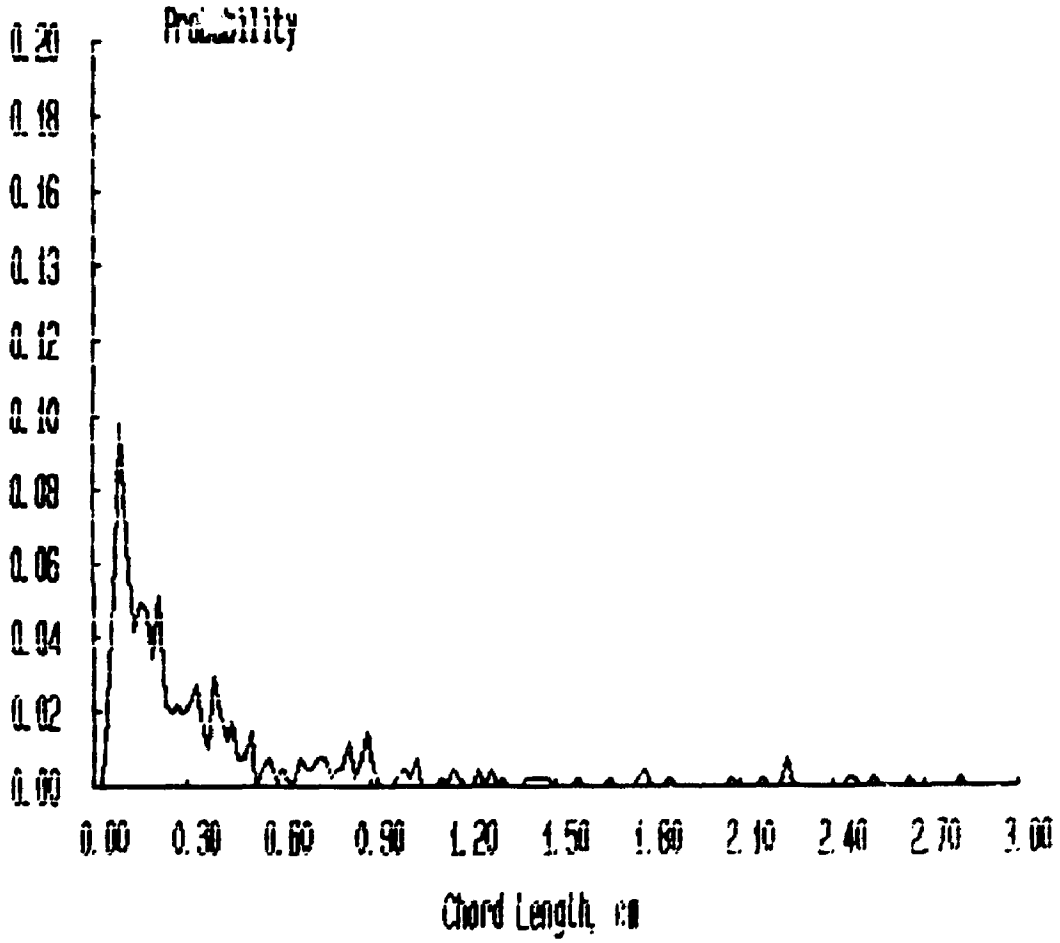

****** FILENAME ****** : JAN16D5A

**** Bubbles detected by probe 1 : 928
**** Percentage of bubbles retained : 46.98
**** Average bubble duration : .004344 s

Probability Distributions

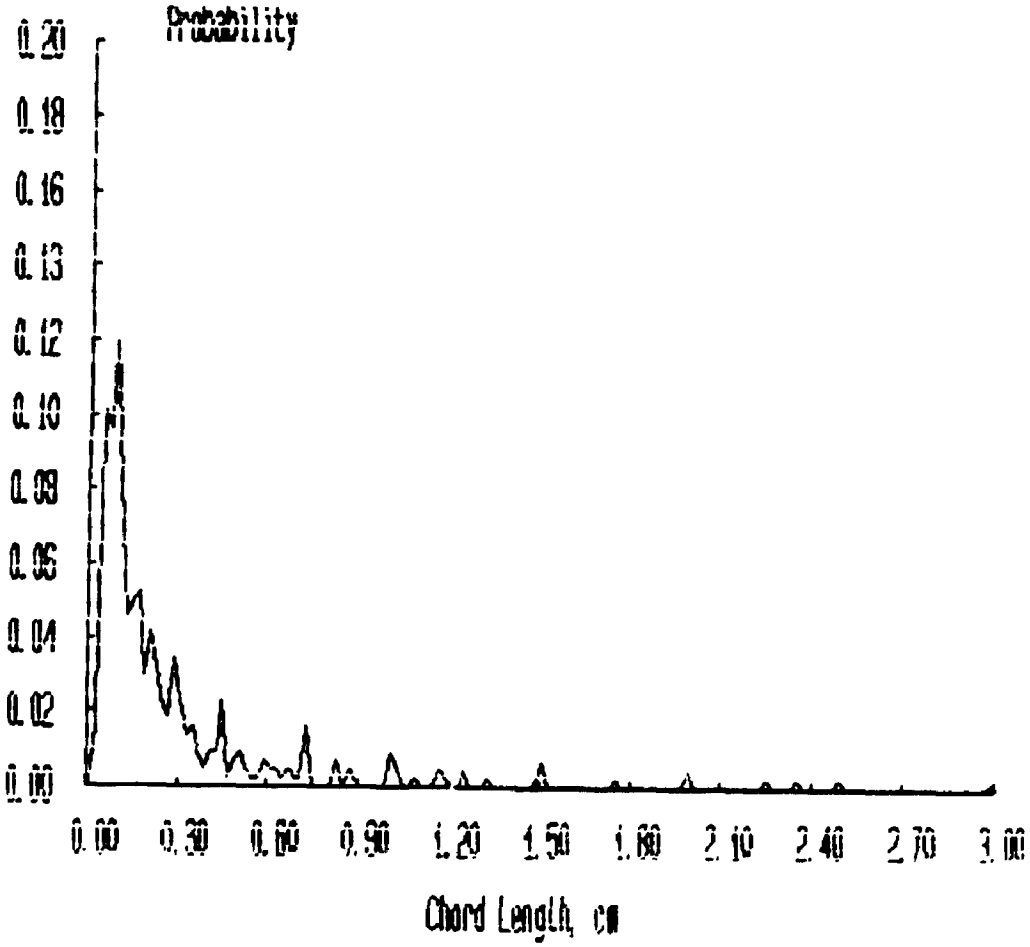

****** FILENAME ****** : JAN16D6A

**** Bubbles detected by probe 1 : 810
**** Percentage of bubbles retained : 41.36
**** Average bubble duration : .004985 s

Probability Distributions

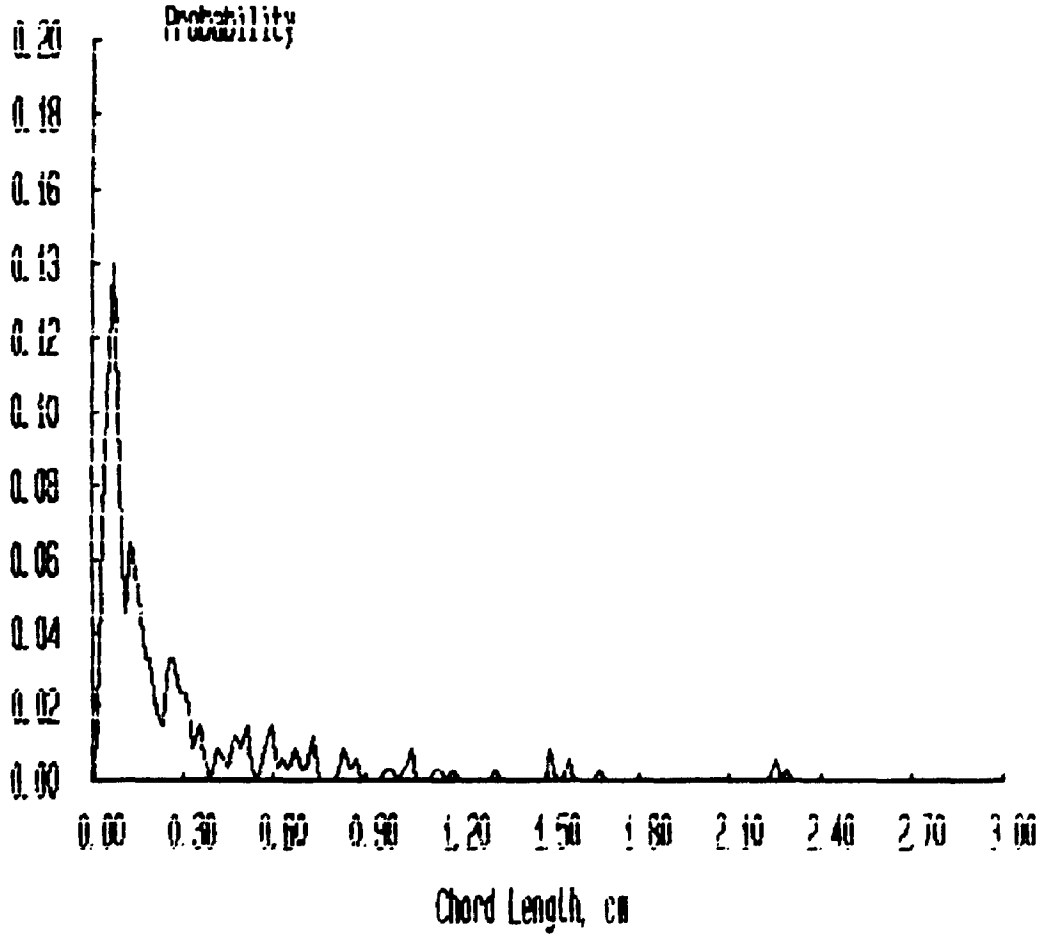

****** FILENAME ****** : JAN16E1A

**** Bubbles detected by probe 1 : 1144
**** Percentage of bubbles rete ned : 52.97
**** Average bubble duration : .UU6408 s

Probability Distributions

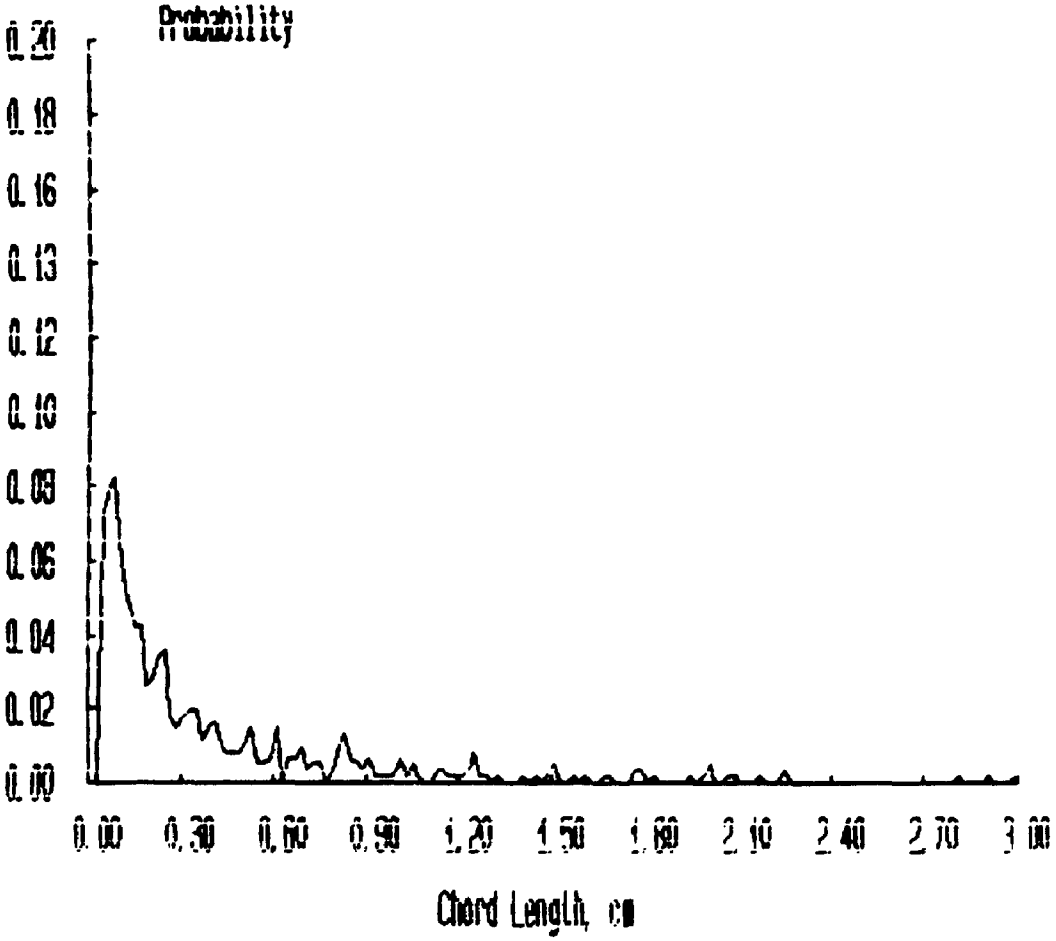

****** FILENAME ****** : JAN16E2A

**** Bubbles detected by probe 1 : 1208
**** Percentage of bubbles retained : 47.76
**** Average bubble duration : .006707 s

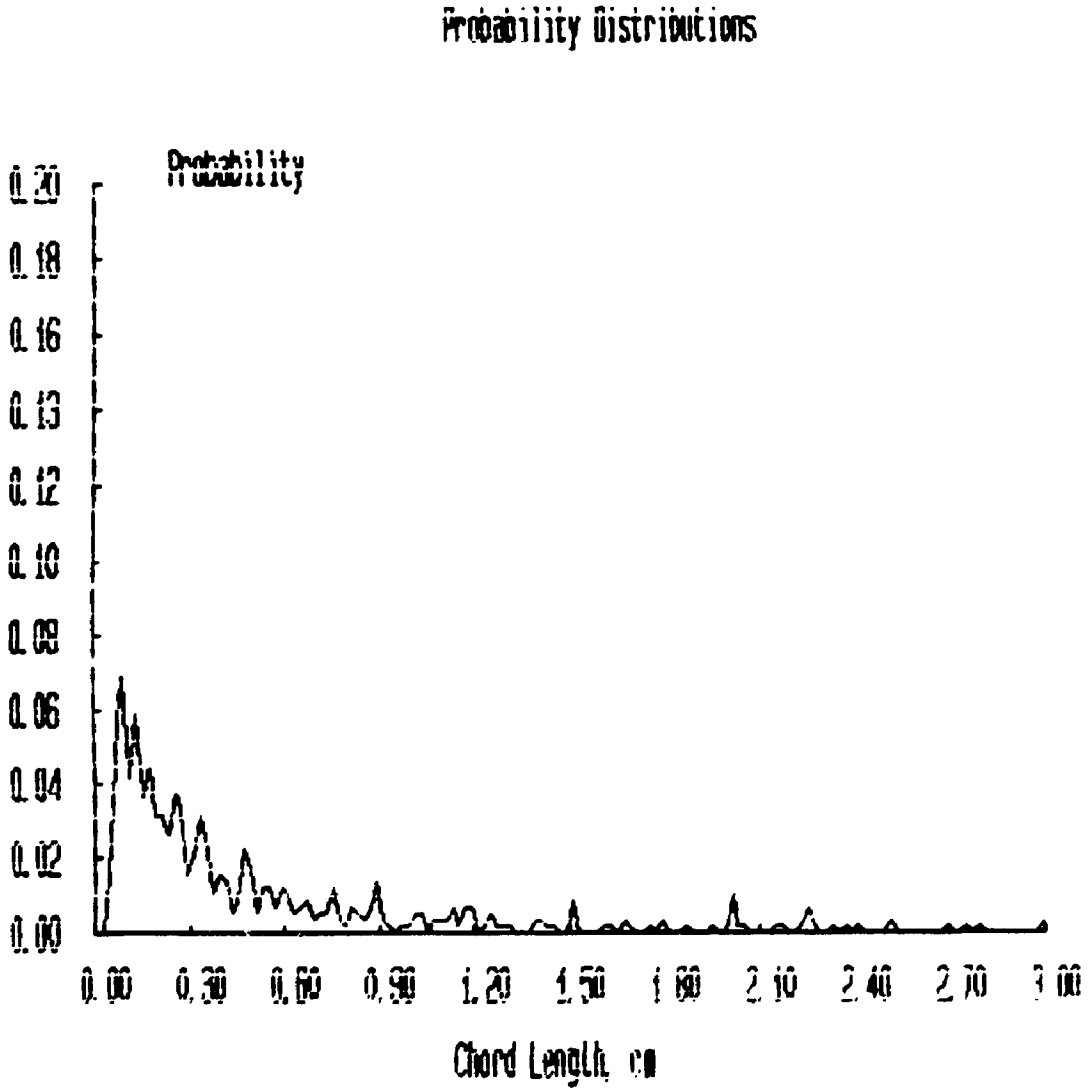

****** FILENAME ****** : JAN16E3A

**** Bubbles detected by probe 1 : 1213
**** Percentage of bubbles retained : 44.35
**** Average bubble duration : .UU6439 s

Probability Distributions

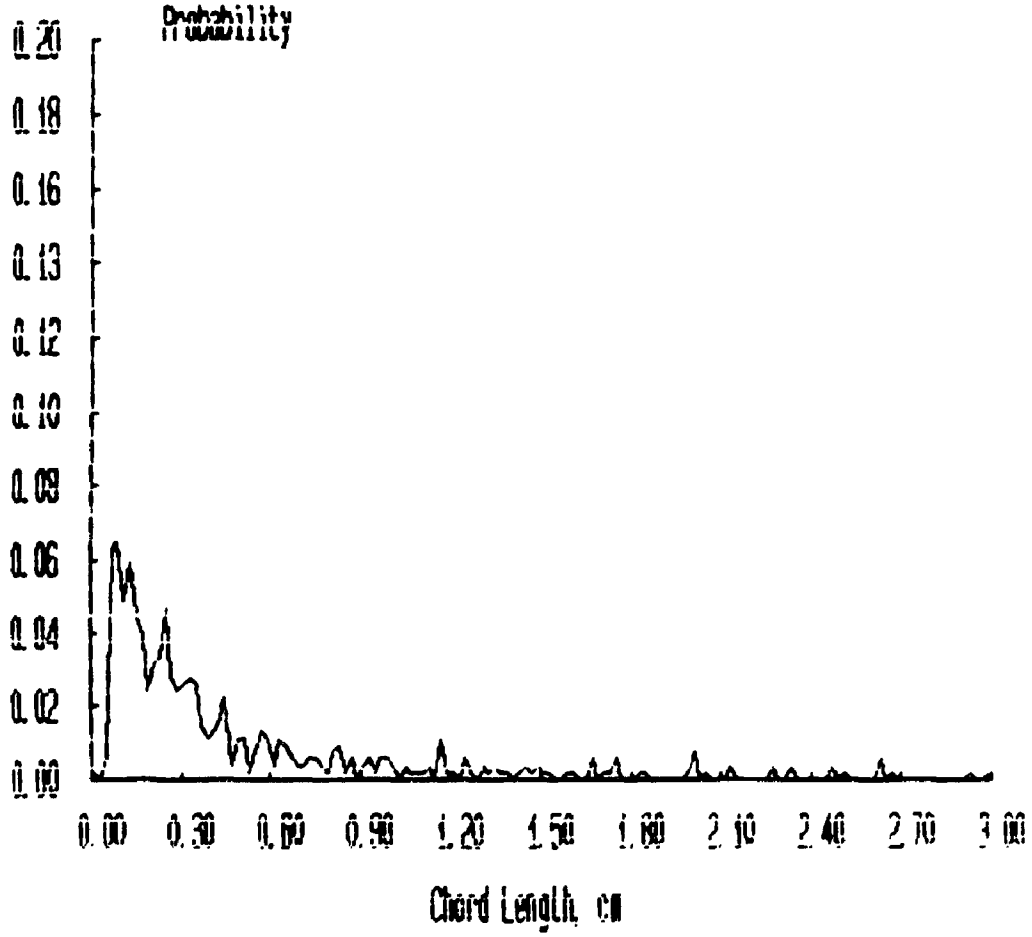

****** FILENAME ****** : JAN16E4A

**** Bubbles detected by probe 1 : 1155
**** Percentage of bubbles retained : 38.10
**** Average bubble duration : .0064UU s

Probability Distributions

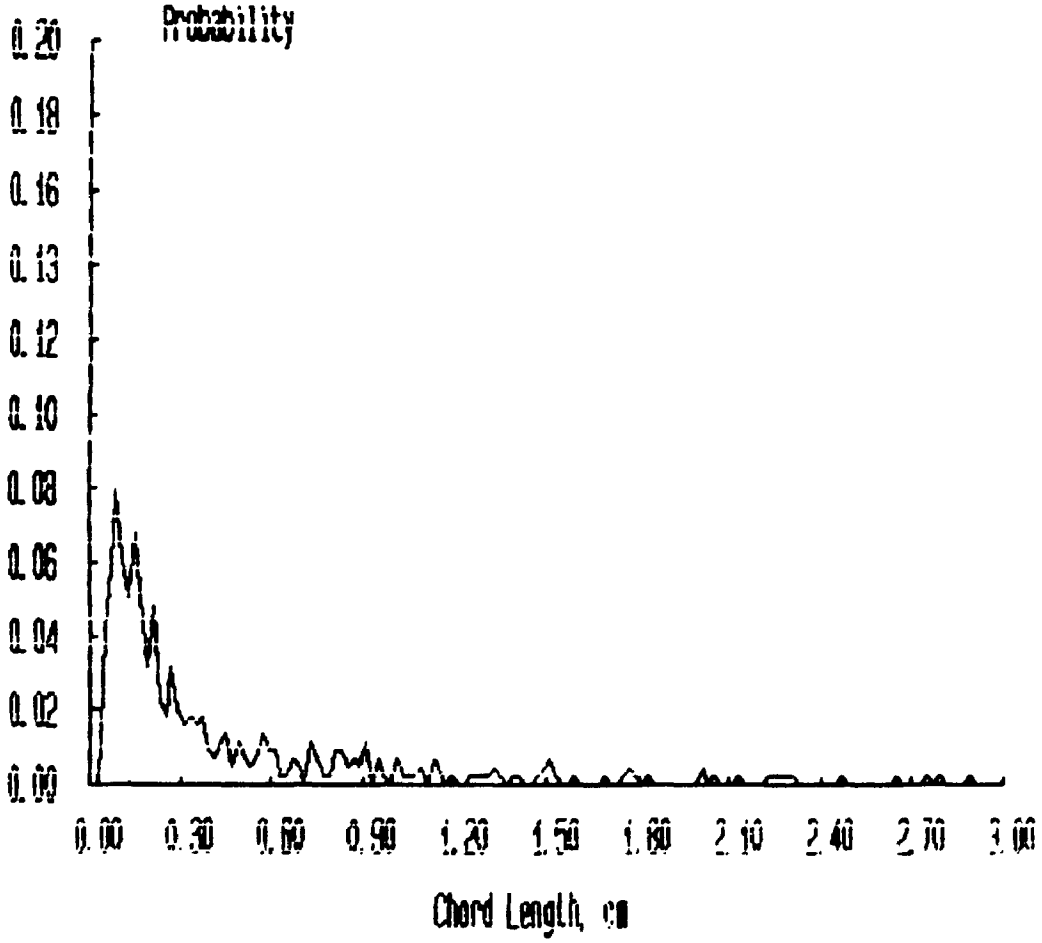

****** FILENAME ****** : JAN16E5A

**** Bubbles detected by probe 1 : 886
**** Percentage of bubbles retained : 44.13
**** Average bubble duration : .006151 s

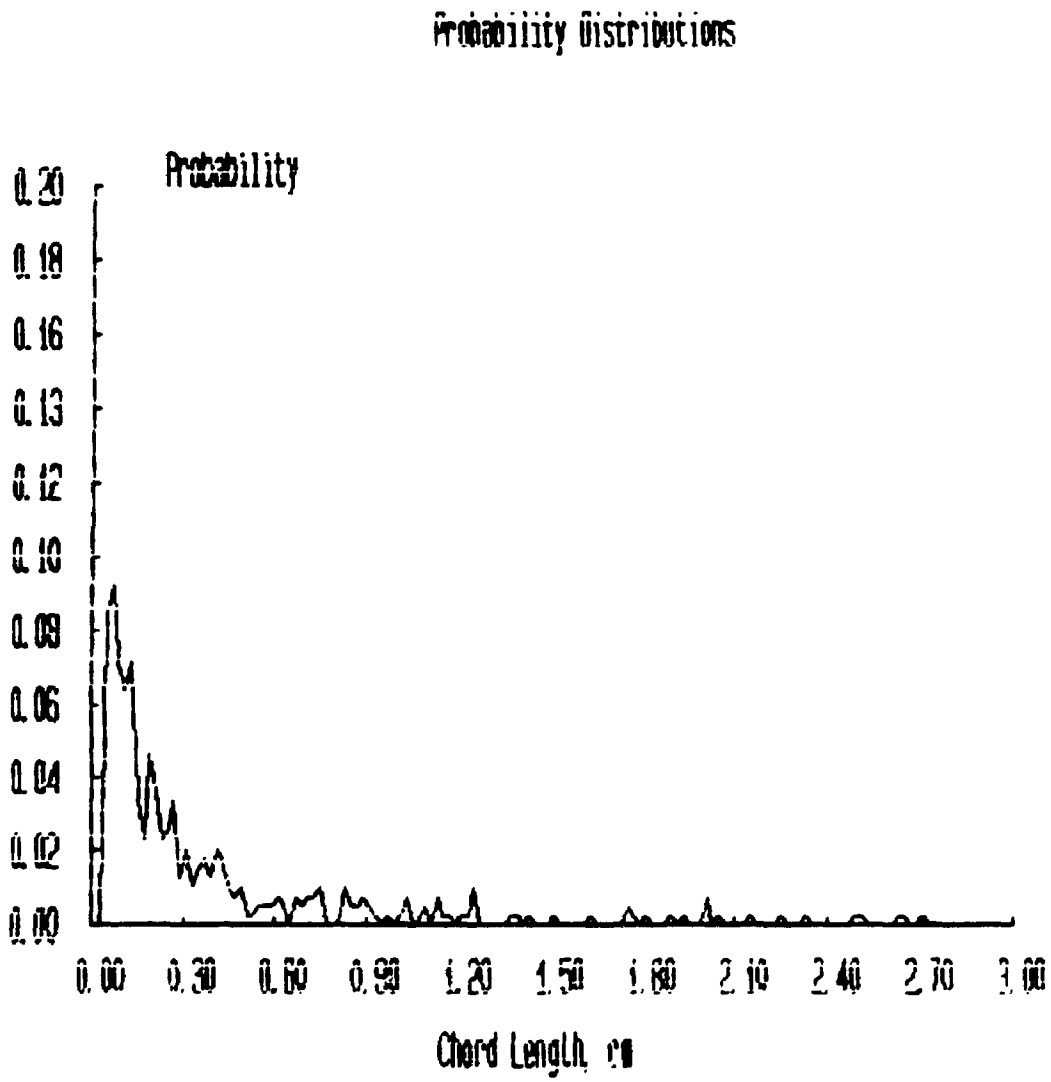

****** FILENAME ****** : JAN16E6A

**** Bubbles detected by probe 1 : 685
**** Percentage of bubbles retained : 35.58
**** Average bubble duration : .00589/ s

Probability Distributions

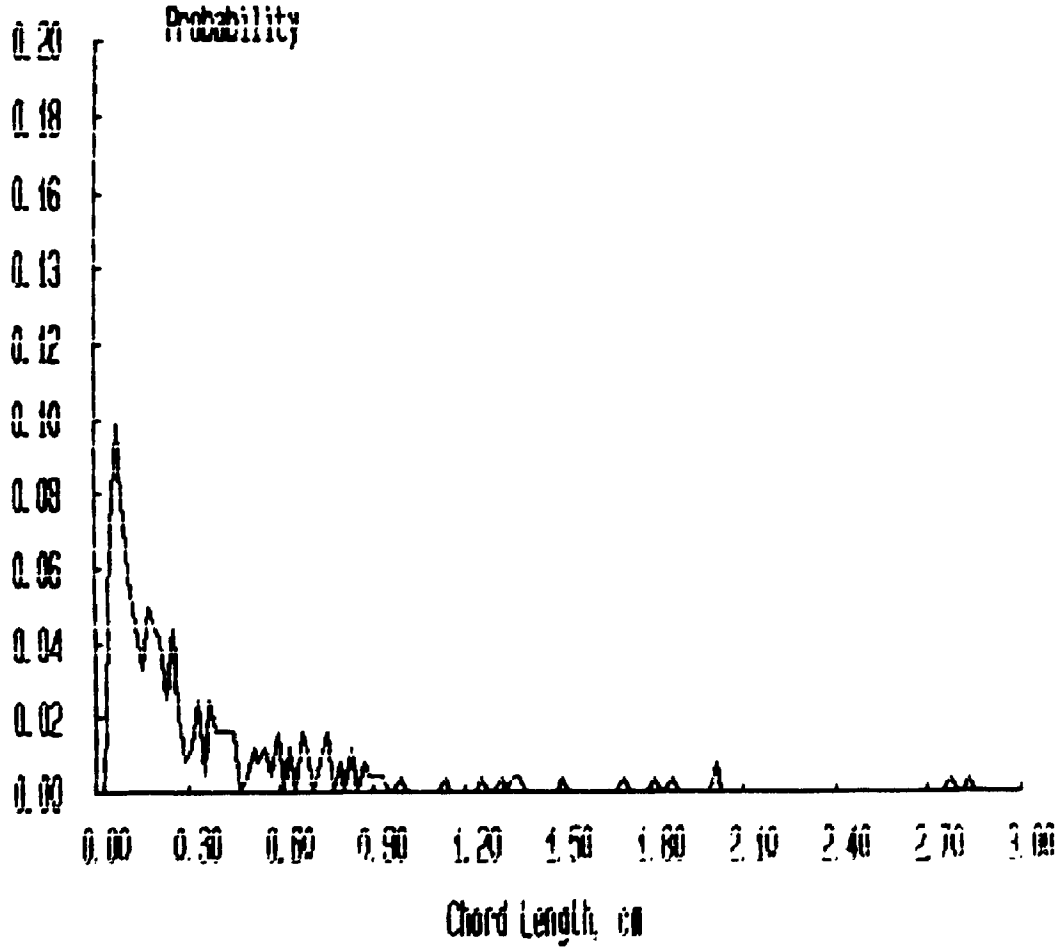

****** FILENAME ****** : JAN17A1A

**** Bubbles detected by probe 1 : 1647
**** Percentage of bubbles retained : 65.57
**** Average bubble duration : .006097 s

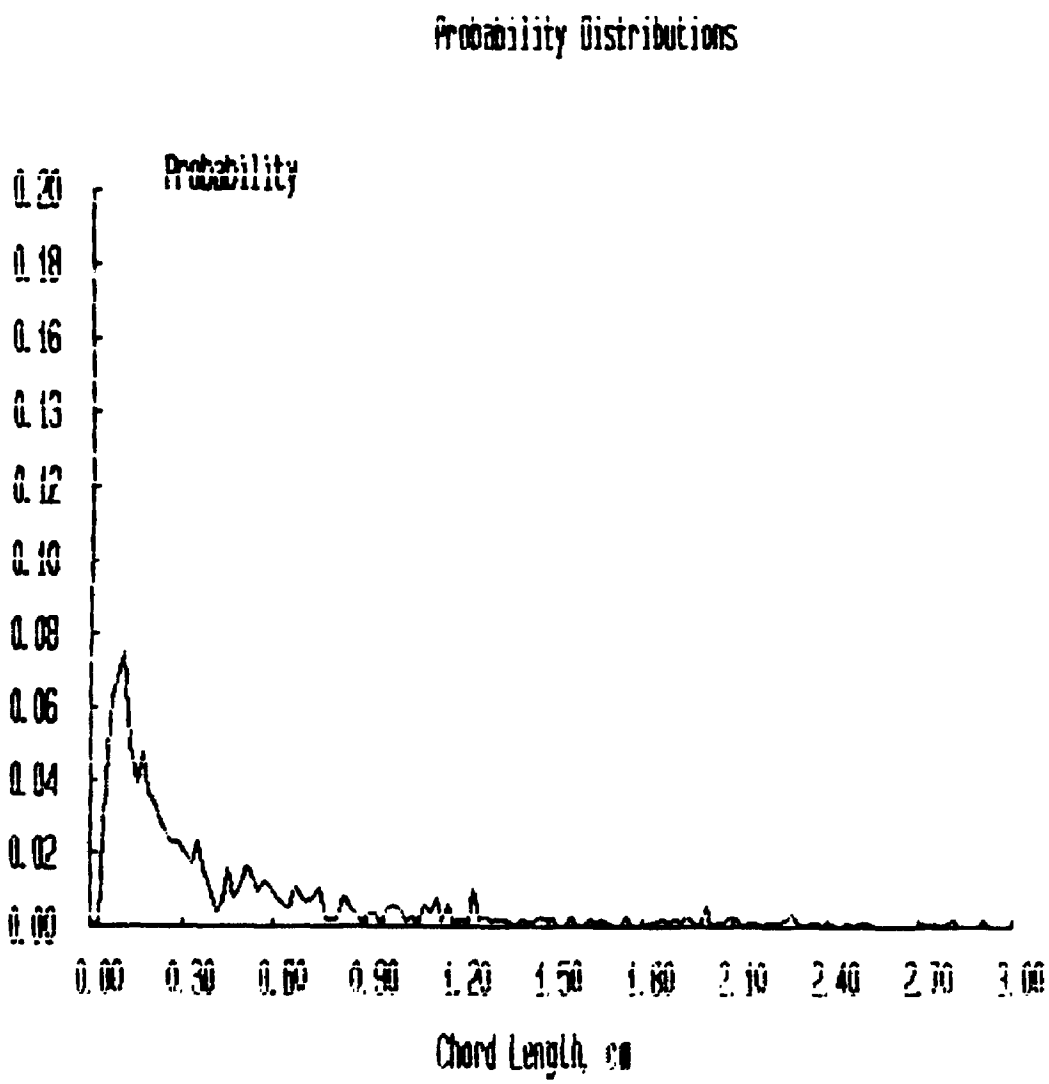

****** FILENAME ****** : JAN17A2A

**** Bubbles detected by probe 1 : 1/86
**** Percentage of bubbles retained : 56.66
**** Average bubble duration : .UU6359 s

Probability Distributions

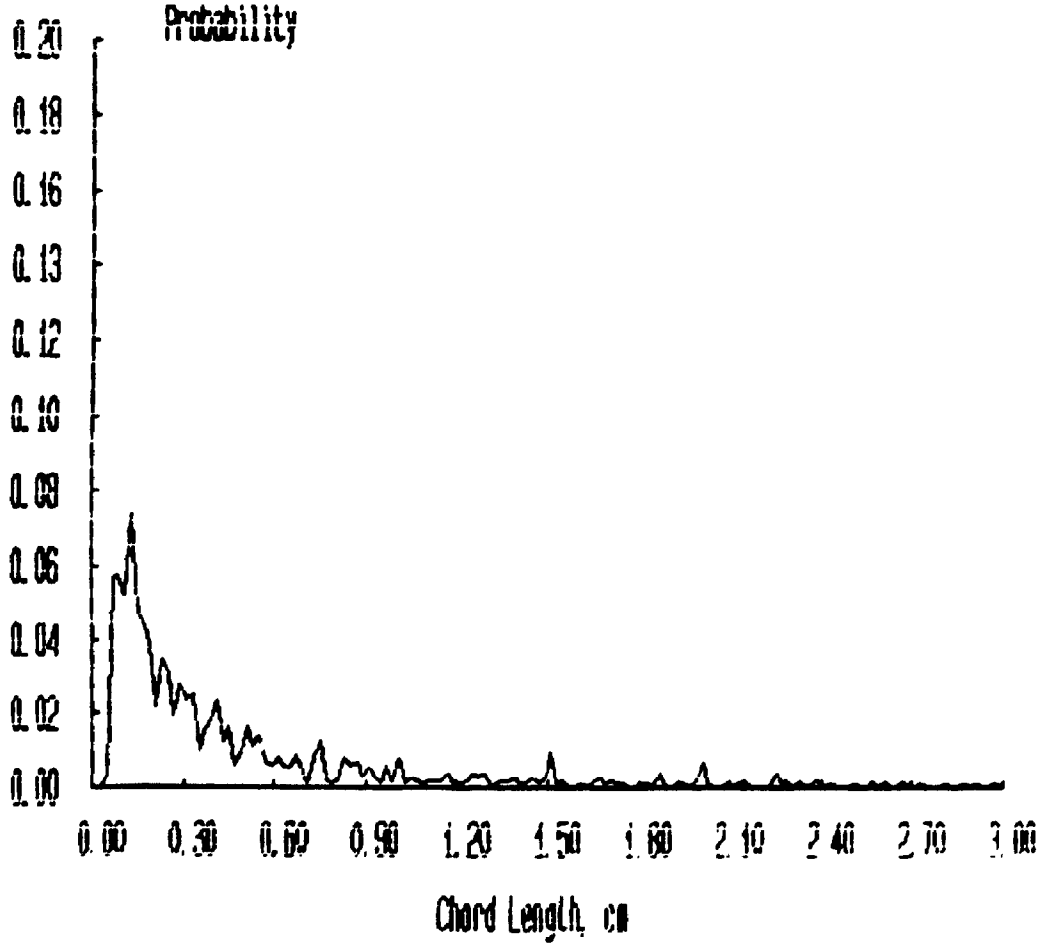

****** FILENAME ****** : JAN17A3A

**** Bubbles detected by probe 1 : 1659
**** Percentage of bubbles retained : 54.85
**** Average bubble duration : .005864 s

Probability Distributions

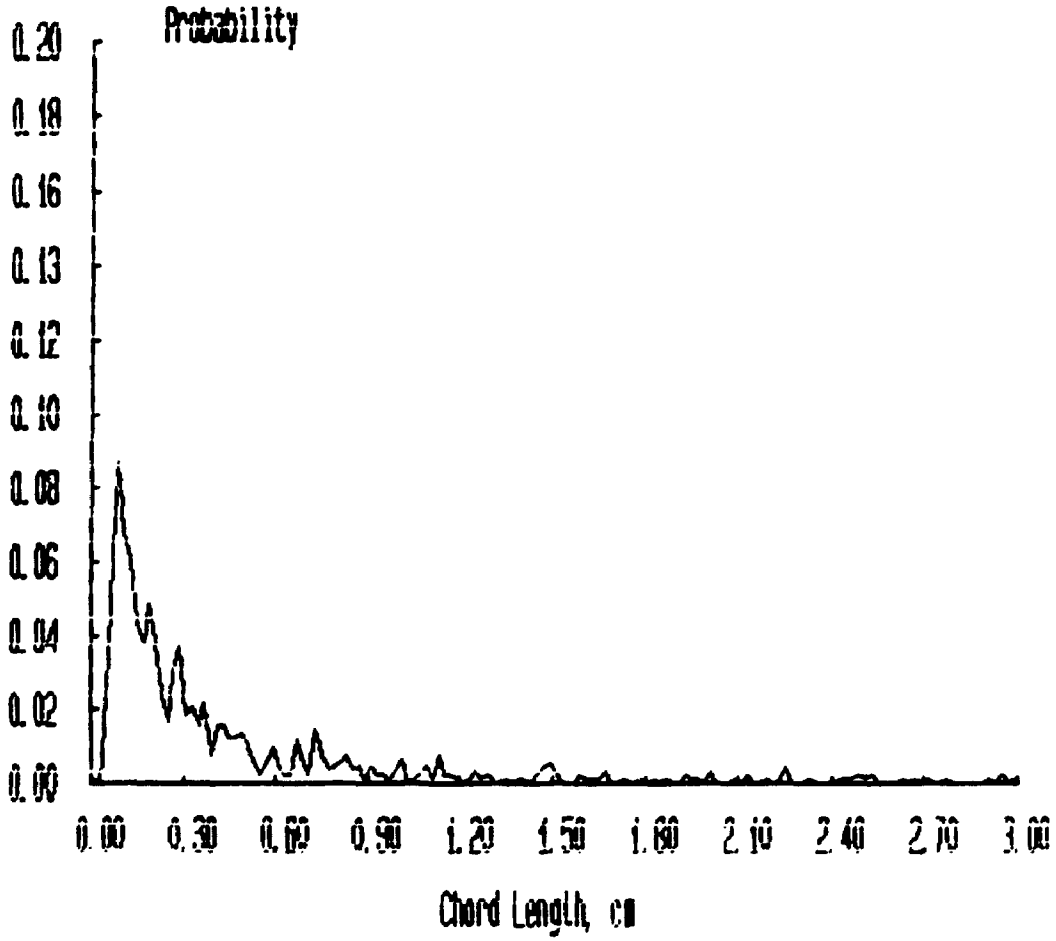

****** FILENAME ****** : JAN17A4A

**** Bubbles detected by probe 1 : 1186
**** Percentage of bubbles retained : 38.95
**** Average bubble duration : .005513 s

Probability Distributions

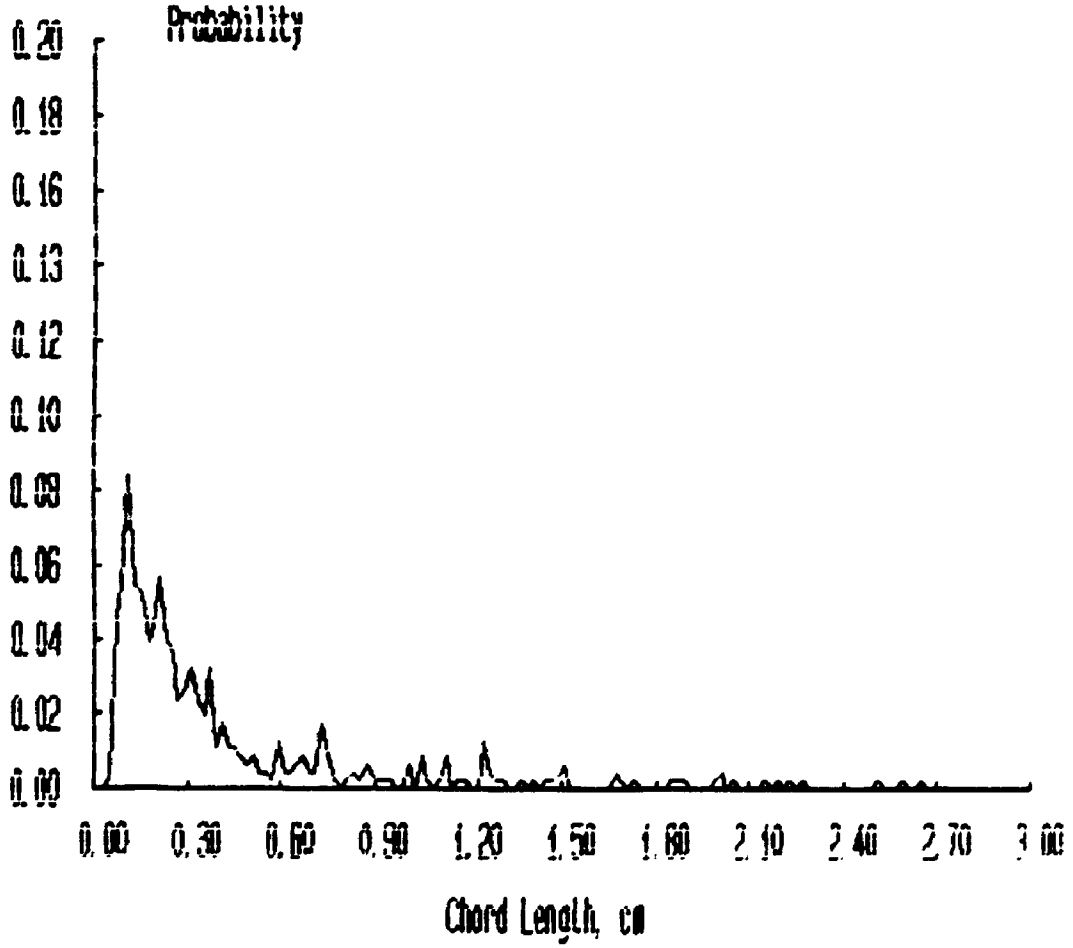

****** FILENAME ****** : JAN17A5A

**** Bubbles detected by probe 1 : 1059
**** Percentage of bubbles retained : 28.52
**** Average bubble duration : .005119 s

Probability Distributions

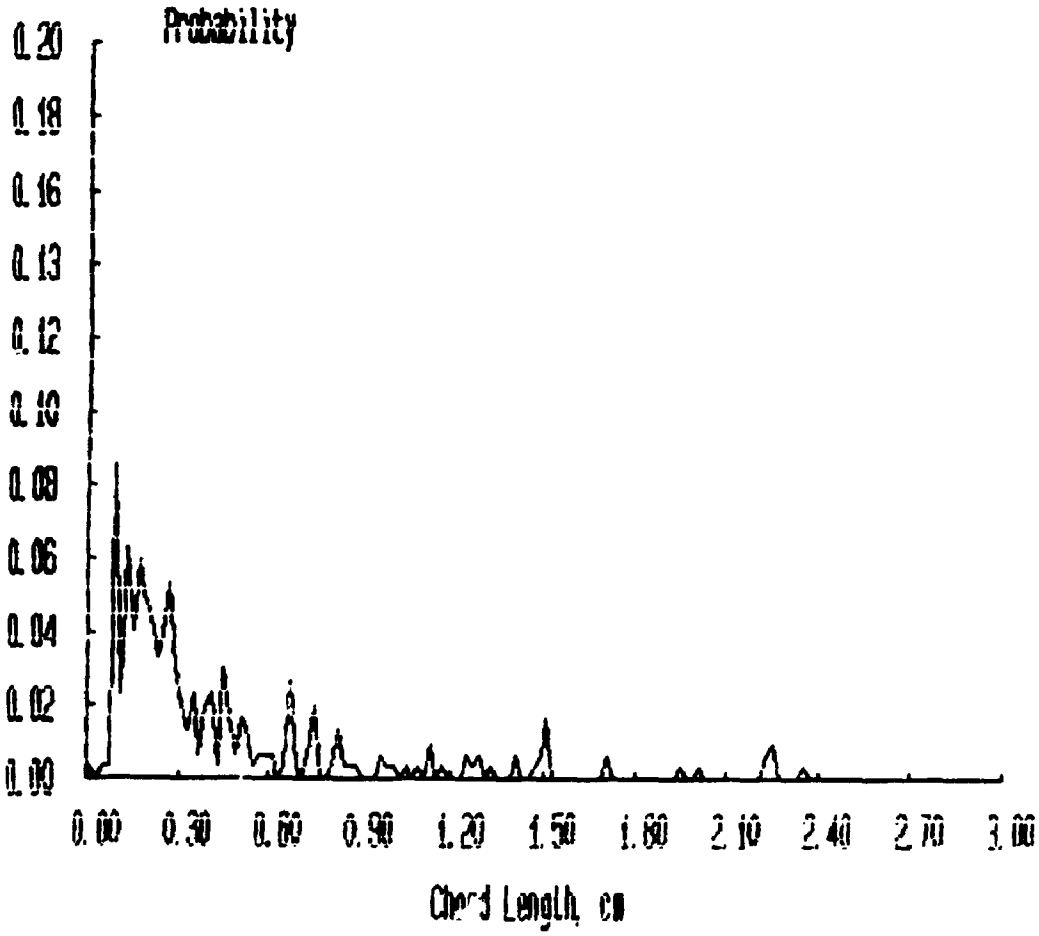

****** FILENAME ****** : JAN17A6A

**** Bubbles detected by probe 1 : 1086
**** Percentage of bubbles retained : 47.88
**** Average bubble duration : .004350 s

Probability Distributions

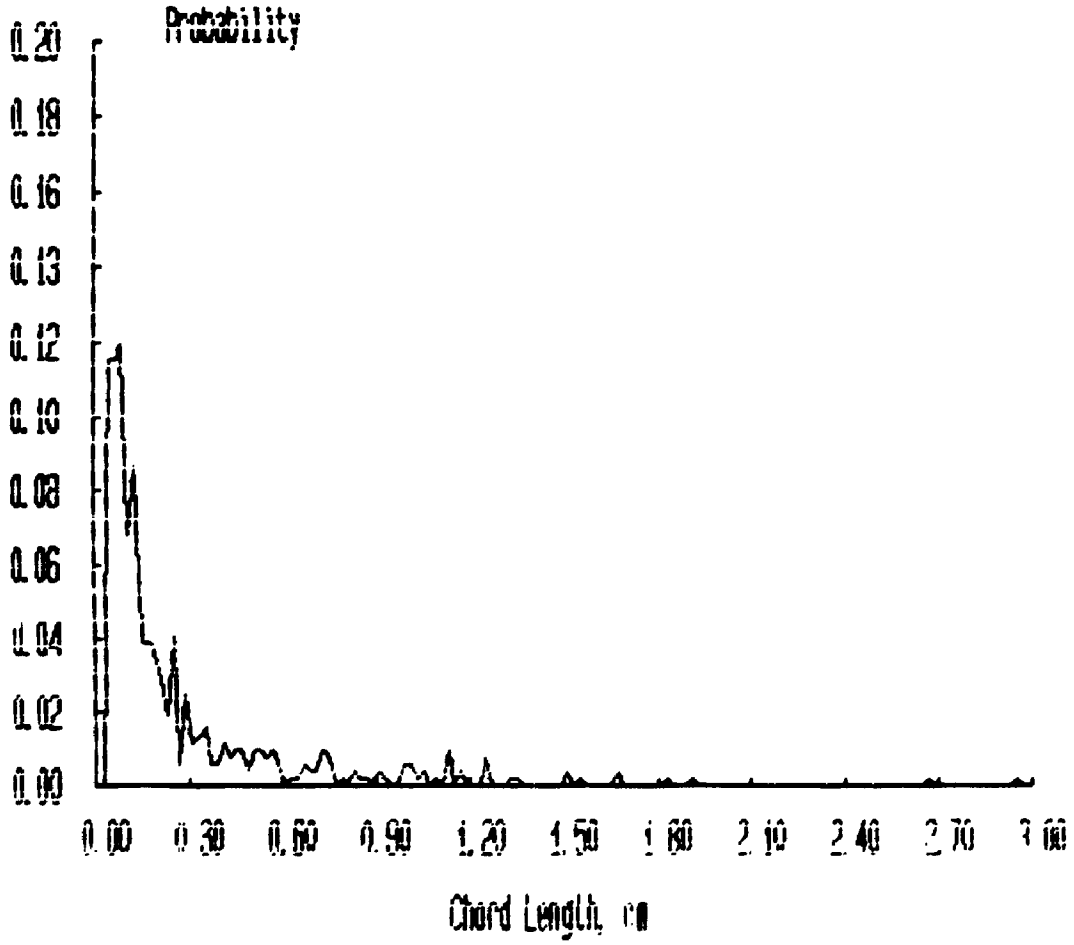

****** FILENAME ****** : JAN17B1A

**** Bubbles detected by probe 1 : 2425
**** Percentage of bubbles retained : 62.60
**** Average bubble duration : .005628 s

Probability Distributions

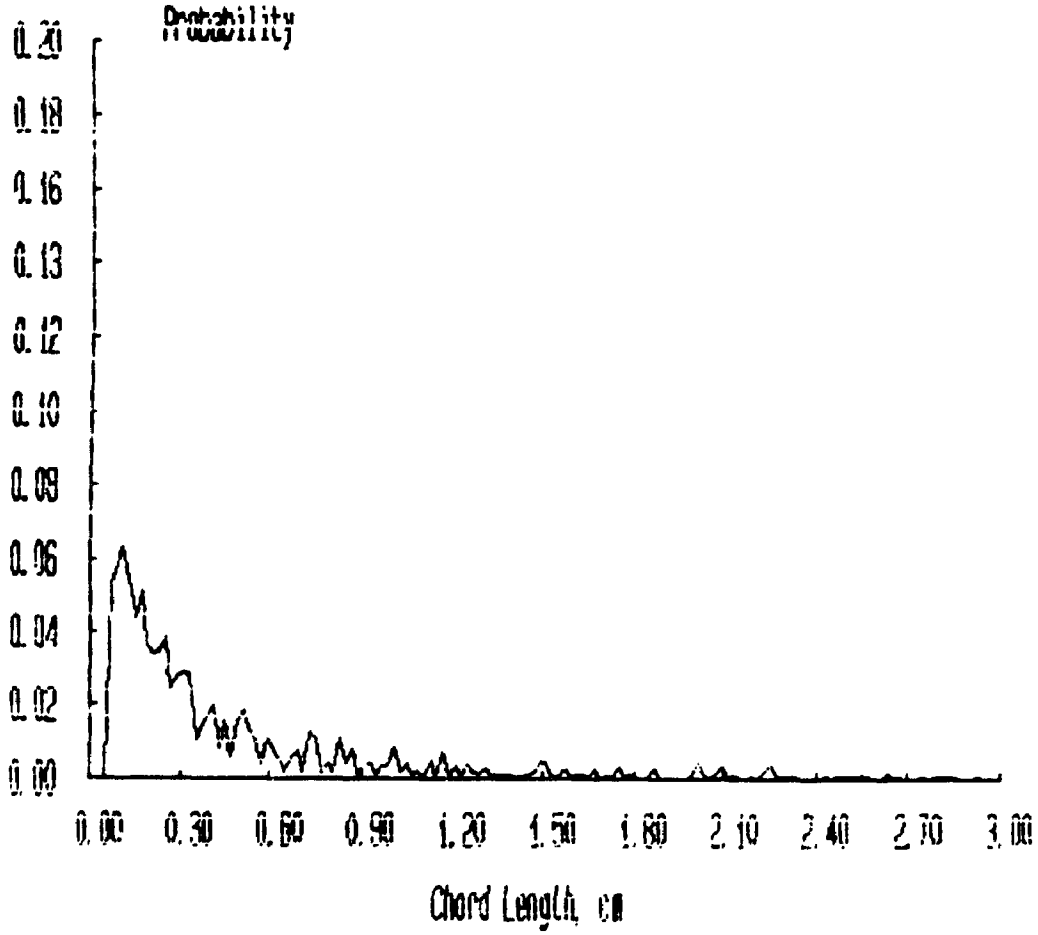

****** FILENAME ****** : JAN17B2A

**** Bubbles detected by probe 1 : 2345
**** Percentage of bubbles retained : 56.25
**** Average bubble duration : .005464 s

Probability Distributions

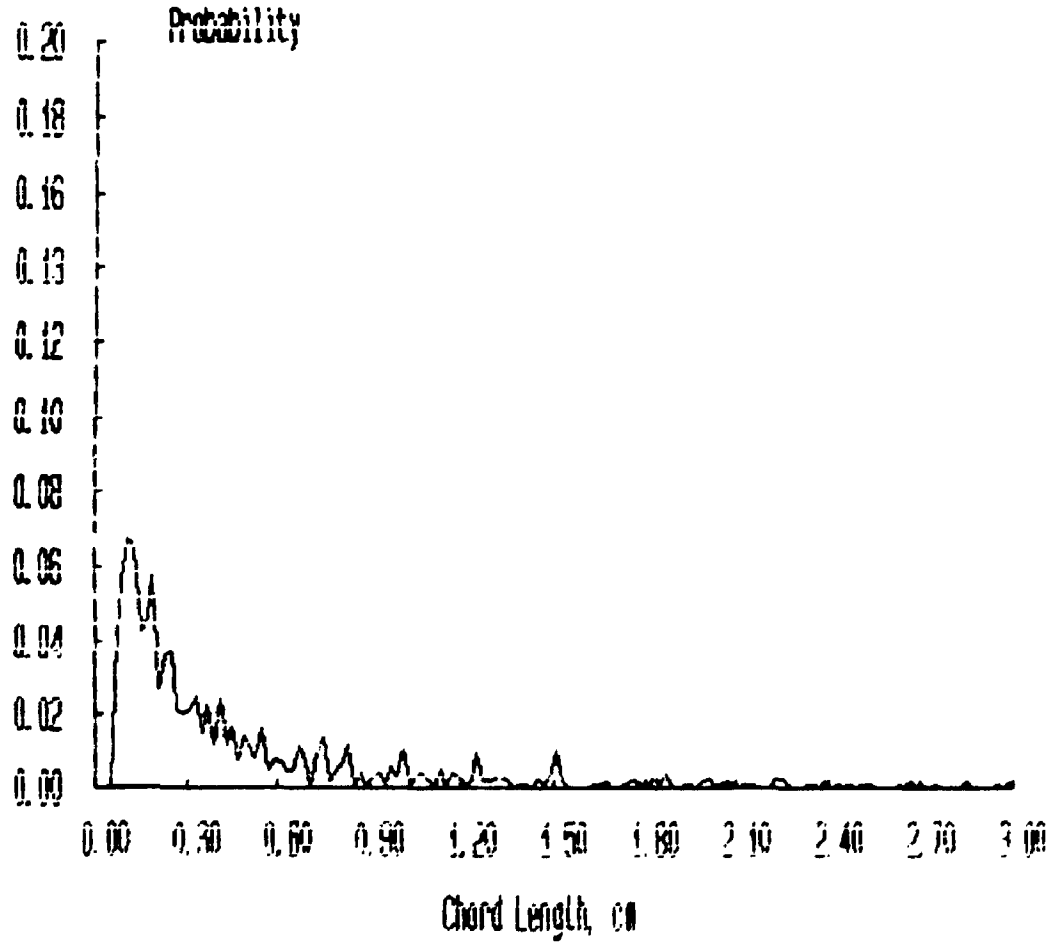

****** FILENAME ****** : JAN1783A

**** Bubbles detected by probe 1 : 1845
**** Percentage of bubbles retained : 53.71
**** Average bubble duration : .005333 s

Probability Distributions

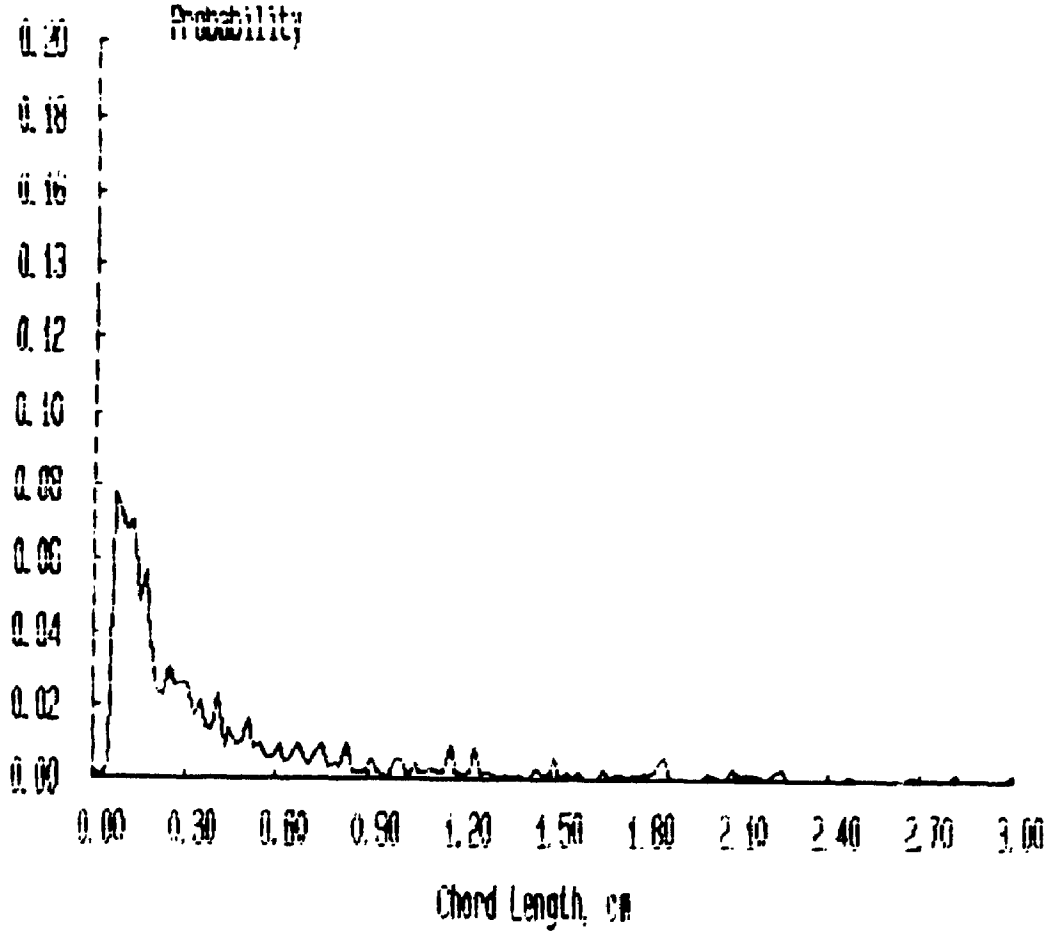

****** FILENAME ****** : JAN17B4A

**** Bubbles detected by probe 1 : 1657
**** Percentage of bubbles retained : 45.08
**** Average bubble duration : .004929 s

Probability Distributions

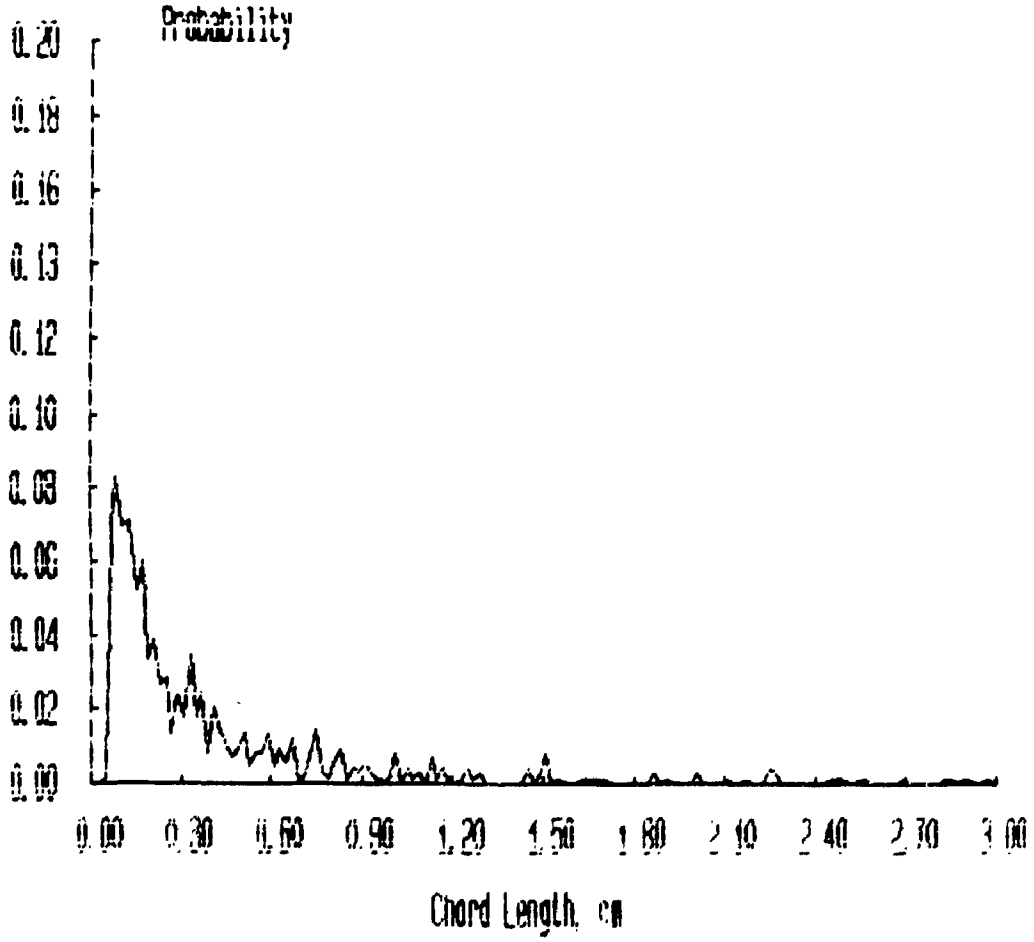

****** FILENAME ****** : JAN1785A

**** Bubbles detected by probe 1 : 1244
**** Percentage of bubbles retained : 41.24
**** Average bubble duration : .004320 s

Probability Distributions

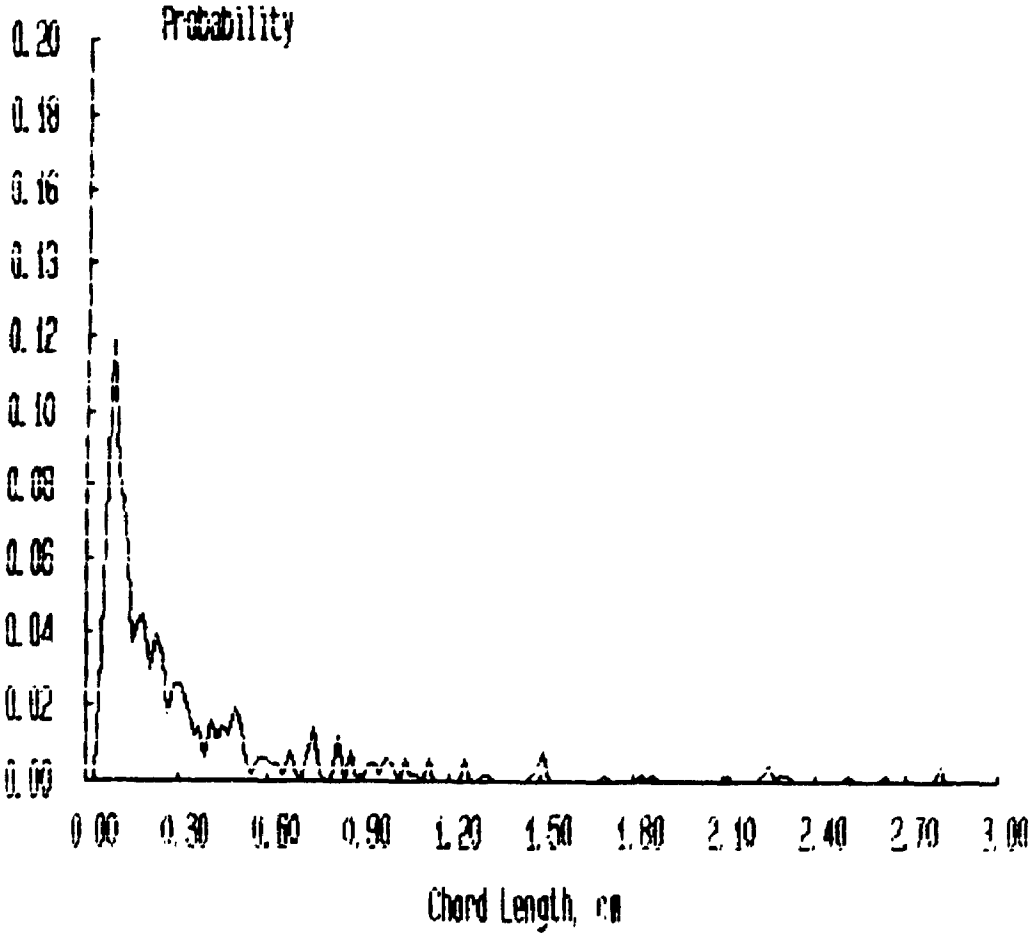

***** FILENAME ****** : JAN17B6A

**** Bubbles detected by probe 1 : 1131
**** Percentage of bubbles retained : 48.72
**** Average bubble duration : .003824 s

Probability Distributions

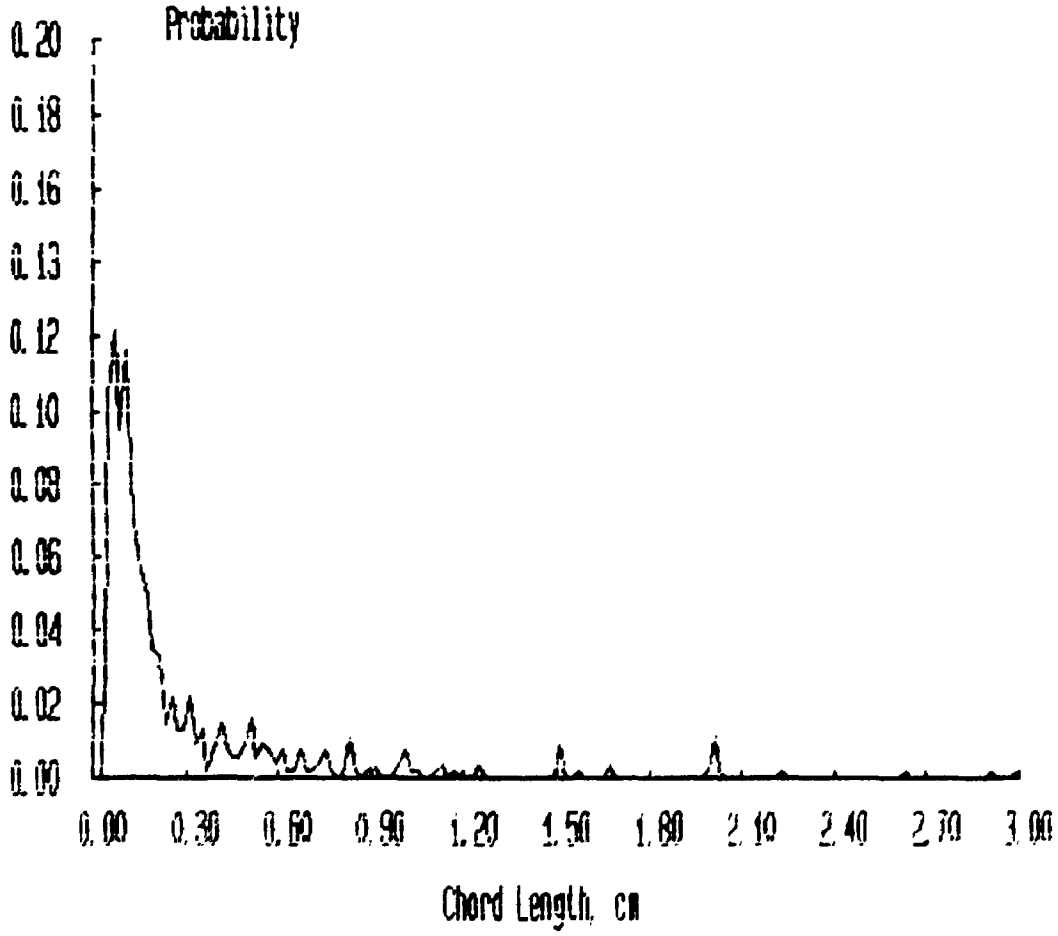

****** FILENAME ****** : JAN17C1A

**** Bubbles detected by probe 1 : 2779
**** Percentage of bubbles retained : 69.49
**** Average bubble duration : .005418 s

Probability Distributions

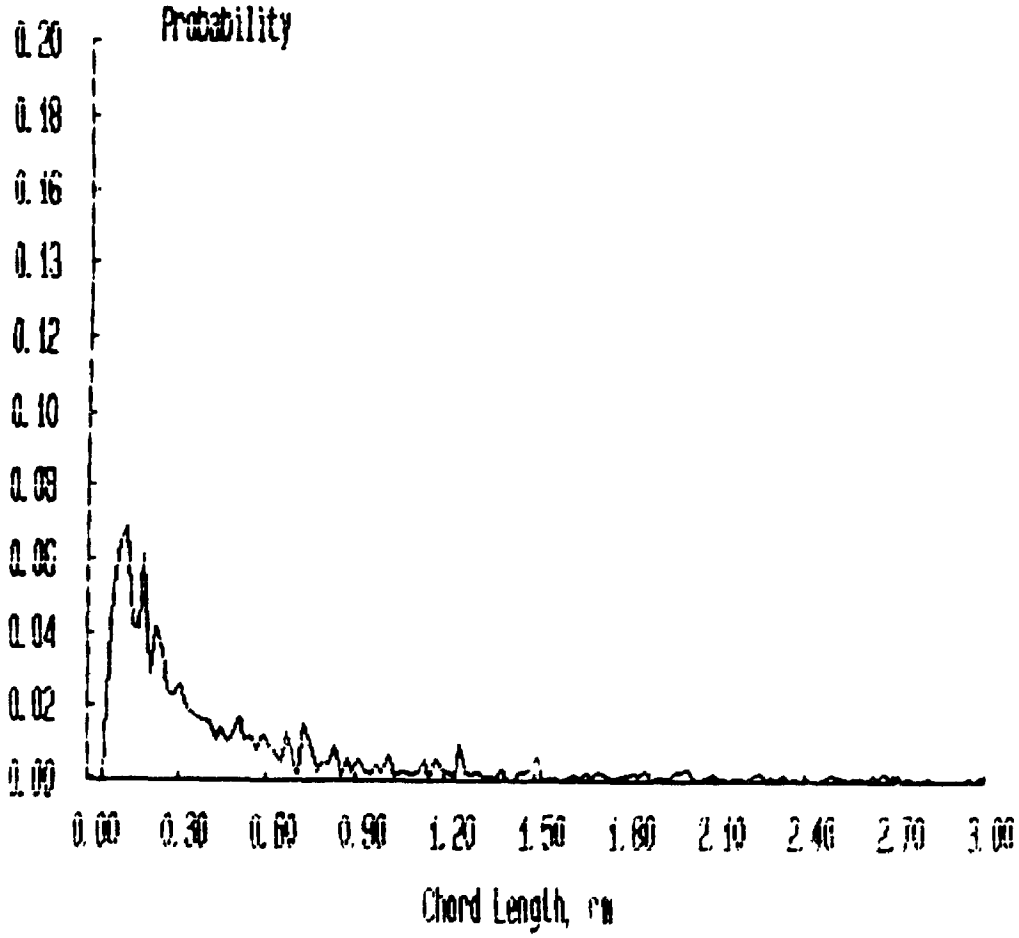

****** FILENAME ****** : JAN17C2A

**** Bubbles detected by probe 1 : 2739
**** Percentage of bubbles retained : 68.49
**** Average bubble duration : .005489 s

Probability Distributions

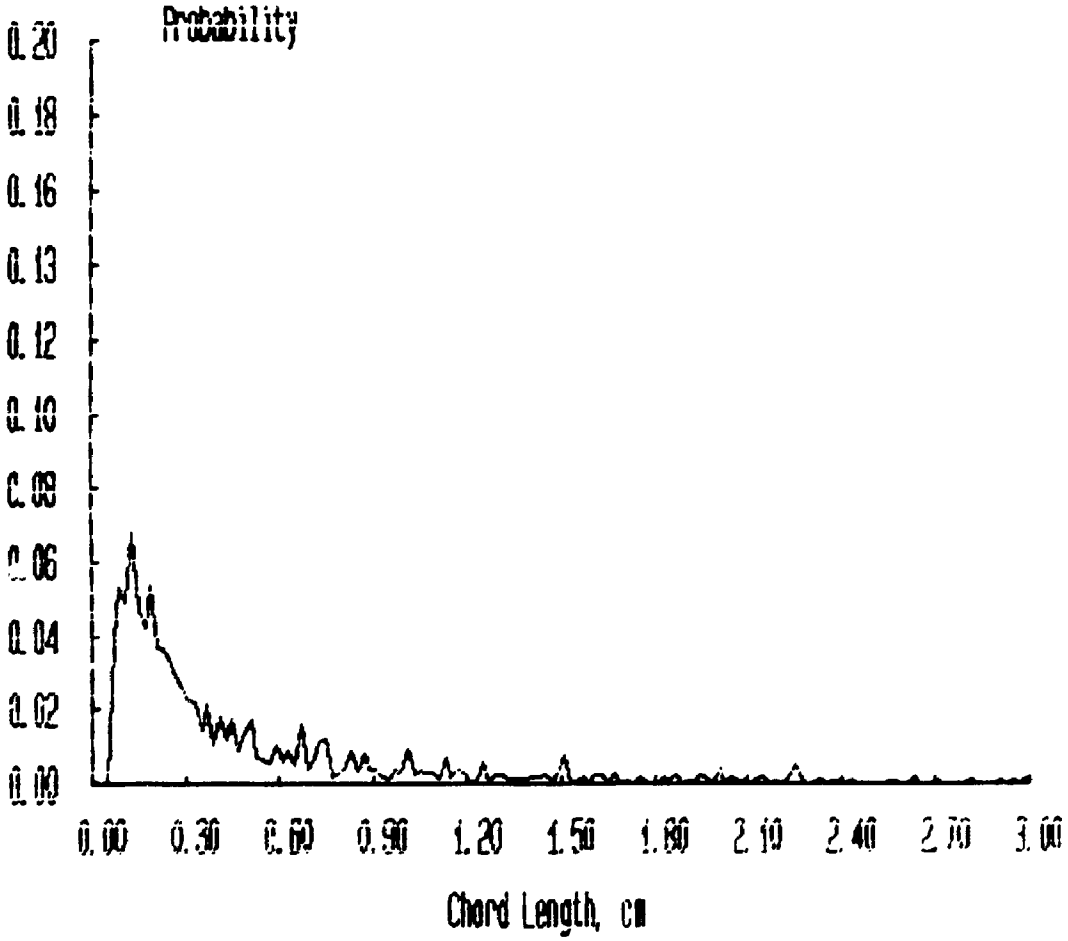

****** FILENAME ****** : JAN17C3A

**** Bubbles detected by probe 1 : 2325
**** Percentage of bubbles retained : 56.99
**** Average bubble duration : .005165 s

Probability Distributions

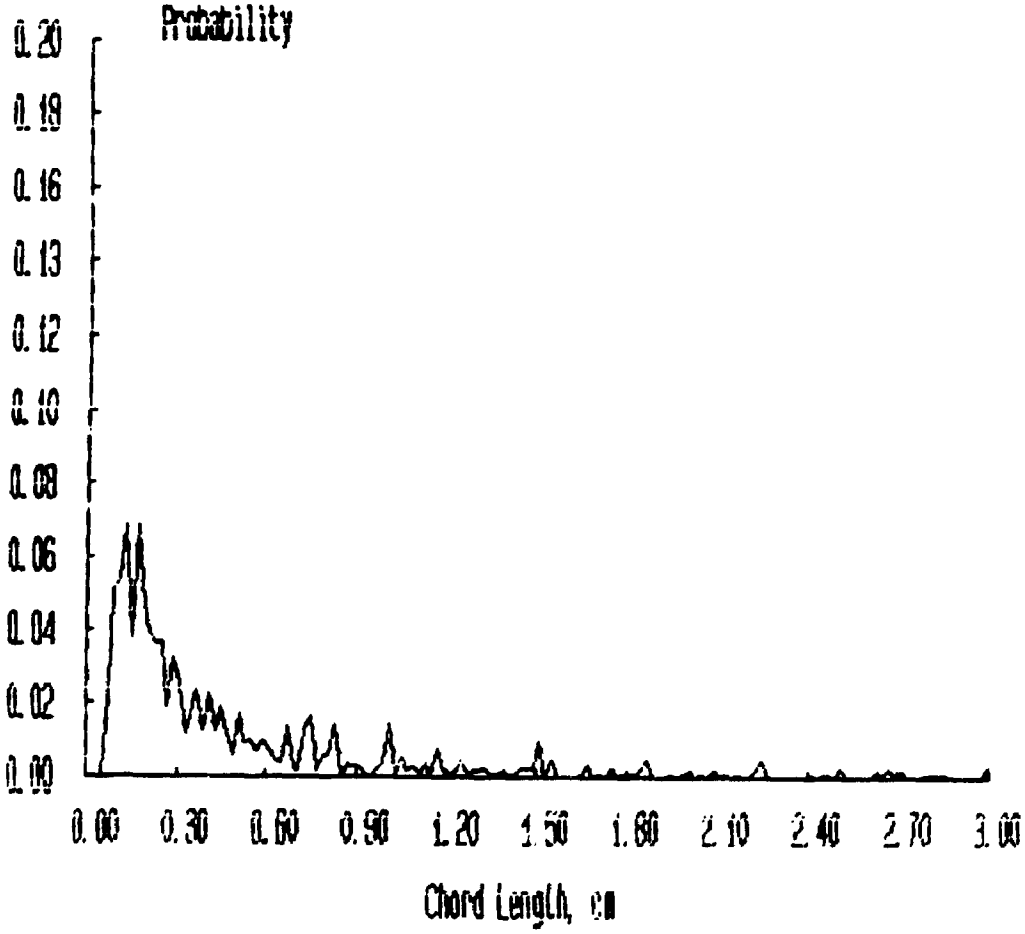

****** FILENAME ****** : JAN17C4A

**** Bubbles detected by probe 1 : 1639
**** Percentage of bubbles retained : 43.75
**** Average bubble duration : .004725 s

Probability Distributions

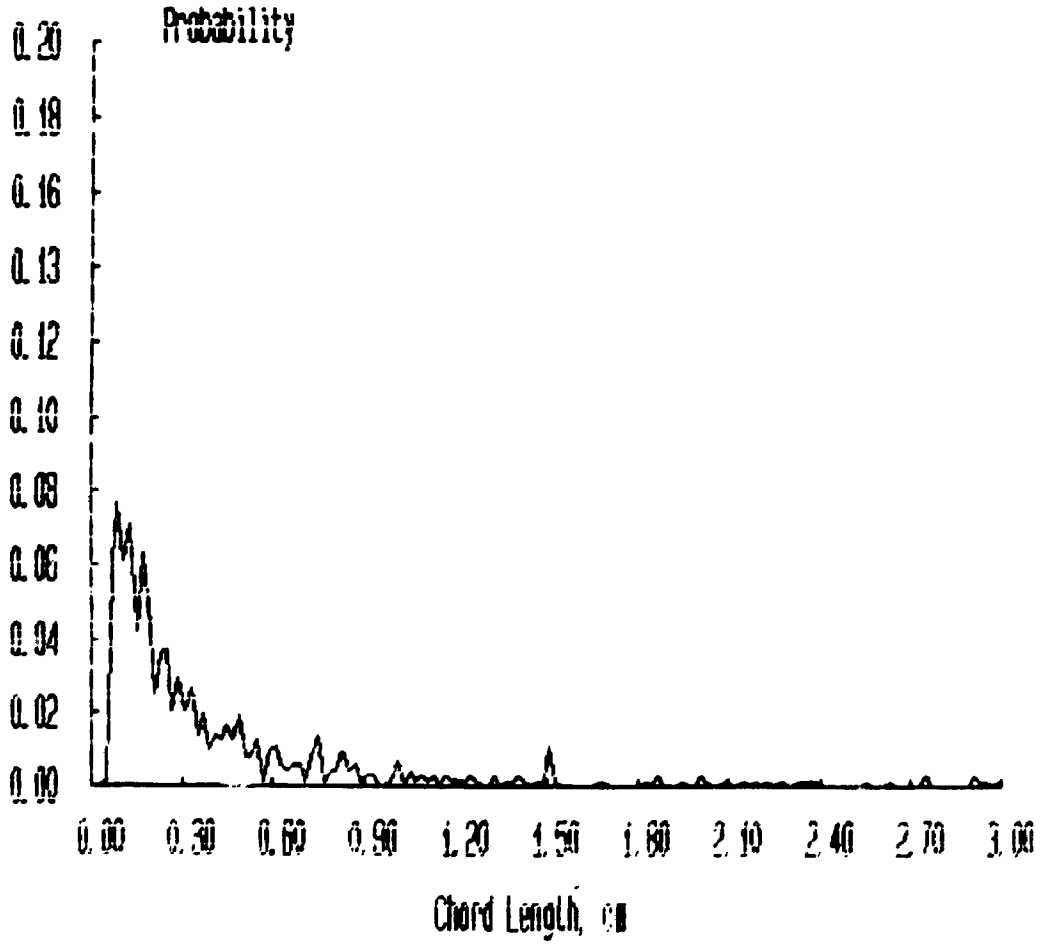

****** FILENAME ****** : JAN17C5A

**** Bubbles detected by probe 1 : 1348
**** Percentage of bubbles retained : 43.84
**** Average bubble duration : .004460 s

Probability Distributions

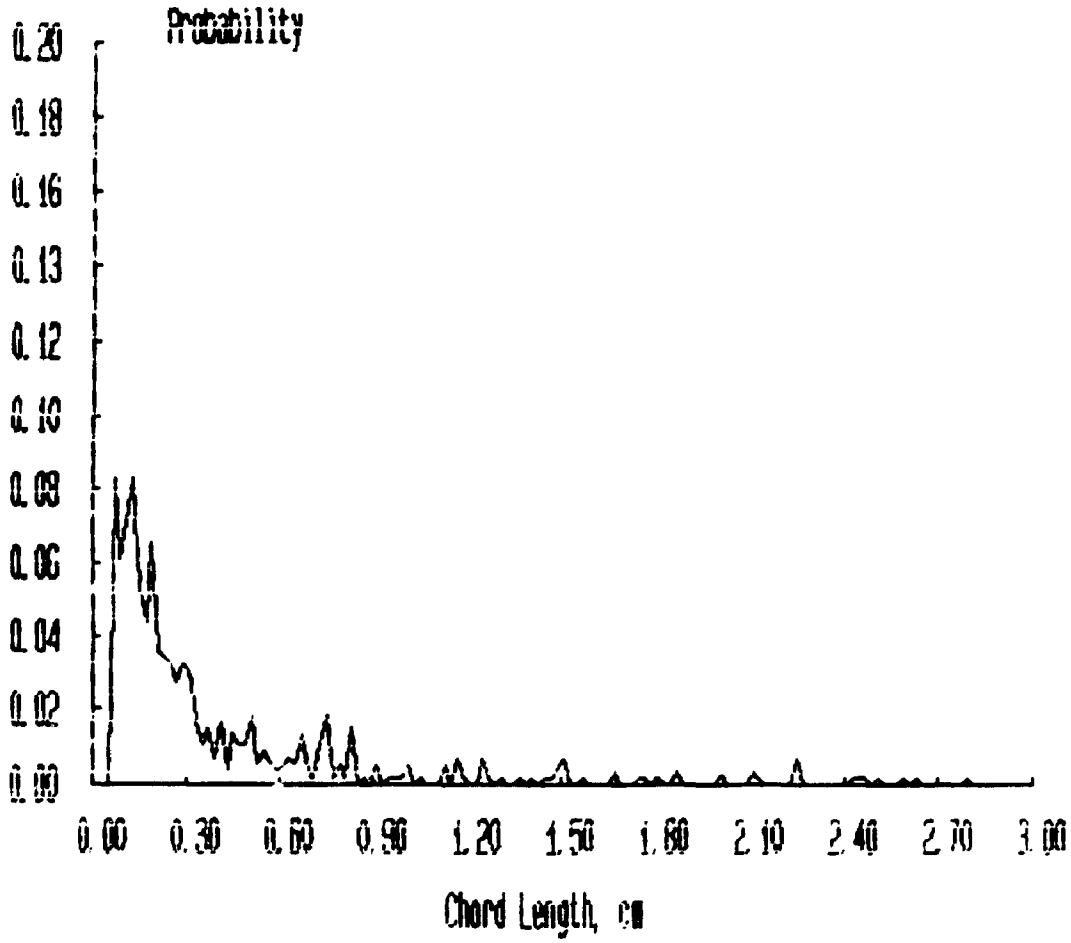

****** FILENAME ****** : JAN17C6A

**** Bubbles detected by probe 1 : 1126
**** Percentage of bubbles retained : 39.08
**** Average bubble duration : .004216 s

Probability Distributions

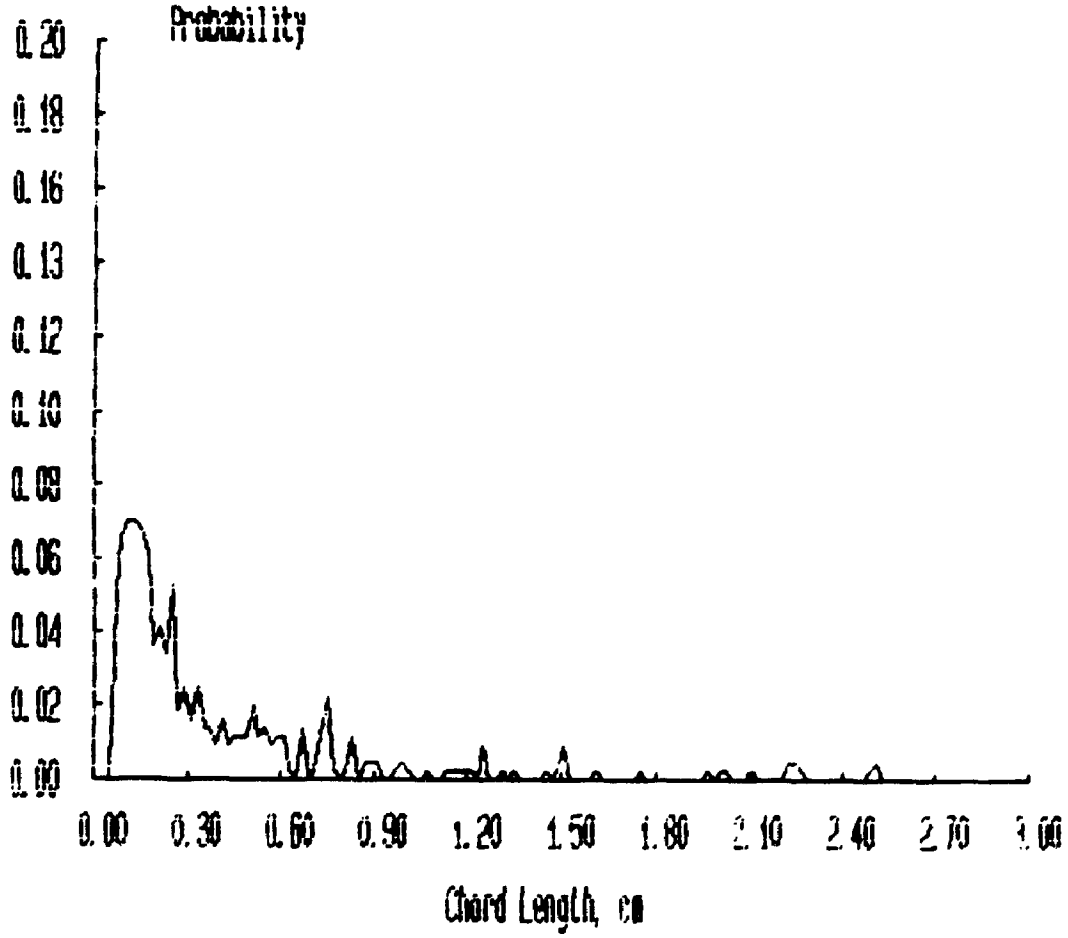

****** FILENAME ****** : JAN17D1A

**** Bubbles detected by probe 1 : 3437
**** Percentage of bubbles retained : 67.70
**** Average bubble duration : .005273 s

Probability Distributions

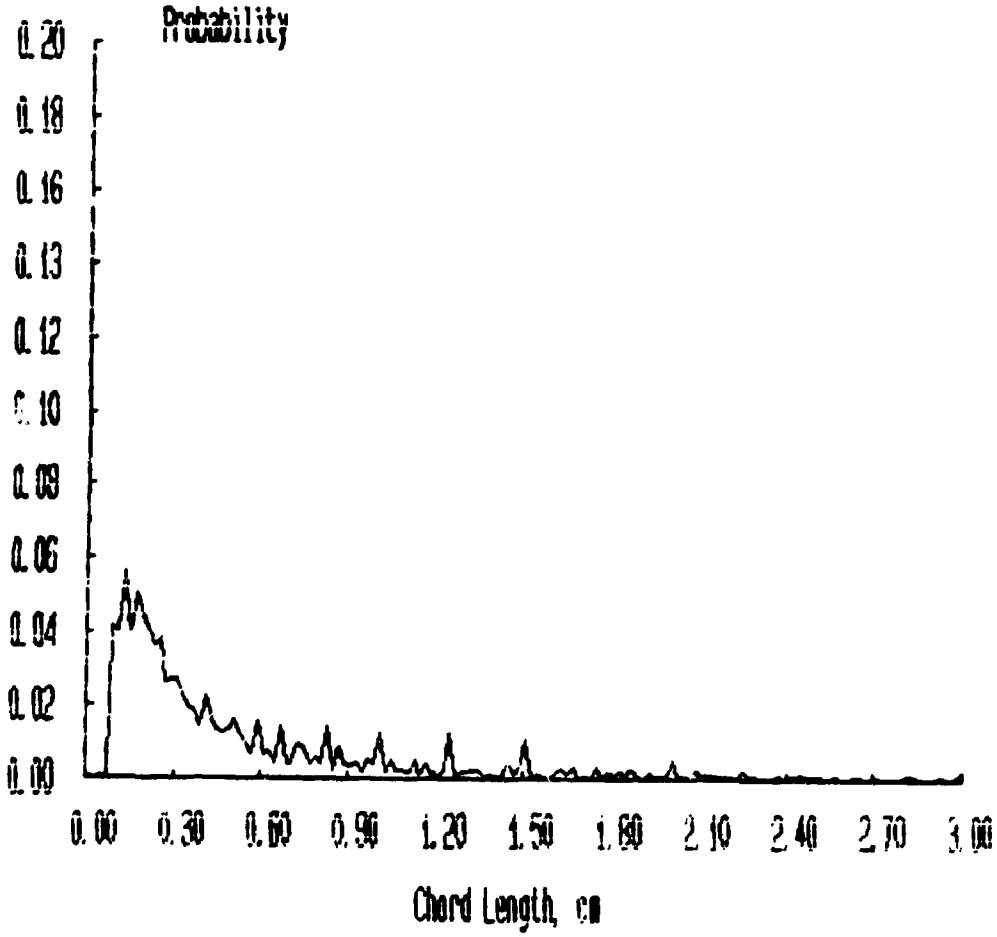

****** FILENAME ****** : JAN17D2A

**** Bubbles detected by probe 1 : 3037
**** Percentage of bubbles retained : 62.63
**** Average bubble duration : .005255 s

Probability Distributions

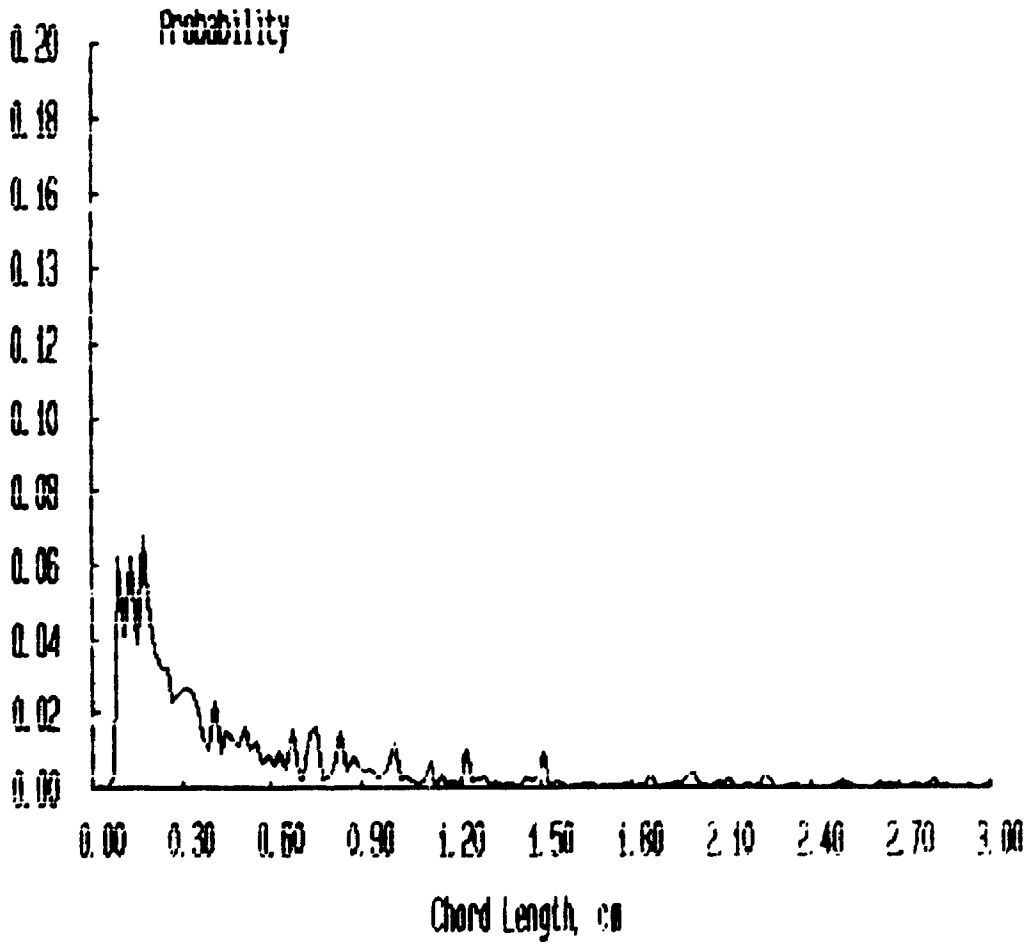

****** FILENAME ****** : JAN17D3A

**** Bubbles detected by probe 1 : 2579
**** Percentage of bubbles retained : 60.45
**** Average bubble duration : .005026 s

Probability Distributions

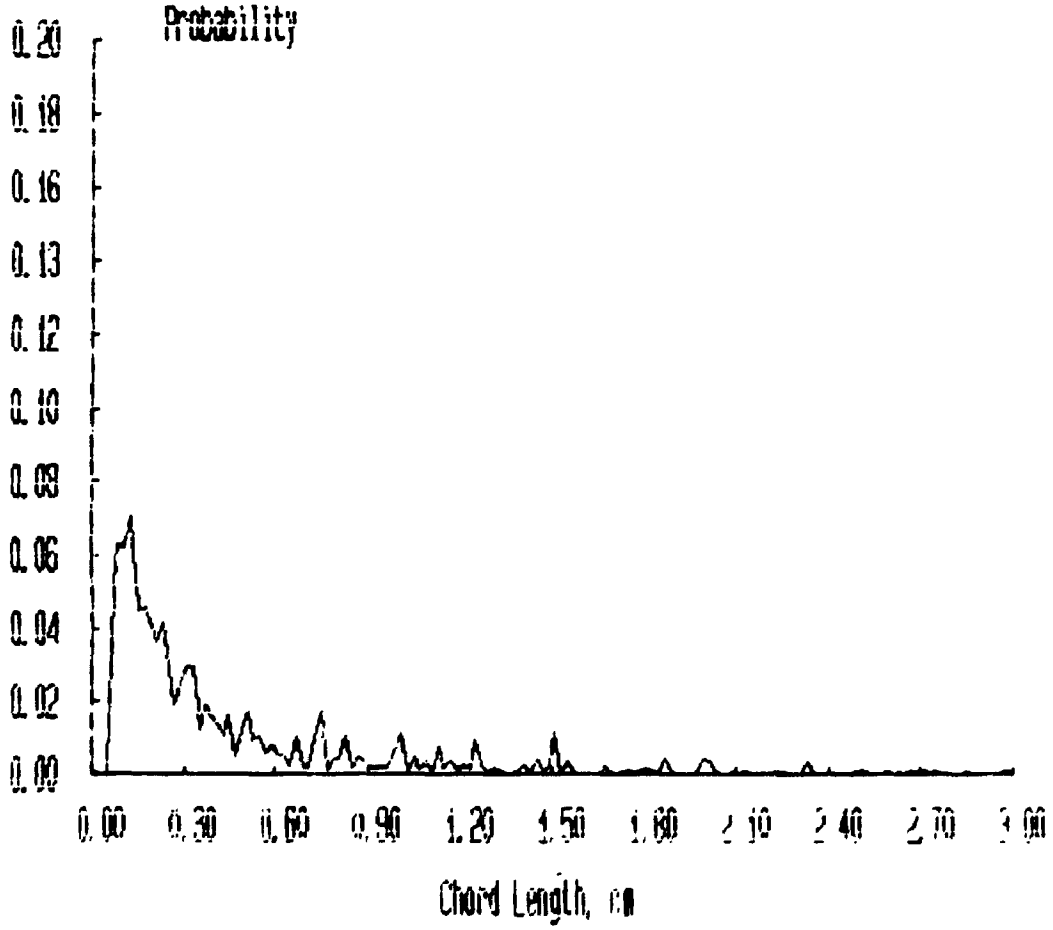

****** FILENAME ****** : JAN17D4A

**** Bubbles detected by probe 1 : 1784
**** Percentage of bubbles retained : 50.45
**** Average bubble duration : .004636 s

Probability Distributions

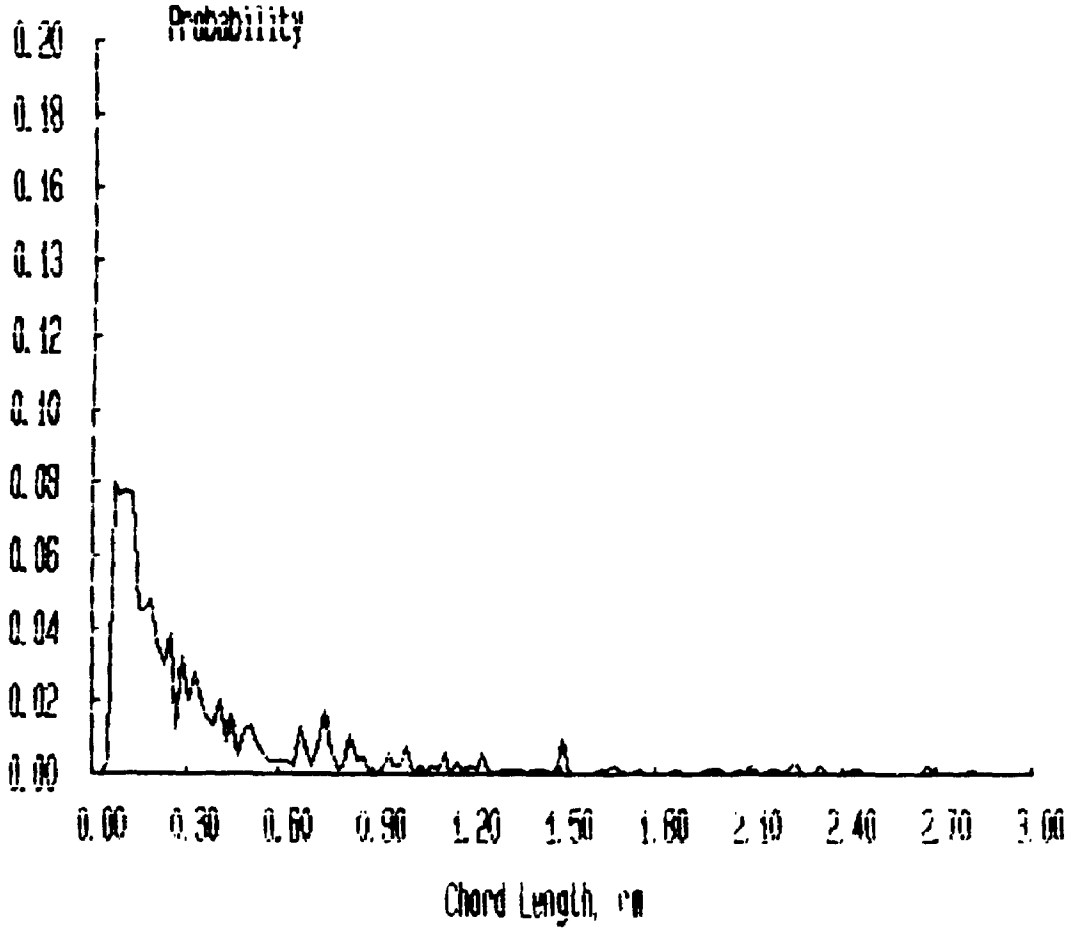

****** FILENAME ****** : JAN17D5A

**** Bubbles detected by probe 1 : 1364
**** Percentage of bubbles retained : 43.91
**** Average bubble duration : .004538 s

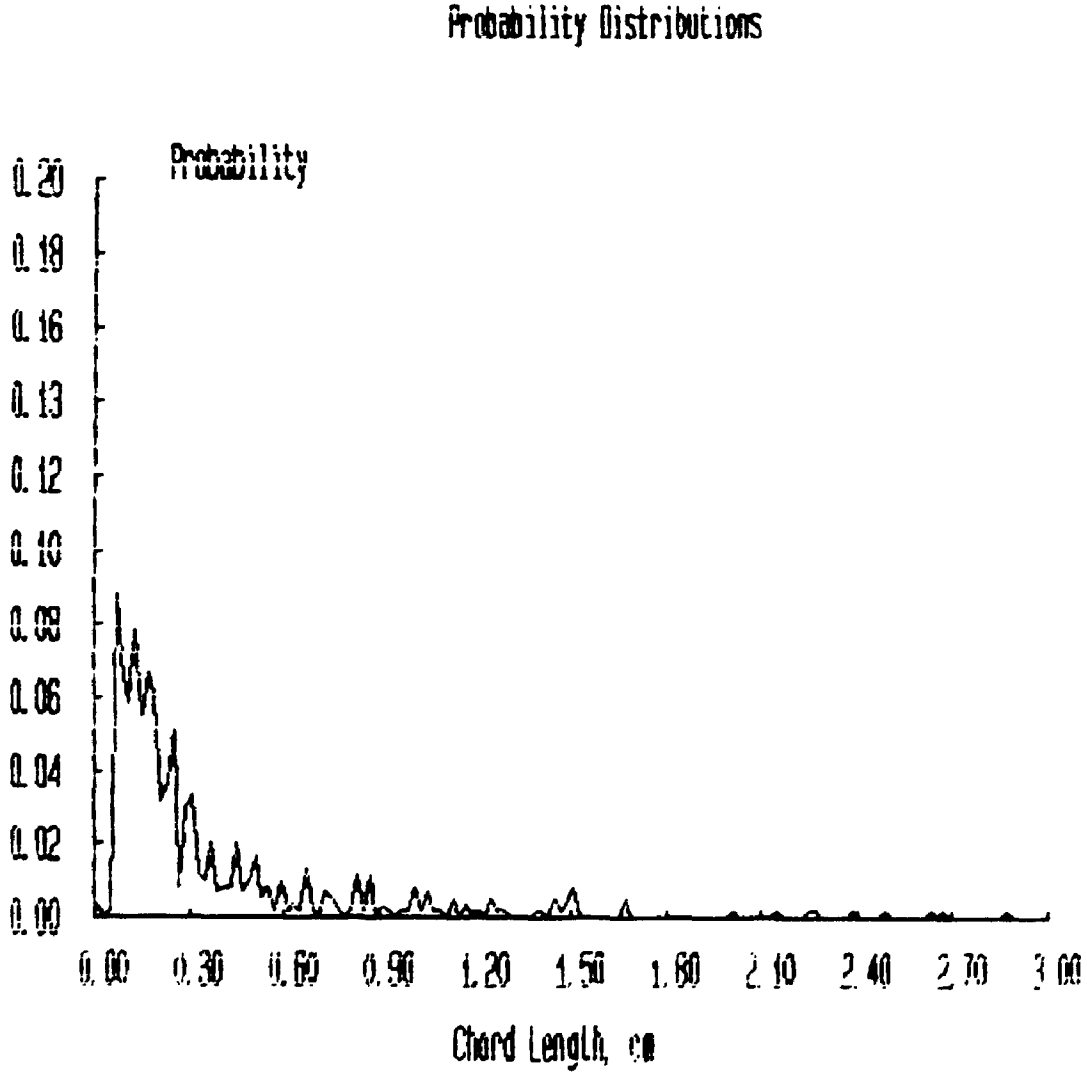

****** FILENAME ****** : JAN17D6A

**** Bubbles detected by probe 1 : 1436
**** Percentage of bubbles retained : 56.06
**** Average bubble duration : .004143 s

Probability Distributions

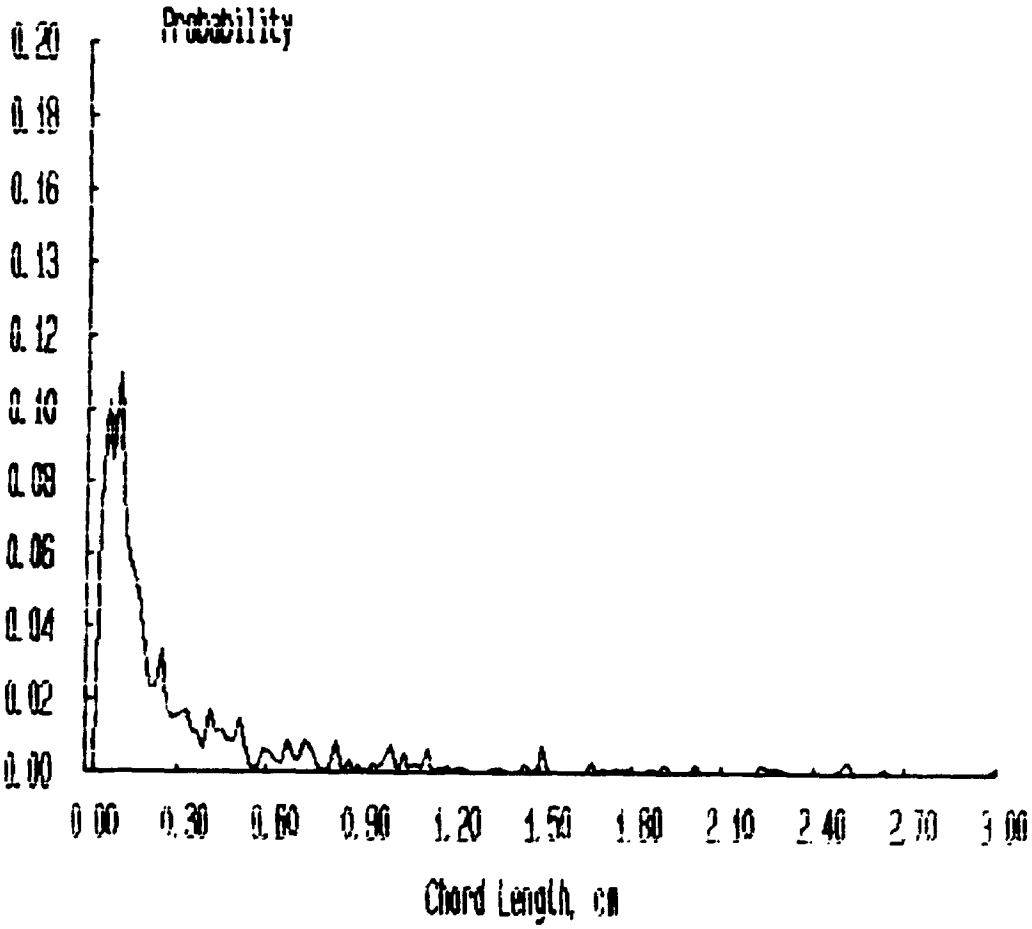

****** FILENAME ****** : JAN17E1A

**** Bubbles detected by probe 1 : 3612
**** Percentage of bubbles retained : 71.01
**** Average bubble duration : .005174 s

Probability Distributions

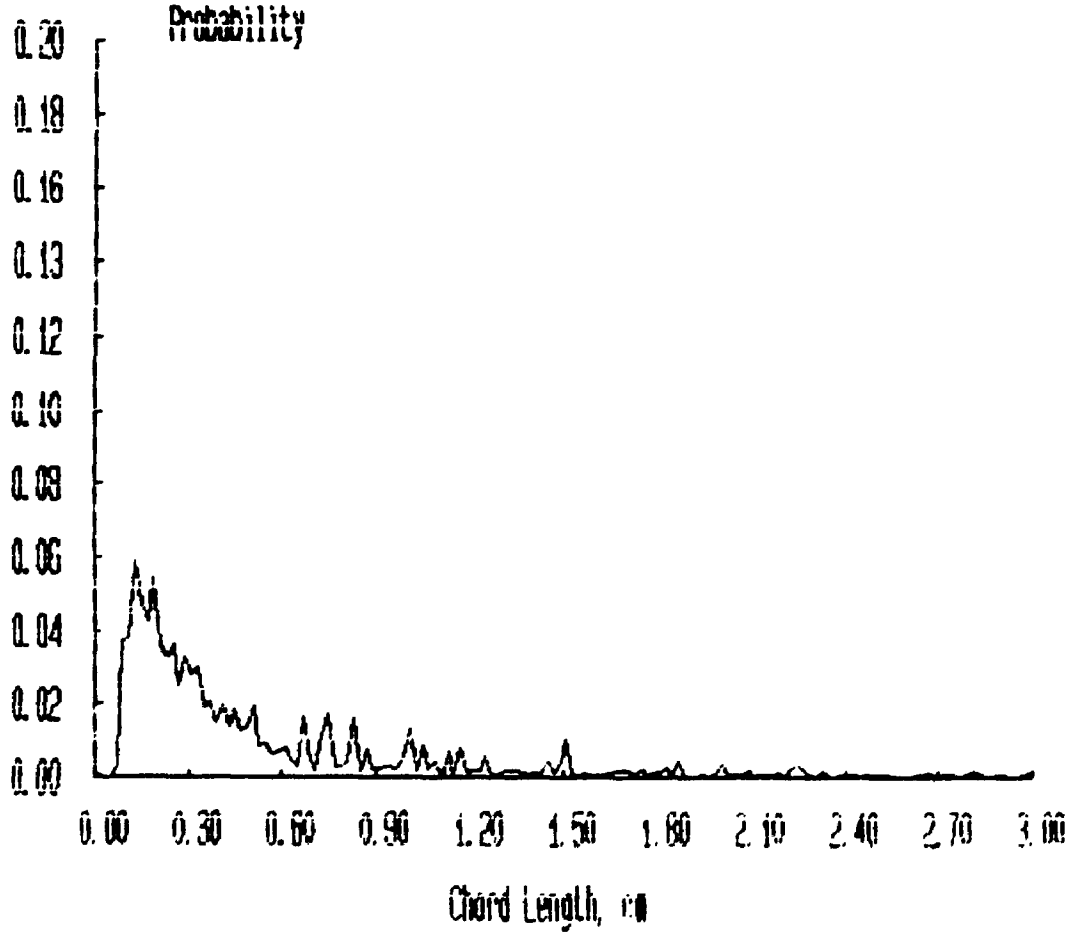

****** FILENAME ****** : JAN17E2A

**** Bubbles detected by probe 1 : 3091
**** Percentage of bubbles retained : 64.80
**** Average bubble duration : .005250 s

Probability Distributions

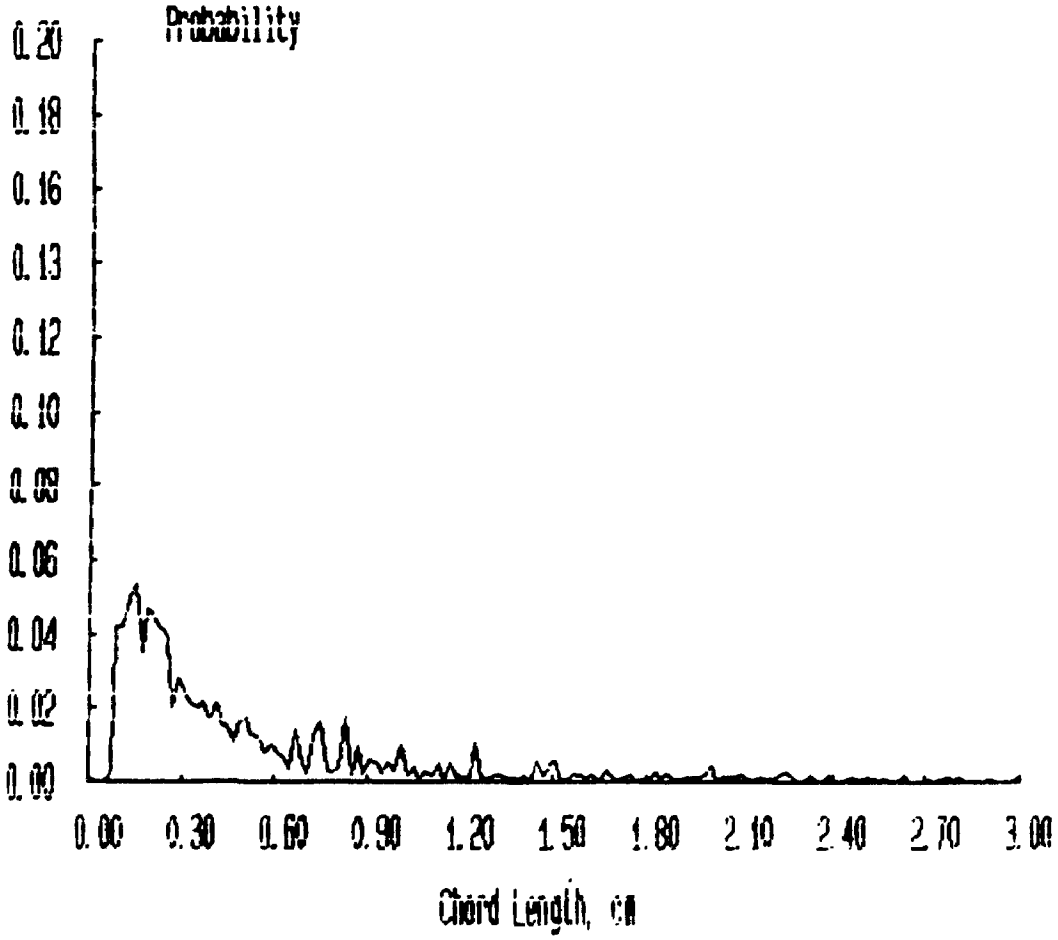

****** FILENAME ****** : JAN17E3A

**** Bubbles detected by probe 1 : 2317
**** Percentage of bubbles retained : 59.39
**** Average bubble duration : .004642 s

Probability Distributions

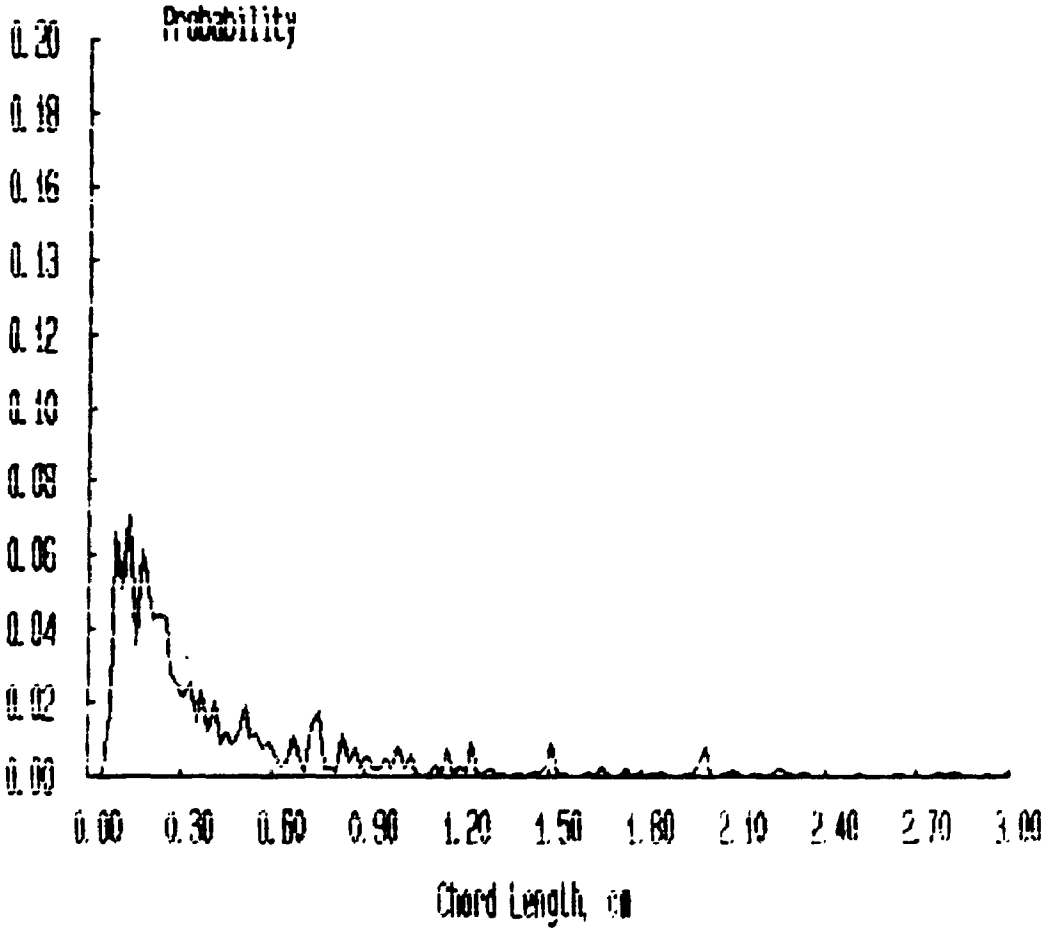

****** FILENAME ****** : JAN17E4A

**** Bubbles detected by probe 1 : 1975
**** Percentage of bubbles retained : 52.96
**** Average bubble duration : .004346 s

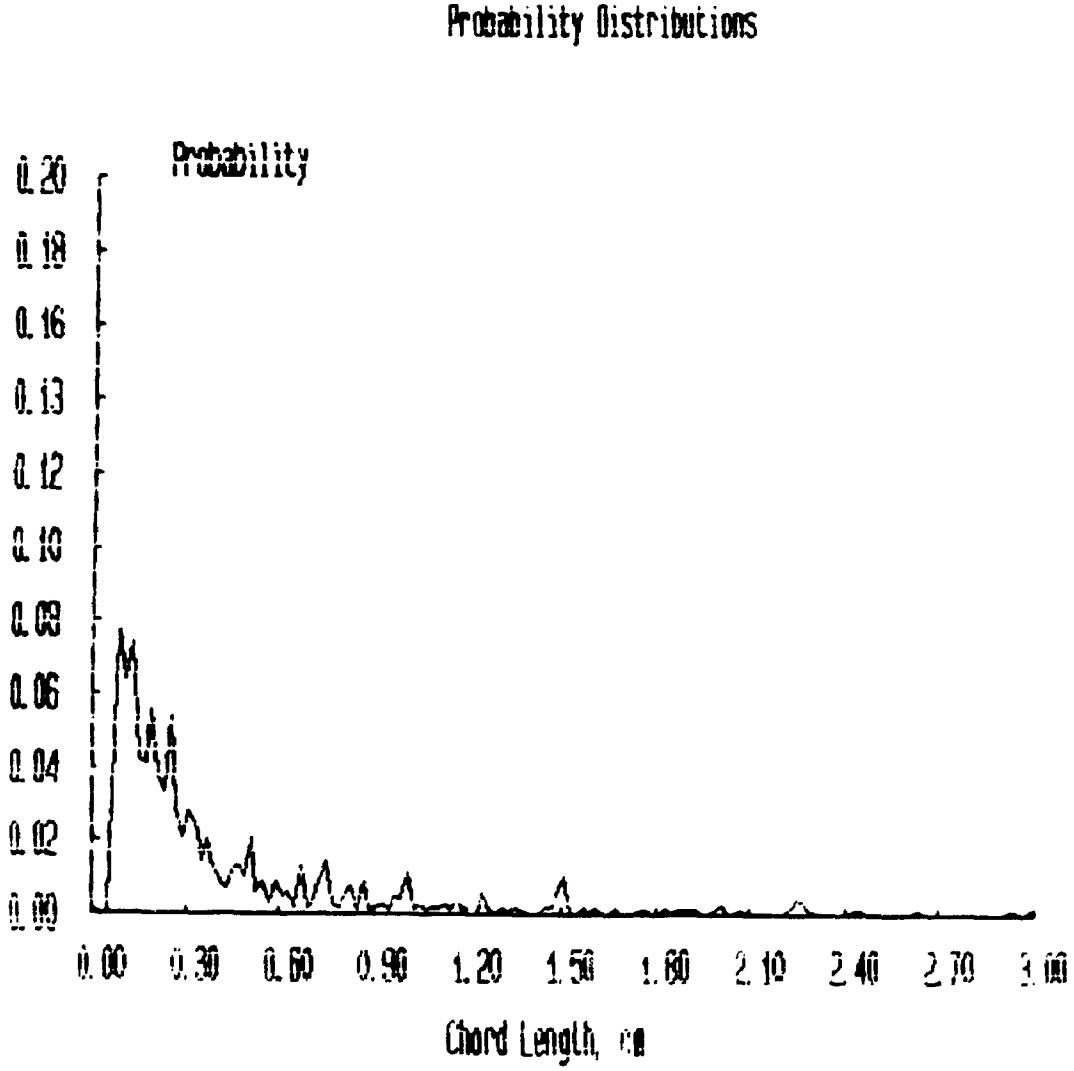

****** FILENAME ****** : JAN17E5A

**** Bubbles detected by probe 1 : 1422
**** Percentage of bubbles retained : 39.03
**** Average bubble duration : .003955 s

Probability Distributions

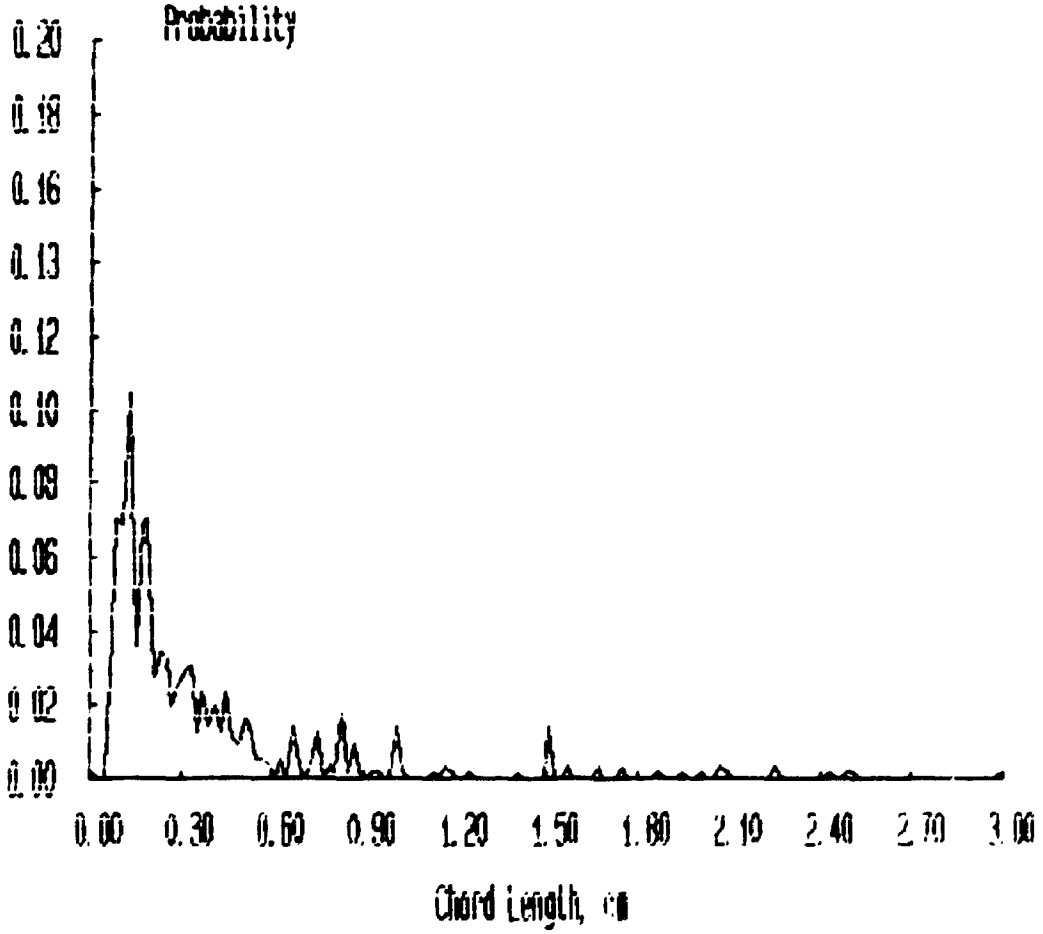

****** FILENAME ****** : JAN17E6A

**** Bubbles detected by probe 1 : 1065
**** Percentage of bubbles retained : 47.89
**** Average bubble duration : .003725 s

Probability Distributions

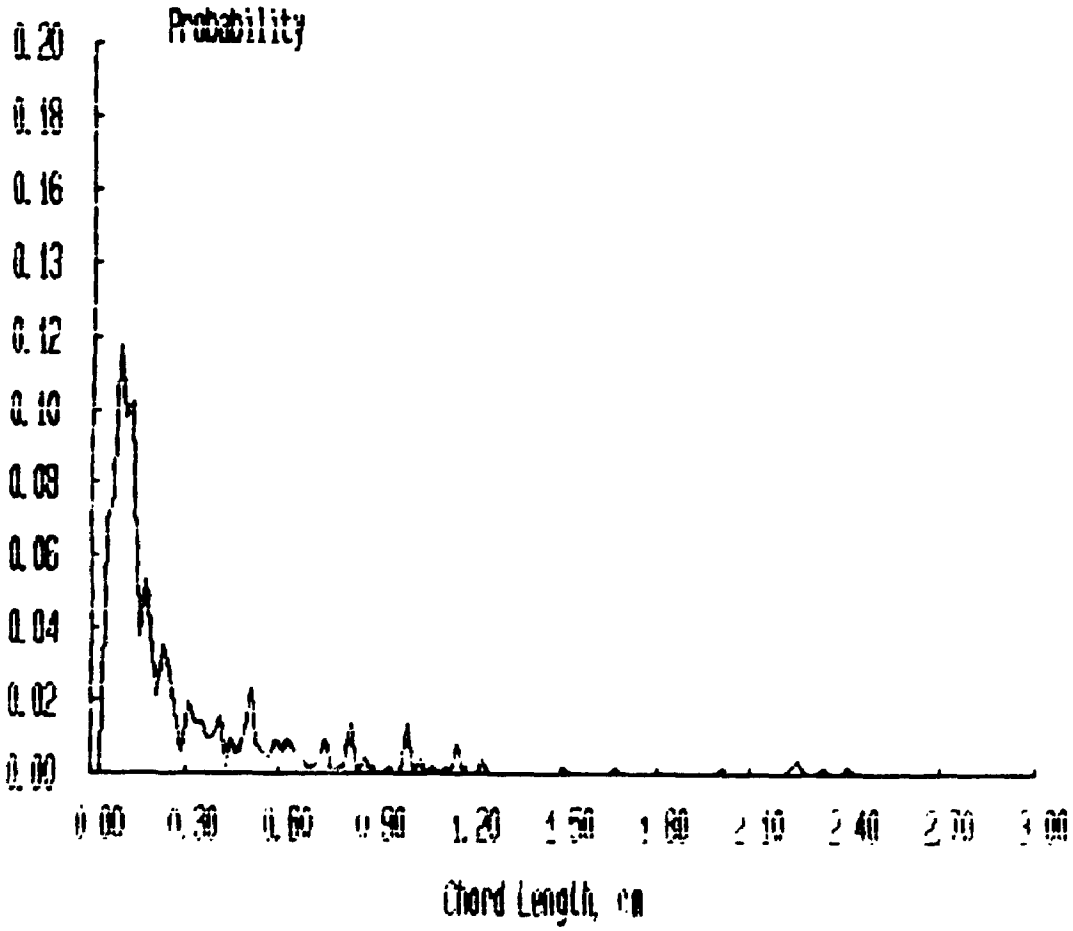

****** FILENAME ****** : JAN18A1A

**** Bubbles detected by probe 1 : 903
**** Percentage of bubbles retained : 53.82
**** Average bubble duration : .006210 s

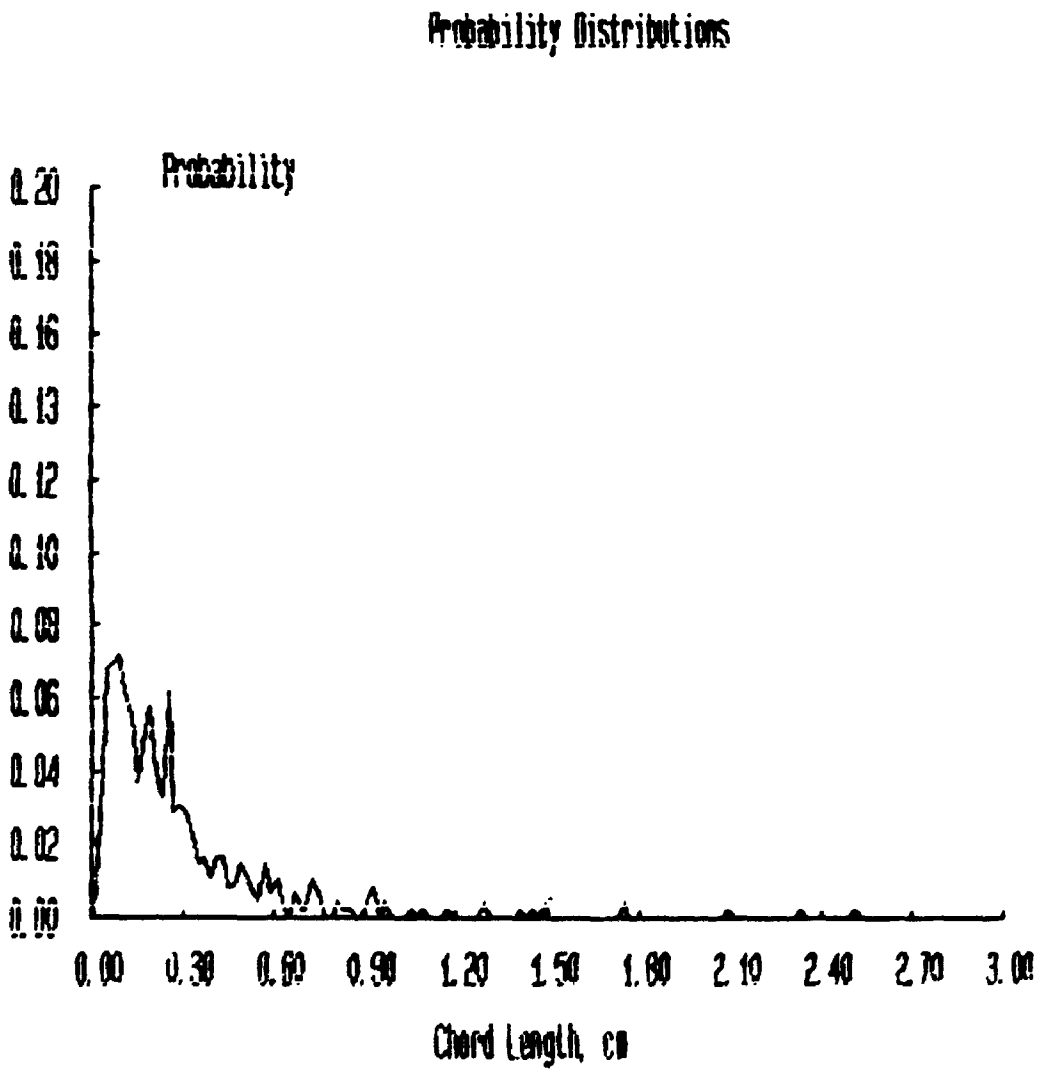

****** FILENAME ****** : JAN18A2A

**** Bubbles detected by probe 1 : 919
**** Percentage of bubbles retained : 56.37
**** Average bubble duration : .006008 s

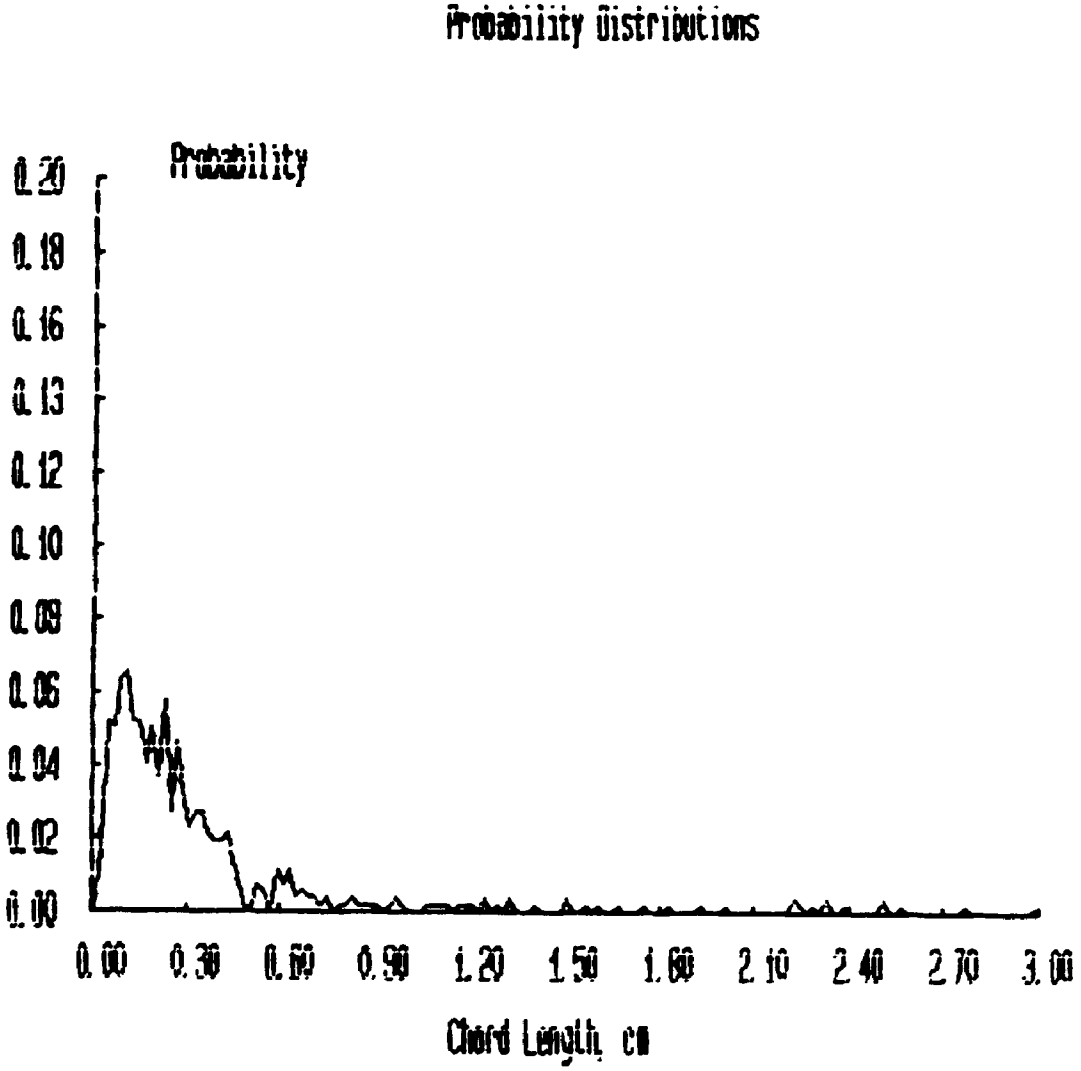

****** FILENAME ****** : JAN18A3A

**** Bubbles detected by probe 1 : 801
**** Percentage of bubbles retained : 48.69
**** Average bubble duration : .005892 s

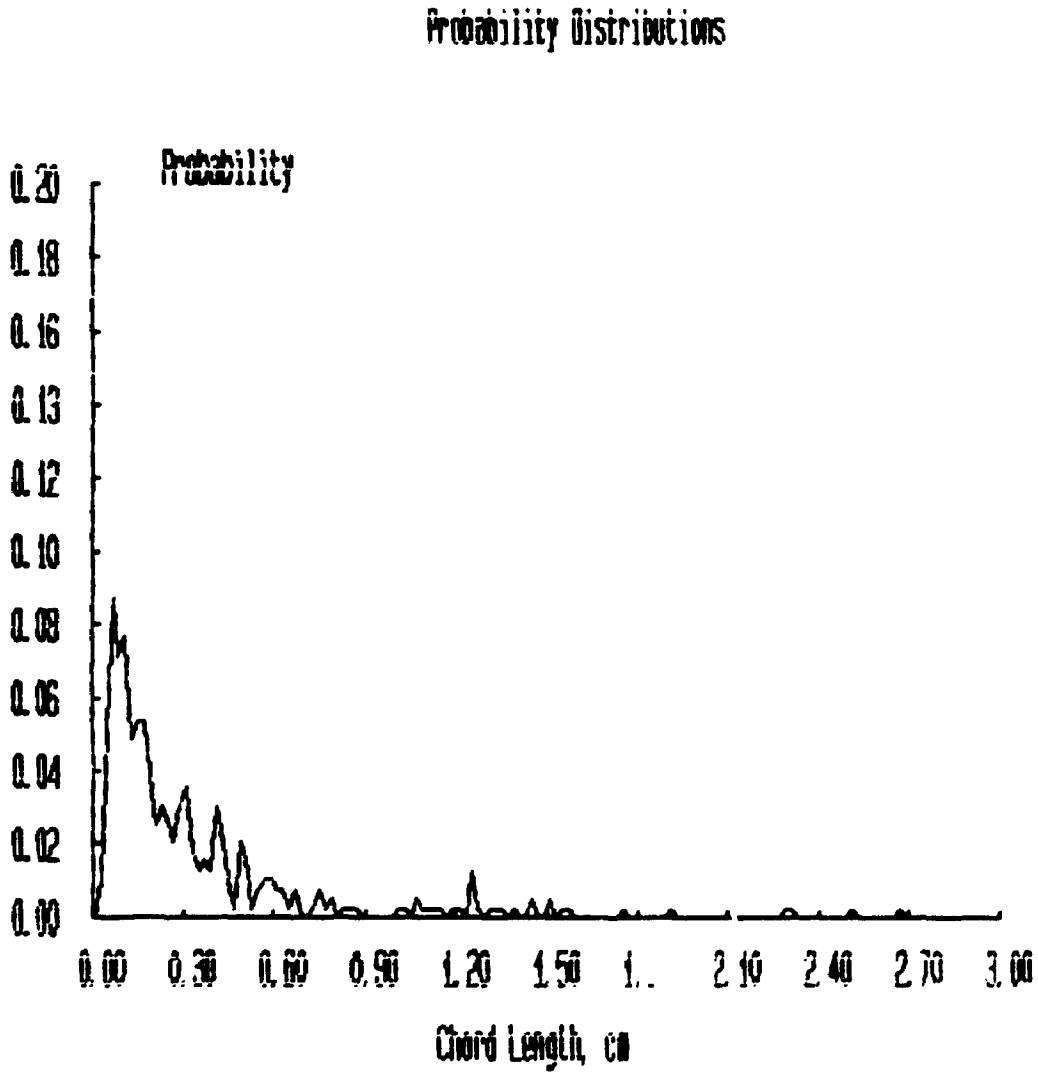

****** FILENAME ****** : JAN18A4A

**** Bubbles detected by probe 1 : 617
**** Percentage of bubbles retained : 38.09
**** Average bubble duration : .006251 s

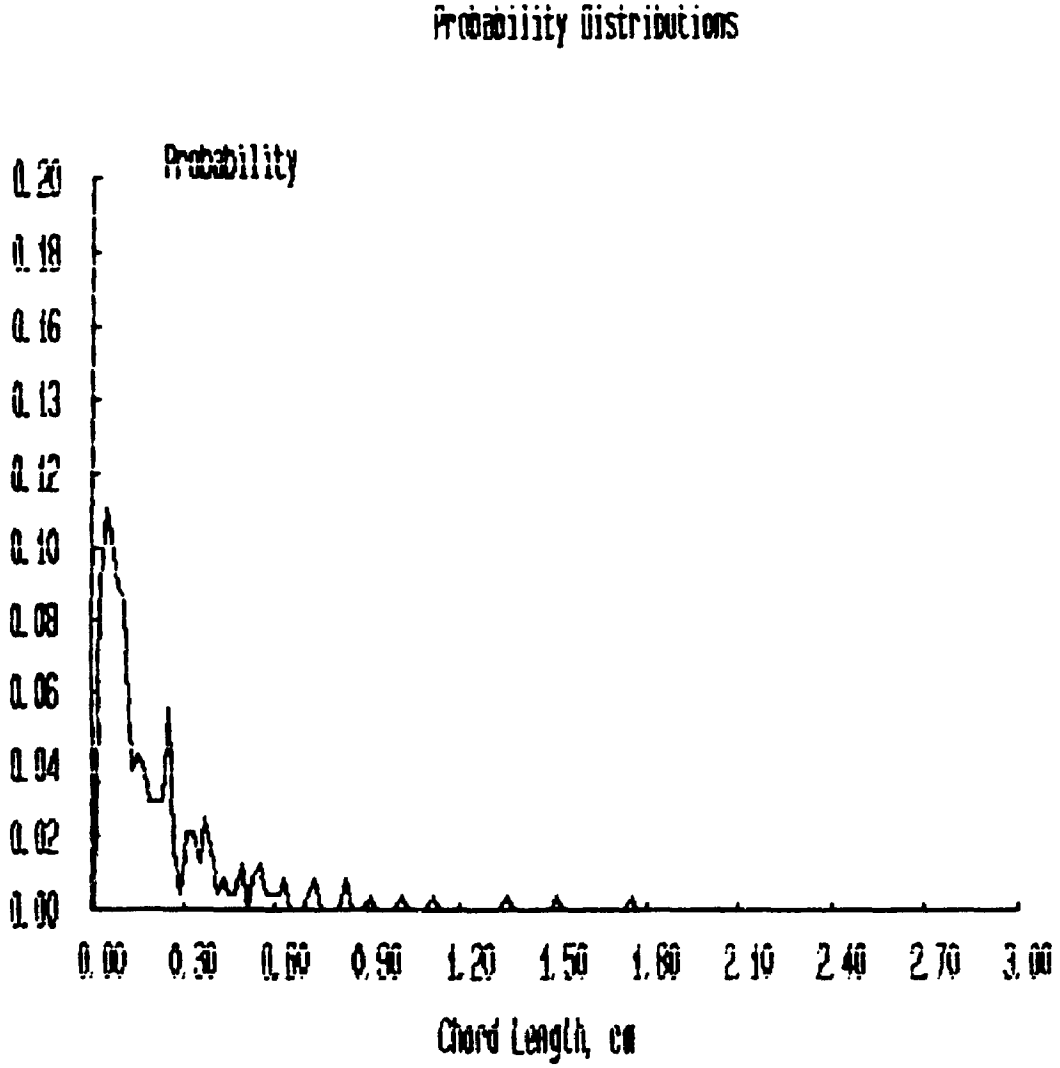

****** FILENAME ****** : JAN18A5B

**** Bubbles detected by probe 1 : 592
**** Percentage of bubbles retained : 36.66
**** Average bubble duration : .006258 s

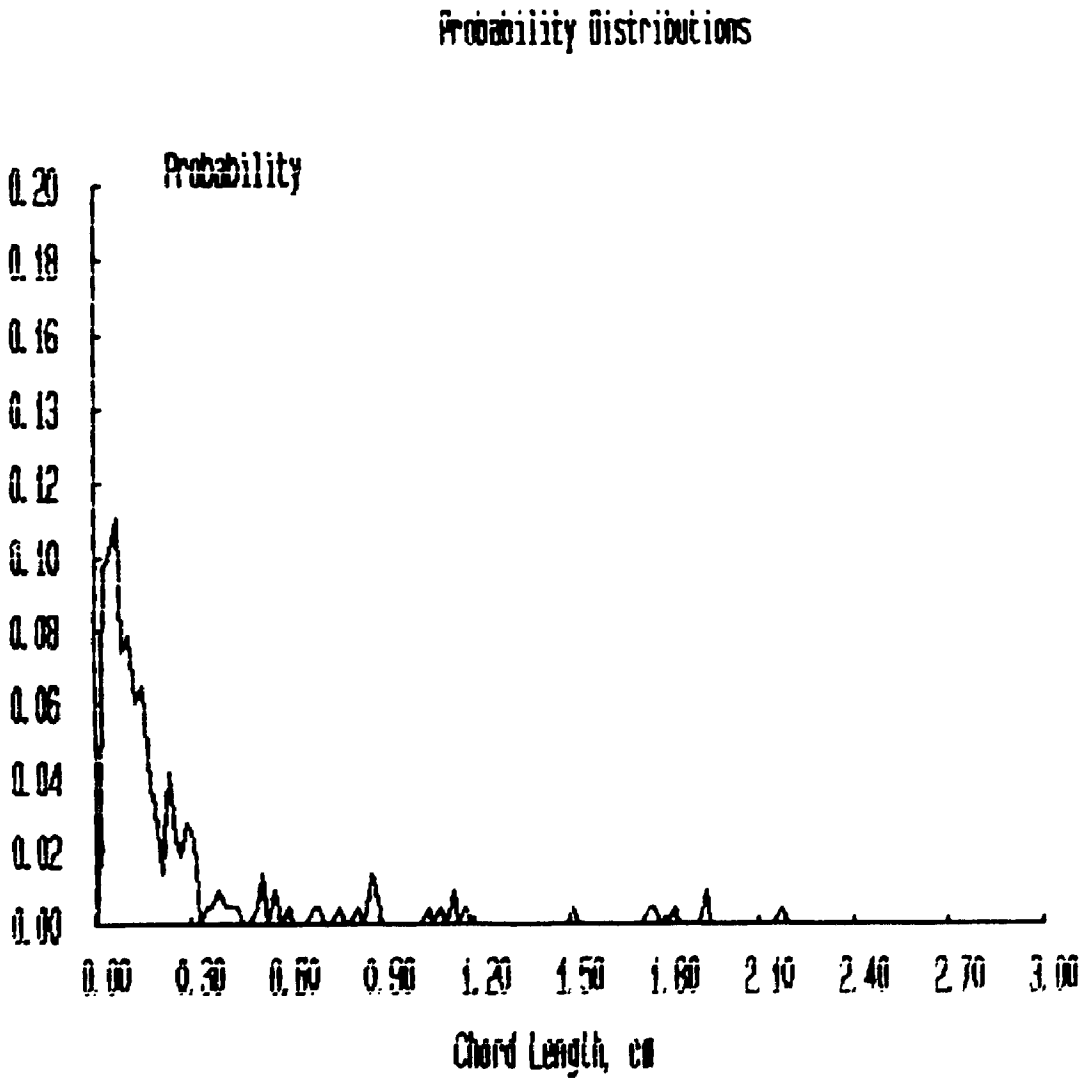

****** FILENAME ****** : JAN18A6A

**** Bubbles detected by probe 1 : 469
**** Percentage of bubbles retained : 35.82
**** Average bubble duration : .006327 s

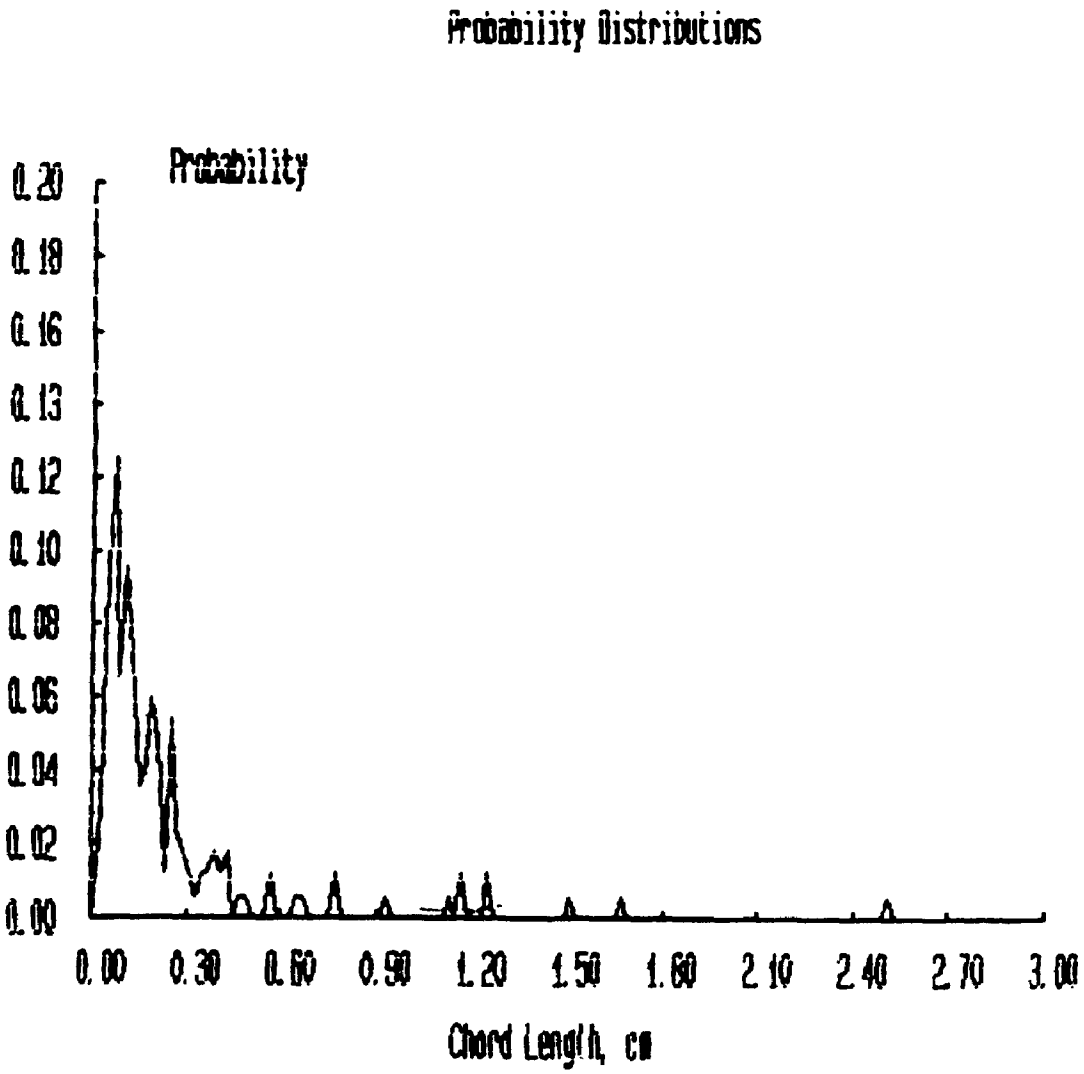

****** FILENAME ****** : JAN18B1A

**** Bubbles detected by probe 1 : 891
**** Percentage of bubbles retained : 55.22
**** Average bubble duration : .005988 s

Probability Distributions

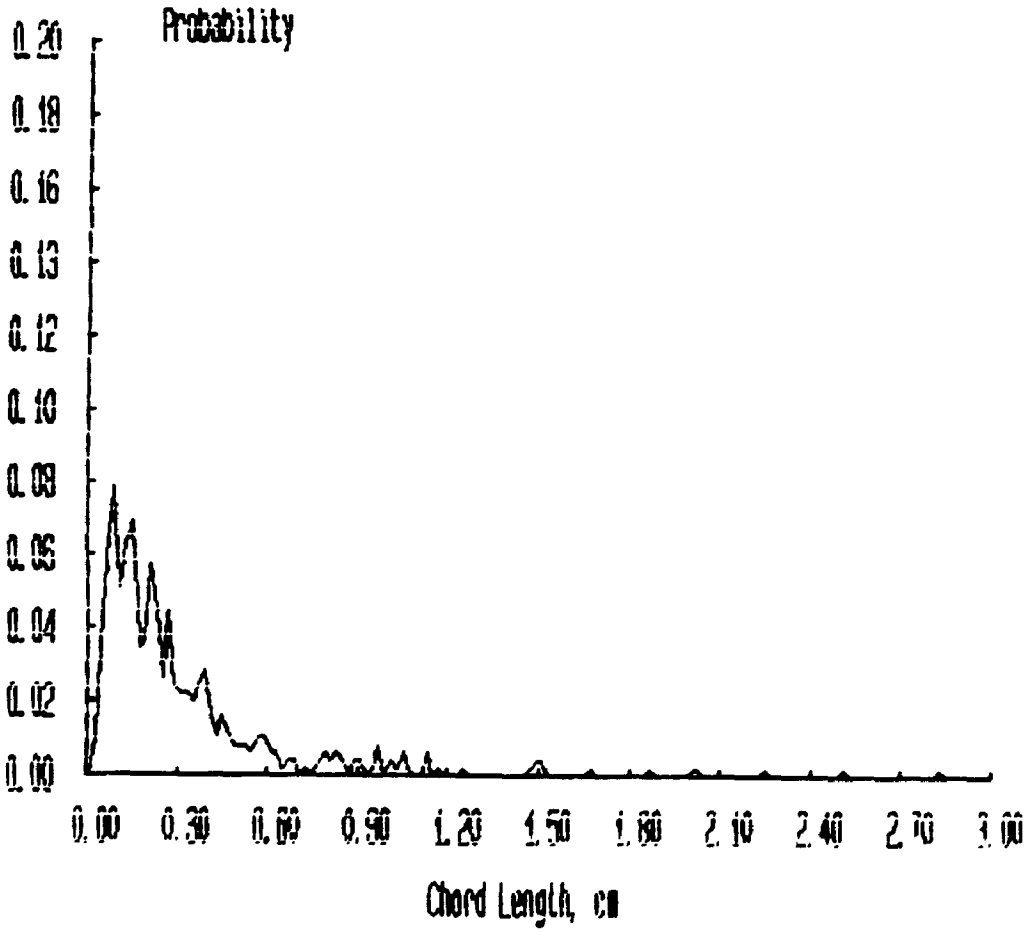

****** FILENAME ****** : JAN1882A

**** Bubbles detected by probe 1 : 956
**** Percentage of bubbles retained : 57.85
**** Average bubble duration : .005944 s

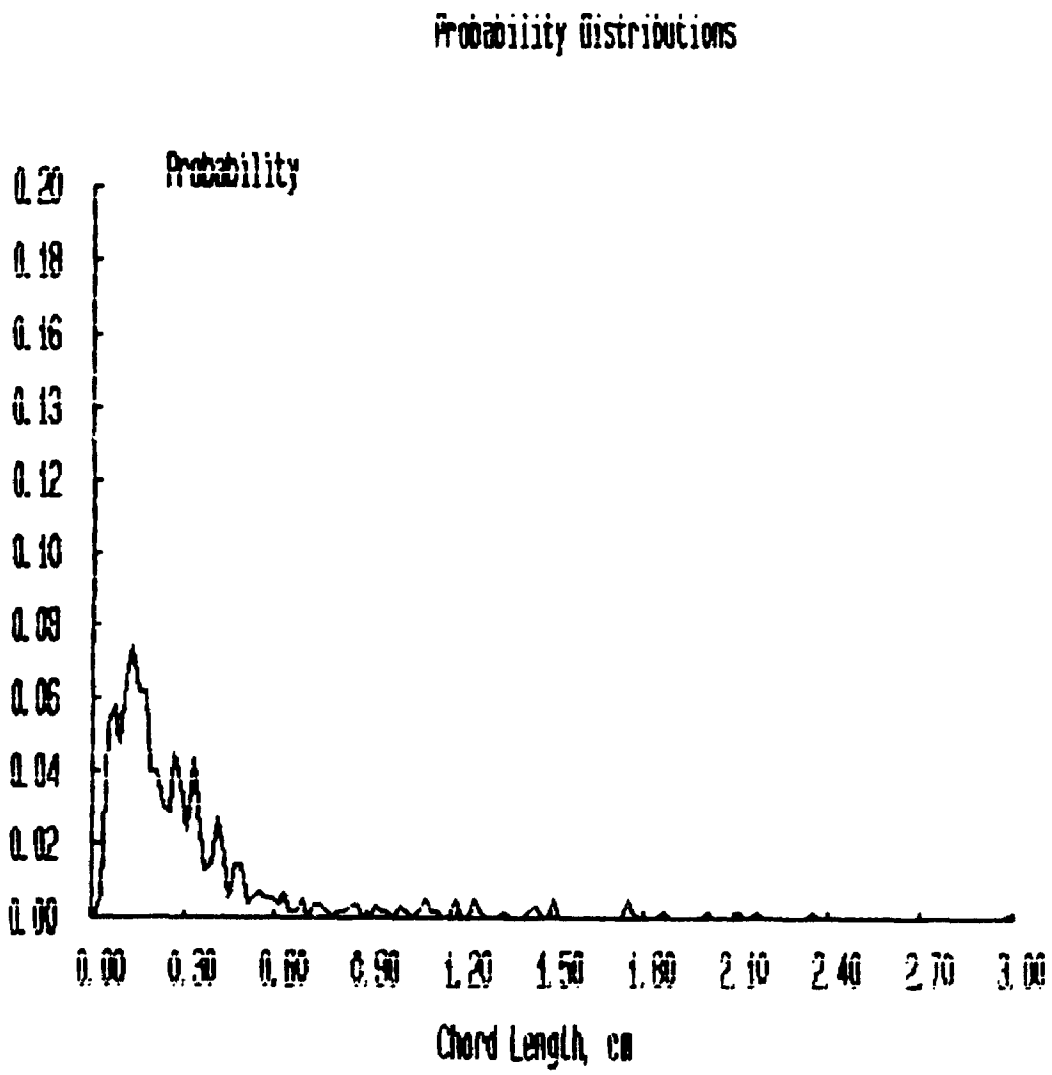

****** FILENAME ****** : JAN18B3A

**** Bubbles detected by probe 1 : 796
**** Percentage of bubbles retained : 42.21
**** Average bubble duration : .006342 s

Probability Distributions

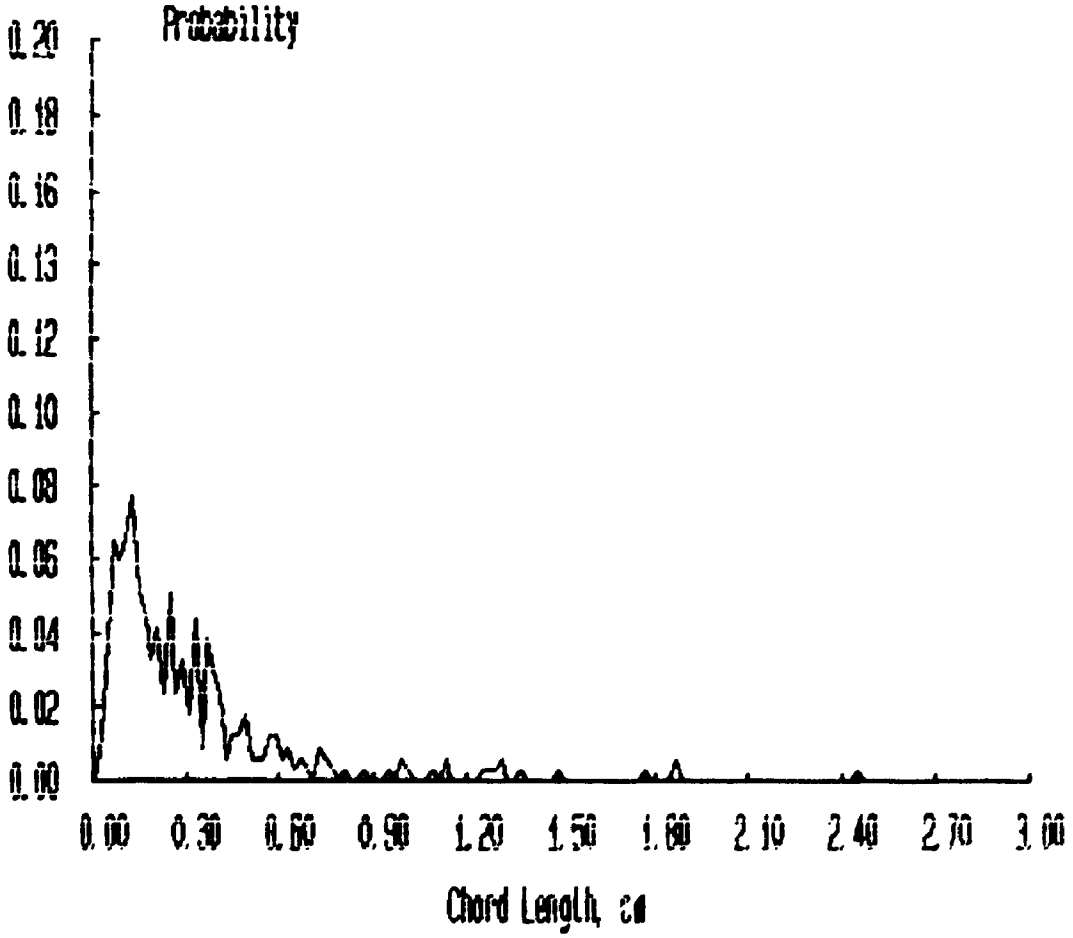

****** FILENAME ****** : JAN1884A

**** Bubbles detected by probe 1 : 680
**** Percentage of bubbles retained : 41.76
**** Average bubble duration : .006518 s

Probability Distributions

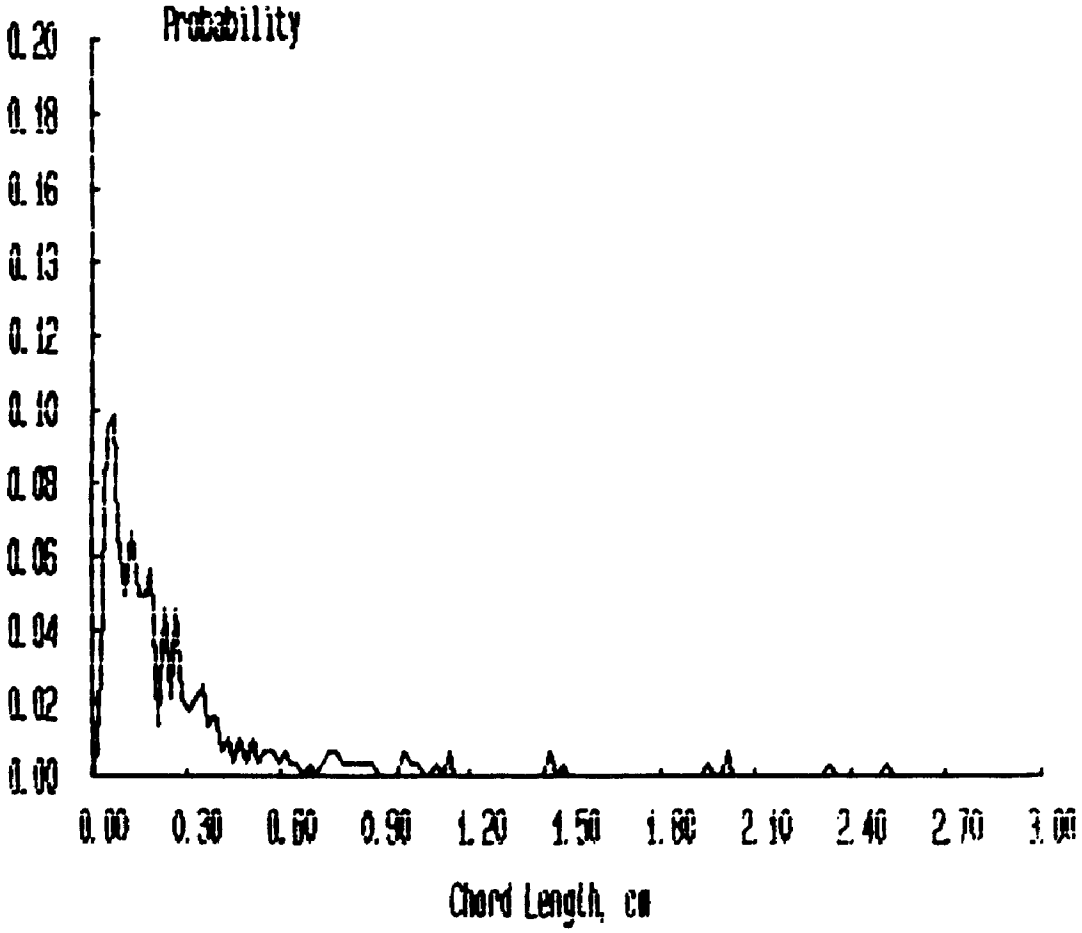

****** FILENAME ****** : JAN1885A

**** Bubbles detected by probe 1 : 425
**** Percentage of bubbles retained : 29.65
**** Average bubble duration : .006476 s

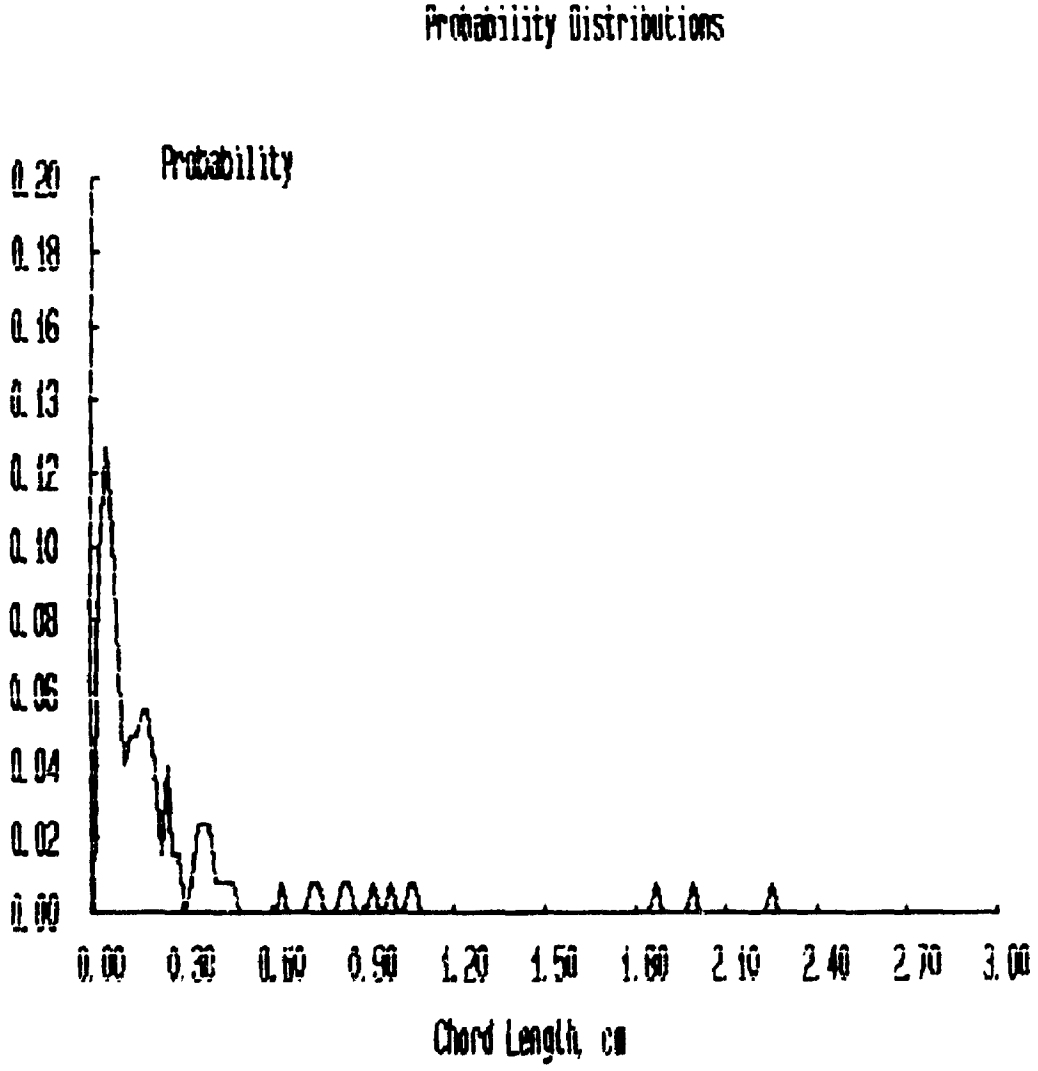

****** FILENAME ****** : JAN18B6A

**** Bubbles detected by probe 1 : 509
**** Percentage of bubbles retained : 41.85
**** Average bubble duration : .006455 s

Probability Distributions

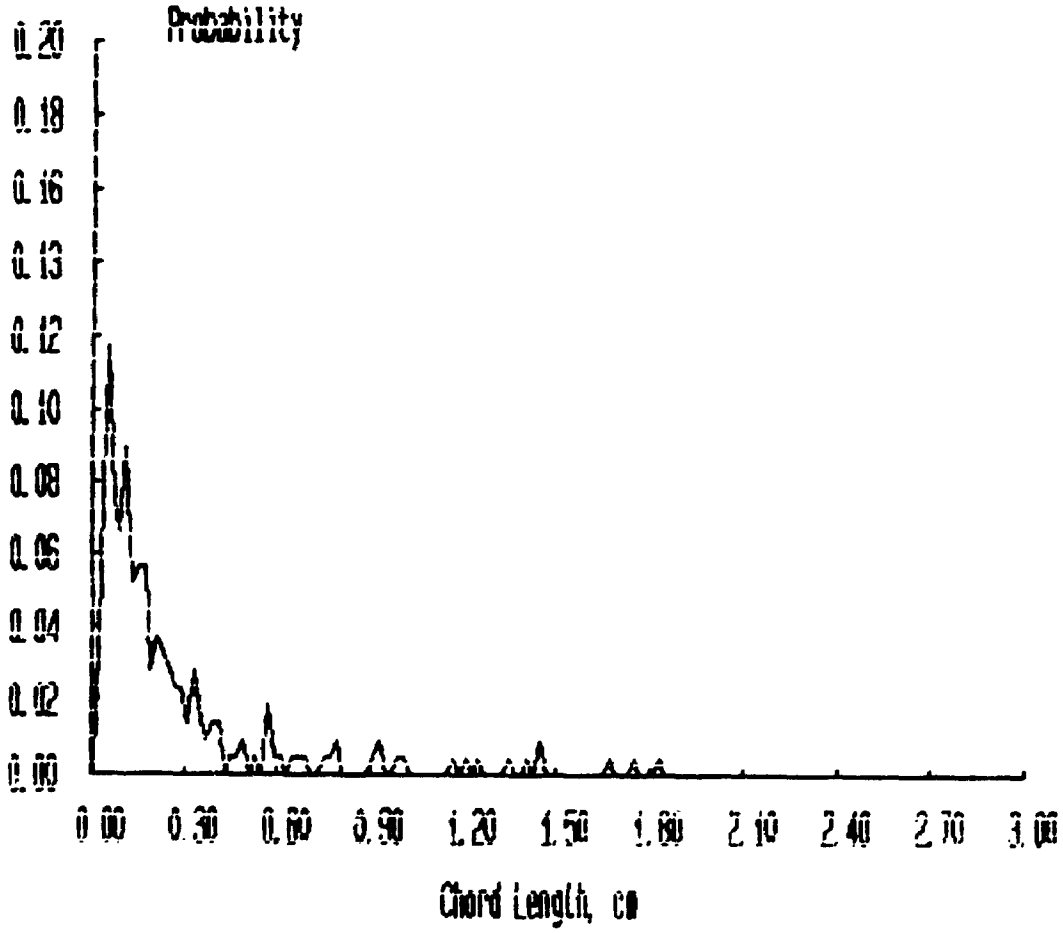

****** FILENAME ****** : JAN18C1A

**** Bubbles detected by probe 1 : 769
**** Percentage of bubbles retained : 47.98
**** Average bubble duration : .006035 s

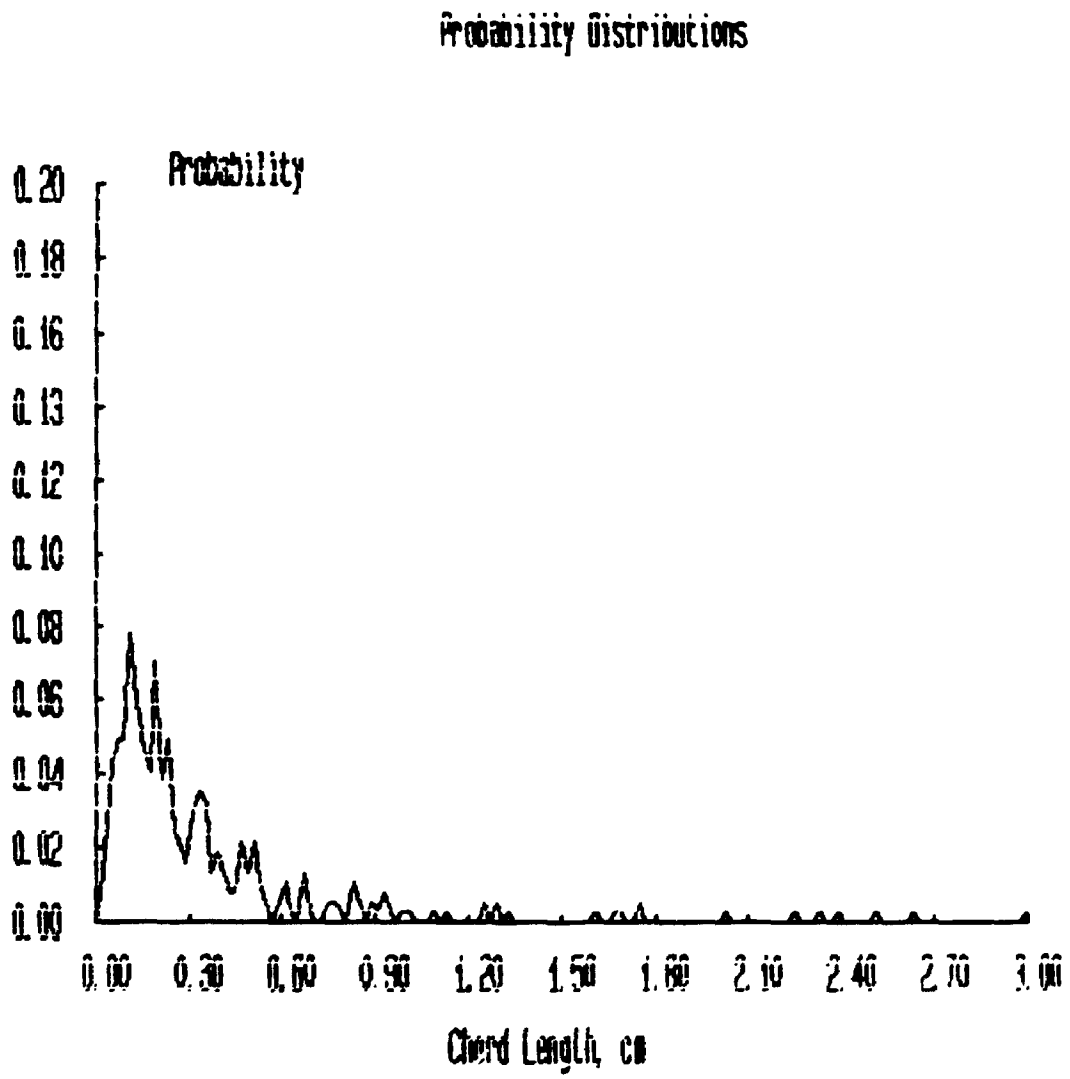

****** FILENAME ****** : JAN18C2A

**** Bubbles detected by probe 1 : 859
**** Percentage of bubbles retained : 56.11
**** Average bubble duration : .006322 s

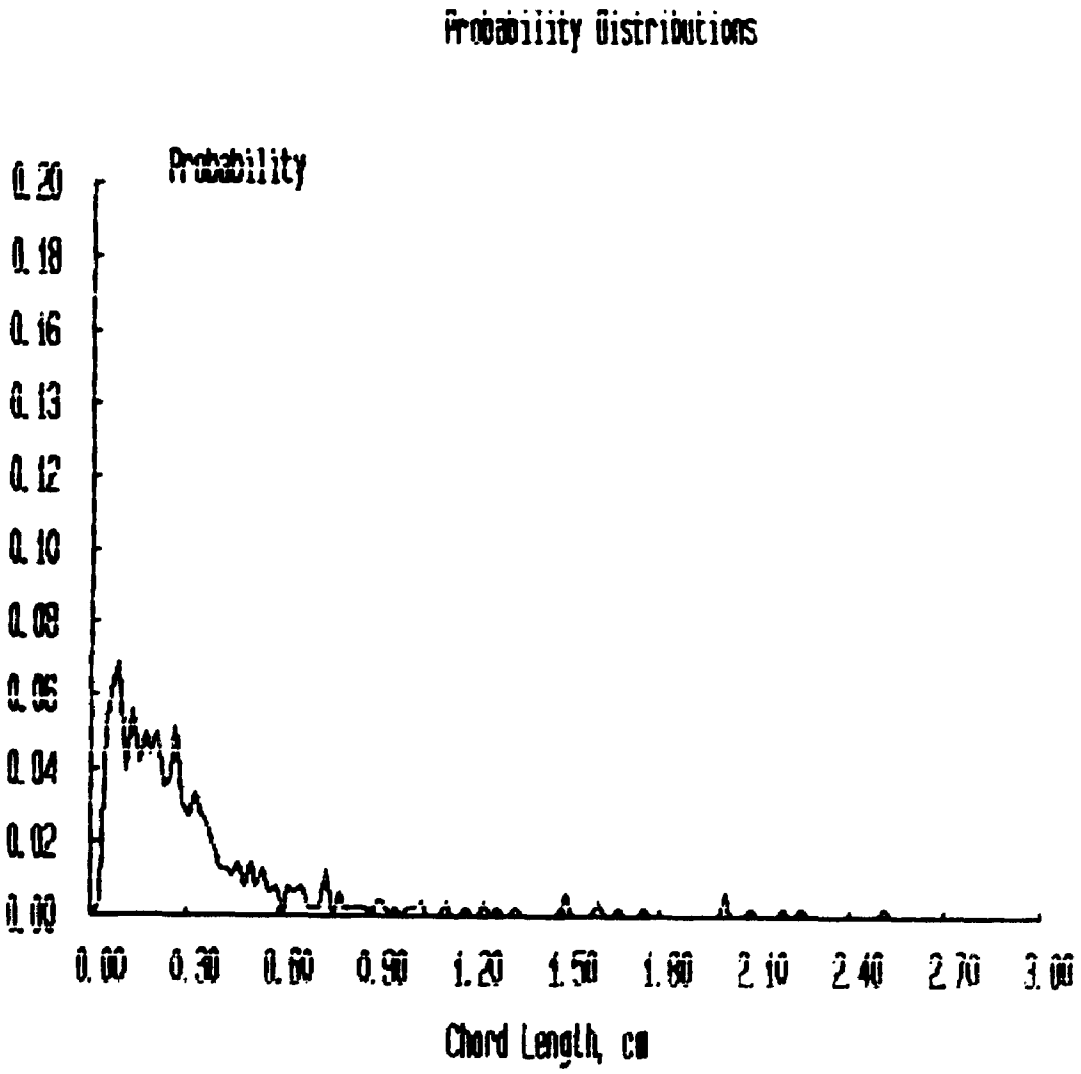

****** FILENAME ****** : JAN18C3A

**** Bubbles detected by probe 1 : 869
**** Percentage of bubbles retained : 46.03
**** Average bubble duration : .006355 s

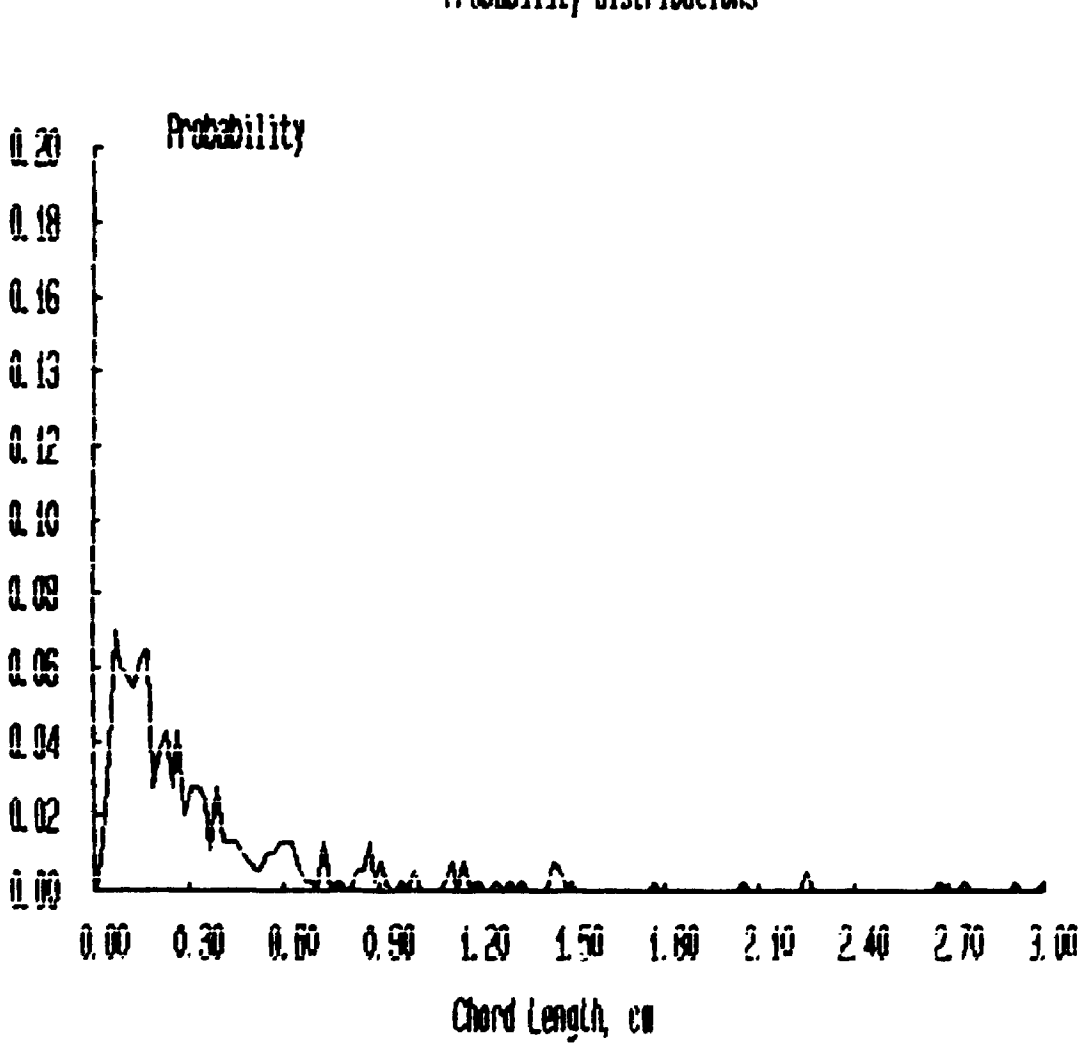

****** FILENAME ****** : JAN18C4B

**** Bubbles detected by probe 1 : 595
**** Percentage of bubbles retained : 34.45
**** Average bubble duration : .006702 s

Probability Distributions

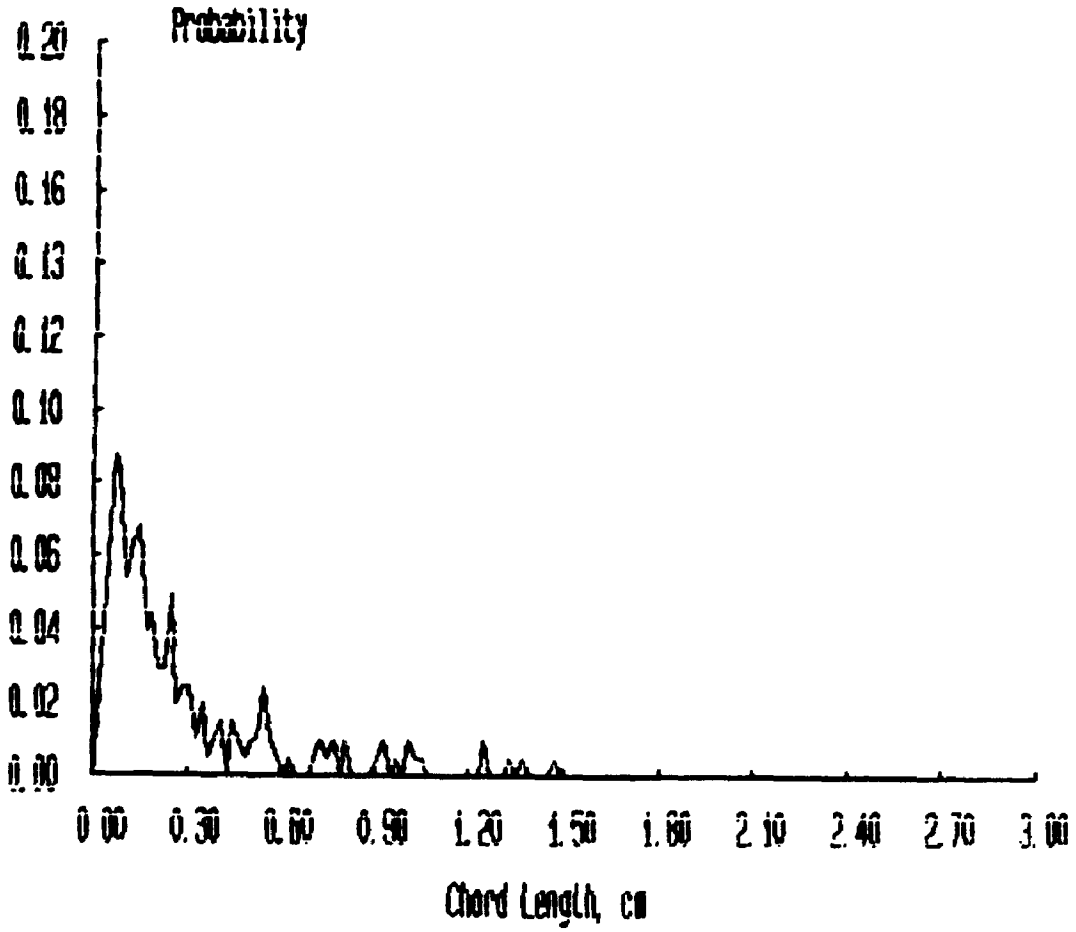

****** FILENAME ****** : JAN18C5B

**** Bubbles detected by probe 1 : 505
**** Percentage of bubbles retained : 37.62
**** Average bubble duration : .006342 s

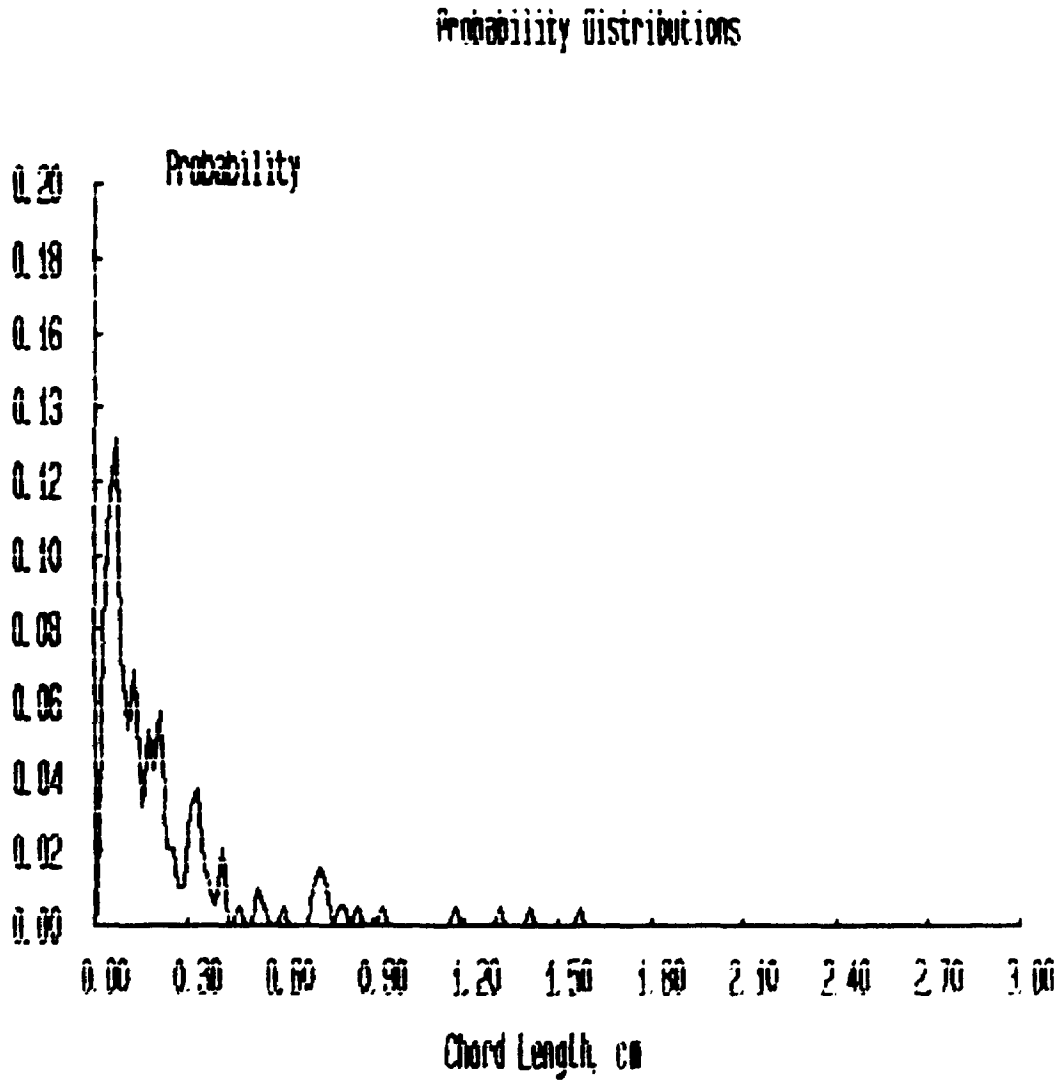

****** FILENAME ****** : JAN18C6A

**** Bubbles detected by probe 1 : 438
**** Percentage of bubbles retained : 35.84
**** Average bubble duration : .006382 s

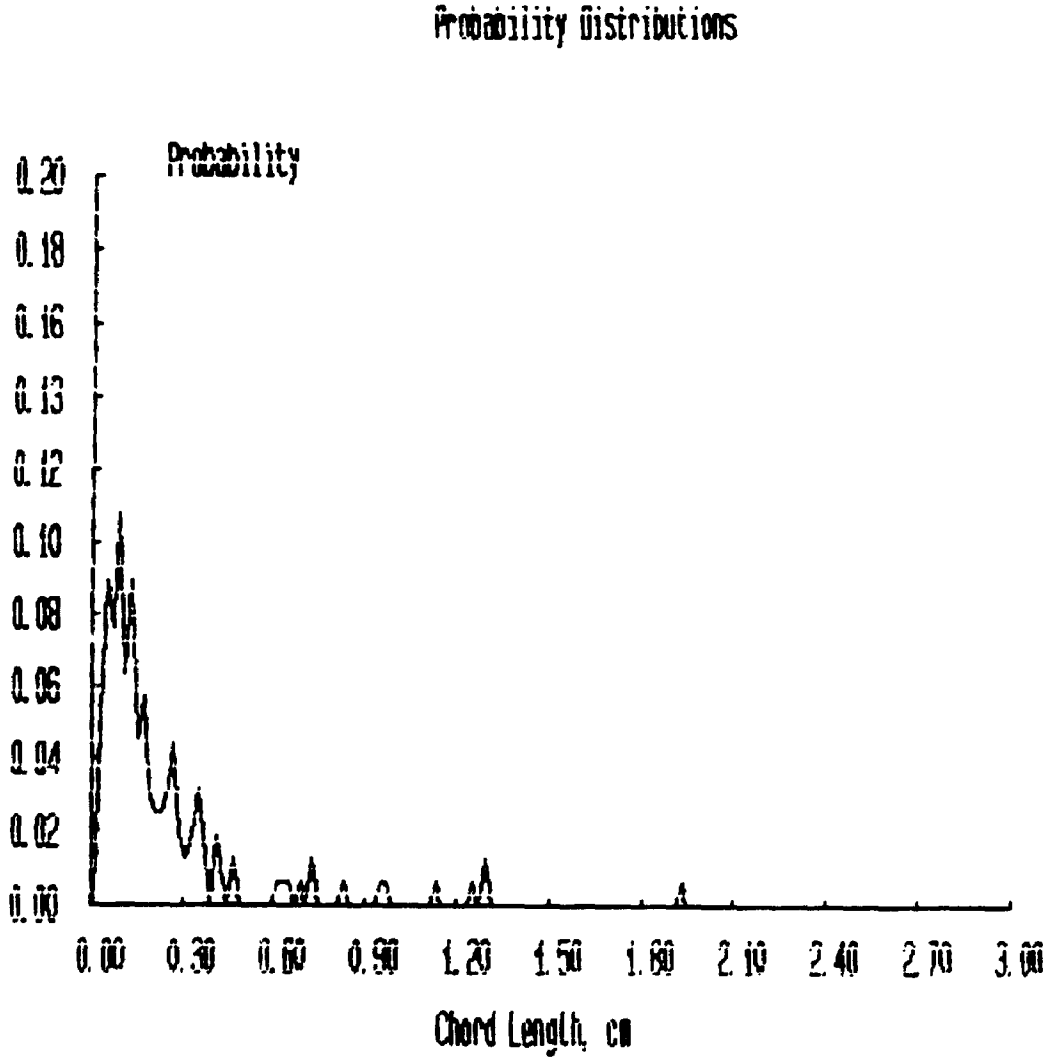

****** FILENAME ****** : JAN18D1B

**** Bubbles detected by probe 1 : 629
**** Percentage of bubbles retained : 54.69
**** Average bubble duration : .006747 s

Probability Distributions

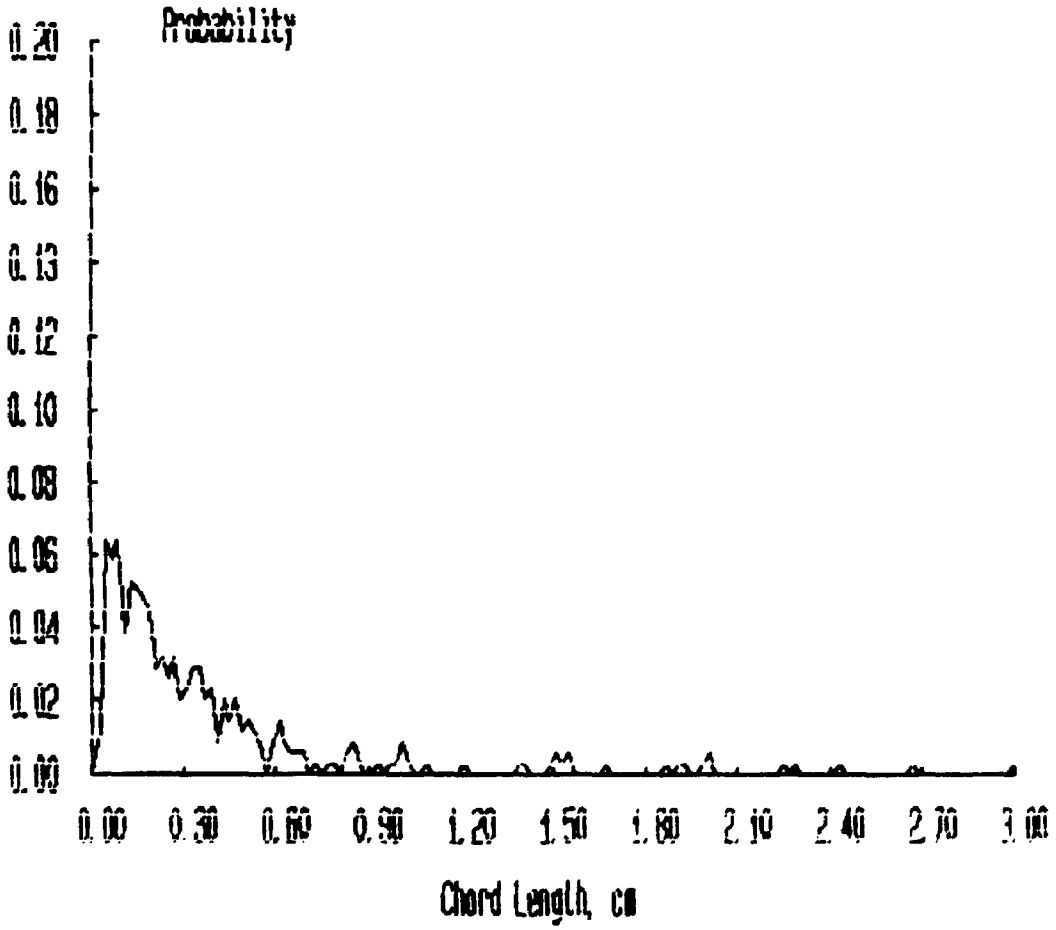

****** FILENAME ****** : JAN18D2A

**** Bubbles detected by probe 1 : 694
**** Percentage of bubbles retained : 53.03
**** Average bubble duration : .007255 s

Probability Distributions

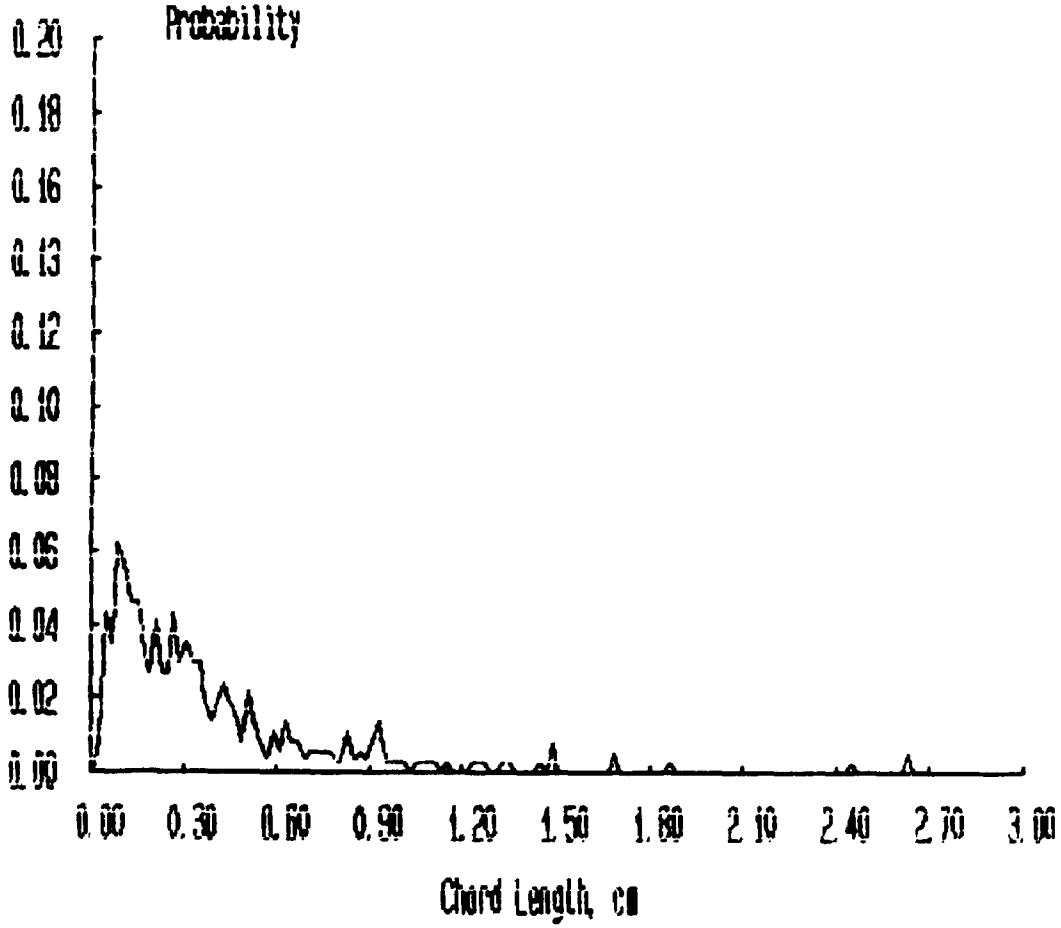

****** FILENAME ****** : JAN18D3A

**** Bubbles detected by probe 1 : 623
**** Percentage of bubbles retained : 41.09
**** Average bubble duration : .006898 s

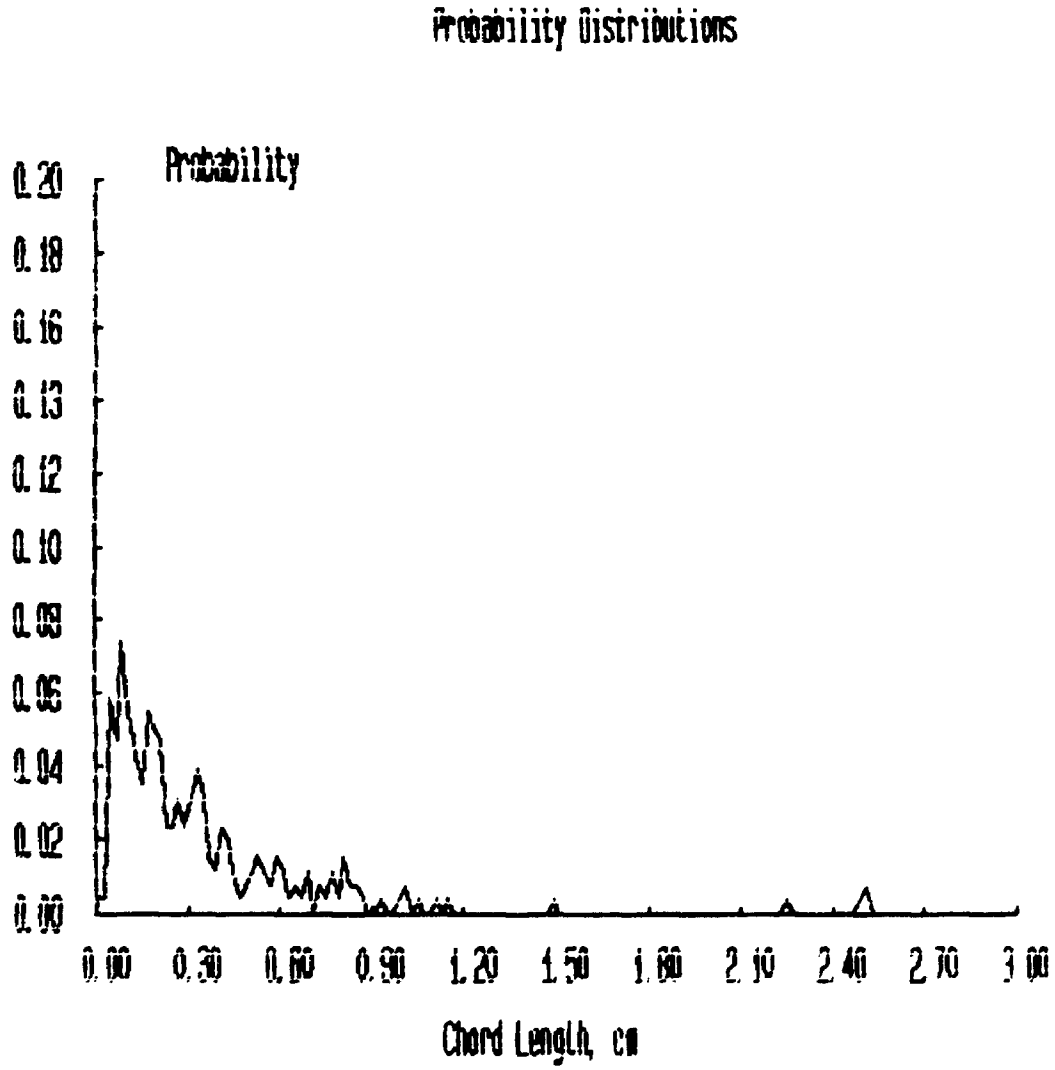

****** FILENAME ****** : JAN18D4B

**** Bubbles detected by probe 1 : 469
**** Percentage of bubbles retained : 36.89
**** Average bubble duration : .007110 s

Probability Distributions

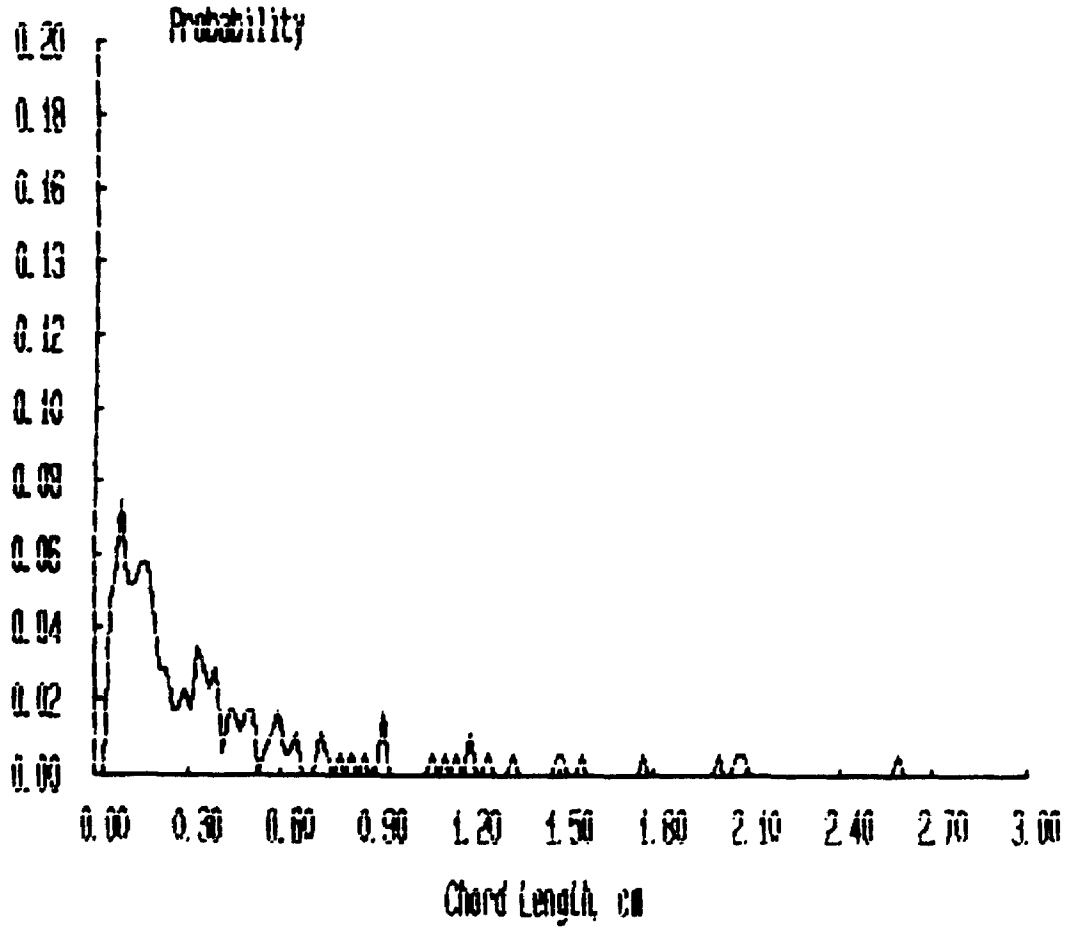

****** FILENAME ****** : JAN18D5B

**** Bubbles detected by probe 1 : 437
**** Percentage of bubbles retained : 29.75
**** Average bubble duration : .006500 s

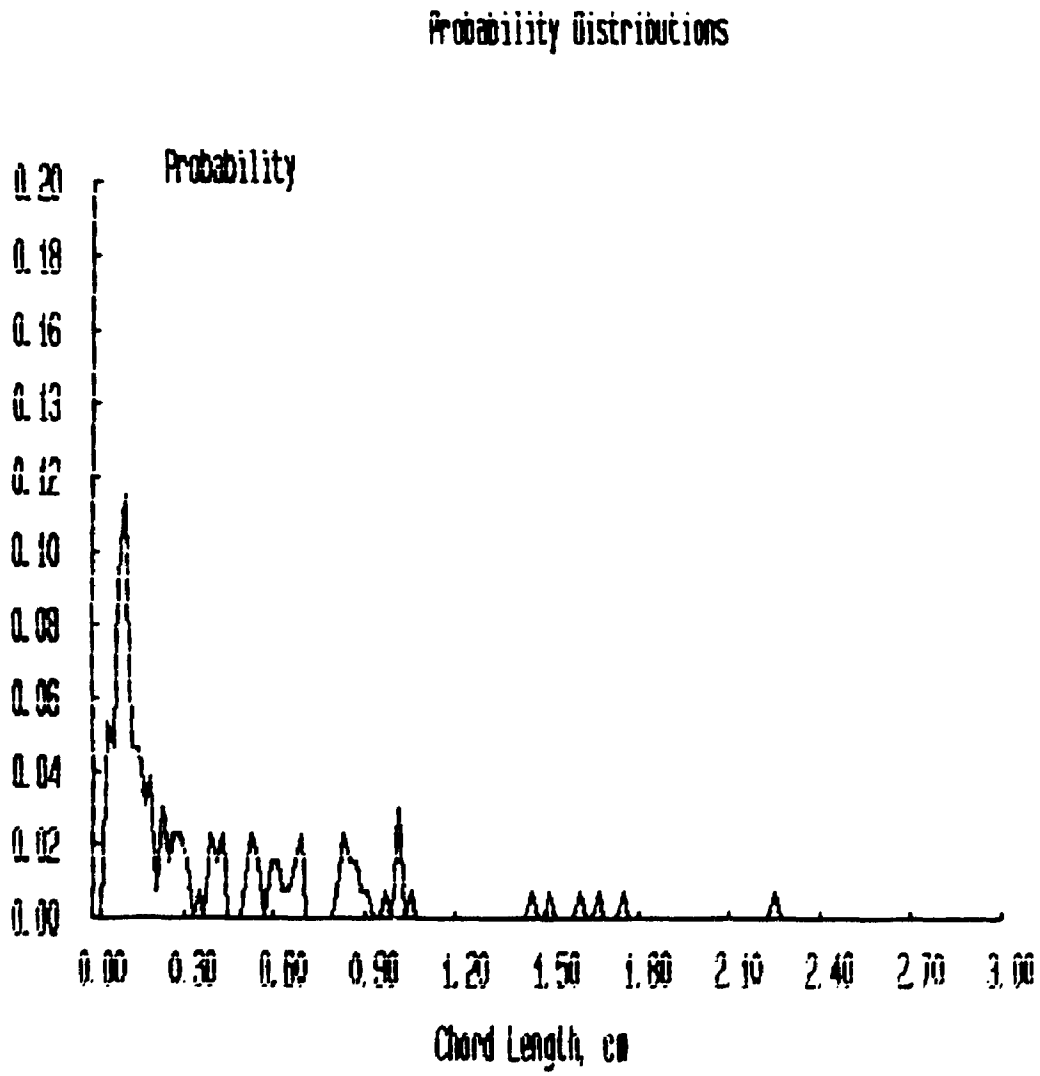

•••••• FILENAME •••••• : JAN18D6A

•••• Bubbles detected by probe 1 : 383
•••• Percentage of bubbles retained : 25.59
•••• Average bubble duration : .006571 s

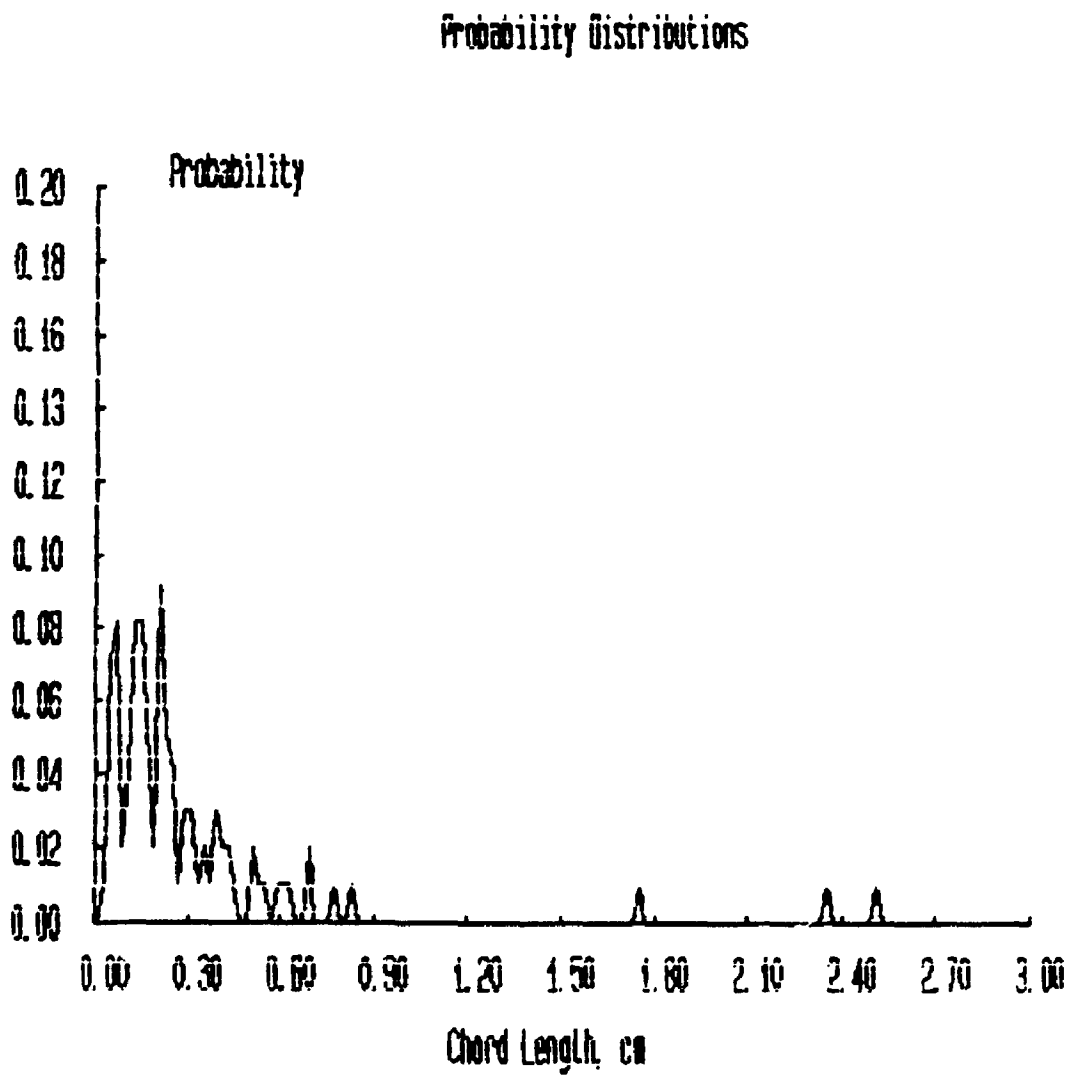

****** FILENAME ****** : JAN18E1A

**** Bubbles detected by probe 1 : 522
**** Percentage of bubbles retained : 46.74
**** Average bubble duration : .0069/5 s

Probability Distributions

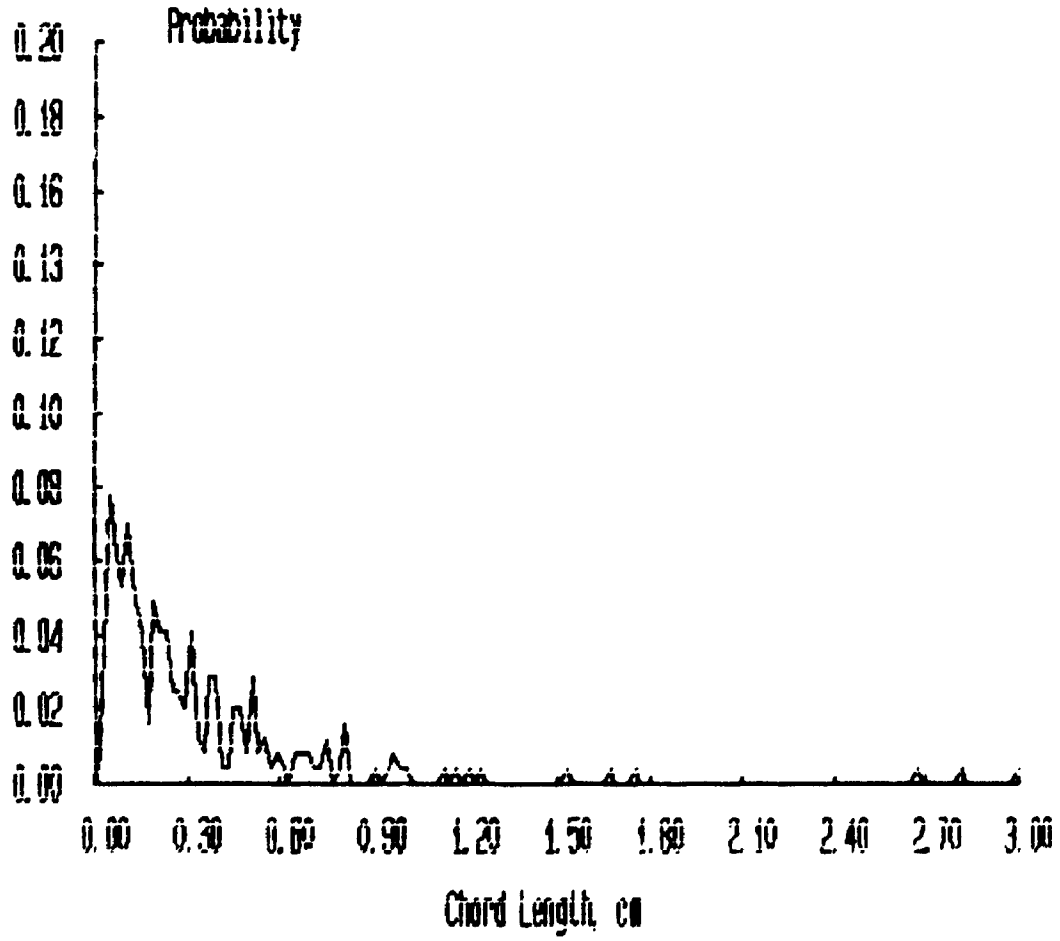

****** FILENAME ****** : JAN18E2A

**** Bubbles detected by probe 1 : 538
**** Percentage of bubbles retained : 44.61
**** Average bubble duration : .007579 s

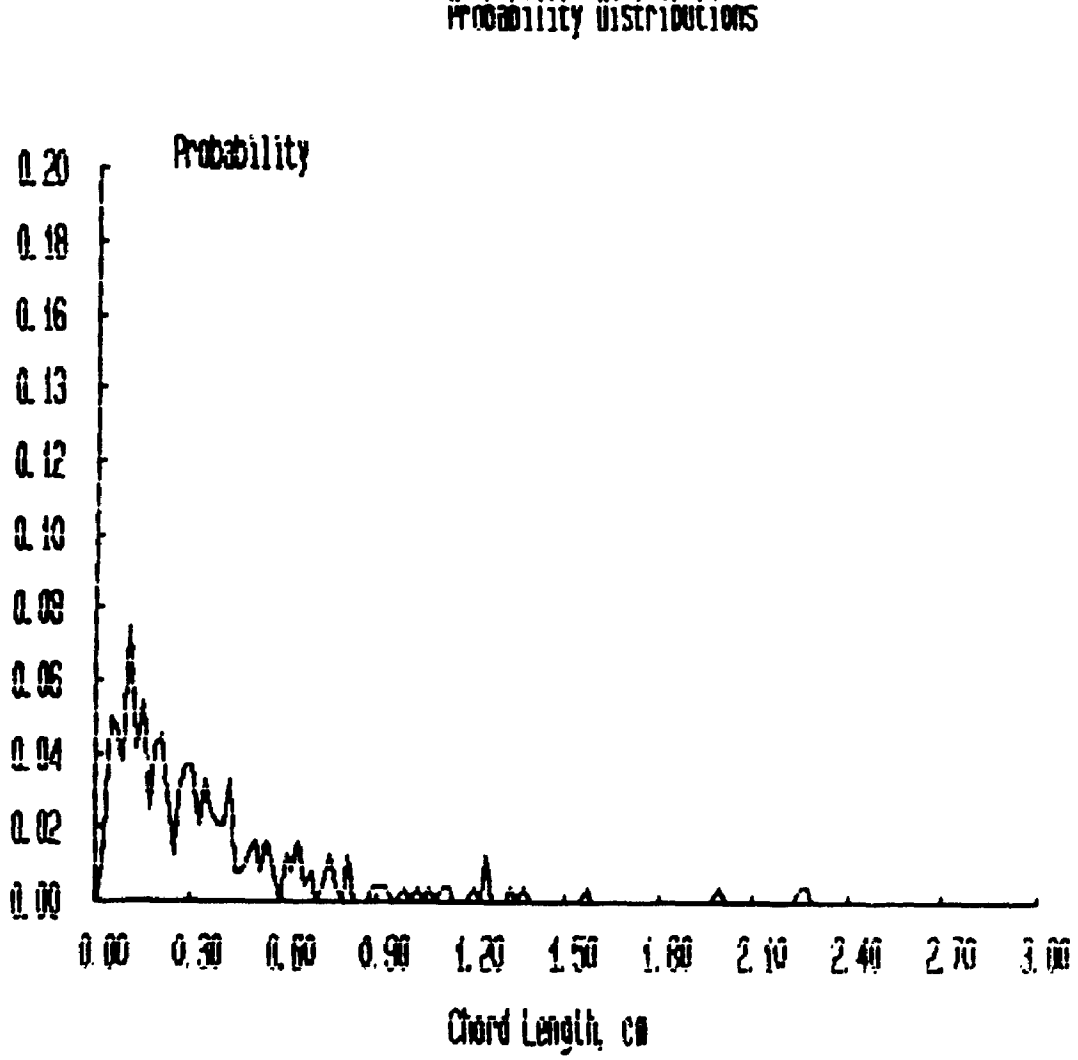

****** FILENAME ****** : JAN18E3A

**** Bubbles detected by probe 1 : 643
**** Percentage of bubbles retained : 45.26
**** Average bubble duration : .006773 s

Probability Distributions

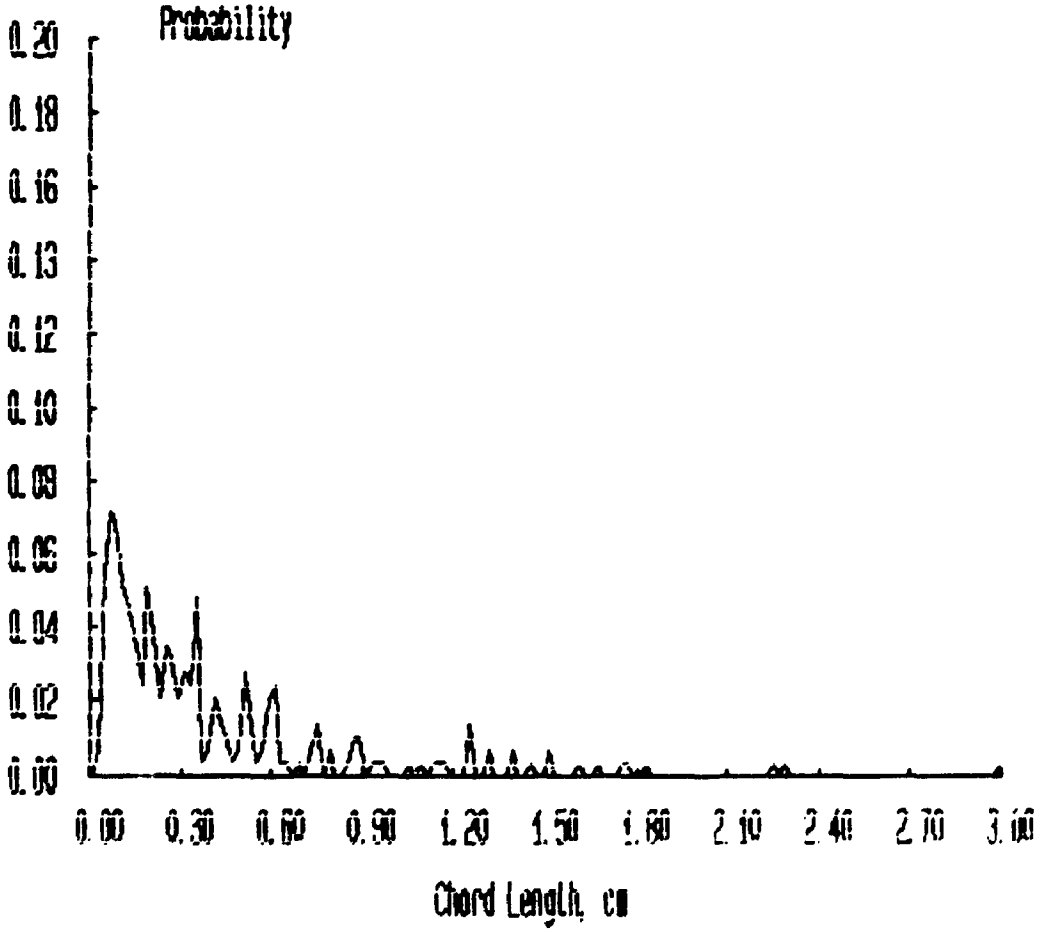

•••••• FILENAME •••••• : JAN18E4A

•••• Bubbles detected by probe 1 : 504
•••• Percentage of bubbles retained : 40.87
•••• Average bubble duration : .006786 s

Probability Distributions

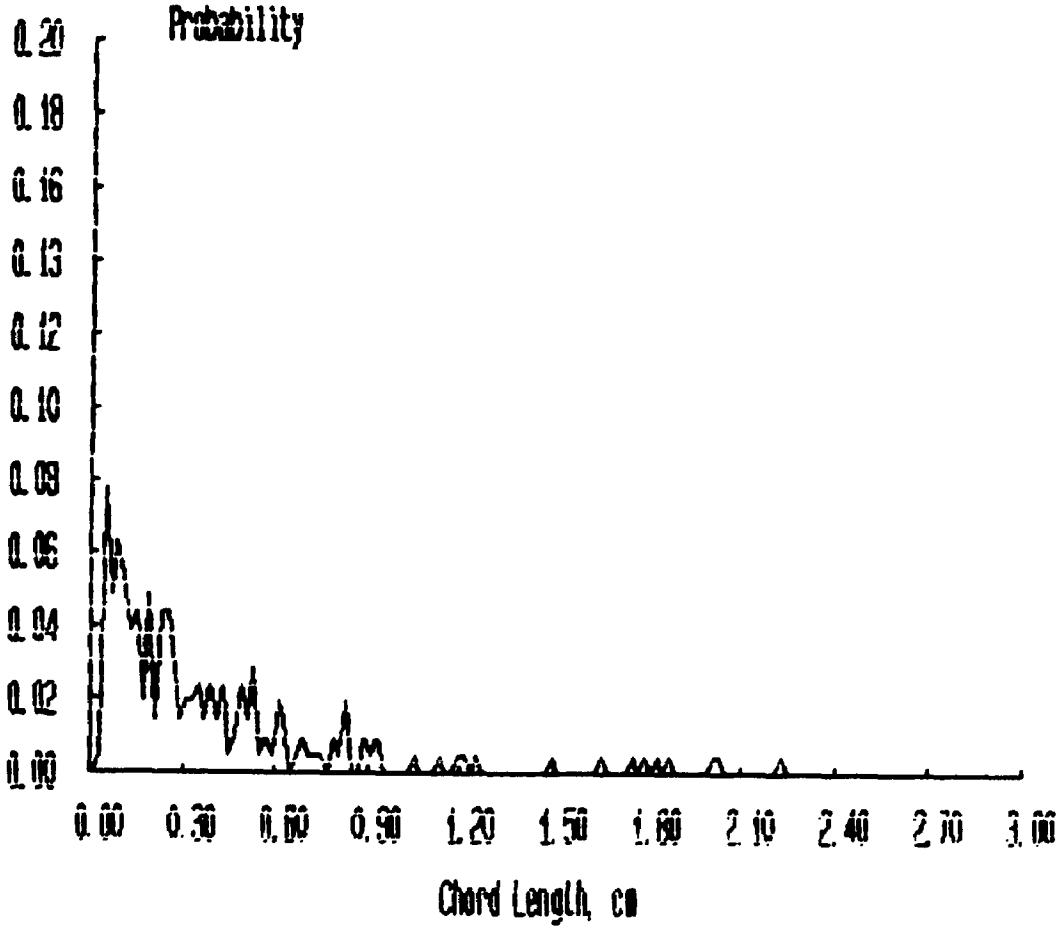

****** FILENAME ****** : JAN18E5B

**** Bubbles detected by probe 1 : 526
**** Percentage of bubbles retained : 55.51
**** Average bubble duration : .006736 s

Probability Distributions

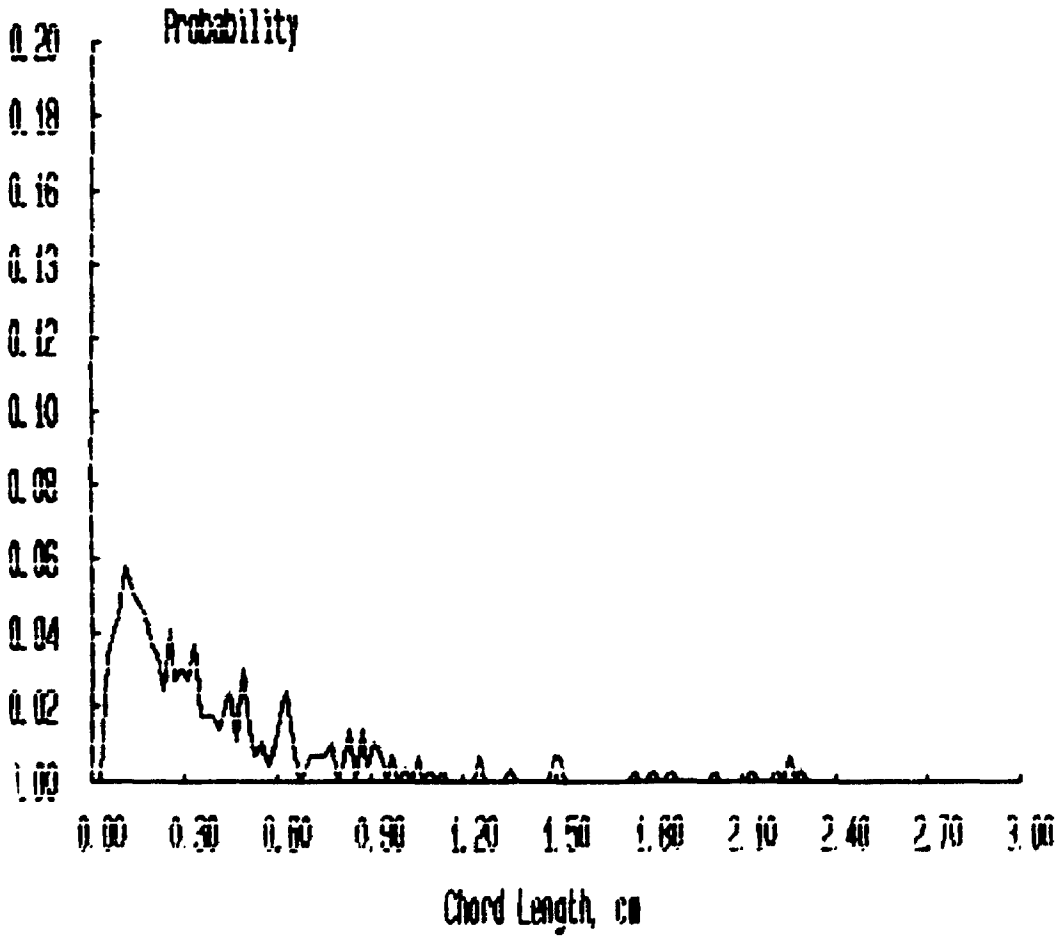

****** FILENAME ****** : JAN18E6A

**** Bubbles detected by probe 1 : 363
**** Percentage of bubbles retained : 41.60
**** Average bubble duration : .007166 s

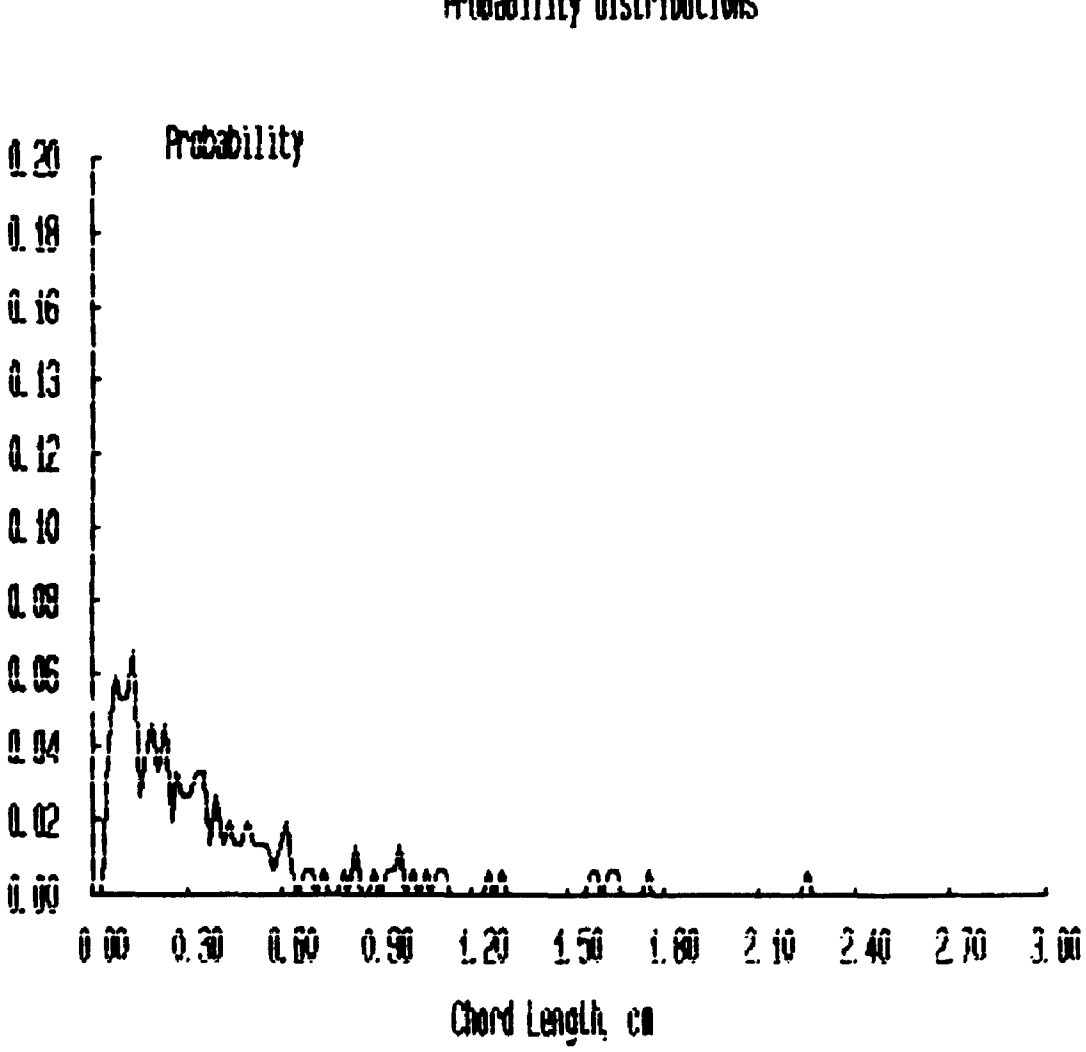

****** FILENAME ****** : JAN20A1A

**** Bubbles detected by probe 1 : 913
**** Percentage of bubbles retained : 56.08
**** Average bubble duration : .006455 s

Probability Distributions

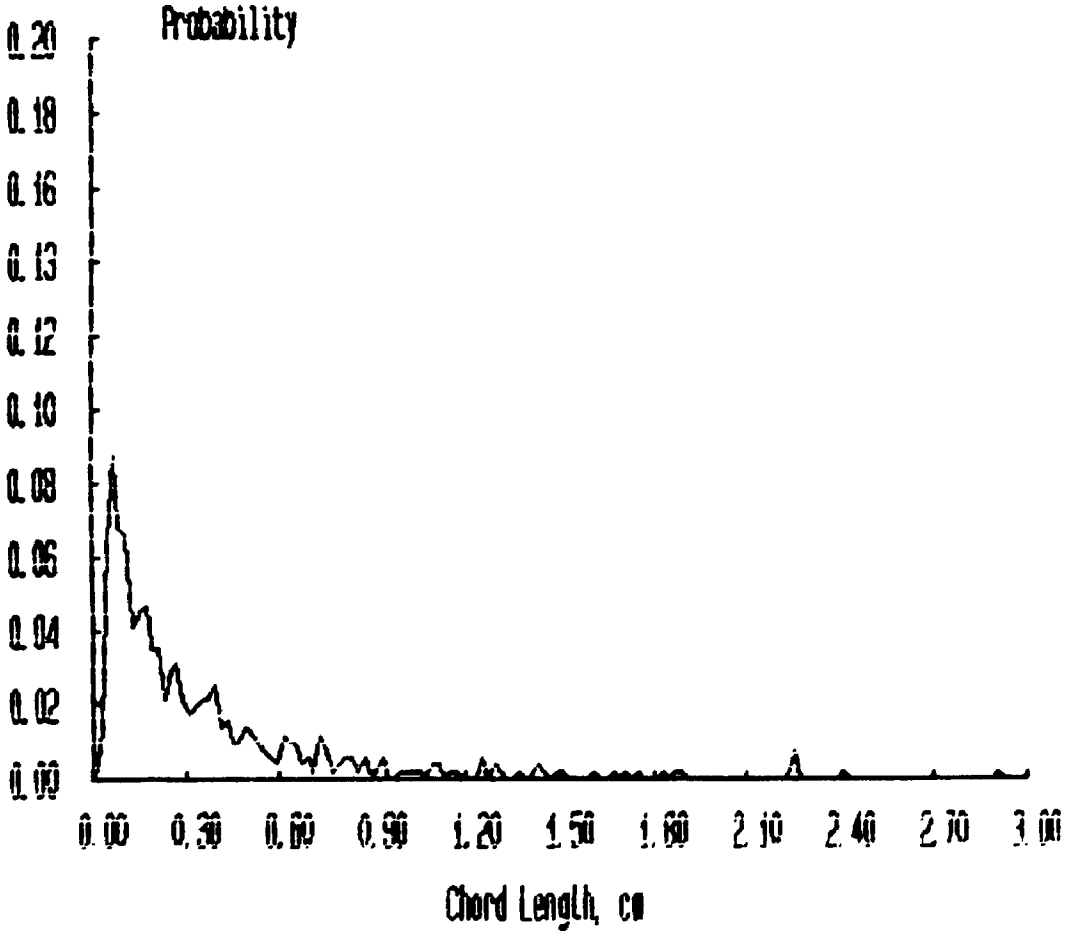

****** FILENAME ****** : JAN20A2A

**** Bubbles detected by probe 1 : 979
**** Percentage of bubbles retained : 53.32
**** Average bubble duration : .006762 s

Probability Distributions

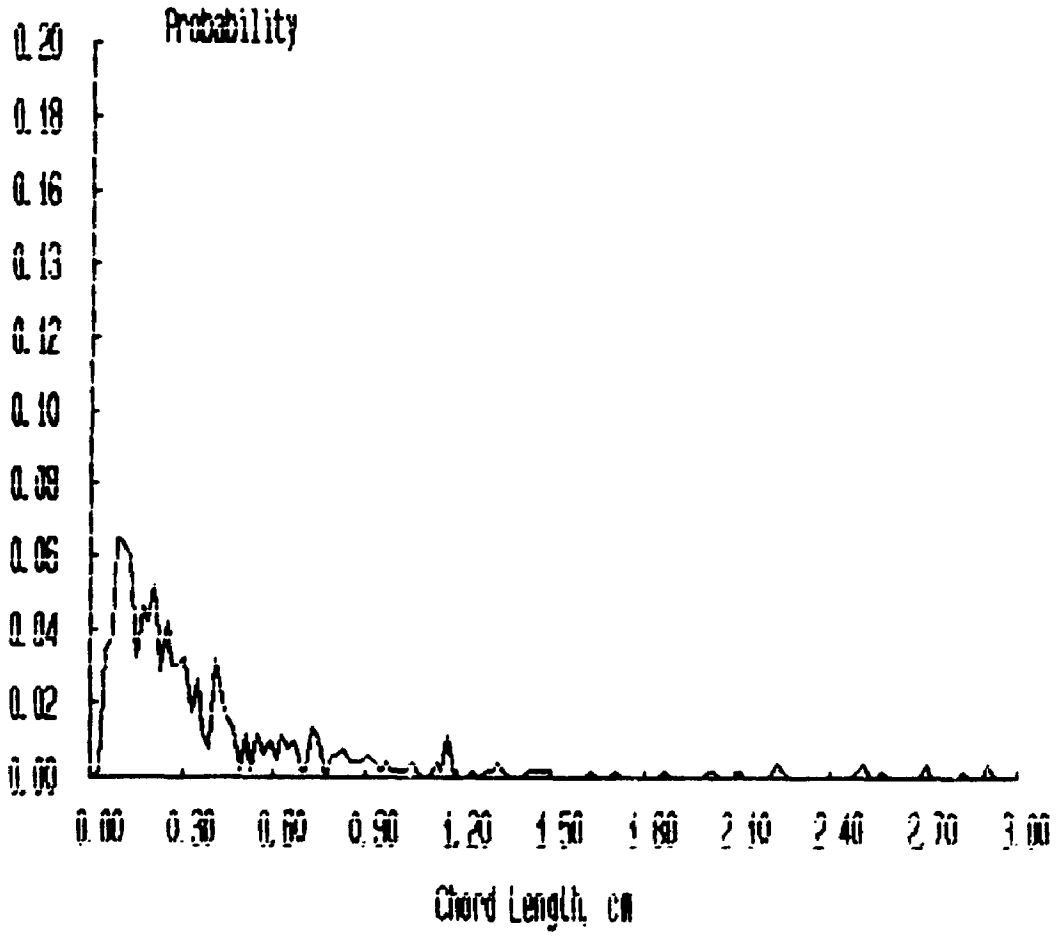

****** FILENAME ****** : JAN20A3A

**** Bubbles detected by probe 1 : 812
**** Percentage of bubbles retained : 43.97
**** Average bubble duration : .006941 s

Probability Distributions

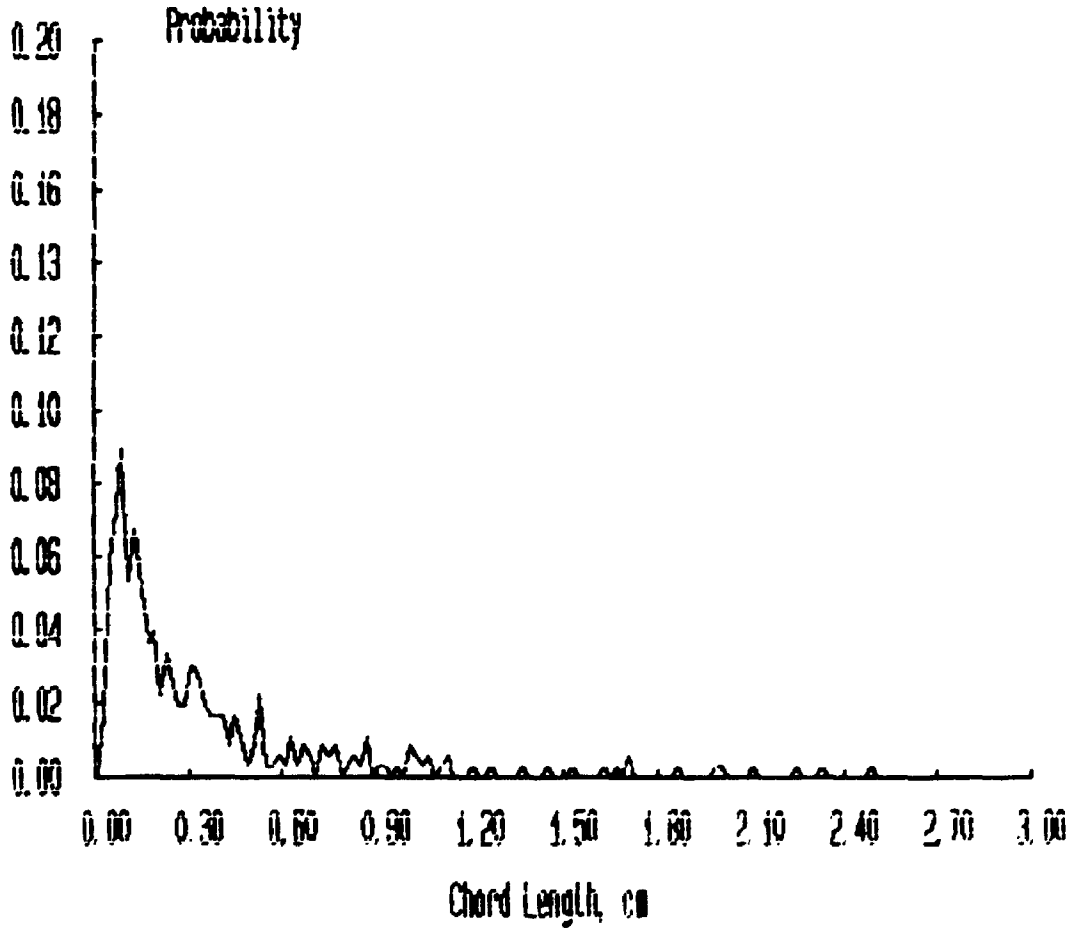

****** FILENAME ****** : JAN20A4A

**** Bubbles detected by probe 1 : 697
**** Percentage of bubbles retained : 37.73
**** Average bubble duration : .007042 s

Probability Distributions

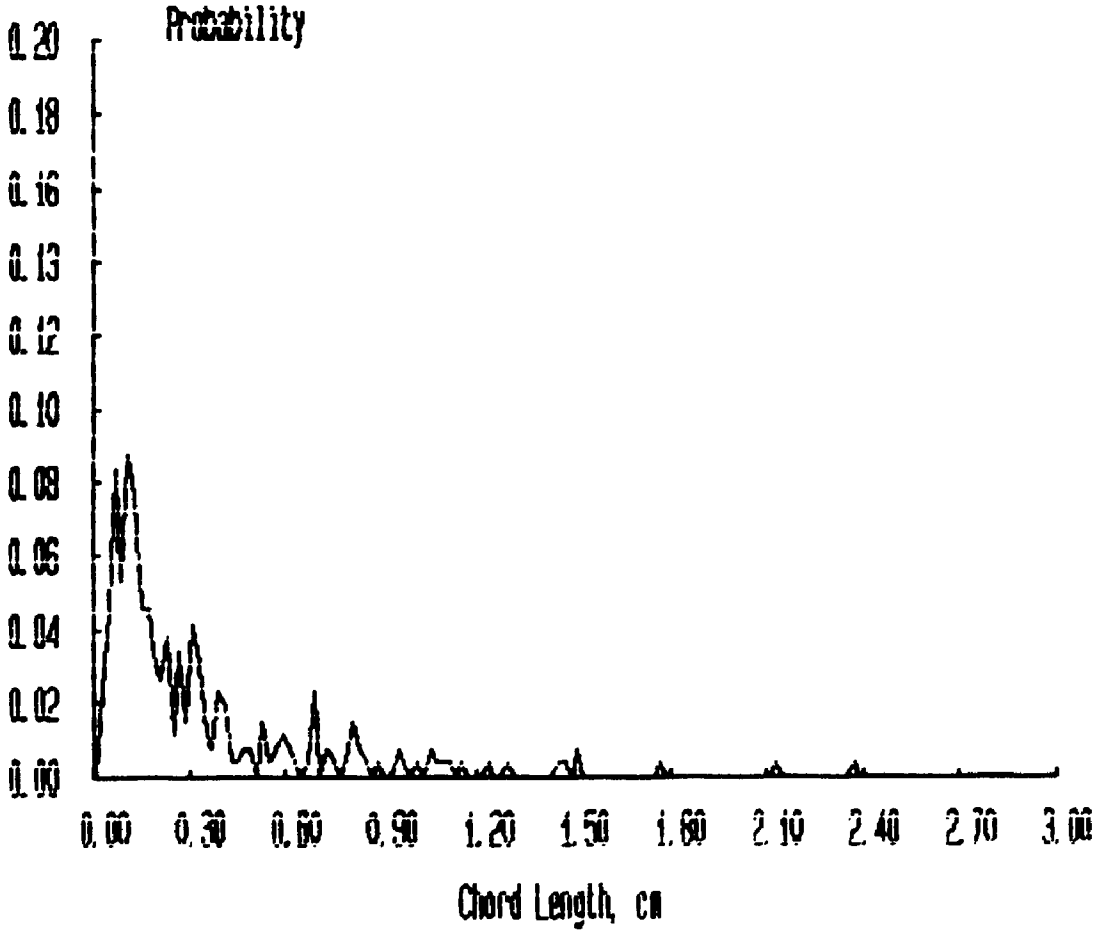

****** FILENAME ****** : JAN20A5A

**** Bubbles detected by probe 1 : 442
**** Percentage of bubbles retained : 24.89
**** Average bubble duration : .007056 s

Probability Distributions

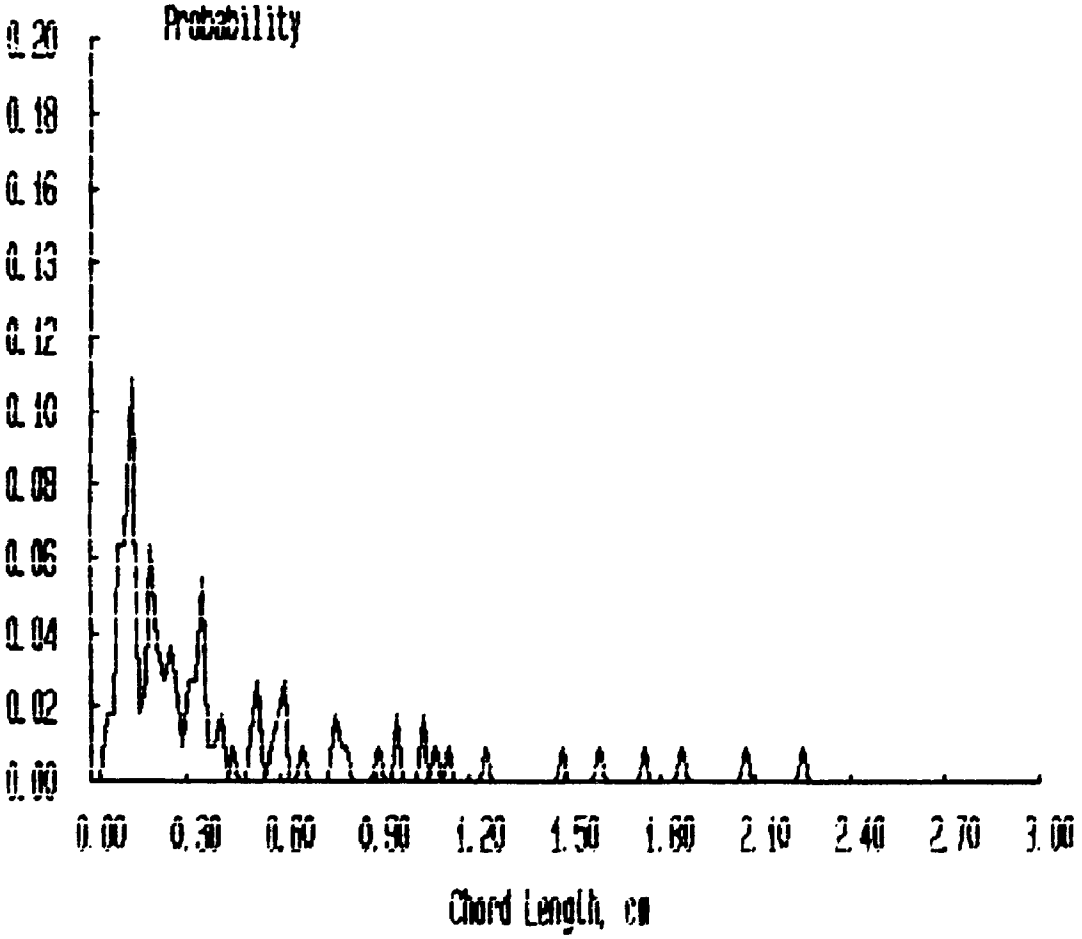

****** FILENAME ****** : JAN20A6A

**** Bubbles detected by probe 1 : 584
**** Percentage of bubbles retained : 40.41
**** Average bubble duration : .006881 s

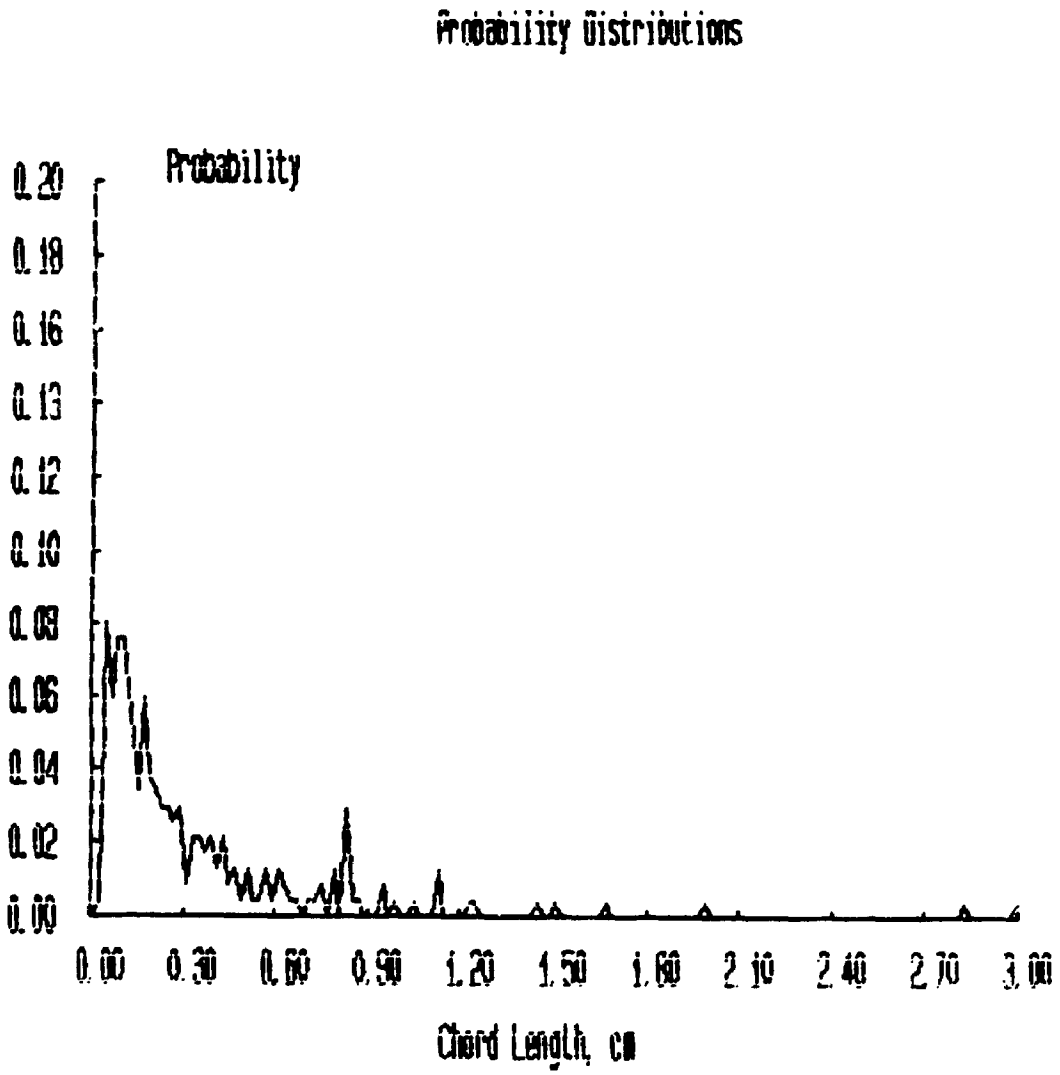

****** FILENAME ****** : JAN20B1A

**** Bubbles detected by probe 1 : 1135
**** Percentage of bubbles retained : 56.83
**** Average bubble duration : .006166 s

Probability Distributions

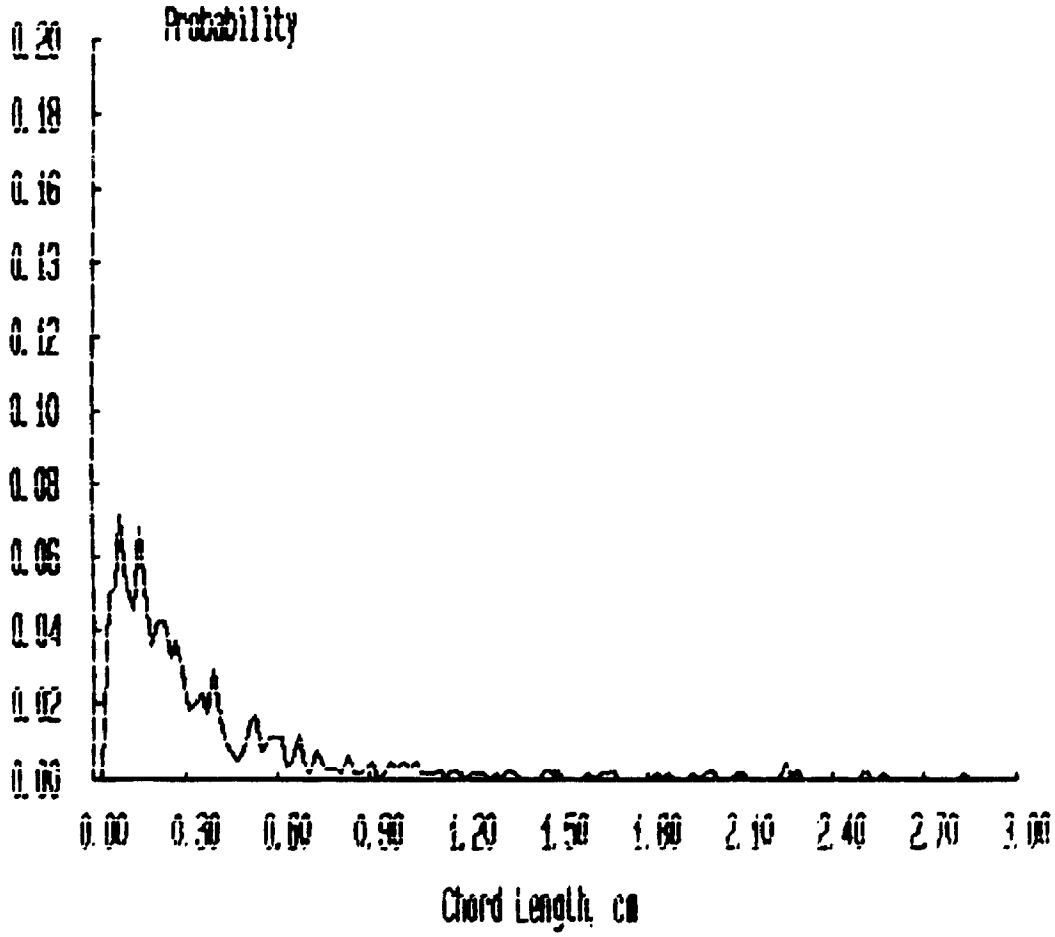

****** FILENAME ****** : JAN20B2A

**** Bubbles detected by probe 1 : 1122
**** Percentage of bubbles retained : 54.99
**** Average bubble duration : .006426 s

Probability Distributions

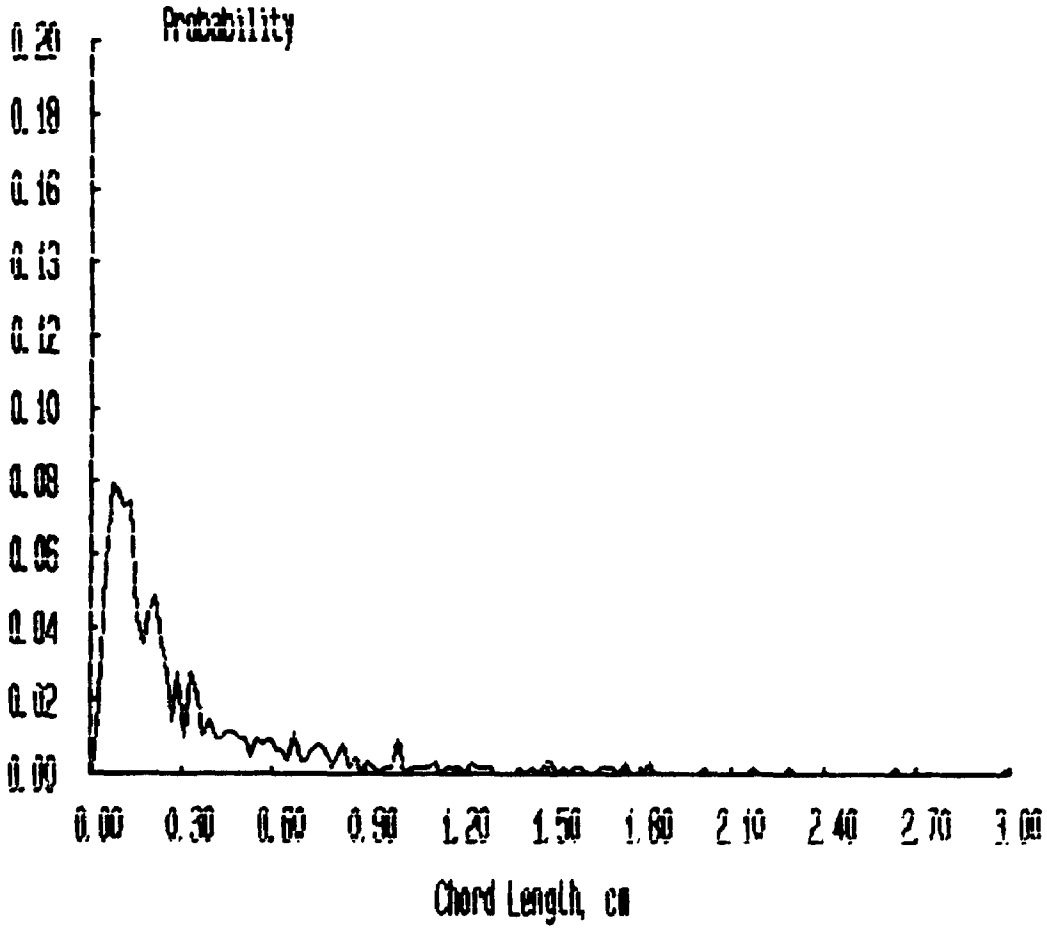

****** FILENAME ****** : JAN20B3A

**** Bubbles detected by probe 1 : 1058
**** Percentage of bubbles retained : 46.98
**** Average bubble duration : .006143 s

Probability Distributions

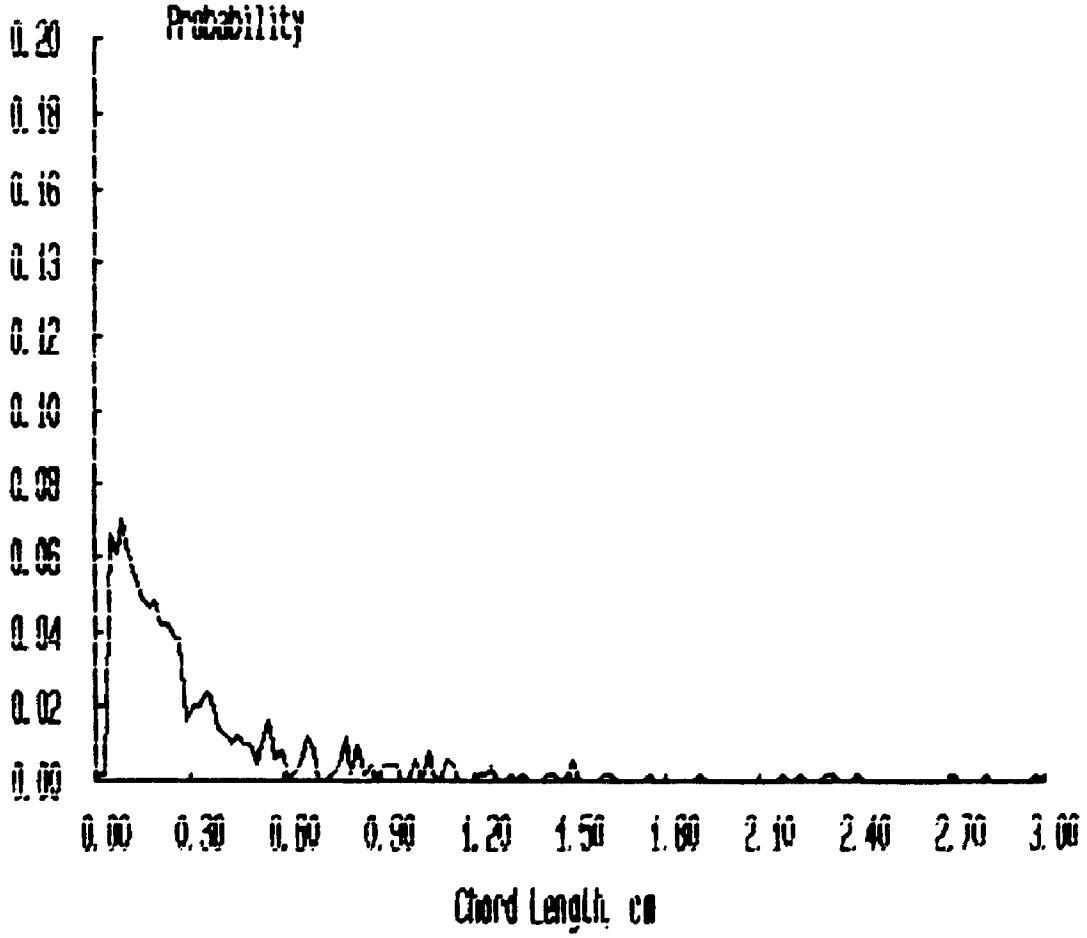

****** FILENAME ****** : JAN20B4A

**** Bubbles detected by probe 1 : 790
**** Percentage of bubbles retained : 38.23
**** Average bubble duration : .006066 s

Probability Distributions

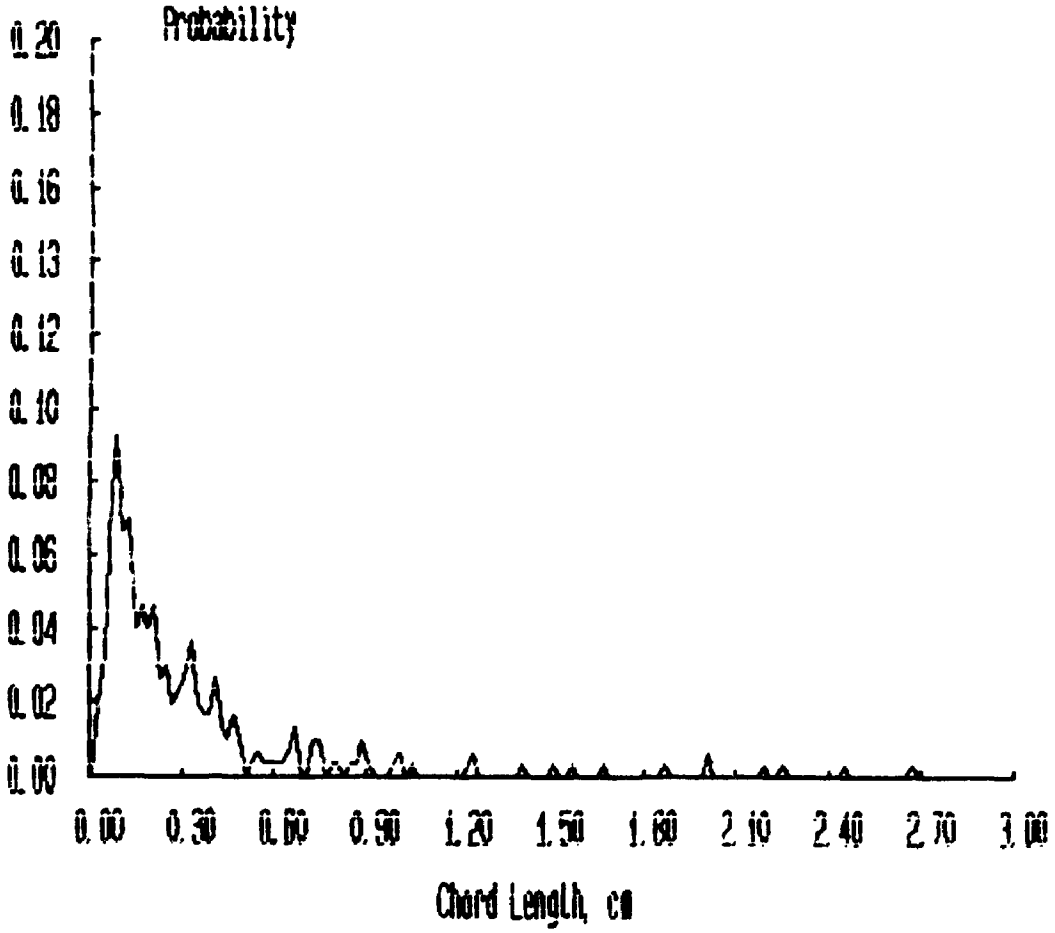

****** FILENAME ****** : JAN20B5A

**** Bubbles detected by probe 1 : 569
**** Percentage of bubbles retained : 58.14
**** Average bubble duration : .006521 s

Probability Distributions

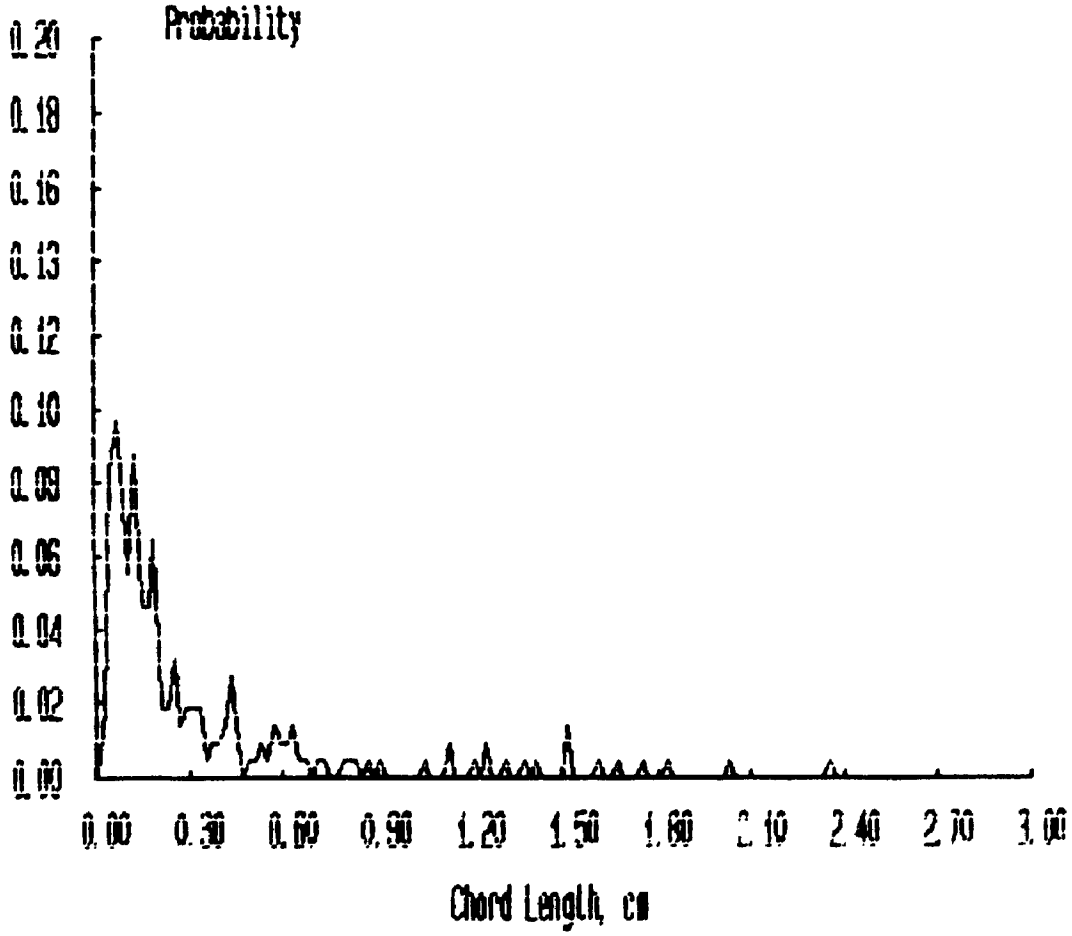

****** FILENAME ****** : JAN20B6A

**** Bubbles detected by probe 1 : 653
**** Percentage of bubbles retained : 47.78
**** Average bubble duration : .005774 s

Probability Distributions

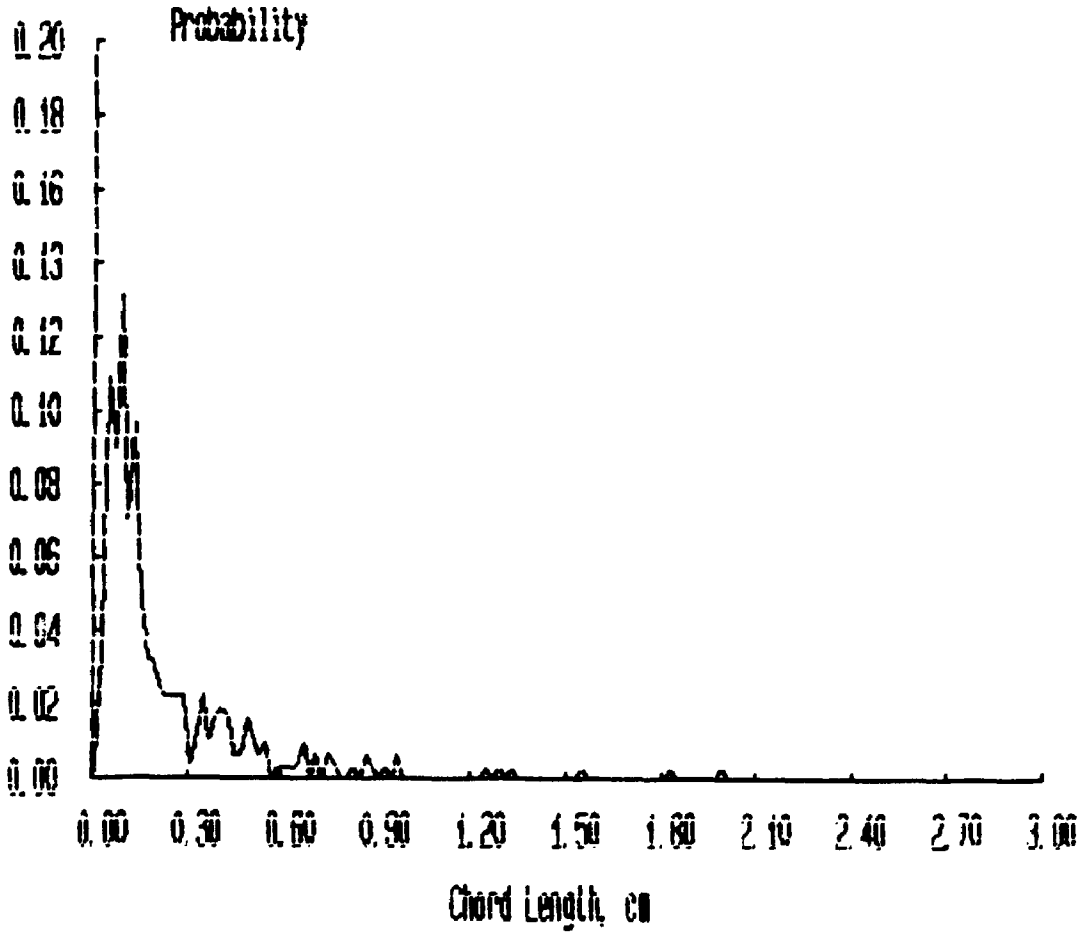

****** FILENAME ****** : JAN20C1A

**** Bubbles detected by probe 1 : 1578
**** Percentage of bubbles retained : 53.93
**** Average bubble duration : .005730 s

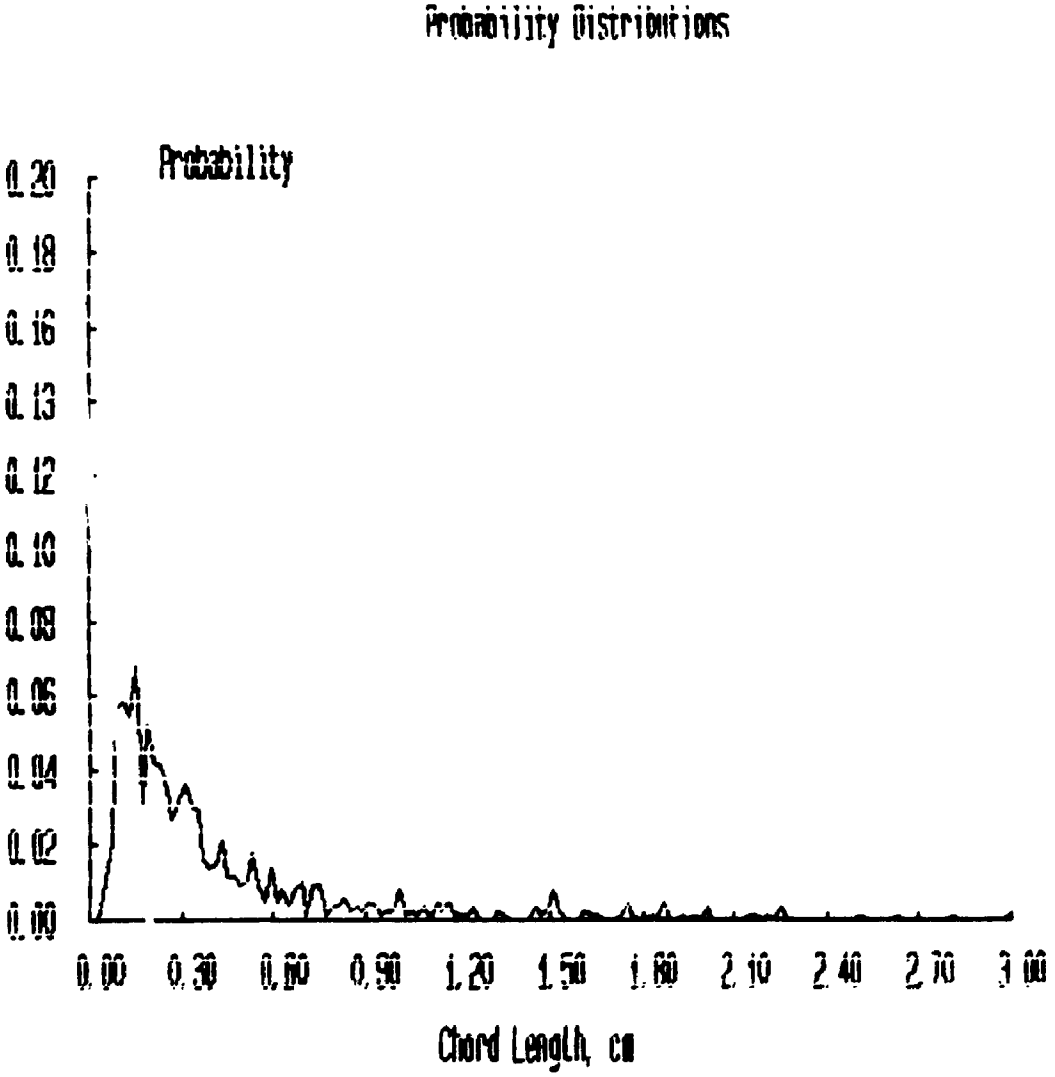

****** FILENAME ****** : JAN20C2A

**** Bubbles detected by probe 1 : 1427
**** Percentage of bubbles retained : 57.95
**** Average bubble duration : .005686 s

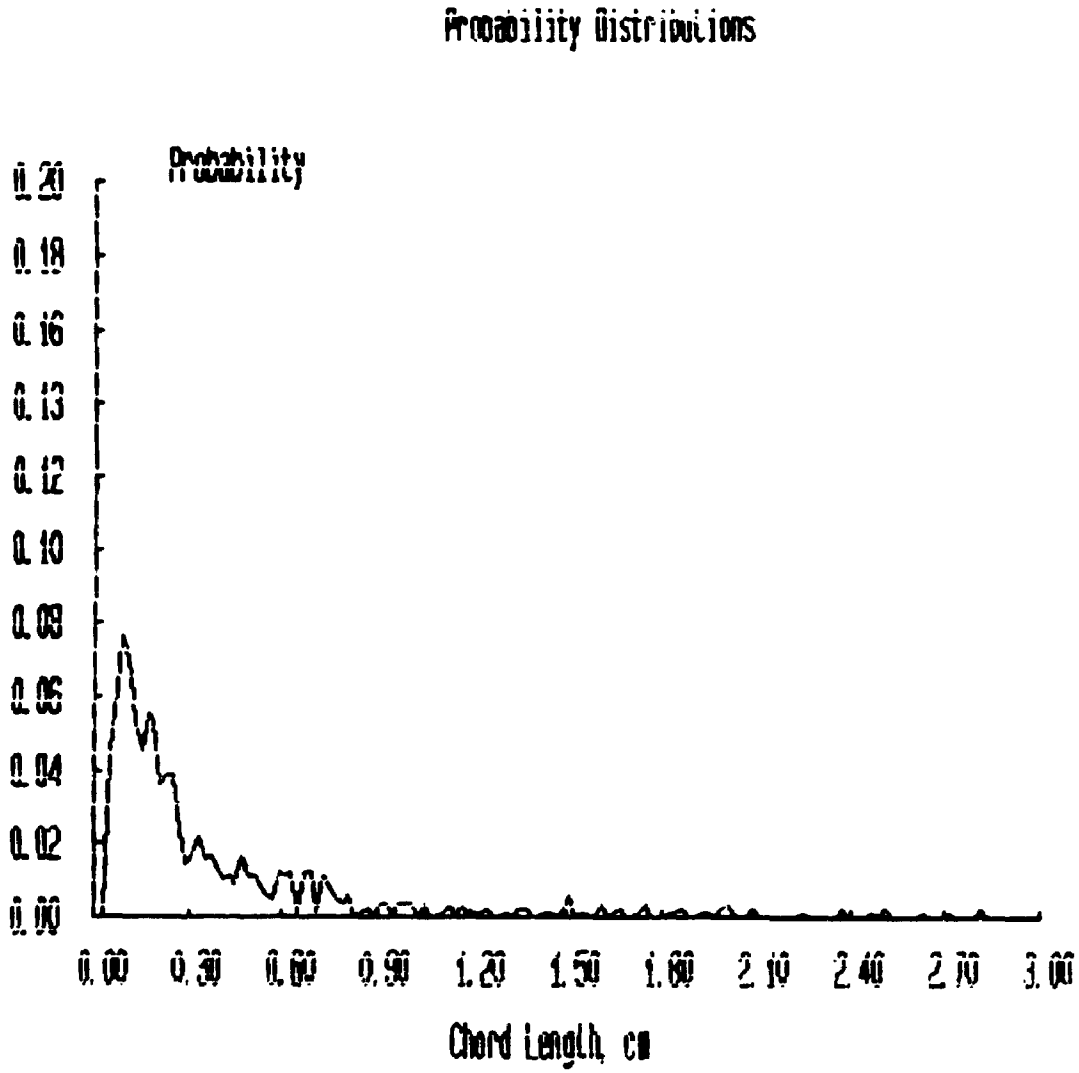

****** FILENAME ****** : JAN20C3A

**** Bubbles detected by probe 1 : 1403
**** Percentage of bubbles retained : 46.33
**** Average bubble duration : .005615 s

Probability Distributions

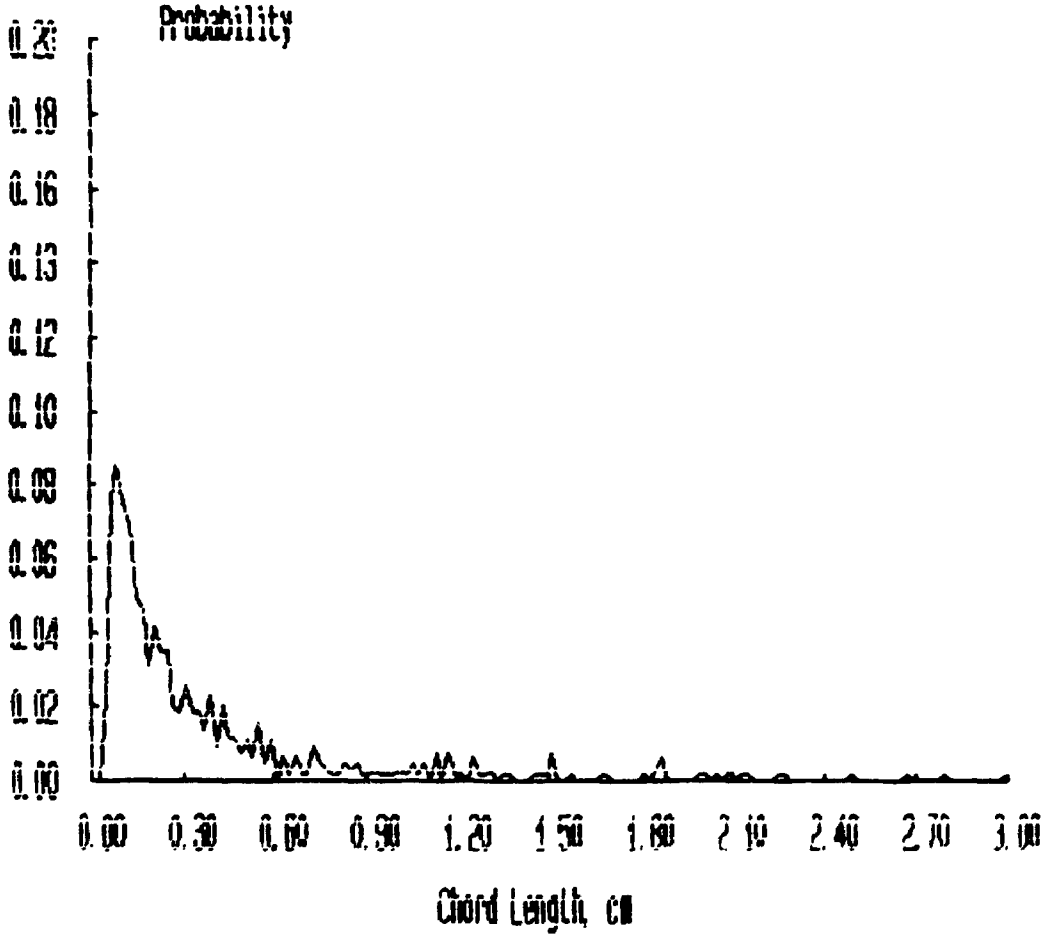

****** FILENAME ****** : JAN2UC4A

**** Bubbles detected by probe 1 : 1297
**** Percentage of bubbles retained : 39.71
**** Average bubble duration : .005955 s

Probability Distributions

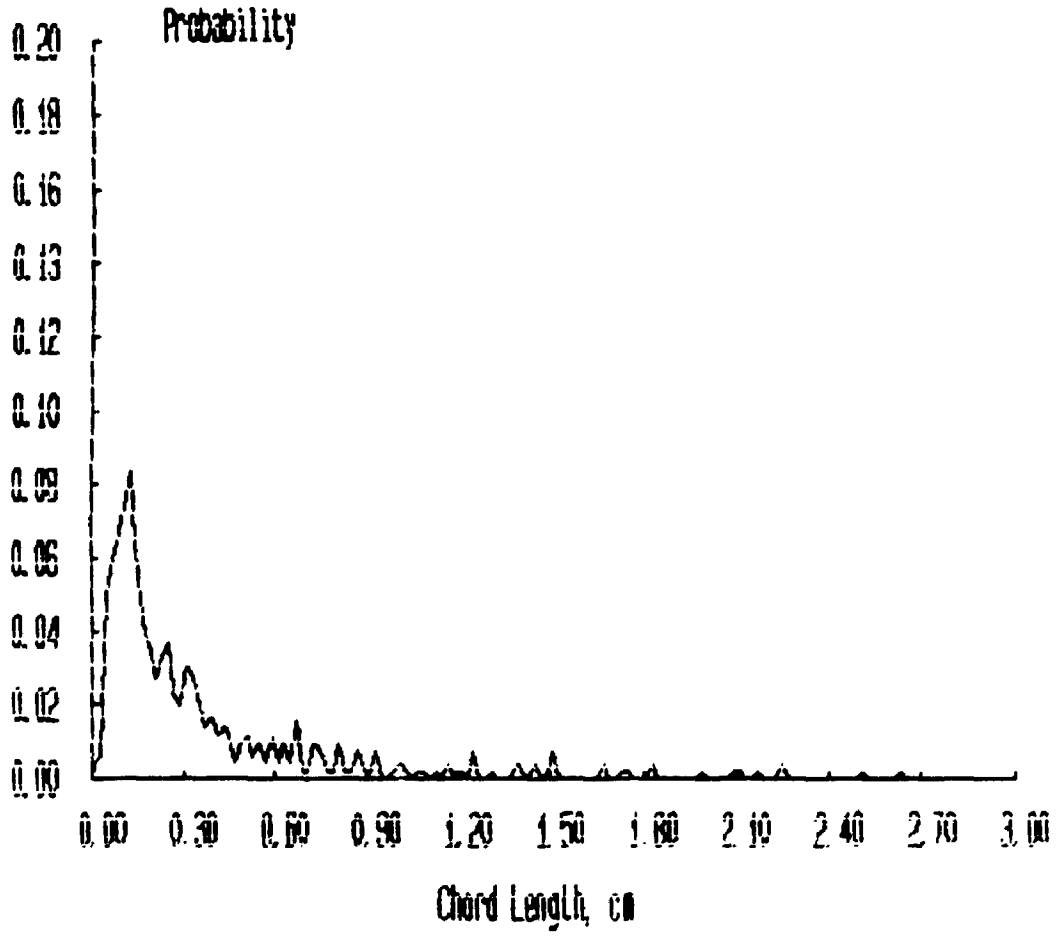

****** FILENAME ****** : JAN20C5A

**** Bubbles detected by probe 1 : 852
**** Percentage of bubbles retained : 44.37
**** Average bubble duration : .006206 s

Probability Distributions

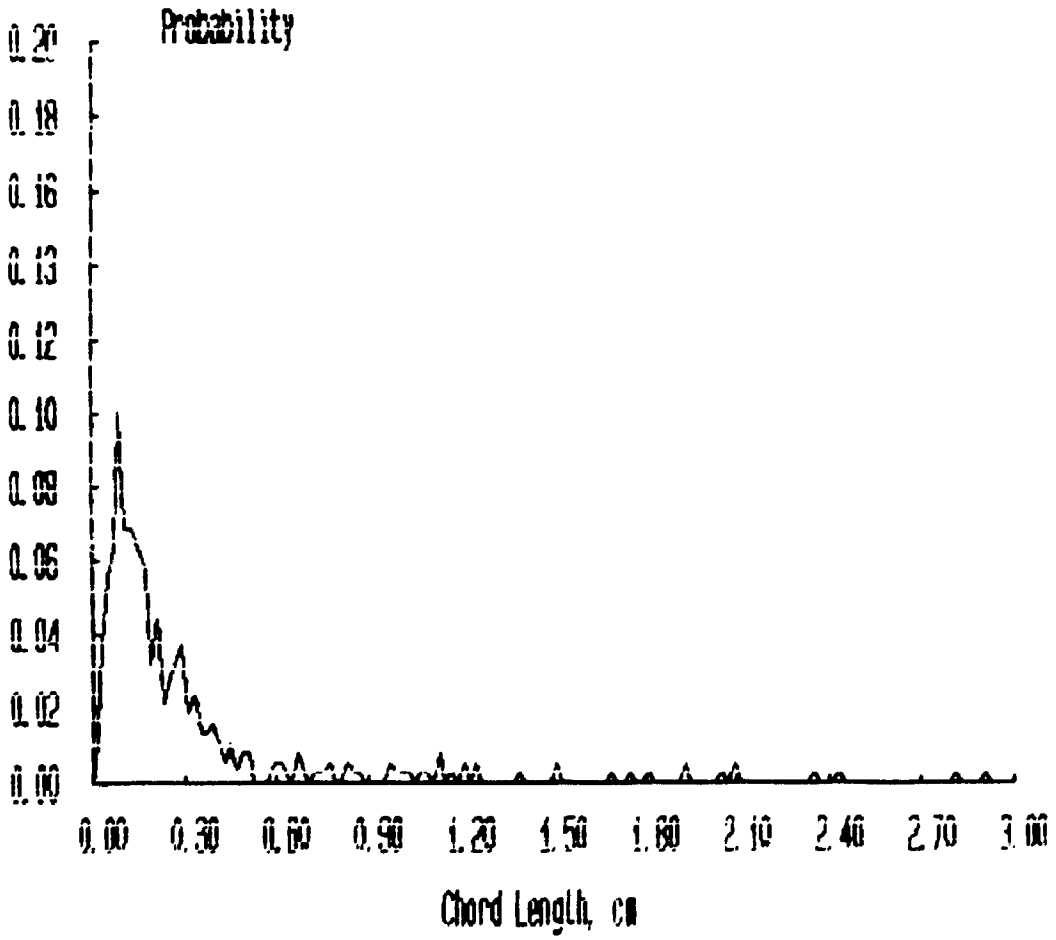

****** FILENAME ****** : JAN20C6B

**** Bubbles detected by probe 1 : 599
**** Percentage of bubbles retained : 43.07
**** Average bubble duration : .005217 s

Probability Distributions

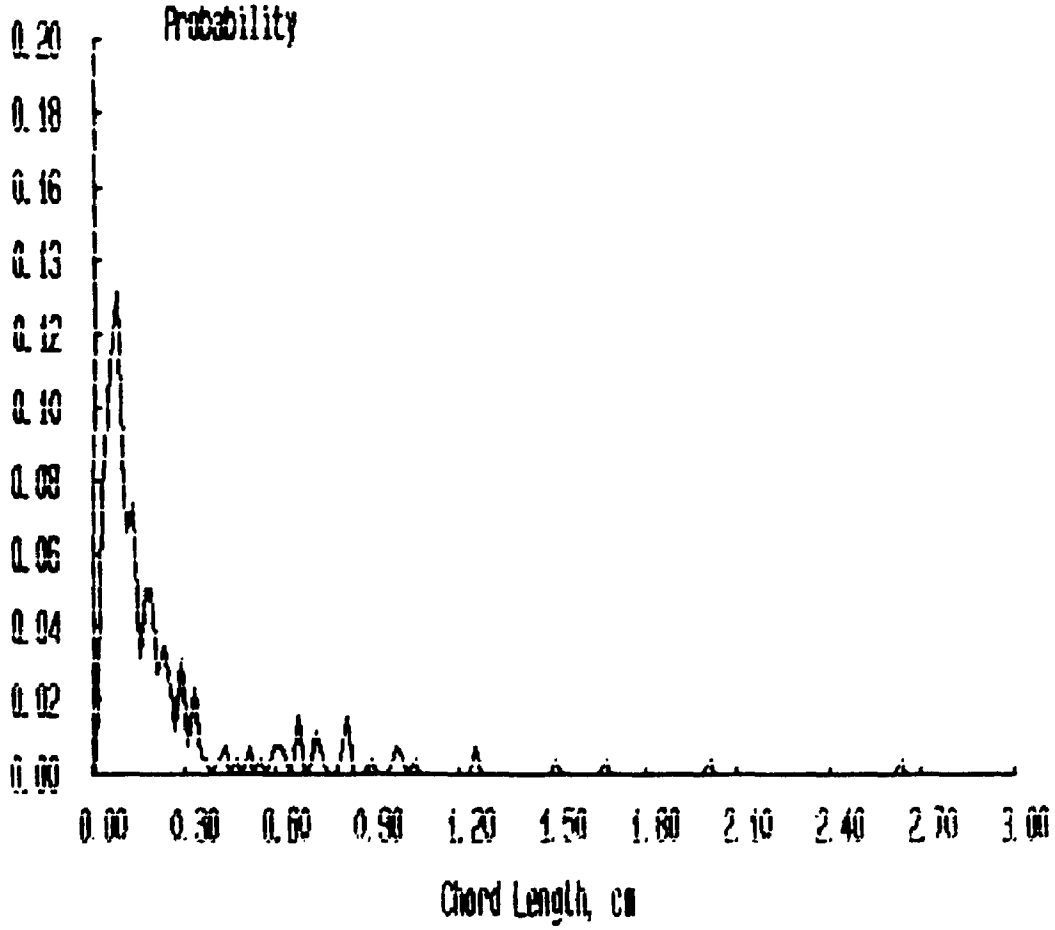

****** FILENAME ****** : JAN20D1A

**** Bubbles detected by probe 1 : 1810
**** Percentage of bubbles retained : 61.82
**** Average bubble duration : .005550 s

Probability Distributions

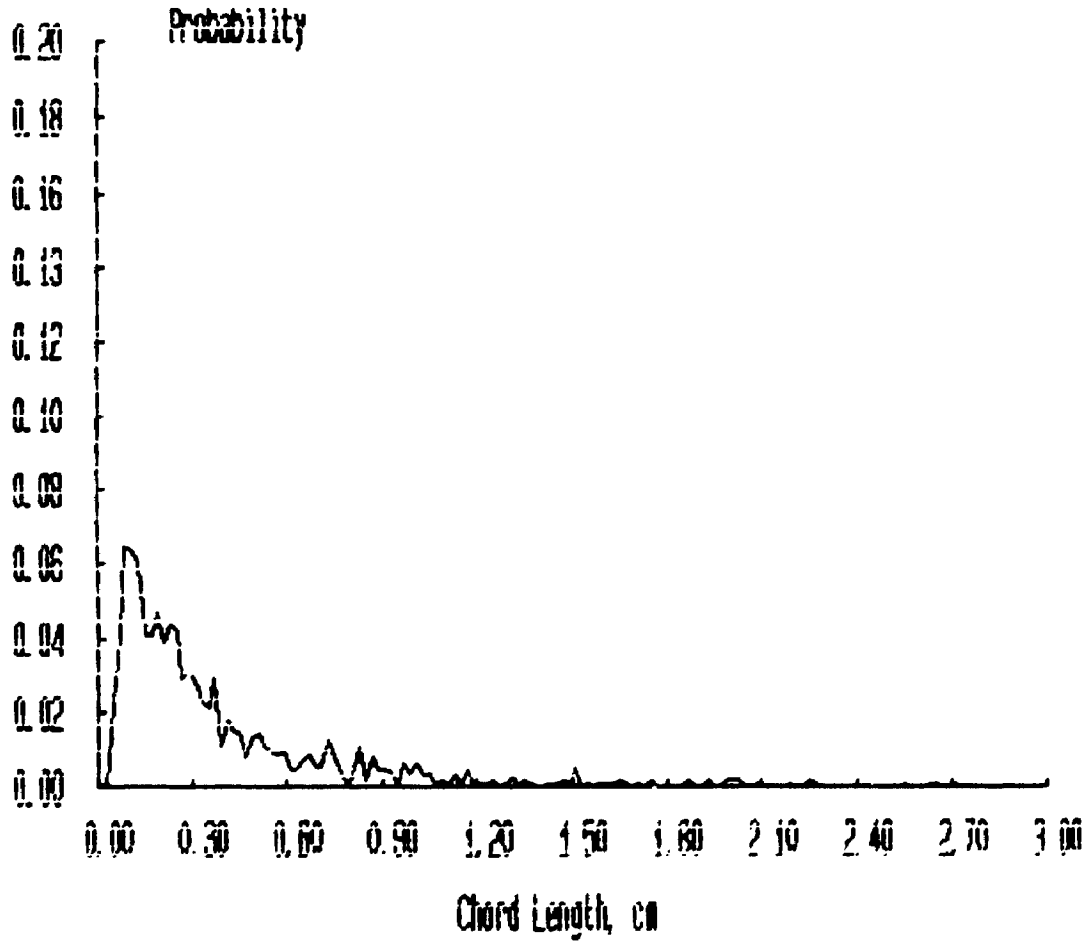

****** FILENAME ****** : JAN20D2A

**** Bubbles detected by probe 1 : 1786
**** Percentage of bubbles retained : 59.01
**** Average bubble duration : .005615 s

Probability Distributions

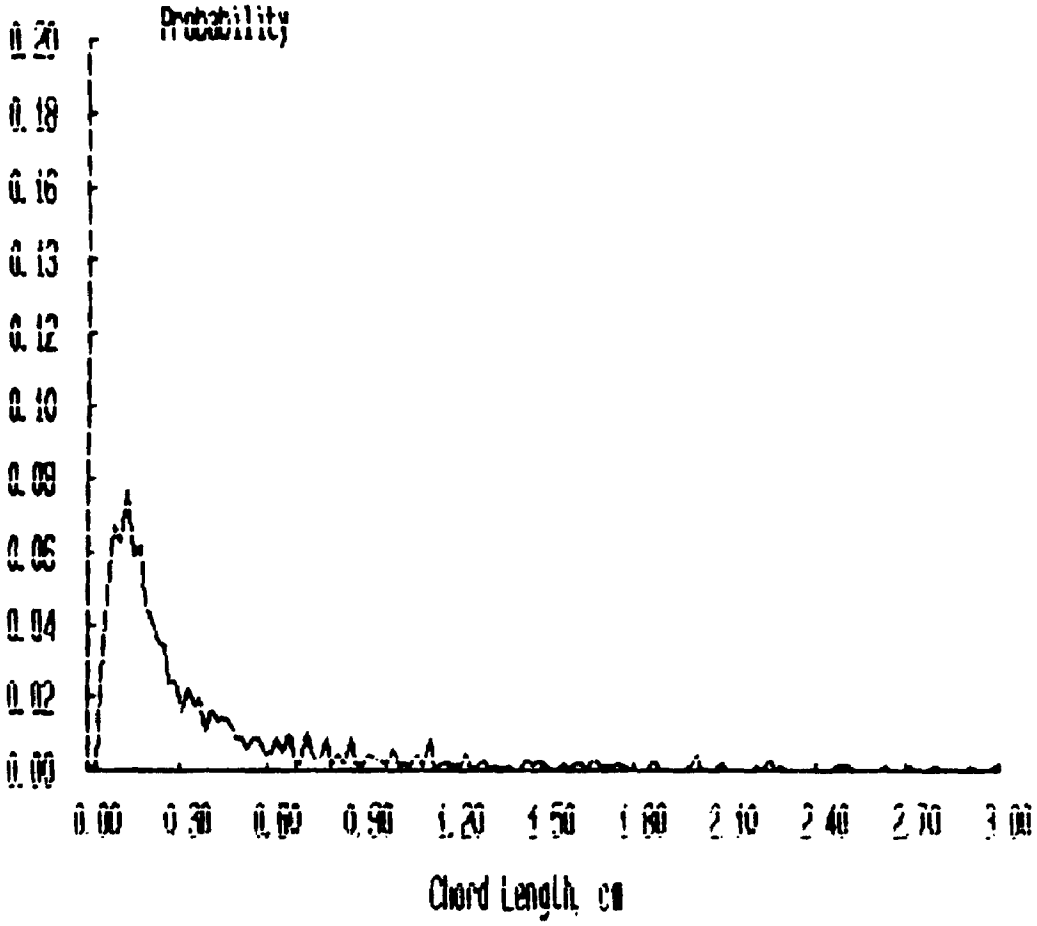

****** FILENAME ****** : JAN20D38

**** Bubbles detected by probe 1 : 1295
**** Percentage of bubbles retained : 46.33
**** Average bubble duration : .005633 s

Probability Distributions

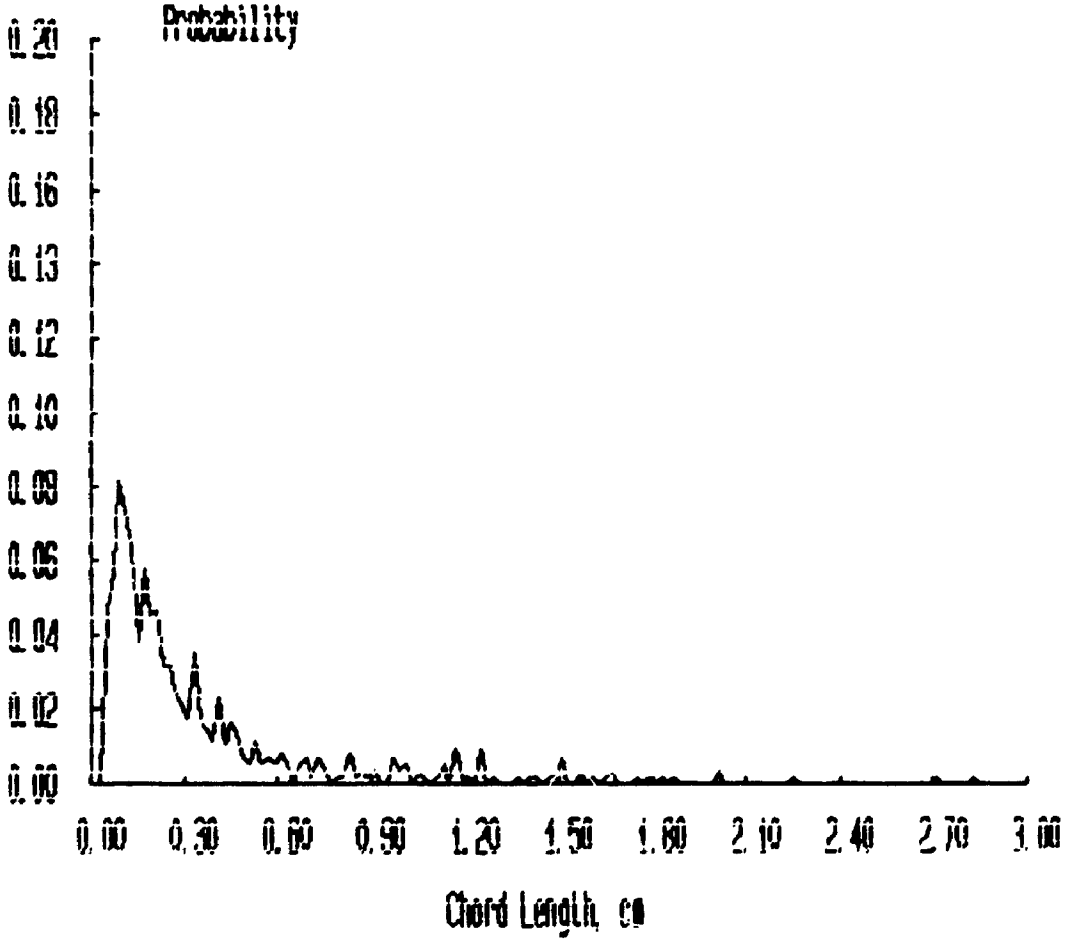

****** FILENAME ****** : JAN20U4A

**** Bubbles detected by probe 1 : 1214
**** Percentage of bubbles retained : 43.99
**** Average bubble duration : .UU5569 s

Probability Distributions

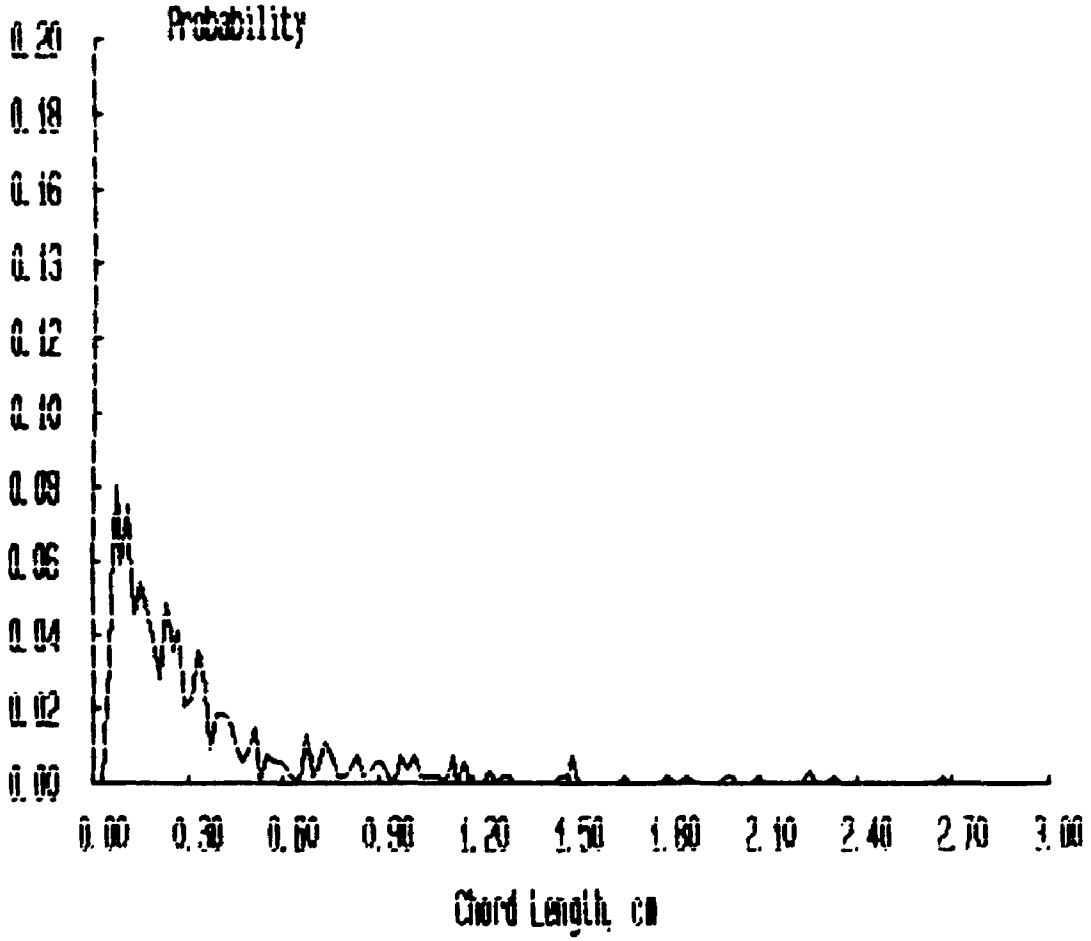

****** FILENAME ****** : JAN2005A

**** Bubbles detected by probe 1 : 867
**** Percentage of bubbles retained : 42.79
**** Average bubble duration : .005547 s

Probability Distributions

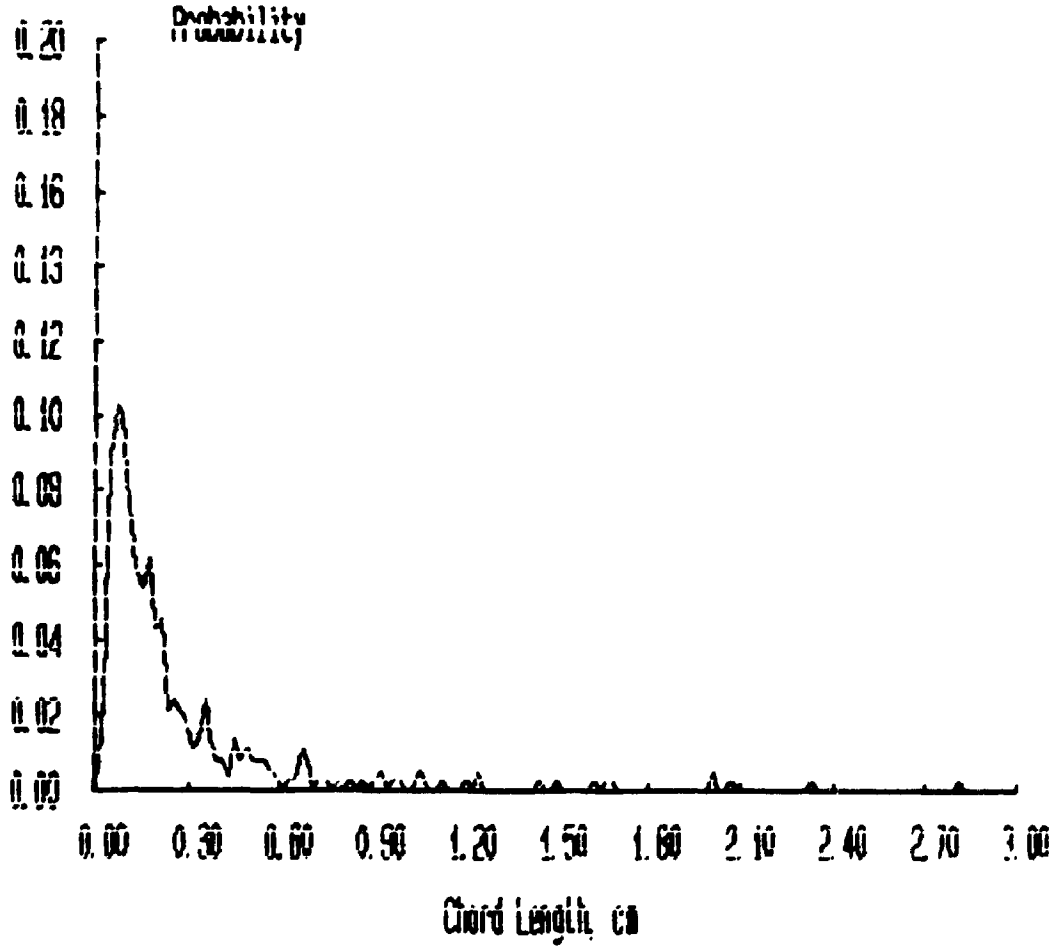

****** FILENAME ****** : JAN20D6A

**** Bubbles detected by probe 1 : 911
**** Percentage of bubbles retained : 50.82
**** Average bubble duration : .005775 s

Probability Distributions

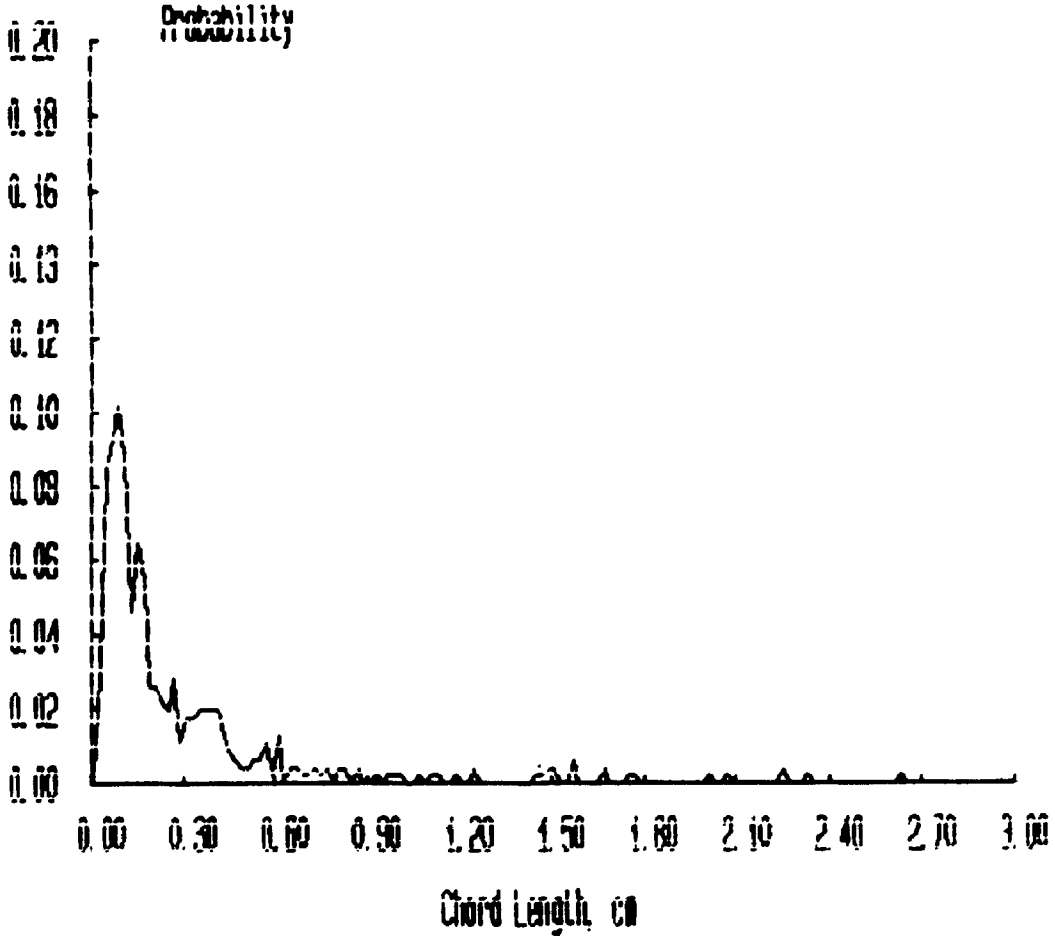

****** FILENAME ****** : JAN20E1B

**** Bubbles detected by probe 1 : 2111
**** Percentage of bubbles retained : 70.01
**** Average bubble duration : .00537B s

Probability Distributions

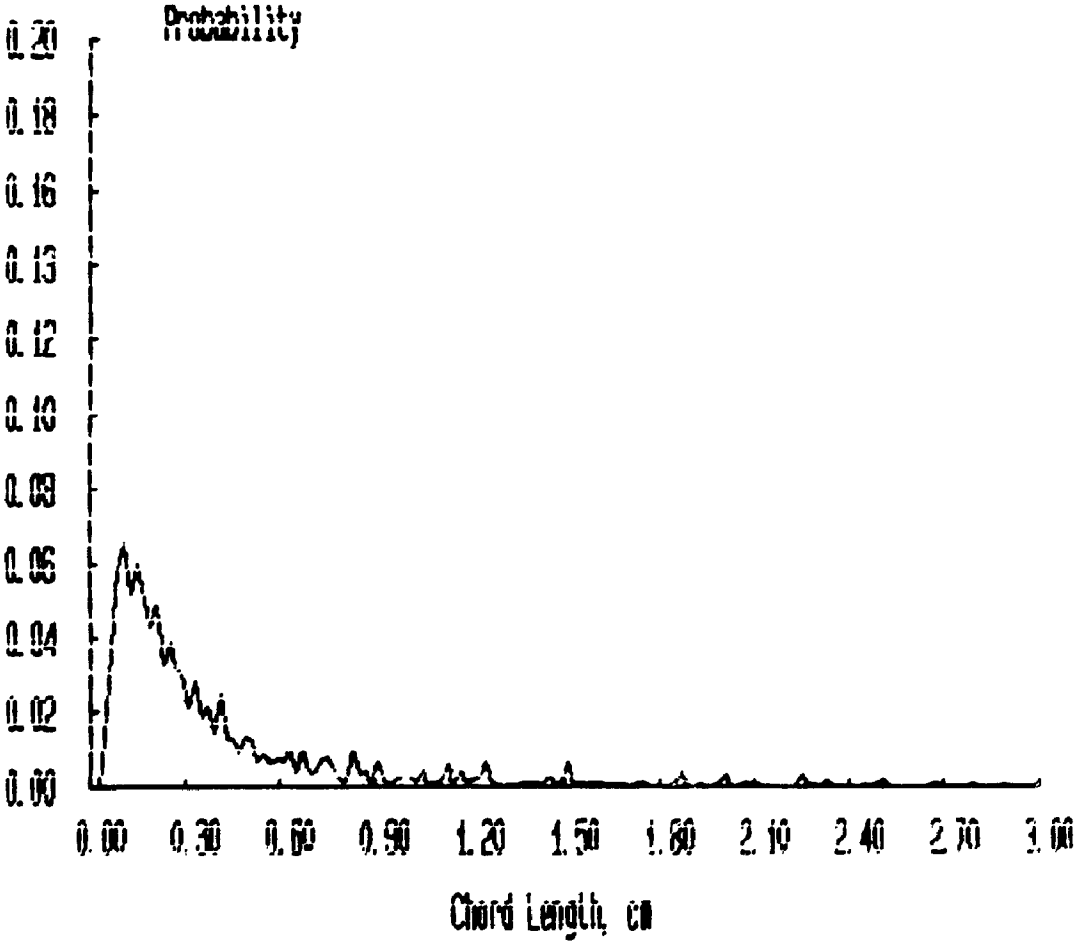

****** FILENAME ****** : JAN20E2A

**** Bubbles detected by probe 1 : 1735
**** Percentage of bubbles retained : 64.03
**** Average bubble duration : .00555 s

Probability Distributions

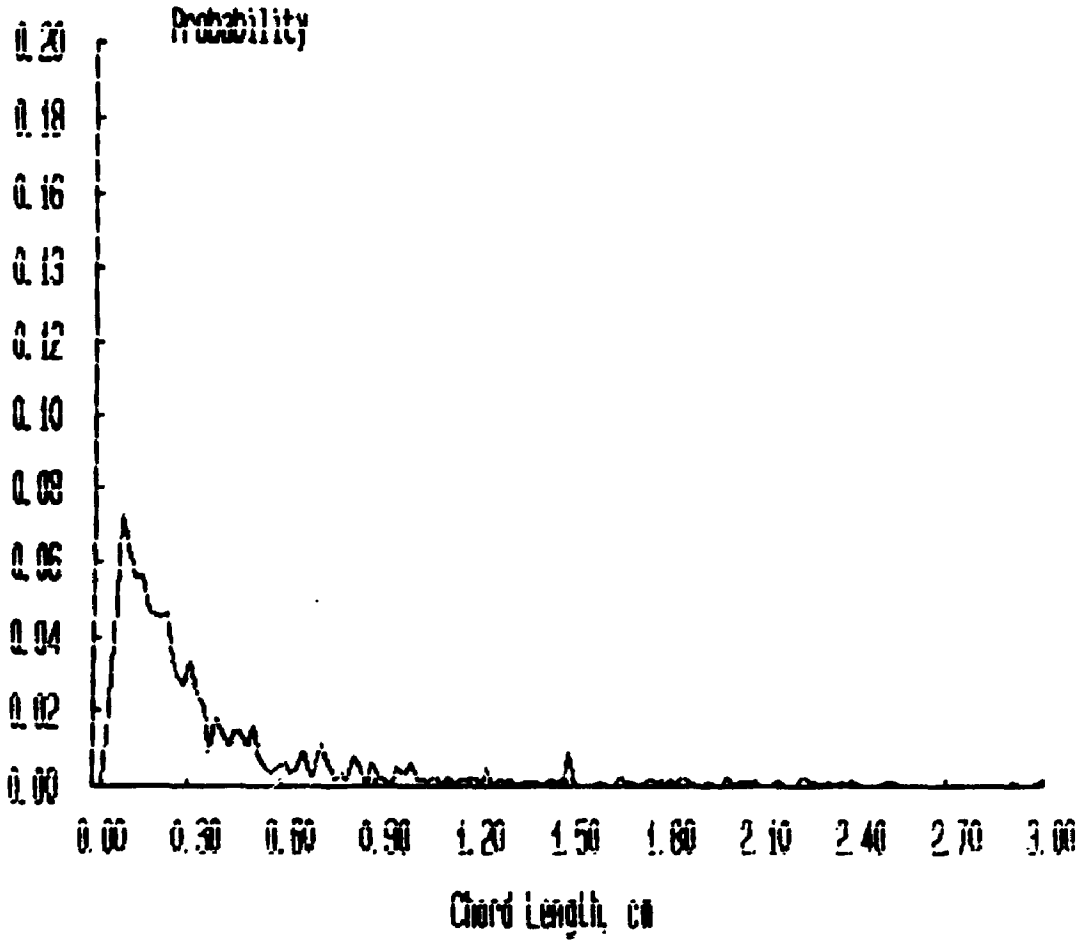

****** FILENAME ****** : JAN20E3A

**** Bubbles detected by probe 1 : 1664
**** Percentage of bubbles retained : 60.40
**** Average bubble duration : .00532 s

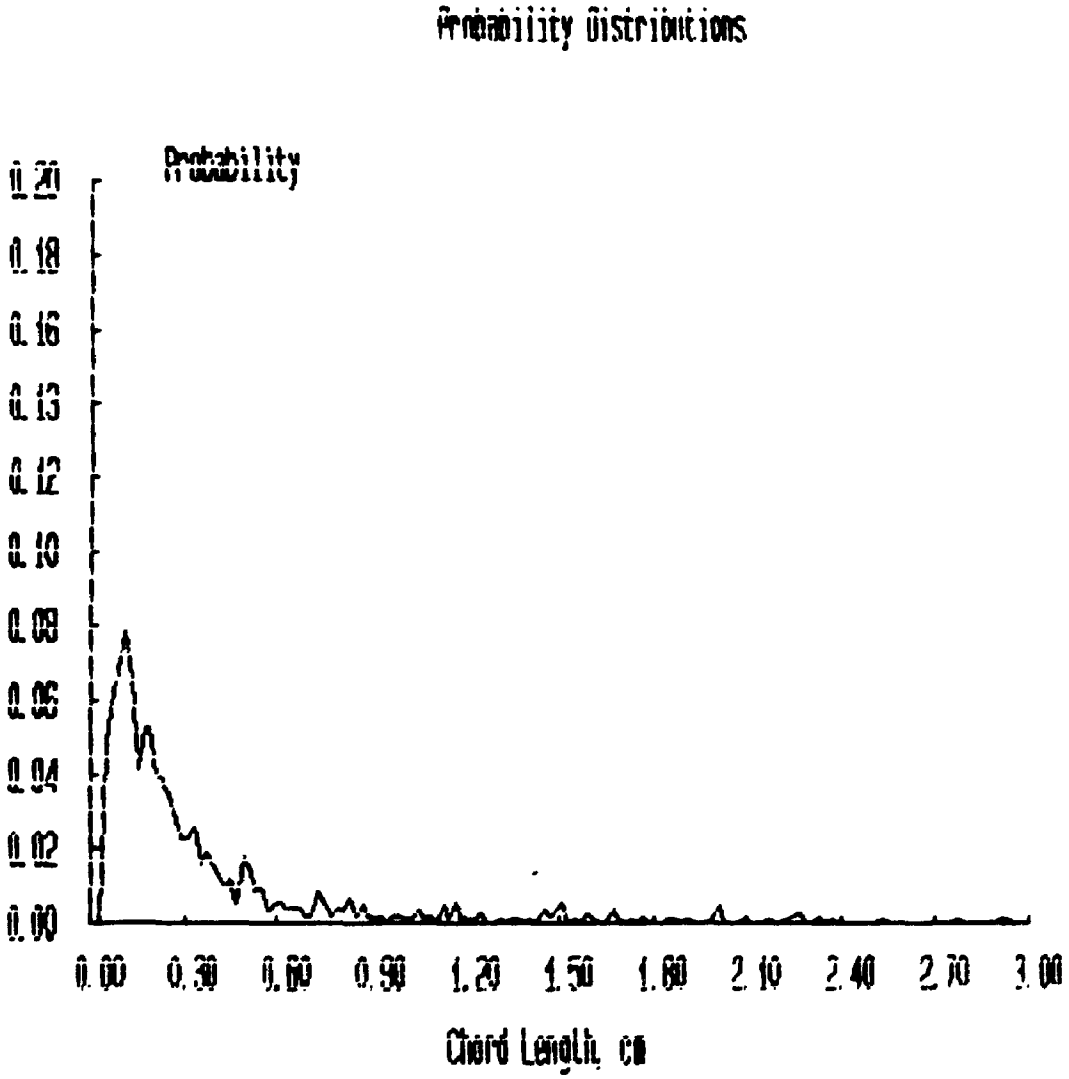

****** FILENAME ****** : JAN20E4A

**** Bubbles detected by probe 1 : 1561
**** Percentage of bubbles retained : 55.99
**** Average bubble duration : .005542 s

Probability Distributions

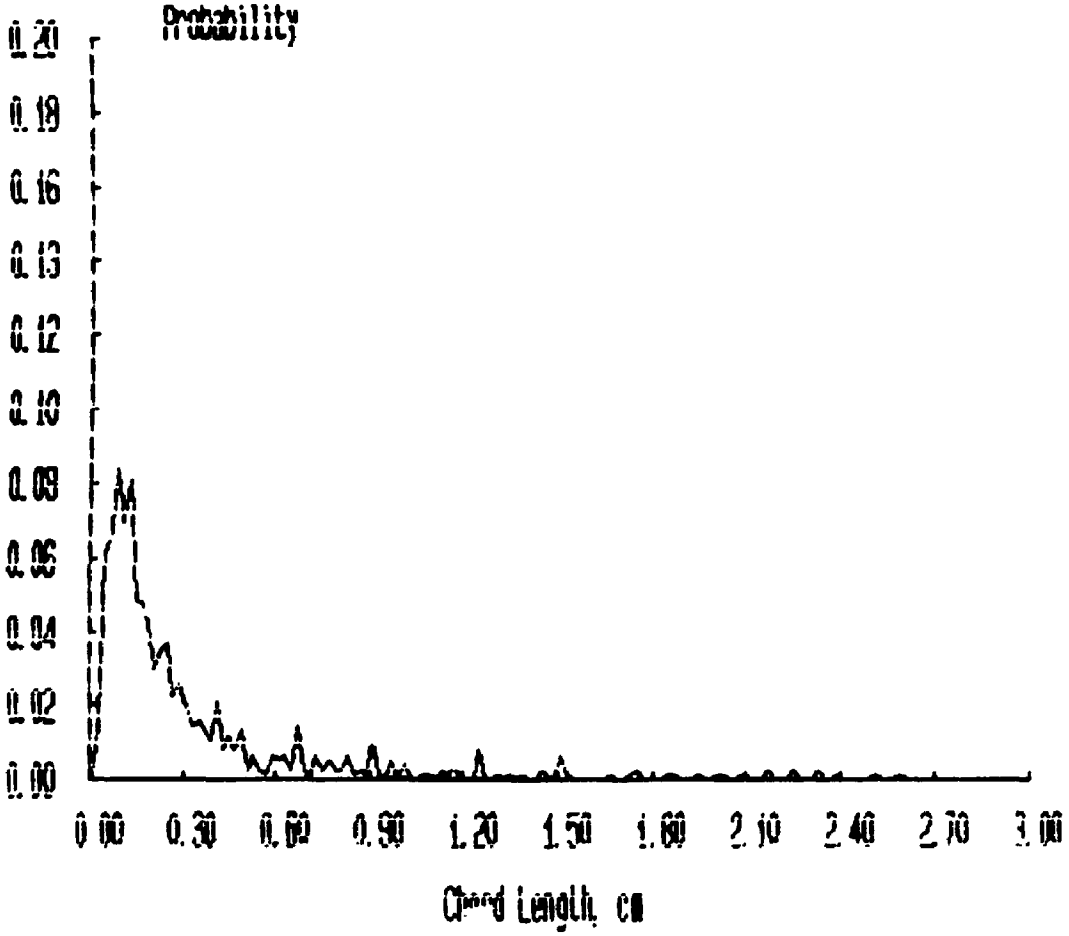

****** FILENAME ****** : JAN20ESA

**** Bubbles detected by probe 1 : 1027
**** Percentage of bubbles retained : 54.92
**** Average bubble duration : .005243 s

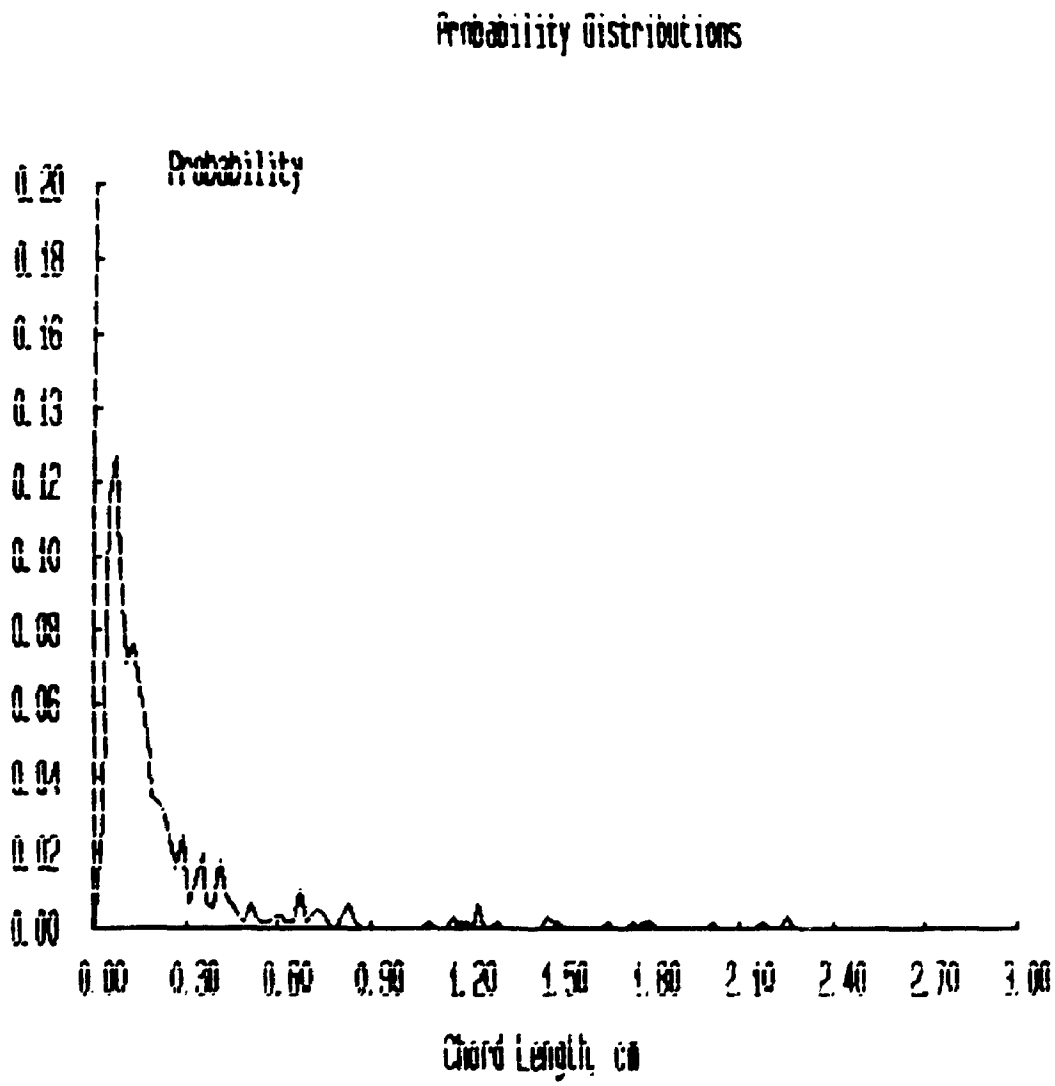

****** FILENAME ****** : JAN20E6A

**** Bubbles detected by probe 1 : 921
**** Percentage of bubbles retained : 56.24
**** Average bubble duration : .005239 s

Probability Distributions

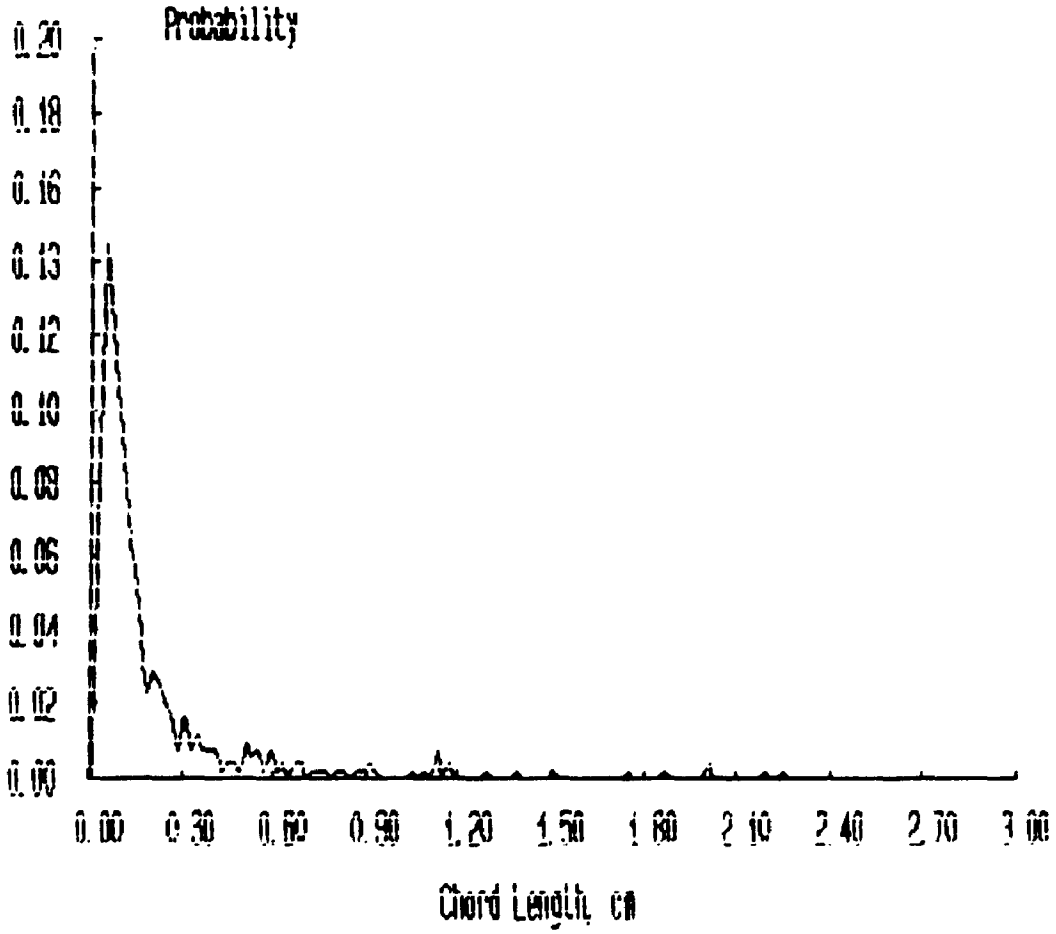

****** FILENAME ****** : JAN21A1A

**** Bubbles detected by probe 1 : 4847
**** Percentage of bubbles retained : 80.92
**** Average bubble duration : .00453/ s

Probability Distributions

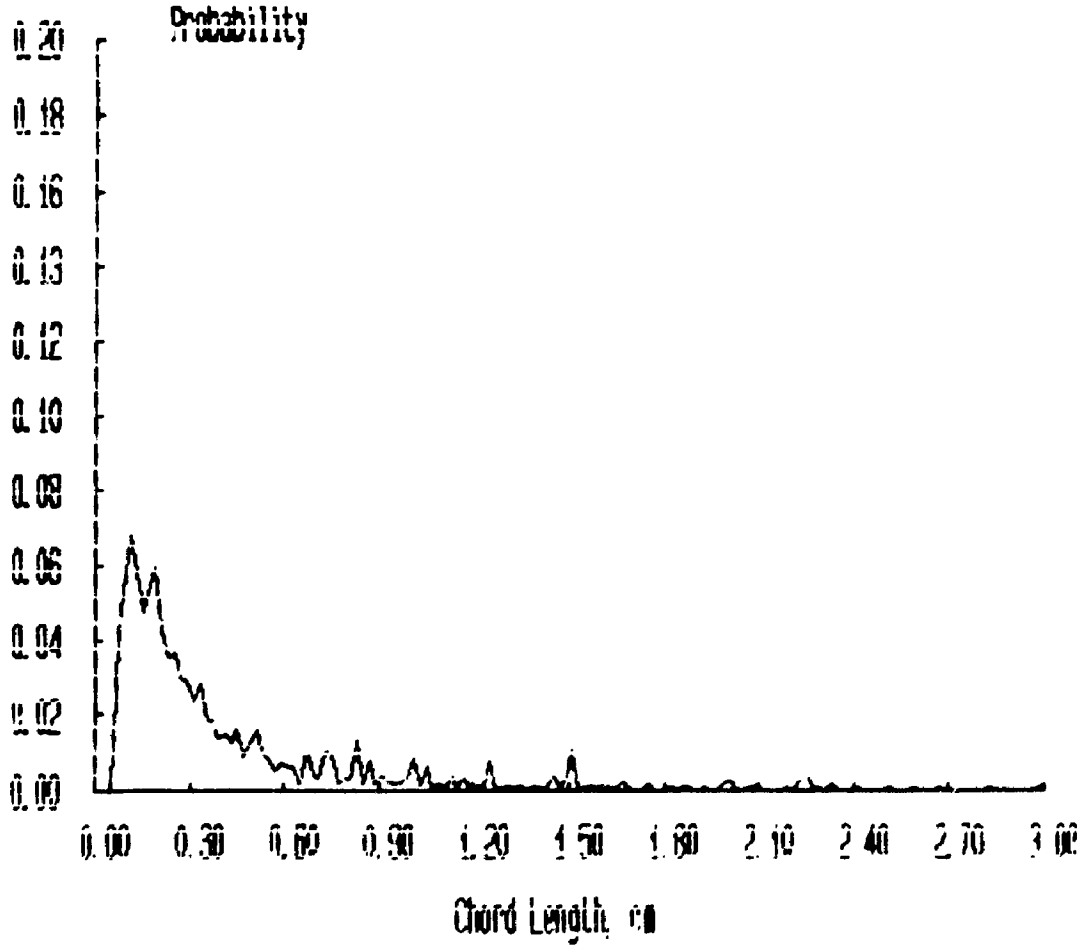

****** FILENAME ****** : JAN21A2A

**** Bubbles detected by probe 1 : 4020
**** Percentage of bubbles retained : 78.76
**** Average bubble duration : .004528 s

Probability Distribution

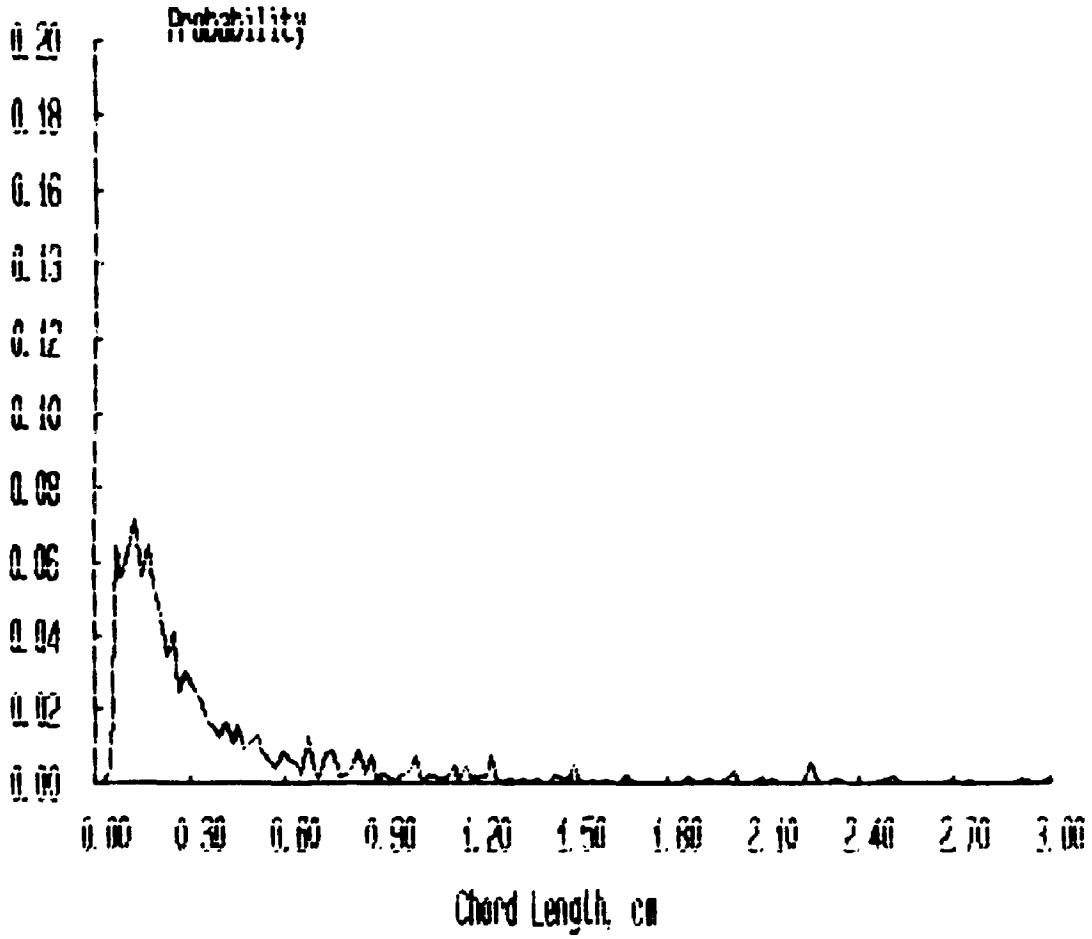

****** FILENAME ****** : JAN21A3A

**** Bubbles detected by probe 1 : 3560
**** Percentage of bubbles retained : 72.67
**** Average bubble duration : .004434 s

Probability Distributions

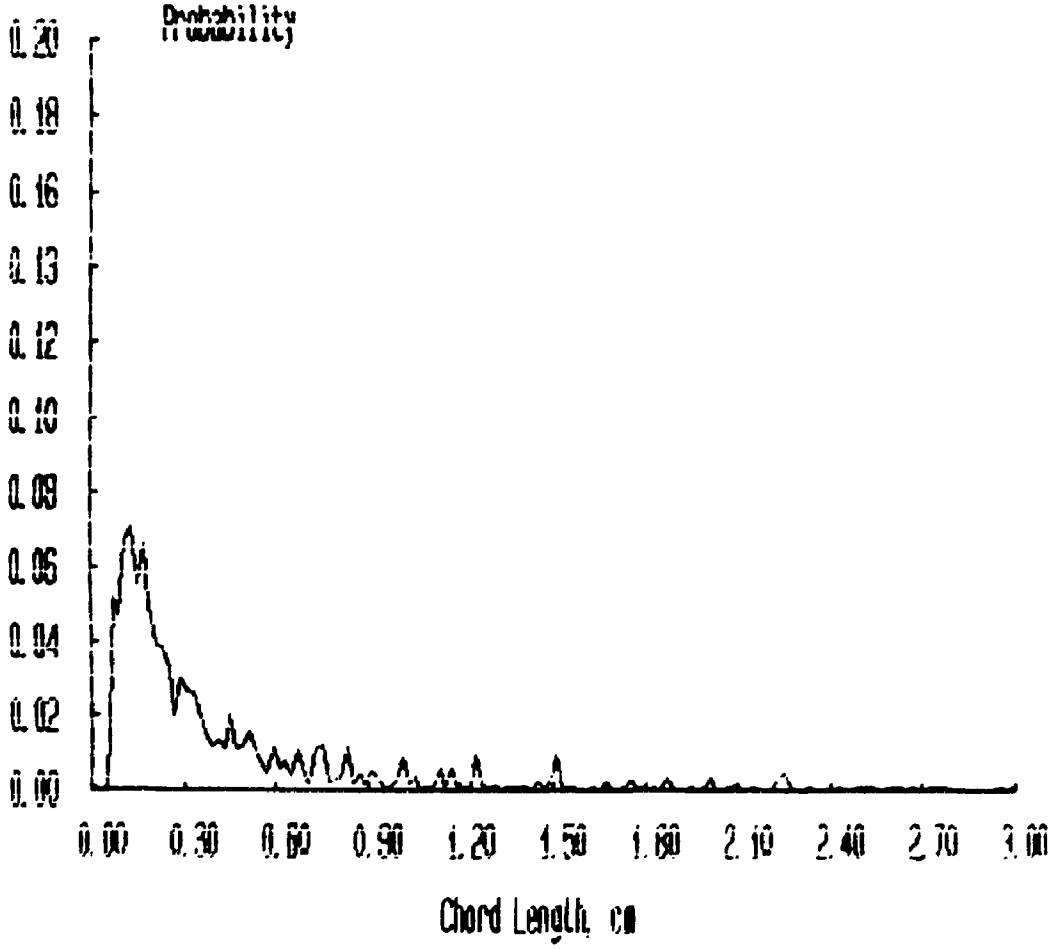

****** FILENAME ****** : JAN21A4A

**** Bubbles detected by probe 1 : 2795
**** Percentage of bubbles retained : 72.74
**** Average bubble duration : .004384 s

Probability Distributions

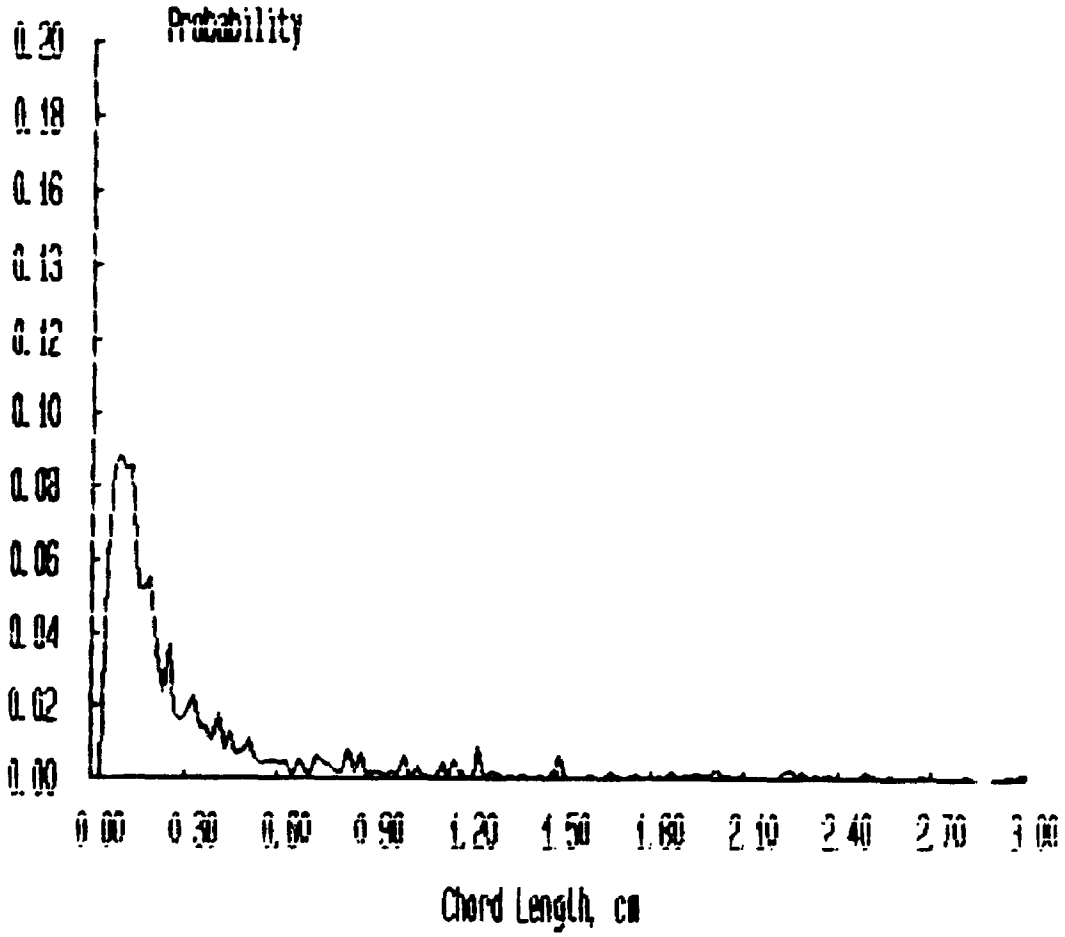

•••••• FILENAME •••••• : JAN21A5A

•••• Bubbles detected by probe 1 : 2169
•••• Percentage of bubbles retained : 80.36
•••• Average bubble duration : .0041/8 s

Probability Distributions

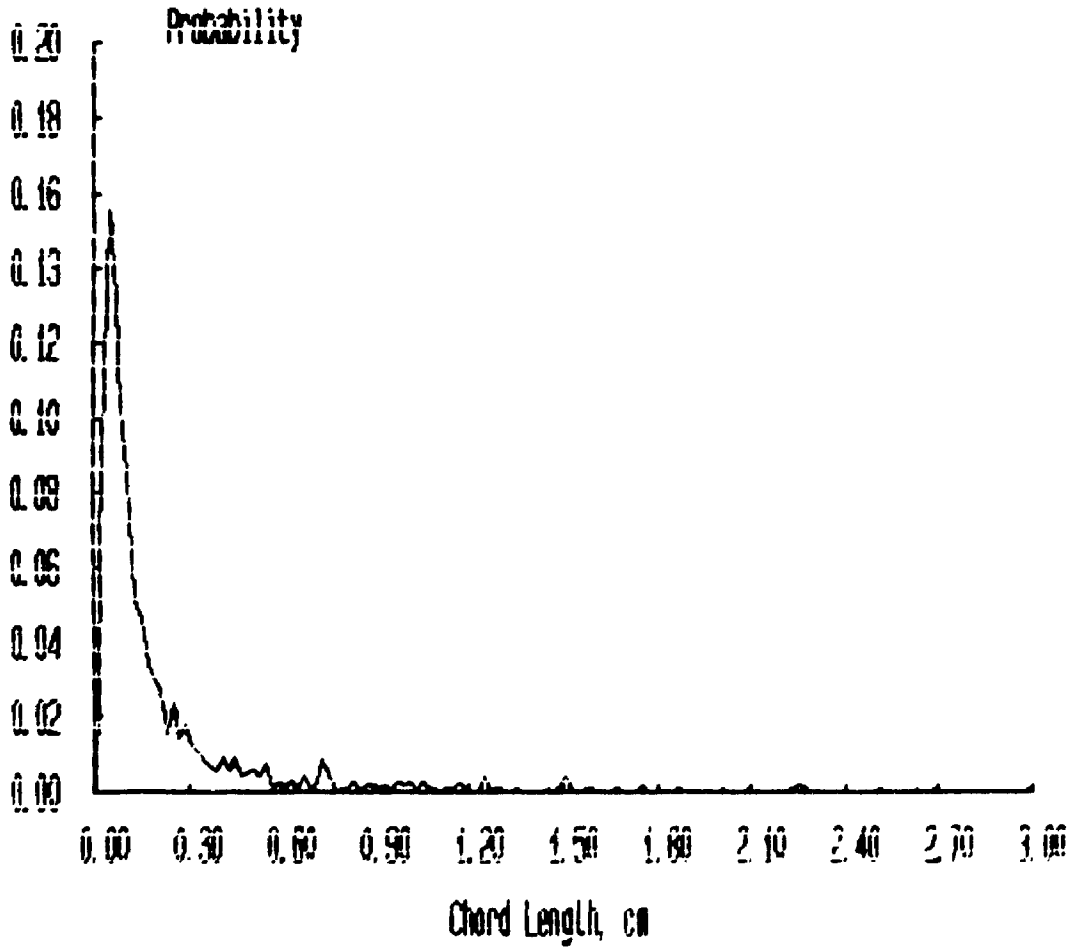

****** FILENAME ****** : JAN21A6A

**** Bubbles detected by probe 1 : 1695
**** Percentage of bubbles retained : 74.16
**** Average bubble duration : .004154 s

Probability Distributions

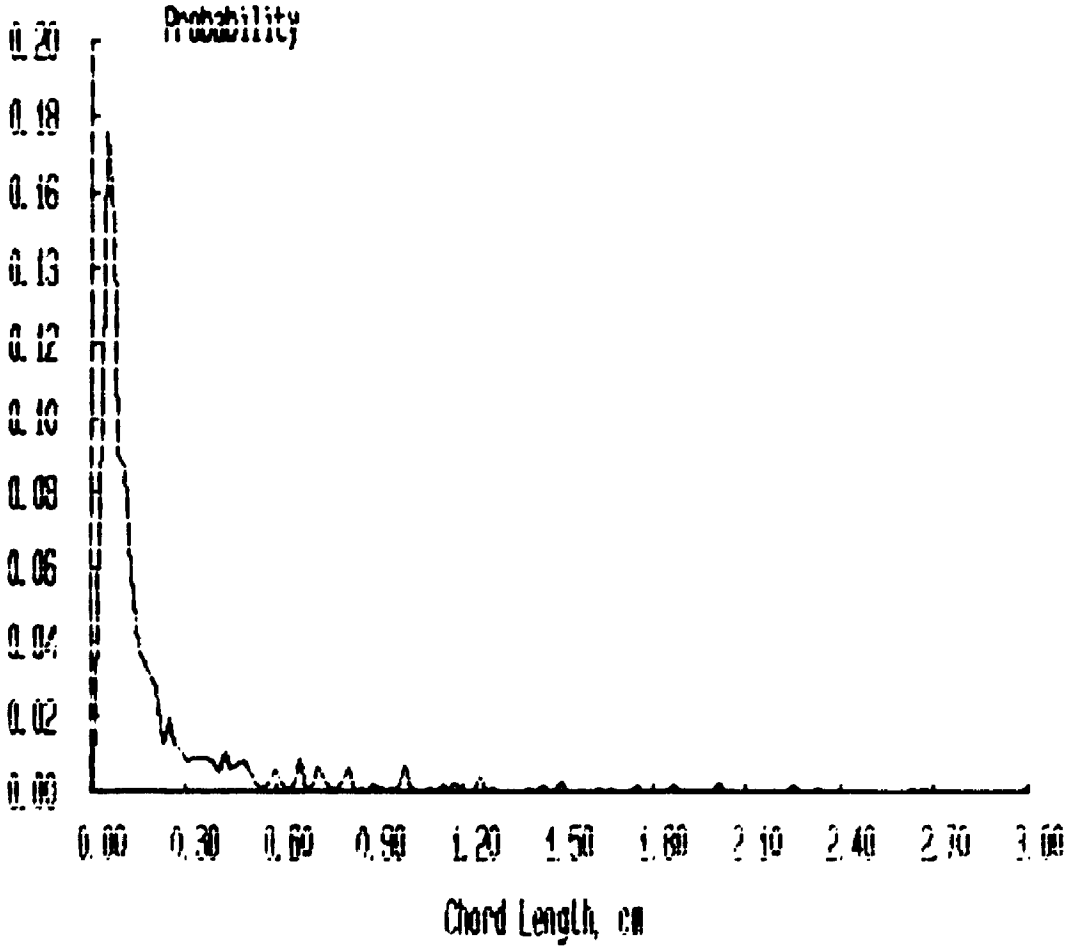

****** FILENAME ****** : JAN2181A

**** Bubbles detected by probe 1 : 4031
**** Percentage of bubbles retained : 77.28
**** Average bubble duration : .004811 s

Probability Distributions

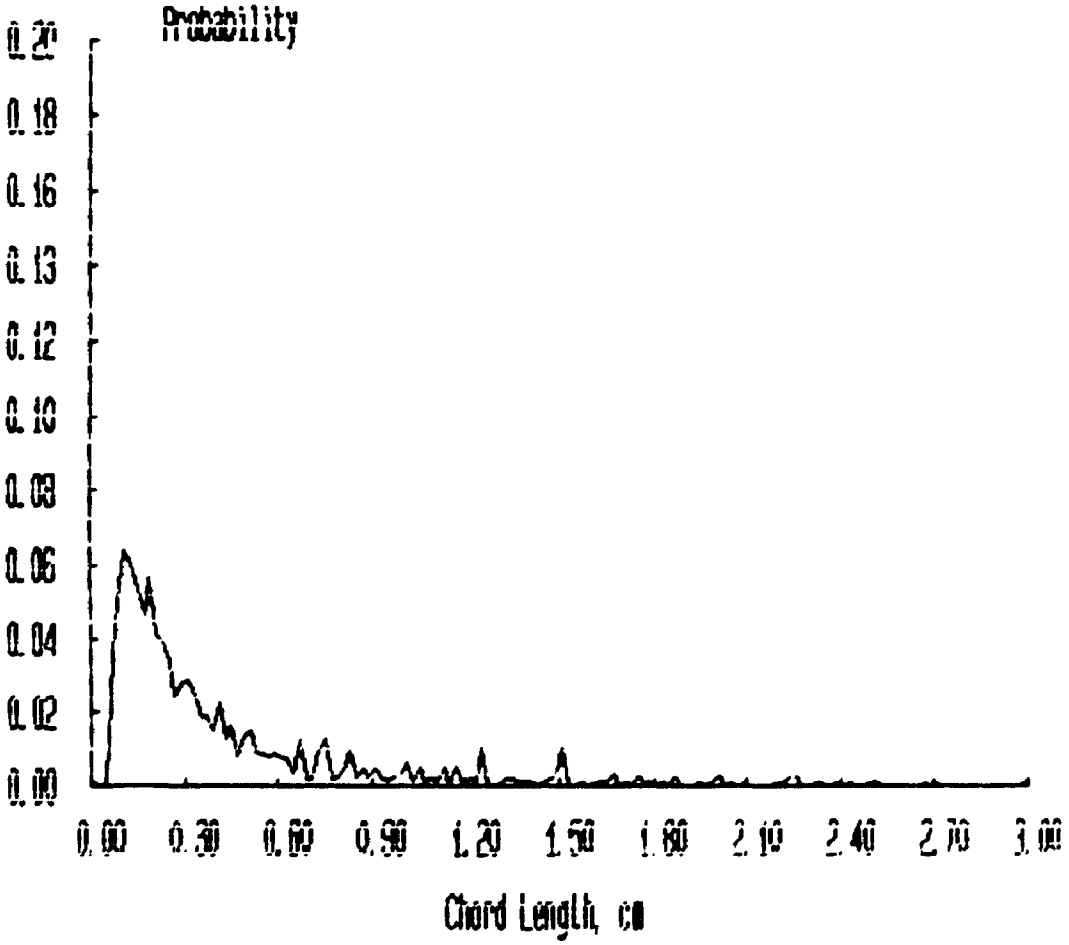

•••••• FILENAME •••••• : JAN21B2A

•••• Bubbles detected by probe 1 : 3796
•••• Percentage of bubbles retained : 77.82
•••• Average bubble duration : .004673 s

Probability Distributions

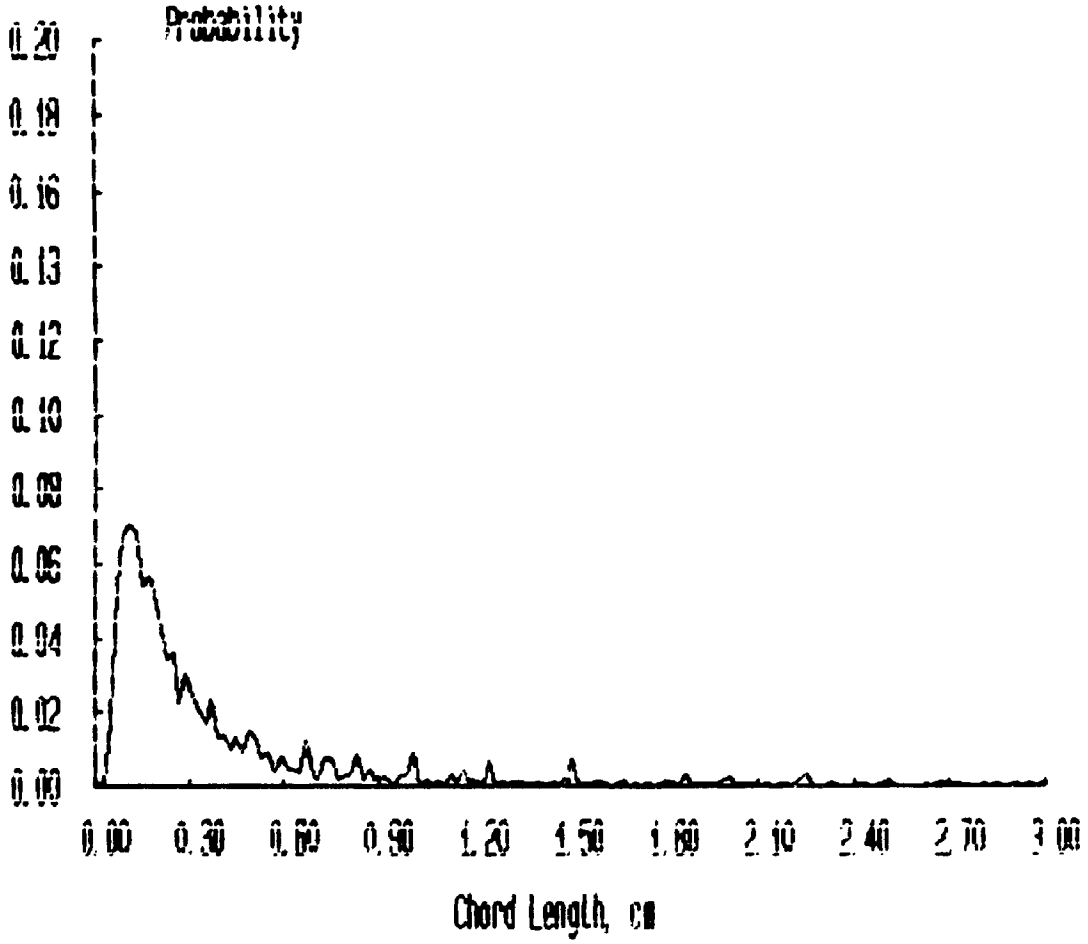

****** FILENAME ****** : JAN21B3A

**** Bubbles detected by probe 1 : 3153
**** Percentage of bubbles retained : 69.84
**** Average bubble duration : .UU4451 s

Probability Distributions

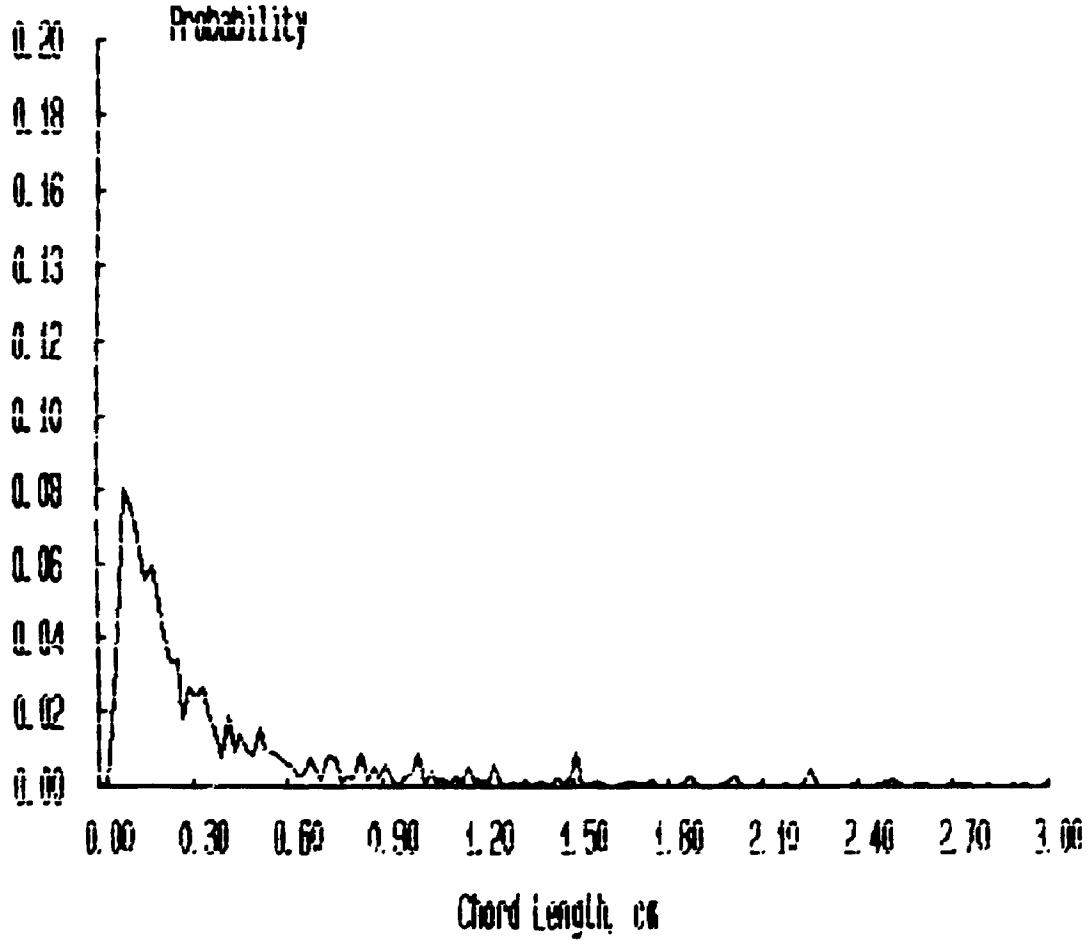

****** FILENAME ****** : JAN2184A

**** Bubbles detected by probe 1 : 2659
**** Percentage of bubbles retained : 71.68
**** Average bubble duration : .004359 s

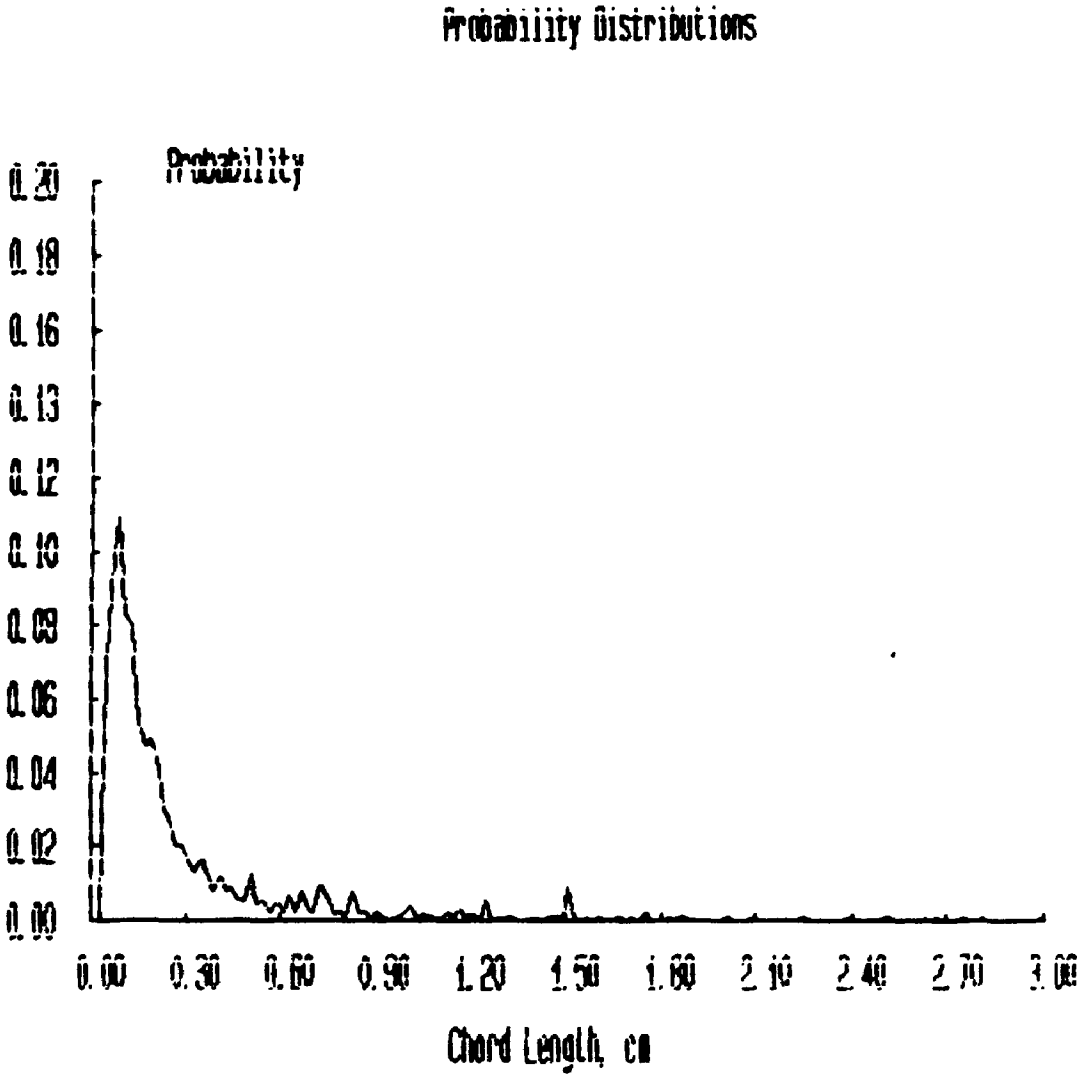

****** FILENAME ****** : JAN2185A

**** Bubbles detected by probe 1 : 1/58
**** Percentage of bubbles retained : 61.21
**** Average bubble duration : .004479 s

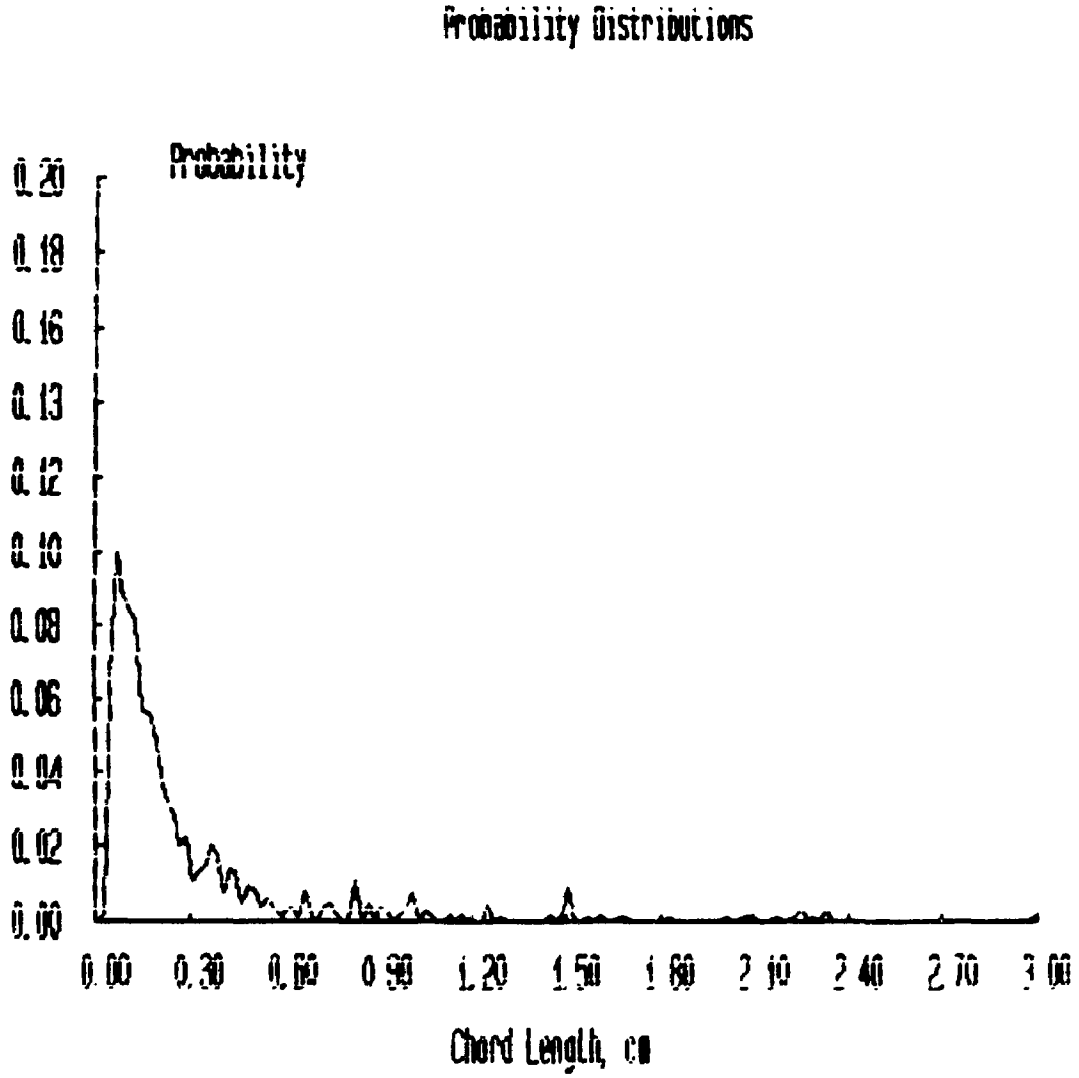

****** FILENAME ****** : JAN2186A

**** Bubbles detected by probe 1 : 1476
**** Percentage of bubbles retained : 58.88
**** Average bubble duration : .004478 s

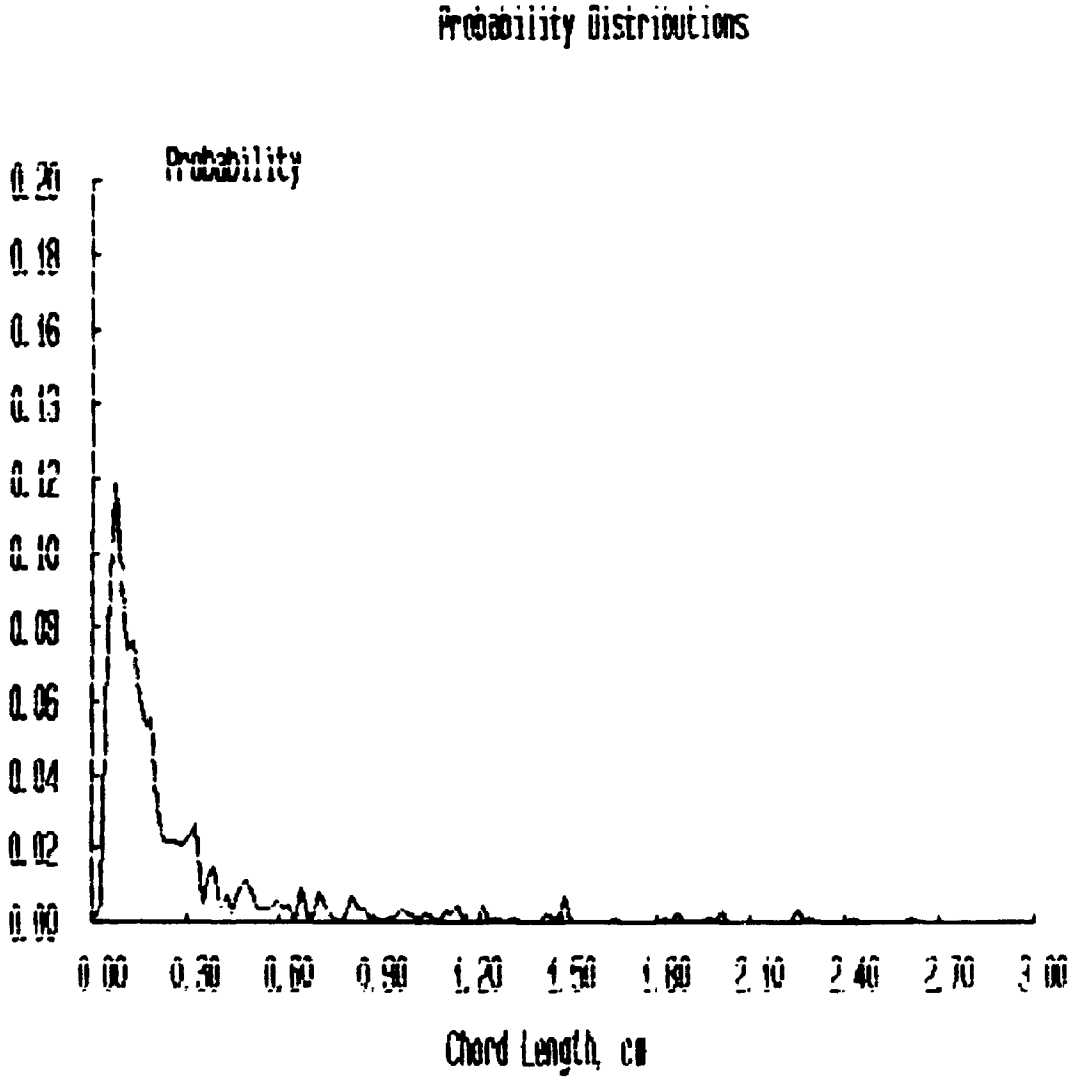

•••••• FILENAME •••••• : JAN21C1A

•••• Bubbles detected by probe 1 : 3273
•••• Percentage of bubbles retained : 73.45
•••• Average bubble duration : .004875 s

Probability Distributions

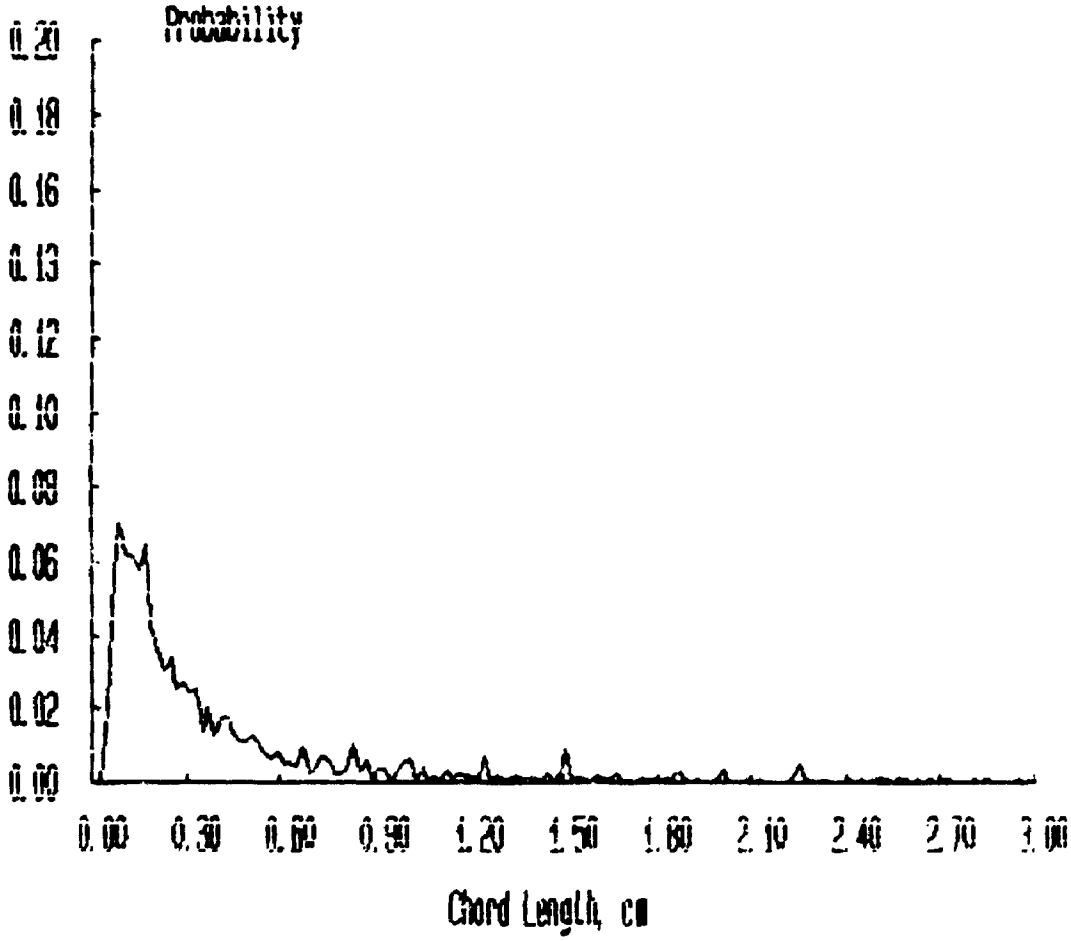

****** FILENAME ****** : JAN21C2A

**** Bubbles detected by probe 1 : 3227
**** Percentage of bubbles retained : 75.67
**** Average bubble duration : .004974 s

Probability Distributions

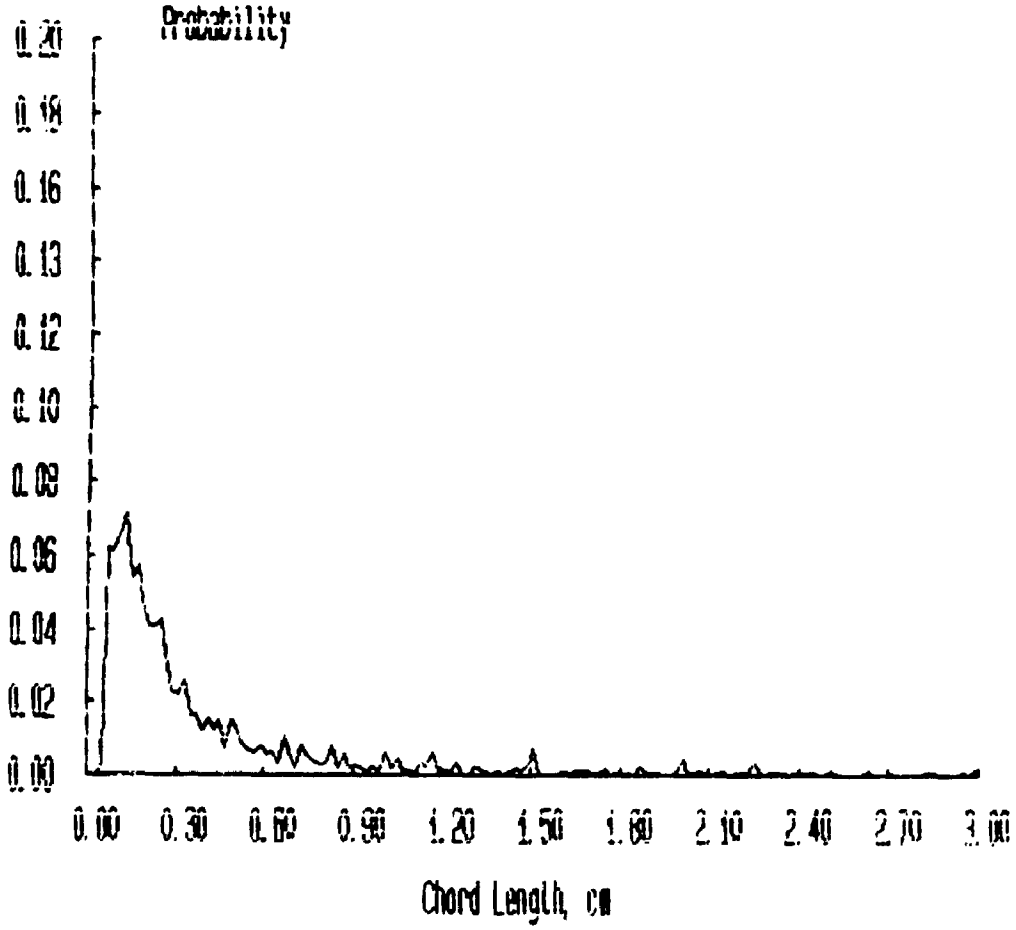

****** FILENAME ****** : JAN21C3A

**** Bubbles detected by probe 1 : 2881
**** Percentage of bubbles retained : 67.82
**** Average bubble duration : .004785 s

Probability Distributions

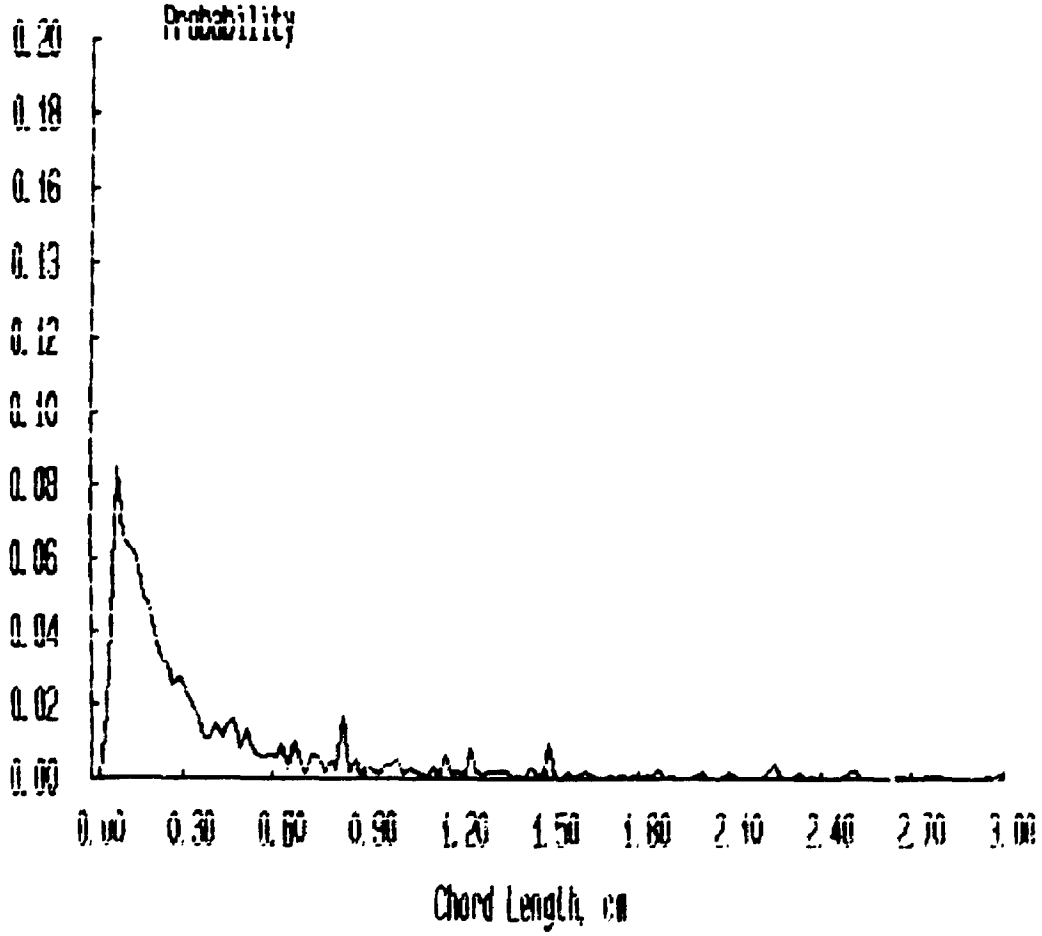

****** FILENAME ****** : JAN21C4A

**** Bubbles detected by probe 1 : 2355
**** Percentage of bubbles retained : 60.13
**** Average bubble duration : .004629 s

Probability Distributions

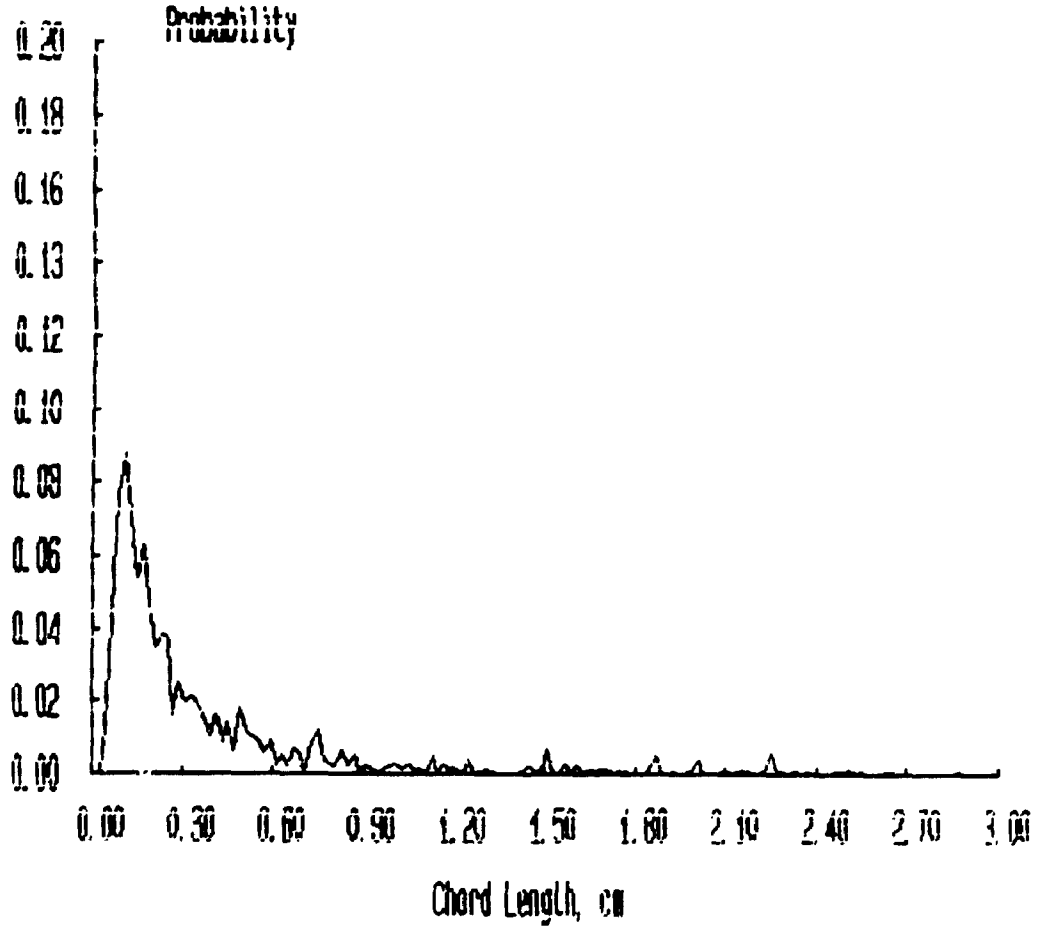

****** FILENAME ****** : JAN21C5A

**** Bubbles detected by probe 1 : 1509
**** Percentage of bubbles retained : 57.06
**** Average bubble duration : .004567 s

Probability Distributions

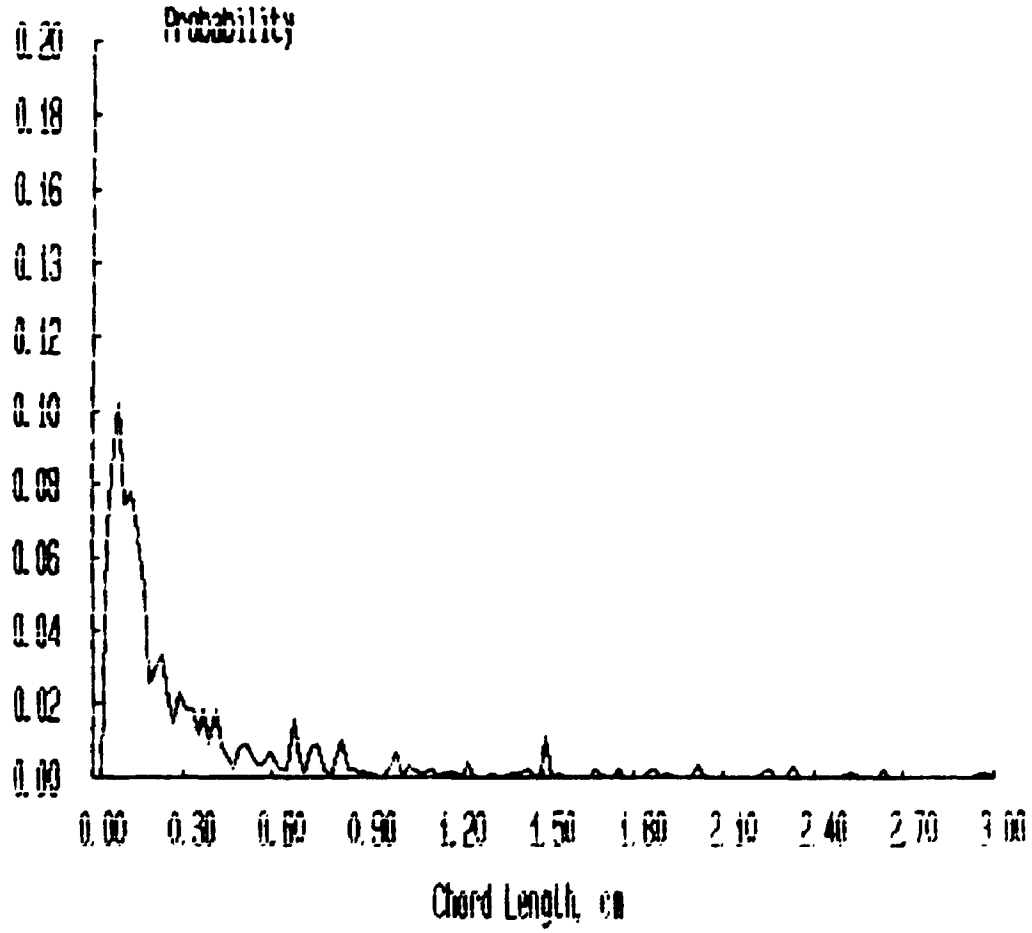

****** FILENAME ****** : JAN21C6A

**** Bubbles detected by probe 1 : 1251
**** Percentage of bubbles retained : 59.38
**** Average bubble duration : .004741 s

Probability Distributions

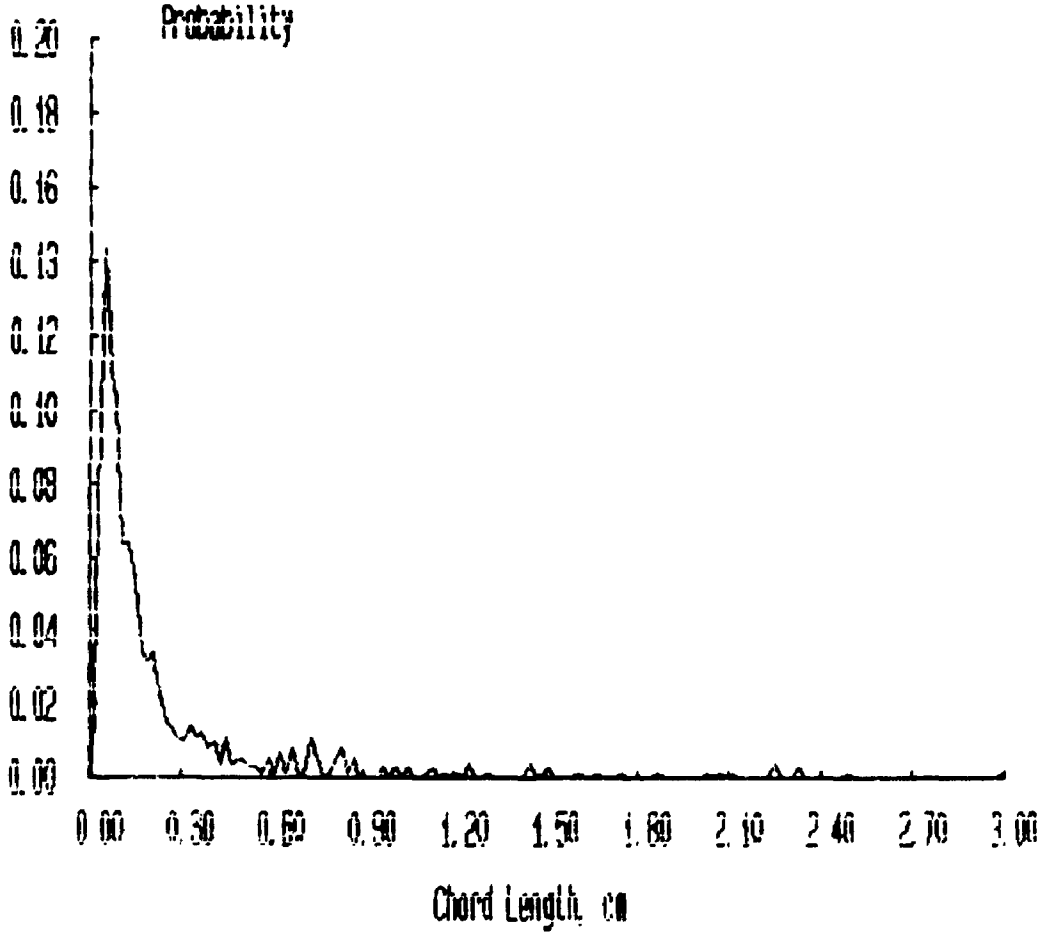

****** FILENAME ****** : JAN21D1A

**** Bubbles detected by probe 1 : 2536
**** Percentage of bubbles retained : 65.10
**** Average bubble duration : .005176 s

Probability Distributions

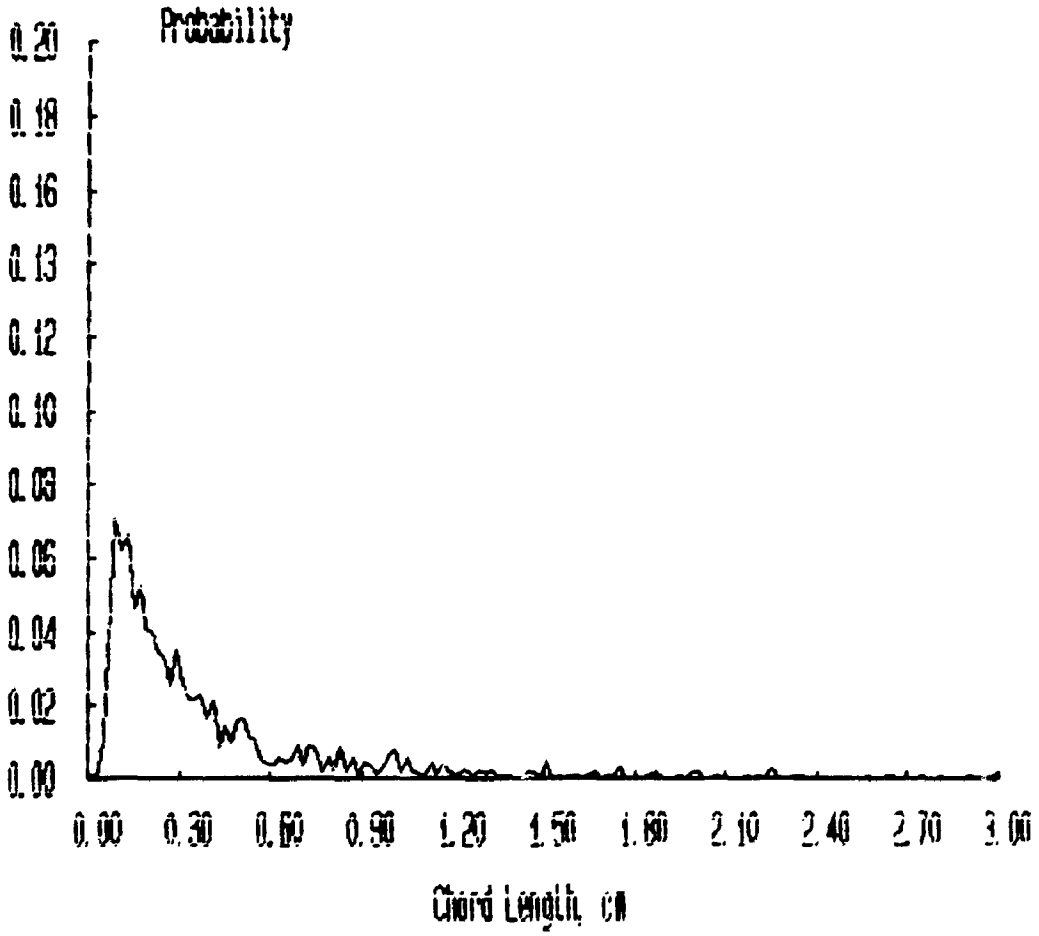

****** FILENAME ****** : JAN21D2A

**** Bubbles detected by probe 1 : 2622
**** Percentage of bubbles retained : 68.65
**** Average bubble duration : .005159 s

Probability Distributions

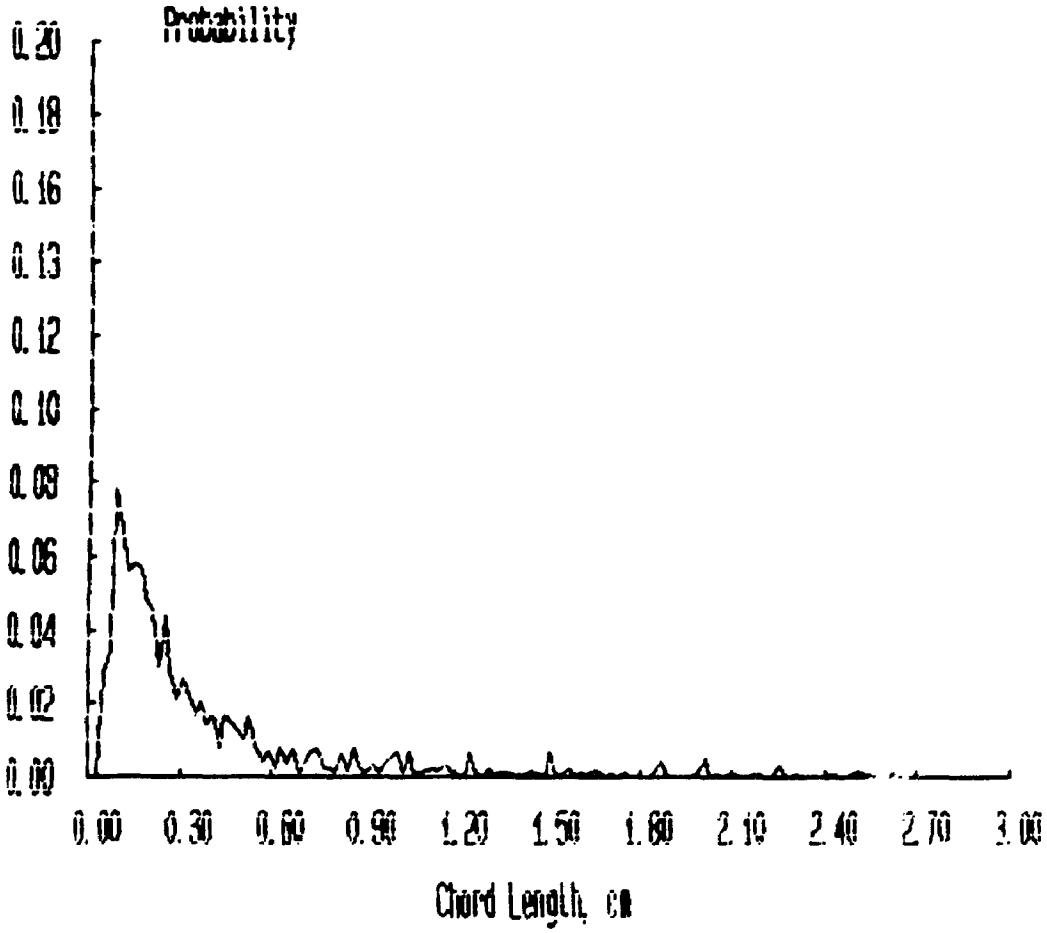

****** FILENAME ****** : JAN21D3A

**** Bubbles detected by probe 1 : 2330
**** Percentage of bubbles retained : 61.20
**** Average bubble duration : .005231 s

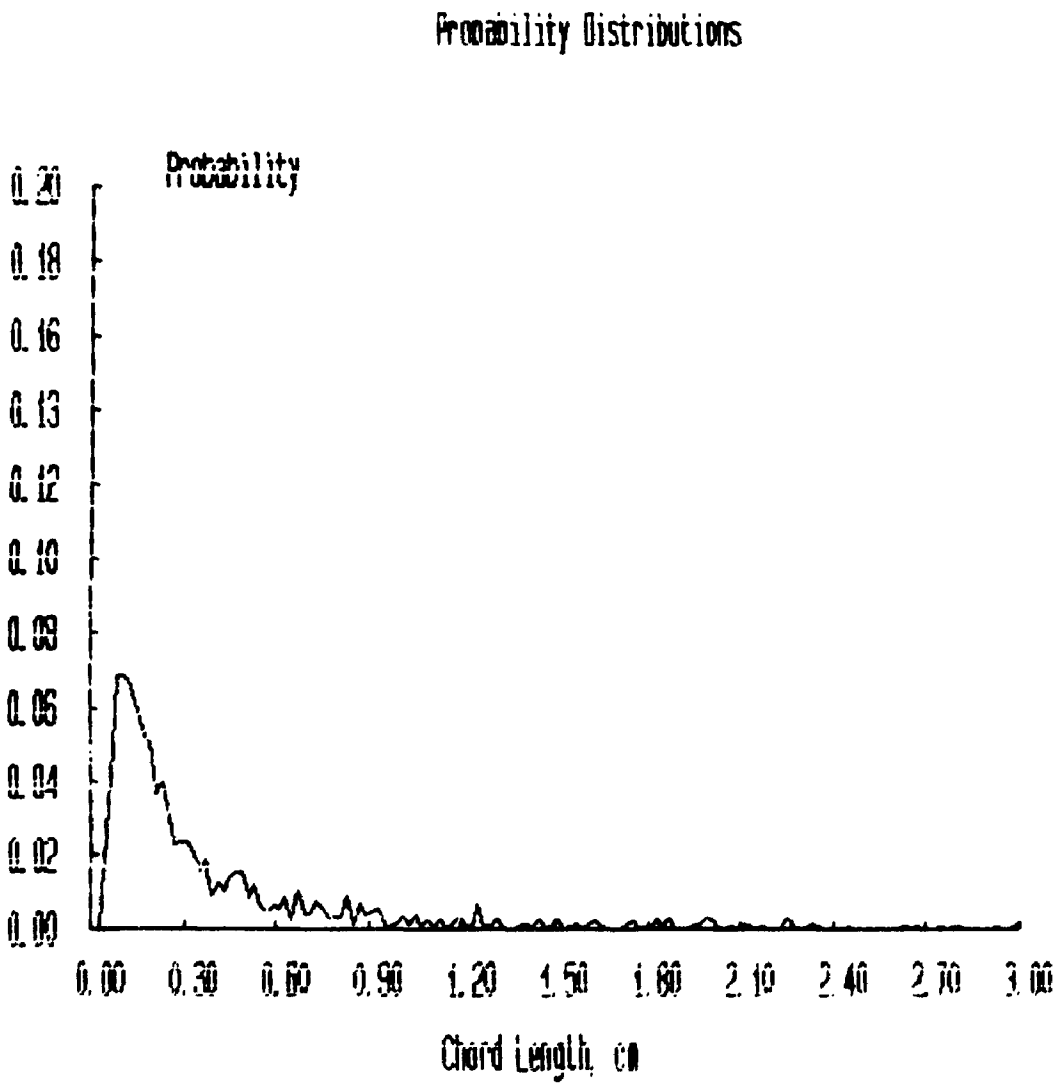

****** FILENAME ****** : JAN21D4A

**** Bubbles detected by probe 1 : 1900
**** Percentage of bubbles retained : 58.79
**** Average bubble duration : .005280 s

Probability Distributions

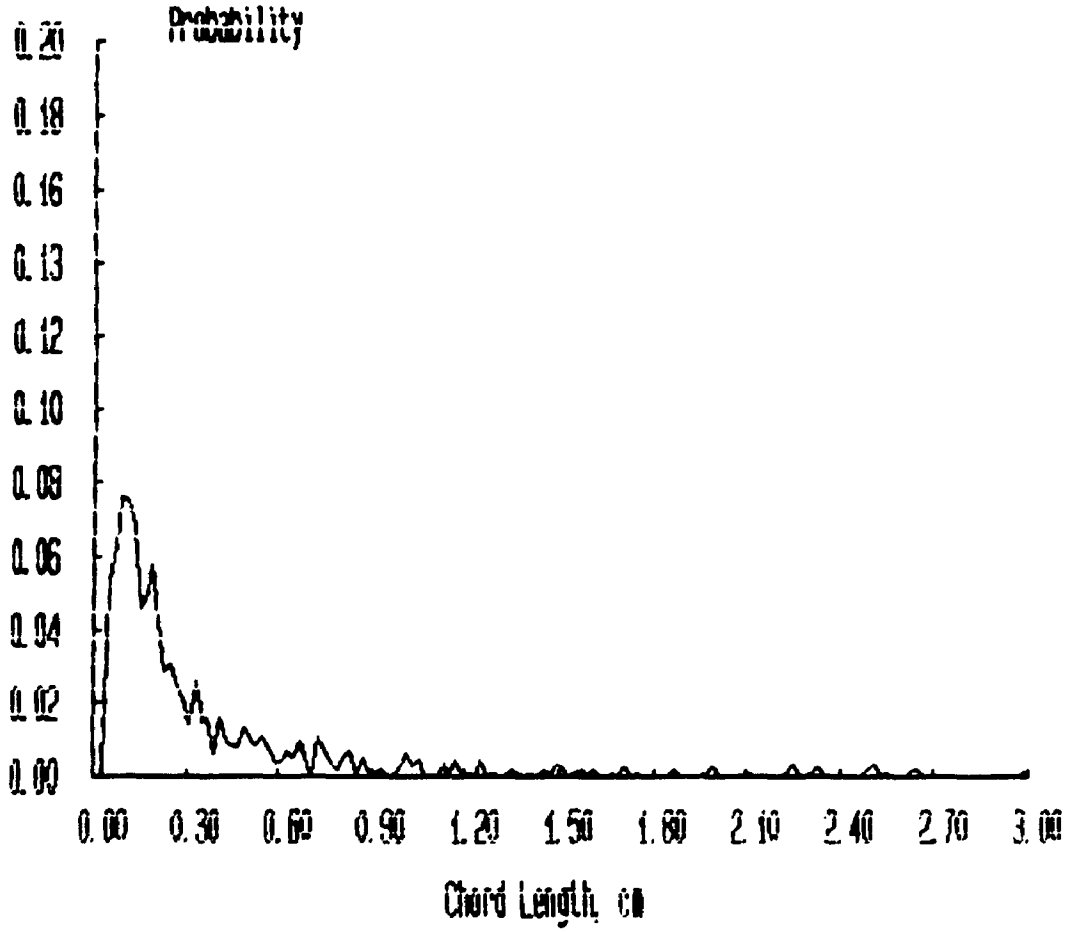

****** FILENAME ****** : JAN21D5A

**** Bubbles detected by probe 1 : 1392
**** Percentage of bubbles retained : 55.96
**** Average bubble duration : .004897 s

Probability Distributions

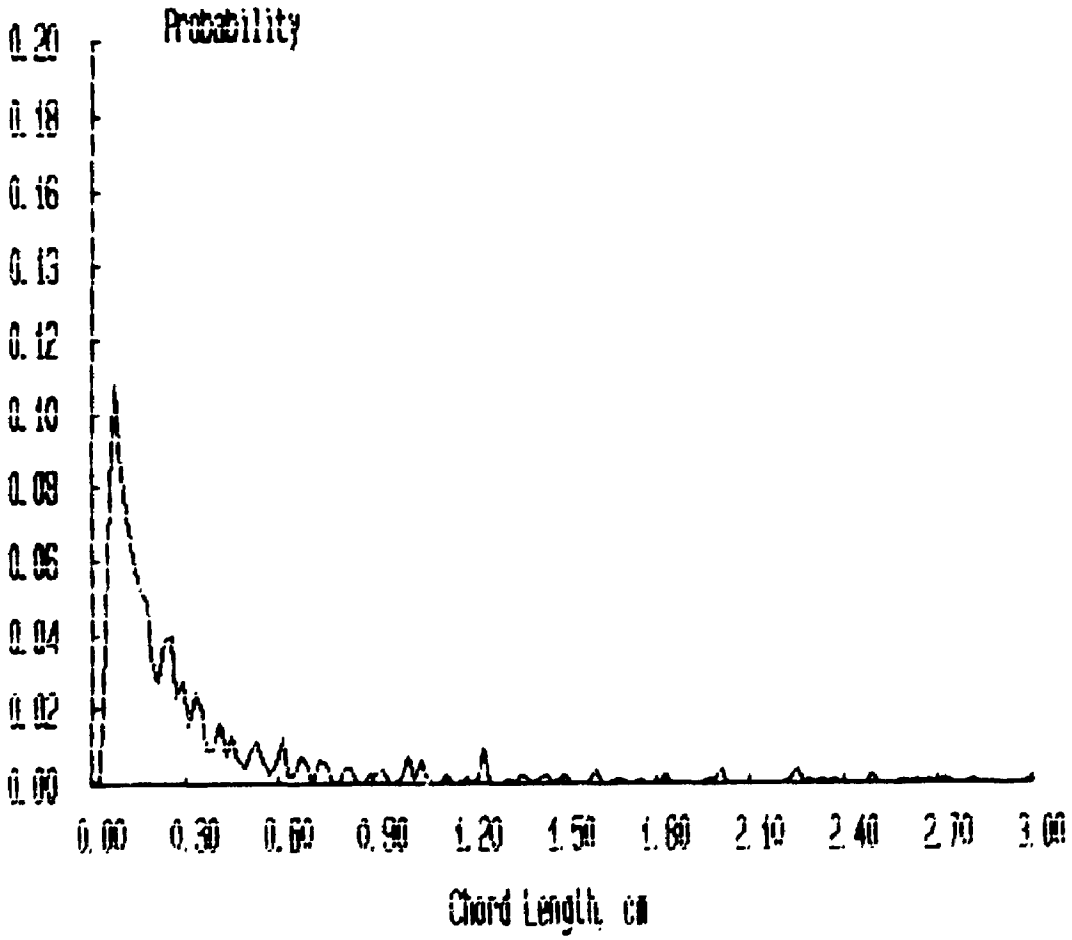

****** FILENAME ****** : JAN21D6A

**** Bubbles detected by probe 1 : 1096
**** Percentage of bubbles retained : 49.54
**** Average bubble duration : .004650 s

Probability Distributions

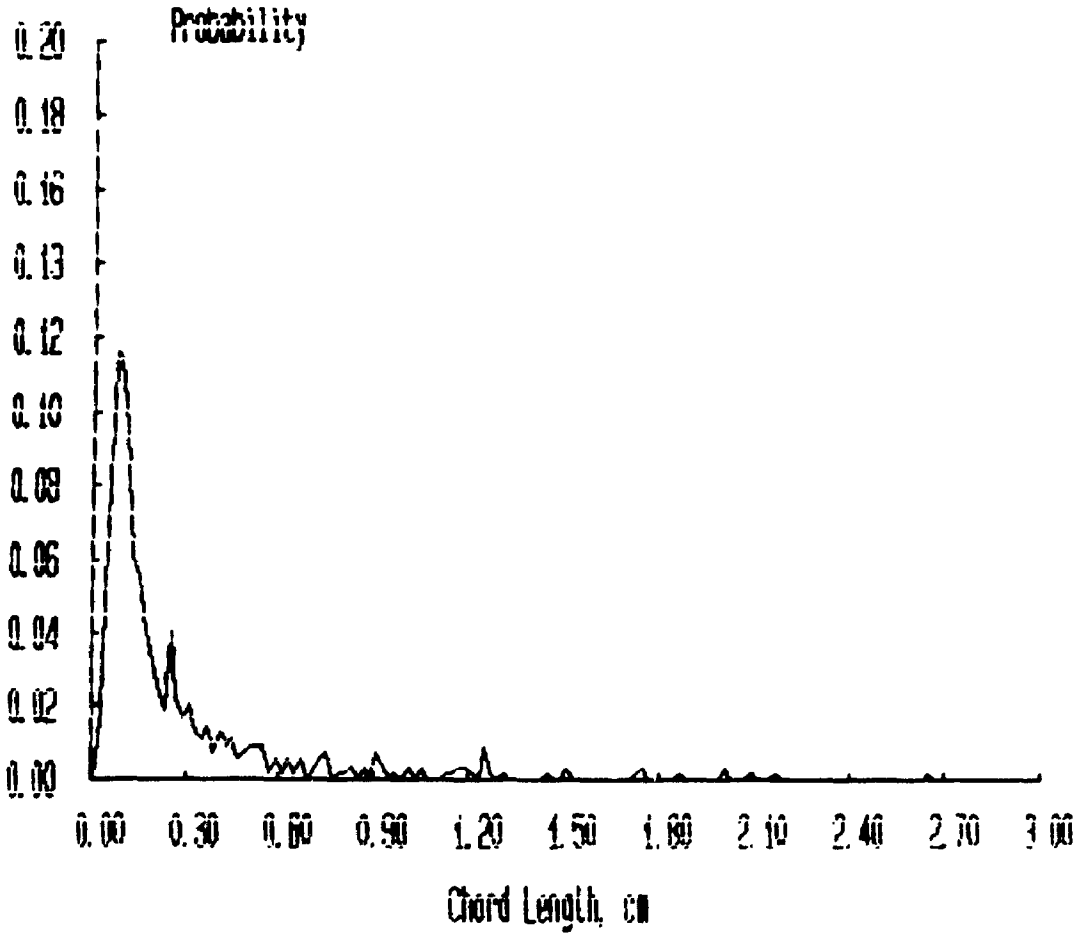

****** FILENAME ****** : JAN21E1A

**** Bubbles detected by probe 1 : 1616
**** Percentage of bubbles retained : 54.39
**** Average bubble duration : .0058UU s

Probability Distributions

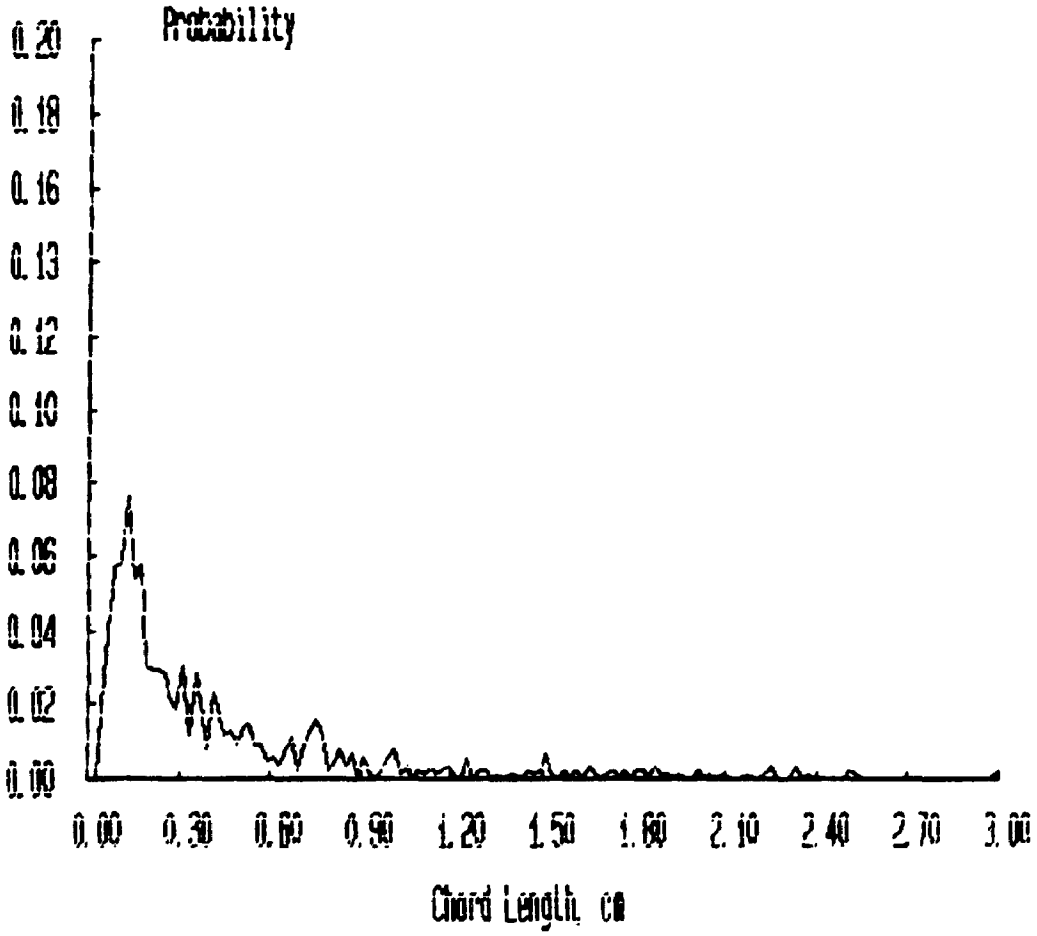

****** FILENAME ****** : JAN21E2A

**** Bubbles detected by probe 1 : 2264
**** Percentage of bubbles retained : 58.26
**** Average bubble duration : .005661 s

Probability Distributions

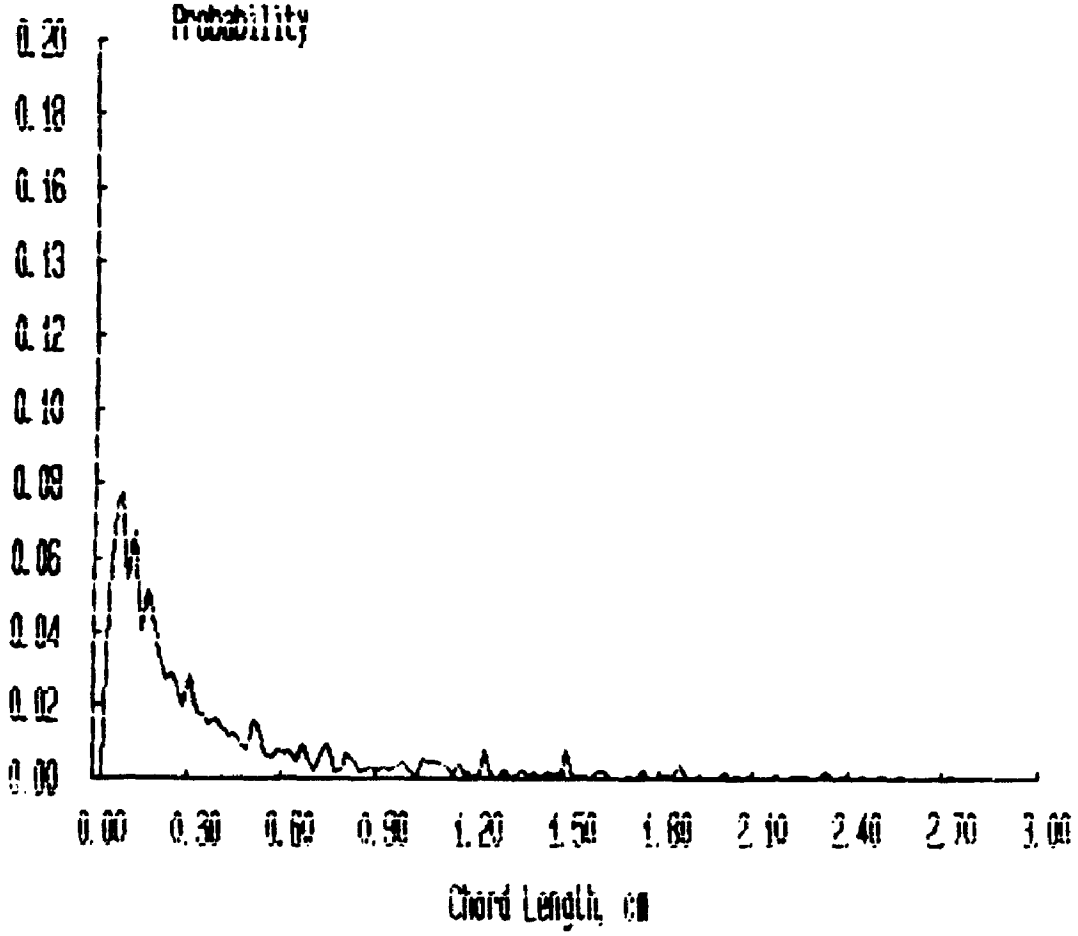

****** FILENAME ****** : JAN21E3A

**** Bubbles detected by probe 1 : 1904
**** Percentage of bubbles retained : 61.13
**** Average bubble duration : .005696 s

Probability Distributions

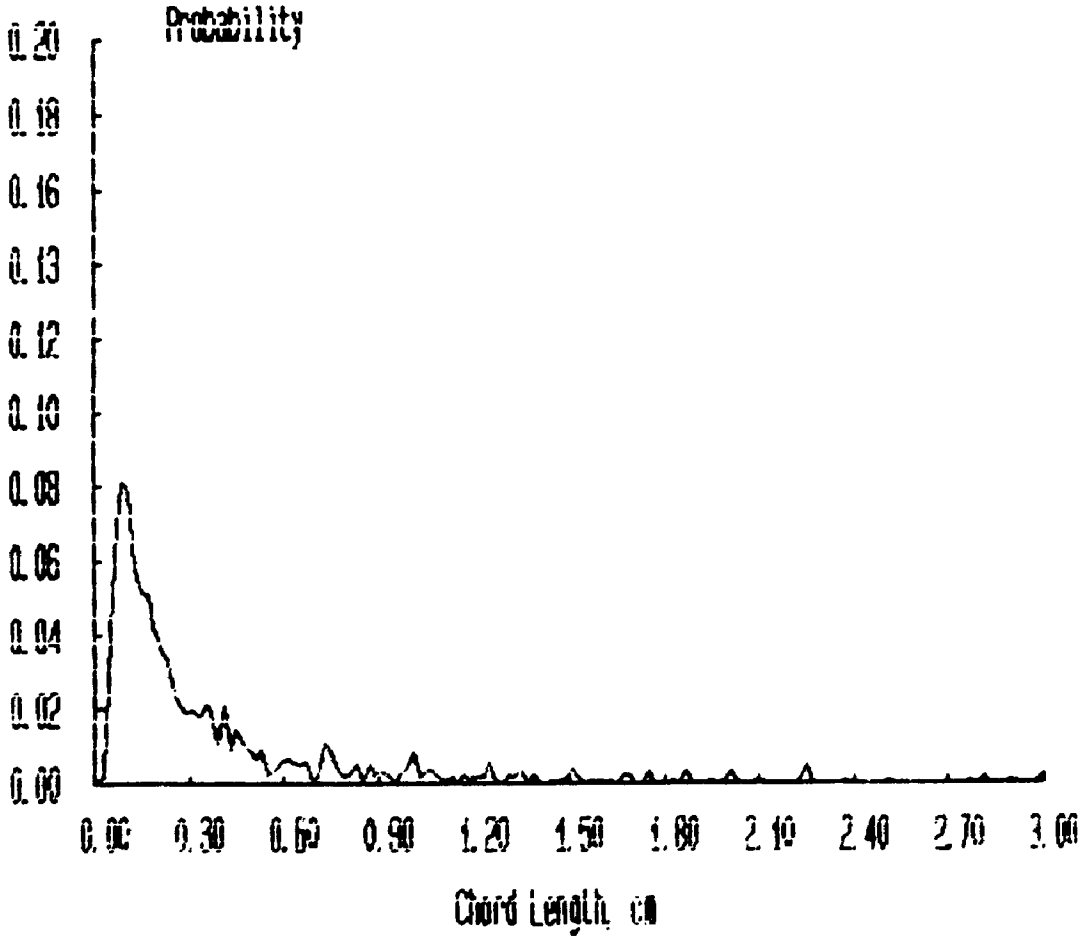

****** FILENAME ****** : JAN21E4A

**** Bubbles detected by probe 1 : 1841
**** Percentage of bubbles retained : 58.45
**** Average bubble duration : .005843 s

Probability Distributions

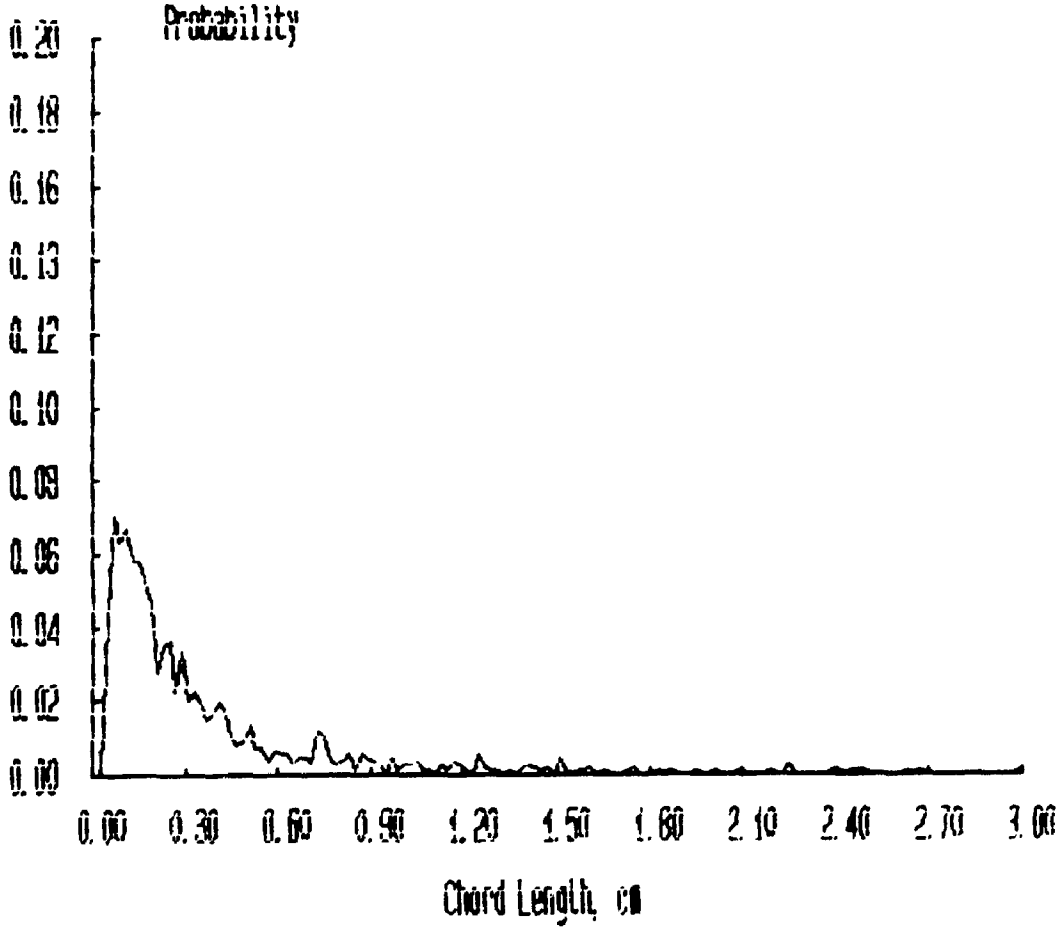

****** FILENAME ****** : JAN21E5A

**** Bubbles detected by probe 1 : 1266
**** Percentage of bubbles retained : 40.44
**** Average bubble duration : .005691 s

Probability Distributions

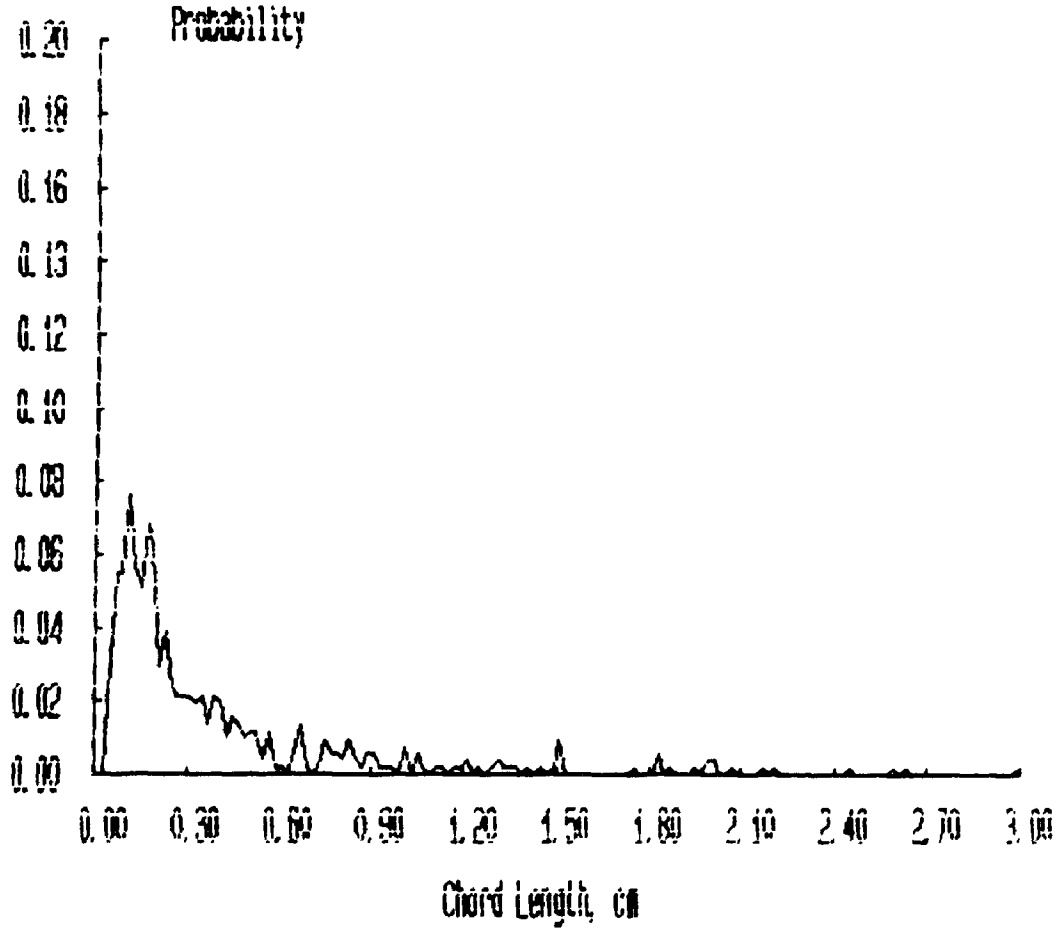

****** FILENAME ****** : JAN21E6A

**** Bubbles detected by probe 1 : 1109
**** Percentage of bubbles retained : 40.94
**** Average bubble duration : .005176 s

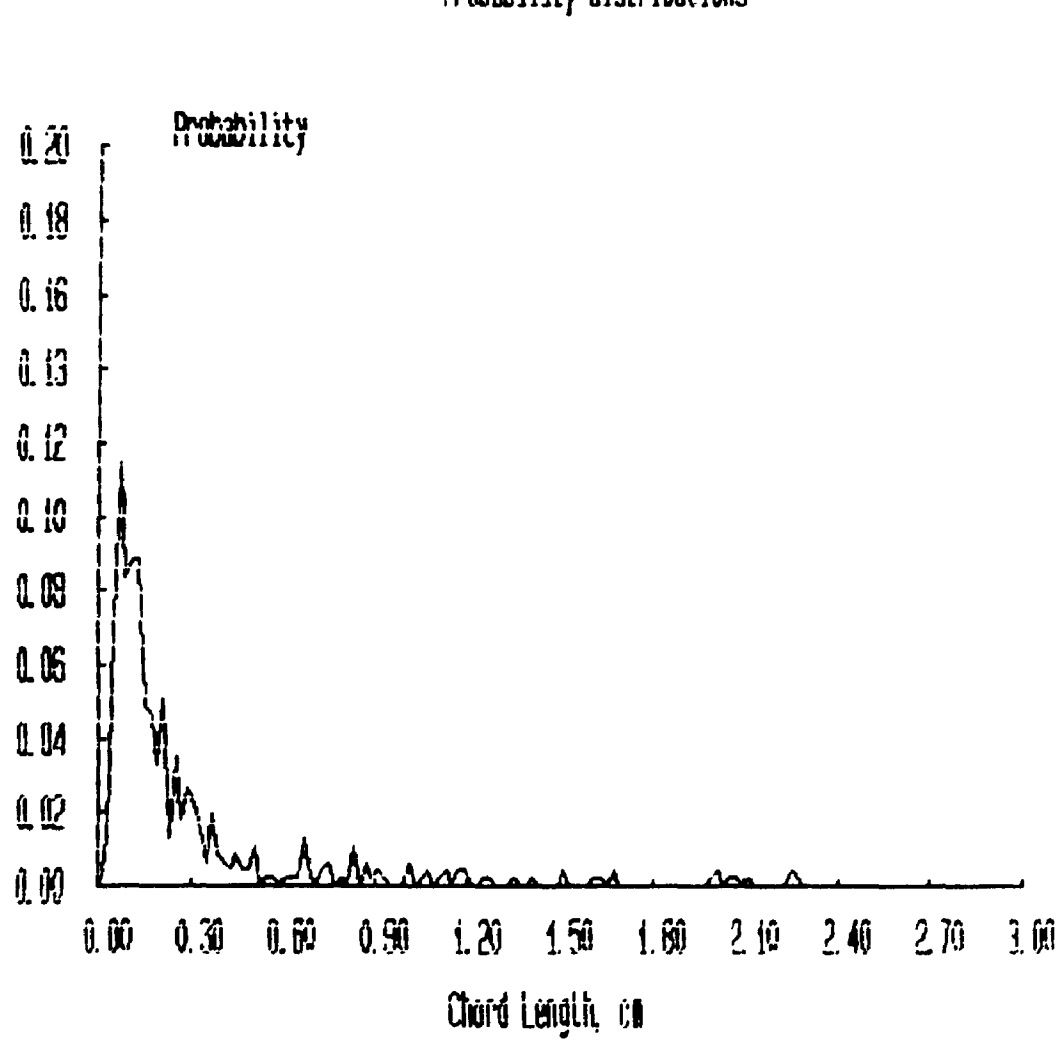

****** FILENAME ****** : JAN22A1A

**** Bubbles detected by probe 1 : 2474
**** Percentage of bubbles retained : 69.64
**** Average bubble duration : .005244 s

Probability Distributions

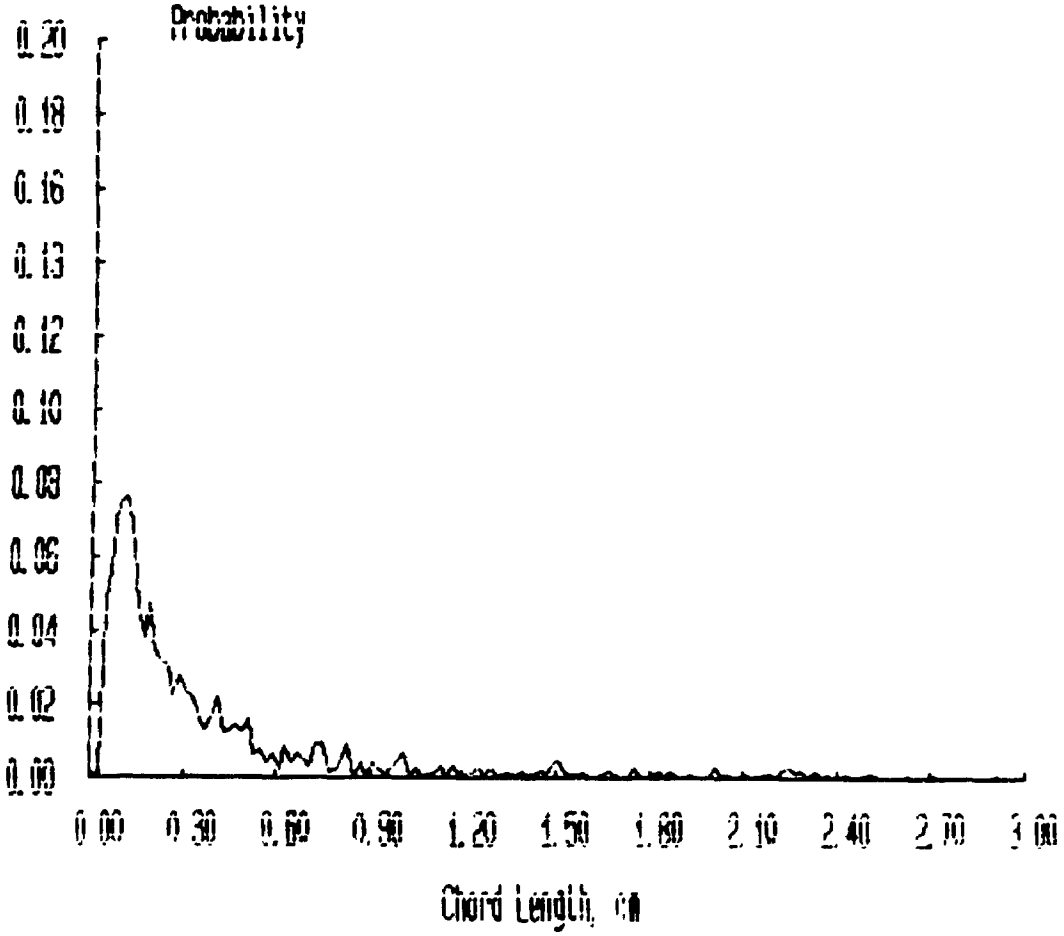

****** FILENAME ****** : JAN22A2A

**** Bubbles detected by probe 1 : 2626
**** Percentage of bubbles retained : 66.34
**** Average bubble duration : .005718 s

Probability Distributions

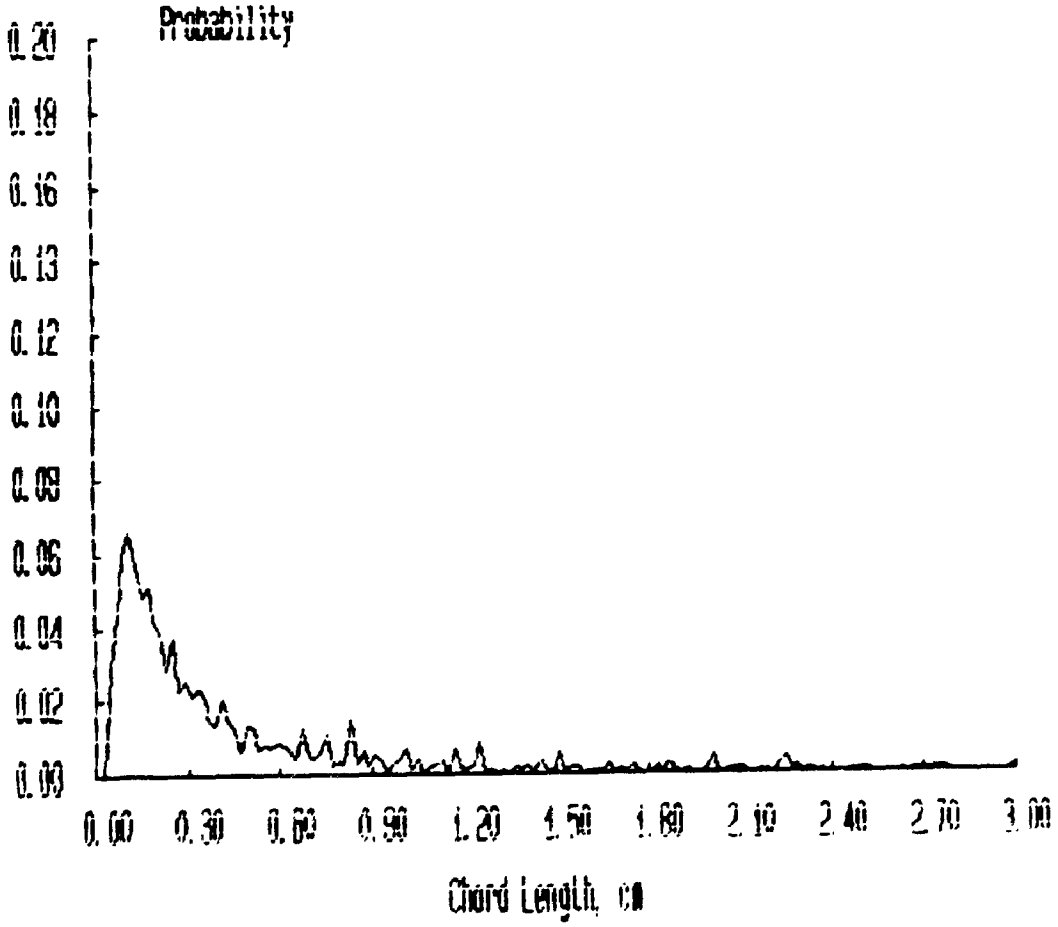

****** FILENAME ****** : JAN22A3A

**** Bubbles detected by probe 1 : 3256
**** Percentage of bubbles retained : 63.97
**** Average bubble duration : .005067 s

Probability Distributions

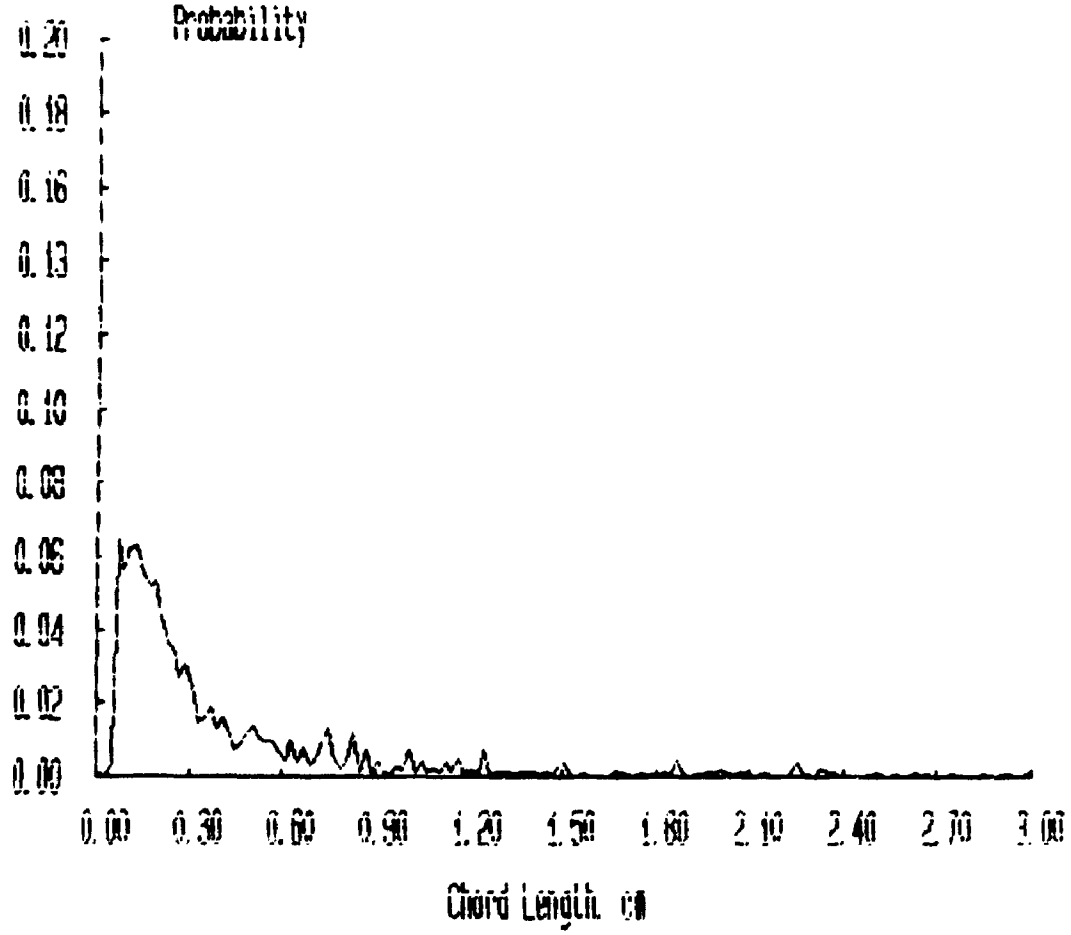

****** FILENAME ****** : JAN22A4A

**** Bubbles detected by probe 1 : 2729
**** Percentage of bubbles retained : 69.26
**** Average bubble duration : .005317 s

Probability distributions

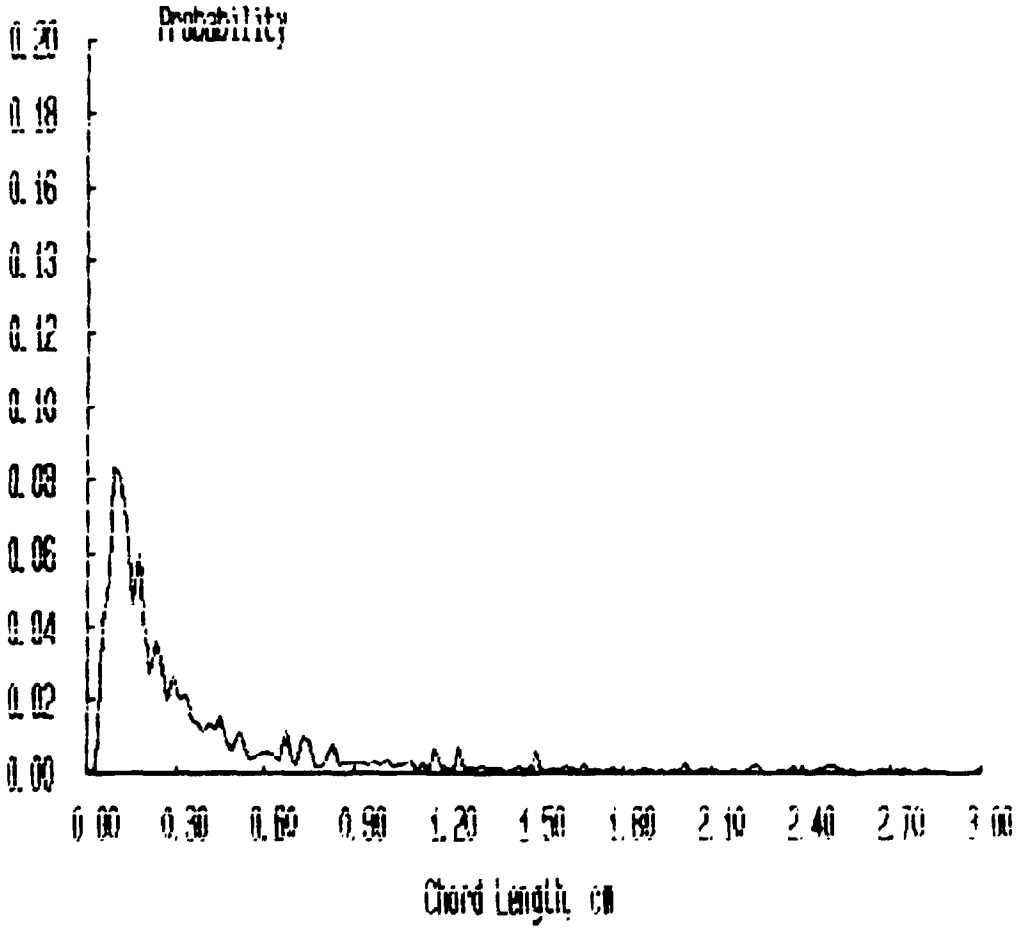

****** FILENAME ****** : JAN22A5A

**** Bubbles detected by probe 1 : 2239
**** Percentage of bubbles retained : 54.76
**** Average bubble duration : .005357 s

Probability Distributions

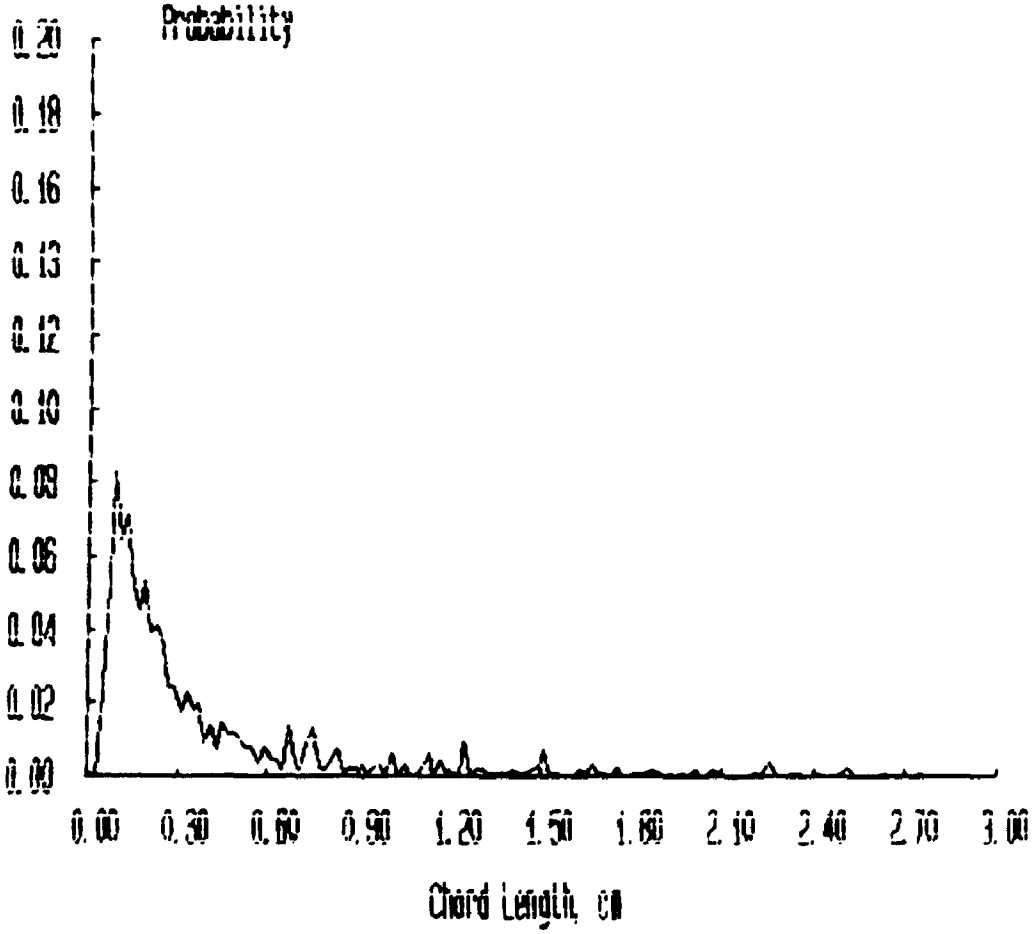

****** FILENAME ****** : JAN22A6A

**** Bubbles detected by probe 1 : 1764
**** Percentage of bubbles retained : 57.54
**** Average bubble duration : .004641 s

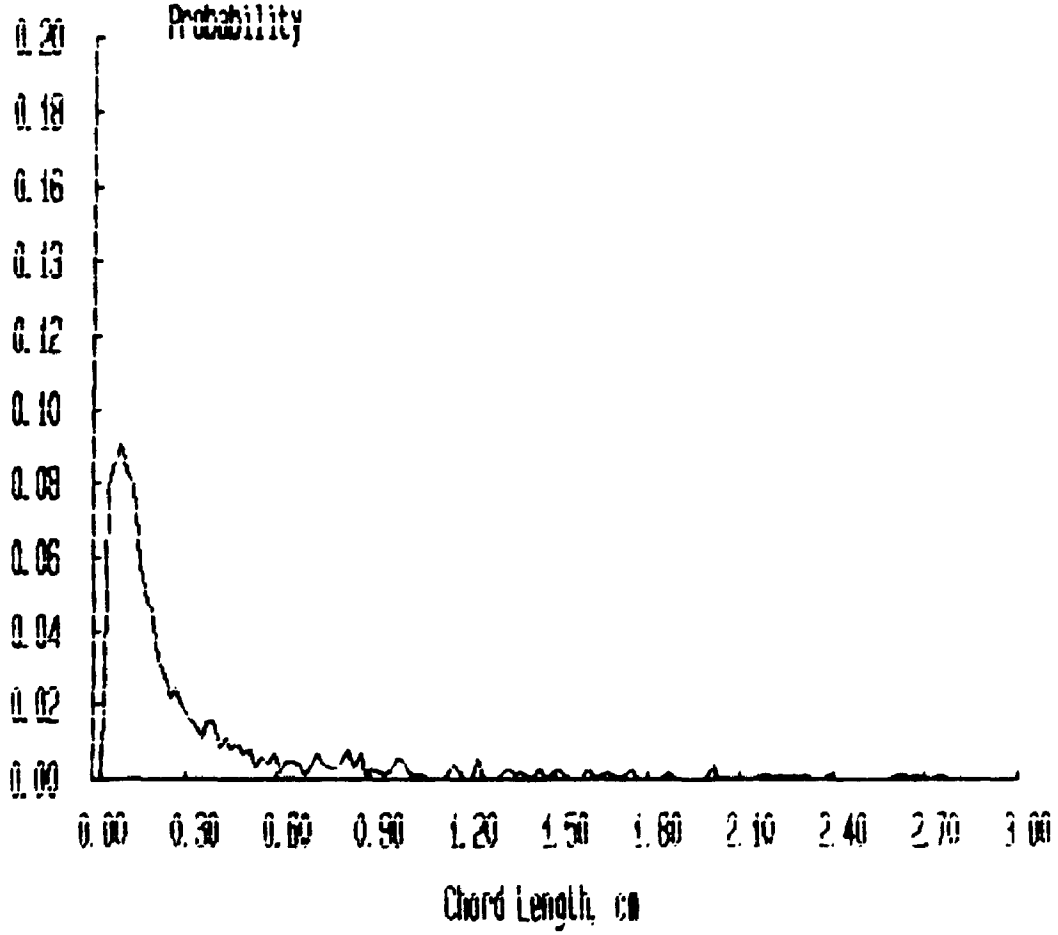

** *** FILENAME ****** : JAN22B1A

**** Bubbles detected by probe 1 : 5445
**** Percentage of bubbles retained : 72.51
**** Average bubble duration : .004759 s

Probability Distributions

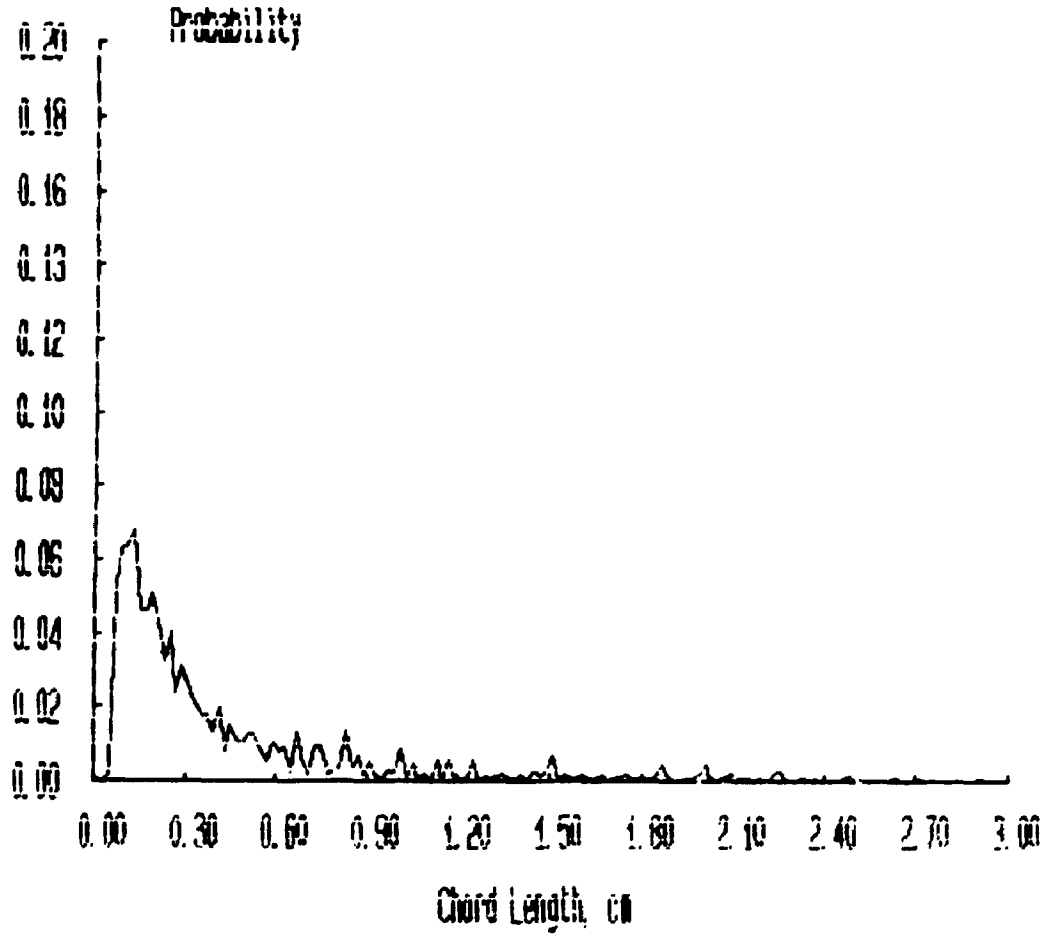

****** FILENAME ****** : JAN22B2A

**** Bubbles detected by probe 1 : 3449
**** Percentage of bubbles retained : 74.40
**** Average bubble duration : .004942 s

Probability Distributions

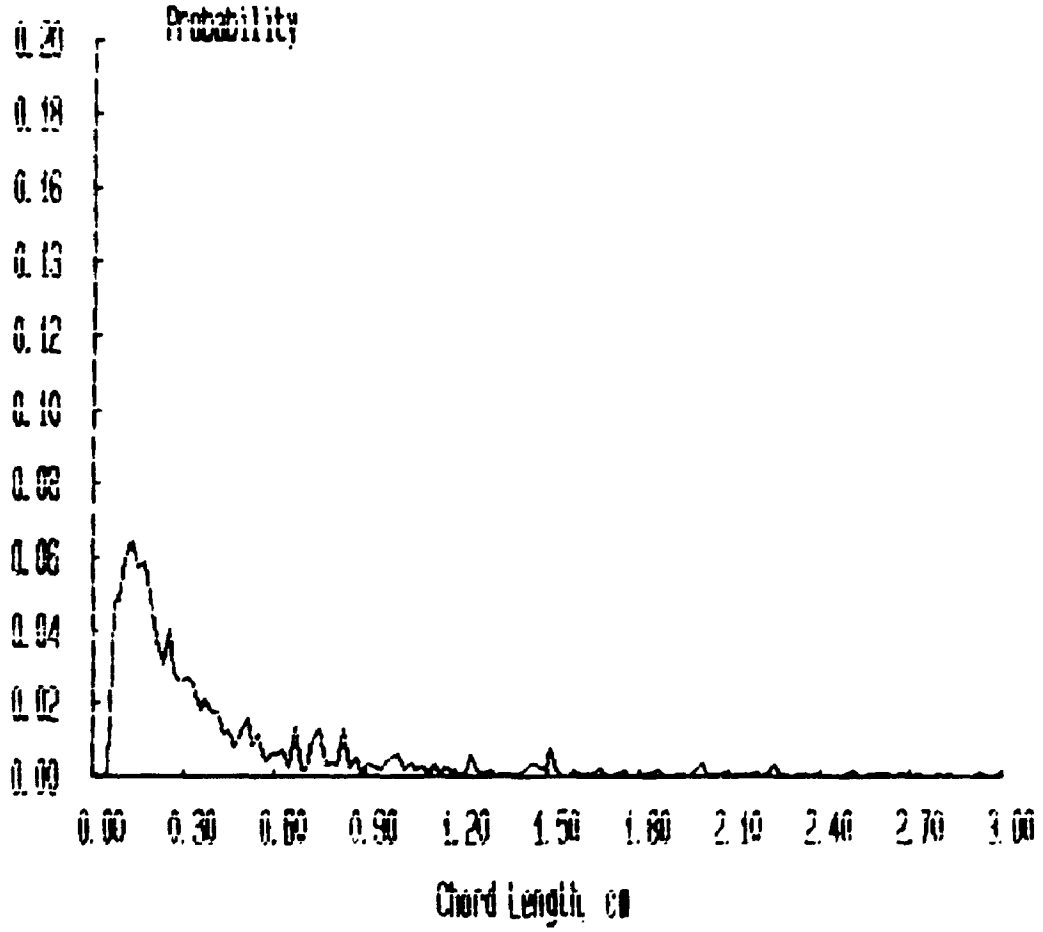

****** FILENAME ****** : JAN22B3A

**** Bubbles detected by probe 1 : 3630
**** Percentage of bubbles retained : 73.42
**** Average bubble duration : .004886 s

Probability Distributions

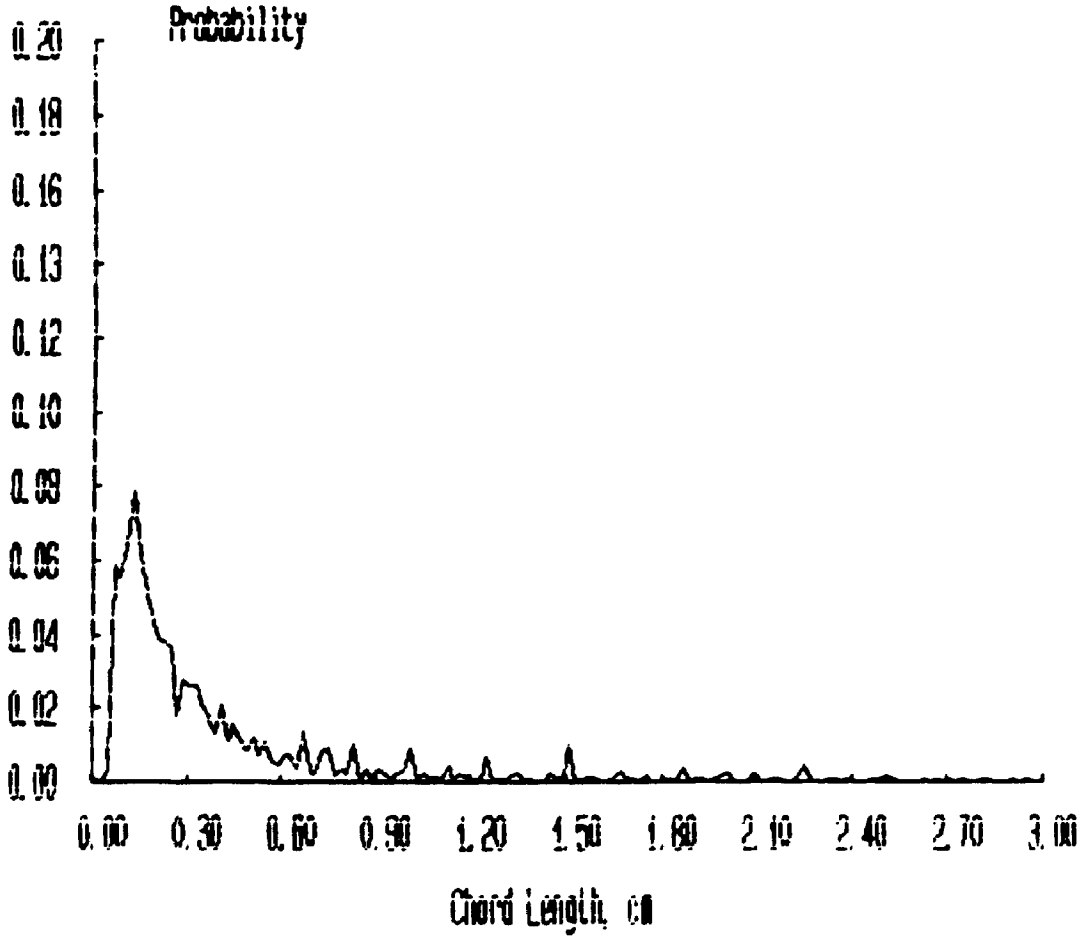

****** FILENAME ****** : JAN22B4A

**** Bubbles detected by probe 1 : 2849
**** Percentage of bubbles retained : 58.30
**** Average bubble duration : .004747 s

Probability Distributions

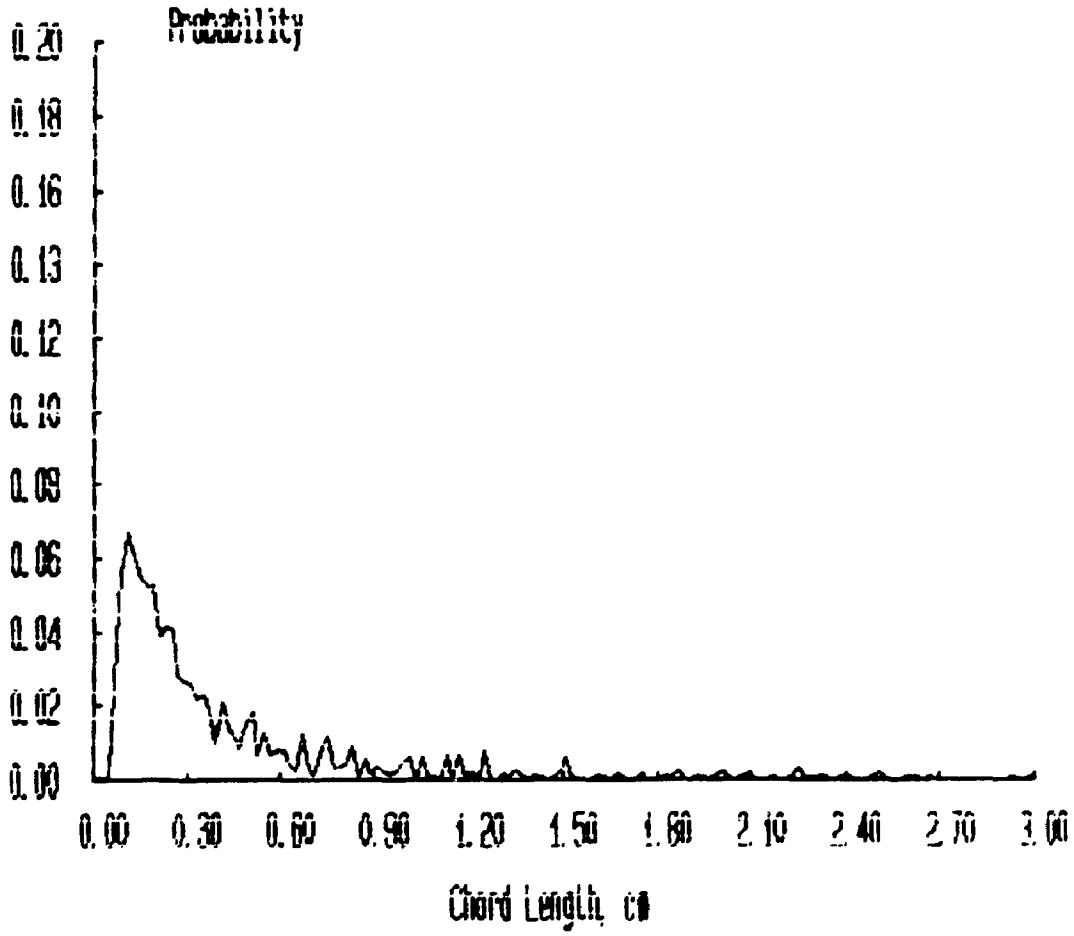

****** FILENAME ****** : JAN2285A

**** Bubbles detected by probe 1 : 2548
**** Percentage of bubbles retained : 54.67
**** Average bubble duration : .004304 s

Probability Distributions

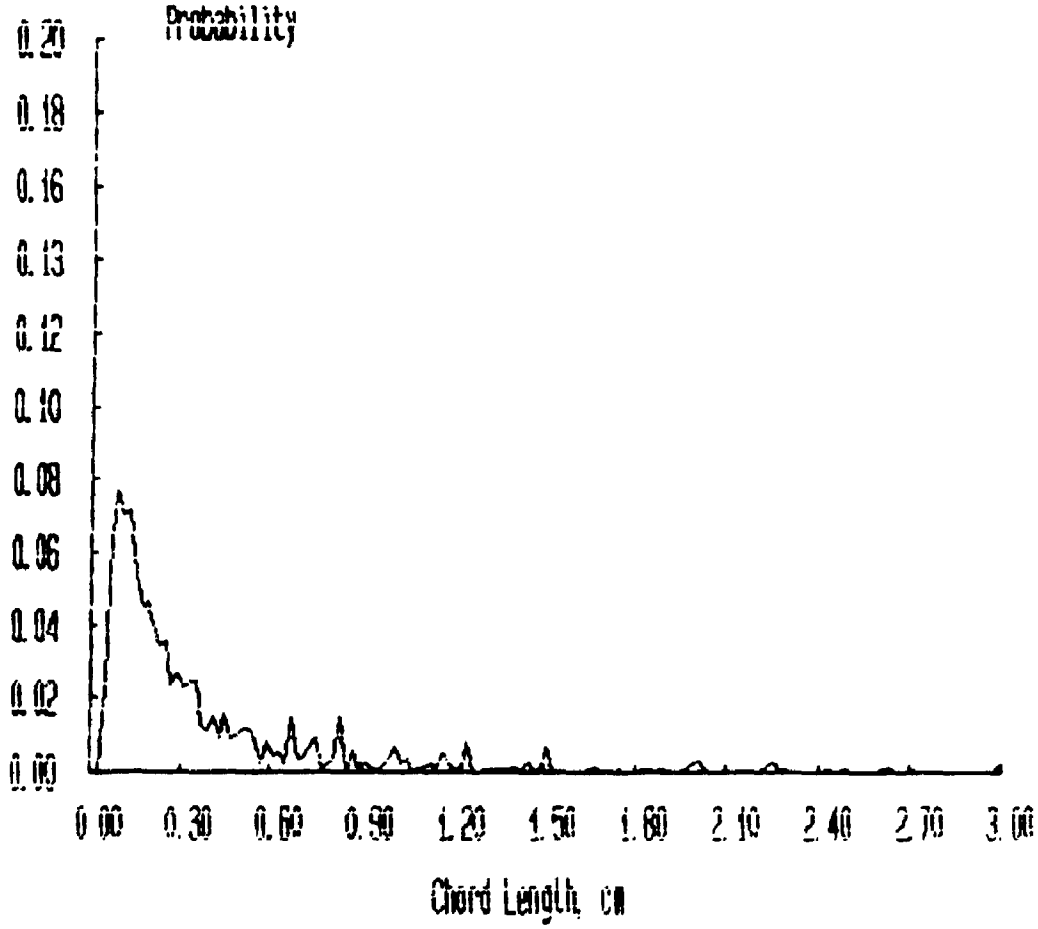

****** FILENAME ****** : JAN2286A

**** Bubbles detected by probe 1 : 1908
**** Percentage of bubbles retained : 55.35
**** Average bubble duration : .004216 s

Probability Distributions

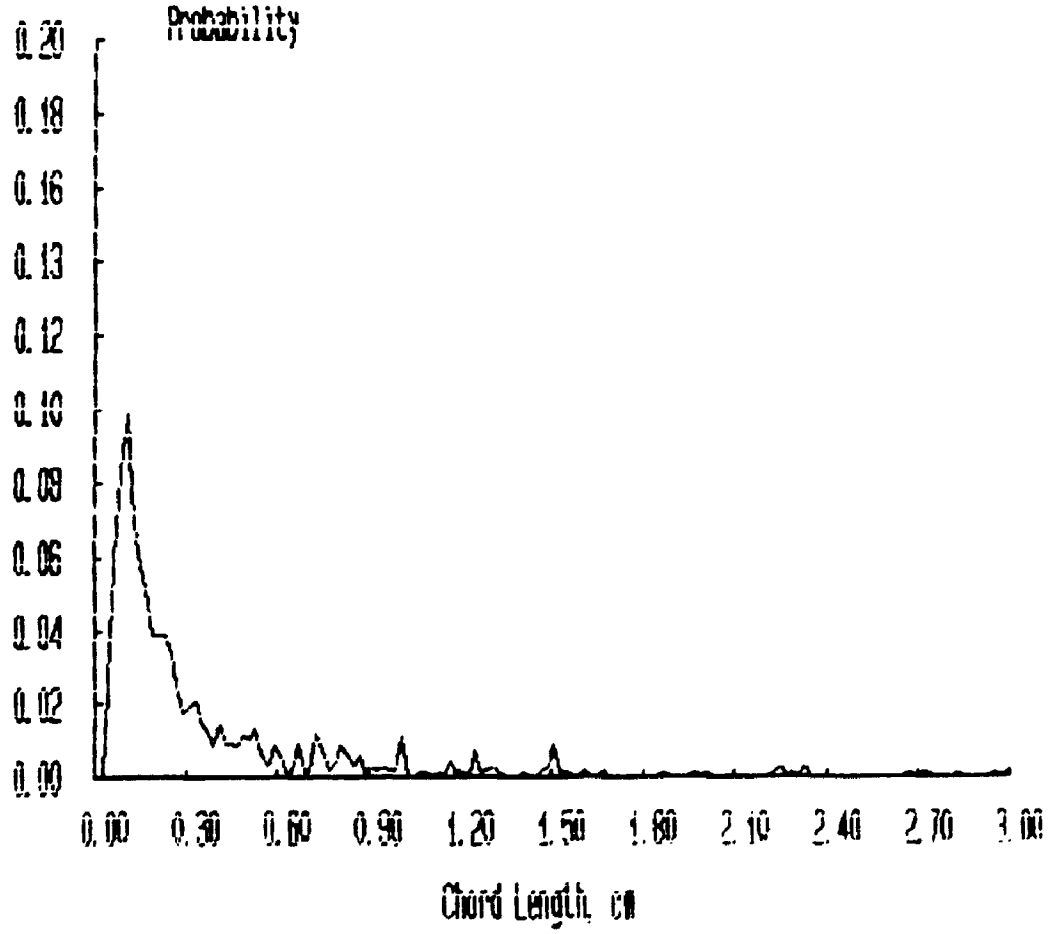

****** FILENAME ****** : JAN22C1A

**** Bubbles detected by probe 1 : 4617
**** Percentage of bubbles retained : 80.72
**** Average bubble duration : .004607 s

Probability Distributions

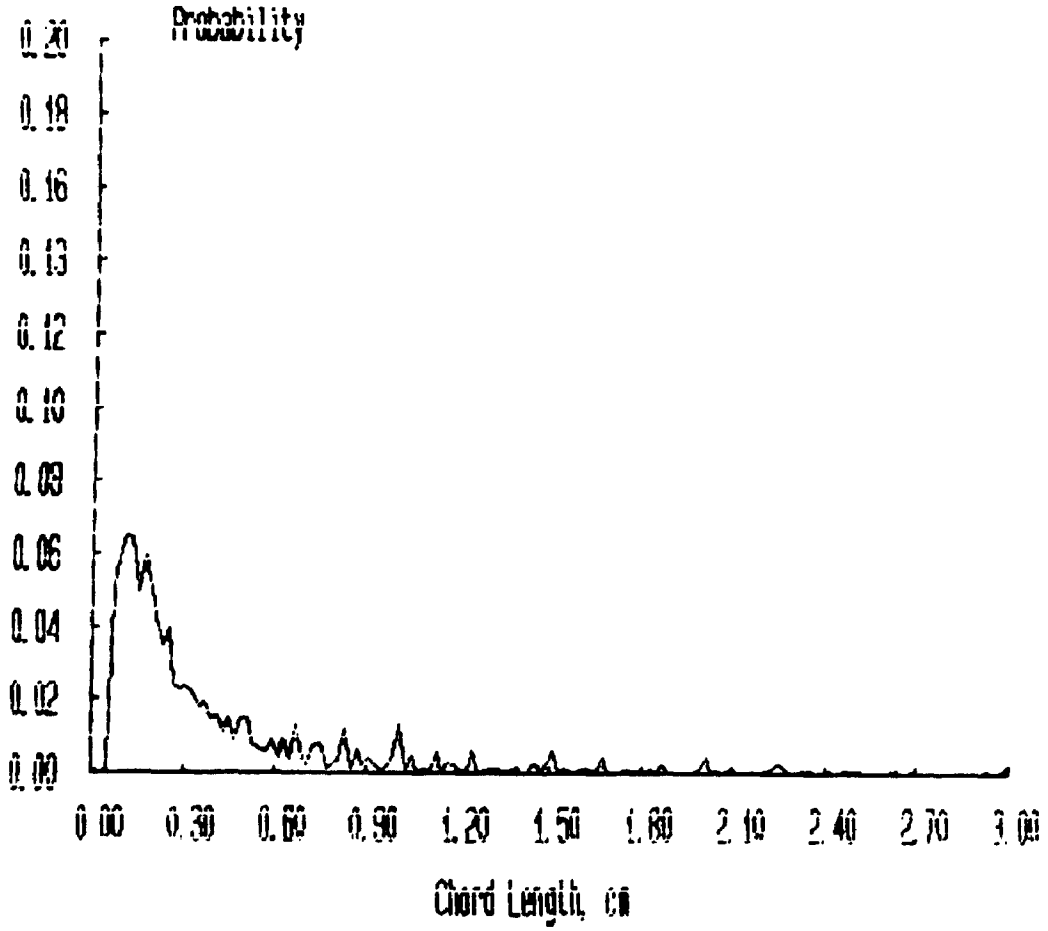

****** FILENAME ****** : JAN22C2A

**** Bubbles detected by probe 1 : 5923
**** Percentage of bubbles retained : 76.34
**** Average bubble duration : .004648 s

Probability Distributions

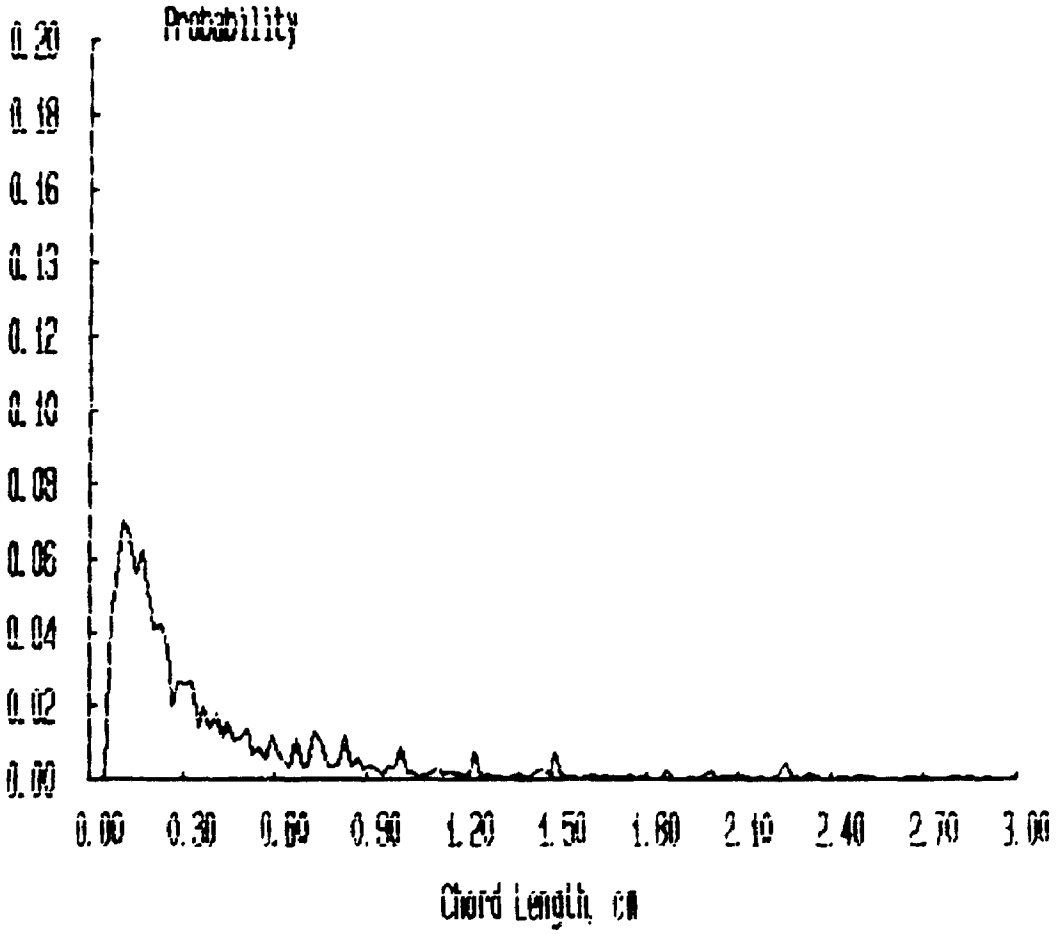

****** FILENAME ****** : JAN22C3A

**** Bubbles detected by probe 1 : 3388
**** Percentage of bubbles retained : 72.31
**** Average bubble duration : .004862 s

Probability Distributions

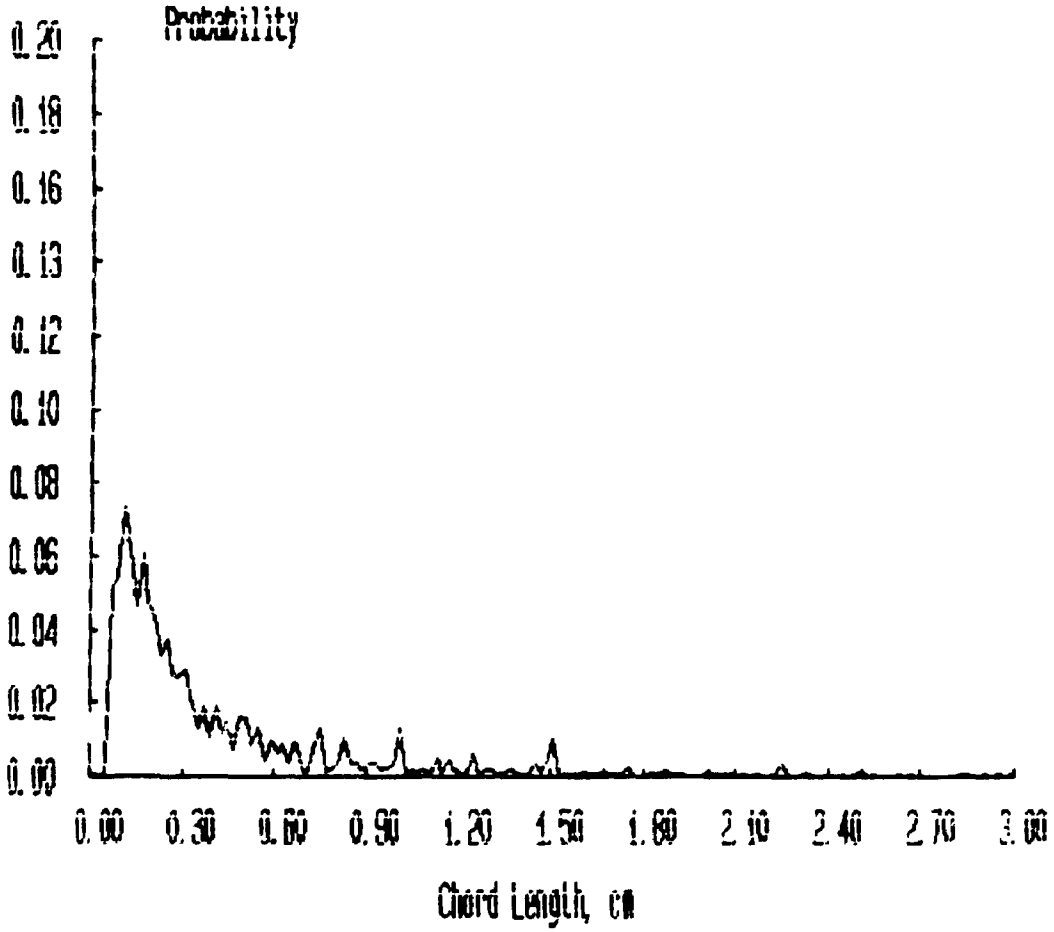

****** FILENAME ****** : JAN22C4A

**** Bubbles detected by probe 1 : 2980
**** Percentage of bubbles retained : 66.38
**** Average bubble duration : .004613 s

Probability Distributions

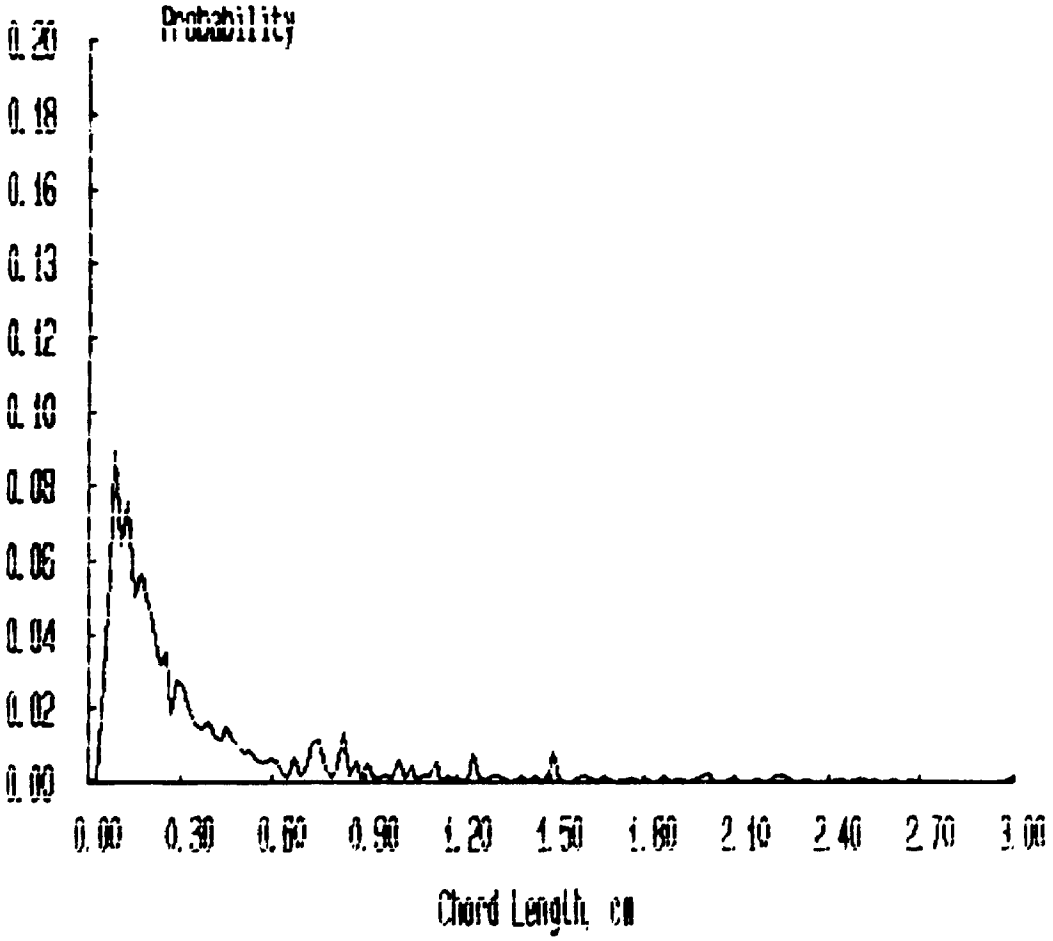

****** FILENAME ****** : JAN22C5A

**** Bubbles detected by probe 1 : 2447
**** Percentage of bubbles retained : 54.03
**** Average bubble duration : .004004 s

Probability Distributions

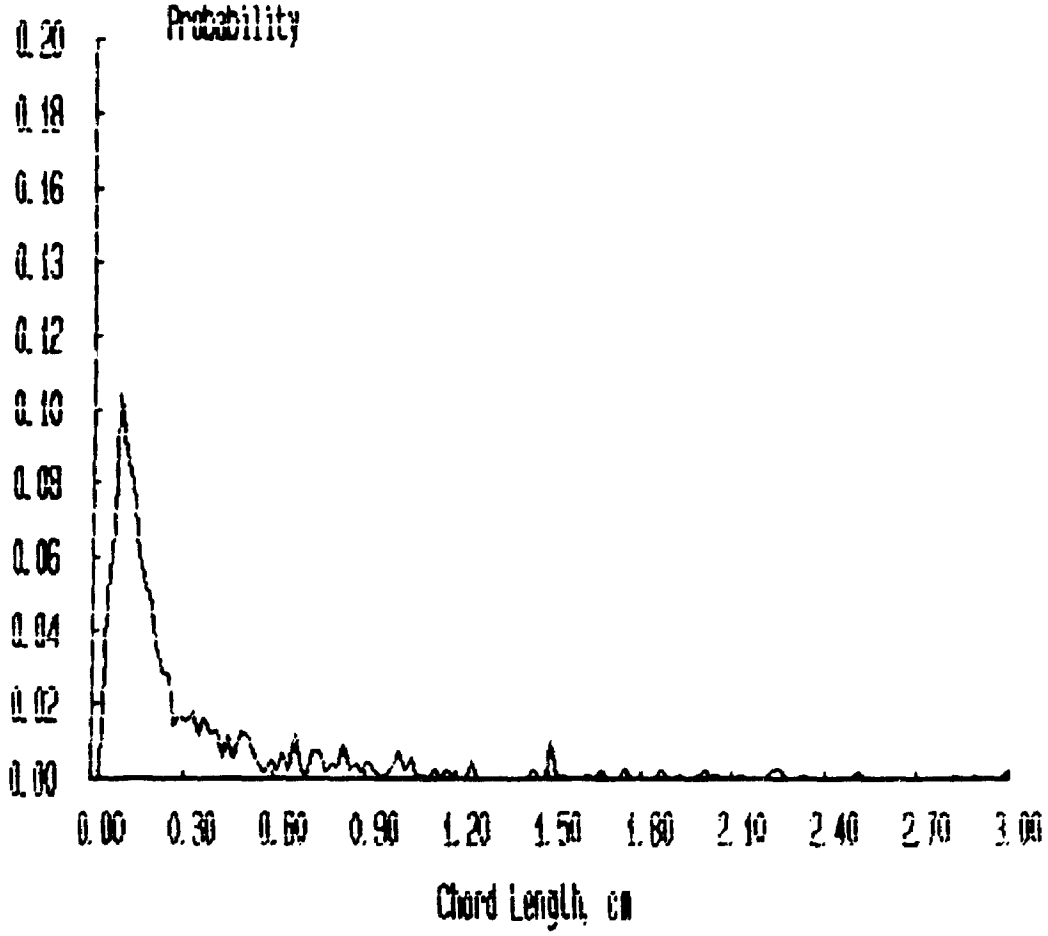

B61

****** FILENAME ****** : JAN22C6A

**** Bubbles detected by probe 1 : 1537
**** Percentage of bubbles retained : 55.63
**** Average bubble duration : .004340 s

Probability Distributions

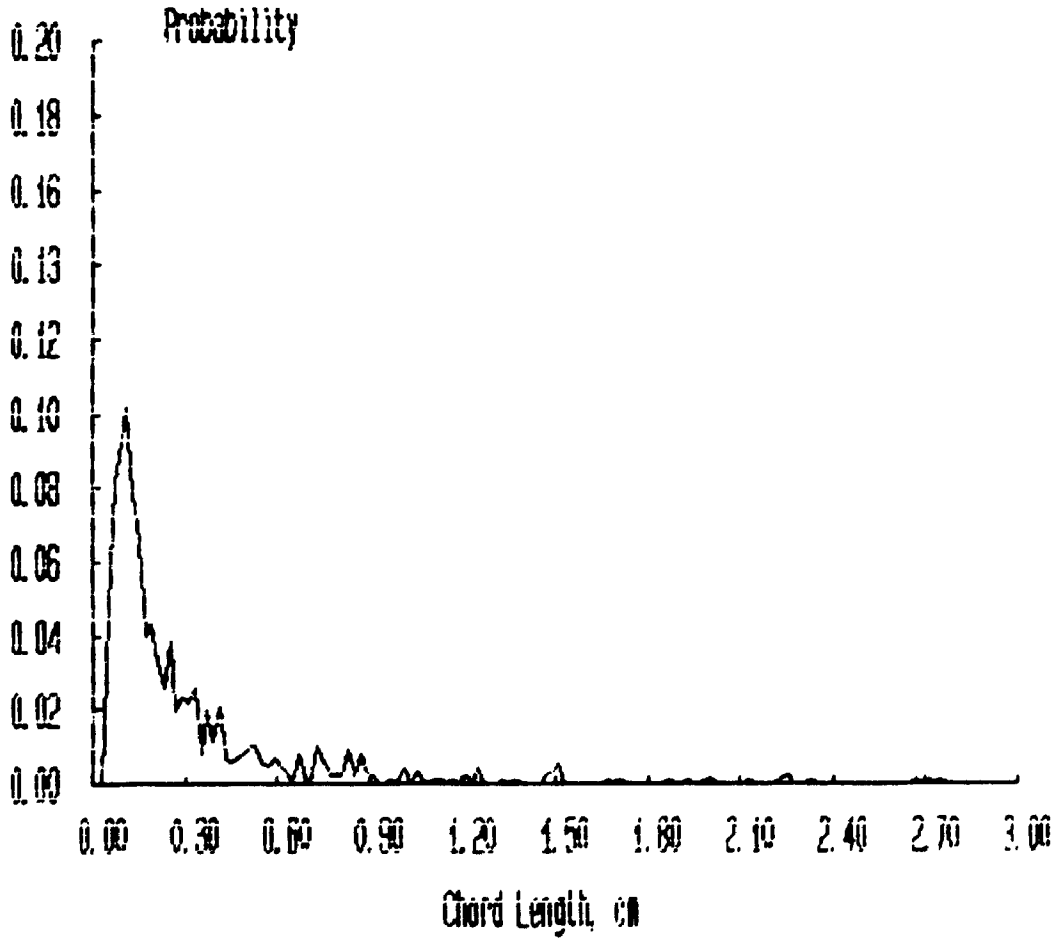

****** FILENAME ****** : JAN22D1A

**** Bubbles detected by probe 1 : 4754
**** Percentage of bubbles retained : 75.47
**** Average bubble duration : .004580 s

Probability Distributions

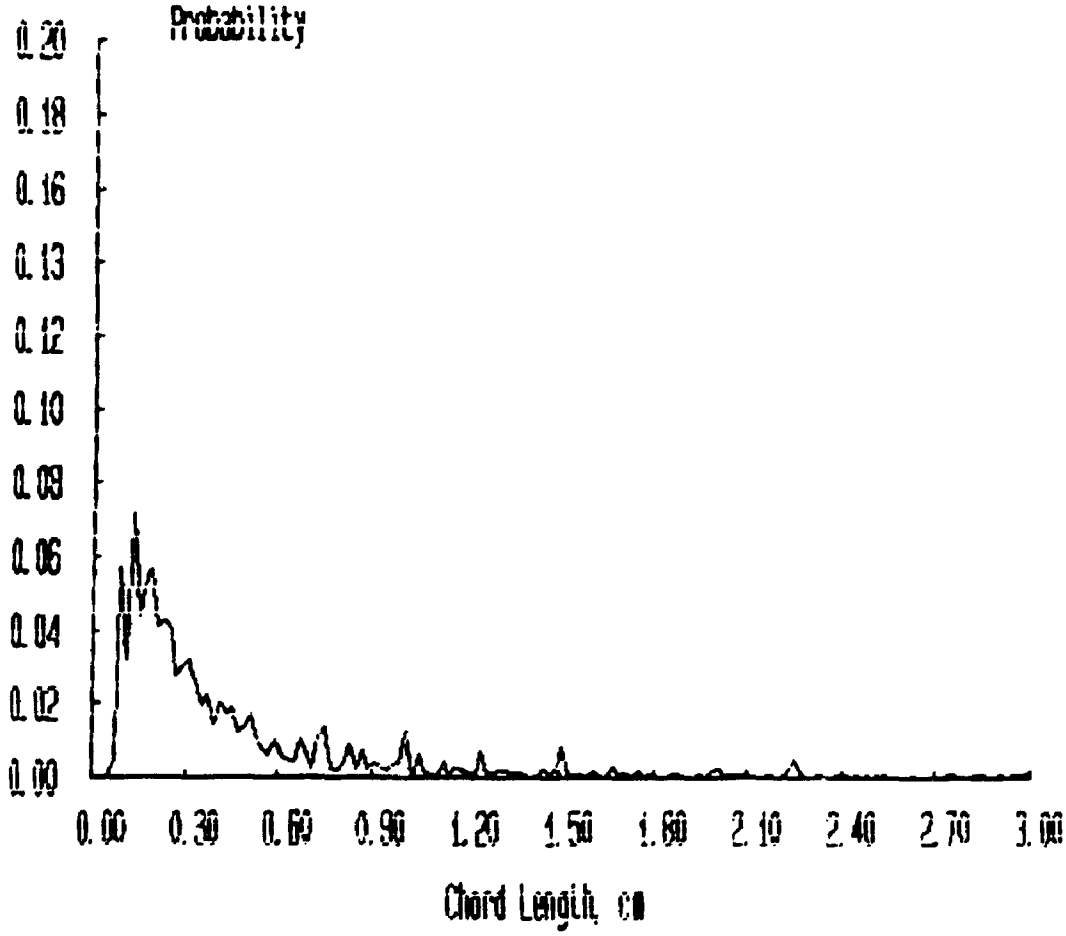

****** FILENAME ****** : JAN22D2A

**** Bubbles detected by probe 1 : 4377
**** Percentage of bubbles retained : 75.71
**** Average bubble duration : .004571 s

Probability Distributions

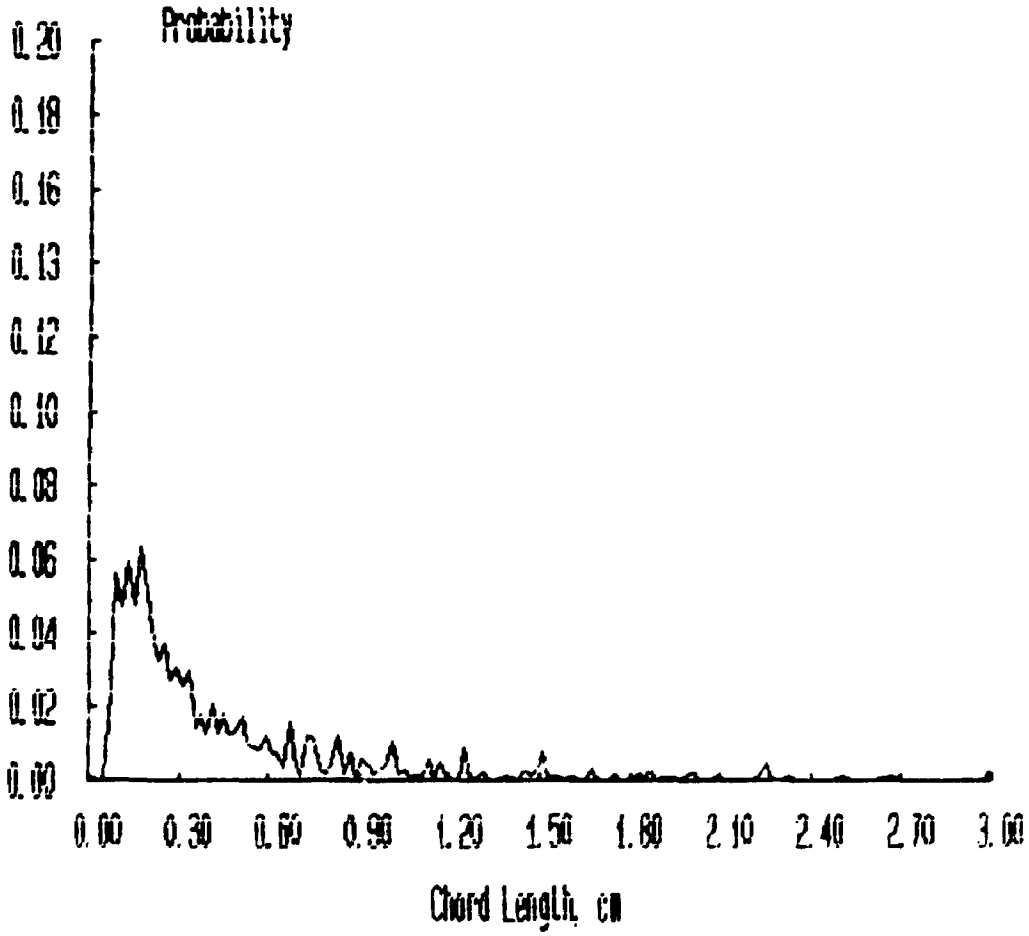

****** FILENAME ****** : JAN22D3A

**** Bubbles detected by probe 1 : 3284
**** Percentage of bubbles retained : 66.99
**** Average bubble duration : .004460 s

Probability Distributions

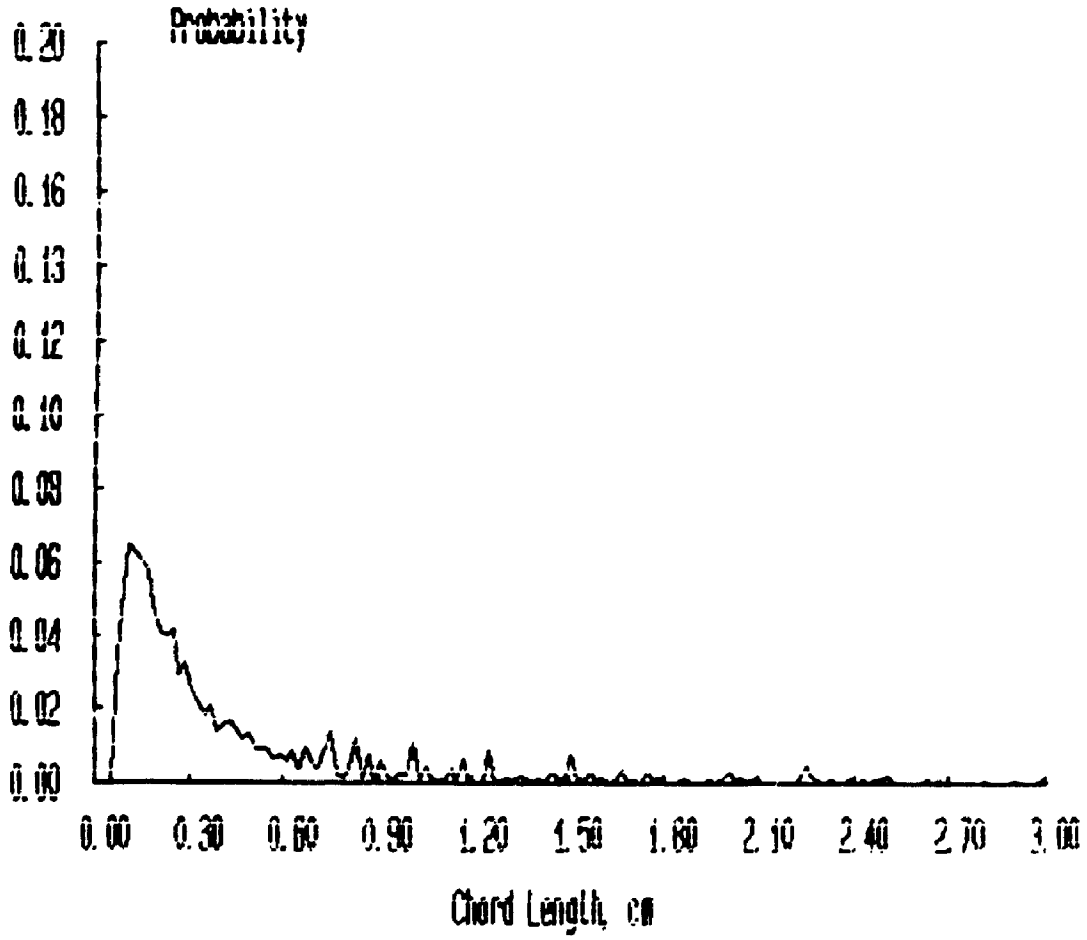

****** FILENAME ****** : JAN22D4A

**** Bubbles detected by probe 1 : 3261
**** Percentage of bubbles retained : 63.54
**** Average bubble duration : .004317 s

Probability Distributions

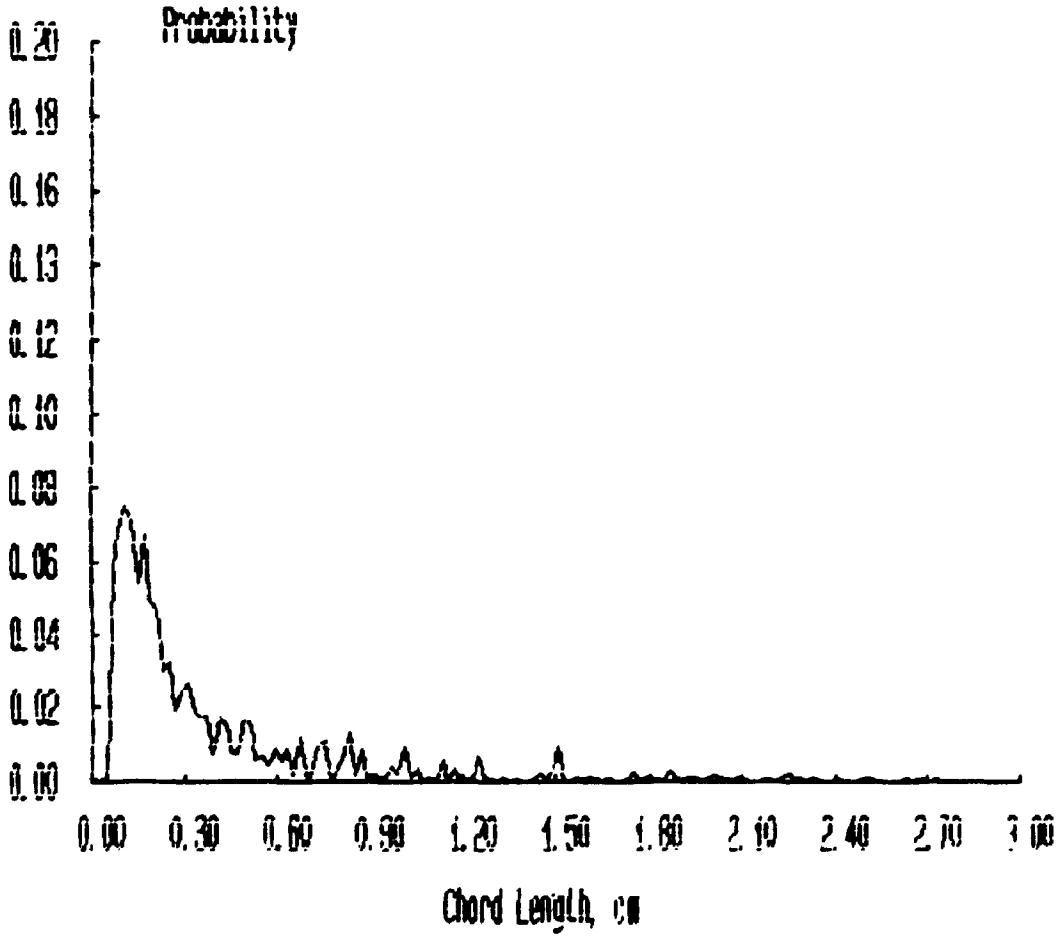

****** FILENAME ****** : JAN22D5A

**** Bubbles detected by probe 1 : 1992
**** Percentage of bubbles retained : 56.93
**** Average bubble duration : .004341 s

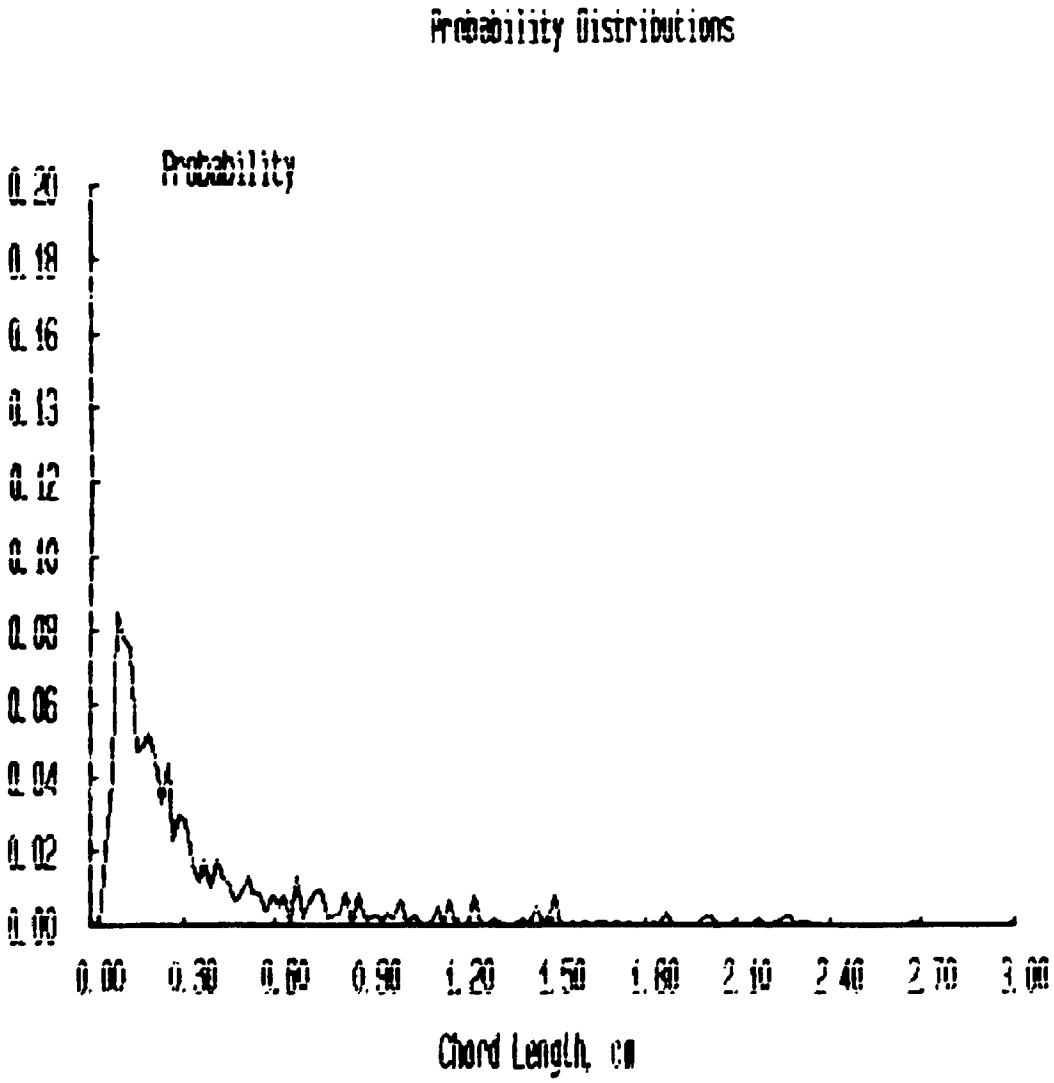

****** FILENAME ****** : JAN22D6A

**** Bubbles detected by probe 1 : 1618
**** Percentage of bubbles retained : 54.0%
**** Average bubble duration : .0040/0 s

Probability Distributions

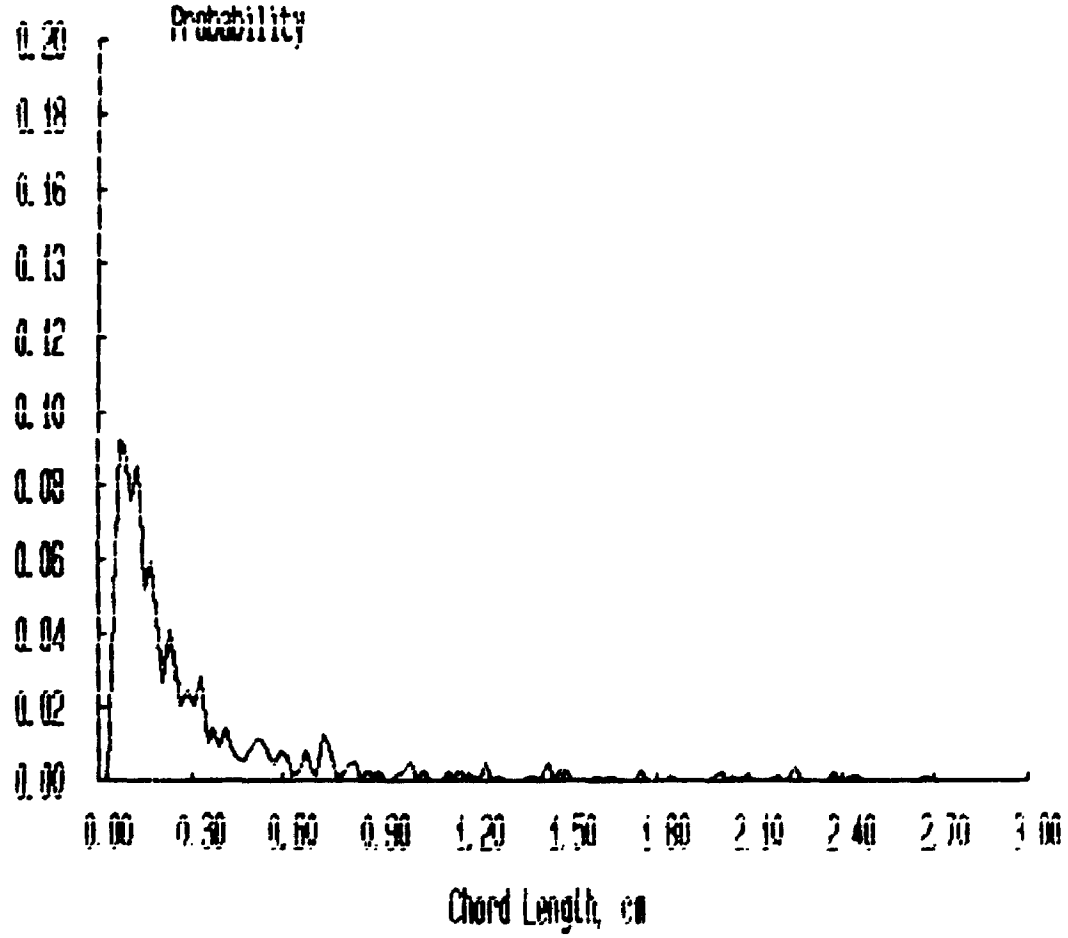

****** FILENAME ****** : JAN22E1A

**** Bubbles detected by probe 1 : 4423
**** Percentage of bubbles retained : 74.75
**** Average bubble duration : .004779 s

Probability Distributions

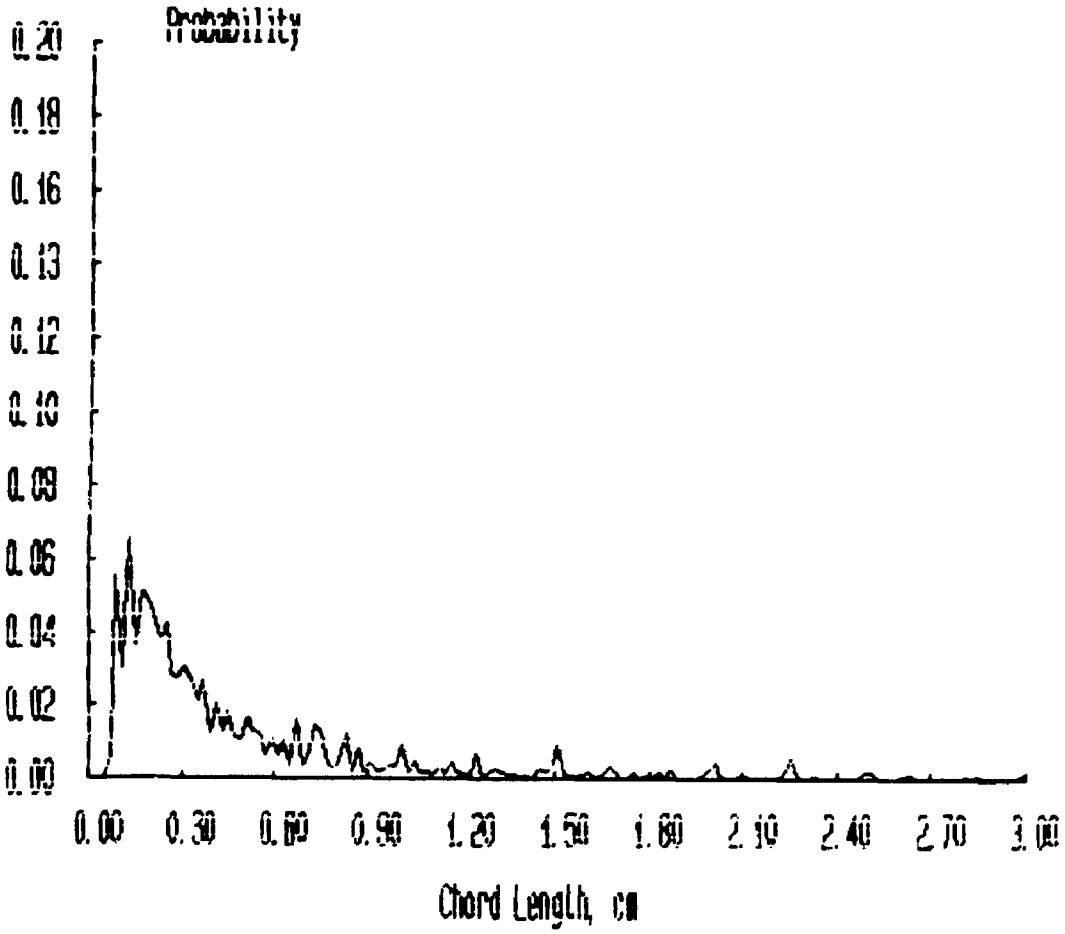

****** FILENAME ****** : JAN22E2A

**** Bubbles detected by probe 1 : 4385
**** Percentage of bubbles retained : 76.62
**** Average bubble duration : .004485 s

Probability Distributions

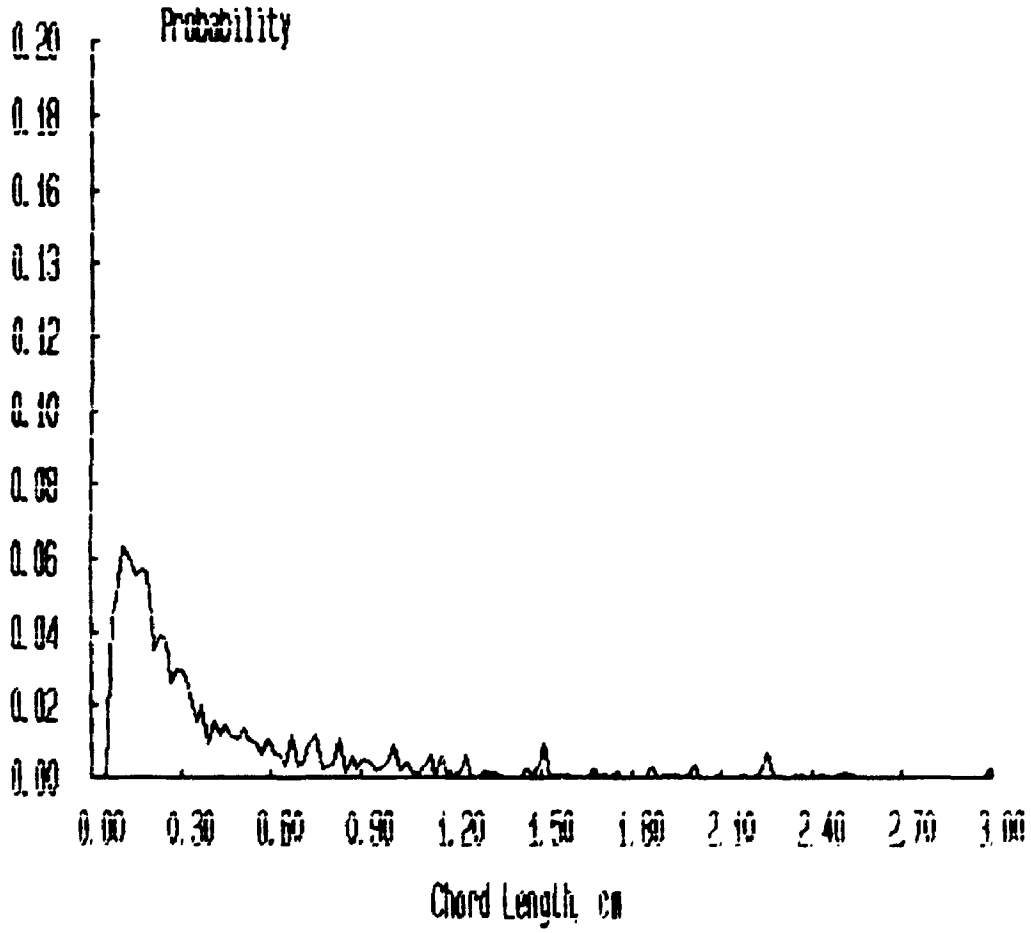

****** FILENAME ****** : JAN22E3A

**** Bubbles detected by probe 1 : 3236
**** Percentage of bubbles retained : 68.29
**** Average bubble duration : .004348 s

Probability Distributions

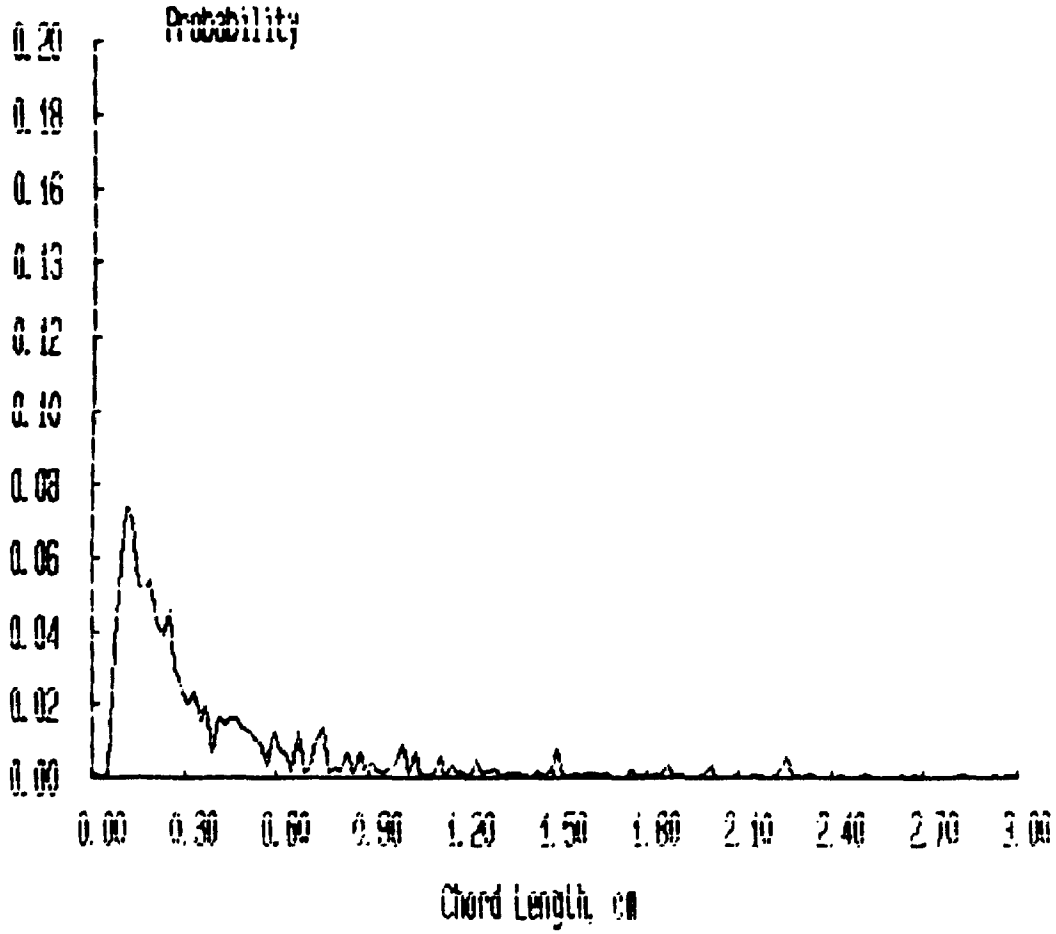

****** FILENAME ****** : JAN22E4A

**** Bubbles detected by probe 1 : 2851
**** Percentage of bubbles retained : 66.51
**** Average bubble duration : .004033 s

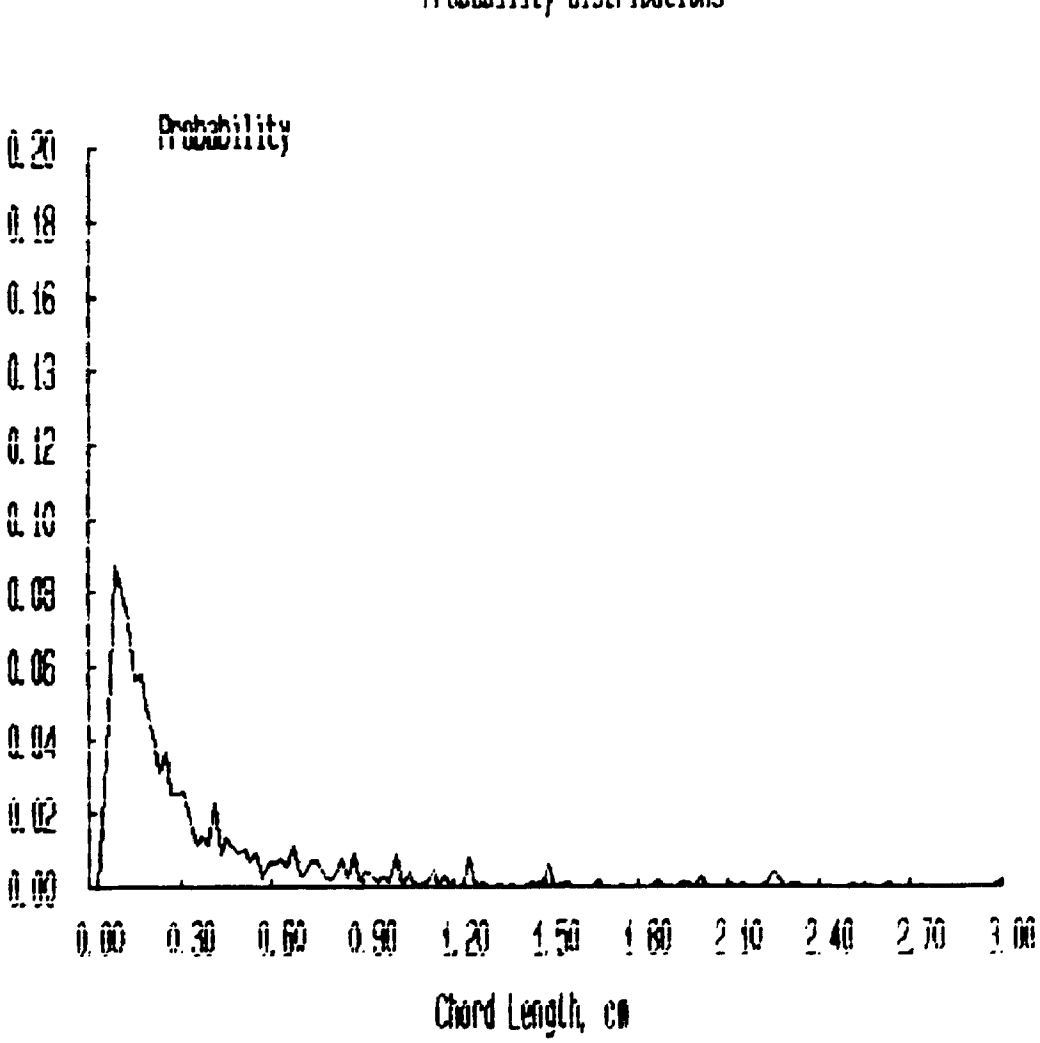

****** FILENAME ****** : JAN22E5A

**** Bubbles detected by probe 1 : 1966
**** Percentage of bubbles retained : 60.53
**** Average bubble duration : .004085 s

Probability Distributions

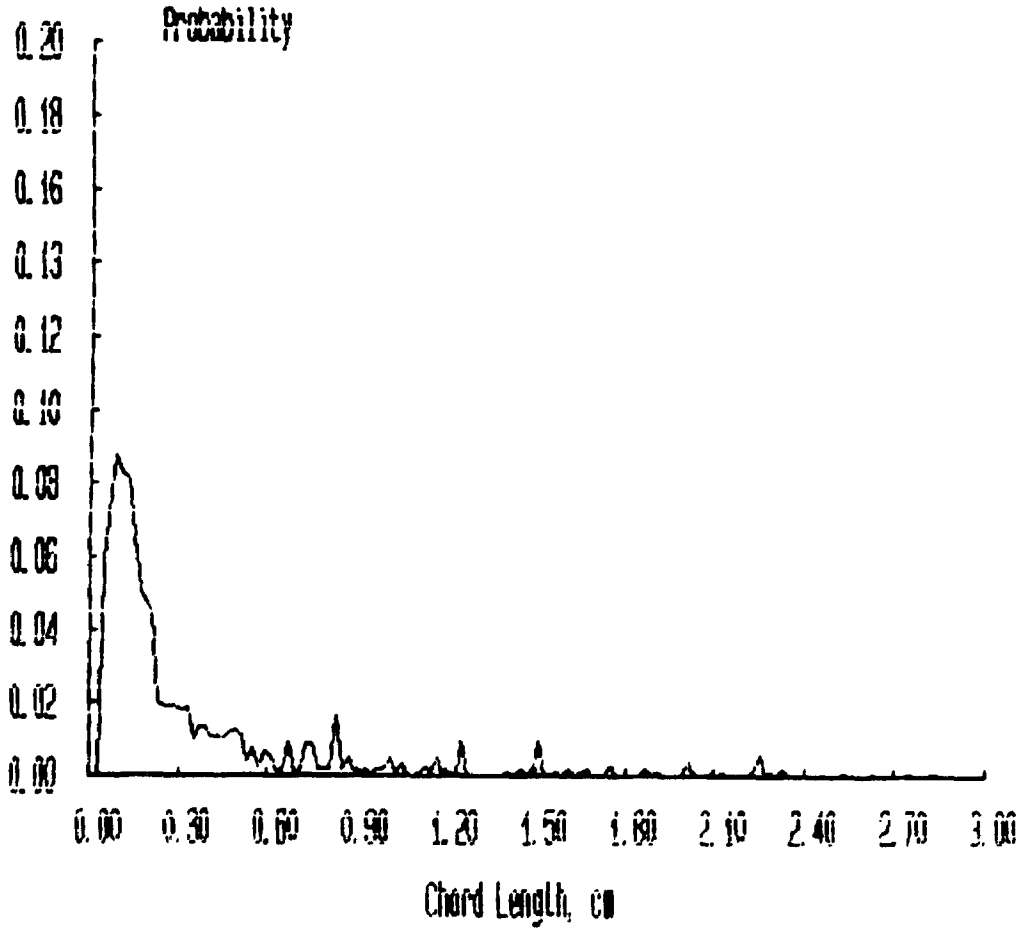

****** FILENAME ****** : JAN22E6A

**** Bubbles detected by probe 1 : 1355
**** Percentage of bubbles retained : 61.70
**** Average bubble duration : .004156 s

Probability Distributions

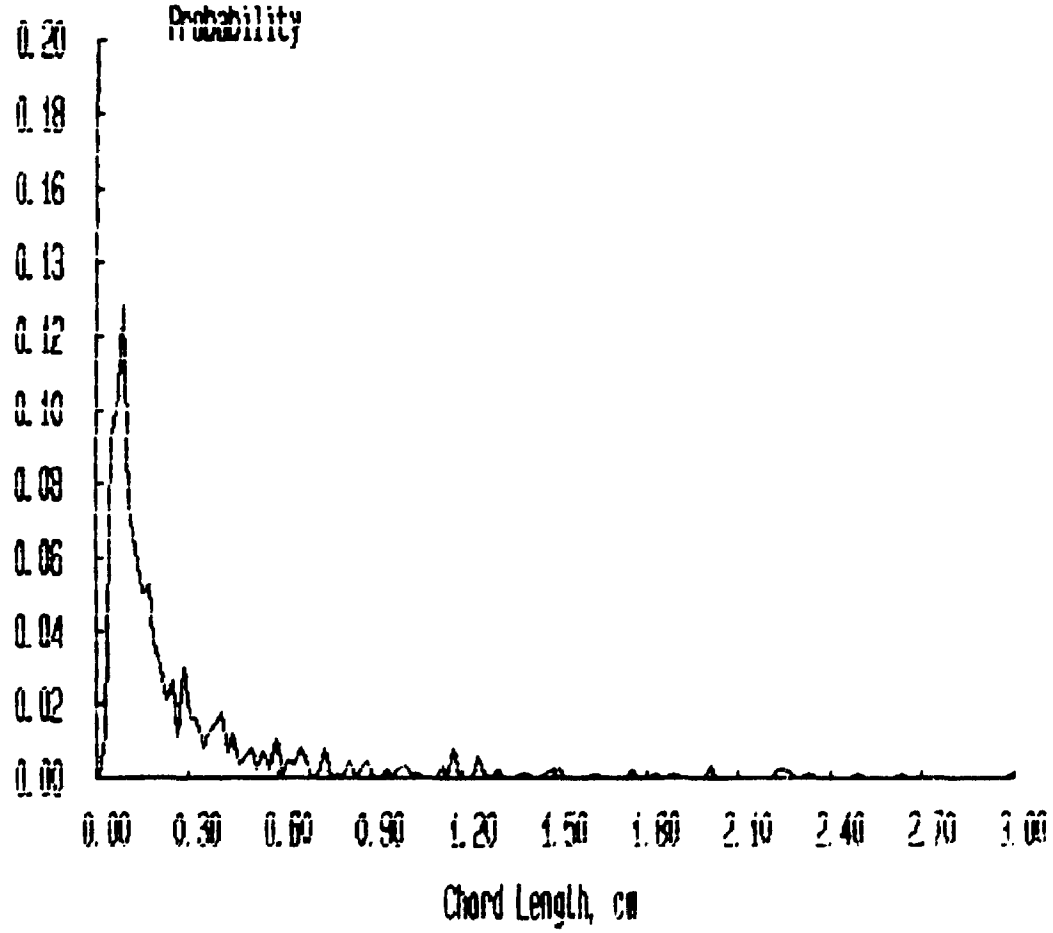

APPENDIX 9

BUBBLE CHORD LENGTH DISTRIBUTION
INVERSE GAUSSIAN DISTRIBUTION FUNCTION PARAMETERS

Table A9.1
Summary of inverse gaussian bubble chord length distribution function (T=100°C, V_s=2.2 cm/s)

Filename	α	α, s.d.	τ	τ, s.d.
jan13d1a	0.4142	0.0679	0.1745	0.0110
jan13d2a	0.5338	0.1354	0.2600	0.0151
jan13d3a	0.4576	0.0595	0.3070	0.0219
jan13d4a	0.4551	0.1390	0.2498	0.0166
jan13d5a	0.6337	0.1607	0.2555	0.01925
jan13d6a	0.4763	0.4710	0.2378	0.0189
jan13c1a	0.3994	0.0682	0.2515	0.0182
jan13c2a	0.4571	0.04982	0.2679	0.0155
jan13c3a	0.4620	0.0811	0.2171	0.0146
jan13c4a	0.4228	0.0746	0.2727	0.0231
jan13c5a	0.4885	0.0536	0.2434	0.0195
jan13c6a	0.3756	0.0832	0.2659	0.0238
jan13b1a	0.3901	0.0214	0.3044	0.0149
jan13b2a	0.4375	0.0339	0.2367	0.0108
jan13b3a	0.4042	0.0213	0.2847	0.0151
jan13b4a	0.3604	0.0389	0.2360	0.0131
jan13b5a	0.3949	0.0820	0.1804	0.0129
jan13b6a	0.3016	0.0129	0.2564	0.0142
jan13a1d	0.4613	0.0146	0.2994	0.0102
jan13a2a	0.4443	0.0195	0.3098	0.0126
jan13a3a	0.3622	0.0112	0.3381	0.0186
jan13a4a	0.2394	0.0133	0.1748	0.0078
jan13a5a	0.3377	0.0258	0.1510	0.0081
jan13a6a	0.3849	0.0199	0.1789	0.0089
jan13e1a	0.3575	0.0196	0.2653	0.0116
jan13e2a	0.4659	0.0212	0.3303	0.0142
jan13e3a	0.4110	0.0389	0.2609	0.0125
jan13e4a	0.1508	0.0208	0.2714	0.0158
jan13e5a	0.1990	0.0129	0.2010	0.0113
jan13e6a	0.2353	0.0181	0.1533	0.0089

Table A9.2
Summary of inverse gaussian bubble chord length distribution function (T=100°C, V_s=4.1 cm/s)

Filename	α	α, s.d.	τ	τ, s.d.
jan11a1a	0.4393	0.0371	0.1712	0.0081
jan11a2a	0.3942	0.0363	0.1896	0.0082
jan11a3a	0.3461	0.0195	0.2120	0.0126
jan11a4a	0.4544	0.0214	0.2779	0.0153
jan11a5a	0.5441	0.3130	0.1693	0.0094
jan11a6a	0.5654	0.1421	0.2271	0.0151
jan11b1a	0.4086	0.0534	0.1878	0.0093
jan11b2a	0.5566	0.0364	0.2444	0.0107
jan11b3a	0.4334	0.0476	0.2073	0.0127
jan11b4a	0.5791	0.0207	0.2441	0.0134
jan11b5a	0.3630	0.0339	0.1696	0.0108
jan11b6a	0.4289	0.0276	0.1611	0.0079
jan11c1a	0.4729	0.0171	0.2661	0.0113
jan11c2a	0.3608	0.0153	0.2651	0.0107
jan11c3a	0.3359	0.0114	0.2902	0.0156
jan11c4a	0.3767	0.1299	0.2742	0.0111
jan11c5b	0.3759	0.0492	0.1485	0.0064
jan11c6a	0.3593	0.0127	0.2297	0.0109
jan11d1a	0.4469	0.0121	0.2577	0.0083
jan11d2a	0.4695	0.0163	0.2674	0.0096
jan11d3a	0.3750	0.0157	0.2725	0.0098
jan11d4a	0.2759	0.0059	0.2082	0.0079
jan11d5a	0.2133	0.0056	0.1971	0.0071
jan11d6a	0.2072	0.0035	0.1709	0.0054
jan11e1a	0.4274	0.0101	0.3626	0.0117
jan11e2a	0.4634	0.0118	0.3570	0.0117
jan11e3a	0.4084	0.0094	0.2448	0.0083
jan11e4a	0.2973	0.0063	0.1477	0.0046
jan11e5a	0.1825	0.0018	0.1255	0.0030
jan11e6a	0.2458	0.0077	0.1440	0.0072

Table A9.3
Summary of inverse gaussian bubble chord length distribution function (T=100°C, V_t=9.0 cm/s)

Filename	α	α, s.d.	τ	τ, s.d.
jan16e1a	0.4658	0.0160	0.2371	0.0089
jan16e2a	0.5579	0.0301	0.3026	0.0129
jan16e3a	0.5352	0.0242	0.3355	0.0152
jan16e4a	0.4131	0.0145	0.2906	0.0112
jan16e5a	0.4821	0.0174	0.2301	0.0103
jan16e6a	0.4037	0.0182	0.2410	0.0117
jan16d1a	0.4798	0.0159	0.3066	0.0132
jan16d2a	0.5173	0.0122	0.3251	0.0112
jan16d3a	0.5493	0.0162	0.2889	0.0111
jan16d4a	0.5716	0.0145	0.3041	0.0145
jan16d5a	0.2924	0.0065	0.2443	0.0094
jan16d6a	0.2889	0.0098	0.1876	0.0079
jan16c1a	0.5160	0.0158	0.3604	0.0166
jan16c2a	0.5836	0.0178	0.3778	0.0166
jan16c3a	0.5494	0.0133	0.3992	0.0174
jan16c4a	0.4275	0.0086	0.3361	0.0144
jan16c5a	0.3454	0.0092	0.2793	0.0106
jan16c6a	0.3547	0.0063	0.3397	0.0159
jan16b1a	0.5528	0.0179	0.4274	0.0198
jan16b2a	0.5060	0.0129	0.3559	0.0151
jan16b3a	0.4865	0.0138	0.3639	0.0181
jan16b4a	0.3403	0.0103	0.2597	0.0099
jan16b5a	0.3868	0.0077	0.2768	0.0107
jan16b6a	0.3511	0.0075	0.3036	0.0134
jan16a1a	0.5586	0.0134	0.4452	0.0181
jan16a2a	0.5354	0.0145	0.4006	0.0155
jan15a3a	0.5040	0.0148	0.4625	0.0285
jan16a4a	0.4494	0.0165	0.4719	0.0284
jan16a5a	0.3101	0.0066	0.2536	0.0097
jan16a6a	0.3136	0.0079	0.2466	0.0119

Table A9.4
Summary of inverse gaussian bubble chord length distribution function (T=100°C, V_s=14.7 cm/s)

Filename	α	α, s.d.	τ	τ, s.d.
jan17a1a	0.5127	0.0181	0.2756	0.0090
jan17a2a	0.5798	0.0196	0.3548	0.0157
jan17a3a	0.4810	0.0128	0.3177	0.0129
jan17a4a	0.4357	0.0116	0.4188	0.0186
jan17a5a	0.5459	0.0202	0.5008	0.0384
jan17a6a	0.3125	0.0053	0.2650	0.0121
jan17b1a	0.5664	0.0165	0.3732	0.0147
jan17b2a	0.5872	0.0173	0.3874	0.0170
jan17b3a	0.4962	0.0141	0.3357	0.0156
jan17b4a	0.4940	0.0115	0.3637	0.0179
jan17b5a	0.4013	0.00949	0.3082	0.0146
jan17b6a	0.3023	0.0048	0.2776	0.0111
jan17c1a	0.5491	0.0185	0.4025	0.0171
jan17c2a	0.5619	0.0149	0.4054	0.0149
jan17c3a	0.5782	0.0159	0.4515	0.0219
jan17c4a	0.5143	0.01203	0.3787	0.0170
jan17c5a	0.4241	0.0135	0.3671	0.0189
jan17c6a	0.4047	0.0108	0.4136	0.0192
jan17d1a	0.6495	0.0161	0.5165	0.0218
jan17d2a	0.5993	0.0207	0.4658	0.0259
jan17d3a	0.5297	0.0152	0.3770	0.0163
jan17d4a	0.4411	0.0114	0.3570	0.0174
jan17d5a	0.3825	0.0111	0.3819	0.0205
jan17d6a	0.3518	0.0061	0.2835	0.0105
jan17e1a	0.5983	0.0168	0.5270	0.0237
jan17e2a	0.6269	0.0165	0.5188	0.0229
jan17e3a	0.5168	0.0124	0.4718	0.0224
jan17e4a	0.4299	0.0131	0.3942	0.0187
jan17e5a	0.3744	0.0115	0.4482	0.0265
jan17e6a	0.2978	0.0061	0.3190	0.0152

Table A9.5
Summary of inverse gaussian bubble chord length distribution function (T=175°C, V_t=2.2 cm/s)

Filename	α	α, s.d.	τ	τ, s.d.
jan18e1a	0.3500	0.0437	0.1999	0.0090
jan18e2a	0.3829	0.0346	0.2888	0.0147
jan18e3a	0.4645	0.0367	0.2485	0.0129
jan18e4a	0.4152	0.0567	0.2365	0.0129
jan18e5b	0.4150	0.0225	0.3513	0.0149
jan18e6a	0.4299	0.0263	0.3057	0.0135
jan18d1a	0.3962	0.0199	0.2830	0.0110
jan18d2a	0.3948	0.0252	0.3130	0.0121
jan18d3a	0.3853	0.0207	0.2868	0.0128
jan18d4b	0.4325	0.0187	0.2943	0.0129
jan18d5a	0.3399	0.0831	0.1709	0.0102
jan18d6b	0.3449	0.0229	0.2730	0.0162
jan18c1a	0.4045	0.0183	0.3151	0.0137
jan18c2a	0.3387	0.0151	0.3014	0.0114
jan18c3a	0.3812	0.0132	0.3052	0.0108
jan18c4b	0.3353	0.0121	0.2348	0.0085
jan18c5b	0.2181	0.0099	0.1632	0.0069
jan18c6a	0.2049	0.0084	0.2202	0.0090
jan18b1a	0.3126	0.0106	0.3085	0.0104
jan18b2a	0.3332	0.0102	0.3378	0.0124
jan18b3a	0.3706	0.0129	0.3226	0.0141
jan18b4a	0.2819	0.0149	0.2087	0.0079
jan18b5b	0.2445	0.0101	0.1485	0.0039
jan18b6b	0.2030	0.0077	0.1797	0.0060
jan18a1a	0.2961	0.0120	0.2526	0.0088
jan18a2a	0.3565	0.0136	0.3019	0.0101
jan18a3a	0.3692	0.0142	0.2612	0.0091
jan18a4b	0.2408	0.0057	0.1983	0.0058
jan18a5b	0.3261	0.0096	0.1483	0.0048
jan18a6a	0.2520	0.0080	0.2336	0.0106

Table A9.6
Summary of inverse gaussian bubble chord length distribution function (T=175°C, V_g=4.1 cm/s)

Filename	α	α, s.d.	τ	τ, s.d.
jan20a1a	0.3464	0.0156	0.2313	0.0067
jan20a2a	0.4147	0.0162	0.3464	0.0136
jan20a3a	0.4183	0.0146	0.2429	0.0082
jan20a4a	0.3217	0.0193	0.2561	0.0119
jan20a5b	0.4771	0.0422	0.3233	0.0226
jan20a6a	0.3662	0.0179	0.2480	0.0109
jan20b1a	0.4270	0.0143	0.3058	0.0101
jan20b2b	0.3577	0.0106	0.2623	0.0069
jan20b3a	0.4144	0.0122	0.2762	0.0085
jan20b4a	0.3294	0.0104	0.2925	0.0112
jan20b5b	0.3854	0.0115	0.2179	0.0070
jan20b6a	0.2499	0.0060	0.2332	0.0094
jan20c1a	0.4975	0.0115	0.4518	0.0167
jan20c2a	0.4257	0.0097	0.3040	0.0089
jan20c3a	0.3782	0.0112	0.3155	0.0119
jan20c4a	0.4278	0.0124	0.2896	0.0099
jan20c5a	0.3913	0.0078	0.2706	0.0093
jan20c6b	0.2435	0.0060	0.1827	0.0060
jan20d1a	0.4480	0.0101	0.3744	0.0103
jan20d2a	0.4146	0.0085	0.3450	0.0104
jan20d3a	0.4058	0.0097	0.3004	0.0092
jan20d4a	0.4097	0.0155	0.3042	0.0120
jan20d5b	0.3040	0.0049	0.2400	0.0066
jan20d6b	0.2785	0.0083	0.2670	0.0119
jan20e1b	0.4404	0.0077	0.3827	0.0093
jan20e2a	0.4377	0.0079	0.3669	0.0096
jan20e3a	0.3893	0.0072	0.3157	0.0080
jan20e4a	0.3886	0.0037	0.2351	0.0063
jan20e5a	0.2364	0.0027	0.1729	0.0034
jan20e6a	0.2075	0.0061	0.3190	0.0152

Table A9.7
Summary of inverse gaussian bubble chord length distribution function (T=175°C, V_t=9.0 cm/s)

Filename	α	α, s.d.	τ	τ, s.d.
jan21e1a	0.4454	0.0154	0.3392	0.0132
jan21e2a	0.4278	0.0116	0.2765	0.0081
jan21e3a	0.4575	0.0082	0.2972	0.0083
jan21e4a	0.3916	0.3206	0.0084	0.3002
jan21e5a	0.4310	0.0122	0.3436	0.0129
jan21e6a	0.3314	0.0055	0.2788	0.0101
jan21d1a	0.4604	0.0095	0.3789	0.0115
jan21d2a	0.4271	0.0087	0.3790	0.0120
jan21d3a	0.4502	0.0070	0.3576	0.0088
jan21d4a	0.4015	0.0073	0.3035	0.0085
jan21d5a	0.3765	0.0077	0.2712	0.0098
jan21d6a	0.3093	0.0056	0.2694	0.0096
jan21c1a	0.4536	0.0074	0.3622	0.0098
jan21c2a	0.4571	0.0074	0.4100	0.0132
jan21c3a	0.4296	0.0099	0.3474	0.0116
jan21c4a	0.4096	0.0068	0.3805	0.0127
jan21c5a	0.3840	0.0058	0.2906	0.0102
jan21c6a	0.2807	0.0038	0.1758	0.0044
jan21b1a	0.4992	0.0104	0.4333	0.0142
jan21b2a	0.4429	0.0063	0.3839	0.0099
jan21b3a	0.3981	0.0065	0.3688	0.0109
jan21b4a	0.3062	0.0043	0.2973	0.0085
jan21b5a	0.3102	0.0042	0.3032	0.0079
jan21b6a	0.3147	0.0045	0.2840	0.0089
jan21a1a	0.4844	0.0102	0.4303	0.0146
jan21a2a	0.4279	0.0078	0.4127	0.0139
jan21a3a	0.4545	0.0101	0.4246	0.0165
jan21a4a	0.3361	0.0045	0.3153	0.0089
jan21a5a	0.2285	0.0028	0.1698	0.0038
jan21a6a	0.2319	0.0030	0.1967	0.0065

Table A9.8
Summary of inverse gaussian bubble chord length distribution function (T=175°C, V_g=14.7 cm/s)

Filename	α	α, s.d.	τ	τ, s.d.
jan22a1a	0.3867	0.0097	0.2935	0.0079
jan22a2a	0.4839	0.0126	0.3318	0.0091
jan22a3a	0.4793	0.0094	0.3896	0.0135
jan22a4a	0.4491	0.0096	0.3164	0.0105
jan22a5a	0.4660	0.0091	0.3495	0.0115
jan22a6a	0.3772	0.0053	0.2772	0.0077
jan22b1a	0.4836	0.0109	0.3906	0.0139
jan22b2a	0.4993	0.0098	0.4254	0.0143
jan22b3a	0.4527	0.0095	0.4016	0.0149
jan22b4a	0.4698	0.0093	0.4352	0.0141
jan22b5a	0.4317	0.0079	0.3418	0.0102
jan22b6a	0.3886	0.0072	0.3279	0.0110
jan22c1a	0.4762	0.0096	0.4097	0.0142
jan22c2a	0.4443	0.0086	0.4294	0.0144
jan22c3a	0.4874	0.0107	0.4070	0.0155
jan22c4a	0.3937	0.0089	0.3398	0.0111
jan22c5a	0.3570	0.0058	0.3289	0.0113
jan22c6a	0.3416	0.0059	0.3232	0.0110
jan22d1a	0.5393	0.0134	0.0.5292	0.0245
jan22d2a	0.4958	0.0120	0.4640	0.0176
jan22d3a	0.4713	0.0078	0.4695	0.0148
jan22d4a	0.4129	0.0086	0.4081	0.0166
jan22d5a	0.4227	0.0093	0.3804	0.0148
jan22d6a	0.3357	0.0058	0.3138	0.0099
jan22e1a	0.5620	0.0162	0.5143	0.0237
jan22e2a	0.4645	0.0098	0.4282	0.0145
jan22e3a	0.4622	0.0089	0.4517	0.0167
jan22e4a	0.3677	0.0067	0.3576	0.0108
jan22e5a	0.3717	0.0064	0.3052	0.0099
jan22e6a	0.3331	0.0056	0.2569	0.0093

APPENDIX 10

TIME SERIES ANALYSIS

TIME SERIES ANALYSIS

The first and essential operation in processing the fibre optic sensors' time series is to identify the individual bubble detection peaks and their individual characteristics (start point, end point, duration, maximum amplitude, average amplitude ...). Such identification was done using a methodology based on the variation of the time series slope. Each and every data points present in a given time series (50000 data points / time series) was read. When a positive change of slope between two adjacent data points was perceived, the following analysis method was activated: When the change of slope was superior to a preset value (criterion #1), the presence of a bubble detection peak was suspected. If the slope of the signal (positive slope) was maintained for one more time interval above a preset value (criterion # 2), a bubble was identified. The ascending portion of the bubble detection peak was monitored until a change of slope was encountered (negative slope). The descending section of the detection peak was monitored until a change in the sign of the slope was encountered. The determination of the end of the bubble detection peak was identified with the help of two supplementary criteria (criteria # 3 and 4). These criteria ensure that the determination of the end of the bubble detection peak was not affected by the presence of oscillations in the bubble detection peak. The four criteria were selected based on the individual response of the sensor

(studied during a pre-testing phase) and the noise present in the system. The criteria, for a given sensor and given operating conditions (temperature, gas superficial velocity) were further validated performing a visual analysis of the time series: Small sections of the time series were printed. For each section printed, visual inspection of the time series allowed to identify every bubble detection peaks present. These observations were then compared to the identification of the bubble detection peak found using the methodology previously described, as shown in a typical example presented in Figure A10.1.

After all the gas bubble detection peaks and their characteristics were identified, important fluid dynamic parameters could be derived. The gas holdup was determined by doing the summation of the duration of every gas bubble detection peak (time during which the fibre optic sensor's detecting tip was in contact with gas) divided by the total data acquisition time, as indicated in Equation 4.1 (Chapter 4). The precise identification of all the bubble detection peaks present in a given time series was also used in the determination of the bubble chord length. As mentioned in Chapter 4, the average bubble chord length at a particular location in the column, under a particular set of operating conditions, is the product of the average bubble rise velocity (obtained from the application of the cross correlation technique to the lower and upper fibre optic sensors' time

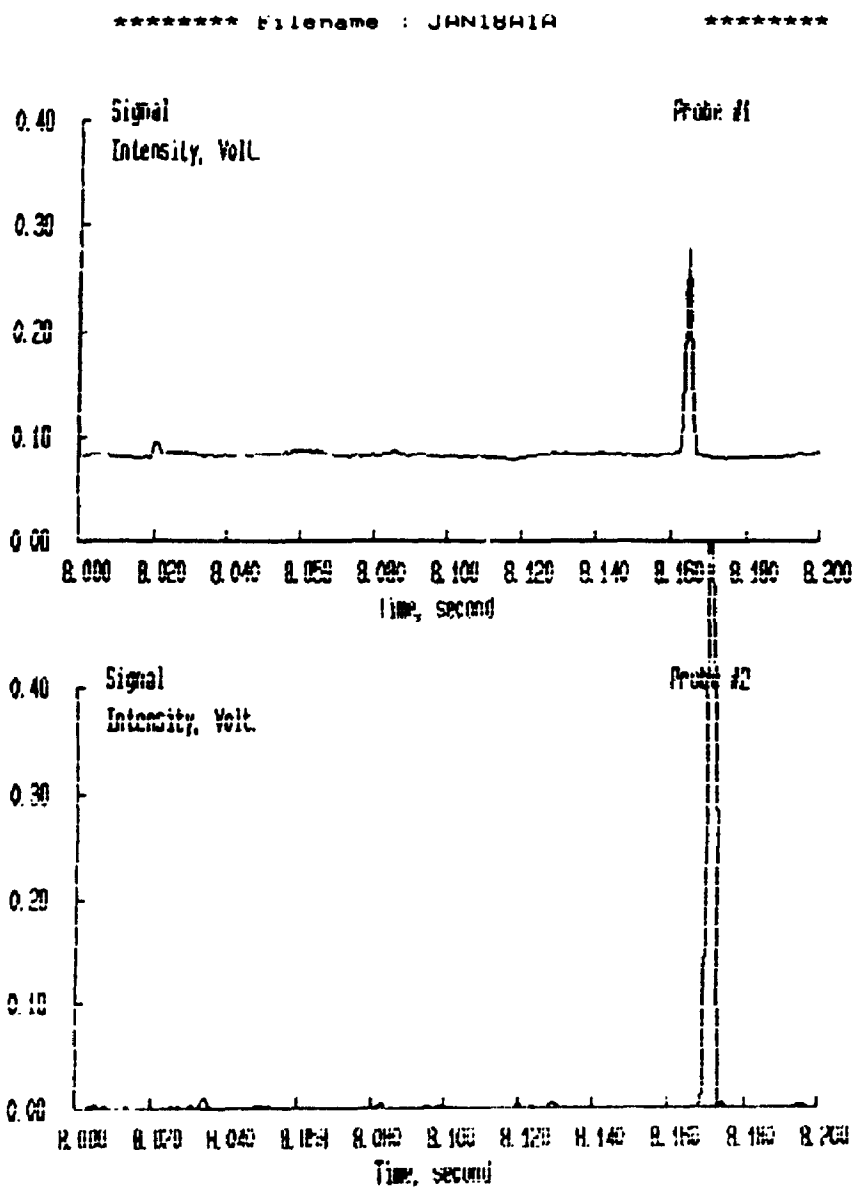


```
******** Probe No : 1 ********

* Bubble # 1  ** Start:  8019  ** End:  8023
* Bubble # 2  ** Start:  8162  ** End:  8167

******** Probe No : 2 ********

* Bubble # 1  ** Start:  8033  ** End:  8036
* Bubble # 2  ** Start:  8168  ** End:  8173
```

Figure A10.1: Typical criteria verification

series, as discussed in Chapter 4) and the average bubble-probe contact time (average duration of all the gas bubble detection peaks) detected by the lower fibre optic sensor (information obtained from the lower fibre optic sensor is less affected by possible bubble flow hindrance than the upper fibre optic sensor). The identification of the individual characteristics of every bubble detection peaks (start point, end point, duration ...) was also used in the bubble chord length distribution analysis, as described in Chapter 4. More details concerning the time series analysis could be found in Appendix 3, where the detailed time series processing softwares are presented.